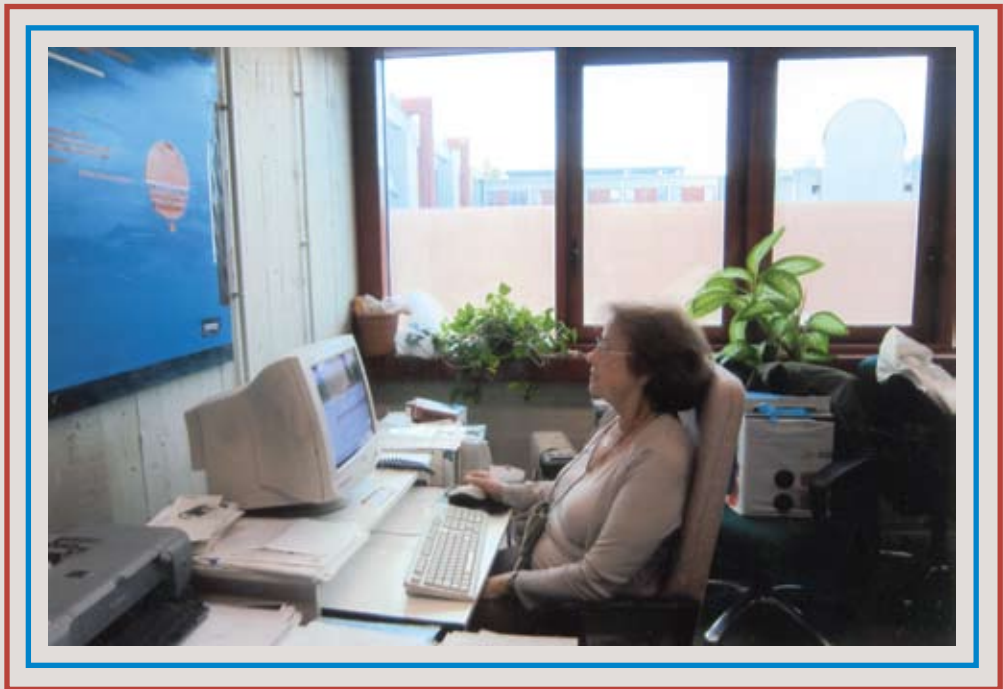


Discoglossus pictus fertilization and other stories

Selected publications and memories of Chiara Campanella



Discoglossus pictus fertilization and other stories

Selected publications and memories of Chiara Campanella

A big thank to Paolo G. for his welcome suggestions, and to Paolo T. for lovingness permeating the composition of this text.

Editorial coordination
doppiavoce
www.doppiavoce.it

English revision
Mark J. Walters

N.B. Some texts and in particular the references were cut for editorial reasons.

*Dedicated to my daughter Elisabetta and my son Paolo
for their well-trying patience waiting for their mother to get back from work.*



Contents

| | |
|--|-----|
| The study of <i>Discoglossus pictus</i> fertilization | 7 |
| The calcium and ER story | 225 |
| Our work on oocytes | 301 |
| The vitelline envelope and jelly coats of <i>D. pictus</i> egg | 339 |
| Eif6 in <i>Xenopus</i> oogenesis and embryogenesis | 405 |
| Final remarks | 463 |

The study of *Discoglossus pictus* fertilization

Cecilia was looking at *Discoglossus pictus* egg insemination through the stereomicroscope. Eventually she was able to see the sperm bundle opening in the jelly plug and exclaimed: "Gosh, I can't believe it! It's the most beautiful thing I've ever seen".

I was moved by her enthusiasm because that was really how I felt too. What she was describing, and the fertilization of *D. pictus* in general, had inspired more than 40 years of research, involving many students and researchers in Italy, Switzerland, the USA and in Japan. The egg of *D. pictus* has a restricted site where fertilization may occur in contrast to the egg of most animals. It is therefore ideal for investigating the characteristics that underlie sperm entry and the activation of development using complementary approaches, thus contributing to the understanding of the fertilization process.



Fig 1.

The story of this research started in the USA. I was sitting in the laboratory room next to Dr. George Nace's office at the Department of Zoology of the University of Michigan. It was a chilly winter day in 1967. Pryambada (Mini) Hejmadi was working with her protein electrophoresis apparatus in a corner of the laboratory. Jack Hegenauer was coming and going, engaged in mysterious activities. I was doing my experiments which involved pre-treatment of *Rana pipiens* eggs with nicotine. My determination to find the ultrastructure of sperm penetration in amphibian eggs had suggested that I induced polyspermy through the use of nicotine to increase the chance of finding the 1 μ m-thick sperm head on the surface of the 1.8-mm large egg. I had promised to achieve this goal both to myself and to Carlo Taddei, during my *degree thesis* while working at the Hitachi microscope at the University of Naples in 1965. Chiaki Katagiri was sitting in front of my bench watching me in silence. Suddenly, Chiaki told me that he had read about a strange European frog, *Discoglossus pictus*. In the thirties, according to two French researchers, namely Wintrebert and Hibbard, its egg has, at the animal hemisphere cen-



Fig. 2. Circa 1975. At the front door of the Centre for the study of electron Microscopy, immersed in the Botanical Garden of Naples, most of the Institute of Histology and Embryology components and many guests. On my right Ettore Olmo, Silvana Filosa, Carlo Taddei, on my left Piero Andreuccetti, behind, among others, Mario de Vincentiis, Giuseppina Barsacchi, Linda Limatola and Elio Parisi. In the front line Franca Andronico, Gianfranco Ghiara, Giovanni Chieffi, Aldo Merola, Sandro Morescalchi. Also, Giovanni Giudice, Vittorio D'Uva, Virgilio Botte, Rakesh Rastogi and on the opposite side Alberto Monroy and Franco Giorgi.

tre, a site predetermined for sperm penetration. "If I've understood correctly the French of the authors, this species should be available in Mediterranean countries and should offer a really convenient model for your study" continued Chiaki. I still remember his smiling face while he was saying that to me. Chiaki died in 2010. His input has been inspirational for my research.

Back in Naples in 1968 to the Institute of Histology and Embriology (later called Department of Comparative and Evolutionary Biology) of the University of Naples Federico II, I found out that Gianfranco Ghiara, the head of the Institute, had indeed worked on the *D. pictus* egg. He had studied the unusual jelly investment of this species. I paid a visit to Reverberi's laboratory at the University of Palermo, where *D. pictus* was normally used after capture in the countryside. I was given help to organize frog shipments to Naples.

There was so much to study and learn about *D. pictus* gametes and fertilization that I had serious difficulties programming a single experiment be-

cause I could not perform at the same time many other experiments I had in mind. I used to spend a long time getting ultrathin sections of *D. pictus* eggs and sperm bundles. A student with boundless enthusiasm, Umberto Atripaldi, was working with me at that time and we spent many days observing the samples under the electron microscope of the Centre for the study of Electron Microscopy. The Centre was founded by Gianfranco Ghiara in the late sixties and was one of the first in Italy, equipped with excellent instruments and taken care by expert technicians. With skill and patience, Gennaro Cafiero, Giuseppe Orsello and Enzo Esposito taught us how to use the microscope. By 1975, most of the ultrastructural study of acrosome reaction and sperm penetration had been completed. I presented the data at the La Jolla meeting on fertilization (1975), yet they were only published 15-22 years later!

The first paper on *D. pictus* egg described the morphology of the dimple, the site of fertilization, also using a scanning microscope belonging to the palaeontologists in our faculty and used for the first time by a biologist in Italy (1974-75). Later Piero Andreuccetti (Institute of Histology and Embryology) joined these ultrastructural studies and together we wrote papers dealing with the formation and localization of cortical granules in the germinative area, and with vitellogenesis, which was to play a key role in the *D. pictus* story later on. Meanwhile the world of embryologists was shaken by the simple, yet little explored, idea contained in the papers by Tom Shroed-



Fig. 3. 1977. Christine Chaponnier with Jean Claude Rumbeli at the Département de Pathologie General, Université de Genève.



Fig. 4. 2001. This picture collected several researchers who had visited Gabbiani laboratory in the 70th -90th. The occasion was the Cytoskeleton Club meeting held in Nyon (Switzerland), chairman Cristine Chaponnier, at the centre of picture. Behind her, with dark dress, Giulio Gabbiani. In the front line, third on the left, his wife and researcher Françoise Gabbiani.

er and Lewis Tilney that eggs (and spermatozoa) could have features quite similar to those of other cells, in particular the cytoskeleton. I was awarded a two-year EMBO fellowship, to be spent in Giulio Gabbiani's laboratory in Geneva University, Institute of Pathology, for studying the cytoskeleton of gametes. In that laboratory I met Christine Chaponnier and thanks to her and Giulio I learnt immunofluorescence techniques in addition to basic biochemistry. We published several papers on the cytoskeleton of the egg before and after fertilization and on the sperm cytoskeleton. Indeed several cytoskeletal features we described explained some interesting motile properties of *D. pictus* spermatozoa. This line of research was the source of several other papers in the following years. I worked in collaboration with researchers such as Baccio Baccetti and Anna Burrini (University of Siena), Roberto Gualtieri (University of Naples), Carla Tatone, Rosella Colonna and Gianna Rossi (University of L'Aquila), Rosa Carotenuto, who developed this line of research at the University of Naples and Loredana Chierchia in her PhD thesis.

We found that during the transition from the disk-shaped germinative area to the funnel-shaped dimple, the actin microfilaments of the bundles embedded in the oocyte microvilli acquire new physical characteristics and are associated to different actin-binding proteins. Spectrin appears in the cortex



Fig. 5. 1987. The University of L'Aquila. In my lab, on my left Carla Tatone, Gianna Rossi and a student of mine.



Fig. 6. 1987. With Carla Tatone, Gianna Rossi and a student of mine.

when the oocyte segregates the animal and the vegetal hemisphere during oogenesis and may be associated to the new arrangement of Cl⁻ channels (the fertilization channels) occurring during the formation of the dimple. Evidently, the cytoskeleton is associated to cell shape and functional roles in preparation to fertilization. Overlapping with these studies, a new branch of research attracted my attention. Indeed, in studying the changes occurring in the dimple at activation, a student of mine, Riccardo Talevi, and I were astonished by the complexity of the phenomena we were observing and predicted that a physical approach such as electrophysiology could unravel many uncertainties about the timing of the observed events with respect to the onset of activation. At the Anton Dohrn Marine Biology Station in Naples, we met Brian Dale a scientist who broadened our scientific horizons. With great generosity Brian and Amedeo De Santis trained us in electrophysiology until we could show that the activation response occurred practically only in the dimple. Indeed, activation by pricking at different angles to the dimple produces a contraction wave (of activation). When the wave arrives in the dimple an activation potential (AP) is produced together with cortical granule exocytosis. Moreover, Riccardo promptly took advantage of the fact that the jelly plug that makes sperm converging into the dimple may dislocate laterally with respect to the dimple centre, following imbibitions in Ringer saline. In this condition, spermatozoa converge into different portions of the dimple where they do not elicit normal FP, but small steps of depolarization. In these regions, the sperm start penetration, but they are stopped and undergo cytological changes similar to blebbing caused by apoptosis. The dimple appears to be a highly regionalized egg territory, being able to respond to sperm penetration only at its centre D1. It has many features that appear to distribute as a gradient starting from D1. Roberto Gualtieri, Gennaro and Piero showed that D1 has intramembrane particles with higher concentration and opposite repartition in the two leaflets with respect to the rest of the egg membrane. We wondered whether these particle were molecules involved in sperm reception or chloride channels, the ionic channels typically involved in amphibian fertilization potential. At about that time Rosa Carotenuto stepped into my laboratory. Since then, she has been party to all the activity in my laboratory where she graduated and then became a researcher.

In 1983, at the Gordon Conference, Rich Nuccitelli, impressed by the Calcium release-connected events occurring in the dimple at activation and in particular by the changes in the endoplasmic reticulum (ER), invited us to the Department of Zoology of the University of California, Davis, with the project of detecting the activation current in the dimple. At the same time

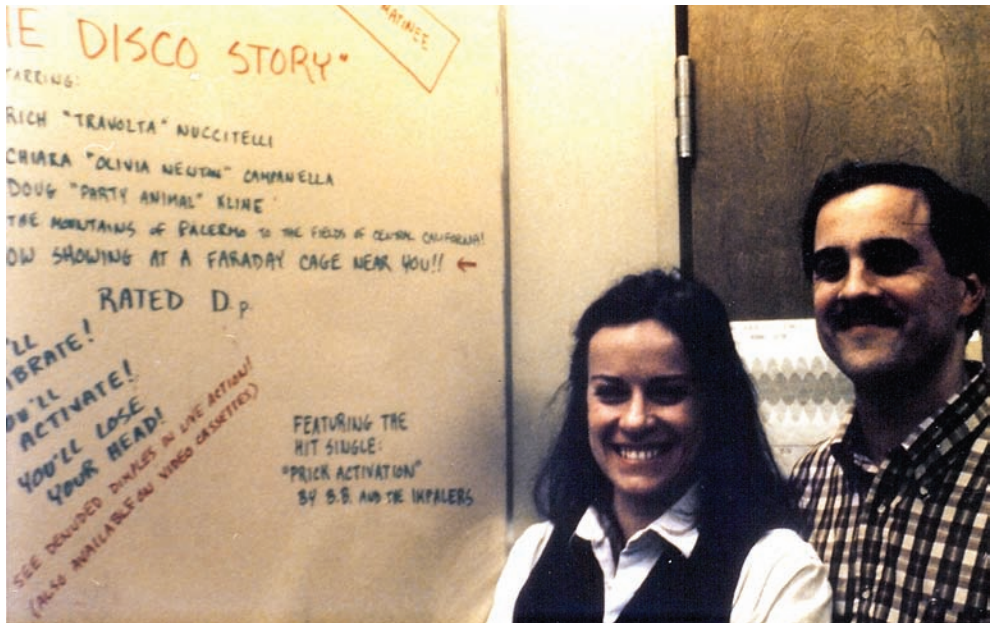


Fig. 7. 1984. With Rich Nuccitelli. Together with Bill Busa we had just written at the blackboard a funny story about *D. pictus* in California.

Jerry Hedrick invited me to give talk at a meeting he organized in Davis. I worked there in 1984 together with Riccardo Talevi who was working on his PhD thesis. It was wonderful to stay in Davis because there was a concentration of persons interested in Amphibian fertilization: Jerry Hedrick and his group, Nick Cross, Doug Kline, Bill Busa, Bob Grey, John Savage and others. We were talking the same 'language'. I worked a lot there and it was a real pleasure. I came back in 1985 to conclude the project. Together with Rich and Doug Kline we found a Cl^- -transported inward current only in D1: we were able to precisely measure D1 as a disk of about $200\ \mu\text{m}$. Because of these experiments and the fact that only D1 was stained by the Cl^- channel-binding DIDS, we were able to conclude that there are only channels in D1. Therefore, the intra-membrane particles detected in the over-mentioned paper, are most probably Cl^- channels. Moreover, we found that the endoplasmic reticulum changes were driven by a combination of the current crossing the dimple and the release of calcium at activation. Thanks to Bill Busa we were able to measure an eight-fold calcium increase at activation, which was crossing the egg from the IP3 injection site to the antipode. When the wave arrives in D1, calcium is able to activate the Cl^- channels, the cortical granules are exo-



Fig. 8. 1986. Mini in my house with me and Elisabetta, my daughter.



Fig. 9. ... and with my son Paolo.



Fig. 10. 1986. Mini gave a seminal Class on Sex Determination at the University of Naples. Here, the Department member were at party in her honour. Behind Riccardo Talevi (first row, light blue shirt) from far left: Roberto Gualtieri, Gaetano Odierna, Piero Andreuccetti, Rakesh Rastogi, Teresa Capriglione, Mini next to me and Gianfranco Ghiara



Fig. 11. 1993. I reciprocated Mini's visit in Naples and I visited her in Bhubaneswar. Here at the main door of her Department of Zoology, Utkal University, Orissa.

cytosed, and whorls of endoplasmic reticulum open and invade the peripheral cytoplasm of D1.

I was invited in 1987 at the Gordon Conference on Fertilization and Activation of Development. I showed these experiments and the audience welcomed the *D. pictus* data with enthusiasm.

There are still many questions that would deserve more attention. Indeed, in particular, we were unable to understand whether IP₃/Calcium were the only molecules involved in activation. We suspected that an unknown signal induced by pricking precedes the calcium wave, because we observed that if the egg is pricked simultaneously at opposite sides, two equal contraction waves are generated. However, when pricking is first conducted at one side and about 20 sec later at the opposite side, the second wave never develops.

In the 1980s and 1990s an important theory about sperm-egg interaction suggested that sperm activates a membrane receptor transducing the signal through IP₃/calcium. In the same period integrins were found in the egg and



Fig. 12. 1987. At the Gordon Conference. From the left Jerry Hedrick, Richard Elinson, next to me N. Yoshizaki, and Yasuhiro Iwao. The picture was taken by Chiaki.

dis-integrins in the sperm. However, a few years later the integrin model was proved to be not necessary for sperm binding and egg activation, with some exceptions. We thought that the egg of *D. pictus*, where successful fertilization occurs only in the small D1, was a convenient model for the study of molecules involved in sperm binding. When we started this work, no molecule at the egg membrane had yet been identified as the first sperm binder. A long period of research then started involving the patience of many students, such as Enzo Infante, Mariangela Caputo, Loredana Tretola and young researchers such as Rosa Carotenuto, Vania Maturi, Maria Grazia De Santo and Carmen Vaccaro. Part of this topic was covered by Vania's PhD thesis and later by that of Enzo. Thousands of gel stripes had to be cut from SDS-PAGE gels.

Finally, also thanks to suggestions made by Floriana Rosati and Riccardo Focarelli (Department of Evolutionary Biology, University of Siena) about technical approaches on large glycoconjugates, we were able to identify high-Mr glycoproteins exposed only at the dimple and able to bind sperm in *in vitro* assays. This was also possible because much earlier, in 1977, together with



Fig. 13. 1993. A meeting in the 'Auletta' of the Department of Biologia Evolutiva e Comparata. In this crowded smiling group I can recognize from left, first row, Roberto Gualtieri and Gina Santella; second row, Gianna Rossi, Paolo Abrescia (hiding Rosa Carotenuto), Rosaria De Sanctis, Carla Tatone, Rosaria Pinto, Sandra Cecconi. In the back, next to me, Brian Dale. Riccardo was the photographer.



Fig 14. 1994. At the University of Naples in the lab with Enzo Infante and Vania Maturi.



Fig 15. 1994. Enzo Infante party in occasion of his Laurea degree. With Vania, Anna Savarese Roberta Poulet and Enzo.

Suzanne Denis (L.E.M., CNR, Naples), I found that the D1 external membrane has a natural marker, terminal fucose, evidently characterizing specific glycoconjugates. The next step was even more difficult and took a long time to be carried through. I remember that at the end of his smart PhD thesis, Enzo and I were guessing that the glycoconjugates at the D1 surface had to be molecules closely related to lipovitellin. This finding was quite unexpected and had to be carefully demonstrated to persuade a sceptical scientific community. Surely the identified D1 glycoconjugates were not contamination from yolk platelets! Enzo and I visited Laura Camardella's laboratory at CNR IBPE to have the N-terminus of D1 glycoconjugates measured. In doing so, we followed some suggestions Vic Vacquier gave us with his usual friendly aptitude of an elder brother. Laura's analyses showed the N-terminus highly similar to that of vitellogenin and lipovitellin 1! Next, Maldi/MS analyses carried out at CEINGE by Angela Flagiello and fluorescent/ultrastructural data fully demonstrated that D1 glycoconjugates are glycoforms of a lipovitellin 1 (DpLIV) located at the egg surface only in D1. Thanks to Carmen Vaccaro's expertise in molecular biology acquired in Teresa Capriglione's laboratory, these data were correctly adopted in our research. The work that Suzanne and I had carried out in 1977 also meant that we could figure out that DpLIV is oocyte-synthesized and becomes external to the dimple during its formation. In fact, the ovarian germinative area undergoes a 10-fold increase in surface area during its post-ovulatory transformation into a dimple. This is due to active exocytosis and surface re-shaping.

At the time these results were published, it was commonly accepted that the egg is activated not because of a receptor in the egg membrane, but because of introduction into the egg of an enzyme able to start development. In *D. pictus*, at the egg membrane (in the glycocalyx) DpLIVs appear to be necessary for sperm adhesion and fusion and not for signal transduction. When spermatozoa reach the egg plasma membrane they have attained the final stages of acrosome reaction and acrosome enzymes (trypsin, chymotrypsin and plasminogen activator activity, as determined by Enzo) are released in close proximity of the membrane. Our ultrastructural data and timing between insemination-AP arousal (electrophysiologically recorded), strongly suggest that the sperm first bind the glycocalyx at the egg membrane and then the acrosome enzymes digest the glycocalyx. Probably enzyme digestion uncovers the molecule able to start egg activation.

The old dream of understanding the morphology of sperm penetration and the more recent hope to understand the molecules involved in sperm-egg interaction were finally largely fulfilled!

Further research on *D. pictus* fertilization was not possible for several reasons. Most importantly, the animals have suffered from urbanization of rural areas and are now listed as protected species. Overall, the study of *D. pictus* fertilization has lent insights into the mechanism of egg activation and the poorly represented number of molecules involved in sperm-egg adhesion at the membrane surface.

I remember the many discussions conducted by Alberto Monroy and his group in the 1980s dealing with the understanding of the fertilization process, in particular in Ascidians. At that time the in vitro techniques for assisted reproduction had not been developed and understanding this complex and difficult process was top priority. He often wondered whether the many sperm do not enter the egg only because they are inhibited by polyspermy blocks. He supposed that this inhibition occurs also because sperm from one or many individuals in one species could be more or less compatible with individual eggs. His curiosity and questions were a guideline for many of us. In 2008, in the Vic Vacquier laboratory, important data were found to support his predictions. Indeed several molecular mechanisms (i.e. positive selection, alternative splicing, recombination) can create thousands of variants in the sperm molecule that binds the egg in oyster and sea urchin fertilisation. Alberto would have been immensely happy to know about the current state of the field.

THE EFFECTS OF NICOTINE
ON INSEMINATED AND ARTIFICIALLY ACTIVATED
RANA PIPIENS SCHREBER EGGS *

CHIARA CAMPANELLA

Istituto di Istologia ed Embriologia
Laboratorio di Anatomia Comparata dell'Università di Napoli

Received 25 October 1971

| | |
|---|----------|
| I. Introduction | page 195 |
| II. Materials and methods | » 197 |
| III. Results | » 198 |
| A. Nicotine fertilization tests | » 198 |
| 1. Effect of nicotine on sperms | » 198 |
| 2. Effect of nicotine on eggs | » 200 |
| 3. Paraffin sections of <i>pretreatment</i> and <i>treatment</i> eggs | » 200 |
| 4. Observations of embryos, nicotine-treated at blastula stage | » 202 |
| B. ES of nicotine-treated eggs | » 202 |
| C. Nicotine-treated and pricked eggs | » 203 |
| IV. Discussion | » 206 |
| <i>Summary</i> | » 208 |
| <i>Riassunto</i> | » 209 |
| <i>References</i> | » 210 |

I. INTRODUCTION

Several drugs have been known to induce polyspermy in the sea urchin egg (CLARK, 1936). Among these, nicotine has been used by several investigators (CLARK, 1936; ROTHSCHILD & SWANN, 1950; ROTHSCHILD,

*The experimental work was conducted in the laboratory of Prof. George W. Nace, the Department of Zoology and Center for Human Growth and Development, the University of Michigan, with the support of National Science Foundation grants NSF GB 4677 and NSF GB 8187, Damon Runyon Memorial Fund grant DRG 980, and National Science Foundation Institutional Grant No. 108. Data collation and analysis were conducted in the Laboratorio di Anatomia Comparata of the Università di Napoli, directed by Prof. Gianfranco Ghiara.

The Site of Spermatozoon Entrance in the Unfertilized Egg of *Discoglossus pictus* (Anura): An Electron Microscope Study

CHIARA CAMPANELLA

Istituto di Istologia ed Embriologia—Via Mezzocannone, 8, Napoli, Italy

Accepted November 5, 1974

The egg of *Discoglossus pictus* has an animal dimple, a pit located at the animal hemisphere pole, which is the only site successfully penetrated by the sperm. Ultrastructural analysis of the unfertilized egg surface reveals unique features characterizing the animal dimple. They are: 1) regularly spaced, finger-like microvilli supported by bundles of fibers which appear to be microtubules and surrounded by antennular glycocalyx, present at the surface of the animal dimple. The orientation and distribution of the fibers suggest that they may play an essential rôle in maintenance of the shape of the animal dimple; 2) granules present in the peripheral cytoplasm of the animal dimple whose characteristics are somewhat different from those of the typical Anuran cortical granules and which are absent from the rest of the peripheral cytoplasm of the egg. The unique presence of these granules at the animal dimple and their apparent loss at the time of fertilization suggest that they might actively participate in the fertilization process.

Freshly laid eggs of *Discoglossus pictus* (painted frog) exhibit a depression (the animal depression) at the animal hemisphere whose center part is invaginated and forms the animal dimple. The animal depression is filled with a gelatinous lens-shaped material forming the animal plug, which protrudes at the surface of the egg (Hibbard, 1928). The eggs are further covered with four gelatinous envelopes with different chemical compositions. The innermost envelope is made up of two membranous layers E_1 and E_2 and strictly adheres to the egg surface, except over the animal dimple where they are separated from the egg surface by a substance of glycoprotein nature (Ghiara, 1960). The nucleus, arrested in metaphase of the 2nd meiotic division, is located in the cortical cytoplasm of the area germinativa which is the bottom of the animal dimple. In sections of eggs at the level of the animal dimple, and particularly at its basal portion, one can clearly distinguish striations which are perpendicular to the egg surface (Hibbard, 1928).

This type of organization at the animal pole of the *Discoglossus* egg is interesting because it seems to be connected with a

peculiar type of fertilization. Indeed, while in all the Anurans studied thus far, sperm penetration may occur anywhere at the animal hemisphere, in *Discoglossus*, the sperm-egg interaction seems to be restricted to the animal dimple where spermatozoa arrive after passing through the animal plug (Hibbard, 1928, Wintrebert, 1930) (Fig. 1).

In the context of a program of investigation on the physiology of fertilization in *Discoglossus*, the ultrastructure of the peripheral cytoplasm of the mature unfertilized egg has been studied with particular reference to the animal dimple in the hope of understanding why the animal dimple is the only possible place for sperm penetration.

These observations have shown that the animal dimple is in fact characterized by certain structural peculiarities which may be related to its physiological role as the site of interaction with the spermatozoa. A brief report on this subject has been published elsewhere (Campanella Trautteur, 1970).

MATERIALS AND METHODS

Adult *Discoglossus pictus* (painted frog) females, captured in the neighborhood of Palermo (Italy), were

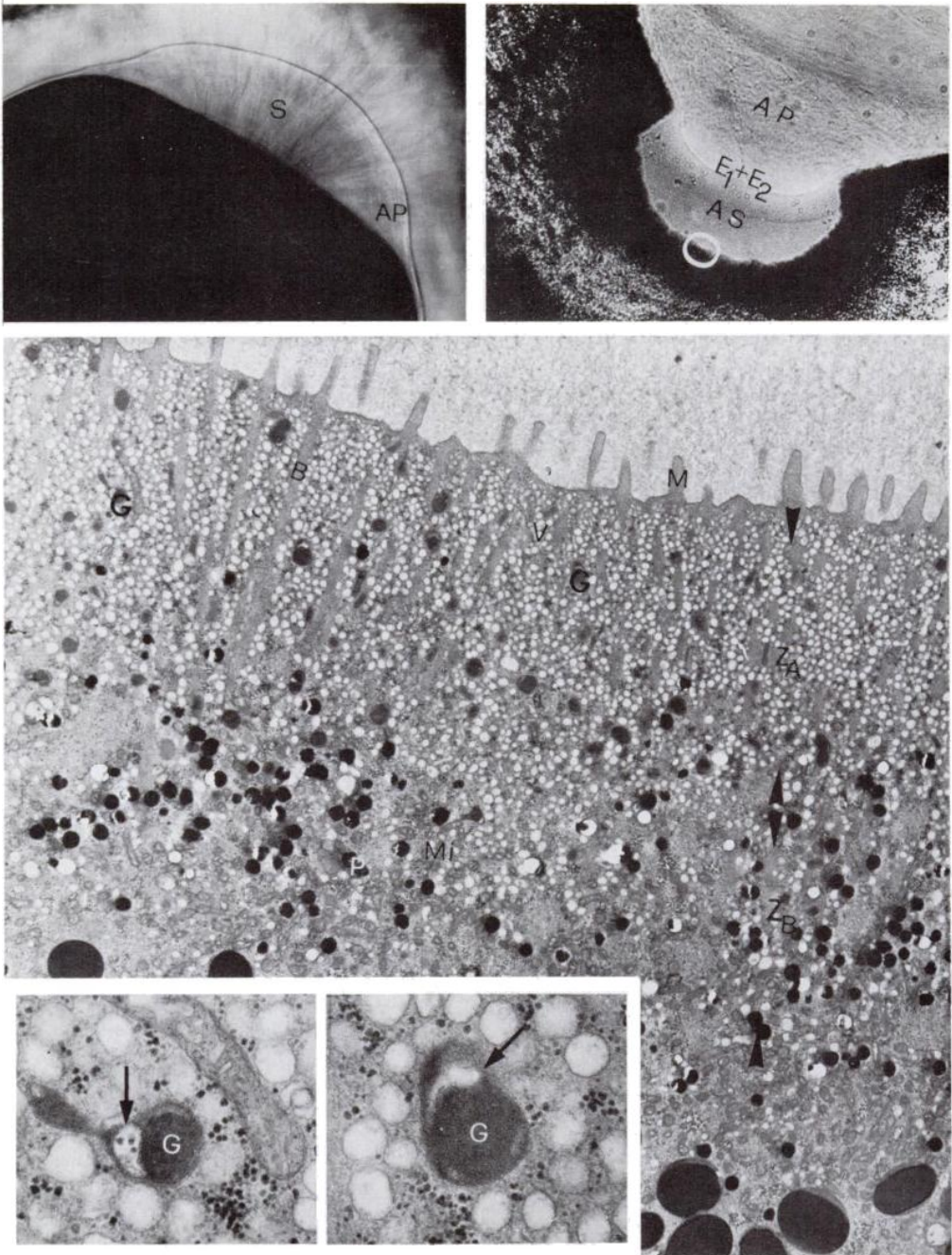


FIG. 1. (upper left) A side-view of the animal pole of a living *Discoglossus* egg showing a bundle of spermatozoa (S) engaged in the penetration of the egg through the animal plug (AP). $\times 40$.

FIG. 2. (upper right) Light microscope micrograph of a sagittal open thick section of egg showing the animal dimple. E_1 = envelope 1; E_2 = envelope 2; AP = animal plug, here considerably reduced in size by dehydration. The animal dimple is filled with a rather amorphous substance (AS). $\times 80$.

FIG. 3. Electron micrograph of the animal dimple in the region encircled in Fig. 2. Z_A = zone A; Z_B = zone B; the four arrowheads delimit Z_A and Z_B . In Z_A there are fingershaped microvilli (M), granules (G), fiber bundles (B), vesicles (V). In Z_B pigment granules (P) appear together with an abundance of mitochondria (MI). Note the rather regularly spaced insertion of microvilli and their conic bases in a cortical cytoplasmic layer and the orientation of the fibers. The general vacuolar aspect of the granules (G) results from a difference in electron density between the core and the periphery of the granules. Note the presence of inner vacuoles (arrow) in some granules (G). $\times 5,500$ and $\times 32,000$.

injected, with 250-350 U Coriovis (Vister) in Amphibian Ringer's solution during February-May. Egg deposition was obtained by abdominal massage. Both oocytes dissected from the oviduct and freshly laid eggs were studied. For transmission electron microscopy they were fixed either in 2.5-3 percent glutaraldehyde in 0.1-0.2M phosphate buffer at pH 7.3-7.4 (Millonig, 1964) or in phosphate buffered formaldehyde-glutaraldehyde (Karnovsky, 1965). They were then post-fixed in 2 percent osmium tetroxide in phosphate buffer, dehydrated and flat embedded in Araldite Epon. Areas to be sectioned were located by means of thick resin sections obtained by free hand razor blade cutting. Ultrathin sections were stained with uranyl acetate followed by lead citrate (Reynolds, 1963) and observed with a Siemens Elmiskop 1A. For scanning electron microscopy, the jelly envelopes were partially removed by a 15 min treatment with 0.1 percent crude papain solution containing 2 percent cysteine (Kalt and Tandler, 1971). They were then rinsed and immersed in 2.5 percent glutaraldehyde in 0.2M phosphate buffer and dehydrated in alcohol or acetone. E_1 and E_2 were then removed manually with forceps. The eggs were then air-dried, coated with a mixture of gold and copper and examined with a Jeol JSM-2 scanning electron microscope.

RESULTS

Animal Dimple

The animal dimple is a pit whose walls may exhibit more or less conspicuous protrusions (Figs. 2 and 9). The size of the animal dimple varies somewhat in different egg clutches. On thick resin sections its average size is approximately 150 μ in depth and 300 μ in width. The surface of the animal dimple shows finger-shaped microvilli that are not found elsewhere on the egg surface (Figs. 3, 5, 6 and 7). The microvilli have a conical shape and protrude into the animal dimple either singly or in pairs. Their bases are protrusions of a cortical cytoplasmic layer, characterized by a fine homogeneous granular matrix and by the absence of vesicles and mitochondria (this layer is present in the entire *Discoglossus* egg and is particularly evident at the vegetative hemisphere). Microvilli are fairly regularly spaced on the animal dimple surface, as can be seen in the images obtained with the scanning electron microscope (Fig. 8) and in Fig. 3. At the bottom of the animal dimple the microvilli may

reach a length of 1.7 μ and a width of 0.3 μ . Their plasma membrane has an average thickness of 10.5 nm: its outermost and innermost layers appear to be equally electron dense. An antennular glycocalyx radiates from the outer surface of the membrane and its branches interdigitate with those of the adjacent microvilli (Figs. 3, 5, 6 and 7). Bundles of straight parallel fibers run along the longitudinal axis of the microvilli and extend into the peripheral cytoplasm for a length of at least 10 μ , while keeping an almost straight orientation (Figs. 3 and 6). These fibers appear to be sections of microtubules although a final statement of their nature must wait further studies.

Another peculiarity of the *Discoglossus* egg is the absence of typical Anuran cortical granules (Wischnitzer, 1966) over the whole periphery of the egg, as already observed by Ghiara and De Miro (1962). Irregularly shaped granules with an average diameter of 0.5 μ , having a vacuolar appearance, are other typical components of the peripheral cytoplasm of the animal dimple (Figs. 3, 4, 5 and 7). They have an electron dense core, suggesting in some in-

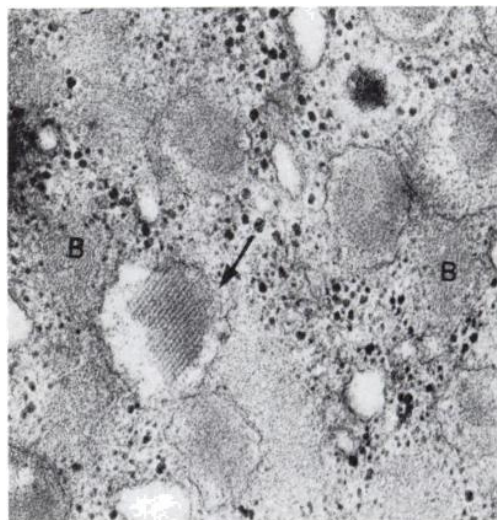


FIG. 4 Peripheral cytoplasm of animal dimple. In favorable sections the granule core shows a crystalline arrangement (arrow). Fiber bundles in oblique and cross sections (B). $\times 42,500$.

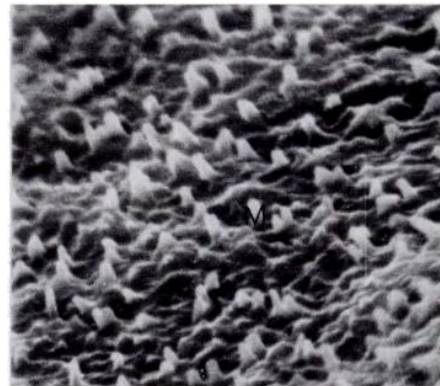
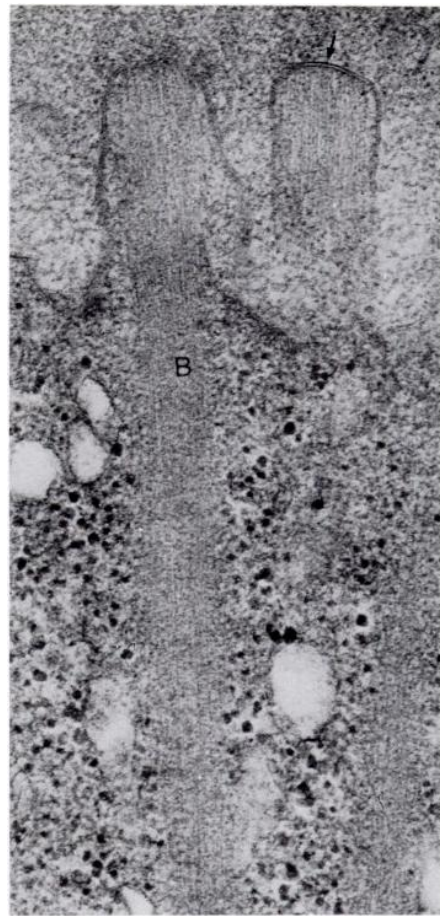
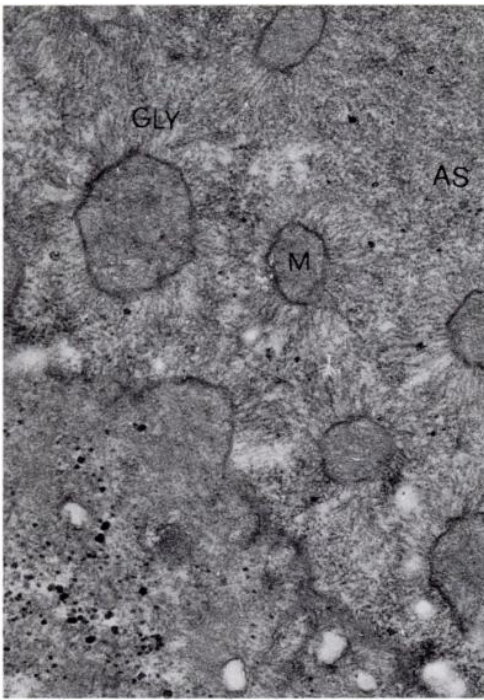


FIG. 5. (upper left) The antennular glycocalyx (GLY) of the animal dimple radiating from the plasma membrane and particularly evident in microvilli (M) cross sections. Microvilli are embedded in the animal dimple content (AS) composed of filamentous material. $\times 28,000$.

FIG. 6. (upper right) The animal dimple fiber bundles (B) run within the microvilli axis and are surrounded by a sheath of cytoplasm. The innermost and outermost layers of the plasma membrane (arrow) appear to be equally electron dense. $\times 50,000$.

FIG. 7. (lower left) Animal dimple. Granules are often found arranged in linear arrays directed towards the egg periphery. Some may be found very close to the egg plasma membrane (arrow). Their periphery may vary in electron density (compare G_1 with G_2). $\times 28,000$.

FIG. 8. (lower right) Animal dimple lateral wall, examined with the scanning electron microscope. Microvilli (M) project from rather uneven prominences of the surface singly or in pairs. $\times 7,000$.

stances a crystalline arrangement (Fig. 4), surrounded by a finely granular matrix. Furthermore, the granules vary considerably with regard to their shape and in the presence of inner vacuoles resembling the above mentioned vesicles (Fig. 3). They are arranged in single file intermingled with an abundance of vesicles and alternating with bundles of fibers with which they may exhibit close contact (Fig. 11). Some granules lie close to the inner aspect of the plasma membrane (Fig. 7). They are not visible in the animal dimple of freshly fertilized eggs in the area close to the entry of the spermatozoon (Campanella, manuscript in preparation). In the peripheral cytoplasm of the animal dimple two zones may thus be distinguished (Fig. 3): 1) *zone A*, which includes the above mentioned cortical cytoplasmic layer and in which bundles of fibers and granules are present together with an abundance of vesicles and glycogen; 2) an underlying *zone B* characterized by the presence of pigment granules; mitochondria are more abundant here than in *zone A*. In the cytoplasm underlying *zone B* pigment granules are scarcer and yolk platelets appear.

The contents of the animal dimple, which consist of glycoproteins, can be observed as rather coarse fibers (Fig. 5). At the upper edges of the animal dimple, where E_1 and E_2 come close to the egg surface, microvilli, fibers and granules disappear gradually. All of the animal dimple features just described are already present in eggs in the lower third of the oviduct (Figs. 9 and 10), whereas in the ovarian oocyte, in which the area germinativa has not yet become invaginated to form the bottom of the animal dimple, this structural organization is not present (Campanella Trautteur, 1970).

Animal Hemisphere

A section through the upper edge of the animal depression shows a surface with few protrusions (Fig. 11). Underneath the plasma membrane there is a thin cortical cytoplasmic layer; pigment granules and mitochondria lie just underneath this layer.

Vegetative Hemisphere

The cortical organization of the vegetative hemisphere does not differ significantly from that of the animal hemisphere (Fig. 12). The asymmetrical configuration of the plasma membrane is here evident, with its innermost layer more electron dense than its outermost layer (Fig. 13). The cortical layer is easily distinguished (Fig. 13), has a thickness of about 4.3μ and is filled with finely granular material. Yolk platelets, mitochondria and lipid droplets can be seen just underneath this layer (Figs. 12 and 13).

Glycocalyxes at the plasma membrane level of the animal and vegetative hemisphere are much less conspicuous than those radiating from the animal dimple membrane.

DISCUSSION

Two findings that have emerged from the ultrastructural analysis of the unfertilized egg of *Discoglossus pictus* deserve special comment as they represent unique features of the animal dimple, the pit located at the center of the animal depression:

1) the presence at the surface of the animal dimple of regularly spaced finger-like microvilli, supported by bundles of fibers and surrounded by antennular glycocalyx extending into the glycoprotein content of the animal dimple;

2) the presence in the peripheral cytoplasm of the animal dimple of granules, whose organization is somewhat different from that of the typical Anuran cortical granules and which are lacking in the rest of the peripheral cytoplasm of the egg.

With regard to 1) it is known that inconspicuous protrusions, similar to those observed at the surface of *Discoglossus* egg outside of the animal dimple, are present in the uterine (Hebard and Herold, 1966; Wischnitzer, 1966; Kemp and Istock, 1967) and oviducal (Hope *et al.*, 1963) eggs of several amphibian species. Regularly shaped microvilli have been described in the unfertilized eggs of *Bufo regularis* and

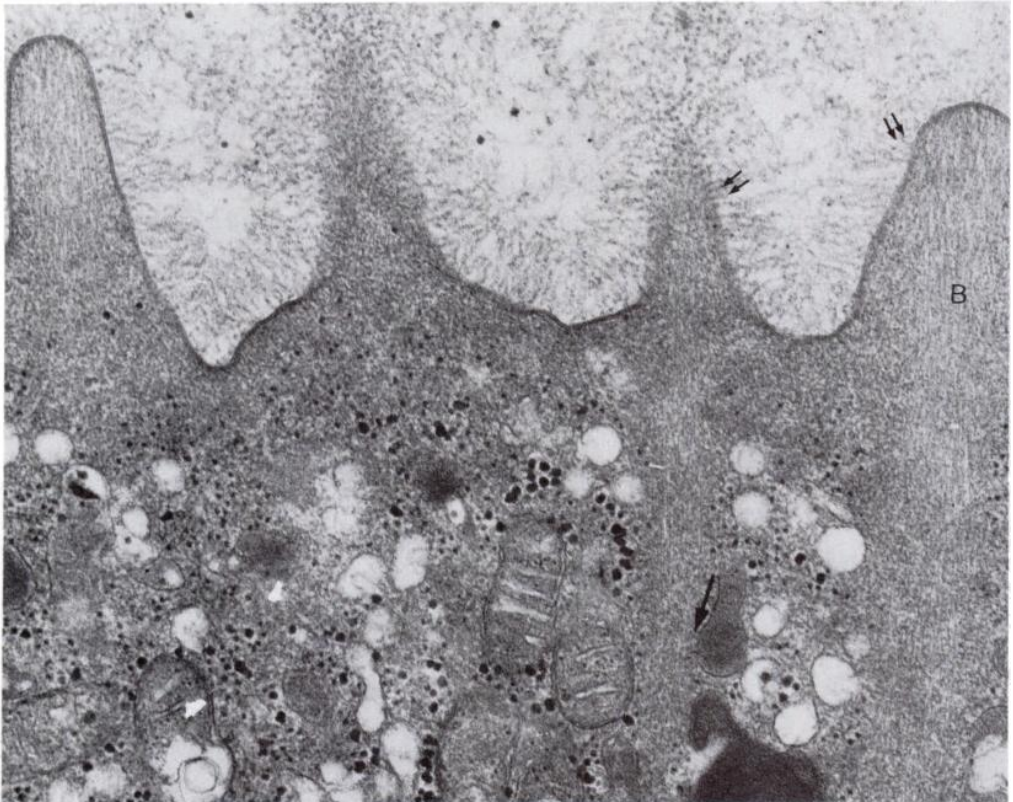
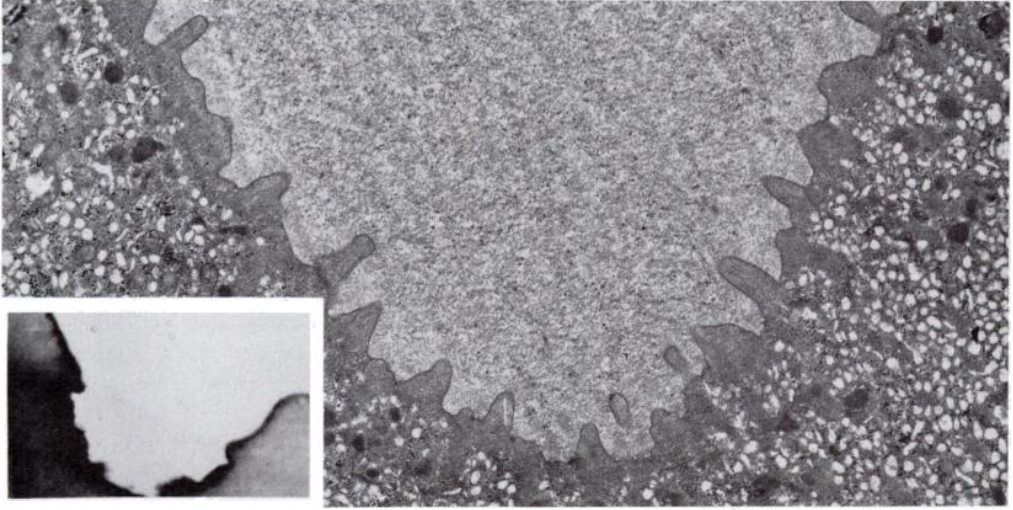


FIG. 9. (upper figure) Oocyte from the lower third of the oviduct. One of the invaginations of the animal dimple (see insert) is shown here, in which the typical animal dimple features are present and arranged as in the laid egg. $\times 65$ and $\times 8,000$.

FIG. 10 (lower figure) Animal dimple from the lower third of the oviduct. Typical fiber bundles (B), as in laid eggs, are evident here. A granule is shown exhibiting close contact with a fiber bundle (arrow). Note glycocalyx insertion on the plasma membrane (double arrows). $\times 40,000$.

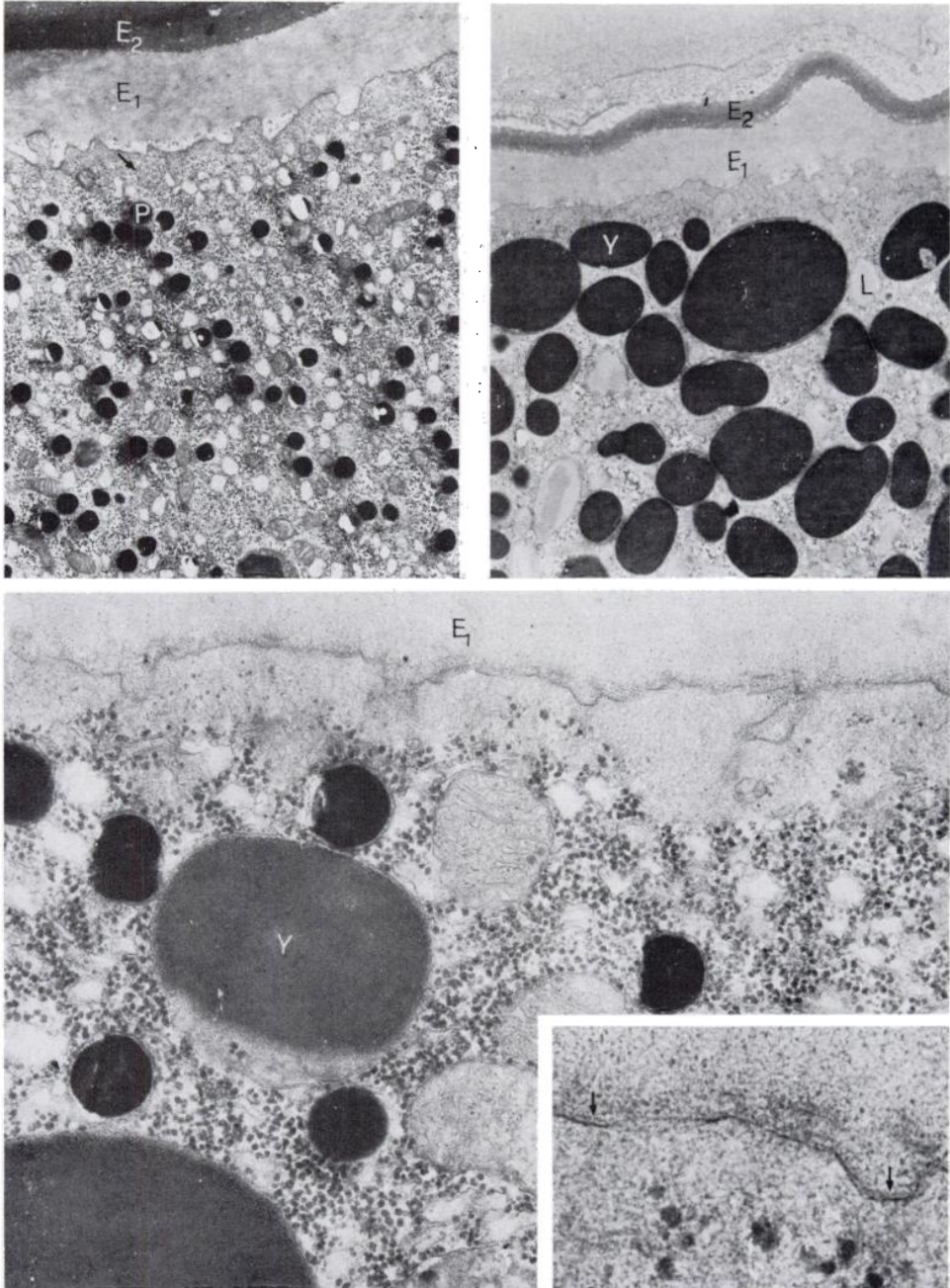


FIG. 11. (upper left) Animal hemisphere. The egg surface has small and irregular protrusions. Pigment granules (P) and few scattered granules with a finely granular matrix are present (arrow) underneath a cortical cytoplasmic layer (see also Fig. 13). E_1 = envelope 1; E_2 = envelope 2. $\times 7,500$.

FIG. 12 (upper right) Vegetative hemisphere. The egg surface has a cortical cytoplasmic layer. Yolk platelets (Y) and lipid droplets (L) are visible underneath. E_1 = envelope 1; E_2 = envelope 2. $\times 7,500$.

FIG. 13. (lower figure) Vegetative hemisphere. A cortical layer with a fine homogeneous granular matrix forms prominences on the egg periphery. E_1 = envelope 1; Yolk (Y). The innermost layer of the plasma membrane is denser than the outermost layer (arrow). $\times 30,000$ and $\times 90,000$.

Xenopus laevis (Balinsky, 1966; Grey *et al.*, 1974). However, to our knowledge, finger-shaped microvilli with antennular glycolyces and supported by bundles of fibers, have not yet been observed in the amphibian unfertilized egg.

The regular spacing of the bundles of microtubules and their perpendicular orientation to the egg surface suggest that they may function as a kind of scaffolding for the cortical cytoplasm, thus playing a role in the shaping of the animal dimple.

The presence of numerous vesicles all along the fibers suggests the possibility that bundles of fibers might also be involved in fluid exchange. The regular organization of fibers is no longer found in freshly fertilized eggs (Campanella, manuscript in preparation) where, as a result of activation, the animal dimple starts rising in a process that, together with the dissolution of the animal plug, makes the egg completely spherical within 15 min after fertilization (Wintrebert, 1929, 1930).

Fuzzy coats, among which are included antennular glycolyces, are composed of heteroglycans (Bennet, 1969) and could have an antigenic and/or an enzymatic function (Rambourg, A., 1971). The conspicuous antennular glycolyx of the animal dimple, radiating from the egg plasma membrane, is the first site of contact with the spermatozoon membranes and with its above mentioned properties might be directly involved in the acrosomal reaction and in the process of egg activation.

With regard to 2), the situation in *Discoglossus* is more similar to the one found in the Urodeles *Triton alpestris* (Wartenberg and Schmidt, 1961) and *Triturus viridiscens* (Hope *et al.*, 1963) than the one generally found in Anurans. The latter have cortical granules with a round shape, a finely granular and homogeneous aspect, a diameter of about 2 μ and are arranged in a single layer underneath the egg plasma membrane (Wischnitzer, 1966). Recently Grey *et al.* (1974) described two kinds of cortical

granules in the *Xenopus laevis* egg. The smaller ones differ slightly from the previously cited cases (Wischnitzer, 1966) in the presence of inner patches of less electron dense material (see also Kotani *et al.*, 1973). The larger ones are found mostly at the vegetative hemisphere where they can be found arranged in more than one layer. *Discoglossus* granules have an irregular shape and there is a difference in density between the core and the periphery; they measure about 0.5 μ in diameter, are located only in the cortical cytoplasm of the animal dimple and precisely in the whole thickness of zone A where they are often found to be arranged in single files and are in close contact with the fibers and vesicles. This irregular shape and the variable presence of inner vacuoles suggest that, in the unfertilized egg, they are not resting structures but are in an active state of exchange with the surrounding cytoplasm. However the fact that these granules are found only in the animal dimple, which is the unique area of the egg surface receptive to a fertilizing spermatozoon and in which much fewer granules are found following fertilization, indicates that the granules might have a role in the process of fertilization similar to that of the Anuran typical cortical granules.

It would be very interesting to check for the presence of proteolytic enzymes in these granules. In fact, the experiments of Wintrebert (1929) in *Discoglossus* have suggested that the animal plug is dissolved by proteolytic enzymes during egg activation. Recently in Echinoderms (Shuel *et al.*, 1973) and also in mammals (Gwatkin *et al.*, 1973), trypsin-like proteases have been reported to localize in cortical granules and their importance in the fertilization process has been suggested (Vacquier *et al.*, 1973).

Studies are in process to ascertain the changes undertaken by the animal dimple at fertilization, and the granules origin, histochemical nature and participation in the egg activation process.

ACKNOWLEDGMENTS

This research was supported by the following CNR grants: 70.00977/04/115.1124; 70.00971/04; 71.00897/04.

I am most grateful to Professor Gianfranco Ghiara for his stimulating discussion in the preparation of this work and for his criticism in reading the manuscript. I am indebted to Prof. Angela Maria Maccagno of the Istituto di Paleontologia of the University of Naples for the use of the scanning microscope. I am also deeply indebted to Professor Alberto Monroy for his suggestions after reading the manuscript. I also wish to acknowledge the expert technical assistance rendered by the "Centro di Microscopia Elettronica" of the University of Naples.

REFERENCES

- BALINSKY, B. I. (1966). Changes in the ultrastructure of Amphibian eggs following fertilization. *Acta Embryol. Morphol. Experim.* 9, 132-154.
- BENNET, H. S. (1969). The cell surface: components and configurations. In "Handbook of Molecular Cytology" (A. Lima-De Faria ed.), pp. 1261-1293. North Holland Publishing Company, Amsterdam-London.
- CAMPANELLA TRAUTTEUR, C. (1970). Osservazioni degli strati superficiali e corticali di ovociti e di uova di *Discoglossus pictus* Otth. (Anfibio Anuro). *Boll. Zool.* 37, 481.
- GHIARA, G. (1960). Ricerche intorno alla struttura microscopica submicroscopica ed istochimica ed alle funzioni degli involucri ovariali di *Discoglossus pictus* Otth e di altre specie di Anfibi. *Arch. Zool.* 45, 9-92.
- GHIARA, G. AND DE MIRO, M. (1962). Le cellule follicolari nell'ovogenesi degli Anfibi. *Atti Soc. Pel. Sc. Fis. Mat.* 8, 155-176.
- GREY, R. D., WOLF, D. P. AND HEDRICK, J. L. (1974). Formation and structure of the fertilization envelope in *Xenopus laevis*. *Dev. Biol.* 36, 44-61.
- GWATKIN, R. B. L., WILLIAMS, D. T., HARTMANN, J. F. AND KNIAZUK, M. (1973). The zona reaction of hamster and mouse eggs: production in vitro by a trypsin-like protease from cortical granules. *J. Reprod. Fert.* 32, 259-265.
- HEBARD, C. N. AND HEROLDS, R. C. (1967). The ultrastructure of the cortical cytoplasm in the unfertilized egg and first cleavage zygote of *Xenopus laevis*. *Exptl. Cell Res.* 46, 554.
- HIBBARD, H. (1928). Contribution à l'étude de l'ovogenèse de la fécondation et de l'histogenèse chez *Discoglossus pictus* Otth. *Arch. Biol.* 38, 251-326.
- HIBBARD, H. AND WINTREBERT, P. (1928). La formation des membranes et les changements d'aspects de l'oeuf de *Discoglossus pictus* Otth. avant la ponte. *C. R. Soc. Biol.* 98, 1521-1523.
- HOPE, J., HUMPHRIES, A. A., JR. AND BOURNE, G. H. (1963). Ultrastructural studies on developing oocytes of the Salamander *Triturus viridiscens*. I. The relationship between follicle cells and developing oocytes. *J. Ultr. Res.* 9, 302-324.
- KALT, M. R. AND TANDLER, B. (1971). A study of fixation of early Amphibian embryos for electron microscopy. *J. Ultrastruct. Res.* 36, 663-645.
- KARNOVSKY, M. J. (1965). A formaldehyde-glutaraldehyde fixative of high osmolality for use in electron microscopy. *J. Cell Biol.* 27, 137A-138A.
- KEMP, N. E. AND ISTOCK, N. L. (1967). Cortical changes in growing oocytes and in fertilized or pricked eggs of *Rana pipiens*. *J. Cell Biol.* 34, 111-122.
- KOTANI, M., IKENISHI, K. AND TANABE, K. (1973). Cortical granules remaining after fertilization in *Xenopus laevis*. *Dev. Biol.* 30, 228-232.
- MILLONIG, G. (1964). Studio sui fattori che determinano la preservazione della ultrastruttura. In "From molecule to cells". Symposium on electron microscopy. pp. 347-362. Roma, C.N.R.
- RAMBOURG, A. (1971). Morphological and histochemical aspects of glycoproteins at the surface of animal cells. In "International Review of Cytology" (G. H. Bourne and J. F. Danielli ed.) 31, pp. 57-114. Academic Press, New York and London.
- REYNOLDS, E. S. (1963). The use of the lead citrate at high pH as electron opaque stain in electron microscopy. *J. Cell Biol.* 17, 208-212.
- SHUEL, H., WILSON, W. L., CHEN, K. AND LORAND, L. (1973). A trypsin-like proteinase localized in cortical granules isolated from unfertilized sea urchin eggs by zonal centrifugation. Role of the enzyme in fertilization. *Dev. Biol.* 34, 175-186.
- VACQUIER, V. D., TEGNER, M. J. AND EPEL, D. (1973). Protease released from sea urchin eggs at fertilization alters the vitelline layer and aids in preventing polyspermy. *Exptl. Cell Res.* 80, 111-119.
- WARTENBERG, H. AND SCHMIDT, W. (1961). Elektronenmikroskopische Untersuchungen der Strukturellen Veränderungen im Rindenbereich des Amphibiencyclus in Ovar und nach der Befruchtung. *Z. Zellforsch.* 54, 118-146.
- WINTREBERT, P. (1929). La digestion de l'enveloppe tubaire interne de l'oeuf par des ferments issus des spermatozoides et de l'ovule, chez *Discoglossus pictus* Otth. *C. R. Acad. Sc.* 188, 97-100.
- WINTREBERT, P. (1930). Phénomènes d'attraction réciproque des gamètes, de captation et de réception du spermatozoïde par l'ovule chez *Discoglossus pictus* Otth. *C. R. Soc. Biol.* 105, 520-524.
- WISCHNITZER, S. (1966). The ultrastructure of the cytoplasm of the developing Amphibian egg. In "Advances in Morphogenesis" (M. Aberchrombie and J. Brachet ed.) 5, pp. 131-179. Academic Press, New York and London.

Ultrastructural and Lectin Binding Changes during the Formation of the Animal Dimple in Oocytes of *Discoglossus pictus* (Anura)

SUZANNE DENIS-DONINI*¹ AND CHIARA CAMPANELLA†

*CNR Laboratory of Molecular Embryology, 80072 Arco Felice, Naples, and †Institute of Histology, University of Naples, Italy

Received January 19, 1977; accepted in revised form June 30, 1977

In *Discoglossus pictus* eggs, the animal dimple is the only place where fertilization can occur. The carbohydrate composition of the dimple membrane was investigated using fluorescent-labeled lectins. Receptors for soybean agglutinin (SBA) and wheat germ agglutinin (WGA) are specifically localized on the dimple walls, whereas fucose-like residues are only present at the bottom of the dimple. This lectin binding pattern is transient since it only appears when the dimple is completely formed and disappears immediately after fertilization. The formation of the dimple requires an increase in surface. Our ultrastructural studies suggest that membrane growth occurs through the insertion of vesicles into the plasma membrane. We hypothesize that the lectin-binding glycocomponents that we observed are inserted along with the vesicles which fuse into the membrane. These vesicles most probably originate from the annulate lamellae and cisternal stacks present in full-grown oocytes. The possibility that the surface features of the dimple, such as the microvilli, the complex glycocalyx, and particularly the neutral carbohydrate residues (fucose-like), might favor sperm-egg fusion is discussed.

INTRODUCTION

The egg of *Discoglossus pictus* (Anura) differs in several respects from other Amphibian eggs. It can only be fertilized in a restricted zone of the animal hemisphere: the animal dimple. This is a funnel-shaped pit which forms in the germinative area² region during the passage of the oocytes through the oviduct. At the same time, part of the surrounding animal hemisphere becomes concave, and this concavity is maintained by the deposition of a heavy gelatinous animal plug (Hibbard and Wintrebert, 1928). The animal plug as well as the gelatinous layers enclosing the egg are secreted by the oviduct cells. The animal dimple is filled with a glycoprotein-rich fluid (Ghiara, 1970). Ultrastructural studies (Campanella, 1975) have

shown that the surface of the dimple is covered with finger-shaped microvilli, whereas the rest of the surface is smooth. The dimple plasma membrane is peculiar in that both leaflets have the same electron density, and that a conspicuous antennular glycocalyx radiates from the external one. Both the animal dimple and the depression are transient features of the egg which disappear shortly after fertilization when the egg reassumes a spherical shape.

It was interesting to see whether these changes in surface organization are accompanied by changes in glycoprotein composition that might make the dimple membrane recognizable by the spermatozoa. Since formation of the dimple requires an increase in surface, the ultrastructural changes that occur during dimple formation were investigated in order to throw some light on the processes through which surface increase may occur. These observations are correlated with changes in the

¹ To whom all correspondence should be addressed.

² The germinative area has only been described in *Discoglossus*. It includes the animal pole and is largely depigmented.

carbohydrate composition of the plasma membrane as visualized with fluorescent lectins.

MATERIALS AND METHODS

Adult *Discoglossus pictus* (painted frog) captured in the neighborhood of Palermo (Italy) were injected during February–May with 250–300 U of Coriovis (Vister) diluted in amphibian Ringer's solution. Egg deposition was obtained by abdominal massage. Spermatozoa were obtained by squeezing the "seminal vesicles" (Mann, 1973), and artificial insemination was performed. Oocytes were recovered from the coelom as well as from the various oviduct tracts of females sacrificed 6–8 hr after hormone injection. The oviduct has been subdivided into four segments which have been individualized morphologically, histochemically, and according to the number and thickness of the gelatinous layers surrounding the oocytes (Campanella *et al.*, 1972). Namely, in oviduct I, the oocytes are only enclosed in the ovarian envelope: the vitelline membrane. In oviduct II, part of the animal plug as well as the innermost jelly coat (J1) are deposited. In oviduct III, the animal plug is completely formed, and a second jelly layer (J2) is deposited. In oviduct IV, the outermost jelly layer (J3) is deposited.

Transmission electron microscopy. Oocytes and eggs were fixed either in 2.5% glutaraldehyde in 0.1–0.2 M phosphate buffer, pH 7.3 (Millonig, 1964), or in phosphate-buffered formaldehyde–glutaraldehyde (Karnovsky, 1965). Some samples were fixed in Kalt and Tandler's trialdehyde fixative (1971). They were then post-fixed in 2% osmium tetroxide in phosphate buffer, dehydrated, and flat embedded in Araldite-Epon. Ultrathin sections were stained with uranyl acetate followed by lead citrate (Reynolds, 1963) and were observed under a Siemens Elmiskop 1A.

Lectin-binding experiments. The eggs were freed from the gelatinous layers by treatment with 0.02 M dithiothreitol (DTT)

in 0.1 M Tris, pH 8.5, for about 15 min and then were thoroughly washed in Ringer's. DTT has the advantage in that it dissolves both the jelly layers and the thick animal plug. This treatment makes the dimple more superficial and, therefore, more accessible. For easier manipulation, the eggs were fixed briefly in 4% formaldehyde in Ringer's, pH 7.4. Since the dimple fluid precipitates in the fixative and could produce artifacts, the vitelline envelope was removed with watchmaker's forceps after three rinses in Ringer's, and part of the precipitated fluid was washed away. This process, fixing and washing, was repeated until the surface appeared clean under the binocular. Removal of the jelly layers with DTT as well as repeated fixing and washing does not affect the pattern and intensity of the lectin binding to the rest of the surface. In order to study accurately the dimple surface, some eggs were split in half with a razor blade after fixation.

The following fluorescent lectins (FITC conjugates) from Miles Yeda were used: soybean agglutinin (SBA), wheat germ agglutinin (WGA), concanavalin A (Con A), and a fucose-binding protein from lotus (FBP). They were used at a concentration of 60 µg/ml of amphibian Ringer's. Incubation time was 10 min. The eggs and oocytes were then rinsed three times in Ringer's and were observed under a Zeiss microscope equipped with epifluorescent illumination using the appropriate filters for fluorescein fluorescence. Controls contained 0.1 M of the appropriate saccharide inhibitor in staining and washing solutions, e.g., *N*-acetylgalactosamine for FITC-SBA and fucose for FBP. Since WGA binds not only to *N*-acetylglucosamine residues (GlcNAc) but also to sialic acid residues (Greenaway and Le Vine, 1973; Zalik and Cook, 1976), some eggs were first treated with vibrio cholera neuraminidase (Sigma) at a concentration of 5 U/ml of Tris-buffered Ringer's, pH 7.4, for 3 hr. They were then stained with WGA in the presence or absence of GlcNAc.

RESULTS

Uterine eggs after deposition are shown in Fig. 1A. The concavity and the animal dimple are clearly visible. Figure 1C shows the dimple in section. We first studied the outer surface of the dimple and concavity as they appear after DTT treatment (Fig. 1B). Both bind SBA and WGA. The binding pattern is complex and suggests a distribution gradient of the lectin binding sites. The lobes of the dimple (Fig. 2A, B) present a globular pattern of fluorescence. They are surrounded by a compact ring of smaller fluorescent particles (Fig. 2C). Further away from the dimple, a small dot pattern can be observed in the concavity (Fig. 2D). The rest of the egg surface is almost negative. The fluorescence, therefore, is at its maximum close to the dimple and decreases toward the end of the depression. The pattern obtained is the same with both lectins, although it is more fuzzy with WGA. The binding specificity will be discussed later. Both the concavity and the outer surface of the dimple are negative with Con A and FBP. In order to study the dimple surface more accurately, the eggs were split in half, incubated in the presence of lectins,

and observed. The dimple sides are positive with SBA and WGA (Fig. 3A). The bottom of the dimple, on the other hand, is negative with these two lectins and is only stained with the one (FBP) recognizing fucose-like residues (Fig. 3B).

Since these results show that the dimple membrane has a mosaic glycoprotein composition, it was interesting to see when, during dimple formation, this membrane specialization occurs. The pattern of dimple formation was also investigated ultrastructurally since we found that dimple formation requires about an 11% increase in surface. In fact, when one measures the diameter of coelomic oocytes and uterine eggs and calculates their surface areas, one finds that the average surface area of an oocyte is $9.25 \pm 0.8 \text{ mm}^2$, whereas the surface of an egg, including dimple and concavity, is $10.92 \pm 0.5 \text{ mm}^2$.

In coelomic oocytes, the depigmented germinative area is only slightly depressed. Therefore, the animal hemisphere appears flat (Fig. 4B). Ultrastructural studies show that the germinative area still has long and irregular microvilli (Fig. 4A), whereas the rest of the surface has become smooth as a consequence of

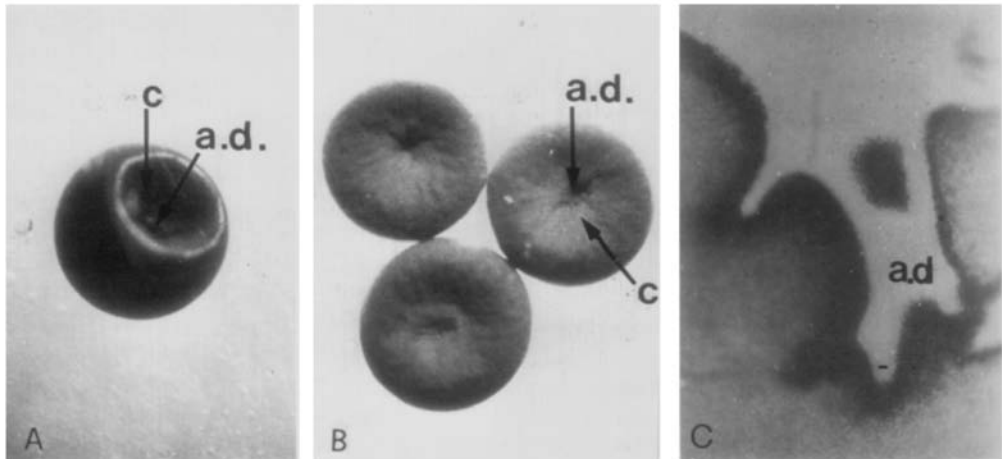


FIG. 1. (A) Deposited uterine egg. The jelly layers are present but not visible because of the horizontal light orientation. a.d., animal dimple; c, concavity. $14 \times$. (B) Deposited uterine egg after DTT treatment. The jelly layers and the animal plug are dissolved. The animal dimple (a.d.) is more superficial, and the concavity (c) is only slightly depressed. $14 \times$. (C) Thick Epon section of the animal dimple (a.d.). $200 \times$.

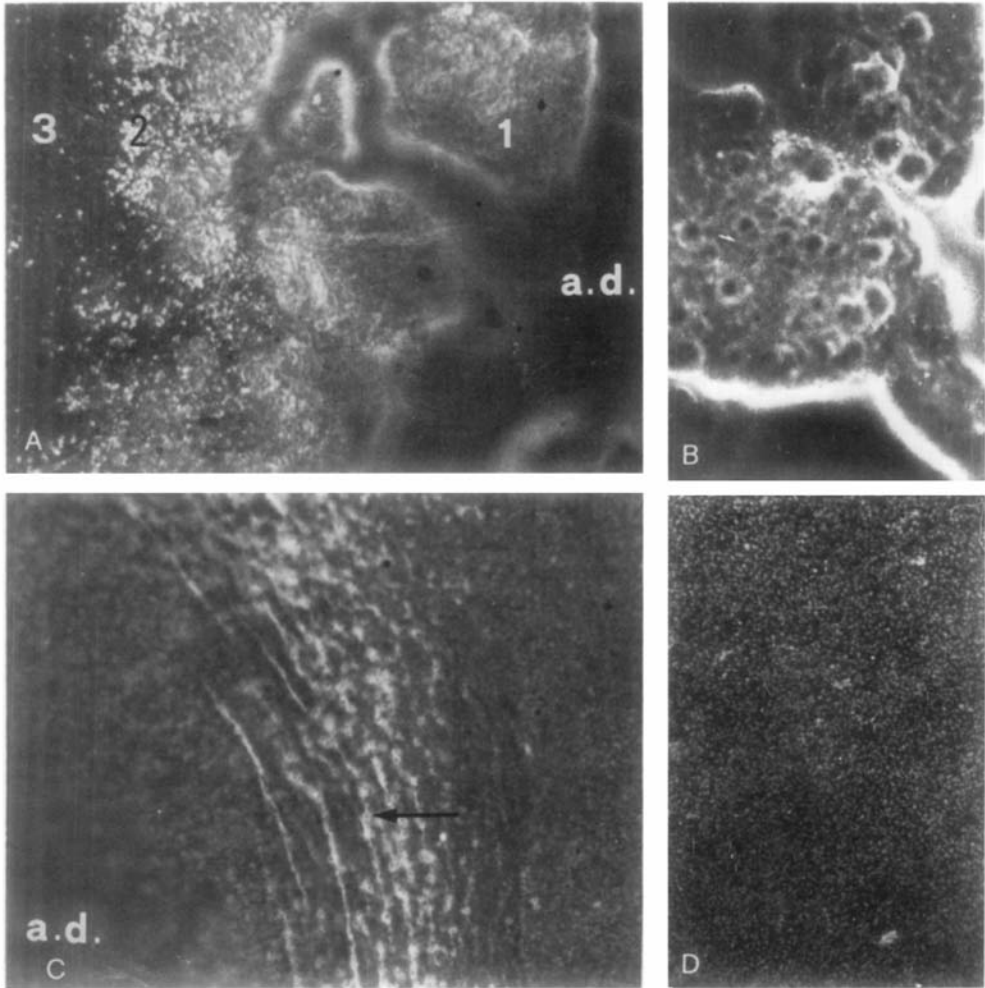


FIG. 2. (A) The external surface of the animal dimple and concavity after exposure to FITC-SBA. Three zones of fluorescence differing in pattern and intensity are noticeable. 1, The lobes of the dimple; 2, ring of fluorescent particles surrounding the dimple; and 3, the concavity surface. 216 \times . (B) Detail of the lobes of the animal dimple (A. 1) after exposure to SBA. Note the globular pattern of fluorescence. 540 \times . (C) Ring of fluorescent particles (A. 2) surrounding the dimple. 540 \times . (D) The concavity surface (A. 3). Small fluorescent dots are noticeable. 540 \times .

ovarian microvilli regression. The glycocalyx is loose without any special organization. A few small vesicles, scattered randomly in the underlying cytoplasm, are noticeable. The annulate lamellae and the cisternal stacks present in the full-grown ovarian oocytes (Andreuccetti and Campanella, 1976) are no longer observable at this stage. When lectin binding experiments are performed, one observes that

the germinative area stains very poorly with SBA and WGA. The rest of the animal hemisphere stains more intensely, mostly at the edges (Fig. 4C). Coelomic oocytes are completely negative with Con A or FBP.

In sections of oocytes withdrawn from the upper part of oviduct II, in which the maturation division occurs and the first polar body is extruded, one can observe no

great change as compared to coelomic eggs, except that the glycocalyx has become somewhat more organized (Fig. 5A). At this time, the dimple and depression are only outlined and are still quite shallow (Fig. 5B). Lectin binding experiments show that the oocytes present only a few lectin receptors for SBA and FBP at the center of the "white spot," where the first polar body has been extruded (Fig. 5C). However, by the time the oocytes have reached the lower part of oviduct II, the exposed carbohydrate residues (*N*-acetylgalactosamine and fucose-like) that could be detected earlier are no longer present. The whole germinative area is negative with FBP, whereas a faint staining is still observed with SBA (Fig. 5D).

In sections of oocytes collected from oviduct III, in which dimple formation occurs, one can see, at the bottom of the dimple that the shape of the microvilli undergoes a gradual transformation. While some of them are indistinguishable from ovarian microvilli (Fig. 6A), others are already fingershaped with an organized glycocalyx (Figs. 6C D). At the same time, many vesicles have migrated close to the surface. In regions where the ovarian-like microvilli are still predominant, exocytotic processes involving fusion between the membrane of the vesicles and the oocyte plasma membrane occur (Fig. 6B). Blebs are also visible and seem to give rise to the vesicles observed in the fluid contained in the animal dimple (Fig. 6A). In the region where

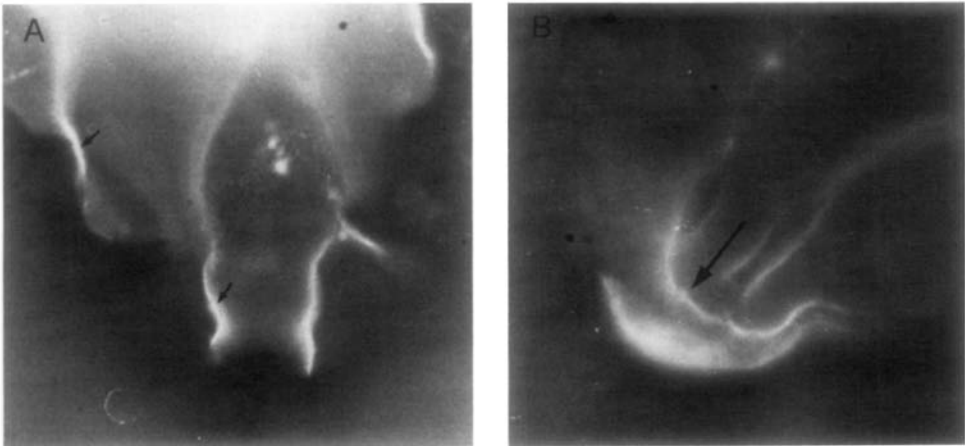
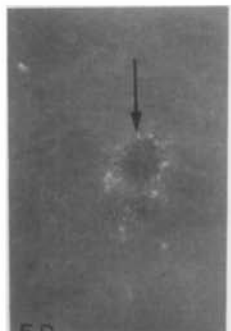
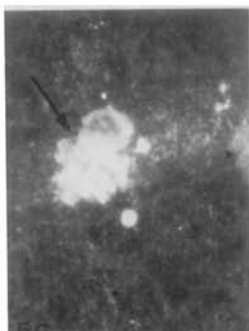
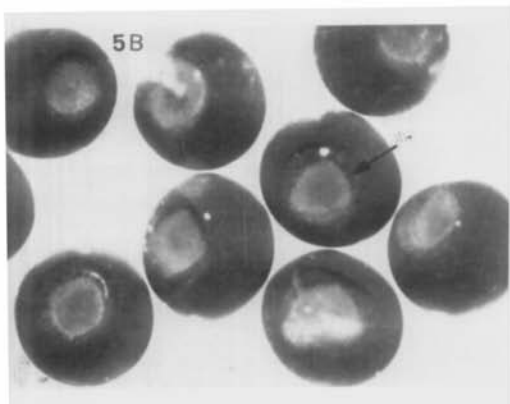
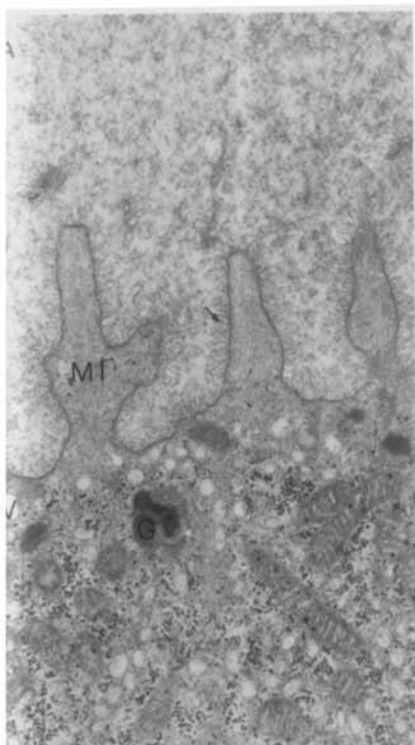
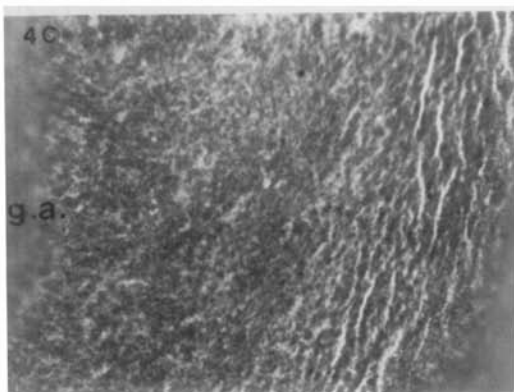
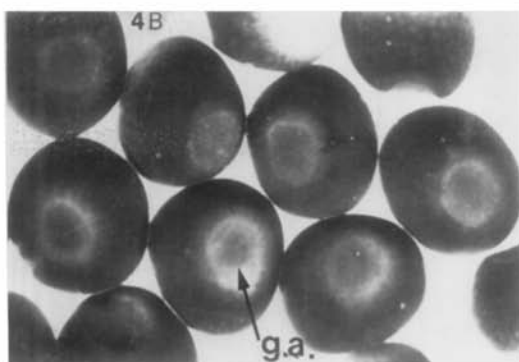
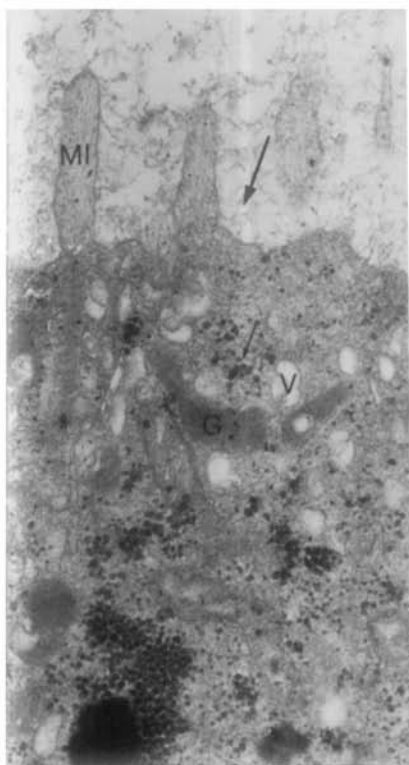


FIG. 3. (A) Split animal dimple exposed to FITC-SBA. The dimple walls are stained (small arrow), whereas the dimple bottom is negative. 375 \times . (B) Split animal dimple after exposure to FITC-FBP. Only the bottom of the dimple is fluorescent (arrow) 375 \times .

FIG. 4. (A) Ultrathin section of the germinative area of coelomic oocytes. The plasma membrane, microvilli (MI), and glycocalyx (arrow) are similar to the ovarian ones. Several vesicles (V), as well as "cortical granules" (G) and glycogen granules (small arrow), are seen in the peripheral cytoplasm. 36,000 \times . (B) Coelomic oocytes. The germinative area (g.a.) is only slightly depressed. 14 \times . (C) Coelomic oocyte after exposure to FITC-SBA. The germinative area (g.a.) is negative. The edges of the animal hemisphere are slightly fluorescent. 240 \times .

FIG. 5. (A) Ultrathin section of oocytes withdrawn from the oviduct II. The antennular glycocalyx (arrow) has become partially organized. V, vesicles; G, animal dimple granules; MI, microvilli. 15,000 \times . (B) Oocytes from oviduct II. Part of the animal hemisphere surrounding the germinative area (g.a.) has become depressed (arrow). 14 \times . (C) Animal hemisphere of oocytes withdrawn from the upper tract of oviduct II, after exposure to FITC-SBA. Bright fluorescent area (arrow) in the "white spot" region where the first polar body has been extruded. 375 \times . (D) "White spot" region of oocytes withdrawn from the lower tract of oviduct II, after exposure to FITC-SBA. Most SBA receptors present during extrusion of the first polar body have disappeared. Only a faint crown of fluorescence is now observable in this region (arrow). 375 \times .



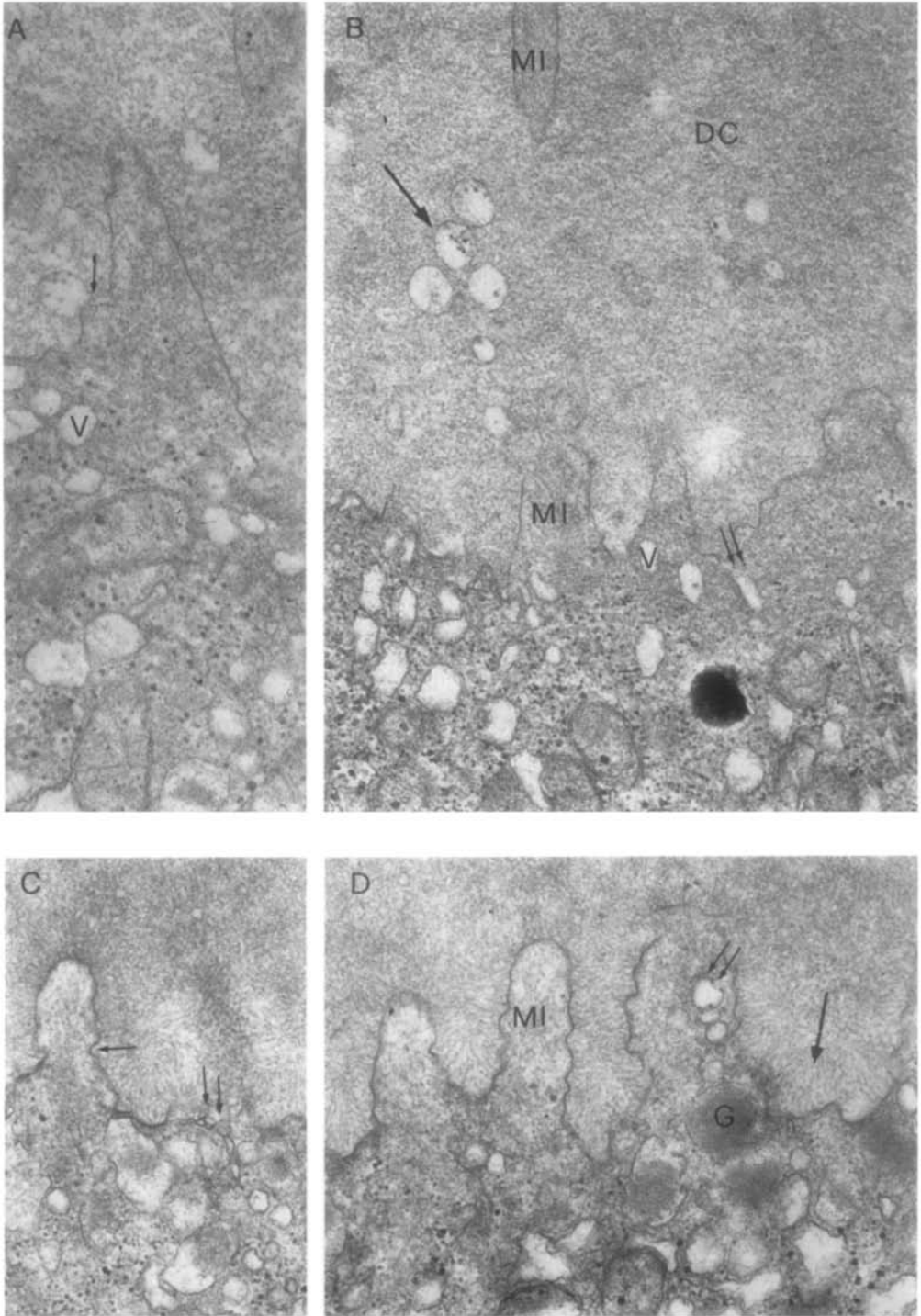


FIG. 6.

the finger-shaped microvilli are present, some of them are invaded by vesicles (Fig. 6D), whereas, at their base, chains of flattened vesicles contiguous with the plasma membrane are often noticeable (Fig. 6C). At this time, the most salient features of the uterine egg dimple, which we have described previously, can be observed with lectins, i.e., intense staining at the bottom with FBP, whereas the sides are stained with SBA and WGA.

In oocytes collected from oviduct IV as well as in uterine eggs, the dimple surface is covered with regular and finger-shaped microvilli. A conspicuous antennular glycocalyx radiates from the plasma membrane as already described (Campanella, 1975). A 0.90- μ m-thick band of vesicle-free cytoplasm is observed immediately below the plasma membrane, whereas the vesicles are more restricted in depth (Fig. 7).

The other point to check was whether this complex membrane architecture maintains itself or disappears after the resorption of the dimple that follows fertilization. A few minutes after fertilization (Fig. 8), great changes in the ultrastructural surface organization are already noticeable; most animal dimple granules (Campanella, 1975) have exocytosed, the antennular glycocalyx has disintegrated, and the microvilli features have changed. They are irregular in shape and are longer than they are in the unfertilized egg dimple. Thirty minutes after fertilization, when the concavity and the dimple have completely regressed and the animal hemisphere has become spherical, one observes, with SBA and WGA, a dark circu-

lar zone at the animal hemisphere surrounded by a slightly fluorescent zone (Fig. 9). The dark central zone is the former dimple bottom, and the brighter zone corresponds to the lateral walls. The intensity of fluorescence, however, is already fainter than on the dimple surface itself. No binding occurs with FBP. It should be noted here that no correlation at all can be observed between pigment distribution and lectin binding. One hour after fertilization, when the ejection of the second polar body takes place, a small area of the animal pole stains with SBA, WGA, and FBP (Fig. 10). The binding pattern is again complex. A bright fluorescent area in a faintly stained "spider web" is now observed. The exposure of these residues is transient, since, a short time later, the whole surface is completely negative with the four lectins used. (For a summary of the ultrastructural and lectin binding changes occurring during formation and regression of the animal dimple, see Fig. 11.) One has to wait for the first cleavage (2.30 hr after fertilization) to be able to observe again some lectin binding with SBA and WGA in the furrow region (Fig. 12).

Binding Specificity

SBA binding could be completely reversed by the addition of *N*-acetylgalactosamine. FBP binding is competed by fucose. On the other hand, WGA binding could not be completely reversed by the addition of sugar. Therefore, we treated the eggs with neuraminidase (5 U/ml for 3 hr) in order to remove the sialic acid terminal; in this case, *N*-acetylglucosamine

FIG. 6. Ultrathin section of oocytes withdrawn from oviduct III. (A, B) Region where the ovarian-like microvilli are still predominant. Numerous vesicles (V) have migrated toward the surface. Blebbing of the plasma membrane is indicated by a small arrow in A. 36,000 \times . In B, exocytotic process is marked by a double arrow. Note the numerous vesicles (large arrow) present in the animal dimple content (DC). Both blebs and extracellular vesicles contain electron-dense granules. Microvilli, MI. 35,000 \times . (C, D) Region where the finger-shaped microvilli have already been formed. In C, chains of flattened vesicles (double arrow) that will probably be inserted in the plasma membrane are observable. In some regions, both inner and outer leaflets of the plasma membrane have the same electron density (arrow). 34,500 \times . In D, microvilli are invaded by vesicles (double arrow). The antennular glycocalyx is indicated by an arrow. G, cortical granules. 34,500 \times .

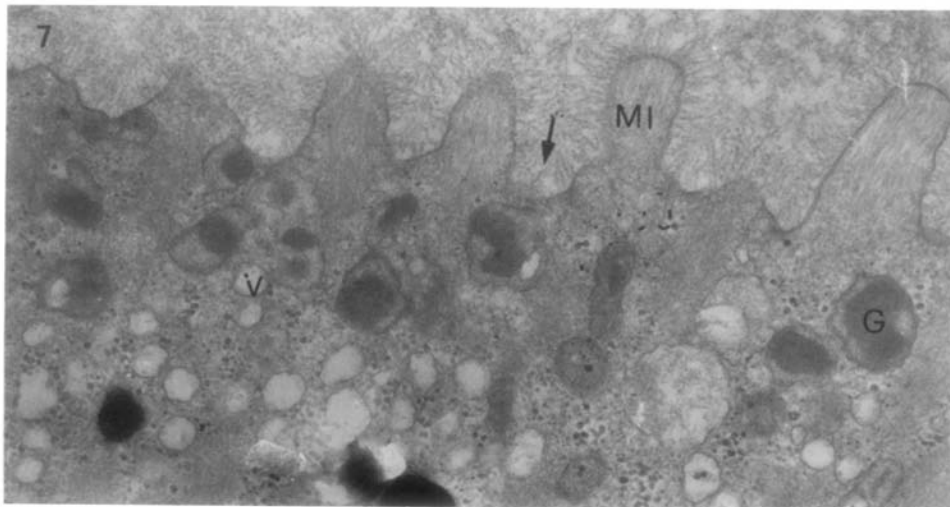


Fig. 7. Ultrathin section of the animal dimple bottom in uterine eggs. Typical finger-shaped microvilli (MI) and organized glycocalyx (arrow). G, cortical granules; V, vesicles that are absent from the cortex. 32,000 \times .

(GlcNAc) reversed the binding. Sialic acid and GlcNAc residues, therefore, are responsible for the staining obtained with WGA.

Since the binding patterns obtained with WGA and SBA are quite similar, experiments were performed to see whether the receptors for these two lectins are the same. Eggs were preincubated for 10 min in a 100- μ g/ml unlabeled WGA solution and, then, were incubated for an additional 10 min in the presence of FITC-SBA. No inhibition of SBA binding occurs under such conditions.

DISCUSSION

It has been known for a long time that sperm penetration occurs only at the dimple bottom (Wintrebert, 1933). To our knowledge, *Discoglossus* eggs are the only ones, among those of vertebrates, which possess such a specialized device for fertilization. This might be correlated with the fact that the spermatozoa are almost immotile, another peculiarity of the genus *Discoglossus*. It has been speculated that the jelly layers and, in particular, the ani-

mal plug are involved in sperm attraction (Hibbard and Wintrebert, 1928; Campanella and Atripaldi, in preparation). Our results show that, during dimple formation and regression, the plasma membrane is subjected to a series of rapid changes. The oocytes, while passing from the coelom to the oviduct II, maintain most of the ovarian ultrastructural organization with regard to the plasma membrane, glycocalyx, and microvilli. In the lower tract of oviducts II and III, where dimple formation occurs, the plasma membrane and the glycocalyx already acquire the characteristics of the uterine egg animal dimple, which, subsequently, will be lost soon after fertilization.

The lectin experiments show that the dimple and the depression have a complex mosaic glycoprotein composition which is established concurrently with dimple formation, i.e., during the final steps that prepare the oocytes for fertilization. The most interesting fact is that the exposed carbohydrate residues (fucose-like) on the membrane of the dimple bottom, which is the region where the membranes of both gametes will fuse, are unique to that area

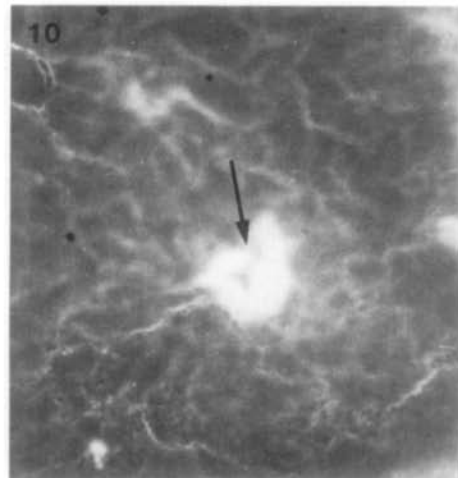
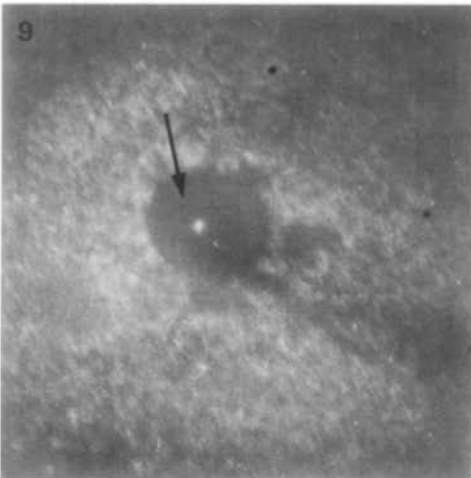
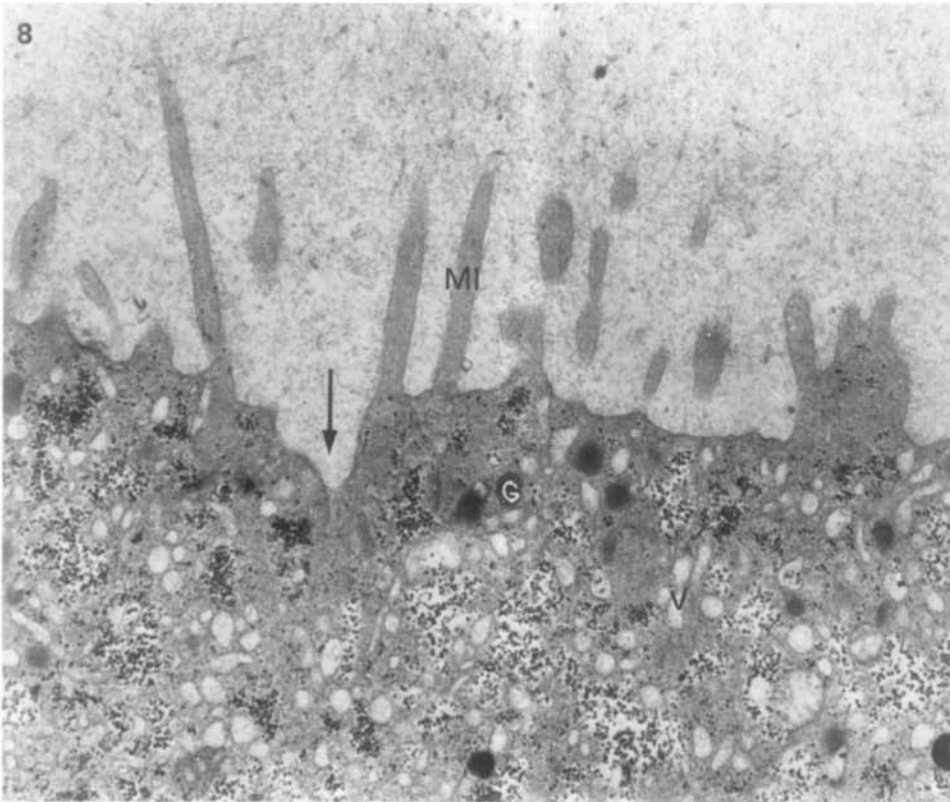


FIG. 8. Ultrathin sections of eggs, a few minutes after fertilization. The glycocalyx has no apparent organization (arrow), and the microvilli (MI) are again very irregular in shape. G, cortical granule that was not extruded; V, vesicles. 7500 \times .

FIG. 9. Animal hemisphere of an egg, 30 min after fertilization following exposure to SBA. The dark central area (arrow) is the former dimple bottom. 375 \times .

FIG. 10. Animal hemisphere of an egg, 1 hr after fertilization when emission of the second polar body takes place. Abundant SBA receptors (arrow) at the center of the white spot. 375 \times .

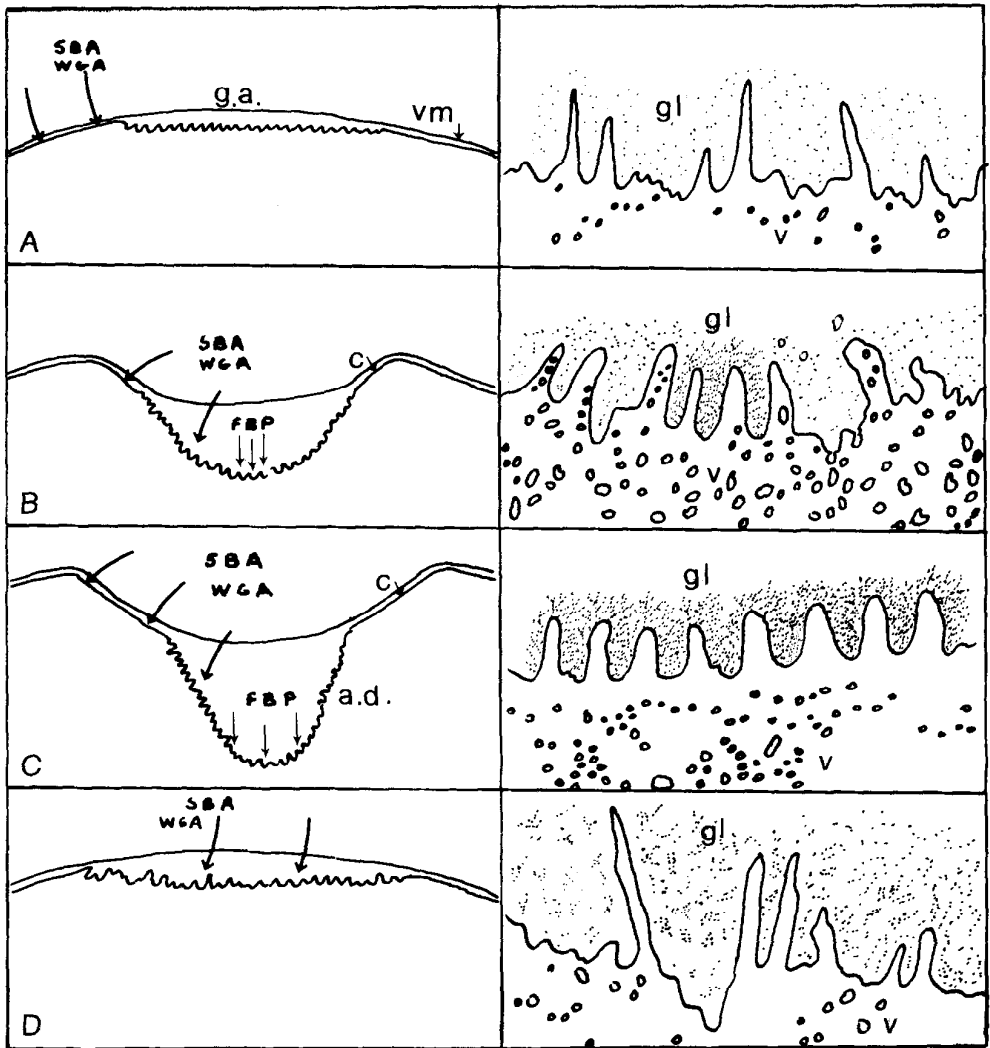


FIG. 11. Schematic diagram illustrating the ultrastructural (right) and lectin binding (left) changes during formation and regression of the animal dimple. (A) Section of coelomic oocyte. The germinative area is the only region covered with long and irregular microvilli and is only slightly depressed. The glycocalyx is loose. Few vesicles scattered in the cytoplasm are noticeable. 8100 \times . The germinative area is negative with the lectins used, whereas the rest of the animal hemisphere stains slightly with SBA and WGA. g.a., germinative area; v.m., vitelline membrane; gl, glycocalyx; v, vesicles. For details, see Fig. 4A, B, C. (B) Section of oocyte collected from oviduct III. This is an active stage in dimple formation. The microvilli undergo a gradual transformation and the glycocalyx becomes organized. Numerous vesicles have migrated close to the surface where they are involved in exocytotic process. Some of them are found in the dimple fluid. 8100 \times . For details, see Fig. 6. The walls of the dimple bind SBA and WGA, whereas the bottom of the dimple binds FBP.c, concavity. (C) Section of uterine egg. The dimple is formed. The microvilli are fingershaped, and the glycocalyx is antennular. A band of vesicle-free cytoplasm is observed underneath the plasma membrane. 8100 \times . For details, see Fig. 7. The lectin binding pattern is the same as the one observed in oviduct III oocytes. a.d., animal dimple. For details, see Fig. 3. (D) Section of an egg, 30 min after fertilization. The dimple is not apparent any more. The microvilli are extremely long and irregular. The glycocalyx has disintegrated. 4050 \times . Only a few receptors for SBA and WGA are still present at the surface and probably represent the former dimple walls. Fucose-like residues that were present at the bottom of the dimple are not detectable any more.

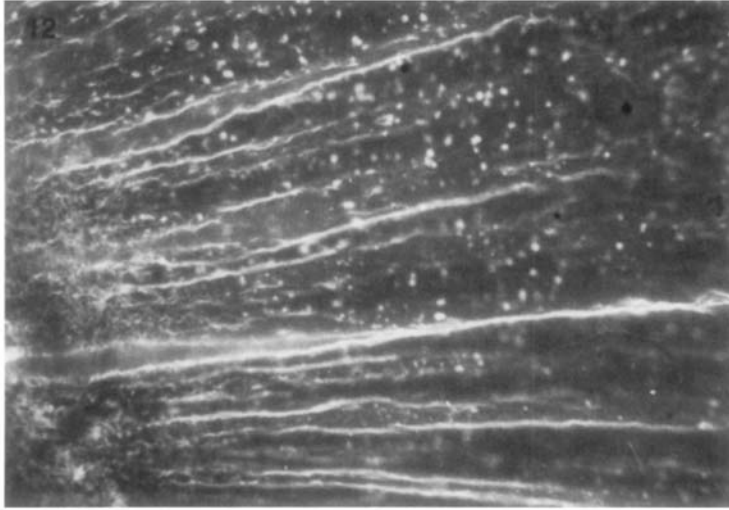


FIG. 12. First cleavage furrow stained with FITC-SBA. The furrow folds are brightly fluorescent. 338.

since they are not found elsewhere on the egg surface, and since, among all lectins used, no other binds to that area. The fact that the FBP receptors, as well as the antennular glycocalyx and the finger-shaped microvilli, disappear very rapidly after fertilization suggests that these three factors might be instrumental in the process of gamete interaction. Poste and Allison (1971) have postulated that some precise requirements must be fulfilled for membrane fusion to occur. One of these is the formation of microvilli that would permit a closer apposition of the two membranes.

Our measurements indicate that dimple formation requires an 11% increase in surface area. Ultrastructural studies clearly show that dimple formation is not a passive event, nor simply an invagination of the membrane and the underlying cytoplasm. In fact, the symmetrical dimple membrane and the antennular glycocalyx seem to originate from an active mechanism of membrane insertion and secretion. During the passage of the oocytes from the coelom to the uterus, an increased number of vesicles are observed close to the surface, while the annulate lamellae and the cisternal stacks present in full-grown ovarian oocytes (Campanella & Andreuc-

cetti, 1976) have disappeared. Therefore, one could imagine that the vesicles originate from these structures. Our data suggest that, during dimple formation, the vesicles participate in many processes which seem to occur in a precise sequence. When the microvilli still have an ovarian-like configuration, the exocytosis of vesicles would contribute to the formation of the glycocalyx and to the dimple fluid. At the same time, during the exocytotic process, insertion of the vesicle membrane into the oocyte plasma membrane would contribute to the surface increase required for dimple formation. On the other hand, the blebs might represent an intermediate step in the extrusion of intracellular material into the dimple fluid. Since the blebs as well as the vesicles found outside contain electron-dense granules, one could imagine that the external vesicles are blebs which have detached from the surface. The chains of flattened vesicles observed in continuity with the plasma membrane might play some role in the formation of the symmetrical dimple membrane, as well as in the process of membrane increase.

Changes in lectin binding during surface increase have already been observed

by Denis-Donini *et al.* (1977) in the cleaving *Xenopus* embryo, and a correlation between the presence of microvilli and lectin binding was observed. Such a correlation is also evident during the gastrulation process in *Xenopus* (O'Dell *et al.*, 1974; Monroy *et al.*, 1976). Similarly, in the case of *Discoglossus*, changes in the glycoprotein composition of the dimple membrane are probably not only associated with the composition and organization of the antennular glycocalyx, but might also reflect a new membrane insertion process. The lectin binding pattern observed during meiotic divisions is strikingly similar to the one shown in *Xenopus* by Denis-Donini *et al.* (1977). Again, it might be considered as a case of new membrane insertion after pinching off of the polar body.

We would like to thank Dr. J. Brachet, Dr. G. Ghiara, and Dr. A. Monroy for their helpful comments during the preparation of this manuscript.

REFERENCES

- ANDREUCCETTI, P., AND CAMPANELLA, C. (1976). The annulate lamellae in *Discoglossus pictus* oogenesis. Submitted.
- CAMPANELLA, C. (1975). The site of spermatozoa entrance in the unfertilized egg of *Discoglossus pictus* (Anura): An electron microscope study. *Biol. Reprod.* 12, 439-447.
- CAMPANELLA, C., ANZISI, A., AND BELLINI, L. (1972). Studio sulla deposizione della gelatina e sull'ovidutto di *Discoglossus pictus*. *Boll. Zool.* 39, 599.
- DENIS-DONINI, S., BACCETTI, B., AND MONROY, A. (1977). Morphological changes on the surface of the egg of *Xenopus laevis* in the course of development. II. Cytokinesis and early cleavage. *J. Ultrastruct. Res.* 56, 104-112.
- GHIARA, G. (1970). Osservazioni sugli strati superficiali e corticali di ovociti e di uova di *Discoglossus pictus* (Otth) e di altre specie di Anfibi. *Arch. Zool.* 45, 9-92.
- GREENAWAY, P. J., AND LE VINE, D. (1973). Binding of *N*-acetyl-neuraminic acid by wheat germ agglutinin. *Nature New Biol.* 241, 191-192.
- HIBBARD, H., AND WINTREBERT, P. (1928). La formation des membranes et les changements d'aspects de l'oeuf de *Discoglossus pictus* (Otth) avant la ponte. *Compt. Rend. Soc. Biol.* 98, 1521-1523.
- KALT, M., AND TANDLER, B. (1971). Improved preservations of Amphibian embryos for electron microscopy. *J. Ultrastruct. Res.* 36, 633-645.
- KARNOVSKY, M. Y. (1965). A formaldehyde-glutaraldehyde fixative of high osmolarity for use in electron microscopy. *J. Cell Biol.* 27, 137A-138A.
- MANN, P., LUTWAK-MANN, C., AND HAY, C. M. F. (1973). A note on the so-called seminal vesicles of the frog *Discoglossus pictus*. *Acta Embryol. Morphol.* 6, 21-25.
- MILLONIG, G. (1964). Studio sui fattori che determinano la preservazione della ultrastruttura. In "From Molecule to Cells Symposium on Electron Microscopy," pp. 347-362. CNR, Roma.
- MONROY, A., BACCETTI, B., AND DENIS-DONINI, S. (1976). Morphological changes of the surface of the egg of *Xenopus laevis* in the course of development. III. Analysis of the process of gastrulation. *Develop. Biol.* 49, 250-259.
- O'DELL, D. S., TENCER, R., MONROY, A., AND BRACHET, J. (1974). The pattern of Concanavalin A binding sites during the early development of *Xenopus laevis*. *Cell Differ.* 3, 193-198.
- POSTE, G., AND ALLISON, A. C. (1971). Membrane fusion reaction: A theory. *J. Theor. Biol.* 32, 165-184.
- REYNOLDS, E. S. (1963). The use of lead citrate at high pH as electron opaque stain in electron microscopy. *J. Cell Biol.* 17, 208-259.
- WINTREBERT, P. (1933). La mécanique du développement chez *Discoglossus pictus* Otth, de l'ovogénèse à la segmentation. *Arch. Zool. Exp. Genet.* 75.
- ZALIK, S. E., AND COOK, G. M. W. (1976). Comparison of early embryonic and differentiating cell surfaces. Interaction of lectins with plasma membrane components. *Biochim. Biophys. Acta* 419, 119-136.

ACTIN AND MYOSIN IN THE VERTEBRATE ACROSOMAL REGION

C. CAMPANELLA *, G. GABBIANI *, B. BACCETTI **, A. G. BURRINI **
and V. PALLINI **

* Department de Pathologie, Université de Genève, 40 Boulevard de la Cluse,
1211 Genève 4, Suisse; ** Istituto di Zoologia, Università di Siena,
Via Mattioli 4, 53100 Siena, Italy

SUMMARY - Actin and myosin are present in the subacrosomal region of the human spermatozoon, as demonstrated by immunofluorescent staining using specific antibodies. The occurrence of both contractile proteins in human spermatozoa is indicated also by SDS-polyacrylamide gel electrophoresis. The above mentioned methods detect the presence of only actin in testicular (but not in epididymal) rat spermatozoa and in the perforatorium of turkey spermatozoa.

KEY WORDS *bird and mammalian spermatozoa - perforatorium - acrosome - actin and myosin*

INTRODUCTION

In the recent years the problem of the structure and function of the rod-like organelle located under the acrosome and generally called perforatorium (Baccetti and Afzelius, 1976) has been approached with electron microscopy and chemical analysis of purified samples. Almost all the results have been obtained in marine invertebrates spermatozoa, where the perforatorium elongates at the time of the acrosome reaction, emerging, as a process, from the sperm surface. Actin was demonstrated to be the most important protein in the process (Tilney *et al.*, 1973; Jespersen *et al.*, 1973). Two conditions have been recognized by Tilney (1975, 1976a and b). In the arthropod *Limulus* the subacrosomal bundle of filaments pre-exists in a coiled form, and the elongation is due to a changed packing of the actin microfilaments from a supercoil with hexagonal array (De Rosier *et al.*, 1977) to a parallel bundle.

When supercoiled, actin is glued by other proteins: scruin (55,000 m.w.) and α -actinin (95,000 m.w.) (Tilney, 1975a, b). In the unreacted perforatorium of *Thione* and *Asterias* (Echinoderms) spermatozoa, actin is trapped in a «storage form» neither globular, nor filamentous (Tilney *et al.*, 1973), bound to other proteins *i.e.* spectrin-like molecules (250,000 and 230,000 m.w.) (Tilney, 1976b, in *Thione*) and profilin (16,000 m.w.) (Carlsson *et al.*, 1976a, b). Actin polymerizes upon a pH rise and separation from the inhibitory proteins (Tilney, 1976b). Moreover Mabuchi and Mabuchi (1976a) have detected myosin in the heads of *Asterias* spermatozoa and localized it in the acrosomal region by immunofluorescence. It is also suggested that myosin accelerates the acrosomal process elongation (Mabuchi, 1976). In the more evolved terrestrial animals the situation seems to be somewhat changed; but only few data are available. Millipeds exert a conspicuous acrosome reaction, but actin seems to be absent from the acrosome complex, where a 60,000 m.w. proteins is prominent (Baccetti *et al.*, 1977). No data

Motile Properties and Localization of Contractile Proteins in the Spermatozoon of *Discoglossus pictus*

C. Campanella and G. Gabbiani

Department of Pathology, University of Geneva

Ejaculated spermatozoa from *Discoglossus pictus* are grouped in bundles, where they are embedded in a network of interwoven threads. Their heads and tails move when exposed to the outermost egg jelly layer, when the bundles are spread across a glass slide or a poly-L-lysine-coated polystyrene tissue culture dish. While moving, single spermatozoa emerge from the bundle and eventually become able to fuse with egg.

Spermatozoa were studied by means of immunofluorescent staining, using specific antibodies against actin, myosin, and tubulin, and by means of electron microscopy. Antiactin antibodies stain both the heads and the ridge (which contains the axoneme) of the tail's undulating membrane. Antimyosin antibodies stain the head segment covered by the acrosome cap, and antitubulin antibodies stain the axoneme. The presence of actin and myosin in the spermatozoon head may provide the molecular basis for a cytoskeletal and/or a contractile system which could be involved in the motion sequence as well as subsequent steps of fertilization.

Key words: spermatozoon, fertilization, contractile proteins, Anura

INTRODUCTION

Adult males of the painted frog (*Discoglossus pictus*), like other amphibia, show glandular dilations of the mesonephric duct [Mann et al, 1963; N'Diaye et al, 1973] which have been referred to as "seminal vesicles" in spite of marked differences from the corresponding mammalian organs [Mann, 1964]. Following injection of gonadotropic hormones, the seminal vesicles become full of seminal fluid [N'Diaye et al, 1974] containing bundles of spermatozoa. Spermatozoa of *Discoglossus* have been studied by several investigators [Ballowitz, 1904; Hibbard, 1928; Favard, 1955] not only on account of their extraordinary length (the longest vertebrate spermatozoon so far reported) but also because their basic mechanism of approach to the eggs is not known. Indeed, *Discoglossus*

Received October 10, 1978; accepted April 17, 1979.

Address reprint requests to C. Campanella, Istituto di Istologia ed Embriologia, University of Naples, Via Mezzocannone 8, 80134 Naples, Italy.

spermatozoa have been described as immotile in spite of the well-developed flagellum and in contrast to spermatozoa from other amphibia [Hibbard, 1928; Favard, 1955]. Our preliminary observations have indicated that this is not the case.

In this study, we have examined some conditions evoking movement and the distribution of contractile and cytoskeletal proteins in *Discoglossus* spermatozoa. Our results indicate that 1) the head and tail of ejaculated spermatozoa move for a limited time, and 2) the head and tail of spermatozoa contain contractile and cytoskeletal proteins which may represent the molecular basis for this movement.

MATERIALS AND METHODS

Adult *Discoglossus pictus* males and females were captured in the neighborhood of Palermo (Italy) from February to May. They were injected in the dorsal lymphatic sac with 200 units of Pregnyl (chorion gonadotropin, Organon Oss, Holland) in amphibian Ringer's solution. The males were utilized 24–48 hours later. Following injection the seminal vesicles become filled with about 3 ml of seminal fluid containing bundles of spermatozoa. We obtained spermatozoa either by squeezing the abdomen, or by pricking the seminal vesicles after opening the male abdomen.

Antisera

Antibodies against actin (AAA), tubulin (ATA), and smooth muscle myosin (AMA) were obtained from patients with chronic aggressive hepatitis (AAA) or from rabbits injected with pig brain tubulin (ATA) or with myosin (AMA) from rat or human uterus. The specificity of these antibodies was tested as previously described [Gabbiani et al, 1977; Chaponnier et al, 1977; Gabbiani et al, 1978].

In the immunofluorescence staining, the AAA and the AMA were fixed on *Discoglossus* oviduct smooth muscle and uterine eggs and the ATA on *Discoglossus* oviduct cilia and uterine eggs [Campanella and Gabbiani, manuscript in preparation]. The cell staining was abolished by prior incubation of the antibody solution with actin for AAA and with tubulin for ATA.

Immunofluorescent Staining

A drop of seminal fluid was applied or gently smeared with a wooden stick on microscope slides, dried, and fixed for 30 seconds in absolute ethanol (for AAA and AMA) or for 20 minutes in 3.7% formaldehyde prepared from paraformaldehyde and diluted in phosphate-buffered saline (PBS) followed by acetone (for ATA). The smears were then incubated with AAA, ATA, or AMA for 15 minutes. After incubation the smears were washed in PBS and then stained for 15 minutes with either fluorescein-conjugated IgG fraction of goat antiserum to human IgG (code No. 64.1070, Miles Seravac, Lausanne, Switzerland) for AAA or with fluorescein-conjugated IgG fraction of sheep antiserum to rabbit IgG (code No. 65-173-1, Miles) for AMA and ATA. In order to learn whether AAA and AMA stain the same sperm region, the smears were incubated with the following agents: 1) AMA; 2) sheep antiserum against rabbit IgG (SARIG) conjugated with rhodamine [Cebra et al, 1965; Lamelin et al, 1972]; 3) AAA; 4) antihuman IgG conjugated with fluorescein (Miles, Seravac). After washing with PBS and mounting in 90% glycerol in PBS, the level of fluorescence was compared with that found in control smears treated in an identical manner with human γ -globulins (code No. 48990, Fluka) (for AAA), rabbit γ -globulins (code No. 22540, Serva, Heidelberg) (for ATA) and rabbit normal serum (for

AMA). For the second step of indirect staining 10% Discoglossus serum was routinely added to the sera used in order to eliminate nonspecific background. Some smears were stained with hemallume and periodic acid-Schiff (PAS) for polysaccharide detection.

Photographs were taken on a Zeiss UV photomicroscope, using Anscochrome color slide film 500 daylight (GAF Corporation, New York) or Ilford black-and-white HP5 film (Ilford, Basel).

Electron Microscopy

Spermatozoa were fixed for 1 hour in 3% glutaraldehyde in cacodylate buffer, pH 7.2, followed by postfixation in 1% OsO₄ in collidine buffer at pH 7.4 for 1 hour, dehydrated in graded ethanol, and embedded in Epon 812. Thin sections were cut with diamond knives, stained with uranyl acetate and lead citrate, and examined in a Philips EM-300 electron microscope.

SDS Electrophoresis on Polyacrylamide Gels

After removal of the seminal fluid by low-speed centrifugation, the spermatozoa pellet was resuspended in a buffer (10 mM NaCl, 10 mM Tris-HCl, 3 mM MgCl₂, 1 mM phenylmethanesulfonylfluoride, pH 7.4) [Bray and Thomas, 1976] containing 0.05% Nonidet (Nonidet P40, BDH Chemical Ltd. Poole) and 0.1% Triton, and then homogenized and centrifuged at 10,000 g. In order to preserve actin and myosin we used mild solubilization conditions. As a result many tail fragments were found in the pellet after centrifugation. Hence supernatants should be considered to contain only part of the axoneme tubulin. The supernatants were boiled with sample buffer (0.05% SDS, 0.07% mercaptoethanol, 0.010% bromophenol blue, 50% glycerol in Tris-H₃PO₄, pH 6.91). About 70 μg of proteins in 100 μl [Bradford, 1976] were subjected to 10% polyacrylamide gel electrophoresis (PAGE) in 0.1% SDS [Laemmli, 1970]. This protein concentration was necessary in order to clearly visualize bands present in the upper portion of the gels. After completion of electrophoresis, gels were stained in 5% methanol plus 10% acetic acid containing 0.1% Coomassie Brilliant Blue. Molecular weight evaluation was made using as markers myosin heavy chain from human uterine muscle (about 220,000), phosphorylase (94,000), pyruvate kinase (57,000), and actin from rabbit skeletal muscle (43,000).

RESULTS

General Features

Discoglossus spermatozoa measure approximately 2.3 mm in length and have a thickness ranging from 1 μm (at the head base) to approximately 0.2 μm (at the head tip). Their main constituents are the head, the "neck" region, and the tail with an undulating membrane supported by the axial rod (Fig. 1). At the tip of the head, the slender, conical "apical rod" can be distinguished (Fig. 1). An acrosomal cap covers the nucleus except for its posterior edge (Fig. 1).

Spermatozoa collected from the seminal vesicles are associated in register in bundles of 20 or more in which spermatozoa are entwined (Figs. 1 and 2a). The bundles are held together by interwoven threads (4 μm thick) of unknown nature (Fig. 2a). The threads are found throughout the entire bundle and are particularly evident around the apical region of the heads and around the "neck" region (Fig. 2a). Furthermore the heads

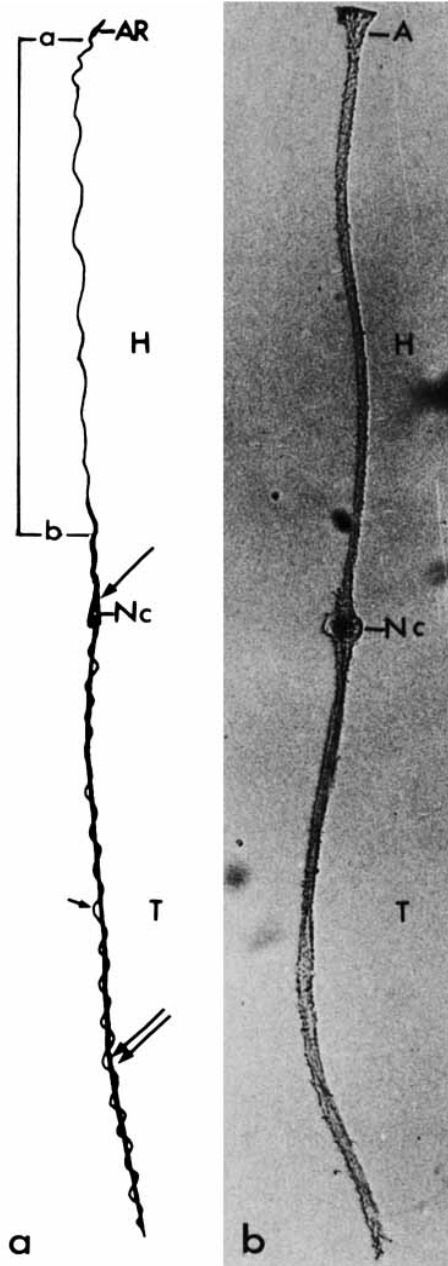


Fig. 1. (Left): Schematic drawing of a *Discoglossus* spermatozoon. The spermatozoon segments of the head and tail have been drawn not to scale, in order to show some morphologic details better. AR, apical rod. a-b, acrosomal cap extension over the nucleus. The nucleus basal portion is thicker (about 1μ) (single large arrow) than the apical one (about 0.2μ) covered by the acrosomal cap, which is not shown. Nc, "neck" region; double large arrow, axial rod; small arrow, axoneme limiting the undulating membrane. (Right): Unfixed ejaculated spermatozoa bundle. A, funnel-shaped terminal part of the heads containing the apical rods; H, heads; Nc, "neck" region; T, tails. $\times 80$.

separate at their apical ends, forming a funnel-shaped structure (Fig. 1). The "neck" region is easily distinguished in such bundles since each spermatozoon shows, at that level, a cytoplasmic droplet (10 μm in diameter), which is strongly PAS-positive (Fig. 2a).

Movement

Discoglossus spermatozoa do not move as long as they are kept in samples of seminal fluid. However, when spermatozoa bundles are exposed to uterine eggs, they are seen to move very rapidly for a short time if they come in contact with or close to the outermost layer of egg jelly. This reaction is difficult to follow in detail, since the jelly is only slightly transparent so that one can establish neither the pattern of the motion nor whether contact with the jelly is needed to trigger movement. However, it can be clearly observed that only single spermatozoa penetrate the gelatinous animal plug (Fig. 2b) into the animal dimple, the site of spermatozoon fusion with the egg [Campanella, 1975]. This process of penetration into the jelly takes place a few seconds after the first contact with the jelly. We have performed a number of experiments aiming at understanding the processes underlying the release of the spermatozoa from the bundles. The following ones are worthy of mention. When a drop of seminal fluid is placed on a glass micro slide the spermatozoa appear immobile. However, if a very small amount of seminal fluid is smeared with a wooden stick across the slide, several bundles rapidly unwind (2–3 seconds after application). Meanwhile the axoneme and the undulating members of single spermatozoa move in a sinuous fashion around the axial rod. As a result single heads move abruptly. Thereafter groups of spermatozoa begin to escape from the apex of the bundle (Fig. 2c, d, e). Once free in the medium, the heads move with both a to-and-fro and a rotating pattern. Most spermatozoa, however, are prevented from proceeding further as they wind round each other (Fig. 2e). The tip of the head of the freely moving spermatozoon ceases to move 1–2 seconds later than the basal portion. The number of moving spermatozoa is greatly enhanced if a coverslip is applied to the upper surface of the sample.

As a result of these events single spermatozoa become free (Fig. 2e) from the bundle, leaving a clear area which retains the shape of the spermatozoon within the bundle (Fig. 2c). The bundle at this time consists of a network of interwoven threads and of the cytoplasmic droplets left by the ejected spermatozoa (Fig 2c, d, e). These processes occur so quickly (approximately 14 seconds) that it is difficult to describe them in greater detail.

To determine the influence of surface charge in the motion of spermatozoa, these cells were applied as a monolayer on a surface showing negative charge (a polystyrene tissue culture dish treated with sulfuric acid; Greiner and Söhne, 7740 West Germany). The spermatozoa do not move at all. However, if on the same petri dish a film of 0.5% poly-L-lysine in PBS is sprayed and dried before spermatozoa are applied, the cells move as previously described. Furthermore, when such a surface is utilized more than two or three times for this study, a further application of sperm does not permit movement of spermatozoa.

Immunofluorescent Staining and Electron Microscopy

Upon incubation with AMA, the heads are made highly fluorescent by anti-rabbit IgG conjugated with fluorescein or rhodamine (Fig. 3a, b, c). The label is absent however, from the "apical rods" (compare Fig. 3a with Fig. 3b) and from the head basal portion which is not covered by the acrosomal cap (Fig. 3d). Controls incubated with normal rabbit serum are not stained (Fig. 3c). In the case of incubation with AAA, a fluorescence weaker than with AMA is observed on the whole head with the exception of the "apical

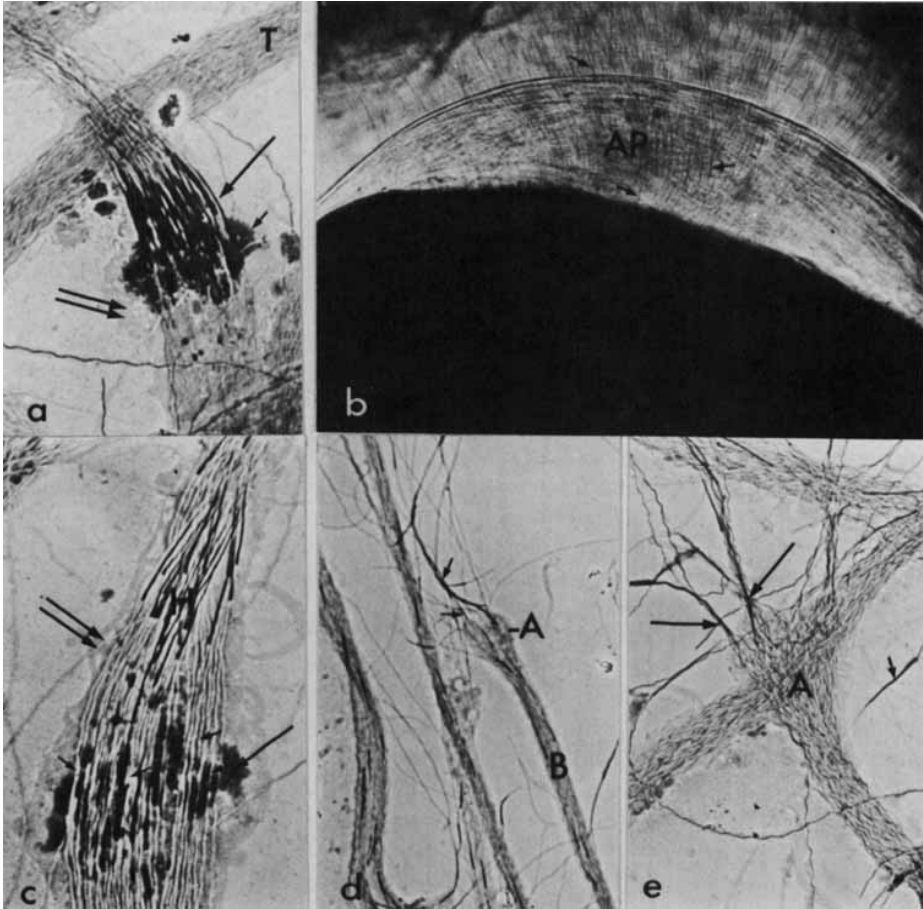


Fig. 2. a: Smear of spermatozoa bundles stained with PAS-hemallume. Single large arrow, basal nucleus portion; small arrow, PAS-positive cytoplasmic droplets; T, bundles of tails; double large arrow, threads surrounding the spermatozoa in the bundle, particularly evident around the "neck" region. $\times 330$. b: Unfixed, whole uterine egg showing the gelatinous animal plug (AP). In the plug no bundles but numerous filiform single spermatozoa (small arrows) are seen. $\times 60$. c-e: Spermatozoa bundles dried while spermatozoa were in the process of ejection and stained with PAS-hemallume. c: note the tightly interwoven threads of the bundle (double large arrow), and the cytoplasmic droplets (large arrow) left over by the displaced heads (H). The original places of the heads now empty are clearly distinguishable (small arrow) among the cytoplasmic droplets. $\times 450$. d: A, apical head region. Several spermatozoa heads (small arrows) are partially ejected from a bundle (B). $\times 130$. e: Some spermatozoa partially outside the bundle apical portion (A) are wound around each other (large arrow) and stuck together. Note one spermatozoa (small arrow) free in the medium. $\times 300$.

rod" (Figs. 3e, f). The fluorescence is particularly strong at the anteriormost portion of the nucleus. Controls exposed to human γ -globulins are negative (Fig. 3g). Furthermore, the tails are also positive to the AAA immunofluorescent staining: An undulating pattern is evident corresponding to the undulating membrane ridge and also to the "neck" region (Fig. 4a, b). Controls incubated with human γ -globulins are not stained (Fig. 4c).

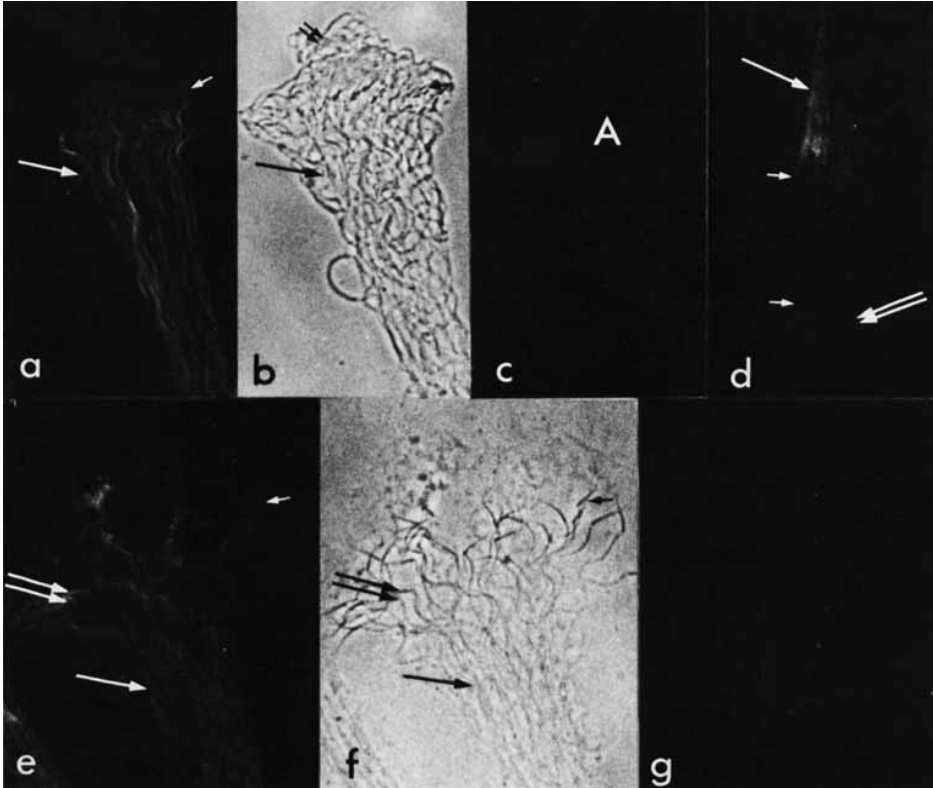


Fig. 3. a: AMA immunofluorescence staining. The label is on the heads (single large arrow). $\times 480$. Small arrow, apical rod, which appears unstained. b: Phase contrast micrograph of the bundle of spermatozoa in Fig. 3a. Small arrow, apical rod corresponding to that indicated in Fig. 3a. Note the threads around the spermatozoa anteriormost region (double small arrows). $\times 480$. c: Control incubated with normal rabbit serum: no label. A, heads funnel-shaped separation. $\times 480$. d: The head fluorescent label after incubation with AMA (single large arrow) is absent in the posteriormost head region (small arrows). Double large arrow, cytoplasmic droplets. $\times 480$. e: Spermatozoa heads incubated with AAA. The label is on the heads (single large arrow) and particularly on the anteriormost region (double large arrow). The apical rod (small arrow) is unstained, $\times 680$. f: Phase contrast of the bundle of spermatozoa in Fig. 3e. Large arrow, heads; double large arrow, anteriormost head region; small arrows, apical rods. The labels indicate corresponding structures of Fig. 3e, $\times 680$. g: Control incubated with human γ -globulins. The heads are not stained. $\times 680$.

When spermatozoa are incubated with ATA, a positive staining occurs on the axoneme with a localization similar to that obtained with AAA (Fig. 4d).

No changes in these patterns are observed in bundle-free spermatozoa. The present experiments were performed with freshly obtained males. With regard to this point, it should be pointed out that in spermatozoa from animals kept in the laboratory for a period longer than one month, the pattern of AAA localization changes. A label is present uniformly on the heads, which are not particularly positive in the apical region, and is absent in the tails. Such spermatozoa are also less motile if compared to spermatozoa from freshly obtained males.

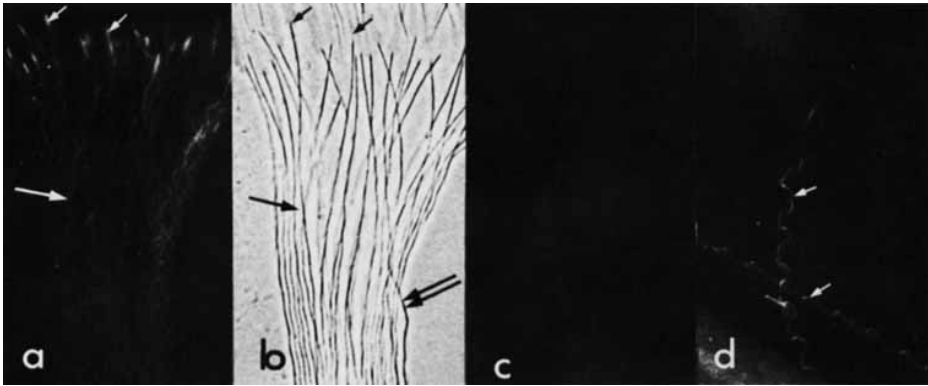


Fig. 4. a, b: Spermatozoa tails incubated with AAA. a: Single spermatozoa are distinguishable as the bundle is loose. The undulating membrane ridge, corresponding to the axoneme and probably to part of the membrane itself, is positive (large arrow). Note an intensely stained segment in the "neck" region (small arrows). b: Phase contrast of the bundle of spermatozoa in Fig. 4a. Small arrows, "neck" regions; single large arrow, axoneme; double large arrows, axial rods. The labels indicate corresponding structures of Fig. 4a. c: Control smear incubated with human globulins: no staining. d: Smear incubated with ATA. Two spermatozoa tails are present. Immunofluorescent staining is shown on the axoneme (small arrows), whose path corresponds to the undulating membrane one. $\times 500$.

Under the electron microscope, the spermatozoon head appears as a rather complex structure. Figure 5a is a cross section of the anterior head portion. Below the plasma membrane is located the acrosomal cap. A space — the subacrosomal space — is present between the inner acrosome membrane and the nuclear envelope, and it contains only very sparse electron-dense material (Fig. 5a). In the acrosomal cap, two components (A and B) can be distinguished. An electron-dense material aggregated in filaments about 80–90 Å thick is present (Fig. 5a) in component B. The nucleus occupies the entire head with the exception of the "apical rod." Along the whole nucleus, an endonuclear canal is present (Fig. 5a) formed from the apical invagination of the nuclear envelope (for the origin of this structure, see Sandoz [1970]). In the canal some electron-dense material is apposed to the invaginate external nuclear membrane (Fig. 5a) and some discontinuous and sparse material is also present (Fig. 5b).

Figure 6 shows a cross section of a tail where the axial rod, the undulating membrane, and the axoneme are present. In the axial rod, around a dense core, a less compact zone is visible. The material composing this layer extends to the undulating membrane and it is present also in the cup-shaped structure adjacent to the axoneme (Fig. 6).

SDS Gel Electrophoresis

By SDS-PAGE it is shown that in the 10,000g spermatozoa homogenate supernatant a band migrating with actin is present (Fig. 7). Since tubulin monomers have a molecular weight of 55,000–60,000 (see Luduena and Woodward [1975]), the band migrating with pyruvate kinase (57,000) (Fig. 7) is probably tubulin.

In Figure 7, one can observe a protein band with an apparent molecular weight in the range of 200,000 (compare gel B with gel A, which contains 220,000 myosin).

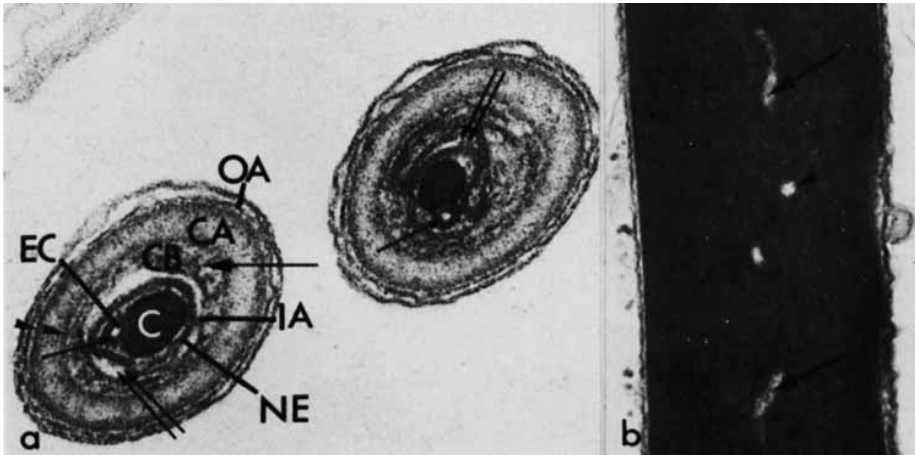


Fig. 5. a: Electron micrograph of the anterior portion of two heads. OA, outer acrosome membrane; IA, inner acrosome membrane; NE, nuclear envelope; EC, endonuclear canal; C, chromatin, CA, acrosome component A; CB, acrosome component B; double arrow, subacrosomal space containing very sparse material. Observe the electron-dense rims (arrowheads) underneath the outer acrosome membrane and separating the acrosome CA from CB. The rims mimic the aspect of a cytomembrane. In CB electron-dense material appears aggregated in filaments about 80–90 Å thick (single large arrow), whereas CA content is more dispersed. In the endonuclear canal some electron-dense material (single small arrows) is present. $\times 100,000$. b: Longitudinal section of a head basal portion where the acrosomal cap is absent. The endonuclear canal internal membrane is decorated with some electron-dense material (arrowhead), which is also found in the canal (arrows). $\times 54,000$.

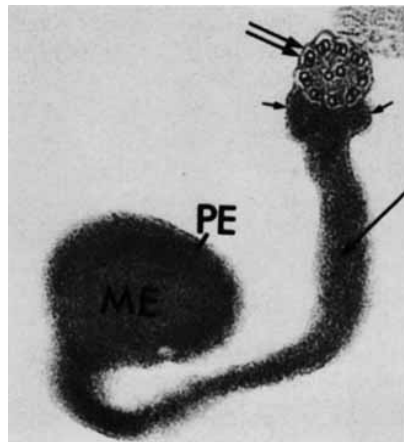


Fig. 6. Cross section of a tail. The axial rod is constituted by a medullar-dense core (ME) and by a dense compact peripheral layer (PE). The material composing the peripheral layer extends to the undulating membrane (single large arrow) and is present also in the cup-shaped structure (small arrows) adjacent to the axoneme (double large arrow). $\times 55,000$.

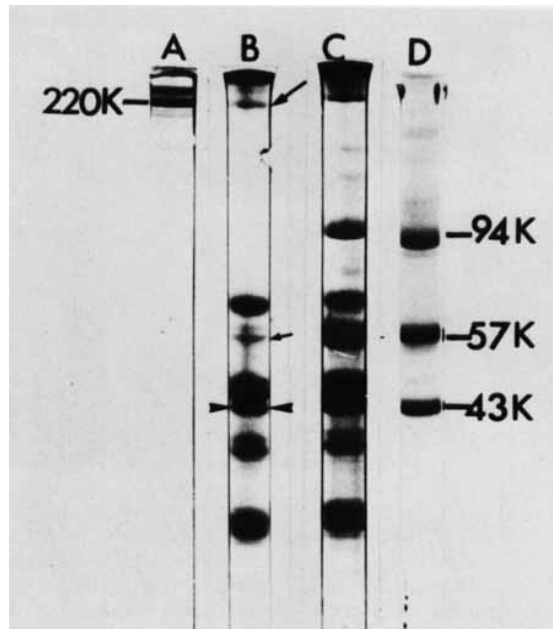


Fig. 7. SDS-PAGE of a 10,000g spermatozoa supernatant. A: human uterine myosin, 200,000. D: phosphorylase, 94,000; pyruvate kinase, 57,000; actin, 43,000. B, and C: spermatozoa. Actin migrates with a band present in the spermatozoa homogenate (arrowheads). Pyruvate kinase migrates with a band (small arrow) probably corresponding to tubulin. The large arrow shows a band with an apparent molecular weight in the range of 200,000. $\times 1.30$.

DISCUSSION

The present studies reveal that ejaculated spermatozoa of *Discoglossus* are organized in bundles consisting of tightly interwoven fibers of unknown composition in which spermatozoa are enveloped. This organization is acquired when spermatozoa are in the seminal vesicles (see N'Diaye et al [1974], and Campanella and Atripaldi, unpublished). In addition we have found three conditions under which ejaculated spermatozoa of *Discoglossus* became motile, namely, by exposure to the egg jelly (see also Furnari [1963]), by smearing on a glass surface, and by smearing on a surface with positive charges.

Under the influence of these stimuli movement occurs in two distinct forms: Escape from the sperm bundle and independent movement of each free spermatozoon in the surrounding fluid.

The phenomenon of escape from the bundle involves abrupt synchronous movements of head and tail which increase in intensity, duration, and frequency until sufficient force is achieved to permit groups of spermatozoa to leave the bundle. The second form of movement is seen in individual spermatozoa after escape from the bundles and involves to-and-fro movement of heads together with rotation of the spermatozoon on its longitudinal axis. It cannot be determined at present whether or not movements of the head are entirely dependent upon prior movement of the tail, or whether the anterior end of the head has the capacity for independent motion. After most of the spermatozoa have left the bundle, the latter remains in its original shape with the constituent threads in place and contains the cytoplasmic droplets and a few remaining spermatozoa.

The present studies provide some insight into the initiation of spermatozoon movement in *Discoglossus*. Movement is not seen when spermatozoa are studied in seminal fluid suspension, which accounts for the reputation for immotility which these spermatozoa have gained [Hibbard, 1928; Favard, 1955]. Evidently the presence of a solid surface facilitates spermatozoon movement of the two types described above, since these movements are seen when sperm bundles are spread across a glass slide. Moreover, the number of moving spermatozoa is greatly enhanced by use of a coverslip on smeared spermatozoa. Presumably, this increases surface available for attachment.

Surface charge is also important, since movement is not seen when polystyrene is used (negatively charged) but is seen to occur rapidly when the same surface is rendered positive by poly-L-lysine. It is interesting that when a poly-L-lysine surface has been used for such a study it will no longer permit movement of spermatozoa if a new sample is applied, presumably because the positive charges of poly-L-lysine have been covered.

Furthermore, we have observed abrupt motion of spermatozoa occurring as soon as the bundles are placed in contact with the egg jelly. Following this interaction, they escape from the bundle and in consequence single spermatozoa are seen in the animal plug in the process of penetrating the egg. It might be postulated that positive charges may be involved in triggering spermatozoon motility also in this fertilization sequence.

It is now becoming increasingly apparent that cellular movements can result from processes involving the interaction between actin and myosin or sometimes polymerization of actin G to F actin [Tilney, 1975; Korn, 1978]. Actin is present in nonmuscle cells both in polymerized form (the microfilaments) visible at the electron microscope, and in monomeric form [Tilney, 1975; Korn, 1978]. Myosin filaments (100–120 Å in diameter) such as these occurring in skeletal muscle are difficult to localize at the electron microscope level.

Our immunofluorescence results indicate that in *Discoglossus* spermatozoa actin is present in the head as well as in the tail. Furthermore a band migrating with rabbit skeletal muscle actin has been detected on SDS-PAGE of spermatozoa homogenates.

Spermatozoa from *Discoglossus* show an undulating membrane coiling around the axial rod. The ridge of this membrane is formed by the axoneme and is stained both by antitubulin and antiactin. Tubulin is known to occur in the axoneme (see also Weber et al [1977]); actin may reside in the axoneme itself or in the adjacent cup-shaped structure (Fig. 6). Nelson [1966] extracted an actin (flactin) from the flagellum of invertebrate spermatozoa. A positive reaction to the antiactin staining has been found in tails of other vertebrates spermatozoa [Talbot and Kleve, 1978; Campanella et al, 1979]. Furthermore, HMM-decorated microfilaments have been detected in the flagellum of an insect spermatozoon [Behnke et al, 1971; Forer and Behnke, 1972].

The fluorescence stain in the head is generalized throughout the segment containing the nucleus. The exact localization of actin within the head is difficult to establish at this time as the presence of microfilaments has not been determined. In other species of invertebrates, nonfilamentous actin has been reported to be present in the electron-dense subacrosomal material or perforatorium which is associated with specialized portions of the nucleus and the acrosome membrane [Tilney, 1975, 1976a, 1976b]. Actin has been recently localized in the acrosomal region of some vertebrate spermatozoa [Talbot et al, 1978; Campanella et al, 1979]. In *Discoglossus* the content of the endonuclear canal which crosses the entire nucleus, is probably analogous to the perforatorium [Sandoz, 1970]. By analogy with these data, it appears that the electron-dense materials in the endonuclear canal and in the subacrosomal space are good candidates for antiactin localiza-

tion. The fact that the immunofluorescent stain is stronger in the anterior region of the head suggests that most actin is localized in this segment where motion takes place for longer time than in the posterior region.

By means of immunofluorescence, myosin is localized in the whole heads with the exception of the apical rod and the posteriormost segment. The stained segment corresponds to the acrosomal cap. The acrosome contains electron-dense material aggregated in filaments which are too thin for the generally accepted size of myosin filaments. Mabuchi and Mabuchi [1976] have found that myosin is present in the starfish spermatozoon acrosomal region. Myosin has been also localized in the acrosomal complex of human spermatozoa [Campanella et al, 1979]. In *Discoglossus* the subacrosomal space is shallow, as the inner acrosome membrane is almost adherent to the nuclear envelope and contains only some inconspicuous material. However, it cannot be excluded that myosin is present in the subacrosomal space, similarly to actin.

The presence of actin and myosin in the spermatozoon head offers the molecular basis for a cytoskeletal and/or contractile system. Therefore one can suppose that such a system may be involved in the *Discoglossus* motion sequence as well as subsequent stages of the fertilization process.

It is well known that spermatozoa from mammalian species undergo a process called capacitation in the female reproductive tract before displaying the acrosomal reaction and fertilizing the egg. Capacitation is associated with increased motility (for reviews see Barros [1974], and Bedford [1974]).

In amphibians, spermatozoa become able to fertilize following exposure to the jelly layers surrounding the egg, which are a product of the female reproductive tract. This process has been called capacitation [Shivers and James, 1970] but has been not clearly separated from the acrosomal reaction. In *Discoglossus*, the spermatozoa contacting the egg jelly become motile, enter the jelly layers, where they undergo the acrosomal reaction [Campanella and Atripaldi, 1974], and during this process acquire a fertilizing ability. We have shown that the acquisition of motility can be studied separately from the jelly presence, ie, by smearing the spermatozoa on a glass surface. Hence the spermatozoon of *Discoglossus* appears particularly suitable for detailed studies on the relationship between capacitation and acrosomal reaction in amphibian spermatozoa.

ACKNOWLEDGMENTS

This work was performed under a European Molecular Biology Organization (EMBO) fellowship 1976–1978 (ALTF 90-1976) and was supported by the Swiss National Science Foundation (grant no. 3.692-0.76) and by the Consiglio Nazionale delle Ricerche grant of the 'Biology of Reproduction Project.'

We thank Drs. P. Hall and A. Monroy for advice and revision of the manuscript, Dr. U. Atripaldi for discussion, and Messrs J.-C. Rumbeli and E. Denking for photographic work.

REFERENCES

- Ballowitz E (1904): Die merkwürdigen $\frac{2}{4}$ millimeter langen Spermien des Beträchier *Discoglossus pictus* Oth. Arch Mikrosk Anat 63:343–364.
- Barros C (1974): Capacitation of mammalian spermatozoa. In Coutinho EM, Fuchs F (eds): "Physiology and Genetics of Reproduction." New York: Plenum, Part B, pp 3–24.
- Bedford JM (1974): Report of a workshop. Maturation of the fertilizing ability of mammalian spermatozoa in the male and female reproductive tract. Biol Reprod 11:346–362.
- Behnke O, Forer A, Emmersen J (1971): Actin in sperm tails and meiotic spindles. Nature 234:408–410.

Cytoskeletal and Contractile Proteins in Coelomic Oocytes, Unfertilized and Fertilized Eggs of *Discoglossus pictus* (Anura)

C. Campanella and G. Gabbiani

Department of Pathology, University of Geneva

The distribution of actin, myosin, and tubulin has been investigated in coelomic oocytes, unfertilized and fertilized eggs of *Discoglossus pictus* utilizing: 1) immunofluorescence; 2) electron microscopy; 3) incubation with heavy meromyosin (HMM), and 4) SDS-polyacrylamide gel electrophoresis (PAGE). In coelomic oocytes the germinative area (GA) has long, irregular microvilli containing microfilaments. In the rest of the oocyte, the microvilli are shallow. During the transit of the oocyte in the oviduct, a dimple forms by the invagination of the GA. A palisade of microfilament bundles is present in the finger-shaped microvilli of the dimple and extends for about 10 μm in the cytoplasm. In the rest of the egg, microvilli are absent and only random filaments appear in the cortex. Following HMM incubation, the dimple microfilaments are decorated with arrowheads pointing toward the bulk of the cytoplasm. SDS-PAGE of egg extracts shows bands co-migrating with actin (43K), pyruvate kinase (57K), and phosphorylase (94K). As a result of fertilization, the pattern of microfilament bundles in the dimple disappears in parallel with the dimple invagination itself. Generally, the entire oocyte cortex is positive to immunofluorescent staining with anti-actin, antimyosin, and antitubulin antibodies. However, the pattern of distribution and intensity of immunofluorescent staining changes for each antiserum, during different stages. It is concluded that a contractile system is present in *Discoglossus* eggs, and it is particularly developed in the dimple. The dimple is probably a major cellular compartment for the storage of unpolymerized tubulin.

Key words: coelomic oocytes, uterine eggs, contractile proteins, Anura

INTRODUCTION

Contractile and cytoskeletal proteins have been extensively described in marine invertebrate eggs. An actomyosin apparatus [Begg and Rebhun, 1979; Burgess, 1977; Byrd et al, 1977; Mabuchi, 1973; Spudlich and Spudlich, 1979] plays a prominent role in cell

Received October 8, 1979; accepted in final form October 22, 1979.

Address reprint requests to C. Campanella, Istituto di Istologia ed Embriologia, University of Naples, Via Mezzocannone, 8, 80134 Naples, Italy.

cleavage and could be implicated in sperm penetration and post-fertilization cortical contractions [for a review, see Burgess and Schroeder, 1979]. Microfilaments (50 Å) are present in unfertilized eggs as well as in microvilli of fertilized eggs [Burgess, 1977; Burgess and Schroeder, 1977]. Microtubules have been described in connection with the mitotic apparatus of fertilized eggs; however, an unpolymerized form of tubulin competent to polymerize is also present in such eggs [Kuriyama, 1977; Pfeffer et al, 1976; Weisenberg, 1972].

A large amount of G and F actin (8.8% of total soluble proteins) has been detected in *Xenopus laevis* oocytes [Clark and Merriam, 1978; Merriam and Clark, 1978]. Actin has been localized as well in the ovarian cortex in several amphibian species by means of immunofluorescent staining [Franke et al, 1976]. Microtubules [Dumont and Wallace, 1972] as well as tubulin synthesis [Moreau and Gounon, 1977] have been described in oocytes of Anura and Urodele, respectively.

Those studies so far reported concerning the distribution of cytoskeletal or contractile proteins in amphibians were conducted on ovarian oocytes. In contrast, there is no available information concerning these systems in uterine eggs at which stage the cortical organization greatly changes as a result of ovulation [see Wischnitzer, 1966].

The germinative area (GA) of the ovarian oocyte in the anuran *Discoglossus* is a portion of the animal hemisphere programmed for the selective accumulation of structures such as cortical granules (CG) and, particularly, prominent microvilli [Andreuccetti and Campanella, 1980; Campanella, 1975; Denis-Donini and Campanella, 1977]. The microvilli of the GA do not regress during ovulation in contrast with those present elsewhere on the oocyte surface which considerably shorten. During the oocyte transit in the oviduct, the GA transforms into a funnel-shaped *animal dimple* [Denis-Donini and Campanella, 1977] where finger-shaped microvilli contain bundles of filaments arranged along their longitudinal axis [Campanella, 1975]. The dimple, where the egg spindle is found in meiotic metaphase II, is the only site of successful spermatoc penetration [Hibbard, 1928]. The rest of the egg cortex, in which CG are absent, does not show microvillar protrusions [Campanella, 1975].

In this study, we have compared the distribution of actin, myosin, and tubulin in the highly specialized region of the dimple versus the remaining cortex of *Discoglossus* uterine eggs by means of immunofluorescence with purified antisera, electron microscopy, heavy meromyosin (HMM) decoration, and SDS-polyacrylamide gel electrophoresis (PAGE). The study has been partially extended to ovulated oocytes collected from the coelom (coelomic oocytes) where the dimple is not yet present, and to fertilized eggs where the dimple has been resorbed. Our results indicate that the investigated proteins are present in the cortex as well as in the dimple where they are more abundant and organized in a highly ordered cytoarchitecture. Some differences in the distribution of these proteins have been observed between coelomic oocytes and uterine eggs, and also between uterine and fertilized eggs.

MATERIALS AND METHODS

Adult *Discoglossus pictus* (painted frog) males and females were captured in the neighborhood of Palermo (Italy) during the period February 1979 through May 1979. They were injected in the dorsal lymphatic sac with 200 U Pregnyl (chorion gonadotropin, Organon Oss., Holland) in amphibian Ringer's solution. Coelomic and uterine eggs were collected, respectively, from the body cavity 12 hours later and from the uterus 24 hours later.

Seminal fluid containing spermatozoa was obtained by squeezing the males abdomen 24–48 hours after the hormone injection.

Groups of eggs were inseminated by exposure to the seminal fluid and were processed for electron microscopy and immunofluorescence 5, 20, 30, and 60 minutes after insemination, as well as at early blastula stage.

Electron Microscopy

Coelomic oocytes, unfertilized and fertilized eggs were fixed for five hours in 3% glutaraldehyde in cacodylate buffer at pH 7.2, followed by postfixation in 1% OsO₄ in collidine buffer at pH 7.4 for one hour. The fixed preparations were stained en bloc with uranyl acetate in Tris-Maleate at pH 5.2, dehydrated in graded ethanol, and embedded in Epon 812. Alternatively, samples were fixed in 3% glutaraldehyde in 0.2 M phosphate buffer at pH 7.4. Thin sections were cut with diamond knives, stained with uranyl acetate and lead citrate, and examined in a Philips EM 300 electron microscope.

Heavy Meromyosin

HMM was prepared according to the method of Woodrum et al [1975] by limited digestion of rabbit skeletal myosin [Richards et al, 1967], and stored in 50% glycerol in 0.01 M phosphate containing 0.6 M KCl. Before use, HMM was dialyzed for 48 hours against 0.01 M phosphate containing 0.015 M KCl and concentrated to approximately 6 mg/ml. *Animal dimples* and peripheral portions of eggs were manually isolated in standard salt solution (0.006 M phosphate buffer at pH 7.0) (SSS) containing 0.1 M KCl and 0.005 M MgCl₂, and incubated with decreased glycerol concentrations in the same buffer (50% for 24 hours; 25% for 24 hours, and 5% for five hours). They were then rinsed in 0.01 M phosphate buffer pH 7.0 and incubated for 40 hours in the HMM-containing solution, and processed for electron microscopy. In the control samples HMM incubation was omitted.

SDS-Polyacrylamide Gel Electrophoresis

Uterine eggs were immersed in 0.005 M DTT in 0.1 M NaCl-0.005 M Tris-HCl (pH 8.0) to dissolve the outermost jelly layers (J₃, J₂) as well as the *animal plug* [Denis-Donini and Campanella, 1977]. After several rinses in amphibian Ringer, the eggs were placed in a cold Nonidet (0.005%) containing buffer (10 mM NaCl, 10 mM Tris-HCl, 3 mM MgCl₂ and 1 mM phenylmethanesulfonyl fluoride, pH. 7.4 [Bray and Thomas, 1976]). The eggs were manually denuded of the innermost jelly coat (J₁) and the vitelline envelope, and subsequently homogenized (about 500 μ l).

After dissolution of the *animal plug*, the dimple flattens almost completely and can be easily excised from the naked egg by means of watchmaker forceps. The isolated dimples were reversed and cleaned of excess cytoplasm. Pieces of peripheral cytoplasm were also excised from eggs, cleaned of excess cytoplasm by gentle aspiration, then released from a Pasteur pipette and rinsed in fresh buffer. The resulting strands of cortical material can be considered as a cortex-enriched egg fraction. Both dimples and cortex-rich fractions were homogenized under the same conditions as the whole eggs and were centrifuged at 10,000g for ten minutes at 4°C in parallel with total egg homogenates. In the case of total eggs, a pellet was obtained containing mostly pigment, yolk, and mitochondria. A thin layer of lipids formed at the top, and the remaining total eggs supernatant is referred to as TES. From dimple and cortex-rich fractions a pellet was obtained containing mostly pigment, mitochondria, some yolk, as well as a clear supernatant. The *animal dimple* supernatant will be referred to as ADS, and the cortex-rich fraction supernatant as CRS. Protein concentrations of TES, ADS, and CRS were determined with the Coomassie brilliant blue micromethod [Bradford, 1976]. Samples were heated to 100°C in sample buffer (0.05%

SDS, 0.07% mercaptoethanol, 0.01% bromophenol blue, 50% glycerol in Tris- H_3PO_4 , pH 6.9) pH 6.9) and, in aliquots of 25–30 μ m, subjected to 10% PAGE in 0.1% SDS [Benzonana et al, 1979]. After fractionation, the gels were stained in 0.1% Coomassie brilliant blue in 10% acetic acid and 5% methanol, and destained in 7% acetic acid.

The following molecular weight protein markers were used: phosphorylase (94K); pig brain tubulin (55–60K) [Ludueno and Woodward, 1975]; pyruvate kinase (57K), and rabbit skeletal muscle actin (43K).

Antisera

Anti-smooth muscle myosin antibodies (AMA) were raised in rabbit after four subcutaneous injections of 1 mg of purified myosin from pregnant rat uterus [Gabbiani et al, 1978]. The titer of the antibody-containing serum was 1/1280 as judged by immunofluorescence staining of rat intestinal muscle. The specificity of these antibodies was tested by immunofluorescence, immunoadsorption, and immunodiffusion, employing the myosin utilized for immunization. Immunofluorescent staining was positive for rat and *Discoglossus* smooth muscle, human platelets, and cultivated mouse embryo fibroblasts [Gabbiani et al, 1978], but not for striated and cardiac rat muscle. Incubation with purified myosin abolished the capacity of the antibody-containing sera to stain rat smooth muscle, human platelets, and mouse fibroblasts. Immunodiffusion against crude and purified myosin gave a single precipitation line.

Purified anti-actin (AAA) and antitubulin (ATA) antibodies were obtained, respectively, from the sera of a patient with chronic aggressive hepatitis containing specific anti-actin antibodies [Chaponnier et al, 1977] and from sera of rabbit repeatedly immunized with pig brain tubulin absorbed to alum [Gabbiani et al, 1977]. These sera were passed through columns of sepharose covalently linked with, respectively, rabbit skeletal muscle actin and pig brain tubulin followed by elution of the absorbed antibody at pH 2.7. The specificity of these antibodies was shown by immunodiffusion where a single precipitation line against the antigens was observed, as well as by immunoelectrophoresis and immunofluorescence. With this test, the AAA was fixed on rat smooth muscle, human platelets, I-bands of rat striated muscle, and on *Discoglossus* oviduct smooth muscle. The ATA was fixed on mouse fibroblasts, mitotic spindles, cultivated mouse fibroblasts, and on *Discoglossus* oviducal cilia. Cell staining was abolished by prior incubation of the antibody solution with actin and with tubulin, respectively.

Immunofluorescent Staining

Before freezing for cryostat sectioning, coelomic oocytes, unfertilized or fertilized eggs were fixed for 15 minutes with 3.7% formaldehyde prepared from paraformaldehyde and diluted in phosphate buffered saline (PBS). This procedure does not alter significantly the immunological reaction and improves the quality of the sections. Frozen 4- μ m sections were fixed in acetone at $-20^\circ C$ for five minutes, dried, and incubated with AAA, ATA, or AMA for 15 minutes. After incubation the sections were washed in PBS and then stained for 15 minutes with either fluorescein-conjugated IgG fraction of goat antiserum to human IgG (Code Nr 64.1070, Miles Seravac, Lausanne, Switzerland) for AAA, or with fluorescein-conjugated IgG fraction of sheep antiserum to rabbit IgG (Code Nr 65-173-1, Miles) for AMA and ATA. After rewashing with PBS and mounting in 90% glycerol in PBS, the level of fluorescence was compared with that found in control sections treated in parallel with human γ -globulins (Code Nr 48990, Fluka) (for AAA), rabbit γ -globulins (Code Nr 22540, Serva, Heidelberg) (for ATA) and rabbit normal serum (for AMA). Ten percent *Discoglossus*

serum was routinely added to the sera used for the second step of indirect staining in order to eliminate nonspecific background.

Photographs were taken on a Zeiss UV photomicroscope, using Anscochrome color slide film 500 daylight (Gaf Corporation, New York, NY) or Ilford black-and-white HP5 film (Ilford, Basel, Switzerland).

RESULTS

I. Uterine Eggs

a. Ultrastructure. The structure characterizing the dimple as well as the cortex in eggs of *Discoglossus* have been reported in detail earlier [Campanella, 1975].

At the bottom of the dimple, finger-shaped, microvilli approximately $1.7\ \mu\text{m}$ long are implanted at regular intervals (Fig. 1a). Bundles of parallel filaments run along the longitudinal axis of microvilli and extend into the peripheral cytoplasm for a depth of about $10\ \mu\text{m}$. It has been observed that most fiber bundles merge together at their basal portion in groups of two or three (Fig. 1a). This reflects the slightly different orientation of microvilli (and related fiber bundles) at the dimple surface. No terminal web is present. Pigment granules and large glycogen islets are found mostly at the base of the bundles. At higher magnification (Fig. 1b) the filaments ($50\text{--}70\ \text{\AA}$ in diameter) within microvilli can be observed to run parallel to one another, with an average distance of $140\ \text{\AA}$. Some filaments bend laterally toward the plasma membrane and appear in close contact with the plasmalemma. Aggregates of electron-dense material $90\ \text{\AA}$ thick bridge the filament bundles and are also present in the cytoplasm close to the plasma membrane.

The peripheral cytoplasm of the dimple contains a network of $50\text{--}70\ \text{\AA}$ filaments (Fig. 1b). The cortex of the rest of the egg periphery is clearly distinguishable, particularly at the vegetative hemisphere where a particle-free layer measuring $0.3\ \mu\text{m}$ is present. In this region 50-\AA filaments are randomly distributed (Fig. 1c). In no instance have microtubules been observed.

b. Heavy Meromyosin. After incubation with HMM, the dimple filaments are decorated with arrowheads having a periodicity of $250\ \text{\AA}$ (Fig. 2) which point toward the bulk of the cytoplasm. A similar decoration is randomly encountered under the same conditions throughout the entire cortex. In control sections not incubated with HMM, the filaments are not decorated with arrowheads.

c. Immunofluorescence. Following exposure to AAA, the dimple peripheral cytoplasm is brightly fluorescent; a pattern of fluorescent rods oriented perpendicularly or obliquely with respect to the dimple surface is visible (Fig. 3a). The peripheral cytoplasm of the rest of the egg periphery is also positive, but the fluorescence is less intense than in the dimple (Fig. 3b). A slight positivity to AAA is detectable in the cytoplasm (Fig. 3b), particularly in the vegetative hemisphere. Control sections incubated with human γ -globulins are negative (Fig. 3c). Sections incubated with AMA (Figs. 3d,e) or ATA (Figs. 4a,b) show a positive reaction in both the cortex and the dimple, but which is generally stronger in the dimple. The cytoplasm is slightly stained after ATA incubation (Figs. 4a,b). Control sections incubated with NRS (for AMA) or with rabbit γ -globulins (for ATA) are negative (Figs. 3f and 4c).

d. SDS-Polyacrylamide Gel Electrophoresis. Electrophoretic fractionation of both TES and ADS shows a prominent band which co-migrates with actin (Fig. 5 A–E). Bands co-migrating with tubulin and/or pyruvate kinase are also present (Fig. 5 B–F). Three bands of proteins with similar molecular weights are visible in the upper portion of the gels.

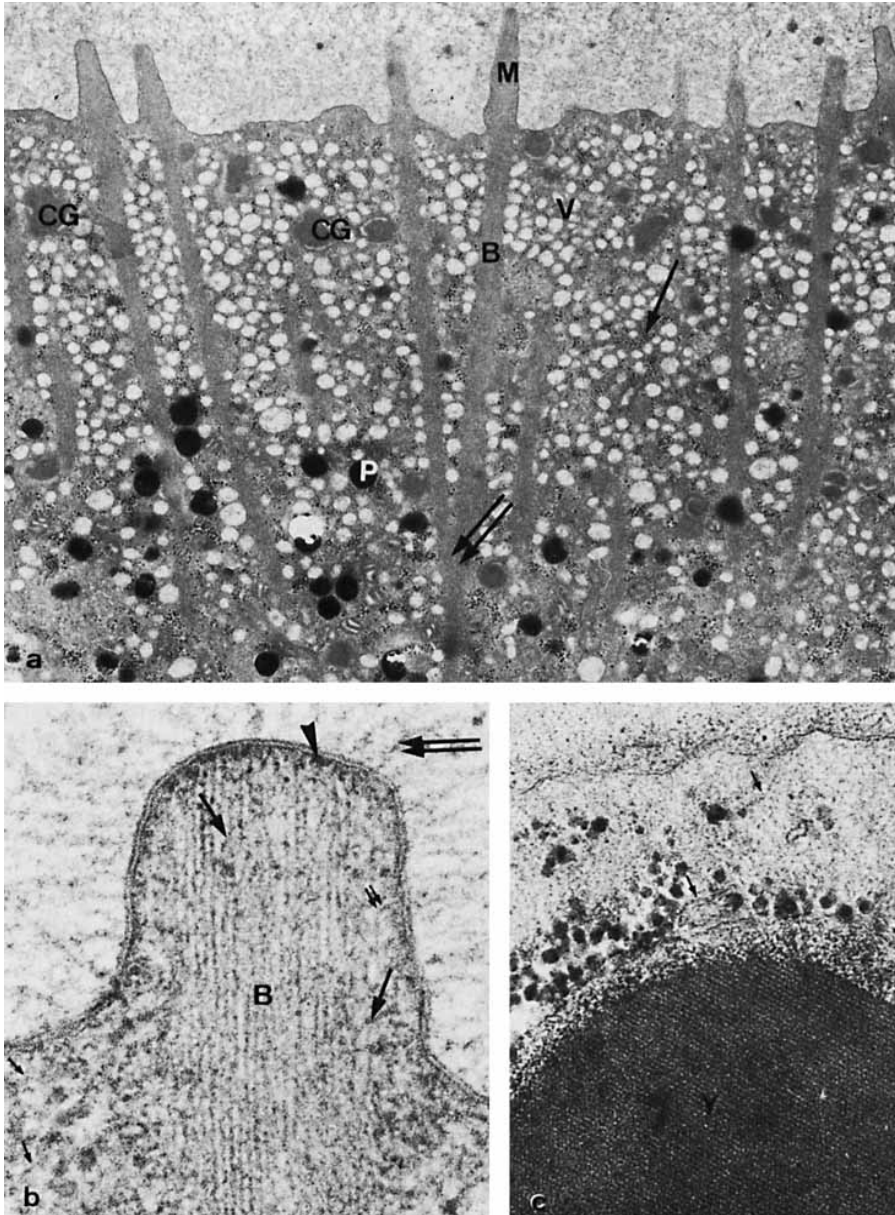


Fig. 1. Ultrastructure of uterine egg animal dimple. a: Filament bundles (B) scan the peripheral cytoplasm: They are located in the finger-shaped microvilli (M) and in the cortical cytoplasm for a depth of about $10\ \mu\text{m}$. Two or three bundles merge at their basal end (double large arrow). Only inconspicuous glycogen islets (large arrow) are present in this layer. P = pigment; CG = cortical granules; V = vesicles (courtesy of Dr. P. Andreuccetti) ($\times 9,000$). b: From the microvillus plasma membrane, a conspicuous glycocalyx radiates (double large arrow). B = microfilament bundle; large arrows = bridges of $90\ \text{\AA}$ thick electron-dense clusters; arrowhead = electron-dense material close to the plasma membrane; double small arrow = microfilament bending toward the plasma membrane: A close contact is apparent among plasmalemma and microfilament; small arrows = $50\text{--}70\ \text{\AA}$ filaments in the peripheral cytoplasm of the dimple ($\times 112,000$). c: Uterine egg cortex at the vegetative hemisphere. Small arrows = microfilaments; Y = yolk ($\times 74,000$).

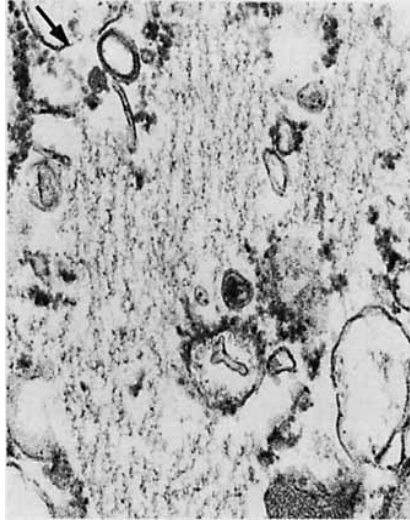


Fig. 2. Uterine egg dimple incubated with HMM. The microfilaments are decorated by arrowheads oriented toward the cytoplasm bulk and having a period of about 250 Å. Large arrow = egg plasma membrane ($\times 51,000$).

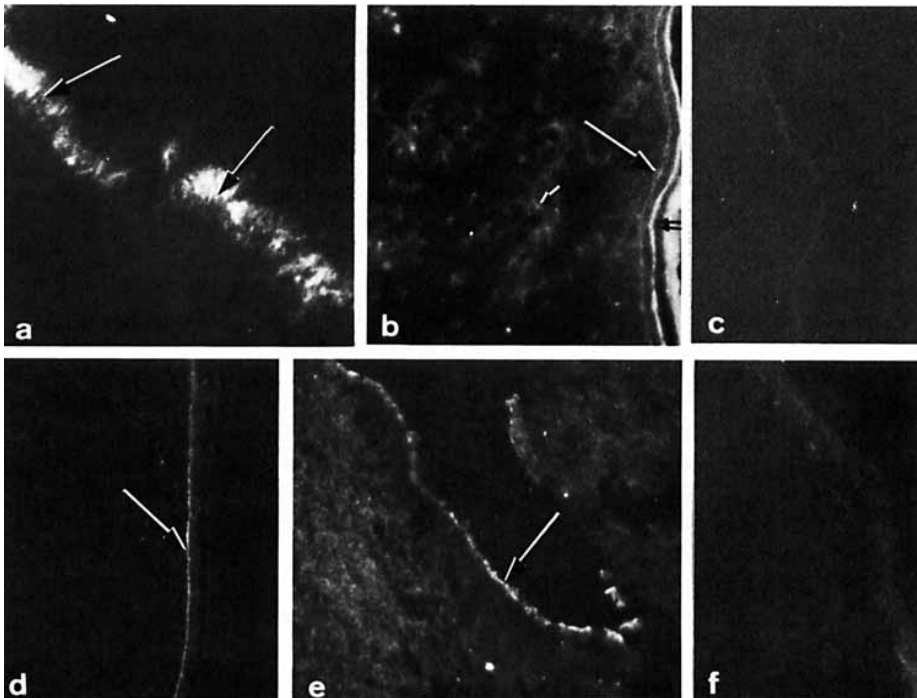


Fig. 3. Immunofluorescent staining of actin and myosin in *Discoglossus* egg periphery. a,b: Sections incubated with AAA. (a) A rod-like pattern (large arrow) is evident at the dimple cortical cytoplasm ($\times 500$). (b) A thin rim of fluorescence is present (large arrow) at the egg cortex. The cytoplasm is also slightly positive (small arrows). Double small arrow = positive staining of the jelly coat which will be described elsewhere ($\times 320$). c: Control section of a cortex incubated with γ -globulin: No staining ($\times 300$). d,e: Uterine eggs incubated with AMA. (d) In the cortex, a rim of positivity (large arrow) is present next to the egg surface ($\times 300$). (e) Band of positivity (large arrow) at the peripheral cytoplasm of the dimple which is here laterally sectioned ($\times 380$). f: Control section of an egg cortex incubated with NRS: No staining ($\times 500$).

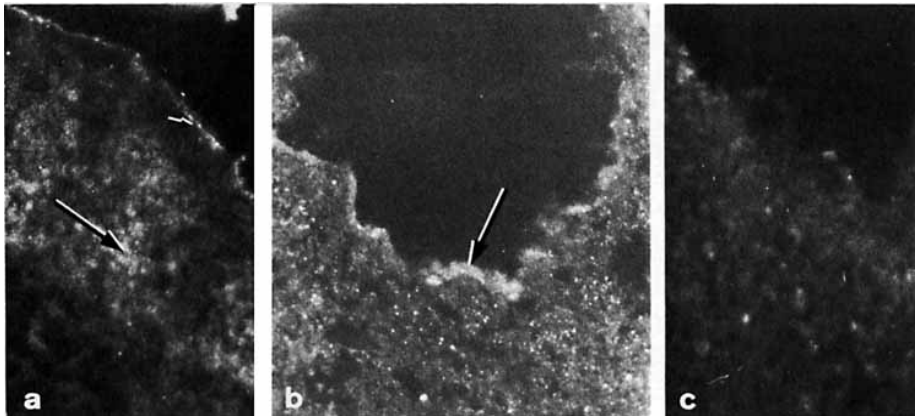


Fig. 4. Immunofluorescent staining of tubulin in *Discoglossus* egg periphery. a,b: Sections incubated with ATA. (a) A thin band of positivity is present in the cortex next to the plasma membrane (small arrow). Some positivity is also detectable in the cytoplasm (large arrow) ($\times 350$). (b) A band of positivity, thicker than that found in the cortex, is detected in the dimple peripheral cytoplasm ($\times 350$). c: Section of the dimple incubated with rabbit γ -globulins: No staining ($\times 350$).

The intermediate band co-migrates with phosphorylase (Fig. 5 A–E). Bands of proteins with molecular weights higher than 100K (as judged by comparison with phosphorylase and myosin) are also present (Fig. 5, double small arrow). The CRS fractionation (not shown) shows essentially the same protein pattern as observed in the TES and ADS gels.

II. Coelomic Oocytes

a. Ultrastructural Observations. In oocytes collected from the body cavity, the GA is a slightly pigmented zone visible in the central portion of the heavily pigmented animal hemisphere.

Ultrathin sections of the GA show (Fig. 6a) slender and irregularly long microvilli which are similar to those present in the ovarian oocyte [Andreuccetti and Campanella, 1980]. Microfilament bundles are present in the microvilli as well as in the peripheral cytoplasm of the GA (Fig. 6b) where they are irregularly arranged. Cytoplasmic inclusions within the GA such as pigment granules and glycogen islets are closer to the plasmalemma than those residing in the peripheral cytoplasm of the uterine eggs dimple (Fig. 6a, and compare with Fig. 1a). The rest of the oocyte surface shows filaments containing microvilli (Fig. 6c) which are shallow when compared to those of ovarian oocytes. Microtubules have not been observed.

b. Immunofluorescence. Upon incubation with AAA, AMA, and ATA, the cortex and the GA are positive (Figs. 6d-f); the cytoplasm is only slightly fluorescent (Fig. 6d, AMA and ATA not shown). In general, the intensity of cortex staining after incubation with the antibodies is stronger in coelomic oocytes than in uterine eggs. In particular, the fluorescent stain of ATA is very intense over the entire animal hemisphere cortex (Fig. 6f). Moreover, following incubation with AAA, the fluorescent rod-like structures of the dimple are not found in the GA (Fig. 6d). Control sections are not stained as a result of incubation with human γ -globulins (for AAA), NRS (for AMA), and rabbit γ -globulins (for ATA).

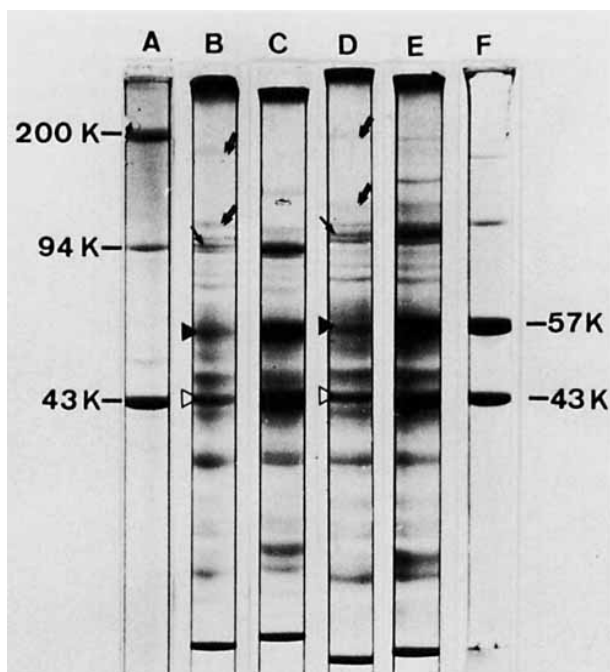


Fig. 5. SDS-PAGE of *Discoglossus* egg homogenate. A = myosin (220K), phosphorylase (94K), actin (43K). B and C = TES. In C, TES has migrated with phosphorylase, pyruvate kinase and actin. D and E = ADS. In E, ADS has migrated with phosphorylase, pyruvate kinase and actin. F = pyruvate kinase (57K) and actin. In both TES and ADS, a prominent band co-migrates with actin (black arrowheads) and polypeptide bands co-migrate with pyruvate kinase (white arrowheads) and with phosphorylase (small arrows). Some faint bands are also present in the upper gel portions of the egg extracts (double small arrows), having an apparent molecular weight greater than 100K ($\times 1.30$).

III. Fertilized Eggs

a. Ultrastructural Observations. Five minutes after insemination, many CG and vesicles have been exocytosed from the dimple, and microvilli have become thinner and longer than before fertilization. Filaments are still present in the microvilli and form randomly oriented bundles in the peripheral cytoplasm (Fig. 7a). Pigment granules, glycogen islets are closer to the egg surface when compared to the unfertilized dimple (Figs. 7a and 1a). Within 20 to 30 minutes, the dimple has completely regressed as the animal hemisphere has become almost spherical. The peripheral cytoplasm is now similar to that of the remaining egg cortex and vesicle, and CG exocytosis is terminated (Fig. 7b). Microvilli have considerably shortened but some microfilaments are still visible within their interior, whereas no microfilament bundles are detectable in the peripheral cytoplasm (Fig. 7b). Pigment granules are situated only a short distance (about $0.6 \mu\text{m}$) (Fig. 7b) from the plasma membrane.

b. Immunofluorescence. By 15 minutes after insemination, AAA fluorescence in the dimple has decreased in sharpness and in intensity when compared to the unfertilized eggs. Thirty minutes after insemination, the dimple is indistinguishable from the rest of the egg

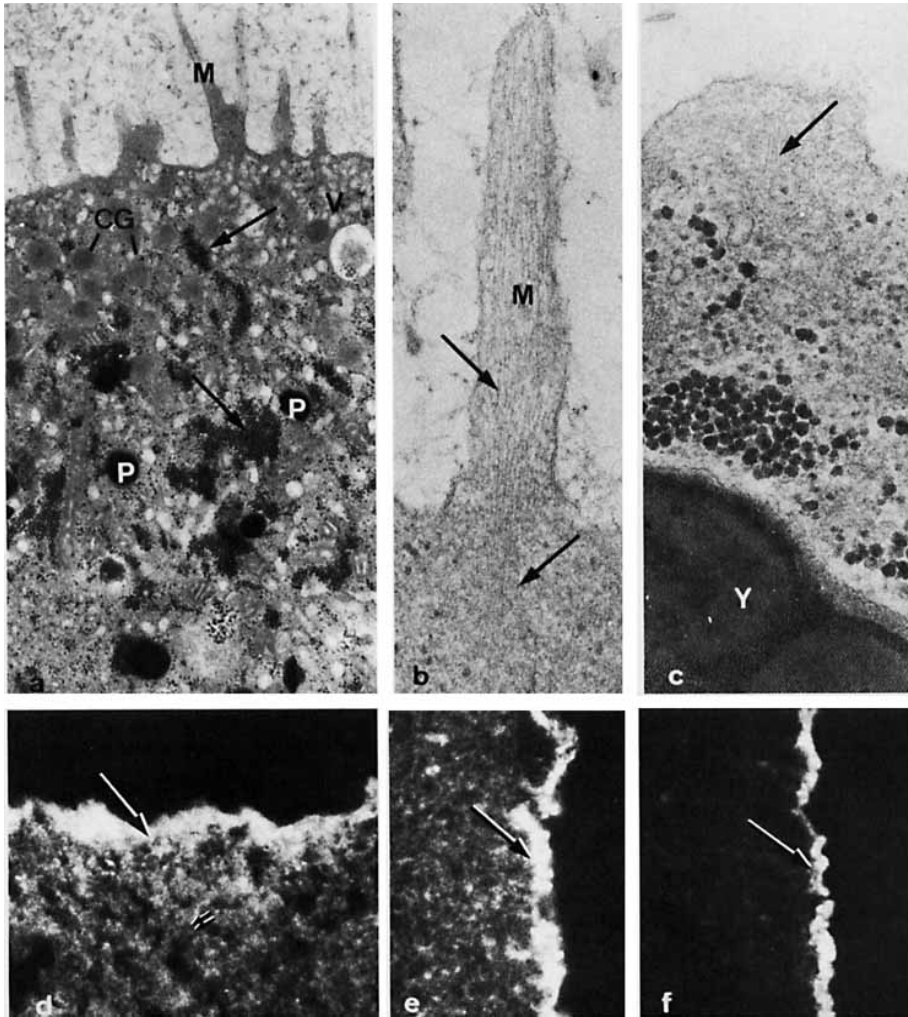


Fig. 6. Ultrastructure and immunofluorescent staining of cytoskeletal elements in *Discoglossus* coelomic oocytes. a: Slender microvilli (M) are present at the oocyte periphery. CG = cortical granules; V = vesicles; large arrow = large glycogen islets; P = pigment ($\times 12,000$). b: In the microvilli (M) and in the cortex, a microfilament bundle is present (large arrows) ($\times 68,000$). c: In the unobscured microvilli of the oocyte cortex, microfilament bundles (large arrow) are observed. Y = yolk ($\times 68,000$). d: GA; the positivity to AAA is in the peripheral layer (arrow) and partially in the cytoplasm (double arrow) ($\times 350$). e: A bright fluorescence is observed in the oocyte cortex (arrow) upon incubation with AMA; some staining is also in the cytoplasm ($\times 550$). f: Same as in (e) but upon incubation with ATA. Arrow = cortex positivity ($\times 350$).

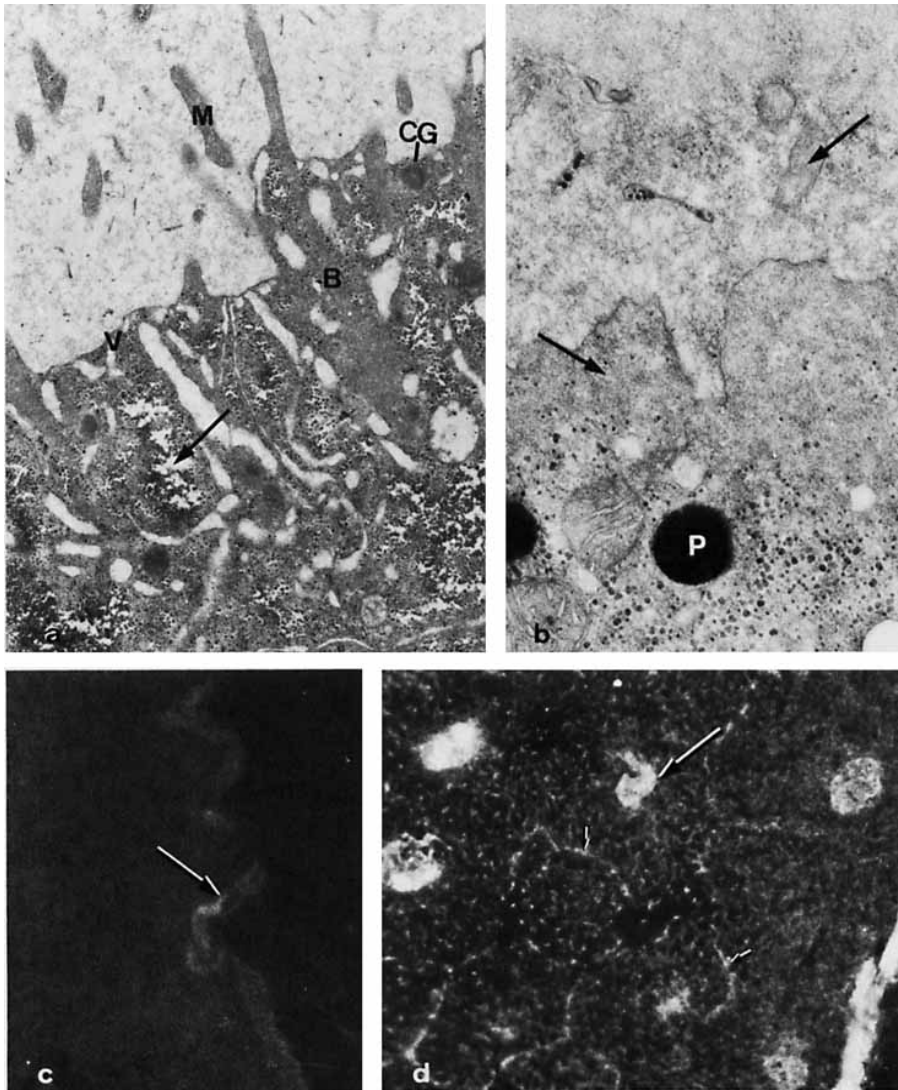


Fig. 7. Ultrastructure and immunofluorescent staining of cytoskeletal elements in *Discoglossus* fertilized egg. a: About five minutes after insemination, vesicles (V) and CG have migrated closer to the plasma membrane where exocytosis occurs. Large arrow = large glycogen islets. The microvilli (M) are long and irregular. Microfilament bundles (B), not uniformly distributed, are present in the peripheral cytoplasm ($\times 9,000$). b: The dimple 20–30 minutes after insemination. The peripheral cytoplasm is now similar to the remaining cortex of the egg. The arrows indicate microfilaments in the cortex as well as in the interior of a microvillar remnant. P = pigment ($\times 28,000$). c: About 20 minutes after insemination, the dimple periphery is almost negative following AAA incubation (arrow) ($\times 350$). d: At blastula, the positivity to AAA is in the blastomere cortex (small arrows) and in the nuclei (large arrow) ($\times 450$).

cortex and most staining has disappeared (Fig. 7c). A clear positivity is detectable at blastula stage in the nuclei as well as in the blastomeres cortex (Fig. 7d).

Upon AMA incubation, no remarkable changes occur as a result of fertilization. In the blastula, a positive staining is observed in the cortex as well as in the nuclei of the blastomeres (Fig. 8).

Thirty minutes after fertilization, the dimple has lost a great deal of ATA positivity when compared to unfertilized eggs (Fig. 9a), while the bulk of the cytoplasm retains its original fluorescence and a slight positivity is still detectable in the cortex. A strong stain is observed in the blastomere nuclei (Fig. 9b). Control sections are negative to the immunofluorescent staining.

DISCUSSION

Our results show actin, myosin, and tubulin present in *Discoglossus* eggs, leading to the conclusion that a contractile system is present in the cortical cytoplasm of the entire egg; particularly developed in the dimple.

Filaments are found in both the coelomic oocyte and the egg periphery. They are randomly distributed in the cortex or associated in bundles when microvilli are present at the oocyte surface, and are most probably F-actin-containing microfilaments as suggested by the corresponding positivity to AAA immunofluorescence staining.

In the GA and cortex of body-cavity oocytes, microfilaments are found in the longitudinal axis of microvilli as well as in the peripheral cytoplasm where they are grouped as irregularly arranged bundles. In both cases, they are positive to AAA immunofluorescence staining, which is similar to ovarian oocytes of other species [Franke et al, 1976].

The positive staining of the cortex is maintained, though at a reduced level, in unfertilized and fertilized eggs. This is probably due to the fact that microvilli have completely disappeared in this region and that microfilaments are no longer organized in bundles but, rather, in a network of filaments.

In the dimple, where finger-shaped microvilli are found, the basal confluence of two or three microfilament bundles (Fig. 1a) may constitute an anchorage system for the microfilaments which might partially substitute for the observed absence of a terminal web. These ultrastructural features are paralleled by a brilliant, rod-like pattern of fluorescence to AAA staining. The pattern and intensity of this staining appear to be strictly correlated with the regularity of arrangement of microfilament bundles in the dimple; that characteristic staining is not yet found in the GA where microfilament bundles are present as well, but in less orderly cytoarchitecture. We do not know whether, at the time of dimple formation, actin is recruited from other cytoplasmic compartments to supplement that already present in the GA or whether a new synthesis of actin occurs during the dimple shaping.

As a result of fertilization, a loss of the dimple rod-like fluorescence occurs. This is documented by the gradual disappearance of the microfilament bundle arrangement which is concomitant to the regression of the dimple itself. Therefore, it appears that the particular distribution of the microfilament bundles in the dimple probably exerts a cytoskeletal role in modeling the shape of the dimple itself [see also Campanella, 1975].

The microfilament pattern, in both the GA and the dimple, may represent a barrier for the penetration of some cytoplasmic inclusion into the cortex (ie, pigment, large glycogen islets). This is suggested by the arrangement of the microfilament bundles of the unfertilized dimple, where they form a 10 μ m palisade.



Fig. 8. Immunofluorescent staining of myosin in blastula. Following incubation with AMA, the positivity is in the blastomere cortex (small arrows) and in the nuclei (large arrow) ($\times 350$).

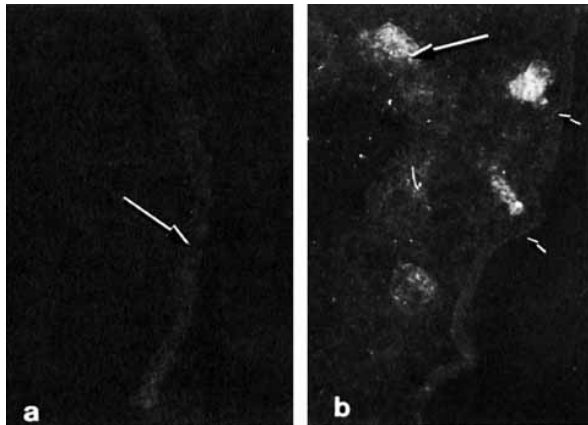


Fig. 9. Immunofluorescent staining with ATA of fertilized eggs. a: About 30 minutes after insemination, the dimple is regressed and is not stained (large arrow) ($\times 350$). b: The positivity is in the blastula nuclei (large arrow). The blastomeres cortex is hardly positive to the stain (small arrows) ($\times 350$).

Since the dimple is the site of spermatric penetration, its surface might bear receptors for sperm entrance similar to those reported for some invertebrate eggs [Glabe and Vacquier, 1978; Schmell et al, 1977; Tsuzuki et al, 1977]. In *Discoglossus*, the presence of receptor sites for spermatozoa binding has not yet been demonstrated. However, it has been shown that fucose-like residues are located only on the dimple surface and appear in the GA during dimple formation. The fucose-like residues are disaggregated after fertilization [Denis-Donini and Campanella, 1977] as are the regular bundles of microfilaments. The assemblage of a large amount of peripheral microfilaments corresponding to the segregation of fucose residues on the egg surface suggests the possibility that microfilaments play a role in this phenomenon of segregation.

The predominant band of protein co-migrating with rabbit skeletal muscle actin in

SDS-PAGE gives support for the presence of actin in the egg, and is in agreement with the findings of Merriam and Clark [1978] who used *Xenopus* oocytes.

Thanks to the HMM decoration of the dimple microfilaments, we have an additional indication for the presence of actin in the filaments. Furthermore, we have observed that microfilaments are unidirectionally oriented toward the bulk of the cytoplasm. This is similar to what has been found in other systems such as the intestinal mucosa [Mooseker and Tilney, 1975] and sea urchin eggs [Burgess and Schroeder, 1977]. Moreover, in both dimple and intestinal mucosa microvilli, we observe the following features: 1) the microfilaments are connected with the plasma membrane of the microvillus at its tip as well as at its lateral walls; 2) bridges of electron-dense material are evident in the cytoplasm around the bundle and crossing the bundle itself, and 3) at the microvillus tip, the bundle is embedded in some electron-dense material.

Mooseker et al [1978] have demonstrated the presence of myosin in the intestinal microvilli terminal web. As already mentioned, we have not observed a terminal web in the dimple. However, myosin appears to be present (as judged by immunofluorescence) in the entire cortex of coelomic oocytes, fertilized and unfertilized eggs, as a thin band close to the egg plasma membrane. This is similar to results obtained in mammalian oocytes [Amsterdam et al, 1977]. A decrease in the staining intensity of the entire cortex is observed in uterine eggs when compared to coelomic oocytes. A possible factor involved in this comparison could be the increase of surface area (about 11%) occurring during the formation of the egg dimple and depression [Denis-Donini and Campanella, 1977], which would require a redistribution of myosin along a larger cortical layer.

Tubulin has been localized by means of immunofluorescence in the entire peripheral cytoplasm of the oocyte in all observed stages and, to a minor extent, in the internal cytoplasm. A band co-migrating with tubulin or with pyruvate kinase, which has a molecular weight in the range of that of tubulin, has been detected.

Our ultrastructural observations do not show microtubules in the periphery of both coelomic oocytes and uterine eggs. This result could be artefactual due to the fixation procedure limits or, alternatively, could indicate that tubulin is present in the egg in an unpolymerized form, reflecting observations made on eggs of other species [Kuriyama, 1977; Pfeffer et al, 1976]. Microtubules have been observed in ovarian oocyte of *Discoglossus* after employing the same fixation procedure [Campanella, unpublished results]. Following incubation with ATA, tubulin appears to be preferentially located in the animal hemisphere peripheral cytoplasm of coelomic oocytes. In the uterine eggs, this preferential staining is further restricted to the dimple and is lost when the dimple regresses following fertilization. A strong staining reappears in the blastomeres nuclei.

It has been shown that after fertilization, tubulin subunits are recruited by the spermatozoon aster and in the mitotic apparatus [Aronson, 1973]. The *Discoglossus* dimple is the site of both maternal and paternal pronuclei initial swelling and migration [Hibbard, 1928]. Our results show that the dimple is positive after ATA staining; hence, the dimple could be considered as an important cellular compartment for the storage of mitotic apparatus tubulin which is later mobilized during the stage of pronuclear shift in the deeper cytoplasm. The dimple is nearly negative to ATA staining one hour following fertilization, before the sperm nucleus and middle piece are ready to begin migration [Wintrebert, 1933]. Perhaps the dimple tubulin could participate in mechanisms other than aster formation and pronuclear migration. For example, it may be involved in the maintenance of dimple structure, since ATA fluorescence staining disappears in parallel with dimple regression.

The contractile system present in the cortex of eggs from different species has been demonstrated or postulated to be active in several events, among which is the well known CG exocytosis process which occurs following egg activation [for a review, see Burgess and Schroeder, 1979]. The cortex of *Discoglossus* appears to contain an actomyosin contractile system but, with the exception of the dimple area, does not contain CG. Similarly, the cortex of *Xenopus laevis* uterine eggs also fluoresces after incubation with AAA and AMA [Campanella, unpublished observations]. However, in this species, CG are present in the entire egg cortex as is the case for most anuran eggs. Since the contractile system is present in anuran eggs independently from the presence of CG, we assume that the principal role of such an apparatus is not CG exocytosis. In the case of *Discoglossus*, however, CG are closely related to the well-developed bundles of microfilaments within the dimple and, at fertilization, the disaggregation of filament bundles could favor an approach of CG and vesicles to the plasma membrane where exocytosis occurs.

Post-scriptum: After this paper was submitted several related reports appeared in the literature such as: DA Begg and LI Rebhun 1979 (*J Cell Biol* 83:241–248); A Spudich and JA Spudich 1979 (*J Cell Biol* 82:212–226). They showed that actin is present in a non-filamentous state in the cortex of unfertilized sea urchin eggs and is induced to assemble in bundles at fertilization when a large number of microvilli extend at the egg surface. Actin polymerization may participate in this process of microvillar elongation. The increase in cytoplasmic pH, which occurs following fertilization in this species, is most probably responsible for actin polymerization in the egg cortex.

ACKNOWLEDGMENTS

This work was performed under an EMBO fellowship 1976–1978 (ALTF 90–1976) and was supported by the Swiss National Science Foundation (grant No. 3.445–0.79) and by a grant from the “Progetto Finalizzato del Consiglio Nazionale delle Ricerche (CNR) sulla Biologia della Riproduzione.”

We thank Drs. C. Chaponnier and E. Rungger-Brändle for discussion, Dr. K. Drury for revision of the manuscript, Mrs. M. Redard for preparation of ultrathin sections, and Messrs. J.-C. Rumbeli and E. Denking for photographic work.

REFERENCES

- Amsterdam A, Lindner HR, Gröschel-Stewart U (1977): Localization of actin and myosin in the rat oocyte and follicular wall by immunofluorescence. *Anat Rec* 187:311–328.
- Andreuccetti P, Campanella C (1980): Origin and cytochemistry of animal dimple granules in *Discoglossus pictus* (Anura) eggs. *J Embryol Exp Morphol* (in press).
- Aronson JF (1973): Nuclear membrane fusion in fertilized lytechinus variegatus eggs. *J Cell Biol* 58:126–134.
- Begg DA, Morell RC, Rebhun LI (1977): Studies of actin in two model systems from sea urchin eggs. *J Cell Biol* 75:256a.
- Benzonana G, Campanella C, Gabbiani G (1979): Supercontraction in crayfish muscle: Correlation with a peculiar actin localization. *Histochem* 60:21–41.
- Bradford MM (1976): A rapid and sensitive method for the quantitation of microgram quantities of protein utilizing the principle of protein-dye binding. *Analyt Biochem* 72:248–254.
- Bray D, Thomas C (1976): Unpolymerized actin in fibroblasts and brain. *J Mol Biol* 105:527–544.
- Burgess DR (1977): Polymerized actin in the isolated sea urchin egg cortex. *J Cell Biol* 75:254a.
- Burgess DR, Schroeder TE (1977): Polarized bundles of actin filaments within microvilli of fertilized sea urchin eggs. *J Cell Biol* 74:1032–1037.
- Burgess DR, Schroeder TE (1979): The cytoskeleton and cytomusculature in embryogenesis. An overview. In Gabbiani G (ed): “Methods and Achievements in Experimental Pathology, The Cyto-

- skeleton in Normal and Pathologic Processes: Cell Biology." Basel: S. Karger, vol 8, pp 171–189.
- Byrd W, Perry G, Weidner E (1977): Role of the egg cortex and actin in fertilization of the sea urchin egg. *J Cell Biol* 75:267a.
- Campanella C (1975): The site of spermatozoon entrance in the unfertilized egg of *Discoglossus pictus* (Anura): An electron microscope study. *Biol Reprod* 12:439–447.
- Chaponnier C, Kohler L, Gabbiani G (1977): Fixation of human anti-actin auto-antibodies on skeletal muscle fibres. *Clin exp Immunol* 27:278–284.
- Clark TG, Merriam RW (1978): Actin in *Xenopus* oocytes. I. Polymerization and gelation in vitro. *J Cell Biol* 77:427–438.
- Denis-Donini S, Campanella C (1977): Ultrastructural and lectin binding changes during the formation of the animal dimple in oocytes of *Discoglossus pictus* (Anura). *Dev Biol* 61:140–152.
- Dumont JN, Wallace RA (1972): The effects of vinblastine on isolated *Xenopus* oocytes. *J Cell Biol* 53:605–610.
- Franke W, Rathke PC, Seib E, Trendelenburg MF, Osborn M, Weber K (1976): Distribution and mode of arrangement of microfilamentous structures and actin in the cortex of the amphibian oocyte. *Cytobiol* 14:111–130.
- Gabbiani G, Chaponnier C, Zumbe A, Vassalli P (1977): Actin and tubulin co-cap with surface immunoglobulins in mouse B lymphocytes. *Nature* 269:697–698.
- Gabbiani G, Chaponnier C, Hüttner I (1978): Cytoplasmic filaments and gap junctions in epithelial cells and myofibroblasts during wound healing. *J Cell Biol* 76:561–568.
- Glabe CG, Vacquier VD (1978): Egg surface glycoprotein receptor for sea urchin sperm binding. *Proc Natl Acad Sci USA* 75:881–885.
- Hibbard H (1928): Contribution à l'étude de l'ovogénèse de la fécondation et de l'histogénèse chez *Discoglossus pictus* Otth. *Arch Biol* 38:251–326.
- Kuriyama R (1977): In vitro polymerization of marine egg tubulin into microtubules. *J Biochem* 81:1115–1125.
- Luduena RF, Woodward DO (1975): α - and β -tubulin: Separation and partial sequence analysis. *Ann NY Acad Sci* 253:272–283.
- Mabuchi I (1973): A myosin-like protein in the cortical layer of the sea urchin egg. *J Cell Biol* 59:542–547.
- Merriam RW, Clark TG (1978): Actin in *Xenopus* oocytes. II. Intracellular distribution and polymerizability. *J Cell Biol* 77:439–447.
- Mooseker MS, Tilney LG (1975): Organization of an actin filament-membrane complex. Filament polarity and membrane attachment in the microvilli of intestinal epithelial cells. *J Cell Biol* 67:725–743.
- Mooseker MS, Pollard TD, Fujiwara K (1978): Characterization and localization of myosin in the brush border of intestinal epithelial cells. *J Cell Biol* 79:444–453.
- Moreau N, Gounon P (1977): Synthèse de la tubuline au cours de l'ovogénèse de *Pleurodeles waltii* (amphibien, urodèle). *Biol Cell* 28:19–22.
- Pfeffer TA, Asnes CF, Wilson L (1976): Properties of tubulin in unfertilized sea urchin eggs. Quantitation and characterization of the colchicine-binding reaction. *J Cell Biol* 69:599–605.
- Richards EG, Chung CS, Menzel DB, Olcott HS (1967): Chromatography of myosin on Diethylaminoethyl-Sephadex A-50. *Biochem* 6:528–540.
- Schmell E, Earles BJ, Breaux C, Lennarz WJ (1977): Identification of a sperm receptor on the surface of the eggs of the sea urchin *Arbacia punctulata*. *J Cell Biol* 72:35–46.
- Tsuzuki H, Yoshida M, Onitake K, Aketa K (1977): Purification of the spermbinding factor from the egg of the sea urchin, *Hemicentrotus pulcherrimus*. *Biochem Biophys Res Commun* 76:502–511.
- Weisenberg RC (1972): Changes in the organization of tubulin during meiosis in the eggs of the surf clam, *Spisula solidissima*. *J Cell Biol* 54:266–278.
- Wintrebert P (1933): La mécanique du développement chez *Discoglossus pictus* Otth, de l'ovogénèse à la segmentation. *Arch Zool Exp Genet* 75:501–539.
- Wischnitzer S (1966): The ultrastructure of the cytoplasm of the developing Amphibian egg. In Abercrombie M, Brachet J (eds): "Advances in Morphogenesis." New York: Academic Press, vol 5, pp 131–179.
- Woodrum DT, Rich SA, Pollard TD (1975): Evidence for biased bidirectional polymerization of actin filaments using heavy meromyosin prepared by an improved method. *J Cell Biol* 67:231–237.

PIERO ANDREUCCETTI and CHIARA CAMPANELLA

REGIONAL DIFFERENCES IN THE PATTERN OF VITELLOGENESIS IN THE PAINTED FROG *DISCOGLOSSUS PICTUS*

Key words: *Discoglossus pictus*, vitellogenesis, pinocytosis, multivesicular bodies, yolk platelets.

ABSTRACT. During oocyte growth in the frog *Discoglossus pictus* two patterns of vitellogenesis are described. The first one consists of the transformation of multivesicular bodies into yolk platelets; the second is the result of a typical endocytotic process, as described in other species. The peculiarity in *Discoglossus* vitellogenesis consists of a regional difference of these features of vitellogenesis in vitellogenic oocytes: the multivesicular bodies transforming into yolk platelets are found only in the germinative area—the central portion of the animal half—whereas deep crypts with numerous endocytotic pits are found only in the vegetal half. The probable meaning of this regional difference in vitellogenic oocytes is discussed.

Introduction

The origin and formation of yolk platelets has been described in a variety of amphibian species.

From these studies it appears that the most important yolk constituent is liver-derived vitellogenin, which is absorbed by the oocyte through a process of pinocytosis (Dumont, 1978). The resulting endosomes constitute the main source of both proteins and membranes for yolk platelet formation. This process has been studied extensively in *Xenopus laevis* (for a review see Wallace, 1978).

In other amphibian species, additional cell constituents such as multivesicular bodies (Balinsky and Devis, 1963; Hope *et al.*, 1964; Kessel and Ganion, 1980; Kress and Spornitz, 1972; Lanzavecchia, 1966; Spornitz and Kress, 1973; Ward, 1964; Ward, 1978a, b; Wartenberg, 1962) or mitochondria

(Balinsky and Devis, 1963; Kessel, 1971; Kress and Spornitz, 1972; Lanzavecchia, 1966; Massover, 1971a, b; Spornitz and Kress, 1971, 1973) appear to participate in the vitellogenic process since yolk proteins gradually accumulate in them.

At the end of oocyte growth yolk platelets vary in size and, in fact, an animal-vegetal gradient is evident with the largest at the vegetal pole and the smallest at the animal pole (Brachet, 1960).

In this paper we have studied oocyte growth in *Discoglossus pictus* by ultrastructural and cytochemical methods. In agreement with other amphibian species, the egg of *Discoglossus pictus* has a distribution of yolk platelets along the animal-vegetal axis (Hibbard, 1928; Klag and Ubbels, 1975). The egg of *Discoglossus pictus* is exceptional among Anurans owing to the presence of the animal dimple, a restricted and funnel-shaped region of the animal hemisphere, where spermatozoon entrance occurs. This structure is formed, following ovulation, in the *germinative area* (GA), a wide portion of the animal hemisphere, which appears as a slightly depressed disc in the vitellogenic oocyte (Andreuccetti and Campanella, 1980).

Institute of Histology and Embryology, Faculty of Sciences, Naples, Italy.

Address for correspondence: Istituto di Istologia ed Embriologia, Via Mezzocannone n.8, 80134 Napoli, Italy.

Received 20 January 1982.

Revised 28 June 1982.

Fertilization and Activation Potentials in *Discoglossus pictus* (Anura) Eggs: A Delayed Response to Activation by Pricking¹

R. TALEVI,² B. DALE, AND C. CAMPANELLA²

Stazione Zoologica, Villa Comunale, Naples, Italy

Received November 26, 1984; accepted in revised form April 12, 1985

We have studied the electrical and morphological changes in the egg of the anuran *Discoglossus pictus* during fertilization and activation by pricking. Despite its atypical structure the fertilization potential (FP) in this egg resembles that of other anurans, consisting of a rapid, Cl⁻ dependent, depolarization of some 40 mV, accompanied by a 10- to 100-fold increase in conductance. Pricking eggs at the predetermined site of sperm entry, the dimple, causes an immediate depolarization, similar to the FP, and a wave of contraction can be seen to spread from the dimple to the antipode. When eggs are pricked outside the dimple a contraction wave spreads from the puncture site to the antipode, however, the activation potential (AP) is not generated until the wave reaches the dimple. Thus the farther the puncture site from the dimple the longer the delay in the generation of the AP. Our results suggest that the contraction wave reflects a propagating Ca²⁺ wave and the channels activated during the AP are localized within the dimple. As there is no obvious ultrastructural change in the dimple region until several seconds after the generation of the AP it is probable that the ion channels preexist in the egg plasma membrane and are not inserted by membrane fusion. © 1985 Academic Press, Inc.

INTRODUCTION

One of the first events in sperm-egg interaction is a rapid depolarization of the egg plasma membrane called the fertilization potential. The origin of this electrical event is unknown. There is increasing evidence to suggest that many basic cell processes are regulated by ionic signals (Boynton *et al.*, 1982) and therefore it would be important to know more about channels activated during fertilization. One unanswered question concerns the spatial distribution of fertilization channels; where are they located on the egg surface with regards to polarity and the area of sperm entry, and what is their density? In the worm *Urechis* there is evidence, albeit indirect, that the ion channels activated during fertilization are relatively localized to the area of sperm attachment (Gould-Somero, 1981). More recently, fertilization channels in the ascidian egg were studied directly using the patch clamp technique (Dale and De Felice, 1984), and it was estimated that at most 2000 are activated during fertilization.

In many marine invertebrates it is not possible to predict the area of sperm entry, which makes a systematic study of fertilization channels difficult. To circumvent this problem, we selected the egg of the amphibian *Discoglossus pictus* (Anura) where the sperm entry site is predetermined. This site, a specialized

region of the animal hemisphere, called the animal dimple (Hibbard, 1928), has a fine structural organization different from that of the rest of the egg (Campanella, 1975; Denis Donini and Campanella, 1977; Campanella and Gabbiani, 1980). Although the egg surface outside the dimple is not destined to react with spermatozoa it has been shown that pricking in these regions with a tungsten needle will lead to artificial activation (Talevi *et al.*, 1983). It would be of interest, therefore, to study prick activation and, in particular, how an activating signal is transmitted to other parts of the egg. Taken together, these facts favor the *Discoglossus* egg as a model system for the study of the ionic mechanisms regulating egg activation. This preliminary report, the first of a series on the physiology of egg activation in *Discoglossus*, describes voltage and resistance changes during fertilization and artificial activation. We have also correlated these electrical events with morphological events and our data suggests that the fertilization channels are located within the animal dimple.

MATERIALS AND METHODS

Adult *D. pictus* were captured near Palermo, Italy, during February and March. To induce ovulation, females were injected in the dorsal lymph sac with 250 IU human chorionic gonadotropin (Prophase, Serono) in amphibian Ringer containing (mM): NaCl 111.0, CaCl₂ 1.3, KCl 2.0, MgSO₄ 0.8, and Hepes 25.0 (final pH 7.8). Eggs were surgically removed 18 hr later from

¹ A preliminary report has been presented to the ABCD Congress, Siena, 21 October, 1984.

² Permanent address: Department of Evolutionary and Comparative Biology, Via Mezzocannone, 8, Naples, Italy.

the ovisac. Spermatozoa were obtained by puncturing the seminal vesicle of a male 24–48 hr after injection of 250 IU Prophase. Batches of eggs were controlled for viability by spreading undiluted semen over the eggs. Successful sperm–egg interaction is indicated by the regression of the animal dimple 6 min after insemination. Fertilization was carried out in 10% Ringer solution containing (mM): NaCl 11.1, KCl 0.2, CaCl₂ 0.13, MgSO₄ 0.08, Hepes 2.5 (final pH 7.8) using eggs with intact jelly layers. In contrast, for artificial activation the jelly layers, J₃, J₂, and the animal plug, were removed by a 5-min exposure to 5 mM dithiothreitol (DTT) in 100 mM NaCl and 5 mM Tris at pH 8.0 (see Denis Donini and Campanella, 1977). Following treatment with DTT the dimple is everted somewhat. Eggs were then washed several times in 10% Ringer and kept in full strength Ringer until use. For ion substitution experiments the following solutions were used: *Low Cl⁻ Ringer*: (mM)—Na₂SO₄ 11.1, K acetate 0.2, MgSO₄ 0.08, Ca(NO₃)₂ 0.13, CaCl₂ 1.3 mM, Hepes 2.5 final pH 7.8 *Na⁺-free Ringer* (mM): choline chloride 11.1, KCl 0.2, CaCl₂ 0.13, MgSO₄ 0.8, Hepes 2.5, final pH 7.8. *K⁺-free Ringer*: standard 10% Ringer minus KCl, pH 7.8. Two methods of activation were employed. The first was pricking DTT-treated eggs in 10% Ringer containing 1.3 mM CaCl₂ using a fine tungsten needle. (This CaCl₂ concentration is necessary for the activation of such partially dejellied eggs.) In several experiments eggs with intact jelly layers were pricked in 10% normal Ringer. The second was exposing eggs to 12 to 37 μM of the Ca²⁺ ionophore A23187 (Sigma St. Louis; 2 mM stock solution in dimethyl sulfoxide) in 10% Ringer.

For electrical measurements the eggs were placed on a glass petri dish containing 10% Ringer at 18°C. Microelectrodes filled with 3 M KCl, of 10–30 MΩ resistance, were used for intracellular recording. Membrane resistance was measured using a single electrode of 1–3 MΩ resistance both for recording voltage and passing current. The electrode impedance was compensated by a bridge circuit (WPI Instruments Conn.). Signals were recorded on an oscilloscope, and either stored on FM tape or on paper (Gould, Ohio). Impaled eggs were also fixed for transmission electron microscopy at various times following activation by the addition of 2.5% V/V glutaraldehyde in 0.2 M phosphate buffer (see Campanella, 1975 for details). The eggs were postfixed in 2% OsO₄ W/V in phosphate buffer, dehydrated in ethanol, and embedded in Epon 812. Sections were cut with an LKB Ultramicrotome, stained with uranyl acetate and lead citrate, and observed using a Siemens Elmiskop 1A electron microscope. For scanning electron microscopy, eggs fixed in a similar manner, were dehydrated in increasing ethanol concentrations and Freon 113. The samples were dried by the critical-

point method, coated with gold, and examined with an autoscan EDEC Siemens electron microscope.

RESULTS

1. Fertilization

Mature *Discoglossus* have a mean resting potential of -17.8 ± 2.8 mV ($N = 37$; 14 females) and an input resistance of 0.25 to 3 MΩ (egg diameter 1.4 to 2 mm). Within 15 to 40 sec of insemination the potential rapidly depolarized to reach a new stable level of $+19.5 \pm 6.8$ mV ($N = 25$; Fig. 1a). The potential remained at this plateau level for several minutes and then slowly hyperpolarized reaching its original resting potential after about 60 min. In 10 experiments we observed a small, 1–2 mV, step depolarization which preceded the larger fertilization potential by 5–7 sec. This preliminary step depolarization was accompanied by a 50% decay in input resistance (Fig. 1b). During the fertilization potential the input resistance decreased to 5–100 KΩ; remained at this level for 5–10 min and then gradually increased as the potential hyperpolarized. In eggs from most batches we observed a characteristic oscillation of the membrane potential, of 4–8 mV amplitude, which started about 20 sec after the initial rise of the fertilization potential and lasted for 40–120 sec (Fig. 1a). Oscillation of the fertilization potential appears to be related to the age of eggs since eggs from oscillation incompetent batches gave rise to this phenomenon following a period of 6–7 hr *in vitro*. Batches of eggs which did not give rise to oscillation of the fertilization potential did, however, develop normally.

In order to gain an insight into the ionic basis of the fertilization potential of *Discoglossus* eggs, we carried out some simple ion substitution experiments. Removal of K⁺ and Na⁺ had little effect ($N = 6$), except in the latter case where the fertilization potential was usually preceded by several abortive spikes similar to those observed in immature eggs (see Fig. 1d). The amplitude of the fertilization potential is Cl⁻ dependent. Increasing external Cl⁻ either by the addition of choline chloride (concentrations used: 2.2, 55, or 111 mM) to the low Cl⁻ Ringer solution, or by using 50–100% Ringer resulted in a reduced fertilization potential ($N = 6$). For example, in one experiment where we added 55 mM of choline chloride to the low Cl⁻ Ringer solution, the peak amplitude of the fertilization potential was -4 mV, whereas control eggs from the same batch in 10% Ringer gave rise to fertilization potentials of $+16$ mV amplitude. In contrast, in low Cl⁻ Ringer the fertilization potential overshoot zero by $+50$ to $+60$ mV (Fig. 1c).

Twice we obtained immature batches of eggs by precociously removing the eggs from the female 14–15 hr following hormone injection. Such eggs had similar

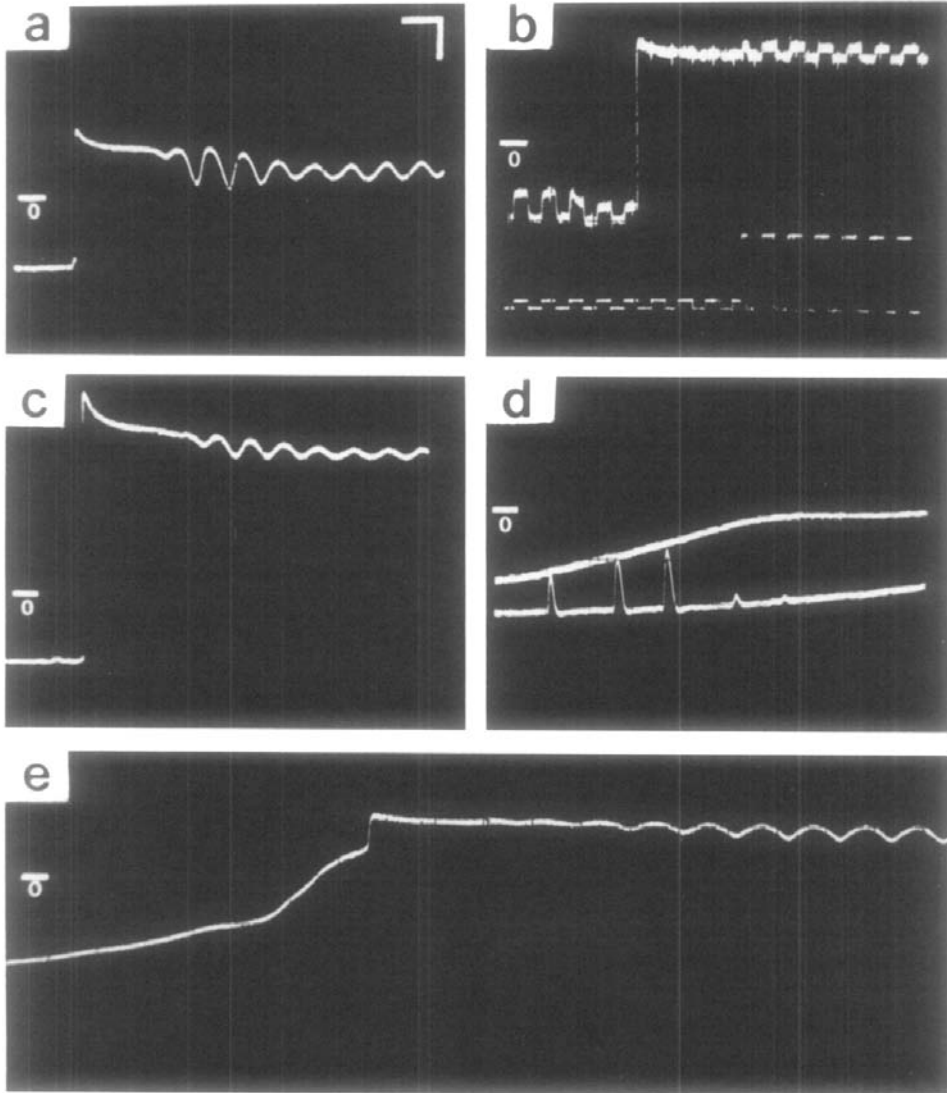


FIG. 1. Fertilization and activation potentials in eggs of *Discoglossus pictus*. (a) Control response in 10% Ringer (11 mM Cl^-). (b) Measurement of membrane resistance during the fertilization potential. Note the drop in resistance 7 sec before the depolarization and the large decay in resistance following the generation of the potential. The lower trace shows amount of injected current; 5×10^{-9} A, then 4×10^{-8} A. (c) Response in low Cl^- Ringer (2.2 mM Cl^-). (d) Response in an immature egg. The top trace is the continuation of the lower trace. (e) A typical activation potential in an egg pricked in the vegetal pole. Note the gradual depolarization. In all traces zero is indicated. Horizontal bar represents 5 sec; vertical bar represents 10 mV.

resting potentials to mature eggs, in the range of -15 to -25 mV, however, the response to insemination was different. Characteristically, we observed several spikes of 1 to 10 mV amplitude and 1-sec duration which

occurred approximately every 4 sec. Some 30–60 sec following insemination the egg depolarized slowly, at about 1 mV/sec, reaching a plateau level of $+10$ to $+15$ mV ($N = 5$; Fig. 1d).

2. Activation

Discoglossus eggs may be activated by pricking with or without jelly layers, however, it is not possible to observe surface changes in intact eggs. For this reason we removed the jelly layers J_3 , J_2 , and the animal plug by a brief exposure to DTT. Such treatment may alter the egg surface to some extent and in fact such partially dejellied eggs had significantly lower resting potentials (mean = -13.1 ± 4.6 mV, $N = 34$) than control eggs (mean = -17.8 ± 2.8 mV, $N = 37$). Nevertheless, DTT does not affect development, since fertilized eggs exposed for similar brief periods to DTT developed into normal embryos.

Pricking in the dimple induced an immediate activation potential, for all intents and purposes, similar to the fertilization potential ($N = 5$), although, always a few millivolts lower in plateau potential. For example, in one batch pricking gave rise to an activation potential of +11 mV, amplitude, whereas the control egg gave rise to a fertilization potential of +25 mV amplitude. The rise time of the potential was similar in the two cases. Pricking outside the dimple resulted in a different type of response. First, there was an immediate hyperpolarization of 2-4 mV accompanied by a decrease in input resistance to less than 1 K Ω (we were not able to measure lower levels owing to the characteristics of our equipment). This was followed by a gradual depolarization and a concomitant increase in resistance (presumably due to sealing of the damage) which terminated in a small activation potential (Fig. 1e; $N = 25$). There was much variation in the absolute value of the plateau of the activation potential, which ranged from -8 to +25 mV; however, in all cases this was significantly lower than that of the fertilization potential. The potential also oscillated, as in the case of

fertilization, however, these oscillations often started concomitantly with the generation of the activation potential. This is in contrast to the fertilization potential where there was always a 20-sec delay before the onset of oscillation (see Fig. 1a). We also noted a correlation between the site of pricking and the delay in generation of the activation potential; the farther away from the dimple, the longer the delay (4 batches; 12 eggs). There was considerable variation between batches, however, within each batch there was always a positive correlation between the delay period and the distance from the prick site to the dimple. For example, an egg from one batch pricked in the dimple generated an activation potential immediately, compared to 1 min 25 sec for an egg pricked in the animal hemisphere, and to 5 min when pricked in the equator. The longest delay occurred when an egg was pricked at the vegetal hemisphere when it took 7 min for the generation of the potential. Corresponding times for a second batch were 0 sec (dimple); 2 min 45 sec (animal hemisphere); 3 min 28 sec (equator); and 4 min (vegetal hemisphere).

Pricking results in extensive but localized damage to the egg surface. Shortly after puncture in the dimple a wave of contraction can be seen to spread slowly over the egg surface from the pricking site toward the antipode (Fig. 2). Pricking outside the dimple induces a contraction wave to travel from the site of puncture to the opposite antipode (Fig. 3). In all cases ($N = 25$) the activation potential was generated when this contraction wave reached the dimple which started regressing as a consequence. We also attempted to correlate the electrical events of activation with ultrastructural changes in the dimple by fixing eggs at various times during electrical recording. In the dimple

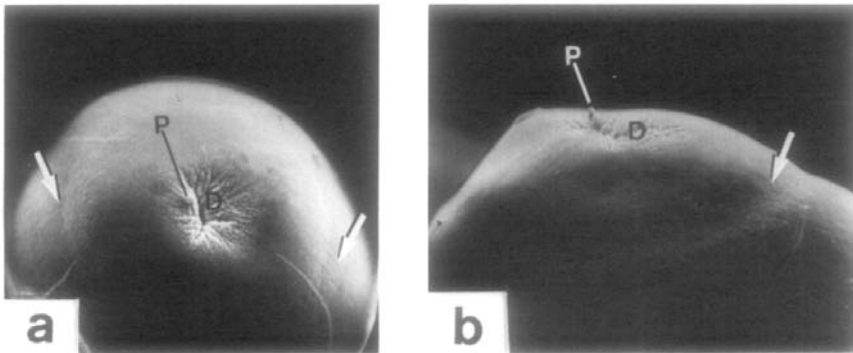


FIG. 2. Scanning electron micrographs of eggs pricked in the dimple (D). P = site of pricking. (a) Upper view of an egg fixed 2 min 30 sec after pricking. The arrows show the wave of cortical contraction which has spread from the site of pricking. $\times 61$. (b) Lateral view of an egg activated as in (a). One can observe that the front of the wave (arrow) has a different morphology from the rest of the egg surface. $\times 90$.

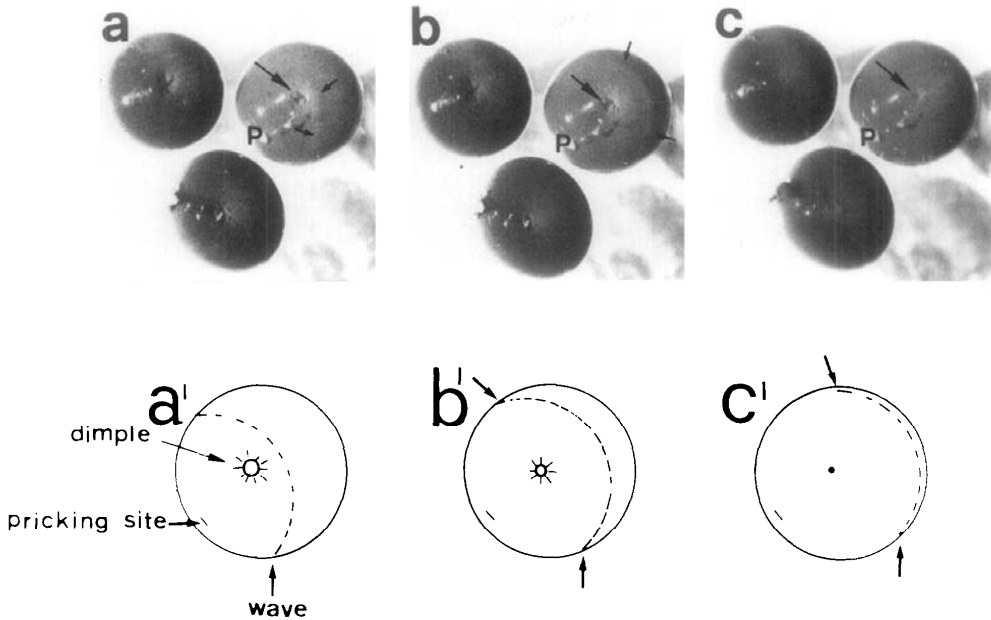


FIG. 3. The contraction wave and disappearance of the dimple. (a-c) Progressive stages of dimple (arrow) regression following the arrival of the contraction wave (small arrows). P = site of pricking. The wave is visible only on one of the three eggs shown which were all pricked at the equator. $\times 15$.

of unfertilized eggs there are regularly spaced microvilli each containing bundles of microfilaments. These bundles penetrate about $12 \mu\text{m}$ into the peripheral cytoplasm and among their roots there are cortical granules of $0.5 \mu\text{m}$ diameter and vacuoles of $0.3 \mu\text{m}$ diameter (Fig. 4; see also Campanella, 1975; Andreuccetti and Campanella, 1980; and Campanella *et al.*, in press). The density of all components is at a maximum at the geometrical center of the dimple and gradually decreases toward the lateral portions of the dimple (Campanella, 1975). Exocytosis of cortical granules in this egg manifests as a rapid disruption of the plasma membrane and opposing cortical granule membrane. At the site of disruption an electron-dense material can be seen and sometimes small vesicles. Such vesicles are hybrids derived from the fusion of the opposing plasma and cortical granule membranes (Campanella *et al.*, in press). The first signs of exocytosis of vacuoles or cortical granules were observed in eggs fixed approximately 15–20 sec after the generation of the activation potential, at the onset of the voltage oscillation. In eggs fixed from 1 min after the generation of the activation potential, toward the end of the oscillation period, the exocytotic process was more evident. Figure 4 shows initial stages of two cortical granules and one vacuole exocytosing in an egg fixed about 2 min after the generation of the activation

potential. The sites of membrane fusion are obscured by the presence of amorphous electron-dense material. Only in one of the granules (small arrow and inset) small vesicles can be seen next to the site where the cortical granule opens in the extracellular space (dimple content). The presence of vesicles within the dimple content (Fig. 4) is an additional sign that exocytosis has occurred.

Finally, activation of *Discoglossus* eggs using the Ca^{2+} ionophore A23187 was less efficient than pricking ($N = 7$). Dimple regression was slower and often incomplete. At lower concentrations of ionophore ($12 \mu\text{M}$) the membrane potential depolarized slowly and regularly reaching a maximum of +25 to +35 mV. The dimple regressed very slowly during this depolarization. At higher concentrations ($37 \mu\text{M}$) the depolarization was more rapid involving a decrease in input resistance and often resulting in a small activation potential. A23187 was also effective in Ca^{2+} -free medium causing similar electrical changes and dimple regression. Dimethyl sulfoxide had no effect at the concentrations used.

DISCUSSION

The egg of the amphibian *D. pictus* is highly polarized both with regard to the fine structure of its surface and to the site of sperm entry. Although an anuran,

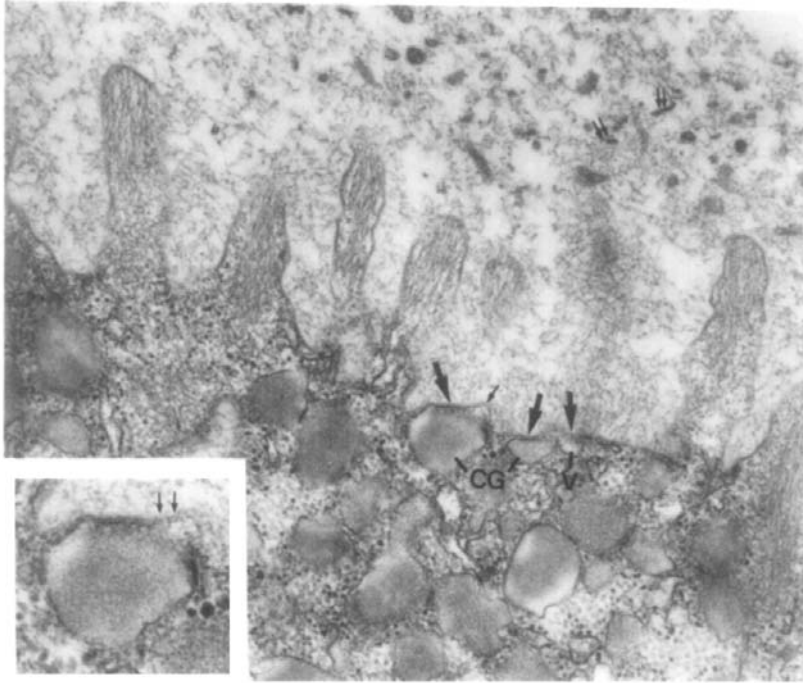


FIG. 4. Central portion of the dimple of an egg fixed 2 min 30 sec after the onset of the AP. Arrows = exocytosis of cortical granules (CG) and a vacuole (V). The sites of membrane fusion are obscured by the presence of amorphous electron-dense material. Only in one of the granules (small arrow and inset) small vesicles can be seen next to the site where the granule opens in the extracellular content. Externally, hybrid vesicles deriving from the fusion of plasma and cortical granule membranes are present (double small arrows). $\times 35,000$. Inset $\times 70,000$.

the egg of this species has characteristics pertaining to both urodele and anuran classes. For example, eggs of anurans have a layer of cortical granules around the cell periphery (Wischnitzer, 1966), whereas urodele eggs do not possess cortical granules (Wartenberg and Schmidt, 1961; Picherai, 1977). In *Discoglossus* there are few cortical granules arranged in columns directly in the animal dimple (Campanella, 1975). There are many differences in the mechanism of fertilization of urodeles and anurans, and recently this has been extended to include their electrical response to fertilization. Charbonneau *et al.* (1983a) have shown that whereas anuran eggs give rise to a rapid depolarization shortly after insemination, urodele eggs do not. In the present study we have shown that, despite its unusual structure, the egg of *Discoglossus* gives rise to a typical anuran fertilization potential (for comparison see Maeno, 1959; Ito, 1972; Cross and Elinson, 1980; Grey *et al.*, 1982; Schlichter and Elinson, 1981; Charbonneau *et al.*, 1983a; Charbonneau and Grey, 1984; Iwao *et al.*, 1981; Webb and Nuccitelli, 1981). This consists of a rapid depolarization accompanied by a decrease in

membrane resistance which is probably the result of the activation of ion channels specific for Cl^- .

The fertilization potential in *Discoglossus* is preceded, by several seconds, by a smaller step depolarization of 1–2 mV. A similar preliminary electrical event has been observed in sea urchins (Dale *et al.*, 1978), ascidians (Dale, 1983; Dale *et al.*, 1983) and an increase in voltage noise noted 10–40 sec before the fertilization potential in *Rana temporaria* (Charbonneau *et al.*, 1983b). The origin of this preliminary event is unknown, however, there is evidence to suggest that it is the result of sperm-egg fusion (Dale and Santella, 1985). Cytoplasmically immature eggs of *Discoglossus*, upon insemination, give rise to small spikes of short duration, at a frequency of one every 5 sec, which probably indicate the interaction of several spermatozoa. A similar phenomenon was observed in meiotically immature oocytes of *Rana pipiens*, where in fact each spike was correlated with a sperm entry (Schlichter and Elinson, 1981). At present we have no evidence in *Discoglossus* that each spike is correlated with a sperm entry, however, experiments in progress should elucidate this problem.

We have shown that *Discoglossus* eggs may be activated by pricking in regions of the egg surface which are not destined to interact with spermatozoa. Furthermore, activation by pricking has allowed us to dissect out various component events of fertilization. Pricking induces a contraction wave to spread over the egg surface, which, on arrival at the animal dimple coincides temporally with the generation of an activation potential, not dissimilar to the fertilization potential. This raises several important questions. First, it is generally accepted that in most eggs, the spermatozoon induces a transient release of intracellular Ca^{2+} that starts at the site of sperm entry and spreads around the egg cortex in a wave-like fashion (Jaffe, 1983). It is possible that the contraction wave observed in *Discoglossus* is the consequence of a propagating Ca^{2+} wave, since there is much evidence to indicate that cellular cytoskeletal systems, particularly actinomyosin are regulated by levels of intracellular Ca^{2+} (Schroeder and Strickland, 1974; Elinson, 1975; Christensen *et al.*, 1984) and it is known that this egg possesses a contractile actinomyosin system (Campanella and Gabbiani, 1980). Cortical waves have been described by several authors in amphibian eggs (Hara and Tydeman, 1979; Elinson, 1980; Stewart-Savage and Grey, 1982; Iwao, 1982; Kline and Nuccitelli, 1983; Takeichi and Kubota, 1984). We do not know how this wave of intracellular Ca^{2+} release is initiated by pricking, nor how it is propagated, however, it is noted that high levels of external Ca^{2+} are required (see also Wolf, 1974). In the *Xenopus* eggs an extensive cortical endoplasmic reticulum found all around the egg periphery may be a site of Ca^{2+} storage (Campanella and Andreuccetti, 1977; Grey and Gardiner, 1983; Andreuccetti *et al.*, 1984; Campanella *et al.*, 1984; Charbonneau and Grey, 1984). In *Discoglossus* the endoplasmic reticulum is more abundant in the dimple than the rest of the egg (Campanella *et al.*, in press) which does not preclude it as a site of Ca^{2+} storage, however, there may be an alternative site. Independently of this, it would be interesting to study the ultrastructure at the site of pricking in *Discoglossus* and also in the cortex during the progression of the contraction wave. When eggs are pricked directly in the dimple a contraction wave passes from the animal to the vegetal pole (see Fig. 2). Preliminary experiments with ion-selective microelectrodes show that there is a transient increase in intracellular Ca^{2+} during fertilization in *Discoglossus* (W. B. Busa, R. Nuccitelli, and C. Campanella, preliminary results) and therefore it is possible that at fertilization the spermatozoon induces a wave of Ca^{2+} release to propagate from animal to vegetal poles. Since in *Discoglossus* the cortical granules are found only in the dimple then this Ca^{2+} wave and/or parallel propagative events may serve to trigger other events such as the metabolic activation of the rest of the egg.

Second, as the activation potential is generated when the contraction wave reaches the dimple it is likely that the channels are localized within this structure and are probably activated by Ca^{2+} . Cross (1981) has shown that iontophoretic injection of Ca^{2+} into *R. pipiens* eggs will induce a Cl^- -dependent depolarization of the membrane that is slower when the Ca^{2+} is injected in the vegetal pole than in the animal pole. The author suggested that one possibility for this difference is that the animal half contains a greater density of Cl^- channels (Cross, 1981).

It has been shown that the cytoplasmic components of the dimple are arranged in a density gradient, being aggregated in the center and sparser toward the lateral portions (Campanella *et al.*, in press). This raises the possibility that the Cl^- channels may also be distributed in the dimple in such a manner and a systematic study using the patch clamp and vibrating probe techniques should answer this question.

The ion channels activated at fertilization probably preexist in the egg in an inactive state and are not inserted by a process of membrane fusion. This is supported by our observations that there are no obvious structural changes in the dimple plasma membrane until several seconds after the generation of the activation potential when exocytosis of vacuoles and cortical granules were observed (see also Campanella *et al.*, in press). This also agrees with the experiments of Jaffe and Schlichter (1985) who show, using capacitance measurements as an indication of cortical exocytosis, that the conductance increase during fertilization in *R. pipiens* precedes the capacitance increase by several seconds. Exocytosis does, however, correspond temporally with characteristic oscillations of the membrane potential and therefore these two events may be linked. Oscillation of the membrane potential following activation has been observed in other amphibian eggs (Cross and Elinson, 1980; Charbonneau *et al.*, 1983a) and in ascidian eggs (Dale *et al.*, 1983), however, its role, if any, is unknown. Finally, it is tempting to speculate as to why the fertilization channels are localized to the sperm entry site. One possibility is that localized changes in the ionic constitution of the dimple region prepare the cytoplasm for later events such as sperm entry, decondensation of the sperm nucleus, and migration of the pronuclei.

Part of this work was carried out in the "Centro di Microscopia Elettronica," Faculty of Science, University of Naples. We thank the staff of this center for assistance, G. Princivalli for typing, and Carlo Tommasino for assistance. This work was supported partially by MPI grants to G. Ghiara and C. Campanella.

REFERENCES

- ANDREUCCETTI, P., and CAMPANELLA, C. (1980). Origin and cytochemistry of the animal dimple granules in *Discoglossus pictus* (Anura) egg. *J. Embryol. Exp. Morphol.* 56, 239-252.

- ANDREUCCETTI, P., DENIS-DONINI, S., BURRINI, A. G., and CAMPANELLA, C. (1984). Calcium ultrastructural localization in *Xenopus laevis* eggs following activation by pricking or by calcium ionophore A23187. *J. Exp. Zool.* **229**, 295-308.
- BOYNTON, A. L., MCKEEHAN, W. L., and WHITFIELD, J. W. (1982). "Ions, Cell Proliferation and Cancer." Academic Press, New York.
- CAMPANELLA, C. (1975). The site of spermatozoon entrance in the unfertilized egg of *Discoglossus pictus* (Anura): An electron microscope study. *Biol. Reprod.* **12**, 439-447.
- CAMPANELLA, C., and ANDREUCCETTI, P. (1977). Ultrastructural observations on cortical endoplasmic reticulum and on residual cortical granules in the egg of *Xenopus laevis*. *Dev. Biol.* **56**, 1-10.
- CAMPANELLA, C., ANDREUCCETTI, P., TADDEI, C., and TALEVI, R. (1984). The modifications of cortical endoplasmic reticulum during *in vitro* maturation of *Xenopus laevis* oocytes and its involvement in cortical granule exocytosis. *J. Exp. Zool.* **229**, 283-293.
- CAMPANELLA, C., and GABBIANI, G. (1980). Cytoskeletal and contractile proteins in coelomic oocytes, unfertilized and fertilized eggs of *Discoglossus pictus* (Anura). *Gamete Res.* **3**, 99-114.
- CAMPANELLA, C., TALEVI, R., ATRIPALDI, U., and QUAGLIA, L. (in press). The cortical endoplasmic reticulum and its possible role in activation of *Discoglossus pictus* (Anura) eggs. In "Molecular and Cellular Biology of Fertilization" (J. L. Hedrick, ed.). Plenum Press, New York.
- CHARBONNEAU, M., and GREY, R. D. (1984). The onset of activation responsiveness during maturation coincides with the formation of the cortical endoplasmic reticulum in oocytes of *Xenopus laevis*. *Dev. Biol.* **102**, 90-97.
- CHARBONNEAU, M., MOREAU, M., PICHÉRAL, B., and GUERRIER, P. (1983a). Fertilization of amphibian eggs: A comparison of electrical responses between anurans and urodeles. *Dev. Biol.* **98**, 304-318.
- CHARBONNEAU, M., MOREAU, M., PICHÉRAL, B., GUERRIER, P., and VILAIN, J. P. (1983b). Voltage noise changes during monospermic and polyspermic fertilization of mature eggs of the anuran *Rana temporaria*. *Dev. Growth Differ.* **25**(5), 485-494.
- CRISTENSEN, K., SAUTERER, R., and MERRIAM, R. (1984). Role of soluble myosin in cortical contractions of *Xenopus* eggs. *Nature (London)* **310**, 150-151.
- CROSS, N. L. (1981). Initiation of the activation potential by an increase in intracellular calcium in eggs of the frog *Rana pipiens*. *Dev. Biol.* **85**, 380-384.
- CROSS, N. L., and ELINSON, R. P. (1980). A fast block to polyspermy in frogs mediated by changes in the membrane potential. *Dev. Biol.* **75**, 187-198.
- DALE, B. (1983). "Fertilization in Animals" (E. Arnold, ed.), The Institute of Biology's Studies in Biology No. 157, London.
- DALE, B., and DE FELICE, L. J. (1984). Sperm activated channels in ascidian oocytes. *Dev. Biol.* **101**, 235-239.
- DALE, B., DE FELICE, L. J., and TAGLIETTI, V. (1978). Membrane noise and conductance increase during simple spermatozoon-egg interactions. *Nature (London)* **275**, 217-219.
- DALE, B., DE SANTIS, A., and ORTOLANI, G. (1983). Electrical response to fertilization in ascidian oocytes. *Dev. Biol.* **99**, 188-193.
- DALE, B., and SANTELLA, L. (1985). Sperm-oocyte interaction in the sea urchin. *J. Cell Sci.*, in press.
- DENIS-DONINI, S., and CAMPANELLA, C. (1977). Ultrastructural and lectin binding changes during the formation of the animal dimple in oocytes of *Discoglossus pictus* (Anura). *Dev. Biol.* **61**, 140-152.
- ELINSON, R. P. (1975). Site of sperm entry and a cortical contraction associated with egg activation in the frog *Rana pipiens*. *Dev. Biol.* **47**, 257-268.
- GARDINER, M. D., and GREY, R. D. (1983). Membrane junctions in *Xenopus* eggs: Their distribution suggests a role in calcium regulation. *J. Cell Biol.* **96**, 1159-1163.
- GOLDENBERG, M., and ELINSON, R. P. (1980). Animal/vegetal differences in cortical granules exocytosis during activation of the frog egg. *Dev. Growth Differ.* **22**, 345-356.
- GOULD-SOMERO, M. (1981). Localized gating of the egg Na channels by sperm. *Nature (London)* **291**, 254-256.
- GREY, R. D., BASTIANI, M. S., WENN, D. J., and SCHERTEL, E. R. (1982). An electrical block is required to prevent polyspermy in eggs fertilized by natural mating of *Xenopus laevis*. *Wilhelm Roux'Arch. Dev. Biol.* **186**, 91-94.
- HARA, K., and TYDEMAN, P. (1979). Cinematographic observation of an "activation wave" (AW) on the locally inseminated egg of *Xenopus laevis*. *Wilhelm Roux's Arch.* **186**, 91-94.
- HIBBARD, H. (1928). Contribution à l'étude de l'ovogenèse de la fécondation et de l'histogenèse chez *Discoglossus pictus* Otth. *Arch. Biol.* **32**, 251-326.
- ITO, S. (1972). Effects of media of different ionic composition on the activation potential of anuran egg cell. *Dev. Growth Differ.* **14**, 217-227.
- IWAQ, Y. (1982). Differential emergence of cortical granule breakdown and electrophysiological responses during meiotic maturation of *Toad* oocytes. *Dev. Growth Differ.* **24**(5), 467-477.
- IWAQ, Y., ITO, S., and KATAGIRI, C. (1981). Electrical properties of *Toad* oocytes during maturation and activation. *Dev. Growth Differ.* **23**(2), 89-100.
- JAFFE, L. F. (1983). Sources of calcium in egg activation: A review and hypothesis. *Dev. Biol.* **99**, 265-276.
- JAFFE, L. A., and SCHLICHTER, L. C. (1985). Fertilization induced ionic conductances in eggs of the frog, *Rana pipiens*. *J. Physiol.* **358**, 299-319.
- KLINE, D., and NUCCITELLI, R. (1984). Activation current and contraction waves in *Xenopus* eggs. West Coast Amphibian Develop. Conference, May 9-10, Fallen Leaf Lake.
- MAENO, T. (1959). Electrical characteristics and activation potential of *Bufo* eggs. *J. Gen. Physiol.* **43**, 139-157.
- PICHÉRAL, B. (1977). La fécondation chez le Triton Pleurodele II. La pénétration des spermatozoïdes et la réaction locale de l'oeuf. *J. Ultrastruct. Res.* **60**, 181-202.
- SCHLICHTER, L. C., and ELINSON, R. P. (1981). Electrical responses of immature and mature *Rana pipiens* oocytes to sperm and other activating stimuli. *Dev. Biol.* **83**, 33-41.
- SCHROEDER, T. E., and STRICKLAND, D. L. (1974). Ionophore A23187, calcium and contractility in frog eggs. *Exp. Cell Res.* **83**, 139-142.
- STEWART-SAVAGE, J., and GREY, R. D. (1982). The temporal and spatial relationships between cortical contraction, sperm trail formation, and pronuclear migration in fertilized *Xenopus* eggs. *Wilhelm Roux's Arch. Dev. Biol.* **191**, 241-245.
- TAKEICHI, T., and KUBOTA, H. Y. (1984). Structural basis of the activation wave in the egg of *Xenopus laevis*. *J. Embryol. Exp. Morphol.* **81**, 1-16.
- TALEVI, R., QUAGLIA, L., and CAMPANELLA, C. (1983). Rallentamento della risposta corticale nelle uova di *Discoglossus pictus* attivate mediante puntura al di fuori della fossetta. Atti A.B.C.D. pp. 96, 2-4 Maggio 1983, Bressanone.
- WARTENBERG, H., and SCHMIDT, W. (1961). Elektronen mikroskopische Untersuchungen der strukturellen Veränderungen im Rindenbereich des Amphibieneies im Ovar und nach der Befruchtung. *Z. Zellforsch. Mikrosk. Anat.* **54**, 118.
- WEBB, A., and NUCCITELLI, R. (1981). Direct measurement of intracellular pH changes in *Xenopus* eggs at fertilization and cleavage. *J. Cell Biol.* **91**, 562-567.
- WISCHNITZER, S. (1966). The ultrastructure of the cytoplasm of the developing Amphibian egg. In "Advances in Morphogenesis" (M. Abercrombie and J. Brachet, eds.), Vol. 5, pp. 131-179. Academic Press, New York.
- WOLF, D. P. (1974). The cortical response in *Xenopus laevis*. *Dev. Biol.* **40**, 102-115.

A Highly Localized Activation Current yet Widespread Intracellular Calcium Increase in the Egg of the Frog, *Discoglossus pictus*

RICHARD NUCCITELLI, DOUGLAS KLINE,¹ WILLIAM B. BUSA,² RICCARDO TALEVI,* AND CHIARA CAMPANELLA†

Department of Zoology, University of California, Davis, California 95616, *Department of Evolutionary and Comparative Biology, University of Naples, Naples, Italy 80134, and †Department of Biomedical Sciences and Technologies and of Biometry, University of L'Aquila, L'Aquila, Italy 67100

Accepted July 22, 1988

Sperm entry in the egg of the painted frog, *Discoglossus pictus*, occurs only at a specialized region of the animal hemisphere called the animal dimple, a structure not found in other species of frog. An extracellular vibrating electrode was used to measure the activation current to determine if the ion channels that open to generate the fertilization potential are localized in this region. Eggs that were activated by microinjecting inositol-1,4,5-trisphosphate (Ins(1,4,5)P₃) exhibited activation potentials very similar to those of fertilized eggs. There was a delay between the time of Ins(1,4,5)P₃ injection and the initiation of the activation potential that was proportional to the distance between the site of the activating stimulus and the animal dimple, similar to the delay previously observed in prick-activated eggs (R. Talevi, B. Dale, and C. Campanella (1985). *Dev. Biol.* 111, 316-323). The delay lasted 30 sec when the stimulus site was 20° (300 μm) from the animal dimple and 14 min when it was 150° from the dimple. Once the activation potential was initiated, there was an excellent temporal correlation between the time of depolarization and the time of the first detectable current entering the dimple region. This inward current was typically 60 μA/cm² in amplitude and was found only in the central 200 μm of the dimple region. The outward current was distributed over the remainder of the egg surface and was much smaller in amplitude. The activation current was carried by Cl⁻ efflux in the animal dimple region, and was reduced by DIDS and reversed by high external Cl⁻ or I⁻. The occurrence of inward current only at the dimple region indicates that Cl⁻ channels which open to produce the activation potential are localized there. Using Ca²⁺-specific microelectrodes, we found that [Ca²⁺]_i increased from 0.25 to 2 μM following both fertilization and activation and returned to the unactivated level after about 37 min. Immature oocytes of *D. pictus* were also studied with the vibrating probe and the inward current in these cells was much less localized than that in the activating egg. A steady transcellular current of up to 4 μA/cm² entered the entire animal hemisphere of the oocyte and exited the vegetal hemisphere. © 1988 Academic Press, Inc.

INTRODUCTION

The large egg (1.6 mm in diameter) of the painted frog, *Discoglossus pictus*, is particularly interesting for the study of egg activation because sperm entry is restricted to a relatively small indentation in the animal hemisphere called the animal dimple which is not found in other species of frog (Hibbard, 1928; Campanella, 1975). This functional polarization is also evident in the external jelly organization which is asymmetric due to the presence of a jelly plug located on the top of the dimple (see Figs. 1A and 1D) (Ghiara, 1960). The dimple has associated with it a specialized peripheral cytoplasm that is rich in endoplasmic reticulum and vacuoles (Campanella *et al.*, 1986). Activating the egg by pricking at the dimple elicits an immediate depolarization resembling the fertilization potential, whereas

pricking elsewhere on the surface results in a wave of cortical contraction that spreads across the surface from the prick site; an activation potential occurs only when the wave reaches the dimple region (Talevi *et al.*, 1985). Here we describe investigations of the egg of *D. pictus* with the extracellular vibrating probe and intracellular Ca²⁺-specific microelectrode. These data reveal that the activation potential is due to the opening of Cl⁻ channels that are localized in the animal dimple region. A increase in intracellular free Ca²⁺ occurs in the cytoplasm, but is not correlated with a ring-shaped wave of ionic current as found in other frog and fish eggs (Kline and Nuccitelli, 1985; Jaffe and Schlichter, 1985; Nuccitelli, 1987). A companion paper considers the relationship between the ionic events described here and the cortical changes that occur at activation (Campanella *et al.*, 1988).

MATERIALS AND METHODS

Fifty adult *Discoglossus pictus* were collected near Palermo, Italy during May of 1984 and, again, March of

¹ Present address: Physiology Department, University of Connecticut Health Center, Farmington, CT 06032.

² Present address: Biology Department, Johns Hopkins University, Baltimore, MD 21218.

TABLE 1
COMPOSITION OF SOLUTIONS USED

| Component | Ringers (mM) | 10% Ringers (mM) | 10% Na ⁺ 10% Ringers (mM) | 12% Cl ⁻ 10% Ringers (mM) | 5× Cl ⁻ 10% Ringers (mM) | 10× K ⁺ 10% Ringers (mM) |
|-----------------------------------|--------------|------------------|--------------------------------------|--------------------------------------|-------------------------------------|-------------------------------------|
| NaCl | 111 | 11.1 | — | — | — | 11.1 |
| KCl | 2 | 0.2 | 0.2 | — | — | 2 |
| CaCl ₂ | 1.3 | 0.13 | 1.4 | 0.7 | 0.7 | 0.13 |
| Ca(NO ₃) ₂ | — | — | — | 0.7 | 0.7 | — |
| MgSO ₄ | 0.8 | 0.08 | 0.08 | 0.08 | 0.08 | 0.08 |
| NaOH | 12 | 1.2 | 1.2 | 1.2 | 1.2 | 1.2 |
| Choline-Cl | — | — | 11.1 | — | 55 | — |
| Na-methanesulfonate | — | — | — | 11.1 | 11.1 | — |
| K-methanesulfonate | — | — | — | 0.2 | 0.2 | — |
| Hepes | 25 | 2.5 | 2.5 | 2.5 | 2.5 | 2.5 |

1985. To induce ovulation, females were injected in the dorsal lymph sac with 250 IU of human chorionic gonadotropin (Prophase, Serono) in amphibian Ringer solution adjusted to a pH of 7.8 (Table 1). Eggs were surgically removed 18 hr later from the ovisac. The data reported here are the results from the study of 131 eggs in 1984 and 179 eggs in 1985. Spermatozoa were obtained by puncturing the seminal vesicle of a male 24–48 hr after injection of 250 IU human chorionic gonadotropin. Fertilization was carried out in 10% Ringer solution (Table 1) using eggs with intact jelly layers (Figs. 1A and 1B). All of the artificial activations were carried out on eggs that were either partially or completely dejellied (Fig. 1C). The jelly layers, J₃ and J₂, and the animal plug were removed by a 5-min exposure to 5 mM dithiothreitol in 100 mM NaCl and 5 mM Tris at pH 8.0 (see Denis-Donini and Campanella, 1977). Eggs were then washed several times in 10% Ringers and kept in full strength Ringers until use. As a result of this treatment the dimple regresses slightly and becomes more superficial (Fig. 1C). To permit the extracellular electrode to be positioned even closer to the plasma membrane, the vitelline envelope (VE) and J₁ (the innermost jelly layer) were also removed with forceps for most of the experiments, resulting in a denuded egg with a dimple that is almost completely flattened. All experiments were conducted at a room temperature of 22–24°C.

Solutions. The solutions used in these experiments are listed in Table 1. Chloride was replaced by methanesulfonate when low Cl⁻ solutions were required, Na⁺ was replaced by choline, and K⁺ by Na⁺. All solutions were adjusted to pH 7.8 with NaOH.

Inositol-1,4,5-trisphosphate (Ins(1,4,5)P₃) iontophoresis. All iontophoresis electrodes were backfilled with 1 mM solutions of either Ins(1,4,5)P₃ (Sigma Chemical Co., St. Louis, MO) or fructose-1,6-bisphosphate, as specified. These solutions were adjusted to pH 7.8 using

0.1 mM Hepes buffer. Electrical connection with this filling solution was made via an Ag/AgCl wire. Negative current was injected between the iontophoresis

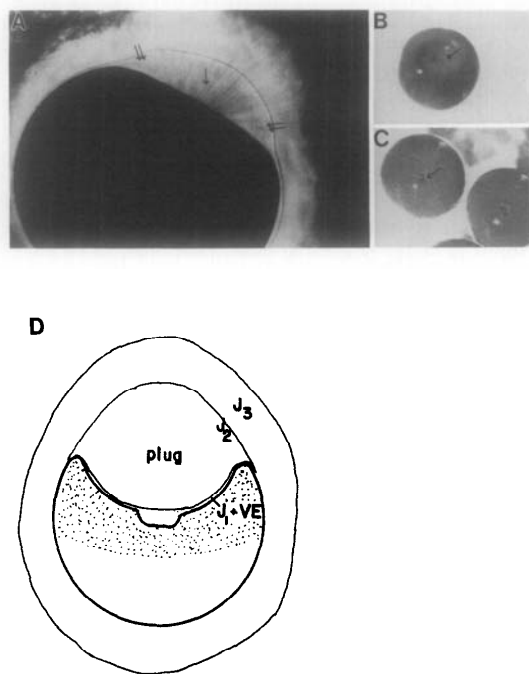


FIG. 1. (A) Oviposited egg of *D. pictus* (1.6 mm in diameter) covered with its jelly investments. Double arrows point to the animal plug; single arrow points to region where a high density of spermatozoa is evident. (magnification, ×40) (B) The animal dimple (arrow) which lies at the center of a large concavity and is seen through the thick animal plug. (X12) (C) Dimple (arrow) in partially dejellied egg surrounded only by its vitelline envelope and closely associated J₁ layer. (X12). (D) Drawing of the egg with the three jelly layers.

electrode and bath ground using the constant current injection circuit of a Biodyne AM-4 preamplifier (Santa Monica, CA), and current commands were supplied to the amplifier through a stimulus isolator by an Anapulse stimulator (Model 301, W-P Instruments, Inc., New Haven, CT). The injected current was monitored at the current monitor output of the amplifier using an oscilloscope. Insertion of the iontophoresis electrode was achieved with the aid of a custom-built piezoelectric advancer that rapidly advanced the electrode about 20 μm to achieve shallow impalements. A second electrode was used with the second channel of the AM-4 preamplifier to monitor membrane potential, and it was inserted into the egg by transiently increasing the negative capacitance on the preamplifier.

Calcium-sensitive microelectrodes. These were fabricated as described previously (Busa, 1986) using a liquid ion exchanger (Fluka Chemical, Hauppauge, NY). The tips were then briefly dipped twice into poly(vinyl chloride)-gelled Ca^{2+} sensor to provide mechanical stability during impalement. The electrodes were calibrated before and after impaling the egg in solutions of known Ca^{2+} concentrations using the buffer, EGTA, as described in detail previously (Busa, 1986).

Vibrating Probe Technique. The extracellular vibrating probe was used to measure steady electrical currents around the *Discoglossus* egg (Jaffe and Nuccitelli, 1974; Nuccitelli, 1986). The probe consists of a solder-filled electrode with a 30 μm platinum-black ball at its tip and a coaxial reference electrode 3 mm behind the tip. It is shown vibrating near the animal dimple of a partially dejellied egg in Fig. 2. Some of the experiments in 1985 used wire probes (Nuccitelli, 1986). The probe is made to vibrate in the horizontal plane by using a piezoelectric bender element to which is applied a sinusoidally varying voltage. The probe is connected

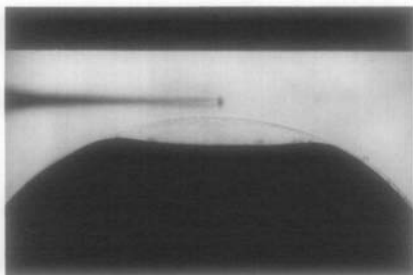


FIG. 2. Photomicrograph of the animal region of a dejellied *Discoglossus pictus* egg with the vibrating probe positioned above the animal dimple region. The vitelline envelope and closely associated J_1 layer (indistinguishable) were left on this egg but were removed for most of the experiments reported here. The ball at the end of the vibrating probe is 30 μm in diameter.

to a lock-in amplifier (Model 5204, Princeton Applied Research, Princeton, NJ). The lock-in amplifier is a voltmeter tuned to the vibration frequency and detects any voltage difference between the extremes of vibration. If there is a net flux of ions into or out of a cell, the movement will generate a local voltage gradient in the extracellular medium, and the probe can detect this gradient with a limiting sensitivity of about 10 nV.

This voltage gradient can then be converted into a current density by using Ohm's law, assuming that the electric field is nearly constant over the small distance of vibration (30 μm). The current density at the center of vibration, in the direction of vibration, is calculated by dividing the peak-to-peak voltage difference by the resistivity of the medium in which the probe is vibrated. One microampere per square centimeter corresponds to a net ion flux of about 10 pmol/cm²-sec, and we use the normal convention here that positive current indicates the flow of positive charge. Inward current indicating an influx of positive ions or an efflux of negative ions is always indicated by an upward deflection in the extracellular current recordings.

During experiments the unactivated egg was dejellied and usually denuded, and gently clamped beneath a loop of 250- μm -thick gold wire with its dimple and animal-vegetal axis in the horizontal, equatorial plane. The gold wire was in turn attached with epoxy to a glass coverslip that formed the bottom of the chamber. The vibrating probe was then positioned at the equator of the spherical egg, either at the dimple region or elsewhere around the circumference, vibrating with an amplitude of 30 μm (see Fig. 2). This resulted in an average distance of 45 μm between the plasma membrane and the center of probe vibration where the measurements were taken.

Electron microscopy. Some of the impaled eggs were also fixed for transmission electron microscopy at various times following activation by the addition of 2.5% (v/v) glutaraldehyde in 0.2 M phosphate buffer (see Campanella, 1975 for details). The eggs were postfixed in 2% OsO_4 (w/v) in phosphate buffer, hydrated in ethanol, and embedded in Epon 812. Sections were cut with an LKB Ultramicrotome, stained with uranyl acetate and lead citrate, and observed using a Philips 301 or 410 electron microscope.

RESULTS

Fertilization and Activation Potentials

We began by studying the electrophysiological changes that accompany natural fertilization in the egg of *D. pictus* (Fig. 1A), confirming the previous findings of Talevi *et al.* (1985). The initial phase of a typical fertilization potential is shown in Fig. 3A. The average

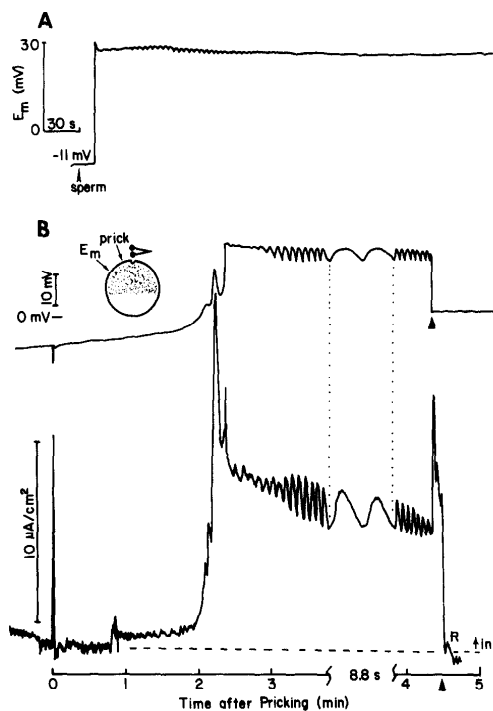


FIG. 3. Fertilization and activation potentials from eggs of *Discoglossus pictus*. (A) Fertilization potential recorded from *Discoglossus pictus* egg. Only the first 5.5 min is shown here, but the potential typically remains positive for 30 min and then slowly begins to recover. (B) Membrane potential (upper) and extracellular current (lower) at dimple in prick-activated *Discoglossus* egg in vitelline envelope and J₁ jelly layer. Activation occurred 2 min after pricking. During the 8.8-sec time interval between the dotted lines the chart recorder speed was increased. The microelectrode measuring membrane potential was removed from the cell shortly thereafter (at arrow on upper trace) and the probe was moved to a reference position (R) at the time marked by the arrow on the time scale. Note the good correlation between inward (upward) current oscillations and membrane depolarization oscillations. The amplitude of this record is smaller than that in most other figures because the probe was about 120 μ m from the egg's surface due to the presence of the vitelline envelope.

initial resting potential was -17 ± 1 (8) mV (SEM, *N*) and the membrane depolarized rapidly upon fertilization to an average peak value of 18 ± 3 (8) mV in 10% Ringers. The membrane potential remained positive for about 30 min before slowly returning to a negative potential and took an additional 30 min to return to the initial resting potential.

It was impossible to use the vibrating probe to detect the fertilization current in jellied eggs because the jelly coat prevented us from placing the probe close enough to the surface of the egg to detect the current. Removal

of the egg jelly layers allowed better probe positioning but we were unable to fertilize a dejellied egg. Consequently, all of the activation current data reported here are from artificially activated eggs, and most of these were denuded.

We activated the eggs by either pricking with a needle or by iontophoresing a small amount of $\text{Ins}(1,4,5)\text{P}_3$ into the egg. We chose this later method of activating eggs because it had been shown previously that $\text{Ins}(1,4,5)\text{P}_3$ activated sea urchin, frog, and fish eggs (Whitaker and Irvine, 1984; Busa *et al.*, 1985; Nuccitelli, 1987). This method has the further advantage that it avoids the large wound currents found at the prick site in prick-activated eggs. Eggs that were activated by pricking (Fig. 3B) or by the injection of $\text{Ins}(1,4,5)\text{P}_3$ (Fig. 4) exhibited activation potentials that were very similar to those of fertilized eggs (see also Talevi *et al.*, 1985). One clear difference between the two was that oscillations in membrane potential were more pronounced and began more rapidly in artificially activated eggs than in fertilized eggs just as Talevi *et al.*, (1985) found in prick-activated eggs.

The amount of $\text{Ins}(1,4,5)\text{P}_3$ required to activate these eggs varied greatly. As little as 3 nC of charge through a pipet filled with 1 mM $\text{Ins}(1,4,5)\text{P}_3$ activated the egg in some instances, but more often about 10 times this amount was required to activate. In contrast, when we iontophoresed fructose-1,6-bisphosphate, no egg activation occurred in the three eggs into which up to 2000 nC of charge was iontophoresed (1 mM of this sugar was in the pipet with 0.1 mM HEPES at pH 7.8). The third of these control eggs was subsequently activated by injecting 30 nC of $\text{Ins}(1,4,5)\text{P}_3$ to assure us that the eggs were indeed activatable.

There was always some delay between the time of either pricking or $\text{Ins}(1,4,5)\text{P}_3$ injection and the initiation of the activation potential when the activating electrode was outside of the dimple region. This delay was a function of the distance between the site of the activating stimulus and the animal dimple (Table 2), lasting about 30 sec when $\text{Ins}(1,4,5)\text{P}_3$ was injected 20° ($300 \mu\text{m}$) from the dimple and 14 min when the egg was activated 150° from the dimple. These delays are substantially longer than reported previously for the delay following prick activation (Talevi *et al.*, 1985).

Once the activation potential was initiated at the animal dimple, there was an excellent temporal correlation between the time of depolarization and the time of the first detectable current entering the dimple region (Figs. 3B and 4). Similarly, oscillations in the activation potential were accompanied by oscillations in the current with the same phase and periodicity. All of our data support the hypothesis that current passing through ion channels in the animal dimple was respon-

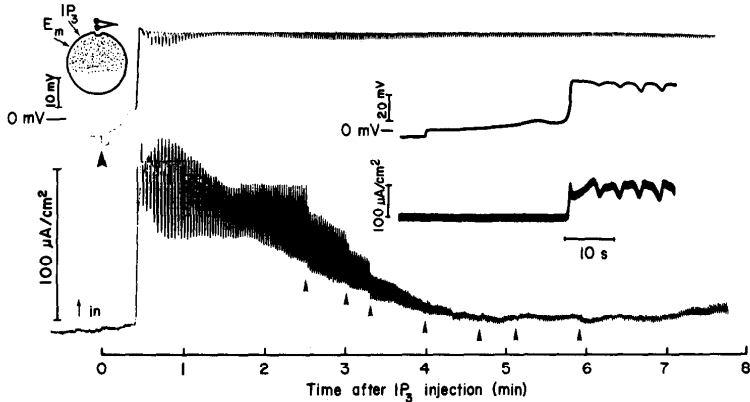


FIG. 4. Membrane potential (upper) and extracellular current (lower) at the dimple in a denuded *Discoglossus* egg that was activated by iontophoresing $\text{Ins}(1,4,5)\text{P}_3$ (6 nA for 6 sec, resulting in 36 nC) 300 μm from the dimple. The $\text{Ins}(1,4,5)\text{P}_3$ injection was begun at the time indicated by the arrow on the upper record. The position of the vibrating probe was adjusted at the times marked by the arrows on the lower trace in an effort to maintain a constant distance between the probe and the surface of the egg during egg shape changes that sometimes follow activation. A 10-msec time constant was used on the lock-in amplifier during this measurement. The insert in the right-center is a photograph of the oscilloscope screen showing the initial part of these two traces on a faster time scale.

sible for the depolarization at activation (Talevi *et al.*, 1985). The amplitude of the activation current varied considerably (Table 3), ranging from 20 to 260 $\mu\text{A}/\text{cm}^2$. The inward current was not uniform over the entire dimple region so we often had to make slight adjustments of the probe position to find the maximum current density. The smaller activation currents recorded from some eggs may have been the result of failing to position the probe over the site of maximum current density. There also appeared to be some variation among females. This spatial variation in the current could be due to uneven channel density, uneven surface topology, or contraction of the dimple at activation (Campanella *et al.*, 1986). The current at the center of the dimple remains inward for the duration of the activation potential, but its amplitude is largest during the first few minutes as seen in Fig. 4.

In order to determine just how localized these channels were, we also measured the extracellular current crossing other regions of the egg during activation. We found that the inward current region was very small, and in 10% Ringers we never recorded inward current anywhere on the egg's surface other than at the central disk of 200 μm across which is the dimple bottom and a very small portion of this large egg with a diameter of 1600 μm (Fig. 5, inset). Figure 5 presents one such study of two different eggs that were both activated at the equator. When the probe was positioned at the animal dimple in Fig. 5A, current was not detected until the sharp change in membrane potential, even though there was a very gradual depolarization prior to this sharp change. On another egg, the probe was positioned at the

equatorial region next to the $\text{Ins}(1,4,5)\text{P}_3$ injection electrode (Fig. 5B) and a small outward current was detected at about the same time as the sharp change in membrane potential, but no inward current was ever measured there. While a wave of cortical contraction was usually visible and could be seen spreading from the activation site towards the animal pole, no transmembrane current was correlated with it. The inward-outward current transition region was found to be sharply delineated by the original walls of the animal dimple. Thus, when the probe was positioned just beyond the 200 μm disk, outward current was detected at activation (Fig. 6), and, when moved over the dimple center, inward current was detected. The inward current region is highly localized, suggesting that the ion channels that generate the activation potential are all located in the animal dimple region.

The Intracellular Free Calcium Concentration Increases in the Egg following Activation

Intracellular free calcium was measured in a total of 11 eggs (7 jellied, 4 dejellied) activated with $\text{Ins}(1,4,5)\text{P}_3$

TABLE 2
 $\text{Ins}(1,4,5)\text{P}_3$ -ACTIVATION DELAY AS A FUNCTION OF POSITION ON EGG

| Position of iontophoresis electrode | Time to peak E_m |
|-------------------------------------|------------------------|
| 250–300 μm from dimple | 26 \pm 9 (6) sec |
| 45° from dimple | 5.3 \pm 3.1 (4) min |
| 90° from dimple | 8.9 \pm 2.4 (11) min |
| 150° from dimple | 14.4 \pm 1.6 (2) min |

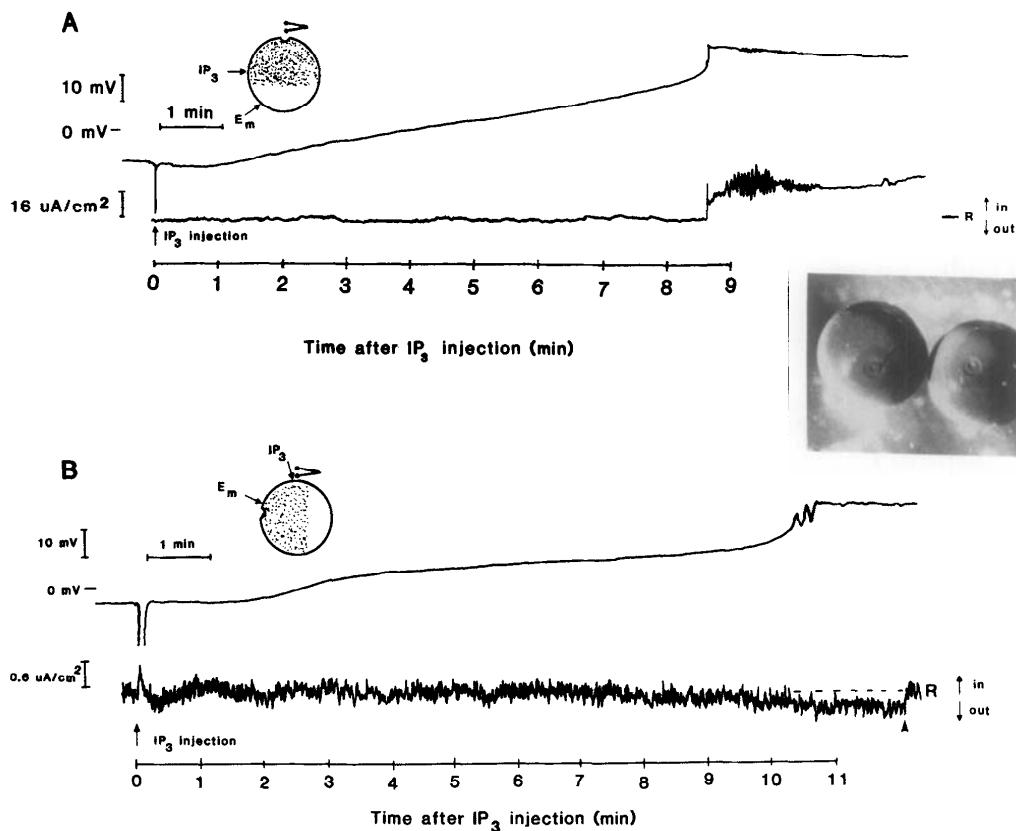


FIG. 5. Membrane potential (upper) and current record (lower) from two denuded *Discoglossus* eggs activated by iontophoresis at the equator of the egg. (A) Activation using 3 nC Ins(1,4,5)P₃ with the vibrating probe measuring current at the animal dimple. (B) Activation using 3 nC Ins(1,4,5)P₃ with the probe measuring current near the injection site at an increased sensitivity. At the arrow on the right, the probe was moved to a reference position far from the egg, indicating that a small component of outward current was present at the equator during activation, but no inward current was ever detected there. Photomicrograph inset: actual appearance of unfertilized, denuded eggs. The most central disc surrounding the animal pole (arrow) is the only region where inward current has been detected at activation. In the jellied egg, this corresponds to the central region at the bottom of the dimple ($\times 11$).

and in one that was fertilized. A Ca²⁺-sensitive microelectrode was inserted into the dimple region (8 eggs) or into the animal hemisphere outside of the dimple region (4 eggs). In the fertilized egg, the Ca²⁺ electrode was inserted about 100 μ m deep at the equator of the egg and sperm were added at the animal dimple (Fig. 7A). The [Ca²⁺]_i increased at the equator 4.5 min after the initiation of the fertilization potential. The rise time from the resting pCa of 6.4 (0.4 μ M) to the peak of 5.9 (1.3 μ M) was 2 min and the [Ca²⁺]_i recovered to the unfertilized level after 50 min. This 4.5-min delay between activation by the sperm at the animal pole and the increase in [Ca²⁺]_i at the equator suggests that the increase in [Ca²⁺]_i might spread slowly throughout the

egg. The absence of a recalibration of the Ca²⁺-sensitive electrode after it was removed from the fertilized egg in this particular record means that these data cannot be relied on quantitatively, but they are an accurate qualitative indication that a transient increase in the cytoplasmic free calcium level accompanies fertilization.

The remainder of the data come from eggs that were activated by Ins(1,4,5)P₃ injection. Figure 7B shows a typical result for an egg impaled with a Ca²⁺ electrode in the subcortical cytoplasm in the center of the animal dimple region and with the Ins(1,4,5)P₃ electrode just above the equator. Note that there is a 3.7-min delay between the initiation of the fertilization potential and the beginning of this increase in [Ca²⁺]_i in the subcorti-

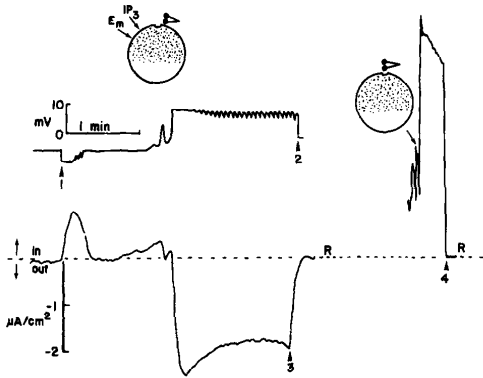


FIG. 6. Membrane potential (above) and current record (below) from a denuded *Discoglossus* egg activated by a second injection of $\text{Ins}(1,4,5)\text{P}_3$ (300 nC injected at arrow 1) (100 nC had been injected 3 min prior to this and failed to activate the egg). This large iontophoresis current was detectable by the vibrating probe as inward current on the lower trace. The probe was initially positioned at one side of the dimple region and detected outward current in that position upon activation. At arrow 2, the membrane potential electrode was removed from the cell, and at arrow 3 the probe was moved to a reference position and subsequently to the center of the animal dimple where inward current was detected. At arrow 4, the probe was again moved to a reference position far from the egg.

cal region. Since there is reason to believe that a $[\text{Ca}^{2+}]_i$ increase triggers the activation potential in frog eggs (Cross, 1981), this record implies that the $[\text{Ca}^{2+}]_i$ increase reached a section of the dimple region containing Cl^- channels before reaching the Ca^{2+} -sensitive microelectrode, suggesting that the concentration increase might spread as a wave through the cytoplasm. In nine eggs from five females, resting $[\text{Ca}^{2+}]_i$ before activation was $0.25 \mu\text{M}$ ($p\text{Ca } 6.6 \pm 0.1$). The mean peak $[\text{Ca}^{2+}]_i$ after activation was $2 \mu\text{M}$ ($p\text{Ca } 5.7 \pm 0.1$) and within a mean recovery time of 37 ± 4 (5) min the $[\text{Ca}^{2+}]_i$ had recovered to approximately the preactivation value. All of these measurements were made in the subcortical region of the animal hemisphere and seven of them were in the animal dimple region. No significant difference was detected between the absolute levels of the $[\text{Ca}^{2+}]_i$ increases in these two regions. Thus, the intracellular free Ca^{2+} concentration increases eightfold following activation and remains elevated for a much longer time than in other frog, sea urchin, or fish eggs (Busa and Nuccitelli, 1985; Eisen *et al.*, 1985; Ridgway *et al.*, 1977; Gilkey *et al.*, 1978).

The wave-like propagation hypothesis is also supported by the fact that the delay between the time of the activation stimulus (sperm or $\text{Ins}(1,4,5)\text{P}_3$) and the time that $[\text{Ca}^{2+}]_i$ increased in a particular region was pro-

portional to the distance between the activation site and the Ca^{2+} electrode. In two cases, the distance between the $\text{Ins}(1,4,5)\text{P}_3$ pipet and the Ca^{2+} electrode was carefully measured and the wave velocity was 2.2 and $2.7 \mu\text{m/s}$ for separations of 160 and $560 \mu\text{m}$, respectively. In these cases the delay between activation at the $\text{Ins}(1,4,5)\text{P}_3$ electrode and the increase in Ca^{2+} at the Ca^{2+} electrode was proportional to the distance between the two: 1.1 and 3.5 min, respectively. For comparison, the wave of cortical contraction exhibits a velocity of about $25 \mu\text{m/s}$ in the dimple region and $2 \mu\text{m/s}$ in the remainder of the animal hemisphere.

The rise time between the initiation of the increase in $[\text{Ca}^{2+}]_i$ and the peak $[\text{Ca}^{2+}]_i$ is somewhat dependent on location. With shallow impalements in the dimple region, the $[\text{Ca}^{2+}]_i$ increased more rapidly than it did outside this region or even in the "deeper" cytoplasm (greater than $100 \mu\text{m}$ deep) in the dimple region. The total rise time to the peak Ca^{2+} concentration was 60 ± 15 (3) sec with shallow impalement in the dimple, but took 174 sec in the one measurement using a deeper impalement there. This can be compared with the average rise time outside of the dimple region of 139 ± 11 (3) sec using a shallow impalement. Therefore, while there is no significant difference between the peak $[\text{Ca}^{2+}]_i$ increases in the cortical region below the dimple and that elsewhere in the animal hemisphere, the $[\text{Ca}^{2+}]_i$ reaches this peak level twice as fast in the dimple region.

Ionic Composition of the Current

Chloride. Eggs were activated in media with varying ion concentrations in order to determine which ions were carrying the inward current (Table 3). As found in other amphibian eggs, Cl^- efflux appears to carry most of this inward positive current. The maximum inward current over the central dimple region, $35 \mu\text{m}$ from the plasma membrane was first measured in control media composed of 10% Ringers for a group of eggs from a single female, and then other eggs from the same female were activated in a medium to which an anion channel blocker was added or in which the concentration of Cl^- was modified. The mean amplitude of the inward current decreased by 95% when the external $[\text{Cl}^-]$ was increased 5-fold. Moreover, the inhibitor of anion exchange and anion channels in frog eggs (Webb and Nuccitelli, 1985), DIDS, greatly reduced both the amplitude of the activation potential and the mean peak inward current in six of the seven eggs treated (Fig. 8). The mean amplitude of the inward current increased by 60% when the extracellular $[\text{Cl}^-]$ was reduced from 11.5 to 0.2 mM. Finally, the current and activation potential reversed direction when the external Cl^- was increased 10-fold (in 100% Ringers) or when 55 mM of the anion,

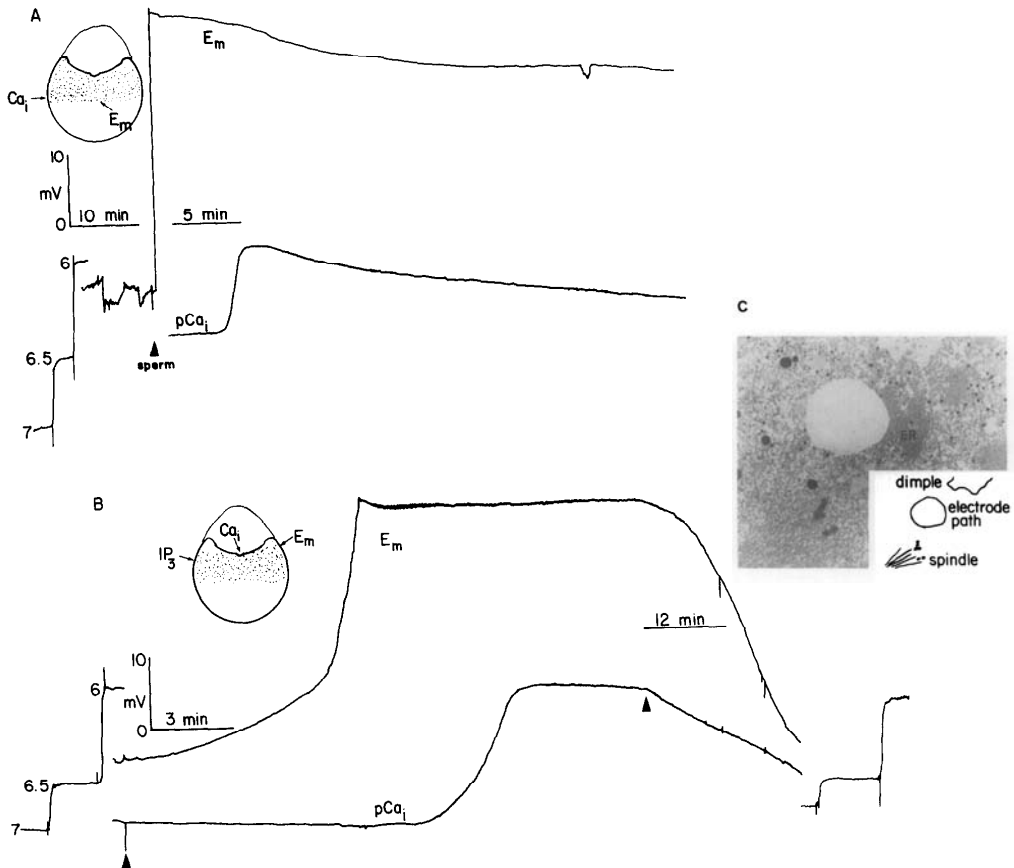


FIG. 7. Membrane potential (E_m) and intracellular free Ca^{2+} measured in *Discoglossus* eggs (not dejellied). Traces at the bottom left and right show Ca^{2+} electrode calibrations (pCa 7.0, 6.5, and 6.0) before and after egg impalement. (A) At the point indicated by the arrowhead, sperm was added and the chart speed was increased as indicated. The Ca^{2+} electrode was inserted about $100\ \mu m$ into the egg at the equator. (B) In this case, the Ca^{2+} electrode was inserted about $100\ \mu m$ into the egg at the animal dimple region. At the point indicated by the left arrowhead, $30\ nA$ of $Ins(1,4,5)P_3$ was injected for 3 sec. At the right arrowhead, the chart speed was decreased to give the new time bar as indicated. (C) Electron micrograph taken from another egg into which the Ca^{2+} electrode was inserted in about the same position as in (B). The path of the electrode is very near to both the dimple and the meiotic spindle. ER is endoplasmic reticulum ($\times 2070$).

I^- , was added to the external medium (Fig. 9). All of these data point to the involvement of an anion channel in the dimple current that allows Cl^- to leave the egg in this region at activation.

Sodium. There was no significant change in either the current density at the dimple or the mean peak activation potential when 90% of the extracellular Na^+ was replaced by the impermeant cation, choline. We therefore conclude that Na^+ is not carrying a significant amount of the current.

Potassium. The removal of external K^+ had no significant effect on the amplitude of the inward current, but significantly increased the peak of the activation po-

tential. This is a surprising result because the internal K^+ concentration is high in frog eggs and reductions in external concentrations should therefore hyperpolarize the membrane. If K^+ channels were opened upon activation, one would expect less depolarization rather than more as observed. Perhaps the reduction in external K^+ results in an increase in input resistance, leading to the increased potential. We did not routinely measure input resistance during these experiments, so we cannot be sure of this.

Increasing the external K^+ significantly increased the amplitude of the inward dimple current. Raising external $[K^+]$ should reduce the net K^+ efflux. If some of

TABLE 3
EXPERIMENTS TO DETERMINE THE IONIC COMPOSITION OF THE INWARD CURRENT

| Solution change ^a | Peak current in experimental solution | Control ^b | Peak act. pot. in exp. soln. | Peak act. pot. in control soln. |
|------------------------------|---|---|-------------------------------------|-------------------------------------|
| | $I_e, \mu\text{A}/\text{cm}^2 \pm \text{SEM} (N)$ | $I_e, \mu\text{A}/\text{cm}^2 \pm \text{SEM} (N)$ | $E_e, \text{mV} \pm \text{SEM} (N)$ | $E_e, \text{mV} \pm \text{SEM} (N)$ |
| 12% Cl^- | 106 \pm 9 (6) | 67 \pm 26 (2) | 47 \pm 1 (4) | 27 \pm 4 (3) |
| 5 \times Cl^- | 14 \pm 1 (2) | 259 \pm 79 (2) | -7 \pm 1 (3) | 14 \pm 4 (2) |
| 1 mM DIDS | 9.3 ^c \pm 6 (2) | 65 \pm 19 (2) | -10 \pm 1 (2) | 25 \pm 1 (2) |
| 100% Ringers | -71 \pm 21 (4) | 65 \pm 19 (2) | -20 \pm 1 (4) | 25 \pm 1 (2) |
| 55 mM NaI | -54 \pm 2 (2) | 74 \pm 21 (6) | -30 \pm 2 (2) | 31 \pm 2 (6) |
| K^+ -free | 70 \pm 13 (4) | 74 \pm 21 (6) | 42 \pm 1 (4) | 31 \pm 2 (6) |
| 10 \times K^+ | 168 \pm 17 (4) | 63 \pm 2 (4) | — | — |
| 10% Na^+ | 142 \pm 23 (3) | 123 \pm 5 (3) | 29 \pm 2 (5) | 29 \pm 2 (4) |

Note. Mean maximum inward current measured at the animal dimple 35 μm from the plasma membrane in 10% Ringers and in experimental solutions following activation by $\text{Ins}(1,4,5)\text{P}_3$ iontophoresis. Inward current is indicated by a positive sign, outward current by a negative sign.

^a Additions or changes to 10% Ringers, except 100% Ringers as indicated.

^b Maximum current in 10% Ringers for eggs of the same females used in the experimental solution.

^c Seven eggs from four females were studied and six showed a reduced current density of which these data are a representative sample. All the data could not be grouped together in this average because there was a substantial difference in the average current densities exhibited by the controls in the three groups.

this efflux occurs in the dimple region near the Cl^- channels, it would mask some of the Cl^- current and a reduction in the K^+ efflux should unmask a portion of the Cl^- current to give the measured increase in amplitude. Thus, this result would suggest that K^+ channels are present in the dimple region along with the Cl^- channels. An alternative explanation is that the K^+ channels at the outer rim of the dimple generate an outward current that is sufficiently large and close

enough to the inward current region that it contributes to the signal detected by the probe. This would reduce the measured inward current under normal conditions, and this reduction would be smaller if the outward current were smaller.

TMB-8 Effects

We ran out of eggs before studying the role of Ca^{2+} in the current, but were able to study the response to a compound that blocks intracellular calcium release in skeletal and smooth muscle, TMB-8 (8-diethylamino)-octyl 3,4,5-trimethoxybenzoate HCl (Chiou and Malagodi, 1975). TMB-8 also blocks Ca^{2+} release from an $\text{Ins}(1,4,5)\text{P}_3$ -sensitive calcium store obtained from sea urchin egg homogenates (Clapper and Lee, 1985). Although we have not shown directly that TMB-8 inhibits calcium release in the *Discoglossus* egg, this lipid-soluble substance dramatically changed the activation current and potential (Fig. 10) in the four eggs studied. Rather than depolarizing to a steady plateau, the activation potential was composed of a series of discrete spikes with a lower frequency than the normal oscillations. The dimple current similarly turned on and off in discrete episodes rather than being composed of a long, steady component. This effect was only observed after the eggs were exposed to 1 mM TMB-8 in 10% Ringers for at least 20 min. Thus, TMB-8 dramatically changed the pattern of ion channel opening in the dimple region. Moreover, this effect could be highly localized since the amplitude of the current measured at the probe position often did not correspond to the amplitude of the membrane potential change, indicating "hot spots" of current flow.

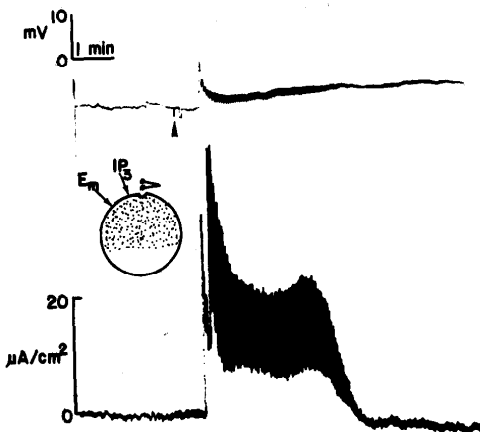


FIG. 8. Membrane potential (upper trace) and extracellular current at dimple (lower trace) in 10% Ringers plus 1 mM DIDS. The amplitudes of the activation potential and extracellular currents are greatly attenuated. At the time marked by the arrow in the upper trace, 10 nC of $\text{Ins}(1,4,5)\text{P}_3$ was injected, followed shortly by 30 nC more.

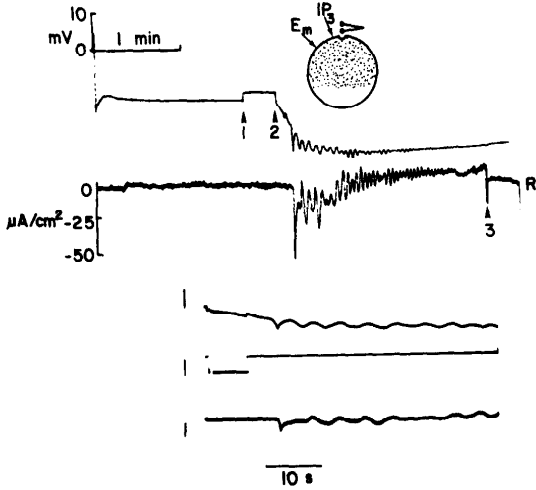


FIG. 9. Membrane potential (upper trace) and extracellular current at the center of the animal dimple (lower trace) in 55 mM NaI plus 10% Ringers. The Ins(1,4,5) P_3 -containing electrode was inserted into the egg at the time marked by arrow 1 and 6 nA of Ins(1,4,5) P_3 was injected for 6 sec at arrow 2. The activation potential reverses direction in this medium, hyperpolarizing rather than depolarizing. The dimple current also reverses direction, leaving the dimple. The probe was moved to a reference position at arrow 3. The egg had rotated slightly during activation so that the probe detected some of the inward current at the side of the dimple for about a minute prior to moving it to the reference position. Inserted on the bottom is the oscilloscope trace of the beginning of the same recordings on a faster time scale. The upper trace is the membrane potential (vertical bar on left is 15 mV with the top of the bar placed at 0 mV), the middle trace is the iontophoresis current (bar represents 6 nA), and the bottom trace is the current detected by the vibrating probe (bar indicates 50 $\mu\text{A}/\text{cm}^2$ and the top of the bar marks the reference position.)

Steady Currents Measured in Immature Oocytes

At the end of oogenesis, a disk-shaped germinative area (GA) is found at the center of the animal hemisphere in the oocytes of *D. pictus*. After germinal vesicle breakdown and first polar body extrusion, a profound remodeling of the GA occurs which leads to the differentiation of the dimple (Denis-Donini and Campanella, 1977). As found for *Xenopus* (Robinson, 1979), no steady currents could be detected around mature oocytes. However, we examined 13 immature oocytes and found an average current of about 4 ± 1 (10) $\mu\text{A}/\text{cm}^2$ entering their animal poles, 3 ± 1 (2) $\mu\text{A}/\text{cm}^2$ entering at 45° with no significant current crossing the equator. Current exited the vegetal pole (-4 ± 1 [6] $\mu\text{A}/\text{cm}^2$) at least as far as 135° (-1 ± 0.2 [3] $\mu\text{A}/\text{cm}^2$) (Fig. 11B). The main difference between this current pattern in the immature oocytes and that observed during activation of the mature egg (Fig. 11A) is the much broader region into

which current flows in the immature oocyte. This suggests that during maturation, the Cl^- channels must become localized to the dimple region. It is possible that they are inserted into the dimple through exocytosis (Denis-Donini and Campanella, 1977).

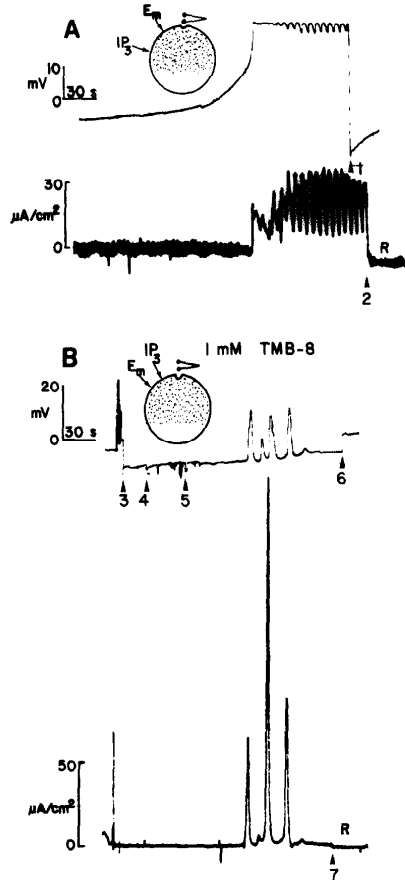


FIG. 10. Membrane potential (above) and current record (below) from two denuded *Discoglossus* eggs from the same female activated by Ins(1,4,5) P_3 iontophoresis. (A) Control in 10% Ringers solution. Ins(1,4,5) P_3 was iontophoresed 11 min prior to the segment of the record shown here (10 nC, 800 μm from dimple). At the time marked by arrow 1, the electrode was pulled out of the egg and, at arrow 2, the vibrating probe was moved to a reference position. (B) After approximately 1 hr in 1 mM TMB-8 in 10% Ringers, a microelectrode to measure membrane potential (arrow 3) and then a microelectrode to inject Ins(1,4,5) P_3 (arrow 4) were inserted into the egg, and it was activated by Ins(1,4,5) P_3 injection (40 nC about 400 μm away from the dimple) at the time marked by arrow 5. The membrane potential electrode was removed from the cell at the time marked by arrow 6. The lower trace indicates the current measured by the probe which was moved to a reference position at the time marked by the arrow 7.

DISCUSSION

New Findings

We have applied the extracellular vibrating probe and intracellular Ca^{2+} -specific microelectrode techniques to study activation in the egg of *D. pictus*. These studies have revealed several new findings: (1) Iontophoresing $\text{Ins}(1,4,5)\text{P}_3$ into the egg artificially activates the egg of *D. pictus*; (2) this triggers the activation potential after a delay that is proportional to the distance between the site of activation and the animal dimple as previously reported in prick-activated eggs (Talevi *et al.*, 1985); (3) the inward activation current is localized to the central portion of the animal dimple region (a 200- μm disc) and is carried by Cl^- efflux; outward currents are found over the remainder of the egg's surface; (4) activation is accompanied by an eightfold increase in $[\text{Ca}^{2+}]_i$ with a mean recovery time of 37 min, and the $[\text{Ca}^{2+}]_i$ increase appears to spread as a wave through the egg; (5) immature oocytes drive a steady current of 4 $\mu\text{A}/\text{cm}^2$ into their entire animal hemisphere and out of their vegetal hemisphere.

Ionic Components of the Activation Current

The changes in the activation current and activation potential when extracellular Cl^- is raised or lowered, or when DIDS or I^- is added to the external medium, all support a major role for Cl^- efflux in the activation current at the animal dimple. This Cl^- efflux has also been found to carry the activation current in several other amphibian eggs (Ito, 1972; Cross and Elinson, 1980; Schlichter and Elinson, 1981; Grey *et al.*, 1982; Charbonneau *et al.*, 1983; Jaffe and Schlichter, 1985; Webb and Nuccitelli, 1985). The only other common ions that might carry an inward current are Na^+ , Ca^{2+} , and Mg^{2+} . Since there was no significant change in the mean inward current amplitude when external Na^+ was decreased by 90%, it is unlikely that Na^+ is carrying much of this current. No experiments to test for the involvement of Ca^{2+} and Mg^{2+} fluxes were conducted.

The only other ion that was investigated was K^+ . K^+ is the only ion with a reversal potential that would allow it to carry outward positive current during activation, so it is very likely that K^+ is carrying the outward activation current. The increase in the inward activation current observed when external $[\text{K}^+]$ is increased to reduce net K^+ efflux suggests that K^+ channels are also present in the dimple region.

The Increase in Intracellular Free Ca^{2+}

The eightfold increase in intracellular free Ca^{2+} that follows activation was measured in several regions of the animal hemisphere and lasts longer than any previously reported increase in other activating eggs.

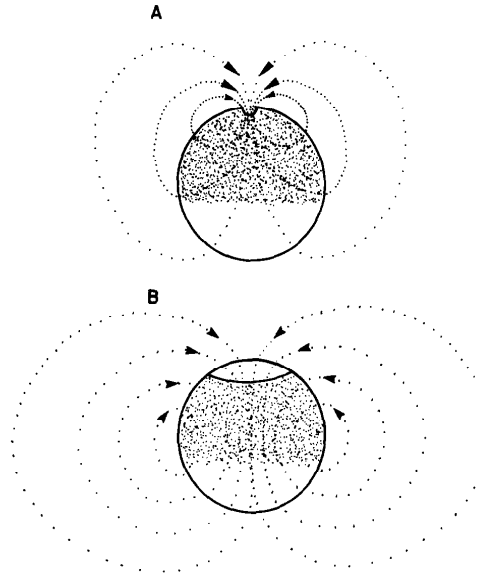


FIG. 11. Extracellular current patterns measured around activating eggs and immature oocytes of *Discoglossus pictus*. (A) Activation current pattern around a denuded egg. Current enters only the central portion of the original animal dimple region and no wave of current is detected. (B) Transcellular ionic current pattern around the immature oocyte.

These include the wave of increased intracellular free Ca^{2+} in the eggs of *Xenopus* (Busa and Nuccitelli, 1985; Kubota *et al.*, 1987), medaka (Ridgway *et al.*, 1977; Gilkey *et al.*, 1978), sea urchins (Eisen and Reynolds, 1984; Swann and Whitaker, 1986), starfish (Eisen *et al.*, 1984), and hamster (Miyazaki *et al.*, 1986). In at least the frog and fish eggs, these waves appear to precede vesicle fusion and may be an integral part of the fusion mechanism. In *D. pictus* the first exocytotic events occur in the dimple about 20 sec following the activation potential and continue over a long period. In the animal and vegetal hemispheres, exocytosis of granules and vacuoles lasts for at least 30 min. (Talevi *et al.*, 1985; Campanella *et al.*, 1986). Therefore, the period of high cytoplasmic free $[\text{Ca}^{2+}]_i$ matches the period of exocytosis quite well.

A second role for the increase in $[\text{Ca}^{2+}]_i$ may be to stimulate the activation potential. Evidence for calcium-activated ion conductance increases at fertilization has been obtained for the nemertean worm, *Cerebratulus* (Kline *et al.*, 1986) and the hamster (Igusa and Miyazaki, 1983, 1986). There is also good evidence in both *Rana* and *Xenopus* eggs that the Cl^- conductance increase at fertilization requires an increase in $[\text{Ca}^{2+}]_i$ (Cross, 1981; Kline, 1988). Furthermore, Cl^- conductances in the *Xenopus* oocyte are also activated by increases in $[\text{Ca}^{2+}]_i$ (Robinson, 1979; Dascal *et al.*, 1985;

Miledi, 1982; Barrish, 1983; Miledi and Parker, 1984; Young *et al.*, 1984). Therefore, the increase in $[Ca^{2+}]_i$ in *D. pictus* may also stimulate the increased Cl^- conductance reported here. The dramatic effect of TMB-8 on both the activation potential and the current also supports a role for Ca^{2+} in the control of Cl^- conductance. This compound reduces intracellular Ca^{2+} release in other cells and appears to greatly reduce the steady current entering the dimple region, turning the activation current into a series of discrete pulses. It also reduces the activation current in the *Xenopus* egg (Kline and Nuccitelli, 1985). However, TMB-8 may have other effects (see Brand and Felber, 1984), and we have not directly demonstrated that it disrupts Ca^{2+} release in *D. pictus*.

There is also an interesting correlation between the morphology of the egg and the rate of rise of the $[Ca^{2+}]_i$. The rate of rise in the dimple cortical region is faster than that elsewhere in the egg, suggesting that the cytoplasm beneath the dimple contains a greater concentration of Ca^{2+} stores. Electron microscopy reveals a higher density of cisternae and vesicles in this region than elsewhere in the egg, so it is likely that these organelles are storage sites for the Ca^{2+} (Andreuccetti and Campanella, 1985; Campanella *et al.*, 1988).

Activation Currents in Other Systems

Three other vertebrate systems have been investigated with either the extracellular vibrating probe or patch clamp techniques during fertilization, the eggs of both *Xenopus* and *Rana pipiens* and the egg of the medaka fish (Kline and Nuccitelli, 1985; Kline, 1986; Jaffe *et al.*, 1985; Nuccitelli, 1987). In all of these, the activation current was found to enter the activation site, but rather than remaining localized there, the current spread across the egg in a ring-shaped wave. Therefore, the egg of *D. pictus* is unique in this regard, and the Cl^- channels appear to be more highly localized than those in any of these other three vertebrates. This egg appears to be the only one studied thus far that exhibits such a striking localization of the channels responsible for the fertilization potential. The only other case in which the fertilization-gated channels appear to be localized is in the invertebrate, *Urechis caupo* (Gould-Somero, 1981).

Physiological Significance of the Activation Current

The two main consequences of the activation current are the accompanying changes in the membrane potential (fertilization potential) and the intracellular concentrations of the ions carrying the current. In many species, the fertilization potential provides a fast block to polyspermy (Jaffe and Cross, 1986); however, the egg of *D. pictus* appears to be polyspermic (Talevi, in prepara-

tion). What is the advantage of concentrating the Cl^- channels in the animal dimple region? If the activation potential played the role of signalling that fertilization has occurred (such as in the fast block to polyspermy), and if the activation of the Cl^- channels were chemically mediated (gated by a chemical messenger such as Ca^{2+}), it would make sense to concentrate them near the region of sperm-egg fusion and fastest $[Ca^{2+}]_i$ increase to minimize the time between sperm-egg fusion and the opening of these channels. However, in this polyspermic egg, it is not clear that the fertilization potential has a signalling function at all.

Other questions arise. How do the channels become localized to the animal dimple during maturation? What holds them in that region and prevents lateral diffusion? The cytoskeletal protein, spectrin, co-localizes in the dimple region and may be involved in anchoring membrane proteins including the chloride channels (Campanella and Gabbiani, 1988). Actin is also found in the dimple region both in the microvilli and in the cortex (Campanella and Gabbiani, 1980). We feel that this is an important area for further study.

This work was supported by grants from NSF (PCM 81-18174) and NIH (HD19966) to R. Nuccitelli and from MPI, 60% to C. Campanella and 40% to S. Filosa.

REFERENCES

- ANDREUCCETTI, P., and CAMPANELLA, C. (1985) Ca^{2+} -antimony deposits in *Discoglossus pictus* eggs during activation. *Cell Diff.* 16, abstr. No. 455.
- BARISH, M. E. (1983). A transient calcium-dependent chloride current in the immature *Xenopus* oocyte. *J. Physiol.* 342, 309-325.
- BRAND, M. D., and FELBER, S. M. (1984). The intracellular calcium antagonist TMB-8 [8-(N,N-diethylamino)octyl-3,4,5-trimethoxybenzoate] inhibits mitochondrial ATP production in rat thymocytes. *Biochem. J.* 224, 1027-1030.
- BUSA, W. B., and NUCCITELLI, R. (1985). An elevated free cytosolic Ca^{2+} wave follows fertilization in eggs of the frog, *Xenopus laevis*. *J. Cell Biol.* 100, 1325-1329.
- CAMPANELLA, C. (1975). The site of spermatozoon entrance in the unfertilized egg of *Discoglossus pictus* (Anura): An electron microscopy study. *Biol. Reprod.* 12, 439-447.
- CAMPANELLA, C., and GABBIANI, G. (1979). Motile properties and localization of contractile proteins in the spermatozoon of *Discoglossus pictus* (Anura). *Gamete Res.* 2, 163-175.
- CAMPANELLA, C., and GABBIANI, G. (1980). Cytoskeletal and contractile proteins in coelomic, unfertilized and fertilized eggs of *Discoglossus pictus* (Anura). *Gamete Res.* 3, 99-114.
- CAMPANELLA, C., CAROTENUTO, R., and GABBIANI, G. (1988). Anti-spectrin antibodies stain the nucleus and the site of *Discoglossus pictus* egg where anionic channels are segregated. *Dev. Biol.*, in review.
- CAMPANELLA, C., TALEVI, R., ATRIPALDI, U., and QUAGLIA, L. (1986). The cortical endoplasmic reticulum and its possible role in activation of *Discoglossus pictus* (Anura) egg. In "Molecular and Cellular Biology of Fertilization" (J. L. Hedrick, Ed.). Plenum, New York.
- CAMPANELLA, C., TALEVI, R., KLINE, D., and NUCCITELLI, R. (1988). The cortical reaction in the egg of *Discoglossus pictus*: A study of the changes in the endoplasmic reticulum at activation. *Dev. Biol.* 130, 108-119.

Fertilization in *Discoglossus pictus* (Anura)

I. Sperm-Egg Interactions in Distinct Regions of the Dimple and Occurrence of a Late Stage of Sperm Penetration¹

R. TALEVI AND C. CAMPANELLA¹

Dipartimento di Biologia Evolutiva e Comparata, Università di Napoli, Via Mezzocannone 8, Naples 80134, Italy

Accepted July 14, 1988

The heterogeneity of the egg surface with respect to receptivity to sperm was investigated in *Discoglossus pictus*; in this species fertilization occurs only in an indentation called the *dimple*, at the center of the animal hemisphere. Following insemination sperm are seen in the outermost jelly layers and in the lens-shaped jelly plug, converging to the dimple center, D1. A fertilization potential (FP) is recorded 30 sec following insemination. About 30 min after fertilization, when fertilization cones can be detected easily, immotile sperm are found at the center of the cone, where 10 min later they accomplish penetration. After 15 min the cone regresses and the second polar body is extruded. In eggs where the plug was experimentally displaced with respect to the dimple, spermatozoa contacted the sides of the dimple and simple protrusions formed but not cones. Spermatozoa do not elicit a normal FP in these regions but small step depolarizations which may be followed by a gradual rise to a positive plateau potential. Such eggs do not develop. In the protrusions, sperm may be only partially incorporated and the unpenetrated portion appears to degenerate. We conclude that at least two regions exist in the dimple: D1, where the FP is triggered, cones are formed, sperm penetration is fully accomplished and development is initiated; and D2 + D3 where the electrical response is not a normal FP, cones do not form, total sperm penetration does not occur, and development is not initiated. © 1988 Academic Press, Inc.

INTRODUCTION

Polarity in oocytes and eggs has been well documented and appears in general to be related to gradients of cytoplasmic organelles. Studies have been carried out to determine whether the plasma membrane is also regionalized in territories reflecting the internal cytoplasmic organization and/or correlated to specific functions of the egg at fertilization or during early development (Nuccitelli, 1978; Jaffe and Guerrier, 1981; Kline *et al.*, 1983; Dictus *et al.*, 1984; Nuccitelli and Wiley, 1985; Talevi and Dale, 1986; De Felice *et al.*, 1986). While the existence of membrane domains in the unfertilized eggs is still uncertain, this feature has been demonstrated in fertilized eggs with a variety of experimental approaches. Regionalization has been demonstrated in terms of differences of membrane fluidity which become extreme after fertilization (Dictus *et al.*, 1984 in *Xenopus laevis*) or of ionic channels distribution, as in the case of *X. laevis* cleavage (Kline *et al.*, 1983) and *Dentalium* where the polar lobe has electric characteristics different from the rest of the egg (Jaffe and Guerrier, 1981).

Fertilization offers an appropriate subject for determining the existence of specific domains of the egg

plasma membrane. The region where fertilization occurs, in some species, is restricted to one-half of the egg; this is best documented in anuran amphibians where sperm entry is restricted to the animal hemisphere (Newport, 1854; Elinson, 1975). In ascidians, sperm entry is reported to be restricted to the vegetal pole (Conklin, 1905), although this conclusion has recently been questioned (C. Sardet personal communication). Therefore the plasma membrane itself may be regionalized in territories according to its ability for successful sperm-egg interaction. In eggs with micropyles (i.e., insects and teleosts), or where sperm are guided to the egg by chemoattractants (i.e., hydroids, for a review see Miller, 1977), fertilization occurs in a much more restricted area of the egg. However, in such cases, the restriction for gamete interaction in the micropyle appears to depend upon the egg investments, while the specificity of the site in the plasma membrane where interaction occurs has been postulated (Freeman and Miller, 1982) but not yet proved. Furthermore fertilization channels in unfertilized ascidian eggs are not regionalized (Talevi and Dale 1986; DeFelice *et al.*, 1986), although the contrary may be true in Anellid eggs (Gould Somero, 1981). Other studies have lead authors to postulate the existence of "hot spots," i.e., sites on the membrane where specific and successful fusion between gamete occurs (see Dale and Monroy 1981).

¹ Present address: Dipartimento di Scienze e Tecnologie Biomediche e di Biometria, Università dell'Aquila, L'Aquila 67100, Italy

We have selected the egg of *D. pictus* to further study this problem, because spermatozoa converge and fuse at a restricted region of the egg, the animal dimple. The dimple membrane might have specific properties that allow the successful fusion with spermatozoa. The dimple is an indentation about 300 μm in diameter and 150 μm deep, located at the center of a large concavity at the animal hemisphere (Figs. 1a and b). It is filled with a fibrillar electron-dense material. The vitelline layer and innermost jelly coat (J1) cover the whole egg plasma membrane except in the region of the dimple where they span the depression (Campanella, 1975). The jelly coat investments reflect the polarization of the egg as they are thicker in correspondence with the dimple. Particularly, the lens-shaped jelly plug is exclusively found in the concavity. At insemination spermatozoa become embedded in the thick jelly coats which cover the dimple where they converge, most probably because of specific characteristics of the plug (Campanella 1975; Campanella and Gabbiani 1979).

The dimple has features not found elsewhere in the egg (Campanella, 1975; Denis-Donini and Campanella, 1977; Campanella *et al.*, 1986); however, the basis of the selectivity of this site with respect to spermatozoa interaction has not been determined. It remains to be ascertained whether the egg investments and particularly the plug, are responsible for restricting the site of

fertilization, or whether in the dimple, specific factors are segregated, which enable fusion and incorporation of spermatozoa.

We studied the possible functional regionality of the dimple through *in vivo* observations, electron microscopy, and electrophysiology. We have shown that, while the plug is able to convey spermatozoa to the dimple, the dimple itself is regionalized in two domains: one where spermatozoa induce a fertilization potential (FP), fertilization cones, and the onset of development, and another where spermatozoa induce small depolarizations, do not produce typical cones, and are not able to initiate development. In this study we also found that sperm heads, which start to penetrate the egg within the first min after insemination (Campanella, unpublished), are completely incorporated only 45 min following fertilization, after a period of apparent inactivity.

MATERIALS AND METHODS

Collection and Viability of Gametes

Adult *Discoglossus pictus* were collected near Palermo, during February and September, and kept in an aquarium at room temperature.

To induce ovulation, females were injected in the dorsal lymph sac with 250 IU of human chorionic gonadotropin (Prophase, Serono) in Amphibian Ringer

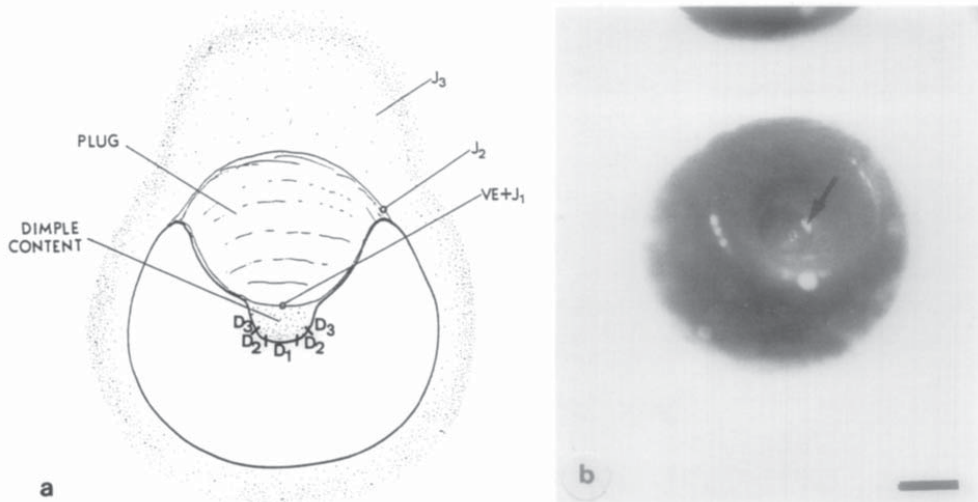


FIG. 1. Unfertilized egg of *Discoglossus pictus*. (a) Drawing of a longitudinal section. VE, vitelline envelope; J1, innermost jelly coat tightly connected to the VE. VE and J1 surround the whole egg and they span the depression. J2, Jelly coat surrounding the gelatinous plug. J3, anteriormost jelly coat. The plug sits in the animal concavity. All the jelly layers and particularly J3 are thicker in correspondence with the dimple. The dimple is filled with amorphous material. (b) Micrograph of an unfertilized egg. The arrow indicates the dimple. D1, deep portion of the dimple and site of physiological sperm-egg fusion; D2, adjacent region to D1 at the dimple wall; D3, uppermost portion of the dimple wall. Bar: 270 μm .

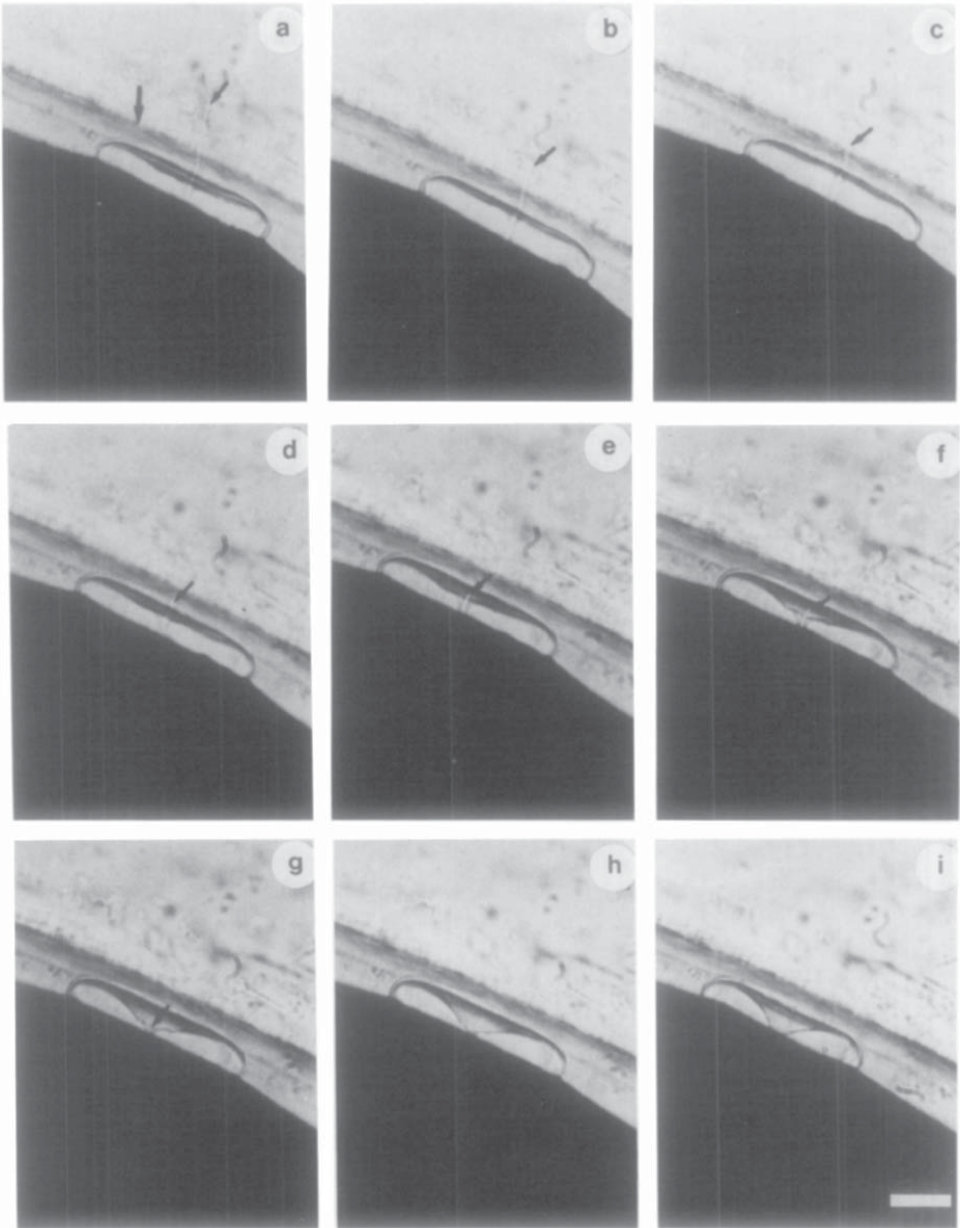


FIG. 2. Photographic sequence of the final stages of sperm incorporation occurring 40-45 min after insemination. (a) Spermatozoon (small arrow) in the cone. Arrow, fertilization envelope (FE) about $10\ \mu\text{m}$ apart from the cone (b-i). Spermatozoon penetrating the cone; its posteriormost region is labeled by a small arrow. In Fig. 2e the sperm has passed through the FE. In Figs (d-e), a weak invagination appears in the cone center and becomes more pronounced toward the end of incorporation (Figs. 2g-i). The process of incorporation takes about 5 min. Bar: $15\ \mu\text{m}$.

containing (mM): NaCl, 111.0; CaCl₂, 1.3; KCl, 2.0; MgSO₄, 0.8; and Hepes, 25.0; final pH 7.8. After 18 hr, the females were anesthetized with 0.1% MS222 and the eggs were removed from the ovisac and stored in a humid chamber at room temperature. The eggs are viable for 8–9 hr.

To obtain spermatozoa, 24–48 hr after the males were injected with 250 IU of HCG, seminal vesicles (Mann *et al.*, 1963) were punctured, and the semen was stored in a petri dish at room temperature, where they are viable for 7–8 hr.

Gametes were checked to verify their normal morphology and physiology. Batches of eggs which showed variabilities in dimension, in pigmentation, or in the distribution of jelly were discarded. Spermatozoa viability was verified by checking the motility upon dilution in 1/10 Ringer solution. The percentage of normal fertilization was then determined. The eggs were put in a petri dish and covered with 1/10 Ringer solution containing (mM): NaCl, 11.1; KCl, 0.2; CaCl₂, 0.13; MgSO₄, 0.08; Hepes, 2.5; pH 7.8. A drop of semen was added on the eggs. Successful sperm-egg interaction was indi-

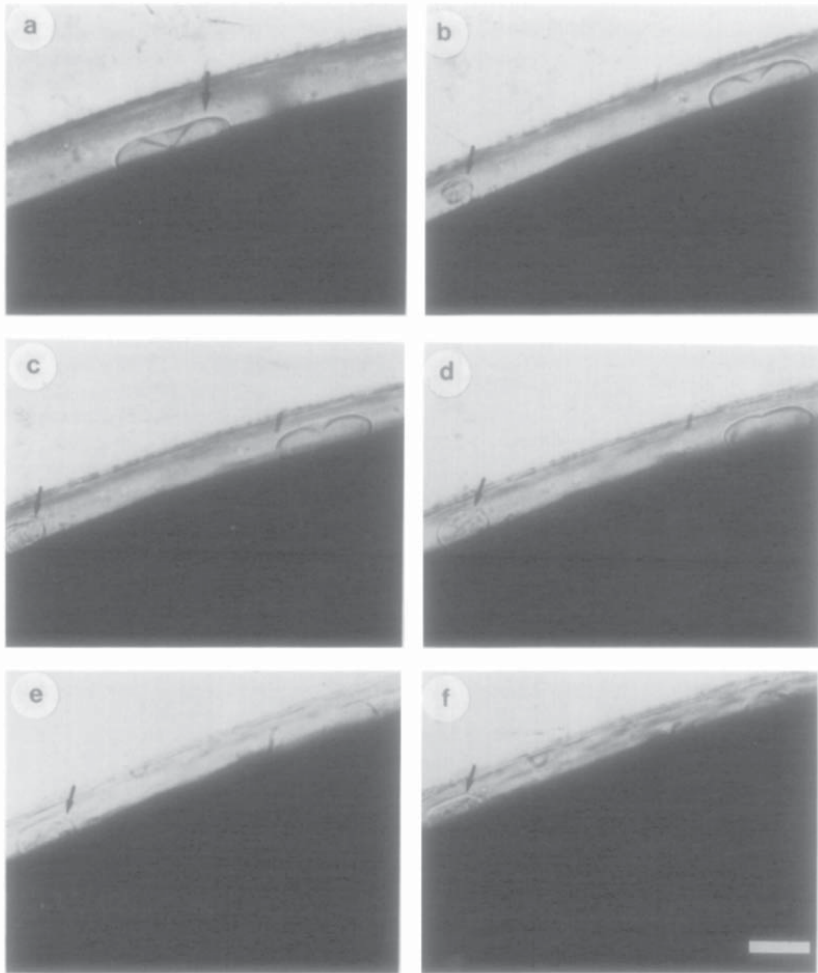


FIG. 3. Photographic sequence depicting the reabsorption of the fertilization cone. In (a) the cone with its funnel, typical of this stage, is seen (about 60 min from insemination). In (b) the second polar body has appeared at the egg surface (small arrow) while the funnel at the center of the cone starts regressing. (c-f) Final stages of cone reabsorption. The sequence takes about 15 min. Bar: 25 μ m.

cated by the regression of the animal concavity about 20 min after insemination.

Fertilized eggs were stored in 1/10 Ringer solution and checked after 3-4 hr to verify the occurrence of cleavage.

Jelly Shifting

In multilayered clusters of eggs stored in a humid chamber for a minimum of 4 hr, eggs of the bottom layer displayed a lateral shift of the jelly so that the dimple and the plug were no longer aligned. Displacement of the jelly occurred spontaneously, due to prolonged pressure of the eggs in the upper layer on eggs of the lower layer. The degree of such displacement was variable and was quite pronounced when the eggs, and therefore the plugs, were oriented with their polar axis perpendicular or oblique with respect to the petri dish. Upon insemination most of the eggs displaying the jelly shift did not cleave. Eggs from the same dish that did not show such displacement were selected as controls and upon insemination they cleaved normally.

In Vivo Observations

Eggs were placed in microslides with a central hole. Upon positioning of the egg, with a lateral view of the dimple, the development of the cones was followed. Photographs were made using a Leitz Orthomat microscope and Ilford Pan F film.

Electron Microscopy

Eggs were fixed at different times following fertilization with 2.5% (v/v) glutaraldehyde in 0.2 M phosphate buffer, postfixed in 2% OsO_4 (w/v) in phosphate buffer, dehydrated in ethanol, and embedded in Epon 812. Sec-

tions were cut with an LKB ultramicrotome, stained with uranyl acetate and lead citrate, and observed using a Philips 301 transmission electron microscope. For scanning electron microscopy, eggs fixed in a similar manner were dehydrated in increasing ethanol concentrations and Freon 113. The samples were critical-point dried, coated with gold, and examined with a Cambridge scanning electron microscope.

Electrical Recording

Eggs were placed in a plastic petri dish containing 10% Ringer at room temperature. Microelectrodes filled with 3 M KCl or 1.25 M K-citrate, of 10-30 M Ω were used for intracellular recording. Signals were amplified (WPI Instruments, Conn.), recorded on an oscilloscope, and stored on FM tape or a chart recorder (Gould, OH).

RESULTS

Sperm Penetration and Fertilization Cone

The conformation of the dimple, the opacity of the dimple contents and the thickness of the jelly layers over the dimple make it difficult to observe the first events of fertilization. The whole surface of the animal hemisphere becomes easier to observe only about 20-30 min after fertilization. By this time the dimple has regressed, the large concavity has rounded out, and the animal plug has dissolved (Wintrebart, 1933; Campanella in preparation).

About 30 min following fertilization one can observe, in the live egg with the compound microscope, one or more fertilization cones (Talevi, in preparation) which have shown to develop within the first 6 min of fertilization (Hibbard and Wintrebart, 1928). At this time

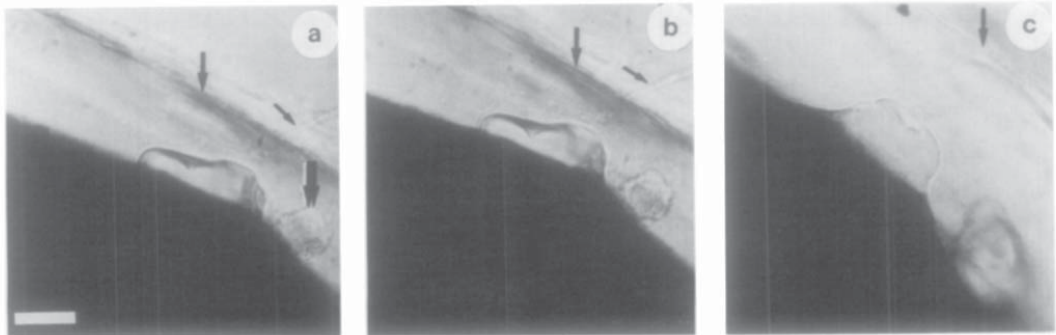


FIG. 4. (a-c) Sperm penetration in a cone which was 70 μm away from the fertilization envelope (arrow). The small arrow indicates the final portion of the sperm head. Double arrow, first polar body. In (b) and (c) the cone has further protruded out of the dimple surface. When the picture shown in (c) was taken, the spermatozoon was seen penetrating in the cone, while at the base of the cone actively moving cytoplasm was observed. Bar: 20 μm .

the cone is 45 to 70 μm in width and about 10 μm in height, and is composed of pigment-free cytoplasm. Its transparency allows the observation of the final stages of sperm penetration. Figure 2 shows the entrance of the sperm through the fertilization cone starting at 40

min after insemination and completed at 45 min. The cone is located about 10 μm below the fertilization membrane (FM). The first micrograph (Fig. 2a) depicts the sperm which was immotile at this time and located in the central portion of the cone. The head protrudes

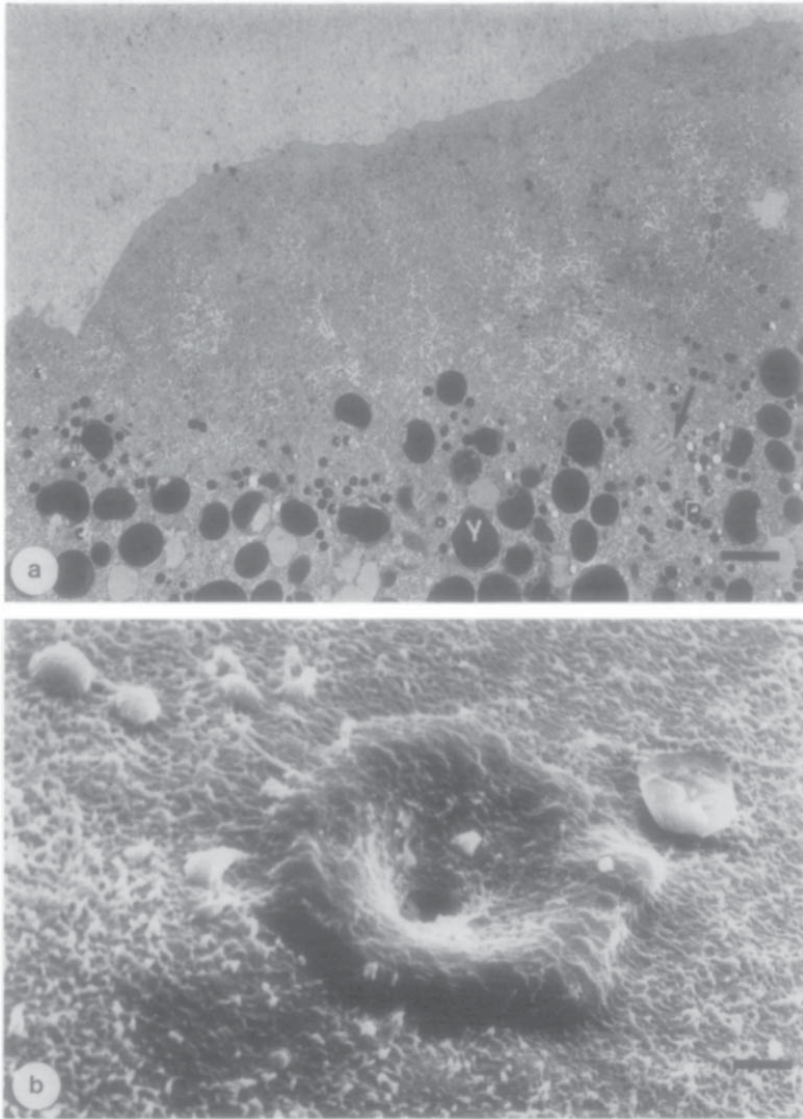


FIG. 5. Fertilization cone (a) TEM micrograph of a lateral section. The surface of the cone is microvilli free. Large cytoplasmic organelles such as yolk platelets (Y) and pigment granules (P) are segregated at the base of the cone. Arrow, portion of penetrated spermatozoon. Bar: 3 μm . (b) SEM micrograph showing the cone with the large funnel at its center corresponding to the micrographs of Figs. 2, 3, 4. Bar: 8 μm .

into the perivitelline space and into the FM and its posteriormost portion extends about $50\ \mu\text{m}$ into the jelly layer. As the sperm head is $900\ \mu\text{m}$ long (Campanella and Gabbiani, 1979), it can be inferred that most of the head has been already incorporated in earlier stages. In Figs. 2b-c the spermatozoon starts progressing into the cone. In Fig. 2d the posteriormost portion of the sperm is close to the FM and in Fig. 2d has passed through this layer. In Fig. 2e (about 3 min from the beginning of this stage of sperm penetration) a weak invagination is visible at the center of the cone, which is the site of sperm entrance. Gradually the invagination becomes more pronounced (Figs. 2f, g, h, i). The sperm tail never penetrated. Evidently it becomes separated at an earlier stage from the sperm head.

The fertilization cone remains quiescent, for 15 min, then about 60 min following insemination, it is reabsorbed, at the time of second polar body extrusion. The process of reabsorption takes 15 min. As shown in Fig. 3 the invagination in the cone gradually regresses. The cone flattens and is completely resorbed toward the end of first polar body extrusion.

The sequence described above was seen in 18 of the 21 eggs we observed. In the other three cases, the distance between the FM and the fertilization cone was wider, about $70\ \mu\text{m}$, and the penetration process was slightly different. As shown in Fig. 4 during the formation of the invagination caused by the sperm ingress, the cytoplasm under the cone lifts and in doing so causes the cone to approach the FM. From now on the process appears identical to that shown in Fig. 2. Both patterns of cone morphology are followed by normal embryo development.

Ultrastructure of the Fertilization Cone

Figure 5 shows the ultrastructural organization of the fertilization cone. The surface of the cone is smooth, without microvilli. Pigment granules, yolk platelets, and lipid droplets are segregated at the base of the cone (Fig. 5a). Figure 5b is a SEM micrograph of a cone, 45 min following insemination, where a wide funnel-shaped invagination produced by the sperm is clearly visible. This invagination is $42\ \mu\text{m}$ wide, on the surface of a $71\text{-}\mu\text{m}$ -wide cone.

Regional Reactivity of the Dimple to Spermatozoa

The dimple has a central flat portion (D1 region) which is flanked by steep lateral walls (D2 and D3 regions) (Figs. 1a and b). The D1 region is $200\ \mu\text{m}$ in diameter and is centered at the animal pole, where the first polar body was extruded before dimple formation. It is also characterized by regularly shaped and numerous microvilli (Fig. 6) which have been described in de-

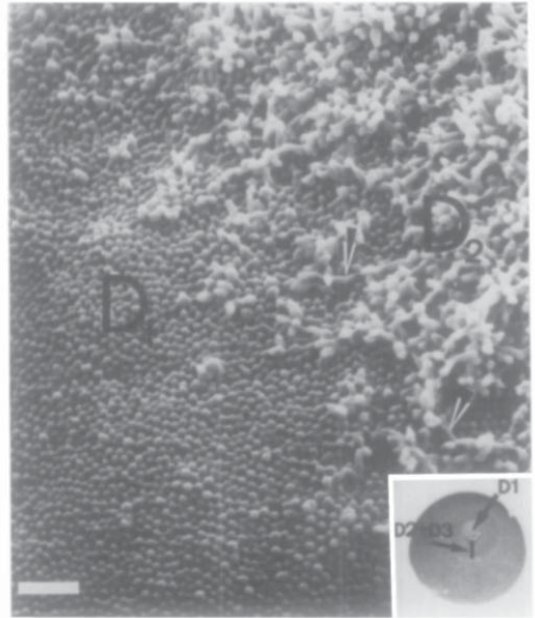


FIG. 6. SEM of the dimple surface. The micrograph shown in the insert ($\times 10$) indicates the regionalization of the dimple which here is flat because of the removal of the egg coats. D1 is the centrally located disk which corresponds in the SEM micrograph to the carpet of highly concentrated microvilli. D2 + D3 constitute the dimple walls. In the SEM micrograph, D2, contiguous to D1, is characterized by tufts of microvilli on shallow ridges (arrows). Bar: 1, $2\ \mu\text{m}$.

tail elsewhere (Campanella, 1975; Campanella and Gabbiani, 1980). Fertilization cone formation occurs in the D1 region only. About 20 min after insemination, it is occasionally possible to detect sperm in protrusions of variable size in the D2 and D3 regions. Such protrusions do not develop to cones even in later stages and were not seen in D1. SEM micrographs show that in D2 + D3 microvilli are sparser than in D1 and protrude on shallow ridges of the unfertilized dimple surface (Fig. 6).

In order to understand better the dimple organization with respect to sperm interaction and penetration, we examined eggs in which the plug was experimentally displaced with respect to the dimple (see Materials and Methods) (Fig. 7a). In such eggs the interaction between sperm and D2 + D3 region generated small cytoplasmic protrusions (Figs. 7b, c, d). Occasionally, under such conditions of plug displacement, fertilization cones are observed in D1 (Fig. 7b). This may be related to the particular position that the plug assumes with respect to the dimple, such that sperm converge both in D1 and D2 + D3. In the protrusions, in most cases, we did not

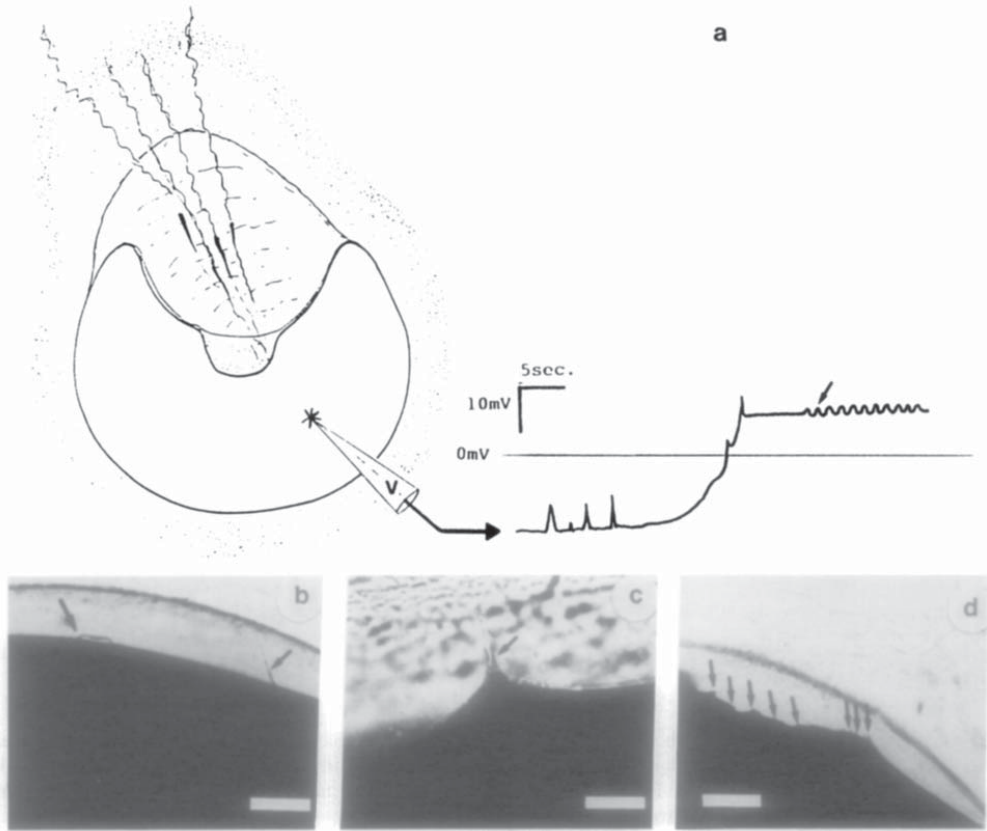


FIG. 7. Eggs with experimentally displaced coats. (a) Schematic drawing of an egg showing that when the coats are not aligned with D1, spermatozoa converge to D2 + D3. When such eggs are impaled, the resulting voltage recordings show brief depolarizations of 3-7 mV for 1-3 sec, which is later followed by a gradual rise to a positive plateau potential. Small arrow indicates oscillations. Eggs 40 min after fertilization. (b) When sperm convergence occurs both in D1 and in D2 + D3, a cone (arrow) and protrusions (small arrow) are seen respectively in D1 and D2. The sperm in the protrusions (small arrow) did not penetrate into the egg, while the sperm in the cone was incorporated. This egg developed. Bar: 100 μ m. (c) This sperm protruding at the surface of D2 (small arrow) was incorporated. This egg did not develop. Bar: 30 μ m. (d) The arrows indicate protrusions in D2 + D3 where the last stage of spermatozoa incorporation did not occur. The egg did not develop. Bar: 100 μ m.

observe entry of the sperm into the egg (Fig. 7d) even when sperm were incorporated in cones of the same egg (Fig. 7b). Protrusions eventually disappear.

We noted that many eggs with a displaced plug did not cleave. Therefore we followed the early development of 26 eggs with a displaced plug. Ten of these eggs with cones and protrusions developed normally; the other 16 eggs with protrusions only did not develop. This shows that sperm interactions leading to protrusions in the D2 + D3 region do not support development, but do not prevent normal development if a cone is present in D1.

Electrical Measurements

To examine the electrical characteristics of the plasma membrane after sperm interaction with D2 + D3, we recorded membrane potential from eggs with a displaced plug. Following insemination we recorded a large number of brief depolarizations of 3-7 mV for 1-3 sec ($N = 9$ eggs) (Fig. 7a), most probably caused by the interaction of spermatozoa with the D2 + D3 area of the dimple as the number of protrusions we observed in such eggs correlated with the number of step depolarizations. Following these brief depolarizations, a large

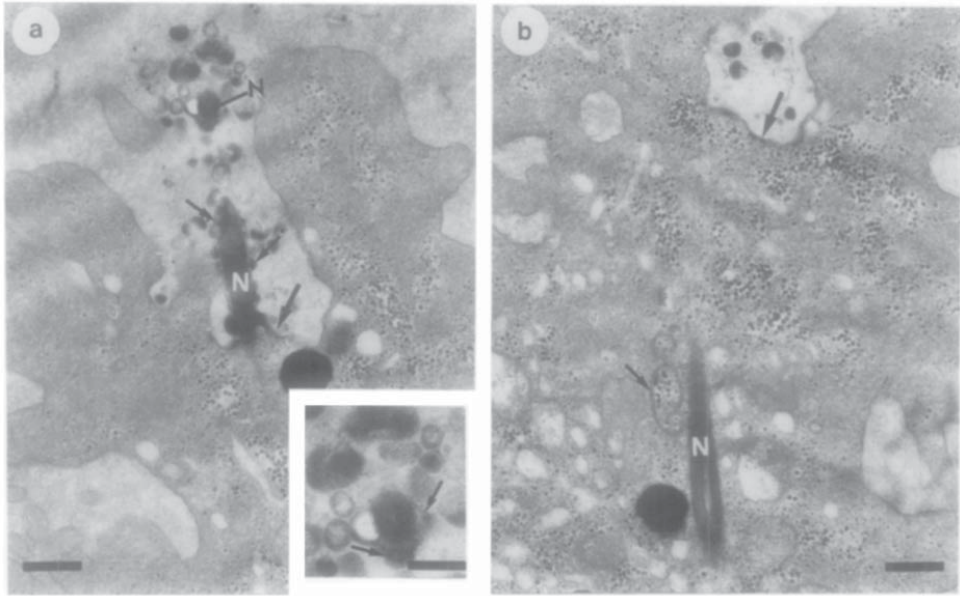


FIG. 8. Serial sections of a protrusion in D2 containing a sperm about 15 min after insemination. Bar: $0.5 \mu\text{m}$. (a) The protrusion is composed of several outfoldings. The site of fusion between the gamete membranes shows electron-dense thickening at the zygote surface (arrow). Around the sperm nucleus (N) are blebs (small arrows) as shown in the inset. Inset bar: $0.25 \mu\text{m}$. (b) The same sperm appears to have penetrated the cytoplasm where it has lost the nuclear envelope (small arrow). The arrow indicates the site of sperm-egg membrane fusion.

depolarization occurred (Fig. 7a) which oscillates similarly to the fertilization and activation potentials of *Discoglossus* eggs (Talevi *et al.*, 1985). It appears that while a single event of sperm-egg interaction in D2 + D3 cannot cause the positive plateau potential, the sum of several events may trigger this response. The eggs displaying such electrical events, when observed under microscope 40 min following fertilization, showed sperm interactions in D2 + D3 and no cone in D1 (Fig. 7a).

Ultrastructure of Spermatozoa in the Protrusions

The next question we asked was whether spermatozoa fused with the D2 + D3 areas. Ultrastructural observations show that the site of such interaction is a protrusion composed of several outfoldings (Fig. 8a). The membrane of the spermatozoon at the center of the protrusion is fused to that of the dimple, at a site which appears to be labeled by patches of electron-dense material. Around the nucleus several vesicles are seen with a content of variable electron density. The vesicles appear to be derived from blebs which bulge out of the sperm nucleus; this appearance suggests nuclear degeneration. Serial sections of the same sample (Fig. 8b) show that such spermatozoa have partially penetrated

into the egg, because the nucleus, deprived of its envelope, is found in the peripheral cytoplasm. We have observed three more cases of sperm under a similar condition.

In conclusion, these observations show that in the protrusions spermatozoa are partially incorporated into the cytoplasm after fusion of their membranes with that of the egg and suggest that, at least in those cases where spermatozoa do not undergo the final stages of penetration, a degeneration of the unpenetrated external portion of the sperm may occur.

DISCUSSION

In this study a functional regionalization of the animal dimple has been established by observing the late events of sperm penetration, and the following new findings have emerged: (1) A late stage of sperm incorporation, following a period of sperm inactivity has been described. (2) Morphological changes in the fertilization cone corresponding to sperm entry in the egg have been observed. (3) A role of the animal plug has been established, in determining the convergence of spermatozoa in the dimple. (4) The dimple may be divided in two regions (Fig. 9) functionally and morphologically distinguishable, i.e., D1, a disk $200 \mu\text{m}$ in diam-

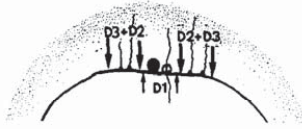


FIG. 9. Schematic drawing of the dimple about 40 min. after insemination, summarizing the functional regionalization of the dimple. In D1, where the 1st polar body (black sphere) is found at the time of insemination, the cone (empty sphere) forms upon insemination and the spermatozoon is incorporated in at least two steps, the first at fertilization and the second 40 min following insemination. In D2 + D3 spermatozoa induce the formation of protrusions and they generally do not undergo the second step of incorporation.

eter, at the center of the dimple, where sperm penetration induces a typical fertilization potential and fertilization cone; and the dimple walls (D2 + D3), where complete or partial penetration is characterized by the generation of step depolarizations which may be followed by a gradual rise to a positive plateau potential, and where sperm induce cytoplasmic protrusions. (5) In such protrusions spermatozoa fuse by their membrane with the dimple membrane and are partially incorporated into the egg. The unpenetrated region of the sperm head appears to degenerate.

D. pictus spermatozoa start to penetrate the egg at the time of their initial interaction with the dimple surface (Campanella, unpublished) and the penetration cone is fully formed in about 6 min (Wintrebert, 1933). We do not know how many steps the penetration process includes. However, we can say that at 30 min following fertilization the spermatozoon is apparently inactive while 10 min later, it appears to be again engaged in penetrating the egg. At this stage, the fertilization cone of *D. pictus* is conspicuously larger and more prominent than that detected in *Rana pipiens* (Elinson and Manes, 1978); however, its smooth surface and internal organization (homogeneous core content free of large organelles) is quite similar to that described in *Pleurodeles* by Picheral (1977). The large size of the cone and its internal invagination appears to match well the extreme length of the sperm (2.33 mm long). Only the head region is incorporated into the egg membrane. The existence of a late stage of incorporation is an unusual feature, not previously described in other amphibians and it may be related to sperm length as well as to the morphology of the egg where the distance between the dimple bottom and the vegetal pole is about 1000 μm . It is evident that the strategy for sperm incorporation must include a lateral shift of the spermatozoon in the subcortical region. Indeed it has been observed by Wintrebert (1933) that the spermatozoon is positioned in the cytoplasm parallel to the egg surface in late stages of fertilization. The occurrence of a large deformation

of the cone, that we observed at the final stage of sperm incorporation, suggests relative plasticity of its contents. Particular conditions of the cone and/or the underlying cytoplasm achieved 40 min after fertilization (see Elinson, 1983) may facilitate the accommodation in the egg of the residual external portion of the sperm head.

The association of the final regression of the cone with the extrusion of second polar body in *D. pictus* has been described by Elinson and Manes (1978) in *R. pipiens* and suggests a coordinate mechanism which could be part of a general physiological change of the egg.

By comparing physiological conditions (where the animal plug is positioned at the center of the dimple) and the experimental conditions (where the plug was displaced with respect to the egg axis) it is evident that the plug is a highly specialized jelly coat programmed for converging spermatozoa to the center of the dimple, i.e., to the site for optimal sperm-egg interaction. Such interaction has been investigated here and in a previous publication (Talevi *et al.*, 1985) in terms of the generation of fertilization potentials, cone formation, and development of the zygote. D1 appears to be the site of the egg where these conditions are satisfied. To our knowledge, this is the only case reported in the literature of a restricted predetermined site for sperm-egg interaction, which depends primarily upon the egg membrane itself and secondarily upon the external investments. This also suggests that "hot spots" (Dale and Monroy, 1981; Dale, 1987) programmed for the acceptance of spermatozoa are available in D1. In this connection, the plug may have a function similar to a lens, adjusted to convey sperm to position avoiding an excessively close convergence of spermatozoa in D1.

The dimple regionalization indicated by the present study is in agreement with previous data. D1 surface displays fucose residues, whereas D2 + D3 displays other sugar residues (Denis-Donini and Campanella, 1977). It has been hypothesized for other species that fucose has a specific role in sperm-egg interactions (see Hoshi, 1984). Electrophysiological observations have shown that the activation potential is due to the activation of channels found only in the dimple (Talevi *et al.*, 1985) and that Cl^- permeable channels (the most common anuran egg channels activated at fertilization) are present at a high concentration in D1, whereas D2 + D3 displays other channels (Nuccitelli, Kline, Busa, Talevi, and Campanella, in preparation). The dimple cortical cytoplasm is characterized by a specific organization of the cytoskeleton in actin bundles (for more details see Campanella and Gabbiani, 1980, Campanella *et al.*, 1982). Furthermore in D1, the transformation of the endoplasmic reticulum at activation and the exocytosis of cortical granules is different from that in D2 + D3

(Campanella *et al.*, 1986; Campanella, Talevi, Kline, and Nuccitelli, in preparation).

In other anurans, the region of the egg surface that can incorporate sperm is much larger as it covers the whole animal hemisphere. Calcium activated Cl^- channels are more abundant in this half than in the vegetal hemisphere (Cross 1981; Kline and Nuccitelli, 1985; Jaffe *et al.*, 1985). A close association is evidently present in *D. pictus* and other anuran eggs between the site of successful sperm-egg interaction and the location of Cl^- channels. Sperm entrance into the egg is associated with a release of intracellular Ca^{2+} which is then propagated to the rest of the egg (for a review see Jaffe, 1983). Given the undetectability of Cl^- channels in D2 + D3, the step depolarizations leading to a positive plateau potential which were observed when sperm penetrated this region might correspond to the propagation of the calcium wave shown to proceed from the site of $\text{Ins}(1, 4, 5)\text{P}_3$ injection to D1 (Nuccitelli, Kline, Busa, Talevi, and Campanella in preparation).

What leads to the formation of cones in D1 and protrusions in D2 + D3? The fusion between sperm and egg is a multiple-step process which includes fusion of membranes and interaction with the cytoskeleton. One hypothesis could be that the presence of fucose in D1 may be relevant in inducing correct sperm-binding necessary for subsequent formation of a cone. Since D1 peripheral cytoplasm is highly differentiated, one can also suggest that specific molecules are present only in this region, which are able to interact with the sperm and produce a fertilization cone. These interactions should be metabolically important because only upon cone formation is development activated, as we have shown here. Interestingly, cone formation is not necessarily connected with initial stages of sperm entrance but rather to final stages of sperm penetration and to the onset of development, since spermatozoa start penetrating also in the protrusions. However, the later sperm incorporation in the cones is either impaired and is accompanied by the apparent degeneration of the unpenetrated portion of the nucleus or is accomplished but not followed by zygote development. Finally, the channel distribution in the dimple, as measured by the vibrating probe show an activation current loop which enter the dimple in D1 and leaves it in D2 + D3. The current lasts about 40 min (Nuccitelli, Kline, Busa, Talevi, and Campanella, in preparation), i.e., before or contemporaneously with the last stage of sperm incorporation. In D1, where the current enters the dimple, cones are formed and sperm are found perpendicularly traversing the cortex. In D2 + D3 where the current leaves the egg, cones are not formed and penetration is generally impaired. Perhaps the microenvironment generated by ionic diffusion in the dimple content or the

current itself may be a driving force with a role in sperm penetration.

Electron microscopy was carried out at the "Centro interdipartimentale di ricerca sulle ultrastrutture biologiche" at the University of Naples. Electrophysiology was carried out at the "Stazione Zoologica" of Naples. We are grateful to Professors G. Ghiara and B. Dale for suggestions and to Mrs. G. Falcone and G. Argenzio for photographic work. This work was supported by the Ph.D. program fund "Biologia Evolutiva e del Differenziamento" and a CNR project on the Biology of Fertilization to Professor G. Ghiara.

REFERENCES

- CAMPANELLA, C. (1975). The site of spermatozoon entrance in the unfertilized egg of *Discoglossus pictus* (Anura): An electron microscopy study. *Biol. Reprod.* **12**, 439-447.
- CAMPANELLA, C., and GABBIANI, G. (1979). Motile properties and localization of contractile proteins in the spermatozoon of *Discoglossus pictus*. *Gamete Res.* **2**, 163-175.
- CAMPANELLA, C., and GABBIANI, G. (1980). Cytoskeletal and contractile proteins in coelomic, unfertilized and fertilized egg of *Discoglossus pictus* (Anura). *Gamete Res.* **3**, 99-114.
- CAMPANELLA, C., RUNGGER-BRANDLE, E., and GABBIANI, G. (1982). Immunolocalization of alpha-actinin in an amphibian egg (*Discoglossus pictus*). In "Embryonic Development" (M. M. Burger, Ed.), Part B, pp 45-53. A. R. Liss, New York.
- CAMPANELLA, C., TALEVI, R., ATRIPALDI, U., and QUAGLIA, L. (1986). The cortical endoplasmic reticulum and its possible role in activation of *Discoglossus pictus* (Anura) egg. In "Molecular and Cellular Biology of Fertilization" (J. L. Hedrick, Ed.), pp. 185-203. Plenum, New York.
- CONKLIN E. G. (1905). The organization and cell-lineage of the Ascidians egg. *J. Acad. Natl. Sci. Philadelphia* **13**, 1-119.
- CROSS, N. L. (1981). Initiation of the activation potential by an increase in intracellular calcium in eggs of the frog *Rana pipiens*. *Dev. Biol.* **85**, 380-385.
- DALE, B. (1987). Mechanism of fertilization. *Nature (London)* **325**, 762-763.
- DALE, B., and MONROY A. (1981). How is polyspermy prevented? *Gamete Res.* **4**, 151-169.
- DE FELICE, L. J., DALE, B., and TALEVI, R. (1986). Distribution of fertilization channels in ascidian oocyte membranes. *Proc. R. Soc. London. B* **229**, 209-214.
- DENIS DONINI, S., and CAMPANELLA, C. (1977). Ultrastructural and lectin binding changes during the formation of the animal dimple in oocytes of *Discoglossus pictus* (Anura). *Dev. Biol.* **47**, 257-268.
- DICTUS, W. J. A. G., VAN ZOELLEN, E. J. J., TETTEROO, P. A. T., TER-TOOLEN, L. G. J., DE LAAT, S. W., and BLUEMINK, J. G. (1984). Lateral mobility of plasma membrane lipids in *Xenopus* eggs: Regional differences related to animal/vegetal polarity become extreme upon fertilization. *Dev. Biol.* **101**, 201-211.
- ELINSON, R. P. (1975). Site of sperm entry and a cortical contraction associated with egg activation in the frog *Rana pipiens*. *Dev. Biol.* **47**, 257-258.
- ELINSON, R. P. (1983). Cytoplasmic phases in the first cell cycle of the activated frog egg. *Dev. Biol.* **100**, 440-451.
- ELINSON, R. P., and MANES, M. E. (1978). Morphology of the site of sperm entry on the frog egg. *Dev. Biol.* **63**, 67-75.
- FREEMAN, G., and MILLER, R. (1982). Hydrozoan eggs can only be fertilized at the site of polar body formation. *Dev. Biol.* **94**, 142-152.
- GOULD-SOMERO, M. (1981). Localized gating of the egg Na channels by sperm. *Nature (London)* **291**, 254-256.
- HIBBARD H., and WINTREBERG, P. (1928). La formation des membranes et les changements d'aspect de l'oeuf de *Discoglossus pictus* Othh. avant la ponte. *C. R. Soc. Biol.* **98**, 1521-1523.

- HOSHI, M. (1984). Roles of sperm glycosidases and proteases in the ascidian fertilization. In "Advances in Invertebrate Reproduction" (W. Engels *et al.*, Eds.), Vol 3 pp. 27-40. Elsevier Science Publishers B. V., New York.
- JAFFE, L. F. (1983). Sources of calcium in egg activation a review and hypothesis. *Dev. Biol.* **99**, 265-276.
- JAFFE, L. A., and GUERRIER, P. (1981). Localization of electrical excitability in the early embryo of *Dentalium*. *Dev. Biol.* **83**, 370-383.
- JAFFE, L. A., KADO, R. T., and MUNCY, L. (1985). Propagating potassium and chloride conductances during activation and fertilization of the egg of the frog *Rana pipiens*. *J. Physiol.* **368**, 227-242.
- KLINE, D., and NUCCITELLI, R. (1985). The wave of activation current in the *Xenopus* egg. *Dev. Biol.* **111**, 471-487.
- KLINE, D., ROBINSON, K. R., and NUCCITELLI, R. (1983). Ion currents and membrane domains in the cleaving *Xenopus* egg. *J. Cell. Biol.* **97**, 1753-1761.
- MANN, T. LUTWAK-MANN, and HAY, M. F. (1963). A note on the so-called seminal vesicles on the frog *Discoglossus pictus*. *Acta Embryol. Morphol. Exp.* **6**, 21-25.
- MILLER, R. L. (1977). Distribution of sperm chemotaxis in the animal kingdom. In "Advances in Invertebrate Reproduction" (K. G. Adiyodi and R. G. Adiyodi, Eds.), Vol. 1, pp. 99-119. Peralam-Kentk, Kerala, India.
- NUCCITELLI, R. (1978). Ooplasmic segregation and secretion in the *Pelvetia* egg is accompanied by a membrane-generated electrical current. *Dev. Biol.* **62**, 13-33.
- NUCCITELLI, R., and WILEY, L. M. (1985). Polarity of isolated blastomeres from mouse morulae: detection of transcellular ion currents. *Dev. Biol.* **109**, 452-463.
- NEWPORT, G. (1854). Research on the impregnation of the ovum in amphibia, and on the early stages of development of the embryo (third series) *Phil. Trans. R. Soc. London* **144**, 229-244.
- PICHERAL, B. (1977). La fécondation chez le triton *Pleurodèle* II. La pénétration des spermatozoïdes et la réaction locale de l'oeuf. *J. Ultrastruct. Res.* **60**, 181-202.
- TALEVI, R., DALE, B., CAMPANELLA, C. (1985). Fertilization and activation potentials in *Discoglossus pictus* (Anura) eggs: A delayed response to activation by pricking. *Dev. Biol.* **111**, 316-323.
- TALEVI, R., and DALE, B. (1986). Electrical characteristics of Ascidian egg fragments. *Exp. Cell Res.* **162**, 539-543.
- WINTREBERT, P. (1933). La mécanique du développement chez *Discoglossus pictus* oth, de l'ovogenèse à la segmentation. *Arch. Zool. Exp. Genet.* **75**, 501-539.

Different Cytoskeletal Organization in Two Maturation Stages of *Discoglossus pictus* (Anura) Oocytes: Thickness and Stability of Actin Microfilaments and Tropomyosin Immunolocalization

CHIARA CAMPANELLA,¹ CHRISTINE CHAPONNIER,² LUCIA QUAGLIA,³ ROBERTO GUALTIERI,³ AND GIULIO GABBIANI²

¹Dipartimento di Scienze e Tecnologie Biomediche e di Biometria, Università de l'Aquila, L'Aquila, Italy;

²Departement de Pathologie, Université de Genève, Genève, Switzerland;

³Dipartimento di Biologia Evolutiva e Comparata, Università di Napoli, Napoli, Italy

ABSTRACT In *Discoglossus pictus* oocytes, the germinative area (GA) contains long and irregular microvilli where actin microfilaments are located. In the egg, the funnel-shaped dimple that originates by invagination of the GA is present. In the dimple both microvilli and microfilament bundles have a very orderly appearance. This report extends previous observations (Campanella and Gabbiani, *Gamete Res* 3:99-114, 1980) and shows that GA microfilaments are thinner (36 Å average) than dimple microfilaments (60 Å average), as measured in ultrathin section. Moreover, the interfilament distance is smaller in GA bundles than in the dimple bundles. To get an insight into actin organization in oocytes and eggs, we used an actin-depolymerizing factor (ADF) in which cryostat sections were incubated prior to immunofluorescent staining with antiactin antibodies. The microfilaments of the GA microvilli and partially of the oocyte cortex are resistant to ADF when compared to those in the dimple and the rest of the egg cortex. We also investigated immunocytochemically the presence of tropomyosin and found that this protein is localized in the dimple and in the cortex of oocytes and eggs but is absent in the GA.

Key Words: Frog, Germinative area, Dimple, Microfilaments

INTRODUCTION

Discoglossus pictus is the only amphibian species that has a small indentation in the egg animal hemisphere, the dimple, where fertilization occurs (Hibbard, 1928; Campanella, 1975; Talevi and Campanella, 1988). In coelomic oocytes, the precursor site of the dimple is the germinative area (GA), a disk 900 µm in diameter, which, after first polar body extrusion, transforms in the dimple through profound remodeling of its surface

and cortex (Denis-Donini and Campanella, 1977). Studies have shown that in the dimple a palisade of microfilaments is present, which may be responsible for modeling the shape of the dimple itself. Furthermore the GA, the dimple, as well as oocyte and egg cortex have distinct types of actin microfilament organization (Campanella and Gabbiani, 1980). Therefore *D. pictus* oocytes and eggs represent convenient models for investigating distinct cytoskeletal organizations in well defined stages of maturation and functional adaptation of amphibian oocytes. As regards other amphibian species the morphology of actin organization has been described in oocytes (Franke et al., 1976) and eggs (which are oocytes arrested at second meiotic metaphase) (Gall et al., 1983). However, a comparative study between oocytes and eggs has not been conducted.

Actin, myosin, tubulin, and alpha-actinin have been immunolocalized in oocytes and eggs (Campanella and Gabbiani, 1980; Campanella et al., 1982). The actin content of *Discoglossus* microfilaments has been demonstrated in coelomic oocytes and in eggs also by other approaches. The GA, dimple, and cortex all stain positively for actin, and generally more intensely where microfilaments are arranged in bundles (Campanella and Gabbiani, 1980). During that study we observed that actin microfilaments in the GA have a thinner diameter than those in the egg dimple. In the present work we compared in detail the dimensions and the interfilament spacing of microfilaments in coelomic oocytes with those in eggs and found significant differences both in the thickness and in the center-to-center distance of such microfilaments. This suggests that GA and dimple microfilaments are discriminated by fixa-

Received January 23, 1989; accepted July 31, 1989.

Address reprint requests to Chiara Campanella, Dipartimento di Scienze e Tecnologie Biomediche e di Biometria, Università de l'Aquila, Collemaggio, 67100, L'Aquila, Italy.

tion and/or that the organization of actin is different in these two distinct meiotic stages of oogenesis.

In order to get an insight into actin organization we utilized a plasma-derived actin-depolymerizing factor (ADF) (Chaponnier et al., 1979, 1985), also called brevin (Harris and Schwartz, 1981) or plasma gelsolin (Yin et al., 1984) in which cryostat sections were incubated prior to immunofluorescent staining with anti-actin antibodies (Low et al., 1981; Gabbiani et al., 1984). Moreover, we also investigated the presence of tropomyosin by means of immunofluorescence with a polyclonal antibody. This protein has been localized in sea urchin eggs (Ischimoda-Tagagi, 1979).

MATERIALS AND METHODS

Adult *D. pictus* (the painted frog) of both sexes were collected in the neighborhood of Palermo (Italy) from February to May. Females were injected in the dorsal lymphatic sac with 200 IU Pregnyl (chorion gonadotropin; Organon, Oss, The Netherlands) in amphibian Ringer's solution. Eight hours later coelomic oocytes and eggs were collected from the body cavity and the ovisac, respectively, of the same female. Coelomic oocytes were utilized after a brief rinse in Ringer's, whereas uterine eggs were first immersed in 5 mM dithiothreitol (DDT) in 0.1 M NaCl, 5 mM Tris HCl (pH 8.0) to dissolve jelly layers.

Electron Microscopy

According to Temmink and Spiele (1979), microfilament preservation does not depend upon the method of fixation. However, it has also been reported that high osmium concentration (i.e., 1%), non-phosphate buffers, alkaline pH, and relatively high temperatures may destroy microfilaments, which do not have a regular distribution (Maupin-Szamier and Pollard, 1978). Therefore, to test whether the method of fixation influences microfilament preservation in our material, we tested fixatives routinely used for ultrastructural studies, as well as a fixation method with low osmium concentration and phosphate buffer at pH 6.0. In addition, the influence of Ca^{2+} ions on the preservation of the oocyte cortical regions was tested by adding EGTA to the fixation buffer. The following methods of fixation were used. A) 3% glutaraldehyde in 0.1 M cacodylate buffer pH 7.3 at room temperature followed by several rinses in the same buffer at 4°C. The samples were postfixed in S-collidine buffer containing 1% OsO_4 for 90 min. B) Same conditions as in A but with cacodylate and S-collidine buffers containing 1 mM EGTA. C) 2.5% glutaraldehyde in 0.2 M phosphate buffer pH 7.2 (Millonig, 1964) for 3 hr to overnight at 4°C. After several rinses the samples were postfixed in 1% OsO_4 in the same buffer for 90 min. D) 2.5% glutaraldehyde, in 0.1 M phosphate buffer pH 6 at 4°C. After several rinses the samples were postfixed in 0.1% OsO_4 in the same buffer for 90 min (Maupin-Szamier and Pollard, 1978). After fixation all samples were dehydrated in

the same way in a graded series of ethanol and embedded in Epon 812. Thin sections were stained with uranyl acetate and lead citrate.

Electron micrographs were obtained on a Philips EM 301 microscope at 80 kV at a magnification of 34,000 or 45,000. Magnifications were controlled with a calibrated grid containing 2160 lines per millimeter (Balzer Union) and were found to be constant with a variation of 2%. Measurements of microfilament thickness and center-to-center distance were performed on micrographs of cross and longitudinal sections at a final magnification of 68,000 or 90,000 with the aid of an ocular micrometer (Bima).

Statistical Analysis

The average values of microfilament thickness and center-to-center distance were compared using Student's t test.

Immunofluorescence and Sensitivity to ADF

Human antiactin antibodies (HAA) were obtained from the serum of a patient with chronic aggressive hepatitis (Chaponnier et al., 1977; Gabbiani et al., 1977). The antibodies were affinity purified using a virosine-F-Actin Sepharose column (Chaponnier et al., 1985). Rabbit antiactin antibodies (RAA) were raised using chicken gizzard actin (Suzuki et al., 1978) as antigen. F-actin was cross linked with glutaraldehyde (Lehrer, 1972) and extensively dialyzed against phosphate-buffered saline (PBS) before injection. Rabbits were subcutaneously and intradermally injected in several regions of the back with 0.5 mg actin emulsified with complete Freund's adjuvant. The procedure was repeated every 2 weeks. Ten days after the third injection, rabbits were bled, and the serum was tested by immunofluorescence and immunoblotting. The specific antiactin antibodies were purified with ion-exchange chromatography and actin-affinity chromatography, as previously described (Gabbiani et al., 1977). Antitropomyosin antibody (a gift from Dr. W. Wnuck, Department of Biochemistry, Faculty of Sciences, University of Geneva, Switzerland) was raised in guinea pig against chicken gizzard tropomyosin, and was utilized as previously described (Kocher et al., 1984).

For immunofluorescent staining, frozen 4 μm sections were used unfixed or fixed in acetone at -20°C for 5 min, dried, and incubated with HAA or RAA. Fluorescein-conjugated goat IgG fraction to human IgG (Miles Severac, Lausanne, Switzerland) or to rabbit IgG (Behringwerke AG, Malburg/Lahn, FRG), were used as secondary antibodies. The level of fluorescence was compared with that in control sections treated in parallel with human gamma-globulins (Fluka Buchs, Switzerland) or rabbit gamma-globulins (Serva, Heidelberg, FRG). ADF is a protein normally present in plasma or serum of humans and small laboratory mammals and has been utilized to investigate actin

organization (Chaponnier et al., 1979, 1985; Low et al., 1981; Gabbiani et al., 1984).

To determine the sensitivity of cytoplasmic actin to ADF, cryostat sections of oocytes and eggs were incubated with ADF or with normal rabbit or human 1/10 in PBS containing ADF (Low et al., 1981; Gabbiani et al., 1984) and stained for actin as described above. As an additional control, sections were preincubated with inactivated normal sera where the activity of ADF was abolished by heating for 60 min at 56°C and by dilution in PBS containing 3 mM EGTA (Chaponnier et al., 1979). The sections were then processed for immunofluorescence staining. Photographs were taken on a Zeiss UV photomicroscope using Ilford black-and-white HP5 or Agfapan vario-XL films.

RESULTS

General Features of Microfilaments

A summary is reported below of the microfilament features in *D. pictus* oocytes and eggs, according to Campanella and Gabbiani (1980). In coelomic oocytes the GA contains long and irregular microvilli (Fig. 1a). Bundles of microfilaments are present in the microvilli, as well as in the peripheral cytoplasm of the GA, where they are irregularly arranged. In the egg the dimple has microvilli (Fig. 1b), with microfilament bundles having a very orderly appearance and extending into the cytoplasm, at regular intervals with a depth of about 10 μm . They segregate underlying organelles such as pigment granules (Fig. 1b). In the cortex of oocytes and eggs, microfilaments are arranged in an apparently randomly organized peripheral network. Moreover, in coelomic oocytes some microfilament bundles are observed in short oocyte protrusions (Campanella and Gabbiani, 1980).

In the GA the most effective fixative for microvillar microfilaments was C: in the tight microfilament bundles, microfilaments were well preserved, as well as transverse stripes with a 150–160 Å repeat (Fig. 2a). When fixed in A (Fig. 2b) or in B, the entire tissue, including the microfilaments, were scantily preserved. In fixation D, microfilaments were hardly distinguishable. The microfilament cortical network of the oocyte showed similar fixation characteristics (Fig. 2a).

In the dimple fixation B gave the best preservation of microfilament bundles; here lateral arms are particularly clear and transverse stripes with a 150–160 Å repeat are discernible (Fig. 3a). In this fixation, however, microvilli appeared to have collapsed slightly. This suggests that Ca^{2+} is necessary during fixation for the maintenance of microvillus shape. In fixations A and C, where microvillus shape was well preserved, microfilaments were similarly well distinguishable. However lateral arms are not as evident as in B-fixed samples (Fig. 3b). When fixed in D, the tissues, and particularly the microfilaments, were not preserved. Similar fixation characteristics have been found for the egg cortical network of microfilaments (Fig. 3a).

Dimension of Microfilaments and Center-to-Center Interfilament Distance

Table 1 shows the thickness of microfilaments in the microvilli as measured in both the coelomic oocyte GA and the egg dimple for fixations A, B, and C. Fixation D was discarded because of poor tissue preservation. Standard deviations are reported for each set of samples. They are rather high in the case of oocytes (more than 20% of mean values) probably due to a varying degree of preservation of the microfilaments. Furthermore the thickness of the microfilaments varies according to the fixation method in oocytes as well as in eggs (significant at the level of probability $P < 0.05$). However, regardless to the fixation method, it is evident in Table 1 that the diameter of oocyte microfilaments (mean value 36 Å) is always less than that of corresponding egg microfilaments (mean value 60 Å). To test the significance of this observation, oocyte and egg average values reported in Table 1 have been compared by the t test for each method of fixation. Differences in the thickness of oocyte and egg microfilaments are highly significant (level of probability $P < 0.001$) for the three fixation methods used (Table 1).

Microfilaments were also measured in the cortex of oocytes and eggs, where, however, they are difficult to visualize because of their organization. The results were similar to those described above.

In cross sections of the GA microvilli, about 35 microfilaments are arranged hexagonally in each bundle (inset 2, Figure 2a). In these bundles the interfilament separation (center-to-center distance) ranges from 75 to 110 Å (mean value 92). In the dimple, bundles of 80 microfilaments or more are also hexagonally packed. The center-to-center distance ranges from 90 to 135 Å (mean value 122) (inset 2, Fig. 3a) (Table 2). t tests indicate that the center-to-center distance of microfilaments in oocytes is significantly less than that in eggs (level of probability $P < 0.001$) (Table 2).

Immunofluorescence Staining

Antiactin staining and sensitivity to ADF. We have shown elsewhere (Campanella and Gabbiani, 1980) that cryostat sections of the GA, dimples and cortices of both oocytes and eggs are positive to immunostaining with antiactin antibodies. In the present work, when coelomic oocytes were first incubated with normal sera (which contain ADF) and then with antiactin antibodies (HAA or RAA) the GA was stained (Fig. 4a). The intensity of this staining was only slightly lower compared to preparations preincubated with PBS (Fig. 4b) or inactivated normal serum. Similarly, in the cortex, the immunostaining for actin was detectable after preincubation with ADF (Fig. 4c). However the antiactin staining was remarkably stronger in preparations preincubated with PBS or inactivated normal serum (Fig. 4d). When egg sections were first incubated with ADF or with normal serum and

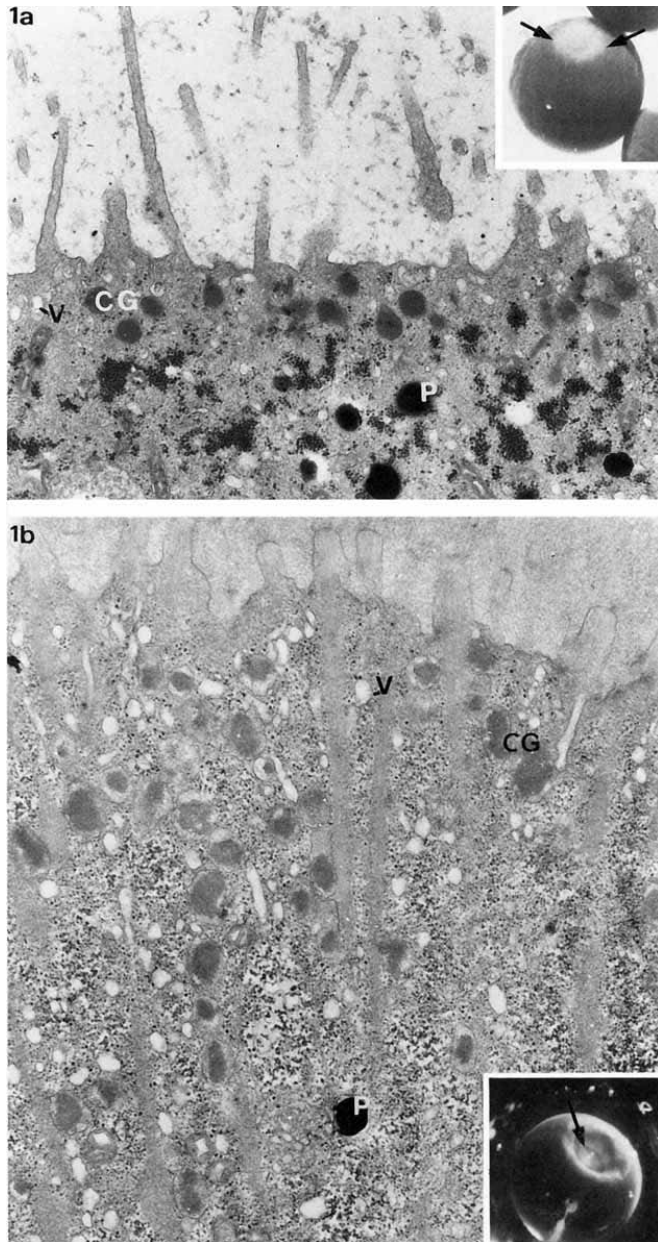


Fig. 1. a: Coelomic oocyte germinative area (GA). Long and irregular microvilli are present at the GA surface. GC, cortical granules; V, vacuoles; P, pigment granules. $\times 18,500$. **Inset:** The GA is indicated by the arrows. $\times 10$. **b:** Uterine egg dimple. Finger-shaped microvilli,

about $0.3 \mu\text{m}$ thick outline the dimple surface. CG, cortical granules; V, vacuoles, P, pigment granule. $\times 18,500$. **Inset:** The dimple is indicated by the arrow. $\times 10$.



Fig. 2. Oocyte GA. **a:** This sample is fixed with method C. Microvillus containing a microfilament bundle. Small arrows, lateral arms; arrows, cortical network of microfilaments. $\times 68,000$. **Inset 1:** Detail of the microvillus tip. Arrows, transverse stripes. $\times 85,000$. **Inset 2:** Cross section of a microfilament bundle (arrowheads). The micro-

filaments are hexagonally arranged in bundles of about 35. The interfilament separation ranges from 75 to 110 Å. $\times 100,000$. **b:** Sample fixed by method A. Such a fixation does not seem to have well preserved cytoplasmic components. Arrow, actin microfilament bundle in the central core of the microvillus. $\times 68,000$.

then with antiactin antibodies (HAA or RAA), the dimple was practically negative (Fig. 5a). Following exposure to the antibodies alone or preincubation with inactivated normal serum, this egg region appeared strongly stained with the typical rod-like pattern previously reported (Campanella and Gabbiani, 1980) (Fig. 5b). The same results were obtained for the egg cortex (Fig. 5c,d). Moreover, the actin immunofluorescent staining was constantly more pronounced in the dimple than in the cortex (compare Fig. 5b with Fig. 5d). No staining was observed in control sections incubated with the corresponding gamma-globulins. These results are summarized in Table 3.

Antitropomyosin Staining

The GA was negative for antitropomyosin (Fig. 6a,b) whereas the oocyte cortex showed a rim of intense positivity (Fig. 6c). The control section of the oocyte animal hemisphere incubated with normal guinea pig serum was negative (Fig. 6d).

In the dimple, a specific positivity for tropomyosin was observed with the same rod-like pattern as for actin (Fig 6e,g, and compared with Fig. 5b). The layer displaying such positivity (Fig. 6c,f, small arrows) has been characterized in a previous publication (Campanella and Gabbiani, 1980) by the presence of microfilament bundles, whose rootlets penetrate the cyto-

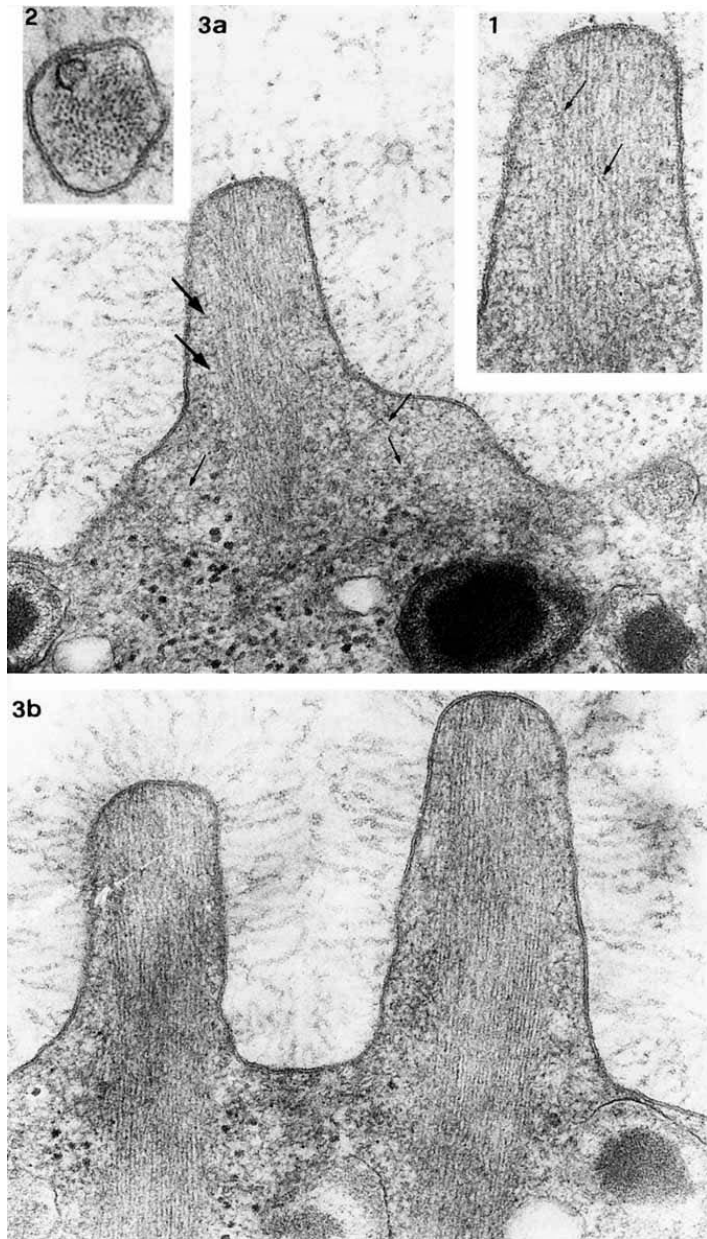


Fig. 3. Egg dimple. **a:** This sample is fixed with method B. Lateral arms (arrows) are also present. The base of the microvillus is slightly enlarged, most probably as a result of fixation, thus giving rise to a rather short microvillus. Small arrows, cortical network of microfilaments. $\times 68,000$. **Inset 1:** A detail of the microvillus tip is shown. Transverse stripes are seen (small arrows) in the microfilament bundle. One can observe that the plasma membrane of this kind of microvilli has little asymmetry as previously reported (Campanella and

Gabbiani, 1980). $\times 85,000$. **Inset 2:** Cross section of microfilament bundles. The bundle is hexagonally packed and contains more than 80 microfilaments. The interfilament distance ranges from 90 Å to 135 Å. $\times 100,000$. **b:** This sample is fixed with method C and is similar to samples fixed with A. The microvillus shape is well preserved, as well as most features of its cytoskeleton. However, lateral arms and transverse stripes are not as evident as in B-fixed samples. $\times 68,000$.

TABLE 1. Microfilament Measurements (Å)*

| | No. samples | No. measurements | Value | | | SD | t | P |
|------------|-------------|------------------|-------|-----|------|------|------|--------|
| | | | Min | Max | Mean | | | |
| Fixative A | | | | | | | | |
| Oocytes | 3 | 17 | 29 | 58 | 37 | 9.8 | 10.6 | <0.001 |
| Eggs | 3 | 29 | 55 | 88 | 68 | 9.0 | | |
| Fixative B | | | | | | | | |
| Oocytes | 3 | 19 | 29 | 58 | 38 | 13.8 | 6.3 | <0.001 |
| Eggs | 3 | 22 | 44 | 73 | 62 | 10.2 | | |
| Fixative C | | | | | | | | |
| Oocytes | 3 | 23 | 14 | 58 | 34 | 11.4 | 7.6 | <0.001 |
| Eggs | 3 | 26 | 29 | 73 | 50 | 9.6 | | |

*Calculated measurements of oocyte and egg microfilaments with their standard deviations and t test values for the means and corresponding levels of probability (P) for each fixation method (A, B, C; see Materials and Methods).

TABLE 2. Microfilament Center-to-Center Measurements (Å)*

| | No. samples | No. measurements | Value | | | SD | t | P |
|---------|-------------|------------------|-------|-----|------|------|-----|---------|
| | | | Min | Max | Mean | | | |
| Oocytes | 3 | 28 | 75 | 110 | 92 | 10.3 | 9.7 | <0.0001 |
| Eggs | 3 | 29 | 90 | 135 | 122 | 13.3 | | |

*Calculated measurements of oocyte and egg microfilaments center-to-center distance in B fixed samples. Standard deviations, t test values for the means, and corresponding levels of probability have been calculated.

plasm for 10–12 µm and segregate pigment granules (Fig. 6f, arrow) of the deeper cytoplasm. A positivity to antitropomyosin was found also in the egg cortex (data not shown). Both in oocytes and eggs the cytoplasm was only slightly positive (Fig. 6). These results are summarized in Table 3.

DISCUSSION

Our results show that actin microfilaments located in microvilli of coelomic oocytes have an apparent thickness of 36 Å, whereas those located in microvilli of eggs have a thickness of about 60 Å. In classic studies on sections or negatively stained microfilaments the actin microfilament thickness ranges from 50 to 70 Å (Huxley, 1957; Knappes and Carlsen, 1962; Hanson and Lowry, 1963). In the present work, the size of the microfilaments in the oocytes or eggs vary according to the fixation procedure utilized. However, the thickness of microfilaments in the oocytes is always less than that measured in the egg, regardless of the fixative used. As was mentioned above, Temnick and Spiele (1979) claim that microfilament preservation does not depend on the fixation method. On the other hand, according to Maupin-Szamier and Pollard (1978), when arranged in a network, microfilaments are better preserved by fixative D, which under our conditions gave the poorest preservation. We have no explanation of this discrepancy, but we have studied microfilaments of different origin and species from those described by these authors.

We have observed that actin microfilaments have different thickness in different oocyte stages (i.e.,

oocyte GA and egg dimple) after being fixed with the same fixative and processed in the same way. We do not know whether our measurements correspond to the real value. Irrespective of the fact that these values may be apparent, our electron microscope observations suggest that microfilament bundles are not in the same biophysical and/or biochemical conditions in oocytes and eggs. Moreover, the fact that the dimple and not the GA is positive to antitropomyosin staining suggests that the presence of tropomyosin may be an important factor involved in the stabilization of actin microfilaments to fixatives, in agreement with the results of Maupin-Szamier and Pollard (1978) and Lehrer (1972).

Two other results suggest that there is a different organization of actin microfilament bundles in the GA versus the dimple and in the oocyte cortex versus the egg cortex: 1) *Distance between microfilaments in microvilli*. The center-to-center measurements of microfilaments (92 Å in the GA and 122 Å in the dimple, as averages) indicate that more microfilaments per unit area are packed in the GA compared to the microfilaments in the dimple. According to Matsudaira et al. (1983), X-ray measurements of variously processed samples show that the interfilament distance may vary with actin cross-linking proteins (for fimbrin 111–120 Å and for villin 120–130 Å). Further work is needed to detect the actin cross-linking proteins in *Discoglossus* oocytes and eggs. 2) *Resistance of actin filaments to ADF*. Surprisingly, the unusually thin microfilaments in the GA bundles are more resistant to the destabilizing action of ADF compared to the putatively tropomy-

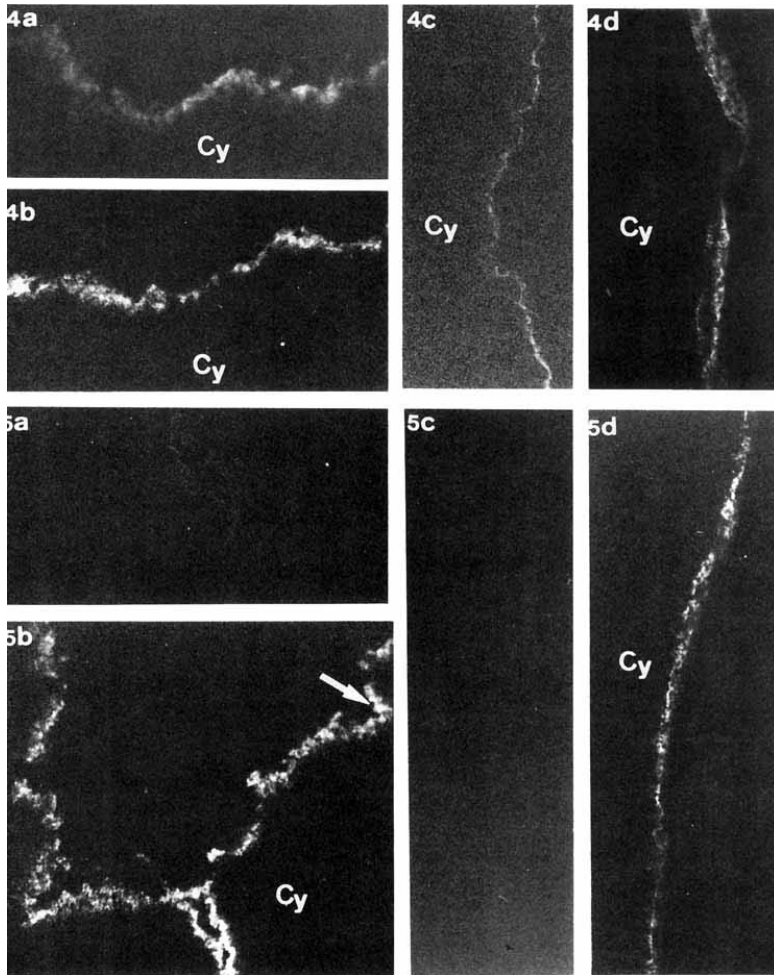


Fig. 4. Oocyte immunofluorescent staining with antiactin antibody. Cy, cytoplasm. **a:** GA preincubated with ADF before the immunostaining with RAA. $\times 350$. **b:** GA incubated only with RAA. $\times 350$. **c:** Cortex preincubated with ADF before the immunostaining with RAA. $\times 350$. **d:** Cortex incubated only with RAA. $\times 350$.

Fig. 5. Egg immunofluorescent staining with antiactin antibody. Cy, cytoplasm. **a:** Dimple preincubated with ADF followed by incubation with RAA. $\times 250$. **b:** Dimple incubated with RAA. Arrow, rod-like pattern of fluorescence. $\times 250$. **c:** Cortex preincubated with ADF followed by incubation with RAA. $\times 350$. **d:** Cortex incubated with RAA. $\times 350$.

osin-stabilized microfilaments of usual size in the dimple bundles. We have previously observed that the *Discoglossus* intestinal mucosa, which has a microfilament bundle organization similar to the dimple, is also sensitive to ADF (unpublished observations). In the cortex of coelomic oocytes, actin immunostaining is partially retained following ADF incubation compared to the egg cortex; this probably correlates with the presence of microfilament bundles in short superficial pro-

trusions, which represent the remnants of ovarian microvilli, whereas the egg cortex contains only a network of microfilaments (Campanella and Gabbiani, 1980). Thus ADF appears to discriminate not only between different types of actin organization, i.e., microfilaments arranged in networks or bundles (Low et al., 1981), but also between different types of microfilament bundles in microvilli. The resistance of microfilaments to depolymerization by ADF is likely dependent on their

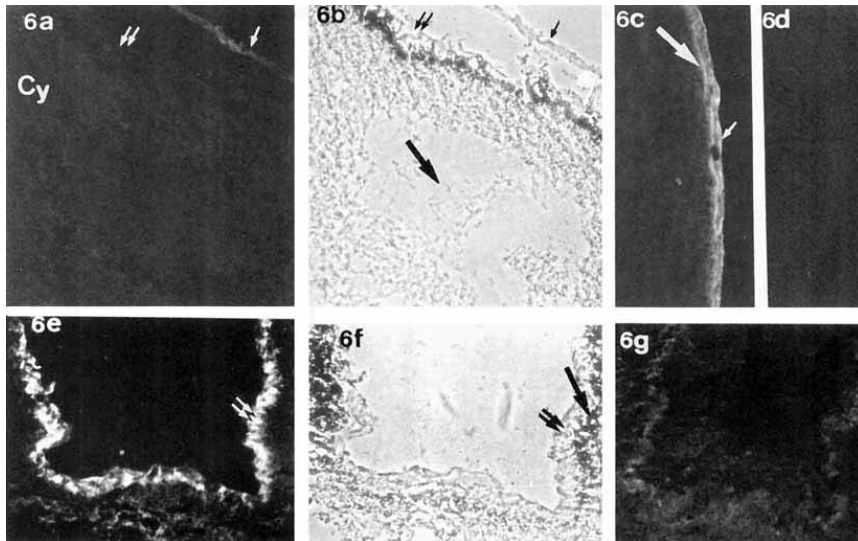


Fig. 6. Oocyte and egg immunofluorescent staining with antitropomyosin antibody. $\times 250$. Cy, cytoplasm. **a:** GA incubated with antitropomyosin. Arrow, vitelline envelope. Double arrow, peripheral cytoplasm of the GA. **b:** Phase contrast micrograph of the same section of **a**. Large arrow, germinal vesicle. Small arrow, vitelline envelope. Double arrow, peripheral cytoplasm of the GA. **c:** Oocyte animal hemisphere incubated with antitropomyosin. A rim of cortical positivity is evident in the cortex (large arrow). The vitelline envelope

positivity (small arrow) will be described elsewhere. **d:** Control section incubated with normal guinea pig serum. **e:** Egg dimple incubated with antitropomyosin. A rod-like pattern of fluorescence (double arrow) is present in the peripheral cytoplasm (compare with **f**). **f:** Phase-contrast micrograph of the same section shown in **3**. Double arrow, peripheral cytoplasm. Arrow, layer of pigment granules located in the deeper cytoplasm. **g:** Dimple control section incubated with normal guinea pig serum.

TABLE 3. Positivity to the Immunostainings and the Variable Resistance to ADF*

| | ADF + antiactin | HAA or RAA | Inactivated NS ^b and HAA or RAA | Anti- tropo- myosin |
|---------------|-----------------------|------------------|--|---------------------------|
| GA | ++ | +++ | +++ | 0 |
| Oocyte cortex | + or ++ | +++ | +++ | + |
| Dimple | 0 | ++++ | ++++ | +++ |
| Egg cortex | 0 | +++ | +++ | ++ |

*We used an arbitrary scale of 0 to + + + + to indicate relative staining intensity.

HAA, human antiactin; RAA, rabbit antiactin.

^bIn the NS, the ADF activity was abolished (see Materials and Methods).

association with actin stabilizing proteins (Low et al., 1981; Korn, 1982; Weeds, 1982; Stossel et al., 1985; Pollard and Cooper, 1986). According to our results, tropomyosin is not a likely candidate for the stabilization of microfilaments in our samples. Neither the actin microfilaments of the egg cortex nor those in the dimple are resistant to ADF despite the presence of tropomyosin in both regions. In oocytes, both GA and cortex microfilaments are resistant to ADF, yet tropomyosin has been localized only in the cortex (see Table 2).

Taken together our data suggest that both the resis-

tance to ADF and the difference in the interfilament distance between dimple and GA microfilament may be explained in terms of actin-associated proteins, most of which remain presently unknown.

The different localizations of tropomyosin in oocytes and eggs indicate that a redistribution of such a protein occurs during the meiotic transition from primary oocytes to oocytes in metaphase II. These changes in tropomyosin distribution mainly involve the region of the GA during its transformation into dimple. During this process, the microvilli bundles are profoundly remodeled by the insertion of new vesicles in the plasma membrane of the GA (Denis-Donini and Campanella, 1977). Particularly, in this transitional stage, the forming microvilli lack bundles of microfilaments and exhibit a tight network of microfilaments at their center. The microfilament bundles appear when the dimple formation is complete (Campanella, unpublished observations). In the present work, we have shown that a new organization of microfilament bundles occurs as a result of these changes. In addition to tropomyosin, also spectrin (Campanella et al., 1988) as well as Cl⁻ channels (Nuccitelli et al., 1988) become segregated in this region. These are all manifestations of pronounced specialization during the preparation of the oocyte for fertilization.

In conclusion, by various experimental approaches, we have assessed different types of cytoskeletal organization in two maturation stages of *D. pictus* oocytes. Further work is needed to elucidate the mechanism responsible for these differences.

ACKNOWLEDGMENTS

We acknowledge Dr. R. Mazzarella for suggestions, Messrs J.C. Rumbeli and E. Denking for expert photographic work, and Dr. A. Cirillo for revising the manuscript. Part of this work was carried out at the "Centro di Microscopia Elettronica," Faculty of Science, University of Naples. This work was supported by the Swiss National Science Foundation (grant 3.107-0.85) and by a 40% MPI of the Italian Ministry of Education.

REFERENCES

Campanella C, Gabbiani G (1980): Cytoskeletal and contractile proteins in coelomic oocytes, unfertilized and fertilized eggs of *Discoglossus pictus* (Anura). *Gamete Res* 3:99-114.

Campanella, C (1975): The site of spermatozoon entrance in the unfertilized egg of *Discoglossus pictus* (Anura): An electron microscopy study *Biol. Reprod.* 12:439-447.

Campanella C, Rungger-Brandle E, Gabbiani G (1982): Immunolocalization of α -actinin in an amphibian egg (*Discoglossus pictus*). In M.M. Burger, R. Weber (eds): "Embryonic Development, Part B: Cellular Aspects." New York: Alan R. Liss, pp 45-53.

Campanella C, Carotenuto R, Gabbiani G (1988): Anti-spectrin antibodies stain the oocyte nucleus and the site of *Discoglossus pictus* egg where anionic channels are segregated. Submitted.

Chaponnier C, Kohler L, Gabbiani G (1977): Fixation of human anti-actin auto-antibodies on skeletal muscle fibres. *Clin Exp Immunol* 27:278-284.

Chaponnier C, Borgia R, Rungger-Brandle E, Weil R, Gabbiani G (1979): An actin-destabilizing factor is present in human plasma. *Experientia* 35:1030-1040.

Chaponnier C, Patebex P, Gabbiani G (1985): Human plasma actin-depolymerizing factor. Purification, biological activity and localization in leucocytes and platelets. *Eur J Biochem* 146:267-276.

Denis-Donini S, Campanella C (1977): Ultrastructural and lectin-binding changes during the formation of the animal dimple in oocytes of *Discoglossus pictus* (Anura). *Dev Biol* 61:140-152.

Franke W, Rathke PC, Seib E, Trendelenburg MF, Osborn M, Weber K (1976): Distribution and mode of arrangement of microfilamentous structures and actin in the cortex of the amphibian oocyte. *Cytobiology* 14:111-130.

Gabbiani G, Chaponnier C, Zumbe C, Vassalli P (1977): Actin and tubulin co-cap with surface immunoglobulins in mouse B lymphocytes. *Nature* 269:679-698.

Gabbiani G, Gabbiani F, Heimark RL, Schwartz SN (1984): Organi-

zation of actin cytoskeleton during early endothelial regeneration in vitro. *J. Cell Sci* 66:39-50.

Gall L, Picheral B, Gounon P (1983): Cytochemical evidence for the presence of intermediate filaments and microfilaments in the egg of *Xenopus laevis*. *Biol Cell* 47:331-342.

Hanson J, Lowry Y (1963): The structure of F-actin filaments isolated from muscle. *J Mol Biol* 6:46-80.

Harris DA, Schwartz JH (1981): Characterization of brevin, a serum protein that shortens actin filaments. *Proc Natl Acad Sci USA* 78: 6798-6802.

Hibbard H (1928): Contribution à l'étude de l'ovogenèse de la fécondation et de l'histogenèse chez *Discoglossus pictus* Otth. *Arch Biol* 38:251-326.

Huxley HE (1957): The double array of filaments in cross-striated muscle. *J Biophys Biochem Cytol* 3:631-647.

Ischimoda-Tagagi T (1979): Localization of tropomyosin in sea urchin eggs. *Exp Cell Res* 119:423-428.

Knappes GG, Carlsen F (1962): The ultrastructure of the Z disc in skeletal muscle. *J Cell Biol* 13:323-335.

Kocher O, Shalli O, Bloom WS, Gabbiani G (1984): Cytoskeleton of rat aortic smooth muscle cells. Normal conditions and experimental intimal thickening. *Lab Invest* 50:645-652.

Korn ED (1982): Actin polymerization and its regulation by proteins from non-muscle cells. *Physiol Rev* 62:672-737.

Lehrer SS (1972): The crosslinking of actin and tropomyosin by glutaraldehyde. *Biochem Biophys Res Commun* 48:967-976.

Low RB, Chaponnier C, Gabbiani G (1981): Organization of actin in epithelial cells during regenerative and neoplastic conditions. *Lab Invest* 44:359-367.

Matsudaira P, Mandelkow E, Renner W, Hesterberg LK, Weber K (1983): Role of fimbrin and villin in determining the interfilament distances of actin bundles. *Nature* 301:209-214.

Maupin-Szamier P, Pollard TD (1978): Actin filament destruction by osmium tetroxide. *J Cell Biol* 77:837-852.

Nuccitelli R, Kline D, Busa W, Talevi R, Campanella C (1988): The activation current and intracellular calcium increase in the egg of the frog *Discoglossus pictus*. *Dev Biol* (in press).

Pollard TD, Cooper JA (1986): Actin and actin-binding proteins. A critical evaluation of mechanism and functions. *Annu Rev Biochem* 55:987-1035.

Stossel TP, Chaponnier C, Ezzel RM, Hartwig JH, Janmey PA, Kwiatkowski DL, Lind SE, Smith DB, Southwick FS, Yin HL, Zamer KS (1985): Nonmuscle actin-binding proteins. *Annu Rev Cell Biol* 1:353-402.

Suzuki K, Yamaguchi M, Sekine T (1978): Two forms of chicken gizzard F-actin depending on preparation with or without added calcium. *J Biochem* 83:869-878.

Talevi R, Campanella C (1988): Fertilization in *Discoglossus pictus* (Anura). I. Sperm-egg interactions in distinct regions of the dimple and occurrence of a late stage of sperm penetration. *Dev Biol* 130: 524-535.

Temink JHM, Spiele H (1979): Preservation of cytoskeletal element for electron microscopy. *Cell Biol Int Rep* 2:51-59.

Weeds A (1982): Actin-binding proteins-regulators of cell architecture and motility. *Nature* 296:811-16.

Yin HL, Kwiatkowski DJ, Mole JE, Cole FS (1984): Structure and biosynthesis of cytoplasmic and secreted variants of gelsolin. *J Biol Chem* 259:5271-5276.

Antispectrin Antibodies Stain the Oocyte Nucleus and the Site of Fertilization Channels in the Egg of *Discoglossus pictus* (Anura)

CHIARA CAMPANELLA,¹ ROSA CAROTENUTO,² AND G. GABBIANI³

¹Dipartimento di Scienze e Tecnologie Biomediche e di Biometria, Università di L'Aquila, Collemaggio, L'Aquila, Italy;

²Dipartimento di Biologia Evolutiva e Comparata, Napoli, Italy;

³Departement de Pathologie, Université de Genève, Genève, Switzerland

ABSTRACT In *Discoglossus pictus* eggs, only the dimple contains ionic channels active at fertilization; in particular, chloride channels are found in the central portion of the dimple, which is also the site of sperm penetration. Moreover the dimple hosts an imposing cytoskeleton, consisting of a cortical network and bundles of microfilaments extending from the microvilli. Since spectrin cross links actin and is connected through ankyrin to anion transporters in the plasma membrane of erythrocytes as well as to anion channels in other cells, we studied, in *D. pictus* egg, the relationship between the localization of spectrin and the high polarization of ionic channels and cytoskeletal organization. By means of immunocytochemistry, we localized spectrin exclusively in the egg dimple. In an attempt to trace back the source of spectrin localization, we immunostained sections of *D. pictus* ovary and localized spectrin in the nuclei of previtellogenic oocytes, where actin is also present. Antispectrin staining remained until germinal vesicle breakdown. By contrast, a cortical localization was found only when the oocytes divided into two hemispheres and into the germinative area (GA), which, after germinal vesicle breakdown, gives rise to the dimple. At this stage the antispectrin signal was particularly strong in the GA. Using Rho-pialloidin, we also established that spectrin is generally present where F-actin is found. However, spectrin and F-actin do not have the same pattern of fluorescence. In conclusion, our data suggest that spectrin may play a role in oocyte and egg polarity. In eggs, it could be instrumental in anchoring to the cytoskeleton membrane proteins such as receptors and ionic channels, including chloride-permeable channels.

Key Words: Spectrin, Ionic channels, Dimple

INTRODUCTION

Unique among amphibians, the egg of *Discoglossus pictus* has an indentation at the center of the animal

hemisphere, known as "the animal dimple" (Hibbard, 1928; Campanella, 1975). The dimple is about 300 μm wide and 150 μm deep and is the site of sperm penetration. It forms, after ovulation and first polar body extrusion, from the invagination and the reshaping of the oocyte disk-shaped germinative area (GA), which is typical of this species (for further details, see Denis-Donini and Campanella, 1977).

In the dimple, specific factors are segregated that enable fusion of spermatozoa and egg activation and that define the highly polarized organization of *D. pictus* egg (Talevi and Campanella, 1988). In particular, a specific cytoskeletal organization is found in the dimple. Actin microfilament bundles extend from the central core of finger-shaped microvilli into the peripheral cytoplasm for about 12 μm (Campanella and Gabbiani, 1980). Actin, myosin, and alpha-actinin, as well as tubulin, have been localized in this region. These proteins are found also in the GA, where, however, they are associated with a different type of microvilli and with a different cytoplasmic organization (Campanella and Gabbiani, 1980; Campanella et al., 1982).

More recently, electrophysiologic studies have revealed chloride channels in the central portion of the dimple membrane (D_1) a disk of 200 μm , where fertilization occurs. Other channels are present in the lateral walls of the dimple (Nuccitelli et al., 1988). In the eggs of other anuran species, chloride-permeable channels are generally located all over the plasma membrane, with the highest concentration occurring at the site of fertilization, the animal hemisphere (Kline and Nuccitelli, 1985; Jaffe and Schlichter, 1985; Jaffe et al., 1985; see also Cross and Elinson, 1980).

In erythrocytes, the anion transporters, which are integral membrane proteins, are linked to a cytoplas-

Received August 4, 1989; accepted December 21, 1989.

Address reprint requests to Chiara Campanella, Dipartimento di Scienze e Tecnologie Biomediche e di Biometria, Università di L'Aquila, Collemaggio, L'Aquila, Italy.

mic protein meshwork composed of ankyrin, spectrin, and actin (for reviews, see Branton et al., 1981, Marchesi, 1985). Spectrin-like proteins (i.e., brain fodrin and the terminal web protein TW260/240) have been described in several cells. Like erythrocyte spectrin, they all bind actin and calmodulin (for a review, see Lazarides and Nelson, 1982). In particular, spectrin has been localized in kidney cells together with the anion transporter and ankyrin-like molecules (Drenckhahn et al., 1985). Both fodrin (Schatten et al., 1986) and spectrin (Fishkind et al., 1987) are present in the cortex of sea urchin eggs and of mouse eggs (Damjanov et al., 1986; Schatten et al., 1986).

In the dimple, the highly polarized localization of actin microfilaments in the cortex and of ionic channels in the plasma membrane prompted us to ask whether the cytoskeleton plays a role in maintaining these ionic channel domains. In particular, we investigated whether spectrin is present in *D. pictus* egg. Using an antibody against brain spectrin, we found a relationship between the presence of spectrin and polarity of *D. pictus* egg, the protein being localized exclusively in the peripheral cytoplasm of the dimple. We next investigated where and when during oogenesis spectrin is present. A similar relationship between polarity and cortical localization of spectrin was found in growing oocytes. Moreover, spectrin was also detected in the oocyte nucleus. Finally, following phalloidin staining, we found a relationship between spectrin and cortical actin localization.

MATERIALS AND METHODS

Animals and Samples

Adult females *D. pictus* were collected in the neighborhood of Palermo, Italy, during February–March. Oocytes of various sizes were obtained by excision of pieces of ovaries. To obtain coelomic oocytes and eggs, females were injected in the dorsal lymphatic sac with 200 U Prohase (Serono, Italy) in amphibian Ringer solution. About 8 hr later, coelomic oocytes were recovered from the body cavity; eggs were collected from the ovisac about 18 hr after hormone injection.

Antispectrin Antibody and Phalloidin

Affinity-purified antibodies raised in rabbit against human brain spectrin (a gift from Dr. V. Marchesi, Department of Pathology, Yale University School of Medicine, New Haven, CT) were used as previously described (Pratt et al., 1984). Rhodamine-phalloidin (Rho-phalloidin) (Molecular Probes, Inc., Eugene, OR) (100 U/ml) was diluted from 1:100 to 1:1,000 V/V with phosphate-buffered solution (PBS) before being used.

Immunofluorescent and Phalloidin Staining

A total of 80 oocytes and 29 eggs from 21 females were examined in this study. Five micrometer frozen sections were utilized unfixed or fixed either in acetone at 20°C for 5 min or in 1% formaldehyde prepared from

paraformaldehyde (PFA) and diluted in PBS for 8 min. The sections were dried and then incubated either with antispectrin for 45 min or with Rho-phalloidin for 30 min. The same incubation times were used for all the sections.

The samples were incubated with fluorescein-conjugated IgG fraction to rabbit IgG (Behringwerke AG, Marburg/Lahn, Federal Republic of Germany). The sections were rinsed with PBS and mounted in 90% glycerol in PBS, after which the level of fluorescence was compared with that in control sections treated in parallel with rabbit gamma globulins (Serva, Heidelberg, Federal Republic of Germany). Thus the antispectrin fluorescence was specific in all the examined samples. Alternatively, the fluorescence was compared with that obtained after Rho-phalloidin staining in parallel sections.

Sections were also incubated with antispectrin antibodies, then with Rho-phalloidin, and finally were exposed to fluorescein-conjugated IgG. However, this procedure rarely gave satisfactory results; both “stainings” were markedly attenuated compared with samples incubated separately with the antibodies or with Rho-phalloidin. Photographs were taken on a Zeiss or a Leitz UV photomicroscope using Ilford black and white HP5 film.

RESULTS

Ovarian Oocytes

In all the egg batches studied, antispectrin and Rho-phalloidin staining first appeared in oocytes that had a diameter of 200 μm and continued throughout oogenesis. It was related to both nucleus and cortex.

Nucleus. The nucleus of both previtellogenic and vitellogenic oocytes up to the end of their growth period showed spots of intense antispectrin staining (Fig. 1a). Control sections incubated with rabbit gammaglobulins were negative (Fig. 1c). Some spots were also observed around the nucleus (Fig. 1a and b) and at the periphery of previtellogenic oocytes. They do not derive from shift of the grains from the nucleus into the cytoplasm, caused by the sectioning procedure, since they were also seen in oocyte sections where the nucleus is absent. A comparison of Figure 1d with Figure 1e shows that the fluorescent grains are located on strands of nuclear contents. They do not seem to be related to any grain-like structure. Phalloidin also stained the nuclei. However, unlike antispectrin staining, it revealed fibrillar material (Fig. 1f).

Cytoplasm. In late-stage oocytes, the cytoplasm was lightly stained with antispectrin. A rim of spectrin was clearly visible in the cortex of 900 μm oocytes that were regionalized in animal and vegetal halves (Fig. 2a). The fluorescence was more evident in the animal hemisphere (Fig. 2b) than in the vegetal half (Fig. 2c). The ovarian tissue that surrounds the oocyte was also lightly stained with antispectrin (Fig. 2b,c). The 900 μm oocytes differentiate a disk, the GA, at the center of

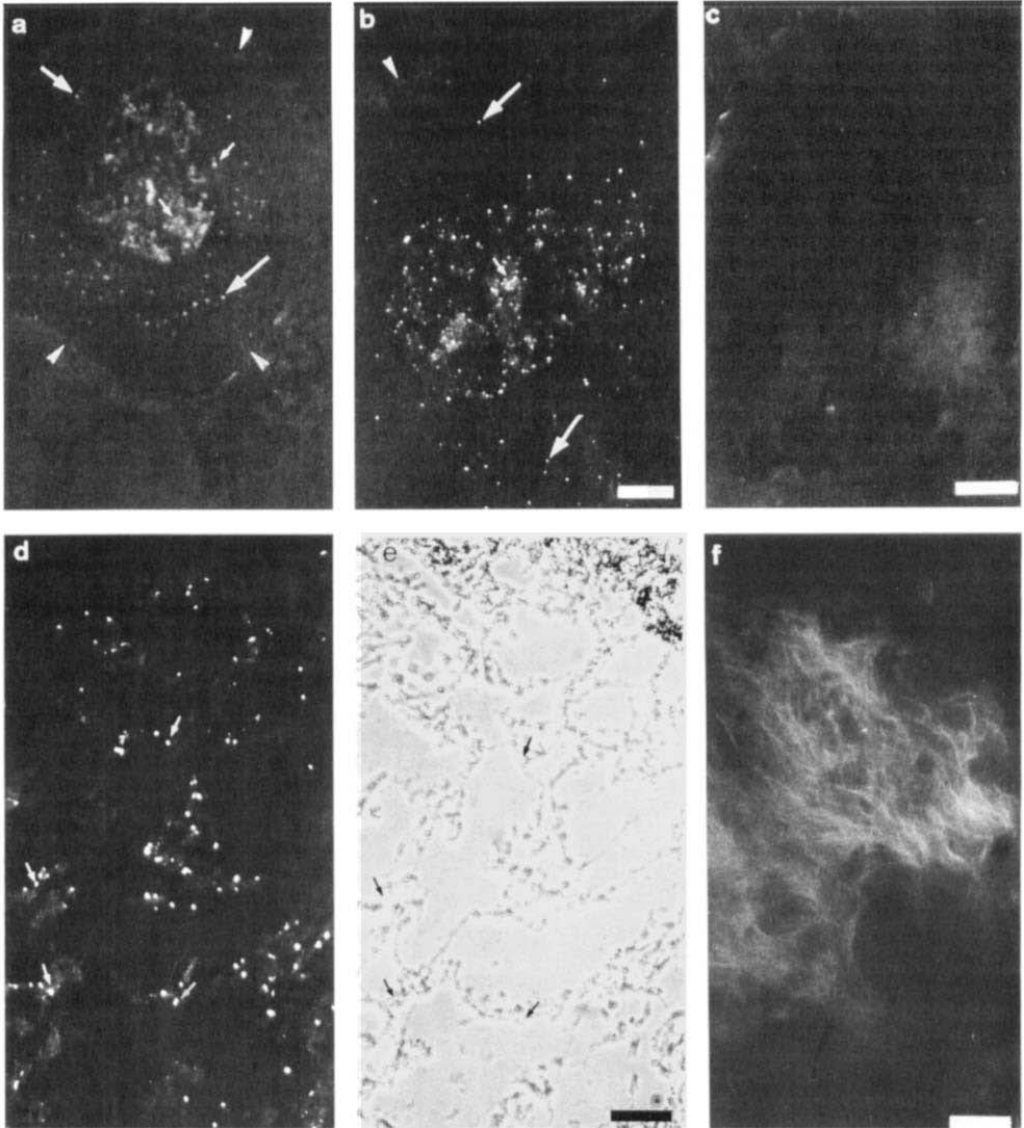


Fig. 1. Oocyte nuclei. **a,b:** Previtellogenic oocytes incubated with antispectrin. The fluorescence is in spots in the nucleus (small arrows). Some spots are seen also in the perinuclear cytoplasm (arrows). The arrowheads indicate the oocyte boundary. $\times 270$. Bar = $37 \mu\text{m}$. **c:** Control section incubated with rabbit gammaglobulins: no staining. $\times 270$. Bar = $37 \mu\text{m}$. **d:** Nucleus of a fully grown oocyte incubated with antispectrin. **e:** Phase-contrast micrograph of the

same section. $\times 270$. Bar = $37 \mu\text{m}$. An examination of **d** and **e** shows that the fluorescent spots are on strands of the nuclear contents (small arrows). There are no grain-like structures corresponding to the fluorescent spots. **f:** Rho-phalloidin staining of a fully grown oocyte nucleus. A network of fluorescent fibrils is seen in the nucleus. $\times 590$. Bar = $18 \mu\text{m}$.

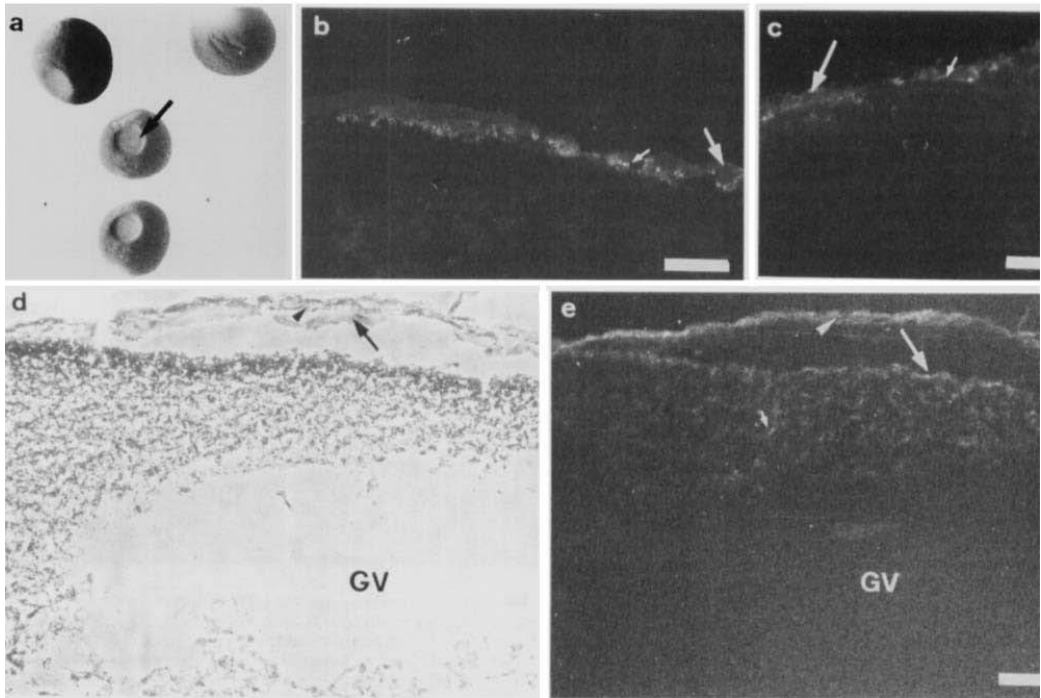


Fig. 2. a: Oocytes showing regionalization in animal hemisphere, vegetal hemisphere, and GA. $\times 12$. b–e: Fully grown oocytes incubated with antispectrin antibodies. b: Animal half. There is a thin rim of fluorescence in the cortex (small arrow), whereas the ovarian tissue is only slightly positive (arrow). $\times 390$. Bar = 25 μm . c: Vegetal half. A rim of fluorescence is barely discernable in the cortex (small arrow). Large arrow, ovarian tissue. $\times 390$. Bar = 25 μm . d: Contrast micrograph of the central portion of the germinative area. Arrowhead, ovarian tissue; arrow, vitelline envelope; GV, germinal vesicle. e: Same section incubated with antispectrin. Arrow, cortical positivity; small arrow, fluorescence in the cytoplasm. Arrowhead, ovarian tissue; GV, germinal vesicle. $\times 240$. Bar = 41 μm .

the animal half (Fig. 2a). The germinal vesicle is located in the cytoplasm below this region (Fig. 2d,c). At the level of the GA, the vitelline envelope and the ovarian tissue are separated by the perivitelline material (Andreuccetti and Campanella, 1980) from the oocyte surface (Fig. 2d,e). The GA cortex was less positive to antispectrin than the rest of the animal hemisphere cortex (Fig. 2e).

As is shown in Figure 3a, Rho-phalloidin stained the cortex of oocytes in advanced stages of vitellogenesis (about 600 μm in diameter), when microfilament bundles appear in microvilli (Andreuccetti and Campanella, 1982). The fluorescent staining remained from this stage of growth throughout oogenesis and was more intense in the animal half than in the vegetal half (Fig. 3b,d).

Figures 3b and c are micrographs of the same section incubated with Rho-phalloidin (Fig. 3b) and antispectrin antibodies (Fig. 3c). Note the difference between the filamentous pattern of the Rho-phalloidin-treated

sample and the amorphous pattern deriving from antispectrin incubation. The staining pattern observed in the GA cortex was similar to that of the rest of the animal hemisphere (data not shown; see also Campanella and Gabbiani, 1980).

Coelomic Oocytes

In freshly ovulated coelomic oocytes, the nucleoplasm is found in the position previously occupied by the intact germinal vesicle, although at this stage the nuclear envelope has already dissolved. In oocytes where meiosis has progressed further and the first polar body has already extruded, the dimple starts forming by gradual invagination and extension of the GA plasma membrane (Denis-Donini and Campanella, 1977) (Fig. 4a–c). Antispectrin (Fig. 4b, and cf. Fig. 2e) and Rho-phalloidin staining were greatly enhanced in the GA of these sections with respect to ovarian GA

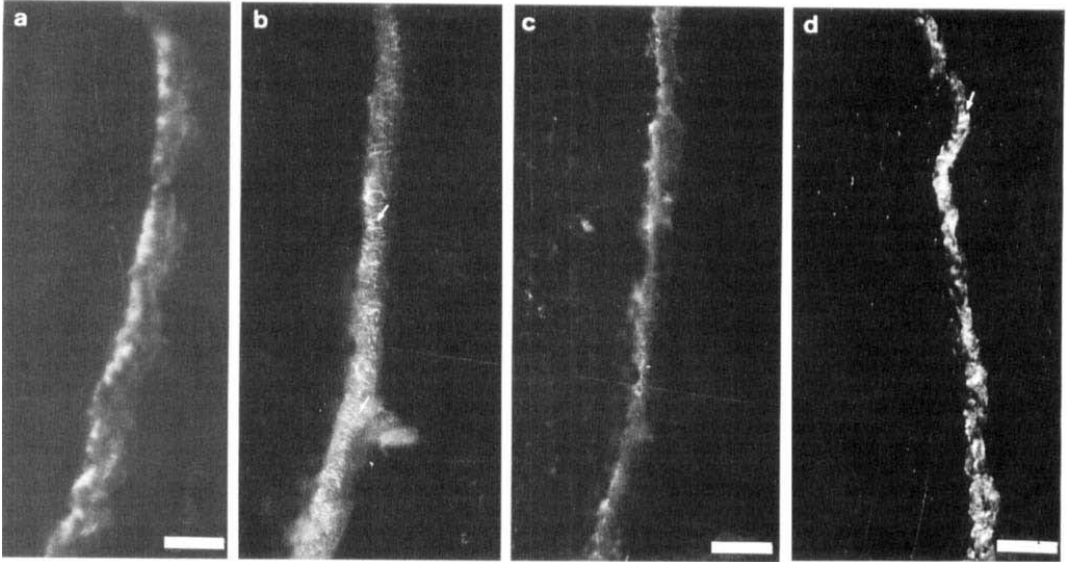


Fig. 3. a: Vitellogenic oocyte stained with Rho-phalloidin. $\times 390$. Bar = 25 μm . The section shown in b and c is of a fully grown oocyte and has been incubated with both Rho-phalloidin and antispectrin. Note the weak fluorescence. b: Rho-phalloidin fluorescence. c: Positivity to antispectrin. b Shows thin fluorescent filaments (small arrows) in the oocyte cortex, perpendicular to the plasma membrane.

These probably correspond to the actin F microfilaments present in the ovarian microvilli core. Note the different staining patterns arising from Rho-phalloidin (b) and antispectrin staining (c). $\times 390$. Bar = 25 μm . d: Vegetal hemisphere. Here the fluorescent filaments stained by Rho-phalloidin are shorter than in the animal half (b). $\times 390$. Bar = 25 μm .

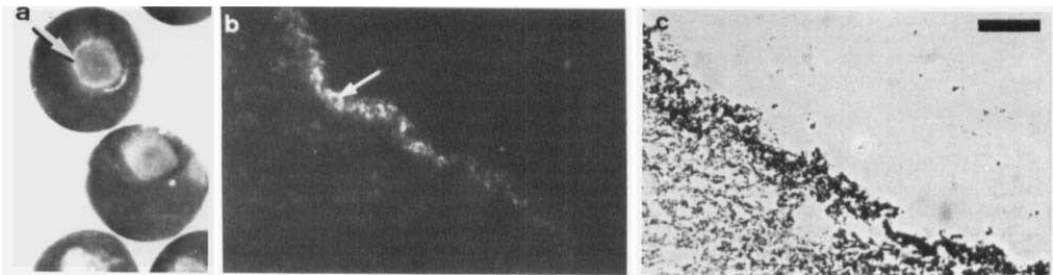


Fig. 4. a: Oocyte with GA (arrow) in the early stages of its transformation into a dimple. A comparison of this micrograph with Figure 2a showing an ovarian GA illustrates well the process of invagination undergone by the GA. $\times 12$. b: GA transforming into a dimple in a

coelomic oocyte section incubated with antispectrin antibody. Arrow, antispectrin staining. c: Phase contrast of a serial section. Arrow, surface of the GA. $\times 390$. Bar = 25 μm .

sections. The cortex of these oocytes retained the antispectrin staining (data not shown).

Uterine Eggs

The dimple forms during the transition of the oocytes in the oviduct. Therefore, eggs collected from the ovisac display their final features (inset, Fig. 5a). In sections of uterine eggs, the dimple was intensely stained with

antispectrin (Fig. 5a), whereas no fluorescence was observed in the rest of the egg (Fig. 5c) or in control sections treated in parallel with rabbit gammaglobulins (Fig. 5b). Rho-phalloidin strongly stained the dimple (Fig. 5d,e) (see also Campanella and Gabbiani, 1980). Our data on the localization and intensity of spectrin and actin staining during the different stages of oogenesis are presented in Figures 6 and 7.

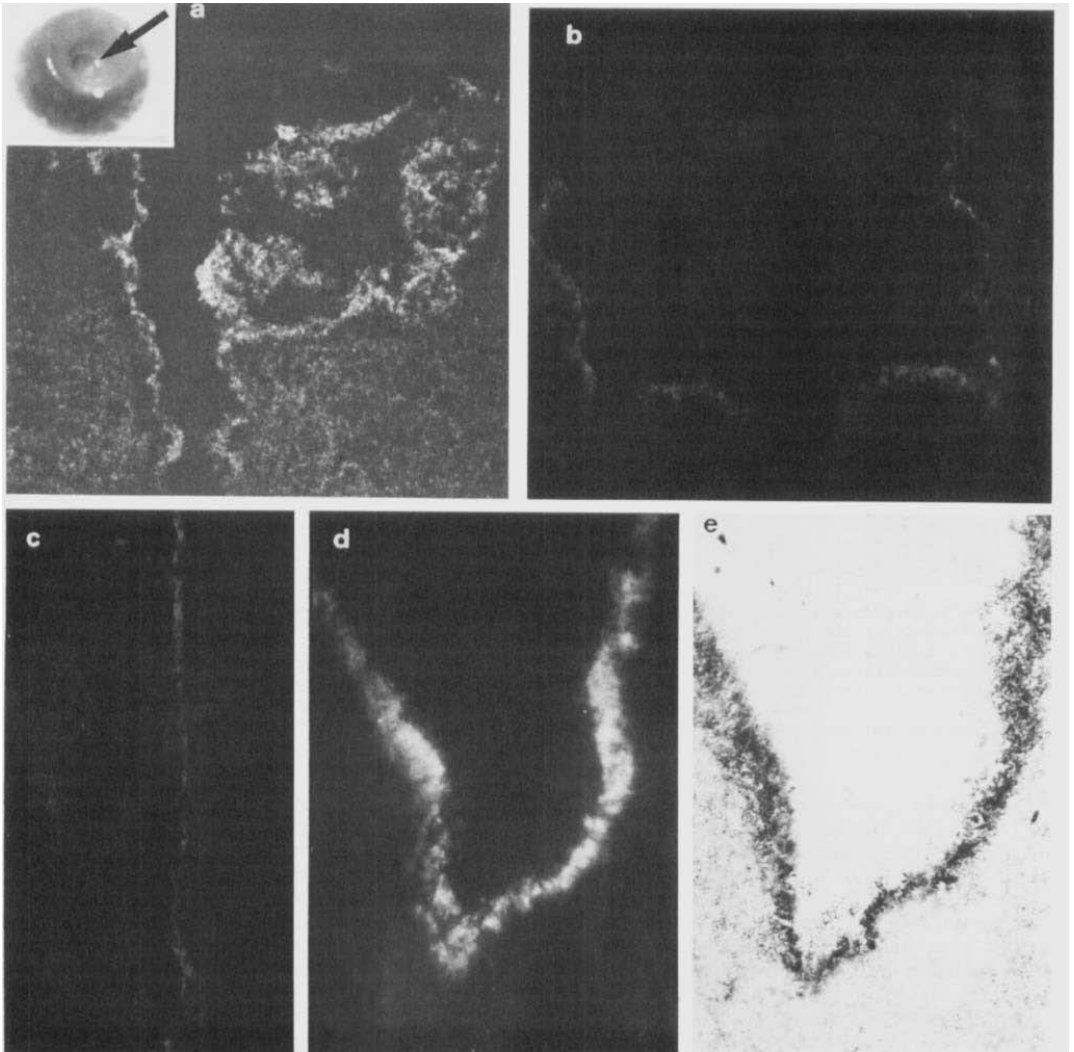


Fig. 5. Egg collected from the ovisac. **a:** Intense antispectrin staining in the dimple cortex. The shape of the dimple in this micrograph is tubular rather than hemispherical because it has been sectioned laterally. $\times 310$. **Inset:** The arrow shows the dimple at the center of the egg animal half. $\times 12$. **b:** Control dimple section incubated

with rabbit IgG. No staining. $\times 310$. **c:** Cortex incubated with anti-spectrin showing no staining. $\times 310$. **d:** Dimple stained with Rhodalloidin. Note the strong fluorescence in the dimple cortex. **e:** Corresponding phase contrast. $\times 500$.

DISCUSSION

In this study antispectrin immunostaining was followed throughout *D. pictus* oocyte growth and was shown to be localized first in the nucleus, then later in oogenesis also in the cortex, and finally only in the egg dimple. In the nucleus of previtellogenic oocytes—

which are blocked in diplotene and display lampbrush chromosomes—the fluorescent spots observed are similar in size to the spheres present in *Discoglossus* lampbrush chromosomes (Capriglione, 1984). However, at our level of resolution, the fluorescence did not appear to be related to any discrete structure. Rho-

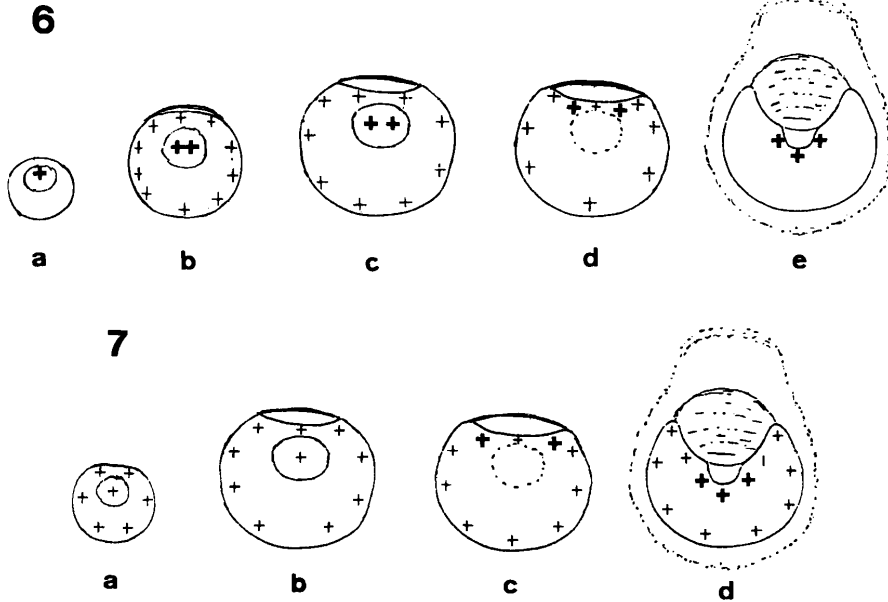


Fig. 6. Antispectrin staining in growing oocytes. Light crosses, medium-low antispectrin staining; dark crosses, intense antispectrin staining. In b, c, and d, the vitelline envelope is evident because it has lifted off the germinative area. In d, the germinative vesicle has broken down, and the GA starts transforming into dimple. In e, an ovoided egg is shown. This is covered by jelly coats. The lens-shaped "jelly plug" lies in a large concavity at the animal hemisphere. At its

center, the concavity is further indented by the presence of the dimple. Size of oocytes as follows: a, 250 μm; b, 1,000 μm; c,d,e, 1,800 μm.

Fig. 7. Rho-phalloidin staining in growing oocytes. Light crosses, Rho-phalloidin staining; dark crosses, very intense Rho-phalloidin staining. Size of oocytes as follows: a, 600 μm; b,c,d, 1,800 μm.

phalloidin staining showed a fine fibrillar network (see also Gounon and Karsenti, 1981, and Parfenov and Galaktionov, 1987), which indicates that F-actin and spectrin do not have the same staining pattern.

Several cytoskeletal proteins, particularly actin, tubulin, and myosin, have been shown in the nucleus of amphibian oocytes (Clark and Merriam, 1977; Clark and Rosebaum, 1979). To our knowledge, the intranuclear localization of spectrin is reported here for the first time. A 240×10^3 Mr calmodulin-binding protein has been found in liver cell nuclei (Bachst and Carafoli, 1987). It is feasible that spectrin, because of its ability to cross-link actin, participates in the regulation of actin functions (Lestourgeon et al., 1975; Paulin et al., 1976; Goldstein et al., 1977; Karsenti et al., 1978; Rungger et al., 1979; Scheer et al., 1984).

In amphibians, the growing oocytes have a polarized organization. Indeed, during oogenesis, many cell components become organized along a gradient (for reviews, see Vacquier, 1981; Elinson, 1980), the center of the gradient being the animal pole. In the specific case of *Discoglossus*, the program of polarization of primary oocytes terminates with the differentiation of the animal and vegetal hemispheres and of the GA disk,

whereas that of oocytes arrested in metaphase II (normally described as "eggs"), terminates with the formation of the dimple. As the dimple is derived from the GA, it is evident that the GA contains several constituents necessary for the dimple formation.

While Rho-phalloidin staining first appeared in oocytes in the early stages of growth, antispectrin staining appeared in more advanced stages of oogenesis, when in the oocyte pigment becomes segregated in the animal half, and the GA is differentiated. Rho-phalloidin staining appeared as filaments perpendicular to the oocyte surface and was related to the microfilament bundles located in the cortical cytoplasm, particularly in the microvilli (Wischnitzer, 1966; Franke et al., 1976). Spectrin was localized mostly in the animal hemisphere cortex, including the GA cortex, where it probably cross links the cytoplasmic rootlets as well as the network of actin microfilaments located in the cortex of the whole oocyte (see Campanella and Gabbiani, 1980). Therefore, it appears that spectrin is first localized in the cortex when the oocyte achieves cortical polarity.

The connection between cell polarity and spectrin localization is more evident in the egg, where spectrin

is localized only in the dimple. In this site there is a specific actin microfilament arrangement (this paper and Campanella and Gabbiani, 1980). It has been suggested that this organization constitutes a stable cap that serves to maintain the prerequisites for sperm-egg fusion and for the onset of development (Campanella and Gabbiani, 1980; Talevi and Campanella, 1988). We know that chloride channels are present in the plasma membrane of D_1 because, upon activation, a large chloride-transported current is detected at this site, whereas other ionic channels are present in the plasma membrane of the dimple walls (Nuccitelli et al., 1988). Therefore, spectrin could serve to anchor these channels to the rest of the cytoskeleton, in a fashion similar to the anion transporters.

In developing erythroids (for a review, see Lazarides and Moon, 1984) and myotubes (Nelson and Lazarides, 1985), the final assembly of newly synthesized spectrin subunits occurs after the synthesis of anion transporters. The overall assembly process was postulated to depend on the number of anion channels available for binding to the cytoskeleton (Lazarides and Moon, 1984). In *D. pictus* is the final spectrin localization in the cortex related to the final ionic channels distribution in the membrane? Chloride channels are generally present in anuran oocytes late in oogenesis (Robinson, 1979; Barish, 1983; Miledi and Parker, 1984). Although data are lacking on ionic channels in *D. pictus* oocytes, preliminary findings indicate that active channels, whose nature has yet to be determined, are more numerous at the GA of oocytes than in the dimple, suggesting that a redistribution or an insertion of channels occurs when the GA transforms into the dimple (Nuccitelli et al., 1988). During dimple formation, vesicles are inserted in the GA plasma membrane, thus leading to a substantial change in the composition of the plasma membrane (Denis-Donini and Campanella, 1977). We show that the transforming GA is more positive to antispectrin antibodies than is the ovarian GA. This suggests that spectrin gradually increases in the GA during its transformation into dimple. Therefore, changes in the membrane, possibly involving rearrangement or insertion of new chloride channels, and the increase of spectrin in the GA both occur during the GA-dimple transition.

What is the source of the spectrin that enters the differentiating dimple? Spectrin might redistribute along the oocyte cortex and segregate in the dimple. A second possibility is that spectrin might migrate to the GA from the germinal vesicle. In fact, we found that antispectrin staining was maintained in the germinal vesicle until the last stages of oogenesis. It disappeared following dissolution of the nuclear envelope, at which point staining became more intense in the overhanging GA cortex. This implies a direct participation of the nucleus content in the polarization of stage II oocytes. Interestingly, in mouse eggs, fodrin localizes at the animal pole at the site of the first polar body extrusion

(Schatten et al., 1986), suggesting a relationship with egg polarity. Furthermore, changes in spectrin distribution have been observed in the mouse during blastomere polarization at compaction (Reima and Lethonen, 1985; Sobel et al., 1988). Further studies are required to test these hypotheses and to investigate the chemical nature of the molecules that cross react with antispectrin in our samples.

ACKNOWLEDGMENTS

We thank Dr. R. Nuccitelli whose conversation prompted this study and Dr. B. Dale for reading the manuscript and making suggestions. This study was supported by 40% grants of the Italian Ministry of Public Education.

REFERENCES

- Andreuccetti P, Campanella C (1980): Origin and cytochemistry of the animal dimple granules in *Discoglossus pictus* (Anura) egg. *J Embryol Exp Morphol* 56:239-252.
- Andreuccetti P, Campanella C (1982): Regional differences in the pattern of vitellogenesis in the painted frog *Discoglossus pictus*. *Tissue Cell* 14:681-690.
- Bachst O, Carafoli E (1987): Calmodulin and calmodulin-binding proteins in liver cell nuclei. *J Biol Chem* 262:10786-10790.
- Barish ME (1983): A transient calcium-dependent chloride current in the immature *Xenopus* oocyte. *J Physiol* 342:309-325.
- Branton D, Cohen CM, Tyler J (1981): Interaction of cytoskeletal proteins on the human erythrocyte membrane. *Cell* 24:24-32.
- Campanella C (1975): The site of spermatozoon entrance in the unfertilized egg of *Discoglossus pictus* (Anura): An electron microscope study. *Biol Reprod* 12:439-447.
- Campanella C, Gabbiani G (1980): Cytoskeletal and contractile proteins in coelomic oocytes, unfertilized and fertilized eggs of *Discoglossus pictus* (Anura). *Gamete Res* 3:99-114.
- Campanella C, Rungger-Brandle E, Gabbiani G (1982): Immunolocalization of alpha-actinin in an amphibian egg (*Discoglossus pictus*). In M Burger and R Weber (eds): "Embryonic Development. Part B: Cellular Aspects." New York: Alan R. Liss, pp 45-53.
- Capriglione T (1984): Dati preliminari sui cromosomi lampbrush di *Discoglossus pictus*. *Boll Zool* 51:24.
- Clark TG, Merriam RW (1977): Diffusible and bound actin in nuclei of *Xenopus laevis* oocytes. *Cell* 12:883-891.
- Clark TG, Rosebaum JL (1979): An actin filament matrix in hand isolated nuclei of *X. laevis*. *Cell* 18:1101-1108.
- Cox JV, Moon RT, Lazarides E (1985): Anion transporter: Highly cell-type-specific expression of distinct polypeptides and transcripts in erythroid and nonerythroid cells. *J Cell Biol* 100:1548-1557.
- Cross NL (1981): Initiation of activation potential by an increase in intracellular calcium in eggs of the frog *Rana pipiens*. *Dev Biol* 85:380-384.
- Cross NL, Elinson RP (1980): A fast block to polyspermy in frogs mediated by changes in the membrane potential. *Dev Biol* 75:187-198.
- Damjanov I, Damjanov A, Letho VP, Virtanen I (1986): Spectrin in mouse gametogenesis and embryogenesis. *Dev Biol* 114:132-140.
- Denis-Donini S, Campanella C (1977): Ultrastructural and lectin binding changes during the formation of the animal dimple in oocytes of *Discoglossus pictus* (Anura). *Dev Biol* 61:140-152.
- Drenckhahn B, Schluter K, Allen BP, Bennett V (1985): Colocalization of band 3 with ankyrin and spectrin at the basal membrane of intercalated cell in rat kidney. *Science* 230:287-289.
- Elinson RP (1980): The amphibian cortex in fertilization and early development. In S Subteny and NK Wessels (eds): "The Cell Surface: Mediator of Developmental Processes." New York: Academic Press, pp 217-234.
- Fishkind DJ, Bonder EM, Begg DA (1987): Isolation and character-

- ization of sea urchin egg spectrin: Calcium modulation of spectrin-actin interaction. *Cell Motil Cytoskel* 7:304-314.
- Franke W, Rathke PC, Seib E, Trendelenburg MF, Osborn M, Weber K (1976): Distribution and mode of arrangement of microfilamentous structure and actin in the cortex of amphibian oocyte. *Cytobiology* 14:111-130.
- Goldstein L, Ko C, Errick J (1977): Nuclear actin: An apparent association with condensed chromatin. *Cell Biol Int Rep* 1:511-515.
- Gounon P, Karsenti E (1981): Involvement of contractile proteins in the changes in consistency of oocyte nucleoplasm of the newt *Pleurodeles waltii*. *J Cell Biol* 88:410-421.
- Grey RD, Bastiani DJ, Webb, Schertel ER (1982): An electrical block is required to prevent polyspermy in eggs fertilized by natural mating of *Xenopus laevis*. *Dev Biol* 89:475-484.
- Hibbard H (1928): Contribution à l'étude de l'ovogénèse, de la fécondation et de l'histogenèse chez *Discoglossus pictus* Otth. *Arch Biol* 32:251-326.
- Jaffe LA, Kado RT, Muncy L (1985): Propagating potassium and chloride conductances during activation and fertilization of the egg of the frog, *Rana pipiens*. *J Physiol* 368:227-242.
- Jaffe LA, Schlichter LC (1985): Fertilization-induced ionic conductances in eggs of the frog, *Rana pipiens*. *J Physiol* 258:299-319.
- Karsenti E, Gounon P, Bornens M (1978): Immunocytochemical study of lampbrush chromosomes: Presence of tubulin and actin. *Biol Cell* 31:219-224.
- Kline D (1988): Calcium-dependent events at fertilization of the frog egg: Injection of the calcium buffer blocks ion channels opening, exocytosis, and formation of pronuclei. *Dev Biol* 126:346-361.
- Kline D, Nuccitelli R (1985): The wave of activation current in the *Xenopus* egg. *Dev Biol* 111:471-487.
- Lazarides E, Moon RT (1984): Assembly and topogenesis of the spectrin-based membrane skeleton in erythroid development. *Cell* 37:354-356.
- Lazarides E, Nelson WJ (1982): Expression of spectrin in nonerythroid cells. *Cell* 31:505-508.
- Lestourgeon WM, Totten R, Forer A (1975): Major components of nuclear and chromosome non histone proteins. *Biochim Biophys Acta* 379:529-552.
- Marchesi VT (1985): Stabilizing infrastructure of cell membranes. *Annu Rev Cell Biol* 1:531-561.
- Miledi R, Parker I (1984): Chloride current induced by injection of calcium into *Xenopus* oocytes. *J Physiol* 351:173-183.
- Nelson WJ, Lazarides E (1985): Posttranslational control of membrane-skeleton (ankyrin and α -spectrin) assembly in early miogenesis. *J Cell Biol* 100:1726-1735.
- Nuccitelli R, Kline D, Busa W, Talevi R, Campanella C (1988): A highly localized intracellular calcium increase in the egg of the frog, *Discoglossus pictus*. *Dev Biol* 130:120-132.
- Paulin D, Nicolas JF, Jaquet M, Jakob H, Gros F, Jacob F (1976): Comparative protein patterns in chromatins from mouse teratocarcinoma cells. *Exp Cell Res* 102:169-178.
- Parfenov VN, Galaktionov KI (1987): Intracellular actin microfilaments in the oocytes of the common frog. *Tsitologia*, 29:142-149.
- Pratt VM, Harris AS, Morrow JS, Madri JA (1984): Mechanism of cytoskeletal regulation. Modulation of aortic endothelial cell spectrin by extracellular matrix. *Am J Pathol* 117:349-354.
- Reima I, Lethonen L (1985): Localization of nonerythroid spectrin and actin in mouse oocytes and preimplantation embryos. *Differentiation* 30:68-78.
- Robinson KR (1979): Electrical currents through full-grown and maturing *Xenopus* oocytes. *Proc Natl Acad Sci USA* 76:837-841.
- Rungger D, Rungger-Brandl E, Chaponnier C, Gabbiani G (1979): Intracellular injection of anti-actin antibodies into *Xenopus* oocytes blocks chromosomes condensation. *Nature* 277:320-321.
- Schatten H, Cheney R, Balczon R, Willard M, Cline C, Simerly C, Schatten G (1986): Localization of fodrin during fertilization and early development of sea urchins and mice. *Dev Biol* 118:457-466.
- Scheer U, Hinssen H, Franke WW, Jockusch BM (1984): Microinjection of actin-binding proteins and actin antibodies demonstrate involvement of nuclear actin in transcription of lampbrush chromosomes. *Cell* 39:111-122.
- Sobel JS, Goldstein EG, Venuti JM, Welsh MJ (1988): Spectrin and calmodulin in spreading mouse blastomeres. *Dev Biol* 126:47-56.
- Talevi R, Campanella C (1988): Fertilization in *Discoglossus pictus*. I. Regionalization of sperm-egg interaction site and occurrence of a late stage of sperm penetration. *Dev Biol* 130:524-535.
- Vacquier VD (1981): Dynamic changes of the egg cortex. *Dev Biol* 84:1-26.
- Wischnitzer S (1966): The ultrastructure of the cytoplasm of developing amphibian egg. In M Abercrombie and J Brachet (eds): "Advances in Morphogenesis." Vol. 5. New York: Academic Press, pp 131-179.

THE CONTRIBUTION OF *Discoglossus pictus* FERTILIZATION IN THE STUDY OF AMPHIBIAN SPERM-EGG INTERACTION

Campanella C.*, Talevi R., Gualtieri R., Andreuccetti P.

Dipartimento di Biologia Evolutiva e Comparata,
via Mezzocannone 8, 80134 Napoli, Italy

* Dipartimento di Scienze e Tecnologie Biomediche e di Biometria, Collemaggio
67100, L'Aquila.

KEYWORDS: Amphibians, gametes, fertilization, Discoglossus pictus.

ABSTRACT We have here raised the following questions which deserve attention in the study of amphibian fertilization: 1. How do sperm acquire motility and what is the action of the jelly coat on sperm; 2. What are the egg surface properties that enable sperm fusion; 3. How is a localized stimulus transmitted to the rest of the egg; 4. What is the role of cortical organelles at activation; 5. How is excess of sperm entrance avoided. Fertilization in Discoglossus pictus may contribute to the understanding of these mechanisms.

INTRODUCTION

Recently, amphibian gametes have provided remarkable contribution to our understanding of gametogenesis and fertilization. The control of G2-metaphase transition at maturation through an histone protein kinase, which appears to be similar from yeast to somatic cell lines (among many references : Arion et al, 1988; Dunphy et al, 1988; Labbé et al, 1988; Lohka et al, 1988; Gautier et al, 1988) has its basis in the discovery of the maturation promoting factor (MPF) in Rana pipiens oocytes by Masui and Market (1971).

The expression of heterologous m-RNA in fully grown oocytes offered the basis of elegant experimentation which suggests the presence of sperm receptors

at the egg plasma membrane, of signal transduction through G-proteins and of endogenous hydrolysis of IP₃ (McIntosh and Catt, 1987; Kline et al, 1988).

The finding that the vitelline envelope (VE) changes its composition following ovulation (first evidences given by Elinson, 1973; Katagiri, 1974; Grey et al, 1977; Miceli et al, 1978) thus acquiring its full ability to interact with sperm, has now been discovered in other classes, such as mammals (Oikawa et al 1988).

Interesting evolutionary interpretations of the fertilization process have been inspired by the sharp differences between urodele and anuran fertilization and the variation with respect to "orthodox patterns" in some species belonging to the most ancient families of the two orders, (Elinson, 1986).

However it is also true that many fundamental points of the fertilization process in amphibians have not been explored or require more experimentation. Among these, how do sperm acquire motility and what is the action of jelly coats on sperm; what are the egg surface properties that enable sperm fusion with the egg; how localized stimuli can be transmitted to the rest of the egg; what are the molecules involved in signal-transduction and the chain of metabolic events initiated at activation; what is the role of cortical organelles in egg activation; how excess of sperm entrance or multiple fusion with the female pronucleus is avoided.

The study of fertilization in the anuran *Discoglossus pictus*, belonging to the ancient superfamily *Discoglossidae*, has provided new data that can be useful for understanding the mechanism of fertilization. We shall first review the main features of the "Discoglossus model" and then examine some of the overmentioned points in the light of what we have learned from this species.

GENERAL FEATURES OF GAMETES AND FERTILIZATION IN *DISCOGLOSSUS PICTUS*

Many functional and morphological characteristics of gametes and gametic interaction are unique to this species, while other features are shared with anuran or urodele species. Among the features typical of *D.pictus* there are: 1. egg morphology (egg diameter: 1.6 mm). The animal hemisphere is indented by a jelly component, the "animal plug" (Ghiara, 1960). The center of this concavity is further invaginated and forms the cup-shaped dimple (Hibbard, 1928; Campanella, 1975) (fig 1). 2. Spermatozoa length and arrangement in bundles. Sperm are 2.33 mm long and are ejaculated in bundles of about 20. They are embedded in a shell made of orderly arranged filaments (Campanella et al, 1979) (figs 2 and 3).

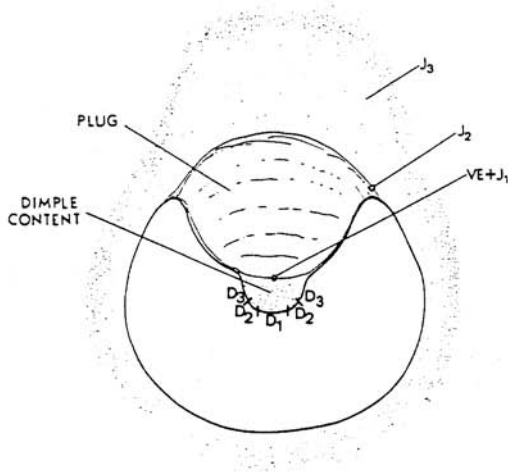


Fig 1. Schematic drawing of a longitudinal section of *D. pictus* egg. J1; J2; J3 indicate jelly coats; VE= vitelline envelope. The "plug" sits in the animal concavity. In the dimple, D1 is the 200 μm disk where fertilization occurs. D2 and D3 are the dimple walls.

3. Sperm behaviour at insemination. When sperm come into contact with the surface of J3 (the outermost jelly layer) the filament shell sticks to the jelly. Sperm acquire motility, come out of their shells and become embedded in the thick jelly coat facing the dimple. Indeed, they converge, through the plug, at the center of the dimple, D1, which is a disk 200 μm in diameter (Campanella and Gabbiani, 1979; Talevi and Campanella, 1988) (figs 1 and 5). D1 is the only site of the egg where fertilization occurs (Campanella, 1975; Talevi and Campanella, 1988) and has regularly arranged microvilli (fig 4). At the dimple walls (fig 1), D2 has less orderly arranged microvilli and D3 has short microvilli (Campanella et al, 1988). Moreover D1 is endowed with special properties with respect to the rest of the egg, as will be reported in the next pages.

Table I summarizes the main events occurring at fertilization in *D. pictus*. Cortical granules (CG) are present only in the dimple and the fertilization envelope does not lift at activation, being already far apart the dimple plasma membrane (see fig 1 and table I). What are then the signs of activation in this egg? They consist mainly in two groups of phenomena: 1) a cortical contraction wave which starts in the dimple a few minutes following fertilization and then spreads to the rest of the egg. As a consequence the dimple regresses (Talevi et al, 1985) (see table I). 2) About 15 min from insemination the concavity disappears as a result of the plug liquefaction. Similarly to urodeles, a capsular chamber is formed in which - the egg with its VE and J1 is free to rotate (see table I).

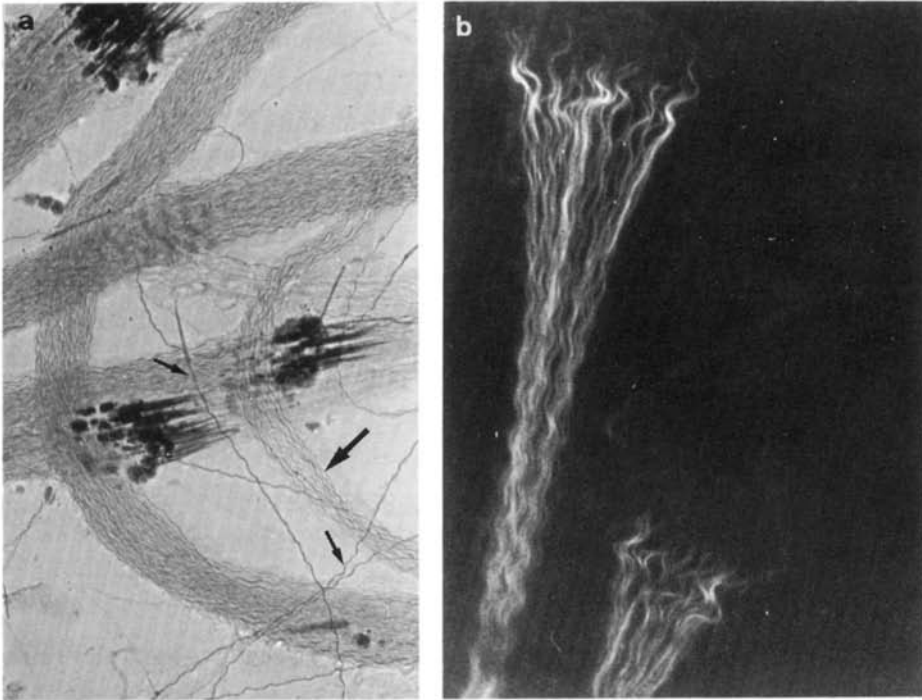


Fig 2. Sperm bundles. a: The very long threads are the heads, which are about $900\ \mu\text{m}$ long (arrow), or the tails (small arrows). The strongly stained segments are the posteriormost portions of the head. The arrowheads indicate the fibrillar matrix where sperm bundles are embedded. $\times 1,000$. b: Sperm stained with anti-actin antibody to show the sperm heads (for details see Campanella and Gabbiani, 1979). $\times 2,000$.

Such a phenomenon is a consequence of the release of peripheral vacuole contents from the egg and involves the reduction of disulphide bonds present in the plug macromolecules (Pitari et al, 1987).

HOW DO SPERM ACQUIRE MOTILITY AND WHAT IS THE ACTION OF JELLY COAT ON SPERM

The acquisition of sperm motility or the variations in the motility pattern is linked to a change in salinity of the medium or to interaction with substances deriving from the female gamete or the genital tract. In amphibians, sperm become motile following release in the external medium (see also Morisawa's report in this volume). In *D. pictus*, in addition to this, contact of the bundle shell with J3 or with a polylysine coated dish triggers initiation of motility and liberation of sperm from the shell (Campanella and Gabbiani, 1979).

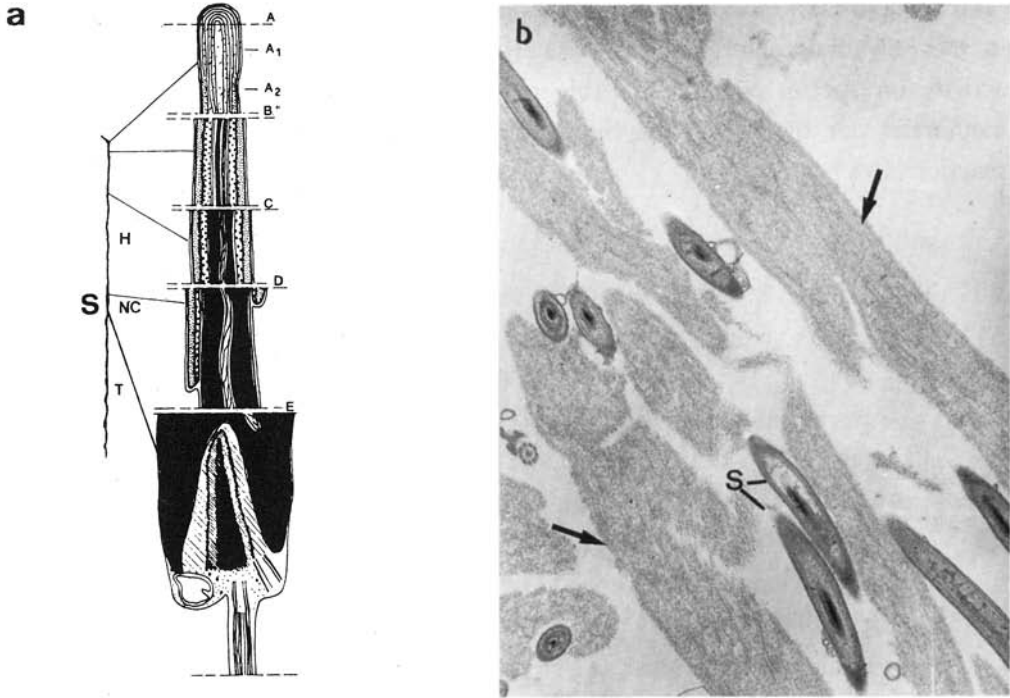


Fig 3. a: Schematic drawing of *D. pictus* sperm (S) where a head (H) with an apical rod, a "neck" (N) and a tail (T) are distinguishable. From A to B= apical rod; from B to E= nucleus covered by the acrosomal cap. Note the presence of an endonuclear canal, well distinguishable at the posteriormost portion of the sperm, approximately at the E level (see Gabbiani and Campanella, 1979, for details). **b:** TEM micrograph showing an oblique section of a sperm bundle. The arrows indicate the fibrillar matrix (the shell) where sperm (S) are embedded. x 12,000.

The shell is made of filaments which come to surround sperm in the "seminal vesicles", a wolffian duct specialization of this species (Mann et al, 1963) (fig 2). This phenomenon raises the following questions: Can external matrix or surface molecules in sperm plasma membrane function as target for environmental signalling to be transduced to the sperm cell? Can such molecules be considered ancestral precursors of mammalian epididymal products?

The mechanism of sperm penetration in amphibian jelly coat is unknown and should not involve acrosome content, as the acrosome reaction generally occurs at the VE. In particular, *D.pictus* sperm - whose motility expires in about 15 s- are able to penetrate the thick jelly layer facing the dimple in as little as 2-3 min. What are the biophysical and/or biochemical properties that make this penetration possible?

When sperm come into contact with the jelly, they acquire the ability to perform the acrosome reaction. Both cations (Ca, Mg) present in the jelly at

relatively elevated concentration (Ishihara et al, 1984), and a 500 dalton molecule in the jelly dialyzable fraction (Katagiri, 1973) have a fertilization-supporting activity on sperm. Neither the role of such jelly components on the sperm membrane nor the biophysical-biochemical changes occurring at the acrosome reaction have been studied.

WHAT ARE THE EGG PROPERTIES WHICH ENABLE SPERM FUSION

A) Vitelline coat and egg surface

In invertebrate and mammalian fertilization, sperm-egg recognition and attachment are based on the interaction between sperm proteins and complementary glycoconjugates in the egg extracellular coat. The binding of these complementary molecules generally triggers the acrosome reaction. In a wide range of species, fucose is involved in this interaction (for reviews see Hoshi, 1984 and Macek and Shur, 1988).

In amphibians, a protease secreted by the oviducal "pars recta" modifies the coelomic oocyte VE. As a consequence the number of exposed ligands for the 32 Kdalton VE sperm lysin (Yamasaki et al, 1988) is increased following passage of the oocyte through the oviduct (Miceli et al, 1980; Takamune et al, 1986; Gerton and Hedrick, 1986). The nature of such ligands and/or sites for sperm attachment has not been investigated. However lectins, thanks to their properties of binding specific saccharides, were used to characterize the carbohydrate moieties of glycoproteins involved in sperm-egg interaction. In Bufo and Xenopus, incubation of dejelled eggs with ConA, WGA, SBA or PHA-P, inhibits fertilization (Charbonneau et al, 1986; del Pino and Cabada, 1987) and in Bufo renders the VE resistant to digestion by both proteolytic enzymes and sperm lysin (del Pino and Cabada, 1987). In Xenopus, the inhibition of fertilization could be due to an effect of lectins on sperm (Charbonneau et al, 1986).

In Discoglossus denuded egg, as a result of maturation, D1 surface acquires the ability of binding FBP. Following fertilization the affinity for such a lectin is lost. By contrast, fertilization does not change the ability of the rest of the egg surface to bind WGA and SBA (Denis-Donini and Campanella, 1977). Indeed, this work suggests that fucose residues have a role in fertilization because they are expressed on D1 during maturation and disappear following fertilization. In D.pictus, they are localized at the dimple surface. More experimentation in D.pictus, as well as in other species should define the glycoconjugates containing

fucose residues and their involvement in sperm binding at the VE and/or the egg surface.

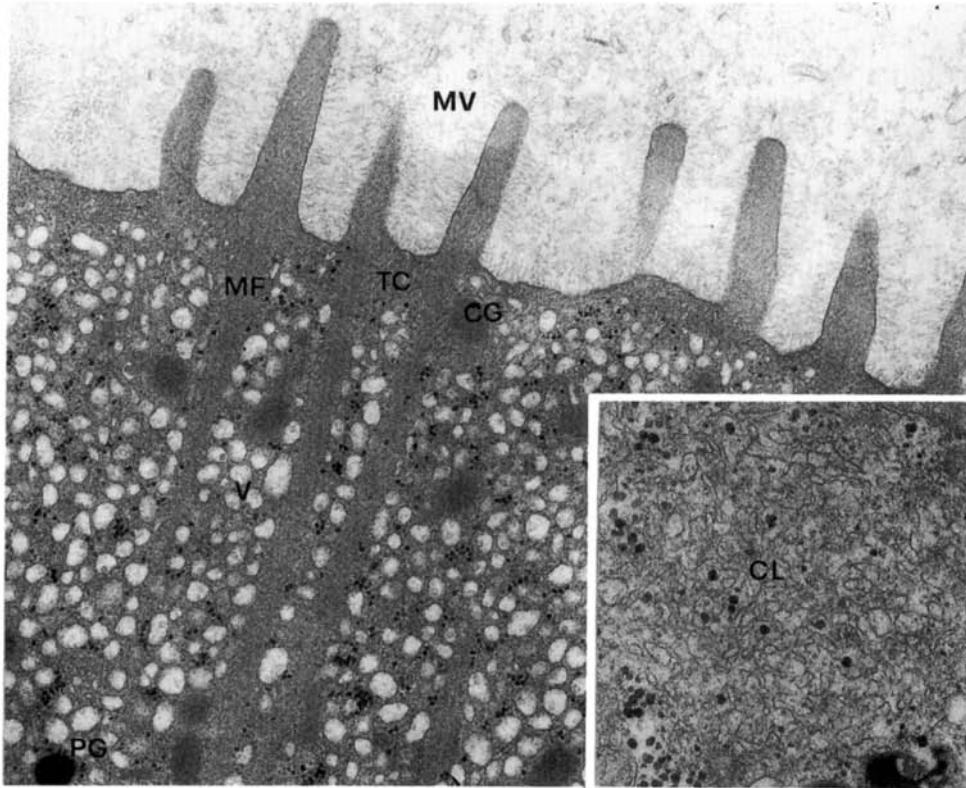


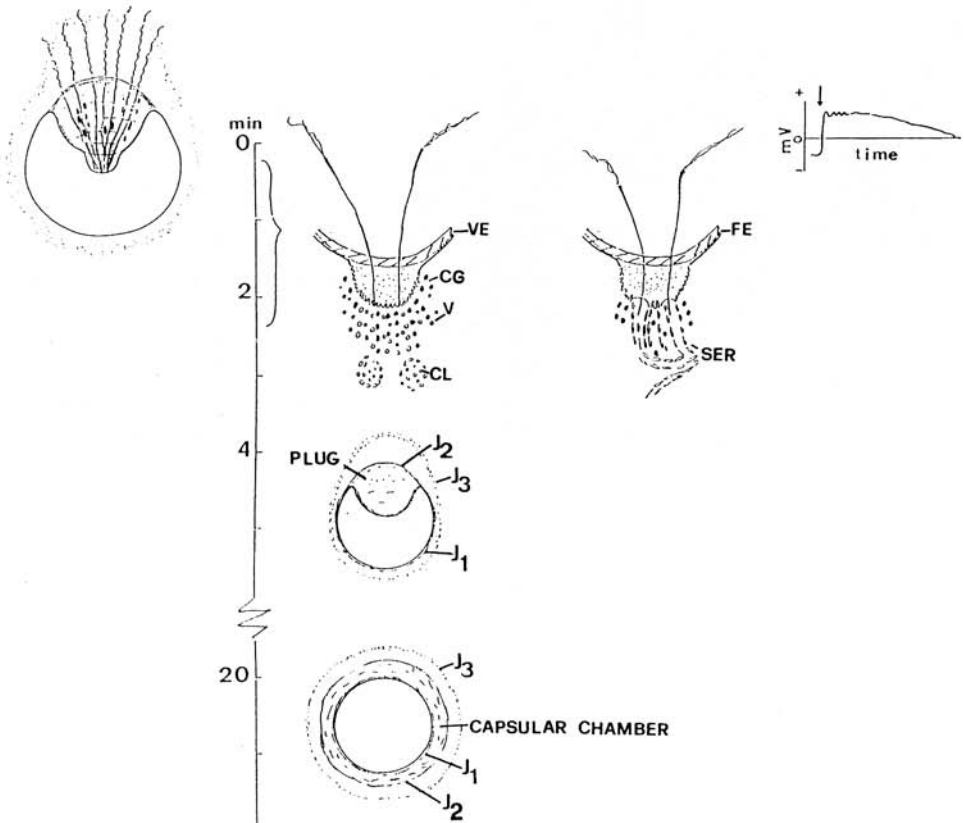
Fig 4. Unfertilized egg of *D. pictus*. Sperm entrance site (D1). Microfilament bundles (MF) inside microvilli (MV) are clearly discernable. The smooth endoplasmic reticulum is arranged in cortical tubular cisternae (TC), peripheral vacuoles (V) and subperipheral clusters of tubular cisternae (inset, CL). CG= cortical granule; PG= pigment granule. x 25,000; inset, x 45,000. (From Gualtieri et al., 1989 with permission of Dev. Gr. Differ.).

B) Plasma membrane-cortex

In anurans, the region where successful sperm-egg interaction occurs is restricted to the animal hemisphere. The plasma membrane and/or cortical features that render this region capable of fusing with sperm are still unknown. In the animal half plasma membrane, lipids have a smaller coefficient of mobility (Dictus et al, 1984) and the Cl^- channels responsible for membrane depolarization at fertilization are more concentrated than in the vegetal half (Cross, 1981; Jaffe et al, 1985). Furthermore, microvilli are distributed at a higher density in the animal hemisphere than in the vegetal hemisphere (Grey et al, 1974). In *D. pictus*, further

restriction of such a privileged area to the dimple, may give some clue for studying the prerequisites for the accomplishment of fertilization.

Table I. Summary of fertilization events in *D. pictus*. On the upper left side sperm penetration through the jelly envelope is schematically outlined. At the upper right side a typical fertilization potential, as recorded at 0 time fertilization, is drawn. SER= smooth endoplasmic reticulum; CL= clusters of SER; V= vacuoles; FE= fertilization envelope; VE= vitelline envelope, CG= cortical granules.



In the dimple, D1, D2 and D3 can be distinguished into three domains on the basis of their surface and cytoplasmic features (Campanella et al., 1988). The dimple regionalization includes functional characteristics: D1 is the only site in the egg, where electrical responses can be elicited by the sperm or by activating agents.

In physiological conditions, the jelly and particularly the plug make spermatozoa converge into D1 (fig. 5a). Gamete interactions occurs only in this area leading to the generation of the fertilization potential (FP), to fertilization cone formation and to the onset of development (Hibbard, 1928; Campanella, 1975; Talevi et al, 1985; Talevi and Campanella, 1988). When the plug is not in axis with the center of the dimple, sperm converge into the dimple walls, D2 and D3 (fig 5b). In these regions, sperm interaction with the plasma membrane leads to small cytoplasmic protrusions and brief depolarizations of few mV (Talevi and Campanella, 1988). A fertilization potential, similar in intensity, delay and shape to the activation potential elicited by pricking (see below) is recorded only when multiple sperm interactions occur in the D2 and D3. In these regions sperm partially penetrate into the egg where, however, degenerate; development is not initiated (Talevi and Campanella, 1988).

Studies on parthenogenetic stimuli have furnished further data on the egg response at activation (Talevi et al, 1985). Activation of the dimple by pricking or by injection with inositol 1,4,5-triphosphate (IP3) in the dimple causes an immediate depolarization, similar to the FP. A wave of contraction that reflects a propagation of $[Ca^{2+}]_i$ (Nuccitelli et al, 1988), spreads from the dimple to the antipode. When eggs are stimulated outside the dimple, a contraction wave spreads from the site of stimulus application to the antipode. In this case, the activation potential (AP) is not generated until the wave reaches the dimple (Talevi et al, 1985; Nuccitelli et al., 1988). As the Cl^- channels are Ca^{2+} -activated (Cross, 1981; Young et al, 1984; Kline, 1988), these data strongly suggest that Cl^- channels are present only in the dimple. On the other hand, by the vibrating probe a large Cl^- -transported inward current has been detected only in the D1 domain, further suggesting that Cl^- channels are located only in this region (Nuccitelli et al, 1988). The above mentioned parthenogenetic experiments allow us to hypothesize that sperm may act as activating stimuli in D2 and D3, and that the stimulus has to be transmitted to D1 to elicit a full FP. In the whole dimple the features which enable sperm penetration and the onset of development are probably distributed according to a gradient which has its highest intensity and threshold values in D1. In this respect in the dimple, a similar gradient of distribution concerns also cytoplasmic organelles such as CG, as well as cisternae, vacuoles and clusters of smooth endoplasmic reticulum (SER), potential sources of $[Ca^{2+}]_i$ to be released at fertilization (fig 4).

Freeze-fracture quantitative analysis of *D. pictus* egg membrane show that D1 has intramembranous particles with higher concentration and opposite ripartition in the two leaflets with respect to the rest of the egg membrane

(Gualtieri et al, 1989). Such a structural polarity of the egg plasma membrane settles during the oocyte maturation at the time of the first polar body extrusion (Gualtieri et al, 1988; Gualtieri et al, in press) (fig 6). Are these particles sperm receptors and/or Cl^- channels? The biochemical and functional analysis of such plasma membrane domains might offer important information on the study of sperm-egg interaction.

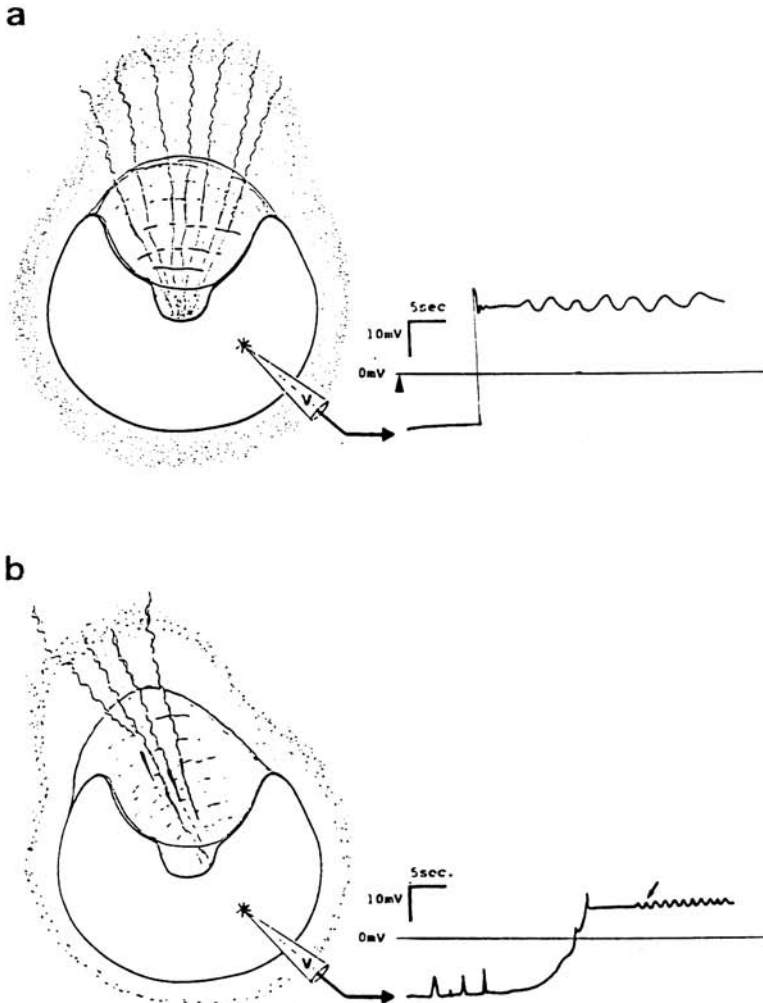


Fig 5. a: On the left, schematic drawing of an egg inseminated in physiological conditions and, on the right, the corresponding fertilization potential. The arrowhead indicates the time of sperm addition. b: On the left, schemating drawing of an egg with the plug not in axis with the center of the dimple. Upon insemination sperm converge into D2 or D3. On the right, corresponding variations of the membrane potential. Explanations in the text.

In conclusion, in D.pictus the multi-step process of fusion between sperm and egg involves specific features to be found only in the dimple. One can also suggest that specific molecules are present only in this region able to interact with sperm, to produce fertilization cones and to start development.

3) HOW IS A LOCALIZED STIMULUS TRANSMITTED TO THE REST OF THE EGG

The fine molecular events related to sperm-egg interaction and the triggering of activation are still one of the most important pitfall of the study of fertilization. Most probably sperm release a substance which is able to start PIP₂ hydrolysis. In sea urchin, a sperm soluble factor is able to initiate activation when injected into the cytoplasm (Dale et al, 1985), and in Urechis a protein has been isolated from the sperm which triggers membrane depolarization upon addition to the egg (Gould and Stephano, 1987) (see articles by Dale, by Kline and by Whitaker, in this volume). In amphibians sperm contribution to gametic fusion has been investigated. It has been postulated that sperm inserts into the egg membrane either receptors which interact with G proteins or factors which directly activate such proteins (Kline et al, 1988; Iwao and Jaffe, 1989). However, it remains to be demonstrated why such putative factor cannot be effective in promoting sperm fusion at the vegetal hemisphere, or in the case of D.pictus, in the regions outside the dimple.

The indication that G proteins are involved in the activation process fits well with the knowledge that, in anurans, stimulation of the egg by sperm or parthenogenetic agents (pricking, IP₃ injection etc.) is followed by an increase of cytosolic calcium which is propagated from the site of activation to the rest of the egg through a Ca²⁺ release (Busa and Nuccitelli, 1985; Busa et al, 1985; Kubota et al, 1987). Extracellular calcium is not needed during such a release, however, in its absence, activation by sperm or by pricking does not occur. Presently, there is not full explanation of such a limited and precise need for extracellular calcium.

Many events, such as ion channels opening, exocytosis and formation of pronuclei are calcium-dependent (Kline, 1988). More work is needed to understand whether the important changes which accompany activation, namely changes in pHi (Webb and Nuccitelli, 1981; Grandin and Charbonneau, 1989 and see Charbonneau, this volume) and in protein phosphorylation (Bement and Capco, 1989) are directly related to the increase in cytosolic calcium.

Among the numerous questions concerning the first stages of activation, one is whether the increase of intracellular Ca^{2+} can be considered as the first signal which travels through the cortex or the whole egg.

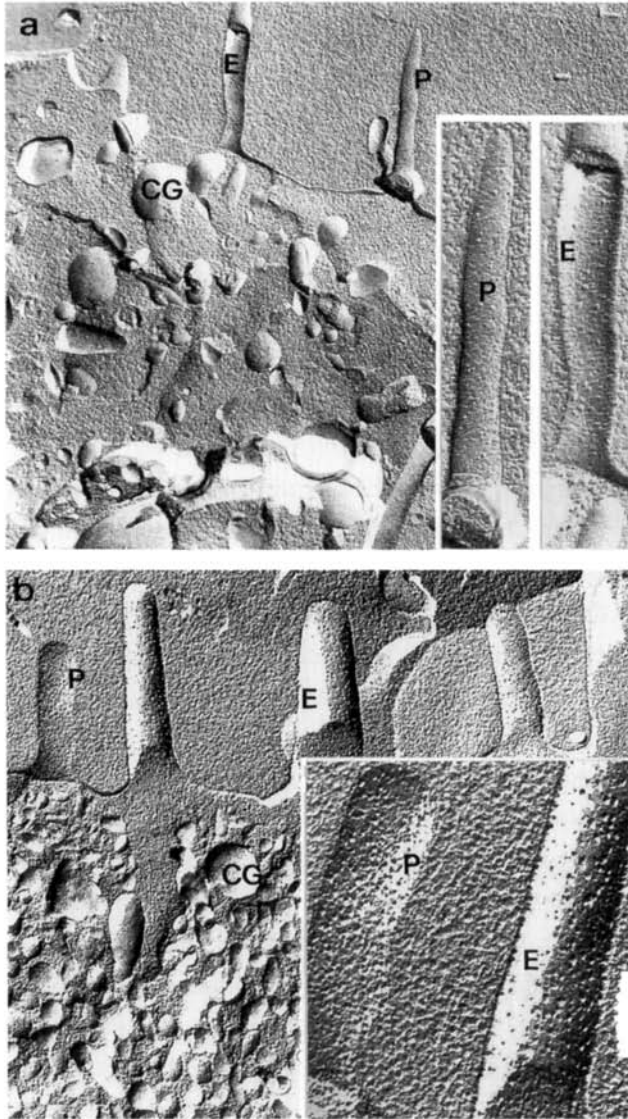


Fig 6. a: Replica of the germinative area in *D. pictus* coelomic oocytes. Insets: P and E face of two microvilli. b: Replica of the sperm entrance site (D1) in *D. pictus* egg. Inset: P and E face of two microvilli. The intramembrane particle density in D1 is markedly increased with respect to the maturing oocyte. a and b, x 25,000; insets, x 60,000. CG= cortical granule. (From Gualtieri et al., 1989 with permission of Dev. Gr. Differ.).

In *D. pictus* egg, the contraction wave elicited by parthenogenetic stimulation, starts egg activation at its arrival in the dimple. This indicates that a

subcortical mechanism of stimulus transmission can work in both direction: from the dimple to the rest of the egg, at fertilization, and from the egg regions outside the dimple to the dimple as a consequence of experimental activation. The particular organization of *D.pictus* egg permits the following experiment: pricking the denuded egg at the equator in two opposite sites gives rise to two distinct contraction waves in case that the stimuli are applied almost contemporaneously.

They reach the dimple after a time that varies from 5 to 15 min according to the egg clutch. However, when pricking is first conducted at one side and about 20 s later at the opposite side, the second wave never develops; the first wave regularly reaches the dimple where the activation is elicited (Campanella, unpublished). What is the nature of such an early signal which inhibits the second wave formation and travels along the egg cortex or plasma membrane? Is it present in other anuran species where it might not be depicted because of the different egg organization?

4) WHAT IS THE ROLE OF CORTICAL ORGANELLES

A) Cortical endoplasmic reticulum (SER).

Cortical constituents, such as vesicles and cisternae, have been extensively studied in *Xenopus laevis* eggs. They are commonly considered SER because they derive from annulated lamellae (Campanella et al, 1984; Larabell and Chandler, 1988) which in germinal as well as in somatic cells transform into rough or smooth endoplasmic reticulum (Kessel, 1985). The cisternae form a continuous network in the cortex and particularly surround CG as a shell (Grey et al, 1974), thus suggesting they might be related to CG exocytosis and be site of accumulation and release of Ca^{2+} at activation (Campanella and Andreuccetti, 1977; Andreuccetti et al, 1984). Furthermore, vacuoles are in close contact with the plasma membrane in loci, where the presence of junctions reminiscent of the triads junctions in striated muscle has been suggested (Gardiner and Grey, 1983). Biochemical analysis is needed to study the characteristics of the peripheral vacuoles and cisternae and their possible analogy with calciosomes (Volpe et al, 1988). The cortical SER anastomoses with whorls of cisternae located in the subcortical layer. Shortly following CG exocytosis, the SER rearranges, and chains of cisternae are transiently seen crossing the egg periphery where later only vacuoles are found (Campanella and Andreuccetti, 1977). The anatomical organization of such probable calcium reservoirs, the dynamic of their transformations as well as

electrophysiological measurements of free Ca^{2+} following IP3 injection, suggest that Ca^{2+} release is a complex, multi-step event involving an IP3-sensitive pool and an IP3-insensitive pool (Busa et al, 1985; Parker and Miledi, 1986 ;Berridge, 1988).

In this context several specific points need explanation. It is known that Cl^- channels are activated by an increase of free calcium and that, as a consequence, the plasma membrane depolarizes. The FP is recorded always before the changes in free calcium concentrations, and this might be due to limits of the utilized techniques (i.e. diffusion time from sites of liberation to the Ca^{2+} -selective electrode). However, it cannot be excluded that a minor release of Ca^{2+} responsible for Cl^- channels activation precedes the larger increase of cytosolic Ca^{2+} . In this respect we hypothesize that the vacuoles next to the plasma membrane are specialized in the first release of Ca^{2+} while the rest of the cortical SER is involved in the transmission of the measurable increase of Ca^{2+} as suggested by electrophysiological work (Busa et al, 1985). A second point is: How can the IP3 injection determine Ca^{2+} release in the cytoplasm where very few vacuoles (SER or calciosomes?) are found? A possible answer is suggested by somatic cells where the IP3-induced Ca^{2+} release does not appear to be the property of a single organelle but of specialized regions of rough and smooth ER and other smooth surfaced structures (Ross et al, 1989).

The function of the subcortical SER clusters has been studied in D.pictus eggs (fig 4, table I). In this species, an eightfold increase of internal Ca^{2+} has been measured at fertilization. It starts in the dimple and then propagates to the rest of the egg (Nuccitelli et al, 1988). In the dimple there are tubular cisternae close to the plasma membrane, vacuoles intermingled with CG and more deeply located cisternae clusters (Campanella et al, 1988). They have a peak of concentration in D1, and are scanty present in the rest of the egg (Campanella et al, 1986; Campanella et al, 1988). The tubular cisternae are equivalent in position and, in our opinion, in function, to X.laevis sub-plasmalemma vacuoles. Following fertilization D.pictus vacuoles become an anastomosed cortical network of SER (similar to that present in unfertilized X.laevis eggs), which migrates towards the plasma membrane. At the same time the cisternae clusters transform into whorls of cisternae which become part of the cortical network (table I). Such transformation occurs only in the dimple, but it can be induced experimentally also in those cisternae clusters located next to the point of IP3 injection. Furthermore cisternae deriving from the clusters participate in plasma membrane wound healing. It has been hypothesized that the clusters open as a consequence of a

physiological or artificially induced increase of Ca^{2+} concentration and that their cisternae might constitute reservoirs of membranes (Campanella et al, 1988a and 1988b; Gualtieri et al, in press; Bracci Laudiero et al, in press).

B) Cortical cytoskeleton and territorial compartmentalization

Eggs, as most cells, are able to maintain compartmentalization at the plasma membrane as well as in the cytoplasm. How is this achieved?

In amphibian eggs, cytoskeletal proteins, such as actin, villin, prekeratin, myosin, tubulin, actin-binding protein and vimentin were depicted (Palecek et al, 1982; Gall et al, 1983; Corwin and Hartwig, 1983; Christensen et al, 1984; Tang et al, 1988). No differences have been reported in the distribution of such proteins between the animal half, the region where sperm penetrate into the egg and the vegetal half, except for a general more abundant presence in the animal hemisphere.

As previously mentioned, D.pictus eggs show an evident compartmentalization of both surface and plasma membrane constituents (sugar residues, intramembranous particles and ionic channels) and cytoplasmic territories within the dimple. In this region, 10 μm long actin microfilament bundles, appear to compartmentalize organelles (i.e. vacuoles, CG) along and between the bundles. Furthermore, in D3, which is located at the boundary of the dimple with the rest of the animal half, mitochondria are found below the bundles palisade, in significantly larger amount than in D1 and D2. Actin, myosin, alfa-actinin, tropomyosin have been immunocytologically defined in the whole egg cortex (Campanella and Gabbiani, 1980; Campanella et al, 1982; Campanella et al, in press) while spectrin has been found only in the dimple peripheral cytoplasm (Campanella et al, submitted) and a positivity to anti-gelsolin antibodies only in D1 (Campanella, unpublished results). This suggests that the cytoskeleton may play a role in organelle distribution. Furthermore, localized cytoskeletal functionality may actively contribute to CG, vacuoles and cisternae locomotion at activation, and, in general, in egg contraction. In particular, spectrin might stabilize plasma membrane domains thanks to its sites of interaction with actin and, as recently suggested (Campanella et al, submitted) with receptors or ionic channels in the plasma membrane. It would be interesting to study whether in other anurans eggs spectrin is similarly found in the region where fertilization occurs and fertilization channels are found.

6) HOW IS EXCESS OF SPERM ENTRANCE AVOIDED

In anuran eggs, fertilization is characterized by the relatively limited area of sperm interaction, the long-lasting membrane depolarization, and the exocytosis of CG at fertilization. These features seem to be the factors responsible for maintaining monospermy in eggs. In urodeles, where eggs are physiologically polyspermic, sperm entrance can occur all over the egg, the membrane does not depolarize, or even hyperpolarize at fertilization, and CG are absent (for reviews see Schmell et al, 1984; Elinson, 1986).



Fig 7. *D. pictus* cleaving eggs. Three irregular furrows are present. x 10.

Is this sharp distinction between the two orders a general rule? Are there alternative mechanisms present in anuran eggs that avoid excess of sperm entrance?

In *D. pictus*, a fast long-lasting depolarization as well as CG exocytosis occurs at fertilization. Yet, recent work has shown that multiple sperm penetration occurs in eggs with normal membrane depolarization and which develop into tadpoles, evidencing an interesting feature of this egg: the voltage independence of sperm penetration. Indeed, this was shown in eggs where the voltage was kept either positive through current injection or negative by bathing the eggs in high NaI Ringer (Talevi, 1989). However, the number of sperm penetrating polyspermic eggs is generally low and normal development is compatible in eggs penetrated by two up to five sperm. Moreover, in spite of the high frequency of polyspermy found (36%), not all egg clutches display polyspermy. The occurrence of this condition does not depend upon sperm "efficiency", but is correlated with characteristics of some egg clutches (Talevi, 1989). Extracellular mechanisms could play an important role in regulating sperm entrance in *D. pictus* egg. In this regard the jelly coat is a good candidate. The plug is made of fibrillar material, and, as previously described, conveys sperm to the D1 area; the fibrillar matrix of the plug

is probably organized in a series of set routes which support sperm penetration. In polyspermic egg clutches this structure may be altered, increasing the number of sperm entering the plug and reaching the VE.

Two further blocks to sperm entrance are present in this species. In experiments of reinsemination, the newly added sperm encounter two barriers i.e. the sperm bundle shells which cover the J3 surface, and the VE which has changed into fertilization envelope as a consequence of fertilization (Campanella, unpublished results).

An important point to be still investigated in fertilization of D. pictus polyspermic clutches is the behaviour of supernumerary sperm in the dimple cytoplasm and how this can be compatible with normal development. Occasionally, upon raising tadpole in laboratory, cleaving embryos with irregular furrows have been observed (fig 7), suggesting that in polyspermic zygotes supernumerary sperm decondense, develop two asters and participate in mitosis (see also Elinson, 1986).

D. pictus is not the only species, among anurans, to display polyspermic fertilization. Recently, a high frequency of polyspermy with normal development has been found in the terrestrial breeding frog Eleutherodactylus coqui (Elinson, 1987).

With respect to urodeles, monospermy has been described in the primitive family Hinobiliae, where a fast membrane depolarization at fertilization has been reported. Furthermore in Hynobius nebulosus the outermost jelly layer constitutes the normal barrier to polyspermy (Iwao, 1989).

These new findings represent important exceptions to the schematic distinction between the two orders, and provide new data for the general understanding of amphibian fertilization. They suggest that several mechanisms can be called into action to guarantee the achievement of the final goal of fertilization: amphimixis of the female aploid genome with one paternal aploid genome.

REFERENCES

- Arion D, Meijer L, Brizuela L, Beach D (1988) CDC2 is a component of the M phase-specific histone H1 kinase: evidence for identity with MPF. *Cell* 55:371-378
- Bement WM, Capco DG (1989) Activators of protein kinase C triggers cortical granule exocytosis, cortical contraction, and furrow formation in Xenopus oocytes and eggs. *J Cell Biol* 108:885-892

- Berridge MJ (1988) Inositol triphosphate-induced membrane potential oscillations in Xenopus oocytes. *J Physiol* 403:589-599
- Bracci Laudiero L, Gualtieri R, Andreuccetti P Possible role of the smooth endoplasmic reticulum during the early stages of development in the painted frog Discoglossus pictus (Anura). In press on *Acta Embr Morph Exp ns*
- Busa WB, Nuccitelli R (1985) An elevated free cytosolic Ca^{2+} wave follows fertilization in eggs of the frog Xenopus laevis. *J Cell Biol* 100:1325-1329
- Busa WB, Ferguson JE, Joseph SK, Williamson JR, Nuccitelli R (1985) Activation of frog (Xenopus laevis) eggs by inositol triphosphate. I. Characterization of Ca^{2+} release from intracellular stores. *J Cell Biol* 101:677-682
- Campanella C, Andreuccetti P, (1977) Ultrastructural observation on the cortical and subcortical endoplasmic reticulum and on residual cortical granules in the egg of Xenopus laevis. *Dev Biol* 56:1-10
- Campanella C (1975) The site of spermatozoon entrance in the unfertilized egg of Discoglossus pictus (Anura): an electron microscope study. *Biol Reprod* 12:439-447
- Campanella C, Gabbiani G (1979) Motile properties and localization of contractile proteins in the spermatozoon of Discoglossus pictus. *Gamete Res* 2:163-175
- Campanella C, Gabbiani G (1980) Cytoskeletal and contractile proteins in coelomic oocytes, unfertilized and fertilized eggs of Discoglossus pictus (Anura). *Gamete Res* 3:99-114
- Campanella C, Rungger-Brandle E, Gabbiani G (1982) Immunolocalization of alfa-actinin in an amphibian egg (Discoglossus pictus). In "Embryonic Development" Part B: Cellular Aspects (M Burger and R Weber eds), 45-53. Alan Liss New York
- Campanella C, Andreuccetti P, Taddei C, Talevi R (1984) The modifications of the cortical endoplasmic reticulum during "in vitro" maturation of Xenopus laevis oocytes and its involvement in cortical granules exocytosis. *J Exp Zool* 229:283-294
- Campanella C, Talevi R, Atripaldi U, Quaglia L (1986) The cortical endoplasmic reticulum and its possible role in activation of Discoglossus pictus (Anura) egg. In "Molecular and Cellular Biology of Fertilization" (JL Hedrick eds) Plenum Press New York
- Campanella C, Kline D, Nuccitelli R (1988) The cortical reaction in the egg of Discoglossus pictus: Changes in the cisternae clusters at activation. In "Cell Interactions and Differentiation" (G Ghiara eds) University of Naples
- Campanella C, Talevi R, Kline D, Nuccitelli R (1988) The cortical reaction in the egg of Discoglossus pictus: A study of the changes in the endoplasmic reticulum at activation. *Dev Biol* 130:108-119
- Campanella C, Chaponnier C, Quaglia L, Gualtieri R, Gabbiani G Different cytoskeletal organization in two maturation stages of Discoglossus pictus (Anura) oocytes: Thickness and stability of actin microfilaments and tropomyosin immunolocalization. In press on *Gamete Res*

CHIARA CAMPANELLA

Fertilization in amphibians

ABSTRACT

The physiology of reproduction as well as the cytological characters of the gametes of urodeles and anurans constitute important features distinguishing the two orders. Recent studies report relevant variations of the cytological pattern of fertilization in species, such as *Eleutherodactylus coqui*, *Discoglossus pictus* and *Hynobius retardatus*, belonging to the two orders. This paper reviews the early events of fertilization in the two orders and pays special attention to the anuran *D. pictus* fertilization, in which features coexist typical of both anuran and urodele patterns of fertilization. *D. pictus* belongs to the oldest superfamily of anurans and *H. retardatus* to the oldest urodele family. While the possible evolutionary significance of these variations needs comparison with other species of the most primitive families, it is tentatively concluded that they might have been secondarily acquired. Future studies should establish which are the stable characters that are constantly found in urodele or in anuran fertilization.

Key words: fertilization, anurans, urodeles, eggs, sperm.

Introduction

Fertilization in amphibians has been studied in details only in urodeles and anura where it is so different to be considered an important character distinguishing the orders. The differences are related to behaviour and physiology of reproduction as well as to fine plasma membrane and cytoplasmic characteristics of the gametes. Recent studies have shown interesting variations with respect to the typical pattern of fertilization as investigated in the major groups of anurans and urodeles. These researchs are related to species belonging to the most primitive families in each orders.

Before introducing exceptions to the rule, I shall first summarize those features which appear to characterize fertilization in anurans and in urodeles. Attention will be paid to the cytological characters of fertilization which have been so far studied, namely to early changes occurring in both the gametes i.e. acrosome reaction, fertilization potential, ionic channels related to fertilization, monospermy and polyspermy changes in cytosolic calcium concentration, cortical reaction, changes of the egg surface, formation of the fertilization envelope, cortical contraction and early changes in cytoplasm consistency. For extensive reviews on these subjects the reader is addressed to Elinson (1986) and Katagiri (1987). Subsequently most attention will be paid to a species, *Discoglossus pictus*, belonging to the oldest superfamily among anurans, *Discoglossidea*, which has cytological characters related to fertilization more similar to urodeles than to anurans. These deviations from the pattern characteristic of anurans suggest that fertilization should be examined in other species belonging to *Leiopelmatidea* and *Discoglossidea*

as well as in primitive urodele families to better define differences in fertilization between the two orders.

Fertilization in anurans

Spermatozoa in anurans have a small apical acrosome granule (in *Rana*, Poirer & Spink, 1971) or an acrosomal cap of various morphology which generally covers the nucleus (in *Bufo*, Pugin-Rios, 1980 and in *Xenopus*, Bernardini et al., 1986). Generally, the undulating membrane is absent in the tail.

Eggs are surrounded by a variable number of jelly layers with specific macromolecular composition (usually glycoproteins) (Fig 1a). Sperm traverse the

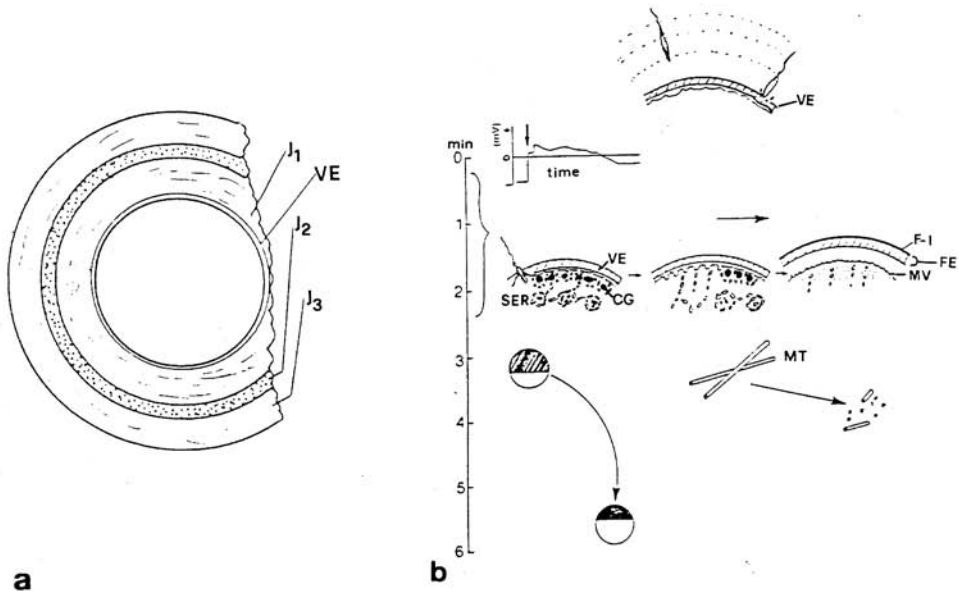


Fig. 1-a - Schematic drawing of an anuran egg. J1, J2 and J3 indicate jelly coats: Ve = vitelline envelope. b: summary of events occurring as a consequence of fertilization in anurans; explanation in the text. SER = smooth endoplasmic reticulum; MT = microtubules. (Modified from Elinson, 1986).

jelly coats in a matter of seconds (2-3). The jelly coat is essential for preparing sperm to the acrosome reaction, most probably because it provides proper ionic environment (Ishihara et al., 1984). While helping the sperm in getting ready for fertilization, the jelly also limits access to the egg as hydrates rapidly upon exposure to low ionic strength solutions, such as pond water and becomes a barrier to sperm. Also the number of sperm which reach the egg plasma membrane is relatively small thus indicating that jelly, even before hydration, may act by

sharply cutting down the number of sperm on their way to the egg surface. Sperm undergo the acrosome reaction at the vitelline envelope (VE). A 32 kdalton lysin released from *Bufo japonicus* sperm is most probably an acrosomal enzyme involved in sperm penetration through the VE (Yamasaki et al., 1988). Sperm always penetrate the egg in the animal hemisphere.

Microvilli cover both animal and vegetal hemispheres, but are longer at the animal half. In the microvilli actin and villin have been described (Franke et al., 1978; Corwin & Hartwig, 1983), whereas in the cortex actin and cytokeratin immunolocalized (Gall et al., 1983).

Among the lectins utilized for investigating saccharides at the egg surface, only WGA and SBA are bound by the dejelled egg (Charbonneau et al., 1986) thus indicating the presence of N-acetyl glucosamine residues. The plasma membrane of the animal half has slightly more intramembraneous particles, typically at the E surface (Bluemink & Tertoolen, 1978) and less lateral mobility of lipids (Dictus et al., 1984) compared to that of the vegetal half.

In the egg cortex there are cortical granules (CG) up to 2-2.5 μm in diameter with a fine homogeneous content surrounded by vesicles and/or cisternae of the smooth endoplasmic reticulum (SER) (Grey et al., 1974; Gomez et al., 1984) which are part of a network of cortical SER indicated to be the site of storage and release of Ca at activation (Campanella & Andreuccetti, 1977; Gardiner & Grey, 1983; Campanella et al., 1984; Andreuccetti et al., 1987). CG as well as cisternae are more concentrated in the animal hemisphere than in the vegetal hemisphere. This distribution pattern is a sign of the egg structural and functional organization whereby the animal hemisphere contains a number of organelles higher than in the vegetal hemisphere or molecules specific for one of the two hemispheres (King, 1985; Weeks & Melton, 1987). This distribution appears to operate along the animal-vegetal axis.

Early fertilization events

Figure 1b (modified from Elinson, 1986) indicates early events occurring at fertilization. The first measurable event is a change in membrane conductance which can be detected electrophysiologically as a depolarization of the plasma membrane, due primarily to the opening of chloride-permeable channels (Cross, 1980; Young, 1988). The activation of such channels depends upon an increase of intracellular calcium which ranges from 0.42 μM to 1.6 μM (in *Xenopus*, Busa & Nuccitelli, 1984). At this time chloride ions leave the eggs as first shown a long time ago by Maeno (1959) and by Ito (1972). Also potassium ions leave the egg at activation (Jaffe & Schlichter, 1985). Both K^+ and Cl^- channels open in a wave-like pattern which propagates along the egg plasma membrane (Jaffe et al., 1985; Kline & Nuccitelli, 1985).

Anuran eggs are monospermic. It has been suggested that the fertilization potential (FP) provides for the defense from polyspermy, which would make development abnormal or impossible. It has been found that by holding the membrane potential positive through injection of current, sperm are unable to enter the egg. When eggs are exposed to high external concentration of halides,

normal membrane depolarization is prevented and more than one sperm penetrate into the egg (Cross & Elinson, 1980; Grey et al., 1982; Charbonneau et al., 1983b; Jaffe et al., 1983). At present there is no way to test at a more direct level whether this hypothesis is correct as the molecular events leading to sperm and egg membrane fusion and to the egg membrane depolarization are still matter of speculation. Both the electrically recorded membrane noise (Charbonneau et al., 1983a) and the presence of small depolarization steps before the main depolarization event (Charbonneau et al., 1983b; Webb & Nuccitelli, 1985) suggest that at least a two steps reaction takes place at this stage (Dale et al., 1978; Dale & De Santis, 1981; De Felice & Dale, 1979). It has been hypothesized that the sperm inserts a protein in the plasma membrane (Jaffe & Cross 1986) or a molecule injected into the cytoplasm (Dale et al., 1985). Recently it has been shown that *Urechis* sperm release a protein from the acrosome (Gould & Stephano, 1897), which is able to depolarize the plasma membrane before intergametic fusion occurs. In myoblasts culture a surface kinase activity has been found to play a key role in intercellular fusion (Lognonne & Wahrmann, 1986). One may wonder whether a similar activity, to be found in the acrosome content or membrane, might play a similar role in intergametic fusion.

Sperm may interact with the egg surface through specific receptors. Although up to date any definitive evidence is available in this respect an elegant work by Kline et al. (1988) in *Xenopus*, shows that receptors might be involved in fusion and their occupancy may be perceived by the egg through a G-protein system. The transduced signal might then bring to the inositide hydrolysis (Busa et al., 1985; Turner et al., 1987). The deriving increase in cytosolic calcium has manyfolds consequences such as the activation of the Cl^- permeable channels, CG exocytosis and cortical contraction. Several further events, i.e. the depolymerization of microtubules and the inactivation of the cytostatic factor (see below) are consequent on such an increase, while the triggering of many others is still to be determined (see Charbonneau, 1989).

A shallow fertilization cone forms at the site of sperm entry which is generally transformed into a clump of microvilli and collapses into the cytoplasm.

Next to the site of sperm penetration the CG exocytosis takes place and propagates in 2-3 min to the antipode. The rate of propagation is shorter in the animal half compared to the vegetal half. This can be considered as a character denoting polarized functionality and most probably reflects the high concentration of SER cisternae in the animal hemisphere. As a consequence of CG exocytosis the egg microvilli elongate and the cortex stiffness increases as indicated by the fact that the cortex can be dissected from the cytoplasm as a sheet (Elinson, 1983).

A lectin released from the CG at the time of their exocytosis passes through the VE and reacts at the VE-jelly interface with the galactose residues present either in J_1 , the innermost jelly layer (Wyrick et al., 1974; Greve & Hedrick, 1978) or in a pre-fertilization layer secreted by the *pars recta* during the oocyte transit through the oviduct (Yoshizaki & Katagiri, 1984; Yoshizaki, 1984). Such interaction produces the electron-dense fertilization layer (F-layer) which consists of a thin and very electron-dense layer located over the VE. The F-layer formation produces an osmotic barrier; the water is trapped between the egg surface and the

fertilization envelope (FE) thus producing the perivitelline space and the lifting of the FE from the egg plasma membrane (Nishihara & Hedrick, 1977; Schmell et al., 1985). In the CG content proteases are also present which directly modify two components of the VE by producing a limited hydrolysis which changes their molecular weight. Furthermore new glycoproteins are added to the envelope. The result of such irreversible changes is the FE, constituted by the modified VE + the F-layer. Sperm are blocked at the FE at the time of its formation, i.e. within five min from egg activation. It is generally thought that as the membrane partially returns to negative values within 30 min from sperm entry, it is substituted in its role of polyspermy prevention, by the block operated by the FE. Such a block is permanent.

Several contraction waves run over the egg a few min following fertilization. The cortex first contracts towards the animal hemisphere, thus reducing the pigmented area, the peak of such contraction occurring at about 5 min after fertilization, then slowly relaxes. According to Elinson (1983, 1986) at the time of cortical contraction the cytoplasm changes from a gel consistency to a sol consistency, probably reflecting a change in the egg cytoskeleton. The main change detected in the cytoskeleton at this stage is the depolymerization of microtubules (Elinson, 1985).

Late fertilization events

The FE and perivitelline space formation permits the rotation of the egg with respect to gravity which is completed about 15 min following fertilization. Completion of meiosis, at the time of polar body extrusion, occurs at variable times according to the species, at about one fifth of the way through the first cell cycle (see Elinson, 1986). Meiosis is resumed because of the inactivation of the cytostatic factor which is responsible for the arrest at metaphase II. The grey crescent formation, which denotes the acquisition of embryonic dorso-ventral polarity, starts about half-way through the zygote cycle (Manes & Elinson, 1980). Cleavage starts at 1.5-3.5 hours after fertilization at 18°C, this large variation in time depending upon species.

Fertilization in urodeles

Spermatozoa in Urodeles have an acrosomal cap, and an undulating membrane substained by an axial rod. This structure is anchored to the nucleus in the implantation *fossa* and the region where both the posterior portion of the nucleus and the axial rod are found is called «neck». Sperm are clustered in the so-called spermatophores that female picks up in her cloaca where the sperm become stored in the spermatheca. Therefore fertilization is internal.

The jelly layers which surround the eggs (Fig. 2a) have variable density, in some species they do not have gelatinous, rather a coriaceous consistency (Salthe, 1963). Their role with respect to sperm is probably similar to that described for anurans.

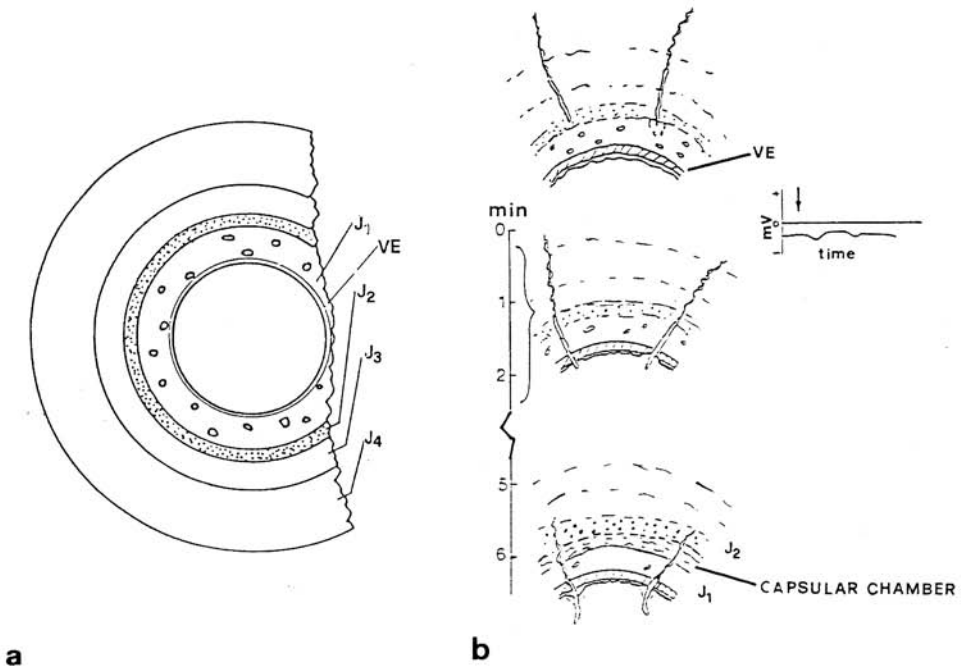


Fig. 2-a - Schematic drawing of an urodele egg. J₁, J₂, J₃ and J₄ indicate jelly coats; VE = vitelline envelope. b: summary of early events at fertilization; explanation in the text. (Modified from Elinson, 1986).

The acrosome reaction appears to start in the innermost jelly coat (Picheral, 1977). Sperm pass through the egg investments in a matter of minutes (5-10). Hydration causes the swelling of the jelly, as in anurans. Such hydration inhibits progression of sperm. Fertilization is physiologically polyspermic; sperm entry occurs in both hemispheres. However, the number of sperm compatible with normal development is relatively small and depends upon the species (four in *Cynops pyrrhogaster*, thirteen in *Notophtalmus viridiscens*, see Elinson's review, 1986). Practically there is not much information about the characteristics of the egg surface. CG are absent. Similarly, a cortical smooth endoplasmic reticulum has not been described.

Figure 2b indicates what is known about early events occurring at fertilization.

Upon fertilization there are practically no changes in the membrane potential, but small and short-lasting hyperpolarizations (Charbonneau et al., 1983 & Iwao, 1985). Also Cl⁻ permeable and Ca²⁺ activated channels are absent (Baud & Barish, 1984). By clamping the egg at a positive membrane potential sperm penetration does not appear to be impaired (Charbonneau, 1983b). No studies are available on changes in Ca²⁺ concentration at activation. Also changes in microvilli and the occurrence of cortical contractions have not been described.

Entry of sperm causes the formation of a shallow penetration cone devoid of microvilli which does not protrude out of the egg surface, rather is partially invaginated into the eggs. The cone is devoid of organelle inside (Picheral, 1977b). Taken together these data, it is not surprising to learn that there is neither elevation of the VE or its transformation into FE.

It is possible to acknowledge activation of the egg essentially for three phenomena: 1. The release of the II polar body; 2. the invasion of pigment in the previously pigment-free germinative area (the region around the animal pole); the formation of fluid-filled capsular chamber from the innermost jelly layer (Salthe, 1963; Picheral, 1977; McLaughlin & Humphries, 1978). This chamber appears to play a functional role similar to the perivitelline space of the anuran egg. In urodeles, as a consequence of the chamber formation, the egg is able to rotate according to gravity with its VE in the capsular chamber fluid and within the rest of the jelly envelopes. Most probably an osmotic barrier forms so that water is retained in the chamber. According to Jago et al. (1986), a precipitation layer occurs because of a lectin-ligand interaction deriving from the innermost and medium jelly layer. This reaction is reminiscent of the above mentioned CG lectin and pre-fertilization layer interaction in anuran eggs. Furthermore this layer appears to play an important role in blocking the penetration into the egg of a number of sperm over the critical one compatible with normal development. In *Ambystoma* there is not coincidence between the layer of precipitation and the layer where sperm are blocked (at the limit between jelly layer 3 and jelly layer 4) (Jago, 1986).

The final defense from polyspermy occurs in urodele eggs because of a mechanism which inhibits the fusion of more than one sperm pronucleus with the female pronucleus (Batallion, 1929; Fankouser, 1932; Fankouser & Moore, 1941).

Fertilization in *Discoglossus Pictus*

In *Discoglossus* many functional and morphological features of the gametes and of gametic interaction are unique of this species. By contrast, other features are shared with anuran or urodele species. Among the features typical of *D. pictus* there are: 1. egg morphology (egg diameter: 1.6 mm). The animal hemisphere is indented by a jelly component the animal plug (Ghiara, 1960). The center of this concavity is further invaginated and forms the cup-shaped *dimple* (Hibbard, 1928; Campanella, 1975) (Fig 3). 2. Spermatozoa length and arrangement in bundles. Sperm are 2.33 mm long (the longest vertebrate known) and are ejaculated in bundles of about 20. They are embedded in a shell made of orderly arranged filaments (Campanella et al., 1979) (Fig 4 and 5). 3. Sperm behaviour at insemination. When sperm come into contact with the surface of J_3 (the outermost jelly layer) the filament shell sticks to the jelly, particularly in the region overhanging the jelly plug (Fig 6a). Two or three seconds later sperm acquire motility and in a matter of seconds they come out of their shells and become embedded in the thick jelly coat facing the dimple. Indeed, they converge through the plug in the center of the dimple, D_1 , which is a disk 200 μm in diameter (Campanella & Gabbiani, 1979; Talevi & Campanella, 1988) (Fig 6b).

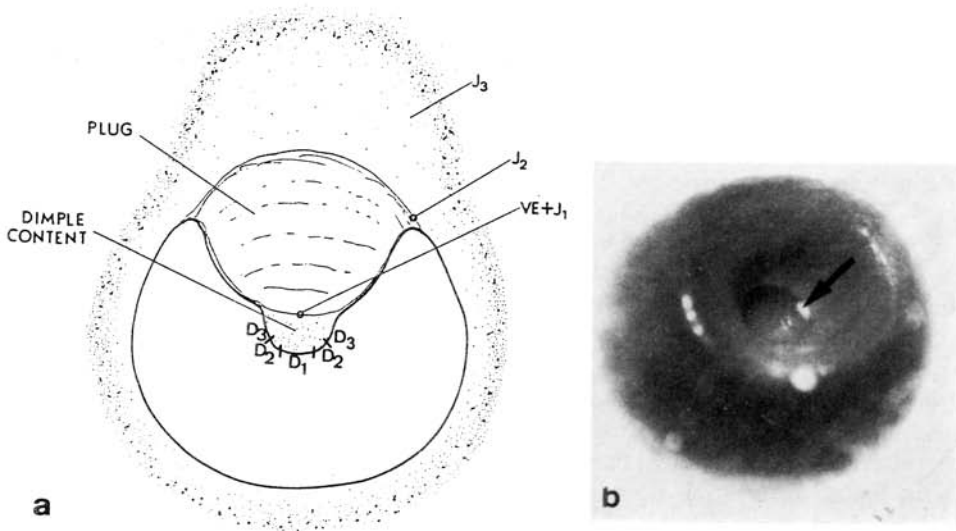


Fig. 3-a - Schematic drawing of a longitudinal section of *D. pictus* egg. J1 to J3 indicate jelly coats. The plug sits in the animal concavity. D₁ is the 200 μ m disk where fertilization occurs. D₂ and D₃ are the dimple walls. b = *D. pictus* egg. The dimple is indicated by the arrow and is located at the center of the animal concavity. X 27.

The plug appears to be the major responsible for this convergence. D₁ is the only site of the egg where fertilization occurs (Talevi & Campanella, 1988).

I shall now summarize the early events occurring at fertilization in *D. pictus* and described in Figure 7, which should also offer easy comparison with the corresponding events described in Figures 1b and 2b.

Some experimental evidence has shown that the acrosome reaction is triggered by the jelly coat, namely J₃, as for urodele sperm (Campanella, unpublished results).

We found that D₁ is endowed with special properties, with respect to D₂ and D₃, the dimple walls. More specifically, it is the only site where the egg can respond to an activating stimulus, including injection of IP₃ (Talevi et al., 1985; Nuccitelli et al., 1988). It has regularly arranged microvilli, while D₂ has less orderly microvilli implanted on the top of shallow cytoplasmic ridges and D₃ has short microvilli (Campanella et al., 1988). In the whole dimple a specific cytoskeletal organization is found having the highest complexity and extension in D₁. Actin, myosin, alfa-actinin, tropomyosin have been localized in the whole egg periphery (Campanella & Gabbiani, 1980; Campanella et al., 1982; Campanella et al., in press), whereas spectrin has been immunolocalized only in the dimple (Campanella et al., submitted).

D₁ surface binds FBP, thus denoting the presence of fucose residues, while the rest of the dimple binds WGA and SBA (Denis-Donini & Campanella 1977). Moreover D₁ has intramembrane particles with higher concentration and opposite polarization with respect to the rest of the dimple (Gualtieri et al., in press).

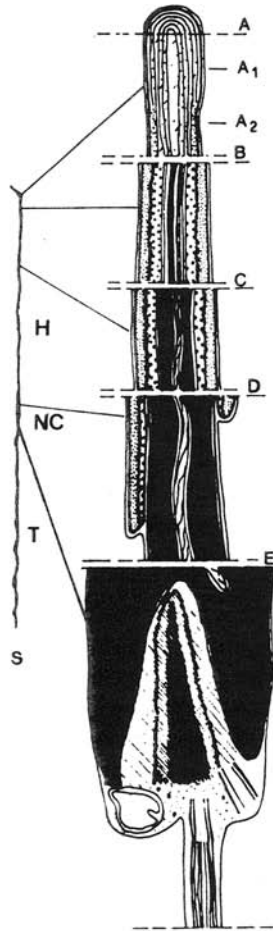


Fig. 4 - Schematic drawing of *D. pictus* sperm (S), where a head (H) with an apical rod, a neck (N) and a tail (T) are distinguishable. From A to B = apical rod; from B to E = nucleus covered by an acrosomal cap. The endonuclear canal is well distinguishable at the posteriormost portion of the sperm, approximately at E level (see Gabbiani & Campanella, 1979 for more details).

In physiological conditions (Fig. 7) sperm converge in D_1 where they elicit: 1) 30 sec to 1 min after insemination a FP which is Cl^- -dependent as in the other anuran eggs; 2) about 3 min later, fertilization cones practically identical to the cones of urodele eggs (Fig. 7 and 9); 3) the onset of development.

If the plug is experimentally displaced so that is not in axis with the dimple, sperm coverage in the dimple walls, induce unusual depolarizations of the plasma membrane, the formations of cytoplasmic protrusions instead of fertilization cones, and do not initiate development (Talevi & Campanella, 1988). At activation a fertilization current, Cl^- transported, is found only in D_1 and does not

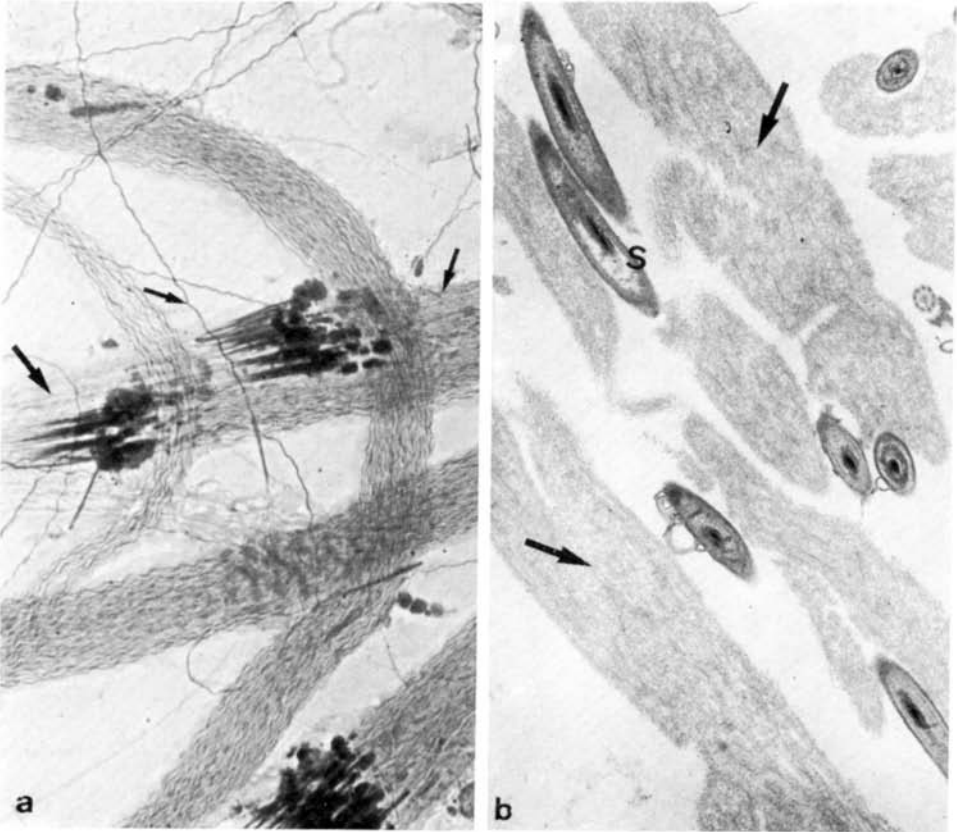


Fig. 5 - Sperm bundles. a: The very long threads are the heads, which are about $900\ \mu\text{m}$ long (arrow), or the tails (small arrows). The strongly stained segments are the posteriormost portions of the head. X1000. b: The arrows indicate the fibrillar matrix where sperm (S) are embedded. X 12000.

propagate to the rest of the egg. Therefore Cl^- channels localization in *D. pictus* is restricted to the dimple central domain (Nuccitelli et al., 1988). Apparently, the characteristics of anuran egg animal half are restricted in this species to a very limited region, i.e. D_1 . The rest of the egg appears quite comparable to urodele eggs; such similarity includes also the absence of CG. In fact CG are present only in the dimple, with a peak of concentration in D_1 .

Three kinds of SER, i.e. vacuoles, cisternae and clusters of cisternae, are also found in the dimple where they have a specific distribution related to the cytoskeleton organization. They are probable site of calcium storage and release at activation (see below). In the rest of the egg such components are scantily present (Andreucetti & Campanella, 1985; Campanella et al., 1988).

An eightfold increase of calcium has been measured at activation. The calcium release starts at the dimple and propagates to the rest of the egg. It transmits to the rest of the egg the stimulus perceived in the dimple, a second

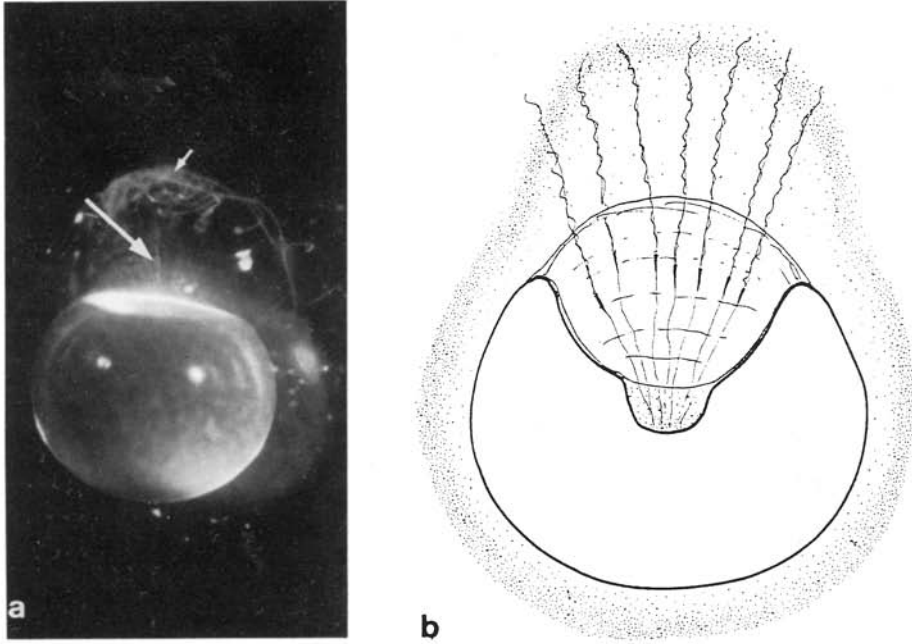


Fig. 6-a - *Discoglossus pictus* egg, few sec following insemination. Sperm bundles stick at the surface of J3 (small arrow), whereas single sperm are in the jelly over the dimple. X 20. b: schematic drawing of *D. pictus* egg showing sperm convergence through the plug in D1.

messenger role as in other anuran eggs. It has been hypothesized that the level of calcium is much higher in the dimple region where the highest concentration of putative sites of calcium stores is found (Nuccitelli et al., 1988). Such transient is 40 min long and is apparently responsible for the exocytosis of CG and vacuoles and for the transformations of the SER clusters at activation (see Figs 7 and 8) (Campanella et al., 1988).

Like in urodeles the eggs are physiologically polyspermic, however the membrane is depolarized at fertilization quite similarly to anurans eggs. It has been demonstrated, by holding the potential at positive values or by the use of high concentrations of halides, that there is no relationship between membrane potential and sperm penetration (Talevi, 1989). The number of sperm admitted in D_1 is never higher than 8. This limitation is probably due to the D_1 size and by the fact that sperm converge in this site. Also egg investments may have a role in cutting down the number of sperm that reach the plasma membrane (Talevi, 1989). There is also a late block to sperm entrance occurring at the fertilization envelope, which forms by the interaction of the vitelline envelope with products of the exocytotic phenomena occurring at activation (Campanella, unpublished results). The FE fails to lift over the egg as it is already far apart from the plasma membrane (see Figs 3 and 7).

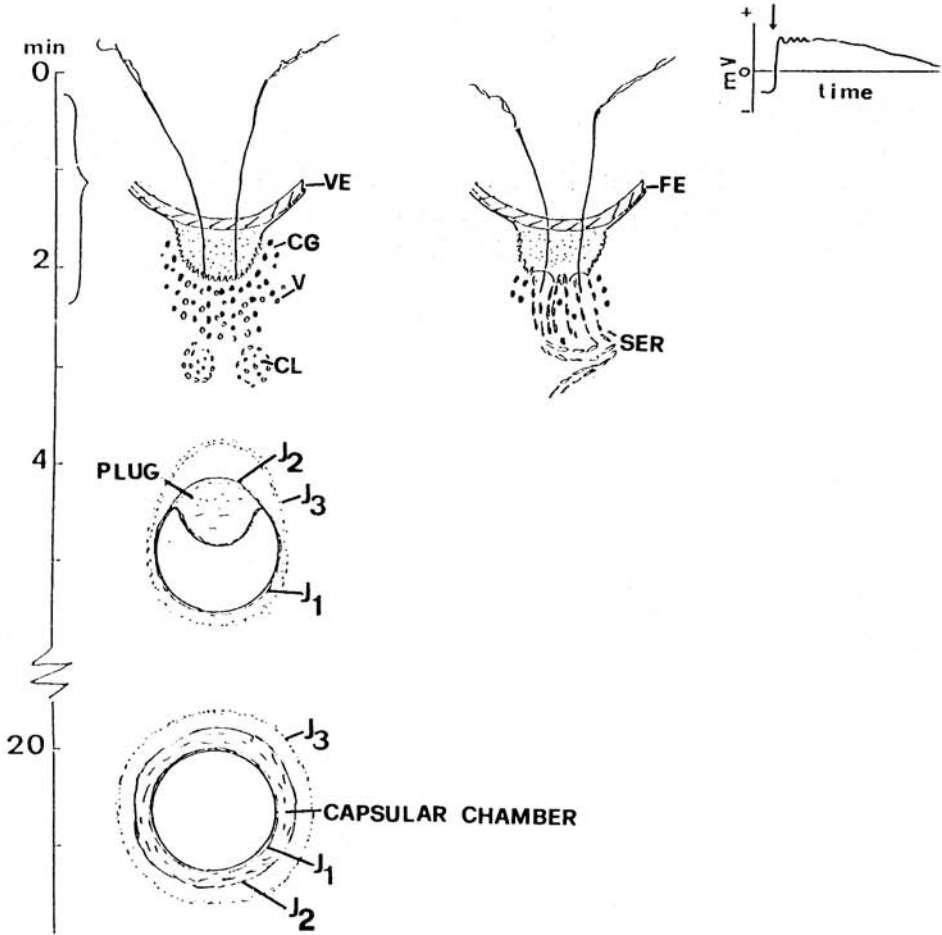


Fig. 7 - Summary of fertilization events in *D. pictus*. Explanation in the text. SER = smooth endoplasmic reticulum; CL = clusters of endoplasmic reticulum. (Modified from Elinson, 1986).

Another peculiarity of *D. pictus* is that sperm penetrate into the egg at least in two steps, the first occurring at the initial gametic fusion and the second occurring about 40 min after fertilization (Talevi & Campanella 1988).

Which are the signs of activation in this egg? They consist mainly in two groups of phenomena: 1) a cortical contraction which occurs in the dimple a few min following fertilization and then spreads to the rest of the egg. As a consequence the dimple regresses (Talevi et al., 1985) (see Fig 7). 2) About 15 min from insemination the concavity disappears as a result of the plug liquefaction. Like in urodeles a capsular chamber is formed in which the egg with its VE and J₁ is free to rotate (see Fig 7). Such a phenomenon is a consequence of the release of

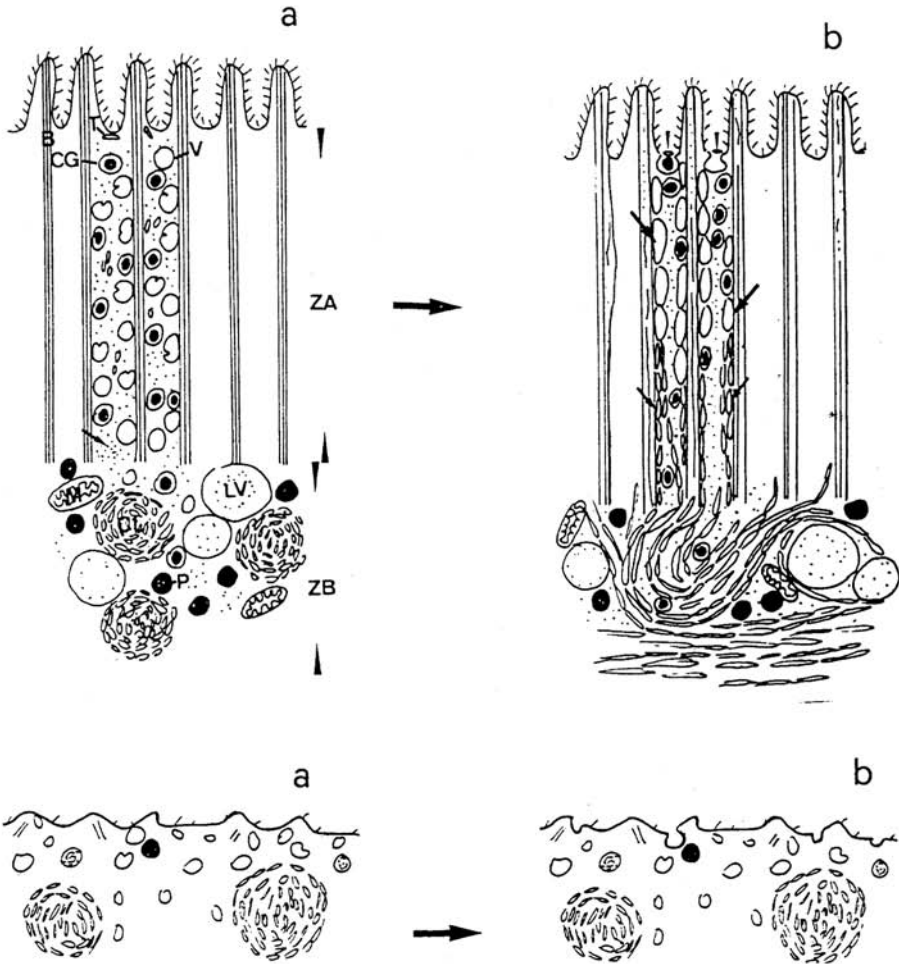


Fig. 8 - Cortical reaction in *D. pictus*, in the dimple (upper row) or outside the dimple (lower row). In the dimple CG and vacuoles exocytose and the clusters of the endoplasmic reticulum in ZB undergo chains of cisternae which migrate toward the plasma membrane. Outside the dimple the clusters do not change, only a few exocytoses of vacuoles occur.

peripheral vacuoles content from the egg and involves the reduction of disulphide bonds present in the plug macromolecules (Pitari et al., 1987).

Recent findings in other anuran and urodele species

Among anurans, *Ascaphus truei* (*Leiopelmatidae*) has internal fertilization and, among urodeles, the most primitive fertilization. Furthermore, in addition to *D. pictus*, a second species appears to constitute an important exception to the

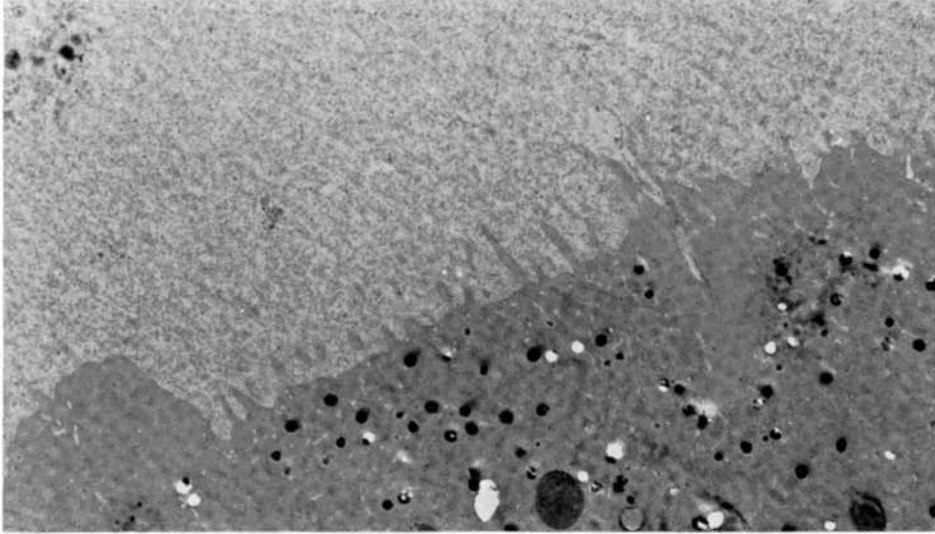


Fig. 9 - Early stages of sperm-egg interaction (about 3 min following insemination). On the left a fertilization cone is observed, on the right a second fertilization cone where a sperm (arrow) is engaged in penetrating into the egg. X 5200.

polyspermy prevention pattern of the anuran egg. Elinson (1987) has reported that in *Eleutherodactylus coqui*- a frog of the *Leptodactylinae* family displaying internal fertilization and development on land-fertilization is restricted to a limited portion of the animal hemisphere. Although eggs have CG, polyspermic cases of fertilizations have been found, which are compatible with normal development. On the urodeles side, in *Hynobius nebulosus* eggs, the fertilizing spermatozoon or Ca-ionophore elicit a positive FP mediated by an increased permeability to Cl^- . Furthermore the egg is monospermic and a relationship has been described between potential and polyspermic block as for anuran eggs. On the other hand, the egg has no CG, and jelly coats appear to have a role in the maintenance of monospermy by reducing sperm access to the egg (Iwao, personal communication). *H. nebulosus* belongs to *Hynobiidae*.

Concluding Remarks

D. pictus in the anuran and *H. nebulosus*, in the urodeles, belong to the most ancient families of the orders. Therefore it would be tempting to speculate that putative ancestor species might have carried eggs with mixed fertilization patterns and that the fertilization model of anuran and urodele eggs may have become stabilized in the more recent families of the order. However the hypothesis appears to be quite improbable. In fact, in the same family of *D. pictus*, *Bombina* and *Alytes* display fertilization features of the typical anuran pattern, with the

exception of the capsular chamber formation in *Alytes* (Salthe, 1963). Future studies on species belonging to the most ancient families of the two orders, should help in clarifying the history of the divergence between the fertilization patterns of the most recent urodeles and anurans. Particularly the study of *D. montalenti* egg and fertilization would offer special interest as this species diverged from the common ancestor of the other *Discoglossus* species 6,000 millions years ago (Lanza et al., 1986).

In the case of anuran *D. pictus* I have described the characters typical of the species, namely the organization of the jelly coat, the modality of sperm-egg interactions, and the two stages of sperm penetration into the egg. If one eliminates the above mentioned hypothesis, such characters might represent secondary adaptations to environmental conditions. In my opinion, also the partition of the egg in two territories, one with typical anuran features and the other with urodele characters, as well as the fertilization come organization, might be well considered part of the above mentioned characters. For example the restriction in the central part of the dimple of the properties which enable successful sperm-egg interaction appears related to the organization of the jelly coat. Furthermore, the capsular chamber of *D. pictus* cannot be considered homologous to the chamber of urodele eggs as the chambers form in different ways. Most probably *D. pictus* capsular chamber substitutes the perivitelline space which does not form because of the absence of CG in most of the egg cortex.

Special attention deserves physiological polyspermy that is generally considered the most relevant character of distinction between urodele and anuran fertilization. It is therefore noteworthy that, both *D. pictus* and *E. coqui*, two anurans, display eggs which may admit more than one sperm. Such eggs do survive and give rise to normal tadpoles, provided that the number of sperm is limited (dispermic or trispermic eggs in *D. pictus*) (Elinson, 1987; Talevi, 1989). Given that *E. coqui* belongs to the family of *Leptodactylinae*, which is much more recent than the *Discoglossidae*, the most reasonable conclusion is that also physiological polyspermy was fixed randomly as secondary adaptation. At this point the question arises whether characters related to fertilization do exist in anuran and urodele eggs, which define sharp distinctions between the two orders even in those species which secondarily acquired features generally present in the other order. It does not seem to be the case of internal and external fertilization for several exceptions are known; some of them have been here mentioned. As suggested by Elinson (1986), a main point could be the destiny of supernumerary sperms in polyspermic zygotes which appear to be related to different cytoplasmic characteristics of the zygotes in the two orders. In urodeles supernumerary sperms develop a single aster and degenerate. Only one sperm fuses with the egg nucleus. Cleavage is regular and blastomeres are diploid. In anurans, polyspermy can be experimentally induced. Every sperm develops two asters and do not degenerate. At the first cleavage a variable number of furrows and of aploid or diploid blastomeres is found. Future study should establish whether in anuran species carrying eggs with polyspermy compatible with development (*D. pictus* and *E. coqui*) and in urodele species with monospermic eggs (*H. nebulosus*), the destiny of supernumerary sperms follows the pattern typical of the order.

REFERENCES

- Andreuccetti P., Denis Donini S., Burrini M.G., Campanella C., 1984 - Calcium ultrastructural localization in *Xenopus laevis* eggs following activation by pricking or by calcium ionophore A23187. *J. exp. Zool.*, 229: 295-308.
- Andreuccetti P., Campanella C., 1985 - Ca-antimony deposits in *Discoglossus pictus* egg during activation Differentiation, 16: 455 (Abstr.).
- Baud C., Barish M.E., 1984 - Changes in membrane hydrogen and sodium conductance during progesterone-induced maturation in *Ambystoma* oocytes. *Dev. Biol.*, 105: 423-434.
- Bernardini G., Stipani R., Melone G., 1986 - The ultrastructure of the spermatozoon of *Xenopus laevis*. *J. Ultrastruct. Res. mol. Struct.*, 94: 188-194.
- Busa W.B., Nuccitelli R., 1985 - An elevated free cytosolic Ca^{2+} wave follows fertilization in eggs of the frog, *Xenopus laevis*. *J. Cell Biol.*, 100: 1325-1329.
- Campanella C., Andreuccetti P., 1977 - Ultrastructural observation on the cortical and subcortical endoplasmic reticulum and on residual cortical granules in the egg of *Xenopus laevis*. *Dev. Biol.*, 56 1-10.
- Campanella C., 1975 - The site of spermatozoon entrance in the unfertilized egg of *Discoglossus pictus* (Anura): an electron microscope study. *Biol.Reprod.*, 12: 439-447.
- Campanella C., Gabbiani G., 1979 - Motile properties and localization of contractile proteins in the spermatozoon of *Discoglossus pictus*. *Gamete Res.*, 2: 163-175.
- Campanella C., Gabbiani G., 1980 - Cytoskeletal and contractile proteins in coelomic oocytes, unfertilized and fertilized eggs of *Discoglossus pictus* (Anura). *Gam. Res.*, 3: 99-114.
- Campanella C., Atripaldi U., Gabbiani G., 1981 - Osservazioni sugli spermatozoi di *Discoglossus pictus* (Anuro) con particolare riferimento alle caratteristiche motorie. *Quaderni di «La Ricerca Scientifica»*, 110: 239-246.
- Campanella C., Ruggeri-Brandle E., Gabbiani G., - 1982. Immunolocalization of alfa-actinin in an amphibian egg (*Discoglossus pictus*). In: M. Burger & R. Weber (eds). *Embryonic development. Part B: Cellular Aspect: Alan Liss, New York*, pp 45-53.
- Campanella C., Andreuccetti P., Taddei C., Talevi R., 1984 - The modifications of the cortical endoplasmic reticulum during «in vitro» maturation of *Xenopus laevis* oocytes and its involvement in cortical granules exocytosis. *J. exp.Zool.*, 229: 283-294.
- Campanella C., Talevi R., Kline D., Nuccitelli R., 1988 - The cortical reaction in the egg of *Discoglossus pictus*: A study of the changes in the endoplasmic reticulum ièat activation. *Dev. Biol.*, 130: 108-119.
- Charbonneau M., 1989 - Weak bases mimic the fertilization-associated chloride-conductance increase and induce morphologicak changes in the cortex of *Xenopus laevis* eggs. *Cell Differ. Dev.*, 26: 39-52.
- Charbonneau M., Moreau M., Picheral B., Guerrier P., Vilain J.P., 1983a - Voltage noise changes during monospermic and polyspermic fertilization of the mature egg of the anuran *Rana temporaria*. *Dev. Growth Differ.*, 25: 485-494.
- Charbonneau M., Moreau M., Picheral B., Vilain J.P., Guerrier P., 1983b - Fertilization of Amphibian eggs: A comparison of electrical responses between anurana and urodeles. *Dev. Biol.*, 93: 304-318.
- Charbonneau M., Dufresne-Dube, Guerrier P., 1986 - Inhibition of the activation reaction of *Xenopus laevis* eggs by the lectins WGA and SBA. *Dev. Biol.*, 114: 347-360.
- Corwin H.L., Hartwig J.H., 1983 - Isolation of actin-binding protein and villin from toad oocytes. *Dev. Biol.*, 99: 61-74.
- Cross N.L., 1981 - Initiation of activation potential by an increase in intracellular calcium in eggs of the frog *Rana pipiens*. *Dev. Biol.*, 85: 380-384.

Spectrin and Ankyrin-like Proteins in the Egg of *Discoglossus pictus* (Anura): Their Identification and Localization in the Site of Sperm Entrance versus the Rest of the Egg

(spectrin/ankyrin/anuran eggs/fertilization)

Carla Tatone, Rosa Carotenuto¹, Rosella Colonna, Christine Chaponnier*, Giulio Gabbiani*, Mauro Giorgi and Chiara Campanella¹

Dipartimento di Scienze e Tecnologie Biomediche, Università di L'Aquila, Italy.

*Department de Pathologie, Université de Geneve, Geneve, Switzerland.

¹Present address: Dipartimento di Biologia Evolutiva e Comparata, Università di Napoli, Italy.

The *Discoglossus pictus* egg has a specific site of sperm-egg interaction, the dimple, which has a well-defined cytoskeleton. We studied whether there are cytoskeletal and cytoskeleton-related proteins typically involved in the polarization of plasma membrane proteins. The identity and the localization of the molecules cross-reacting with antispectrin, antifodrin and antiankyrin antibodies were investigated by immunofluorescence and immunoblotting of the proteins of the dimple (D) and of the rest of the egg (dimple-less-egg; DLE). Two polypeptides of about 254- and 246-kD were detected in the D and DLE, and localized in the egg cortex. A third molecule, weakly cross-reacting with antispectrin and antifodrin, was found in the subcortical cytoplasm. The 246-kD polypeptide was labile in samples prepared for SDS-PAGE; a mild pre-fixation of eggs prevented its dispersion. Mild fixation was also needed to retain antispectrin reactivity in cryostat sections of the DLE cortex, while this is not necessary in D. A molecule of about 204-kD, cross-reacting with antiankyrin, was detected in the cortex of the whole egg. These data and the finding that the concentrations of both the 254-kD polypeptide and ankyrin are about 12-fold higher in D than in the DLE, suggest that, in D, spectrin has a specific organization.

Introduction

Various ionic channels are present in the egg plasma membrane, some of which are involved in membrane depolarization at fertilization (for a review, see 39). G proteins and probably sperm receptors (24, 25) occur in the egg plasma membrane and they might coincide with the fertilization channels (see 19). A key question in fertilization is: which of the molecules present in the membrane is involved in sperm-egg interaction? An important, yet unexplored, approach to this problem would be the search for a cortical organization providing the plasma membrane with the anchoring of such molecules.

The egg of *Discoglossus pictus* lends itself to this studies because it is endowed with a specific site of sperm penetration, the dimple, which has the prerequisites for sperm-egg interaction (47), a high concentration of fertilization channels (38) and

intramembrane particles (20), as well as a specific cytoskeleton organization. The cytoskeleton consists of actin microfilaments that extend from the central core of the microvilli of this region into the peripheral cytoplasm, and that form a cortical network. Myosin, tropomyosin, alpha-actinin and tubulin are also present in the dimple (for a review, see 9).

The analysis of the molecules present in the dimple plasma membrane and cortex and absent from or differently organized in the rest of the egg periphery may provide data on the molecules involved in the fertilization process. Particularly, the present paper raises the question whether proteins, such as spectrin (alpha-spectrin, Mr 240,000 and beta-spectrin Mr 220,000) and ankyrin (Mr 210,000, in human erythrocytes) are present in the cortex of these two regions of the *D. pictus* egg, which might account for the anchoring and compartmentalization of intrinsic proteins in the dimple and/or in the rest of the egg. Indeed, in erythrocytes as well as in other cells (i.e., in the

Correspondence should be addressed to Chiara Campanella

kidney, 14; in epithelial cells, 37; in the muscle, 36; in neurons, 35) spectrin connects the cortical cytoskeleton with plasma membrane proteins, such as channels and receptors, mainly through the bridging protein, ankyrin (for reviews, see 29, 1, 34, 12). The presence of ankyrin has not been investigated in eggs, through spectrin has been detected in echinoderms and mammals eggs (15, 27, 44, 45). In *Xenopus laevis* eggs, Giebelhaus et al. (17) have demonstrated the presence of a spectrin-like molecule showing a good degree of analogy with human erythrocyte alpha-spectrin and whose synthesis is developmentally regulated. However, these authors have not advanced hypotheses on the possible presence of a companion subunit of spectrin and on the role of the spectrin-like molecule they detected.

Previously we studied the immunolocalization of spectrin in oocyte and egg sections of *D. pictus*, and found that in sections of unfixed oocytes, cross-reactivity to antispectrin is detectable in the cortex of polarized oocytes, and during the transformation of the flat germinative area (GA) into the concave dimple such positivity concentrates exclusively in this region (10). The present paper aims at identifying and localizing the molecules that cross-react with antispectrin, and to map the presence of ankyrin in *D. pictus* eggs.

Materials and Methods

Animals: Adult females and males of *D. pictus* were collected in the neighborhood of Palermo, Italy. Females were injected with 250 UI Profase (Serono, Italy) in Amphibian Ringer solution in the dorsal lymphatic sac, so that, about 18 hrs later,

eggs could be collected from the ovisac (47).

Solutions and Buffers: Amphibian Ringer: NaCl 111 mM; CaCl_2 1.3 mM; KCl 2 mM; MgSO_4 0.8 mM; Hepes 25 mM pH 7.8. Dejellinging buffer: NaCl 100 mM; DTT 5 mM; 50 mM Tris-HCl pH 8.0. Homogenization buffers: (1) 25 mM HB: 900 mM glycerol; 0.02 mM NaN_3 ; 1 mM ATP; 1 mM DTT; 5 mM EGTA; HEPES 25 mM pH 7.5. (2) modified De Boer's: 110 mM NaCl; 1.3 mM KCl; 5 mM EDTA; NaHCO_3 to pH 7.4. This solution was utilized only for the sample shown in Fig. 2 (lane b).

The following protease inhibitors were added to these buffers: 0.5 mM PMSF or 0.1 mM DFP; 2 mM TAME; 5 $\mu\text{g/ml}$ SBTI; 5 $\mu\text{g/ml}$ aprotinin; 25 $\mu\text{g/ml}$ leupeptin.

Preparation of the samples:

GHOSTS: Human erythrocyte ghosts were prepared according to Marchesi (33). Aliquots were suspended in electrophoresis buffer and stored at -80°C .

EGGS: Eggs were dejellied in dejellinging buffer. After manual removal of the vitelline envelope (VE), the eggs were homogenized as follows:

A. **Total eggs:** whole eggs were centrifuged at 15,000 g for 30 min and the supernatant (S1) was used for electrophoresis.

B. **Cortex-enriched eggs:** eggs were broken in 25 mM HB and aspirated back and forth in a Pasteur pipette to separate the peripheral portion of the egg, which was then collected. Dimples were dissected out of the rest of the egg with watchmaker's forceps as shown in Fig. 1. Samples were centrifuged at 15,000 g for 30 min and the supernatant (D S2 and DLE S2) was used for electrophoresis.

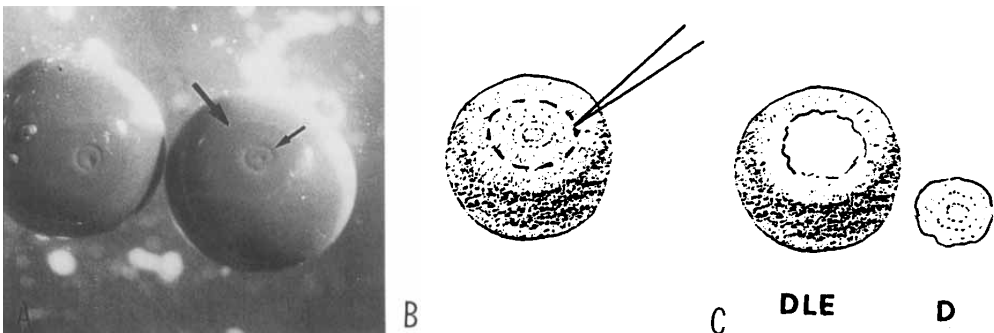


Fig. 1. A partially dejellied egg, endowed with vitelline coat and the innermost jelly layer. The dimple, which is a large indentation in the intact egg, becomes flushed to the egg surface after DTT treatment. The smaller arrow indicates D1 (the central portion of the dimple), the larger arrow the concentric boundaries, the dimple walls. b and c=manual dissection of the dimple (D) from egg to obtain a dimple-less egg (DLE).

C. *Partially-cleaned-cortices*: D and DLE were separated and spread on glass petri dishes containing 25 mM HB on ice. Under these conditions some cytoplasm spreads into the medium. After one rinse in fresh buffer, D and DLE were collected, centrifuged at 15,000 g for 30 min and analyzed for electrophoresis.

D. *Cortices*: D and DLE were separated and spread on glass petri dishes containing 25 mM HB on ice. After repeated rinses in the fresh buffer, the whole cytoplasm was lost and cortices were collected, homogenized and analyzed with electrophoresis. Alternatively they were pelleted at 1,500 g for 10 min before SDS-PAGE (see Electrophoretic Analysis of Cortices). When indicated, eggs were fixed before collection of the cortices for 1, 3 and 10 min in 1% formaldehyde (see Immunofluorescence and Microscopy).

E. *ZnCl₂-cortices*: 10 mM ZnCl₂ were added to 25 mM HB, and the eggs were soaked for about 30 min in this medium. The cortices appeared somehow hardened by the treatment and were then easily peeled from the eggs with forceps as entire sheets. In contrast to untreated cortices, they do not release cytoplasm upon soaking in 25 mM HB. They were pelleted at low speed; the supernatant did not contain proteins.

Electrophoresis sample buffer (28) containing mercaptoethanol was added to the samples, which were then boiled for 3 min.

Protein determination, electrophoresis and densitometric analysis: The protein concentration of ghosts, S1 and S2 eggs, was measured with the Bio-Rad assay. 50–60 µg proteins were loaded for each electrophoretic run, as detailed for each experiment. About 10 D and 5 DLE cortices, with one exception (see Fig. 8), were used for each run when whole cortices were analyzed.

Protein samples were analyzed with SDS-PAGE using Laemmli's Tris-glycine buffer system (28). The running gel contained 6% or 5% acrylamide; the stacking gel contained 3% acrylamide. 5–20% gradients were also used.

Coomassie blue-stained gels were analyzed with an LKB 2202 Ultrascan Laser Densitometer.

Antibodies: Affinity-purified antibodies against spectrin from human erythrocytes raised in rabbits, were a gift from Dr. V. Marchesi, antihuman brain fodrin raised in rabbit from Dr. A. Harris, and antihuman erythrocyte ankyrin raised in rabbit from Dr. J. Morrow (V. M., A. M. and J. M. are from the Department of Pathology, Yale University, School of

Medicine, New Haven, CT).

Immunological detection on nitrocellulose of spectrin and ankyrin: Proteins subjected to SDS-PAGE were electrophoretically transferred to nitrocellulose sheets according to Towbin *et al.* (48) for 6 hrs at 400 mA. The efficiency of the transfer was evaluated by staining the nitrocellulose sheets with Neutral Red and Coomassie blue of the corresponding gel. The nitrocellulose sheets were then incubated with 5% fat-free milk (Milupa, Verona, Italy) to saturate additional protein binding sites, rinsed in saline and incubated with antispectrin, antifodrin, antiankyrin or non-immune rabbit serum. Human erythrocyte ghosts or *D. pictus* blood were used as positive controls. Antibody binding was detected by anti-rabbit IgG, raised in goat and conjugated to alkaline phosphatase, using the Protoblot Immunoscreeing system (Promega, Madison, U.S.A.).

Immunofluorescence microscopy: Eggs were dejellied and immersed for 10 min in 1% formaldehyde prepared from paraformaldehyde (PFA) and diluted in 1/10 Ringer. After several rinses the eggs were frozen, sectioned and fixed in acetone at 20°C for 5 min. The 5-µm sections were dried and then incubated with antispectrin, antifodrin or antiankyrin for 45 min. The samples were then incubated with fluorescein-conjugated anti-rabbit IgG. Ten per cent *D. pictus* serum was added to the sera used for the second incubation to eliminate possible cross-reactivity with *D. pictus* tissues. The sections were rinsed in PBS and mounted in 90% glycerol in PBS pH 9, after which the level of fluorescence was compared with that in control sections treated with rabbit gamma globulins for antispectrin, or normal rabbit serum for antifodrin and antiankyrin.

Pelleted cortices were fixed in 2% glutaraldehyde in 0.2 M phosphate buffer pH 7.4, post-fixed in 1% osmium tetroxide and, after dehydration in alcohol, embedded in epon. Thick sections were obtained by a Porter ultramicrotome and stained with toluidine blue.

Photographs were taken with a Leitz UV microscope, using Kodak Tmax p3200.

Results

Electrophoretic analysis of total or cortex-enriched homogenates. Immunoblots obtained with anti-spectrin and antifodrin

Fig. 2 shows a detail of an SDS-PAGE gradient

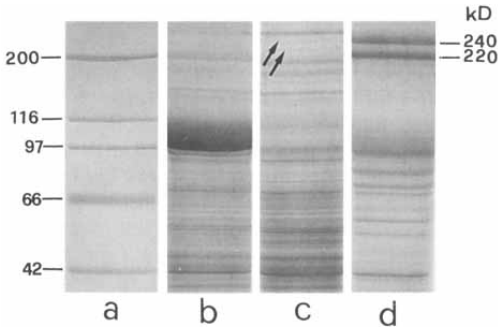


Fig. 2. Upper portion of an SDS-PAGE 5–20% gradient. Lane a=Reference molecular weights (kD). Lane b=S1 of eggs (68 μ g) homogenized in De Boer's. Lane c=S1 of eggs (68 μ g) homogenized in 25 mM HB. The arrows indicate two bands with an Mr in the range of spectrin. Lane d= α and β spectrin of erythrocyte ghosts (kD).

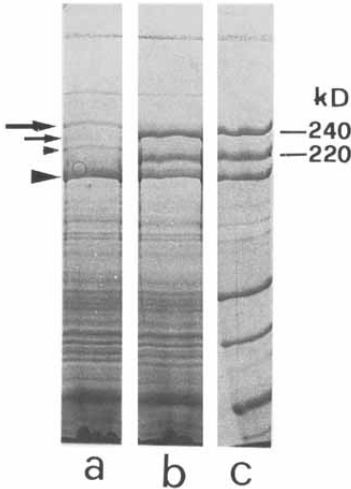


Fig. 3. Comigration of S2 with α and β spectrin of erythrocyte ghosts. The samples were separated on an SDS/5% acrylamide gel. Lane a=S2 (60 μ g); lane b=S2 (60 μ g) and ghosts; lane c=ghosts and reference molecular weights (spectrin=240- and 220-kD). Larger arrow=band of about 254,000 Mr; smaller arrowhead=band of about 225,000 Mr; larger arrowhead=band of about 204-kD; smaller arrow=minor band of about 246-kD.

of the supernatant of the total egg homogenate (S1) and of human erythrocyte ghosts (lanes b, c and d respectively). With 25 mM HB as homogenization buffer, two bands were present with an Mr in the range of spectrin (220,000–240,000 daltons), whereas, these bands did not appear with De Boer's as homogenization buffer. To get a better resolution of these proteins, we used S2 (B procedure) and 5% SDS PAGE (Fig. 3).

Comigration of S2 and erythrocyte ghosts (Fig. 3) and Rf calculation in the D and DLE samples

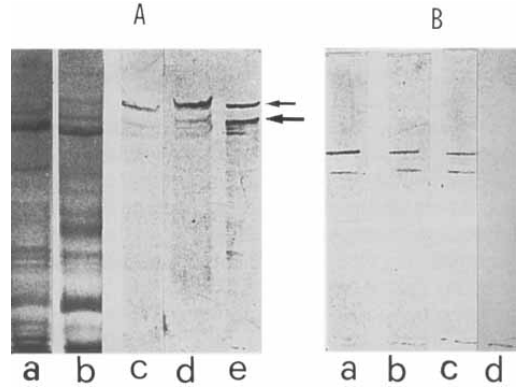


Fig. 4. Western blots with antispectrin and antifodrin. A. Lane a=Dimple S2 (51 μ g), Coomassie blue staining; lane b=dimple-less-egg S2 (66 μ g), Coomassie stained; lanes c, d, e=samples transferred onto nitrocellulose paper and incubated with anti-human erythrocyte spectrin. Lane c=D (50 μ g); lane d=DLE (60 μ g); lane e=human erythrocyte ghost. Smaller arrow= α -spectrin; larger arrow= β -spectrin. Both the 254- and the 225-kD bands are immunoreactive. Note the light degradation of spectrin in e. B. Lanes a, b, c=samples transferred onto nitrocellulose paper and incubated with anti-fodrin; a=human erythrocyte ghosts; b=DLE (56 μ g); c=D (54 μ g). Both the 254- and the 225-kD bands are positive. d=DLE (58 μ g) incubated with normal rabbit serum; no reactive bands are present.

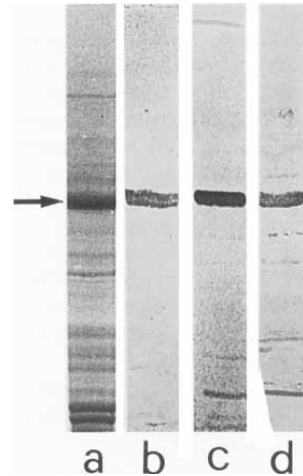


Fig. 5. Detection of ankyrin in D and DLE. Lane a=Coomassie blue staining pattern of DLE (60 μ g); the arrow indicates a band of about 204-kD. Lanes b, c, d=western blots probed with antibody to human erythrocyte ankyrin. Lanes b (D) (58 μ g of proteins) and c (DLE) (61 μ g of proteins) are reactive to this antibody on the 204-kD band. Lane d (ghosts) ankyrin (210-kD) is reactive to the antibody.

indicated that the two bands had an apparent Mr of approximately 254- and 225-kD; in addition a minor band of about 246-kD was also present (Fig. 3). Moreover, a prominent band of about 204-kD appeared in the 5% polyacrylamide gels (Figs. 3 and 5).

Dimple and DLE S2 were transferred onto nitrocellulose sheets and probed with antispectrin or antifodrin. In the immunoblots (Fig. 4), anti-spectrin reacted with the alpha and beta subunits

of erythrocyte spectrin, the 254-kD protein and, to a lesser extent with the 225-kD protein in both D and DLE S2. Antifodrin reacted with spectrin from human ghosts, and with 254- and -225 kD proteins (Fig. 4).

When the nitrocellulose sheets were incubated with anti-ankyrin, the 204-kD band reacted positively (Fig. 5). No cross-reactive bands were detected (Fig. 4d), when the transferred samples were exposed to rabbit serum.

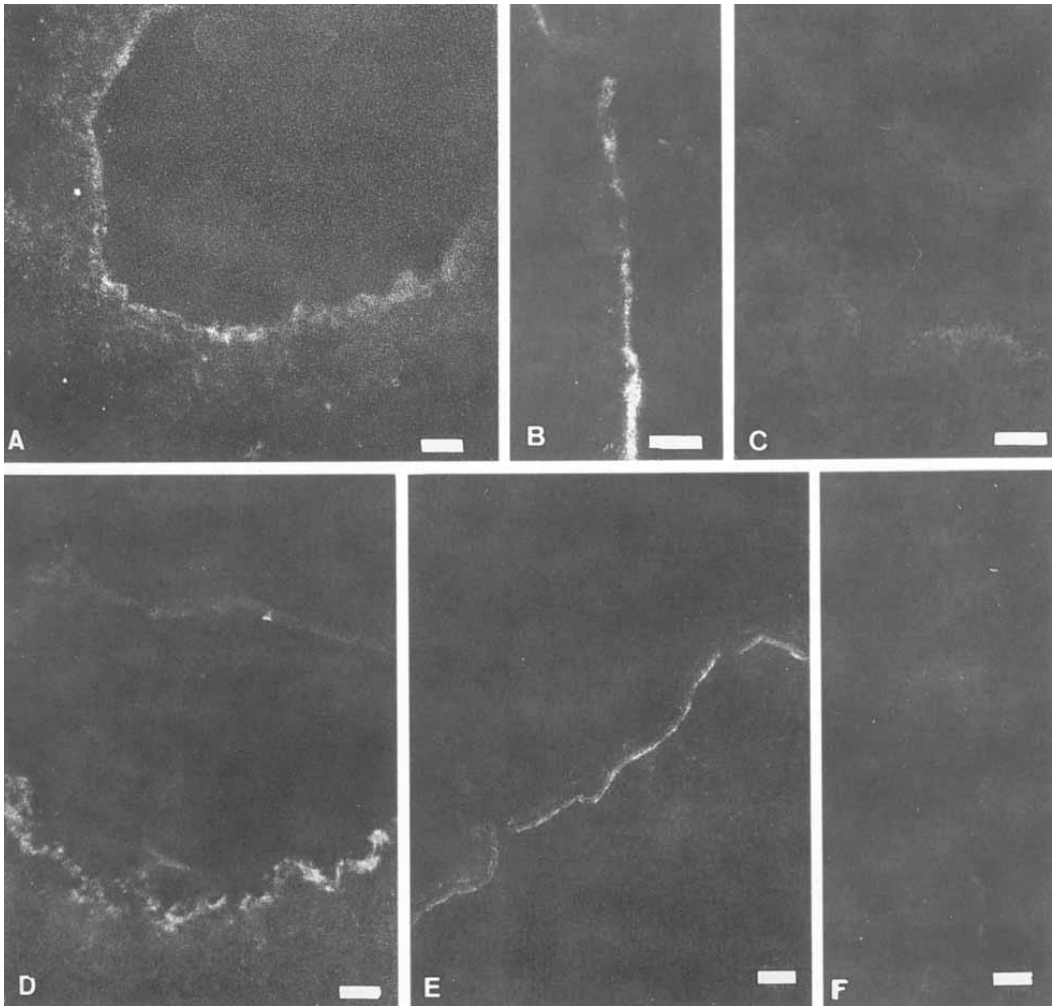


Fig. 6. Immunofluorescence on cryostat sections of eggs fixed with PFA. a and b=sections incubated with antispectrin. a: there is a rim of fluorescence at the dimple border ($\times 300$); b: similar fluorescence in the animal hemisphere cortex. ($\times 400$). c=control section of the dimple (half dimple) incubated with anti-rabbit IgG ($\times 400$). d and e=sections incubated with anti-ankyrin. The cortices of both the dimple (d) and the animal half (e) are fluorescent ($\times 300$). f=cortex of the animal half incubated with normal rabbit serum ($\times 300$). Horizontal bar=20 μm .

Densitometric analysis of the gradient shown in Fig. 2, indicates that the 254-kD band in the total egg supernatant accounts for 0.028% of total soluble proteins per egg, the 225-kD band for 0.038% and the 204-kD for 0.24%.

Immunofluorescence

Frozen sections of eggs prefixed in PFA were incubated with anti-human erythrocyte spectrin, the antibody that we used for immunoblotting, and subsequently with fluorescein-conjugated antirabbit IgG. The sections, examined under a light microscope equipped with epifluorescence optics, showed a thin rim of reactive material in the cortex of the egg, and some positive signals scattered in the cytoplasm (Fig. 6). Similar results were obtained with antifodrin. Because in unfixed sections, incubation with antifodrin gave a fluorescent staining only in the dimple (10) we conclude that prefixation prevents the loss of antigenicity from the egg cortex during sample processing.

Following section incubation with antiankyrin, fluorescent staining was found in the whole egg cortex including the dimple (Fig. 6).

With the antibodies tested, the fluorescence was intenser in the dimple peripheral cytoplasm than in the cortex of the DLE.

Electrophoretic analysis of cortices

In the light of the immunofluorescence results and in order to get a further insight into spectrin and ankyrin localization in *D. pictus* eggs, we utilized the cortices of D and DLE. On electrophoretic analysis, erythrocyte ghosts treated with $ZnCl_2$ for 30 min were undistinguishable from untreated samples. In particular, the 240- and the 220-kD spectrin dimers were unaffected by the treatment (data not shown). Cortices of untreated (procedure D) and $ZnCl_2$ -treated eggs (procedure E) were about 6 μm thick, and during sample

preparation they became spotted with yolk platelets (Fig. 7).

$ZnCl_2$ -cortices of D and DLE were pelleted at 1,500 g and supplemented with sample buffer. The 254-kD band appeared in both D and DLE cortex (Fig. 8); this protein, together with the 204-kD, appeared to be the major high molecular weight protein of the cortex. The 225-kD protein was absent. Western blots of $ZnCl_2$ -cortices and of untreated cortices showed cross-reactivity of the 254-kD band when incubated with antispectrin, and cross-reactivity of the 204-kD band, when incubated with antiankyrin (see Fig. 10). It is possible that the 225-kD protein was weakly bound to the cortical cytoskeleton, and was thus lost during centrifugation of the sample. To test this hypothesis, we analyzed supernatants of 1,500 g-centrifuged dimple cortices (procedure D) and found that the 225-kD protein was absent from both the supernatant and the pellet, while the 254-kD protein was present in both samples. Both samples also showed a weak band of about 246 kD (Fig. 9A). The 225-kD band appeared in supernatants of the dimples partially cleaned from their cytoplasm (procedure C; Fig. 9B).

The gel shown in Fig. 8 was analyzed densitometrically. We have utilized $ZnCl_2$ cortices for this analysis because they do not release cytoplasm upon soaking in 25 mM HB. Spectrin accounted for 3.2% and 3.9%, respectively, of the total protein in the 9 D and the 10 DLE cortices used in the gel. The area of a single dimple was 0.6 mm² (dimple diameter, 900 μm) and that of DLE was 7 mm² (egg diameter, 1.6 mm). Thus, the amount of 254-kD proteins per unit area in the dimple cortex was approximately 12-fold as high as in the DLE cortex. The same calculation made for the 204-kD protein (4.7% in D and 4.8% in DLE cortices), showed a 12-fold concentration in D with respect to DLE and a greater amount of this

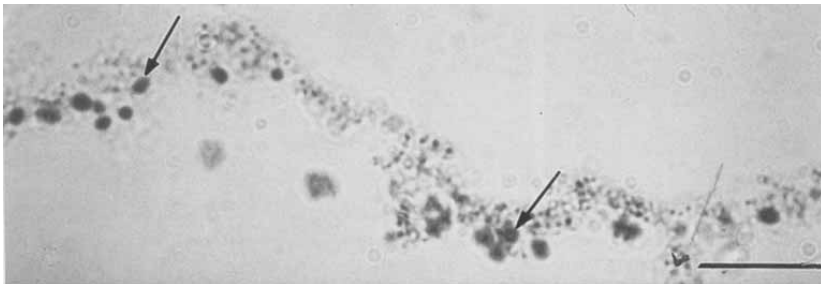


Fig. 7. Thick section of a cortex prepared for PAGE. Staining with toluidine blue. The arrows indicate yolk platelets. $\times 4,000$. Horizontal bar = 10 μm .

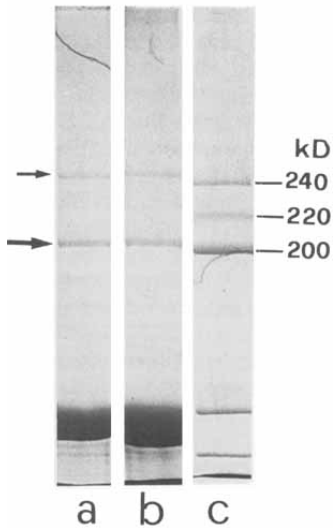


Fig. 8. SDS-PAGE of cortices of $ZnCl_2$ -treated eggs. Lane a=cortices of 10 DLE; lane b=cortices of 9 D; lane c=ghosts and reference molecular weights. The 254-kD (smaller arrow) and the 204-kD (larger arrow) proteins are the major high molecular weight bands present in these gels.

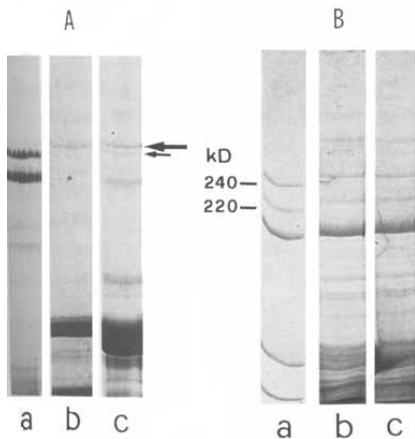


Fig. 9. A Separation by SDS-PAGE of the supernatant and the pellet of dimple cortices centrifuged at 1,500 g. Lane a=ghosts. Lane b=supernatant, the 254-kD band is present as in the pellet (lane c) (larger arrow), while the 225-kD band is absent. The minor band of about 246 kD (smaller arrow) is also present. B. Supernatant of D and DLE cortices partially clean of the internal cytoplasm, separated by SDS-PAGE; the 225-kD band is present (arrowhead) together with the 254-kD band (larger arrow). Lane a=ghosts and reference molecular weights; Lane b=D; lane c=DLE.

ankyrin-like protein than the 254-kD polypeptide in the cortex.

These results indicate that the 254-kD protein

is cortical being more concentrated in the dimple, while the 225-kD is localized in the subcortical cytoplasm, thus contrasting with the typical dimeric organization of spectrin-like molecules. To examine whether these findings were attributable to a leakage of proteins from our samples into the medium, as observed for frozen sections (see previous paragraph), we prefixed the eggs in formaldehyde for 1, 3, 10 min. At 1 and 3 min the protein pattern of the gels was unchanged, while in 10-min fixed eggs, the 246,000 Mr protein became more evident in D (Fig. 10) and in DLE (data not shown). In these samples, the 204-kD band was present and the 225-kD absent.

5% SDS PAGEs of 10-min fixed egg cortices and unfixed eggs were transferred onto nitrocellulose sheets and probed with antispectrin and antifodrin. In fixed cortices, the 254- and the 246-kD bands reacted equally with antifodrin. Also in unfixed cortices, the 246-kD band, although faint, reacted with antifodrin (Fig. 10A).

When similar gels were transferred onto nitrocellulose sheets and probed with anti-ankyrin, the 204-kD band appeared in both D and DLE cortices (Fig. 10B).

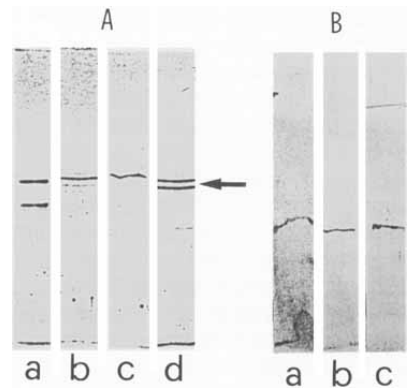


Fig. 10. Western blots of D and DLE cortices probed with anti-fodrin (A) or anti-ankyrin (B). A. Lane a=human erythrocyte ghosts: alpha and beta spectrin is stained. b (D) and c (DLE) lanes=cortices of unfixed eggs. The staining is on the 254-kD band and mildly on the 246-kD band. Lane d=D cortex of eggs fixed with PFA for 10 min; the 254- and the 246-kD bands (arrow) are equally immunoreactive to anti-fodrin. B. Lane a=*D. pictus* blood. Lanes b (D) and c (DLE)=cortices of unfixed eggs. In lanes b and c the 204-kD band is immunoreactive; a similar band is stained in the blood.

Discussion

General conclusions

We found two spectrin-like polypeptides in the

cortices of D and DLE the *D. pictus* egg. A third molecule reacting with anti-spectrin was localized in the subcortical cytoplasm and an ankyrin-like molecule was also identified and localized in the egg cortex. This is the first report of molecules that anchor intrinsic plasma membrane proteins to the cortical cytoskeleton in gametes. Cortical spectrin and ankyrin-like molecules were remarkably more concentrated in the dimple rather than in the rest of the egg, which suggests they play a specific role in the organization and function, or both, of the site of sperm entrance in the egg.

Spectrin and ankyrin identification and localization

The 254,000- and 246,000-Mr polypeptides were localized in the cortex and identified as "spectrin-like" because of their apparent Mr, and because they cross-reacted with both antihuman erythrocyte spectrin and antihuman brain fodrin. These 254- and 246-kD-polypeptides of the *D. pictus* egg are probably subunits of a molecule with typical spectrin-like heterodimeric organization. We refer to this molecule as a "spectrin-like" protein, which is not incompatible with "fodrin".

Beside *Xenopus* egg spectrin (17), spectrin-like dimers of 237–234 kD and 240–235 kD have been detected in sea-urchin and in the mouse eggs, respectively (27, 15, 44, 46). Our results add to the body of evidence that spectrin occurs in eggs of evolutionary distant species, and thus it should be included among proteins of general interest for the female gamete.

An intriguing characteristic of the 254- and the 246-kD molecules is their articulate lability during sample preparation. Only the dimple cortices of unfixed uterine eggs stain with antispectrin, the rest of the egg is negative (10). However, sections from PFA-fixed eggs incubated with the same antibodies are positive throughout the whole egg cortex. This suggests that, in DLE, the linkage between spectrin and plasma membrane or cortical proteins is unusually weak. Alternatively, the linkage could be susceptible to intrinsic enzymatic degradation escaping the protease inhibitors used in this study. Therefore, the spectrin in the dimple could differ from DLE spectrin not only in concentration but also in linkages with specific proteins. Furthermore, D spectrin might differ from DLE spectrin in characteristics other than PAGE-determined molecular weight. In echinoderm and mammal eggs, spectrin seems to have polarized distribution, because it is more concentrated at the site of polar body extrusion, and later, during cleavage, is preferentially localized in the regions

of blastomere contact (43–46).

The 254-kD polypeptide of *D. pictus* seems to be the major antispectrin-crosslinker in the unfixed egg cortical preparation for SDS-PAGE. The 246-kD polypeptide concentration in polyacrylamide gels of cortices significantly increased after the eggs were given mild pretreatment with PFA, i.e. the same fixation conditions that allowed the visualization of fodrin by immunofluorescence in the whole egg cortex. This indicates that the putative non-covalent bonds that connect the two polypeptides in spectrin dimers, are labile under the isolation conditions used. Non-erythroid spectrin is particular labile during sample preparation in *Dictyostelium* and *Acanthameba* (42, 4). Furthermore in the latter, a second spectrin-like polypeptide was identified by immunoreactivity on immunoblots of a polypeptide that was not Coomassie blue stained. It was hypothesized that, in the case of mouse embryos, where spectrin localization is stage-dependent, a specific membrane domain influences the stability of the association of spectrin with cortical proteins (46). The gradual loss of cortical immunoreactivity to anti-spectrin observed in unfixed oocyte sections during maturation of the *D. pictus* oocyte (for more details see ref. 10), could reflect a gradual change in molecules associated to spectrin. Interestingly, in the *D. pictus* egg, actin microfilaments crosslink proteins different from those in the oocyte (11).

The third molecule we observed, which cross-reacts with antispectrin and antifodrin, has an apparent Mr of 225,000 and was localized in the subcortical layer by electrophoretic analysis of distinct peripheral egg layers. Different forms of spectrin are segregated in restricted domains in such somatic cells as neurons (31) and in the intestinal brush border (18). Furthermore, there is evidence that spectrin acts as a filament cross-linker (the TW 240/260; 18) and as vesicle-associated cytoplasmic protein, whose function is unknown (5). In sea urchin eggs, spectrin has been localized around vacuoles and granules, including cortical granules (CG) (6, 16). However, the cross-reactivity in the immunoblot of the *D. pictus* 225-kD polypeptide was weak. This indicates a scarce immunoreactivity rather than a low concentration of the polypeptide in the gels. In fact, in total egg extracts, the concentration of the 225-kD polypeptide was slightly greater than that of the 254-kD polypeptide.

Ankyrins are a family of closely related polypeptides that is found in the plasma membrane of cells in several tissues and that has

binding sites for beta-spectrin. In human erythrocytes, ankyrin is a monomer of 210,000 Mr (2, 3), while in non-erythroid cells it is a dimer of 210- and 220-kD subunits and occurs in three-fold excess over spectrin. The latter finding has been associated to other functions ankyrin might have in cell regions dislocated from plasma membrane (for reviews, see 1, 12). In our samples, the 204-kD band was immunolocalized in sections and in immunoblots of both the S2 preparation and the cortices. It is about eight-fold more concentrated than spectrin-like proteins in total egg supernatant, while it is only slightly in excess of the 254-kD protein in the cortices. Therefore, the 204-kD band of S2 preparations might contain either several comigrating proteins, or predominantly subcortically localized ankyrin.

Different ankyrin isoforms occur in the same tissue; each form might contribute to the accumulation of different integral proteins to particular membrane domains (26). Further studies are required to establish whether in *D. pictus* egg, the ankyrins found in D and DLE is the same isoform, or whether the 12-fold excess in D might reflect a specific ankyrin isoform restricted to this membrane domain.

Predictable roles of spectrin and ankyrin

The plasma membrane and the cortex of the *D. pictus* egg have a functional and structural mosaicism that is acquired during the formation of the dimple after the first polar body extrusion. Fucose residues are segregated at the surface of its central portion, D1 (13), and at the same time, intramembrane particles become more concentrated and invert polarity in D1 (21) (see ref. 23, for a review of the role of fucose in sperm-egg interaction). The function and distribution of Cl^- channels, which are necessary for membrane depolarization at fertilization in anurans, change at the end of maturation; Cl^- channels have been detected only in D1 of uterine eggs, while other ionic channels are present in the plasma membrane of the rest of the animal half (38). The prerequisites for sperm-egg entrance and initiation of development are also acquired during maturation and have a gradient-like distribution in the dimple, that reaches its maximum in D1 (47). During the dimple formation, the cortical actin microfilaments form a cap of bundles. The latter are 10–12 μm long in D1 and gradually shorter towards the lateral walls of the dimple (D2 and D3) (7, 8). It has yet to be established whether any of the properties of D1 described above can be attributed to the higher

concentration of the molecules in this site or to segregation of specific molecules uniquely present in D1.

The overall conclusion is that D1 is a specific site in the egg because of the structural and functional polarity of the egg and that this polarity is established in the oocyte during dimple formation. The cytoskeleton may play an important role in this process. After fertilization, the microfilament cap disaggregates (8), the dimple regresses, and the organization of the fucose residues and intramembrane particles are rearranged (13, 21).

Our results indicate that in the *D. pictus* egg spectrin is an important submembrane cytoskeleton constituent; we hypothesize that, through ankyrin, it links channels and/or receptors of the egg plasma membrane. Like ankyrin, spectrin is more concentrated in the dimple region than in the rest of the egg. This suggests that a higher number of intramembrane proteins, such as those constituting Cl^- channels or intramembrane particles, can be anchored to the cytoskeleton in this region than anywhere else in the egg. Our data are in agreement with the hypothesis (10) that during dimple formation, spectrin together with other constituents such as actin, plays an active role in establishing the specialized domain of the dimple. This hypothesis stems from evidence that spectrin is involved in the active mobility of membrane proteins during receptor capping (32, 35), and from the observation that antispectrin cross-reactivity present throughout the oocyte cortex becomes restricted to GA during dimple formation in unfixed samples (10).

Spectrin is probably present also in deeper cytoplasmic regions; the putative 225 kD spectrin-like polypeptide has been found only subcortically. Therefore, spectrin may be linked to vacuoles and CG destined to be exocytosed after activation, as seen in the brush border (22, 40) and the sea urchin egg (6, 15, 16); CGs are present only in the dimple while vacuoles occur all around the egg periphery (8). Moreover, spectrin might play a similar role in the second burst of exocytosis (about 15 min after fertilization (41), involving deeply localized vacuoles that become more superficial after fertilization.

Acknowledgements: We are grateful to Ms G. Rossi for her excellent laboratory work, to Dr. T. Petrucci for her suggestions, to Dr. G. D'Andrea for densitometric analysis, and to Mr. G. Cafiero for section preparation at the University of Naples C.I.R.U.B.

Supported by a 40% grant from M.U.R.S.T. (Italy),

by CNR grant 92. 00999. CTO4 (Italy) and by N.S.F. (Switzerland) 3.108-0.88 and 31-26614.89.

References

- Bennett, V., 1985. The membrane skeleton of human erythrocytes and its implications for more complex cells. *Annu. Rev. Biochem.*, **54**, 273-304.
- Bennett, V. and P. J. Stenbuck, 1979. Identification and partial purification of ankyrin, the high affinity membrane attachment site for human erythrocyte spectrin. *J. Biol. Chem.*, **254**, 2533-2541.
- Bennett, V. and P. J. Stenbuck, 1980. Human erythrocyte ankyrin. *J. Biol. Chem.*, **254**, 2533-2541.
- Bennett, V. and J. Condeelis, 1988. Isolation of an immunoreactive analogue of brain fodrin that is associated with the cell cortex of *Dictyostelium* Amoebae. *Cell Motil. and Cytosk.*, **11**, 303-317.
- Black, J. D., S. T. Koury, R. B. Bankert and E. A. Repansky, 1988. Heterogeneity in lymphocyte spectrin distribution: ultrastructural identification of a new spectrin-rich cytoplasmic structure. *J. Cell Biol.*, **106**, 97-109.
- Bonder, E. M., D. J. Fishkind, N. M. Contreras and D. A. Begg, 1989. The cortical actin-membrane cytoskeleton of unfertilized sea urchin eggs: analysis of the spatial organization and relationship of filamentous actin, nonfilamentous actin and egg spectrin. *Develop. Biol.*, **134**, 327-341.
- Campanella, C. and G. Gabbiani, 1980. Cytoskeletal and contractile proteins in coelomic oocytes, unfertilized and fertilized eggs of *Discoglossus pictus* (Anura). *Gam. Res.*, **3**, 99-114.
- Campanella, C., R. Talevi, D. Kline and R. Nuccitelli, 1988. The cortical reaction in the egg of *Discoglossus pictus*: A study of the changes in the endoplasmic reticulum at activation. *Develop. Biol.*, **130**, 120-132.
- Campanella, C., R. Talevi, R. Gualtieri and P. Andreuccetti, 1989. The contribution of *Discoglossus pictus* fertilization in the study of Amphibian sperm-egg interaction. *In* Mechanisms of Fertilization, Vol. H45 (Ed. B. Dale), Nato ASI Series. Springer-Verlag.
- Campanella, C., R. Carotenuto and G. Gabbiani, 1990a. Antispectrin antibodies stain the oocyte nucleus and the site of fertilization channels in the egg of *Discoglossus pictus*. *Mol. Reprod. and Develop.*, **26**, 134-142.
- Campanella, C., C. Chaponnier, L. Quaglia, R. Gualtieri and G. Gabbiani 1990b. Different cytoskeletal organization in two maturation stages of *Discoglossus pictus* oocytes: Thickness and stability of actin microfilaments and tropomyosin immunolocalization. *Mol. Reprod. and Develop.*, **25**, 110-121.
- Coleman, T. R., D. J. Fishkind, M. S. Mooseker and J. S. Morrow, 1989. Functional diversity among spectrin isoforms. *Cell Motil. and Cytosk.*, **12**, 225-247.
- Denis-Donini, S. and C. Campanella, 1977. Ultrastructural and lectin binding changes during the formation of the animal dimple in oocytes of *Discoglossus pictus* (Anura). *Develop. Biol.*, **61**, 140-152.
- Drenckhahn, B., K. Schluter, B. P. Allen and V. Bennett, 1985. Colocalization of band 3 with ankyrin and spectrin at the basal membrane of intercalated cells in rat kidney. *Science*, **230**, 287-289.
- Fishkind, D. J., E. M. Bonder and D. A. Begg, 1987. Isolation and characterization of sea urchin egg spectrin: calcium modulation of spectrin-actin interaction. *Cell Motil. and Cytosk.*, **7**, 304-314.
- Fishkind, D. J., E. M. Bonder and D. A. Begg, 1990. Subcellular localization of sea urchin spectrin: evidence for assembly of the membrane -skeleton on unique classes of vesicles in eggs and embryos. *Develop. Biol.*, **142**, 439-452.
- Giebelhaus, D. H., B. D. Zelus, S. K. Henchman and R. T. Moon, 1987. Changes in the expression of alpha-fodrin during embryonic development of *Xenopus laevis*. *J. Cell Biol.*, **105**, 843-853.
- Glenney, J. R. Jr., P. Glenney and K. Weber, 1983. Mapping the fodrin molecule with monoclonal antibodies. A general approach for rod-like multidomain proteins. *J. Cell Biol.*, **96**, 1491-1496.
- Gould Somero, M., 1981. Localized gating of egg Na⁺ channels by sperm. *Nature*, **291**, 254-256.
- Gualtieri, R., G. Cafiero and P. Andreuccetti, 1989. Plasma membrane domains and the site of sperm entrance in *Discoglossus pictus* (Anura) oocytes. *Develop. Growth. & Differ.*, **31**, 485-491.
- Gualtieri, R., G. Cafiero and P. Andreuccetti, 1991. Surface and cortex regionalization during 'in vivo' maturation in *Discoglossus pictus* (Anura) oocytes. *In* International Symposium on the Evolution of Terrestrial Vertebrates, Collana U.Z.I., Selected Symposia and Monographs, (Eds. G. Ghiara et al.), Edizione Mucchi, Modena.
- Hirokawa, N., R. E. Cheney and M. Villard, 1983. Localization of a protein of the fodrin-spectrin-TW 260/240 family in the mouse intestinal brush border. *Cell*, **32**, 953-965.
- Hoshi, M., 1984. Roles of sperm glycosidases and proteases in the ascidian fertilization. *In* Advances in Vertebrate Reproduction, Vol. 3 (Eds. W. Engels et al.), pp. 27-40. Elsevier Science Publishers. B. V., New York.
- Kline, D., 1988. Calcium-dependent events at fertilization of the frog egg: injection of the calcium buffer blocks ion channels opening exocytosis, and formation of pronuclei. *Develop. Biol.*, **126**, 346-361.
- Kline, D., G. S. Kopf and L. F. Muncy, 1991. Evidence for the involvement of a pertussis toxin-insensitive G-protein in egg activation of the frog, *Xenopus laevis*. *Develop. Biol.*, **143**, 1218-1229.
- Kordeli, E. J. and V. Bennett, 1991. Distinct ankyrin isoforms at neuron cell bodies and nodes of Ranvier resolved using erythrocyte ankyrin-deficient mice. *J. Cell Biol.*, **114**, 1243-1259.
- Kuramochi, K., I. Mabuchi and K. Owaribe, 1986. Spectrin from sea urchin eggs. *Biomed. Res.*, **7**, 65-68.
- Laemmli, U. K., 1970. Cleavage of structural proteins during the assembly of the head bacteriophage T4. *Nature*, **227**, 680-685.
- Lazarides, E. and W. J. Nelson, 1982. Expression of spectrin in non-erythroid cells. *Cell*, **31**, 505-508.
- Lazarides, E. and W. J. Nelson, 1983. Erythrocyte and brain forms of spectrin in cerebellum distinct membrane-cytoskeletal domains in neurons. *Science*, **220**, 1295-1296.
- Lazarides, E., W. J. Nelson and K. Kasamatsu, 1984. Segregation of two spectrin forms in the chicken optic system: a mechanism for establishing restricted membrane cytoskeletal domains in the chicken optic system. *Cell*, **36**, 269-278.
- Levine, J. and M. Villard, 1983. Redistribution of fodrin accompanying capping of cell surface molecules. *Proc. Natl. Acad. Sci. USA*, **80**, 191-195.
- Marchesi, V., 1971. Isolation of spectrin from erythrocyte membranes. *Meth. in Enzymol.*, **344**, 275-277.
- Marchesi, V. T., 1985. Stabilizing infrastructure of cell membrane. *Ann. Rev. Cell Biol.*, **1**, 531-561.
- Nelson, W. J., C. L. S. Colaco and E. Lazarides, 1983.

Sperm-Egg Interaction in the Painted Frog (*Discoglossus pictus*): An Ultrastructural Study

C. CAMPANELLA,* R. CAROTENUTO, V. INFANTE, G. MATURI, AND U. ATRIPALDI

Dipartimento di Biologia Evolutiva e Comparata Università di Napoli Federico II, Naples, Italy

ABSTRACT The ultrastructure of sperm changes and penetration in the egg was studied in the anuran *Discoglossus pictus*, whose sperm have an acrosome cap with a typical tip, the *apical rod*. The first stage of the sperm apical rod and acrosome reaction (AR) consists in vesiculation between the plasma membrane and the outer acrosome membrane. The two components of the acrosome cap are released in sequence. The innermost component (component B) is dispersed first. The next acrosome change is the dispersal of the outermost acrosome content (component A). At 30 sec postinsemination, when the loss of component B is first observed, holes are seen in the innermost jelly coat (J1), surrounding the penetrating sperm. Therefore, this acrosome constituent might be related to penetration through the innermost egg investments. At 1 min postinsemination, during sperm penetration into the egg, a halo of finely granular material is observed around the inner acrosome membrane of the spermatozoon, suggesting a role for component A at this stage of penetration.

Gamete-binding and fusion take place between D1 (the egg-specific site for sperm interaction) and the perpendicularly oriented sperm. Spermatozoa visualized at their initial interaction (15 sec postinsemination) with the oolemma are undergoing vesiculation. The first *interaction* is likely to occur between the D1 glycocalyx and the plasma membrane of the hybrid vesicles surrounding the apical rod. As *fusion* is observed between the internal acrosome membrane and the oolemma, it can be postulated that gametic interaction might be followed by fusion of the latter with the apical rod internal membrane that extends posteriorly into the inner acrosome membrane.

Insemination of the outermost jelly layer (J3) dissected out of the egg, and observations of the ultrastructural changes of spermatozoa in this coat, indicate that J3 rather than the vitelline coat (VC) induces the AR. Interestingly, at the late postinsemination stage, VC fibrils are seen crosslinking the inner acrosome membrane. The role of this binding is here discussed. *Mol. Reprod. Dev.* 47:323-333, 1997. © 1997 Wiley-Liss, Inc.

Key Words: fertilization; amphibians; acrosome reaction

INTRODUCTION

The ultrastructure of the fertilization process in echinoderms and mammals was extensively studied about 20 years ago. Since then, research has been focused on the molecules involved in this process. Recently, in the sea urchin, a glycoprotein having a transmembrane domain (Ohlendieck and Lennarz, 1995) that interacts with acrosome-reacted sperm has been detected on the egg surface (Ohlendieck et al., 1994; Foltz et al., 1993). In mammals, the interaction of sperm *fertilin*, located in the plasma membrane of the postacrosomal cap (Primakoff et al., 1987; see Myles, 1993), with integrins at the egg plasma membrane appears to ensure sperm binding to the oolemma (Fusi et al., 1993; Tarone et al., 1993; Almeida et al., 1995). Apparently, sperm-egg binding differs between echinoderms and mammals in the location of the active molecules in the spermatozoa, as well as in the nature of the interacting molecules. The molecular mechanisms elucidated by these studies are also difficult to compare, due to the evolutionary distance between echinoderms and mammals. In this context, a study of sperm-egg interaction in amphibians appears useful, to gain a more general understanding of fertilization in vertebrates. Furthermore, the biology of reproduction and ease in gamete handling are well-known in this class, although no information is yet available on the ultrastructure of fertilization and on the gamete surface molecules involved in this process.

In amphibians, at gamete interaction, sperm swim in the jelly coat, pass through the vitelline coat (VC), and arrive in a matter of minutes at the egg plasma membrane where gametes fuse. Jelly presence around the egg is necessary for fertilization to occur (Wolf and Hedrick, 1971; Katagiri, 1974; reviewed in Katagiri, 1987; Elinson, 1986). A fundamental role for the molecules of the jelly coat is the ability to retain calcium and/or magnesium ions (Ishihara et al., 1984). Upon jelly removal by disulphide bond reducing agents, sperm bind to the VC (Grey et al., 1976), much as in mammalian fertilization.

Contract grant sponsor: CNR and MURST.

*Correspondence to: C. Campanella, Dipt. di Biologia Evolutiva e Comparata, Università di Napoli "Federico II," Via Mezzocannone 8, 80134 Naples, Italy.

Received 25 September 1996; Accepted 17 December 1996

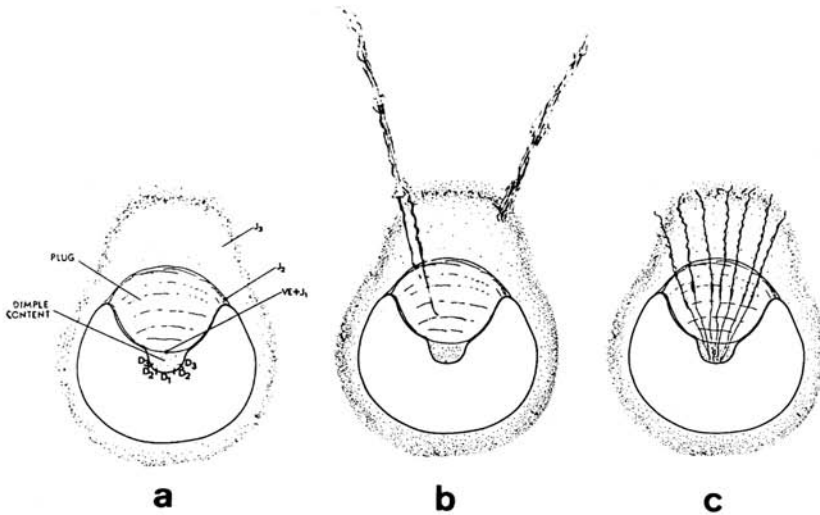


Fig. 1. Schematic drawing of *D. pictus* egg. **a:** Dimple is located at the center of a large concavity of the animal half. Dimple regions D1, D2, and D3 are indicated. Jelly layers J1, J2, and J3 surround the whole egg. J3 is about threefold thicker at the animal half, in correspondence with the jelly plug, than in the rest of the egg. The

gelatinous plug is located uniquely in the egg concavity. VC and J1 are separated from the dimple surface by the dimple content, consisting of finely granular material. **b:** At insemination, spermatozoa are ejected from their bundle into the jelly. **c:** Sperm become embedded along their whole length in the jelly layers.

So far, the role of jelly coats and VC in sperm activation and acrosome reaction (AR) is still rather controversial. In *Rana pipiens*, *Bufo arenarum*, and *Xenopus laevis*, jelly may promote the AR (Shivers and James, 1970; Elinson, 1971; Wolf and Hedrick, 1971; Miceli et al., 1987). In *Pleurodeles waltlii*, this process occurs before the passage through the innermost jelly layer (Picheral, 1977). In *Bufo japonicus*, the pars recta secretion is able to induce the AR (Katagiri et al., 1982; Yoshizaki and Katagiri, 1982). *Bufo* sperm, as analyzed during their passage through the innermost jelly layer, have intact acrosome (Omata, 1993), suggesting that the AR occurs after sperm passage through this coat next to or in the VC. In this case, the jelly would have the role of "capacitating" the sperm (Shivers and James, 1970; Elinson, 1971, 1973; Barbieri and Otenino, 1972).

The present paper describes the fine structure of the AR sequential stages and of sperm penetration into the egg of *Discoglossus pictus*, to gain a further understanding of sperm-egg interaction in anurans. This species has been chosen because it has a distinct jelly layer, where the 2.3-mm-long sperm converge (the *plug*, Ghara, 1960), and a predetermined site of sperm entrance, the *dimple* (Hibbard, 1928; Campanella, 1975). These features render the ultrastructural detection of sperm relatively easy. In other anurans, such as *Xenopus laevis*, fertilization occurs along the entire animal half (see Elinson, 1986), and spermatozoa are about 60 μm long (Bernardini et al., 1988). *Discoglossus* sperm ultrastructure and acquisition of motility (Campanella and

Gabbiani, 1979; Campanella et al., 1981), as well as several features concerning dimple properties and egg activation (Campanella and Talevi, 1988; Campanella et al., 1990, 1992; Gualtieri and Andreuccetti, 1996), have been previously reported. The *D. pictus* sperm anteriormost portion is constituted of the apical rod, a specialization of the acrosome formed by concentric membrane-like sheets, and posteriorly covered by the acrosome cap. The nucleus is located behind the apical rod; it is covered by the acrosome cap throughout its surface except for its posterior edge. Sperm are entwined in bundles that are held together by interwoven threads (the bundle matrix). Figure 1a is a schematic drawing of the egg longitudinal section, showing the organization of jelly layers 1–3, the lens-shaped plug, the VC, and the dimple located at the center of the animal hemisphere.

Earlier studies established that one or more sperm can undergo successful egg penetration into D1, the region 200 μm in diameter constituting the dimple bottom; only in this region are fertilization cones formed. A first step of sperm penetration occurs within the the first 6 min postinsemination. Penetration of the posteriormost head region (uncovered by the acrosome) is resumed about 35 min postinsemination (Wintrebert, 1933; Campanella et al., 1981; Talevi and Campanella, 1988; Talevi, 1989) after the dimple and the animal hemisphere concavity have regressed, and the egg has assumed a spherical shape (Campanella et al., 1992; Pitari et al., 1993).

MATERIALS AND METHODS

Animals and Gametes

Adult *Discoglossus pictus* males and females were captured in the neighborhood of Palermo, Italy from 1975–1986. They were injected in the dorsal lymphatic sac with 200–250 units of Profasi HP (Serono, Rome, Italy) in amphibian Ringer's solution (111 mM NaCl, 1.3 mM CaCl₂, 2 mM KCl, 0.8 M Mg₂SO₄, in 25 mM HEPES). The eggs were obtained about 18 hr later. Similarly, following hormone treatment, the seminal vesicles (see Campanella and Gabbiani, 1979) became filled with about 3 ml of semen (sperm and seminal fluid) that could be recovered in the next 24–48 hr by squeezing the abdomen, or by pricking the seminal vesicles after opening the abdomen of males anesthetized with MS222.

Insemination was performed by addition of a drop of semen to uterine eggs. Variations of this procedure will be described in Results.

Electron Microscopy

Inseminated eggs were fixed from 15 sec to 20 min following insemination. When sperm ultrastructure in J3, J2, or the plug was not to be investigated, these jelly layers were manually removed from the egg to improve fixative penetration. Alternatively, the eggs were cut in halves, 1 hr after immersion in the fixative.

The fixative was 2.5% glutaraldehyde in 0.2 M phosphate buffer for 3 hr at room temperature. Following several rinses, the samples were kept overnight in buffer at 4°C and postfixed in 2% OsO₄ in the same buffer.

Sperm were similarly fixed or, alternatively, were for 1 hr in 3% glutaraldehyde in cacodylate buffer, pH 7.2, followed by postfixation in 1% OsO₄ in collidine buffer at pH 7.4 for 1 hr, at 4°C.

Dehydration in graded ethanol at 4°C was followed by embedding in Epon 812. Thick and thin sections were cut with diamond knives, stained with uranyl acetate and lead citrate (Fluka Chemie Ag Buchs, Switzerland), and examined in a Siemens Elmiscop 1A or in a Philips EM-300 microscope at the Centro Interdipartimentale Ricerche Ultrastrutturali Biologiche (C.I.R.U.B.) of the University of Naples.

RESULTS

Timing of Sperm-Egg Interaction

Previous experiments have shown that, when sperm bundles come into contact with J3, sperm start moving and single spermatozoa are ejected from the bundles into the jelly in about 4–5 sec. In diluted saline, unfastening of sperm from their bundle is activated either immediately upon dilution or a few seconds later, depending on the concentration of the bundles, i.e., on the chance that the bundles are fully surrounded by the medium. Sperm motion lasts only 14 sec (Campanella and Gabbiani, 1979).

In the present work, observations at the dissecting microscope showed that spermatozoa become fully em-

bedded in the jelly coats facing the animal dimple (J3, J2, and the plug) 2–3 sec after ejection from the bundles (Fig. 1b,c), i.e., 7 sec from insemination. At this time, sperm still have 7 sec to move. Thin sections indicate that the sperm tip (the apical rod) (Fig. 2a) gains the dimple content (DC) at the earliest fixation time, i.e., 15 sec after insemination. Therefore, it appears that the remaining 7 sec of motility are sufficient for the sperm to pass through the J1-VC complex and the DC, and to engage in fusion with the oolemma. Moreover, as a consequence of gamete morphology and of the velocity of sperm penetration, single spermatozoa, which gain the oolemma in about 10 sec, are contemporaneously embedded in the DC and in all the egg investments (Fig. 1b,c).

Ultrastructural Observations

The apical rod and the acrosome reaction. Sequences of acrosome changes could be reconstructed by comparing electron micrographs of samples fixed at increasing time intervals starting from egg insemination. No relationship was found between ultrastructural changes occurring in the reacting sperm and the specific jelly layer in which a sperm segment is embedded. In the present work, most of the micrographs represent sperm sections located in the plug whose matrix is made of layers of fine and coarse fibers. Figure 2b is a cross section of the anterior portion of the intact sperm head where acrosome components A and B and their electron-dense borders are shown. Figure 2c–e indicates the fine changes in sperm undergoing the acrosome reaction. The outer membrane of the acrosome cap fuses with the plasma membrane. Several small vesicles, as well as long sheets of fused membranes, are formed (Fig. 2c–e). The sperm surface is thus constituted of the outermost electron-dense rim that delimits acrosome component A. This reaction is already underway 15–20 sec from insemination (Fig. 2c), and can be accomplished about 30 sec later (Fig. 2d).

Loss of the inner component of the acrosome (component B) follows the first stages of vesiculation, as indicated in Figure 2d, which shows samples fixed 50 sec postinsemination. Lastly, at about 60 sec from insemination, component A is similarly lost, and the nucleus is surrounded by the inner acrosome membrane (Fig. 2e). Interestingly, at a given time, spermatozoa may be at different stages of the acrosome reaction, as can be seen in Figure 2e.

The apical rod displays vesiculation between the plasma membrane and the outermost of its membranes (Fig. 2a). The newly exposed membrane is continuous with the inner acrosome membrane (Fig. 3). This reaction could be observed only in the DC, because the apical rod is the anteriormost portion of the sperm and, being the first to reach this region, can be more easily detected there than in the egg investments. The sequence of the acrosome and apical rod reaction is summarized in Figure 3.

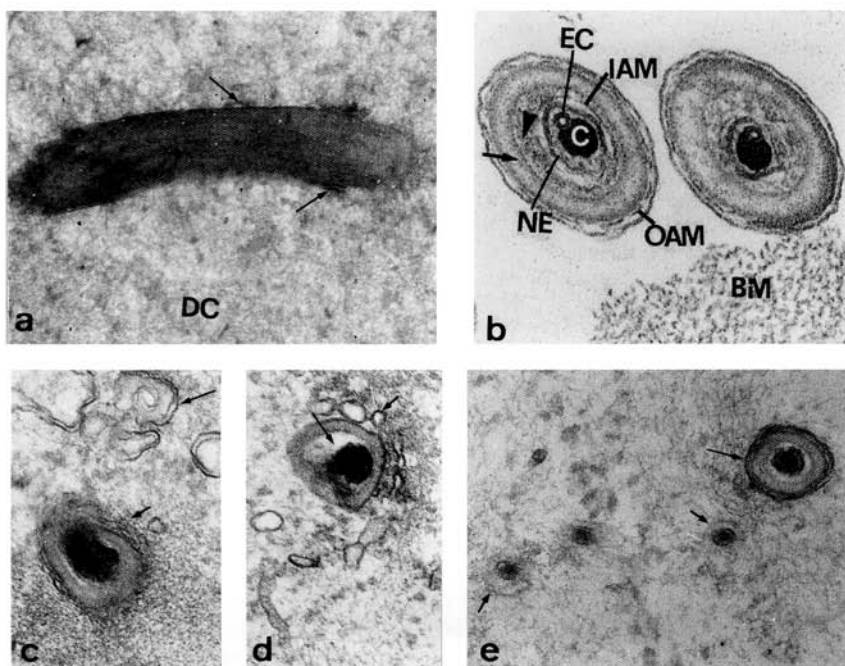


Fig. 2. Acrosome and apical rod reaction. **a:** Apical rod at 15–20 sec following insemination, in the DC, which is made of finely granular material. This structure is characterized by concentrically arranged membrane layers. Arrows indicate hybrid vesicles at the apical rod surface ($\times 60,000$). **b:** Unreacted sperm cross section. The bundle matrix (BM) thin fibrils are indicated. OAM, outer acrosome membrane; arrow, acrosome component A surrounded by electron-dense rims; arrowhead, component B; IAM, inner acrosome membrane; NE, nuclear envelope; C, chromatin; EC, endonuclear canal ($\times 67,000$). **c–e:** Sections of reacting sperm at the plug level. **c:** Vesiculation between

the sperm plasma and the outer acrosome membranes at 20 sec after insemination. Small vesicles (small arrow) and long sheets of fused membranes (arrow) are formed ($\times 50,000$). **d:** At about 50 sec after insemination, the acrosome has lost most of component B (arrow). Hybrid vesicles surround the sperm (small arrow) ($\times 52,000$). **e:** The acrosome is completely absent and the thin nuclei are surrounded by the inner acrosome membrane (small arrows). In the same micrograph, a spermatozoon at the initial stage of the AR is present (arrow) (60 sec after insemination, $\times 52,000$).

Jelly and VC changes occurring upon sperm passage. Sections of sperm localized between the plug and J1 indicate some disappearance of the contacting array of the plug fibers and the J1 matrix. An apparent orderly arrangement of the plug coarse fibers occurs at the site of close contact of sperm with the plug thin fibers. The sperm are at early stages of plasma membrane fusion with the outer acrosome membrane (Fig. 4).

Serial sections of an obliquely cut spermatozoon (30 sec postinsemination) show that, at early stages of vesiculation, the transit through the tight matrix of J1 and of VC allows the separation of vesicles from the sperm surface (Fig. 5a–c). At this stage, as well as at a more advanced stage of the AR, when the sperm surface consists of component A outermost electron-dense rim (Fig. 5d,e), J1 contains sperm-derived vesicles and a few holes. In samples where the dimple has completely regressed, causing spreading of DC on the animal half concavity, a decrease in the distance between the fertilization membrane and the dimple plasma mem-

brane occurs. As a consequence, when the first stage of penetration into the egg is over, the spermatozoon in the fertilizing cone is subjected to an increase in mechanical pressure. A lateral section of sperm facing D1 indicates that VC fibrils crosslink the outermost sperm membrane, which, at this stage, is the inner acrosome membrane. As a result, the sperm are caught in a J1-VC fold (Fig. 6).

Sperm in the dimple content and at the oolemma. Fifteen to 25 sec after insemination, the anterior-most sperm head region located in the DC is at an early stage of vesiculation. DC is made of a finely granular matrix (Figs. 2a, 7a). It is noteworthy that most of the sperm plasma membrane and of the underlying outer acrosome membrane are unusually electron-dense in the DC. Spermatozoa, when in close contact with one another, may also fuse. Their surface is constituted either of remnants of the plasma membrane or of the outermost electron-dense rim of component A (Fig. 7a).

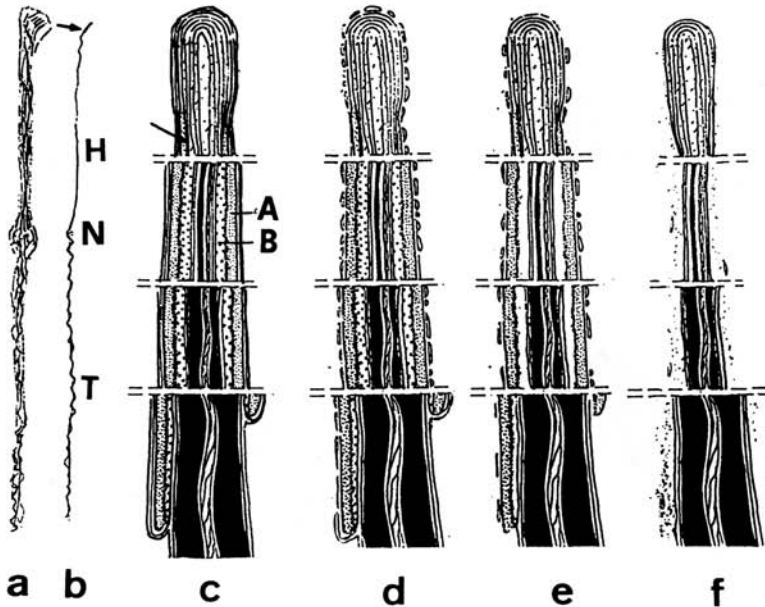


Fig. 3. Schematic drawing of the apical rod and acrosome reaction in *D. pictus* sperm. **a:** Sperm bundle. **b:** Single spermatozoan. It has a thickness ranging from 1 μm (at the head base) to 0.2 μm (at the head tip). The head is about 1 μm long. The neck, where a single mitochondrion is present, is followed by a 1.33- μm -long tail with an undulating membrane. Arrow, apical rod; N, neck; H, head; T, tail. **c:** Intact sperm head. The apical rod is a sort of specialization of the acrosome cap, made of concentric membrane. At its basal portion, acrosome cap component A is present and is bordered by two mem-

branes which extend posteriorly into the outer and the inner acrosome membranes. Small arrow indicates the inner acrosome membrane at the apical rod level. Posteriorly, the acrosome is made of finely granular component A (A) delimited by electron-dense rims and by coarse granule-containing component B (B). In the thin nucleus, chromatin and an endonuclear canal are present. **d:** Vesiculation between the plasma membrane and the outermost membrane in the apical rod and between the plasma membrane and the outer acrosome membrane. **e:** Loss of component B. **f:** Loss of component A.

Due to its length, the penetration of *D. pictus* sperm into the egg lasts several minutes. Few cases of sperm-egg fusion at an early stage (1 min postinsemination) were observed. The anteriormost portion of a spermatozoon head engaged in fusion with the oolemma is perpendicular to the egg surface, and is located in a narrow egg invagination (Fig. 7b). In the head, the slender nucleus is surrounded by the nuclear envelope, the inner acrosome membrane, and a halo of finely granular material, which is most probably acrosome component A, being dissimilar to the DC content. The inner acrosome membrane is parallel to and in close contact with the oolemma in the invagination. In a deeper portion of the invagination, the oolemma fuses with the inner acrosome membrane. The ooplasm surrounding the spermatozoon is finely granular and organelle-free (Fig. 7b). It will later extend to form the penetration cone (see Campanella et al., 1981).

Where the acrosome reaction is elicited. It is possible that the acrosome reaction starts simultaneously with sperm release from the bundles. This is also likely in view of the extreme velocity at which sperm penetrate after ejection. To test this hypothesis, semen was mixed with diluted Ringer's solution. As a

consequence, single spermatozoa were partially or completely released into the medium and, in this process, part of them came into reciprocal contact. The samples were fixed for electron microscopy either immediately or 10 min after getting free of the bundles. In the former case, thin sections indicated that some spermatozoa reacted, leading to the formation of large sheets of plasma and outer acrosome membranes, as well as to the loss of component B. Vesiculation of the external membranes was not observed (Fig. 8a). The acrosome reaction was complete in samples fixed 10 min later; the nucleus was exposed, surrounded by plasma and acrosome membranes (Fig. 8b). Only a small number of sperm showed such changes.

In a second set of experiments, it was tested whether sperm are triggered for the acrosome reaction on contact with the outermost jelly layer. J3 was removed from eggs ($n = 10$) and, upon insemination (Fig. 8c), spermatozoa readily became embedded in this coat. The excised J3 was processed for electron microscopy about 1 min after insemination. In the corresponding thin sections, typical vesiculation of the external membrane and dispersal of acrosome component B was found (Fig. 8d,e).



Fig. 4. Cross section of a sperm in the plug at 30 or 50 sec postinsemination. The plug is made of coarse and fine fibers organized in alternating layers. The sperm displace the plug thin fibers. The adjacent plug coarse fibers appear arranged in an orderly fashion around the sperm (small arrows). The sperm are in the process of vesiculation and are next to J1. The plug (P) and the J1 matrix are partially dispersed (arrow) at contact sites with sperm-derived vesicles ($\times 30,000$).

DISCUSSION

In this paper, the approximate timing of penetration of *D. pictus* sperm was traced through direct observation and thin section micrographs. The AR and the initial stages of sperm penetration into the egg of *D. pictus* were reconstructed through sections of samples fixed during the early stages of insemination and fertilization.

At insemination, sperm become embedded along their whole length in the jelly layers in 2–3 sec, and their arrival at the egg surface coincides with the end of their motility.

An important characteristic of *D. pictus* sperm is the short duration of their motion (14 sec, Campanella and Gabbiani, 1979), which is nonetheless sufficient for the sperm to reach the egg plasma membrane. Upon egg insemination, sperm bundles stick to the surface of J3. As a consequence, sperm are ejected from the bundle in about 5 sec and penetrate into the egg investments and the DC in about 10 sec, as the apical rod is seen next to

the oolemma 15 sec postinsemination. Electrophysiological measurements of *D. pictus* eggs record fertilization potentials from 15–40 sec following insemination (Talevi et al., 1985; Talevi and Campanella, 1988). These data are consistent with the timing of sperm penetration into the egg that we have calculated here. Recordings longer than 15 sec might be ascribed mainly to sperm deriving from bundles with delayed activation. Moreover, a latent period may exist between the initial interaction of sperm with the glycocalyx of the dimple microvilli (Campanella, 1975), and the onset of the oolemma depolarization (reviewed in Whitaker and Swann, 1993). In *D. pictus*, a 5–7-sec step depolarization was found to precede the main depolarization event in several eggs (Talevi et al., 1985), and might reflect the length of this latent period.

The acrosome and apical rod reaction is triggered by J3 and consists of vesiculation of the plasma membrane and outer acrosome membrane, as well as in the sequential release of the acrosome constituents.

The vesiculation of external membranes during the AR, as is here shown to occur in *D. pictus* sperm, is a process common to both vertebrates and invertebrates. In amphibians, it has been described in *Bufo bufo japonicus* (Yoshizaki and Katagiri, 1982) and in *Pleurodeles waltlii* (Picheral, 1977). Generally, it is during this process that the acrosome content, including proteolytic enzymes, is released.

Vitelline coat or jelly layers might be the substrata of *D. pictus* acrosome components A and B, similar to what has been postulated for the acrosome enzymes of *Pleurodeles waltlii* (Picheral, 1977). An early study by Hibbard (1928) demonstrated a jelly coat-dispersing activity in *D. pictus* sperm. In other amphibian species, a VC-lysing activity has been found in sperm (Raisman and Barbieri, 1969), namely, in *Bufo arenarum*. The acrosomal localization of trypsin-like activity has been demonstrated in *Rana pipiens* and *Leptodactylus chaquensis* (Penn and Glenhill, 1972; Raisman et al., 1977). Iwao and Katagiri (1982) isolated the VC lysin of *Bufo bufo japonicus*; it is a proteinase sharing several properties with serine-protease (see also Yamasaki et al., 1988).

The loss of acrosome component B, observed in *D. pictus* about 30 sec postinsemination, suggests that this component is involved in the interaction between sperm and jelly coat. Spermatozoa at early stages of component B loss either displace the plug matrix where partial rearrangement occurs, or produce holes in J1. However, at initial stages of jelly and VC penetration, sperm are seen in these coats before any visible loss of component B. We surmise that, in the first 10 sec, sperm open their way in the jelly and pass through the tightly interwoven J1-VC, thanks to its active motion. Acrosome enzyme might have a role in sustaining the sliding of the immotile sperm during their subsequent penetration into the egg. However, the possibility exists that enzymes, whose leakage from the sperm is of

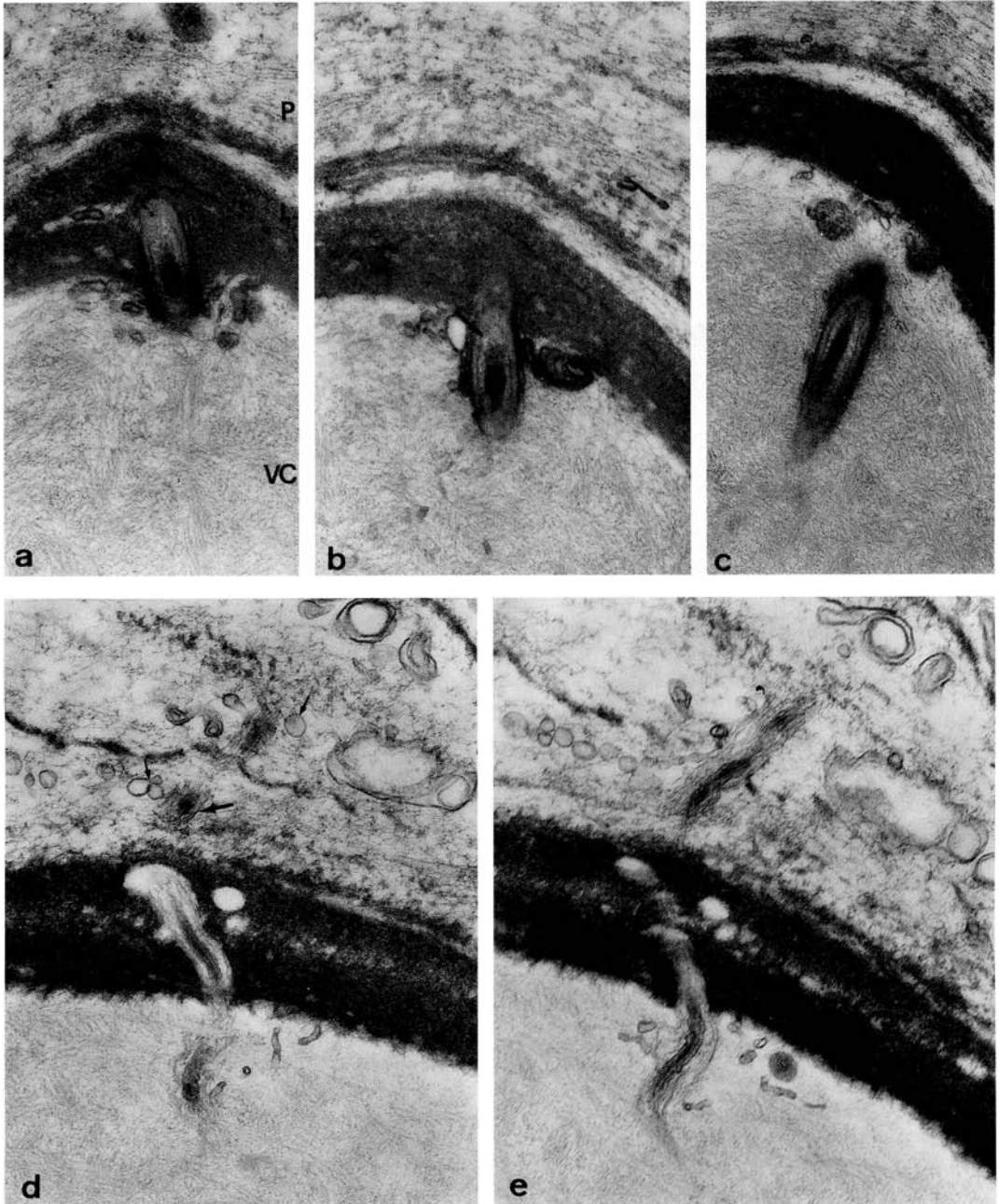


Fig. 5. a-c: Serial sections of an obliquely cut sperm at 30 sec postinsemination indicate that, at early stages of vesiculation, the transit through the highly electron-dense J1 and VC allows some separation of vesicles from the sperm surface. Arrow indicates initial acrosome component B loss. P, plug matrix ($\times 30,000$). d,e: Serial

sections showing a spermatozoan that has lost acrosomal component B, exposing the component A electron-dense rim (arrow), which is still surrounded by vesicles (small arrows). This sperm segment is visualized while crossing the plug and J1, which contains sperm-derived vesicles and a few holes ($\times 30,000$).

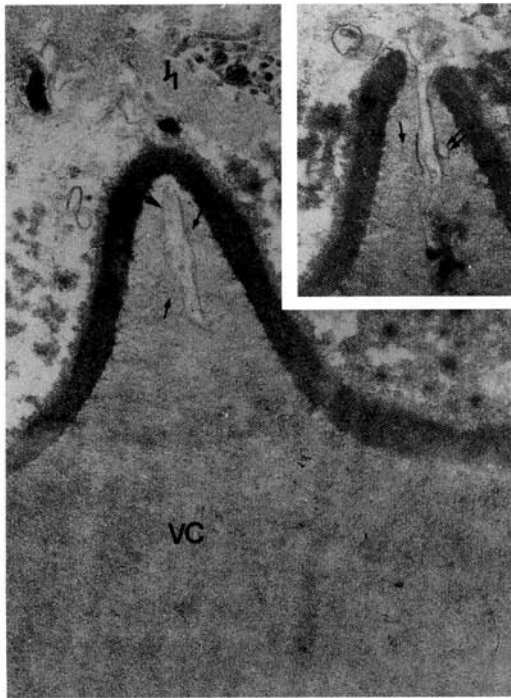


Fig. 6. Sperm segment crossing the VC, 6 min following insemination. P, jelly plug; J1, jelly layer 1. Arrow indicates inner acrosome membrane. Small arrows indicate VC fibrils bound to sperm membrane. **Inset:** Serial section. Double small arrows indicate sperm hybrid vesicle ($\times 18,000$).

difficult ultrastructural detection, are released on the earliest sperm contact with the egg investments. In mice, *acrosin* gene knockout experiments indicate that the zona pellucida penetration is a mechanochemical process (Baba et al., 1994).

In *D. pictus*, the sequence of sperm penetration into the egg investments is in agreement with the observation that the AR stages are independent of the interaction with the specific jelly layer in which a sperm segment is embedded, i.e., the AR occurs along a single sperm in a sequence depending on the arousal time of the reaction. The AR may either occur contemporaneously all over the sperm or start at the apical rod and then spread along the rest of the sperm. In both cases, the observed presence in the same section of sperm at more or less advanced stages of AR could be explained by hypothesizing that sperm might derive from different bundles penetrating the jelly with slight delay. The site where the AR is triggered does not appear to be the innermost jelly coat or the VC, unlike what has been observed in *Bufo japonicus* (Katagiri et al., 1982; Yoshizaki and Katagiri, 1982; Omata, 1993) and in agreement with work in other species (Wolf and Hedrick, 1971 in *Xenopus*; Elinson, 1971 in *Rana pipiens*; Picherat, 1977 in *Pleurodeles waltlii*). In *D. pictus*, all

the stages of AR were observed in isolated J3, strongly suggesting that, during penetration of entire eggs, this jelly coat triggers the AR. The fact that in amphibians the AR can be triggered in the VC or in the jelly coat may reflect differences among species, similar to what has been found in mammals (reviewed in Ward and Kopf, 1993). Moreover, we found that, simply upon dilution of the bundles, some sperm coming out of the bundle matrix undergo changes practically identical to the AR, except for the in toto removal of external membranes without vesiculation (AR*). Sperm freed in the external medium would undergo the AR*, while sperm embedded in the jelly coat would start the AR. We showed that spermatozoa, in the absence of the egg jelly matrix, may interact with one another, coming out of the bundles. Probably the AR* occurs in such sperm.

While the VC does not seem to trigger the AR in *D. pictus*, evidence was found that binding occurs between the sperm and this coat. Indeed, in a fold of the VC, fibrils were observed connecting the external sperm surface at a postinsemination time when all sperm had undergone AR. It is unclear whether sperm binding to the VC occurs at earlier stages and whether it occurs for all the inseminating sperm. However, it is known that the fertilizing sperm are caught in a VC fold at the second stage of penetration into the egg (see Talevi and Campanella, 1988). A simple interpretation of this phenomenon is that the binding occurs during the AR, when the inner acrosomal membrane becomes exposed. The binding could be clearly seen only when changes of pressure occurred in the perivitelline space and on the sperm themselves. Accordingly, this binding might be instrumental for maintaining fertilizing sperm attached to the fertilization membrane when their penetration into the fertilization cone is temporarily blocked and conformational changes occur in the dimple.

Furthermore, the observed binding does not seem to be related to sperm binding occurring on the external surface of isolated VC (Grey et al., 1976 in *Xenopus*), but it reflects what appears to occur in the sperm penetration of undissected eggs.

In the dimple, where fusion between spermatozoa may occur, sperm fuse with the oolemma by the inner acrosome membrane, and the acrosome content is released at the fusion site.

On its arrival in the dimple content, the apical rod is at the earliest stages of vesiculation. The acrosome content is almost unchanged; therefore, the head surface is constituted by hybrid vesicles (plasma membrane + outer acrosome membrane) and by the component A external rim. The sperm surface is probably quite sticky in the DC, as spermatozoa may interact or fuse in this environment; it is not clear whether a relationship exists between this ability and the observed intense electron-density of the sperm surface (Fig. 7).

We could not detect the initial stage of interaction of the sperm tip with the oolemma. However, we established that the spermatozoon interacts apically with

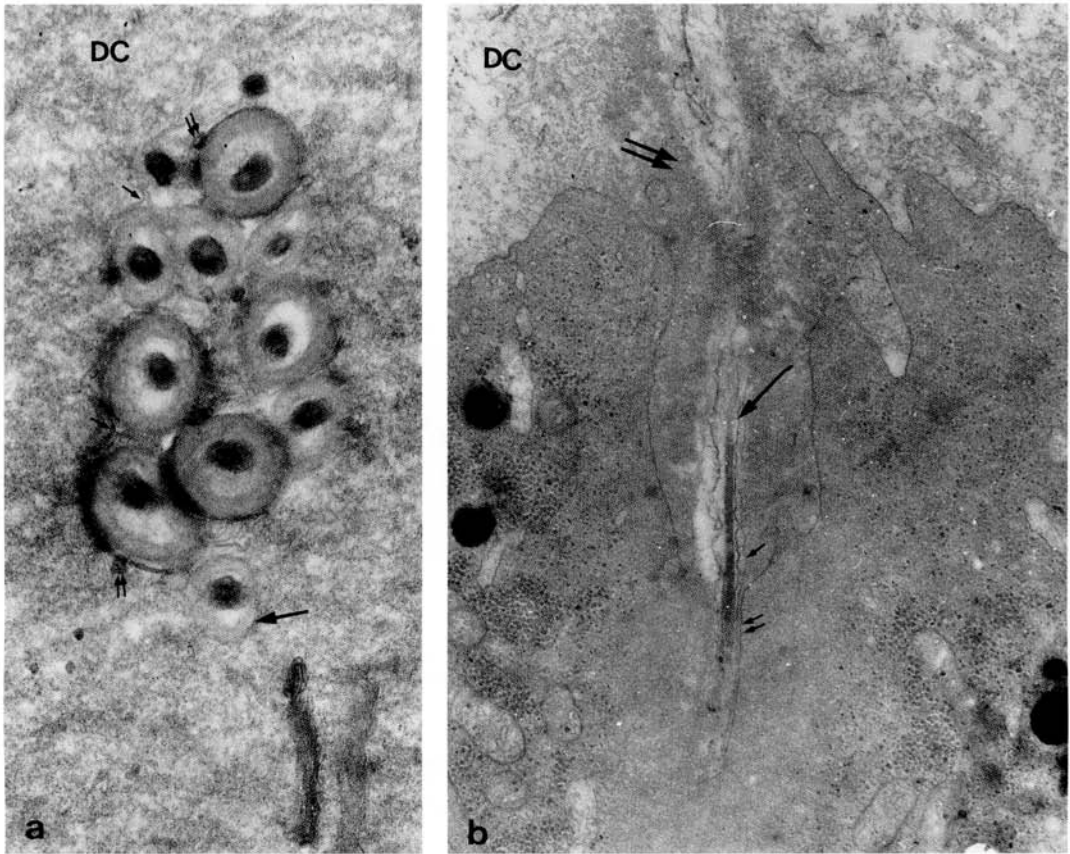


Fig. 7. a: Cross sections of sperm in the DC about 50 sec postinsemination. The sperm surface consists of electron-dense hybrid vesicles (double small arrows) and of a component B electron-dense rim (arrows). Sperm in close contact show sites of fusion (small arrows) ($\times 56,000$). **b:** Fusions between sperm and egg membranes at 1 min postinsemination. The anteriormost portion of the sperm head is engaged in fusion with the oolemma in a narrow egg invagination. The

spermatozoan is surrounded by a halo of finely granular material (double arrows), which is probably acrosome component A. Its nucleus is surrounded by the nuclear envelope (arrow). Fusion occurs at the tip of the invagination, and it is not clearly visible because of the section orientation. Small arrow, inner acrosome membrane; double small arrows, oolemma; DC, dimple content ($\times 32,000$).

the oolemma, and its initial fusion involves the inner acrosome membrane, which is dissimilar to the mammalian pattern of interaction (reviewed in Yanagimachi, 1994). Initial binding probably occurs between the surface of the apical rod and the antennular glycocalyx that surrounds the dimple (D1) microvilli (Campanella, 1975). Fusion happens at the apical rod membrane, which extends into the inner acrosome membrane; at that time, the subsequent sperm head still contains most of the acrosome content. In this work we observed that, about 30 sec later, the penetrating sperm are surrounded by a halo of finely granular material, which has the appearance of acrosomal constituents rather than of DC. As the sperm are delimited by the inner acrosome membrane, and in view of the temporal sequence of the acrosome reaction, it is highly probable that the surrounding halo consists of acrosome component A. Therefore, this acrosomal content appears to

support the penetration of the head region, while, at the very initial stages, component B may also participate in this process. The penetrating sperm undergo morphological changes indistinguishable from those described as stages of the acrosome reaction.

Fusion between the innermost acrosome membrane and the oolemma occurs at the bottom of the funnel, where the acrosomal content is absent. The enormous length of sperm membrane to be incorporated is striking; as a consequence, the penetration funnel reaches a final depth of at least 50 μm during the penetration of the head region covered by the acrosome (Talevi and Campanella, 1988).

The following new findings are reported in this study: 1) the sequential stages of the AR in the jelly coats; 2) a novel interaction between the VC and penetrating sperm; and 3) the fine structure of sperm penetration into the egg in amphibians.

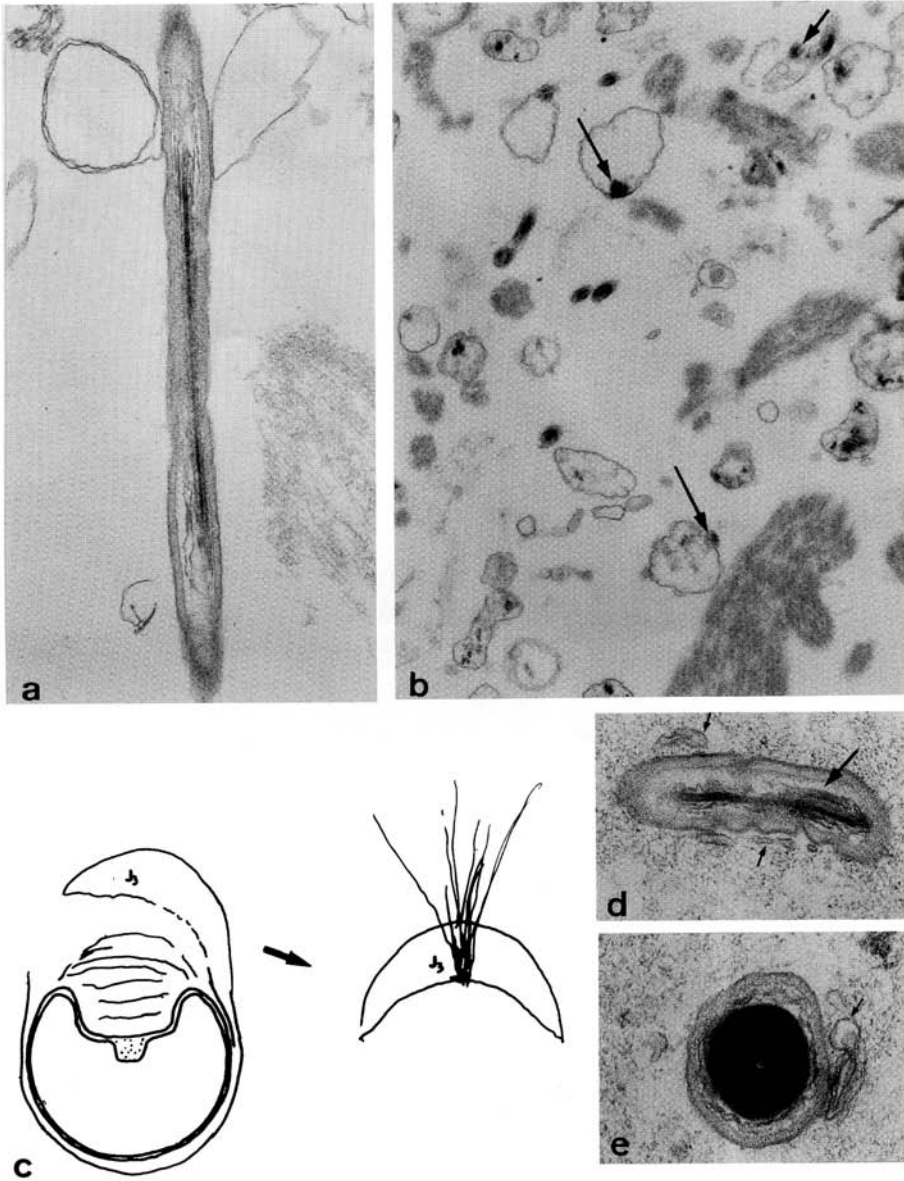


Fig. 8. Sperm bundles fixed after dilution in 10% Ringer's solution. **a:** Sperm fixed immediately after ejection from the bundles. Depletion of large sheets of plasma membrane and outer acrosome membrane has occurred ($\times 12,000$). **b:** Sperm fixed 10 min after getting free of the bundles. Nuclei (arrows) are surrounded by similar membrane sheets

($\times 9,000$). **c:** Schematic drawing of J3 removal from the egg and of its insemination. **d,e:** Sections of sperm in the excised J3 showing the acrosome reaction. Small arrows, hybrid vesicles; arrow, component B depletion (d, $\times 68,000$; e, $\times 50,000$).

ACKNOWLEDGMENTS

We thank Drs. P. Andreuccetti, R. Gualtieri, J.L. Hedrick, C. Katagiri, W.L. Lennarz, and R. Talevi for their comments and suggestions. The authors are also indebted to Messrs. G. Cafiero and A. Ciarletta for

technical help, and to Mr. G. Falcone for printing the micrographs. This research was supported by Consiglio Nazionale Delle Ricerche (C.N.R.) and Ministero Dell' Università E Della Ricerca Scientifica e Tecnologica (MURST) grants to C.C.

REFERENCES

- Almeida EAC, Huovila J, Sutherland AE, Stephens LE, Calarco PG, Shaw LM, Mercurio AM, Sonnenberg A, Primakoff P, Myles DG, White JM (1995): Mouse egg integrin $\alpha 6 \beta 1$ functions as a sperm receptor. *Cell* 81:1095-1104.
- Baba T, Azuma S, Kashiwabara S, Toyoda Y (1994): Sperm from mice carrying a targeted mutation of the acrosin gene can penetrate the oocyte zona pellucida and effect fertilization. *J Biol Chem* 269:31845-31849.
- Barbieri FD, Oterino JM (1972): A study of the diffusible factor released by the jelly of the egg of the toad, *Bufo arenarum*. *Dev Growth Differ* 14:107-117.
- Bernardini G, Andrietti F, Camatini M, Cosson MP (1988): *Xenopus spermatozoon*: Correlation between shape and motility. *Gamete Res* 20:165-175.
- Cabada MO, Mariano MI, Raisman JS (1978): Effect of trypsin inhibitors and concanavallin A on the fertilization of *Bufo arenarum* coelomic oocytes. *J Exp Zool* 204:409-416.
- Campanella C (1975): The site of spermatozoa entrance in *Discoglossus* (Anura) unfertilized egg: An electron microscope study. *Biol Reprod* 12:439-447.
- Campanella C, Gabbiani G (1979): Motile properties and localization of contractile proteins in the spermatozoon of *Discoglossus pictus*. *Gamete Res* 2:163-175.
- Campanella C, Atripaldi U, Gabbiani G (1981): Osservazioni sugli spermatozoi di *Discoglossus pictus* (Anuro) con particolare riferimento alle caratteristiche motorie. Quaderni di "La Ricerca Scientifica" n. II. Atti del Convegno Progetto Finalizzato Biologia della Riproduzione, 5-7 febbraio 1979, pp 239-246.
- Campanella C, Talevi R, Gualtieri R, Andreuccetti P (1990): *Discoglossus pictus* fertilization as a model for the study of amphibian sperm-egg interaction. In B. Dale (ed) "Mechanism of fertilization: from Plants to Humans. NATO ASI series, vol H45. Plenum Press New York. pp. 180-195.
- Campanella C, Amore F, Pitari G, Fusco C, Maurizi G, Dupre S (1992): Post-fertilization changes in *Discoglossus pictus* (Anura) eggs result in the formation of a capsular chamber where the egg rotates. *Int J Dev Biol* 36:413-422.
- Elinson RP (1971): Fertilization of partially jellied and jellyless oocytes of the frog *Rana pipiens*. *J Exp Zool* 176:415-428.
- Elinson RP (1973): Fertilization of frog body cavity eggs enhanced by treatments affecting the vitelline coat. *J Exp Zool* 183:291-302.
- Elinson RP (1986): Fertilization in amphibians: The ancestry of the block to polyspermy. *Int Rev Cytol* 101:59-100.
- Foltz KR, Partin JS, Lennarz WJ (1993): Molecular characterization of the sea urchin egg receptor for sperm. *Science* 259:1421-1425.
- Fusi FM, Vignali M, Gailit J, Bronson RA (1993): Mammalian oocytes exhibit specific recognition of the RGD (Arg-Gly-Asp) tripeptide and express oolemmal integrins. *Mol Reprod Dev* 36:212-219.
- Ghiara G (1960): Ricerche intorno alla struttura microscopica, submicroscopica ed istochimica ed alle funzioni degli involucri ovariali di *Discoglossus pictus* Oth e di altre specie di Anfibi. *Arch Zool* 45:9-92.
- Grey RD, Working PK, Hedrick JL (1976): Evidence that the fertilization envelope blocks sperm entry in egg of *Xenopus laevis*: Interaction of sperm with isolated envelopes. *Dev Biol* 54:52-60.
- Gualtieri R, Andreuccetti P (1996): Localization of egg-surface carbohydrates and fertilization in *Discoglossus pictus* (Anura). *Cell and Tissue Research* 283:173-181.
- Hibbard H (1928): Contribution à l'étude de l'ovogenèse, de la fécondation, et de la histogénèse chez *Discoglossus pictus*. *Arch Biol* 38:251-322.
- Ishihara K, Hosono J, Kanatani H, Katagiri C (1984): Toad egg-jelly as a source of divalent cations essential for fertilization. *Dev Biol* 105:435-442.
- Iwao Y, Katagiri C (1982): Properties of the vitelline coat lysin from toad sperm. *J Exp Zool* 219:87-95.
- Katagiri C (1974): A high frequency of fertilization in premature and mature coelomic toad eggs after enzymic removal of vitelline membrane. *J Embryol Exp Morphol* 31:573-581.
- Katagiri C (1987): Role of oviductal secretions in mediating gamete fusion in anuran amphibians. *Zool Sci* 4:1-14.
- Katagiri C, Yoshizaki N, Iwao Y (1982): Participation of oviductal pars recta secretions in inducing the acrosome reaction and release of vitelline coat lysin in fertilizing toad sperm. *Dev Biol* 94:1-10.
- Miceli DC, Fernandez SN, Mansilla ZC, Cabada MO (1987): New evidence of anuran oviductal pars recta involvement on gamete interaction. *J Exp Zool* 244:125-132.
- Myles GD (1993): Molecular mechanism of sperm-egg membrane binding and fusion in mammals. *Dev Biol* 158:35-45.
- Ohlndieck K, Lennarz WY (1995): Role of the sea urchin egg receptor for sperm in gamete interactions. *TIBBS* 20:29-33.
- Ohlndieck K, Partin JS, Lennarz WJ (1994): The Biological active form of the sea urchin egg receptor for sperm is a disulfide-bonded homo-multimer. *J. Cell Biol* 125:817-824.
- Omata S (1993): Relative roles of jelly layers in successful fertilization of *Bufo japonicus*. *J Exp Zool* 265:329-335.
- Penn A, Glenhill BL (1972): Acrosomal proteolytic activity of amphibian sperm. *Exp Cell Res* 74:285-288.
- Picheral B (1977): La fécondation chez le triton pleurodèle. *J Ultrastruct Res* 60:106-120.
- Pitari G, Dupré S, Fusco C, Maurizi G, Campanella C (1993): Jelly plug dissolution in *Discoglossus pictus* eggs (Anura) involves peroxidase-like activity and oxidative opening of disulphide bonds. *Zygote* 1:61-69.
- Primakoff P, Hyatt H, Tredick-Kline J (1987): Identification and purification of a sperm surface protein with a potential role in sperm-egg membrane fusion. *J Cell Biol* 104:141-149.
- Raisman JS, Barbieri FD (1969): Lytic effects of sperm suspensions on the vitelline membrane of *Bufo arenarum* oocytes. *Acta Embryol Exp* 1:17-26.
- Raisman JS, Mariano MI, Cabada MO (1977): Effect of trypsin inhibitors and concanavallin A on *Bufo arenarum* fertilization. *Dev Growth Differ* 19:119-123.
- Shivers CA, James JM (1970): Capacitation of frog sperm. *Nature* 227:183-184.
- Talevi R (1989): Polyspermic eggs in the anuran *Discoglossus pictus* develop normally. *Development* 105:123-130.
- Talevi R, Campanella C (1988): Fertilization in *Discoglossus pictus*. I: Regionalization of sperm-egg interaction site and occurrence of a late stage of sperm penetration. *Dev Biol* 130:524-535.
- Talevi R, Dale B, Campanella C (1985): Fertilization and activation potentials in *Discoglossus pictus* eggs: A delayed response to activation by pricking. *Dev Biol* 111:316-323.
- Tarone G, Russo MA, Hirsch E, Odoriso T, Altruda F, Silengo L, Siracusa G (1993): Expression of B1 integrin complexes on the surface of unfertilized mouse oocyte. *Development* 117:1369-1375.
- Ward CR, Kopf GS (1993): Molecular events mediating sperm activation. *Dev Biol* 158:9-34.
- Whitaker M, Swann K (1993): Lighting the fuse at fertilization. *Development* 117:1-12.
- Wintrebert P (1933): La mécanique du développement chez *Discoglossus pictus* Oth, de l'ovogenèse à la segmentation. *Arch Zool Exp Genet* 75:501-539.
- Wolf DP, Hedrick JL (1971): A molecular approach to fertilization. II. Viability and artificial fertilization of *Xenopus laevis* gametes. *Dev Biol* 25:348-359.
- Yanagimachi R (1994): Mammalian Fertilization. In E Knobil, J Neill (eds): "The Physiology of Reproduction." New York: Raven Press, pp 189-317.
- Yamasaki H, Takamune K, Katagiri C (1988): Classification, inhibition and specificity studies of the vitelline coat lysin from toad sperm. *Gamete Res* 20:287-300.
- Yoshizaki N, Katagiri C (1982): Acrosome reaction in sperm of the toad, *Bufo bufo japonicus*. *Gamete Res* 6:343-352.

Specific Glycoconjugates Are Present at the Oolemma of the Fertilization Site in the Egg of *Discoglossus pictus* (Anurans) and Bind Spermatozoa in an *in Vitro* Assay

G. Maturi, V. Infante, R. Carotenuto, R. Focarelli,*
M. Caputo, and C. Campanella

Dipartimento di Biologia Evolutiva e Comparata, Università di Napoli, via Mezzocannone n.8,
80134, Napoli, Italy; and *Dipartimento di Biologia Evolutiva, Università di Siena,
Via Mattioli n.4, Siena, Italy

In the egg of the anuran *Discoglossus pictus*, the site of fertilization is restricted to the central portion of an animal hemisphere indentation (the *dimple*). Previous studies showed that the acrosome reaction of *D. pictus* sperm is triggered in the jelly, and yet sperm arrive at the dimple surface with the plasma membrane at an early stage of vesiculation. Reactivity of the dimple surface with specific lectins suggests that fucose might be utilized as a marker of glycoproteins located at the dimple surface. In this paper, proteins of the egg surface were labeled with the membrane impermeable sulfo-NHS-biotin. Four main bands of 200, 230, 260, and 270 kDa labeled only at the dimple surface, although they were detected in the cortex of the whole egg. The 270-kDa band reacted with *Galanthus nivalis* agglutinin only in the cortex of the dimple, suggesting that this band is differently glycosylated according to its localization. The α -L-fucose-specific lectin *Ulex europaeus* agglutinin I was utilized both in lectin blotting and in affinity chromatography and cross-reacted with the 200- and 270/260-kDa bands. Furthermore, two polypeptides were obtained by exposure of intact eggs to lysylendoproteinase C. They were also reactive to *Ulex europaeus* agglutinin I. The 200- and 270/260-kDa bands were eluted from the acrylamide gels and adsorbed to polystyrene beads. An assay for sperm binding to 200-kDa glycoprotein-bound beads was developed. Sperm stuck to the beads before but not after Ca-ionophore treatment. When the beads were coated with the 270/260-kDa glycoproteins, binding occurred after ionophore treatment. In these assays, the 200- and 270/260-kDa glycoproteins competitively inhibited sperm binding to the beads coated with the corresponding glycoprotein. These results indicate that the assayed glycoproteins, located either in the glycocalyx or in the plasma membrane of the fertilization site, are involved in sperm binding. © 1998 Academic Press

INTRODUCTION

Membrane fusion between sperm and eggs is preceded by a coordinated series of reactions involving egg envelopes. The egg extracellular coat possesses ligands that are able to interact with the sperm, causing the acrosome reaction and the binding of the sperm membrane to the vitelline envelope (VE) or zona pellucida; thus the sperm may proceed toward the oolemma where intragametic fusion occurs. While the interaction with external coats has been investigated in detail both in invertebrates (for reviews, see Foltz and Lennarz, 1993; Rosati, 1995) and vertebrates (see Barros *et al.*, 1996; Hedrick and Nishihara, 1991), the chemical colloquium taking place between sperm and egg surface at

the time of fusion is largely unknown. At present, the challenge is to understand what molecular interaction occurs between sperm and egg surface after the former has attained the ability to bind and fuse with the oolemma by interaction with extracellular coats.

In the anuran egg, two main territories are present, the whitish vegetal hemisphere and the pigmented animal hemisphere where fertilization occurs. This remarkable compartmentalization is extreme in the genus *Discoglossus*, where the predetermined site of fertilization is further concentrated in the center of the animal half. Indeed, in the egg of *Discoglossus pictus*, fertilization takes place in the dimple, while, in the rest of the egg (DLE, dimpleless egg), sperm do not activate development. *D. pictus* has several

advantages over other species for detecting the surface molecules that take part in the fertilization process. First, experimental evidence indicates that, in the dimple, ionic channels, intramembrane particles, and cortical cytoskeleton are highly concentrated, which provides favorable conditions for biochemical analysis of cortex and plasma membrane (Talevi *et al.*, 1985; Talevi and Campanella, 1988; Nuccitelli *et al.*, 1988; Gualtieri *et al.*, 1989; Tatone *et al.*, 1993). Second, a glycoprotein content (dimple content) keeps the dimple surface apart from the vitelline envelope (VE) for a depth of about 300 μm . This makes it possible to pinch off the VE manually, and to proceed to biochemical analysis of the dimple versus the DLE, cleared of the extracellular component of the egg. Third, the presence of terminal fucose has been histologically determined only at the surface of the dimple center. This natural marker can be utilized for the identification of glycoconjugates typical of this region and probably involved in the fertilization process: in fact, fucose-containing components settle at the surface of the dimple during its formation, and disappear after fertilization (Denis-Donini and Campanella, 1977). Fourth, the acrosome reaction of *D. pictus* sperm has been studied in its natural environment, and the membranes interacting and fusing with the oolemma have been determined (Campanella *et al.*, 1997). The jelly coat, and particularly the *plug*, is essential for sperm convergence into the dimple center. Electrophysiological experiments have shown that the dimple center is endowed with the specific ability to generate typical fertilization potentials upon insemination, followed by the formation of the fertilization cone and the onset of development. Elsewhere in the dimple, initial sperm penetration occurs but this event does not produce either typical fertilization potentials or the onset of development (Talevi and Campanella, 1988).

In this paper, we identified glycoproteins present at the dimple surface. From biotin labeling and terminal fucose lectin binding experiments, we determined the presence of four fucosylated proteins, 200, 230, 260, and 270 kDa. The major glycoproteins (200, 270, 260 kDa) were tested for their ability to function in sperm binding.

MATERIALS AND METHODS

Animals

Adult females and males of *D. pictus* were collected in the neighborhood of Palermo, Italy. They were injected with 250 IU Profasi (Serono, Italy) in amphibian Ringer (111 mM NaCl, 1.3 mM CaCl_2 , 2 mM KCl, 0.8 mM MgSO_4 , 25 mM Hepes, pH 7.8) in the dorsal lymphatic sac, and their gametes were collected about 18 h later, as indicated in a previous paper (Campanella *et al.*, 1997).

Preparation of Eggs and "Cortex" (Plasma Membrane with a Thin Layer of Underlying Cytoplasm)

Eggs were dejellied in dejellifying buffer (100 mM NaCl, 5 mM DTE, 50 mM Tris-HCl, pH 8.5) and transferred to ice-cold 25 mM

Hepes, pH 7.5, containing 900 mM glycerol, 0.02 mM NaN_3 , 1 mM ATP, 1 mM DTT, 5 mM EGTA (HB) and the following protease inhibitors: 2 mM TAME (Sigma Chemical Co., St. Louis, MO), 5 mg/ml SBTI, 5 $\mu\text{g}/\text{ml}$ aprotinin (Sigma), and 10 μM E64 (Calbiochem-Novabiochem Corp., San Diego, CA).

After manual removal of the VE and of the innermost jelly layer, the eggs were homogenized in HB containing 1% SDS, centrifuged at 15,000g, and prepared for electrophoresis. For cortex preparation, the dimple and DLE were separated by manual dissection (for more details, see Tatone *et al.*, 1993) and spread on glass petri dishes containing fresh HB on ice. After several rinses in fresh buffer, dimple and DLE cortices were homogenized in HB and prepared for electrophoresis as described for the eggs. A concentration of 0.3 M NaCl was added to the samples during homogenization, prior to SDS-PAGE analysis under nonreducing conditions. Samples of the dimple content were collected by pricking the VE facing the dimple.

Protein Determination, SDS-PAGE, and Gel Staining

Protein concentration of the samples was determined with the BCA or Micro BCA protein assay reagent (Pierce Chemical Co., Rockford, IL). After being mixed with sample buffer (Laemmli, 1970) and boiled for 3 min, 1 to 60 μg proteins was loaded for each electrophoretic run, as detailed for each category of experiments. In case of total egg supernates, the optimal amount of total egg soluble proteins applied to the gels was 40–60 μg per lane, which corresponds to about 1 egg.

Protein samples were analyzed with SDS-PAGE using Laemmli's Tris-glycine buffer system (Laemmli, 1970). The running gel either contained 4, 5, 7.5, or 10% acrylamide or was a 5–12% gradient. Molecular mass standards (200, 116, 97, 45, 31, or 21 kDa) (Bio-Rad, Hercules, CA) and human spectrin dimer (220 and 240 kDa) derived from erythrocyte ghosts (Marchesi, 1971) were used as reference markers. After fixation in methanol/acetic acid, gels were stained with either Coomassie blue or the silver method.

Biotinylation

Sulfo-NHS-biotin (Pierce Chemical Co.) was used as a membrane-impermeable, biotinylating agent for labeling surface proteins. Small wells were molded in agar-containing petri dishes. The wells were filled with 5 ml of freshly prepared sulfo-NHS-biotin in 8.3 mM phosphate buffer, pH 8.0. Eggs, deprived of their external investments, were deposited in the wells. After a 30-min incubation at 4°C, the solution was replaced with 40 mM lysine in phosphate buffer to stop the reaction. Following incubation in this medium, the dimple and DLE regions were manually divided and separately homogenized in phosphate buffer containing proteases inhibitors. As controls, a set of eggs was directly homogenized in phosphate buffer containing sulfo-NHS-biotin. In both experimental and control samples, 1% SDS was added to phosphate buffer at homogenization. The samples were then centrifuged at 15,000g, prepared for SDS-PAGE by addition of sample buffer with or without 5% β -mercaptoethanol, and blotted on nitrocellulose sheets.

Affinity Chromatography

After removal of jelly and VE, eggs were homogenized in buffer A (0.5 M NaCl, 20 mM Tris-HCl, pH 7.4) containing 1.5% β -octylglucoside and protease inhibitors. Following centrifugation at 15,000g, 50–100 μg of the supernate glycoproteins was diluted 1:40 (v/v) with the same buffer and incubated overnight with gentle

shaking with UEA-I agarose [Sigma]. The lectin matrix was allowed to settle on ice and the supernate was carefully removed. Following washing in buffer A and A' (0.15 M NaCl, 20 mM Tris-HCl, pH 7.4), batch elution was accomplished by incubating *Ulex europaeus* (UEA-I) agarose with 250 mM fucose in buffer A' for 20 min. The eluate was analyzed by SDS-PAGE.

Western Blot and Lectin Blot Detection on Nitrocellulose

Proteins subjected to SDS-PAGE were electrophoretically transferred to nitrocellulose sheets, according to Towbin *et al.* (1979), overnight at 180 mA (for more details, see Tatone *et al.*, 1993). Biotinylated samples were incubated with 5% fat-free milk (Milupa, Verona, Italy) and, following several rinses in saline, were exposed to streptavidin conjugated with alkaline phosphatase, using the Protoblot Immunoscreeing system (Promega, Madison, WI). In some experiments, blots were stained with 1% amido black. Likewise, for lectin blotting, transferred proteins were first blocked in 2% BSA in PBS, incubated in α -L-fucose-specific UEA-I agglutinin conjugated with biotin and exposed to avidin-alkaline phosphatase. Blotting was also performed with biotinylated *Arachis hypogea* peanut agglutinin (PNA) for general identification of O-linked sugar chains, and with concanavalin A (Con A) and *Galanthus nivalis* agglutinin (GNA) for N-linked sugar chains. Negative control runs consisted of the addition of fucoidan or fucosyl lactose, D-mannose, and D-galactose to UEA-I, Con A, GNA, or PNA, respectively.

Lysylendoproteinase C Treatment

After being dejellied, the eggs were transferred to Ringer and the VEs were manually removed. Undamaged eggs were transferred to a fixed volume of fresh Ringer containing lysylendoproteinase C (3 U in 100 ml Ringer, Boehringer Mannheim, Germany). The digestion was monitored under a dissecting microscope. As soon as egg surface brightness started changing, the reaction was stopped by the addition of aprotinin (20 U/100 ml Ringer).

The Ringer containing the enzyme digestion products was concentrated using a 3000 MW cutoff Microcon (Amicon, Beverly, MA) and processed for electrophoresis and Western blotting.

Microscopy

Eggs were fixed, frozen and sectioned for fluorescence microscopy, as described by Tatone *et al.* (1993). The sections were incubated with UEA-I conjugated with fluorescein isothiocyanate (UEA-I FITC, Sigma), extensively rinsed in PBS and mounted in 90% glycerol in PBS; afterward the level of fluorescence was compared with that in control sections treated with UEA-I preincubated with 1 mg/ml fucosyl-lactose.

Photographs were taken with a Leitz UV microscope using Ektachrome 320 T.

For electron microscopy, eggs, dimple and DLE were fixed as indicated in a previous publication (Campanella *et al.*, 1988).

Electroelution

Egg proteins were separated by SDS-PAGE and the resulting bands were visualized by staining with 0.3 M CuCl₂. The area of the selected bands was cut out, and the gel slices were electroeluted with 25 mM Tris-HCl, pH 8.3, containing 1.44% glycine. Electro-

eluted glycoproteins were dialyzed at 4°C against distilled water and concentrated in a Savant speed vacuum concentrator. In some experiments, E64 was added to buffer D and to distilled water. The protein content and the purity of each sample were checked either by SDS-PAGE or by Micro BCA protein assay.

In Vitro Sperm Binding Assay

The eluted molecules were diluted with 2× buffer B, 1:1 (v/v). Protein binding on 300- to 400- μ m polystyrene beads was performed as suggested by the supplier (Polysciences, Warrington, PA), utilizing 0.1 M borate buffer, pH 8.5. About 800 beads were used for each adsorption experiment. Equimolar amounts of the 200- and 270/260-kDa glycoproteins, BSA, and lipovitellin were employed. A specific sperm binding assay was developed, which may underestimate the number of sperm bound to the beads, but has the advantage of not selecting as "bound" those sperm trapped around the beads because of their length.

Sperm suspensions recovered from the seminal vesicle were diluted, and large sperm clumps were discarded. About 100 μ l sperm suspension was diluted in 1/10 Ringer and gently smeared on microslides to induce unraveling of the sperm bundles and sperm ejection. Sperm stop moving in 15 s (Campanella and Gabbiani, 1979). About 100 protein-coated beads were released onto the spermatozoa and incubated for 5 min, with gentle rocking. After being rinsed in Ringer, beads were removed from the petri dish with watchmakers' forceps and observed at a light transmission microscope to score beads with sperm. The microslide carrying the beads was shaken by moving the microscope translation table. Sperm attachment to the beads that had resisted such treatment was assessed as sperm binding. Parallel assays were performed utilizing spermatozoa exposed to 25 μ M calcium ionophore A23187. For each assay, the percentage of beads with sperm was counted on 80 beads.

For competition assays, 200- or 270/260-kDa electroeluted proteins were diluted in 1/10 Ringer at decreasing concentrations, starting from the concentration utilized for adsorption to the beads. They were then preincubated with sperm for 15 min. The sperm binding assay was subsequently performed as described.

Beads were photographed with a Leitz UV microscope directly or following exposure to 95% ethanol, staining for 20 min with 1.6 μ M DAPI, and mounting in PBS-glycerol.

RESULTS

Biotinylation of Surface Protein and SDS-PAGE of Labeled Dimple and DLE Indicate that Four Major Proteins Are Present at the Dimple Surface

Labeled eggs were divided into dimple and DLE regions and subjected to SDS-PAGE. Figures 1A and 1B show the blotted gels after incubation with streptavidin-alkaline phosphatase. Under nonreducing conditions, four high-molecular-weight bands, having the apparent M_r of 200, 230, 260, and 270 kDa and a minor band of about 250 kDa, labeled only at the dimple surface (Fig. 1A, compare lane a, DLE, with lane b, dimple). In addition, a conspicuous band having an M_r of about 140 kDa was present in both dimple and DLE blots, while a minor band of 100 kDa was found only in the dimple blot (Fig. 1A, b). Previous experiments revealed that these bands cross-react directly with strepta-

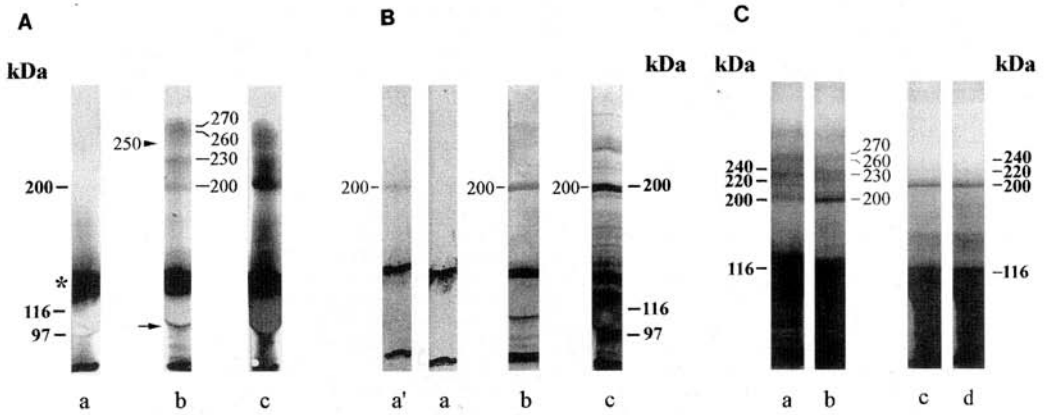


FIG. 1. [A, B] Western blots of sulfo-NHS-biotin-labeled proteins of dimple and DLE regions as transferred onto nitrocellulose sheet and revealed by streptavidin-alkaline phosphatase. The polyacrylamide concentration used was 5%, and 40 μg of samples per lane was loaded on the gels. (A) Blot of samples under nonreducing conditions. (Aa, blot of DLE) Ab, blot of dimple) Bands of 270/260, 230, and 200 kDa are indicated, as well as a minor 250-kDa band (arrowhead). These proteins are not found in the DLE sample (compare Aa with Ab). Asterisk, band of about 140 kDa; arrow, band of 100 kDa. Ac, Blot of control eggs broken while in sulfo-NHS-biotin. (B) Blots of samples under reducing conditions. Ba, Blot of DLE; Bb, blot of dimple. By comparing dimple and DLE blots, a 200-kDa protein is only in the dimple blot. Ba', this is the same blot as DLE in Ba, restained with amido black; the 200-kDa band is stained. Bc, blot of control egg broken while in sulfo-NHS-biotin. (C) SDS-PAGE of dimple and DLE cortex, silver stained (40 μg proteins/sample) Ca and Cb, electrophoresis under nonreducing conditions. Ca, DLE; Cb, dimple. The 200-, 230-, 260-, and 270-kDa bands are present both in D and in DLE; Cc and Cd, electrophoresis under reducing conditions. The 200-kDa band is present both in the dimple (Cd) and in DLE (Cc). Reference molecular mass proteins are indicated.

vidin and anti-biotin antibodies, indicating that they are endogenous biotinylated proteins [Infante *et al.*, 1995].

In control experiments, where the eggs were broken and homogenized in sulfo-NHS-biotin, thus allowing labeling of internal proteins, a larger number of labeled proteins were found on the blots (Fig. 1A, c).

Under reducing conditions, a 200-kDa band (Fig. 1B) and minor bands of low M_r were found, indicating a change in the electrophoretic pattern of the high M_r molecules of the dimple surface due to mercaptoethanol.

The electrophoretic patterns of the dimple cortex and the DLE cortex, under both nonreducing and reducing conditions, are indicated in Fig. 1C; these patterns belong to proteins located in the plasma membrane and the underlying cytoplasm. The only difference in the electrophoretic patterns of dimple and DLE lies in the relative concentration of some proteins. In particular, the 200-, 230-, 260-, and 270-kDa bands are present in the DLE gel (Fig. 1C, a, DLE gel under nonreducing conditions). This indicates that the four bands were present in the DLE but not at its surface (compare the gel of Fig. 1C, a, with the corresponding Western blot of DLE in Fig. 1A, a).

To ascertain whether these bands were present in the DLE blot, though unreactive to streptavidin because they were unlabeled, the DLE blot of Fig. 1B, a, was stained with 1% amido black. The 200-kDa band was clearly present (Fig. 1B, a', sample under reducing conditions).

Dissected samples were processed for electron microscopy particularly to check whether the dimple content was still present at the surface following egg dissection. By comparing Fig. 2b with an undissected egg (Fig. 2a), it is evident that, in the latter, the dimple content was no longer present, while the dimple surface maintained microvilli bordered by typical glycocalyx [Campanella *et al.*, 1988]. The inset of Fig. 2a represents the electrophoretic profile of the dimple content, where the 270-, 260-, 230-, and 200-kDa bands are absent.

Affinity Chromatography and UEA-I Blots Reveal That the High M_r Glycoproteins Detected at the Dimple Surface Are Fucosylated

Total egg supernatant solutions (50 μg) were exposed to UEA-I agarose. About 1/10 of the initial proteins was eluted from agarose beads and loaded on polyacrylamide gels. Mildly reactive 200- and 270/260-kDa bands and a conspicuous 116-kDa band were present in the gels (Fig. 3A). To further investigate on the affinity of these molecules for UEA-I, the dimple and DLE cortex supernates were electrophoretically separated under nonreducing conditions; they were then transferred onto a nitrocellulose sheet and probed with UEA-I. In the lectin blots, the 200-kDa band did not react with lectin, the 230-kDa band reacted mildly, while the large strip including the 260- and 270-kDa bands was

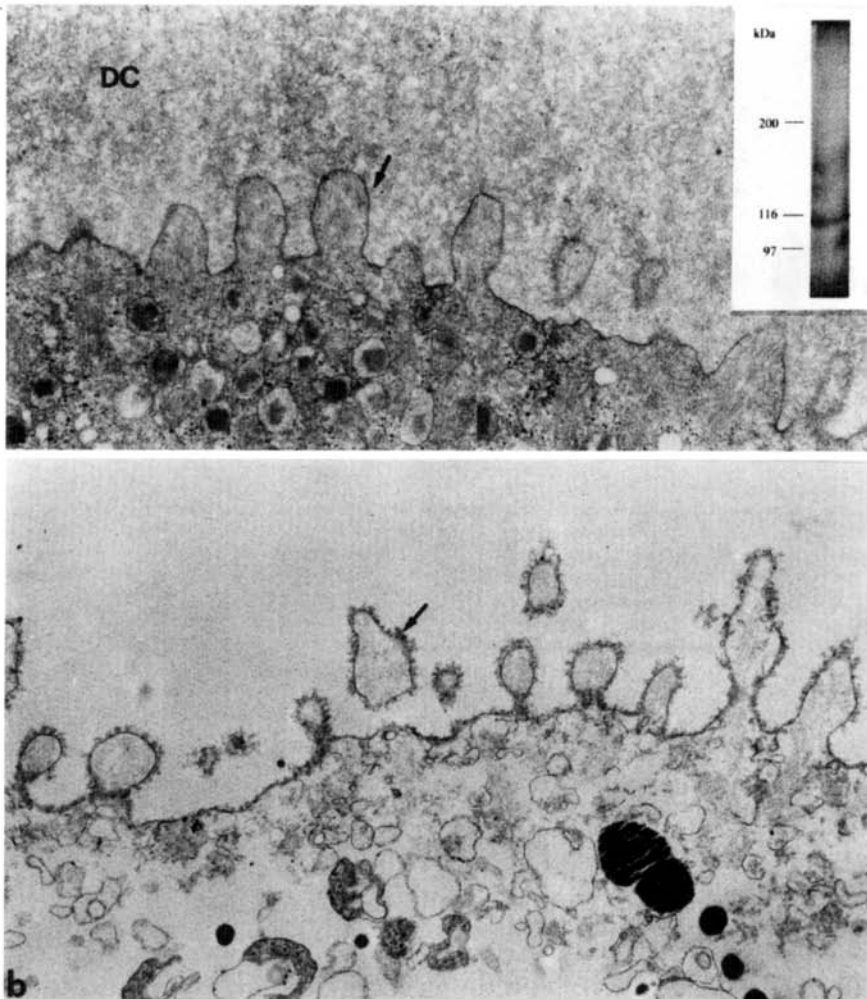


FIG. 2. Thin sections of the dimple. (a) Undisseminated egg. The typical microvilli of the dimple surface are here shown. They are bordered by glycocalyx (arrow). The dimple content is indicated (DC). (Inset) SDS-PAGE of the dimple content showing the absence of high M_r molecules; silver stain. (b) Dissected dimple region, as for the samples utilized for SDS-PAGE. The surface has microvilli bordered by glycocalyx (arrow). The dimple content is absent. $\times 12,000$.

clearly reactive (Fig. 3B). Similar results were obtained when the cortex of the dimple and DLE was homogenized with HB buffer containing 2% NP-40 or 1.5 β -octylglucoside or when whole egg supernate was utilized. Preincubation of lectin with 1 mg/ml fucoidan or 1 mg/ml fucosyl-lactose inhibited the reaction (data not shown).

Frozen sections of the dimple, exposed to UEA-I FITC, showed reactivity to lectin at the border of the dimple center, decreasing along the lateral walls of the dimple and

in small spots of the cortical and peripheral cytoplasm (Figs. 4a and 4b). Control sections, exposed to UEA-I following preincubation with fucosyl-lactose, did not react with lectin (Fig. 4c).

Blots of the egg cortex were further probed with concanavalin A, *G. nivalis* agglutinin, and *A. hypogea* agglutinin. The bands examined did not react with concanavalin A and *A. hypogea* agglutinin in both dimple and DLE domains. However, the 270-kDa band reacted with *G. nivalis*

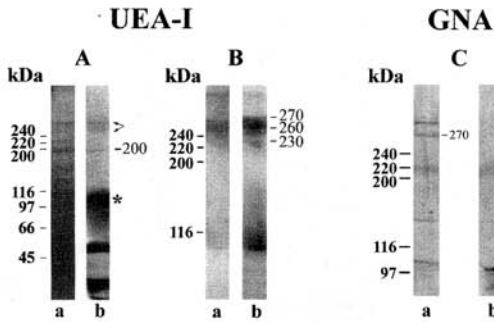


FIG. 3. [A] SDS-PAGE of molecules eluted from agarose-*Ulex europaeus* agglutinin-I (UEA-I) beads under nonreducing conditions; silver-stained 5–12% acrylamide gradients. Aa, total egg supernate. Ab, following elution, a 200-kDa band, several polypeptides and a prominent 116-kDa band (asterisk) were separated. The 270- and 260-kDa bands form a large strip (small arrows). Reference molecular masses are indicated. [B] UEA-I blot of dimple and DLE cortex electrophoretically separated under nonreducing conditions in 5% polyacrylamide gels. Ba, dimple; Bb, DLE. In both samples the 270- and 260-kDa bands form a large strip strongly reactive to lectin. A band of about 230 kDa, as well as other bands, are mildly reactive to UEA-I. Reference molecular mass proteins are indicated. [C] *Galanthus nivalis* agglutinin (GNA) blots of dimple (Ca) and DLE (Cb) cortex electrophoretically separated under nonreducing conditions. The 270-kDa band is reactive in the dimple blot (Ca).

agglutinin only in the dimple territory (Fig. 3C). The addition of 100 mM D-mannose inhibited the reaction of *G. nivalis* agglutinin on the blots (data not shown).

Lysylendoproteinase C Digestion Releases UEA-I-Binding Fragments from the Egg Surface

Upon removal of all their investments, the eggs were exposed to lysylendoproteinase C to release fragments of surface proteins (see Foltz and Lennarz, 1992). After stopping the reaction with aprotinin, the Ringer solution surrounding the eggs was concentrated and analyzed by SDS-PAGE. Part of the sample was electrophoretically transferred to nitrocellulose and incubated with UEA-I gold. One reactive band of about 63 kDa and a second minor band of 118 kDa are depicted in Fig. 5, indicating the presence of surface glycoconjugates containing α -L-fucose.

The Electroeluted 200- and 260/270-kDa Bands Are Able to Bind *D. pictus* Sperm

Following electroelution, the 200-kDa band yielded a 200-kDa band and/or 120- and 66-kDa bands (Fig. 6a), together with polypeptides of lower M_r . The pattern of the separated polypeptides contained the original 200-kDa band when the protease inhibitor E64 was added to buffer D. This suggests that the molecule might change its initial M_r ,

either by the action of exogenous proteases or for a specific fragility of the molecule that splits into two or more polypeptides. Similar results were obtained for the 270/260-kDa band that yielded fragments of lower M_r , including fragments of 118 and 66 kDa (Fig. 6A). Lipovitellin (115 kDa), the most prominent egg lipoglycoprotein, was also electroeluted (Fig. 6A).

Glycoproteins eluted in 8 separate sets of elution were utilized. The electroeluted 200- or the 270/260-kDa band was adsorbed to polystyrene beads. The adsorption was checked by boiling an aliquot of beads in sample buffer and analyzing the released glycoprotein by SDS-PAGE in each binding experiment (Fig. 6B). Lipovitellin and commercial BSA were adsorbed to beads as well. Knowing the concentrations of the glycoprotein in the eluate before and after adsorption and the number of beads per volume unit, the amount of bound 200-kDa band/bead was estimated to be about $0.0039 \mu\text{g}$ (1.18×10^{10} molecules). Similarly, the amount of bound 270/260-kDa band/bead was estimated to be about $0.0045 \mu\text{g}$ (1×10^{10} molecules).

In the binding assays, one or two males were utilized for each experiment. *D. pictus* sperm are 2.3 mm long, the head being about 1 mm long (Fig. 7a). When sperm come out of the bundles, they may get entangled because of their extraordinary length; thus clumps of sperm form, and the resulting suspension of spermatozoa is, therefore, rather uneven. As a consequence, it is impossible to give an appropriate meaning to quantitative counts of sperm bound/bead; i.e., whether more bound sperm mean a greater ability of the beads to bind sperm or more spermatozoa available to the beads cannot be established. Therefore, we measured successful sperm collision (binding) with beads under constant rocking, in terms of percentage of beads with sperm, without considering the number of sperm/bead.

Upon exposure of 200-kDa beads (beads coated with the eluted 200-kDa band), sperm stuck to the beads either at their tip or along bends that are often formed when they are not embedded in the jelly matrix (Figs. 7b and 7c). The mean percentage of beads with sperm was 76%, a value by far higher than that achieved by beads coated with BSA and lipovitellin (Fig. 8A). Binding was stable and sperm were not released from the beads over several hours. The same assay was performed by pretreating sperm with $25 \mu\text{M}$ of calcium ionophore A23187 for 5 min to induce the acrosome reaction in substitution of the jelly coat (see Campanella and Gabiani, 1979; Gualtieri and Andreuccetti, 1996; Campanella *et al.*, 1997). Following several rinses with 1/10 Ringer, sperm were exposed to the 200-kDa beads. Under this condition, a 25% percentage of beads with sperm was observed. This value approaches the values reported for BSA and lipovitellin beads (Fig. 8A).

Upon exposure to 270/260-kDa beads (beads coated with the eluted 270/260-kDa band), sperm stuck to the beads when they were pretreated with A23187 (Fig. 7d). On average, the percentage of beads with sperm was 73%, a much higher value than the corresponding values of control beads. In the absence of A23187 sperm treatment, only 23%

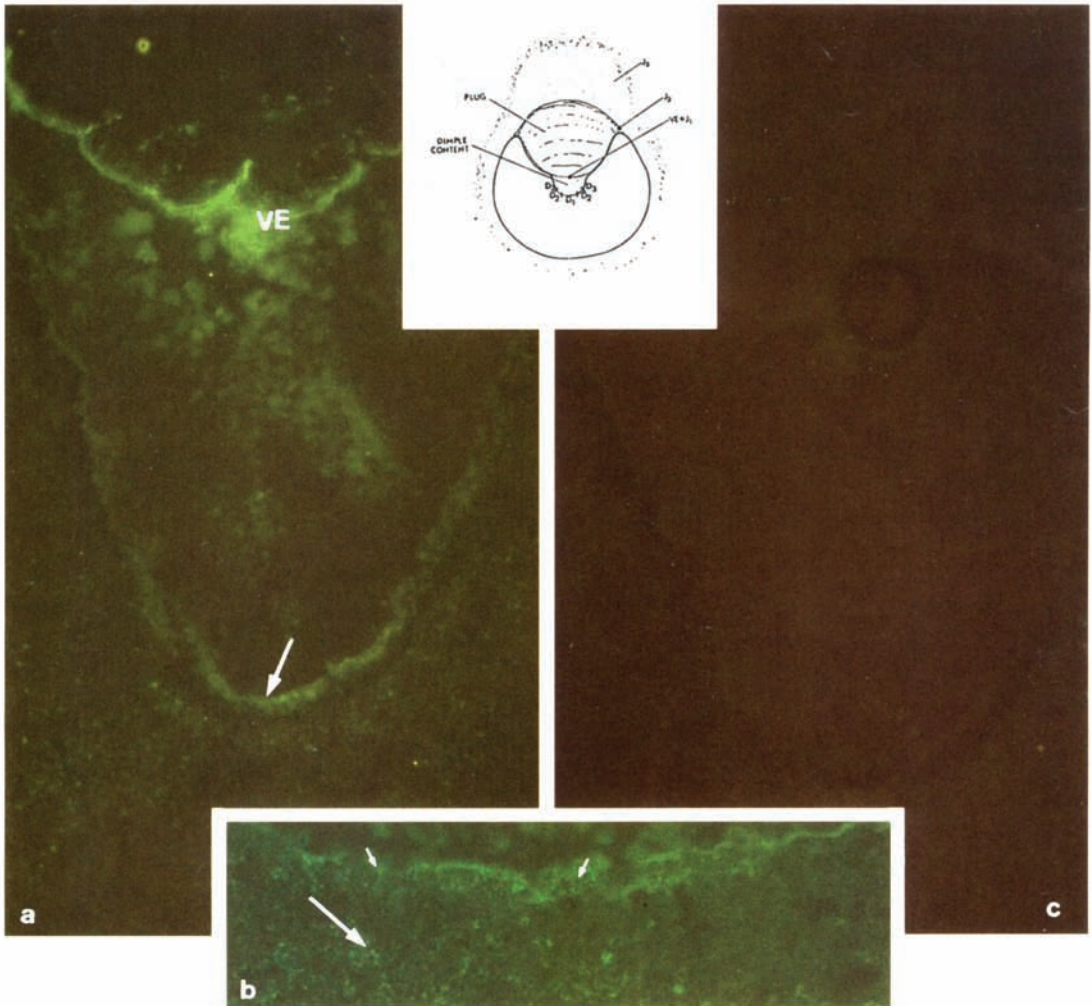


FIG. 4. Frozen section of the dimple incubated with either UEA-I FITC (a and b) or UEA-I FITC after preincubation with fucosyl-lactose (c). In a, the border of the dimple center is reactive (arrow). VE, vitelline envelope. $\times 310$. In b, underneath the reactive border, granules are present in cortical (small arrows) as well as in peripheral cytoplasm (arrow). $\times 500$. In c, there is no reactivity. $\times 310$. Inset, drawing of a longitudinal section throughout the egg, indicating the vitelline envelope, the dimple, the dimple content (DC), and the jelly coats, including the jelly plug.

of the beads had bound sperm (Fig. 8A). Figure 7e is an example of a sperm that, following treatment with Ca ionophore, sticks by its head to a 270/260-kDa bead.

Inhibition of Binding on 200- or 270/260-kDa Beads

The 200- and the 270/260-kDa bands eluted from SDS-polyacrylamide gels were also tested for their ability to

inhibit sperm binding to beads coated with the corresponding glycoproteins, under the conditions described under Materials and Methods and in the previous paragraph. Ringer and BSA were utilized as control media.

Figures 8B and 8C report the percentage of binding between 200- or 270/260-kDa beads and sperm in the presence of the corresponding glycoproteins. For the 200-kDa glycoprotein, the results show that the percentage of beads with sperm decreased with the increase of soluble

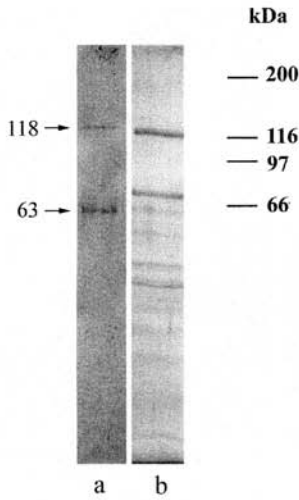


FIG. 5. SDS-PAGE and UEA-I blot of polypeptides released from *D. pictus* eggs following lysyendoproteinase C exposure. (a) UEA-I blot. (b) Corresponding silver-stained proteins. Two fragments of 118 and 63 kDa are shown, that react with UEA-I. Molecular mass standards are indicated.

glycoprotein concentration, indicating that sperm binding might be inhibited in a dose-dependent manner. Maximal sperm-bead binding in these experiments ($74 \pm 4\%$) was

not significantly affected by the 200-kDa glycoprotein up to $0.42 \mu\text{g/ml}$ (Fig. 8A). In contrast, the maximal value of sperm binding was not affected by soluble 270/260-kDa glycoproteins (Fig. 8B).

For the 270/260-kDa glycoproteins, the assays were conducted using A23187-treated sperm. The maximal value in these assays ($73 \pm 4\%$) was not affected until the glycoprotein concentration was $0.5 \mu\text{g/ml}$. A dose-dependent inhibition was observed at concentrations of soluble glycoproteins in the range of $0.5\text{--}1 \mu\text{g/ml}$ (Fig. 8C). Corresponding assays utilizing the 200-kDa soluble glycoprotein indicated that sperm binding to the beads was not significantly affected by this treatment (Fig. 8D).

In control experiments, soluble BSA had little effect on the percentages of binding between sperm and beads (Figs. 8B and 8C).

DISCUSSION

Biochemical approaches to the study of the egg surface are impaired either by the presence of extracellular coats that need to be removed by means of enzymatic agents (echinoderms) or by the large number of eggs necessary for protein purification (mammals). In the amphibian *D. pictus*, the extracellular investments of the numerous eggs can be easily removed manually without enzymatic agents. Therefore, this species gave us the opportunity of studying surface molecules by a simple protein labeling method.

The dimple center is the only site where fertilization occurs and calcium release into the cytosol is triggered as a consequence of either sperm penetration or IP₃ injection

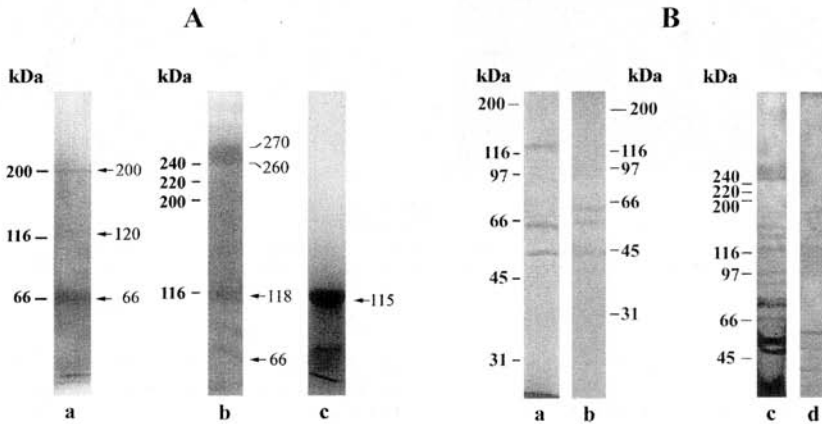
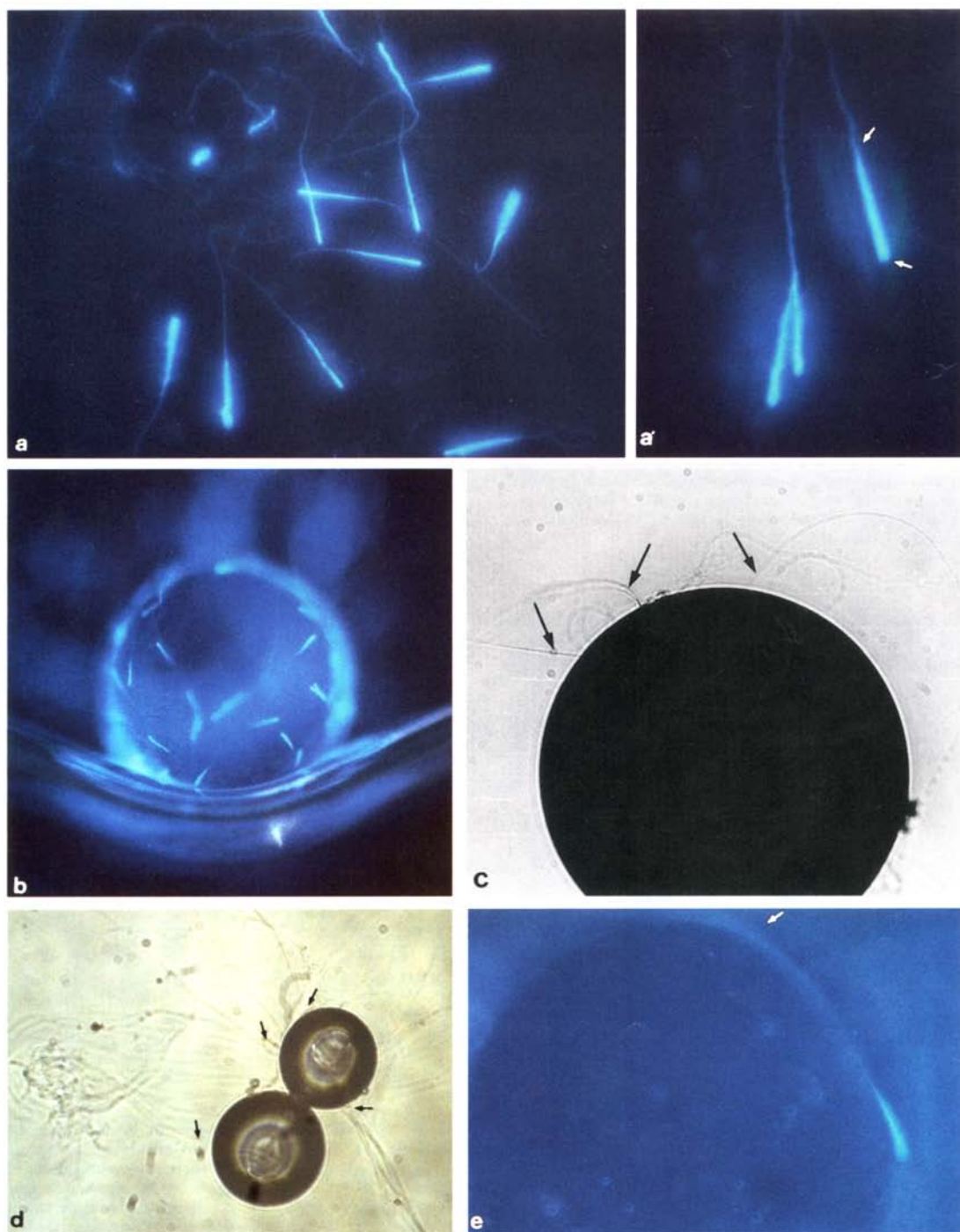


FIG. 6. (A) Electroeluted egg proteins utilized for adsorption to polystyrene beads. Aa, 200-kDa band (about $1 \mu\text{g}$); several bands of lower M_r are also present, including bands of 66 and 120 kDa; Ab, 270/260 kDa band ($1 \mu\text{g}$). The original band is indicated together with 118- and 66-kDa bands and lower M_r bands. Ac, lipovitellin (115 kDa). Reference molecular masses are indicated. (B) SDS-PAGE of polypeptides as recovered following exposure and adsorption to the beads; Ba and Bb, 10% acrylamide gels; Bc and Bd, 5–12% acrylamide gradients. Ba, unbound sample of electroeluted 200 kDa utilized for adsorption to the beads; Bb, corresponding bound sample, as recovered upon boiling of the beads. Bc, unbound sample of electroeluted 270/260 kDa utilized for adsorption to the beads; Bd, corresponding bound sample, as recovered upon boiling of the beads.



(Talevi *et al.*, 1985; Campanella *et al.*, 1988; Nuccitelli *et al.*, 1988; Talevi and Campanella, 1988). In fact, the endoplasmic reticulum reaches the critical concentration that permits the calcium elevation event to occur only in this site (Campanella *et al.*, 1988; Gualtieri *et al.*, 1992). A privileged localization of specific molecules in the dimple center is also supported by the finding that, in this site, the concentration and distribution of intramembrane particles is clearly different from that of the DLE (Gualtieri *et al.*, 1989). In this regard, Cl^- channels, which, in anurans, are calcium-activated and depolarize at fertilization, are located only in the dimple center (Nuccitelli *et al.*, 1988; Talevi *et al.*, 1992). Taken together, these data suggest consistently that, in *D. pictus* eggs, molecules might be present uniquely or at their highest concentration in the central part of the dimple.

Our results showed that the monodimensional electrophoretic patterns of dimple and DLE differ only in the relative concentration of proteins; however, at the dimple surface, at least four molecules (200, 230, 260, and 270 kDa) exist that are not found at the DLE surface. The 270/260- and 230-kDa bands were modified by mercaptoethanol in the sample buffer, suggesting that the molecules present in these bands might have disulfide bonds.

Ultrastructural (Gualtieri and Andreuccetti, 1996) and lectin fluorescence (this paper) studies indicate that UEA-I-binding sites are present in the dimple center. The affinity with UEA-I and LTA, a lectin that similarly binds α -L-fucose, is high in this site and drastically decreases toward the dimple walls (Denis-Donini and Campanella, 1977; Gualtieri and Andreuccetti, 1996). Therefore, in the present paper, the ability to bind UEA-I was considered as a marker for determining which molecule, among those located at the dimple plasma membrane surface, is highly concentrated in the domain of the dimple center. It was found that three (200, 260, and 270 kDa) of the four major molecules detected at the dimple surface, as well as peptide fragments obtained by lysylendoproteinase C treatment of intact eggs, did bind UEA-I. We suppose that the 200- and 270/260-kDa bands are the main glycoproteins responsible for reactivity to UEA-I, histologically localized at the center of the dimple surface.

Some discrepancy exists between affinity chromatography and lectin blot assays. According to affinity chromatography using UEA-I agarose, 200- and 270/260-kDa bands contained α -L-fucose. However, in lectin blots, the 270/260-kDa band readily bound UEA-I, whereas the 200-kDa band did not. The absence of reactivity of the 200-kDa band in

lectin blots was independent of the detergent utilized in the homogenization buffer. This finding, coupled with the observation that the 270/260-kDa band reacted with UEA-I in blotting experiments but bound rather mildly the agarose immobilized lectin, suggests that the 200- and 270/260-kDa bands might have reactive sites for UEA-I differently available or affected according to the method used. This point needs further investigation.

As mentioned, the UEA-I-binding glycoproteins were unexpectedly found both at the dimple surface and in the DLE cortex. The presence of such glycoproteins in the whole egg cortex might be explained by the UEA-I-binding granules and vesicles found in the peripheral cytoplasm of *D. pictus* eggs (Gualtieri and Andreuccetti, 1996; and this paper). Denis-Donini and Campanella (1977) reported that an active vesicle exocytosis reshapes the plasma membrane during dimple formation. As a consequence, fucosylated molecules settle at the center of the forming dimple. It can be hypothesized that surface glycoproteins might be segregated in vacuoles of the peripheral cytoplasm that merge with the oolemma only in the territory of the forming dimple. On the other hand, the 270-kDa band reacted with *G. nivalis* agglutinin, a lectin specific for nonreducing terminal mannose residues present in the high-mannose-type N-linked chains (Shibuya *et al.*, 1998), only in the dimple territory. This suggests that, when exposed at the surface, this band has a different glycosylation with respect to its cytoplasmic form. Interestingly, Ohlendieck *et al.* (1994) found that, in sea urchins, the 350-kDa glycoprotein, located at the egg surface, is also present in the cortical granules. Partin *et al.* (1996) showed that it is apparently similar, if not identical, in these two sites.

Several studies have indicated the presence of fucose, particularly in its sulfated form, in glycoconjugates involved in sperm-egg interaction, although it is not yet clear whether a specific role exists for this sugar (Bowell *et al.*, 1979; Stafford *et al.*, 1992, in *Fucus*; Focarelli and Rosati, 1995, in *Unio*; Segall and Lennarz, 1979; Glabe *et al.*, 1982; De Angelis and Glabe, 1987, 1988; Foltz and Lennarz, 1993; Dhume *et al.*, 1996, in sea urchins; Rosati and De Santis, 1978, 1980; De Santis *et al.*, 1983, in *Ciona*; Ruttenberg-Barnum and Brown, 1983, in *Limulus*; Ahuja, 1982; Dravland and Mortimer, 1988; Jones *et al.*, 1988; and O'Rand *et al.*, 1988, in mammals). However, these studies are mainly concerned with glycoproteins located in extracellular coats, with some exceptions, as *Fucus*, (Bowell *et al.*, 1979; Stafford *et al.*, 1992), having eggs without external investments, and hamster (Dravland and Mortimer, 1988). In the

FIG. 7. Sperm binding to 300- to 400- μ m large beads. [a, a'] *D. pictus* sperm DAPI-stained. In the a', the long and tapered head is shown, whose posteriormost and thickest portion (arrows) is not covered with the acrosome cap. Original magnification: a, $\times 250$; a', $\times 400$. [b, c] 200-kDa band coated beads. [b] DAPI-stained heads bound to the bead surface. $\times 100$. [c] Unstained sperm bound to the beads (small arrows). $\times 200$. [d, e] 270/260-kDa band coated beads. [d] Two beads bearing ionophore treated spermatozoa (small arrows). $\times 60$. [e] DAPI stained nuclei. The arrow indicates the tapered apical portion of the sperm nucleus (ionophore treatment) surrounding the bead. $\times 250$.

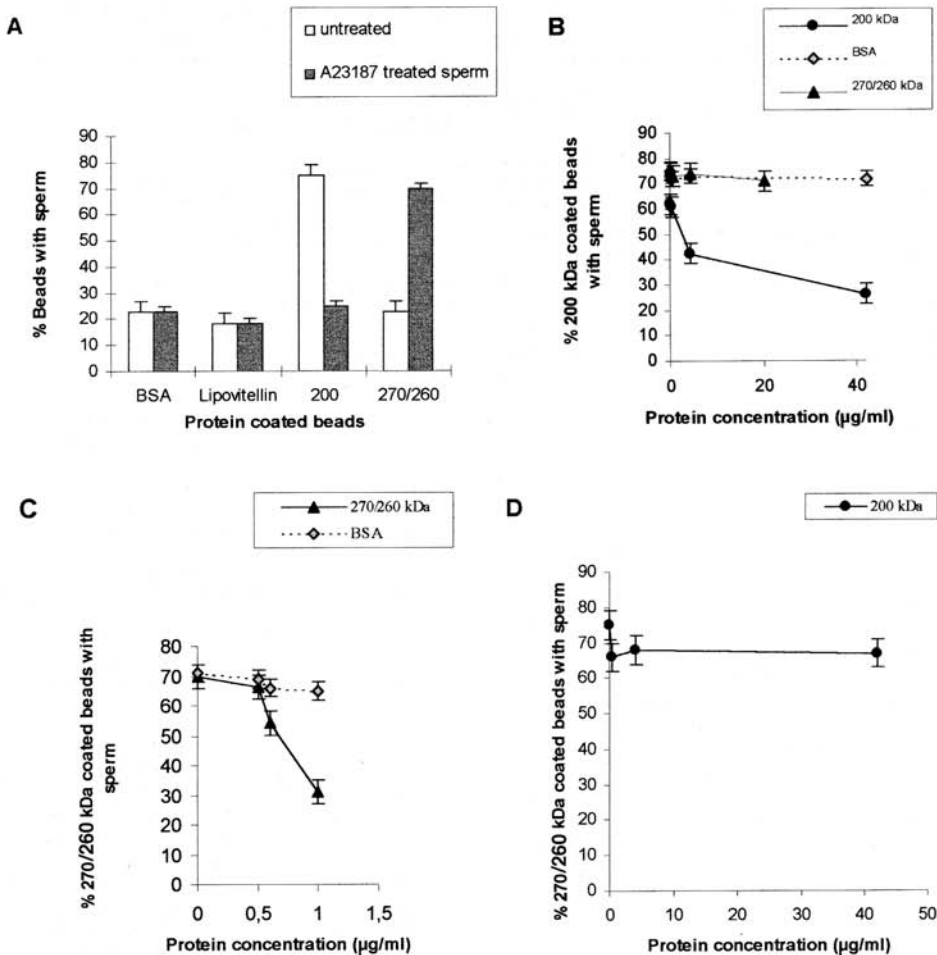


FIG. 8. [A] Quantification of the mean percentage of beads with sperm, as counted in sperm binding assay. A23187-exposed and unexposed sperm were utilized. Beads were coated with BSA, lipovitellin, or 200- or 270/260-kDa glycoproteins. Bars represent standard deviation with $n = 3$. [B, C, D] Dose-dependent inhibition of sperm binding to beads coated with 200-kDa (B) or 270/260-kDa (C) soluble glycoproteins and related controls. The BSA control protein had little effect on sperm binding to the beads. [B] Assay with soluble 200-kDa glycoprotein. Experiments utilizing soluble 270/260 glycoproteins do not affect sperm binding to the 200-kDa glycoproteins. [C] Assay with soluble 270/260 kDa glycoproteins. [D] Experiments utilizing soluble 200-kDa glycoprotein do not affect sperm binding to the 270/260-kDa beads. In B, C, and D bars indicate the standard deviation with $n = 5$.

present report, we detected surface glycoproteins that do not belong to the dimple content, as is shown by the SDS-PAGE pattern of this matrix. They are instead located in the glycocalyx and/or in the egg plasma membrane. The fucosylated fragments shed from the egg surface after lysoendoproteinase C digestion may constitute the extracellular portions of the detected molecules and may be instrumental for their future molecular characterization and

comparison. At present, whether a structural relationship exists between the 200- and the 270/260-kDa bands is not known. Our initial data indicate that the carbohydrate chain of the 270-kDa band is dissimilar to the chain of the 200-kDa one, at least in the dimple region.

The *in vitro* assays indicated that the 200- and the 270/260-kDa glycoproteins are able to bind sperm. Sperm binding to 200-kDa beads was accomplished before the

occurrence of the acrosome reaction, suggesting that spermatozoa bind the 200-kDa glycoprotein through the plasma membrane. By contrast, with the 270/260-kDa beads, spermatozoa bound after calcium ionophore treatment, i.e., following the acrosome reaction. Beads staining with DAPI revealed that sperm bind the beads by their head, thus rendering rather remote the hypothesis that binding might occur in sites where the acrosome is absent. In both cases, the solubilized glycoproteins competitively inhibited the binding between sperm and the corresponding 200- or 270/260-kDa beads in a dose-dependent manner. Inhibition did not occur if either solubilized glycoprotein was replaced by the other in these assays. We suggest that these molecules might have a sperm binding activity in the dimple center, the site where they are exposed at the surface of the egg. Two types of molecular interaction may occur between sperm and egg, one mediated by the 200-kDa glycoprotein and the other mediated by the 270/260-kDa glycoproteins. In its natural environment, the acrosome reaction is triggered when sperm come into contact with the jelly layer. In a few seconds, they become embedded in the thick jelly plug, which sits in a large concavity of the animal hemisphere, and converge into the dimple. Penetration of the egg investments takes about 15 s. When sperm arrive at the dimple surface, they are still at a very early stage of vesiculation (hybrid vesicles of plasma membrane and outer acrosome membrane), as documented by ultrastructural studies [Campanella *et al.*, 1997]. In *D. pictus* fertilization, the first contact is established between sperm plasma membrane in the process of vesiculation and the dimple glycocalyx. Subsequently, fusion occurs between the inner acrosome membrane and the oolemma deprived of the antennular glycocalyx (ultrastructural observations), when an imposing release of acrosome content is observed at the site of gamete interaction. This suggests that acrosomal enzymes may clear the glycocalyx away after binding has occurred, thus permitting a second interaction and fusion [Campanella *et al.*, 1997; and see De Santis *et al.*, 1992].

For mammalian spermatozoa, the presence of several prerequisites for the molecules involved in gamete binding and fusion is well known [Primakoff *et al.*, 1987; Blobel *et al.*, 1992; Myles, 1993; Yuan *et al.*, 1997]. For egg surface, it is not yet clear whether binding and the resulting fusion is a one-step or a multistep process, in which one or more molecules are involved (see also Ohlendieck and Lennarz, 1995; Schultz and Kopf, 1993; Parrington *et al.*, 1996).

At present, this is the first report on the identification and separation of molecules related to the oolemma binding *in vitro* homologous sperm. In this regard, it has been postulated that in *Xenopus*, integrin-like molecules might be able to trigger activation upon binding with disintegrin domains [Iwao and Fujimura, 1996; Shilling *et al.*, 1997], similarly to what has been suggested in mammals [Fusi *et al.*, 1992 and 1993; Tarone *et al.*, 1993; Almeida *et al.*, 1995]. It is noteworthy that the large integrin family includes such glycoproteins as IIb-IIIa that binds to ligands containing the RGD core sequence [Roussanti and Piersch-

bacher, 1987]. Molecular mapping and purification of *D. pictus* 200- and 270/260-kDa bands are under way and might clarify the role of these molecules in fertilization.

ACKNOWLEDGMENTS

We are indebted to Drs. E. Longobardi, R. Poulet, M. G. De Santo, M. Pirozzi, and G. Scarallo for participating in the experiments and to Mr. G. Falcone and Mr. S. Manzella for technical help. We thank Professors W. L. Lennarz, F. Rosati, R. De Santis, and M. Wilding for criticism and suggestions, and Dr. A. Cirillo for editing the manuscript. We are especially grateful to Professor J. L. Hedrick for suggestions and revision of the manuscript.

REFERENCES

- Ahuja, K. K. (1982). Fertilization studies in the hamster. The role of cell-surface carbohydrates. *Exp. Cell Res.* **140**, 353-362.
- Almeida, E. A. C., Huovila, J., Sutherland, A. E., Stephens, L. E., Calarco, P. G., Shaw, L. M., Mercurio, A. M., Sonnenberg, A., Primakoff, P., Myles, D. G., and White, J. M. (1995). Mouse egg integrin $\alpha 6 \beta 1$ functions as a sperm receptor. *Cell* **81**, 1095-1104.
- Barros, C., Crosby, J. A., and Moreno, R. D. (1996). Early steps of sperm-egg interaction during mammalian fertilization. *Cell Biol. Int.* **20**, 33-39.
- Blobel, C. P., Wolfsberg, T., Turck, C. W., Myles, D. G., Primakoff, P., and White, J. M. (1992). A potential fusion peptide and an integrin ligand domain in a protein active in sperm-egg fusion. *Nature* **356**, 248-252.
- Bowell, G. P., Callow, J. A., Callow, M. R., and Evans, L. V. (1979). Fertilization in brown algae. II. Evidence for lectin sensitive complementary receptors involved in gamete recognition in *Fucus serratus*. *J. Cell Sci.* **36**, 19-30.
- Busa, W. B., and Nuccitelli, R. (1985). An elevated free cytosolic Ca^{2+} wave follows fertilization in eggs of the frog *Xenopus laevis*. *J. Cell Biol.* **100**, 1325-1329.
- Campanella, C., Amore, F., Pitari, G., Fusco, C., Maurizi, and Duprè, S. (1992). Postfertilization changes in *Discoglossus pictus* (Anura) eggs result in the formation of a capsular chamber where the egg rotates. *Int. J. Dev. Biol.* **36**, 413-422.
- Campanella, C., Carotenuto, R., Infante, V., Maturi, G., and Atripaldi, U. (1997). Sperm-egg interaction in the painted frog *Discoglossus pictus*: An ultrastructural study. *Mol. Reprod. Dev.* **47**, 323-333.
- Campanella, C., and Gabbiani, G. (1979). Motile properties and localization of contractile proteins in the spermatozoon of *Discoglossus pictus*. *Gamete Res.* **2**, 163-175.
- Campanella, C., Talevi, R., Kline, D., and Nuccitelli, R. (1988). The cortical reaction in the egg of *Discoglossus pictus*: A study of the changes of endoplasmic reticulum at activation. *Dev. Biol.* **130**, 108-119.
- De Angelis, P. L., and Glabe, C. G. (1987). Polysaccharide structural features that are critical to the binding of sulfated fucans to bindin, the adhesive protein from sea urchin sperm. *J. Biol. Chem.* **262**, 13946-13952.
- De Angelis, P. L., and Glabe, C. G. (1988). Role of basic amino acids in the interaction of bindin with sulfated fucans. *Biochemistry* **27**, 8189-8195.
- Denis-Donini, S., and Campanella, C. (1977). Ultrastructural and lectin binding changes during the formation of animal dimple

- in oocytes of *Discoglossus pictus* (Anura). *Dev. Biol.* **61**, 140–152.
- De Santis, R., Pinto, M. R., Cotelli, R., Rosati, F., Monroy, A., and D'Alessio, G. (1983). A fucosyl glycoprotein component with sperm receptor and sperm-activating activities from the VE of *Ciona intestinalis* eggs. *Exp. Cell Res.* **148**, 508–513.
- De Santis, R., Shirakawa, H., Nakada, K., Miyazaki, S., Hoshi, M., Marino, R., and Pinto, M. R. (1992). Evidence that metalloendoproteases are involved in gamete fusion of *Ciona intestinalis*, *Ascidia*. *Dev. Biol.* **153**, 165–171.
- Dhume, S. T., Stears, R. L., and Lennarz, W. J. (1996). Sea urchin egg receptor for sperm: The oligosaccharide chains stabilize sperm binding. *Glycobiology* **6**, 59–64.
- Dravland, J. E., and Mortimer, D. (1988). Role for fucose-sulfareich carbohydrates in the penetration of zona-pellucida-free hamster eggs by hamster spermatozoa. *Gamete Res.* **21**, 353–358.
- Focarelli, R., and Rosati, F. (1995). The 220 kDa vitelline coat glycoprotein mediates sperm binding in the polarized egg of *Unio elongatulus* through O-linked oligosaccharides. *Dev. Biol.* **171**, 606–614.
- Foltz, K. R., and Lennarz, W. J. (1992). Identification of sea urchin egg receptor for sperm using an antiserum raised against a fragment of its extracellular domain. *J. Cell Biol.* **116**, 647–658.
- Foltz, K. R., and Lennarz, W. J. (1993). The molecular basis of sea urchin gamete interactions at the egg plasma membrane. *Dev. Biol.* **158**, 46–61.
- Foltz, K. R., Partin, J. S., and Lennarz, W. J. (1993). Molecular characterization of the sea urchin egg receptor for sperm. *Science* **259**, 1421–1425.
- Fusi, F., Vignali, M., Busacca, M., and Bronson, R. A. (1992). Evidence for the presence of an integrin cell adhesion receptor on the oolemma of unfertilized human oocytes. *Mol. Reprod. Dev.* **31**, 215–222.
- Fusi, F. M., Vignali, M., Gailit, J., and Bronson, R. A. (1993). Mammalian oocytes exhibit specific recognition of the RGD (Arg-Gly-Asp) tripeptide and express oolemmal integrins. *Mol. Reprod. Dev.* **36**, 212–219.
- Glabe, C. G., Gabel, L. R., Vacquier, V. D., and Rosen, S. D. (1982). Carbohydrate specificity of sea urchin sperm binding: A cell surface lectin mediating sperm-egg adhesion. *J. Cell Biol.* **94**, 123–128.
- Gualtieri, R., and Andreuccetti, P. (1996). Localization of egg-surface carbohydrates and fertilization in *Discoglossus pictus*. *Cell Tissue Res.* **283**, 173–181.
- Gualtieri, R., Cafiero, G., and Andreuccetti, P. (1989). Plasma membrane domains and the site of sperm entrance in *Discoglossus pictus* (Anura) eggs. *Dev. Growth Differ.* **31**, 485–491.
- Gualtieri, R., Campanella, C., and Andreuccetti, P. (1992). Cytochemical Ca^{2+} distribution in activated *Discoglossus pictus* eggs: A gradient in the pre-determined site of fertilization. *Dev. Growth Differ.* **34**, 127–135.
- Hedrick, J. L., and Nishihara, T. (1991). Structure and function of the extracellular matrix of anuran eggs. *J. Electron. Microsc. Tech.* **17**, 19–35.
- Infante, V., Maturi, G., Carotenuto, R., and Campanella, C. (1995). "Presenza di proteina biotinata specifica nel sito di fecondazione dell'uovo di *Discoglossus pictus* (Anfibio)." Atti Convegno Conjunto ABCD, AGI, SIBBM, SIMGBM. p. 14.
- Iwao, Y., and Fujimura, T. (1996). Activation of *Xenopus* eggs by RGD-containing peptides accompanied by intracellular Ca^{2+} release. *Dev. Biol.* **177**, 558–567.
- Jones, R., Brown, C. R., and Lancaster, R. T. (1988). Carbohydrate-binding properties of boar sperm proacrosin and assessment of its role in sperm-egg recognition and adhesion during fertilization. *Development* **102**, 781–792.
- Myles, G. D. (1993). Molecular mechanism of sperm-egg membrane binding and fusion in mammals. *Dev. Biol.* **158**, 35–45.
- Nuccitelli, R., Kline, D., Busa, W., Talevi, R., and Campanella, C. (1988). A highly localized intracellular calcium increase in the egg of the frog, *Discoglossus pictus*. *Dev. Biol.* **130**, 120–132.
- Ohlendieck, K., and Lennarz, W. Y. (1995). Role of the sea urchin egg receptor for sperm in gamete interactions. *Trends Biochem. Sci.* **20**, 29–33.
- Ohlendieck, K., Partin, J. S., Stears, R. L., and Lennarz, W. J. (1994). Developmental expression of the sea urchin egg receptor for sperm. *Dev. Biol.* **165**, 53–62.
- O'Rand, M. G., Widgren, E. E., and Fisher, S. J. (1988). Characterization of the rabbit sperm membrane autoantigen, RSA, as a lectin-like zona binding protein. *Dev. Biol.* **129**, 231–240.
- Parrington, J., Swann, K., Shevchenko, V. L., Sesay, A. K., and Lai, F. A. (1996). Calcium oscillations in mammalian eggs triggered by a soluble sperm protein. *Nature* **379**, 364–368.
- Partin, J. P., Ohlendieck, K., and Lennarz, W. L. (1996). Fate of the sea urchin egg receptor for sperm following fertilization. *Dev. Growth Differ.* **38**, 79–86.
- Pitari, G., Dupre', S., Fusco, C., Maurizi, G., and Campanella, C. (1993). Jelly plug dissolution in *Discoglossus pictus* eggs (Anura) involves peroxidase-like activity and oxidative opening of disulfide bonds. *Zigote* **1**, 61–69.
- Primakoff, P., Hyatt, H., and Tredick-Kline, J. (1987). Identification and purification of a sperm surface protein with a potential role in sperm-egg membrane fusion. *J. Cell Biol.* **104**, 141–149.
- Rosati, F. (1995). Sperm-egg interactions during fertilization in invertebrates. *Boll. Zool.* **62**, 323–334.
- Rosati, F., and De Santis, R. (1980). Role of the surface carbohydrates in sperm-egg interaction in *Ciona intestinalis*. *Nature* **283**, 762–764.
- Rosati, F., De Santis, R., and Monroy, A. (1978). Studies on fertilization. II. Lectin binding to the gametes of *Ciona intestinalis*. *Exp. Cell Res.* **132**, 289–295.
- Rouslanti, E., and Pierschbacher, M. D. (1987). New perspectives in cell adhesion: RGD and integrins. *Science* **238**, 491–497.
- Ruttenberg-Barnum, S., and Brown, G. (1983). Effects of lectins and sugar on primary sperm attachment in the horseshoe crab, *Limulus polyphemus* L. *Dev. Biol.* **95**, 352–359.
- SeGall, G. K., and Lennarz, W. J. (1979). Chemical characterization of the component of the jelly coat from sea urchin eggs responsible for induction of the acrosome reaction. *Dev. Biol.* **71**, 33–48.
- Shibuya, N., Goldstein, I. J., Van Damme, E. J. M., and Peumans, W. J. (1988). Binding properties of a mannose-specific lectin from the snowdrop (*Galanthus nivalis*) bulb. *J. Biol. Chem.* **263**, 728–734.
- Shilling, F., Kratzschmar, J., Cai, H., Weskamp, G., Gayko, U., Leibow, J., Myles, D. G., Nuccitelli, R., and Blobel, C. P. (1997). Identification of metalloprotease/disintegrins in *Xenopus laevis* testis with a potential role in fertilization. *Dev. Biol.* **186**, 155–164.
- Schultz, R. M., and Kopf, G. S. (1993). Molecular basis of mammalian egg activation. *Curr. Topics Dev. Biol.* **30**, 21–59.

Sperm Nuclei of *Discoglossus pictus* (Anuran Amphibian) Contain a Unique, Histidine-rich Basic Protein

Toru Itoh¹, Vincenzo Infante², Chiara Campanella² and Chiaki Katagiri^{1*†}

¹Division of Biological Sciences, Graduate School of Science, Hokkaido University, Sapporo 060, Japan and

²Dipartimento di Biologia Evolutiva e Comparata, Università di Napoli Federico II, Naples, Italy

ABSTRACT—Fractionation with reverse-phase HPLC and electrophoretic analyses revealed that the nuclear basic proteins in sperm of an anuran amphibian, *Discoglossus pictus*, consisted of weakly basic proteins without histones. Amino acid analyses indicated that none of these proteins were histones or protamines because of the low amounts of Lys and Arg. The predominant protein among those fractionated possessed an unusually high content of His and extremely low amounts of Arg and Lys, indicating that this is a unique nuclear basic protein not reported previously. The induction of a highly decondensed state of sperm nuclei upon their incubation in egg extract was accompanied by the removal of most, if not all, of this His-rich protein from the nuclei.

INTRODUCTION

In most animals, sperm chromatin is highly condensed by the interaction of DNA with strongly basic proteins that are different from somatic histones. Despite their broad similarity in function to stabilize the nuclear state of sperm, these basic proteins display a surprising diversity both in molecular weights and amino acid sequences, ranging from the highly specialized protamines, as typically found in mammals and fishes, to the sperm-specific histones found in many invertebrates (Poccia, 1986). This diversity is particularly well-illustrated among different genera of amphibians. In *Bufo japonicus*, for instance, sperm nuclear basic protein (SNBP) is comprised exclusively of protamines (Takamune *et al.*, 1991), while in *Xenopus laevis* 6 apparent SBNPs (SP1–6) that exhibit the properties intermediate between protamines and histones coexist with a set of core histones (Yokota *et al.*, 1991). The chromatin of *Rana catesbeiana* sperm, on the other hand, is unique in consisting of an irregularly spaced nucleosomal structure by possessing the special histone H1-variants in addition to a full set of core histones (Itoh *et al.*, 1997).

In our studies on sperm and egg interactions in *Discoglossus pictus*, we found that the SBNPs of this anuran amphibian are comprised of unique proteins that have not been recorded previously in any form of animal. We describe here their amino acid compositions and electrophoretic mobilities, as well as their possible function in maintaining the condensed state of sperm chromatin.

MATERIALS AND METHODS

Materials

Sexually mature painted frogs, *Discoglossus pictus* (hereafter referred to as *Discoglossus*), were captured in the neighborhood of Palermo, Italy. South African clawed frogs, *Xenopus laevis* (referred to as *Xenopus*), were obtained from a colony in our laboratory. Sexually mature toads, *Bufo japonicus* (referred to as *Bufo*), were purchased from commercial dealers in the Tokyo area.

Isolation of nuclei from sperm and somatic cells

Mature sperm were obtained from *Discoglossus* as described by Campanella and Gabbiani (1979) with a minor modification, as follows. Adult male frogs were injected in a dorsal lymphatic sac with 200 IU of human chorionic gonadotropin (HCG; Teikokuzoki, Co. Ltd., Japan) in De Boer's solution (DB; 110 mM of NaCl, 1.3 mM each of KCl and CaCl₂, pH 7.3 with NaHCO₃). Between 24–48 hr later, mature sperm were obtained, either by squeezing the abdomen or by pricking the seminal vesicles after opening the male abdomen, and were suspended in SMT buffer (250 mM sucrose, 2 mM MgCl₂, 10 mM Tris-HCl, pH 7.4). Sperm were obtained from *Bufo* and *Xenopus* by macerating testes in ice-cold DB. Mature sperm cells were isolated by ultracentrifugation in a 70% Percoll (Pharmacia LKB Biotechnology AB, Sweden) solution containing DB (36,000g, 60 min., 4°C) (*cf.*, Yoshizaki, 1987), and were then suspended in SMT buffer.

Mature sperm were demembrated with 0.05% lysolecithin (LC) for 10 min at room temperature as described by Lohka and Masui (1983), and the nuclei were stored at –70°C in SMT buffer at a concentration of 1×10⁷ nuclei/ml (*Discoglossus*) or 1×10⁸ nuclei/ml (*Xenopus* and *Bufo*).

Erythrocytes of *Discoglossus* were LC-permeabilized in the same way, and the isolated nuclei were suspended in SMT and stored at –70°C at a concentration of 1×10⁸ nuclei/ml.

Extraction of nuclear proteins and amino acid analysis

Nuclear proteins were extracted according to Mann *et al.* (1982). Proteins extracted with 0.4 N H₂SO₄ were precipitated with 20% trichloroacetic acid (TCA), washed in cold (–20°C) acetone, and then dried *in vacuo*.

The acid-extracted proteins dissolved in 25 mM Tris-HCl (pH 8.5)

* Corresponding author: Tel. +81-11-861-3388; FAX. +81-11-866-1126.

E-mail. katagiri@bio.sci.hokudai.ac.jp

† Present address: 3-2, 5-chome minami, Hondori, Shiroishi-ku, Sapporo 003-0026 Japan

were mixed with an equal volume of Q-Sepharose Fast Flow gels (Pharmacia). The unabsorbed proteins were collected as acetone powder, and were fractionated by reverse-phase high performance liquid chromatography (RP-HPLC) with a 150×4.6 mm Finepak SIL 300C₁₈-T-7 column (Japan Spectroscopic Co. Ltd., Japan) equilibrated with 0.05% trifluoroacetic acid (TFA). The proteins were eluted with a gradient of acetonitrile (0–50%) in 0.05% TFA at a flow rate of 1 ml/min. The purified proteins were dried *in vacuo*, hydrolyzed with 6 N HCl for 24 hr at 110°C, and subjected to amino acid analysis using a Hitachi-835 amino acid analyzer (Hitachi Co. Ltd., Japan).

Incubation of sperm nuclei in egg-extracts

The egg extract for the incubation of sperm nuclei was prepared as described by Ohsumi *et al.* (1988). Briefly, 10 ml of dejellied mature eggs from *Xenopus* were suspended in ice-cold extraction medium (EM; 100 mM KCl, 2 mM MgCl₂, 10 mM Tris-HCl, pH 7.4), decanted to remove as much of the EM as possible, and then centrifuged at 10,000g for 10 min (2°C). The semitransparent layer between the top (lipid) and the bottom (yolk and pigment granules) was collected, and served as the 'egg extract' (EE). Twenty μl of LC-permeabilized sperm nuclear suspension (2×10⁸ nuclei) was mixed with 200 μl of EE, and incubated at room temperature with frequent vortexing. After the incubation, the nuclei were collected by centrifugation and the proteins were extracted for electrophoretic analyses.

Electrophoresis

Acid/urea/Triton X-100 polyacrylamide gel electrophoresis (AUT-PAGE) was carried out according to Zweidler (1978), using 12% polyacrylamide gels containing 2.5 M urea, 6 mM Triton X-100, and 5% acetic acid. The acetone-dried samples were dissolved in 10 M urea solution. Sodium dodecyl sulfate polyacrylamide gel electrophoresis (SDS-PAGE) was carried out according to Laemmli (1970), using 15% resolving gels and 4.5% stacking gels. The samples were dissolved in SDS-sample buffer (10 mM Tris-HCl, pH 6.8, 1% SDS, 1% 2-mercaptoethanol, 20% glycerol). For two-dimensional analysis, AUT-PAGE was carried out in rectangular tubes (1×2×70 mm), followed by equilibration gels with SDS-sample buffer, and the materials were separated by SDS-PAGE. Gels were stained with 0.05% Coomassie brilliant blue R250.

RESULTS AND DISCUSSION

Fig. 1 shows the AUT-PAGE profiles of nuclear basic proteins from sperm and erythrocytes of *Discoglossus*, in comparison with those from sperm of *Xenopus* and *Bufo*. *Discoglossus* sperm did not possess the core histones that are commonly found in nuclei of somatic cells and sperm of *Xenopus*, but exhibited bands whose mobilities were different from either the sperm-specific proteins (SP1-6) of *Xenopus* or the protamines of *Bufo*. Two dimensional PAGE analyses using AUT- and SDS systems (Fig. 2) also clearly revealed that *Discoglossus* sperm nuclei do not possess either core histones or the H1-type histones found in *Rana catesbeiana* sperm (*cf.*, Itoh *et al.*, 1997). Thus, the nuclear basic proteins of *Discoglossus* sperm appeared unique in that they exhibited electrophoretic mobilities different from those of any sperm nuclear basic proteins recorded previously.

The basic proteins from sperm nuclei and from erythrocyte nuclei of *Discoglossus* were fractionated by reverse-phase HPLC for comparison. All seven fractions obtained from sperm nuclei (designated A–G in Fig. 3) exhibited elution and SDS-PAGE profiles which were distinct from those of the fractions

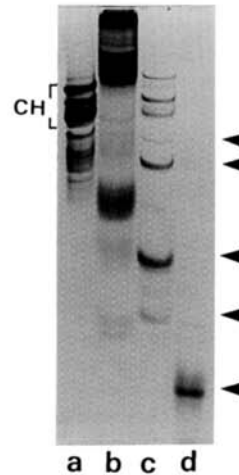


Fig. 1. AUT-PAGE analysis of basic proteins from the nuclei of erythrocytes (a) and sperm (b) of *Discoglossus* in comparison to those from the nuclei of sperm of *Xenopus* (c) and *Bufo* (d). Proteins extracted from 1×10⁶ (a, c and d) or 1×10⁵ (b) nuclei were applied to each lane. Direction of electrophoresis was from top (+) to bottom (-). CH, core histones; Arrow heads, sperm-specific proteins of *Xenopus* and *Bufo*.

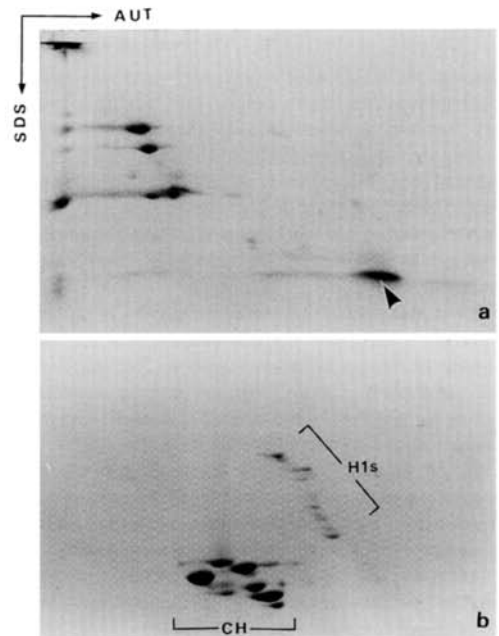


Fig. 2. Two dimensional electrophoresis of acid extracts of the nuclei from sperm (a) in comparison to those of erythrocytes (b) of *Discoglossus*. Proteins were separated by AUT-PAGE in the horizontal direction from left to right, followed by SDS-PAGE in the vertical direction from top to bottom. Arrowhead in a, histidine-rich protein. CH and H1s in b refer to core- and H1 histones, respectively.

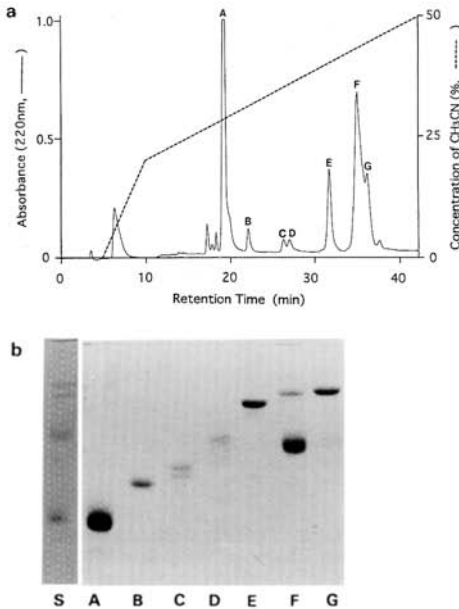


Fig. 3. a: Reverse-phase HPLC profiles of nuclear basic proteins from the nuclei of sperm of *Discoglossus*. Acid extracts of proteins unadsorbed to Q-Sepharose under the conditions given in MATERIALS AND METHODS were loaded on a Finepak SIL 300C₁₈ T-7 column, and elution was carried out by 10–50% acetonitrile linear gradient in 0.05% trifluoroacetic acid for 50 min, at a flow rate of 1.0 ml/min. b: SDS-PAGE analysis of SNBPs (S) and protein fractions A–G shown in a.

obtained from somatic cell nuclei (data not shown). The fractions eluted faster than the fraction A (Fig. 3a) possibly represented fast-moving minor bands in AUT-PAGE profile shown in Fig. 1 (lane b), but these fractions were not processed for further analysis.

In Table 1 are compared the amino acid compositions of fractions A–G shown in Fig. 3 with those of sperm nuclear proteins from other anuran species reported previously (Yokota *et al.*, 1991; Takamune *et al.*, 1991; Itoh *et al.*, 1997). It is clear that none of the proteins from *Discoglossus* sperm were similar in amino acid compositions to those from sperm nuclei from other amphibian species so far reported (cited in Table 1). We could not determine whether the minor fractions (B–G) represented distinct molecular entities or fragments derived from the major fraction A. In any event, all of the minor proteins were of weaker basicity (*i.e.*, they contained a lower amount of total basic amino acids than do somatic histones), and were composed of relatively smaller amounts of Lys than are histones (*cf.*, Itoh *et al.*, 1997). Unlike the sperm from *Bufo* or *Xenopus* which possessed Arg-rich, more typically sperm-specific nuclear basic proteins (Takamune *et al.*, 1991; Yokota *et al.*, 1991), the sperm proteins from *Discoglossus* contained extremely small amounts of Arg. Above all, the predominating basic protein in *Discoglossus* sperm (fraction A, Table 1) was characterized by an unusually high content of His, which is apparently the major contributor to the observed basicity of this protein.

In an attempt to elucidate the role of these unique basic proteins in the condensed state of the sperm chromatin, sperm nuclei were incubated in egg extract from *Xenopus*. The

Table 1. Amino acid composition of fractions A–G (*cf.*, Fig. 3) isolated from the sperm of *Discoglossus pictus*, in comparison with sperm nuclear basic proteins from other anuran amphibians. The numbers indicate the molar percentages of amino acids, calculated from the average of three independent determinations.

| Amino acid | Fraction | | | | | | | <i>Rana</i> ¹ | <i>Bufo</i> ² | <i>Xenopus</i> ³ |
|-------------------|----------|------|------|------|------|------|------|--------------------------|--------------------------|-----------------------------|
| | A | B | C | D | E | F | G | | | |
| Asx | 2.4 | 4.8 | 8.6 | 7.8 | 9.6 | 12.7 | 9.7 | 3.4 | 2.7 | 5.2 |
| Thr | 11.3 | 8.7 | 3.8 | 3.9 | 5.4 | 6.5 | 3.9 | 4.5 | 6.9 | 11.5 |
| Ser | 8.8 | 10.6 | 10.1 | 8.4 | 6.3 | 7.2 | 7.5 | 8.4 | 6.0 | 14.1 |
| Glx | 6.1 | 9.1 | 14.4 | 11.7 | 12.3 | 10.8 | 14.0 | 3.1 | 3.9 | 2.6 |
| Gly | 1.5 | 4.4 | 8.8 | 10.5 | 5.6 | 6.6 | 10.2 | 6.7 | 0.9 | 6.4 |
| Ala | 8.1 | 7.1 | 5.9 | 7.0 | 8.9 | 7.3 | 7.9 | 19.8 | 4.7 | 11.5 |
| Cys | 3.5 | 2.2 | 0.5 | 1.4 | 1.7 | 3.4 | 1.6 | 0 | 0 | 0 |
| Val | 10.9 | 7.9 | 5.8 | 4.8 | 6.8 | 5.3 | 5.9 | 6.0 | 5.1 | 1.3 |
| Met | 1.1 | 0.1 | 1.9 | 2.5 | 1.7 | 1.2 | 0.7 | 0 | 0 | 3.9 |
| Ile | 5.9 | 1.2 | 2.7 | 5.3 | 4.1 | 4.1 | 3.9 | 1.6 | 0 | 0 |
| Leu | 3.7 | 7.2 | 8.8 | 6.8 | 5.3 | 5.9 | 6.1 | 4.0 | 0 | 1.3 |
| Tyr | 2.6 | 2.2 | 1.9 | 1.6 | 4.1 | 6.6 | 3.6 | 0.8 | 2.6 | 2.6 |
| Phe | 0.2 | 0.2 | 1.0 | 1.1 | 3.4 | 4.8 | 3.6 | 0 | 0 | 0 |
| Lys | 2.5 | 15.0 | 7.7 | 8.8 | 8.9 | 7.0 | 5.7 | 29.6 | 5.2 | 1.3 |
| His | 20.8 | 4.4 | 6.3 | 5.6 | 1.8 | 2.4 | 1.3 | 0.7 | 9.7 | 1.3 |
| Arg | 0.6 | 0.5 | 5.9 | 6.1 | 5.8 | 3.8 | 4.1 | 1.5 | 42.3 | 35.9 |
| Pro | 9.9 | 14.2 | 5.7 | 6.8 | 28.3 | 4.7 | 10.5 | 10.1 | 10.0 | 1.3 |
| Basic amino acids | 23.9 | 19.9 | 19.9 | 20.5 | 16.5 | 13.2 | 11.1 | 31.8 | 57.2 | 38.5 |
| Lys/Arg ratio | 4.2 | 30.0 | 1.3 | 1.4 | 1.5 | 1.8 | 1.4 | 19.7 | 0.1 | 0.1> |

¹ Sperm-specific H1 variant in *Rana catesbeiana*, cited from Itoh *et al.* (1997).

² Protamine in *Bufo japonicus*, cited from Takamune *et al.* (1991).

³ Sperm-specific protein SP4 in *Xenopus laevis*, cited from Yokota *et al.* (1991).

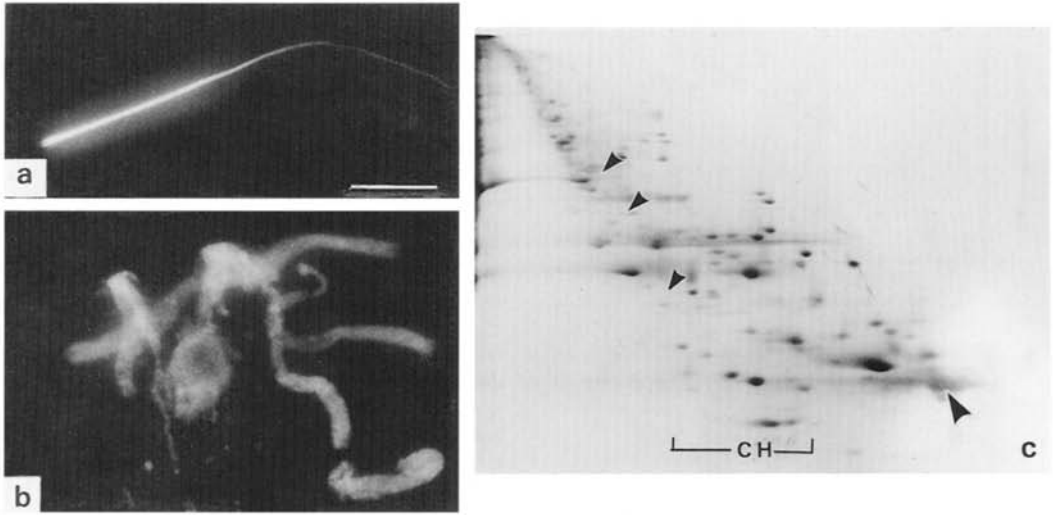


Fig. 4. **a** and **b**, Hoechst-stained sperm nuclei of *Discoglossus* at 0 (**a**) and 60 (**b**) min following incubation with *Xenopus* egg extract, showing prominent decondensation in **b**. bar, 10 μ m; **c**, Two dimensional-PAGE of acid extracts from the nuclei of *Discoglossus* sperm which were incubated with *Xenopus* egg extract, showing a total or partial loss of sperm-specific proteins and accumulation of core histones (CH). Large and small arrowheads indicate the positions of Histidine-rich and other minor sperm proteins, respectively. Electrophoresis conditions same with those given in Fig. 2.

nuclei of *Discoglossus* sperm decondensed well during 60 min of incubation (Fig. 4a, b), as did those of homologous *Xenopus* sperm. Two dimensional PAGE analyses of sperm nuclei after incubation in the egg extracts (Fig. 4c) revealed that Hist-rich protein was reduced but a certain amount remained unremoved, concomitant with a total loss of other minor SNBPs. This loss and/or reduction of the *Discoglossus* sperm proteins was accompanied by the partial acquisition of histones from the egg extracts (Fig. 4c). We also induced the decondensation of *Discoglossus* sperm nuclei without complete loss of Hist-rich protein after incubation in a high concentration of *Xenopus* nucleoplasm (data not shown), a result that is reminiscent of the partial removal of sperm-specific H1-type proteins from *Rana catesbeiana* (*cf.*, Itoh *et al.*, 1997).

Thus, our results demonstrate the existence of a unique type of sperm nuclear basic protein which has not been reported in any form of animal (*cf.*, Kasinsky, 1989). Further studies are needed to clarify both the primary structure of this Hist-rich protein, and how it contributes to the condensation of chromatin in this unusually giant sperm (*cf.*, Campanella and Gabbiani (1979).

ACKNOWLEDGEMENTS

This study was supported in part by The Japan Society for Promotion of Science.

REFERENCES

Campanella C, Gabbiani G (1979) Motile properties and localization of contractile proteins in the spermatozoon of *Discoglossus pictus*.

- Gamete Res 2: 163–175
- Itoh T, Ausio J, Katagiri Ch (1997) Histone H1 variants as sperm-specific nuclear proteins of *Rana catesbeiana*, and their role in maintaining a unique condensed state of sperm chromatin. *Mol Reprod Develop* 47: 181–190
- Kasinsky HE (1989) Specificity and distribution of sperm basic proteins. In "Histones and Other Basic Nuclear Proteins" Ed by LS Helinica, GS Stein, JL Stein, CRC Press Inc, Florida, pp 73–163
- Laemmli UK (1970) Cleavage of structural proteins during the assembly of the head of bacteriophage T4. *Nature* 227: 680–685
- Lohka MJ, Masui Y (1983) Formation *in vitro* of sperm pronuclei and mitotic chromosomes induced by amphibian ooplasmic components. *Science* 20: 719–721
- Mann M, Risley MS, Eckhardt RA, Kasinsky HE (1982) Characterization of spermatid/sperm basic chromosomal proteins in the genus *Xenopus* (anura, pipidae). *J Exp Zool* 222: 173–186
- Ohsumi K, Katagiri Ch, Yanagimachi R (1988) Human sperm nuclei can transform into condensed chromosomes in *Xenopus* egg extracts. *Gamete Res* 20: 1–9
- Poccia D (1986) Remodeling of nucleoproteins during gametogenesis, fertilization, and early development. *Int Rev Cytol* 105: 1–65
- Takamune K, Nishida H, Takai M, Katagiri Ch (1991) Primary structure of toad sperm protamines and nucleotide sequence of their cDNAs. *Eur J Biochem* 196: 401–406
- Yokota T, Takamune K, Katagiri Ch (1991) Nuclear basic proteins of *Xenopus laevis* sperm: Their characterization and synthesis during spermatogenesis. *Develop Growth Differ* 333: 9–17
- Yoshizaki N (1987) Isolation of spermatozoa, their ultrastructure, and their fertilizing capacity in two frogs, *Rana japonica* and *Xenopus laevis*. *Zool Sci* 4: 193–196
- Zweidler A (1978) Resolution of histones by polyacrylamide gel electrophoresis in presence of nonionic detergents. *Methods Cell Biol* 17: 223–233

(Received April 30, 1999 / Accepted June 5, 1999)

Enzyme activity in anuran spermatozoa upon induction of the acrosome reaction

V. Infante¹, R. Amirante¹, M.C. Vaccaro¹, M. Wilding² and C. Campanella¹

University of Naples 'Federico II' and Centre for Reproductive Biology, Naples, Italy

Date submitted: 2.3.01. Date accepted: 14.5.01

Summary

At the time of sperm–egg fusion in *Discoglossus pictus*, a large amount of electron-dense material of an unknown nature is liberated from the sperm. In the present work we studied this material in *D. pictus* sperm, using an assay utilising strips of autoradiographic film as a gelatin substrate for proteolytic enzymes. Upon treatment with A23187, *D. pictus* sperm produced a large halo on the gelatin substrate, indicating the presence of enzymes released by the sperm at the time of the acrosome reaction. In contrast, *Xenopus laevis* sperm did not produce halos upon treatment with A23187. The use of protease inhibitors such as TLCK, leupeptin, chymostatin, SBTI and EACA strongly suggests that the *D. pictus* whole acrosome contains trypsin and chymotrypsin activity while an SBTI-sensitive activity is absent in a small portion of the acrosome, possibly the anteriormost region. Furthermore, the material released at the acrosome reaction also contains an EACA-inhibited activity, indicating the presence of plasminogen activator. We conclude that *D. pictus* sperm release proteolytic enzyme(s) that may act at the egg surface at the time of gamete fusion.

Keywords: Anurans, Fertilisation, Protease inhibitors, Proteolytic enzymes, Sperm acrosomes

Introduction

Several experimental approaches have shown that amphibian sperm contains enzymes with proteolytic activity (Raissman & Barbieri, 1969; Elinson, 1974; Raissman & Cabada, 1977; Iwao *et al.*, 1994; Mizoke *et al.*, 1999), similar to mammalian sperm (for a review see Barros *et al.*, 1996). The vitelline envelope (VE) lysin of the toad *Bufo bufo japonicus* is a trypsin-like protease (Yoshizaki & Katagiri, 1982; Yamasaki *et al.*, 1988). In this toad, as well as in *Bufo arenarum*, the VE lysin is able to digest the VE of uterine eggs and appear to be implicated in fertilisation, according to inhibition assays utilising protease inhibitors (Cabada *et al.*, 1978;

Takamune *et al.*, 1986). Sperm extracts of the urodele *Cynops pyrrhogaster* and the anuran *Xenopus* have a similar proteolytic activity (Iwao *et al.*, 1994, 1995; Mizote *et al.*, 1999). *Cynops* sperm enzyme was putrified as a 100 and a 65 kDa protein with tryptic as well as chymotryptic properties and the ability to activate both *Cynops* and *Xenopus* eggs. Also *Bufo arenarum* sperm lysin is able to activate the corresponding egg (Cabada *et al.*, 1989). Therefore sperm-released enzymes appear to have a role both in the digestion of egg investments and in the process of sperm–egg fusion. However, in particular in the case of *Xenopus*, it is obscure how sperm interact with the VE and the egg plasma membrane, and sperm extracts are unable to activate either heterologous or homologous eggs (Mizote *et al.*, 1999). In this species, a receptor–ligand system is thought to be active at the time of fusion between egg and sperm, involving disintegrin at the sperm plasma membrane and integrins at the oolemma (Iwao & Fujimura, 1996; Shilling *et al.*, 1997, 1998), as for mammals (Blobel *et al.*, 1992; Almeida *et al.*, 1995; Chen & Sampson, 1999).

Sperm enzyme activity is thought to reside in the acrosome, both because of indirect evidence (for

All correspondence to: Prof. Chiara Campanella, Dipartimento di Biologia Evolutiva e Comparata, Università di Napoli Federico II, Via Mezzocannone 8, 80134 Naples, Italy. Tel: +39 081 2528921. Fax: +39 081 2528902. e-mail: Campanella@dgbm.unina.it

¹Dipartimento di Biologia Evolutiva e Comparata, Università di Napoli, via Mezzocannone 8, 80134 Naples, Italy.

²Centre for Reproductive Biology, Clinica Villa del Sole, via Manzoni 15, 80126 Naples, Italy.

Cynops: Iwao *et al.*, 1994; for *Rana*: Penn & Gledhill, 1972) and because in other sperm, such as mammalian sperm, a tryptic protease, acrosin, is associated with the acrosome matrix (Hardy *et al.*, 1991).

In *Discoglossus pictus* fertilisation, ultrastructural observations indicated that a large amount of electron-dense material is liberated from sperm in the process of penetrating into the egg (Campanella *et al.*, 1997). It was hypothesised that enzymes released from the sperm acrosome are able to digest the egg glycocalyx and to uncover the sperm receptor in the egg plasma membrane (Maturi *et al.*, 1998). However, nothing is known about the enzymic nature of the material released from sperm as a consequence of the acrosome reaction (AR) in this species except for an early report that suggests the presence of an enzyme 'similar to pancreas enzymes' in the acrosome (Parat, 1933), and indirect evidence (Campanella *et al.*, 1997).

Discoglossus pictus sperm are 2.33 mm long, the head itself being about 900 µm long. Its anteriormost portion is constituted by the apical rod, a short specialisation of the acrosome, and posteriorly covered by the acrosome cap. The acrosome contains at least two ultrastructurally distinguishable constituents. The nucleus is located behind the apical rod; the acrosome cap covers it throughout its surface except its posterior edge. The acrosome cap is very thin at the sperm anteriormost region (0.02 µm) covering a 0.2 µm thick nucleus, while posteriorly, where the nucleus is about 1 µm thick, it doubles its size (Campanella *et al.*, 1979). Sperm are associated in register, entwined in bundles of 20 or more. When in contact with the egg jelly, sperm are freed from the bundles and enter the jelly coat, where the AR is triggered (Campanella & Gabbiana, 1979; Campanella *et al.*, 1997).

In this work we studied the material released upon induction of the acrosome reaction in *D. pictus* sperm, using an assay first developed in *Rana pipiens* sperm (Penn & Gledhill, 1972) whose acrosomal granule is quite inconspicuous (Poirer & Spink, 1971; Campanella, unpublished data). The assay is sensitive to small amounts of enzymes released by single sperm (Penn & Gledhill, 1972). Furthermore it allows the examination of a direct relationship between release of acrosome content and digestion of a substrate (see also Iwao *et al.*, 1994). The assay was also applied to *X. laevis* sperm.

Materials and methods

Adult *D. pictus* males were injected into the dorsal lymphatic sac with 200–250 IU of Profasi HP (Serono, Italy) diluted in amphibian Ringer's solution 100% (111 mM NaCl, 1.3 mM CaCl₂, 2 mM KCl, 0.8 mM Mg₂SO₄, in 25 mM HEPES-NaOH pH 7.4). Sperm bundles were

obtained by squeezing the animals 24–48 h after hormone injection. Adult *X. laevis* males (Rettilli, Varese, Italy) were decapitated under anaesthesia. Their testes were rinsed in 100% De Boer's solution (110 mM NaCl, 1.3 mM CaCl₂, 1.3 mM KCl, 5.3 mM tris-HCl pH 7.4) and minced in small pieces in 10% De Boer's solution to obtain motile sperm. Strips of autoradiographic film were used as gelatin substrate for proteolytic enzymes, according to Penn & Gledhill (1972). Briefly, the experimental procedure involved a 10 min exposure of Kodak A-25 autoradiographic films to light, followed by a 4 min treatment with Kodak D-19 developer and a 2 min fixation in sodium hyposulphite (1.98 M) and sodium bisulphite (1.64 M). Small strips of exposed film were then spread, emulsion side up, onto microscope slides.

For *D. pictus*, as it was previously shown that, in diluted saline release of sperm from their bundle is activated, drops of semen were added to 10% Ringer (for more details see Campanella *et al.*, 1997). Sperm suspensions were gently brushed onto the strips and then 50 µM calcium ionophore A23187 added (final concentration 25 µM) to trigger the AR (Gualtieri & Andreuccetti, 1996). The whole slide was covered with a coverslip, kept in a moisture chamber at 37 °C and viewed at regular intervals in a compound microscope.

Enzyme inhibitors were mixed with sperm suspension together with A23187 to obtain the following concentrations: 1 mM *N*-tosyl-lys-chloromethyl-ketone hydrochloride (TLCK; inhibitor of serine proteases), 1 mM leupeptin (inhibitor of trypsin-like and cystine proteases), 1 mM chymostatin (inhibitor of chymotrypsin-like serine proteases), 1 mg/ml soybean trypsin inhibitor (SBTI; inhibitor of trypsin, chymotrypsin, kallikrein and plasmin), 1 mM ϵ -amino-*n*-caproic acid (EACA; inhibitor of carboxypeptidase B and of the activator of plasminogen) and 1 mM E64 (inhibitor of cysteine proteases) (Sigma Biochemical, St Louis, MO). Table 1 summarises the enzyme inhibitors utilized and their inhibitory activities.

The inhibitory concentrations were calibrated by exposing film strips to increasing concentrations of commercial enzymes (i.e. trypsin, Sigma) and by adding to the enzyme the corresponding inhibitors (i.e. TLCK or SBTI). Neither the Ringer nor calcium ionophore produce alteration of the gelatin substrate of the Kodak autoradiographic film.

Results

To test the effect of the acrosome reaction on the gelatin-coated strips, *D. pictus* sperm were exposed to 25 µM calcium ionophore A23187. Upon incubation for 10 min at 37 °C, a large halo was observed on the strip where sperm were located (Fig. 1a), indicating diges-

Table 1 The inhibitors used and their inhibitory action

| Inhibitor | Inhibitory action |
|--|--|
| TLCK | Irreversible inhibitor of serine-trypsin proteases. Also inhibits bromelain, endoproteinase Arg-C, endoproteinase Lys-C, papain, plasmin, thrombin and trypsin |
| Leupeptin | Reversible inhibitor of serine-trypsin proteases. Inhibits some cysteine-like proteases including endoproteinase Lys-C, kallikrein, papain, thrombin and cathepsin B |
| SBTI | Reversible inhibitor of serine-proteases. Also inhibits trypsin and factor X |
| Chymostatin | Reversible inhibitor of chymotrypsin-like serine proteases including α -, β -, γ -, δ -chymotrypsin |
| E64 | Irreversible inhibitor of cysteine-proteases |
| ϵ -amino- <i>n</i> -caproic acid (EACA) | Inhibitor of carboxypeptidase B. Inhibitor of the activator of plasminogen |

tion and degradation of the gelatin substrate. By utilising a small aliquot of spermatozoa, we observed that the extension of the halo produced on the gelatin strip is not as long as the sperm (about 200 μ m in contrast to the 2.33 mm of the whole sperm length), indicating that the release of the enzyme occurs in a discrete region of sperm, such as the region where the acrosome is more conspicuous (Fig. 2b). For untreated sperm, similarly incubated on strips, halos were absent (Fig. 1b). On the contrary, *X. laevis* sperm, whether treated with A23187 or not, did not undergo the formation of a halo, even after several hours of incubation.

In experiments utilising enzyme inhibitors, incubation of sperm with TLCK or leupeptin on the gelatin-coated strips resulted in major inhibition of halo formation after AR induction (Fig. 2c, d; and compare with Fig. 2b). In contrast, incubation with SBTI caused partial inhibition of halo formation, as several circular spots of gelatin digestion were observed next to the reacted sperm (Fig. 2f). These data suggest that a partial inhibition of sperm AR enzymes occurs with SBTI and that a discrete segment of sperm is insensitive to this inhibitor.

While the thiol-protease inhibitor E64 is not able to inhibit sperm enzyme action on gelatin (Fig. 2h), chymostatin has a good inhibitory activity (Fig. 2e). Similarly, by using EACA, an inhibitor of plasminogen activator (Huarte *et al.*, 1993), the gelatin was affected by the sperm-released enzymes except in tiny regions visible within or around spermatozoa (Fig. 2g).

Discussion

Our data indicate that substances released by *D. pictus* sperm upon the induction of the AR are enzymes, as they are able to digest a gelatin matrix and enzyme inhibitors impair this ability. Given that TLCK, leupeptin, SBTI and chymostatin are capable of inhibiting halo formation of the gelatin matrix, it can be concluded that the enzymes have tryptic and chymotryptic activity. This is in agreement with data on *Bufo bufo japonicus* (Yamasaki *et al.*, 1988), *Bufo arenarum* (Raissman & Cabada, 1977), *Cynops* and *Xenopus* (Mizote *et al.*, 1999) showing that a serine protease with tryptic activity is present in sperm extracts. Moreover, the chymotryptic activity we found in *D. pictus* sperm can be compared with a similar activity found in *Cynops* sperm (Mizote *et al.*, 1999). *D. pictus* shares several properties with urodele species (Campanella *et al.*, 1991). Although the experimental approach we used allowed the observation of sperm at a low resolution, the morphology of the halo developed by sperm and the location along the sperm strongly suggest that the enzymes are located in the acrosome cap. By comparing the halos produced upon exposure to SBTI with the complete inhibitory activity obtained with the other inhibitors, it can be further hypothesised that the whole acrosome contains trypsin and chymotrypsin activity while the SBTI-sensitive activity is absent in a small portion of the acrosome. The apical rod at the tip of the acrosome is a good candidate for such SBTI-resistant release. This is in agreement with the complex morphology of the acrosome cap, which has two types of granular content, and of the apical rod, which has a fine granular content and several sheets of membranes (Campanella & Gabbiani, 1979). Furthermore, our experimental approach allows us to conclude that *D. pictus* sperm contain EACA-sensitive enzymes, such as the plasminogen inhibitor. Interestingly urokinase can be involved in sperm-egg interaction in a co-operative action with integrin (Huarte *et al.*, 1993; Chapman, 1977) and integrins are thought to be the sperm receptors in vertebrate eggs (Almeida *et al.*, 1995; Shilling *et al.*, 1997, 1998).

The complexity of the enzyme content of *D. pictus* spermatozoa deserves more study. However, the present data suggest that the enzymes packed in the acrosome may have functions directly linked to specific substrates that the sperm interact with during egg investment penetration and egg membrane interaction (see also Hardy *et al.*, 1991). Ultrastructural evidence found that component B, the inner acrosome matrix component, is released before compound A, in close proximity to the egg surface (Campanella *et al.*, 1997). Our results support the hypothesis that the material released by *D. pictus* sperm at the time of fusion with the egg (Campanella *et al.*, 1997) is constituted by

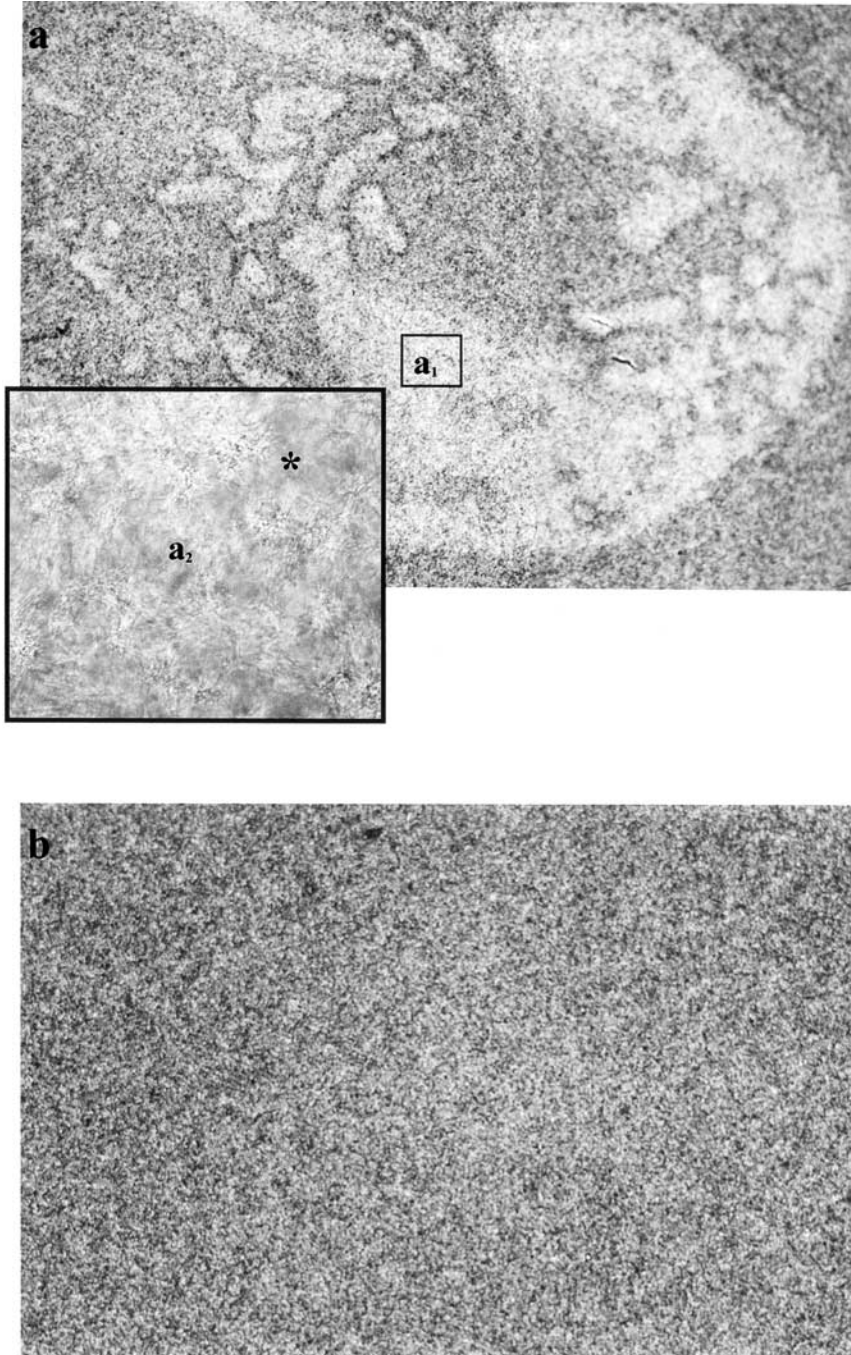


Figure 1 (a) Effect of material released from A23187-treated-sperm on gelatin-coated strips. A large area where gelatin was digested is seen, corresponding to the sperm. $\times 60$. The inset a_2 is a magnification of the detail a_1 , showing sperm (asterisk) in the region where gelatin was digested. $\times 160$. (b) Control strip treated with Ringer-diluted sperm $\times 220$.

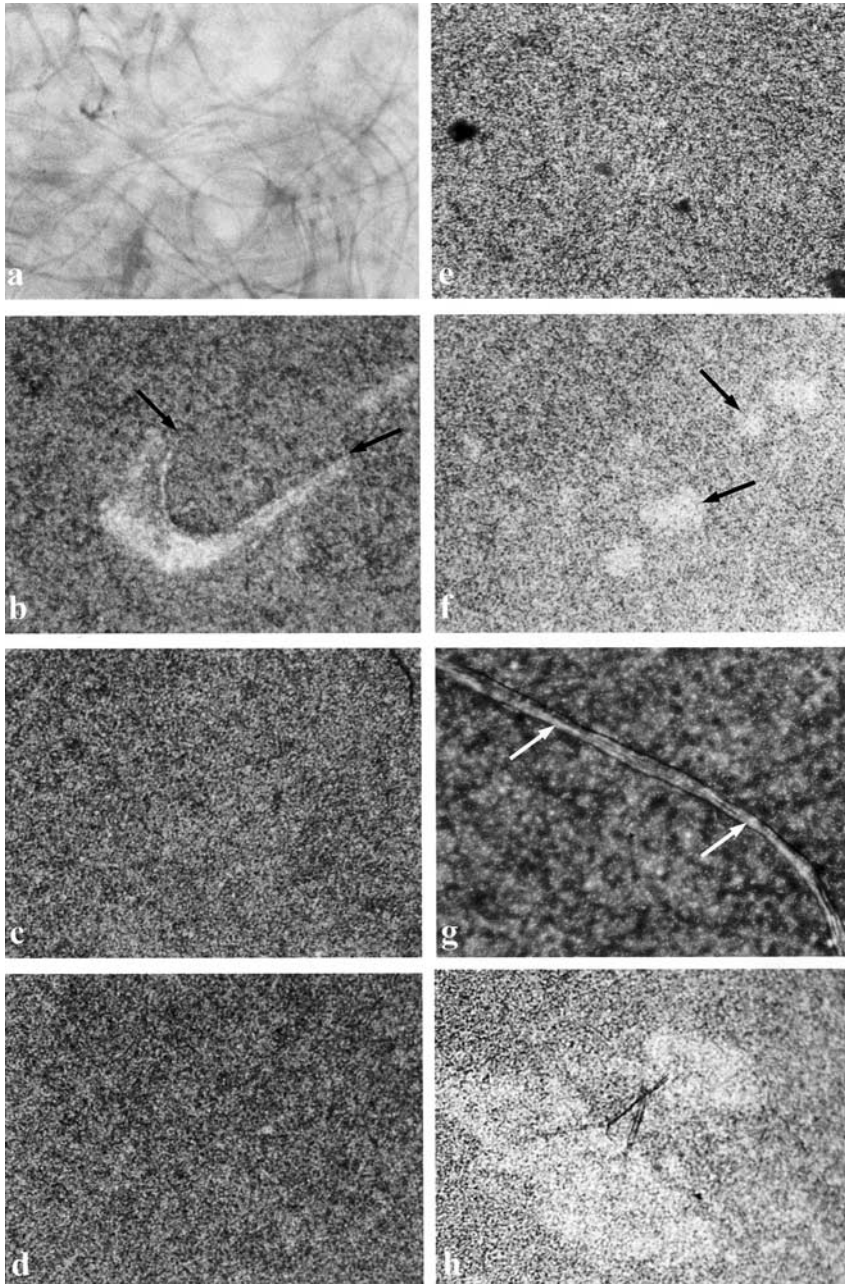


Figure 2 A23187-treated sperm on the gelatin-coated strips. (a) As seen in Nomarski DIC optics. $\times 450$. (b) As seen with normal optics. A halo is seen along part of the sperm length (arrows). $\times 220$. (c) Sperm exposed to TLCK: no halo formation occurred, as in (d) where sperm were incubated with leupeptin, and (e) where the inhibitory action of chymostatin is seen. $\times 220$. (f) SBTI-exposed sperm. The inhibitory action is exerted on sperm but there are small regions where halos are present (arrows). $\times 220$. (g) EACA-exposed sperm. Inhibition occurred except for tiny spots of gelatin digestion along sperm bundles (small arrows). $\times 850$. (h) Sperm exposed to E64: no inhibition occurred and large halos of digested gelatin are seen on the strip. $\times 220$.

trypsin and chymotrypsin-like enzyme(s) with further urokinase activity, that have a role in membrane interaction.

In contrast, *Xenopus* sperm do not release chemicals able to digest gelatin upon treatment with calcium ionophore that is able to provoke the AR in general and in amphibians in particular (Gualtieri & Andreuccetti, 1996; Martinez & Cabada, 1996). This finding may indicate, however, that sperm are not responsive to A23187, or that the assay we used is not sensitive enough to the relatively small amounts of proteolytic enzymes found in *Xenopus* sperm extracts (Mizoke et al., 1999). Alternatively, it may show that the enzymes are not located in the acrosome cap of this species.

References

- Almeida, E.A.C., Huovila, J., Sutherland, A.E., Stephens, L.E., Calarco, P.G., Shaw, L.M., Mercurio, A.M., Sonnenberg, A.P., Myles, D.G. & White, J.M. (1995). Mouse egg integrin $\alpha 6 \beta 1$ functions as a sperm receptor. *Cell* **81**, 1095–104.
- Barros, C., Crosby, J.A. & Moreno, R.D. (1996). Early steps of sperm–egg interactions during mammalian fertilization. *Cell Biol. Int.* **20**, 33–9.
- Blobel, C.P., Wolfsberg, T.G., Turck, C.W., Myles, D.G., Primakoff, P. & White, J.M. (1992). A potential fusion peptide and an integrin ligand domain in a protein active in sperm–egg fusion. *Nature* **356**, 248–52.
- Cabada, M.O., Mariano, M.I. & Raissman, J.S. (1978). Effect of trypsin inhibitors and concanavalin A on the fertilization of *Bufo arenarum* coelomic oocytes. *J. Exp. Zool.* **204**, 409–16.
- Cabada, M.O., Manes, M.E. & Gomez, J.I. (1989). Effect of trypsin inhibitors and concanavalin A on the fertilization of *Bufo arenarum* coelomic oocytes. *J. Exp. Zool.* **204**, 409–16.
- Campanella, C. & Gabbiani, G. (1979). Motile properties and localization of contractile proteins in the spermatozoon of *Discoglossus pictus*. *Gamete Res.* **2**, 163–75.
- Campanella, C. et al. (1999). Fertilization in amphibians. In *Symposium on the Evolution of Terrestrial Vertebrates* (ed. G. Ghiara et al.), pp. 335–34. Modena: Mucchi.
- Campanella, C., Carotenuto, R., Infante, V., Maturi, G. & Atripaldi, U. (1997). Sperm–egg interaction in the painted frog *Discoglossus pictus*: an ultrastructural study. *Mol. Reprod. Dev.* **47**, 323–33.
- Chapman, H. (1997). Plasminogen activators, integrins, and the coordinated regulation of cell adhesion and migration. *Curr. Opin. Cell Biol.* **9**, 714–24.
- Chen, H. & Sampson, N.S. (1999). Mediation of sperm–egg fusion: evidence that mouse egg $\alpha 6 \beta 1$ integrin is the receptor for sperm fertilin beta. *Chem. Biol.* **6**, 1–10.
- Elinson, R.P. (1974). A comparative examination of amphibian sperm proteolytic activity. *Biol. Reprod.* **11**, 401–2.
- Gualtieri, R. & Andreuccetti, P. (1996). Localization of egg-surface carbohydrates and fertilization in *Discoglossus pictus* (Anura). *Cell Tissue Res.* **283**, 173–81.
- Hardy, D.M., Oda, M.N., Friend, D.S. & Huang, T.T.F. (1991). A mechanism for differential release of acrosomal enzymes during the acrosome reaction. *Biochem. J.* **275**, 759–66.
- Huarte, J., Vassalli J.-D., Belin, D. & Sakkas, D. (1993). Involvement of the plasminogen activator/plasmin proteolytic cascade in fertilization. *Dev. Biol.* **157**, 539–46.
- Iwao, Y. & Fujimura, T. (1996). Activation of *Xenopus* eggs by RGD-containing peptides accompanied by intracellular Ca^{2+} release. *Dev. Biol.* **177**, 558–67.
- Iwao, Y., Miki, A., Kobayashi, M. & Ornitake, K. (1994). Activation of *Xenopus* egg by an extract of *Cynops* sperm. *Dev. Growth Differ.* **36**, 469–79.
- Iwao, Y., Miki, A., Kobayashi, M., Miki, A., Kubota, H.Y. & Yoshimoto, Y. (1995). Activation of *Xenopus* eggs by *Cynops* sperm extract is dependent upon both extra- and inter-cellular Ca activities. *Zool. Sci.* **12**, 572–81.
- Martinez, M.L. & Cabada, M.O. (1996). Assessment of the acrosome reaction in *Bufo arenarum* spermatozoa by immunostaining: comparison with other methods. *Zygote* **4**, 181–90.
- Maturi, G., Infante, V., Carotenuto, R., Focarelli, R., Caputo, M. & Campanella de l'oeuf, C. (1998). Specific glycoconjugates are present at the oolemma of the fertilization site in the egg of *Discoglossus pictus* (Anuras) and bind spermatozoa in an *in vitro* assay. *Dev. Biol.* **204**, 210–23.
- Mizote, A., Okamoto, S. & Iwao, Y. (1999). Activation of *Xenopus* eggs by proteases: possible involvement of a sperm protease in fertilization. *Dev. Biol.* **208**, 79–92.
- Parat, M. (1993). L'acrosome du spermatozoïde dans la fécondation et la parthenogénèse expérimentale. *C. R. Soc. Biol.* **112**, 1134–7.
- Penn, A. & Gledhill, B.L. (1972). Acrosomal proteolytic activity of amphibian sperm. *Exp. Cell Res.* **74**, 285–8.
- Poirer, G.R. & Spink, G.C. (1971). The ultrastructure of testicular spermatozoa in two species of *Rana*. *J. Ultrastruct. Res.* **36**, 455.
- Raissman, J.S. & Barbieri, F.D. (1969). Lytic effects of sperm suspensions on the vitelline membrane of *Bufo arenarum* oocytes. *Acta Embryol. Exp.* **1**, 17–26.
- Raissman, J.S. & Cabada, M.O. (1977). Acrosomic reaction and proteolytic activity in the spermatozoa of an anuran amphibian, *Leptodactylus chaquensis* (Ceii). *Dev. Growth Differ.* **19**, 227–32.
- Shilling, F.M., Kratzschmar, J., Cai, H., Wescamp, G., Gayko, U., Leibow, J., Myles, D.G., Nuccitelli, R. & Blobel, C.P. (1997). Identification of metalloprotease/disintegrins in *Xenopus laevis* testis with a potential role in fertilization. *Dev. Biol.* **186**, 155–64.
- Shilling, F.M., Magie, C.R. & Nuccitelli, R. (1998). Voltage-dependent activation of frog eggs by a sperm surface disintegrin peptide. *Dev. Biol.* **202**, 113–24.
- Takamune, K., Yoshizaki, N. & Katagiri, C. (1986). Oviducal pars recta-induced degradation of vitelline coat proteins in relation to acquisition of fertilizability of toads eggs. *Gamete Res.* **14**, 215–24.
- Yamasaki, H., Takamune, K. & Katagiri, C. (1988). Classification, inhibition, and specificity studies of the vitelline coat lysin from toad sperm. *Gamete Res.* **20**, 287–300.
- Yoshizaki, N. & Katagiri, C. (1982). Acrosome reaction in sperm of the toad, *Bufo bufo japonicus*. *Gamete Res.* **6**, 343–52.

THE SEARCH FOR MOLECULES RESPONSIBLE FOR SPERM BINDING AND FUSION TO THE EGG IN VERTEBRATES

C. Campanella* and V. Infante

University of Napoli Federico II,
Dipartimento di Biologia Evolutiva e Comparata
Via Mezzocannone n.8,80 134 Napoli, Italy.

ABSTRACT

The sperm-egg interaction triggers egg activation that increases cytosolic Ca^{++} , increases pH and induces development. The acrosome reaction depends upon highly conserved signal transduction pathways similar to the regulated exocytosis of somatic cells. The fusion of gamete membranes is very much similar to viral function. The main characteristic of fertilization is that due to increase in cytosolic Ca^{++} , eggs are activated which in turn triggers development. Other than calcium, various biochemicals are also involved during fertilization such as PIP_2 , IP_3 , DAG, integrins, oscillin, fertilin etc. Integrins play a significant role during fertilization. The present paper aims to discuss the role of the above mentioned chemicals during fertilization and suggests a new model for the study of fertilization in the egg of *Discoglossus pictus*.

Key words: Fertilization, signal transduction, surface glycoprotein

INTRODUCTION

Sperm-egg interaction is comprised of distinct events. Sperm first passes through the outermost coats of the egg, then binds to the extracellular matrix that surrounds the egg, *i.e.* zona pellucida (ZP) in mammalian eggs and vitelline envelope (VE) or chorion in other eggs. This initial interaction (primary binding) with a ZP glycoprotein (*i.e.* ZP3) may trigger the exocytosis of the acrosomic enzyme content in the sperm that facilitates passage through the zona of the egg. Thanks to the subsequent exposure of the internal sperm membrane; secondary binding occurs between the inner acrosome membrane and a second zona pellucida glycoprotein (*i.e.* ZP2). This binding avoids removal and loss of the reacted sperm from the ZP. Similarly, fusion between sperm and egg membranes is accomplished in two stages: adhesion and fusion. This interaction triggers egg activation that provokes the increase of cytosolic Ca^{++} , pH changes and the onset of development.

* Corresponding Author.

Mechanisms underlying these events are highly conserved in all cells, regardless of their origin, somatic or germinal. Indeed, the sperm-ZP interaction is comparable to adhesion between cell and extracellular matrix occurring during axon growth, lymphocyte migration etc. The acrosome reaction depends upon highly conserved signal transduction pathways similar to the regulated exocytosis of somatic cells such as neurons and mast cells. Furthermore, fusion between gamete membranes shares several features with viral fusion.

The main characteristics of the fertilization process are the high specialization of the gametes, and the ways the molecular basis of the mentioned biological processes are utilized. Eggs are activated by an increase in cytosolic calcium that triggers development. The mechanism that initiates such release is controversial and has been debated in several review articles (Jaffe, 1990; Nuccitelli, 1991; Foltz and Lennarz, 1993; Whitaker and Swann, 1993; Myles, 1993; Schultz and Kopf, 1993). There are two main hypotheses: 1) sperm injection of a factor into the egg to trigger the Ca^{++} increase 2) occupation of an egg receptor by a sperm agonist and hydrolysis of phosphatidylinositol 4,5-bisphosphate [PIP_2]. In the first case Ca^{++} itself could be released from the Ca^{++} -rich sperm. In support of the first hypothesis, the experimental introduction of Ca^{++} into several kinds of eggs provoke an increase of inositol 1,4,5 trisphosphate [IP_3] and subsequent release of more Ca^{++} (Whitaker and Swann, 1993). Other data indicate that injected molecules from sperm homogenate are able to initiate egg development (Dale *et al.*, 1985). In particular, a 33 kDa sperm protein (Oscillin) releases calcium directly from calcium stores in mammalian egg cytoplasm (Parrington *et al.*, 1996). However, further data suggest that this is not the sperm molecule responsible for egg activation (Wolny, 1999).

According to the second hypothesis calcium release might be induced by the hydrolysis of PIP_2 which generates IP_3 and DAG through the action of a phospholipase C [$\text{PIP}_2^{\text{PLC}}$ $\text{IP}_3 + \text{DAG}$]. IP_3 binds to specific receptors located in the endoplasmic reticulum, allowing propagative Ca^{++} release from this storage (Han *et al.*, 1992; Miyazaki *et al.*, 1993). In support of this hypothesis, it was found that IP_3 injection into the egg provokes the release of Ca^{++} that activates the egg (Busa *et al.*, 1985 in *Xenopus*, Nuccitelli *et al.*, 1988 in *Discoglossus*). Also, a strong elevation of PIP_2 and IP_3 was found during fertilization (Snow *et al.*, 1996).

Lately, data coming from several experiments further strengthen the role of IP_3 in fertilization both in mammals and amphibians, and sustain the presence of a receptor,

able to cause its release when occupied by a ligand. PIP2 hydrolysis may be activated along one of the following pathways: 1) a sperm ligand activates a tyrosine kinase receptor that is phosphorylated and binds a phospholipase (PLC γ 1) through its SH2 domains. As a consequence, PLC γ 1 increase its hydrolytic activity on PIP2 (Jaffe, 1990; Creton and Jaffe, 1995; Snow *et al.*, 1996; Kline *et al.*, 1988; Foltz e Lennarz, 1993; Ohlendieck and Lennarz, 1995) as a result of which IP3 and DAG are produced. DAG activates protein kinase C that up to recently was thought to cause intracellular pH release in the sea urchin (Swann and Whitaker, 1985). 2) a sperm ligand activates the classical pathway of PIP2 hydrolysis through the involvement of G proteins. In *Xenopus*, Kline *et al.*, (1991) hypothesized the existence of a G protein typical of the egg and demonstrated that injection of a non-hydrolysable GTP analog triggers egg activation. The involvement of protein G in egg activation was shown in the starfish (Shilling *et al.*, 1994) and in the mouse (Moore *et al.*, 1994).

Integrins (α 6 β 1, in mouse eggs) are possible receptors for spermatozoa, according to immunolocalization and fertilization inhibition assays with specific antibodies (Tarone *et al.*, 1993; Almeida *et al.*, 1995; Chen and Sampson, 1999). Furthermore, synthetic peptides that reproduce the active binding site of integrin ligands (disintegrins) inhibit fertilization (Bronson and Fusi, 1990a,b; Fusi *et al.*, 1992; Myles, 1994). The presence of disintegrins of the ADAM or MDC protein family was clearly demonstrated in mammal spermatozoa (Primakoff *et al.*, 1987; Blobel *et al.*, 1992). In mammalian sperm, fertilin, a heterodimeric molecule composed of α and β fertilin was found in the membrane of the post-acrosomal cap, *i.e.* the region that probably fuses first with the oolemma. Alfa-fertilin has molecular characteristics that may enable membrane fusion, while β -fertilin contains an integrin-binding domain (Primakoff *et al.*, 1987; Blobel *et al.*, 1992). In particular, it was hypothesized that β -fertilin and integrin may represent the functional ligand-receptor system. However, more recently it was found that β -fertilin knock-out mice are fertile, indicating that β -fertilin is not necessarily implicated in sperm egg binding and fusion (Cho *et al.*, 1998). Indeed, a second disintegrin ciritestin was cloned in mouse spermatozoa with a localization in the sperm similar to that of β -fertilin (Yuan *et al.*, 1997). Synthetic peptides that reproduce its disintegrin domain are able to inhibit fertilization.

Recently, Zuccotti *et al.*, (1998) demonstrated that integrin α 6 and β 1 gene expression starts in primordial germ cells in female embryos following the first two weeks of life and goes up to the end of oogenesis. The heterodimer α 6 β 1 was localized at the surface of 25-30 μ m oocytes.

However, integrins are present on the egg membrane also after fertilization in contrast to the current knowledge that receptors used by the sperms are inactivated after fertilization. Indeed, it was shown that integrin $\alpha 6\beta 1$ is involved in the trophoectoderm migration, suggesting a role of this molecule in embryogenesis and shadowing its possible function in fertilization.

Among lower vertebrates, anurans are a useful model for biochemical studies of fertilization because of the ease in manipulation of their numerous and large eggs and the accumulating knowledge of the activation process in the egg. Injection of IP_3 into the egg induces egg activation in *Xenopus* and *Discoglossus* (Busa and Nuccitelli, 1985; Nuccitelli *et al.*, 1988; Nuccitelli *et al.*, 1993). In *Xenopus*, sperms cause hydrolysis of PIP_2 to produce IP_3 (Stith *et al.*, 1993, which has been found to increase after fertilization (Snow *et al.*, 1996) and trigger a transient increase of cytosolic Ca^{++} (Busa and Nuccitelli, 1985; Kline, 1988). These data suggest the involvement of receptors in the sperm-mediated activation signal. According to Yim *et al.*, (1994) tyrosine kinase or G-proteins (Kline *et al.*, 1991) may be implicated in this process. In amphibians, integrins may play a significant role during fertilization. It has been shown that a molecule of the MDC family (MDC16) is present at the surface of the posteriormost head region *i.e.* a region which is however, not competent for initial sperm-egg fusion. Synthetic peptides, comprehensive of the disintegrin domain of MDC16 or of a similar disintegrin domain (RGD) are able to depolarize the egg membrane and induce intracellular Ca^{++} release (Iwao and Fujimura, 1996; Shilling *et al.*, 1997,1998). In *Xenopus*, Sato *et al.*, (1999) showed the role of a non-receptor tyrosine kinase of the (Src) family (p57) for egg activation. It was observed that p57 increases in concentration and is phosphorylated following egg activation by RGD peptide. It has been hypothesized that p57 activity is connected to integrin receptor in signal transmission. Indeed micro-injection of synthetic inhibitors of p57 inhibits egg activation by RGD. However, up to date, integrins have been not found at the egg surface, indicating that many open questions still exist in a possible model implicating a disintegrin-integrin system active at fertilization.

Further research on sperm proteases indicate that *Cynops pyrogaster* sperm extract containing a trypsin-like protease is able to activate the *Xenopus* egg. *Xenopus* sperm extracts have a proteolytic activity whose function in fertilization is unclear. Interestingly, it has been hypothesized that the protease itself may contain a ligand domain for egg receptors or that the protease may hydrolyze the egg receptor exposing an agonistic peptide in the receptor (Mizote *et al.*, 1999). Altogether, these data reveal the complexity of the fertilization process. The study of sperm-egg interaction is flourishing with new data, yet deserve many more integrative experiments.

Introducing a model for the study of fertilization, *Discoglossus pictus*

In anuran eggs, 2 main territories are present, the whitish vegetal hemisphere and the pigmented animal hemisphere where fertilization occurs. This remarkable compartmentalization is extreme in the genus *Discoglossus* where the predetermined site of fertilization is further concentrated in the centre of the animal half. Indeed, in the egg of *Discoglossus pictus*, fertilization takes place in the dimple (D) while in the rest of the egg, sperm cannot activate development (Fig.1). *D.pictus* has several advantages over other species for studies aiming at the detection of the surface molecules that take part in the fertilization process. First, experimental evidence indicates that the dimple is a site where the animal hemisphere molecules are highly concentrated, thus simplifying biochemical studies (Talevi *et al.*, 1985; Talevi and Campanella, 1988; Nuccitelli *et al.*, 1988; Gualtieri *et al.*, 1989; Tatone *et al.*, 1993). Second, in the dimple, glycoprotein content keeps the D surface apart from the vitelline envelope (VE) for a depth of about 300 μm . This makes it possible to pinch off the VE manually and to proceed for biochemical analysis of D versus Dimple-less-egg (DLE) cleared of all the extracellular component of the egg. Third, the presence of terminal fucose has been histologically determined only at the surface of the dimple center, D₁. This natural marker can be utilized for the identification of glycoconjugates typical of this region which are probably involved in the fertilization process as they settle on the D₁ surface during dimple formation (Denis Donini and Campanella, 1977). Fourth, the acrosome reaction of *D. pictus* sperm (Figs. 2,3) has been studied in its natural environment and the membranes interacting and fusing with the oolemma have been determined (Campanella *et al.*, 1997). Sperms arrive at the oolemma (Fig. 4) at the initial stage of acrosome reaction, *i.e.* covered with hybrid vesicles (plasma membrane+outer acrosome membrane) and intragametic fusion occurs between the inner acrosome membrane and the oolemma in a narrow funnel located at the centre of the fertilization cone (Campanella and Gabbiani, 1979; Campanella *et al.*, 1997).

Further data render this egg an interesting model for the study of fertilization. Electrophysiological experiments have shown that while the jelly coat and particularly the *plug*, is essential for sperm convergence on the dimple, the dimple itself is endowed with the specific ability to generate typical fertilization potentials (FP) upon insemination followed by the formation of the fertilization cone and the onset of development. More precisely, this property is possessed only by D₁, whereas elsewhere in the dimple, initial sperm penetration occurs but this event does not evoke either typical FP or the onset of development (Talevi and Campanella, 1988).

In D_1 , calcium release into the cytosol is triggered as a consequence of either sperm penetration or IP3 injection (Talevi *et al.*, 1985; Campanella *et al.*, 1988; Nuccitelli *et al.*, 1988; Talevi and Campanella, 1988). In fact, only in D_1 , the endoplasmic reticulum reaches the critical concentration that permits the calcium elevation event to occur (Campanella *et al.*, 1988; Gualtieri *et al.*, 1992). A privileged localization of specific molecules in D_1 is supported by the finding that in D_1 , the concentration and distribution of intramembrane particles is clearly different from that of DLE (Gualtieri *et al.*, 1989). In this regard, electrophysiological measurements and specific staining showed that Cl^- channels are located only in D_1 ; these are the ionic channels which are depolarized at activation in amphibians and are calcium activated (Nuccitelli *et al.*, 1988 and Talevi *et al.*, 1992). Recently, Maturi *et al.*, (1998) have determined the presence of four glycoproteins of apparent molecular weight of 200,230,260 and 270 kDa on the surface of the egg and precisely only at the dimple territory. Gp200 and gp270/260 are the major glycoconjugates. As these molecules are fucosylated, it is supposed that they constitute the main glycoproteins responsible for the reactivity to UEA I (a lectin binding to terminal fucose), histologically localized at the D_1 surface. Indeed, in ultrastructural and lectin-fluorescence studies, the affinity with UEA I and LTA, a lectin that similarly binds α -L-fucose, is high in D_1 and drastically decreases towards the dimple walls (Denis Donini and Campanella, 1977; Gualtieri and Andreuccetti, 1996). Therefore, the ability to bind UEA I was considered as a marker for determining which molecule among those located at the dimple plasma membrane surface is highly concentrated in the D_1 domain (Maturi *et al.*, 1998).

Several studies have indicated that among the glycoconjugates involved in sperm-egg interaction, fucose is present particularly in its sulfated form, although it is not yet clear whether a specific role exists for this sugar (Bowell *et al.*, 1979 and Stafford *et al.*, 1992, in *Fucus*; Focarelli *et al.*, 1988, 1995 in *Unio*; Segall and Lennarz, 1979, Glabe *et al.*, 1982, De Angelis and Glabe, 1987,1988; Foltz and Lennarz, 1993; Dhume *et al.*, 1996; Rosati and De Santis, 1978, 1980; De Santis *et al.*, 1983 in *Ciona*; Ruttenberg-Barnum and Brown, 1983 in *Limulus*; Ahuja 1982; Dravland and Mortimer, 1988; Jones *et al.*, 1988; O'Rand *et al.*, 1988 in mammals). However, these studies are mainly concerned with glycoproteins located in extracellular coats with some exceptions such as *Fucus* (Bowell *et al.*, 1979; Stafford *et al.*, 1992) and Hamster (Dravland and Mortimer, 1988) whose egg does not have external investments. The fucosylated glycoproteins of D_1 are located in the glycocalyx and/or in the plasma membrane. They are not part of the dimple content, as shown by SDS PAGE pattern on this matrix (Maturi *et al.*, 1998).

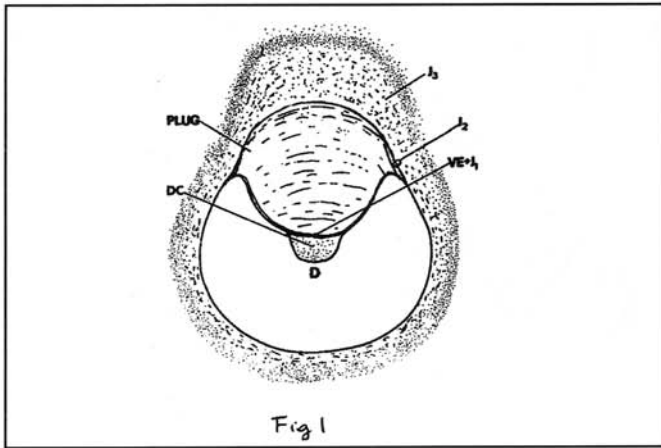


Fig 1

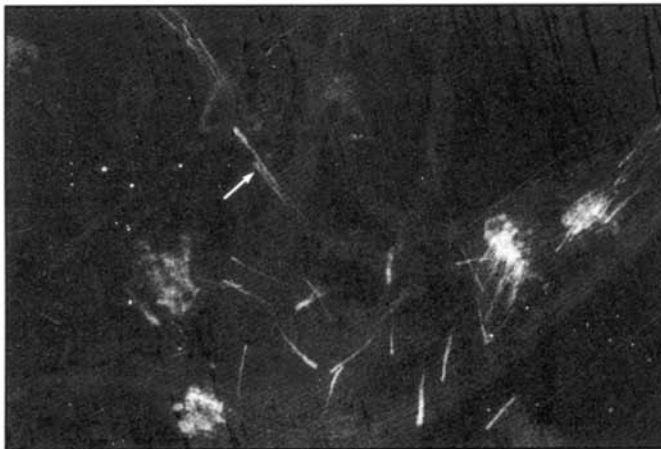


Fig. 3

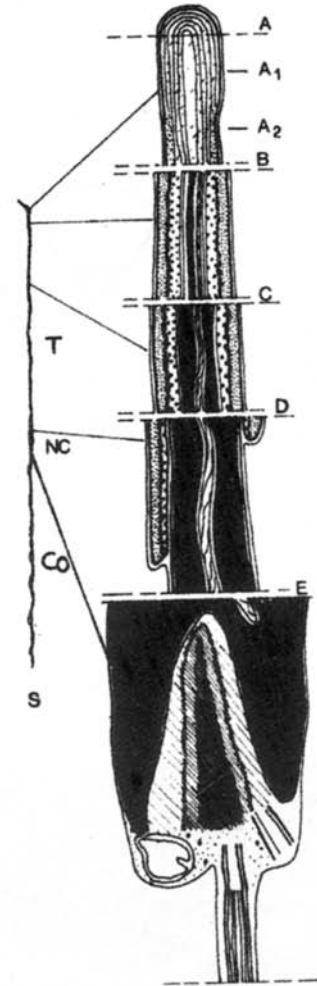


Fig. 2

Fig. 1 : Schematic drawing of a longitudinal section of *D. pictus* egg. D,dimple; DC,dimple content; J3,Jelly 3; J2,Jelly2. J1,jelly1;VE,vitelline envelope. The plug is sitting at the center of the animal hemisphere, in the concavity, which is typical of the eggs belonging to the genus *Discoglossus* ; Fig. 2 : Diagram of a single *D. pictus* sperm (S); T,head; NC,neck; Co,Tail. *D. pictus* sperm head is about 1mm long. Remarkable is the acrosome that covers the whole sperm nucleus except for (A) a short posterior segment (level E). It has an anteriormost specialization, the apical rod, containing several membrane-like structures (A1-A2). The rest of the acrosome cap has two kinds of granular content (levels B-D). Fig. 3: Sperm bundles. Sperms (arrow) are ejaculated in bundles of 20. Smear stained with propidium iodide and PSA. X25.

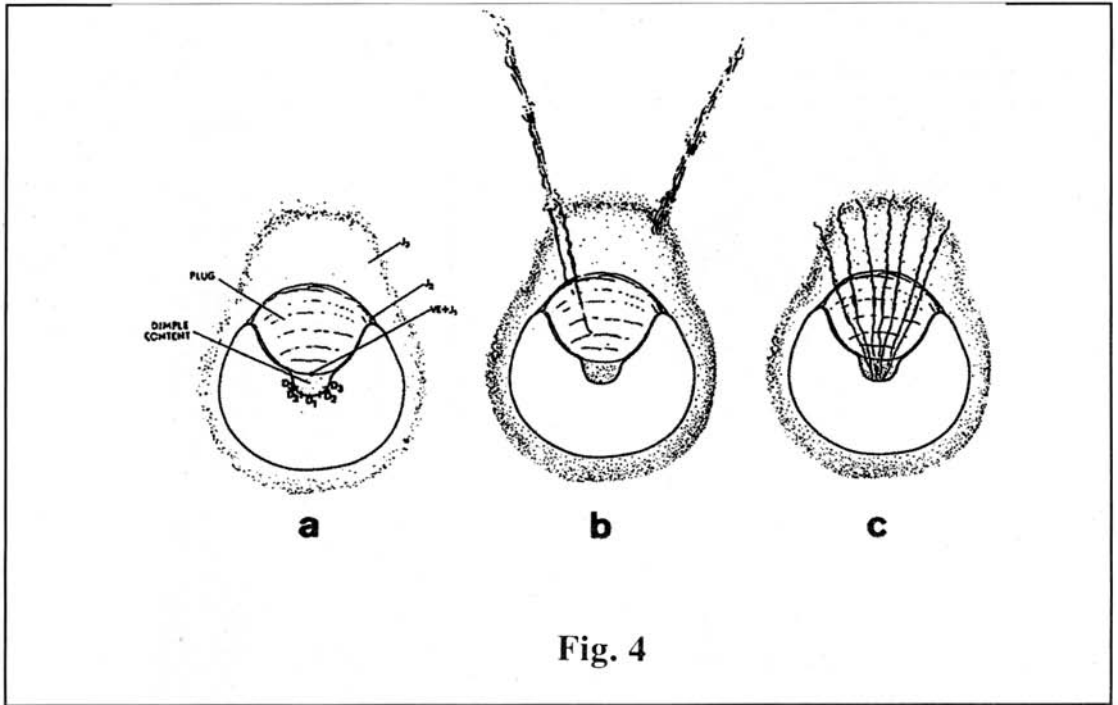


Fig. 4

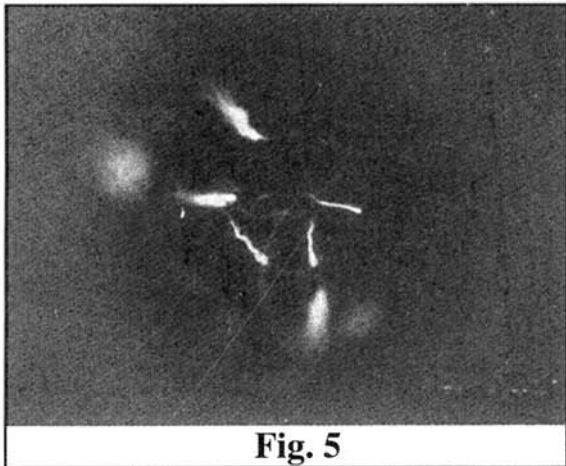


Fig. 5

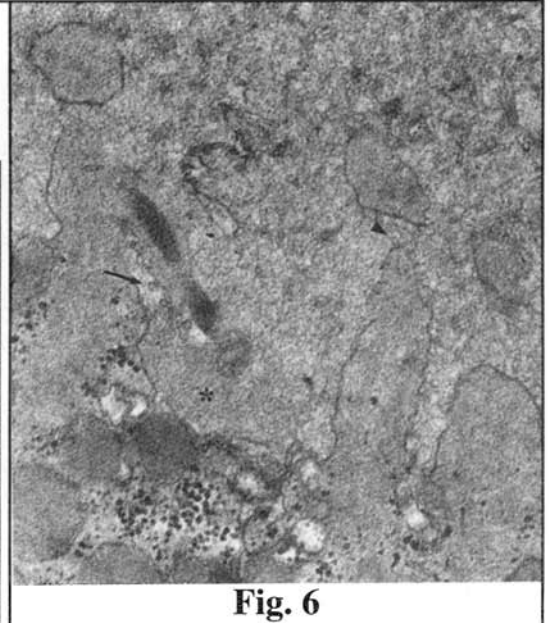


Fig. 6

Fig. 4 : Schematic diagram of *D. pictus* egg before and in two stages of interaction with sperm. **a** Dimple regions D1,D2, and D3 are indicated. D1 is the only site where fertilization can occur. **b**,at insemination sperms are ejected from their bundle into the jelly. **c**,sperms become embedded along their whole length in the jelly layers ; **Fig. 5 :** Sperm heads bound on a polystyrene beads where gp 200 was absorbed. DAPI staining. X250 ; **Fig.6:** Thin section of a sperm at initial stage of penetration. Showing plasma membrane-acrosome vesiculation at the surface of the sperm head (arrow); Sperm content released during the acrosome reaction (asterisk); Oolemma glycocalyx (arrowhead). X 66,000.

Gps 200 and gp 270/260 were excised out of polyacrylamide gels, electrocuted and adsorbed to polystyrene beads. Sperms bind in an *in vitro* assay to the gps-coated beads (Fig. 5) thus discriminating between unreacted sperms and sperms having undergone acrosome reaction following treatment with Ca-ionophore. Sperms stuck to gp200 beads before but not after Ca-ionophore treatment. Conversely, for gp270/260 beads, binding occurred after ionophore treatment. Beads stained with DAPI indicate that sperms bind the beads through their heads, thus rendering rather remote the hypothesis that binding might occur in sites where the acrosome is absent (Fig. 5). In contrast, lipovitellin and BSA coated beads, used as controls did not bind the sperms. Two types of molecular interaction may occur between sperm and egg, one mediated by gp200 and the other mediated by gp270/260. In its natural environment, the acrosome reaction is triggered when sperms come into contact with the jelly layer. In a few seconds, they become embedded in the thick jelly plug which sits in a large concavity of the animal hemisphere, and converge through this jelly coat and the VE into the dimple (Fig. 4). Penetration of egg investments take about 15 sec. When sperms arrive at the dimple surface, they are still at a very early stage of hybrid vesicles formation as documented by ultrastructural studies (Campanella *et al.*, 1977) (Fig. 6). The first contact occurs between sperm plasma membrane in the process of vesiculation and the D₁ glycocalyx while fusion occurs between the inner acrosome membrane and the oolemma deprived of the antennular glycocalyx (ultrastructural observations), when a release of acrosome content is observed at the site of gamete interaction (Campanella *et al.*, 1997) (Fig. 6). This suggests that acrosomal enzymes may clear the glycocalyx after binding has occurred, thus permitting a second interaction and fusion to occur (Maturi *et al.*, 1998; De Santis *et al.*, 1992; Sato *et al.*, 1999). In this connection unpublished observations reveal that, following Ca-ionophore treatment, *D. pictus* sperm release chymotrypsin and trypsin-like proteases (Infante and Amirante, unpublished) similar to *Cynops* (Sato *et al.*, 1999) and *Bufo* (Yamasaki *et al.*, 1988). These data can be compared to the ultrastructurally determined heterogeneous acrosomal content of *D. pictus* sperm (Campanella *et al.*, 1997).

Presently, the research is concentrated to molecular micro-sequencing of *D. pictus* gp200, the most prominent among the D₁ glycoconjugates. Therefore, *D. pictus* model is ready to offer new data on the identification and separation of a molecule related to the oolemma binding *in vitro* homologous sperm. In *Xenopus*, where information is available on MDC16 (Shilling *et al.*, 1997, 1998), it is not clear however, sperm perform an acrosomal reaction. Similarly, the characteristics of this egg surface render practically impossible for the study of surface molecules implicated in sperm-egg interaction. In this regard, it will be interesting to know the possible relationship between *D. pictus* gp200 and integrin-like molecules.

ACKNOWLEDGEMENT

We thank Dr. Martin Wilding for suggestions and revision of the manuscript.

REFERENCES

- Almeida E.A.C., J. Huovila, A.E. Sutherland, L.E. Stephens, P.G. Calarco, L.M. Shaw, A.M. Mercurio, A. Sonnenberg, P. Primakoff, D.G. Myles and J.M. White (1995). Mouse egg integrin $\alpha 6/\beta 1$ functions as a sperm receptor. *Cell*. **81**: 1095-1104.
- Ahuja, K.K. 1982. Fertilization studies in the hamster. The role of cell-surface carbohydrates. *Exp. Cell. Res.* **140**: 353-362.
- Blobel, C.P., T.G. Wolfsberg, C.W. Turck, D.G. Myles, P. Primakoff and J.M. White 1992. A potential fusion peptide and an integrin ligand domain in a protein active in sperm-egg fusion. *Nature*. **356**: 248-252.
- Bowell, G.P., J.A. Callow, M.R. Callow and L.V. Evans. 1979. Fertilization in brown algae II. Evidence for lectin sensitive complementary receptors involved in gamete recognition in *Fucus serratus*. *J. Cell. Sci.* **36**:19-30.
- Bronson, R.A. and F. Fusi. 1990a. Sperm-oolemmal interaction: role of RGD adhesion peptide. *Fertil. Steril.* **54**:527-529.
- Bronson, R.A. and F. Fusi. 1990b. Evidence that an Arg-Gly-Asp (RGD) adhesion sequence plays a role in mammalian fertilization. *Biol. Reprod.* **43**:1019-1025.
- Busa, W.B and R. Nuccitelli. 1985. An elevated free cytosolic Ca^{2+} wave follows fertilization in eggs of the frog *Xenopus laevis*. *J. Cell Biol.* **100**: 1325-1329.
- Busa, W.B., J.E. Ferguson, S.K. Joseph, J.R. Williamson and R. Nuccitelli. 1985. Activation of frog (*Xenopus laevis*) eggs by inositol triphosphate. I. Characterization of Ca^{++} release from intracellular stores. *J. Cell. Biol.* **101**: 677-682.
- Campanella, C. and G. Gabbiani. 1979. Motile properties and localization of contractile proteins in the spermatozoon of *Discoglossus pictus*. *Gamete Res.* **2**:163-175.
- Campanella, C., R. Talevi, D. Kline and R. Nuccitelli. 1988. The cortical reaction in the egg of *Discoglossus pictus*: A study of the changes of the endoplasmic reticulum at activation. *Dev. Biol.* **130**:108-119.
- Campanella, C., R. Carotenuto, V. Infante, G. Maturi and U. Atripaldi. 1997. Sperm-egg interaction in the painted frog *Discoglossus pictus*: An ultrastructural study. *Mol. Reprod. Dev.* **47**: 323-333.
- Chen, H. and N.S. Sampson. 1999. Mediation of sperm-egg fusion: evidence that mouse egg alpha6 beta1 integrin is the receptor for sperm fertilin beta. *J. Chem. Biol* **6**:1-10.
- Cho, C., D. Bunch, J.E. Faure, E.H. Goulding, E.M. Eddy, P. Primakoff, D.G. Myles. 1998. Fertilization defects in sperm from mice lacking fertilin β . *Science*. **281**: 1857-1859.

Lipovitellin Constitutes the Protein Backbone of Glycoproteins Involved in Sperm–Egg Interaction in the Amphibian *Discoglossus pictus*

C. CAMPANELLA,^{1*} M. CAPUTO,¹ M.C. VACCARO,¹ N. DE MARCO,¹ L. TRETOLA,¹ M. ROMANO,² M. PRISCO,² L. CAMARDELLA,³ A. FLAGIELLO,⁴ R. CAROTENUTO,¹ E. LIMATOLA,² A. POLZONETTI-MAGNI,⁵ AND V. INFANTE¹

¹ Department of Structural and Functional Biology, University of Naples Federico II, MSA, Naples, Italy

² Department of Biological Sciences, University of Naples Federico II, Naples, Italy

³ Institute of Protein Biochemistry, CNR, Naples, Italy

⁴ Advanced Biotechnologies, CEINGE, Naples, Italy

⁵ Department of Biology, University of Camerino, Camerino, Italy

SUMMARY

Our knowledge of the molecules that interact with sperm at the egg membrane is restricted to a short list. In the eggs of *Discoglossus pictus*, fusion with sperm is limited to a differentiated structure, the dimple, offering several advantages for detecting molecules involved in fertilization. Previous studies have identified fucosylated glycoproteins of 200, 260, and 270 kDa located at the surface of the dimple that are able to bind sperm in vitro. Here, we show that dimple glycoproteins and a protein represented by a 120-kDa band released following gel-into-gel SDS–PAGE of both glycoproteins share the same N-terminal amino acid sequence, which itself is similar to the N-termini of *Xenopus* liver-synthesized vitellogenin (VTG) and the lipovitellin 1. MALDI/MS mass spectrometry indicated that the 120-kDa band is part of both gps 200 and 270/260. A 117-kDa major protein of the egg lysate exhibits the same MALDI/MS spectrum, and LC-MSMS indicates that this is a lipovitellin 1 (DpLIV) that coincides with the 120-kDa band and is responsible for the formation of the 200–270-kDa dimers. Therefore, lipovitellin 1 constitutes the protein backbone of the dimple glycoconjugates. In vitro assays using polystyrene beads coated with DpLIV or with its dimers indicate that significant sperm binding occurs only with DpLIV dimers. In amphibians, VTG is taken up by the oocyte, where it releases lipovitellins destined to form yolk. In *Discoglossus*, our data suggest that yolk proteins are also synthesized by the oocyte. The dimple forms in the ovulated oocyte following the exocytosis of vesicles that likely expose DpLIVs at their membrane. Indeed, in whole mounts of immunostained eggs, anti-vitellogenin antibodies label only the surface of the dimple.



* Corresponding author:
Department of Structural and
Functional Biology,
University of Naples Federico II,
Complesso Universitario Monte
Sant'Angelo, Via Cinthia, I-80126
Naples, Italy.
E-mail: chiara.campanella@unina.it

Grant sponsor: Regione Campania

Mol. Reprod. Dev. 78: 161–171, 2011. © 2011 Wiley-Liss, Inc.

Published online 14 January 2011 in Wiley Online Library
(wileyonlinelibrary.com).
DOI 10.1002/mrd.21282

Received 4 October 2010; Accepted 23 December 2010

INTRODUCTION

Fertilization is a multi-phase process involving a number of molecules in a coordinated program of step-wise

Abbreviations: anti-TcVTG, antiserum directed against *Triturus* vitellogenin; D1, center of the dimple; gps, glycoproteins; GA, germinative area; MALDI/MS, matrix-assisted laser desorption ionization mass spectrometry; LC-MSMS, liquid chromatography tandem mass spectrometry; LIV, lipovitellins (also DpLIV, *Discoglossus pictus* lipovitellin 1); UEA-I, *Ulex europaeus* agglutinin I; VTG, vitellogenin; ZP, zona pellucida.

interactions. In mammals, sperm bind first to the oviductal and then to the granulosa cells, and finally to the zona pellucida (ZP) of the egg. Different sperm membranes and several interacting molecules (i.e., ZP3, ZP2) are involved in gamete binding. Binding to ZP3 occurs through so-called *primary binding* and to ZP2 through *secondary binding* (for reviews, see Shur et al., 2004; Wassarman et al., 2004).

When acrosome-reacted sperm interact with the egg membrane (*tertiary binding*), adhesion molecules and molecules promoting fusion are called into action. The critical problem in understanding this process is that no surface protein that mediates sperm–egg binding and fusion has been shown to have a link with intracellular signaling; that is, the mode of stimulation of the egg by sperm remains largely unknown (for review, see Miyazaki, 2006).

Data on molecules involved in sperm interactions with the egg membrane focus on the proteins necessary for fusion, that is, members of the tetraspanin family such as CD9 (Ellerman et al., 2003; Zhou et al., 2009), which does not possess receptor properties. However, they interact laterally with other molecules, such as integrin receptors, forming complexes in *cis* referred to as *tetraspanin webs* (Levy and Shoham, 2005). Integrins are not required for fertilization to occur (Cho et al., 1998; Miller et al., 2000; Stein et al., 2004), though they may contribute to sperm adhesion to the egg through disintegrins located in the sperm membrane. A member of the immunoglobulin super family, Izumo, located in the sperm membrane is necessary for sperm–egg fusion, though it does not interact with tetraspanins or integrins (Inoue et al., 2005). *Xenopus* egg activation involves a tyrosine kinase c-Src that interacts with PLC- γ , which is required for calcium release (Sato et al., 1999, 2000, 2003). Uroplakin III (xUPIII; Mahbub Hasan et al., 2007), an egg membrane microdomain-associated protein, is phosphorylated upon fertilization (Sakakibara et al., 2005). Furthermore, sperm peptides containing disintegrins are able to activate the egg (Iwao and Fujimura, 1996; Shilling et al., 1998). In the sea urchin, bindin, an acrosome protein with adhesion properties (Glabe et al., 1982) interacts with EBR1, a 350-kDa protein in which an ADAMTS-like N-terminus is followed by EBR repeats with alternating CUB and thrombospondin type 1 modules (Kamei and Glabe, 2003). Taken together, these data support the concept that the fertilization process is based on the existence of multimeric complexes on both egg and sperm membranes (for a review, see Evans, 2002).

The egg of *Discoglossus pictus* represents an interesting *alter ego* of the main models used for the study of fertilization in vertebrates. This 2-mm diameter egg has a specific site for sperm fusion (the dimple) that is naturally labeled by the presence of terminal fucose (Denis-Donini and Campanella, 1977; Talevi et al., 1985; Gualtieri and Andreuccetti, 1996). The dimple is funnel-shaped, and its membrane is considerably separated from the vitelline envelope, making this site quite suitable for studying the molecules responsible for sperm adhesion and fusion at the egg plasma membrane. The egg surface is endowed with microvilli decorated by a long and ramified glycocalyx. In the center of the dimple (D1), highly concentrated ionic channels exist

that generate a calcium-dependent chloride current upon activation (Talevi et al., 1985; Nuccitelli et al., 1988). Upon insemination, fertilization potentials are elicited in D1, followed by the onset of development (Talevi and Campanella, 1988). Labeling of the egg surface proteins with membrane-impermeable sulfo-NHS-biotin identified four main bands of 200, 230, 260, and 270 kDa exclusive to the dimple surface. They are glycoproteins (gps) containing terminal fucose. Specificity for lectins indicates that glycosylation/fucosylation is more extensive in gps 230, 260, and 270 than in gp 200. In *in vitro* assays, sperm adhered to beads coated with gp 200 before the acrosome reaction occurred whereas only acrosome-reacted sperm bind beads coated with gps 270/260 (Campanella et al., 1997; Maturi et al., 1998). Whether these glycoconjugates have a different protein backbone or are glycoforms of the same polypeptide has yet to be ascertained.

In the present study, we analyzed the protein backbone of gps 200, 260, and 270. Unexpectedly, we found that they are polymers of a molecule of the lipovitellin 1 family that is a homologue of human apolipoprotein B (reviewed in Howell and Herz, 2001). In amphibians, lipovitellins (LIV) are part of vitellogenin (VTG), a high molecular weight lipoglycophosphoprotein synthesized in the liver. In *Xenopus laevis*, lipovitellin 1 (M_r of about 120 kDa) is located at the N-terminus of VTG, and lipovitellin 2 (M_r of about 30 kDa) is at the C-terminus of VTG. Native VTG has a M_r of approximately 400 kDa and, in SDS-PAGE, yields monomers of 197–182 kDa. When endocytosed by the oocyte, VTG splits essentially into fosvitin and lipovitellins, which are later incorporated into yolk platelets (Wiley and Wallace, 1981; Gerber-Huber et al., 1987). Several cases of oocyte-derived VTG components have also been reported (Wallace and Selman, 1990; Yoshitome et al., 2003). Four VTG genes have been found, forming two families (A and B). The *Xenopus* VTGA2 gene has been fully sequenced (Gerber-Huber et al., 1987), whereas the sequence of *D. pictus* VTG is unknown.

RESULTS

N-Terminal, MALDI, and LC-MSMS Analyses Indicate Homology of gps 200, 260, and 270 With Lipovitellin 1

D. pictus egg lysates separated by SDS-PAGE exhibited an electrophoretic pattern with a prominent band in the range of approximately 117 kDa, previously described as the main yolk component lipovitellin, and high M_r bands of gps 200, 230, 260, and 270 (Fig. 1), which are the fucosylated glycoconjugates identified at the dimple surface (Maturi et al., 1998). Here, we characterized the protein portions of gps 200, 260, and 270. N-terminal sequencing of gps 200, 270, and 260 identified the same 11 amino acid residues: EKS_NLVNPFSD. The sequencing did not go beyond the 11th residue because of the low sequencing yield, which was attributed to the large size of these molecules. To improve the N-terminal analysis, gps 200 and 270/260 were excised from the SDS-PAGE gels and several

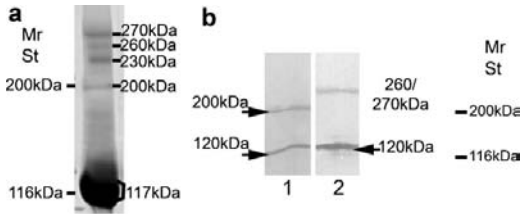


Figure 1. Electrophoresis pattern of *D. pictus* total egg lysate and gel-into-gel results. **a:** SDS-PAGE of total egg supernatant. A prominent band is present of about 117 kDa. Bands of 200, 230, 260, 270 kDa are indicated. **b:** As a result of gel-into-gel experiments, the bands of 200 or 270/260 kDa release a polypeptide of about 120 kDa during electrophoresis. M, standards are indicated.

bands of each of these gps were loaded onto a new gel (gel-into-gel experiments). As a result, the original bands and a main band of approximately 120 kDa were obtained for both the 200 and 270/260 gps (see also Maturi et al., 1998) (Fig. 1). N-terminal sequencing of the 120-kDa polypeptide yielded a sequence of 19 amino acid residues: EKS_NLVNPFSDK_KTYVYNY. This result demonstrated that the 120-kDa band contained the same N-terminus as gps 200 and 270/260 (first 11 residues identical), and extended the sequence. The 19 amino acid residue sequence shows 68% identity with the N-terminus of mature *X. laevis* VTG B2 (accession no.: P19011), 63% identity with the N-terminus of *X. laevis* VTG1 (accession no.: P19010) and 47% with the lipovitellin 1 situated at the N-terminus of VTG A2 (accession no.: P18709). We then performed MALDI/MS analyses of trypsin digests of *D. pictus* gps 270/260, 200 and of the 120-kDa band. The results of these analyses are all super-imposable (Fig. 2a–c), indicating that the 120-kDa band is part of gps 200 and 270/260. Additionally, the MALDI spectrum of the 117-kDa lipovitellin, as separated by SDS-PAGE from the egg extracts, was identical to the spectra for the 120-kDa band and gps 200 and 270/260 (Fig. 2d). A trypsin digest of the 117-kDa polypeptide was further analyzed through LC-MSMS. Five peptides were identified as part of the *X. laevis* VTG A2 precursor sequence (Fig. 3). The amino acid residues identified by the N-terminus analysis were contained in one of the trypsin digest sequences at the N-terminus of *Xenopus* VTG A2, whereas the other sequences corresponded to the amino acid sequences analyzed by LC-MSMS.

Finally, as *Xenopus* phosvitin as well as lipovitellins originates in the oocyte during VTG cleavage, we extracted phosvitin from egg lysates to investigate whether or not it is contained in the MALDI/MS spectra shared by the 117-kDa polypeptide, the 120-kDa band and gps 200–270/260. Separation of the sample by SDS-PAGE identified a molecule of approximately 50 kDa that was heat-stable and typically stained by stains-all due to the high content of phosphorylated amino acids (see Romano et al., 2004). The

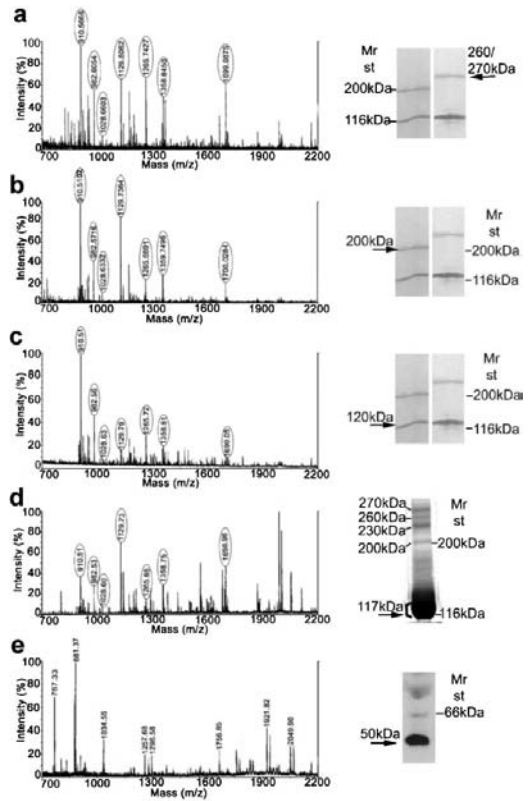


Figure 2. Spectra obtained by MALDI/MS analysis of trypsin digests of gp 270/260 (a), gp 200 (b), gp 120 (c), 117 band (d), and phosvitin (e). Samples of proteins utilized for the analyses are indicated in the corresponding gels on the right side of each diagram, where M_r standards of 66, 116, and 200 kDa are also indicated. Spectra in a, b, c, d are characterized by the same peaks. Some of these peaks are encircled. The spectra are shown from 700 (*m/z*) to 2,200 (*m/z*) because typical peaks are found in this range of values. The phosvitin spectrum in (e) does not show the same peaks as spectra a–d.

analysis by MALDI/MS showed that the *D. pictus* phosvitin spectrum does not share similarities with the previously identified spectra (Fig. 2e). Overall, we concluded that the sequence we analyzed shared by the 120-kDa polypeptide deriving from gps 200 and 270/260 and the 117-kDa lipovitellin represents a single protein of the lipovitellin family, namely a lipovitellin 1 (DpLIV), because of its M_r and its position at the N-terminus, as compared to *X. laevis* VTGA2. Because gps 200–270/260 have spectra super-imposable on DpLIV spectrum, where the phosvitin sequence was not found, the overall data indicate that they are dimers of DpLIV. At present, it cannot be concluded

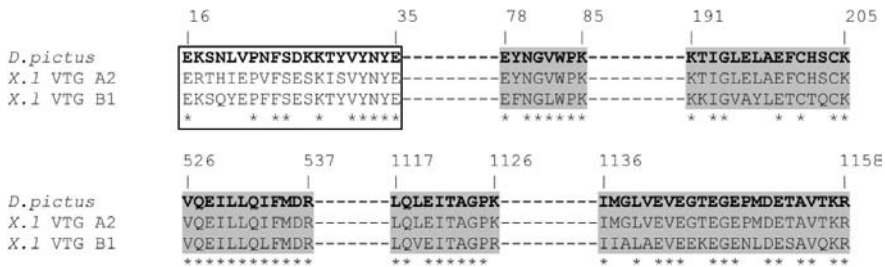


Figure 3. CLUSTAL W alignment of *X. laevis* VTG B1 and VTG A2 amino acid sequences compared with the partial sequence of the *D. pictus* 117 kDa protein obtained by LC-MSMS analysis of the trypsin digest. The 19-aa sequence of *D. pictus* gp 120, 200, and 260/270 obtained by N-terminal sequencing is boxed. The amino acid short sequences detected by LC-MSMS analysis are shaded gray. Amino acids identical in all compared sequences are indicated by asterisks.

whether the dimers are present in natural conditions or are formed during sample preparation. Interestingly, in SDS-PAGE in reducing conditions, the 200, 230, 260, and 270 bands are barely detectable (Maturi et al., 1998). Their different M_r are likely due to the fact that these gps are glycosylated differently, as it has been previously shown (Maturi et al., 1998). Hereafter, the complex of the DpLIV glycoforms will be referred to as DpLIVs.

Sperm Binding Assays

Previous data showed that sperm bind beads coated with the 117-kDa band electroeluted from SDS-PAGE of the egg lysate at a percentage similar to BSA-coated beads (Maturi et al., 1998). This prompted us to compare the sperm-binding ability of beads coated with the 117-kDa band electroeluted from gels of egg lysate, with that of beads coated with the 120-kDa band, gp 200 or gp 270/260 after electroelution from gel-into-gel experiments. We know from earlier work utilizing glycoproteins electroeluted directly from gels of egg lysates, that significant sperm binding to gp200 beads occurs before the acrosome reaction ($76 \pm 5\%$ and $25 \pm 2\%$ for sperm binding after the acrosome reaction), while the opposite is true for gp270/260 beads ($73 \pm 1\%$ for sperm binding after and $23 \pm 4\%$ for sperm binding before the acrosome reaction) (Maturi et al., 1998). Similarly here, for the gp 200 beads, the percentage of beads with untreated sperm was significantly higher than with spermatozoa treated with A23187 Ca-ionophore ($64 \pm 2\%$, vs. $33 \pm 1\%$ for sperm binding after the acrosome reaction) (Fig. 4). For gps 270/260, the percentage of beads with sperm was higher for A23187-treated spermatozoa with respect to the trial with untreated sperm (respectively, $49 \pm 5\%$ and $33 \pm 5\%$) (Fig. 4). However, the percentage of beads with sperm treated with A23187 was evidently lower (about 24%) than in the above-mentioned data from Maturi et al. Therefore we performed experiments where the gps 270/260 were electroeluted directly from the first gel, utilizing the same samples we used for gel-into-gel experiments. The resulting percentage of beads with sperm treated with

A23187 was then $70 \pm 4\%$ versus $31 \pm 3\%$ for untreated sperm (Fig. 4). These data indicate that the sperm-binding ability of the highly glycosylated gps 270/260 is partially impaired following the second gel run, whereas the sperm-binding ability is less affected for the minorly glycosylated gp 200. Overall, this suggests that the glucidic portion of the glycoconjugates may be affected by the second gel run. In the case of the 120-kDa band and of the 117-kDa lipovitellin, the percentage of beads with sperm was barely higher than for BSA-coated beads (Fig. 4). Interestingly, the 120-kDa band is mildly reactive with *Ulex europaeus* agglutinin I

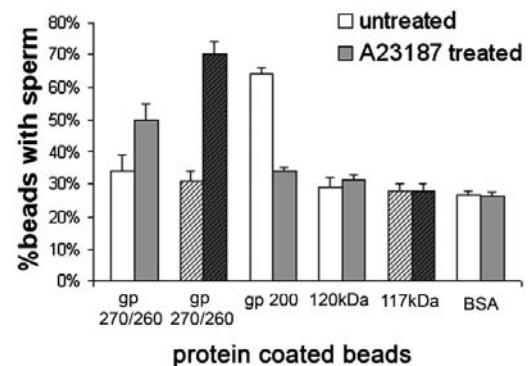


Figure 4. Quantification of the mean percentage of beads with sperm, as counted in sperm-binding assays. A23187-exposed and unexposed sperm were utilized. Beads were coated with gp 270/260, gp 200 or the 120-kDa band electroeluted from gels. Columns without stripes indicate samples obtained by gel-into-gel experiments. Columns with stripes indicate samples obtained from only one gel run. In particular, data concerning the 120-kDa bands deriving from gp 200 and gps 270/260 were pooled together as they were practically indistinguishable. Beads were also coated with the 117-kDa band electroeluted from gels of egg lysates or with commercial BSA. Bars represent standard deviation with $n = 4$.

(UEA-I), while the 117-kDa band is strongly reactive to the same lectin (data not shown and see Fig. 3, Maturi et al., 1998). The data suggest that DpLIVs are active in sperm binding only in dimers and that fucosylation of these molecules is not sufficient for significant sperm binding to occur.

VTG in Blood Serum and Yolk Proteins in Oocytes

To further understand the relationship between DpLIVs and liver-derived VTG, vitellogenin was extracted from serum of *D. pictus* adults following injection with β -estradiol, and analyzed by SDS-PAGE and Western blots with antiserum directed against *Triturus* VTG (anti-TcVTG). Only two bands of 200/210 kDa cross-reacted with anti-TcVTG (Fig. 5a) and have M_r values in the range of those reported for *X. laevis* VTGs (Gerber-Huber et al., 1987; Yoshitome et al., 2003). Therefore, the highly glycosylated 270- and 260-kDa glycoproteins present in *D. pictus* eggs by SDS-PAGE gels were not found in blood. We then analyzed the oocytes to determine when the latter bands become detectable during oogenesis but prior to their final exposure at the membrane surface, where glycosylation may occur as well (Kohler and Bertozzi, 2003). In lysates of pre-vitellogenic oocytes, that is, oocytes not yet able to incorporate VTG from the bloodstream, bands of 117 and 200 kDa were observed, both of which were cross-reactive with anti-TcVTG in Western blots (Fig. 5b,c). In lysates of fully grown oocytes, that is, oocytes where VTG uptake and splicing into lipovitellins and phosvitins had occurred, the pattern of anti-TcVTG-reactive bands found is identical to that found in uterine eggs, comprising bands of 117, 200, 230, 260, and 270 kDa (Fig. 5b,c). These observations suggest that in addition to the typically liver-derived lipovitellin (Andreuccetti and Campanella, 1982), in *D. pictus*, lipovitellin is also synthesized by the early oocytes and that its dimers are detectable in the oocyte later in oogenesis.

Therefore, the fully grown oocyte appears to contain DpLIVs of different origin.

Immunofluorescence and Immuno-Gold

Localization of DpLIVs

The Western blots presented in Figure 5 show that anti-TcVTG specifically binds to the SDS-PAGE-separated bands that were identified in this study as DpLIVs by N-terminal sequencing and MALDI/MS. Frozen sections of *D. pictus* eggs stained with the same antibody show, as expected, strong fluorescence in the yolk platelets (Fig. 6a). Importantly, in Figure 5a, the dimple border is also immunostained by the antiserum. The staining is specific, as shown by comparison to negative controls (Fig. 6b). According to sulfo-NHS-biotin assays (Maturi et al., 1998), gps 200, 260, and 270 are exposed at the dimple surface, and our present data indicate that these gps are DpLIV dimers. Therefore, it appeared of fundamental importance to perform whole-mount immunofluorescence to determine if the gps cross-reacting with the antiserum are located at the surface of the dimple. Upon removal of the external coats, which is necessary for correct preparation of the samples, the dimple becomes superficial and assumes variable configurations. At the egg surface, the antiserum reactive site was D1 (Fig. 6c,d), which is the dimple center, with a diameter of approximately 200 μ m. When samples were tilted to achieve a full upper view of the dimple, strong immunofluorescence was observed in D1, in particular at a spot at its center (see Nuccitelli et al., 1988) (Fig. 6e). This staining was specific (Fig. 6f) and showed a pattern comparable to that obtained following exposure to a terminal fucose-specific lectin (Denis-Donini and Campanella, 1977). Early studies showed that, following ovulation, the dimple forms from the oocyte region at the animal pole (*germinative area*, GA) because of the insertion of peripheral vesicle membranes. As a result, the oocyte membrane

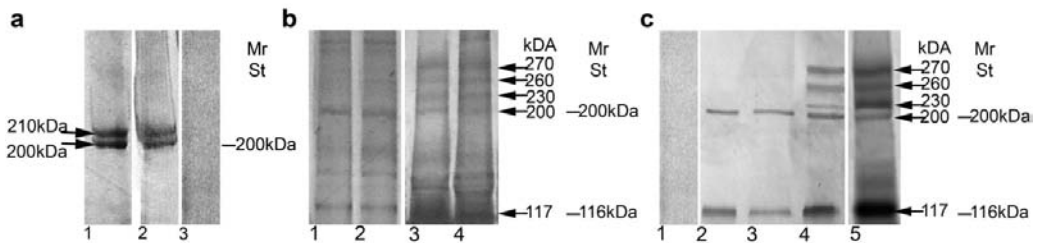


Figure 5. SDS-PAGE and immunoblots of VTG, pre-vitellogenic, vitellogenic oocytes and uterine eggs exposed to anti-TcVTG. **a:** liver-synthesized VTG, as extracted from the serum of estrogen-injected *D. pictus* adults and run in SDS-PAGE (1) shows two bands of 200–210 that are reactive with anti-TcVTG in Western blots, indicating the specificity of the antiserum (2). In Western blot controls exposed to pre-immune serum, the bands are absent (3). **b:** SDS-PAGE of stage I (1), stage II (2), stage VI (3), and uterine eggs (4), indicating that in stage I–II, two bands are present of 200 and 117 kDa, while in stage V and in uterine eggs, gps 230, 260, 270 are also present. **c:** Corresponding Western blots of gels shown in (b). In (1) control blot exposed to pre-immune serum: bands are absent. In (2; stage I oocytes) and (3; stage II oocytes) the 200- and 117-kDa bands cross-react with anti-TcVTG. In stage V oocytes and uterine eggs (respectively 4–5), the 230–260–270 bands cross-react with anti-TcVTG, in addition to bands 117 and 200. M_r standards are indicated.

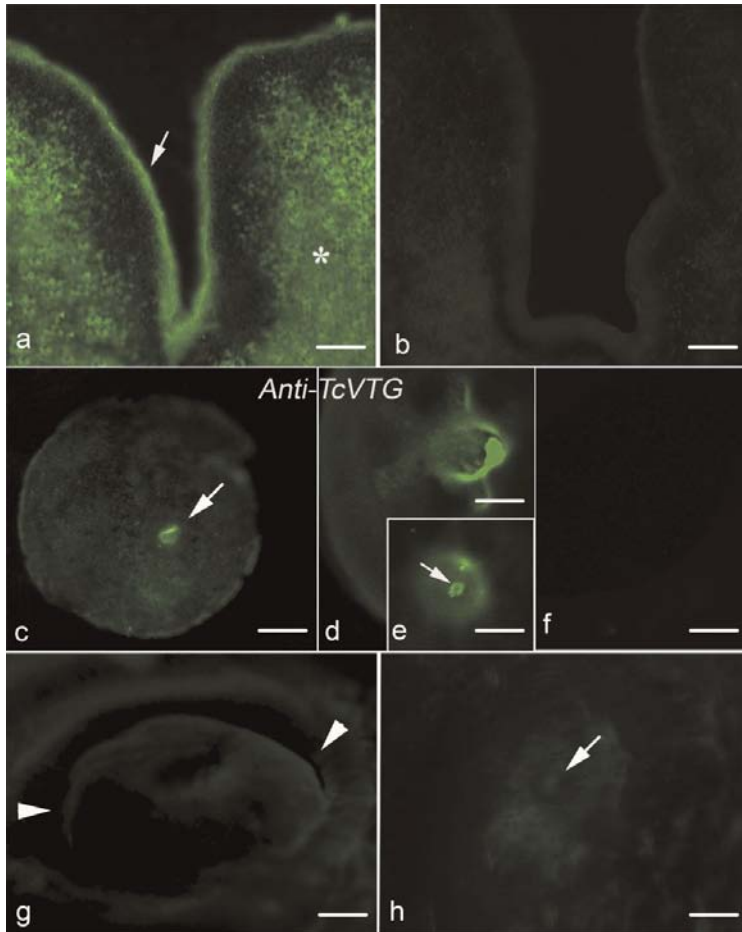


Figure 6. Immunofluorescence in sections or in whole mounts using anti-TcVTG. **a:** In frozen sections of the dimple, immunofluorescence is present in the yolk platelets (asterisk) and in the dimple periphery (arrow). **b:** Control section incubated with pre-immune serum: immunostaining is absent. Bars in **b** and **c** = 40 μm . **c:** Whole mount of uterine eggs. The dimple region is the immunofluorescent area (arrow). Bar = 400 μm . **d,e:** Higher magnifications of the immunoreactive dimple region in a view showing the walls of the dimple (**d**) and an upper view (**e**), where a strongly fluorescent spot is centrally located (arrow). Bars in **d**, **e** = 125 μm . **f:** Control whole mount where the uterine egg was exposed to pre-immune serum. Immunostaining is absent. **g:** Ovarian oocyte area germinativa (arrowheads), which is a disc of approximately 900 μm at the animal pole that is extruded following removal of the vitelline envelope. Immunostaining is practically absent. Bars in **f** and **g** = 160 μm . **h:** Here, the dimple has regressed as a result of fertilization and an inconspicuous immunofluorescence using anti-TcVTG is observed. Bar in **h** = 110 μm .

acquires a new glycocalyx and the ability to bind the lectin specific for terminal fucose (Denis-Donini and Campanella, 1977). Here, we showed that in the GA, there was no immunofluorescence upon staining with anti-TcVTG (Fig. 6g). Moreover, following fertilization and vesi-

cle trafficking (Talevi et al., 1985), most of the dimple region lost the ability to bind anti-TcVTG (Fig. 6h). It was earlier shown that after fertilization, the dimple region loses the affinity for the lectin specific for terminal fucose (Denis-Donini and Campanella, 1977). Therefore

the anti-TcVTG reacting molecules and terminal fucose are transiently present at the surface of the dimple region only in the unfertilized egg.

In ultrathin sections of the dimple processed with an immuno-gold staining procedure, the anti-TcVTG immunostaining was specific, though not abundant (Fig. 7a–c). Interestingly, the 10-nm gold particles were observed in the dimple glycocalyx branching at the plasma membrane, as shown in Figure 7a, where the particles decorate two such branches in a single file arrangement. Significantly, immunostaining was also found in the peripheral vesicles, where previous reports also showed the presence of UEA-I-binding glycoproteins (Gualtieri and Andreuccetti, 1996; Maturi et al., 1998).

DISCUSSION

In *D. pictus*, the 200, 270, and 260 gps are candidate molecules for mediating sperm/egg binding in natural conditions because they specifically bind spermatozoa in *in vitro* assays (Maturi et al., 1998). Here, we characterized the protein backbone of these glycoconjugates. Various molecular approaches lead us to conclude that gps 200 and 270/260 contain the same molecule, a lipovitellin 1. First, N-terminal sequencing of gps 200 and 270/260, as well as the 120-kDa polypeptide derived from our gel-into-gel experiments, indicated that they all contain the same N-terminus. Moreover, the amino acid residue sequence shows identity to that of *X. laevis* VTG B2 and VTGB1, as well as to the lipovitellin 1 located at the N-terminus of VTG A2 (Gerber-Huber et al., 1987). Second,

MALDI/MS analyses of *D. pictus* gps 270/260, gp 200, the 120-kDa band and the 117-kDa lipovitellin derived from egg extracts all presented super-imposable MALDI spectra. Third, a trypsin digest of the 117-kDa lipovitellin analyzed through LC-MSMS resulted in five sequences that were identified as part of the *X. laevis* VTG A2 precursor sequence. The amino acid residues identified by N-terminal analysis align with the N-terminus of *Xenopus* VTG A2. Importantly, the *D. pictus* phospho spectrum was not included in the MALDI/MS spectra of all of the analyzed proteins. We concluded that the 120-kDa polypeptides deriving from gp 200 and gps 270/260 and the 117-kDa lipovitellin are the same molecule, DpLIV. This molecule belongs to the lipovitellin 1 family and is able to form variously glycosylated dimers. DpLIV forms the dimers of 200, 260, 270 and, likely, of 230 kDa either in natural conditions or during sample preparation. The following considerations argue against the possibility that lipovitellin 1 is a contaminant of the PAGE-separated bands that we studied: N-terminal sequencing of the 200-, 260-, and 270-kDa bands after the release of the 120-kDa band identified a single amino-acid sequence showing identity with that of lipovitellin 1, which was further analyzed by MALDI/MS and LC-MSMS; the 200-, 260-, and 270-kDa bands were found in samples of the yolk-poor cortices but not in the yolk-rich bulk of the cytoplasm (Maturi et al., 1998).

As shown through anti-TcVTG Western blots of pre-vitellogenic and vitellogenic oocytes, DpLIVs derive not only from canonical VTG cleavage but also from synthesis occurring in the oocyte before VTG uptake by micropinocytosis. Although present in the cortex of the

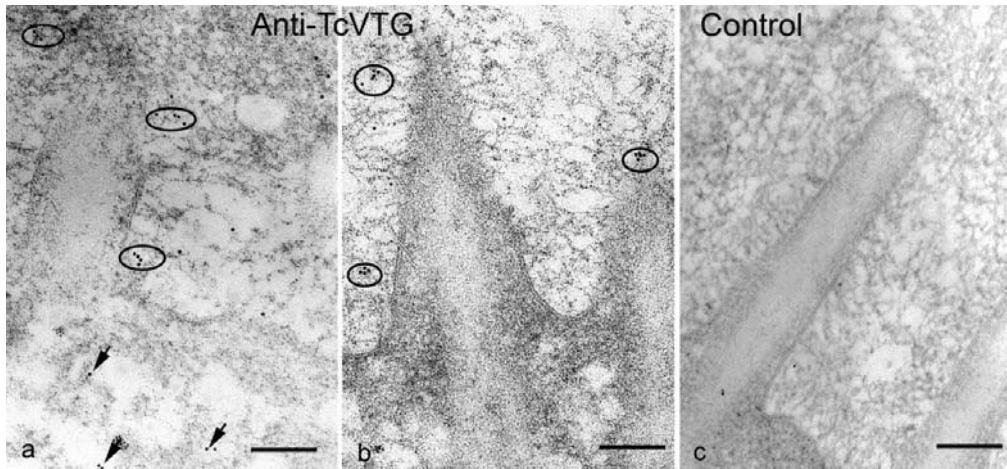


Figure 7. Immunogold labeling of ultrathin sections utilizing anti-TcVTG. **a,b:** Microvilli of the dimple with long branched glycocalyx. Some gold particles are present in the glycocalyx, exhibiting a single file pattern associated with some glycocalyx filaments (circles in a and in b). The arrows indicate gold particles located in cortical vesicles. Bar = 120 nm. **c:** Control section incubated with pre-immune serum. Few gold particles are seen. Bar = 250 nm.

whole egg, gps 200–270 are exposed extracellularly, specifically on the plasma membrane of the dimple (Maturi et al., 1998). It is not clear at present if the ability to form dimers is specific to DpLIVs destined to be exposed at the dimple surface. It was previously shown in *D. pictus* oocytes that the germinative area concentrates numerous actively secreting Golgi apparatuses (Andreuccetti and Campanella, 1980). The dimple forms from this region, exhibiting specifically glycosylated DpLIV dimers: gp 270 rich in terminal mannose (Maturi et al., 1998) and gp 230 rich in sialic acid linked to galactose, as indicated by cross-reactivity to *Maackia amurensis* agglutinin (Campanella, unpublished results). It is important to stress here that the four main bands of 200, 230, 260, and 270 kDa labeled by sulfo-NHS-biotin in our previous studies were derived from the dimple surface of eggs in which the plasma membrane remained in excellent condition during manual operations and, therefore, was not leaking yolk lipovitellins (see Maturi et al., 1998).

The immunostaining data presented in this paper appear to be of particular significance. Experiments using anti-TcVTG in whole-mount samples clearly indicated that the only site where the staining was found was D1, the central portion of the dimple; this staining is absent before the dimple forms, decreases following fertilization and coincides with the cross-reactivity of a lectin specific for terminal fucose and similar to UEA-I (Denis-Donini and Campanella, 1977). In particular, immunogold labeling indicated that the glycocalyx of the dimple microvilli may cross-react with anti-TcVTG. A similar ultrastructural approach showed that the dimple glycocalyx is rich in UEA-I-reactive glycoproteins (Gualtieri and Andreuccetti, 1996). The dimple microvilli form following exocytosis of vesicles labeled with the lectin specific for terminal fucose (Denis-Donini and Campanella, 1977), and our data show that similar vesicles are still present in the dimple and are labeled by anti-TcVTG-gold.

Do DpLIVs originate from the liver, similar to the typical yolk-component lipovitellin 1? In oocytes taking up VTG by receptor-mediated micropinocytosis, yolk proteins are released into multi-vesicular bodies that later coalesce to form primordial yolk platelets in *D. pictus*, as in other amphibian species (Andreuccetti and Campanella, 1982; Opresko and Wiley, 1987). Our data indicate that before incorporation of the 200–210-kDa VTGs, the oocyte lysates already contain anti-TcVTG-reactive bands of 120 and 200 kDa. Therefore, oocyte-synthesized lipovitellin 1 is present in the oocyte together with liver-synthesized lipovitellin 1 (see also Wallace and Selman, 1990). As specific labeling of lipovitellins cannot be performed during the long-lasting amphibian oogenesis, we cannot conclude whether the DpLIVs exposed at the plasma membrane during dimple formation derive from the liver or from the oocyte. However, we reason that liver-synthesized lipovitellin, which is targeted specifically to an intracellular route for yolk formation, should escape the yolk pathway and go back to the Golgi apparatus for further glycosylation to be exposed again to the plasma membrane. The oocyte-synthesized DpLIVs would be expected to follow a more direct pathway of glycosylation and exocytosis.

In conclusion, DpLIVs may have a different origin during oogenesis and a different location in the egg, probably because of specific glycosylation. DpLIV constitutes the protein backbone of the terminal fucose-containing glycoconjugates exposed at the dimple surface. We previously reported that gp 200-coated beads specifically bind acrosome-unreacted sperm, whereas gp 270/260-coated beads bind acrosome-reacted sperm. In these assays, gps 200 and 270/260 competitively inhibited sperm binding to the beads coated with the corresponding glycoprotein. These data suggested that binding to the sperm plasma membrane or inner acrosome membrane may depend upon the types of oligosaccharide exposed by gps 200 and 270/260 (Maturi et al., 1998). Our in vitro sperm-binding assays indicate that DpLIV is not active or sufficient for sperm binding in its monomeric form, nor is the presence of the sugar moiety recognized by UEA-I. New experimentation is needed to ascertain which sugars are necessary for binding reacted or unreacted sperm. Interestingly, we previously observed that terminal fucose of gp 200 cannot be detected by lectin blots but can be by affinity chromatography, in contrast to gps 270/260, suggesting that these glycoproteins might have reactive sites for UEA-I differently available or affected according to the method used (Maturi et al., 1998).

The fact that lipovitellin 1 appears to constitute the backbone of the dimple glycoproteins is certainly surprising. It is similarly surprising that in *Xenopus* oocytes, phosphorylated lipovitellin 1 associates with Grb2 in the cytosol during the G2/M transition and constitutes the starting point for a recently discovered pathway in which PLC- γ 1 binds Grb2 and recruits Sos (Browaeys-Poly et al., 2007). Moreover, for more than two decades, lipovitellin 1 has been known as an efficient binder of ions such as Zn²⁺ and Cd²⁺ (Sunderman et al., 1995) and a natural linker of follistatin (Okabayashi et al., 1996), BMP-4, activin-A (Iemura et al., 1999), and calmodulin (Molla et al., 1983).

MATERIALS AND METHODS

Animals

Adult *D. pictus* were maintained and utilized at the University of Naples Federico II, according to the guidelines of the University Animal Welfare Office and in agreement with international rules. Oocytes were excised from the ovaries of females anaesthetized with MS222 (Sigma Chemical Co, St. Louis, MO). Uterine eggs were obtained about 18 hr following the injection of females with 250 units of Profase HP (Serono, Rome, Italy) in Ringer's solution (111 mM NaCl, 1.3 mM CaCl₂, 2 mM KCl, 0.8 mM MgSO₄, 25 mM HEPES, pH 7.8). Spermatozoa were collected from the male seminal vesicles (see Maturi et al., 1998).

Sample Preparation for SDS-PAGE and Western Blot

We used oocytes in early vitellogenesis, fully grown oocytes, coelomic oocytes and uterine eggs. Somatic tis-

sue (ovarian epithelia, theca and follicle cells) was removed from the oocytes by exposure to 0.04% collagenase Type XI (Sigma Chemical Co), 20 U/ml hyaluronidase and 10 µg/ml proteinase K (Sigma Chemical Co) in Ringer's solution. The oocytes were homogenized in 25 mM HEPES buffer pH 7.5 containing 900 mM glycerol, 0.02 mM Na₃N, 1 mM ATP, 1 mM DTT, 5 mM EGTA 1% SDS and protease inhibitors (2 mM TAME, 5 mg/ml SBTI, 5 µg/ml aprotinin and 10 µM E64, Sigma Chemical Co). Uterine eggs were homogenized following removal of the jelly coats. After centrifugation at 15,000g for 40 min, the supernatant protein concentration of the eggs or oocytes was determined using the BCA protein assay reagent (Pierce, Rockford, IL). Following mixing of the protein with sample buffer and heating at 90°C, aliquots of 40–80 µg were analyzed on a SDS–PAGE 5–10% polyacrylamide gels under non-reducing conditions using standard Tris–glycine buffer and utilizing molecular mass standards (200, 116, 97, 45, 31, 21, 14 kDa; Bio-Rad, Hercules, CA). Proteins were detected by Coomassie or silver staining.

Western blotting on a nitrocellulose membrane was performed as in Maturi et al. (1998). The nitrocellulose membrane was incubated with an antiserum directed against *Triturus carnifex* VTG (anti-TcVTG, 1:500 dilution, v/v; Mosconi et al., 1998) pre-absorbed with *D. pictus* serum, followed by incubation with alkaline phosphatase-conjugated anti-rabbit IgGs. In control experiments, incubation with the primary antibody was omitted or substituted with pre-immune rabbit serum incubation.

N-Terminal Analysis

Following SDS–PAGE in non-reducing conditions, samples of gps 200, 260, and 270 were blotted onto a PVDF membrane (Millipore, Bedford, MA). The transfer buffer contained CAPS 3-(cyclohexylamino)-1-propanesulfonic acid 10 mM pH 11 and 10% methanol in MilliQ water. The PVDF membranes were stained with Coomassie blue, destained with methanol and washed extensively in MilliQ water. The bands of interest were directly loaded onto a Precise 492 automated protein sequencer (Applied Biosystems, Foster City, CA). Additionally, 7–8 bands of gp 200 or gps 270/260 were excised from the gels and charged onto a new gel under non-reducing conditions (gel-into-gel experiments). A 120-kDa polypeptide band was recovered and blotted, and the N-terminal analysis was performed as described.

Matrix-Assisted Laser Desorption Ionization Mass Spectrometry (MALDI/MS) and Liquid Chromatography Tandem Mass Spectrometry (LC-MS/MS) Analyses

Selected protein bands stained with Coomassie were excised from the gels of egg lysates or of gel-into-gel samples. The bands were digested and analyzed as described in the supplementary data of Zito et al. (2007). MALDI mass spectra were recorded on an Applied Biosystem Voyager DE-PRO mass spectrometer equipped with a reflectron analyzer used in delayed extraction mode. The

peptide mixture of the 117-kDa band was also analyzed by LC-MS/MS using the LC/MSD Trap XCT Ultra (Agilent Technologies, Palo Alto, CA) equipped with an 1100 HPLC system and a chip cube (Agilent Technologies) (for more details see Zito et al., 2007).

In Vitro Sperm-Binding Assay

The eluted proteins were adsorbed on 300–400 µm polystyrene beads according to the supplier's instructions (Polysciences, Warrington, PA), utilizing 0.1 M borate buffer, pH 8.5. About 800 beads were used for each adsorption experiment. Equimolar amounts of electroeluted glycoproteins or BSA were used. Glycoproteins eluted in five separate sets of elution were utilized for adsorption. We used a specific assay developed to estimate sperm–egg binding, as thoroughly described in Maturi et al. (1998).

VTG Extraction

VTG was recovered from the blood of ovariectomized females or from males upon injection with β-estradiol (40 µg for 1 g body weight). For extraction of VTG from serum, the method of Wiley and Wallace (1978) was used. For phosphovitin extraction from egg lysates, the procedure of Burley and Cook (1961) was applied following lysis of yolk platelets. Precipitation by (NH₄)₂SO₄, followed by centrifugation at 12 500 g and pellet suspension in Tris–HCl 0.05 M was used for separation and recovery of lipovitellin and phosphovitin (Limatola et al., 2001).

Immunofluorescence and Electron Microscopy

For whole-mount staining, *D. pictus* coelomic oocytes and dejellied unfertilized and fertilized eggs were fixed for 1 hr in 4% formaldehyde at 4°C and stored in 100% MeOH at –20°C. For immunofluorescence experiments, 8-µm-thick frozen sections of samples embedded in Killik (Bio Optica, Milan, Italy) were obtained. Non-specific background staining was blocked by incubating the samples in PBS containing 3% normal goat serum, 0.5% BSA, and 0.1% Triton. The samples were then exposed overnight at 4°C to anti-TcVTG antiserum (1/300, v/v) pre-absorbed with *D. pictus* serum, followed by anti-rabbit goat IgG conjugated with BODIPY FL (Invitrogen Molecular Probes, Carlsbad, CA); 0.5% BSA and 0.1% Tween were added to both primary and secondary antibodies. For whole-mount samples, UEA-I conjugated to fluorescein was also used together with specificity controls (Maturi et al., 1998). The samples were then observed and photographed under a Leica MZ 16F UV stereomicroscope. After mounting in PBS/glycerol (9:1, v/v) the sections were photographed under a Zeiss UV Axioskop microscope equipped with a Progress 3800 color video camera and KS300 image analysis software. For electron microscopy, samples were fixed and embedded in Epon 812 as in Talevi et al. (1985) with omission of OsO₄. Thin sections were collected onto copper grids and deplasticized (Jeffrey and Goodsir, 1996) to optimize antibody penetration into the tissue. Anti-TcVTG antibodies pre-absorbed with *D. pictus* serum were used for incubating the sections

at the dilution of 1:300 (v/v) in 0.1% BSA containing TBS. The secondary antibody was anti-rabbit IgG conjugated with 10-nm colloidal gold.

ACKNOWLEDGMENTS

This paper is dedicated to colleagues who have inspired (N. L. Cross, J. L. Hedrick, D. Epel, Y. Iwao, V. D. Vacquier, and many others) or participated in the study of *D. pictus* fertilization (S. Denis, P. Andreuccetti, R. Talevi, R. Gualtieri, G. Gabbiani, B. Dale, R. Nuccitelli, W. B. Busa, D. Kline, W. J. Lennarz, and others) and to the memory of C. Katagiri, A. Monroy, and G. Ghiara. We thank Dr. Gennaro Marino and Dr. Piero Pucci for suggestions and Mark Walters for editing the manuscript. This work was supported, in part, by AMRA Scarl and Regione Campania (L.5 funds).

REFERENCES

- Andreuccetti P, Campanella C. 1980. Origin and cytochemistry of the animal dimple granules in *Discoglossus pictus* (Anura) eggs. *J Embryol Exp Morphol* 56:239–252.
- Andreuccetti P, Campanella C. 1982. Regional differences in the pattern of vitellogenesis in the painted frog *Discoglossus pictus*. *Tissue Cell* 14:681–690.
- Browaeys-Poly E, Broutin I, Antoine AF, Marin M, Lescuyer A, Vilain JP, Ducruix A, Calliau K. 2007. A non-canonical Grb2–PLC- γ 1–Sos cascade triggered by lipovitellin 1, an apolipoprotein B homologue. *Cell Signal* 19:2540–2554.
- Burley RW, Cook WH. 1961. Isolation and composition of avian egg yolk granules and their constituent α and β lipovitellins. *Can J Biochem Physiol* 39:1295–1307.
- Campanella C, Carotenuto R, Infante V, Maturi G, Atripaldi U. 1997. Sperm–egg interaction in the painted frog *Discoglossus pictus*. *Mol Reprod Dev* 47:323–333.
- Cho C, Bunch DO, Faure JE, Goulding EH, Eddy EM, Primakoff P, Myles DG. 1998. Fertilization defects in sperm from mice lacking fertilin beta. *Science* 281:1857–1859.
- Denis-Donini S, Campanella C. 1977. Ultrastructural and lectin binding changes during the formation of animal dimple in oocytes of *Discoglossus pictus*. *Dev Biol* 61:140–152.
- Ellerman DA, Ha C, Primakoff P, Myles DG, Dveksler GS. 2003. Direct binding of the ligand PSG17 to CD9 requires a CD9 site essential for sperm–egg fusion. *Mol Biol Cell* 14:4098–4103.
- Evans JP. 2002. The molecular basis of sperm–oocyte membrane interactions during mammalian fertilization. *Hum Reprod Update* 8:297–311.
- Gerber-Huber S, Nardelli D, Haefliger JA, Cooper DN, Givel F, Germond JE, Engel J, Green NM, Wahli W. 1987. Precursor-product relationship between vitellogenin and the yolk proteins as derived from the complete sequence of a *Xenopus* vitellogenin gene. *Nucleic Acids Res* 15:4737–4760.
- Glabe CG, Grabel LR, Vacquier VD, Rosen SD. 1982. Carbohydrate specificity of sea urchin sperm bindin: A cell surface lectin mediating sperm–egg adhesion. *J Cell Biol* 62:123–128.
- Gualtieri R, Andreuccetti P. 1996. Localization of egg-surface carbohydrates and fertilization in *Discoglossus pictus*. *Cell Tissue Res* 283:173–181.
- Howell BW, Herz J. 2001. The LDL receptor gene family: Signalling functions during development. *Curr Opin Neurobiol* 11:74–81.
- Iemura S, Yamamoto TS, Takagi C, Kobayashi H, Ueno N. 1999. Isolation and characterization of bone morphogenetic protein-binding proteins from the early *Xenopus* embryo. *J Biol Chem* 274:26843–26849.
- Inoue N, Ikawa M, Isolani A, Okabe M. 2005. The immunoglobulin superfamily protein Izumo is required for sperm to fuse with eggs. *Nature* 434:234–238.
- Iwao Y, Fujimura T. 1996. Activation of *Xenopus* eggs by RGD-containing peptides accompanied by intracellular Ca $^{2+}$ release. *Dev Biol* 177:558–567.
- Jeffrey M, Goodsir M. 1996. Immunohistochemistry of resinated tissues for Light and Electron Microscopy. *Methods Mol Med* 3:301–312.
- Kamei N, Glabe CG. 2003. The species-specific egg receptor for sea urchin sperm adhesion is EBR1, a novel ADAMTS protein. *Genes Dev* 17:2502–2507.
- Kohler JJ, Bertozzi CR. 2003. Regulating cell surface glycosylation by small molecule control of enzyme localization. *Chem Biol* 10:1303–1311.
- Levy S, Shoham T. 2005. Protein-protein interactions in the tetraspanin. *Web Physiol* 20:218–224.
- Limatola E, Rosanova P, Anteo C, De Nardo M, Marciano R, Malanga M, Alviggi E, Romano M. 2001. Oocytes and egg yolk proteins in the lizard *Podarcis sicula*. In: Th Goos HJ, Rastogi RK, Vaudry H, Pierantoni R, editors. *Perspective in comparative endocrinology: Unity and diversity*. Bologna: Monduzzi. pp 1135–1141.
- Mahbub Hasan AK, Ou Z, Sakakibara K, Hirahara S, Iwasaki T, Sato K, Fukami Y. 2007. Characterization of *Xenopus* egg membrane microdomains containing uroplakin Ib/III complex: Roles of their molecular interactions for subcellular localization and signal transduction. *Genes Cells* 12:251–267.
- Maturi G, Infante V, Carotenuto R, Focarelli R, Caputo M, Campanella C. 1998. Specific glycoconjugates are present at the oolemma of the fertilization site in the egg of *Discoglossus pictus* (Anurans) and bind spermatozoa in an in vitro assay. *Dev Biol* 204:210–223.
- Miller BJ, Georges-Labouesse E, Primakoff P, Myles DG. 2000. Normal fertilization occurs with eggs lacking the integrin alpha6-beta1 and is CD9-dependent. *J Cell Biol* 149:1289–1296.

The calcium and ER story

This story also started in the Department of Zoology, Ann Arbor, Michigan, between 1966 and 1968. I was following a class in *Physiology of the Cell* and became quite interested in ionic exchange occurring in the cells, when activated. While working on nicotine-induced-polyspermy in *Rana pipiens* eggs, I started to suspect that nicotine was altering the fertilization potential of the egg, thus making the egg polyspermic. About ten years later Laurinda Jaffe demonstrated that in sea urchins the change in the fertilization potential caused by the penetrating sperm impedes the penetration of other spermatozoa. However, my main 'love' was Ca^{2+} . In the University Library I found some publications by L.V. Heilbrunn who, before the Second War, pioneered theories about the role of the calcium increase in many cell events, including fertilization. His fervour in describing or making conjectures led me even to dream about this event at fertilization. Sometimes I had the impression to be... within the cell and see the dramatic changes in the gel/sol status caused by this ion.

Much of the following story is linked to Alberto Monroy. Together with Albert Tyler, Alberto was one of the first to explore fertilization potential. Through this paper and Alberto's book: "Chemistry and Physiology of fertilization", that was lying on George Nace's desk, I got to know this Italian scientist who was considered one of the foremost scholars in the field of fertilization. I met Alberto and Anna Monroy, as well as Giovanni and Anna Giudice, in Woods Hole, in 1967. I have very pleasant memories about that stay, as Alberto and Anna, Giovanni and Anna were quite informal and friendly to me in a way I had never experienced with senior professors in Italy.

I returned to Naples in 1968. About one or two years later Alberto founded the L.E.M. in Naples and together with Suzanne became interested in the *Xenopus* egg activation reaction. He asked me to do some ultrastructural studies on the *Xenopus* egg before and after fertilization. Piero and I performed that work. I used to watch the micrographs very carefully and I kept on thinking: "how can the cortical granules be extruded following the command of sperm entry?" Suddenly, the penny dropped: the cortical granules were surrounded by an endoplasmic reticulum that was forming an interconnected cisternae system in the cortex and in the deeper peripheral cytoplasm where whorls of cisternae are located. Following fertilization, the granules are exo-

cytozed and, interestingly, the cisternae change their arrangement drastically. It was clear to me that the ER was a reservoir of calcium, as the sarcoplasmic reticulum, and that sperm activation was producing calcium release from the ER, thus making CG exocytosis occur. I ran immediately to Piero and to Gianfranco Ghiara to tell them about this hypothesis.

Months later, while sitting at his desk at the A. Dohrn Marine Biology Station, Alberto informed me of a coming meeting on fertilization organised by David Epel at La Jolla, California. I believe my face turned almost apoplectic with enthusiasm when he told me. To my delight, Gianfranco Ghiara, Alberto, and David suggested I went to the conference! It was one of the most important and exciting events in my scientific life.

At La Jolla, I met all the scientists whose papers I was familiar with. I could not believe that they were all there! Garth L. Nicholson (who had recently authored with S. J. Singer the plasma membrane fluid mosaic model) was chairing the final session. He made several concluding remarks and challenged the audience with important questions. He asked whether anybody guessed what made the cortical granules exocytose at fertilization. I stood up. He invited me to talk, while Alberto, who was sitting next to me, was staring at me both puzzled and concerned. I drew on the blackboard the model I had in mind, while the audience fell completely silent. When I finished, they were all enthusiastic and full of questions.

The paper on the endoplasmic reticulum as source of calcium was published in 1977. At that time I was working in Giulio Gabbiani's lab in Geneva. Alberto told me that at that year's Gordon Conference the topic of the ER as a source of calcium in the eggs was the most popular subject of discussion and people were asking him why Piero and I were not there. Later in the years Piero and I showed that in the oocytes the cortical granules become able to respond to activation by pricking when the ER starts to surround them. Histochemistry quite clearly indicated that calcium is gradually released from the ER on the arrival of the activation stimulus. I showed these data at a meeting in the gorgeous medieval town of Gargonza organized by Émile Baulieu and the Gotha of the calcium-reticulum story (1981). In the concluding remarks Baulieu mentioned our work as one of the most important paper presented in that meeting.

Similar results were obtained for *D. pictus* ER at activation in the work performed by Roberto Gualtieri and Piero. Next, I had the idea to replicate Masui's classical experiment in producing layered *Xenopus* eggs by mild cen-



Fig. 16. 1981. Gargonza meeting on Calcium. Yoshio Masui, Michael Whitaker, David Epel, Marc Moreau, Paul Guerrier, K.S.R. Cutbertson, Gregorio Siracusa, Michael Berridge, Emile Baulieu, Sabine Shorderet-Slatkin, Drs. Allende, Massimo De Felici, Franco Mangia, Jim Maller and many others.



Fig. 17. 1984. Participants of the meeting organized by Jerry Hedrick at Davis. Among them, from left Chiaki Katagiri, Dora Miceli, Alberto Monroy, Jerry. I was the photographer.



Fig. 18. During my presentation at the Davis meeting. I was talking about endoplasmic reticulum in *Xenopus* and in *Discoglossus* eggs.

trifugation. Riccardo and I found the layer full of ER. Measures of calcium release were started in that layer by Bill Busa. This work was later reproduced and published by Rich Nuccitelli and co-workers.

All in all, a tremendous amount of research on the relationship between calcium and the ER took place at the end of the 1970s.

Ultrastructural Observations on Cortical Endoplasmic Reticulum and on Residual Cortical Granules in the Egg of *Xenopus laevis*

CHIARA CAMPANELLA AND PIERO ANDREUCETTI

Istituto di Istologia ed Embriologia, Università di Napoli, Via Mezzocannone 8, Napoli, Italy

Received October 16, 1975; accepted in revised form October 4, 1976

Two kinds of cortical granules (CG) are present in the unfertilized egg of *Xenopus laevis*: CGa and CGv. The cisternae surrounding both CGs have been found to be interconnected through elements of ER. CG cisternae also anastomose with the subcortical ER. It is suggested that these connections establish a functional unity between the CGs and that the cortical network may be involved in the propagation of the activation stimulus leading to the gradual CG activation and rupture. About 2% of the CGs are left in the cortex following activation. They have never been found in the process of extrusion in eggs fixed later than 5 min after pricking. Notable ER modifications occur in the egg cortical cytoplasm within the first 30 min following activation. Residual CGs do not show preferential distribution with regard to their position in the cortical cytoplasm or with regard to their presence in the animal and vegetal hemispheres. Most CGv and a few CGa undergo changes, although the changes are different in the two classes of granules; both CG types lose most of their original contents. CGv eventually disaggregate, whereas CGa show a reduction of their contents and form one or more large invaginations. Autophagosomes are found in the animal hemisphere 20 to 30 min after activation. They are located in the cortical cytoplasm and have a granular content similar to modified CGs.

INTRODUCTION

Among amphibians, the CG ultrastructure has been studied in a variety of species including *Rana pipiens* (Kemp and Istock, 1967) and *Xenopus laevis* (Balinsky, 1966; Grey *et al.*, 1974). In *Xenopus* eggs, two types of CGs are present, differing in size, structure, and distribution. Both types appear to be surrounded by a layer of flat vesicles (Gray *et al.*, 1974). Sulphated mucopolysaccharides have been histochemically identified in *Rana pipiens* CGs (Schuel *et al.*, 1974).

In *Rana pipiens* and *Xenopus laevis*, large amounts of CG components are released into the perivitelline space following activation and they appear to play a role in the formation of a fertilization layer and in polyspermy prevention (Kemp and Istock, 1967; Wolf, 1974a,b,c; Grey *et al.*, 1974; Wyrick *et al.*, 1974).

In sea urchin eggs, Vacquier (1975) has shown that Ca^{2+} ions can trigger the CG

rupture and his data suggest that the activating stimulus propagates as an autocatalytic process in which the Ca^{2+} released from one CG triggers the breakdown of its neighbours. In this connection, it is interesting to remember that Wolf (1974c) has shown that for the propagation of the cortical response in *Xenopus laevis*, extracellular Ca^{2+} is required in the first 5-10 sec following activation.

In *Xenopus*, exocytosis of CGs is completed within 9-10 min after insemination (Gray *et al.*, 1974) or 180 sec after pricking (Wolf, 1974c); in *Rana pipiens*, it is completed within 90 sec after pricking (Kemp and Istock, 1967). However, intact CGs can still be found in the cortex of the blastomeres as late as blastula stage (Katagiri, 1959; Balinsky, 1966; Kotani *et al.*, 1973). Why some CGs (about 1% in *Xenopus* according to Kotani *et al.*, 1973) do not participate in the activation reactions is unknown. One factor may possibly be their

deep location in the egg peripheral cytoplasm (Gray *et al.*, 1974). Furthermore, Kotani *et al.* (1973) postulate that the CG contents also may be released after the cortical reaction has taken place, thus contributing intercellular material during early embryogenesis. These authors also show the presence of a large amount of CG in a single "germ plasm" islet.

One of the major unresolved questions connected with the cortical reaction is the mechanism(s) whereby the CG breakdown propagates from the point of sperm attachment (or of pricking in the case of artificial activation in amphibian eggs) to the rest of the egg. The observations described in this paper show that the CGs are interconnected by components of the endoplasmic reticulum and we suggest that this connection may be instrumental in the propagation of the cortical reaction. Furthermore, our observations show that some of the residual CGs undergo changes in the course of early development, the significance of which is unclear. In any case, we have been unable to see any "late" extrusion of their contents that may participate in the formation of intercellular material.

MATERIALS AND METHODS

Adult *Xenopus laevis* females, injected with 600 U of Coriovis (Vister), were stripped in De Boer's solution (110 mM NaCl, 2.2 mM KCl, 0.44 mM CaCl₂ to pH 7.2 with NaHCO₃; Katagiri, 1961). The intact eggs were pricked at the vegetal hemisphere with a sharpened tungsten needle. They were immersed in fixative 1, 2, 5, 10, 20, 30, 45, and 65 min after pricking. Eggs were also artificially inseminated and fixed after a brief exposure to activated papain (Dawid, 1965) at rotation, first cleavage, and the 32-cell stage. Papain was used to remove egg jelly in order to ensure fixative penetration. The fixative is 2.5% glutaraldehyde in 0.2 M phosphate buffer (final concentration) to which 0.5% NaCl was added (Millonig, 1964). The eggs were postfixed in 2% osmium tetroxide in

phosphate buffer and 0.5% NaCl, dehydrated in alcohol, and embedded in Araldite-Epon. Blocks were sectioned with an LKB ultramicrotome, double stained with uranyl acetate and lead citrate (Reynolds, 1963) and observed with a Siemens Elmiskop 1A electron microscope.

Sections of all of the above-mentioned samples were observed at both the animal and vegetal hemispheres.

RESULTS

(A) ER and CGs in the Unfertilized Eggs

The cortex of *Xenopus laevis* is characterized by the presence of two types of CG (see Grey *et al.*, 1974) (Fig. 1). The so-called CGv type is predominant in the vegetal hemisphere of the egg; they have a diameter of 2 to 2.5 μm , their shape is sometimes irregular, and their contents are flocculent. The so-called CGa type is more abundant in the animal hemisphere; they are smaller than the CGv (about 1.5 μm in diameter) and their contents are denser and more homogeneous. Both types of CGs are surrounded by flattened vesicles, forming a more or less continuous shell around them. The vesicles are separated from the CGs by a thin cytoplasmic layer (Figs. 1, 2, 3, 5, 6, and 7). The flattened vesicles that surround two adjacent CGs are sometimes interconnected by ER elements (Figs. 3, 5, and 6). Furthermore, in some eggs which were serially sectioned, it was observed that the flattened sacs also anastomose with the underlying ER cisternae (Figs. 1, 2, 3, 6, and 7). Moreover, when the cisternal shell around the CG is incomplete, the cortical ER elements themselves may be found immediately adjoining the CG membrane.

Clusters of ER are discernible in the subcortical regions; they are regularly spaced between the yolk and pigment granules (Fig. 1). Similar ER clusters also can be observed in the cortex at the vegetal hemisphere in regions where CGs are lacking (Fig. 4). They occur at a periodicity of about 15 μm .

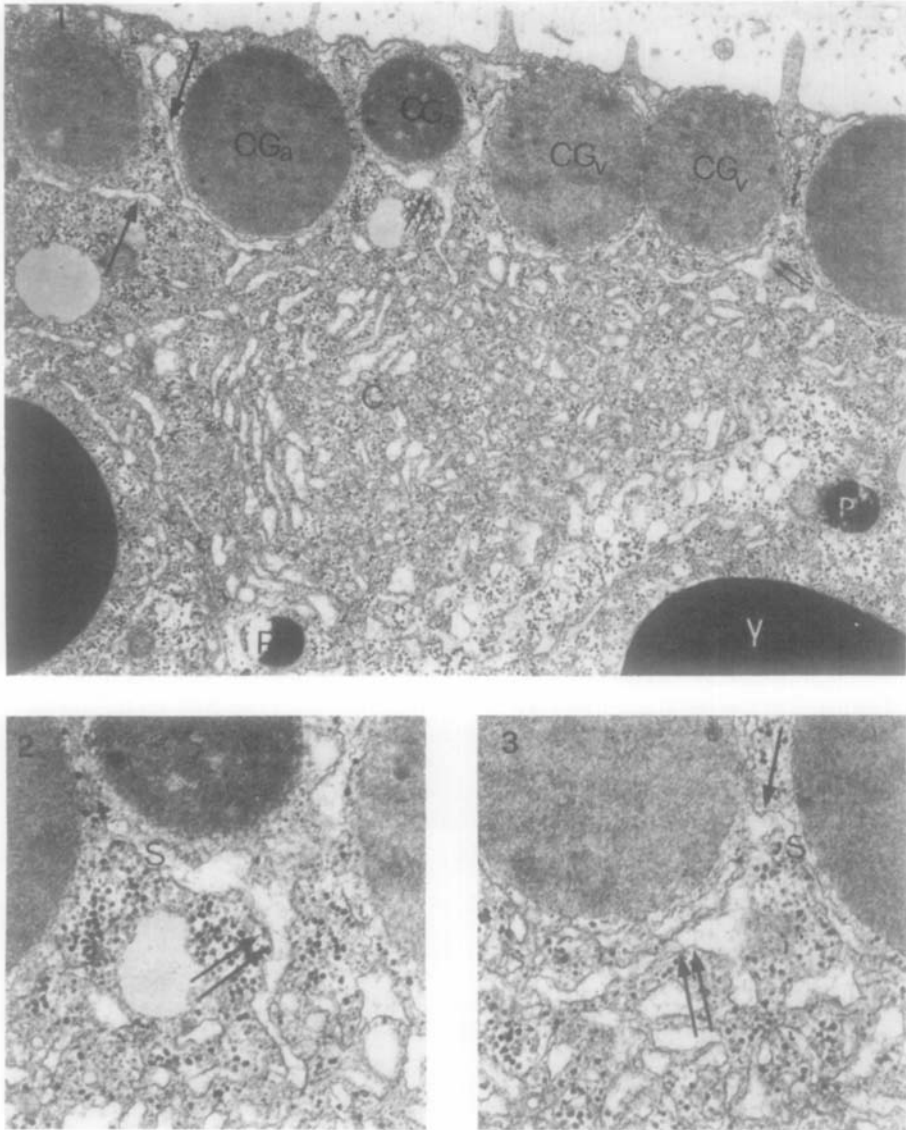


FIG. 1. Animal hemisphere region close to the marginal zone of an unfertilized egg. In the cortex two kinds of cortical granules are evident: CGa and CGv. Distinctions between CGa and CGv are not always clear cut and depend on the fixation quality. The smooth ER system is abundant at the cytoplasm periphery where it may be condensed in clusters (C). The flattened sacs that surround each CG are interconnected by ER cisternae (arrows) and with the underlying ER (double arrows). P, pigment; Y, yolk. $\times 15,000$.

FIGS. 2, 3. Details of Fig. 1 at the double arrow. Figure 2 shows flattened sac(s) surrounding a CG projects in a subcortical ER cluster (double arrow). Figure 3 shows a short cisterna visible among two CG flattened sacs (arrow). It also anastomoses with some subcortical ER (double arrow). $\times 34,000$.

(B) ER Changes after Pricking or Insemination

Figure 8 shows the cortex of an egg 5 min after pricking. Most of the CGs have

already released their contents. ER clusters are no longer present, while ER channels are seen in the peripheral cytoplasm, oriented obliquely toward the egg surface.

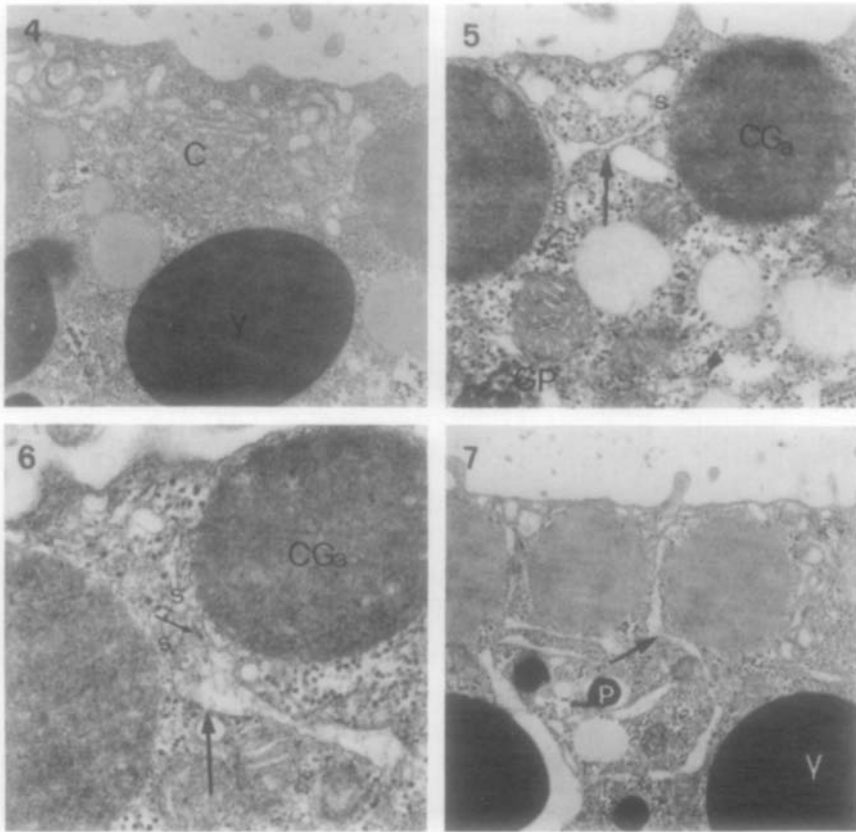


FIG. 4. Vegetal hemisphere of an unfertilized egg. A cluster (C) of ER elements is found in the cortex next to the CG. Y, yolk. $\times 10,000$.

FIGS. 5, 6. Vegetal hemisphere of an unfertilized egg. The flattened sac(s) that partially surround the granules are interconnected by ER cisternae (large arrows). In Fig. 6, a few ribosomes are seen on the cisterna membrane (small arrow). GP, germ plasma. Fig. 5, $\times 19,000$; Fig. 6, $\times 35,000$.

FIG. 7. Animal hemisphere of an unfertilized egg. A CGA cisterna projecting into the subcortical cytoplasm (arrow) is evident. This is one of a very few examples found showing a CG surrounding cisterna in the plane of the section for most of its length. P, pigment granule; Y, yolk. $\times 10,000$.

About 30 min after pricking, the ER arrangement changes considerably; the cisternae are not as abundant as in the unfertilized egg and do not show any preferential orientation (Fig. 9).

(C) Residual CGs and Autophagosomes

In eggs fixed later than 5 min after pricking, few (about 2%) residual CGs are found. They are randomly distributed either in the cortex, close to the plasma membrane, or in the deeper regions of the peripheral cytoplasm. This situation has

been found unchanged as late as the 32-cell stage.

Table 1 summarises the percentages with respect to the unfertilized eggs of residual CGa and CGv in activated eggs at various times after activation. As deducible from the high σ values obtained, the percentage of residual CGs is variable among the eggs examined at the same time interval between activation and pricking. There are no significant differences in the numbers of residual CGs between the animal and the vegetal hemi-

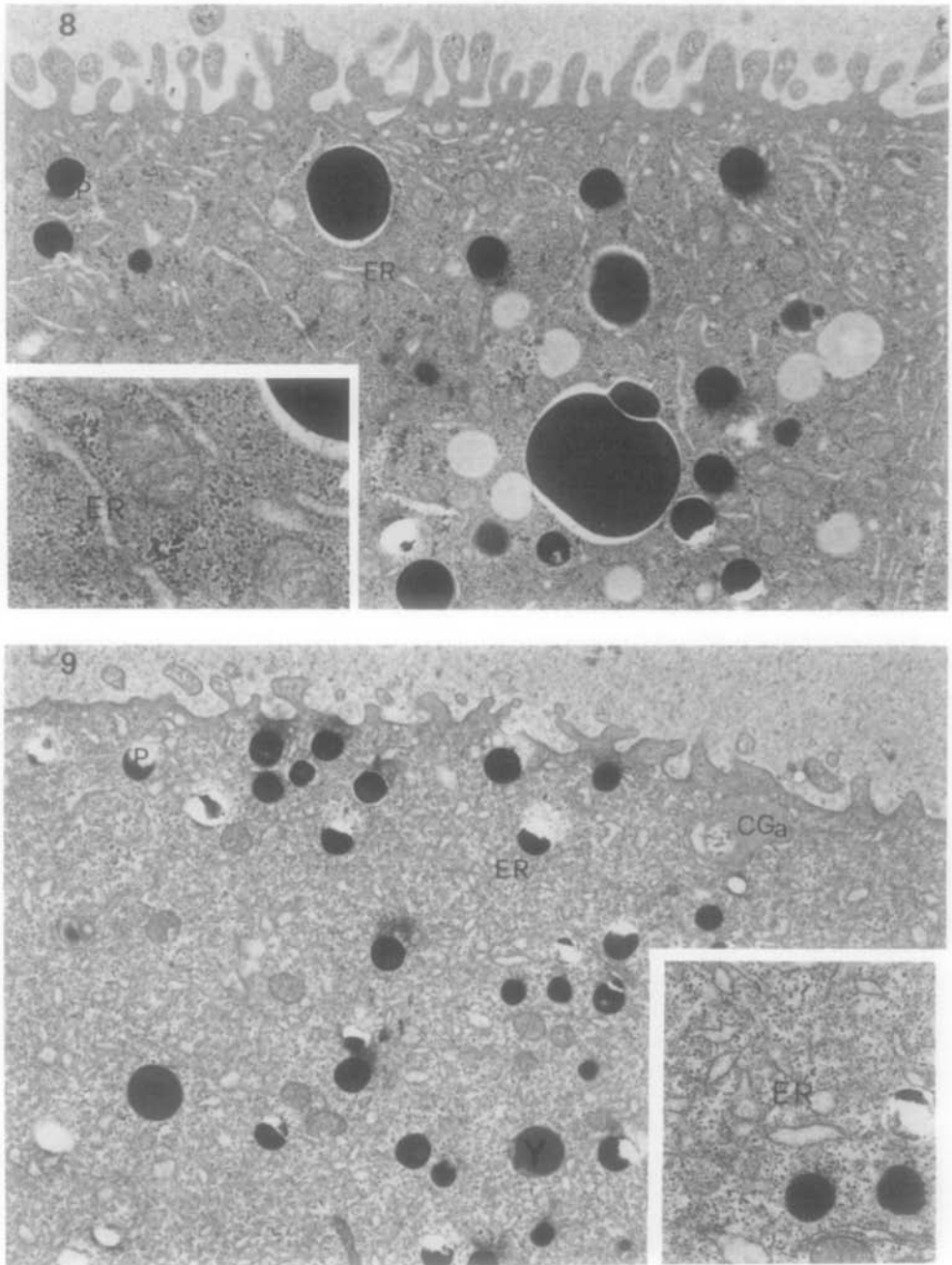


FIG. 8. Animal hemisphere 5 min after pricking. Note the position of the ER channels which are obliquely oriented with respect to the egg surface. No CG is seen in the egg cortex. ER, endoplasmic reticulum; P, pigment. $\times 6000$. *Inset*: Endoplasmic reticulum (ER). $\times 14,000$.

FIG. 9. Animal hemisphere 30 min after pricking. The ER is randomly distributed. A modified CGa is seen in the egg cortex. ER, endoplasmic reticulum; P, pigment; Y, yolk. $\times 7000$. *Inset*: Endoplasmic reticulum (ER). $\times 14,000$.

TABLE 1
PERCENTAGE OF RESIDUAL CGS COUNTED IN ACTIVATED EGGS^a

| Delay between activation and fixation (min) | Percentage CGs ^b | | | | | | | | | |
|---|-----------------------------|------------|-----|----------|-----------|--------------------|----------|-----|----------|-----------|
| | Animal hemisphere | | | | | Vegetal hemisphere | | | | |
| | CGa | σ^c | CGv | σ | Total CGs | CGa | σ | CGv | σ | Total CGs |
| 5 | 1.6 | 1.8 | 1.6 | 1.5 | 3.2 | 0.3 | 0.78 | 1.4 | 1.6 | 1.7 |
| 65 | 1.2 | 1.7 | 1.4 | 2.9 | 2.6 | 0.2 | 0.7 | 2 | 0.1 | 2.2 |
| 300 (32-cells) | 0.2 | 0.6 | 1.3 | 2.3 | 1.5 | 0.3 | 0.9 | 0.9 | 0.2 | 1.2 |

^a Counts were performed on pricked eggs in the case of 5-min eggs, on pricked and inseminated eggs in the 65-min eggs, and on inseminated eggs in the 300-min ones. The numbers are averages of counts performed on thin sections of at least two eggs from the same clutch. Due to the monolayer, and therefore, highly anisotropic distribution of CGs, the usual stereological methods for evaluating the numerical density (e.g., Weibel, 1973, p. 249) are likely to be heavily biased. The following estimate of the percentage of CGs has been developed: $\gamma = [(N_1 \cdot l)/\bar{D}] \cdot k$, where N_1 = actual CG count along a micrograph profile; l = length of the profile; \bar{D} = average diameter of the CGs in same units as l ; k = parameter which estimates (a) the surface of the monolayer scanned by the section and (b) the covering factor of a close hexagonal packing of spheres [$k = 8/(12)^{1/2}$].

^b The percentage of residual CGs is calculated with regard to the unfertilized egg assuming maximum packing of granules; see below. It must be noted that this maximum packing does not always occur at the vegetal hemisphere. Therefore, the value of γ generally will be higher.

^c σ = standard deviation of corresponding columns.

sphere. In eggs fixed later than 5 min after activation, the percentage of residual CGv is greater than that of the CGa. This is particularly evident in the case of the vegetal hemisphere. However, the *t* test does not substantiate any significant difference, at the 5% level, between the percentages of residual CGv and CGa at various times after activation.

Structural changes of residual CGs are evident in eggs fixed from 20 to 65 min after pricking or insemination, whereas very few CGs undergoing changes were observed in later stages, thus suggesting that the process is completed prior to the first cleavage. Such changes are more often detectable in the CGv (70%) than in the CGa (8%). Furthermore, while modified CGa have been observed only at the animal hemisphere, modified CGv are present in both hemispheres.

Residual CGv are surrounded by a clearly distinguishable shell of flattened sac (Fig. 10). Ten minutes after pricking, empty vesicles are seen at the periphery of the granules as well as inside them. Twenty minutes after pricking (or 30 min after insemination) the CGv contents are

scarce and flocculent and may include several invaginations of the CG membrane (Fig. 10). Further stages in this process may be indicated by the discontinuities in the CGv membrane, as shown in Fig. 10, where the CG flattened sac directly binds the CGv contents, and by the appearance in the CGs of granules similar in electron density and size (150 and 350 Å) to the ribosomes and glycogen granules (Fig. 11). Such modified CGv finally disaggregate. CGa are modified differently; 20 min after activation, very large vacuoles in which numerous electron-dense particles are incorporated are observed in them (Fig. 12). At approximately the same time, membrane-bound bodies of variable dimensions are seen at the animal hemisphere in pricked as well as in fertilized eggs. These have been interpreted as autophagosomes because a portion of their content is still recognizable as being cytoplasmic matrix, electron-dense particles can be seen in them, and they are bound by one or more membrane layers of variable thicknesses (75 to 100 Å) (Ericsson, 1969). In Fig. 13 two autophagosomes are shown in which flattened sacs with swollen ends enclose

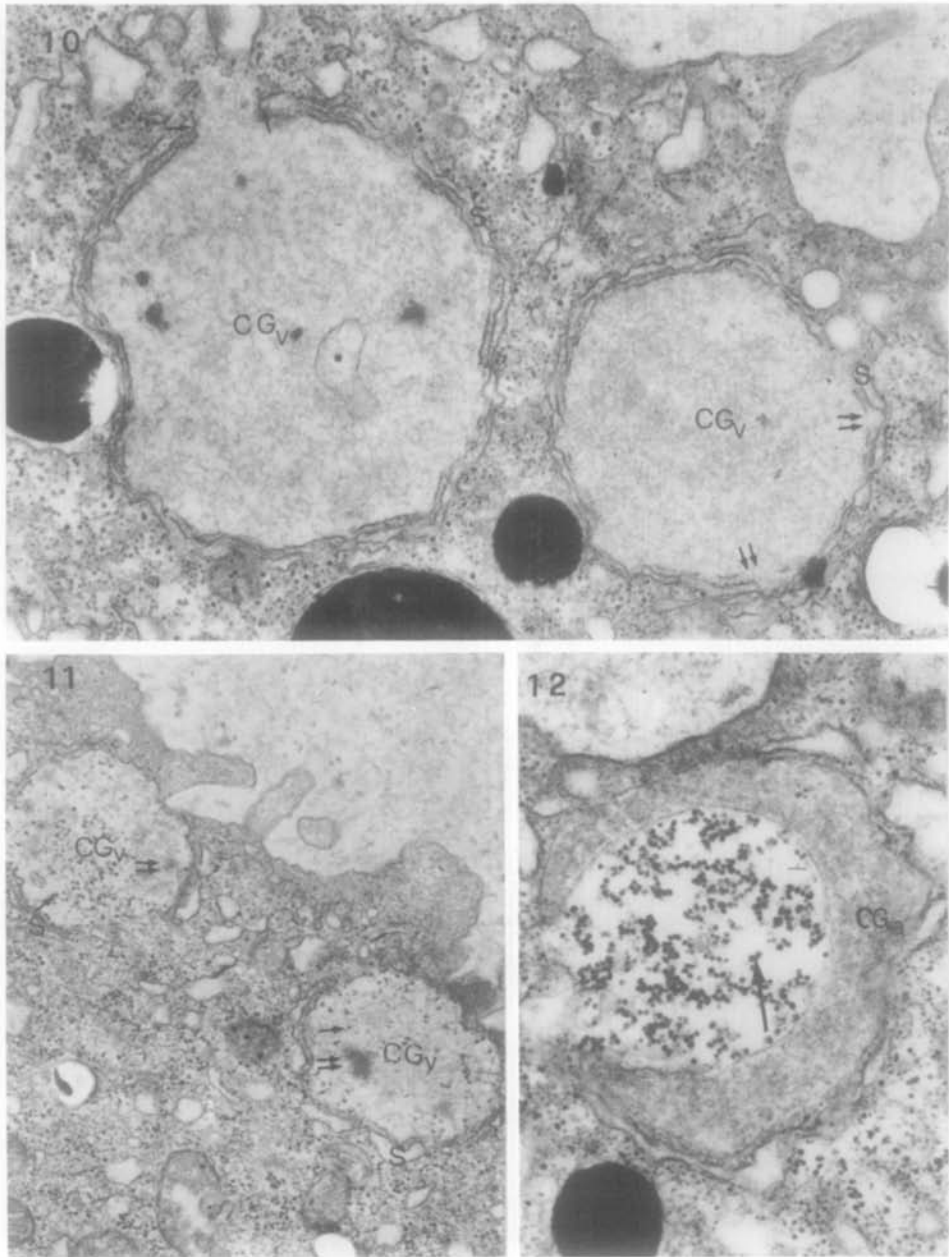


FIG. 10. Animal hemisphere 20 min after pricking. The CG_v content is flocculent. In the granule on the left one can also note an invagination (asterisk) containing some flocculent material. At the granule opening, membrane fusions are seen between the CG_v membrane and the flattened sac membranes (arrows). The granule on the right shows discontinuities in its membrane (double arrows) and is therefore limited by the flattened sac membrane. s, flattened sac. $\times 26,000$.

FIG. 11. Animal hemisphere 30 min after insemination. Some residues of their original content (double arrows) and electron-dense particles (arrows) can be observed in the CG_v. s = flat sac. $\times 16,000$.

FIG. 12. Animal hemisphere 20 min after pricking. A large invagination filled with 320-Å (arrow) particles is located within the CG_a. $\times 28,000$.

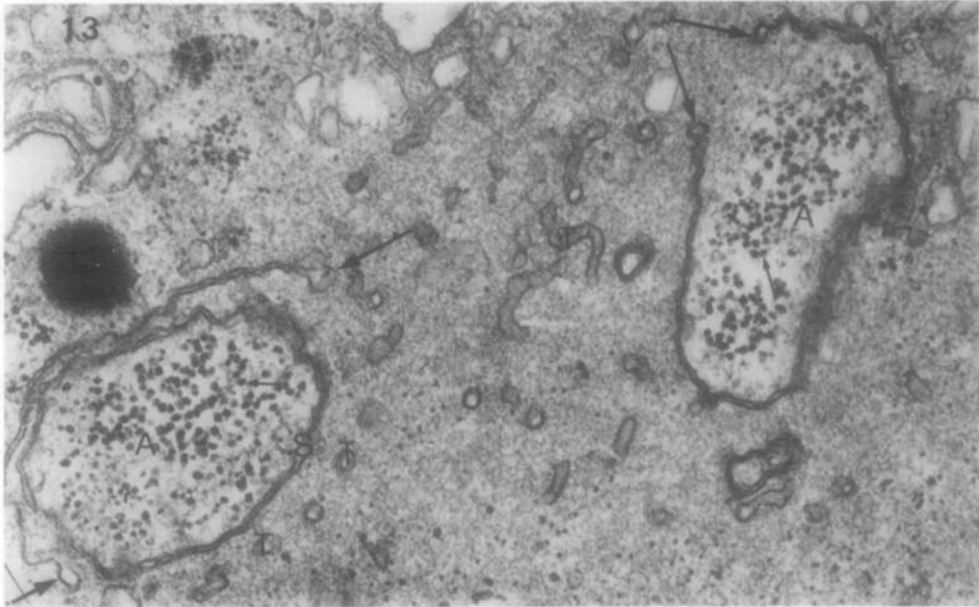


FIG. 13. Animal hemisphere 30 min after insemination. Two autophagosomes (A) are visible. Both are surrounded by a cup-like flattened cisterna with swollen ends (arrows). The one on the left is also surrounded by a full flattened sac (S). Tubules (T) 450 Å in diameter are present in the particle-free cytoplasm between the two autophagosomes. On the left, cross-sectioned tubules also form a regularly arrayed chain in sequence with the autophagosome flattened sac(s) swollen ends. The tubules appear identical to the flattened sac ends. Notice the electron-dense particles abundantly present in the autophagosomes' interiors (small arrows). $\times 28,000$.

250-Å particles; tubules 450 Å in diameter are visible in the cytoplasm close to the autophagosomes. Furthermore, sections of tubules surround the autophagosomes and appear to be in continuity with the autophagosome flattened sac (Fig. 13, arrow). Tubules are seen also in the proximity of disaggregating CGv.

DISCUSSION

(A) ER and CGs

In the cortical cytoplasm of *Xenopus* eggs there are two types of CGs (CGv and CGa) both surrounded by a shell of flattened vesicles; this is in agreement with the observations of Grey *et al.* (1974). In addition, the egg peripheral cytoplasm is rich in ER, as already reported by Balinsky (1966), Van Gansen (1966), and Grey *et al.* (1974). Furthermore, regularly spaced clusters of ER elements in subcortical

areas of the animal hemisphere or in the cortical areas of the vegetal hemisphere have been observed. Our observations also show the presence of an ER network in the cortical and subcortical regions of the unfertilized egg which appears to connect the flattened sacs surrounding adjacent CGs. The CG flattened vesicles also anastomose with subcortical ER components. It is tempting to speculate that this network may play a role in the propagation of the stimulus which is responsible for the breakdown of the CGs. The scanning electron micrographs of sea urchin CGs (Vacquier, 1975) also show strands connecting the CGs to one another.

Our results show that most CGs extrude their contents upon activation, whereas only about 2% are left unbroken. This finding is in agreement with the findings of several authors (Katagiri, 1959; Kotani *et*

al., 1973; Grey *et al.*, 1974). The distance of the granules from the plasma membrane does not seem to be the main factor responsible for CG retention. Indeed, unreacted CGs have been observed both close to the egg plasma membrane and in the deeper cytoplasmic regions. Furthermore, no indication of CG extrusion has been found in eggs fixed later than 5 min after pricking. Therefore, the question as to why some CGs do not participate in the cortical reaction still remains unanswered. One possible cause might be their lack of connection with the cortical ER; the wave of activation would thus skip the unconnected CGs.

The participation of the ER in the changes occurring following activation is also suggested by the observation that at the time the CG reaction is still underway, no ER clusters are present and the cisternae are oriented obliquely toward the egg surface, while at a later stage (30 min after activation) they are randomly distributed. A similar, transient change of orientation of the ER cisternae has been observed in newly fertilized eggs of *Discoglossus pictus* shortly after the breakdown of the *animal dimple* granules (Campanella, 1975, and manuscript in preparation).

(B) *Residual CGs and Autophagosomes*

Residual CGs seem to be randomly detectable in the egg peripheral cytoplasm and persist unchanged, at least until the last developmental stage studied by us, namely, the 32-cell stage. Some residual CGs undergo changes which are different in the CGa and CGv. Such modifications do not seem to be associated with any kind of abnormal process due to pricking since they are also observed in the fertilized eggs. In both cases, the changes mostly occur prior to the onset of cleavage.

We have observed that modified CGa are present only in the animal hemisphere and even there, only a small number of them exhibits the changes. Conversely, the great majority of CGv undergo profound alterations both in the animal and

in the vegetal hemisphere. This may be indirect evidence of their dissimilar nature.

At the final stages of CG modification, while the CGv contents is granular and its membrane breaks into pieces, the CGa becomes filled with large vacuoles and its appearance is very similar to the autophagosomes described in the mouse kidney convoluted tubules (see Ericsson, 1969, p. 376).

Autophagosomes and the tubules located in their proximity have membranes of similar dimensions. This may suggest that tubules derive from the autophagosome membrane, or vice versa. Furthermore, taking into account the similarities that exist between autophagosomes and disaggregating CGs (that is, location in the cortical cytoplasm, contents, and surrounding by flat sac) the possibility cannot be denied that the autophagosomes segregate disaggregating CGs, thus representing a possible mechanism of CG utilization and/or disposal.

In conclusion, residual CGs do not seem to be preferentially located in one or the other of the two egg hemispheres. Our observations show that in the course of early embryogenesis, CGs do not extrude their contents, but most of them are modified in such a way as to suggest that their contents are utilized and/or disposed by the embryo. Whether or not they play any additional role can only be shown by further studies on the presence of CGs in embryonic presumptive areas.

We are most grateful to Professor G. Ghiara for his stimulating discussion and criticism in reading the manuscript. We are also deeply indebted to Professor A. Monroy for his suggestions after reading the manuscript.

We also wish to acknowledge the expert photographic assistance of Mr. G. Falcone and Mr. G. Argenzio.

REFERENCES

- BALINSKY, B. I. (1966). Changes in the ultrastructure of Amphibian eggs following fertilization. *Acta Embryol. Morphol. Exp.* 9, 132-154.
- CAMPANELLA, C. (1975). The site of spermatozoon

- entrance in the unfertilized egg of *Discoglossus pictus* (Anura): An electron microscope study. *Biol. Reprod.* 12, 439-447.
- DAWID, I. B. (1965). Deoxyribonucleic acid in Amphibian eggs. *J. Mol. Biol.* 12, 581-599.
- ERICSSON, J. L. E. (1969). Mechanism of cellular autophagy. In *Lysosomes in Biology and Pathology* (Dingle, J. T., and Fell, H. B., eds.), Vol. II, pp. 368, 376. Amsterdam/London.
- GREY, R. D., WOLF, D. P., and HEDRICK, J. L. (1974). Formation and structure of the fertilization envelope in *Xenopus laevis*. *Develop. Biol.* 36, 44-61.
- KATAGIRI, C. (1959). Cortical changes at fertilization in the egg of the grass frog *Rana temporaria*. *J. Fac. Sci. Hokkaido Univ.* 14, 166-174.
- KATAGIRI, C. (1961). On the fertilizability of the frog egg. I. *J. Fac. Sci. Hokkaido Univ. Ser. VI Zool.* 14, 607-613.
- KEMP, N. E., and ISTOCK, N. L. (1967). Cortical changes in growing oocytes and in fertilized or pricked eggs of *Rana pipiens*. *J. Cell Biol.* 34, 111-112.
- KOTANI, M., IKINISHI, K., and TANABE, K. (1973). Cortical granules remaining after fertilization in *Xenopus laevis*. *Develop. Biol.* 30, 228-232.
- MILLONIG, G. (1964). Studio sui fattori che determinano la preservazione della ultrastruttura. In "From Molecule to Cells," Symposium on Electron Microscopy, pp. 347-362. C.N.R., Rome.
- REYNOLDS, E. S. (1963). The use of lead citrate at high pH as an electron-opaque stain in electron microscopy. *J. Cell Biol.* 17, 208-212.
- SCHUEL, H., KELLY, W. J., BERGER, E. R., and WILSON, W. L. (1974). Sulfated acid mucopolysaccharides in the cortical granules of eggs. *Exp. Cell Res.* 88, 24-30.
- STEINHARDT, R. A., EPEL, D., CARROLL, E. J., and YANAGIMACHI, R. (1974). Is calcium inophore a universal activator for unfertilized eggs? *Nature (London)* 252, 41-43.
- VACQUIER, V. D. (1975). The isolation of intact cortical granules from sea urchin eggs: Calcium ion trigger granule discharge. *Develop. Biol.* 43, 62-74.
- VAN GANSEN, P. (1966). Ultrastructure comparée du cytoplasme périphérique des oocytes mûrs et des oeufs vierges de *Xenopus laevis* (Batracien anoure). *J. Embryol. Exp. Morph.* 15, 335-364.
- WEIBEL, E. R. (1973). Stereological techniques for electron microscopic morphometry. In "Principles and Techniques of Electron Microscopy" (Hayat, M. A., ed.), Vol. 3. Van Nostrand Reinhold Company, New York.
- WOLF, D. P. (1974a). The cortical granule reaction in living eggs of the toad *Xenopus laevis*. *Develop. Biol.* 36, 62-71.
- WOLF, D. P. (1974b). On the contents of the cortical granules from *Xenopus laevis* eggs. *Develop. Biol.* 38, 14-29.
- WOLF, D. P. (1974c). The cortical response in *Xenopus laevis* ova. *Develop. Biol.* 40, 102-115.
- WYRICK, R. E., NISHIHARA, T., and HEDRICK, J. L. (1974). Agglutination of jelly coat granule components and the block to polyspermy in the Amphibian *Xenopus laevis*. *Proc. Nat. Acad. Sci. USA* 71, 2067-2071.

The Modifications of Cortical Endoplasmic Reticulum During In Vitro Maturation of *Xenopus laevis* Oocytes and Its Involvement in Cortical Granule Exocytosis

C. CAMPANELLA, P. ANDREUC CETTI, C. TADDEI, AND R. TALEVI
*Institute of Histology and Embryology, University of Naples, Via
 Mezzocannone 8, 80134 Naples, Italy*

ABSTRACT In *Xenopus laevis* eggs, cisternae shells which surround cortical granules (CG) are part of a cortical endoplasmic reticulum (ER) network. In this paper the origin of such ER shells has been studied in full-grown, progesterone-exposed *Xenopus* oocytes. Furthermore, the possible role of the cortical ER in the activation process has been investigated by pricking maturing oocytes. It has been shown that in full-grown ovarian oocytes ER CG shells are absent and ER cisternae are extensively and randomly distributed throughout the peripheral cytoplasm, where they appear to be continuous with annulate lamellae (AL). Following hormone treatment, the AL completely disaggregate and the ER cisternae gradually migrate to the cortex where they surround the CG constituting the typical cortical network described in uterine eggs. Furthermore, it has been found that 8 h after progesterone treatment (before the first polar body extrusion) the response to pricking (CG exocytosis) occurs only at the animal half; there is no observable response in the vegetal half. At this time ER shells surround CG only in the animal hemisphere. A complete CG exocytosis occurs following the first polar body emission, when the cortical ER is well organized in the whole oocyte cortex. The correlation between the differentiation of the cortical ER and the arousal in the oocyte of the ability to respond to a pricking stimulus is discussed in the light of an involvement of the cortical ER in the propagation of CG exocytosis.

The presence of smooth endoplasmic reticulum (ER) as a shell surrounding each cortical granule (CG) was first reported by Grey et al. ('74) in uterine eggs of *Xenopus laevis*. More recently Campanella and Andreuccetti ('77) have shown that these shells are interconnected and anastomose with clusters of cisternae regularly distributed deeper in the subcortical region, thus indicating that the cortical and subcortical ER of uterine eggs of *Xenopus* forms a continuous network. This organization is unique in *Xenopus* eggs. In other species, including other amphibians, ER vesicles and cisternae are randomly distributed in the cortex. In addition, it was demonstrated that, at activation, in *Xenopus* eggs, cisternae distribution gradually changes following CG exocytosis and eventually becomes random and sparse (Campanella and Andreuccetti, '77).

On the basis of these observations, it was proposed that the cortical network of ER may be involved in the propagation of the activa-

tion stimulus leading to the gradual CG exocytosis through release of Ca^{++} (Campanella and Andreuccetti, '77; see Gilkey et al., '78). This hypothesis is now supported by cytochemical data showing Ca^{++} sequestering ability of ER elements and strongly suggesting the intracellular release of these ions at activation (Andreuccetti et al., '84).

The importance of Ca^{++} in the processes following activation is extensively reported in studies on *Oryzias* (Teleosts) and sea urchin eggs. At activation, Ca^{++} , once liberated from unknown intracellular stores, triggers CG exocytosis, and most probably is also responsible for the propagation of the cortical wave of exocytosis (for reviews, see Epel, '80; Shapiro and Eddy, '80; Vacquier, '81). Although direct evidence is not available, it is conceivable that a similar situation exists in amphibians and, in particular, in *Xenopus* eggs.

We have undertaken this study with the aim to clarify the origin of this ER network

and to understand its possible role in cortical granule exocytosis. Since our preliminary observations on the organization of the cortical region in full-grown *Xenopus* oocytes do not show any ER shell around the CG, we have exposed the oocytes to the progesterone in vitro and examined them with the electron microscope at different time intervals from the hormone exposure. Furthermore, to clarify the function of the reticulum we have undertaken an experimental approach to correlate the differentiation of the ER with the arousal of the oocytes' ability to respond to propagating triggering signals, such as pricking. Indeed, full-grown or maturing amphibian oocytes, unlike eggs, are not capable of propagating pricking stimulation. This capability arises when the oocytes have eliminated the first polar body (Belanger and Shuetz, '75; Hollinger and Shuetz, '76; Hollinger et al., '79). By contrast, CG exocytosis can be induced as early as 1-2 h after the germinal vesicle dissolution both by ionophore treatment, which is a nonpropagating stimulus, in *Rana* oocytes (Belanger and Shuetz, '75) and microinjection of Ca^{++} in *Xenopus* and *Rana* oocytes (Hollinger and Shuetz, '76; Hollinger et al., '79).

We have found that cortical ER develop from annulate lamellae (AL) and, following progesterone treatment, gradually organize into the typical network found in uterine eggs. When maturing oocytes are pricked, CG dehiscence in the animal hemisphere occurs if they are exposed to hormone for at least 8 h (before the first polar body extrusion). In the same oocytes CG are retained at the vegetal hemisphere. At this time in the animal half the cortical network is well organized whereas in the vegetal hemisphere the network is markedly less organized.

MATERIALS AND METHODS

Experimental conditions and treatments

Adult *Xenopus laevis* females were kept during spring in aquaria at a constant temperature of 20°C and fed on calf liver or heart twice a week. Pieces of ovaries were removed from females anesthetized by hypothermia and kept until utilization in sterilized amphibian Ringer's solution (113 mM NaCl; 2.0 mM KCl; 1.2 mM $CaCl_2$; 2.3 mM $NaHCO_3$) containing streptomycin (50 mg/liter). Stage VI (Dumont, '72) oocytes were manually defolliculated with watchmaker's forceps in sterilized Steinberg's solution (46 mM Tris-HCl pH 7.4 containing 58 mM NaCl; 0.67 mM KCl; 3.4 mM $Ca(NO_3)_2 \cdot 4H_2O$; 0.83 mM $MgSO_4$) containing streptomycin and

penicillin. In addition, oocytes were enucleated by making a small puncture at the animal pole and exerting gentle pressure on the sides of the oocyte until the germinal vesicle emerged. When (under the microscope) the germinal vesicles appeared damaged, the enucleated oocytes were discarded. About 250 enucleated and nucleated oocytes were transferred to 5 μM progesterone in Ringer's solution for 10 min, rinsed, and kept in the same medium. The germinal vesicle breakdown (GVBD) was identified by the appearance of the "maturation spot" and further verified by manual dissection of some oocytes. GVBD was in the order of 100% 6 h after progesterone treatment, whereas no spontaneous maturation was observed in the controls.

The entire experimental procedure was performed in a room thermostatically controlled at 20-21°C. Pricking of the oocytes was performed at the animal hemisphere with a tungsten needle in Ringer's solution.

Electron microscopy

Stage VI oocytes were directly immersed in the fixative after excision from the ovary. The isolated oocytes manually defolliculated were fixed at various times (0,1,3,6,7,8,12, 13 h) following progesterone treatment. Concomitantly, some oocytes of each oocyte group were pricked and fixed 5, 15, or 30 min later. Parallel control oocytes were also fixed.

The fixative used was 2.5% glutaraldehyde in 0.2 M phosphate buffer (Millonig, '64) pH 7.2-7.4 at room temperature for 3-4 h. The samples were rinsed thoroughly in the buffer, where they were left overnight at 4°C. They were postfixed in 2% osmium tetroxide in the same buffer, dehydrated in graded cold ethanol, and embedded in Epon. The eggs were oriented in the embedding dishes with the animal hemisphere at the upper side so that both hemispheres of the same oocyte could be sectioned. Thin sections, stained with uranyl acetate and lead citrate, were examined on a Siemens 101A or Philips 301 transmission electron microscope.

RESULTS

Untreated full-grown oocytes

We examined with the electron microscope both ovarian oocytes surrounded by their thecae and those manually defolliculated and kept in Ringer's for not more than 15 min.

In the cortical region of ovarian undefolliculated stage VI oocytes, some cisternae and vesicles are randomly distributed among nu-

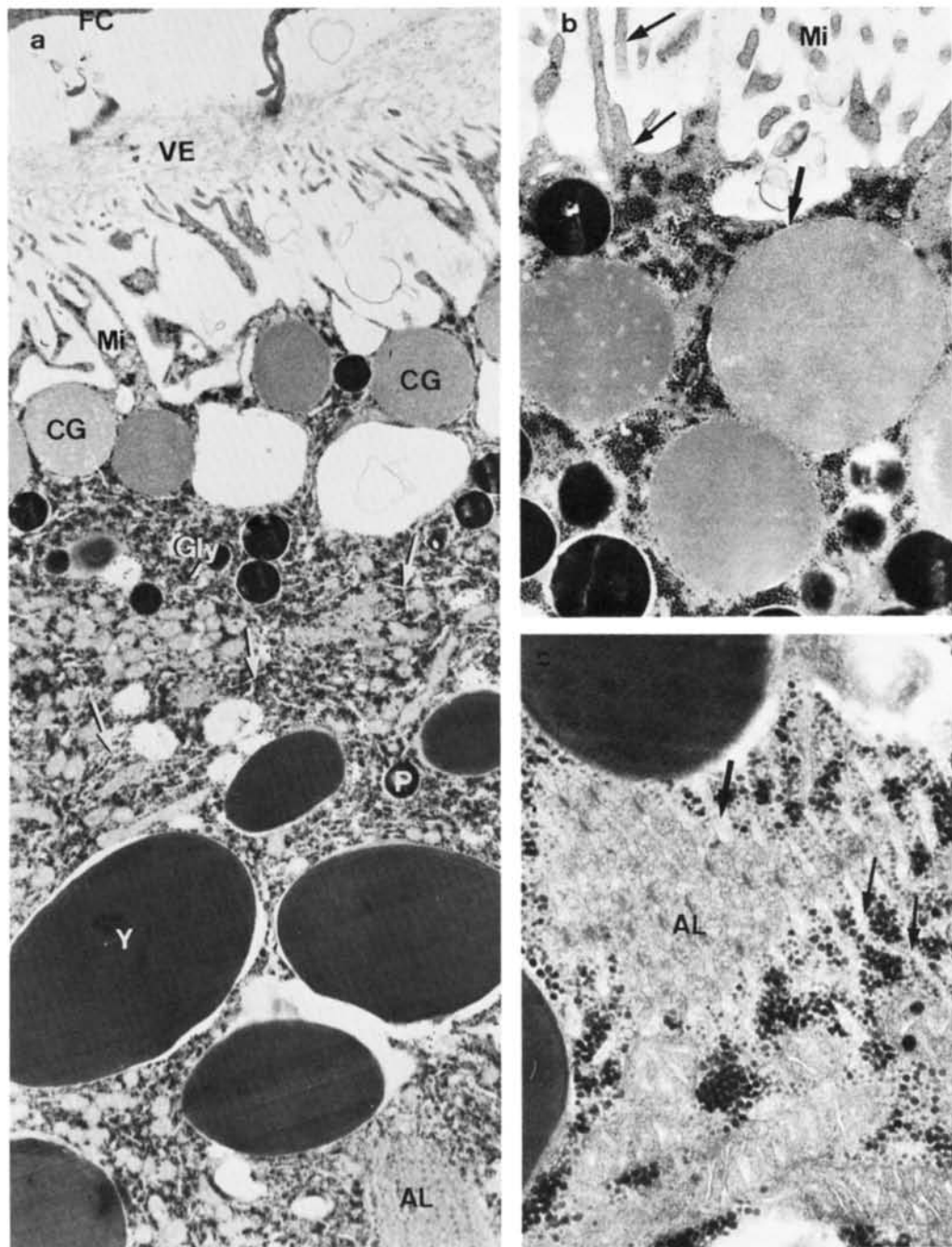


Fig. 1. Ovarian stage VI oocytes. a) ER cisternae (small arrows), glycogen (Gly), and mitochondria occupy the bulk of the cytoplasm. The plasma membrane is folded in long and irregular microvilli (Mi) and invaginations. CG are in the cortex, close to the plasma membrane. A stack of AL is present in a deeper region of the cytoplasm. FC, follicle cells; VE, vitelline envelope; P, pigment granule; Y, yolk platelets. Magnification $\times 9,000$.

b) Cisternae and vesicles are randomly distributed in the cortex. CG are not surrounded by the ER shells and appear to be close (arrow) to the plasma membrane. Glycogen granules are abundantly present. Small arrow = microfilament bundles. $\times 21,600$. c) AL stack depicted in the same region as in a. At their terminal ends the lamellae have lost their pore complex (arrow) and are continuous with ER cisternae (small arrows). $\times 45,000$.

merous glycogen islets. Most CG are in close contact with the plasma membrane, which is folded in numerous and irregular microvilli and in deep invaginations (Fig. 1a, b). Microfilament bundles, which constitute the microvilli core, are also present in the cytoplasm, among the CG (Fig. 1b). In a deeper region of the oocyte, smooth ER cisternae, intermingled with glycogen islets, are tightly embedded in the cytoplasmic matrix where lipid droplets, pigment granules, yolk platelets, and mitochondria are also present (Fig. 1a). If one follows the pathway of these cisternae, it can be seen that they are continuous with the stalks of AL which are located in a deeper ooplasmic region. Indeed, at the end of practically all these AL stacks, each lamella is continuous with an extremely elongated cisterna (Figs. 1a, c), which extends and ramifies in the oocyte subcortical region (Fig. 1a). The AL stacks are numerous and composed of not more than 20 lamellae (Fig. 1c).

In defolliculated oocytes a general ER reorganization is evident (Fig. 2). The CG are separated by more than $0.1 \mu\text{m}$ from the plasma membrane, which has been partially stretched as a result of dissection and shows microvilli and invaginations less conspicuous than in the ovarian oocytes. These features are maintained also in the defolliculated oocytes, not exposed to progesterone, and fixed, as controls, at increasing intervals of time.

Progesterone-treated oocytes

Up to 3 h following hormone treatment, there are no major changes except for a general smoothing of the oocyte surface, where most microvilli have retracted from the vitelline envelope. Furthermore, in the cortex microfilament bundles have been shortened up or rearranged in the typical microfilament network of amphibian egg cortex (Franke et al., '76; Campanella and Gabbiani, '80). The subcortical ER cisternae have diminished in number. Moreover, in these oocytes the AL stacks are no longer evident. The occurrence of islets of ER cisternae or vesicles intermingled with glycogen (Fig. 3) in the areas occupied by the AL in stage VI oocytes leads us to the conclusion that the first derive from the second, as was also seen by several authors in amphibian oocytes (see Shuetz, '74).

Six hours after hormone treatment, when germinal vesicle dissolution was evident, the subcortical ER has further considerably diminished, whereas in the cortex abundant

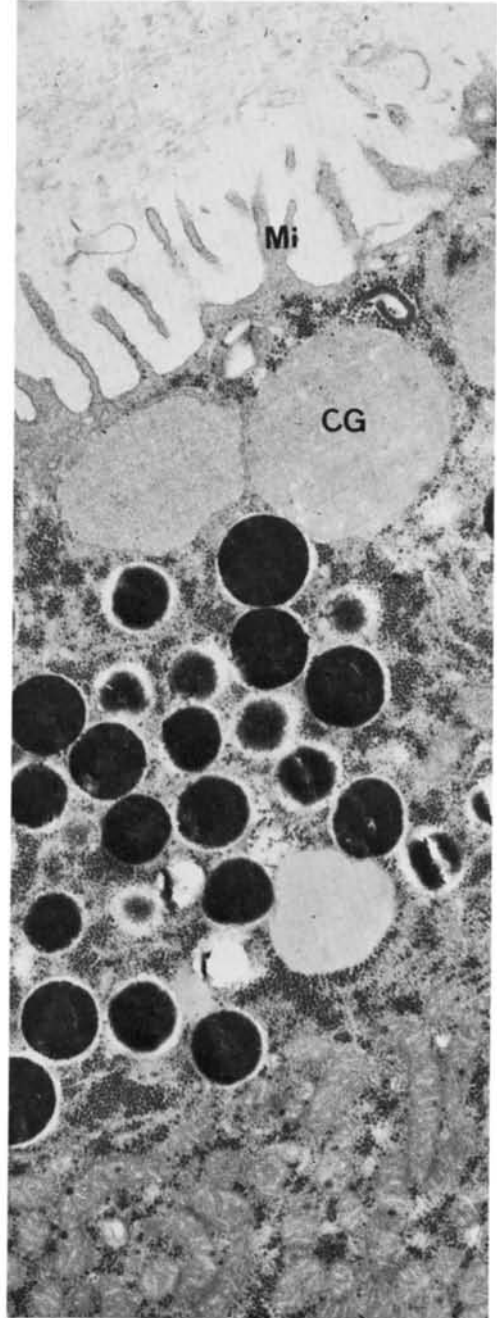


Fig. 2. Defolliculated, untreated stage VI oocyte. A general ER reorganization can be appreciated in the periphery of this oocyte by comparing this micrograph with Figure 1a. Microvilli (Mi) are shorter and the CG are slightly farther apart from the plasma membrane than in the ovarian oocytes covered by their thecae. Magnification $\times 18,000$.

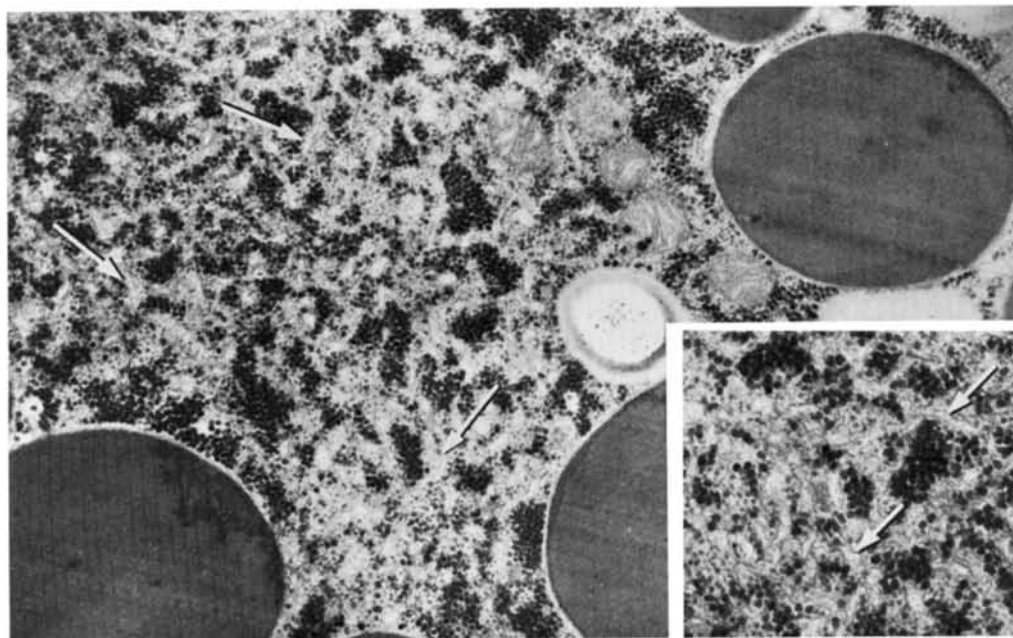


Fig. 3. Oocyte fixed 3 h following progesterone treatment. A cluster of vesicles and cisternae (arrows) intermingled with glycogen is present in the same oocyte

region where AL stacks are observed in untreated oocytes. Magnification $\times 30,000$. Inset: Detail showing cisternae (arrows). $\times 42,000$.

cisternae and vesicles are observed, thus indicating some migration of the ER to this region. CG are now closer to the plasma membrane. In the animal hemisphere, where glycogen becomes sparser than in untreated oocytes, some CG appear to be surrounded by ER shells. In the vegetal hemisphere of the same oocytes, ER is less abundant in the cortex than in the animal hemisphere, or arranged in clusters both in the cortical and in the subcortical regions.

Eight hours after treatment, CG in the animal hemisphere (Fig. 4a) are surrounded by complete ER shells (Fig. 4b). Abundant cisternae and vesicles are observed next to the plasma membrane in the interstices between adjacent CG. In the vegetal half of the same eggs the ER cisternae, which are conspicuously present in the cortex, are parallel to the plasma membrane or still arranged in clusters (Fig. 5a, b) and do not appear to form continuous shells around each CG (Fig. 5b). Glycogen islets are present in both the cortical and subcortical regions and are more nu-

merous in the vegetal hemisphere than in the animal one. Control oocyte appear to be still identical, at this time, to the untreated oocytes (Fig. 6).

About 13 h after treatment (first polar body extruded) throughout the egg the cortical network is well developed: The ER shells surround each CG also at the vegetal hemisphere (Fig. 7). Interestingly, in progesterone-exposed enucleated oocytes the cortical ER became organized in the same way and about at the same time as the nucleated ones.

Pricked oocytes

Oocytes exposed to progesterone for periods less than 8 h and pricked do not show any cortical reaction at either the animal or the vegetal half. At 8 h following hormone exposure, pricking causes exocytosis of CG in the animal half only (Fig. 8); the vegetal half is unchanged. This holds true independently of the time of fixation (5, 15, or 30 min) following pricking.

A complete CG reaction occurs throughout

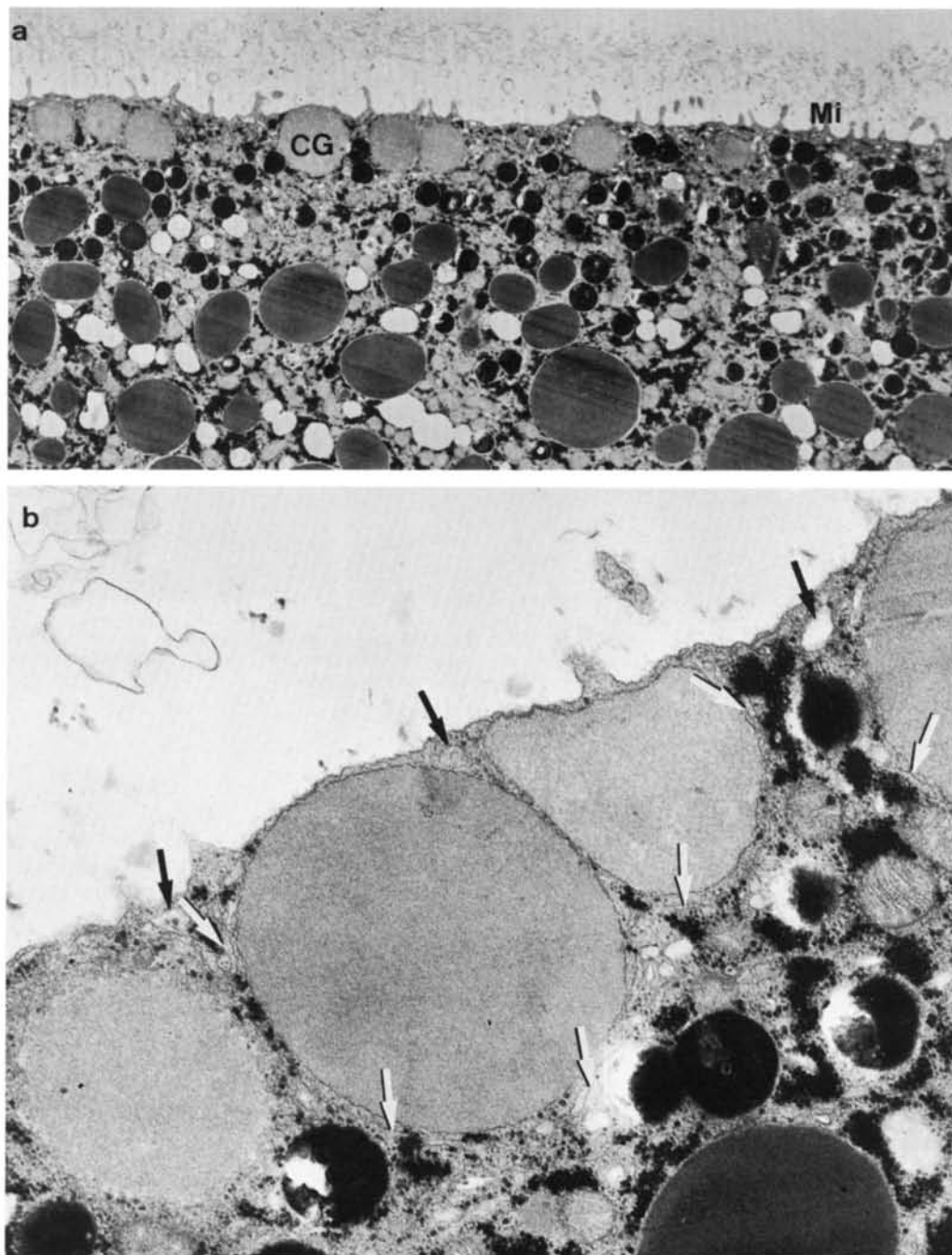


Fig. 4. Animal hemisphere of oocytes fixed about 8 h following progesterone treatment. a) ER vesicles and cisternae are more abundantly present in the cortical region than in the subcortical. The oocyte surface is folded in sparse and short microvilli (Mi). CG = cortical

granules. Magnification, $\times 6,000$. b) Next to the plasma membrane, vesicles and cisternae are observed in the interstices between CG (arrows). Each CG is surrounded by a shell of narrow cisternae (small arrows). $\times 30,000$.

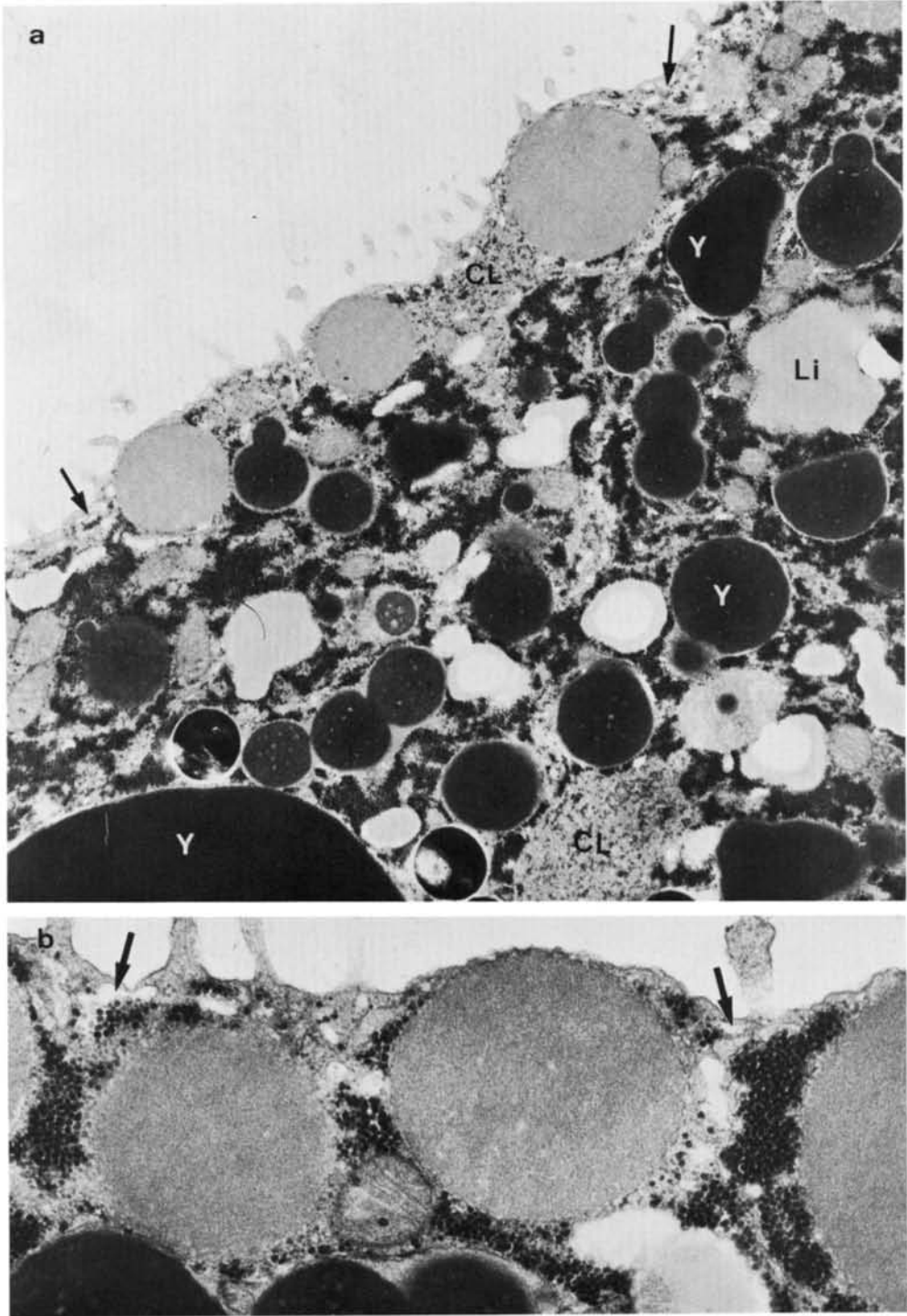


Fig. 5. Vegetal hemisphere of oocyte fixed about 8 h following progesterone treatment. a) Vesicles are abundantly present in the cortex of this oocyte where they are oriented parallel to the plasma membrane (small arrows). Clusters (CL) of ER elements intermingled with glycogen granules are present in the cortex and in the

subcortical region. Y = yolk platelets; Li = liposomes. Magnification, $\times 12,000$. b) CG do not appear to be surrounded by ER shells. Arrows = vesicles next to the plasma membrane. This cortical arrangement does not change following stimulation by pricking. $\times 41,000$.

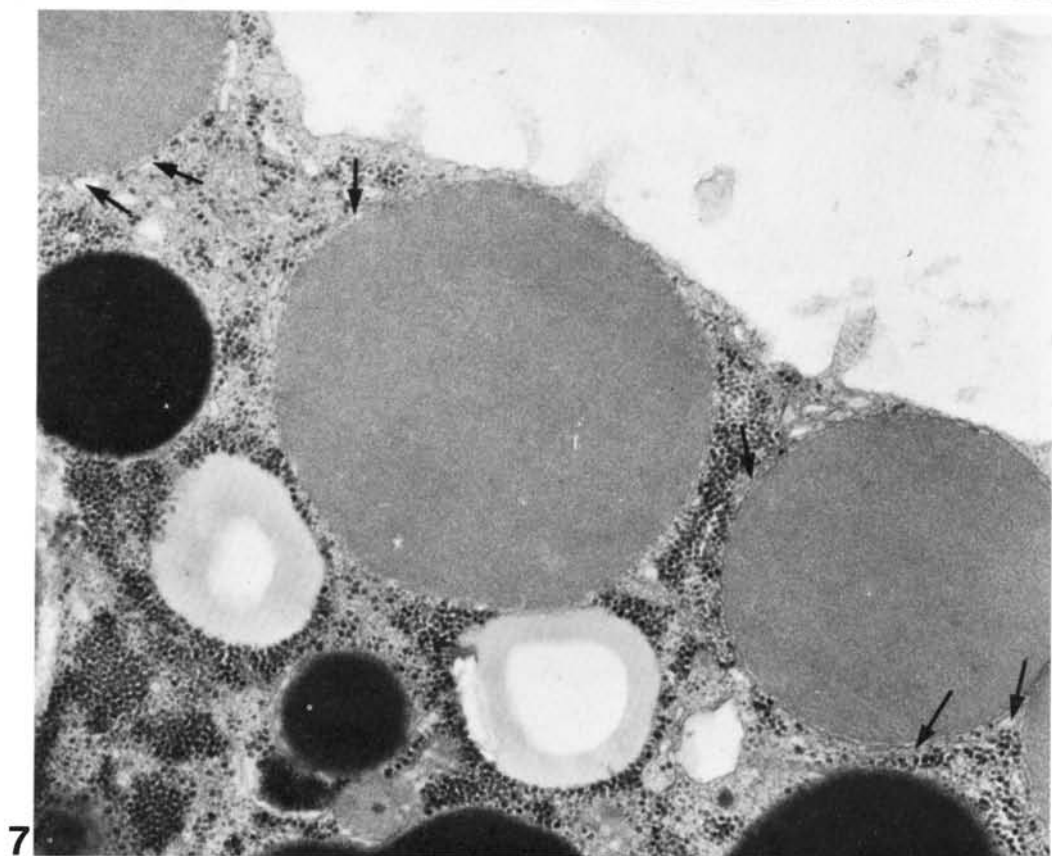
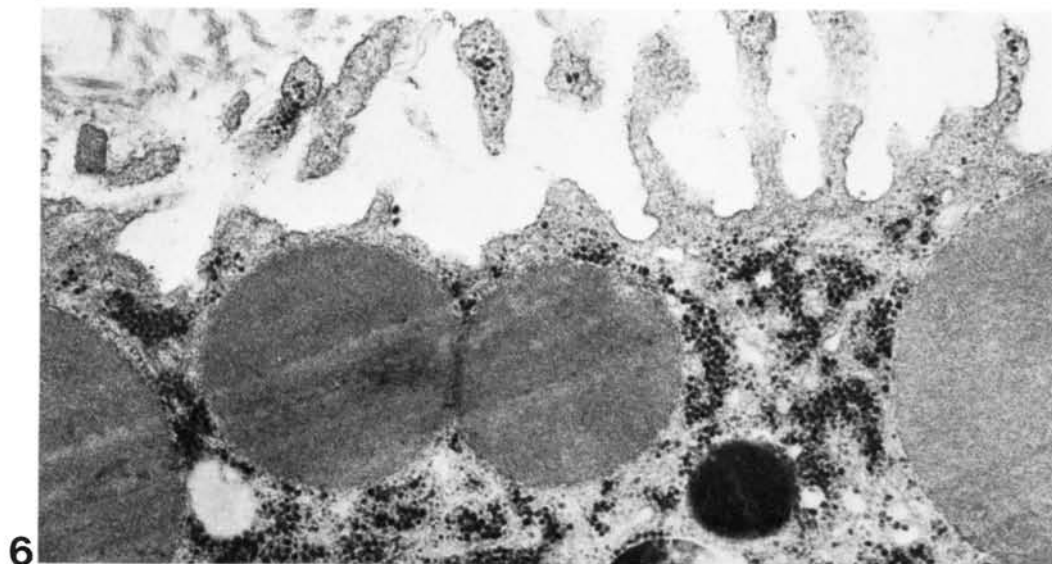
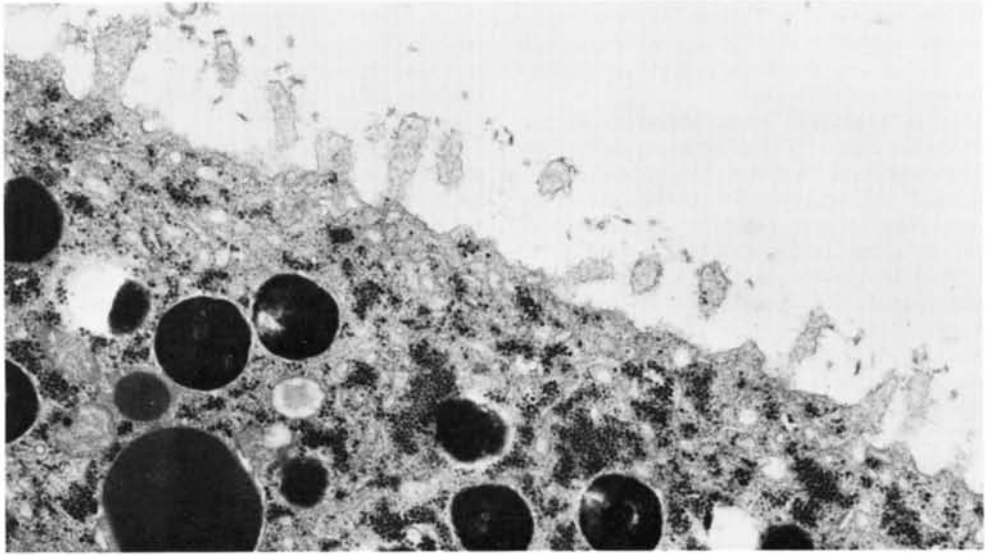
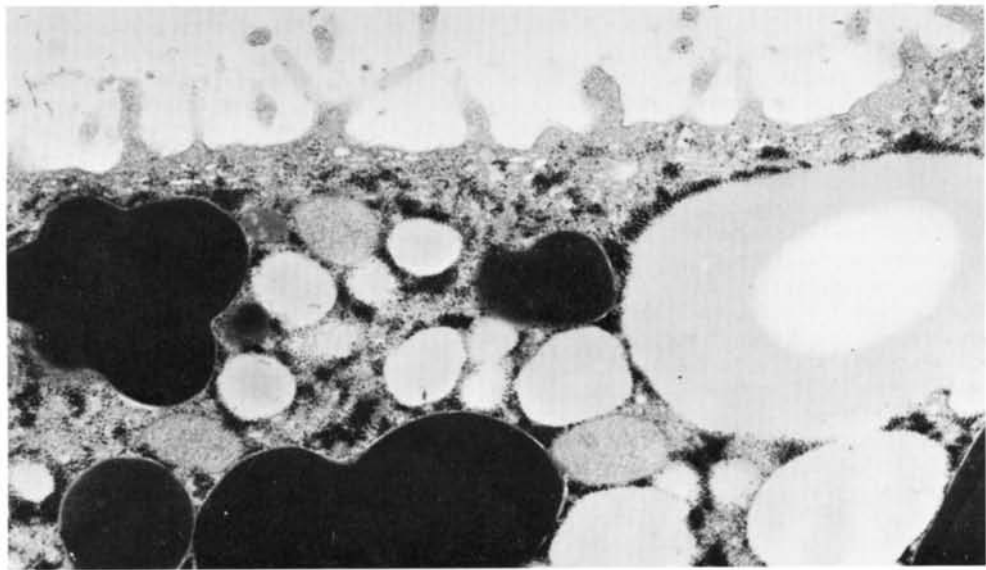


Fig. 6. Control, untreated, defolliculated oocyte kept in Ringer's for 8 h and fixed. The ER elements are randomly distributed in the cortex. Magnification $\times 36,000$.

Fig. 7. Vegetal hemisphere of oocyte fixed 13 h following progesterone treatment, when the first polar body has been extruded. The CGs appear to be covered with ER shells (arrows). Magnification $\times 34,000$.



8



9

Fig. 8. Animal hemisphere of oocyte pricked 8 h following hormone treatment. This cortex is depleted of CG. Magnification $\times 21,000$.

Fig. 9. Vegetal hemisphere of an oocyte pricked 10 h after hormone exposure, when the first polar body has been extruded. Magnification $\times 18,000$.

the cortex of treated oocytes pricked after the appearance of the first polar body (about 13 h after progesterone treatment) (Fig. 9).

DISCUSSION

The data reported show that the ER cortical network and particularly the cisternae which surround CG in *Xenopus* uterine eggs

are gradually organized during oocyte maturation. In ovarian full-grown oocytes ER cisternae are found, before the hormone treatment, in the subcortical region. Here AL are also present and most probably represent the precursor of these cisternae. A transformation of AL in ER is a well-known phenomenon which also occurs in other sys-

tems (for a review, see Maul, '77). Following hormone exposure the ER cisternae migrate to the cortex and AL disaggregate in clusters of cisternae and vesicles.

The ER migration from subcortical to cortical regions and its organization in the cortex of maturing oocytes is a gradual phenomenon, taking about 8 h (in the case of the animal hemisphere). However, numerous ER cisternae stay in the subcortical region, as observed in uterine eggs (Campanella and Andreuccetti, '77). Concomitantly with the ER changes, the oocyte surface becomes smoother and the entire cortical region, including the microfilament bundles, rearranges, thus allowing the ER to settle in the cortex.

The migration and settling of the ER in the cortex might be explained according to Robinson's ('79) findings, which show that during oogenesis, in *Xenopus laevis*, a Cl^- current, probably mediated by Ca^{++} , passes through the oocyte along their animal-vegetal axis. This current accounts for the maintenance of the oocyte polarity, and therefore for the position in the cytoplasm of the nucleus and of other cell components. Following progesterone treatment, this current and the electric field generated by the current terminate. It is possible that, as a consequence of this, the ER and the other cytoplasmic constituent are free to assume a new position in the oocyte (see Robinson, '79).

The disassembly of stacks of AL observed here in maturing *Xenopus* oocytes has also been described by other authors and attributed to the hormone treatment (Balinsky and Devis, in *Xenopus*, '63; Kessel and Subtelny, in *Rana pipiens*, '81). Our data support the hypothesis that the product of AL disaggregation—clusters of vesicles and cisternae—contributes to the organization of the peripheral endoplasmic reticulum of *Xenopus* maturing oocytes. Indeed, in the vegetal hemisphere of maturing oocytes, nests of ER elements identical to those derived from the AL are long stored as such and are observed in positions that will be later (in uterine eggs) occupied by the ER cortical and subcortical network (Campanella and Andreuccetti, '77).

In *Rana*, vesicles are liberated by AL during maturation and some of them are seen next to CG (see Fig. 20 in Kessel and Subtelny, '81). As these vesicles appear to have an origin very similar to those in *Xenopus* oocytes, they probably have similar func-

tions. Interestingly enough, in urodele eggs, where CG are absent, although following progesterone treatment the AL disappear, they undergo neither vesicle nor cisternae formation (Imoh, '82).

From our data and thanks to an adequate examination of control defolliculated oocytes kept in Ringer's, we can conclude that both ER peripheral reorganization and AL disaggregation in maturing *Xenopus* oocytes are phenomena related to progesterone treatment and are among the first signs of cytoplasmic maturation. Furthermore, our observations on the organization of the cortical ER network in the progesterone-treated enucleated oocytes rule out an involvement of the nuclear envelope in this process of cortical ER arrangement.

Our data show a correlation between the differentiation of the cortical ER and the onset of the ability of the oocyte to respond, through CG exocytosis, to a pricking stimulation. In fact, 8 h after progesterone treatment, in the animal half, ER shells are observed around the CG and cisternae and vesicles are seen in the interstices between the CG: It is only in this region that CG exocytosis occurs as a result of pricking. The incomplete differentiation at this stage of cortical ER in the vegetal half might explain the lack of response to the pricking of this region. Since in our experiments we have never observed CG exocytosis in the vegetal half also in the samples fixed 30 min after pricking, a delay in the propagation of the exocytosis stimulus is excluded in the vegetal hemisphere, in contrast to what has been reported by Iwao ('82) in *Bufo bufo* oocytes.

Our result may also partially explain the data by Goldenberg and Elinson ('80), who have similarly shown that, in *Rana pipiens* pricked immature oocytes, the cortical reaction is limited to the animal half cortex. In *Rana pipiens*, however, a cortical ER network is not present in both animal and vegetal halves.

The concomitant differentiation of the cortical ER and the acquisition by the oocyte of the capability to respond to pricking supports the hypothesis that the cortical ER network might be directly involved in the propagation of the activation stimulus. By analogy with the sarcoplasmic reticulum, the ER of *Xenopus* eggs might be the source of intracellular stored Ca^{++} , which is most probably released on activation in this egg (Andreuccetti

et al., in press), as in other species (Steinhardt et al., '77; Gilkey et al., '78).

It is not clear why the ER network is organized faster in the animal half than in the vegetal half. According to Kessel and Subtelny ('81), AL, and therefore the deriving ER vesicles, are more abundant in the region next to the nucleus of maturing *Rana* oocytes. Therefore, one simple explanation could be the unequal closeness of these organelles to the cortex. Furthermore, the unequal responsiveness of maturing oocyte animal and vegetal halves in the fulfillment of ER network organization and in answering to the activation stimuli may be a sign of the functional polarity of the anuran egg, whose typical expression at the time of fertilization consists in the occurrence of egg-sperm fusion only in the animal hemisphere.

ACKNOWLEDGMENTS

This research was carried out at the "Centro di Studio di Microscopia elettronica" of the University of Naples and was supported by the CNR project "Biology of Reproduction" and by an M.P.I. grant.

We thank Dr. Brian Dale for advice and revision of the manuscript, and Messrs. Giuseppe Falcone and Giuseppe Argenzio for photographic work. We also thank Dr. Anna Maria Cirillo for editing the revision of the manuscript.

LITERATURE CITED

- Andreuccetti, P., S. Denis-Donini, A.G. Burrini, and C. Campanella (1984) Calcium ultrastructural localization in *Xenopus laevis* eggs following activation by pricking or by calcium ionophore A 23187. *J. Exp. Zool.* 229:295-308.
- Balinsky, B.A., and Devis, R.J. (1963) Origin and differentiation of cytoplasmic structures in the oocytes of *Xenopus laevis*. *Acta Embryol. Morphol. Exp.*, 6: 66-108.
- Belanger, A.M., and A.W. Schuetz (1975) Precocious induction of activation responses in amphibian oocytes by divalent ionophore A23187. *Dev. Biol.*, 45:378-381.
- Campanella, C., and P. Andreuccetti (1977) Ultrastructural observations on cortical endoplasmic reticulum and on residual cortical granules in the egg of *Xenopus laevis*. *Dev. Biol.*, 56:1-10.
- Campanella, C., and G. Gabbiani (1980) Cytoskeletal and contractile proteins in coelomic oocytes, unfertilized and fertilized eggs of *Discoglossus pictus* (Anura). *Gam. Res.*, 3:99-114.
- Dumont, J.N. (1972) Oogenesis in *Xenopus laevis* (Daudin). I. Stages of oocyte development in laboratory maintained animals. *J. Morphol.*, 136:153-179.
- Epel, D. (1980) Experimental analysis of the role of intracellular calcium in the activation of the sea urchin egg at fertilization. In: *The Cell Surface: Mediator of Developmental Processes*. Subtelny, S. and Wessel, N.K. eds. Academic Press, New York, p. 169.
- Franke, W., P.C. Ratlike, E. Seib, M.F. Trendelenburg, M. Osborn, and Weber (1976) Distribution and mode of arrangement of microfilamentous structures and actin in the cortex of the amphibian oocyte. *Cytobiology*, 14:111-130.
- Gilkey, J., L.F. Jaffe, E.B. Ridgway, and G.T. Reynolds (1978) A free calcium wave traverse the activating egg of the medaka, *Oryzias latipes*. *J. Cell Biol.*, 76: 448-466.
- Goldenberg, M., and R.P. Elinson (1980) Animal/vegetal differences in cortical granule exocytosis during activation of the frog egg. *Dev. Growth Diff.*, 22:345-356.
- Grey, R.D., D.P. Wolf, and J.L. Hedrick (1974) Formation and structure of the fertilization envelope in *Xenopus laevis*. *Dev. Biol.*, 36:44-61.
- Hollinger, T.J., and A.W. Schuetz (1976) Cleavage and cortical granule breakdown in *Rana pipiens* oocytes induced by indirect microinjection of calcium. *J. Cell Biol.*, 71:395-401.
- Hollinger, T.J., J.N. Dumont, and R.A. Wallace (1979) Calcium-induced dehiscence of cortical granules in *Xenopus laevis* oocytes. *J. Exp. Zool.*, 210:107-116.
- Imoh, J. (1982) Occurrence of fine structure of subcortical cytoplasmic islets in fertilized egg of *Cynops pyrrhogaster*. *Dev. Growth Diff.*, 22:153-162.
- Iwao, I. (1982) Differential emergence of cortical granule breakdown and electrophysiological responses during meiotic maturation of toad oocytes. *Dev. Growth Diff.*, 24:467-478.
- Kessel, R.G., and S. Subtelny (1981) Alteration of annulate lamellae in the "in vitro" progesterone-treated full-grown *Rana pipiens* oocytes. *J. Exp. Zool.*, 217: 119-135.
- Millonig, G. (1964) Studio sui fattori che determinano la preservazione della ultrastruttura. In: *From Molecule to Cells. Symposium on Electron Microscopy*. CNR, Rome, pp. 347-362.
- Robinson, K.R. (1979) Electrical currents through full-grown and maturing *Xenopus* oocytes. *Proc. Natl. Acad. Sci. USA*, 76:837-841.
- Schuetz, A.W. (1974) Role of hormones in oocyte maturation. *Biol. Reprod.*, 10:150-178.
- Shapiro, B., and E.M. Eddy (1980) When sperm meets egg: Biochemical mechanisms of gamete interaction. *Int. Rev. Cytol.*, 66:257-295.
- Steinhardt, R.A., R. Zucker, and G. Shatten (1977) Intracellular calcium release at fertilization in the sea urchin egg. *Dev. Biol.*, 25:232-247.
- Vacquier, V. (1981) Dynamic changes of the egg cortex. *Dev. Biol.* 84:1-26.

Calcium Ultrastructural Localization in *Xenopus laevis* Eggs Following Activation by Pricking or by Calcium Ionophore A 23187

P. ANDREUC CETTI, S. DENIS-DONINI, A.G. BURRINI, AND
C. CAMPANELLA

Institute of Histology and Embryology, University of Naples, Via Mezzocanone 8, 80134 Naples (P.A., C.C.), Institute of Molecular Embryology, CNR, 80072 Arco Felice (Naples) (S.D.-D.), and Institute of Zoology, University of Siena, 53100 Siena (A.G.B.), Italy

ABSTRACT In the egg of *Xenopus laevis* a cortical network of smooth endoplasmic reticulum (SER) surrounds and interconnects each cortical granule (CG) (Campanella and Andreuccetti, '77). This network is a possible intracellular site of calcium storage to be called into action for CG exocytosis. In our experiments, *Xenopus* eggs, unfertilized or activated by pricking or by calcium ionophore A 23187, have been fixed in osmium-pyroantimonate for calcium localization.

Our data show that deposits can be detected only in activated eggs. The calcium chelator edetate (EGTA) and x-ray microprobe analysis demonstrate that they contain calcium. Deposits are found on liposomes and on all intracellular cytomembranes, which therefore appear to be possible sites of calcium sequestration. In the case of ionophore-activated eggs, deposits are detectable independently of the presence of extracellular calcium. These data show that in *Xenopus* at activation an intracellular liberation of calcium occurs similar to that described in other species.

Furthermore, the fact that antimony deposits are observed only after activation makes *Xenopus* eggs appropriate material in which to follow the temporal and spatial sequence of appearance of the deposits during the early stages of activation. Our results show that antimony deposits appear first in SER vesicles between the plasma membrane and CGs and then spread to the rest of the egg cytomembranes. These data corroborate our hypothesis that in *Xenopus* the cortical SER network is the first intracellular site where calcium is released at activation. The possible mechanism of calcium release and propagation along the egg cortex is discussed.

The exocytosis of cortical granules (CG) is the most conspicuous event of the activation wave, which is the spreading of an activating stimulus (spermatic or parthenogenetic) along the egg cortex. Studies in *Oryzias* (Teleosts) and in sea urchin eggs have demonstrated that upon activation, Ca^{2+} is released from intraovular sites: about $30 \mu\text{M Ca}^{2+}$ /egg is the value calculated for *Oryzias* eggs (Gilkey et al., '78), whereas in sea urchin eggs, 2.5 to $45 \mu\text{M Ca}^{2+}$ /egg (Steinhardt et al., '77) is released in the cytoplasm and later in the external medium (Nakazawa et al., '79; Arzania and Chambers, '76; Johnston and Paul, '78). The release of this ion is essential both to the initiation of CG exocytosis

and to the exocytosis process itself (Chambers et al., '74; Steinhardt and Epel, '74; Steinhardt et al., '77; Gilkey et al., '78). In agreement with these findings, it has also been shown that Ca^{2+} liberation occurs as a consequence of an autocatalytic process that starts at the site of sperm entrance and slightly precedes the initiation of CG exocytosis (Ridgway et al., '77; Gilkey et al., '78; for reviews: Epel, '80; Shapiro and Eddy, '80; Vacquier, '81). These data strongly suggest that Ca^{2+} also plays a role in the propagation of the activation stimulus and particu-

Address reprint requests to P. Andreuccetti.

larly in the spreading of the wave of CG exocytosis around the egg (Ridgway et al., '77).

One aspect of activation which has been questioned and still remains unknown is where in the egg potentially diffusible calcium ions are stored. The egg of the amphibian *Xenopus laevis* is an interesting model for the study of Ca^{2+} localization, owing to its cortical organization. In this egg, each cortical granule is surrounded by flat vesicles of smooth endoplasmic reticulum (SER) (Grey et al., '74). These cisternae are interconnected through elements of SER and anastomose with subcortical SER clusters (Campanella and Andreuccetti, '77). These observations suggest that the cortical network of *Xenopus laevis* eggs constitutes a functional unit, which upon activation may be involved in the propagation of the stimulus leading to the gradual breakdown of CG. In analogy with the sarcoplasmic reticulum, the SER in *Xenopus* eggs might be the site of intracellular Ca^{2+} storage from where it would be released upon activation (Campanella and Andreuccetti, '77; Andreuccetti et al., '80; and see discussion of Gilkey et al., '78). In amphibians, in contrast to what is known from the studies on sea urchin and *Oryzias* eggs, the role of Ca^{2+} in the activation process has been studied in a rather fragmentary way. In *Rana* eggs, Ca^{2+} introduced into the egg is able to initiate an activation potential (Cross, '81). In the same eggs Wolf ('74) has shown that extracellular Ca^{2+} is required for activation only within the first 5–10 s following pricking. The process of exocytosis taking about 2 min for completion (Kemp and Istock, '67; Grey et al., '74; Wolf, '74); it seems that extracellular Ca^{2+} is required only at the initial stages of activation, whereas it is not required for the propagation of the wave of activation. In *Xenopus* eggs a release of intracellular Ca^{2+} and its implication in activation can be postulated from experiments with Ca^{2+} ionophores whereby the egg can be activated in the absence of extracellular Ca^{2+} (Steinhardt et al., '74). On the other hand, in *Xenopus* immature oocytes, in which the CG have already migrated into the cortex, but are not yet surrounded by SER shells (Campanella et al., '84), microinjected Ca^{2+} triggers only a localized CG breakdown which is not propagated (Hollinger et al., '79).

In the present report we have studied the cytochemical localization of Ca^{2+} in unfertilized and activated *Xenopus laevis* eggs in an

attempt to investigate the presence and the role of this ion in activation.

The cytochemical method we used for Ca^{2+} detection is the pyroantimonate technique with which ions such as Ca^{2+} , Mg^{2+} , and Na^+ are precipitated, with Ca^{2+} as the predominant element in the deposits (Klein et al., '72; Yarom and Chandler, '74; Chandler and Battersby, '76; Weakly, '79). In spite of this possible lack of specificity, the nature of the cation precipitate by pyroantimonate can be determined through the appropriate use of chelators and by x-ray microprobe analysis. We have found that most egg cytomembranes, including ER elements are sites of Ca^{2+} sequestration. However, calcium-antimony precipitates are visualized only in activated eggs. In ionophore-treated eggs this finding appears to be independent of the presence of extracellular Ca^{2+} . Furthermore, our results show that intracellular Ca^{2+} is released at activation first in the SER elements next to the plasma membrane and this release is later extended to all cytomembranes. A brief preliminary report on this subject has been presented elsewhere (Andreuccetti et al., '80).

MATERIALS AND METHODS

Adult *Xenopus laevis* females were kept during spring in aquaria at a constant temperature of 20°C and fed on calf liver or heart twice a week.

Four adult females were injected in the dorsal lymphatic sac with 500 IU Pregnyl (Organon, Oss, Holland) the day before utilization.

Treatment of the egg

Uterine eggs were collected one day after the hormone injection and immersed in 5 mM dithiothreitol (DTT) in 0.1 M NaCl-5 mM Tris (Tris (hydroxymethyl)-aminomethane) HCl (pH 8.0) in order to dissolve the jelly layer. They were then rinsed in Ringer's solution (1.3 mM $CaCl_2$, 113 mM NaCl, 2 mM KCl, 2.3 mM $NaHCO_3$).

A group of eggs was directly fixed for routine electron microscopy or in osmium-pyroantimonate fixative. A second group of eggs was first activated by different procedures as indicated below and then fixed: (1) by pricking in Ringer's; (2) by pricking in Ca-free Ringer's, containing 114.3 mM NaCl and 12 mM EGTA (ethylene-glycol-bis [β -amino ethyl ether N-N' tetracetic acid]) (Wolf, '74),

the specifically Ca²⁺-chelating agent; (3) by exposure to Ringer's containing 10 mM A23187 Ca²⁺ ionophore (Eli Lilly and Company, Indianapolis, Ind.) (Steinhardt et al., '74); or (4) by exposure to A23187 in Ca-free Ringer's containing 12 mM EGTA.

All samples were fixed 30 s to 2 min after application of the stimulus. Ionophore being dissolved in 1.28 mM dimethyl sulfoxide (DMSO), control eggs were exposed to an equal concentration of DMSO in Ringer's for 2 min. Under these conditions, DMSO is not toxic. Some of these control eggs were fixed for routine electron microscopy.

With regard to the characteristics of the stimuli used, it is worth mentioning that the ionophore produces an opening of Ca²⁺ channels in the plasma membrane with which it comes into contact and promotes a local activation response restricted only to the subjacent cytoplasm (see Picheral and Charbonneau, '82; Schroeder and Strickland, '74). By immersing the eggs, as we did, in the ionophore solution, the entire egg surface is exposed to the drug, and therefore the whole egg is activated simultaneously. By contrast, a stimulation by pricking provokes a cell response at the site of pricking, which is then propagated over the entire egg.

Electron microscopy and x-ray microprobe analysis

For routine electron microscopy eggs were fixed in 3% glutaraldehyde in phosphate buffer 0.2 M (Millonig, '64) at pH 7.2-7.4 at room temperature. They were postfixed in 2% OsO₄ in the same buffer, dehydrated in graded alcohols, and embedded in Epon.

Among the various methods for fixation in pyroantimonate-osmium and for tissue processing (Spicer et al., '68; Herman et al., '73; Klein et al., '72), we selected the procedure of Klein et al. ('72), since it gave the most reproducible results and tended to minimize possible cation loss and dislocation. We found that when glutaraldehyde is used as a primary fixative, antimony deposits cannot be observed in the sections (this is in line with the findings of Cardasis et al. ('78). Therefore, the samples were directly fixed in osmium-pyroantimonate. With this fixation the majority of the egg organelles are well preserved. However, a change in the configuration of SER cisternae into vesicles is observed (compare Fig. 1a with Fig. 1b). The fixation procedure we used is the following:

1. Fixation in 2% potassium-pyranthionate containing 1% OsO₄ pH 7.8 for 90 min at 4°C. The slight alkaline pH inhibits the formation of nonspecific precipitation products (Klein et al., '72).

2. Dehydration in graded ethanol during half (50 min) the total time currently used, in order to minimize cation loss and dislocation (Klein et al., '72).

Some of the eggs were purposely broken in the fixative to ensure better exposure of the whole ooplasm to the fixative. Samples were fixed in 2% OsO₄ alone as controls.

Thin sections were observed with a Philips 301 electron microscope either directly or after staining with lead citrate and uranyl acetate. The nature of the antimony deposits was evaluated by treating thin sections showing precipitates with either an aqueous solution containing 5 mM EGTA or distilled water as a control at 60°C (Ravazzola, '76).

For x-ray microprobe analysis, sections approximately 1,000 Å thick were cut and collected on Formvar- and carbon-coated copper grids. They were left unstained and observed with a Philips 300 electron microscope equipped with an EDAX energy dispersive analyzer. The conditions of analysis were an accelerating voltage of 80 kV, 50 eV for the channel, and the time of analysis was 100 s.

Since antimony and calcium emission peaks practically overlap (for calcium the K α peak is 3.7 keV; for antimony the L α peak is 3.6 keV) the presence of calcium cannot be directly estimated with this method, but requires the use of a computer. Therefore, such analysis was performed in order to determine whether, in sections containing antimony deposits, elements such as magnesium and sodium are present, which, apart from calcium, can possibly precipitate with antimony (K α peak of sodium = 1 keV; K α peak of magnesium \cong 1.2 keV).

RESULTS

Unfertilized eggs

Ultrathin sections of unfertilized uterine eggs do not show any electron-dense deposits in the cytoplasm after fixation in antimony osmium (Fig. 1b). Only a few deposits can be observed on the vitelline envelope (data not shown). This result was obtained in all the samples examined that were derived from four independent clutches of eggs, even if the eggs were broken during the fixation procedure in order to ensure full penetration of the fixative in the ooplasm.

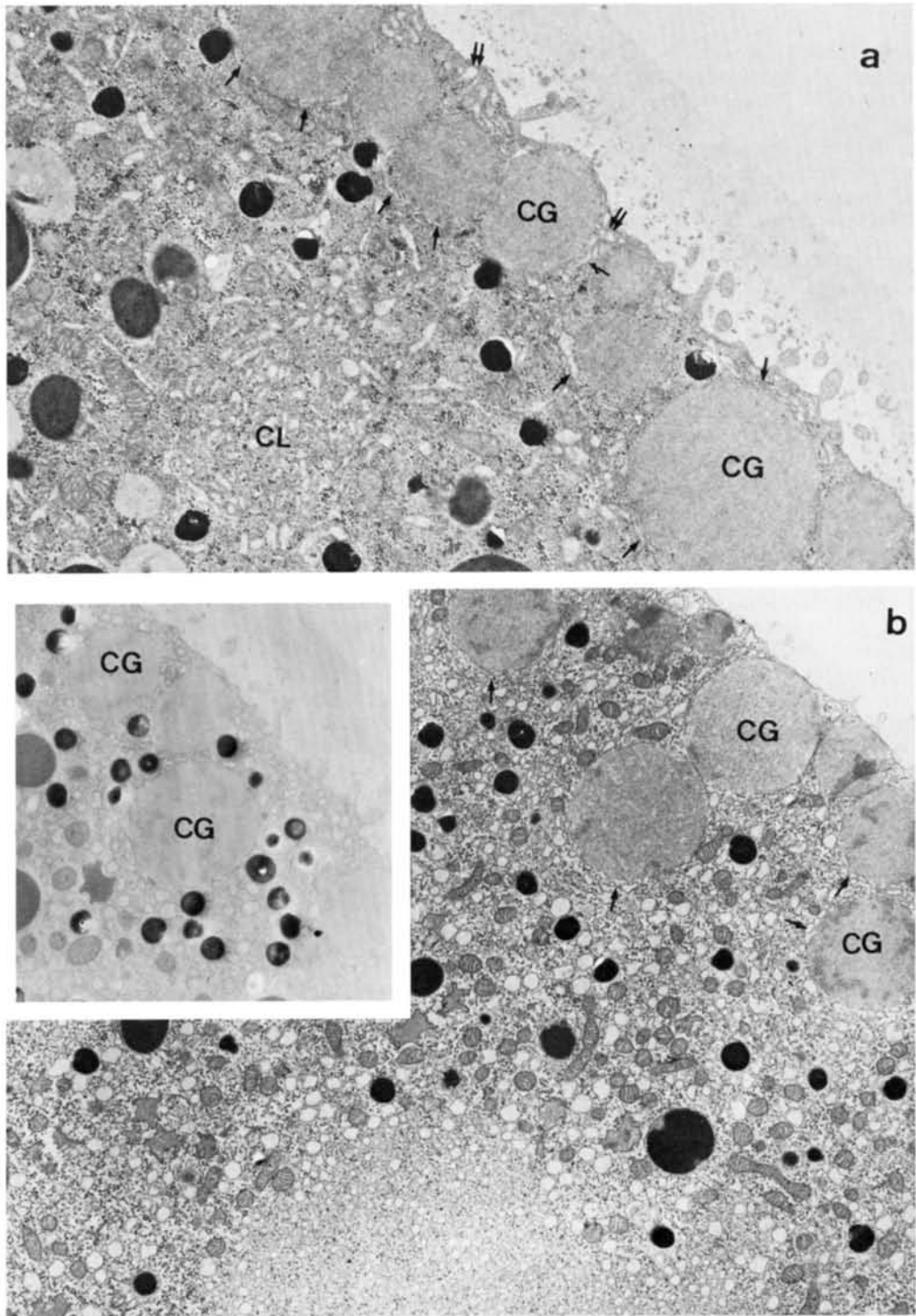


Fig. 1. Unfertilized egg of *Xenopus*. a. Egg fixed in glutaraldehyde for routine electron microscopy. Each cortical granule (CG) is surrounded by a network of SER cisternae elements (small arrows) which anastomose with the cisternae clusters (CL), located in the subcortical cytoplasm. In the interstices between the CGs, note the presence of additional cisternae (double small arrows) close to the plasma membrane. $\times 7,200$. b. Unfertilized

egg fixed with osmium pyroantimonate and stained. Following this kind of fixation most cisternae are converted into vesicles. Particularly, the cisternae shells surrounding CG are converted into chains of vesicles (small arrows) closely apposed to each cortical granule. Antimony deposits are absent. $\times 7,000$. Inset. Unstained unfertilized egg fixed in osmium pyroantimonate. $\times 7,000$.

Activated eggs

By pricking. When eggs are pricked in complete Ringer's, as described in Materials and Methods, and fixed within 1 min from stimulation, no deposits are observed, presumably because the activation response is not yet complete at the time of fixation. On the other hand, when eggs are fixed 1.30–2 min after activation, antimony deposits appear on most cytomembranes (Figs. 2, 3). They are clearly noticeable on vesicles surrounding the CGs that are either intact or at various stages of exocytosis (Figs. 2, 3). Deposits are also present on mitochondria and on the cytomembrane of cortical granules and on pigment granules, as well as on the inner and outer surfaces on the plasma membrane (Figs. 2, 3). In the subcortical layer, deposits are also observed on the surfaces of the liposomes and on vesicles. Larger deposits than the ones found on the egg organelle cytomembranes are present on the fertilization envelope and on the outer surface of the plasma membrane (Fig. 2).

When eggs are pricked in Ca-free-EGTA Ringer's, they are not activated (see also Wolf, '74). Antimony deposits are not observed in thin sections.

By ionophore. In eggs activated by A 23187 in Ca²⁺ complete Ringer's, the process of exocytosis is detectable as early as 30 s following the treatment. In sections in which CGs are still intact, antimony deposits are found only on the vesicles next to the plasma membrane and located in the interstices between the CGs and also on the liposomes (Fig. 4a,b). In sections, where where CGs are either intact or have extruded, the deposits are depicted on all cytomembranes, including those of vesicles located in the subcortical cytoplasm (Fig. 5). This localized or increased positivity could reflect a different timing in ionophore and fixative diffusion through the vitelline envelope and into the cytoplasm.

When the eggs are exposed to ionophore in Ca-free EGTA Ringer's for 30 s, deposits are found, in contrast to what happens in the case of pricking. They are observed on the cytomembranes in the cortical region, whereas in the subcortical region only the liposome surface and mitochondria are "stained" (Fig. 6).

When the treatment with ionophore in Ca-complete Ringer's is prolonged (1–2 min) the peripheral region of the egg where deposits are present does not exceed 3 μ m in depth

(Fig. 7). When such a prolonged treatment with ionophore is performed in Ca-free-EGTA Ringer's, deposit-free sections result, even though the exocytotic reaction has occurred. This could be due to the fact that at this time and under these experimental conditions all available intracellular Ca²⁺ has already been released before fixation.

In control samples exposed to DMSO alone, no deposits are ever found.

In all the samples observed, whether activated by pricking or by ionophore, deposits are always associated with the cytomembranes and are not found free in the cytoplasm. As far as the reaction specificity is concerned, it is of importance to note that the deposits on the cytomembranes can be washed away after treatment of the sections with EGTA (Fig. 8c). On the contrary, some deposits on the fertilization membrane (data not shown) and on the liposomes are not so labile and remain after such treatment (Fig. 8c).

X-ray microprobe analysis

The spectra obtained through x-ray microprobe analysis show an emission in the range of 3.6–3.7 keV in sections where antimony deposits are found. In particular in regions where the precipitates are on vesicles close to the CGs, they produce signals of this range, whereas emission peaks corresponding to magnesium and sodium are practically absent (Fig. 8a). The deposits on plasma membrane were also analyzed, and only in this case are the signals accompanied by peaks corresponding to sodium (data not shown). Osmium M α and L α peaks (respectively 1.9 and 8.9 keV) are present in all the sections analyzed.

In control regions of deposit-free cytoplasm or of unfertilized egg sections, as well as of Formvar coat, the signals in the range of 3.6–3.7 keV are absent (Fig. 8b). Copper (L α = 0.9 keV, K α = 8 keV, K β = 8.9 keV) and several more element peaks are detected both in experimental and control spectra (Fig. 8a,b), but they are due to the copper grids and to metals in the specimens and/or within the microscope.

DISCUSSION

The use of osmium-pyroantimonate fixation has allowed us to localize Ca²⁺-binding sites in the egg of *Xenopus laevis*. These sites are not observed before activation but be-

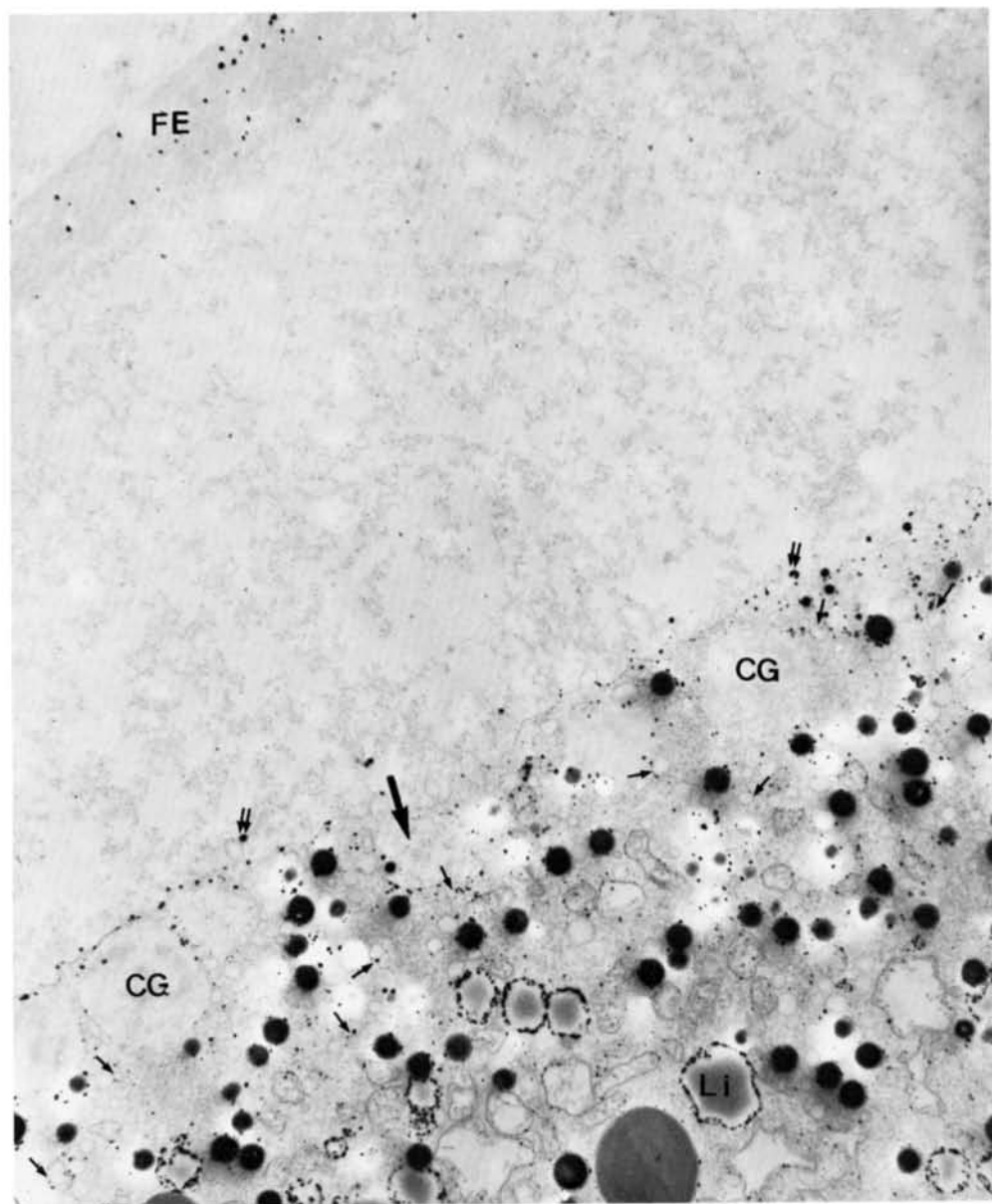


Fig. 2. Unstained section of an egg activated by pricking and fixed in osmium-pyranthimonate 1.30 min later. Deposits are present on the fertilization envelope (FE), on the outer (double small arrows) and inner surface of the plasma membrane, on the cytomembranes of all organelles, as well as on the external shell of the liposomes

(Li). The small arrows indicate deposits on vesicles. Deposits on the FE and on the outer aspect of the plasma membrane are generally larger than the ones on the intraovular organelles. The large arrow indicates a site where exocytosis has occurred. $\times 6,500$.

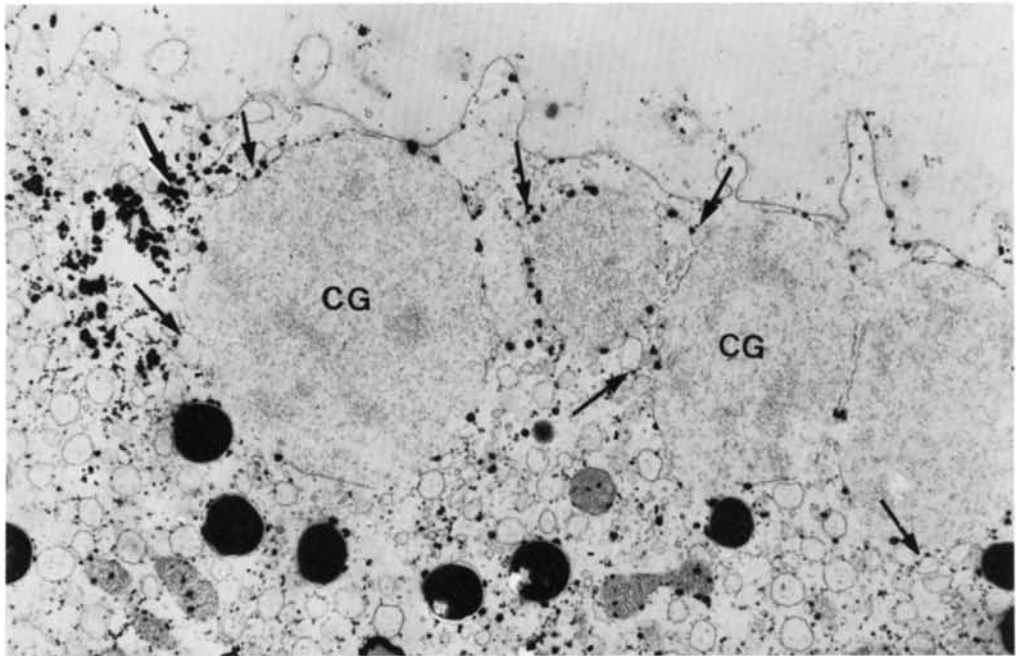


Fig. 3. Stained section of an egg activated by pricking and fixed in osmium-pyroantimonate 1.30 min later. Deposits are located on the plasma membrane, on the cytomembranes of CG, pigment granules, vesicles, and on

mitochondria. The cytomembranes of vesicles next to CG are decorated with antimony deposits (arrows) which, in this section, are particularly abundant on the cluster of vesicles indicated by the large arrow. $\times 14,000$.

come detectable shortly afterward. This situation makes *Xenopus* eggs particularly appropriate for such a study, since it permits observation of the temporal and spatial sequence of the appearance of antimony deposits as a result of activation.

After activation, antimony precipitates are present on the cytomembranes of most membrane-bound organelles including the endoplasmic reticulum vesicles, mitochondria, and the plasma membrane, which are the typical Ca²⁺-sequestering cellular compartments, as well as on the liposome surface. The deposits observed are of two sizes: the smaller ones found on the cytomembranes and the larger ones located predominantly at the fertilization envelope and on the outer surface of the plasma membrane. According to Klein et al. ('72), the site of the deposits reflects primarily the degree of supersaturation achieved by the reagent at various sites prior to precipitation, with an inverse relationship between the degree of supersaturation and deposit size. As we mentioned before, K-pyroantimonate precipitates not only Ca²⁺, but also Mg²⁺ and Na⁺, though to a lesser extent (Spicer and Swanson, '72; Klein et al., '72; Herman et al., '73; Yarom and Chandler, '74; Chandler and Battersby, '76;

Cardasis et al., '78; Weakly, '79). Owing to the use of EGTA and x-ray analysis, we have been able to show that Ca²⁺ is the major component of the precipitate in our material. Indeed, by incubating sections with EGTA, deposits on the cytomembranes are eliminated, whereas few of them remain on the fertilization membrane and the liposomes. These results coincide with those obtained by x-ray microprobe analysis showing that, in sections where antimony deposits are found on the cytomembranes, emission peaks corresponding to Na⁺ and Mg²⁺ are practically absent. A Na⁺ emission was only found in deposits that are located on the external surface of the plasma membrane. Therefore, we conclude that in our preparations, the loci where antimony is deposited (CG membranes and SER shells, pigment granules, vesicles, mitochondria, and liposome surfaces) represent possible sites of Ca²⁺ sequestration. This localization is similar to that found in sea urchin eggs, where Ca²⁺-containing antimony deposits are found on all cytomembranes (Cardasis et al., '78). Whether the observed sites of Ca²⁺ precipitation represent the original sites of Ca²⁺ location "in vivo" is the next point that we will discuss.

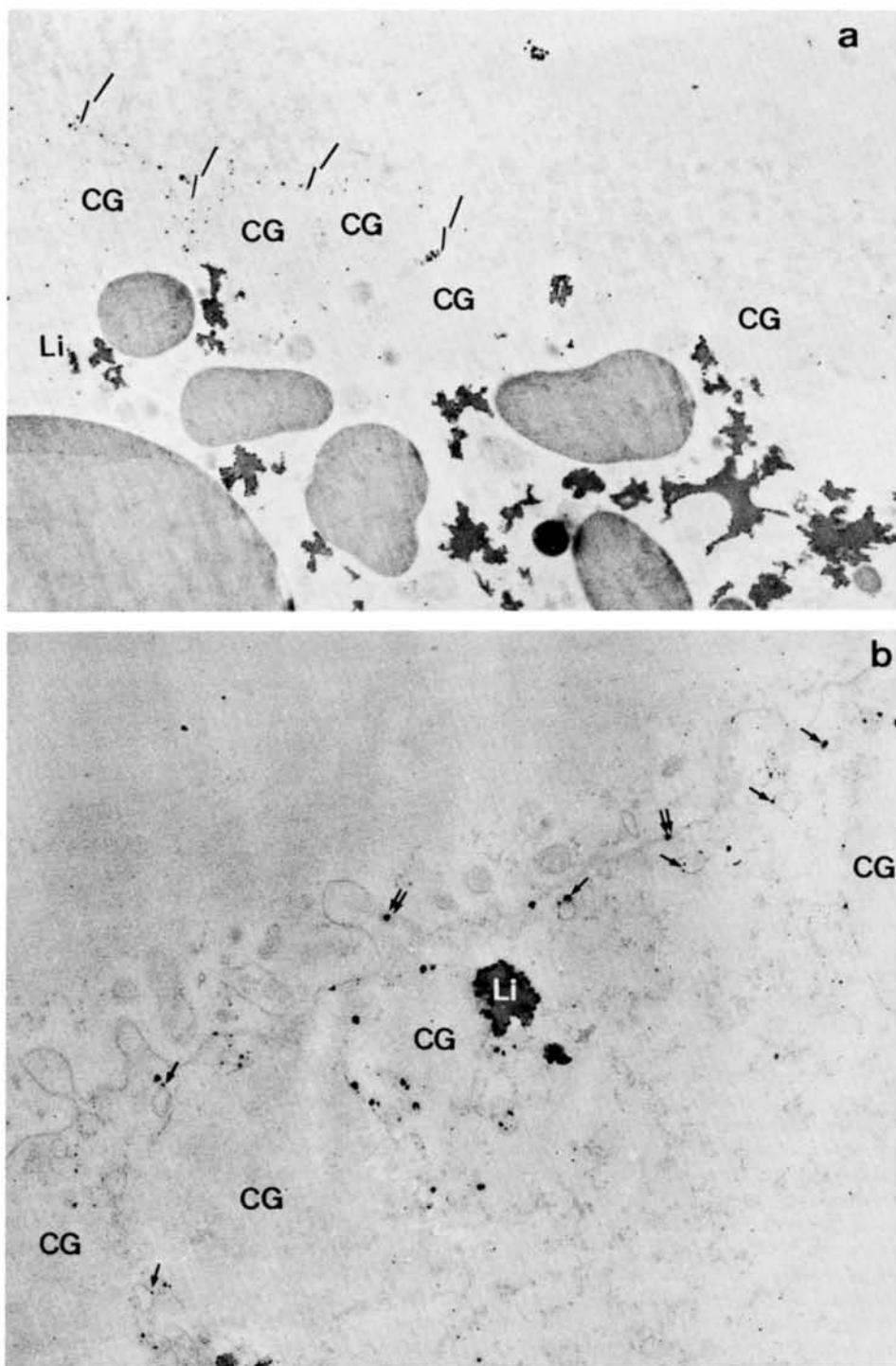


Fig. 4. Unstained section of an egg, fixed 30 s after exposure to ionophore in osmium-pyrosulfonate. a. Deposits are present on the plasma membrane and in the interstices between CGs, only in the sites indicated by the arrows, whereas elsewhere deposits are observed

only on liposomes (Li). $\times 5,000$. b. Deposits are found on the plasma membrane (double small arrows) and on vesicles next to the CGs or to the plasma membrane (small arrows). In this section a few deposits are seen on CG membranes. $\times 24,000$.

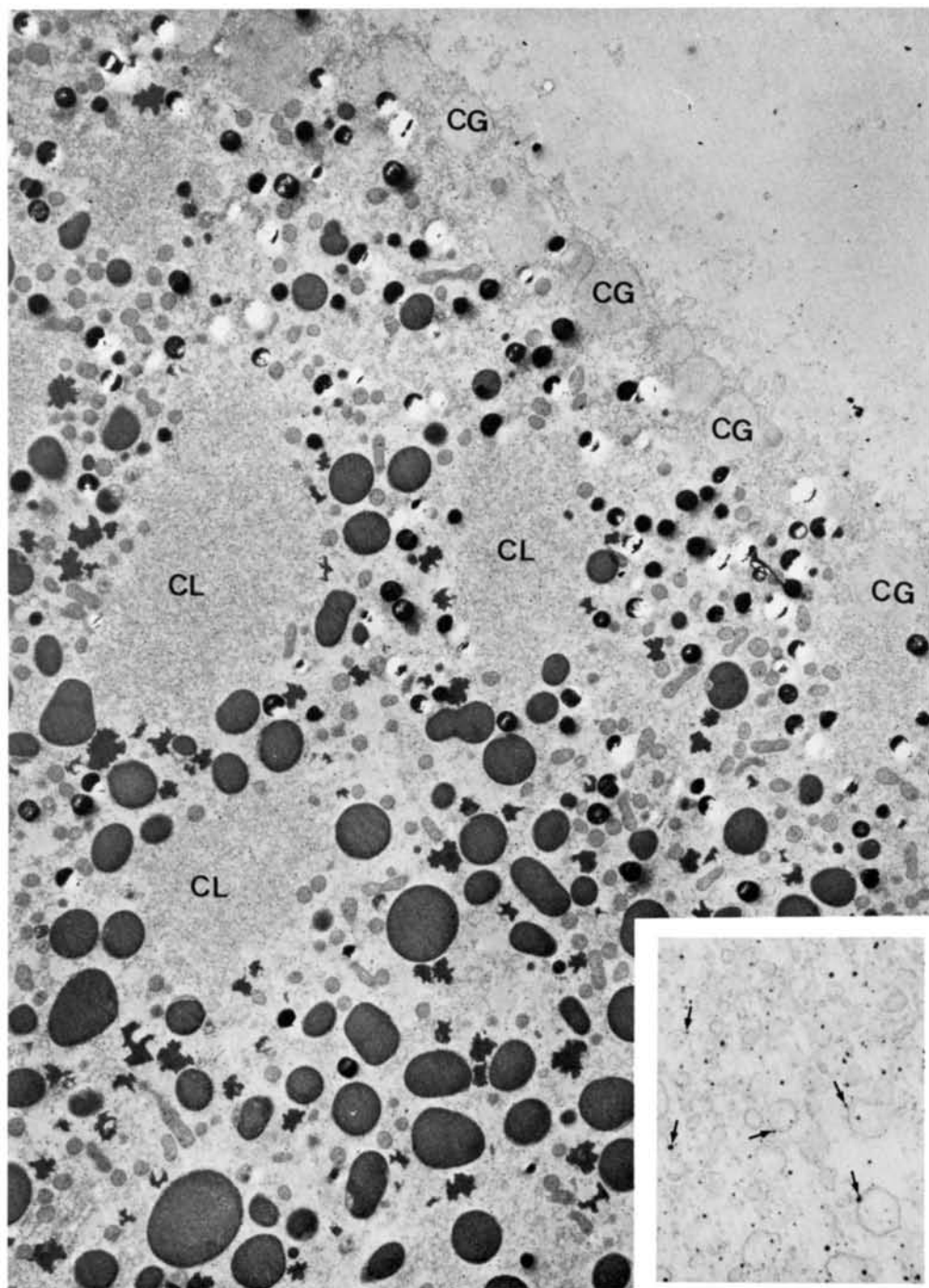


Fig. 5. Unstained section of an egg, fixed 30 s after exposure to ionophore in osmium-pyroantimonate. Deposits are seen on the cytomembrane of the organelles in the entire peripheral cytoplasm. CL = clusters of

vesicles. $\times 4,000$. Inset. Higher magnification of a cluster of vesicles. Small arrows = deposits on the vesicle membranes. $\times 40,000$.

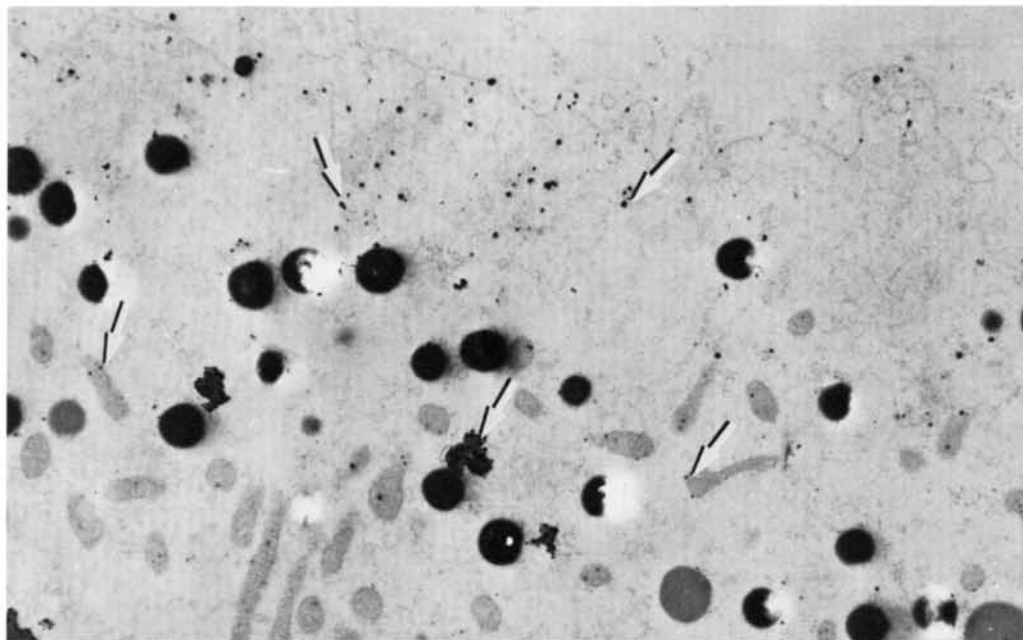


Fig. 6. Unstained section of an egg fixed in osmium-pyranthimonate 30 s after exposure to ionophore in Ca-free-EGTA-Ringer's. The deposits are seen in the cortical

region and on the mitochondria and liposomes (arrows). $\times 11,000$.

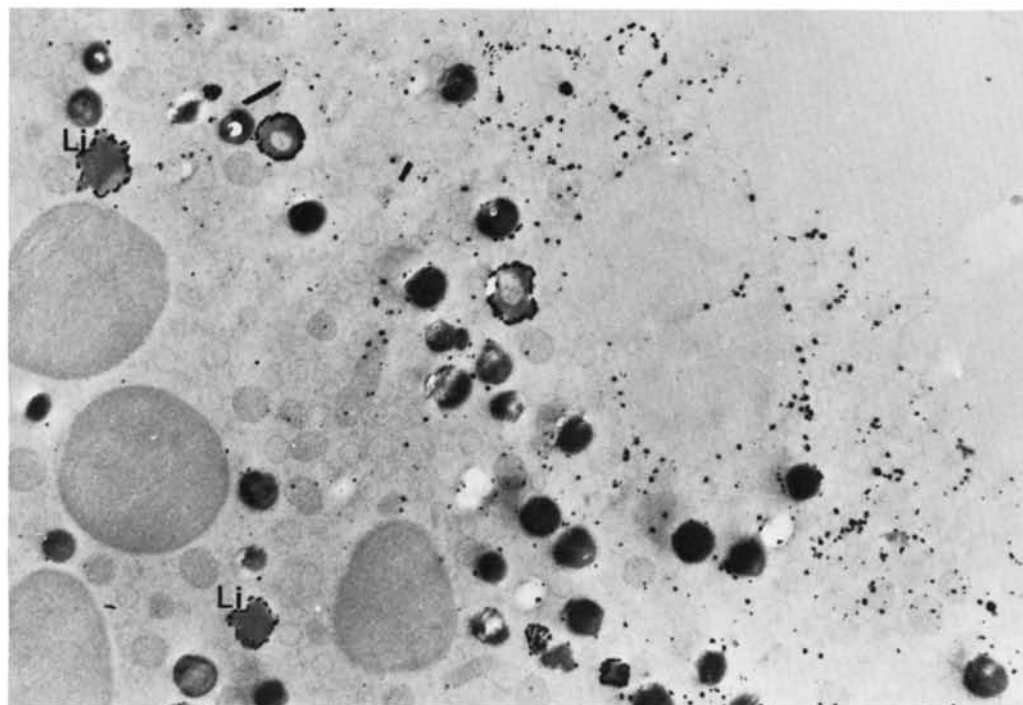


Fig. 7. Unstained section of an egg fixed in osmium-pyranthimonate 30 s after exposure to ionophore in Ca-complete medium. Deposits are observed on the egg cy-

tomembranes of organelles present in a cortical region of about $3\mu\text{m}$, and on liposomes (Li). $\times 9,500$.

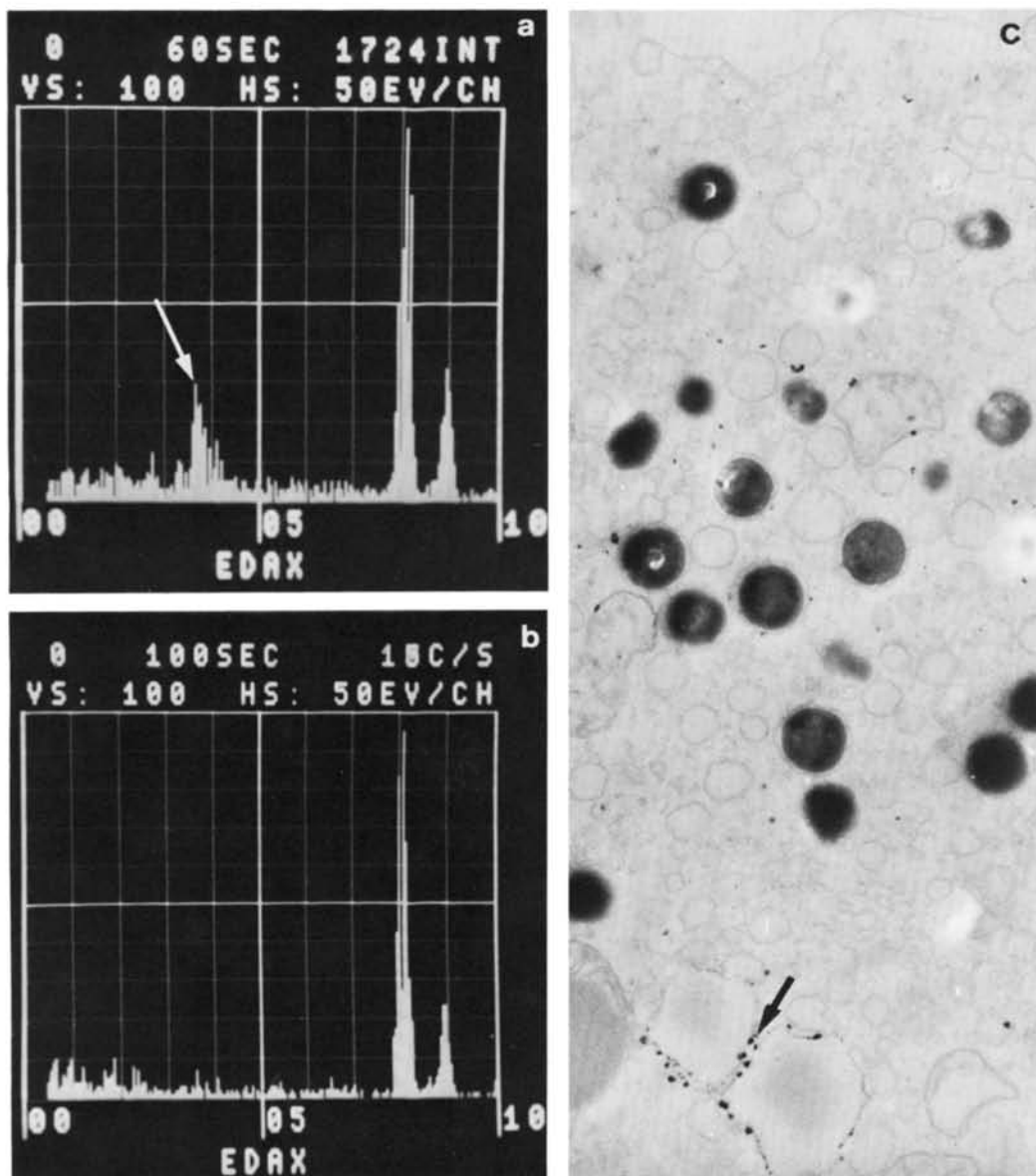


Fig. 8. a. X-ray energy spectrum of a section similar to the one shown in Figure 3. The electron beam was positioned over a region where antimony deposits are on vesicles next to CGs. The x-ray spectrum represents the number of x-ray events (ordinate) versus the individual energies of the x-ray in keV. The arrow indicates a peak representing not only antimony emissions but probably also some calcium emission. b. X-ray energy spectrum of a section of a control region of an unfertilized egg, where no deposits are detectable. The 3.6–3.7 peak is absent.

Both in this figure and in Figure 8a, copper ($K\alpha = 8$ keV, $K\beta = 8.9$ keV, $L\alpha = 0.9$ keV) and osmium ($M\alpha = 1.9$ keV, $L\alpha = 8.9$ keV) are present and partially overlapping. The emissions at 1–1.3 keV (probably related respectively to sodium and magnesium) are low, as is true also in Figure 8a. c. Section unstained and treated with EGTA of an egg pricked in calcium-complete Ringer's and fixed 1.30 min later. Deposits are present only on liposomes (arrows) $\times 25,000$.

In this type of cytochemical study, as well as in others, artifacts in the localization of the reaction product may occur during the fixation procedure. For instance, Ca^{2+} as such, before precipitation with pyroantimonate, might be washed out of the egg during fixation; and/or free Ca^{2+} , as well as depos-

its, might have been translocated from original sites to secondary ones. In order to reduce to a minimum the possible diffusion of deposits from their original sites, we have drastically reduced the total dehydration time (Klein et al., '72). Since we have never found free deposits in the cytoplasm we feel confi-

dent that an artifactual diffusion of the precipitate does not occur in our system (see Debbas et al., '75). It is still possible, however, that during the cytochemical procedure Ca^{2+} has been translocated from original sequestering sites to secondary ones. As will be discussed later, the results obtained with ionophore strongly suggest that the observed localization of antimony deposits coincides with Ca^{2+} localization "in vivo."

A further point to consider is whether the origin of Ca^{2+} precipitate by pyroantimonate is external or internal. The fact that the deposits are also seen in eggs exposed for 30 s to ionophore in Ca-free-EGTA Ringer's indicates that precipitates can be formed even when the source of Ca^{2+} is internal. In such samples when fixation is performed a little later (1.30 min), we have seen that deposits are absent, though they can still be observed when Ca^{2+} is present in the medium. This suggests that when external Ca^{2+} is provided, it does participate in the formation of deposits, which is consistent with the occurrence of a Ca^{2+} influx following activation (Mazia, '37; Nakazawa et al., '79; Paul and Johnston, '78; Arzania and Chambers, '76; in sea urchin eggs).

With regard to the results obtained when eggs are stimulated in Ca-free-EGTA Ringer's, our data emphasize the difference between the two kinds of stimuli used. In fact, they confirm that activation occurs in such conditions only when ionophore is the activating agent (Steinhardt et al., '74; Wolf, '74), and that only in this case can Ca-antimony deposits be detected.

The most intriguing result we have obtained is that antimony deposits are present only in activated eggs. We should have expected that before activation, sites of Ca^{2+} storage could be readily detected by the pyroantimonate method, as has been found in sea urchin eggs (Cardasis et al., '79). Our results cannot be attributed to a lack of permeability of the unactivated egg, which is known to be lower than in activated eggs (Maeno, '59; Webb and Nuccitelli, '81) for the following reasons: (1) permeability characteristics are lost during osmication, which in our samples occurred simultaneously with pyroantimonate exposure; and (2) no deposits have been found even when the eggs are broken in the fixative. It seems, therefore, highly probable that in *Xenopus* eggs, before activation, Ca^{2+} is bound in intracellular compartments where it is not available for

precipitation with pyroantimonate. Immediately following activation, variations in the physicochemical characteristics of the cytoplasm occur. These might involve changes in pH, for instance, (Webb and Nuccitelli, '81) or other changes whereby Ca^{2+} would be released from intracellular compartments, thus becoming accessible for precipitation with pyroantimonate. This hypothesis is in agreement with the data obtained with ionophore activated eggs in the absence of external Ca^{2+} which indicate that Ca^{2+} is released from intracellular stores following activation.

As already mentioned, the pattern and timing of deposit localization in activated eggs suggest that the deposits are directly formed at the sites where Ca^{2+} is released. In fact, in eggs exposed to ionophore for 30 sec, in regions where no sign of exocytosis is detectable, the deposits on cytomembranes are exclusively on the plasma membrane and on the SER elements next to the CGs. In regions where exocytosis takes place, the deposits cover the cytomembranes in the whole cytoplasm, whereas in regions where all CGs have already been extruded, the deposits are again restricted to the cortical region. Such a sequence of events, although reconstructed from static images, suggests that Ca^{2+} is first liberated close to the plasma membrane and in the network of SER interlacing the CGs and subsequently in the cytomembranes in deeper regions of the cytoplasm. This is followed by a centrifugal diffusion of Ca^{2+} , starting in deeper regions, whereas it is still retained on the cytomembranes of the cortical region. This interpretation is compatible with the hypothesis that in *Xenopus*, as in other species (Steinhardt et al., '77; Ridgway et al., '77; Gilkey et al., '78), the Ca^{2+} intracellular release occurring at activation is associated with CG exocytosis.

It is also in agreement with our original hypothesis that the smooth endoplasmic reticulum is the site where Ca^{2+} is released following stimulation, as in the case of the SER of muscle and other excitable cells (Walz, '82). Therefore, we suggest that the interconnected CG shells constitute the cortical egg compartment through which a Ca^{2+} -mediated Ca^{2+} release spreads along the entire egg cortex, starting from the region of sperm penetration. On the other hand, our data show that at the very initial stages of activation, Ca^{2+} deposits are found first in the plasma membrane and in the subjacent SER

cisternae, located in the interstices between CGs. Cisternae are constantly present in these regions, where they establish close contact with the plasma membrane in the earlier phases of meiosis, i.e., following oocyte maturation when the rest of the cortical network becomes organized (Campanella et al., in press). The close relationship between SER cisternae and the plasma membrane is reminiscent of that occurring in the muscle fiber. These considerations would favor, as an alternative hypothesis, the idea that the plasma membrane depolarization which follows activation (Maeno, '59; Ito, '72; Cross and Elinson, '80; Schlichter and Elinson, '81; Grey et al., '82) would be transmitted directly to the subjacent cisternae, which in turn would be stimulated to release Ca²⁺.

NOTE ADDED IN PROOF

Gardiner and Grey (J. Cell Biol., 96:1159-1163, 1983) have recently observed the presence of membrane junctions between the plasma membrane and SER cisternae in *Xenopus* eggs. Most of these junctions form during oocyte maturation, as a consequence of progesterone treatment. These junctions have features which are reminiscent of plasma membrane-sarcoplasmic reticulum junctions present in muscle cells. In *Xenopus* eggs, according to the authors and similarly to the conclusions of the present paper, the cisternae which are part of the junctions are good candidates for storage and release of Ca²⁺ as a consequence of plasma membrane depolarization at fertilization.

ACKNOWLEDGMENTS

This paper is dedicated to Prof. Mario Galgano on the occasion of his seventy-fifth birthday.

We are grateful to Professor Baccio Bacchetti for suggestions and to Dr. A.M. Cirillo for editing and revising the manuscript. We wish to acknowledge the expert assistance of the technical staff of the "Centro di Microscopia Elettronica della Facoltà di Scienze" of the University of Naples, where this work was carried out.

This research was supported by A/4 and 60% MPI grants to Dr. C. Campanella.

LITERATURE CITED

- Andreuccetti, P., A.G. Burrini, S. Denis-Donini, and C. Campanella (1980) Ca²⁺ localization in smooth endoplasmic reticulum in *Xenopus* eggs. Abstracts of the XIV International Embryological Conference, Patras, Greece.
- Arzania, R., and A.L. Chambers (1976) The role of divalent cations in activation of the sea urchin egg. I. Effect of fertilization on divalent cation content. J. Exp. Zool., 198:65-78.
- Campanella, C., and P. Andreuccetti (1977) Ultrastructural observations on cortical endoplasmic reticulum and on residual cortical granules in the egg of *Xenopus laevis*. Dev. Biol., 56:1-10.
- Campanella, C., P. Andreuccetti, C. Taddei, and R. Tal- evi (1984) The modification of cortical endoplasmic reticulum during "in vitro" maturation of *Xenopus laevis* oocytes and its involvement in cortical granules exocytosis. J. Exp. Zool. 229:283-293.
- Cardasis, C.A., H. Schuel, and L. Herman (1978) Ultra- structural localization of calcium in unfertilized sea urchin eggs. J. Cell Sci., 31:301-115.
- Chambers, E.L., B.C. Pressman, and B. Rosen (1974) The activation of sea urchin eggs by the divalent ionophores A23187 and X-537A. Biochem. Biophys. Res. Commun., 60:126-132.
- Chandler, J.A., and S. Battersby (1976) X-ray microanal- ysis of zinc and calcium in ultrastructural sections of human sperm cells using the pyroantimonate tech- nique. J. Histochem. Cytochem., 24:740-748.
- Cross, N.L. (1981) Initiation of the activation potential by an increase in intracellular calcium in eggs of the frog *Rana pipiens*. Dev. Biol., 85:380-384.
- Cross, N.L., and R.P. Elinson (1980) A fast block to poly- spermy in frogs mediated by changes in the membrane potential. Dev. Biol., 75:187-198.
- Debbas, G., L. Hoffman, E.J. London, and L. Hurtwith (1975) Electron microscopic localization of calcium in vascular smooth muscle. Anat. Rec., 182:447-472.
- Epel, D. (1980) Experimental analysis of the role of intra- cellular calcium in the activation of the sea urchin egg at fertilization. In: The Cell Surface Mediator of Devel- opmental Processes. Subtenly, Wessel, A.C. Press, New York, p. 169.
- Gilkey, J., L.F. Jaffe, E.B. Ridgway, and G.Y. Reynolds (1978) A free calcium wave traverses the activating egg of the medaka, *Oryzias latipes*. J. Cell Biol., 76:448-466.
- Grey, R.D., D.P. Wolf, and J.L. Hedrick (1974) Formation and structure of the fertilization envelope in *Xenopus laevis*. Dev. Biol., 36:44-61.
- Grey, R.D., M.J. Bastiani, D.J. Webb, and E.R. Schertel (1982) An electrical block is required to prevent poly- spermy in eggs fertilized by natural mating of *Xenopus laevis*. Dev. Biol. 89:475-484.
- Herman, L., T. Sato, and C.N. Hales (1973) The electron microscopic localization of cations in pancreatic islets of Langerhans and their possible role in insulin secre- tion. J. Ultrastruct. Res., 42:298-311.
- Hollinger, T.G., J.N. Dumont, and R.A. Wallace (1979) Calcium-induced dehiscence of cortical granules in *Xenopus laevis* oocytes. J. Exp. Zool., 210:107-116.
- Ito, S. (1972) Effects of media of different ionic composi- tion on the activation potential of anuran egg cell. Dev. Growth Diff., 14:217-227.
- Johnston, R.N., and M. Paul (1978) Calcium influx fol- lowing fertilization of *Urechis caupo* eggs. Dev. Biol., 57:364-374.
- Kemp, N.E., and N.L. Istock (1967) Cortical changes in growing oocytes and in fertilized or pricked eggs of *Rana pipiens*. J. Cell Biol., 34:101-112.
- Klein, R.L., S.S. Yen, and A. Thureson-Klein (1972) Cri- tique on the K-pyroantimonate method for semiquan- titative estimation of cations in conjunction with electron microscopy. J. Histochem. Cytochem., 20: 65-78.

- Maeno, T. (1959) Electrical characteristics and activation potential of *Bufo* eggs. *J. Gen. Physiol.*, **43**:139-157.
- Mazia, D. (1937) The release of calcium in *Arbacia* eggs on fertilization. *J. Cell Comp. Physiol.*, **10**:291-304.
- Millonig, G. (1964) Studio sui fattori che determinano la preservazione della ultrastruttura. In: *From Molecule to Cells. Symposium on Electron Microscopy*, CNR, Rome, pp. 347-362.
- Nakazawa, J., K. Asami, Shuger R. Fujiwara, and I. Yasumazu (1979) Ca^{2+} uptake, H^+ injection and respiration in sea urchin eggs on fertilization. *Exp. Cell Res.*, **63**:143-146.
- Paul, M., and R.N. Johnston (1978) Uptake of Ca^{2+} is one of the earliest response to fertilization of sea urchin egg. *J. Exp. Zool.*, **203**:143-149.
- Picheral, B., and M. Charbonneau (1982) Anuran fertilization: A morphological reinvestigation of some early events. *J. Ultrastruct. Res.*, **81**:306-321.
- Ravazzola, M. (1976) Intracellular localization of calcium in the chromaffin cells of the rat *Adrenal medulla*. *Endocrinology*, **98**:950-953.
- Ridgway, E.B., J.C. Gilkey, and L.I. Jaffe (1977) Free calcium increases explosively in activating medaka eggs. *Proc. Natl. Acad. Sci. USA*, **74**:623-627.
- Schlichter, L.C., and R.P. Elinson (1981) Electrical responses of immature and mature *Rana pipiens* oocytes to sperm and other activating stimuli. *Dev. Biol.* **83**:33-41.
- Schroeder, T.E., and D.L. Strickland (1974) Ionophore A23187, calcium and contractility in frog eggs. *Exp. Cell Res.*, **83**:139-142.
- Shapiro, B., and E.M. Eddy (1980) When Sperm Meet Egg: Biochemical Mechanisms of Gamete Interaction. *Int. Review of Cytology*. Bourne and Danielli, eds. Academic Press, New York, pp. 257-295.
- Spicer, S.S., and A. Swanson (1972) Elemental analysis of precipitates formed in nuclei by antimony-osmiumtetroxide fixation. *J. Histochem. Cytochem.*, **20**: 518-526.
- Steinhardt, R.A., and D. Epel (1974) Activation of sea urchin eggs by a calcium ionophore. *Proc. Natl. Acad. Sci. USA*, **71**:1915-1919.
- Steinhardt, R.A., D. Epel, E.J. Carroll, and R. Yanagimachi (1974) Is calcium ionophore a universal activator for unfertilized eggs? *Nature*, **252**:41-43.
- Steinhardt, R.A., R. Zucker, and G. Shatten (1977) Intracellular calcium release at fertilization in the sea urchin egg. *Dev. Biol.*, **25**:232-247.
- Vacquier, V.D. (1981) Dynamic changes of the egg cortex. *Dev. Biol.*, **84**:1-26.
- Walz, B. (1982) Ca^{2+} sequestering smooth endoplasmic reticulum in an invertebrate photoreceptor. I. Intracellular topography as revealed by OsFeCN staining and *in situ* Ca accumulation. *J. Cell Biol.*, **93**:839-848.
- Weakly, B.S. (1979) A variant of the pyroantimonate technique suitable for localization of calcium in ovarian tissue. *J. Histochem. Cytochem.*, **27**:1017-1028.
- Webb, A., and R. Nuccitelli (1981) Direct measurement of intracellular pH changes in *Xenopus* eggs at fertilization and cleavage. *J. Cell Biol.*, **91**:562-567.
- Wolf, D.P. (1974) The cortical response in *Xenopus laevis*. *Dev. Biol.*, **40**:102-115.
- Yarom, R., and J.A. Chandler (1974) Electron probe microanalysis of skeletal muscle. *J. Histochem. Cytochem.*, **22**:147-154.

From: THE MOLECULAR AND CELLULAR BIOLOGY OF
FERTILIZATION
Edited by Jerry L. Hedrick
(Plenum Publishing Corporation, 1986)

THE CORTICAL ENDOPLASMIC RETICULUM AND ITS POSSIBLE ROLE IN
ACTIVATION OF DISCOGLOSSUS PICTIS (Anura) EGGS

Chiara Campanella, Riccardo Talevi, Umberto Atripaldi,
and Lucia Quaglia

Dipartimento Di Biologia Evolutiva E Comparata
University of Naples
Naples, Italy

SUMMARY

The role of endoplasmic reticulum was investigated in the egg of Discoglossus pictus; recent findings suggest that this organelle is the source of Ca^{2+} sequestration and release at activation. In the egg of Discoglossus the dimple is the only site where sperm-egg fusion occurs. Microvilli containing microfilament bundles penetrate into the dimple cytoplasm and thus define a cortical layer containing cortical granules, tubular cisternae 35 nm thick and vacuoles. In the underlying cytoplasm are clusters of small cisternae and mitochondria. In the region of the egg cortex outside of the dimple, clusters of cisternae, some vacuoles and a heterogeneous population of small granules are found. In eggs activated by pricking contraction starts from the site of pricking and travels to the antipode. Sections of eggs, fixed 20 to 60 s following fertilization or pricking, show that the tubular cisternae have disappeared and the clusters of cisternae have opened to give rise to longer cisternae arranged in chains. These chains pile up below the vacuoles which are now flat and long because of multiple fusion. A network of cisternae is thus formed whose constituents lean against the microfilament bundles and within 5 min from activation approach the plasma membrane. The flattened vacuoles and the cortical granules are exocytosed. Some cisternae fuse with the microvillar membrane thus participating in microvilli elongation. The microfilament rootlets gradually rearrange and become shorter. In the cortex outside the dimple the cisternae clusters do not open, whereas exocytosis of granules occurs. In eggs treated with A23187, vacuoles and cortical

granules undergo exocytosis; however a cisternal network is not formed.

The possible stimuli that cause the cisternae network to form at activation only in the dimple and in a matter of seconds are discussed. Our observations, namely exocytosis, formation of cortical wave of contraction and changes in the cytoskeleton organization at activation are consistent with an increase of free Ca^{2+} . Vacuoles and cisternae appear to be good candidates for the sequestration and release of Ca^{2+} as well an important source for the increase in total plasma membrane at activation.

INTRODUCTION

Upon fertilization of fish and sea urchin eggs, Ca^{2+} is released from intracellular storage sites, and the resulting rise in the free Ca^{2+} concentration leads to cortical granule (CG) exocytosis and the activation of metabolism (17,19,38). In the fish, Oryzias, a wave of Ca^{2+} release and, following by about 15 sec, of CG exocytosis, spreads from the site of sperm entry to the opposite pole of the egg (19,33). The search for the intracellular site of Ca^{2+} storage and the mechanism of Ca^{2+} release at activation are intriguing lines of research generated by these findings (17,37,41). In the present paper we will describe some recent data related to these questions and describe our recent studies on the egg of the frog, Discoglossus pictus.

A particularly attractive subject for study in this regard has been the egg of Xenopus laevis. The ultrastructure of its cortex suggests that the site of Ca^{2+} storage may be a specialized network of the smooth endoplasmic reticulum (SER). A shell of smooth cisternae surrounds each CG (20). These shells are interconnected and are part of a network of SER which includes clusters of cisternae situated at regular intervals in the subcortical layer, as well as cisternae lying between the CG, in close contact with the plasma membrane (5,18). Junctions between these cisternae and the plasma membrane are similar to those between the sarcoplasmic reticulum and the plasma membrane of muscle cells (18).

The following lines of evidence strongly suggest that the cortical SER network is the cellular compartment which stores and releases Ca^{2+} at fertilization (and is probably involved in the propagation of CG exocytosis). First, during progesterone-stimulated oocyte maturation, the oocyte becomes able to respond to a pricking stimulus at the same time that the cortical SER becomes fully organized (7,11). Second, at fertilization the organization of the network changes and then the network gradually disappears (5). Finally, the results of staining eggs with osmium and pyroantimonate to visualize Ca^{2+} suggest that Ca^{2+} release originates at these cortical cisternae.

There are no calcium antimonate deposits in unfertilized eggs, but in eggs activated by Ca^{2+} ionophore in Ca^{2+} -free Ringer's containing EGTA, deposits are first seen on the plasma membrane and the adjacent smooth cisternae, and later are found over organelles more centrally located (1,2).

In sea urchin eggs, calcium antimonate deposits are found on the cytomembranes of all egg organelles (8). However, according to Poenie and co-workers (32), as a consequence of fertilization these deposits are lost from tubular sacs located in the egg cortex but not from sacs and other vacuoles located in deeper cytoplasm. Therefore also in the sea urchin, tubular sacs located in the egg cortex appear to be good candidates for storage and release of Ca^{2+} at fertilization.

There is as yet no direct evidence that the free Ca^{2+} concentration increases in the cortex of Xenopus eggs, but it seems likely that a wave of Ca^{2+} release starts at the point of sperm penetration and then spreads around the egg, leading to the wave of CG exocytoses. Recently Busa and Nuccitelli (personal communication), using a Ca^{2+} -selective intracellular microelectrode, found that the subcortical free Ca^{2+} level increases from 0.4 to 1.2 μM about 1 min after fertilization. The increase is transient; it begins in the animal hemisphere and traverses the egg as a wave moving at 10 $\mu\text{m}/\text{sec}$. This Ca^{2+} pulse is probably the subcortical extension of a cortical Ca^{2+} wave. Alternatively, a change in membrane occurring when the membrane depolarizes at activation (10,13,21,24,25,28,35) could be transmitted to the subjacent cisternae through the junctions they make with the membrane and stimulate them to release Ca^{2+} . This model has obvious parallels to the release of Ca^{2+} from the sarcoplasmic reticulum upon depolarization of the plasma membrane and transverse tubule system (2,18,19), and is supported by the presence of the plasma membrane-cisternae junctions (18), and by the above mentioned data obtained with pyroantimonate fixation. This hypothesis, however, does not easily explain the fact that CG exocytosis spreads as a wave from the point of sperm entrance (20,44). The factors which cause the propagation of CG exocytosis may be better understood when electrophysiological studies are coupled to an accurate analysis of CG exocytosis.

In contrast to the Xenopus egg, the unfertilized eggs of other amphibians have randomly distributed vesicles in the cortex and they lack the cortical vesicular network. In the present study we describe the presence of numerous, well-organized cisternae in eggs of Discoglossus pictus. Interestingly, this pattern of cisterna organization is first observed shortly after fertilization, and is seen only at the site where the sperm fuses with the egg: the "animal dimple" (4,22). These conditions may aid in further elucidating the role of the SER in egg activation, including its function as a Ca^{2+} sequestering and releasing organelle.

MATERIALS AND METHODS

Adult Discoglossus pictus (the painted frog) were collected near Palermo, Italy, during the period February to May. To induce ovulation, females were injected in the dorsal lymph sac with 100 I.U. of human chorionic gonadotropin (Pregnyl, Organon Oss, Holland) in amphibian Ringer's solution, containing (in mM): NaCl, 111; CaCl₂, 1.3; KCl, 2.0; and NaHCO₃, 2.0. Eggs were surgically removed from the uterus 18 h later. Sperm in seminal fluid was obtained by pricking a male's seminal vesicles 24-48 h after a similar injection of hCG. To insure the optimal percentage of fertilized eggs, this sperm suspension was spread over "dry" eggs.

To artificially activate eggs, the regions of jelly designated J2, J3, and the "animal plug" (14) were first removed by immersing the eggs in a solution of 5 mM dithiothreitol (DTT), 0.1 M NaCl, and 5 mM Tris, pH 8.0. The eggs were then activated in full strength Ringer's by pricking with a tungsten needle, or by exposure to a solution of the Ca²⁺ ionophore, A23187, made by dilution from a stock solution of a 2 mM in absolute ethanol. (See Results for the concentrations used.) At intervals of 30 s to 20 min after insemination or artificial activation, eggs were fixed for electron microscopy as previously described (6).

RESULTS

Unfertilized Eggs

The animal hemisphere of the Discoglossus egg is indented by an asymmetrical jelly component, the "animal plug". The center of this indentation is further invaginated and forms the cup-shaped dimple. The dimple is about 150 μ m in diameter and filled with a colloidal content (Fig. 1, and inset a). In the dimple cytoplasm are finger-shaped microvilli containing microfilament bundles implanted at regular intervals. The bundles penetrate into the cytoplasm for about 12 μ m; contractile protein localization in the dimple has been described elsewhere (6). The thickness of the peripheral layer (zone A), where there are CGs, which are about 0.5 μ m in diameter, tubular cisternae, glycogen, and vacuoles, and where there are few mitochondria, is defined by the presence of the microfilament bundles, and therefore is about 12 μ m deep (Figs. 1 and 2a). The depth of this layer and also the concentration of the vacuoles are maximal at the center of the dimple, where the sperm fuses with the egg, and they gradually decrease toward the perimeter of the dimple (4,6).

The tubular cisternae of zone A have electron-dense contents, and are mostly present just beneath the plasma membrane. They average about 35 nm in thickness. Vacuoles are about 0.2 to 0.3 μ m in diameter, contain sparse material, and are characterized by the

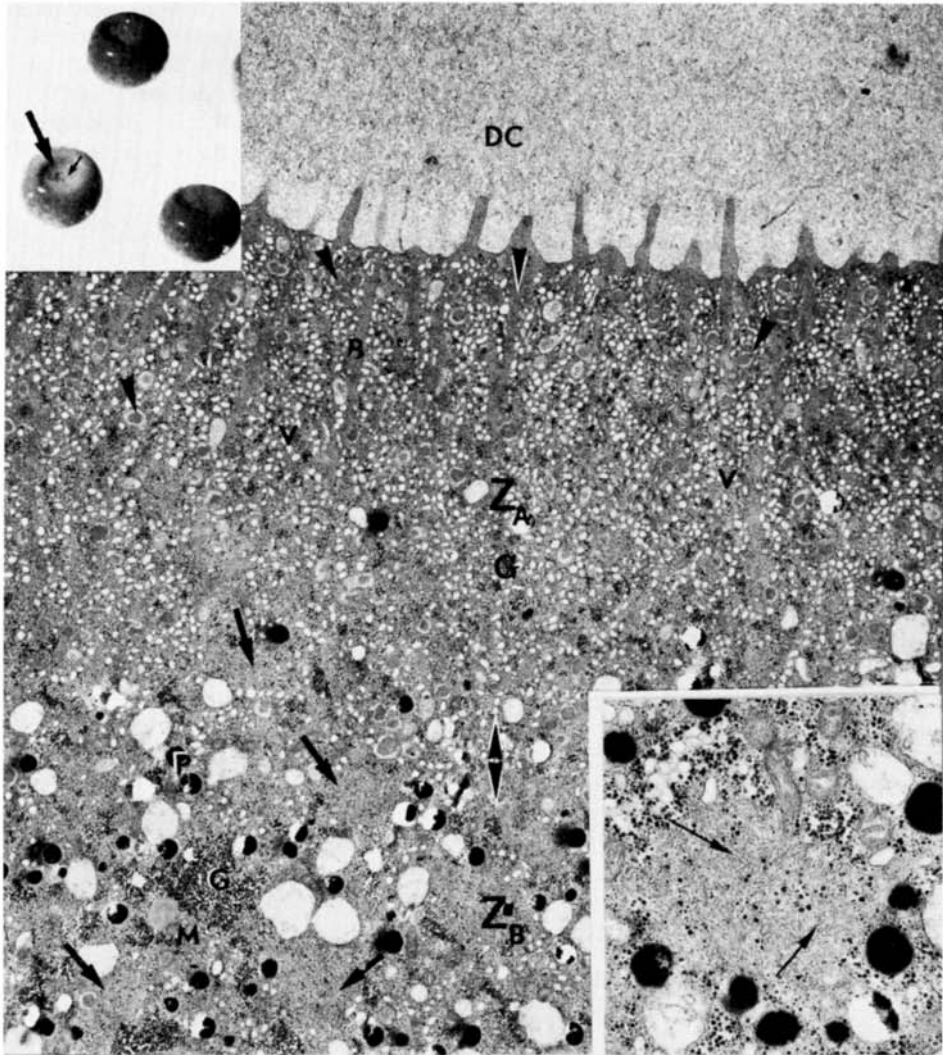


Figure 1. Dimple of unfertilized egg. At the dimple surface are finger-shaped microvilli containing microfilament bundles. In zone A (Z_A), one can observe the bundle rootlets (B), cortical granules (arrowheads), vacuoles (V), and glycogen. In zone B (Z_B) are clusters of cisternae (large arrows), pigment granules (P), mitochondria (M), and large islets of glycogen (G). DC = dimple content x 5000. Inset a: the large arrow points to the indentation at the animal half and the small arrow points to the dimple x 10. Inset b: clusters of small cisternae (arrows) x 14,000.

presence of small electron-dense invaginations (Fig. 2a). In zone B (Fig. 1), several clusters of small cisternae are present, and a few CGs. In the region of the egg cortex outside of the dimple where microvilli and microfilament bundles are short, there are similar clusters of cisternae, vacuoles with invaginations, as well as a heterogenous population of small granules (about $0.3\ \mu\text{m}$ in diameter). These granules differ from the CGs in size and in the structure of their contents (compare Figs. 2a and 2b).

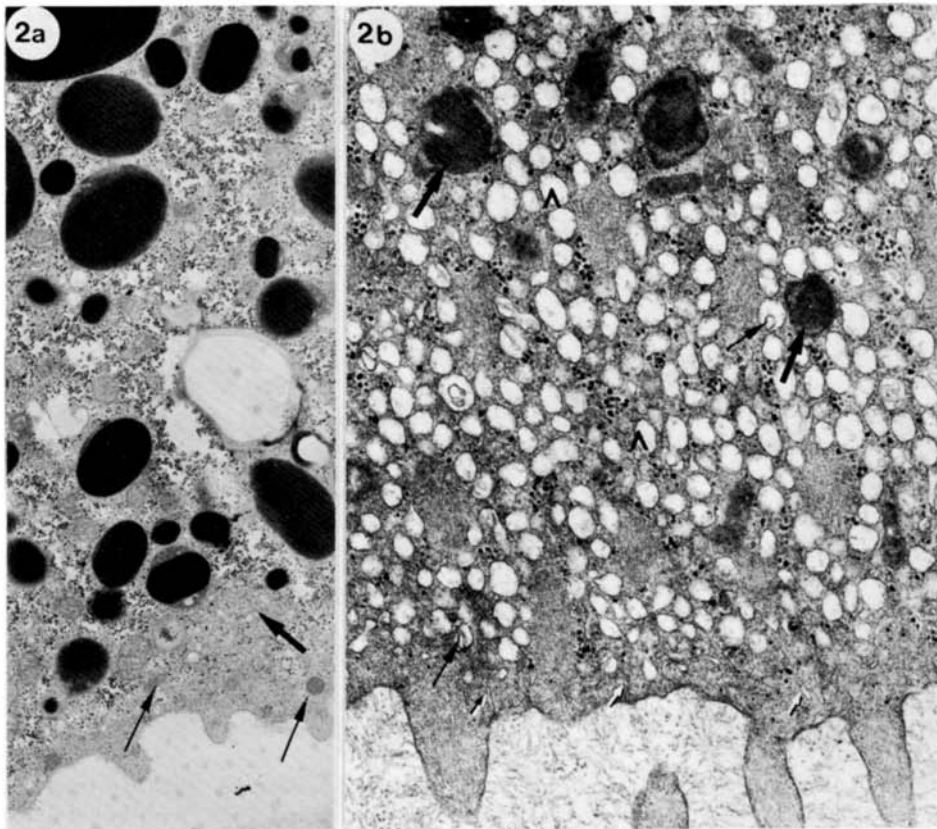


Figure 2. Unfertilized egg. 2a: Dimple. Beneath the plasma membrane are tubular cisternae about 35 nm in diameter (small arrows). Cortical granules (large arrows) and vacuoles (V) containing sparse material and invaginations (arrows), and located among microfilament bundles $\times 26,000$. 2b: Vegetal hemisphere. Small granules (about $0.3\ \mu\text{m}$) (arrows) with variable content and clusters of cisternae (large arrow) are in the egg cortex $\times 7,000$.

Fertilized Eggs

In eggs fixed 30 s to 1 min after sperm addition, conspicuous changes are evident in the central portion of the dimple. In zone B the cisternae have lengthened, and are arranged in chains rather than clusters. The chains of cisternae are parallel to the egg surface, but bend to extend into zone A, where they are perpendicularly oriented with respect to the plasma membrane (Fig. 3). Some chains bend laterally and anastomose with adjacent chains of cisternae (Fig. 4a). The cisterna chains pile up below the vacuoles, which are now flatter and longer than those in the unfertilized egg, so that an apparent continuity is formed between these two kinds of vacuolar structures (Fig. 3). Furthermore, the cisternal chains lean against the microfilament bundles in zone A (Fig. 4a). The CGs and flattened vacuoles are also closely associated with the microfilament bundles (Fig. 4a). Another feature of interest observed at this stage is the absence of the 35 nm thick cisternae.

After insemination, several types of exocytosis are seen. Some of the flattened vacuoles appear to have fused with the plasma membrane by 1 min after fertilization (Fig. 4a). At later stages (1 to 3 min after insemination), when the microfilament bundles have partly disaggregated, flattened vacuoles and/or cisterna chains are seen in the microvilli (Fig. 5). The cisternae appear to fuse with the microvillar membrane, so that they become inserted by exocytosis into the plasma membrane and cause the microvilli to elongate (Fig. 5). Other cisternal chains terminate in close contact with the plasma membrane in the spaces between the microvilli, but we were unable to detect fusion between the plasma membrane and these cisternae. Furthermore, at this stage the number of flattened vacuoles and CGs has decreased. In fact, cases of CG exocytosis are observed: where the CG membrane becomes inserted into the plasma membrane, flat vesicles form which may be hybrid vesicles containing portions of both the CG membrane and the dimple membrane; they are also seen in the dimple contents (Fig. 5).

Later (3 to 5 min after insemination), longer microvilli are observed, and the microfilament rootlets lose their regular orientation in the peripheral cytoplasm. Interestingly, the cisternal clusters in the peripheral cytoplasmic layer outside the dimple do not change following activation. However, about 5 min following insemination, most granules disappear, showing that exocytosis does also occur in these regions of the egg (data not shown).

By about 20 min after fertilization, the microfilament rootlets become shorter, few cisternae are visible in the dimple, and vacuoles are arranged in a layer beneath the plasma membrane (Fig. 6). During this period two other changes also occur: the dimple regresses in the first 6 min after insemination, and the larger concavity gradually rounds out (by 20 min after insemination) as the animal plug

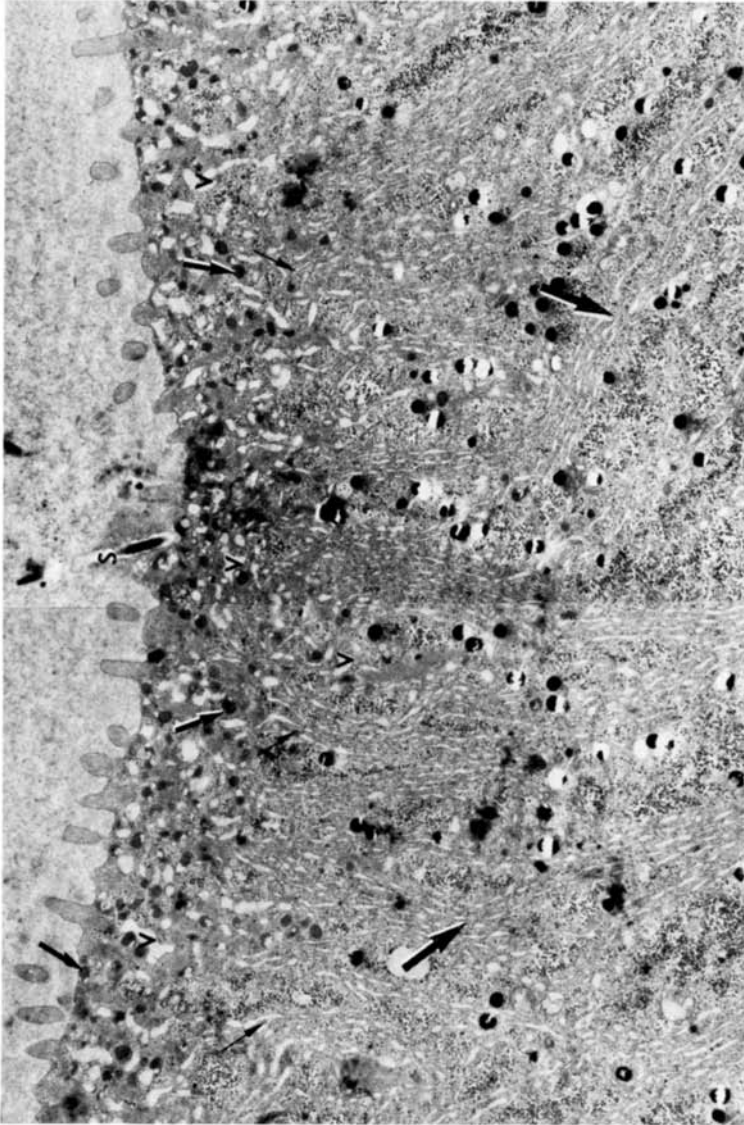


Figure 3. Dimple, 1 min following insemination. Cisternae clusters of zone B have transformed into chains of longer cisternae (large arrows) and are perpendicularly oriented with respect to the plasma membrane. Zone A vacuoles (V) are now flatter and longer than in the unfertilized egg. The small arrows indicate regions of apparent continuity between the two components of this network. Arrows = spermatozoan cortical granules; S = spermatozoan x 6,000.

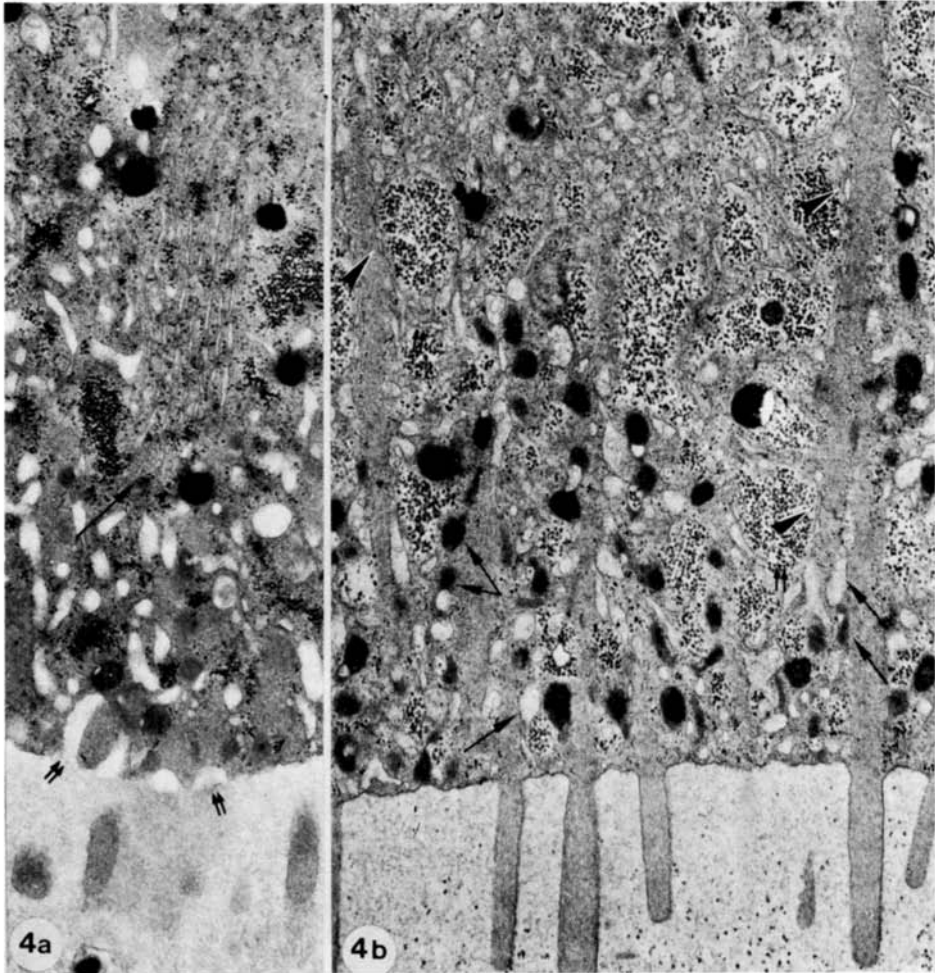


Figure 4. Dimple of fertilized egg. 4a: One min following insemination. Chains of cisternae bend laterally and anastomose with adjacent chains of cisternae (double small arrows). Arrowheads = sites of cisternae and bundle associations. Arrows = association between either cortical granules or flattened vacuoles and microfilament bundles x 10,000. 4b: About 2 min following insemination, flattened vacuoles are undergoing exocytosis (double small arrows). Arrow = region of continuity between flattened vacuoles and cisternae x 10,000.

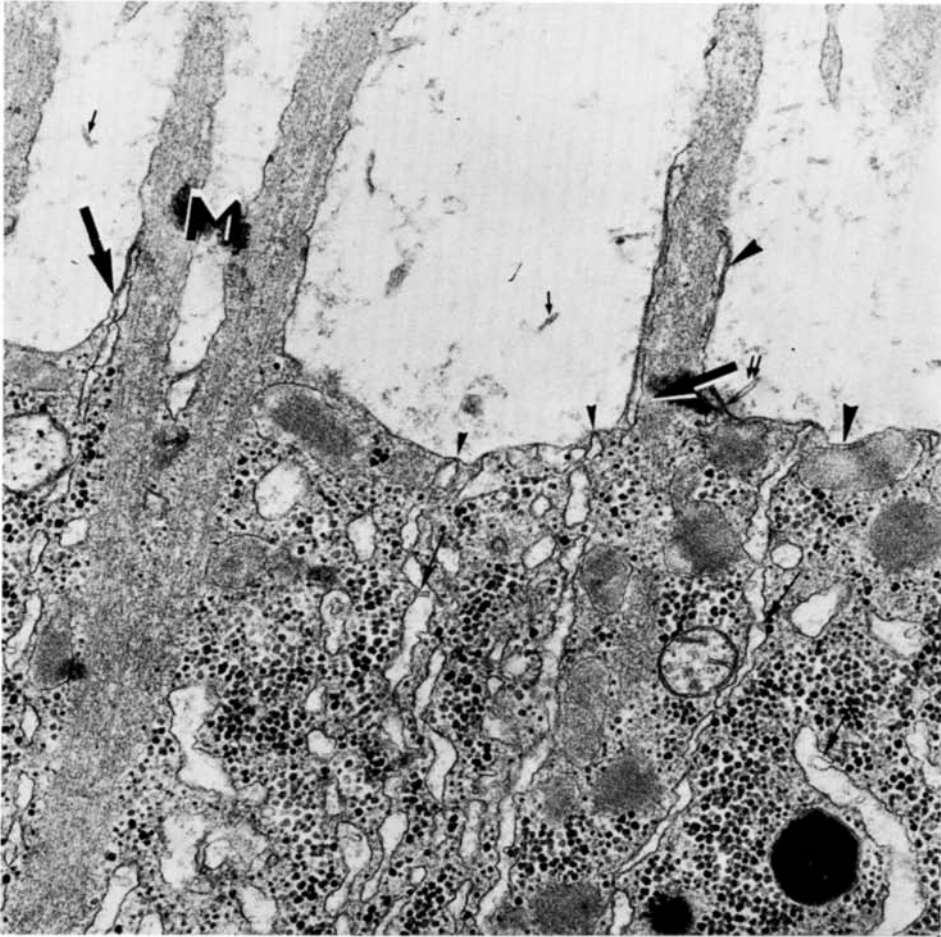


Figure 5. Dimple 3 min following insemination. In the microvilli (M) microfilament bundles are slightly disaggregated. Cisternal chains have entered the microvilli (large arrows). Large arrowheads indicate probable sites of prospective exocytosis of cortical granules and cisternae. Hybrid flat vesicles - deriving from partial fusion of these organelles' membranes with the plasma membrane are observed next to the plasma membrane (double small arrow) or in the extracellular dimple content (small arrow). Small arrowheads = cisternae contacting the plasma membrane. Arrows = invaginations in the cisternae lumen x 38,000.

of jelly dissolves (43). As a result of these changes, the egg loses its asymmetry (Fig. 6, inset) and the dimple surface is now similar to that of the rest of the egg (6).

Pricked Eggs

To provide a more precise timing of the unusual changes occurring in the cisternal clusters and vacuoles immediately following activation, we have examined DTT-treated eggs pricked in the dimple. The first changes occur in the cisternal clusters in zone B. Indeed, within 20 s of pricking, the clusters are less compact and give rise to whorls of longer cisternae, most of which run obliquely to the plasma membrane. The vacuoles lose their spherical shape and become markedly elongated (Fig. 7), because they have fused together. They may also incorporate the invaginations which were present in their lumen before activation (Fig. 7, inset). Furthermore, similar

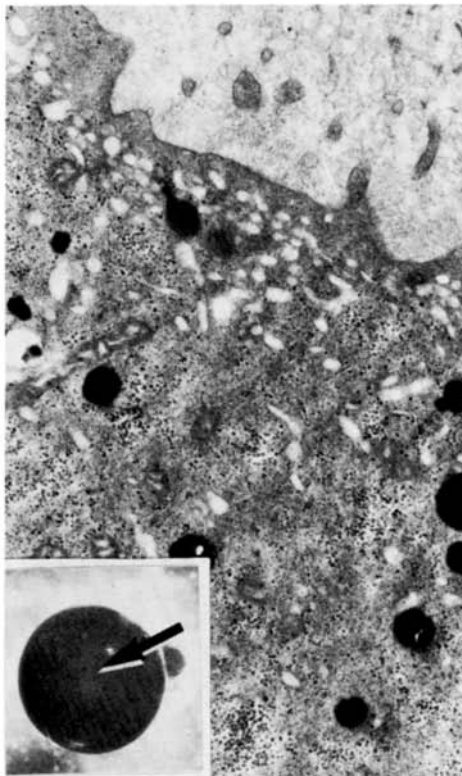


Figure 6. Dimple 20 min after insemination. The cortex is filled with vesicles; at this time both indentation and dimple (arrow) have regressed (inset) x 14,000. Inset x 10.

changes may also occur in the cisternae. These ultrastructural changes, and those observed in pricked eggs at later times, are similar to those described for fertilized eggs.

One interesting difference observed when these partially dejellied eggs were pricked was a wave of cortical contraction, beginning 3-4 min after pricking and spreading over the egg, starting from the site of the stimulus. This wave has not been detected in fertilized eggs, probably because the presence of the plug makes it difficult to observe changes in the dimple.

A23187 Treated Eggs

Eggs treated with DTT and then immersed in 5 μ M ionophore do not show any signs of dimple regression. At 10-12 μ M ionophore, the dimple regresses in about 20-30 min (the exact time depends on the egg clutch). At 35-50 μ M, the dimple starts regressing about 5 min after treatment and there is some variation in the pigmentation around the dimple itself. Such a higher concentration of ionophore is required to obtain a reasonably rapid activation probably because of the presence of the jelly layer J1, the vitelline envelope, and in particular, the dimple contents (see Fig. 1), which could slow down the diffusion of A23187.

In eggs exposed to 35-50 μ M ionophore, vacuoles and CGs undergo exocytosis, even in Ca^{2+} -free Ringer's containing 10 mM EGTA. The reaction of the egg to A23187 is not usually uniform: there are regions of "unreacted" dimple peripheral cytoplasm next to regions where exocytosis is already underway. Again, this may be the result of an unequal diffusion of ionophore and the fact that the response to this drug is not propagated (9).

The time of the first response to ionophore varied with the clutch of eggs; the earliest response found was at 1 min after treatment. Once the response began, most vacuoles and CGs disappeared within the next 5 min (data not shown). Importantly, in only 1 egg of 25 did we observe a network of SER cisternae similar to that found in fertilized eggs. In the remaining eggs neither the transformation nor the re-orientation of the cisternal clusters and vacuoles were detected. Apparently the response of the egg to activation by ionophore is not equivalent to that induced by fertilization or by pricking, as ionophore does not lead to the formation of a cisternal network, at least in our experimental conditions.

DISCUSSION

The most intriguing features of the activation response of Discoglossus eggs are the changes in the morphology and organization of the organelles in the dimple, and the rapidity of these changes.

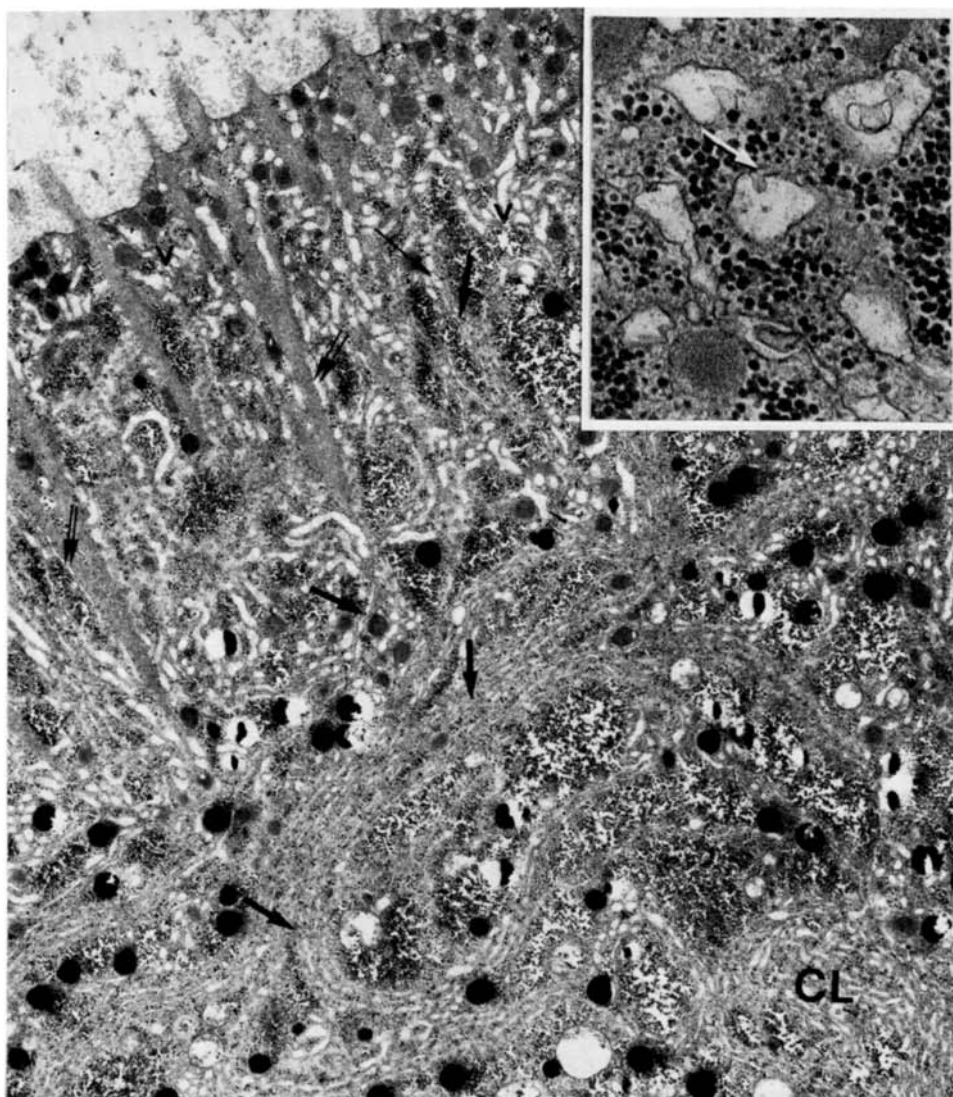


Figure 7. Dimple about 30 sec after pricking. In this early stage of cisternal network formation, zone B clusters (CL) have lost their compactness and are continuous with whorls of cisternae (arrows). Cisternae chains are already in the process of invading zone A, and pile up below the vacuoles (small arrow). Vacuoles (V) have elongated, probably because they have fused together and have incorporated some of the invaginations (inset, arrow) present in their lumen. Double small arrows = sites where either cisternae or flattened vacuoles lean against the microfilament bundles x 7,500. Inset, x 25,000.

Vacuoles and cisternae of the clusters are both competent to respond at the same time to the sperm by transforming into the peripheral network of cisternae. The transformation of the vacuoles consists of their flattening and elongation due to the fusion of vacuoles, and to the incorporation of the invaginations present in the lumen. Similar changes may occur in the cisternae of the clusters during their transformation into arrays of longer cisternae. The elaboration of the peripheral network creates a transient communication to bridge the superficial and the deeper regions of the egg periphery.

It is interesting to compare the formation of this membranous network with the origin of the analogous cortical complex in Xenopus oocytes. The Discoglossus cisternae and vacuoles probably form when the annulate lamellae (AL) disaggregate, as is true for Rana and Xenopus fully grown oocytes following progesterone treatment (26,7). Indeed, in the fully grown Discoglossus oocyte, the AL are located at the future site of the dimple (the "germinative area"). At the same time that the AL disappear following germinal vesicle breakdown, the vacuoles which are later found in oviposited eggs gradually accumulate in the peripheral cytoplasm of the forming dimple (14). The observation that AL in Discoglossus may give rise to both cisternae and vacuoles is in agreement with the situation in Xenopus, where AL disaggregation results in the formation of cisterna clusters as well as the SER shells which surround the CGs (7). However, while in Xenopus the cisternae and shells are already interconnected in oviposited eggs, in Discoglossus the two sets of organelles become continuous only at the time of egg activation. They then regain the association they probably had in the AL of the ovarian oocyte.

There is much indirect evidence suggesting that the free Ca^{2+} concentration increases in amphibian eggs at fertilization and this has recently been confirmed by measurements in Xenopus oocytes using intracellular Ca^{2+} -selective microelectrodes (Busa and Nuccitelli, personal communication). Three lines of evidence suggest that the free Ca^{2+} increases at activation of Discoglossus eggs. First, there is exocytosis of CGs cisternae and vacuoles. Second, there is a cortical contraction wave after activation, which is most likely due to a Ca^{2+} induced contraction of cortical acto-myosin (16,36,39). Actin and myosin are present in the Discoglossus egg cortex (6). Finally, the microfilament bundles gradually disaggregate. They become less compact, less organized, and are shortened, probably due to severing. These effects may be the result of Ca^{2+} regulation of actin-associated proteins (42,29). It is interesting to note, however, that in the Discoglossus egg a wave of contraction spreads over the entire egg from the site of pricking, and exocytosis occurs in both animal and vegetal halves after activation, but only in the dimple is there a transformation of the cisternae and vacuoles. These observations suggest that a transient increase in free Ca^{2+} may propagate from the dimple to the rest of the egg following fertilization, and

that this ionic change alone is not sufficient to cause the transformation of vacuoles and clusters.

What stimulus could reorganize the organelles located in a peripheral region more than $12\ \mu\text{m}$ deep in a matter of seconds? One good candidate is a flow of current through the egg after activation (30). Transcellular currents have been detected at several stages of egg development. In the fully grown, germinal vesicle stage Xenopus oocyte, a Ca^{2+} -mediated Cl^- current enters the oocyte at the animal pole (34). The current is lost during meiotic maturation, but a Cl^- efflux reappears at fertilization (27,30). In Rana eggs the Cl^- channels, which may be more concentrated in the animal hemisphere, can be opened by an increase in free Ca^{2+} (Cross, 1981). Sperm enter the Rana egg throughout the animal hemisphere, but in Discoglossus, the site of sperm entry is restricted to the dimple, which is an expression of the exaggerated polarity of this egg (6). If the Cl^- channels are more concentrated in the dimple than in the rest of the egg, then at activation a current by Cl^- efflux through the dimple membrane would traverse the egg along its polar axis, and this current could reorient the cisternae and vacuoles towards the plasma membrane.

Alternatively, the driving force for reorganizing the dimple cytoplasm might be provided by contractile proteins. It is only in the dimple that there are both the striking rearrangement of membrane-bound organelles and the extensive arrays of microfilament bundles. A role for myosin and for a spectrin-like protein in the movement of vesicles along core rootlets in intestinal epithelial cells has been suggested by Pearl et al. (31) and by Hirowaka et al. (23).

The next obvious question is the role of the constituents of such a network, and of the network itself. From our data it is evident that both transformed vacuoles and cisternae constitute, together with CG membranes, an important source for an increase in total plasma membrane at activation as they are inserted in the egg plasma membrane, and in particular, participate in microvilli elongation. Furthermore, as most vacuoles and cisternae undergo exocytosis, it is highly probable that they may provide the egg surface or the perivitelline space with substances related to fertilization or to later stages of development, as observed in, for example, Acipenser (15) and Limulus (3).

In ionophore-treated eggs, CGs and vacuoles undergo exocytosis, but neither the transformation nor the re-orientation of the cisternal clusters and vacuoles were detected. The fact that exocytosis may occur also when the network fails to form (as in ionophore activation) allows us to distinguish between further possible roles of the network itself and of its constituents. Although other possibilities exist, it may be that vacuoles and cisternal clusters

transform into the network only as a response to stimuli such as fertilization or pricking, in which a propagating reaction spreads from the site of activation. If so, the network may be instrumental in the propagation of the reaction itself. It cannot be excluded, however, that A23187 treatment might be exerting effects in addition to the release of Ca^{2+} from intracellular stores; these additional effects might inhibit the transformation of cisternal clusters and vacuoles into a network.

Even if the organization in a cisternal network is not needed for the exocytotic process, its constituents may well be the source of Ca^{2+} storage and release at activation in view of the above-mentioned analogy to the cortical SER of Xenopus, which, however, in contrast to the Discoglossus organelles, is not exocytosed at activation. Organelles other than the peripheral vacuoles could be totally or partially responsible for Ca^{2+} sequestration and release at activation (for example, mitochondria or the 35 nm thick cisternae observed in the unactivated but not in the fertilized egg cortex). However, at least in the case of mitochondria, this possibility seems less likely because they are predominantly located in zone B, far from the dimple plasma membrane, and also because in sea urchin egg homogenates little of the Ca^{2+} sequestering activity is in the mitochondria (40).

In contrast, the hypothesis that the network constituents are the source of Ca^{2+} release is strengthened by the observation that, as a result of fertilization or of activation by pricking, the network cisternae are in close contact, directly or through interconnections, with the microfilament bundles. This association, which closely resembles that found between sarcoplasmic reticulum cisternae and microfilaments, suggests a calcium release by the cisternae that could account for most of the observed changes in the cytoskeletal organization, and CG exocytosis.

ACKNOWLEDGEMENTS

This paper is dedicated to Professor Mario Galgano on the occasion of his seventy-fifth birthday. We thank Dr. Nicholas L. Cross and Dr. Brian Dale for suggestions on the manuscript. Part of this work was carried out in the Center for Electron Microscopic Studies (Centro per gli Studi di Microscopia Elettronica) of the University of Naples. Supported by a 40 percent M.P.I. grant to Dr. Gianfranco Ghiara.

REFERENCES

1. Andreuccetti, P., Burrini, A.G., Denis-Donini, S., and Campanella, C. 1980. Ca^{2+} localization in smooth endoplasmic reti-

- culum in Xenopus eggs. Abstract of the XLV International Embryological Conference, Patras, Greece.
2. Andreuccetti, P., Denis-Donini, S., Burrine, A.G., and Campanella, C. 1984. Calcium ultrastructural localization in Xenopus laevis eggs following activation by pricking or by Calcium ionophore A23187. *J. Exp. Zool.* 229:295-308.
 3. Bannon, G.A., and Brown, G.G. 1980. Vesicle involvement in the egg cortical reaction of the horseshoe crab, Limulus polyphemus L. *Dev. Biol.* 76:418-427.
 4. Campanella, C. 1975. The site of spermatozoon entrance in the unfertilized egg of Discoglossus pictus (Anura): An electron microscope study. *Biol. Reprod.* 12:439-447.
 5. Campanella, C., and Andreuccetti, P. 1977. Ultrastructural observations on cortical endoplasmic reticulum and on residual cortical granules in the egg of Xenopus laevis. *Dev. Biol.* 56:1-10.
 6. Campanella, C., and Gabbiani, G. 1980. Cytoskeletal and contractile proteins in coelomic oocytes, unfertilized and fertilized eggs of Discoglossus pictus (Anura). *Gam. Res.* 3:99-114.
 7. Campanella, C., Andreuccetti, P., Taddei, C., and Talevi, R. 1984. The modification of cortical endoplasmic reticulum during in vitro maturation of Xenopus laevis oocytes and its involvement in cortical granules exocytosis. *J. Exp. Zool.* 229:283-293.
 8. Cardasis, C.A., Schuel, H., and Herman, L. 1978. Ultrastructural localization of calcium in unfertilized sea urchin eggs. *Cell Sci.* 31:301-315.
 9. Charbonneau, M., and Picheral, B. 1983. Early events in anuran amphibian fertilization: an ultrastructural study of changes occurring in the course of monospermic fertilization and artificial activation. *Dev. Growth and Differ.* 25:23-37.
 10. Charbonneau, M., Moreau, M., Picheral, B., Vilain, J.P., and Guerrier, P. 1983. Fertilization of amphibian eggs: a comparison of electrical responses between Anurans and Urodeles. *Dev. Biol.* 98:304-318.
 11. Charbonneau, M., and Grey, R.D. 1984. The onset of activation responsiveness during maturation coincides with the formation of the cortical endoplasmic reticulum in oocytes of Xenopus laevis. *Dev. Biol.* 102:90-97.
 12. Cross, N.L. 1981. Initiation of activation potential by an increase in intracellular calcium in eggs of the frog Rana pipiens. *Dev. Biol.* 85:380-384.
 13. Cross, N.L., and Elinson, R.P. 1980. A fast block to polyspermy in frogs mediated by changes in the membrane potential. *Dev. Biol.* 75:187-198.
 14. Denis-Donini, S., and Campanella, C. 1977. Ultrastructural and lectin binding changes during the formation of the animal dimple in oocytes of Discoglossus pictus (Anura). *Dev. Biol.* 61:140-152.
 15. Dettlaff, T.A. 1962. Cortical changes in acipenserid eggs during

The Cortical Reaction in the Egg of *Discoglossus pictus*: A Study of the Changes in the Endoplasmic Reticulum at Activation

CHIARA CAMPANELLA,*¹ RICCARDO TALEVI,* DOUGLAS KLINE,^{†2} AND RICHARD NUCCITELLI[†]

*Dipartimento di Biologia Evolutiva e Comparata, via Mezzocannone No. 8, 80134, Napoli, Italy, and [†]Zoology Department, University of California, Davis, California 95616

Accepted July 18, 1988

In *Discoglossus pictus* previous ultrastructural observations have shown that at the animal dimple, where sperm fuse with the egg, cortical granules (CG), vacuoles, and tightly packed clusters of small cisternae are present. At fertilization the clusters open (i.e., become loose) and give rise to longer cisternae arranged in whorls and chains which migrate toward the plasma membrane. The vacuoles fuse to form cisternae and exocytose along with the CG. In the rest of the egg periphery, while exocytosis occurs, the clusters do not open as a result of activation (C. Campanella, R. Talevi, U. Atripaldi, and L. Quaglia (1986). In "Molecular and Cellular Biology of Fertilization" (J. L. Hedrick, Ed.). Plenum, New York). We have recently conducted electrophysiological studies which have detected inward currents at the dimple center, outward current at the rest of the egg surface, and an eightfold increase in $[Ca^{2+}]_i$ which propagates from the site of activation throughout the egg (R. Nuccitelli, D. Kline, W. Busa, R. Talevi, and C. Campanella (1988). *Dev. Biol.* 130, 120-132). In this paper we have asked whether the anionic current and the Ca^{2+} increase could be causally related to the changes of the smooth endoplasmic reticulum (SER) at activation. The results obtained by activating the eggs in ion-substituted Ringers indicate that (1) the migration of cisternae is not dependent on the polarity of the activation current crossing the dimple, but is strongly impaired, together with CG exocytosis, by $5 \times Cl^-$ Ringer; (2) TMB-8, a drug which partially blocks calcium release (C. Y. Chou and M. J. Malagodi (1975). *Brit. J. Pharmacol.* 53, 279-288), partially inhibits opening of cisternae clusters and the formation of an SER network in the dimple. This suggests a causal relationship between the Ca^{2+} rise and the cluster transformation at activation. © 1988 Academic Press, Inc.

INTRODUCTION

The animal dimple of *Discoglossus pictus* eggs is a cup-shaped indentation of the animal hemisphere and is the only region of the egg's surface where sperm fuse with the egg (Hibbard, 1928; Campanella, 1975). Such functional polarity is also indicated by the fact that several types of cytoplasmic organelles are present only in the dimple or are more concentrated there than in the rest of the egg cortex.

In the peripheral dimple cytoplasm are microvilli containing microfilament bundles which penetrate in the cytoplasm and thus define a cortical layer, zone A, where cortical granules (CG), tubular cisternae and vacuoles are present. In the underlying cytoplasm, zone B, are mitochondria, tightly packed clusters of small cisternae and large vacuoles with a sparse electron-dense content (Campanella *et al.*, 1986) (Figs. 1b and 2a). By contrast, in the region of the egg outside the dimple, while cisternae clusters are present, the regular microvilli, the complex cytoskeleton, and CG are not found.

The organization of the dimple changes dramatically at activation. Here is a brief summary of the main events occurring at activation (for more details see Campanella *et al.*, 1986). In the first 20 sec following activation the tubular cisternae disappear. The clusters open (i.e., lose their compactness) while their cisternae swell and elongate thus becoming organized in chains and whorls which migrate towards the plasma membrane. They pile up with the vacuoles which have fused and flattened so that a massive network of smooth endoplasmic reticulum (SER) is seen in the egg periphery. Therefore such a SER network includes vacuoles transformed in cisternae as well as cluster-derived cisternae. Cortical granules and part of the cisternae are exocytosed (Fig. 2b). In the region outside the dimple, vacuoles are exocytosed, while the clusters do not open following activation (Campanella *et al.*, 1986). Therefore one can distinguish between changes occurring at fertilization in the whole egg, i.e., exocytosis, and changes occurring only in the dimple, i.e., opening of the clusters and migration of their components toward the plasma membrane (for more details see also Campanella *et al.*, 1986).

In the companion paper we show that an inward activation current of $65 \mu A/cm^2$ carried by Cl^- efflux is found only in the central dimple region D₁ (Fig. 1a), a

¹ Present address: Dipartimento di Scienze e Tecnologie Biomediche e di Biometria, Università dell' Aquila, Collemaggio 67100, L' Aquila.

² Present address: Physiology Department, University of Connecticut Health Center, Farmington, CT 06032.

disk 200 μm in diameter. These data and the fact that the fertilization potential (FP) can start only in the dimple (Talevi *et al.*, 1985) have led us to conclude that the Cl^- channels are located exclusively in D_1 . In addition, outward current has been found at the rest of the egg surface. This is probably carried by K^+ , as is likely in eggs from both *Xenopus* and *Rana* (Webb, 1984; Kline and Nuccitelli, 1985; Jaffe and Schlichter, 1985). Furthermore, there is a transient increase of free Ca^{2+} at activation in the egg of *D. pictus* as also found in echinoderms (Steinhardt *et al.*, 1977; Eisen and Reynolds, 1984) teleosts (Gilkey *et al.*, 1978; Ridgway *et al.*, 1977), other anurans (Busa and Nuccitelli, 1985; Busa *et al.*, 1985; Kubota *et al.*, 1987) and mammals (Miyazaki *et al.*, 1986). When Ca^{2+} -selective electrodes are inserted in the dimple or in other regions of the egg, a shift of $[\text{Ca}^{2+}]_i$ from 0.25 to 2 μM is recorded shortly after the FP. The Ca^{2+} transient lasts for more than 30 min. Given that the depth of Ca^{2+} -selective electrode insertion was at least 100 μm in all of the measurements, it is likely that the whole egg is exposed for a relatively long time to a high level of free calcium, which might account for the long lasting exocytosis of SER constituents and of CG (Campanella *et al.*, 1986; Nuccitelli *et al.*, 1988). Moreover, the increase in free $[\text{Ca}^{2+}]_i$ may be involved in the generation of the FP, since it has been shown that the FP can be triggered in anuran eggs by an increase in internal free calcium (Cross, 1981), and Cl^- channels are Ca^{2+} -activated at least in an *in vitro* system (Young *et al.*, 1984).

Because of these recent electrophysiological findings, in the present study we investigated whether a causal relationship exists between Cl^- and Ca^{2+} fluxes and SER rearrangement at fertilization. That flows of current may cause vesicle secretion or a rearrangement of cell constituents has been hypothesized for various systems (for a review see Nuccitelli, 1983). Particularly we have asked whether by activating the eggs in Ringers at various Cl^- concentrations, the current generated by the Cl^- efflux through the dimple membrane and thus along the egg's polar axis, could orient the SER network toward the plasma membrane, thus explaining also why in the rest of the egg cortex the typical rearrangement of the SER clusters does not take place.

MATERIALS AND METHODS

All the methods regarding animal and gamete collection, electrophysiological techniques and salines utilized are identical to those described in the accompanying paper (Nuccitelli *et al.*, 1988). Additional methods are here reported on fertilization and on egg-handling procedures.

Egg batches were tested for viability by spreading the semen on the eggs immersed in diluted Ringer. In this

condition, if care is taken to apply the semen very close to the egg jelly, 100% fertilization can be obtained. The semen collected from the seminal vesicles contains 20 mM Na^+ , 19 mM Cl^- for an overall concentration of 40 mM of inorganic ions (Mann *et al.*, 1963). In nature the amplexus of the mating couple occurs in pond water: evidently the eggs are exposed to semen diluted to a concentration that is difficult to estimate. In the laboratory, while fertilization does not occur in undiluted Ringer, spermatozoa are mobile and high percentages of fertilization are ensured upon dilution of Ringer with water to concentrations less than 1:4 (about 80% Ringer). In this paper 10% Ringer was considered as the standard according to observations carried out in previous publications (Talevi *et al.*, 1985). Furthermore it should be mentioned that fertilization occurred normally in all the experimental Ringer solutions here utilized.

For artificial activation the jelly layer, J_3 , the animal plug and J_2 were removed by a 5–10 min exposure to 5 mM dithiothreitol (DTT) in 100 mM NaCl and 5 mM Tris at pH 8.0. The eggs were then washed several times in 10% Ringer and kept in undiluted Ringer until use in 10% Ringer where 1.3 mM CaCl_2 was added (see Talevi *et al.*, 1985). We preferred activation of partially denuded eggs versus fertilization because the presence of the jelly coats necessary for fertilization to occur inhibits an optimal penetration of the fixative and preservation of the tissue which were essential for our ultrastructural observations. Furthermore in a previous study (Campanella *et al.*, 1986) no difference was detected between fertilized and pricked eggs with respect to cortical changes at activation.

Partially dejellied eggs were activated by pricking with a sharpened tungsten wire or by intracellular iontophoresis of $\text{Ins}(1,4,5)\text{P}_3$ (Sigma Chemical Co., St. Louis, MO) in distilled water or in 0.1 mM HEPES (see Nuccitelli *et al.*, 1988).

Use of activation potential (AP) recordings for determining the time of activation was not only optimal, but also necessary for obtaining precisely comparable samples. In fact, in *D. pictus* eggs the first visible effects of activation, such as contraction and wrinkling of the dimple (Campanella, unpublished observations) and the initiation of the activation wave (no elevation of the fertilization envelope occurs in this species), are very attenuated in certain egg batches and therefore hard to detect. The resting potential (RP) and AP reported in the "Results" are an average of a minimum of three eggs.

Electron microscopy. Eggs were fixed for electron microscopy at various intervals (from 30 s to 10 min and in some samples 30 min) following the onset of the activation potential (AP), measured with standard electro-

physiological techniques described in the companion paper (Nuccitelli *et al.*, 1988), by addition of 2.5% (v/v) glutaraldehyde in 0.2 M phosphate buffer (see Campanella, 1975, for details). The average resting potential (RP) before activation as well as the average AP are included in the Results for each set of experiments. The eggs were postfixed in 2% OsO₄ (w/v) in phosphate buffer, dehydrated in ethanol and embedded in Epon 812. Sections were cut with an LKB or Reichert ultramicrotome, stained with uranyl acetate and lead citrate and observed on a Philips 301 or Philips 410 electron microscope. All the fixed samples were sectioned and

examined ($N = 22$ in 1/10 Ringer; $N = 16$ in high Cl⁻; $N = 9$ in 55 mM NaI Ringer; $N = 18$ in low Cl⁻; $N = 12$ in TMB-8). Under Results a summary of the examined micrographs has been reported.

RESULTS

Unfertilized Eggs

The main morphological features of the dimple are summarized in Figs. 1a, 1b and 2a, and are described in detail elsewhere (Campanella, 1975; Campanella and Gabbiani, 1980; Campanella *et al.*, 1986). In the present

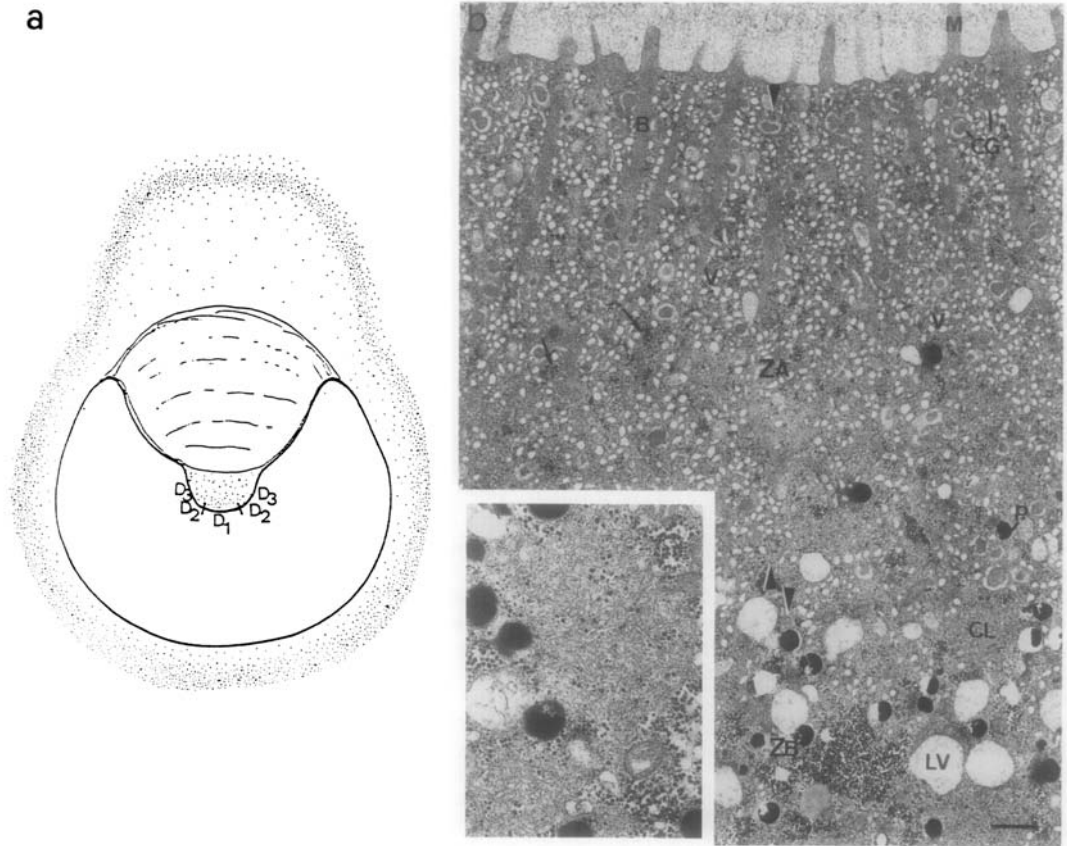


FIG. 1. (a) Schematic drawing of a longitudinal section of *D. pictus* egg. The dimple regions, D₁, D₂, and D₃, are indicated. (b) Unfertilized egg of *D. pictus*: central portion of the dimple (D₁). The small arrows indicate glycogen which is abundant in the whole egg periphery. Cortical granules (CG) are scattered in the cortical cytoplasm, among the microfilament bundles (B). This is a feature unique to the *D. pictus* egg with respect to other anuran eggs where CG are located only in the cortex. Furthermore, *D. pictus* CGs have an electron-dense central core and a fibrillar periphery. They have a diameter of 0.5 μm (for more details see Campanella, 1975). ZA, Zone A; ZB, zone B; M, microvilli; V, vacuoles; LV, large vacuole with sparse electron-dense material; CL, cluster of cisternae; P, pigment granule. ×7000. Horizontal bar, 1 μm (from Campanella *et al.*, 1986). Inset, clusters of cisternae (×15600).

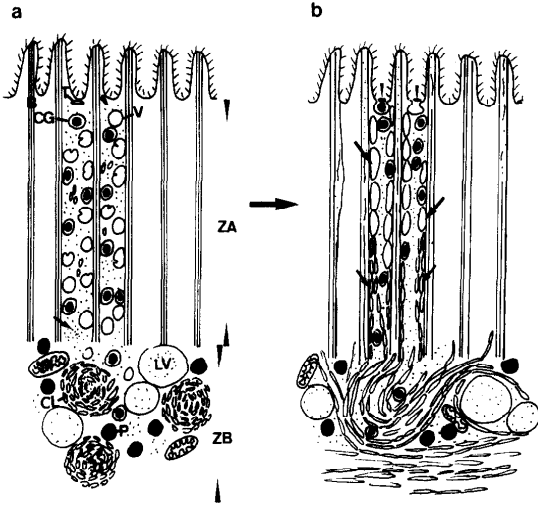


FIG. 2. (a) Schematic drawing of the central portion of the dimple, D_1 , in an unfertilized egg. ZA, Zone A; ZB, zone B; small arrow, glycogen; CG, cortical granules; T, tubular cisternae; V, vacuole with typical small invagination; LV, large vacuole; CL, cluster of cisternae; P, pigment granule; M, mitochondrion. (b) Schematic drawing of D_1 in full strength Ringer or in 1/10 Ringer within the first minute from activation. The tubular cisternae have disappeared. The cisternae clusters have opened. Their cisternae have transformed into whorls of cisternae in ZB and into chains of cisternae in ZA. They become part of a SER network whose more superficial component are the vacuoles which have transformed in cisternae by fusing and flattening. Such cisternae (arrows) are larger than those deriving from the clusters (small arrows). Cisternae and CG have migrated towards the plasma membrane where they exocytose (arrowheads). The microfilament bundles have partially lost their integrity, suggesting a process of solution.

paper we have further examined the distribution of cytoplasmic organelles in the whole dimple and observed that the length of the microfilament rootlets and the concentration of CG and of cisternae clusters gradually decreases from the center to the border of the dimple. In contrast to this graded distribution, the concentration of vacuoles is highest at the center of the dimple and decreases sharply at the dimple's lateral walls. At least three regions can be distinguished (Fig. 1a). These are D_1 , the central portion of the dimple measuring 200 μm in diameter, where zone A is at its maximal depth and the largest concentration of cisternae clusters and vacuoles is found; D_2 next to D_1 and at the beginning of the dimple walls, where a relatively small number of vacuoles is present; D_3 , the most peripheral region of the dimple, where zone A is only about 1 μm deep and a conspicuous concentration of mitochondria is found. D_1 ultrastructure is outlined in Figs. 1b and 2a. The features of D_2 and D_3 are still easily recognized after acti-

vation (Figs. 4b and 4c) and therefore are not shown here. It should also be mentioned that the dimple ultrastructure is not affected upon soaking the eggs in the media we have utilized.

Activated Eggs

10% Ringer. In D_1 , cisternae clusters open (i.e., lose their compactness) and transform into whorls and strands of longer cisternae in the first 20–30 sec following activation when this SER network also starts migrating toward the plasma membrane, as previously reported for eggs activated in undiluted Ringer (Campanella *et al.*, 1986) (Figs. 2b and 3b). Whorls of cisternae are seen at the base of zone A while, in a more superficial region, cisternae are obliquely arranged with respect to the plasma membrane (Fig. 2b). Within the first minute following activation (RP = -15 mV; AP = $+10$ mV) the migration of CG toward the plasma membrane begins (see also Talevi *et al.*, 1985). Furthermore in these conditions and, unless specified, in all the following ones, the microvillar bundles of microfilaments are partially disaggregated, suggesting that a solution of the bundles has occurred (Figs. 2b and 3b and compare with Fig. 3a, which shows a bundle of an unfertilized egg). Ten minutes following activation (RP = -15 mV; AP = $+10$ mV) microvilli have elongated (Fig. 4a) and the length of zone A has decreased predominantly as a consequence of the exocytotic phenomena at the base of the microvilli (Campanella *et al.*, 1986). Some CG are still present, clustered at the egg periphery or in whorls of the SER network. Pigment granules and large vacuoles are in zone B where formerly the cisternae clusters were located (Fig. 4a and compare with Figs. 1b and 2a). At later stages after activation they will migrate to the plasma membrane where the large vacuoles will undergo exocytosis (data not shown). In D_2 of the same egg shown in Fig. 4a, microvilli have not elongated and in fact there is no sign of CG and cisternae exocytosis, but a large number of CG are grouped in zone A (Fig. 4b). Few cisternae are present in zone A. Indeed most of them are still in zone B where they are arranged in clusters, which are either smaller than in the unfertilized egg (as observed in serial sections) or have merged together forming large masses (Inset 2, Fig. 4b). This indicates that a rearrangement of the clusters has occurred which includes little migration of cisternae towards the plasma membrane. In D_3 , while microvilli have slightly changed in shape, as a result of CG exocytosis, cisternae clusters are as compact as in the unfertilized eggs (Fig. 4c, same egg of Figs. 4a and 4b).

The following descriptions of the dimple refer to D_1 only because this is the site where the SER changes

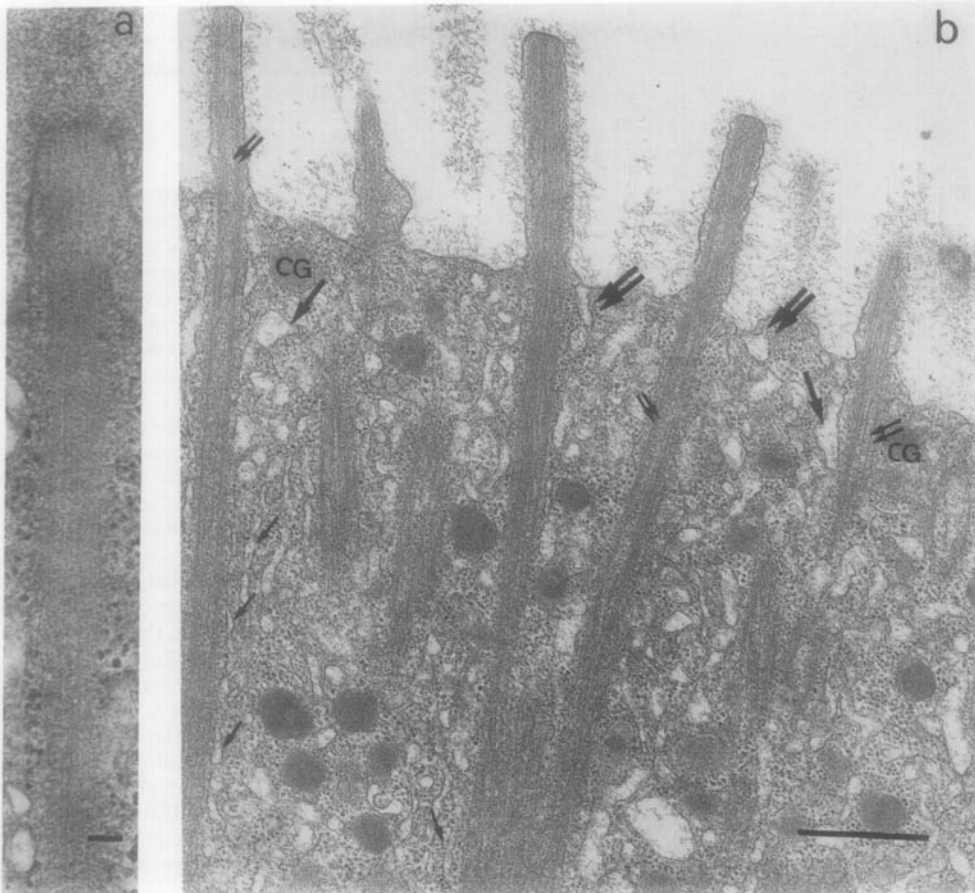


FIG. 3. (a) Microvillus of an unfertilized egg. Microfilaments are homogeneously distributed in the bundle located in the microvillus core and extending in the cytoplasmic rootlet. $\times 55,000$. Horizontal bar, $0.1 \mu\text{m}$. (b) 10% Ringer D_1 activation reaction, about 1 min following AP. The uppermost portion of zone A is here shown. The microvillar bundles have lost their compactness (double small arrows) (compare with Fig. 2a). The cortical granules (CG) are close to the plasma membrane. The SER network is here present: small arrows indicate cisternae derived from the clusters opening as shown in Fig. 1c, while large arrows indicate vacuole derived cisternae two of which are in initial stages of exocytosis (double arrows) $\times 21,000$. Horizontal bar, $1 \mu\text{m}$.

fully develop at activation and where sperm fuse with the egg.

High Cl^- and Γ . In high external Cl^- , the AP is reduced in magnitude or may even change its sign, hyperpolarizing rather than depolarizing, due to a reversal in the net activation current. This is due to the reduced net Cl^- efflux in high external Cl^- (Nuccitelli *et al.*, 1988). In eggs activated in such medium ($5\times \text{Cl}^-$ Ringer composed of 0.7 mM CaCl_2 , $0.7 \text{ mM Ca}(\text{NO}_3)_2$, 0.08 mM MgSO_4 , 1.2 mM NaOH , 55 mM Choline-Cl , $11.1 \text{ mM Na-methane sulfonate}$, $0.2 \text{ mM K-methane sulfonate}$, 2.5 mM Hepes), D_1 shows, 3 min following the initiation of the AP (RP

$= -11 \text{ mV}$; AP $= -9 \text{ mV}$), an impressive amount of SER confined in zone B (Fig. 5a) while only a few cisternae appear to be in the process of migrating toward the plasma membrane (not shown). Several CG are trapped in SER whorls which have slightly invaded zone B (Fig. 5a). At a later stage (10 min) following the initiation of the AP (RP $= -11 \text{ mV}$; AP $= -9 \text{ mV}$), the microvilli have only slightly elongated and many CG are present in zone A (Fig. 5b and compare with Fig. 4a) as, evidently, little exocytosis has occurred. The high Cl^- medium was the only one tested in which there is a clear reduction in cortical granule exocytosis in D_1 , and a

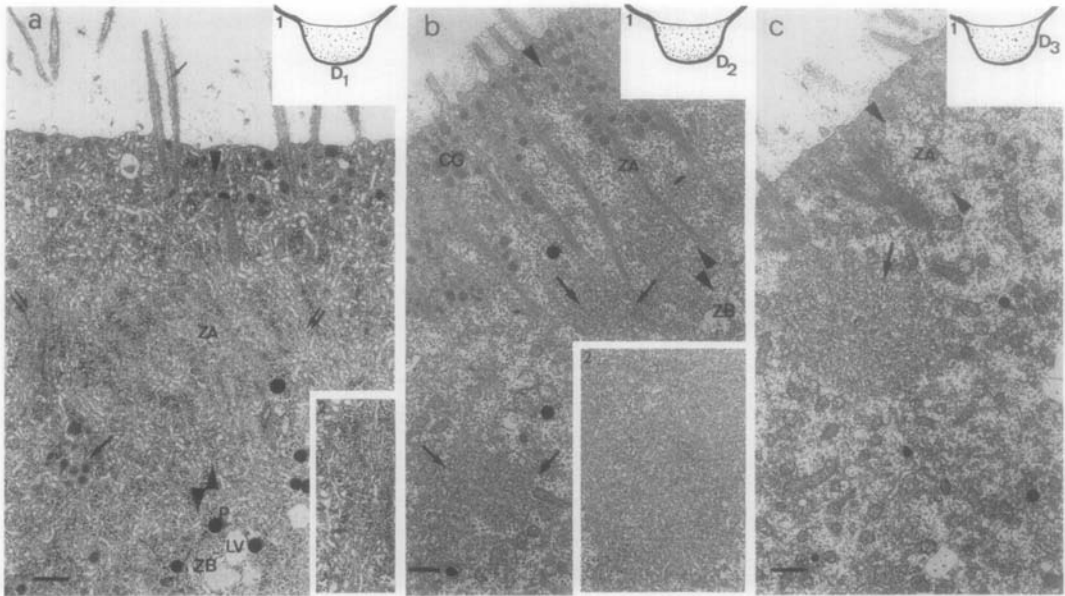


FIG. 4. 10% Ringer dimple 10 min following AP. The three micrographs (a), (b), and (c) are thin sections of the same egg. Upper insets indicate where in the dimple the sections have been taken. Therefore in (a) the inset indicates D_1 ; in (b), D_2 ; and in (c), D_3 . (a) D_1 : The microvilli have elongated. Their central core is partially isolated (small arrow). The network of cisternae derived from the clusters opening is evident in zone A (ZA). A few CG are present; some of them are located within cisternae whorls (arrow). The double small arrow indicates cisternae obliquely oriented with respect to the plasma membrane. Inset 2 is a higher magnification showing such cisternae ($\times 9100$). LV, Large vacuole; P, pigment granule ($\times 5500$). (b) D_2 : In this region, which is continuous with D_1 , microvilli have not elongated and many CG are found in ZA, where they are closely associated with microfilament rootlets (small arrows). In ZB the clusters have rearranged in smaller ones (arrows) with respect to unfertilized eggs or in large masses of cisternae (Inset 2, $\times 5500$). Very little SER network is present in ZA. LV, Large vacuoles ($\times 5500$). (c) D_3 : In this peripheral region of the dimple, the microvilli have changed their shape as a consequence of activation. The cisternae cluster does not appear to have reacted (arrow) ($\times 5500$). Horizontal bars, 1 μm .

remarkable network of cisternae, obliquely or perpendicularly oriented to the plasma membrane, is present mostly below the region where microvilli rootlets are present. In zone B, cisternae clusters are absent and several groups of CG are found confined by SER whorls.

Eggs activated in 55 mM NaI Ringer also display a negative AP (RP = -9 mV; AP = -28 mV) as well as an outward current at the dimple (Nuccitelli *et al.*, 1988). However, despite this current reversal, sections of eggs activated in this medium do not show significant differences in the ultrastructural changes that follow activation (Figs. 6a and 6b) when compared to eggs of the same batch activated in 10% Ringer. Therefore, the reduction in both SER migration to the plasma membrane and CG exocytosis that was observed in high external Cl^- is not due to the reversal in current direction, per se.

Low Cl^- . Eggs activated in this medium containing 12% of the normal Cl^- in 10% Ringer display a 1.6-fold increase of the inward current (Nuccitelli *et al.*, 1988). In

these samples, the microfilament bundle solation is particularly conspicuous in D_1 . Figure 7a depicts an egg fixed 1 min following AP (RP = -14 mV; AP = +21 mV) where the core of both the microvilli and the rootlets appears to have partially dissolved.

Ten minutes following the AP (RP = -20 mV; AP = +17 mV), D_1 is similar to the 10% Ringer eggs fixed at the same interval from activation (Fig. 7b and compare with Fig. 4a). Moreover, one can observe that some pigment granules and large vacuoles have migrated to zone A where they are close to the plasma membrane (Fig. 7b). In eggs activated in 10% Ringer these organelles are found in comparable positions at later times after activation.

TMB-8. TMB-8 blocks intracellular Ca^{2+} release in skeletal and smooth muscle (Chiou and Malagodi, 1975). The addition of 1 mM TMB-8 to 10% Ringer appears to eliminate the steady component of the dimple current, but large, discrete pulses of current are still present (Nuccitelli *et al.*, 1988). Ultrathin sections of the eggs

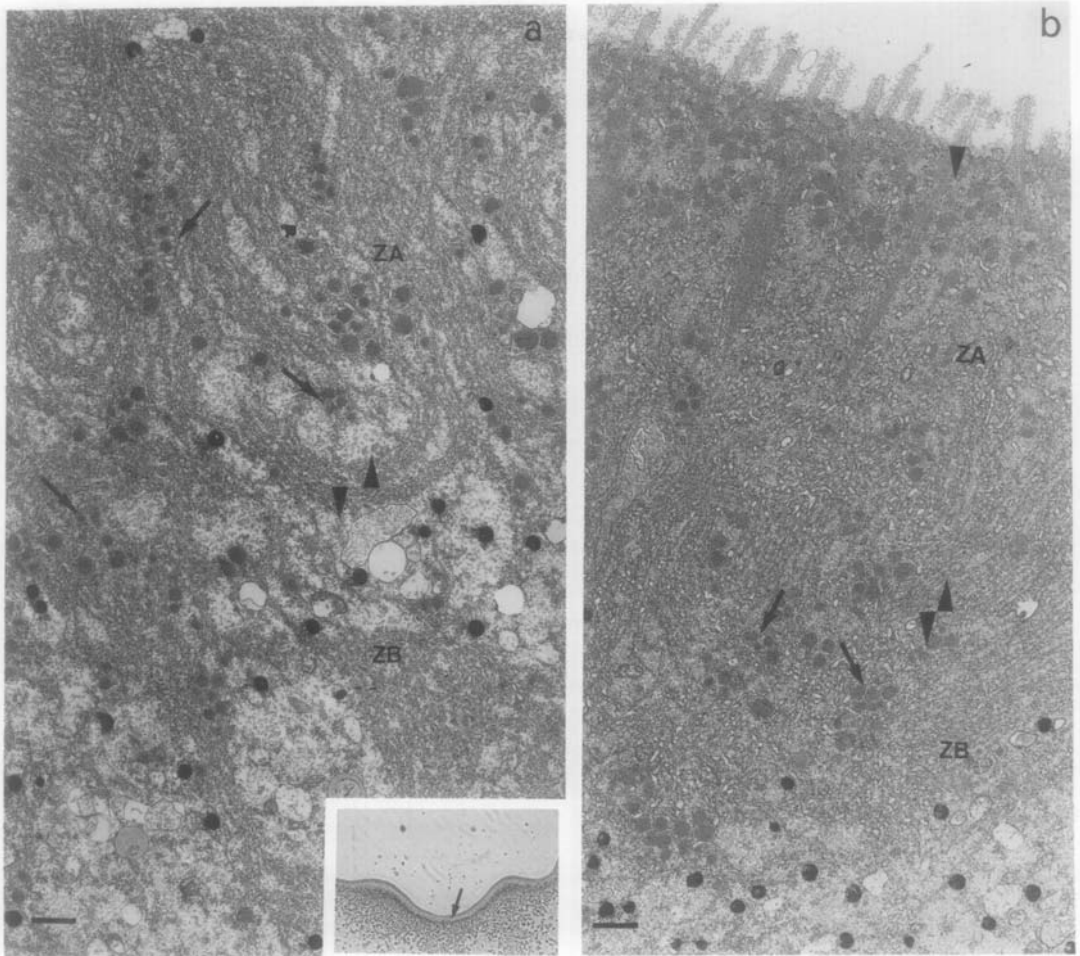


FIG. 5. $5X Cl^-$ Ringer. D_1 following activation. (a) Egg fixed 3 min following AP. The micrograph shows both the lower portion of ZA and the upper portion of ZB in a section obliquely oriented. An impressive amount of cisternae whorls are found, many of them containing nests of CG (arrows) ($\times 7200$). The inset is a light micrograph of D_1 . ZA is the pigment-free region; ZB is the underlying pigment rich region ($\times 50$). The small arrow shows the region of the dimple where Fig. 5 micrograph has been taken. (b) Eggs fixed 10 min following AP. The microvilli are almost unchanged. Several CG are grouped in ZA or in whorls of cisternae (arrows). Most SER network is located below the region where microvilli rootlets are present ($\times 7200$). Horizontal bars, $1 \mu m$.

fixed after AP and current recordings, as reported in Fig. 10 of Nuccitelli *et al.* (1988), show that in eggs activated in TMB-8 unreacted clusters of cisternae are found in D_1 , even 3 min following AP (RP = -8 mV; AP = $+8$ mV) (Fig. 8b). Furthermore, while in the corresponding 10% Ringer-activated eggs the SER develop normally (RP = -8 mV; AP = $+20$ mV) (Fig. 8c), in the TMB-8 exposed eggs a network of SER is not found (Figs. 8a and 8b). This implies that fusion between cis-

ternae deriving from the opening of some clusters or from vacuoles has not fully occurred (compare Figs. 8a and 8b with Fig. 8c).

DISCUSSION

In this paper we have shown that following activation CG and vacuole exocytosis does not propagate evenly in the dimple and, more precisely, from the central portion

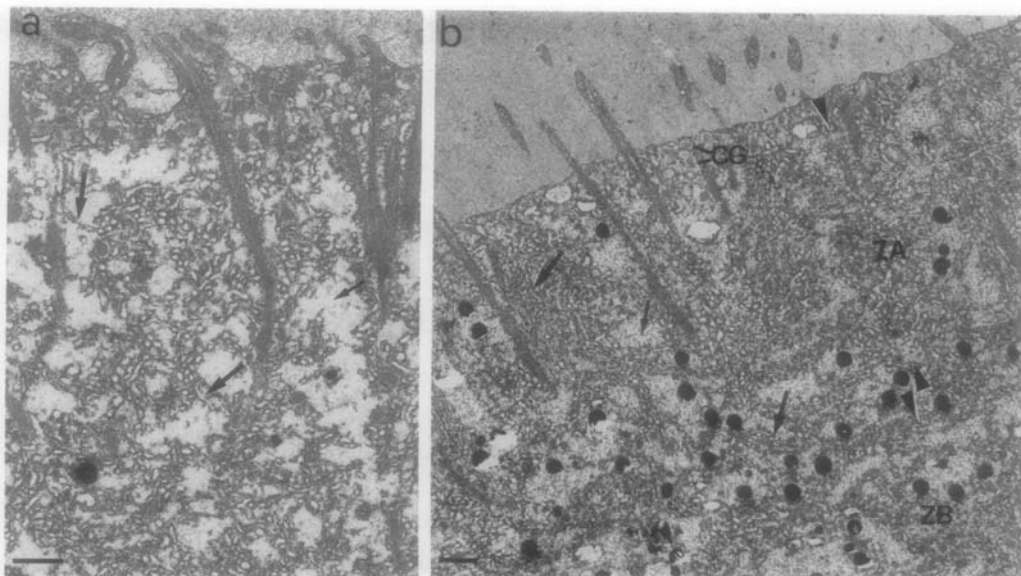


FIG. 6. Fifty-five millimolar NaI Ringer. Following exposure to such medium the glycogen islets are not clearly visible (small arrows). (a) D₁ fixed 1 min following AP. A SER network is present (arrows) in ZA. ($\times 8000$) Horizontal bar, 1 μ m. (b) D₁ fixed 10 min following AP. Microvilli have elongated similarly to eggs activated in 10% Ringer (Fig. 4a). A SER network is in ZA as well as in ZB (arrows). No cluster is present in ZB. CG, Cortical granules. $\times 6000$. Horizontal bar, 1 μ m.

of this region, D₁, to the more peripheral one, D₃. In fact, it appears to skip D₂, which is located between the two. This is a quite unusual situation in eggs and particularly in those of anurans where CG exocytosis appears to spread without discontinuity from the site of sperm penetration to the antipode (Kemp and Istock, 1967; Wolf, 1974; Grey *et al.*, 1974). In *D. pictus*, however, CG are stockpiled among the microfilament rootlets and they have to cover a relatively long distance before reaching the membrane, whereas in the eggs of other anurans, they form a single or a double layer in the cortex (for a review see Elinson, 1980). Therefore the reason whereby any exocytosis of CG (and cisternae) occurs in D₂ could be correlated with the propagation of the activating stimulus as well as to this migration process.

We have also observed that the SER network deriving from the clusters fully migrates toward the plasma membrane only in D₁ where the inward current has been detected at activation, while in D₂ and D₃, where outward currents are found at the same time (Nuccitelli *et al.*, 1988), this migration is only partial in the case of D₂ or absent in the case of D₃, where the cisternae clusters do not change after activation. This might suggest that the inward current could be related to or even

cause the migration of SER to the membrane. However, according to the results obtained with ion-substituted Ringers, SER migration does not appear to be affected by the direction of the anionic current flow which crosses D₁ at activation. In fact, while 5 \times Cl⁻ and 55 mM NaI Ringers both generate a reversal of the current, only 5 \times Cl⁻ Ringer strongly impairs SER migration in D₁. Moreover the latter medium appears to cause a reduced secretion of CG. At present we do not know the mechanism whereby 5 \times Cl⁻ Ringer results in retention of CG and SER. In low Cl⁻ medium, large vacuoles and pigment granules get close to the plasma membrane more readily than in control eggs (Fig. 7b and compare with Fig. 4a), which suggests that when the Cl⁻ conductance increases and more Cl⁻ leaves, migration and exocytosis of zone B components are accelerated. However no relevant effects on CG and SER have been observed in low Cl⁻ Ringer. Perhaps there is no detectable morphological difference between low Cl⁻ and 10% Ringer because the difference in the Cl⁻ concentrations of the two salines is not large enough. However it does appear that Cl⁻ gradients may play a role in the migration activity of zone B constituents. In 10% Ringer the reason for the reduction in SER migration to D₂ plasma membrane could be due to the absence of Cl⁻-permeable

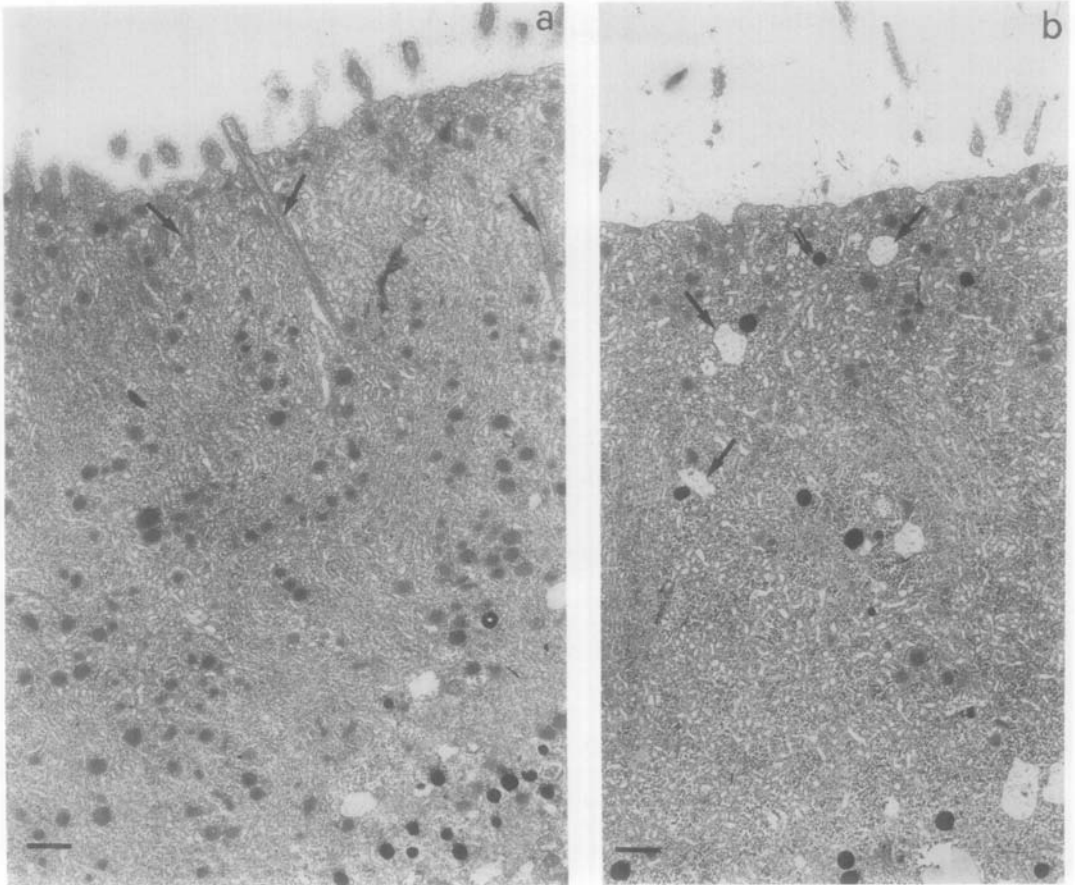


FIG. 7. Low Cl^- Ringer. (a) D_1 fixed 1 min following AP. The core of the microvilli as well as of the rootlets is isolated (arrows) ($\times 7000$). (b) D_1 fixed 10 min following AP. Some pigment granules (double small arrow) and large vacuoles (arrows) have migrated to the plasma membrane ($\times 7000$). Horizontal bars, 1 μm .

channels and of localized Cl^- mobilization in that region of the dimple.

The fact that in D_2 the SER does not fully migrate and the CG fail to exocytose, as well as the retention of CG and inhibition of SER migration in $5\times \text{Cl}^-$ Ringer, also suggests that a functional relationship may exist between SER and CG. This is also stressed by the observation that, at early stages of unravelling of the SER network in zone B, nests of CG appear to be circumscribed by whorls of SER. Indeed in 10% Ringer the abrupt opening of the clusters (within 20 sec from activation) in D_1 and the subsequent development of strands of cisternae directed toward the plasma membrane could furnish the mechanical drive for pushing

CG and vacuoles toward the plasma membrane to an extent which makes them able to undergo exocytosis. During such events, groups of CG may become trapped in the unravelling mass of cisternae. These observations and hypotheses offer some explanations for the mechanism of the exocytotic process and for the fact that nests of CG are found in zone B confined in whorls of SER in eggs activated in all the salines used. It should be mentioned that, given that eggs in $5\times \text{Cl}^-$ Ringer are fertilized and develop normally, CG and SER migration and exocytosis does not seem to be crucial for embryonic development.

The activation experiments conducted in TMB-8 offer more clues for the understanding of early SER changes.

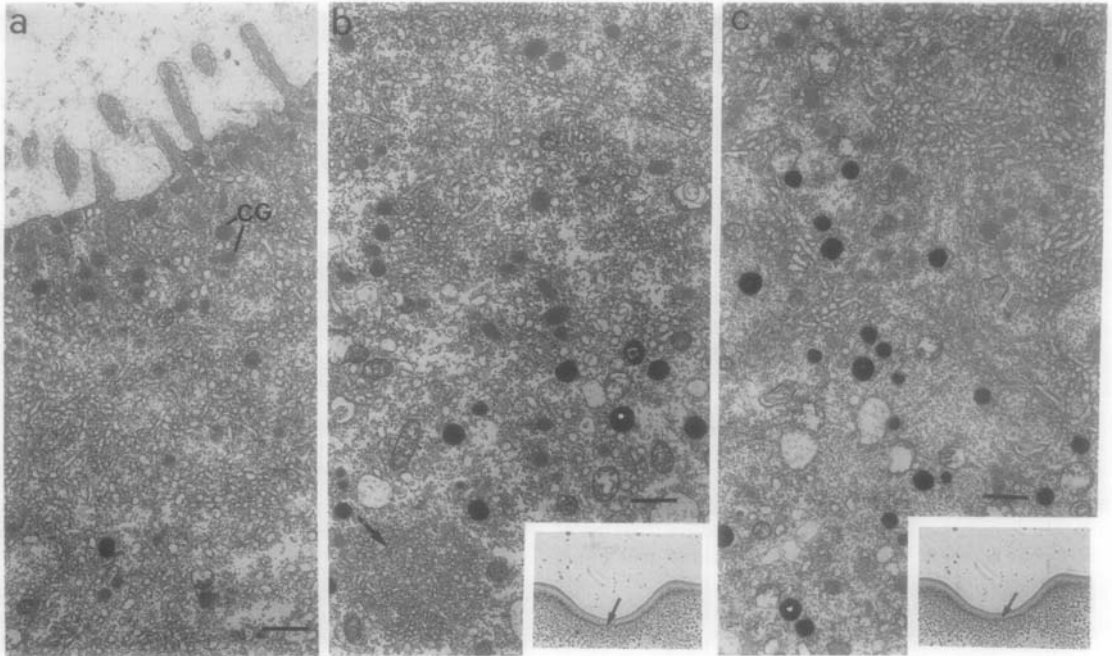


FIG. 8. TMB-8. Eggs fixed 3 min following AP. (a) and (b) D₁ of an egg activated in 1 mM TMB-8. (a) ZA: The microvilli have slightly elongated. A typical network of SER is absent probably because fusion between cisternae deriving from vacuoles or from the opening of some clusters has not fully occurred. CG, Cortical granules ($\times 6900$). (b) The inset shows approximately the region (2A lower portion and 2B) where the section has been taken. The clusters have not reacted (arrow) and a network of cisternae has not formed ($\times 6900$). (c) This is a control egg activated in 10% Ringer showing the same region of the peripheral cytoplasm shown in (b) (inset). The clusters have disappeared and a network has formed ($\times 6900$). Horizontal bars, 1 μ m.

This drug dramatically changes the shape of the activation potential in both *X. laevis* (Kline and Nuccitelli, 1985) and *D. pictus* (Nuccitelli *et al.*, 1988), suggesting that the release of calcium is partially blocked in such eggs as in other tissues (Chiou and Malagodi, 1975) and that the activation channels are consequently only partially activated. Since we find that TMB-8 also reduces cluster opening as well as the fusion of the deriving cisternae and of the vacuoles, a rise in intracellular Ca^{2+} may be causally related to cluster opening. This also leads us to propose that high levels of $[\text{Ca}^{2+}]_i$ are generated at activation in D₁ and D₂ and that such levels might be higher than those reached in the rest of the egg cortex since the clusters do not open there. However, we have no Ca^{2+} measurements to support this hypothesis since the egg cannot be reliably impaled with Ca^{2+} -selective electrodes to a depth as shallow as 15 μ m (the thickness of zone A plus zone B). It would be useful to try another technique for Ca^{2+} detection such as fura-2 or aequorin to determine if there really is more Ca^{2+} release in the dimple cortex than elsewhere

in the egg. There are indeed other indications that this might be the case: (1) the microfilaments in the core of the local microvilli disaggregate following activation and most proteins which sever actin or cause its depolymerization are Ca^{2+} -dependent (for reviews see Weeds, 1982; Stossel *et al.*, 1986). In brush border microvilli, core solation occurs as a consequence of severing actin by villin in the presence of at least 10 μM Ca^{2+} (Keller and Mooseker, 1982; Burgess and Prum, 1982). Villin has been isolated in toad oocytes (Corwin and Hartwig, 1983). (2) When $\text{Ins}(1,4,5)\text{P}_3$ is injected into regions of the egg cortex outside of the dimple, Ca^{2+} release is induced (Busa *et al.*, 1985; Kline and Nuccitelli, 1985; Nuccitelli *et al.*, 1988) and the clusters are observed to open (Campanella *et al.*, 1988). The fact that such a stimulus can produce the opening of clusters and some swelling of their cisternae that would not normally occur upon activation suggests that perhaps the clusters only open in response to an unusually high level of Ca^{2+} release. We suspect that the dimple cortex may see this high level. (3) The velocity of propagation of the

wave of cortical contraction is 10-fold higher in the dimple than in the rest of the egg (Campanella, unpublished observations). Such a wave results from the activation of the cortical cytoskeleton by the intracellular release of Ca^{2+} at fertilization. Therefore it is reasonable to assume that the higher the $[\text{Ca}^{2+}]_i$, the faster the velocity of propagation of the wave (Stewart-Savage and Grey, 1982; Kline and Nuccitelli, 1985; Kubota *et al.*, 1987; Cheer *et al.*, 1987). Furthermore the reduction in cluster opening from D_1 to D_3 can indeed reflect a sort of gradient of calcium concentration with its maximum in D_1 , where a high concentration of vacuoles is found. These organelles are among the best candidates to be Ca^{2+} reservoirs which deliver Ca^{2+} at activation (Campanella and Andreuccetti, 1985; see also Nuccitelli *et al.*, 1988) as does the SER in *Xenopus* (Campanella and Andreuccetti, 1977; Gardiner and Grey, 1983; Andreuccetti *et al.*, 1984). Interestingly the SER also changes its configuration in *Xenopus* eggs, however, only following CG exocytosis. An egg fixed 5 min following pricking at the vegetal hemisphere shows in its animal half chains of cisternae crossing the peripheral cytoplasm (see Fig. 8 in Campanella and Andreuccetti, 1977). Evidently many important questions on the causal and functional roles of the SER at activation should still be answered, particularly those related to the migration of the cisternae to the D_1 membrane. It is highly probable that the cytoskeleton plays an important role in these phenomena, as it has been observed that the dimple contracts upon activation. In the intestinal brush border the terminal web contracts upon chemical stimulation (Rodewald *et al.*, 1976; Keller *et al.*, 1985). In the dimple the web has not been detected morphologically among the microfilament rootlets. However, in the peripheral cytoplasm, actin, myosin, α -actinin, tropomyosin, and spectrin, typical components of the web, have all been detected (Campanella and Gabbiani, 1980; Campanella *et al.*, 1982; Campanella *et al.*, in preparation).

We thank Drs. P. Andreuccetti and A. Sotgiu for suggestions and Ms. R. Harris, G. Falcone, and G. Argenzio for skillful technical assistance. Part of this work was carried out in the "Centro per gli studi di Microscopia Elettronica" of the University of Naples. This work was supported by grants from NSF (PCM 81-18174) and NIH (HD 19966) to R. Nuccitelli and from M.P.I., 60% to C. Campanella and 40% to S. Filosa.

REFERENCES

- ANDREUCCETTI, P., DENIS-DONINI, S., BURRINI, A. G., and CAMPANELLA, C. (1984). Calcium ultrastructural localization in *Xenopus laevis* eggs following activation by pricking or by calcium ionophore A23187. *J. Exp. Zool.* **229**, 295-308.
- BURGESS, D. R., and PRUM, B. E. (1982). Reevaluation of brush border motility: Calcium induces core filament solation and microvillar vesiculation. *J. Cell Biol.* **94**, 97-107.
- BUSA, W. B., and NUCCITELLI, R. (1985). An elevated free cytosolic Ca^{2+} wave follows fertilization in eggs of the frog, *Xenopus laevis*. *J. Cell Biol.* **100**, 1325-1329.
- BUSA, W. B., FERGUSON, J. E., NUCCITELLI, R., JOSEPH, S. K., and WILLIAMSON, J. R. (1985). Activation of frog (*Xenopus laevis*) eggs by inositol triphosphate. I. Characterization of Ca^{2+} release from intracellular stores. *J. Cell Biol.* **101**(2).
- CAMPANELLA, C. (1975). The site of spermatozoon entrance in the unfertilized egg of *Discoglossus pictus* (Anura): An electron microscopy study. *Biol. Reprod.* **12**, 439-447.
- CAMPANELLA, C., and ANDREUCCETTI, P. (1977). Ultrastructural observation on cortical endoplasmic reticulum and on residual cortical granules in the egg of *Xenopus laevis*. *Dev. Biol.* **56**, 1-10.
- CAMPANELLA, C., and GABBIANI, G. (1980). Cytoskeletal and contractile proteins in coelomic, unfertilized and fertilized egg of *Discoglossus pictus* (Anura). *Gamete Res.* **3**, 99-114.
- CAMPANELLA, C., RUNGGER-BRANDLE, E., and GABBIANI, G. (1982). Immunolocalization of alpha-actin in an amphibian egg (*Discoglossus pictus*). In "Embryonic Development. Cellular Aspects" (Burger and Weber, Eds.), Part B, pp. 45-53. Alan R. Liss, New York.
- CAMPANELLA, C., and ANDREUCCETTI, C. (1985). Ca^{2+} -antimony deposits in *Discoglossus pictus* egg during activation. *Cell Diff.* **16**, 1455.
- CAMPANELLA, C., TALEVI, R., ATRIPALDI, U., and QUAGLIA, L. (1986). The cortical endoplasmic reticulum and its possible role in activation of *Discoglossus pictus* (Anura) egg. In "Molecular and Cellular Biology of Fertilization" (J. L. Hedrick, Ed.). Plenum, New York.
- CAMPANELLA, C., KLINE, D., and NUCCITELLI, R. (1989). The cortical reaction in the egg of *Discoglossus pictus*: Changes in the cisternae clusters at activation. In "Cell Interactions and Differentiation" (G. Ghiara, Ed.). Univ. of Naples Press, Naples.
- CHEER, A., VINCENT, J.-P., NUCCITELLI, R., and OSTER, G. (1987). Cortical activity in vertebrate eggs I: The activation waves. *J. Theor. Biol.* **124**, 377-404.
- CROSS, N. L. (1981). Initiation of the activation potential by an increase in intracellular calcium in eggs of the frog *Rana pipiens*. *Dev. Biol.* **85**, 380-385.
- CHIOU, C. Y., and MALAGODI, M. J. (1975). Studies on the mechanism of action of a new Ca^{++} antagonist, (*N,N*-diethylamino)-octyl-3,4,5-trimethoxybenzoate hydrochloride in smooth and skeletal muscles. *Brit. J. Pharmacol.* **53**, 279-288.
- CORWIN, H. L., and HARTWIG, J. H. (1983). Isolation of Actin-binding protein and villin from toad oocytes. *Dev. Biol.* **99**, 61-74.
- EISEN, A., and REYNOLDS, G. T. (1984). Calcium transients during early development in single starfish (*Asterias forbesi*) oocytes. *J. Cell Biol.* **99**, 1878-1882.
- ELINSON, R. P. (1980). The amphibian egg cortex in fertilization and early development. In "The Cell Surface: Mediator of Developmental Processes" (S. Subtelny and N. K. Wessels, Eds.). Academic Press, New York.
- GARDINER, M. D., and GREY, R. D. (1983). Membrane junctions in *Xenopus* eggs: Their distribution suggests a role calcium regulation. *J. Cell Biol.* **96**, 1159-1163.
- GILKEY, J. C., JAFFE, L. F., RIDGWAY, E. B., and REYNOLDS, G. T. (1978). A free calcium wave traverses the activating egg of the medaka, *Oryzias latipes*. *J. Cell Biol.* **76**, 448-466.
- GREY, R. D., WOLF, D. P., and HEDRICK, J. L. (1974). Formation and structure of the fertilization envelope in *Xenopus laevis*. *Dev. Biol.* **36**, 44-61.
- HIBBARD, H. (1928). Contribution à l'étude de l'ovogenèse de la fécondation et de l'histogenèse chez *Discoglossus pictus*. *Oth. Arch. Biol.* **32**, 251-326.
- JAFFE, L. A., KADO, R. T., and MUNCY, L. (1985). Propagating potassium and Chloride conductances during activation and fertilization

Cytochemical Ca^{2+} Distribution in Activated *Discoglossus pictus* Eggs: A Gradient in the Predetermined Site of Fertilization

(amphibians/calcium/egg activation/K-pyroantimonate)

Roberto Gualtieri, Chiara Campanella and Piero Andreuccetti

Dipartimento di Biologia Evolutiva e Comparata, Università degli Studi di Napoli "Federico II", Via Mezzocannone 8, 80134 Napoli, Italy.

The K-pyroantimonate/ OsO_4 (PA) cytochemical method coupled with EGTA and X-ray microanalytical controls has been used to localize Ca^{2+} at egg activation in *Discoglossus pictus* eggs. The results show that: 1) the PA method is able to selectively localize Ca^{2+} pools mobilized by activating stimuli; 2) the smooth endoplasmic reticulum (SER) elements located in the animal dimple region, i.e. in the predetermined site of fertilization, are the first egg components labeled by precipitates; 3) a decreasing gradient of precipitates is present from the center beyond the boundaries of the dimple region; 4) precipitates are lacking in the remainder of the egg even at late times after activation.

The possibilities are discussed that a) SER is the major Ca^{2+} -releasing store at activation in *Discoglossus*, and b) the observed gradient of pyroantimonate-detected Ca^{2+} reflects an ionic Ca^{2+} gradient.

Introduction

At fertilization, eggs from a variety of species show a wave-like propagating Ca^{2+} increase supported by internal stores (28, 11, 12, 5, 23, 27, reviewed in 18 and 19). Such an increase, physiologically triggered by the sperm, functions as a second messenger which mediates many early and late activities of the fertilizing egg (11, 21). Now it is known that Ca^{2+} is mobilized from intracellular storage sites in response to the release of inositol-(1, 4, 5)-triphosphate (IP₃) from the plasma membrane, which is supposed to open IP₃-gated Ca^{2+} -channels located in the store membrane (2, 3, 33, 35, 4, 30, 22). In several species, extensive networks of the smooth endoplasmic reticulum (SER) are arranged in both the cortical and the deeper regions of the egg cytoplasm, thus possibly functioning as Ca^{2+} sources and sinks at activation (6, 13, 29, 24, 14). In particular, in anuran eggs, the SER has been hypothesized to be the major Ca^{2+} store involved in egg activation, since it appears and fully differentiates at the same time the maturing oocyte acquires the ability to respond to activating stimuli (7, 10).

We chose the egg of the amphibian *Discoglossus pictus* (Anura) to study the release of

intracellular Ca^{2+} and its pattern of distribution during egg activation. In this species, indeed, the successful sperm-egg interaction occurs only in a narrow area (D1) located at the bottom of the cup-shaped indentation of the egg animal hemisphere called the animal dimple (32). D1 can be easily distinguished from the rest of the egg since it shows distinctive ultrastructural features. The SER is typically clustered in D1 where it accounts for a large percentage of the peripheral cytoplasm (other organelles are cortical granules and rootlets of microfilaments) (Fig. 1a). It is only in the dimple that the SER shows a very complex organization, being divided into three structural elements with different spatial locations: 1) cortical tubular cisternae; 2) peripheral vacuoles; 3) subperipheral clusters of tubular cisternae (8) (Fig. 1a). Moreover, the concentration of SER elements drastically decreases at the dimple lateral walls (D2 + D3), thus showing a peculiar gradient of distribution (8, see also 9 for a review). The occurrence of such a polarized distribution of the SER in the predetermined site of sperm entry led us to suggest that Ca^{2+} may be released at activation according to a gradient which has its highest level in the dimple region.

In order to get an insight into the temporal and spatial pattern of Ca^{2+} release during activation in *Discoglossus* we used the K-pyroantimonate/ OsO_4 (PA) cytochemical method coupled with

Correspondence should be addressed to R. Gualtieri.

EGTA and X-ray microanalytical controls. The data here reported (part of which presented in a preliminary form; see 16) show that: 1) pyroantimonate-detectable Ca^{2+} (pdCa^{2+}) is absent before egg activation; 2) shortly after activation (1–3 min) the SER elements located in the dimple peripheral cytoplasm are the first egg components labeled by pdCa^{2+} ; 3) later on (5 min), pdCa^{2+} is found on all the dimple organelles, while 4) it is not detected outside the dimple region, even at 10 min after activation. Moreover, our results may provide some clues to the usefulness of the PA method for localizing Ca^{2+} .

Materials and Methods

Collection and viability of gametes: Adult *Discoglossus pictus* were collected in the neighbourhood of Palermo (Italy) during February and September and kept in aquaria. Gamete collection and viability assessments were performed as previously reported (15).

Removal of the jelly coats: The jelly coats were chemically removed in order to improve fixative penetration as well as to allow artificial activation by pricking. The medium consisted of (mM): dithiothreitol 5, NaCl 100, Tris-HCl 50, pH 8.0. After a 10–15 min treatment, dejellied eggs were extensively washed in amphibian Ringer (R) (mM): NaCl 111, CaCl_2 1.3, KCl 2, MgSO_4 0.8, Hepes 25, pH 7.8) diluted ten times with distilled water (1/10R) and kept in this medium until use.

Artificial activation: The removal of the jelly coats renders the egg unfertilizable. In order to activate eggs we used: 1) pricking by tungsten needles in 1/10R supplemented with 1.3 mM CaCl_2 (1/10R+Ca; final Ca^{2+} concentration 2.6 mM); 2) exposure to the Ca^{2+} -ionophore A23187 50 mM in 1/10R or in 1/10R Ca^{2+} -free (1/10R without CaCl_2 and supplemented with EGTA 12.5 mM). Activation was evidenced by the formation of foldings in the dimple surface followed by its progressive flattening during the first 5–6 min after the activation itself. Upon prick activation, a ring of contraction starting from the dimple was observed in some batches (see also 31).

Cytochemistry: Unactivated dejellied eggs were directly fixed for 1.5 hr at 4°C in potassium pyroantimonate 2%, OsO_4 1%, acetic acid 0.01N, pH 7.8 (15 eggs, 5 females). Some of them were purposely broken in the fixative to make sure it

freely penetrated into the ooplasm (6 eggs, 3 females). A second group of eggs was first activated by the different procedures described above and then fixed at 1, 3, 5 and 10 min after activation: 1) eggs pricked in 1/10R+ Ca^{2+} (1 min: 9 eggs, 3 females; 3 min: 7 eggs, 3 females; 5 min: 6 eggs, 3 females; 10 min: 7 eggs, 2 females); 2) eggs exposed to ionophore in 1/10R (1 min: 12 eggs, 4 females; 3 min: 9 eggs, 4 females; 5 min: 8 eggs, 4 females; 10 min: 8 eggs, 3 females), or 3) in 1/10R Ca^{2+} -free after manual removal of the vitelline envelope in order to avoid a retainance of Ca^{2+} inside the vitelline space (1 min: 3 eggs, 1 female; 5 min: 5 eggs, 2 females).

After fixation, eggs were processed as previously described (1). White/gold sections of animal and vegetal halves (AH, VH) were cut with a diamond knife at an LKBIII and observed unstained or slightly double-stained at a Philips EM 301 at 80 kV. In order to study the cytochemical reaction along the egg axis, animal and vegetal halves of the same egg were localized and cut (1 min: 9 ionophore, 6 pricked; 3 min: 8 ionophore, 4 pricked; 5 min: 4 ionophore, 6 pricked; 10 min: 7 ionophore, 4 pricked).

EGTA and X-ray microanalysis controls: EGTA: Serial sections of egg regions containing conspicuous precipitates were treated either with the Ca^{2+} -chelator EGTA 5 mM, pH 8.0 (AH, 7 eggs, 3 females), or with distilled water (serial sections of the same samples) for 5 min at 60°C in order to ascertain the chemical composition of precipitates.

X-ray microanalysis: gold-blue sections (100–250 nm thick) were collected on carbon-coated nylon grids and analysed at a Philips CM12 in STEM mode equipped with an EDS AN 10,000 (Link), a Li/Be window 0.008 mm wide and connected to a Cambridge computer. Acquisition and processing of spectra were made by the program Quantem (Demonplus). We chose the following analysis conditions: accelerating voltage 40 kV, beam current 5 μA , spot size 15 to 100 nm, channel size 20 eV, time of analysis 100–300 sec. Since Sb and Ca emission peaks practically overlap (Ca $K\alpha$ =3.690 keV; Sb L α 1=3.605 keV), in most cases the presence of Ca cannot be unambiguously detected (depending on the ratio of the two elements inside the analyzed area) and could only be revealed using Sb standards to quantify and strip the Sb contribution from the combined Sb/Ca peak. Therefore, in the present paper, X-ray microanalysis was performed in order to determine whether, elements such as Na and

Mg, which also may react with Sb (20), contribute to the precipitates.

Results

Unactivated egg

Dejellied unactivated eggs fixed in PA did not show intracellular precipitates (Fig. 1b) except for dimple liposomes whose edges were heavily labeled (Fig. 1b, inset). The cytochemical pattern was the same in eggs purposely broken during fixation (data not shown). The dimple extracellular content was intensely stained both before and after activation (Fig. 3)

Artificially activated eggs

In the dimple region of eggs activated either by pricking or by ionophore and fixed at about 1 min after activation, liposomes did not show any change of their cytochemical pattern (data not shown). Clusters of precipitates, instead, were unevenly localized, in sites of the ooplasm corresponding to SER elements (Fig. 2a). At 3 min after activation, most SER elements were labeled, while the other organelles still remained unstained (Fig. 2b). At 5 min after activation, the reaction had spread to all the organelles present in the peripheral cytoplasm of the dimple (Fig. 2c). Similar results were obtained up to 10 min after activation (data not shown). Eggs completely denuded and treated with ionophore in 1/10R Ca^{2+} -free did activate and showed essentially the same pattern as the parallel samples activated in 1/10R (Fig. 2d).

The distribution of the precipitates was studied along the animal/vegetal axis of eggs activated either by pricking or by ionophore and fixed up to 10 min after activation. Indeed, in both cases, and at all times studied, precipitates were distributed only along the dimple peripheral cytoplasm and gradually decreased, disappearing approximately at the dimple periphery (Fig. 3a, b, c). At increasing times after activation, the labeled region widened to cover the whole dimple (data not shown). However, at the time studied, precipitates were absent in the rest of the egg (Fig. 4a, c), except for pricked eggs in which they were also found in a narrow region close to the pricking site (7 eggs, 3 females) (Fig. 4b).

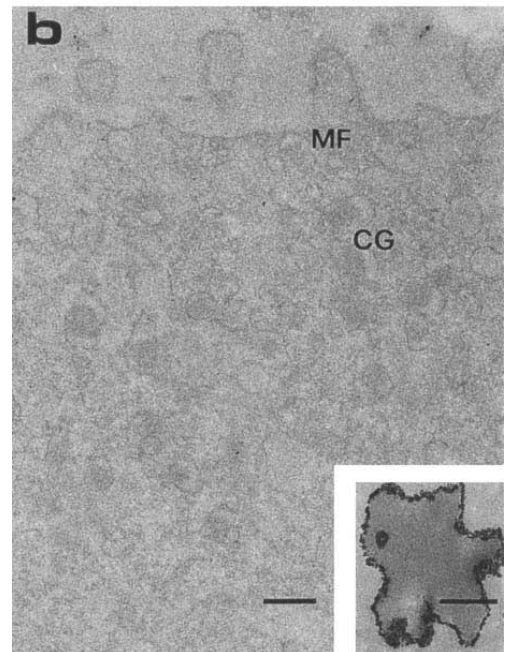
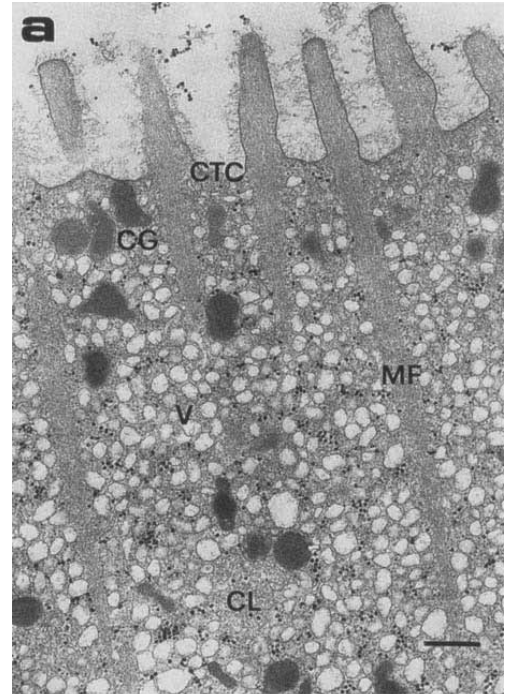


Fig. 1. (a): D1 region in a conventionally fixed unactivated egg. MF: microfilament rootlets. CTC: cortical tubular cisternae. CG: cortical granules. CL: clusters. 17,500 \times ; bar: 0.5 μ m. (b): D1 region in a pyroantimonate-fixed unactivated

egg. Precipitates stain only liposomes (inset). 17,500 \times ; bar: 0.5 μ m. Inset: 30,000 \times ; bar: 300 nm.

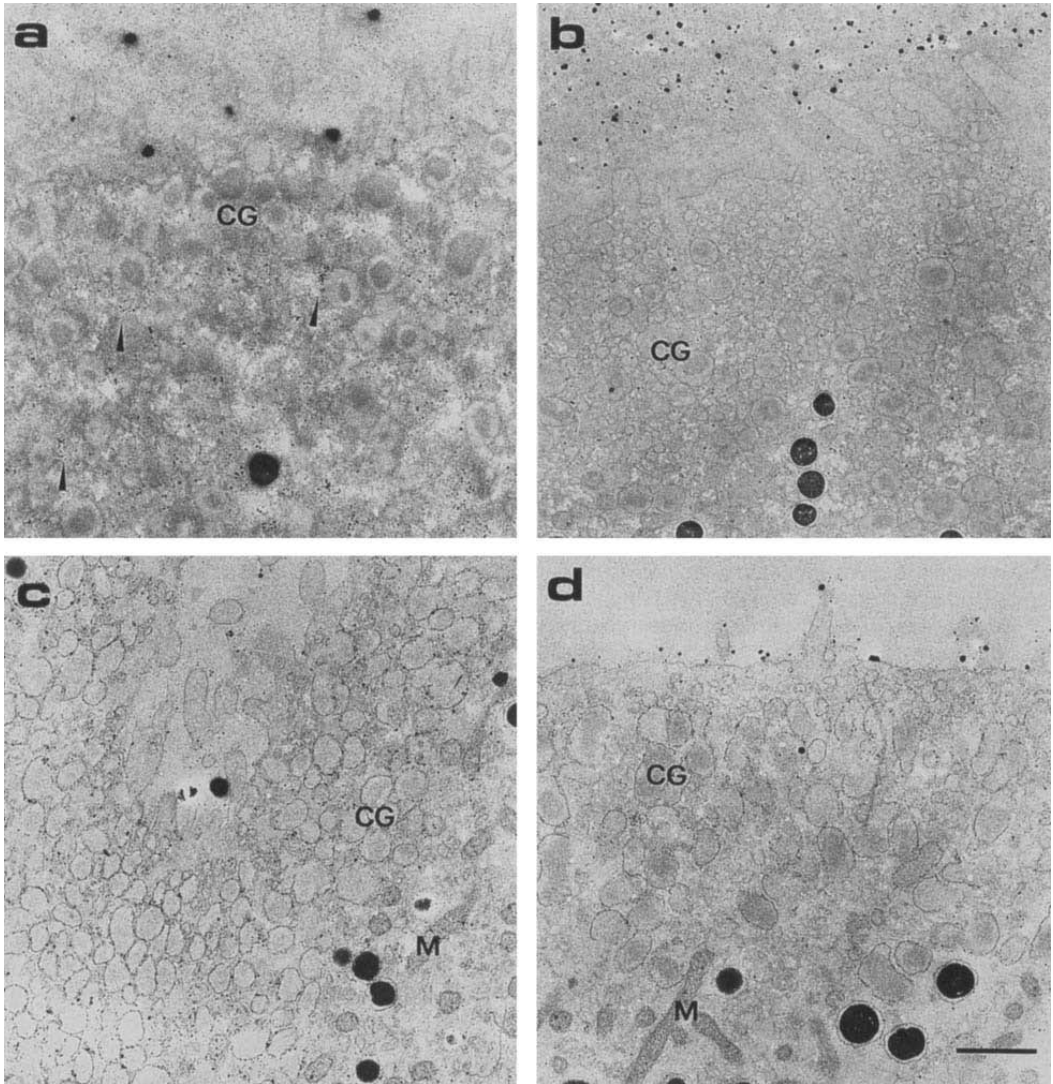


Fig. 2. Dimple region at 1 min (a), 3 min (b) and 5 min (c, d) after ionophore activation in 1/10 R (a, b, c) or in 1/10 R Ca^{2+} -free (d). 12,600 \times ; bar: 1 μm . (a) Only part of the SER is stained. (b) Most SER elements are stained. (c) Precipitates are associated with membranes of all the organelles. (d) The pattern of reaction does not change with respect to Fig. 2c.

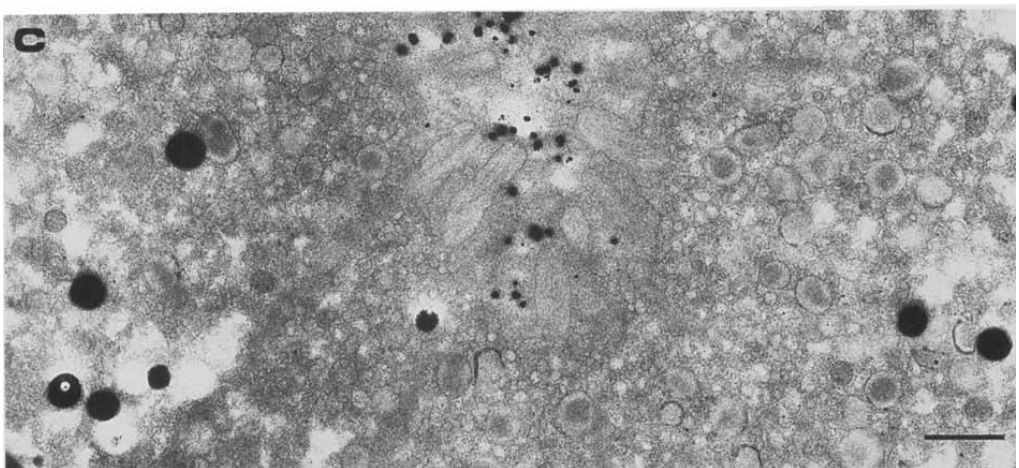
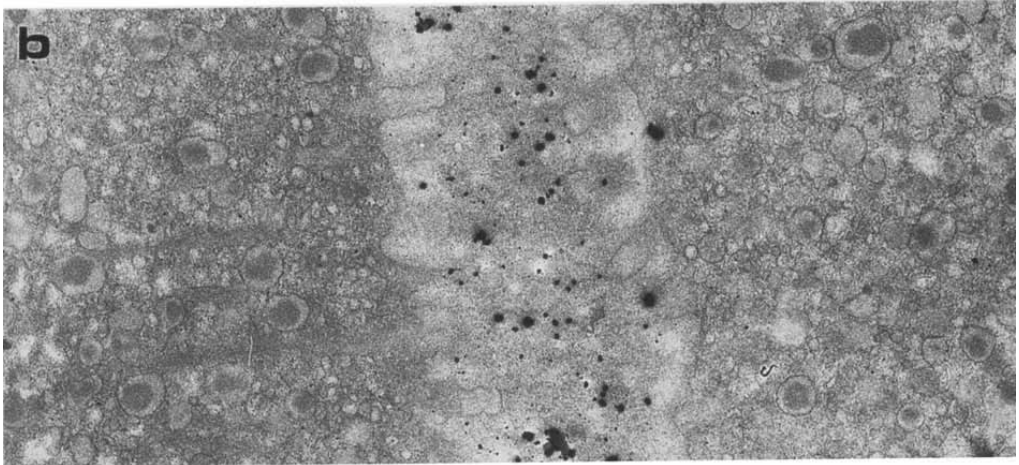
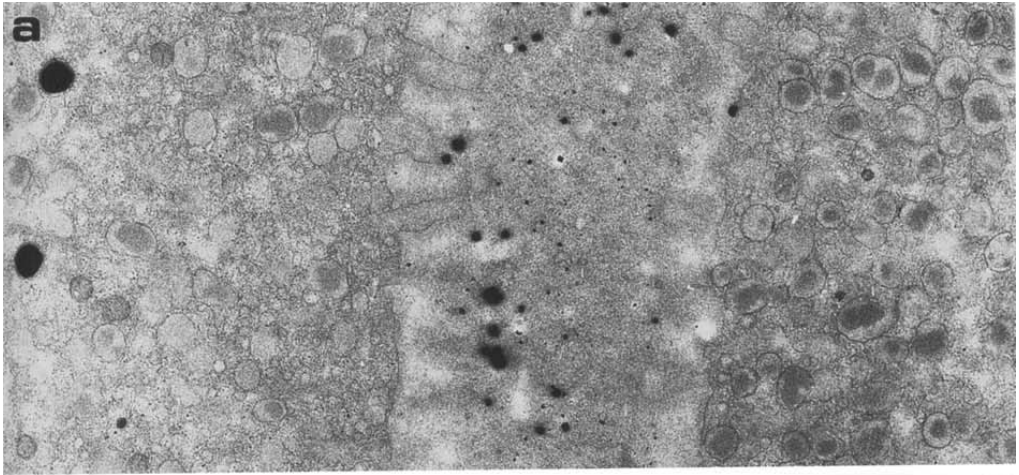
Controls with EGTA and X-ray microanalysis

EGTA: exposure of sections to EGTA 5 mM, pH 8.0 at 60°C for 5 min fully removed both extracellular and intracellular precipitates (Fig. 5b). Serial sections treated in distilled water at 60°C for

5 min (Fig. 5a) did not show any change in the cytochemical pattern compared to untreated sections.

X-ray microanalysis: spectra of both extracellular (45 spectra from 6 eggs) and intracellu-

Fig. 3. Dimple region at 1 min post-activation with ionophore in 1/10 R. The three micrographs show three neighboring regions of a single egg dimple. A decreasing gradient of precipitates is observed from upper (D1: central region of the dimple) to lower left and lower to upper right (D2: more peripheral region of the dimple). Note a corresponding gradient in the concentration of SER vesicles. 12,600 \times ; bar: 1 μm .



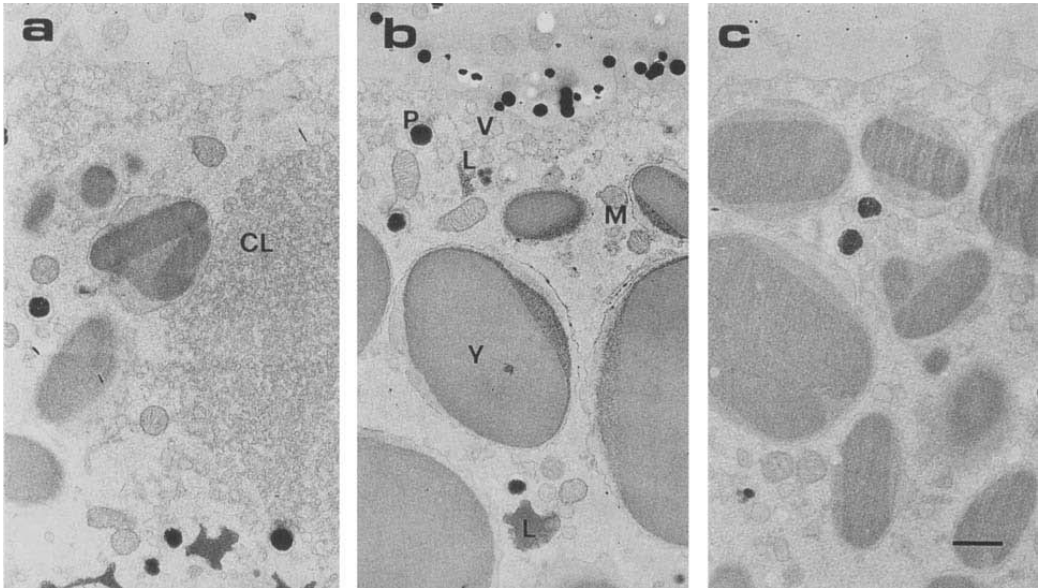


Fig. 4. Three different regions of a single egg at 10 min post-activation by pricking. 17,000 \times ; bar: 0.5 μm . (a) Animal hemisphere far from the dimple region. (b) A region very close to the pricking site (at the equator in this case). (c) Vegetal hemisphere.

lar precipitates (53 spectra from 5 eggs) clearly showed the Sb L alpha 1 and L beta 1 emission peaks respectively at 3.604 and 3.843 keV (Fig. 6a, b). In both cases we failed to detect Na or Mg signals associated with Sb (Fig. 6a, b: large arrowheads). As mentioned above, in most cases the microanalysis set-up did not discriminate between Ca and Sb emissions due to their overlapping. Nevertheless, spectra of dimple pigment granules showed both emissions possibly due to an element ratio more in favour of Ca inside the analyzed area. In fact, focalized spots of the pigment granule content showed that the Ca signal was not associated with the Sb signal (45/63 spectra from 6 eggs) (Fig. 6c). This would support the view that the bulk of Ca in pigment granules is tightly bound and unavailable to precipitate with antimonate.

Discussion

The present data suggest that the SER is the first site which releases Ca^{2+} in response to activating stimuli. In fact, in *Discoglossus pictus* eggs, pdCa^{2+} is first found at activation at the level of SER elements which are devoid of precipitates in the unactivated egg. Under the unactivated condition, the absence of precipitates cannot be due to a poor penetration of the PA across the egg

membrane, since: 1) osmication leads to a loss of the permeability features of the plasma membrane, 2) dimple liposomes are constantly heavily labeled by antimonate, 3) pdCa^{2+} is not found outside the dimple region even in eggs broken into the fixative. Thus, the observed negative reaction seems rather to depend on the inability of Ca^{2+} to precipitate with antimonate under unactivated conditions. This consideration has led us to revisit the literature dealing with the specificity and capability of PA to precipitate cations. According to Klein *et al.* (20) antimonate is able to precipitate Ca^{2+} 1 μM , Mg^{2+} 10 μM and Na^+ 10mM. Standard PA fixation conditions (with OsO_4 as a primary fixative) are considered to selectively detect Ca^{2+} and to allow a considerable loss of Na^+ (25, 26, 34). As regards the state of the Ca^{2+} revealed by the PA method, some authors claim it is ionic and easily exchangeable Ca^{2+} (20, 25, 26). Some authors, instead, believe that the PA method is not likely to detect either free or tightly bound Ca^{2+} , but rather it may mainly reveal pools of easily exchangeable Ca^{2+} ready to be mobilized in order to act as regulator of several cell functions (reviewd in 34). On the basis of our results, the following considerations can be made: 1) both EGTA and X-ray microanalysis controls exclude a contribution of other cations to the precipitates; 2) in pigment granules, the

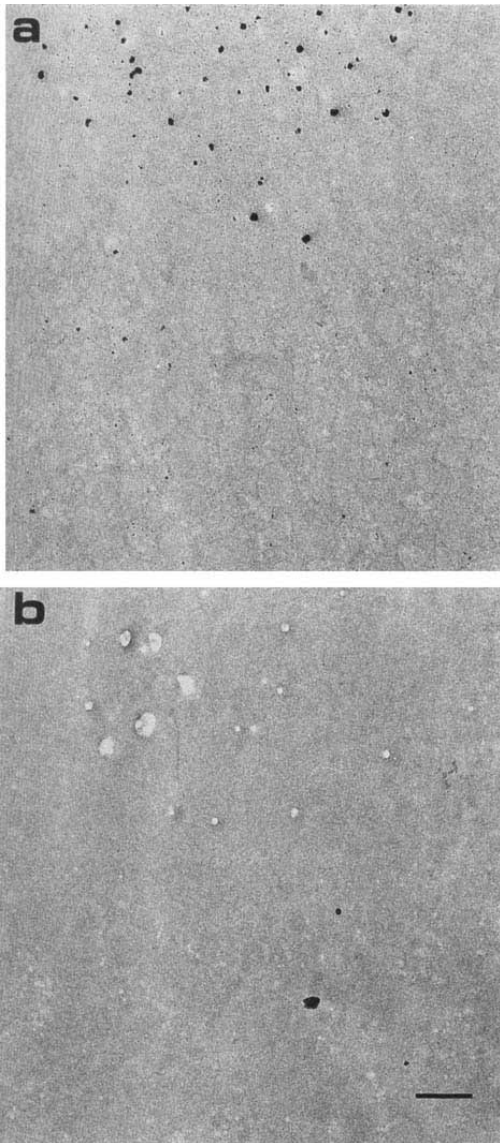


Fig. 5. Dimple region at 3 min post-activation with ionophore after exposure of the sections to distilled water (a) or to EGTA (b). 18,200 \times ; bar: 0.5 μ m.

recording of Ca signals not associated with Sb signals indicates the presence of a Ca^{2+} pool which is neither able to be lost upon fixation procedures nor to react with antimonate and, therefore, can be regarded as tightly bound Ca^{2+} ; 3) though the Ca^{2+} here revealed by the PA

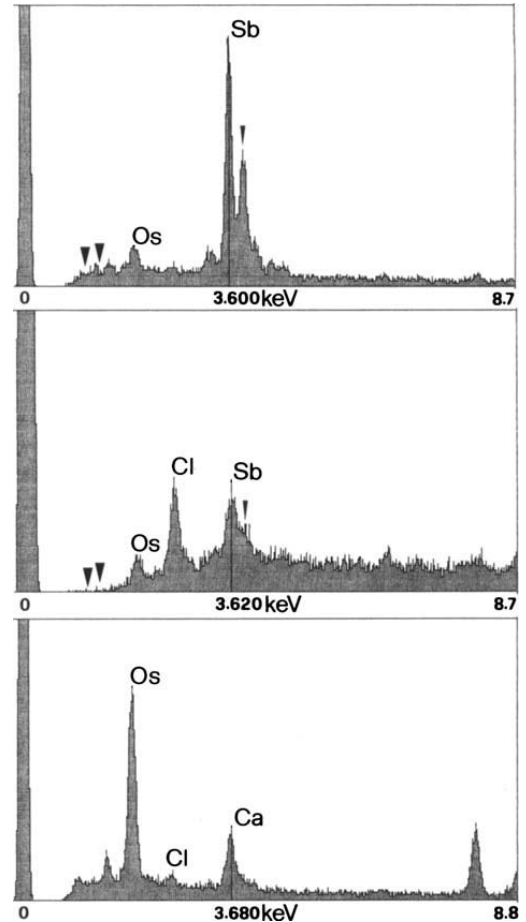


Fig. 6. X-ray microanalysis spectra of extracellular (a), intracellular precipitates (b), and pigment granule content (c) from eggs at 5 min after activation. (a) and (b) show the emission range from 0 to 8.700 KeV and the cursor is respectively at 3.600 and 3.620 KeV. (c) shows the emission range from 0 to 8.800 KeV and the cursor is at 3.680 KeV. Large arrowheads indicate the K alpha regions of sodium and magnesium. The small arrowhead in Fig. 6a and 6b indicates the Sb L beta 1 emission region at 3.843 KeV.

method cannot be unambiguously identified as ionic or easily exchangeable Ca^{2+} , the lack of pdCa^{2+} under the unactivated condition and its specific appearance in response to activating stimuli as well as to sperm interaction (work in progress) strongly indicates we are dealing with the free Ca^{2+} increase taking place at egg activation. From this point of view, it is not surprising that the pdCa^{2+} is lacking in the unactivated egg, where the free Ca^{2+} concentration is about 0.25 μ M (27),

i.e. far below the detection limit of 1 μM described by Klein *et al.* (20).

At activation the early (about 1 min after activation) appearance of pdCa^{2+} in SER elements indicates that in these sites Ca^{2+} pools are specifically mobilized in response to the Ca^{2+} -mobilizing action of the Ca^{2+} -ionophore or to the entrance of external Ca^{2+} caused by pricking. At 1 min after activation only part of the SER elements are labeled, while, later (3 min) the whole SER is labelled, which may indicate that preferential sites of SER release Ca^{2+} at the beginning of activation. We could not detect any obvious difference in the staining pattern of the three distinct SER elements present in the dimple peripheral cytoplasm. Further studies might establish whether the early appearance of pdCa^{2+} in particular sites of the SER and its subsequent spreading to the whole SER may reflect the existence of a multistep mechanism of Ca^{2+} release. Later on (about 5 min), pdCa^{2+} is found on membranes of all the dimple organelles (SER, cortical granules, mitochondria, pigment granules, yolk platelets, liposomes) perhaps indicating a Ca^{2+} -releasing or buffering activity in these sites. Interestingly, both in ionophore and prick activated eggs, the pdCa^{2+} decreases and then disappears as one moves towards the dimple boundaries. We know from a previous work (27), that the free Ca^{2+} -increase at fertilization or IP3-induced activation in *Discoglossus* proceeds as a wave, reaches a peak concentration of about 2 μM and then slowly recovers to the resting level as late as 40 min after activation. The authors did not find any differences in the free Ca^{2+} levels along the activating egg axis. However, it should be noted that the Ca^{2+} registrations were made at about 100 μm below the egg cortex and thus may reflect the diffusion or the autocatalytical regeneration of a cortical free Ca^{2+} release in the deep cytoplasm. Indeed, on the basis of kinetics of Ca^{2+} increase in different egg regions, Nuccitelli *et al.* (27) suggested that "the cytoplasm beneath the dimple contains a greater concentration of Ca^{2+} stores" and that cisternae and vesicles in this region are likely candidates as Ca^{2+} storage sites (see also 8). Since we never found pdCa^{2+} outside the dimple region even at 10 min after activation, as well as in ionophore-activated eggs, i.e. under conditions that should trigger a synchronous Ca^{2+} release, we can maintain that the PA method is not able to reveal a free Ca^{2+} level of 2 μM . It is noteworthy that the dynamic of the pdCa^{2+} increase at fertilization is essentially similar to that here reported at artificial

activation (work in progress). On the other hand, we suppose that upon egg activation the cortical free Ca^{2+} concentration in the dimple region may greatly exceed this value, and thus be detected by the PA method. For this purpose, it may be relevant that in the dimple region the wave of cortical contraction propagates at 25 $\mu\text{m/s}$, while the propagation rate in the remainder of the animal hemisphere is only 2 $\mu\text{m/s}$ (27).

The first appearance of pdCa^{2+} on the SER inside the dimple, the decrease of pdCa^{2+} at (or over) the dimple boundaries, and the lack of pdCa^{2+} in the remainder of the egg, indicate that 1) the SER is the site of activation-induced Ca^{2+} release in *Discoglossus pictus*, 2) this increase is distributed according to a steep gradient along the dimple peripheral cytoplasm (thus reflecting the extreme polarity of SER distribution in this egg) and, finally, 3) outside the dimple region the Ca^{2+} increase may be too low to be detected by the PA method. In this regard, it is noteworthy that recent studies on IP3-induced Ca^{2+} release in stratified eggs of *Xenopus laevis* have demonstrated that although all organelle layers are able to release (and sequester) Ca^{2+} , the reticulum-enriched layer releases ten fold as much Ca^{2+} (17).

In conclusion, our data indicate that the SER is the major Ca^{2+} store involved in the first steps of egg activation and that an animal/vegetal Ca^{2+} gradient may exist at activation in *Discoglossus*. Indeed, the pdCa^{2+} gradient overlaps the unique egg region where the sperm penetrates (32) and anionic channels, reportedly Ca^{2+} -gated (11, 36), and instrumental in the fertilization potential (31, 27), are segregated (27). This overlapping is striking indeed, and suggests that metabolic chains leading to egg activation and to the onset of development are segregated within the dimple according to a similar pattern of distribution.

Acknowledgements: This work was supported by grants of the Italian MURST. We thank Dr. B. Dale and Dr. R. Talevi for reading the manuscript, Mrs. A. Cirillo for English revision, Mr. G. Cafiero for expert technical assistance and advices with X-ray microanalysis and Mr. G. Falcone for printing. Part of this work was carried out at the CIRUB, Via Foria 222, Napoli.

References

1. Andreuccetti, P., S. Denis-Donini, A. G. Burrini and C. Campanella, 1984. Calcium ultrastructural localization in *Xenopus laevis* eggs following activation by pricking or by calcium ionophore A23187. *J. Exp. Zool.*, **229**, 295-308.

Our work on oocytes

Gianfranco Ghiara's group in Naples was working on the relationship between follicle cells and oocytes. My *degree* thesis, tutored by Carlo Taddei, was on cortical granules in the oocytes of Mediterranean amphibians. Much later in the years, several papers of my research group started with analyses related to the oocyte, to be then compared to unfertilized and fertilized eggs. However, we also worked on issues related to oogenesis *per se*. The study of the cytoskeleton and of the electrical properties of the *D. pictus* egg brought our attention to spectrin, because of its properties in retaining ionic channels and/or receptors in the plasma membrane.

In a paper closely related to her PhD thesis in 1997, and keen to discover where spectrin is located in the oocytes of *X. laevis*, Rosa Carotenuto found that its localization is not only cytoplasmic, but nuclear as it surrounds the numerous nucleoli of the growing oocytes. The study was then extended to the expression of spectrin mRNA during *Xenopus* oogenesis, and showed that the mRNA and the protein have a stage-specific asymmetric localisation in the oocyte and in the egg where it is found at the animal half, the region where sperm may penetrate the *Xenopus* egg. A significant contribution to this work was made by Carmen Vaccaro.

These results suggested that, in our system, spectrin is strongly related to cell polarization. At that time, because of my lectures in Developmental Biology, I studied the fascinating role that *gurken* has in eliciting microtubule polarization in *Drosophila*. *Xenopus* at stage III of oogenesis has a comparable microtubule reorganization, hence I supposed that a *gurken*-like molecule was similarly present in *Xenopus*. Trudy Schüpbach kindly sent us anti-*gurken* antibodies. Guided by Franco Graziani and Carla Malva in their IGB laboratory, Carmen screened a *Xenopus* library using that antibody and found colonies positive to it. However, the molecule reactive with anti-*gurken* was indeed XNOA 36 that does not share sequences longer than 5aa with *gurken*. When Carmen presented her interesting thesis, I was overwhelmed by deep-seated emotion. It was the first time that in our lab a research into molecular biology has been carried out. Much of Carmen's PhD thesis and later her post-doc work aimed to throw more light on *Xenopus* oocyte polarization and to understand whether XNOA 36 is involved in oocyte polarization. Indeed, its RNA distribution coincides with that of spectrin protein and bisects

X. laevis stage I oocytes along the future A/V axis. XNOA 36 is also located in the METRO region of the mitochondrial cloud. Therefore it is released in the cortex of the vegetal pole, upon the arrival of the mitochondrial cloud, where it potentially interacts with γ -tubulin. Although not proved, it may be hypothesized that XNOA 36, which interacts with centromeres in mammalian cells, is part of the mechanism that provides microtubule reorganisation in *Xenopus* oocytes.



Fig. 19. 2001. Capri, at the ABCD meeting *Regolazione dello sviluppo* conducted by G. Tocco and myself and organized by Carmen. From left: Irma Nardi, Roberto Perris, Michela Ori, Nadia De Marco, Riccardo Focarelli, Carmen, Mariangela Caputo.

A novel protein cross-reacting with antibodies against spectrin is localised in the nucleoli of amphibian oocytes

Rosa Carotenuto¹, Giovanna Maturi¹, Vincenzo Infante¹, Teresa Capriglione¹, Tamara C. Petrucci² and Chiara Campanella^{1,*}

¹Dipartimento di Biologia Evolutiva e Comparata, Università di Napoli, via Mezzocannone n. 8, 80134 Napoli, Italy

²Istituto Superiore della Sanità, Laboratorio di Biologia Cellulare, viale Regina Elena n.299, 00161 Roma, Italy

*Author for correspondence

SUMMARY

Cytoskeletal proteins such as actin and myosin are important constituents of the nucleoplasm. Spectrin is an actin binding protein typically related to plasma membrane; recently, it has been found that it is widespread and forms distinct membrane protein domains in such organelles as the Golgi. In this paper, the large germinal vesicle of amphibian oocytes was chosen as a particularly suitable system to investigate the presence and location of spectrin in the nucleus. We manually isolated the germinal vesicles of both *Discoglossus pictus* and *Xenopus laevis* oocytes, and processed them for SDS-PAGE, immunoblotting and immunoprecipitation. By the use of an antibody against the general form of brain β spectrin (β II Σ 1) and of an anti- α brain spectrin (α II Σ *), a band of 230 kDa was identified as a nuclear spectrin-like molecule. Moreover the 230 kDa protein was extracted from the nuclei by 1 M KCl, similarly to spectrin in other systems. In oocyte sections and nuclear spreads incubated with anti- α II Σ * and/or anti-

β II Σ 1 antibodies, the immunostain was localised in the nucleoplasm and in the outer shell of the round bodies abundantly present in the germinal vesicle. Sections of the same oocytes, stained with a monoclonal antibody against nucleolar fibrillarin and anti- α II Σ *, showed co-localisation of the two antibodies. It was concluded that, in the germinal vesicle of amphibian oocytes, a spectrin-like molecule is a part of the outer shell of nucleoli. It is hypothesised that spectrin, together with actin, might be instrumental in keeping nucleoli attached to the inner nuclear membrane, as nucleoli migrate during oogenesis to the inner aspect of the nuclear envelope, where they are stably kept until the end of their growth. Furthermore, these results strongly suggest that the 230 kDa band might comprise both an α and a β chain of the same apparent molecular mass, thus constituting a novel form of a spectrin-like molecule.

Key words: Spectrin, Germinal vesicle, Nucleolus

INTRODUCTION

Spectrin has a strategic position and role related to plasma membrane structural organisation in erythrocytes, as well as in other cells. It is made of two distinct α and β subunits which are cross-linked by filamentous actin and other proteins to form an extensive filamentous meshwork. On the other hand, they are associated with membrane proteins, thus maintaining membrane structural integrity and generating distinct membrane protein domains (for a review, see Bennet, 1990). Moreover, spectrin is also associated with the membrane of organelles such as exocytotic vesicles (Hirowaka et al., 1983; Fishkind et al., 1990) or with electron-dense cytoplasmic islets (Black et al., 1988). More recently, a β spectrin homologue (β II Σ *) has been found to be associated with the Golgi apparatus (Beck et al., 1994; Devarajan et al., 1996). The family of spectrin-like molecules appears to be composed of complex and articulated isoforms, each bearing a specific location and function in the cell (see Morrow et al., 1991). In amphibian eggs, a spectrin-like dimer of 254/239 kDa is localised in the cortex, whereas another spectrin-like dimer of

254/225 kDa is present in the subcortical cytoplasm (Tatone et al., 1993; Carotenuto et al., 1994, and unpublished results).

Little is known of the occurrence of spectrin in the nucleus. The large germinal vesicle (GV) of amphibian oocytes is a suitable system for studying nuclear components because of ease in manipulation and abundance of some of its constituents. In a previous study, we showed that the GV of *Discoglossus pictus* oocytes was immunologically stained by antibodies against brain spectrin. The fluorescence depicted in frozen histological sections was spot-like and appeared to be randomly distributed in the nuclear matrix (Campanella et al., 1990; for similar results in *Xenopus* GV see Ryabova et al., 1994). The data were preliminary, since immunolocalisation could not be ascribed to any precise structure and, furthermore, biochemical studies to identify cross-reactive molecules were not carried out. To date, the presence of spectrin in the nucleus of other systems, although suggested, has not yet been fully investigated. Contrary to spectrin, other cytoskeletal proteins such as actin and myosin have been described in the nuclei of germinal and somatic cells (for a review, see De Boni, 1994) where they may constitute aggregates, as it has recently been demonstrated

by confocal immunocytochemistry and ultrastructural immunolocalisation (Milankov et al., 1991). Furthermore, protein 4.1, that in erythrocytes stabilises the complex between spectrin and actin and anchors them to the plasma membrane through interactions with integral membrane proteins, has been detected in the nucleus of human cells (Wald Krauss et al., 1997). Despite the numerous biochemical and immunological studies of cytoskeletal proteins, much work is still needed for understanding their role in the nucleus.

The aim of the present study was to determine which GV constituent of amphibian oocytes is labelled by anti-brain spectrin antibodies and to identify the cross-reacting protein. We depicted a spectrin-like molecule in nuclear preparations, by utilising antibodies against α or β isoforms (α II Σ^* and β II Σ 1, respectively, according to recent nomenclature, see Malchioldi Albedi et al., 1993; Winkelman and Forget, 1993; Devarajan et al., 1996). The immunostain was localised in the GV and in particular in the multiple nucleoli, typically present in growing amphibian oocytes. In this regard, a novel protein of about 230 kDa was identified by immunoblotting and immunoprecipitation in the GV of both *Discoglossus pictus* and *Xenopus laevis* oocytes.

MATERIALS AND METHODS

Animals and samples

Adult *Discoglossus pictus* (painted frog) females were captured in the neighbourhood of Palermo (Italy). Adult *Xenopus laevis* specimens were obtained from 'Rettili' (Varese, Italy).

Groups of oocytes at various stages of oogenesis were excised from the ovaries of females anaesthetised with MS222 and processed for immunocytochemistry or biochemistry.

Antibodies

Rabbit polyclonal antibody against the general form of brain β spectrin (β II Σ 1) was a gift from Dr J. Morrow (Department of Pathology, Yale University School of Medicine, New Haven CT, USA) (see also Malchioldi-Albedi et al., 1993). The IgG fraction of

the antiserum was purified by a Protein A-Tris-acryl (Sigma Chemical Co.) column. Following dialysis in PBS, the purified antibodies were used at varying concentrations (100 μ g/ml for immunofluorescence; 1 μ g/ml for electrophoresis, immunoblotting and immunoprecipitation).

Rabbit polyclonal antibody against bovine brain α spectrin (α II Σ^*) was similarly affinity purified (Di Stasi et al., 1991) and utilised. This antibody recognises both erythroid and non-erythroid α spectrin and, to a lesser extent, erythroid β spectrin.

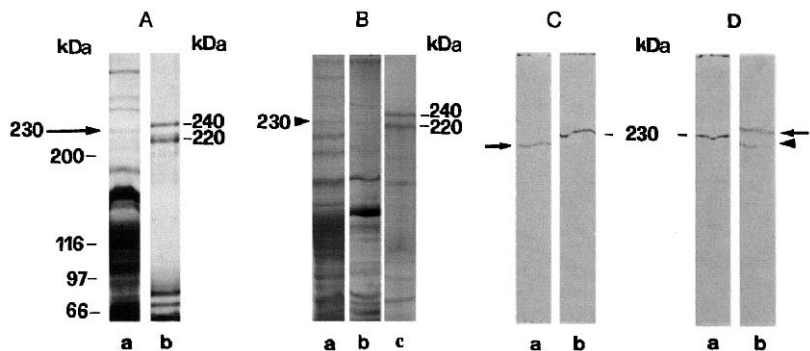
A mouse monoclonal antibody against fibrillarlin (17C12; Hultman et al., 1994) was a gift from Dr K. M. Pollard (Department of Molecular and Experimental Medicine, the Scripps Research Institute, La Jolla, CA, USA). Fibrillarlin is a protein typical of nucleoli (Ochs et al., 1985). 17C12 specifically stains somatic and oocyte nucleoli of *Xenopus laevis*, whereas it fails to stain spheres (Wu et al., 1993; Gall et al., 1995).

Electrophoresis and immunoblotting

GVs of *D. pictus* or *X. laevis* were obtained by gently squeezing the oocyte with watchmaker's forceps and collected in 20 mM Tris-HCl, pH 7.5, containing 2 mM MgCl₂, 75 mM KCl, 0.05 mM PVP, 1 mM DTT at 4°C (see Clark and Merriam, 1977). After several rinses in the same buffer without PVP, a cocktail of protease inhibitors (0.5 mM PMSF, 2 mM EDTA, 5 μ g/ml SBTL, 5 μ g/ml aprotinin, 25 μ g/ml leupeptin) was added to the last rinse. The nuclei were homogenised and boiled for 3 minutes in sample buffer containing 50 mM Tris-HCl, pH 6.8, 69 mM SDS, 0.028 mM Bromophenol Blue, 1 mM DTT. Aliquots of 50 GVs were submitted to SDS 7.5% or 5% polyacrylamide gel electrophoresis (Laemmli, 1970), using human erythrocyte ghost preparations and high molecular mass proteins (Sigma Chemical Co.) as molecular mass standards. In some experiments, 100 GVs were homogenised in homogenisation buffer containing 1 M KCl and centrifuged at 14,000 g. The supernatant was lyophilised after dialysis against 2 mM Tris-HCl, pH 7.4. Equal volumes of the high salt soluble and insoluble extracts were analysed by SDS-PAGE.

The gels were stained with 0.1% Coomassie Brilliant Blue or silver. Part of the samples was transferred electrophoretically to nitrocellulose paper (NC) (Towbin et al., 1979) overnight at 400 mA in a cooling chamber. The efficiency of the transfer was evaluated by staining the NC with Ponceau S and the corresponding gel with Coomassie Brilliant Blue. The NC sheets were then incubated with 5% fat-free

Fig. 1. Samples of oocyte GVs and human erythrocyte ghosts were analysed on 5% SDS-PAGE and stained with Coomassie Blue or transferred to nitrocellulose membrane. (A) Gels stained with 1% Coomassie Blue. Molecular mass standards are indicated on the left. Lane a, total GV preparation. The arrow points to a faint molecule of about 230 kDa. Lane b, 240 and 220 kDa bands are indicated, corresponding to α and β erythroid spectrin subunits in human erythrocyte ghosts. (B) GV extracted in 1 M KCl



containing buffer. Lane a, soluble extract. The 230 kDa band is indicated. Lane b, pellet; the band is undetectable. Lane c, erythrocyte ghosts. (C) Western blot with anti- β II Σ 1 spectrin antibodies showing the immunoreactivity of the GV 230 kDa band and of the spectrin β chain (arrow in a), as control. Lane a, erythrocyte ghosts. Lane b, GV. (D) Western blot with anti- α II Σ^* incubation. Lane a, the 230 kDa band is immunoreactive. Lane b, in human erythrocyte ghosts the spectrin α chain is reactive, while the β spectrin subunit is only slightly positive (arrowhead).

milk (Milupa, Verona, Italy) to saturate additional protein binding sites, rinsed in saline and incubated with antibodies or antisera. Human erythrocyte ghosts were used as controls; the erythroid β chain and partially the erythroid α chain were recognised by anti- α II Σ^* , while with anti- β II Σ 1 only the β -chain was clearly cross-reacting (see Fig. 1). Antibody binding was detected by anti-rabbit IgG, raised in goat and conjugated to alkaline phosphatase, using the Protoblot Immunoscreeing system (Promega, Madison, USA).

Immunoprecipitation

Aliquots of 50 GV, prepared as for SDS-PAGE, were homogenised in buffers containing the cocktail of protease inhibitors previously described. Buffer A (40 mM Tris-HCl, pH 8.8, containing 1 M NaCl, 20 mM Na-pyrophosphate, 40 mM NaF, Triton X-100, 2 mM MgCl₂, 5 mM EGTA and 4 mM EDTA) was mixed with buffer B (20 mM Hepes-NaOH Buffer, pH 6.8, containing 0.5 M NaCl, 10 mM Na-pyrophosphate, 20 mM NaF, 1% Triton X-100, 1 mM MgCl₂, 2.5 mM EGTA, 2 mM EDTA), as previously described (Malchiodi-Albedi et al., 1993) under non-denaturing conditions. Following homogenisation and centrifugation at 13,000 g the supernatant was: (1) incubated with 20 μ l of rabbit IgG (1 mg/ml) in order to precipitate possible aspecifically binding proteins; (2) incubated with 20 μ l of Protein A-Tris-acryl (Sigma Chemical, Co.) for a minimum of 1 hour at 4°C; (3) centrifuged; (4) incubated overnight at 4°C with 20 μ l of anti- β II Σ 1 spectrin (1 mg/ml); then (5) centrifuged. The pellet was first washed several times in PBS, then treated with 50 mM Tris-HCl, pH 7.4, and eventually boiled in sample buffer. After centrifugation, the supernatant was submitted to SDS-PAGE and immunoblotting with anti- β II Σ 1 spectrin antibody.

Immunofluorescence

Preparation of samples

D. pictus GV, obtained as previously indicated, were cleaned from residual cytoplasm in 20 mM KCl and 20 mM NaCl at 4°C (medium A) and transferred into a small chamber glued on a histological slide. The GV's were then deprived of the nuclear envelope in 2% formalin in medium A and stored at 4°C. Nucleoli and lampbrush chromosomes settled on the bottom of the chamber in the following two or three days. The samples were allowed to dry before processing them for immunofluorescence.

X. laevis and *D. pictus* oocytes (stages I to VI) were fixed in 2% formaldehyde, prepared from paraformaldehyde and diluted in PBS, for 1 hour at 4°C. Following rinses in PBS, the oocytes were embedded in Tissue-tek O.C.T. compound (Miles Inc. Elkart Ind. USA), frozen in liquid nitrogen and sectioned with a Jung Frigocut 2800 N cryostat at the thickness of 6 μ m. The sections were dried before incubation with antibodies.

Immunofluorescent staining

Following several rinses in 10 mM Tris-HCl, pH 7.4, the contents of *D. pictus* GV's was exposed in sequence to: (1) 10 mM Tris-HCl, pH 7.4, containing 1% BSA, 0.3% Triton X-100, 1% gelatin, 0.02 M glycine, 5% NaCl; (2) antibody or rabbit IgG as controls (Sigma Chemical Co.); (3) rinses in Tris-HCl; (4) fluorescein-conjugated IgG fraction to rabbit IgG (Sigma Chemical Co.) containing 10% *D. pictus* serum; (5) rinses in Tris-HCl. The chamber was sealed with a coverslip.

Frozen sections from *D. pictus* or *X. laevis* oocytes were similarly incubated through steps 1, 2 and 3 and exposed to anti- α II Σ^* or anti- β II Σ 1 antibody, then to fluorescein-conjugated IgG fraction to rabbit IgG. Frozen sections exposed to anti-fibrillarlin were incubated with fluorescein-conjugated IgG fraction to mouse IgG (Sigma Chemical Co.). Double incubation with anti-brain spectrin antibodies and anti-fibrillarlin followed by FITC anti-rabbit and TRITC anti-mouse IgG was assayed but not utilised, because it resulted in a strong attenuation of fluorescence.

To check the specificity of antibody staining, frozen sections were incubated with anti- α II Σ^* antibody preabsorbed with human erythro-

cyte α and β spectrin. Human erythrocyte ghost extracts were separated on 5% SDS-PAGE and transferred onto NC. The area of nitrocellulose containing the α and β spectrin bands was cut and the NC strips were used to inhibit antibody reactivity.

The sections were eventually mounted in 90% glycerol in PBS containing 0.1% *p*-phenylenediamine. The level of fluorescence derived from incubation with polyclonal antibodies was compared with that in control nuclei or sections treated in parallel with rabbit γ globulins (Sigma Chemical, Co). For the sections exposed to the preabsorbed antibodies, the level of fluorescence was compared with that of sections treated in parallel with unabsorbed anti- α II Σ^* antibodies. The immunofluorescence was specific in all the examined samples.

The samples were observed using a Leitz photomicroscope equipped for epifluorescence. Photographs were taken using an Ektachrome 800-1600.

RESULTS

Electrophoresis, immunoblotting and immunoprecipitation

A band of 230 kDa cross-reacting with anti-brain spectrin antibody is depicted in the GV

Fig. 1 shows the electrophoretic fractionation of *Discoglossus* GV total proteins. A faint band was present with an apparent molecular mass of about 230 kDa (Fig. 1A, arrow) when compared to α and β subunits of human erythrocyte spectrin (220 and 240 kDa) (Fig. 1A). Following extraction in 1 M KCl, the 230 kDa band was highly enriched in the supernatant (Fig. 1B,a) and barely detectable in the pellet (Fig. 1B,b).

After transfer of the separated proteins onto NC, the 230 kDa band was stained by both anti- β II Σ 1 (Fig. 1C,b) and anti- α II Σ^* antibodies (Fig. 1D,a).

Aliquots of 50 *D. pictus* GV's were used to precipitate the 230 kDa protein with antibodies against β spectrin subunit. The experimental conditions used have previously been shown to preserve the association between α and β subunits (Malchiodi-Albedi et al., 1993). The immunoprecipitate pellet was loaded into two wells of a 5% SDS-PAGE gel and, following electrophoresis, one of the two lanes was transferred onto NC and incubated with anti- β II Σ 1 antibody (Fig. 2). The second lane

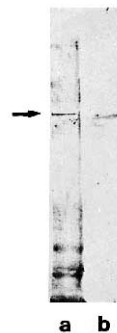


Fig. 2. GV immunoprecipitation with anti- β II Σ 1 antibody. Lane a, immunoblots of the immunoprecipitate transferred onto NC and exposed to anti- β II Σ 1 antibody. The 230 kDa protein is indicated by the arrow. Lane b, human ghost erythrocyte incubated with the same antibody; β spectrin is immunoreactive.

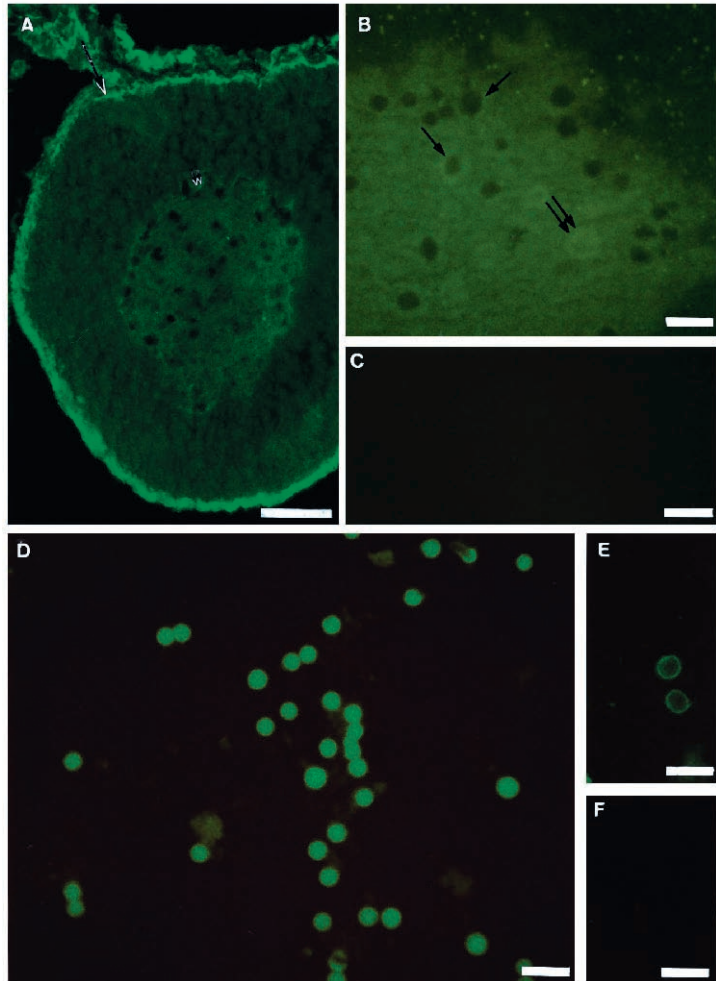


Fig. 3. (A-C) Immunofluorescence of frozen sections of *D. pictus* oocytes at an early stage of vitellogenesis (about 320 μm in diameter). (A,B) Anti- βIIIS1 antibody incubation. (A) The immunostain is present in the cortex and in the surrounding ovarian tissue (arrow). Furthermore, the fluorescence is located in the GV content, particularly surrounding dark spherical organelles. The nuclear envelope is immunoreactive (double small arrows). $\times 310$. (B) The GV matrix is fluorescent. Round bodies are surrounded by a rim of immunostain (arrows), or fully stained, when tangentially sectioned (double arrows) $\times 500$. (C) Control section incubated with rabbit IgG. Immunostain is absent. $\times 500$. (D) GV preparation spread on a microslide and incubated with anti- βIIIS1 antibody. Immunostain is present on the numerous round bodies. $\times 500$. (E) Fluorescence is located around these bodies. $\times 500$. (F) Control GV preparation. Immunostain is absent. $\times 500$. Bars: 50 μm (A,B); 20 μm (C-F).

was stained with Coomassie Brilliant Blue (not shown). The 230 kDa band was present in the immunoprecipitate (Fig. 2a). Other low molecular mass bands were also present. This can be explained by considering that the non-denaturing conditions of the procedure supposedly fails to separate the 230 kDa from other complexing proteins.

Immunofluorescence

Anti- β spectrin stains round bodies located in the GV

Frozen sections of *D. pictus* oocytes incubated with affinity purified anti- βIIIS1 antibody revealed a fluorescence in the GV's of both previtellogenic and vitellogenic oocytes. In oocytes at an early stage of vitellogenesis (about 300 μm in diameter), fluorescence was evident in the nucleoplasm, and appeared to

surround round bodies therein present as a more evident rim of fluorescence (Fig. 3a,b). In Fig. 3b, some of these bodies are tangentially and others longitudinally sectioned. In the former case (double arrows), the immunostain covers the entire round body, in the latter case only its periphery is stained, the central core remaining unstained. Moreover, the immunostain is present on the nuclear envelope (Fig. 3a), as well as in the oocyte cortex and in the surrounding ovarian tissue. Fig. 3c is a control section incubated with non immune rabbit IgG.

In oocytes at more advanced stages of vitellogenesis, the βIIIS1 staining was visible as a fluorescent rim around the round bodies, while it was less evident in the surrounding nucleoplasm (data not shown).

The GV content spread on histological slides was constituted

predominantly by lampbrush chromosomes, nucleoli, B-snurposomes and spheres. Upon incubation with anti- β II Σ 1 antibody, round bodies 8-10 μ m in diameter were specifically stained (Fig. 3d,e). Fig. 3f is a control GV preparation incubated with non immune rabbit IgG. The immunostain covered the whole bodies (Fig. 3d), but, in some nuclear preparations, it could be appreciated that the cross-reactivity was located at the periphery of the bodies (Fig. 3e). Therefore, spectrin appears to be a part of the outer shell of the GV round bodies.

The round bodies surrounded by spectrin appear to coincide with the nucleoli: anti- α II Σ * and anti-fibrillar

Oocyte frozen sections were incubated with anti- α II Σ * or fib-

rillar (Fig. 4). It was found that anti- α II Σ * recognizes the nuclear content similarly to anti- β II Σ 1 (Fig. 4a). Fig. 4a depicts an oocyte at the onset of vitellogenesis; fluorescence surrounds the round bodies scattered in the whole GV. Anti-fibrillar was used on a similar section with the aim of detecting nucleoli among other spherical organelles present in the GV. The immunostain depicted a rim around the nucleoli and, to a lesser extent, was also present in the nucleoplasm (Fig. 4b). Fig. 4c,d are control sections for the anti- α II Σ * antibodies indicating that the immunostain was abolished by preincubating anti- α II Σ * antibodies with human α and β erythroid spectrin.

In order to determine whether the round bodies surrounded by spectrin are nucleoli, serial sections of ovarian oocytes were incubated in an alternating sequence with anti- α spectrin or

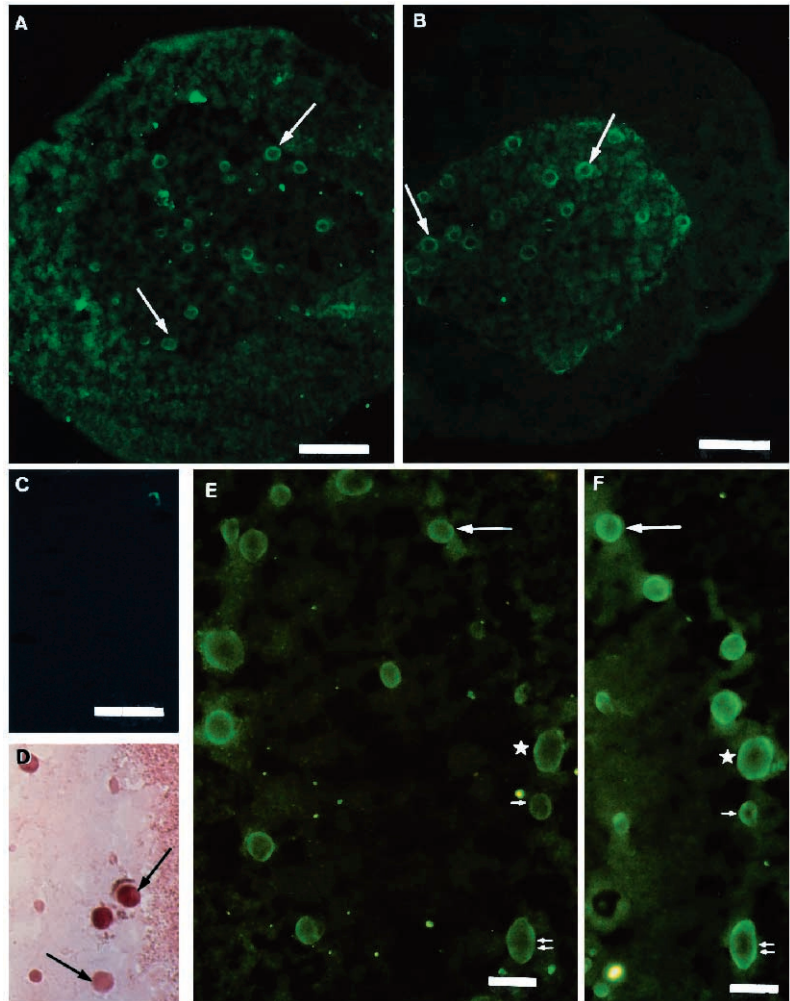


Fig. 4. Frozen sections of *D. pictus* oocytes at early stages of oogenesis. (A) Section of an oocyte of about 300 μ m incubated with anti- α II Σ *. The arrows indicate the rim of immunostain surrounding the round bodies. $\times 310$; (B) Incubation with anti-fibrillar. Immunostain surrounds spherical bodies thus identified as nucleoli (arrows). $\times 310$. (C) Control section exposed to anti- α II Σ * preabsorbed with erythroid α and β spectrin; the immunostain is absent. (D) Light microscopy of the same section as in B. The round bodies are indicated (arrows). The section is lightly stained by *p*-phenylenediamine present in the glycerol-PBS mixture. $\times 310$. (E,F) Serial sections of the same GV from a 500 μ m oocyte. (E) Incubated with anti- α II Σ * antibody; (F) incubated with anti-fibrillar. Corresponding labels (arrow, double small arrows, star, small arrow) indicate the same nucleoli immunostained by both antibodies. $\times 500$. Bars: 50 μ m (A-C); 20 μ m (E,F).

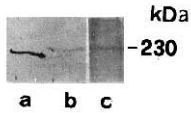


Fig. 5. *Xenopus laevis* GV preparation (lane b) and human erythrocyte ghost (lane a) after western blot with anti- β II Σ 1 antibody. Lane a, immunoreactivity at the 220 kDa β spectrin. Lane b, the GV preparation shows immunoreactivity of the 230 kDa band. Lane c, SDS-PAGE of the GV preparation stained with silver stain. The 230 kDa band is indicated.

anti-fibrillarin. Fig. 4e and f are sections of the same GV stained with anti- α spectrin (Fig. 4e) or with anti-fibrillarin (Fig. 4f). The two immunostains were localised in the same organelles, i.e. the nucleoli, thus indicating that spectrin is part of the nucleoli periphery.

Immunoblots and immunofluorescence in *X. laevis*

The GV 230 kDa band cross-reacts with anti- β spectrin, and immunocytochemistry is localised in the nucleoli of *Xenopus* oocytes

As for *D. pictus* oocytes, a protein of about 230 kDa, present

in the GV homogenate, cross-reacted with anti- β II Σ 1 antibodies following separation through SDS-PAGE and transfer to NC (Fig. 5).

X. laevis frozen sections of oocytes at various stages of oogenesis were incubated with anti-spectrin antibodies. Fig. 6a and b show the specific cross-reactivity with anti- β spectrin. At the oocyte periphery, both cortex and the surrounding ovarian tissue were immunostained. In the GV, fluorescence was present in the nucleoplasm and surrounded the round bodies (Fig. 6a,b). As for *D. pictus* oocytes, the nucleoplasm staining was particularly intense in oocytes at early stages of vitellogenesis.

In the GV, serial sections of the same oocyte incubated with anti- α II Σ * spectrin (Fig. 6c) or with anti-fibrillarin (Fig. 6d), showed an identical pattern of fluorescence at the nucleoli periphery.

DISCUSSION

In amphibian oocytes, cross-reactivity to anti-spectrin antibodies was detected in the nucleoplasm and in the outer shell of the GV round bodies. The protein responsible for such cross-reactivity was identified as a 230 kDa protein by immunoprecipitation and immunoblotting of isolated nuclei. Immunostaining with anti-

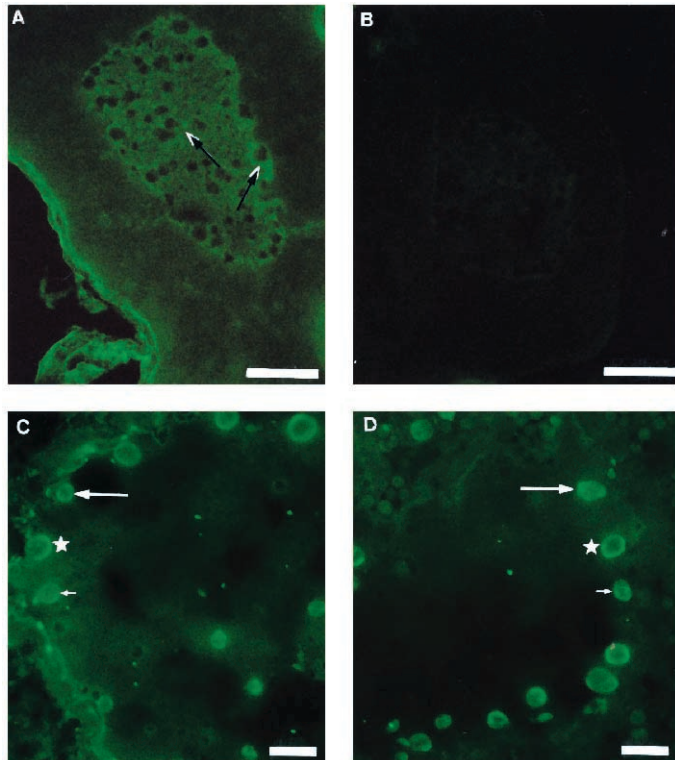


Fig. 6. Frozen oocyte sections of *X. laevis*. (A) 350 μ m oocyte section incubated with anti- β II Σ 1 spectrin. Immunostain is in the ovarian tissue in the GV content and surrounds nucleoli (arrows). $\times 310$. (B) Control section incubated with a fraction of rabbit IgG, showing a slight background of positivity. $\times 310$. (C) A 450 μ m oocyte section incubated with anti- α II Σ * spectrin. In the GV, several nucleoli, as recognised by the corresponding staining with anti-fibrillarin (D), are immunostained. (D) Corresponding labels of C,D (arrows, stars, small arrow) indicate that the same nucleoli are immunostained by this antibody and anti- β II Σ 1. (C,D) $\times 500$. Bars: 50 μ m (A,B); 20 μ m (C,D).

α II Σ^* antibodies was inhibited by preincubation of the antibodies with α and β erythroid spectrin. This result, together with the documented solubility at high salt concentrations, typical of several spectrins (Levine and Willard, 1981; Glenney et al., 1982) led us to identify the 230 kDa molecule as a spectrin-like protein. This is the first characterisation of a spectrin-like molecule localised in the nucleoplasm and in specific nuclear organelles. Preliminary results have been published elsewhere (Carotenuto et al., 1994). In hepatocyte nuclei, Bachst and Carafoli (1987) identified a protein able to bind calmodulin. A site for calmodulin binding does exist in the non-erythroid spectrin α chain (Harris and Morrow, 1988). More recently, Wald Krauss et al. (1997) have demonstrated the presence of protein 4.1 in fibroblast nuclei. Taken together, these findings suggest that isoforms of structural proteins, which are typical partners in membrane skeleton, might perform a common function in the nucleus.

It is well known that spectrin is a heterodimer, composed of two distinct subunits which self-associate to form tetramers. The present data show that a single protein band is immunoreactive to both anti- α and anti- β spectrin antibodies (anti- β II Σ 1 and anti- α II Σ^*). Interestingly, in our samples, these antibodies appear to recognise different molecules located in the oocyte cytoplasm. Anti- β II Σ 1 antibody, recognising the brain β spectrin (Malchiodi-Albedi et al., 1993), cross-reacts with two cytoplasmic molecules of about 239 and 225 kDa in *Discoglossus* oocytes and eggs (Tatone et al., 1993, and unpublished results). Anti- α II Σ^* antibody, which recognises brain and erythroid α spectrin and mildly the erythroid β chain (Di Stasi et al., 1991, and this paper), in *Discoglossus* oocytes and egg cytoplasm, cross-reacts with a band of 254 kDa (Tatone et al., 1993, and unpublished results), indicating that, in our experimental system, this antibody is able to distinguish between α and β subunits. These data do not exclude the possibility that the anti- α spectrin and the anti- β antibodies might recognise the same component in *Discoglossus* GVs. However, alternatively, they might indicate that the 230 kDa band comprises both an α and a β spectrin chain of the same apparent molecular mass, thus constituting a particular form of spectrin-like molecule. In relation to that, the existence of homodimeric spectrin-like molecules in *Acantamoeba castellanii* has been postulated (Pollard, 1984; Bennet and Condelis, 1988).

In a previous paper we reported that, in *D. pictus* GVs, spot-like fluorescence was present after immunostaining with anti-spectrin antibodies (Campanella et al., 1990). In the present work, pre-fixation of the ovarian tissue with paraformaldehyde allowed a better preservation of the GV and clearly showed the presence of round bodies in its contents. The use of a monoclonal antibody specifically staining nucleolar fibrillar (Wu et al., 1993; Gall et al., 1995) led to the identification of the nucleoli, the most conspicuous GV constituents. Incubation of serial sections of the same GV in a sequence alternating the use of anti-fibrillar and of anti-spectrin antibody, showed that the anti-fibrillar-identified bodies are those immunostained by anti-spectrin. In addition, the anti-spectrin antibodies stained round bodies in spread GV contents (see Fig. 3d,e). Based on their morphology, we assume that these bodies represent nucleoli. Taken together, these results indicate that a spectrin-like molecule is a part of the nucleolus periphery.

Nucleoli of the amphibians *D. pictus* and *X. laevis* are the product of the well-known process of genic amplification, typical of the oogenesis of amphibians (Brown and Dawid,

1968). During this process, a large number of nucleoli gradually accumulate at the periphery of the nucleus starting from stages preceding yolk deposition to stages where yolk is at the peak of its concentration and reach the inner aspect of the nuclear envelope. In *X. laevis* and *D. pictus*, the immunostain was detected in the whole nucleoplasm, particularly in oocytes at early stages of vitellogenesis, whereas the reactivity of the nucleoli to anti-spectrin antibodies appears to be independent of the oogenic stages we observed both in nuclei preparations and on frozen sections.

In forming nucleoli, r-DNA is first duplicated and then transcribed. RNA molecules become associated with nucleolar proteins, i.e. fibrillar (Kazimiers et al., 1993), nucleolin (Schmidt-Zachman and Nigg, 1993) and other proteins such as No38 and a 180 kDa protein (Bell et al., 1992). During such processes, the nucleolus keeps a spherical, compact structure. Spectrin probably participates in the framing of the nucleolus and/or in most of its activities; in that, it might be associated with actin, which has a specific binding site in both erythroid and non-erythroid spectrin and is the predominant cytoskeletal protein of the GV. As previously mentioned, several studies have indicated that actin is present in the nuclei either in a diffuse or in a fibrillar form, depending upon the functional stages of the nucleus (see Gounon and Karsenti, 1981; Milankov et al., 1991; Milankov and De Boni, 1993). Three-dimensional reconstruction from confocal images, as well as ultrastructural localisation, depicts actin aggregates at the nucleolus periphery, from where actin extends into the nucleoplasm. Interestingly, a chemically distinct isoform of actin has been found in the nucleus (Bremer et al., 1981; Kumar et al., 1984). Actin has also been localised in *D. pictus* GV (Campanella et al., 1990).

In our samples, immunofluorescence indicates that the spectrin-like antigen is localised in the whole nucleoplasm. Therefore, it can be hypothesised that spectrin and actin might be components of a complex network, which is part of the gelatinous nuclear matrix, and provide for positioning the nuclear constituents in specific sites of the germinal vesicle (see also Benavente et al., 1984; Kazimiers et al., 1993). The fact that, in the isolated nuclear content, nucleoli are immunoreactive to anti-spectrin indicates that this molecule is part of the nucleolus or is tightly bound to it, as is also suggested by the rim of positivity to anti-spectrin antibodies surrounding the nucleoli in histological sections. Furthermore, the localisation of the immunostain at the nucleoli periphery, where actin is also present, and its closeness to the inner aspect of the nuclear envelope, suggest that the 230 kDa antigen might link the nucleoli to specific constituents of such a membrane. This would agree with the typical function of spectrin, i.e. the participation in the segregation of microdomains of membrane through its interaction with specific membrane proteins as well as with cytoskeletal proteins.

We are grateful to Drs Roberta Poulet, Simona Russo and Anna Savarese for assistance and to Dr Gaetano Odierna for suggestions. We thank Drs G. Barsacchi and J. G. Gall for critically reading the manuscript. This research was financially supported by 40% MURST grants to C.C.

REFERENCES

- Bachst, O. and Carafoli, E. (1987). Calmodulin and calmodulin-binding proteins in liver cell nuclei. *J. Biol. Chem.* **262**, 10786-10790.

- Bell, P., Dabauvalle, M. C. and Sheer, U. (1992). In vitro assembly of prenucleolar bodies in *Xenopus* egg extract. *J. Cell Biol.* **118**, 1297-1304.
- Beck, K. A., Buchanan, J. A., Malhotra, V. and Nelson, W. J. (1994). Golgi spectrin: identification of an erythroid β -spectrin homolog associated with the Golgi complex. *J. Cell Biol.* **127**, 707-723.
- Benavente, R., Krohne, G., Schmidt-Zachmann, M. S., Hugle, B. and Franke, W. W. (1984). Karyoskeletal proteins and the organization of the amphibian oocyte nucleus. *J. Cell Sci. Suppl.* **1**, 161-186.
- Bennet, V. and Condeelis, J. (1988). Isolation of an immunoreactive analogue of brain fodrin that is associated with the cell cortex of *Dictyostelium* amoebae. *Cell Motil. Cytoskel.* **11**, 303-317.
- Bennet, V. (1990). Spectrin based skeleton: a multipotential adaptor between plasma membrane and cytoplasm. *Physiol. Rev.* **70**, 1029-1065.
- Black, J. D., Koury, S. T., Bankert, R. B. and Repasky E. A. (1988). Heterogeneity in lymphocyte spectrin distribution: Ultrastructural identification of a new spectrin-rich cytoplasmic structure. *Cell Biol.* **106**, 97-109.
- Bremer, J. W., Busich, H. and Yeoman, L. C. (1981). Evidence for a species of nuclear actin distinct from cytoplasmic and muscle actins. *Biochemistry* **20**, 2013-2017.
- Brown, D. D. and Dawid, I. B. (1968). Specific amplification in oocytes. *Science* **160**, 272-280.
- Campanella, C., Carotenuto, R. and Gabbiani, G. (1990). Antispectrin antibodies stain the oocyte nucleus and the site of fertilization channels in the egg of *Discoglossus pictus* (Anura). *Mol. Reprod. Dev.* **26**, 134-142.
- Carotenuto, R., Maturi, G., Infante, V., Caprigione, T., Odierna, G. and Campanella, C. (1994). Proteine citoscheltriche nucleari: identificazione di una proteina nucleolare fodrino-simile. Atti del convegno congiunto ABCD-AGI-SIBBM-SIMGBM, Montesivano Lido (PE).
- Clark, T. G. and Merriam, R. W. (1977). Diffusible and bound actin in the nuclei of *Xenopus laevis* oocytes. *Cell* **12**, 883-891.
- De Boni, U. (1994). The interphase nucleus as a dynamic structure. *Int. Rev. Cytol.* **150**, 149-171.
- Devarajan, P., Stabach, P. R., Mann, A. S., Ardito, T., Kashgarian, M. and Morrow, J. S. (1996). Identification of a small cytoplasmic ankyrin (AnkG119) in the kidney and muscle that binds β 1S* spectrin and associates with the Golgi apparatus. *J. Cell Biol.* **133**, 819-830.
- Di Stasi, A. M., Gallo, V., Ceccarini, M. and Petrucci, T. C. (1991). Neuronal fodrin proteolysis occurs independently of excitatory aminoacid-induced neurotoxicity. *Neuron* **6**, 445-454.
- Fishkind, D. J., Bonder, E. M. and Begg, D. A. (1990). Subcellular localization of sea urchin spectrin: evidence for assembly of the membrane-skeleton on unique classes of vesicles in eggs and embryos. *Dev. Biol.* **142**, 439-452.
- Gall, J. G., Tsvetkov, A., Wu, Z. and Murphy, C. (1995). Is the sphere organelle/coiled body a universal nuclear component? *Dev. Genet.* **16**, 25-35.
- Glenney J., Glenney P. and Weber, K. (1982). The spectrin-related molecule, TW-260/240, cross-links the actin bundles of the microvillus rootlets in the brush borders of intestinal epithelial cells. *J. Biol. Chem.* **257**, 9781-9790.
- Gounon, P. and Karsenti, E. (1981). Involvement of contractile proteins in the changes in consistency of oocyte nucleoplasm in the newt *Pleurodeles waltii*. *J. Cell Biol.* **88**, 410-421.
- Harris, A. S. and Morrow, J. S. (1988). Proteolytic processing of human brain alpha spectrin (fodrin): Identification of a hyper-sensitive site. *J. Neurosci.* **8**, 2640-2651.
- Hirokawa, N. R., Cheney, E. and Villard, M. (1983). Localization of a protein of the fodrin-spectrin-TW 260/240 family in the mouse intestinal brush border. *Cell* **32**, 953-965.
- Hultman, P., Enestrom, S., Turley, S. J. and Pollard, K. M. (1994). Selective induction of anti-fibrillar autoantibodies by silver nitrate in mice. *Clin. Exp. Immunol.* **96**, 285-291.
- Kazimiers, T. T., Shu, M.-D. and Steitz, J. A. (1993). A small nucleolar RNA is processed from an intron of the human gene encoding ribosomal protein S3. *Genes Dev.* **7**, 1176-1190.
- Kumar, A., Razindin, C., Finlay, T. H., Thomas, J. O. and Szer, W. (1984). Isolation of a minor species of actin from nuclei of *Acanthamoeba castellanii*. *Biochemistry* **23**, 6753-6757.
- Laemmli, U. K. (1970). Cleavage of structural proteins during the assembly of the head of bacteriophage T4. *Nature* **227**, 680-685.
- Levine, J. and Willard, M. (1981). Fodrin: axonal transported polypeptides associated with the internal periphery of many cells. *J. Cell Biol.* **90**, 631-643.
- Malchiodi-Albedi, F., Ceccarini, M., Winkelmann, J. C., Morrow, J. S. and Petrucci, T. C. (1993). The 270 kDa splice variant of erythrocyte β -spectrin (β II Σ 2) segregates in vivo and in vitro to specific domains of cerebellar neurons. *J. Cell Sci.* **106**, 67-78.
- Milankov, K., Amankwah, K. S. and De Boni, U. (1991). Cytochemical localization of actin and myosin aggregates within interphase nuclei of intact neurons. *J. Cell Biol.* **115**, 95a (abstract).
- Milankov, K. and De Boni, U. (1993). Cytochemical localization of actin and myosin aggregates in interphase nuclei in situ. *Exp. Cell Res.* **209**, 189-199.
- Morrow, J. S., Cianci, C. D. and Kennedy, S. P. (1991). Polarized assembly of spectrin and ankyrin in epithelial cells. *Curr. Top. Membr.* **38**, 227-244.
- Ochs, R. L., Lischwe, M. A., Spohn, W. H. and Busch, H. (1985). Fibrillarlin: a new protein of the nucleolus identified by autoimmune sera. *Biol. Cell.* **54**, 123-134.
- Pollard, T. D. (1984). Purification of a high molecular weight actin filament gelation protein from *Acanthamoeba* that shares anti-genic determinants with vertebrate spectrin. *J. Cell Biol.* **99**, 1970-1980.
- Ryabova, L. V., Virtanen, I., Wartiovaara, J. and Vassetzky, S. G. (1994). Contractile proteins and nonerythroid spectrin in oogenesis of *Xenopus laevis*. *Mol. Reprod. Dev.* **37**, 99-109.
- Schmidt-Zachman, M. S. and Nigg, E. A. (1993). Protein localization to the nucleus: a search for targeting domains in nucleolin. *J. Cell Sci.* **105**, 799-806.
- Tatone, C., Carotenuto, R., Colonna, R., Chaponnier, C., Gabbiani, G., Giorgi, M. and Campanella, C. (1993). Spectrin and ankyrin-like proteins in the egg of *Discoglossus pictus* (Anura): their identification and localization in the site of sperm entrance versus the rest of the egg. *Dev. Growth Differ.* **35**, 161-171.
- Towbin, H., Staehelin, T. and Gordon, J. (1979). Electrophoretic transfer from polyacrylamide gels to nitrocellulose sheets: procedure and some application. *Proc. Nat. Acad. Sci. USA* **76**, 4350-4354.
- Winkelmann, J. C. and Forget, B. G. (1993). Spectrin and nonerythroid spectrins. *Blood* **81**, 3173-3185.
- Wu, Z., Murphy, C., Wu, C.-H. H., Tsvetkov, A. and Gall, J. G. (1993). Snurposomes and coiled bodies. *Cold Spring Harb. Symp. Quant. Biol.* **58**, 747-754.
- Wald Krauss, S., Larabell, C. A., Lockett, S., Gascard, P., Penman, S., Mohandas, N. and Chasis, J. A. (1997). Structural protein 4.1 in the nucleus of human cells: dynamic rearrangements during cell division. *J. Cell Biol.* **137**, 275-289.

α -Spectrin Has a Stage-Specific Asymmetrical Localization During *Xenopus* Oogenesis

ROSA CAROTENUTO,¹ MARIA CARMEN VACCARO,¹ TERESA CAPRIGLIONE,¹
TAMARA CORINNA PETRUCCI,² AND CHIARA CAMPANELLA^{1*}

¹Dipartimento di Biologia Evolutiva e Comparata, Università di Napoli, Napoli, Italy

²Istituto Superiore della Sanità, Laboratorio di Biologia Cellulare, Roma, Italy

ABSTRACT *Xenopus* oocyte organization largely depends upon the cytoskeleton distribution, which is dynamically regulated during oogenesis. An actin-based cytoskeleton is present in the cortex starting from stage 1. At stages 4–6, a complex and polarized cytoskeleton network forms in the cytoplasm. In this paper, we studied the distribution of spectrin, a molecule that has binding sites for several cytoskeletal proteins and is responsible for the determination of regionalized membrane territories. The localization of α -spectrin mRNA was analyzed during *Xenopus* oogenesis by in situ hybridization on both whole mount and sections, utilizing a cDNA probe encoding a portion of *Xenopus* α -spectrin. Furthermore, an antibody against mammalian α -spectrin was used to localize the protein. Our results showed a stage-dependent mRNA localization and suggested that spectrin may participate in the formation of specific domains in oocytes at stages 1 and 2 and 4–6. *Mol. Reprod. Dev.* 55:229–239, 2000.

© 2000 Wiley-Liss, Inc.

Key Words: amphibians; oocyte; cytoskeleton; mitochondrial cloud; regionalization; follicle cells

INTRODUCTION

During diplotene, amphibian oocytes undergo important functional and molecular changes related either to oogenesis or to the prospective embryo development. The spatial distribution of organelles and molecules, which is of fundamental importance for oocyte organization, is strictly dependent upon the cytoskeleton.

Several cytoskeletal proteins have been detected in amphibian oocytes, including actin (Franke et al., 1976; Campanella and Gabbiani, 1980; Roeder and Gard, 1994), tubulin (Wylie et al., 1985; Yisraeli et al., 1990; Gard et al., 1995), vinculin (Evans et al., 1990), vimentin (Godsave et al., 1984; Tang et al., 1988; Dent et al., 1989; Torpey et al., 1990), talin (Evans et al., 1990), cytokeratin (Franz et al., 1983; Godsave et al., 1984b; Klymkowsky et al., 1987), spectrin (Campanella et al., 1990; Ryabova et al., 1994; Carotenuto et al., 1997), and myosin (Meeusen and Cande, 1979; Campanella et al., 1980; Christensen et al., 1984; Ezzell et al., 1985). They play a key role in building cytoplasmic cytoarchitecture, which is not competent for contractile activity.

Only following progesterone and protein kinase C stimulation, at maturation, these proteins acquire this competence in preparation of fertilization (Johnson and Capco, 1997).

When the oocyte reaches its final size and polarization (stages 4–6), its animal/vegetal axis can be revealed by the eccentrically located germinal vesicle, which marks the animal side, and by the distribution along the axis of several cytoplasmic constituents, such as yolk platelets and ribosomes. Immunocytochemistry coupled with the use of disruptive drugs has shown that actin, intermediate filaments and microtubules have an important function in the establishment and maintenance of animal/vegetal polarity (Klymkowsky et al., 1987; Gard et al., 1995, 1997). In particular, by linking to cortical and perinuclear actin through their minus end, microtubules form the mechanical and functional scaffolding of the oocyte and regulate the distribution of organelles and molecules (Gard et al., 1995).

Early in oogenesis (stages 2 and 3), a microtubule bundle forms, which transports Vg1 mRNA to the future vegetal half (Melton, 1987; Kloc et al., 1998). Other mRNAs have been found spatially restricted to the vegetal or animal hemisphere: an1 (Linnen et al., 1993); an2 (Weeks and Melton, 1987); Xwnt11 (Ku and Melton, 1993); Xlsirt (Kloc, 1993; Kloc and Etkin, 1994); Xcat2 (Mosquera et al., 1993); Xlan4 (Reddy et al., 1992); Veg T (Zhang and King, 1996); they contribute to the distinct functions of blastomeres deriving from the animal and vegetal halves. Some of them are anchored to the cortex through actin, and, in the case of Vg1 mRNA, the linkage is realized through Xl-sirt mRNA (Kloc et al., 1993; Kloc and Etkin, 1994; Hesketh, 1996). Anchoring of Vg1 to the cortex is also partially dependent upon cytokeratin filaments (Pondel and King, 1988; Klymkowsky et al., 1991). However, it is not yet clear whether other cortical cytoskeletal proteins, such as spectrin, may confer regional specificity to the generic actin localization in the cortex, thereby contributing to the anchoring of mRNAs. By its association

Grant sponsors: CNR and MURST.

*Correspondence to: Chiara Campanella, Dipartimento di Biologia Evolutiva e Comparata, Università di Napoli, Via Mezzocannone n.8, 80134 Napoli, Italy. E-mail: Campanella@dgbm.unina.it

Received 3 August 1999; Accepted 15 October 1999

with membrane proteins, spectrin may indeed generate distinct membrane protein domains, as has been shown in a variety of cells (for a review see Morrow et al., 1991; Winkelman and Forget, 1993). Indeed, during early stages of oocyte polarization, specific domains may be involved in exchanges of signals between the oocyte and follicle cells, as has been demonstrated in *Drosophila* (reviewed by Ray and Schupbach, 1996) but not in vertebrates, and/or in the stabilization of cytoskeletal territories involved in fertilization or tissue specification.

Spectrin is made of two distinct but homologous α and β subunits, self-associating to form tetramers $[(\alpha\beta)^2]$. These tetramers, in turn, are cross-linked by short actin polymers and other proteins to form an extensive filamentous cortical meshwork having an important role in the maintenance of the structural organization of the plasma membrane both in erythrocytes and in other cells. Although α and β subunits of both erythroid and nonerythroid spectrin share high homology, they are encoded by different genes (Winkelman and Forget, 1993), the products of which are subjected to alternative splicing (Moon and McMahon, 1990; Winkelman et al., 1990), with the exception of erythrocyte α -spectrin. This generates additional spectrin diversity, and, therefore, the family of spectrin-like molecules appears to be composed of complex and articulated isoforms, each bearing a specific location and function in the cell (Morrow et al., 1991).

Giebelhaus et al. (1987) demonstrated the presence of polypeptides immunologically related to chicken α -spectrin in oocytes and differentiated tissues of *Xenopus laevis*. They also isolated two cDNA clones for α -spectrin in *Xenopus* and showed that α -spectrin is actively synthesized in oocytes and differentiated tissues, decreasing markedly after fertilization; conversely, transcripts encoding other membrane cytoskeleton proteins (i.e., 4.1 protein; Giebelhaus et al., 1987) remain stable indicating that the steady-state levels of the transcripts encoding membrane cytoskeleton proteins are not coordinately regulated (Giebelhaus et al., 1988).

Spectrin-like molecules have been localized by immunocytochemistry in the cytoplasm of *Xenopus* oocytes and in the peripheral oocyte cytoplasm of another anuran, *Discoglossus pictus* (Campanella et al., 1990; Ryabova et al., 1994a; Carotenuto et al., 1997). They may have a role in stabilizing and supporting cytoskeleton organization (Ryabova et al., 1994b). Recently, a spectrin-like molecule has also been detected in the nucleoli of *Xenopus* and *Discoglossus* germinal vesicles (GV) (Carotenuto et al., 1997). In the egg, where a remarkable reorganization of the cytoskeleton has occurred, spectrin is present (Carotenuto, unpublished observations; Tatone et al., 1993), though it does not appear to be required for egg cortical contraction to occur (Johnson and Capco, 1997).

The aim of the present study was to investigate the localization of α -spectrin mRNA during *Xenopus oogenesis*. By utilizing a cDNA probe encoding a portion of *Xenopus* α -spectrin (Xen α 1), we determined the hybrid-

ization pattern both in whole mount and in sections. A stage-dependent and asymmetrical mRNA distribution was found in oocytes. The protein, which was revealed by using an antibody against mammalian α -spectrin, has a localization consistent with mRNA regionalization.

Our results suggest that spectrin may concur to the formation of specific domains during oogenesis. At stages 1 and 2, an asymmetrical hybridization in the oocyte and the overlying ovarian tissue may be indicative of the presence of specific domains in oocyte and follicle cells. At stages 4–6, mRNA was observed only on the animal hemisphere, a domain where active protein synthesis occurs at maturation (Capco and Mecca, 1988), when it becomes the site for egg fusion with the spermatozoon (for a review see Kline, 1988).

METHODS

Animals and Samples

Adult *Xenopus laevis* females were obtained from Rettilli, Varese (Italy). Groups of oocytes at various stages of oogenesis were excised from the ovaries of females anaesthetized with MS222 (Sigma Chemical Co., St. Louis, MO).

According to Dumont (1972), the stages of oocyte growth are the following: stage 1 (50–300 μ m); stage 2 (300–450 μ m); stage 3 (450–600 μ m); stage 4 (600–1000 μ m); stage 5 (1000–1200 μ m); stage 6 (1200–1300 μ m). Somatic tissue (outer ovarian epithelium, theca and follicle cells) was removed from the oocytes by exposure to 0.04% collagenase Type XI (Sigma), in OR₂ (82.5 mM NaCl, 2.5 mM KCl, 1 mM MgCl₂, 1 mM NaH₂PO₄, 5 mM Hepes, 3.8 mM NaOH, pH 7.8) for 20 min at room temperature. Following several rinses, oocytes were processed for in situ hybridization, immunocytochemistry, and western blots.

In Situ Hybridization

Whole mount. α -Spectrin cDNA, Xen α 1 was utilized for hybridization on whole mount and sections. It was a kind gift by Prof. R.T. Moon, University of Washington (Seattle, WA).

Whole mount in situ hybridization and related controls were performed according to the procedure of Harland (1991). Briefly, oocytes were incubated at room temperature in 10 μ g/ml proteinase K, 2 mg/ml collagenase Type XI, 20 U/ml hyaluronidase (Sigma) in PBS for 10 min. They were then fixed in 2% FAD (flavin adenin dinucleotide), 250 mM NaCl, and 5% acetic acid for 1 hr at room temperature. Just before hybridization, oocytes were treated with 10 μ g/ml proteinase K (Sigma) for 5 min at room temperature, then rinsed with PBST (PBS pH 7.4 and 0.1% Tween 20) and refixed in 2% paraformaldehyde in PBS for 20 min at room temperature. They were briefly rinsed in the hybridizing solution (HS: 5 \times SSC, 50% formamide, 50 μ g/ml heparin, 1 mg/ml DNA *Micrococcus* carrier, 0.1% Tween 20, 0.1% CHAPS, 10 mM EDTA, 1 \times Denhart's), incubated in fresh HS at the hybridizing temperature (60°C) for 6 hr and then hybridized overnight at 60°C, using 1 μ g/ml Xen α 1.

Photographs were taken using a Kodak EPJ 320T film at a stereomicroscope or at a Leitz photomicroscope, using Kodacolor 100.

Sections. Oocytes were fixed in 2% FAD, 250 mM NaCl, 5% acetic acid for 1 hr at 4°C, and processed for embedding in paraffin according to standard techniques. Before sectioning, microslides were immersed in 2% 3-aminopropyltriethoxysilane in acetone and activated with 2% paraformaldehyde. Following attachment to treated microslides, the sections were exposed to proteinase K (3 µg/ml in 1 M Tris-HCl, pH 7.4, containing 0.5 M EDTA) for 15 min at 37°C and post-fixed in 2% paraformaldehyde. Oocyte sections were incubated in the hybridization solution (50% formamide, 1× Denhardt's solution, 4× SSC, 0.5 mg/ml DNA *Micrococcus* carrier) for 1 hr at room temperature. The hybridization solution was then exchanged for fresh solution with the addition of digoxigenin-labeled cDNA probe (Xen α1), and hybridization was continued overnight at 37°C. The sections were washed in 2× SSC, 1× SSC, 0.5× SSC at room temperature, 0.1× SSC at 37°C and incubated for 1 hr at room temperature with anti-digoxigenin alkaline phosphatase conjugated antibody (Boehringer Mannheim, Germany), diluted 1:500 in 100 mM Tris-HCl, pH 7.4, containing 150 mM NaCl and 0.5 % blocking reagent (Boehringer Mannheim). After being washed in 100 mM Tris-HCl, pH 9.5, 100 mM NaCl, 50 mM MgCl₂ (NTM), sections were incubated at room temperature in the developing solution, i.e., 45 µl 4-nitro-blue-tetrazolium chloride (NBT), 35 µl 5-bromo-4-chloro-3-indolylphosphate (BCIP), and 1 mM levamisole in 10 ml of NTM.

Sections were mounted in PBS-glycerol and observed at a Leitz photomicroscope. Photographs were taken using Kodacolor 100 film.

Electron Microscopy

Oocytes were fixed in 2.5% glutaraldehyde in 50 mM phosphate buffer, pH 7.4, post-fixed in 1% OsO₄, dehydrated in alcohol, and embedded in Epon, as previously reported (Maturi et al., 1998). Following staining with uranyl acetate and lead citrate, ultrathin sections were observed at a Philips 410 electron microscope at the Center for Ultrastructure Research (CIRUB) of the University of Naples, Federico II.

Western Blotting

The antibody utilized was anti-bovine brain α-spectrin, affinity purified (Di Stasi et al., 1991). This antibody cross-reacts with the erythroid α and β chains, and with a number of α-spectrin chains, in different tissues and divergent species (Di Stasi et al., 1991) including *Xenopus* (unpublished data).

Collagenase-treated oocytes were grouped according to the stage (1–6) and homogenized in ice-cold 25 mM Hepes, pH 7.5, containing 900 mM glycerol, 0.02 mM NaN₃, 1 mM ATP, 1 mM DTT, 5 mM EGTA (HB), and the following protease inhibitors (Sigma): 2 mM TAME, 5 mg/ml SBTI, 5 µg/ml aprotinin, and 10 µM E64. After

centrifugation at 15,000g for 40 min at 4°C, the supernatants were boiled for 3 min in sample buffer containing 50 mM Tris-HCl, pH 6.8, 69 mM SDS, 0.028 mM bromophenol blue, and 1 mM DTT. Aliquots of protein were submitted to SDS 5% polyacrylamide gel electrophoresis using human erythrocyte ghost (α-spectrin, 240 kDa; β-spectrin, 220 kDa) preparation (Malchiodi-Albedi et al., 1993) and high molecular mass protein standards (200, 116, 97, 45, 31, or 21 kDa) (Bio-Rad, Hercules, CA). Sixty micrograms of proteins from oocytes of all the oogenetic stages were loaded on each gel. The samples were transferred electrophoretically to nitrocellulose paper (see Maturi et al., 1998) overnight at 200 mA in a cooling chamber. The efficiency of the transfer was evaluated by staining the nitrocellulose paper with Ponceau S and the corresponding gel with Coomassie Brilliant Blue. The nitrocellulose paper was then incubated with 5% fat-free milk (Milupa, Verona, Italy) to saturate additional protein binding sites, rinsed in saline, and incubated with anti-bovine brain α-spectrin antibodies. Human erythrocyte ghosts were used as controls; the erythroid α chain and partially the β chain were recognized by anti-bovine α-spectrin. Antibody binding was detected by anti-rabbit IgG, raised in goat, conjugated to alkaline phosphatase, and revealed by NBT and BCIP.

Antibodies Staining

For α-spectrin localization, sections of samples fixed and embedded in paraffin as for in situ hybridization and frozen sections were used.

In sequence, paraffin sections of *Xenopus* oocytes were (1) treated with citrate buffer (pH 6) in a microwave oven for 3 × 7 min to expose the binding sites of antibodies (Gown et al., 1993), (2) incubated in 10 mM Tris-HCl, pH 7.4, containing 1% BSA, 0.3% Triton X-100, 1% gelatin, 0.02 M glycine, 5% NaCl; (3) exposed to anti-bovine brain α-spectrin diluted in TBS (10 mM TRIS, 225 mM NaCl, pH 7.5 containing 0.1% Triton X-100, and 3% BSA) or in alternative, to rabbit IgG as controls (Sigma). Antibody binding was detected by anti-rabbit IgG raised in goat and conjugated to alkaline phosphatase (Sigma), and revealed by NBT/BCIP.

Immunofluorescence was also performed *Xenopus* oocytes were fixed in 2% formaldehyde, prepared from paraformaldehyde and diluted in PBS for 1 hr at 4°C. Following rinses in PBS, the oocytes were embedded in Tissue-tek OCT compound (Miles Inc., Elkart, IN), frozen in liquid nitrogen, and sectioned with a Jung Frigocut 2800N cryostat at the thickness of 7 µm. Following exposure to 10 mM Tris-HCl, pH 7.4, containing 1% BSA, 0.3% Triton X-100, 1% gelatin, 0.02 M glycine, and 5% NaCl, the sections were exposed to anti-bovine brain α-spectrin, or to rabbit IgG as controls (Sigma) containing 15% *Xenopus* serum. Antibody binding was detected by anti-rabbit IgG raised in goat and fluorescein-conjugated.

The sections were eventually mounted in 90% glycerol/PBS containing 1% *p*-phenylenediamine. The samples

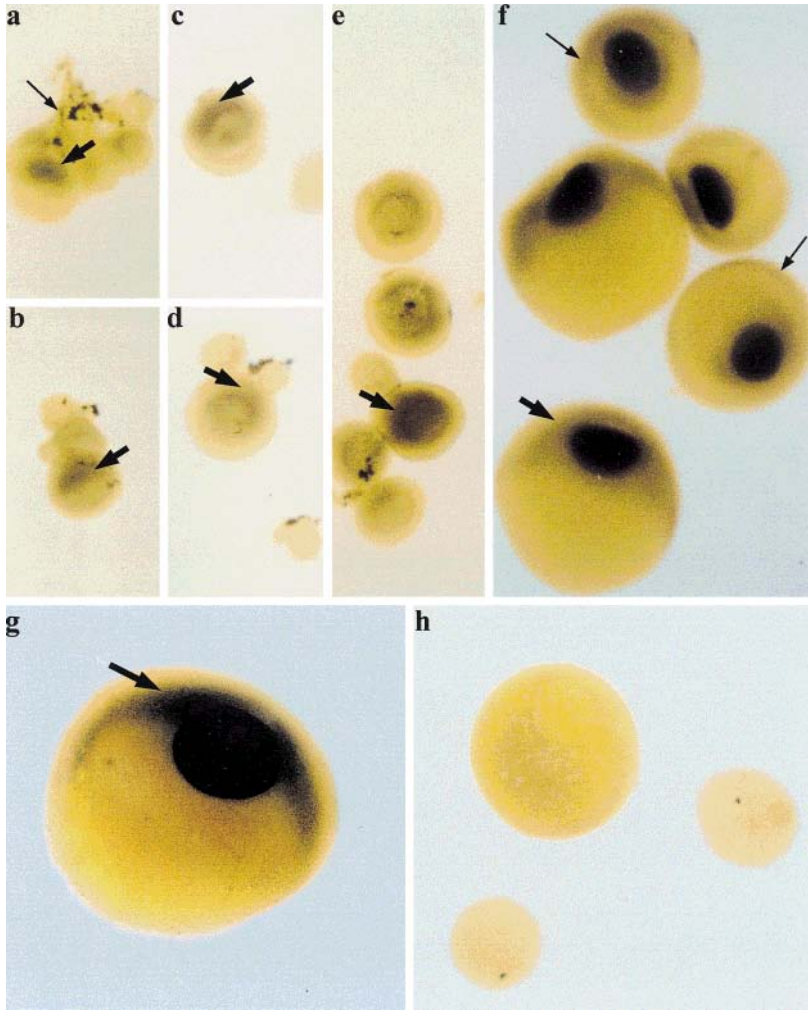


Fig. 1. Whole mount in situ hybridization to Xen $\alpha 1$ cDNA. (a–f) Photos taken with a stereomicroscope. (g, h) Photos taken with a compound microscope. (a, b) Oocytes of 100–130 μm . The hybridization is in the hilum ovarian tissue (small arrow) and in one side of the oocytes (arrow). (c–e) Oocytes of 200–300 μm where the label extends around the germinal vesicle and shows a peak at the center of the

hybridization staining (arrows). (a–e) 55 \times . (f) In the oocytes of 600–750 μm , the probe localization is in and around the germinal vesicle. The oocyte periphery is also labeled (small arrows); 45 \times . In 1000–1200 μm oocytes (f, g), the label is on the animal half (arrows); 50 \times . (h) Control oocyte; the label is absent; 45 \times .

were observed at a Zeiss photomicroscope. Photographs were taken using a Kodacolor 100 or an Ektachrome 800–1600.

RESULTS

In Oocytes, Spectrin mRNA Localization Is Polarized and Stage-Dependent

Oocyte analysis by whole mount in situ hybridization. Figure 1a, b depicts oocytes of about 130 μm in

diameter and held in clusters by ovarian tissue. In oocytes at this stage of growth, the Xen $\alpha 1$ digoxigenin-labeled probe stained a cup-shaped area of cytoplasm located between the GV and the oocyte surface. Therefore, probe hybridization was asymmetrical and located at the site where the oocyte is suspended from the ovarian epithelium (hilum). The somatic tissue of this region was labeled as well (Fig. 1a). When the oocyte size doubled, this asymmetric hybridization peaked at

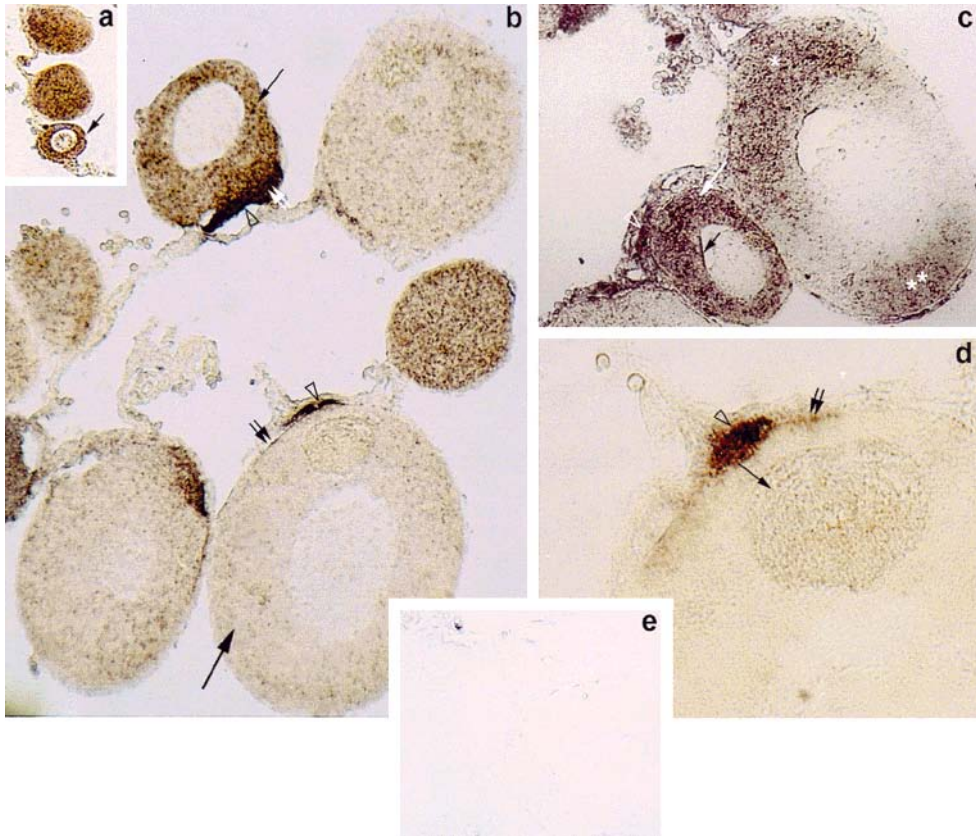


Fig. 2. In situ hybridization to Xen α -1 cDNA on sections. (a) The small arrow indicates an oocyte of about 80 μ m, where the probe hybridizes to the cytoplasm; 160 \times . (b, c) Oocytes of 150–200 μ m (arrow) labeled in the whole cytoplasm and with a peak of hybridization at the hilum (arrowhead) and in the facing region of the oocyte (double arrow in b). In b (large arrow), oocytes of 300–400 μ m also show a peak of hybridization located in the oocyte region (double small

arrows) facing the ovarian tissue that is labeled as well (arrowhead). In an oocyte of c, note the hybridization at the hilum (asterisk) and at its antipode (double asterisk). The small arrows indicate labeling in the nuclear envelope; 130 \times . (d) Hybridization region of a stage 2 oocyte. The label is in the hilum (arrowhead) and faces the oocyte region (small arrow). The mitochondrial cloud (arrow) is located at the hilum side; 350 \times . (e) Control section.

its center and further extended as a thin layer around the GV (Fig. 1c–e). The GV itself was heavily labeled at more advanced stages of oogenesis, such as stages 3 and 4 (600–750 μ m oocytes), when the label was also present in the cortex of the whole oocyte (Fig. 1f). Starting from stages 4–6, hybridization was clearly localized in the nucleus and in the animal half, while absent from the vegetal one (Fig. 1f, g). In control oocytes, alkaline phosphatase staining was not observed (Fig. 1h).

Oocyte analysis by in situ hybridization on sections. Hybridization being more detailed in sections than in whole mounts, the histological sections were exposed in situ to the Xen α 1 probe to analyze spectrin mRNA localization with respect to the oocyte surface and its relationship with the ovarian tissue.

In 80–150 μ m oocytes (Fig. 2a), α -spectrin mRNA was located almost all over the cytoplasm, with a peak in larger oocytes (Fig. 2b, c). In some sections, a second site of hybridization was located at the antipode of the first one (Fig. 2c), suggesting that the sectioning knife cuts a cup-shaped hybridization. The peak of α -spectrin mRNA was also evident in older oocytes of 300–400 μ m (stage 2), where the general cytoplasmic hybridization appears weaker than in younger oocytes (Fig. 2b–d). In the stage 1 and stage 2 oocytes examined ($n = 28$), the hybridization peak was always located in the oocyte region facing the ovarian tissue. Furthermore, the nuclear envelope was also labeled on the GV site facing the cytoplasmic labels (Fig. 2c).

The ovarian tissue hybridized to the probe, particularly at the hilum, just next to the site of highest

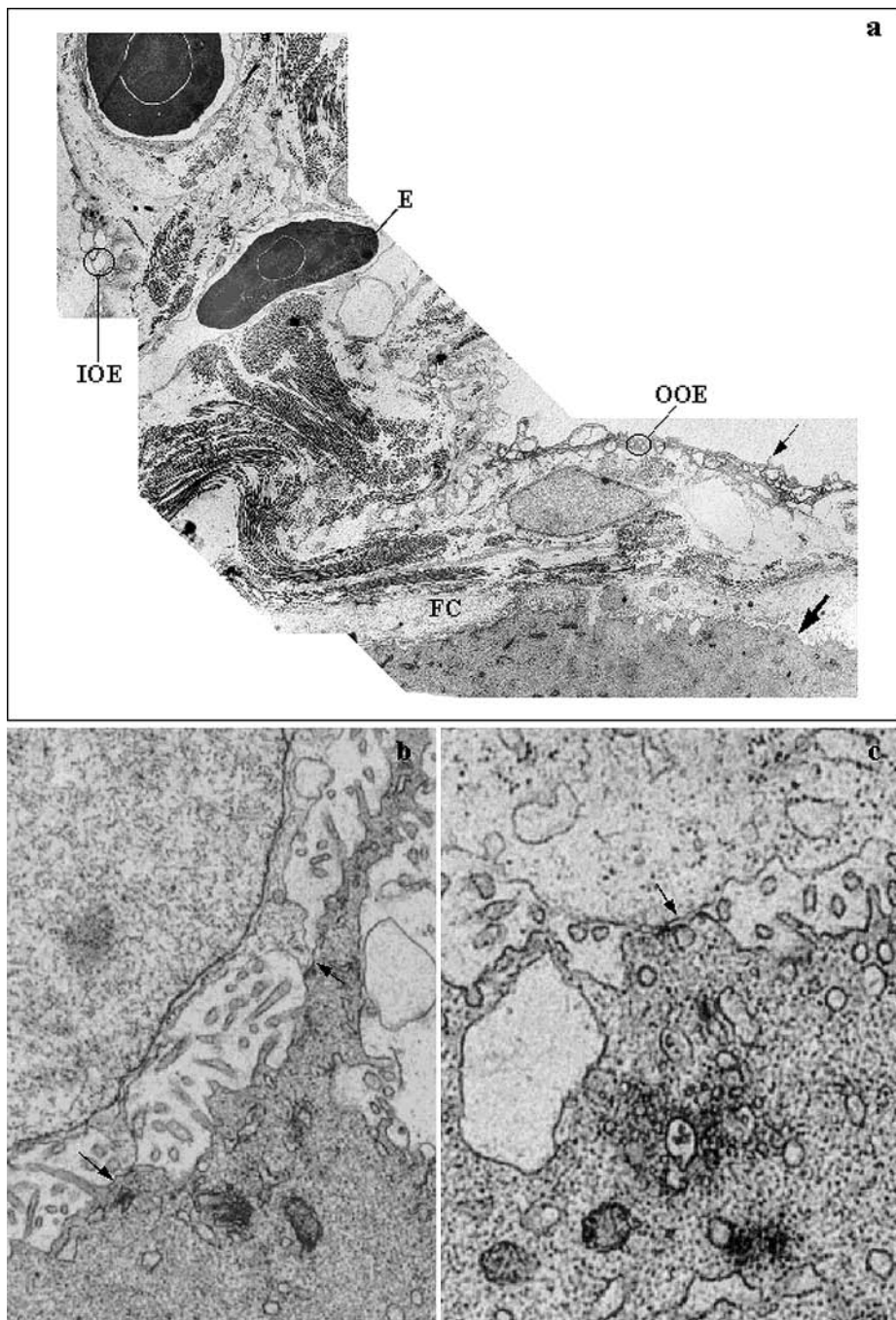


Fig. 3. Thin sections of a 200 μm oocyte. (a) Hilum. Collage of micrographs. In the ovarian tissue of this region, the thin outer ovarian epithelium (OOE) is rather electron-dense and has microvilli (small arrow). Below this layer the theca is present with collagen fibers and small vessels containing erythrocytes (E). The follicle cells

(FC) form a monolayer that surrounds the oocyte (large arrow). The inner ovarian tissue is indicated (IOE); 2,500 \times . (b, c) The oocyte surface shows abundant microvilli. In spots indicated by small arrows, the follicle cell membrane and that of the oocyte are closely apposed; (b) 12,000 \times ; (c) 17,000 \times .

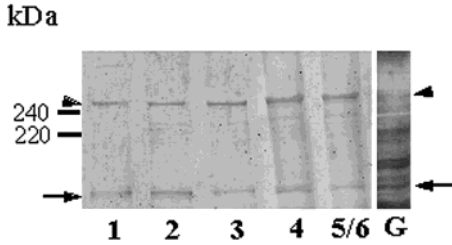


Fig. 4. Immunoblotting utilizing anti-bovine brain α -spectrin on oocytes of stages 1–6. G = silver stained gel of a stage 6 oocyte. On the left, the 220 and 240 kDa human erythrocytes α - and β -spectrins are indicated as *M_r* standards. The arrowhead indicates the 254 kDa oocyte protein cross-reacting with the antibody, and the arrow shows the 140 kDa corresponding product of degradation.

hybridization of the oocyte (Fig. 2b–d). In 20 out of the 23 oocytes examined (190–360 μ m), the cloud was localized at the hilum site, and in the remaining 3 (300 μ m oocytes) a cloud was observed opposite to the hilum. In control sections, alkaline phosphatase staining was not observed (Fig. 2e).

No bridges but sites of close apposition between somatic tissue and oocyte surface are present at the hilum. This ultrastructural analysis was undertaken in order to investigate whether cytoplasmic bridges are present in the hilum between the follicle cells and the oocyte, where α -spectrin mRNA was located.

In the hilum region, the oocyte is surrounded by the outer ovarian epithelium (Dumont and Brummett, 1978). In regions other than the hilum, the oocyte is covered by the theca, the follicle cell layer and the inner ovarian layer. Figure 3a–c depicts ultrathin sections of the hilum region of an about 200 μ m oocyte. Beneath this epithelium there are the theca, containing abundant collagen, fibroblasts, blood vessels, and follicle cells surrounding the oocyte as a single layer. The oocyte surface is rich in microvilli. Serial sections showed no intercellular bridges between somatic constituents and the oocyte at the hilum but did show sites of close apposition between the follicle cells and the oocyte plasma membrane (Fig. 3b, c).

Western blots and immunohistochemistry indicate that an α -spectrin-like protein is present in oocytes throughout oogenesis. Proteins from stage 1–6 oocytes were separated by SDS-PAGE and transferred onto nitrocellulose sheets. Upon incubation with the antibody against bovine brain- α -spectrin, an about 254 kDa band was detected at all the stages of oogenesis, starting from stage 1. A band of about 140 kDa was also stained (Fig. 4), which, in other tissues, appears as product of degradation of α -spectrin (see Di Stasi et al., 1991; Wang et al., 1998).

In paraffin sections of oocytes, the same antibody specifically stains the nuclear envelope and the cytoplasm of stage 1–3 oocytes (Fig. 5a–d). The mitochondrial cloud was also stained. In oocytes of about 80–120 μ m, immunostaining was present in the cytoplasm,

while, at later stages, it was particularly concentrated in the oocyte peripheral cytoplasm (Fig. 5a–d). Interestingly, at the hilum of stage 1 and 2 oocytes, though practically no stain was found in the somatic cells, the protein showed a peak of concentration in the oocyte (Fig. 5d). Erythrocytes of the ovarian tissue were also immunoreactive (Fig. 5d).

For the detection of spectrin in pigmented oocytes (starting from stage 3), we used an FITC-conjugated secondary antibody, as pigment can be mistaken for the purple-red stain of the AP-conjugated antibodies. In Fig. 6, immunofluorescence of 900–1300 μ m oocytes shows a cytoplasmic distribution of spectrin, along filamentous arrays perpendicular to the cortex in the animal side (Fig. 6a, b). An apparent less orderly organization is found in the vegetal cytoplasm (Fig. 6a). Immunostain is also present in the germinal vesicle, as previously reported (Carotenuto et al., 1997) (Fig. 6a) and as a very thin layer in the cortex of the whole oocyte, in the follicle cells and in the rest of the somatic tissue (Fig. 6b). No immunofluorescence was detected when the primary antibody was omitted or substituted with pre-immune IgG (Fig. 6c).

DISCUSSION

We investigated the distribution of the RNA hybridizing to an α -spectrin probe during *Xenopus* oogenesis, showing that mRNA has different patterns of distribution according to the oocyte stage of growth. The α -spectrin cDNA probe used was isolated from *Xenopus* oocytes and identified as encoding portions of *Xenopus* α -fodrin (non erythroid α -spectrin) (Giebelhaus et al., 1987). Moreover, immunofluorescence analysis revealed a similar stage-dependent distribution in the oocytes of a spectrin-like molecule cross-reacting with an antibody against anti-bovine brain α -spectrin. We detected a band of about 254 kDa by cross-reaction with this antibody on western blots of oocytes starting from stage 1 throughout all oogenesis.

In *Xenopus* oocytes, it has been shown that, unlike histone mRNAs (Melton, 1987; Perry and Capco, 1988), the localization of the mRNAs of cytoskeletal proteins (actin and tubulin) and proteins important in development, such as Vg1, may change during oogenesis. Similarly to the expression of many mRNAs in amphibian oogenesis (i.e., *cytokeratin*, Franz et al., 1983; *Xcat-2*, Mosquera et al., 1993; etc.), the hybridization pattern of α -spectrin covers almost the entire oocyte cytoplasm at early stage 1. This suggests that spectrin mRNA is transcribed in a large amount at early stages of diplotene-blocked oocytes. At more advanced stages, when, in the oocyte, molecules are diluted in a larger cytoplasm mass, the hybridization pattern becomes more restricted. In oocytes of about 200–300 μ m, spectrin mRNA is distributed over a cap with a peak at the site where the oocyte is suspended from the ovarian tissue, as is shown in both in toto and section hybridization. A similar peak of hybridization is located in the overlying somatic tissue comprising follicle cells, theca, and outer ovarian epithelium. The spectrin-like protein accumulates in the region facing the hilum, while

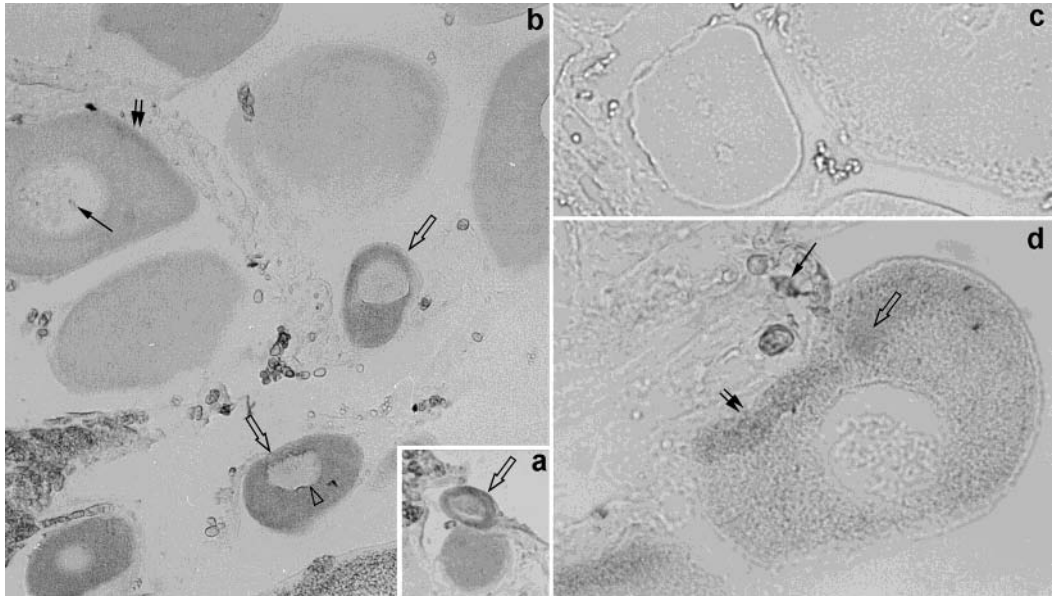


Fig. 5. Immunostain with anti-bovine brain α -spectrin on paraffin sections. (a) The immunostain covers the whole cytoplasm in the 80 μ m oocyte (arrow). (b) Stage 1 and 2 oocytes. The arrows indicate 150- μ m oocytes. In larger oocytes, it is concentrated in the peripheral cytoplasm (small double arrows). The nuclear envelope (arrowhead) cross-reacts with the antibody. (c) Control section incubated with

pre-immune rabbit IgG; no staining is present. (a-c) 125 \times . (d) The double arrow indicates the regions of oocyte peripheral cytoplasm in close contact with the hilum and particularly reactive with the antibody. Arrow = mitochondrial cloud; small arrow = erythrocytes; 312 \times .

practically no protein was detected in the hilum itself. The period of occurrence of clustering of spectrin mRNA and related protein spans from stage 1 to the beginning of stage 2. In this lapse of time, spectrin mRNA distribution substantially differs from the distribution of all forms of *Xenopus* RNA containing poly (A), which includes many mRNAs (Capco and Jeffery, 1982), such as Vg1 (Melton, 1987). This unique pattern precedes the animal-vegetal polarity establishment of the oocyte, suggesting a role of α -spectrin in the oocyte polarization.

Current knowledge indicates intercellular bridges between the oocyte and follicle cells as the only route of mRNA access to the oocyte. We found that in oocytes at the stage corresponding to the spectrin mRNA cap, only closely apposed sites of oocyte and follicle cell membranes are present at the hilum. Gap junctions and desmosomes will form at later stages from similar regions (see Dumont and Brummett (1978) and Villeco et al. (1996) in *Bufo* oogenesis). Conversely, intercellular bridges are absent in the hilum (our data), as in the other regions of the oocyte periphery (Dumont and Brummett, 1978). The signs of spectrin mRNA synthesis in the GV and of its release into the cytoplasm through the nuclear envelope, observed by us, make a spectrin synthesis for the oocyte by somatic tissue a remote hypothesis. Moreover, the lack of cross-reactiv-

ity of the somatic tissue with anti-bovine brain α -spectrin at stages 1 and 2 of oogenesis may indicate that spectrin translation in somatic cells occurs later in oogenesis, as we showed for oocytes at stages 4-6. However, since the antibody was not made against *Xenopus* antigens, we cannot rule out that the antibody might not be effective in the detection of either a low amount of the protein or of a specific *Xenopus* spectrin isoform.

Spectrin presence in the cortical actin-based cytoskeleton determines domains of specific plasma membrane proteins (Morrow et al., 1991). In our samples, at the oocyte periphery, where actin is present early in oogenesis (Roeder and Gard, 1994), spectrin may segregate selective plasma membrane proteins both at the oocyte and follicle cell aspects. This may be instrumental in allowing the clustering of ligands and receptors, as occurs during the determination of dorso-ventrality in *Drosophila* (Shupbach et al., 1991; Hecht and Anderson, 1992). Spazle/Toll function, typical of dorso-ventral signaling in *Drosophila* (reviewed in Morisato and Anderson, 1995), has been shown to be conserved for dorsoventral signaling during *Xenopus* embryogenesis (Armstrong et al., 1998). However, at present nothing is known about the putative activity of this system during oogenesis. Interestingly, in *Drosophila* ovarian follicle, α -spectrin-deficient follicle cells undergo the disruption

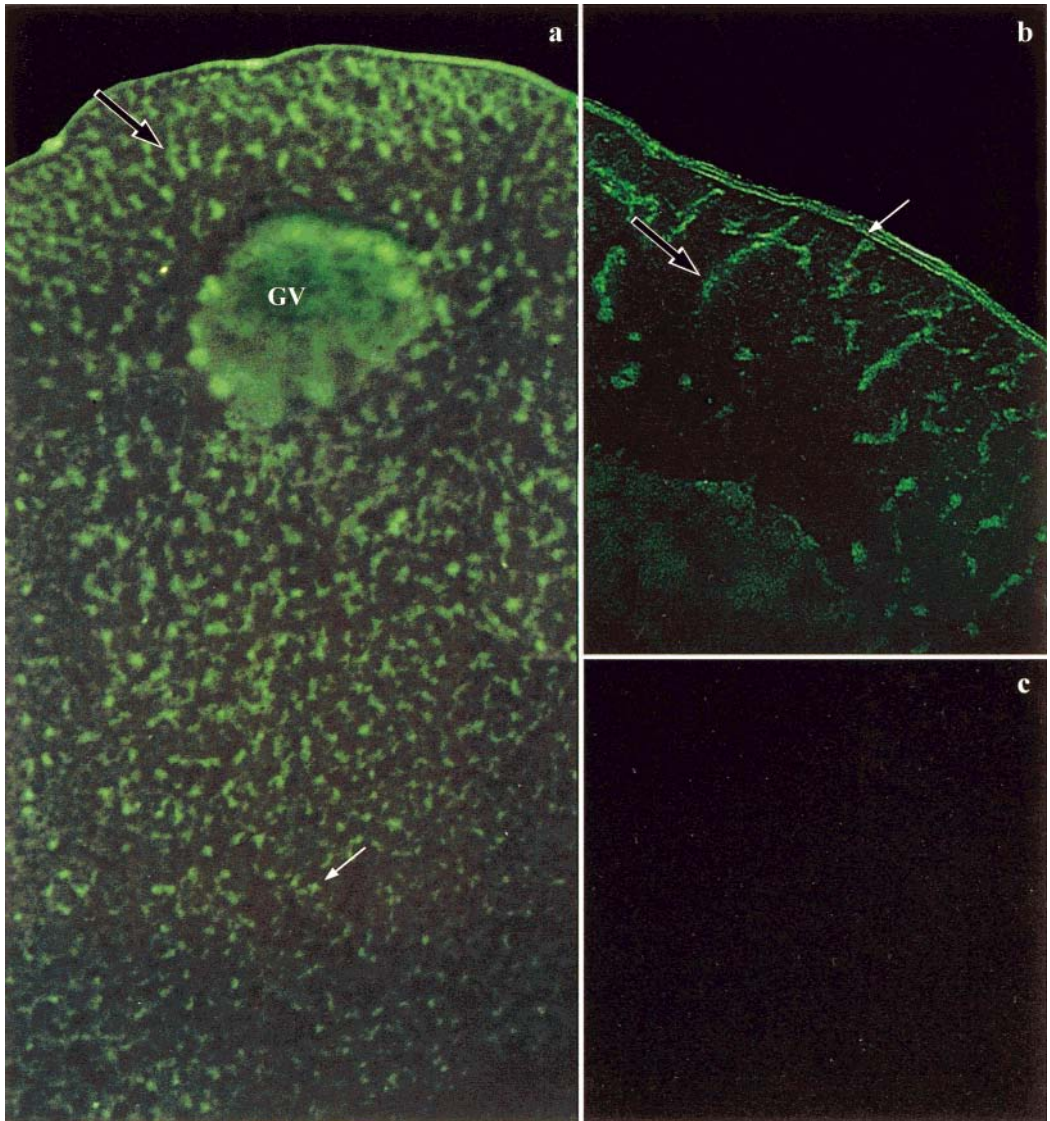


Fig. 6. Frozen sections of stage 6 oocytes, immunostained with anti-bovine brain α -spectrin. (a) GV = germinal vesicle. The GV position indicates the animal half of the oocyte, on the opposite side of the vegetal half. The stain is on the GV, on fibers located perpendicularly to the animal hemisphere surface (arrow), and along fibers with an apparent less orderly organization at the vegetal hemisphere

(small arrow); 220 \times . (b) At a higher magnification of the animal half, one can distinguish three peripheral layers that are stained by the antibody, the innermost being the oocyte cortex (small arrow) and the animal hemisphere fibers (arrow). (c) Control section incubated with rabbit IgG; no stain is evident. (b, c) 450 \times .

of the apical membrane skeleton followed by the loss of the anterior-posterior axis of the oocyte (Dubreuil et al., 1996; Lee et al., 1997).

We also showed that at stages 1 and 2, anti-spectrin antibody labels the mitochondrial cloud where interme-

diated filaments and γ -tubulin are similarly located (Godsave et al., 1984b; Kloc and Etkin, 1998).

At stages 3 and 4, spectrin mRNA spreads around the whole oocyte, particularly at its periphery, while between stages 4 and 6 it accumulates at the oocyte

animal half, reacquiring a regionalized distribution. This suggests that stages 3 and 4 are intermediate stages for the reorganization of spectrin mRNA. Moreover, the segregation of α -spectrin mRNA, at stages 4–6, in the animal hemisphere of the definitively polarized oocyte can be of relevance, because, in this region, during oogenesis and maturation, the oocyte acquires the ability to fuse with the sperm. In this regard, Cl⁻ channels are more concentrated in the animal hemisphere than in the opposite egg half (reviewed by Kline, 1988). In addition, in *Discoglossus* eggs, a 254/239 kDa spectrin heterodimer is tenfold more concentrated at the site of sperm entrance at the animal half, than in the rest of the egg, suggesting that it may anchor to the plasma membrane glycoproteins involved in fertilization (Tatone et al., 1993; Carotenuto, unpublished observations; Maturi et al., 1998). In *Xenopus*, by immunocytochemistry, we found that α -spectrin is located in the cortex, as well as in the cytoplasm of the whole oocytes of stages 4–6. The cytoplasmic localization indicates a different organization of the labeled cytoskeletal network in the animal and vegetal halves, and resembles the distribution of tubulin and cyokeratin detected in the oocyte at the same stages (Gard et al., 1995, 1997) where the cytoskeleton is evidently polarized along the animal/vegetal axis (summarized by Gard et al., 1997). α -Spectrin may derive from the mRNA distributed in the cytoplasm at stages 3 and 4 and/or at stages 4–6, may spread from the animal cap to the whole cytoplasm. A collaboration to this spatial distribution may come from actin microfilaments that, in somatic cells, interact with, or bind to, nascent cytoskeletal proteins during their translation (Singer et al., 1989).

In an attempt to elucidate the capping of mRNA between stages 4 and 6, it can be also hypothesized that a specific spectrin heterodimer is present in the animal hemisphere, i.e., α -spectrin dimerizes with a form of β -spectrin that may concur to the typical organization of the cytoskeleton network in this region. Although at present the β -chain of heterodimeric spectrin has not yet been detected in *Xenopus* oocytes and eggs, the data available on *Discoglossus* indicate that, in addition to the cortical 254/239 kDa heterodimer, a second spectrin is located in the egg periphery (Tatone et al., 1993). It is well known that, in other cells, spectrin isoforms are often segregated within specialized plasma membrane subdomains providing temporally and spatially defined cell functions (Morrow et al., 1991; Malchiodi-Albedi et al., 1993; Wilkeman and Forget, 1993).

ACKNOWLEDGMENTS

We thank Drs. T. Notari, R. Poulet, A. Russo, and D. Capobianco, and Mr. G. Cafiero, Mr. G. Argenzio, and Mr. G. Falcone for help in the laboratory and in photographic preparation. We are grateful to Drs. G. Barsacchi, F. Graziani, and C. Malva for critical reading of the manuscript and to A. Cirillo and M. Wilding for editing. This work was partially supported by CNR and MURST grants to C.C.

REFERENCES

- Armstrong NJ, Steinbeisser H, Prothmann C, DeLotto R, Rupp RAW. 1998. Conserved Spatzle/Toll signalling in dorsoventral patterning of *Xenopus* embryos. *Mech Dev* 71:99–105.
- Campanella C, Gabbiani G. 1980. Cytoskeletal and contractile proteins in coelomic, unfertilized and fertilized eggs of *Discoglossus pictus* (Anura). *Gamete Res* 3:99–114.
- Campanella C, Carotenuto R, Gabbiani G. 1990. Antispectrin antibodies stain the oocyte nucleus and the site of fertilization channels in the egg of *Discoglossus pictus* (Anura). *Mol Reprod Dev* 26:134–142.
- Capco DG, Jeffery WR. 1982. Transient localizations of messenger RNA in *Xenopus laevis* oocytes. *Dev Biol* 89:1–12.
- Capco DG, Mecca MD. 1988. Analysis of proteins in the peripheral and central regions of amphibian oocytes and eggs. *Cell Differentiation* 23:155–164.
- Carotenuto R, Maturi G, Infante V, Caprigione T, Petrucci TC, Campanella C. 1997. A novel protein cross-reacting with antibodies against spectrin is localised in the nucleoli of amphibian oocytes. *J Cell Sci* 110:2683–2690.
- Christensen K, Sauterer R, Merriam RW. 1984. Role of soluble myosin in cortical contractions of *Xenopus* eggs. *Nature (London)* 310:150–151.
- Dent JA, Polson AG, Klymkowsky MW. 1989. A whole-mount immunocytochemical analysis of the expression of the intermediate filament protein vimentin in *Xenopus*. *Development* 105:61–74.
- Di Stasi AMM, Gallo V, Ceccarini M, Petrucci TC. 1991. Neuronal fodrin proteolysis occurs independently of excitatory amino acid-induced neurotoxicity. *Neuron* 6:445–454.
- Dubreuil RR, MacVicar G, Dissanayake S, Liu C, Homer D, Hortsch M. 1996. Neuroglian-mediated cell adhesion induces assembly of the membrane skeleton at cell contact sites. *J Cell Biol* 133:647–655.
- Dumont JN. 1972. Oogenesis in *Xenopus laevis* (Daudin). I. Stages of oocyte development in laboratory maintained animals. *J Morphol* 136:153–180.
- Dumont JN, Brummett AR. 1978. Oogenesis in *Xenopus laevis* (Daudin): V. Relationships between developing oocytes and their investing follicular tissues. *J Morphol* 155:73–98.
- Evans JP, Page BD, Kay BK. 1990. Talin and vinculin in the oocytes, eggs and early embryos of *Xenopus laevis*: a developmentally regulated change in distribution. *Dev Biol* 137:403–413.
- Ezzell RM, Cande WZ, Brothers AJ. 1985. Ca²⁺-ionophore-induced microvilli and cortical contraction in *Xenopus* eggs. Evidence for involvement of actomyosin. *Wilhelm Roux's Arch* 194:140–147.
- Franke WW, Rathke PC, Seib E, Trendelenberg MF, Osborn M, Weber K. 1976. Distribution and mode of arrangement of microfilamentous structures and actin in the cortex of amphibian oocytes. *Cytobiologie* 14:111–130.
- Franz JK, Williams MA, Picherl B, Franke WW. 1983. Intermediate-sized filaments in a germ cell: expression of cytokeratins in oocytes and eggs of the frog *Xenopus*. *Proc Natl Acad Sci USA* 80:6254–6258.
- Gard DL. 1995. Axis formation during amphibian oogenesis: reevaluating the role of the cytoskeleton. *Curr Topics Dev Biol* 30:215–252.
- Gard DL, Cha B-J, Schroeder MM. 1995. Confocal immunofluorescence microscopy of microtubules, microtubules-associated proteins, and microtubules-organizing centers during amphibian oogenesis and early development. *Curr Topics Dev Biol* 31:383–431.
- Gard DL, Cha B-J, King E. 1997. The organization and animal-vegetal asymmetry of cytokeratin filaments in stage VI *Xenopus* oocytes is dependent upon F-actin and microtubules. *Dev Biol* 184:95–114.
- Giebelhaus DH, Zeus BD, Henchman SK, Moon RT. 1987. Changes in the expression of α -fodrin during embryonic development of *Xenopus laevis*. *J Cell Biol* 105:843–853.
- Giebelhaus DH, Eib DW, Moon RT. 1988. Antisense RNA inhibits expression of membrane skeleton protein 4.1 deriving embryonic development of *Xenopus*. *Cell* 53:601–615.
- Godsave SF, Wylie CC, Lane EB, Anderton BH. 1984a. Intermediate filaments in the *Xenopus* oocyte: the appearance and distribution of cytokeratin-containing filaments. *J Embryol Exp Morphol* 83:157–167.
- Godsave SF, Anderton BH, Heasman J, Wylie CC. 1984b. Oocytes and early embryos of *Xenopus laevis* contain intermediate filaments which react with anti-mammalian vimentin antibodies. *J Embryol Exp Morphol* 83:169–187.



A transient asymmetric distribution of XNOA 36 mRNA and the associated spectrin network bisects *Xenopus laevis* stage I oocytes along the future A/V axis

M.C. Vaccaro^{a,*}, S. Gigliotti^b, F. Graziani^b, R. Carotenuto^a, C. De Angelis^a,
M. Tussellino^a, C. Campanella^a

^a Department of Structural and Functional Biology, University of Naples "Federico II", Italy
^b IGB-ABT, CNR Napoli, Italy

ARTICLE INFO

Article history:

Received 14 July 2009
Received in revised form
9 December 2009
Accepted 9 December 2009

Keywords:

Xenopus laevis
mitochondrial cloud
XNOA 36
spectrin
oocyte A/V axis

ABSTRACT

In *Xenopus* oogenesis, the mechanisms governing the localisation of molecules crucial for primary axis determination have been uncovered in recent years. In stage I oocytes, the mitochondrial cloud (MC) entraps RNAs implicated in germ line specification and other RNAs, such as Xwnt-11 and Xsirts, that are later delivered to the vegetal pole. Microfilaments and microtubules gradually develop in the cytoplasm, sustaining organelles as well as the MC. At stage III, other mRNAs migrate to the vegetal hemisphere through a microtubule-dependent mechanism. We report here the isolation of a cDNA encoding XNOA 36, a highly conserved protein, whose function is to date not fully understood. The XNOA 36 transcript is abundantly accumulated in stage I oocytes where it decorates a filamentous network. At the end of stage I the transcript gradually segregates in a sector of the oocyte surrounding the MC and opposite the ovarian hylum. Here, XNOA 36 mRNA distributes in a gradient-like pattern extending from a peripheral network towards the interior of the oocyte. This distribution is similar to that of α -spectrin mRNA. Both mRNAs are segregated in one half of the 250 μ m oocytes, with the MC located between the XNOA 36/ α -spectrin mRNA-labelled and unlabelled regions. XNOA 36 mRNA localisation was uncoupled from that of α -spectrin mRNA by cytochalasin B or ice-nocodazole treatments, suggesting that the two transcripts rely on different mechanisms for their localisation. However, immunolocalisation experiments coupled with *in situ* hybridisation revealed that the XNOA 36 transcript co-localises with the protein spectrin. This observation, together with the finding that XNOA 36 mRNA co-precipitates with spectrin, indicates that these two molecules interact physically.

In conclusion, our data suggest that XNOA 36 mRNA is localized and/or anchored in the oocyte through a cytoskeletal network containing spectrin. The putative implications of this finding are discussed.

© 2010 Elsevier GmbH. All rights reserved.

Introduction

RNA localisation is fundamental for positioning proteins of strategic relevance in cells (for reviews see Kloc et al., 2002; King et al., 2005; Sardet et al., 2005). In recent years, the mechanisms underlying RNA localisation for primary axis determination have been uncovered in *Xenopus laevis* oogenesis (see Kloc et al., 2002; King et al., 2005; Kloc and Etkin, 2005). *X. laevis* oogenesis display a manifest polarity because of the asymmetric localisation of both the fusome and the so-called primordial mitochondrial cloud (Kloc et al., 2004). In stage I oocytes the definitive mitochondrial

cloud (MC), rich in active mitochondria (Wilding et al., 2001), grows anchored to the nuclear envelope. The virtual animal/vegetal axis (A/V) of the oocyte can be traced because of the position of the MC (Heasman et al., 1984). The MC can be considered a package of RNAs held together by a complex network of cytoskeletal proteins, endoplasmic reticulum (ER) and mitochondria, used to transport genetic information to the oocyte cortex. It contains germplasm mRNAs (Xcat2, Xdaz1, Xpat, DEADSouth, etc.) and other molecules such as Xsirts, Xwnt-11, Xotx1 mRNAs (see King et al., 2005 and Tao et al., 2005), cytokeratin (Wylie et al., 1985; Gard and Klymkowsky, 1998; Gard 1999) and spectrin (Kloc and Etkin, 1998). Xcat2 mRNA is entrapped in the germinal granules located in METRO, an ER-rich territory of the MC (Kloc et al., 1996, 1998; Chang et al., 2004). The MC gradually migrates towards the vegetal cortex through an

* Corresponding author. Tel.: +39 081 679200; fax: +39 081 679233.
E-mail address: chiara.campanella@unina.it (M.C. Vaccaro).

unknown mechanism and, at stage II, releases therein its content, thereby marking it as the vegetal pole (King et al., 2005). The mRNAs remain tightly anchored to the vegetal cortex, thanks to cytoskeletal proteins, until the end of oogenesis (Alarcón and Elinson, 2001). A conspicuous network of cytoskeleton components (tubulin, actin, cytokeratin etc.) surrounds, permeates and sustains the MC (see Gard and Klymkowsky, 1998; Gard, 1999) without exerting contractile activity. In fact, this ability is acquired only after oocyte maturation (Johnson and Capco, 1997).

Microtubules have a fundamental role at stage III. Indeed, several mRNAs, such as Vg1 and VegT mRNAs, implicated in body plan formation (Xanthos et al., 2001; Birsoy et al., 2005), localise in the vegetal hemisphere by an ER and microtubule-dependent mechanism which directs them to the territory where the MC has disassembled (Yisraeli et al., 1990; Kloc and Etkin, 1998b). Interactions between mRNA *cis*-acting sequences and *trans*-acting protein factors concur to the correct localisation of the transcripts (for reviews see Kloc et al., 2002; King et al., 2005). A polarised organisation of microtubules starts at the site of Vg1 and VegT migration and spreads in the whole oocyte forming a crown of 'radii' containing not only microtubules but also cytokeratin, spectrin and actin, and connecting the nucleus to the cortex (Gard et al., 1995; Kloc and Etkin, 1998b; Carotenuto et al., 2000). A similar mechanism is well known in *Drosophila*, where microtubule re-organisation, caused by an early signal loop triggered by the TGF α homologue Gurken, underlies the polarisation of the oocyte (Schupbach and Wieschaus, 1986; Nilson and Schupbach, 1999).

In *Xenopus*, previous data indicated that in stage I oocytes, spectrin (mRNA and protein) is mostly segregated in a cap located at the oocyte cortex. This cap is detectable during the translocation of the MC to the cortex and constitutes an early event of cytoskeleton polarisation (Carotenuto et al., 2000).

In this paper we report the isolation of a cDNA encoding a novel protein homologous to NOA 36, a member of a highly conserved protein family displaying characteristic CXXC motifs putatively involved in the formation of zinc-finger structures of the C2-C2 type (Bolivar et al., 1999). NOA 36 was first isolated in *H. sapiens* as an autoimmune antigen in a patient suffering from rheumatoid arthritis and was found to be localised in the nucleolus in G1/G2 or associated with centromeres during metaphase, suggesting that the NOA 36 function is related to cell cycle regulation (Bolivar et al., 1999). Although we did not investigate the function of this protein in *Xenopus laevis*, we followed the distribution of XNOA 36 mRNA as we found that it marks a novel transient asymmetry of stage I oocytes. We also analysed the pattern of distribution of α -spectrin mRNA in *X. laevis* early oogenesis and found that both XNOA 36 and α -spectrin mRNAs undergo a gradual segregation in the oocyte, parallel to the virtual A/V axis, thereby cutting the oocyte in two halves. By cytochalasin B or ice-nocodazole treatment, XNOA 36 mRNA localisation was uncoupled from that of α -spectrin mRNA. On the contrary, it appeared to be linked to the localisation of the spectrin protein. Moreover, XNOA 36 mRNA co-localises with spectrin in thin filamentous structures and co-immunoprecipitates with this protein. These findings suggest the existence of a novel cytoskeletal-dependent process of RNA localisation/anchoring in stage I oocytes of *Xenopus laevis*.

Materials and methods

Animals and oocytes

Adult *X. laevis* females were obtained from Rettili (Varese, Italy). They were kept and utilized at the Department of Structural and

Functional Biology, the University of Naples Federico II, according to the guidelines and policies dictated by the University Animal Welfare Office and in agreement with European Community laws. Groups of oocytes at various stages of oogenesis were excised from the ovaries of females anaesthetized with MS222 (Sigma, St. Louis, MO, USA). The growth stages of the *X. laevis* oocyte are: stage I (50–300 μ m), stage II (300–450 μ m), stage III (450–600 μ m), stage IV (600–1000 μ m), stage V (1000–1200 μ m) and stage VI (1200–1300 μ m) (Dumont, 1972).

Isolation and sequence analysis of *X. laevis* NOA 36 cDNA

A unidirectional cDNA library in pBluescript SK(+) phagemid vector (ZAP Express cDNA cloning kit, Stratagene), constructed using poly(A) mRNA isolated from *X. laevis* oocyte stages 1, 2, 3 (gift of W.J. Lennarz, SUNY, Stony Brook, NY), was screened by using a monoclonal anti-Gurken antibody (gift of T. Schupbach, Princeton University, NJ, and purchased from the Developmental Studies Hybridoma Bank, maintained by the University of Iowa, developed under the auspices of the National Institute of Child Health and Human Development of NIH, Department of Biological Sciences, Iowa City, IA 52242). This antibody recognizes an epitope of *Drosophila melanogaster* Gurken encompassing aa 53–185 upstream of the EGF domain (Nilson and Schupbach, 1999). After overlaying the infected plates with nitrocellulose filters soaked in 10 mM IPTG (isopropyl- β -D-thiogalactopyranoside) (Roche Diagnostics, Mannheim, Germany) at 37 °C O.N. to induce protein translation, the filters were pre-incubated O.N. in TBS containing 5% dry milk (Milupa, Verona, Italy), 0.05% sodium azide, a cocktail of protease inhibitors (10 μ M E64, 2 mM TAME, 5 μ g/ml SBTI and 5 μ g/ml aprotinin, Sigma). After washing in TBS, the filters were incubated with anti-Gurken antibody (1:10, v/v) O.N. at 4 °C in TBS containing 0.5% Triton and 3% BSA (Sigma) and the cocktail of protease inhibitors, followed by incubation with anti-mouse AP-conjugated antibody diluted 1:10 (v/v) in the same solution (Promega, Madison, Wisconsin).

The positive clones obtained were sequenced in both directions by using ³³P-dGTP (Amersham Biosciences, Little Chalfont, UK) and the Thermo Sequenase Radiolabeled terminator cycle sequencing kit (USB, Swampscott, MA USA). cDNA sequence information was processed using BLAST, PSORT II and ScanProsite programs. Multiple alignments were generated with ClustalW. The complete sequence of XNOA 36 was deposited in Gene bank with accession number DQ478933.

Northern blot

For transcript analysis, total RNA from *X. laevis* staged oocytes was isolated using Tri-reagent (Sigma). Twenty micrograms of total RNA per sample were separated on 1% formaldehyde agarose gel and blotted on a nylon membrane (Roche). The XNOA 36 cDNA was labelled using ³²P-labelled dCTP (NEN) and the random primer DNA labelling kit (Roche). The RNA blots were hybridised as previously described (Vaccaro et al., 2001).

Whole mount in situ hybridisation

Somatic tissues (outer ovarian epithelium, theca and follicle cells) were removed from oocytes by exposure to 2 mg/ml Type XI collagenase (Sigma), 20 U/ml hyaluronidase and 10 mg/ml proteinase K (Sigma) in a suitable PBS volume for 10 min at room temperature. Following several rinses, oocytes were fixed in 2% paraformaldehyde (PFA), 250 mM NaCl, 5% acetic acid for 1 hr at room temperature, dehydrated in ethanol and stored at –20 °C.

XNOA 36 cDNA was used as template to synthesise antisense and sense RNA probes, labelled with digoxigenin or fluorescein-conjugated UTP using T3 and T7 RNA polymerase according to the manufacturer's recommendations (RNA T3-SP6 transcription and labelling kit, Roche). Whole mount in situ hybridisation was performed according to the procedure of Harland (1991). After incubation with anti-digoxigenin-alkaline phosphatase (AP)-conjugated antibody the detection was performed using BM-purple (Roche).

In situ hybridisation on sections

X. laevis oocytes were fixed in 2% PFA, 250 mM NaCl, 5% acetic acid for 50 min at room temperature, dehydrated in ethanol and processed for embedding in paraffin according to standard techniques. The 7 μ m thick paraffin sections were placed on Superfrost Plus slides (Carlo Erba, Italy) and processed as previously described (Vaccaro et al., 2001). XNOA 36 and Xen 1 α -spectrin (see Carotenuto et al., 2000) cDNAs were used as template to synthesise digoxigenin-labelled antisense and sense probes, using digoxigenin-labelled UTP and Sp6, T3 and T7 RNA polymerase according to the manufacturer's recommendations (Roche RNA T3-SP6 transcription and labelling kit). After incubation with anti-digoxigenin-alkaline phosphatase (AP)-conjugated antibody the detection was performed using BM-purple (Roche).

For double in situ hybridisation, the oocyte sections were hybridised simultaneously with a digoxigenin and a fluorescein-labelled probe under standard conditions. After incubation with anti-digoxigenin-alkaline phosphatase (AP)-conjugated antibody and detection of the first probe using BM-purple (Roche), AP was inactivated in 100 mM glycine, pH 2.2, 0.1% Tween-20 for 30 min. Following several washes in PBS 1X – 0.1% Tween-20, blocking in 100 mM maleic acid, 150 mM NaCl, pH 7.5 and blocking reagent (Roche), the sections were incubated with anti-fluorescein-AP conjugated antibody (Roche). Vector black kit was used as AP substrate (Vector Laboratories).

Immunofluorescent microscopy

Xenopus oocytes were fixed as for in situ hybridisation on sections. Following rinses in PBS, the oocytes were embedded in Killik (Bio Optica, Italy), frozen and cryostat-sectioned at a thickness of 7 μ m. Aspecific background was blocked by incubating the sections for 20 min at RT in PBS containing 3% normal goat serum, 0.5% bovine serum albumine (BSA), 0.1% Triton-X100 (PBT), prior to exposure O/N at 4 °C to one of the following antibodies diluted in PBT: polyclonal anti- β -spectrin (β IIIS1) antibody directed against the general form of spectrin of human epithelial cells, a gift of Dr J. Morrow (Dept. of Pathology, Yale University, School of Medicine, New Haven); anti-pan-cytokeratin monoclonal antibody (Sigma, C2931) reacting with most type II cytokeratins (K 4,5,6,8) and with type I cytokeratins (K10,13,18); monoclonal anti-acetylated tubulin recognizing the acetylated form of tubulin in many organisms (Sigma, T6793). Control sections incubated with rabbit IgG (Sigma, I5006) or in the absence of primary antibody were included in each experiment. BODIPY FL goat anti-rabbit IgG (H+L) (Molecular Probes, B2766) or BODIPY FL goat anti-mouse IgG (H+L) (Molecular Probes, B2752) diluted in PBT were used as secondary antibody. The sections were eventually mounted in glycerol/PBS 9:1 (v/v). Photographs were taken with a Nikon Eclipse 1000 UV photomicroscope or with a Leica DM6000B photomicroscope equipped with a digital camera.

In situ hybridisation on sections coupled with immunostaining

Following hybridisation, incubation with anti-digoxigenin-AP conjugated antibody and detection using the BM-purple substrate, AP activity was inhibited by treatment with 100 mM glycine pH 2.2, 0.1% Tween-20 for 10 min at room temperature. After extensive washes in PBS1X – 0.1% Tween-20, the sections were (1) pre-incubated in PBS pH 7.4 containing 0.5% BSA, 0.1% Triton X-100 and 3% normal goat serum for 30 min, (2) incubated O.N. at 4 °C with anti- β -spectrin diluted (1:100) in PBT. Goat anti-rabbit IgG conjugated with AP (Sigma) was used as secondary antibody and revealed by using the Vector Black kit (Vector Laboratories) after 30 min incubation in PBS containing 0.5 mg/ml levamisole, 0.1% Tween-20. Negative controls were performed by using a XNOA 36 sense probe and unspecific rabbit IgG.

Ice-nocodazole and cytochalasin treatments

To perturb microtubule organisation, small groups of stage 1–2 oocytes in L-15 medium (50% Leibowitz medium supplemented with 1 mg/ml BSA, 100 μ g/ml gentamicin, 1 U penicillin, 1 μ g/ml streptomycin, 1 mM l-glutamine, 1 μ g/ml insulin, 50 U/ml nystatin, 15 mM HEPES, pH 7.8), were first incubated for 90 min in ice and then for 20 h at 18 °C, after addition of nocodazole, freshly diluted from a 10 mM stock in dimethyl sulfoxide, to a final concentration of 10 μ M, according to Chang et al. (2004). To perturb actin organisation, oocytes were incubated for 20 h at 18 °C in L-15 medium supplemented with 20 μ g/ml of cytochalasin B (Sigma), according to classical experiments of Gard et al. (1997). Control oocytes were incubated for 20 h at 18 °C in L-15 medium.

Immunoprecipitation of mRNA-protein complexes

Stage I oocytes were homogenized in ice-cold NET buffer (50 mM Tris-HCl, pH 7.5, 150 mM NaCl, 0.5% Nonidet P-40, 1 mM EDTA pH 8, 0.25% gelatine, 0.02% NaN3) according to Minshall et al. (2007), supplemented with a cocktail of protease inhibitors: 2 mM TAME, 5 mg/ml SBTI, 5 mg/ml aprotinin and 10 mM E64 (Sigma) and 100 U/ml RNase inhibitor (Roche). After centrifugation at 15,000 g at 4 °C for 45 min, undiluted anti- β -spectrin was added to supernatants (1: 50 v/v) and incubated for 2 h or O.N. under constant agitation at 4 °C. Protein A-Sepharose beads (Sigma) were added to the sample at 1:3 (v/v) and kept under constant agitation for 2 h at 4 °C. Following centrifugation to pellet the beads and several rinses in NET buffer, the recovered precipitate was boiled in sample buffer (1:1 v/v) under reducing conditions and subjected to SDS-PAGE. The proteins were detected by silver staining. Incubation with rabbit IgGs or in absence of primary antibody was performed as general control of the specificity of the immunoprecipitation reaction. For western blots, the samples were transferred electrophoretically to nitrocellulose paper as previously described (Maturi et al., 1998). After anti- β -spectrin incubation, goat anti-rabbit IgG conjugated to AP was used as secondary antibody and revealed by NBT and BCIP.

For RNA detection in the immunoprecipitate, immunoprecipitation reactions were performed as described above. DNase I treatment was carried out by incubating the *Xenopus* oocyte lysate with RNase-free DNase I (Roche, 500 U/ 500 μ l extract) for 15 min at 37 °C, following immunoprecipitation with the anti- β -spectrin antibody. Following four washes in NET buffer, the beads were incubated at 50 °C in NET buffer containing 2% SDS and 200 μ g/ml proteinase K. The RNA was purified by phenol/chloroform extraction and ethanol precipitated in the presence of 20 μ g glycogen. O. N. at –20 °C. Reverse transcription was performed using purified RNA,

oligo-dT primers and the Superscript II reverse transcriptase (Invitrogen). PCR reactions were performed using AmpliTaq Gold (Applied Biosystem, Roche) and the following XNOA 36, or p27^{BBP}/eIF6 specific primers: XNOA 36 Forward:5'-GGGTGCCATTGTGATTCT-3'; XNOA 36 Reverse: 5'-GAATGGCTTTGAGGCTCTTG-3'; XNOA 36 Forward nested: 5'-TTTGAACCAAGCCAGTTG-3'; XNOA 36 Reverse nested: 5'-TGTTCACCAGATGCAAGA-3'; p27^{BBP}/eIF6 Forward 5'-GTGTGCTGCTGAGTGAAGA3'; p27^{BBP}/eIF6 Reverse 5'-CAGTGTCTGCTGAAAGTCCA-3'.

Results

XNOA 36 cloning and Northern blots

The cDNA coding for XNOA 36 was fortuitously isolated by screening a cDNA library of stage I-II *Xenopus* oocytes using an antibody directed against *Drosophila* Gurken. XNOA 36 and Gurken proteins do not share sequences longer than 5 aa. XNOA 36 cDNA encodes a protein of 313 residues with a predicted molecular mass of 36 kDa, similar to the size of other NOA 36 proteins isolated from a variety of living organisms. The deduced protein sequence of XNOA 36 has the typical nine CXXC motifs implicated in the formation of four putative zinc fingers. The sequence shows a putative nuclear localisation signal (PKKKTGARKK) in the N-terminal region (Fig. 1). It has high similarity with NOA 36 proteins from *H. sapiens* (79% identity), *Cricetulus griseus*, *Rattus norvegicus* (80%), *D. melanogaster* (69%) and *Brugia malay* (57%). Multiple alignment of XNOA 36 with *H. sapiens*, *D. melanogaster* and *B. malay* NOA 36 protein sequences indicates high similarity of all these proteins in the zinc-finger region, in the predicted nuclear localisation signal and in the

typical acidic domain, while little similarity is found in the C-terminal region (Fig. 1). Prosite analysis indicates the presence of two putative N-glycosylation sites and several protein kinase C and Casein kinase II phosphorylation sites. Prediction of subcellular localisation, made with the PSORT II program, is as follows: 73.9% nuclear, 17.4% cytoplasmic, 4.3% cytoskeletal and 4.3% mitochondrial, with the putative mitochondrial targeting sequence located in the N-terminal region. While the predicted mitochondrial localisation is shared by all the analysed species, cytoskeletal localisation is hypothesised only for vertebrates. Moreover, with the exception of *Drosophila melanogaster* and *Brugia malay*, there is no predicted localisation in the endoplasmic reticulum.

XNOA 36 mRNA is present throughout embryogenesis and displays an ubiquitous expression pattern (data not shown). On the other hand, Northern blot analysis of RNA extracted from staged oocytes showed a stage-dependent expression of XNOA 36, as the transcript appears highly concentrated in previtellogenic oocytes and little concentrated in vitellogenic oocytes (Fig. 2a,b).

XNOA 36 mRNA distribution matches α-spectrin mRNA localisation in stage I oocytes

In 'whole mount' *in situ* hybridisation experiments using a XNOA 36 antisense riboprobe the transcript appears abundant in stage I oocytes (Fig. 2c-d), whereas from stage II to the end of oogenesis (Fig. 2e) it is only weakly detectable in the entire cytoplasm and in stages IV-VI is mainly restricted to the germinal vesicle (Fig. 2f), as checked by bisecting the oocytes. The specificity of the hybridisation signal was confirmed by using a sense probe (Fig. 2g). Interestingly, in late stage I, a major fraction of XNOA 36 RNA is found in one half of the whole oocyte (Fig. 2d).

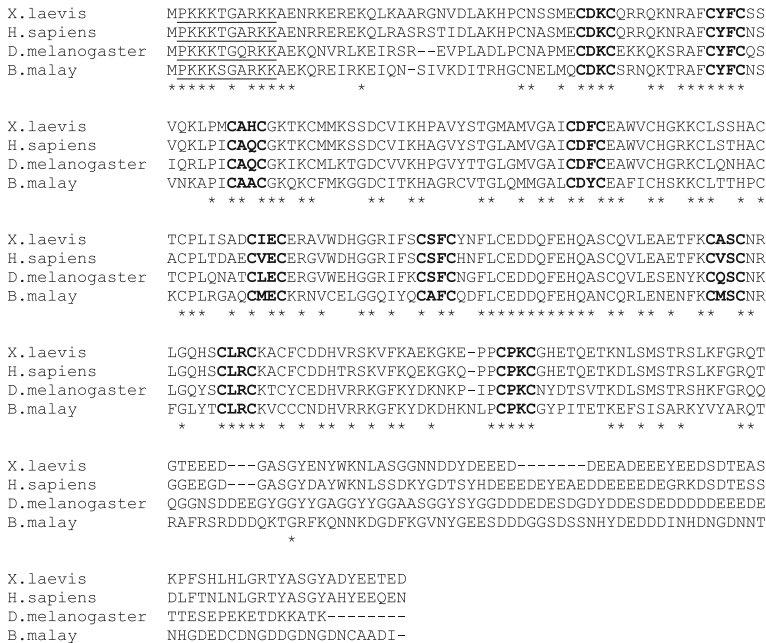


Fig. 1. Multiple sequence alignment: the CXXC motifs are in bold face, the putative nuclear localisation sequence is underlined. The symbol * indicates identical residues.

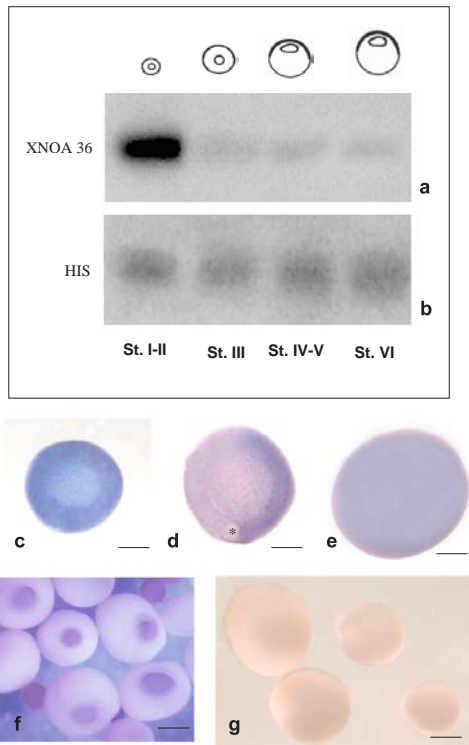


Fig. 2. Northern blot of total RNA from staged oocytes, hybridized with the XNOA 36 cDNA (a) and with the *X. laevis* H1 histone cDNA, as loading control (b). Equivalent amounts of total RNA were loaded. The 1100 nt long XNOA 36 transcript is highly expressed in stage I–II oocytes, while it is present at much lower levels in later stages of oogenesis. c–f. Whole mount *in situ* hybridisation using an antisense XNOA 36 riboprobe. c. In stage I 150 μm oocytes, XNOA 36 mRNA is distributed in the whole cytoplasm. Bar = 60 μm . d. In larger (250 μm) stage I oocytes, the XNOA 36 transcript is segregated in a sector that roughly corresponds to one half of the oocyte (on the right side in the figure) and it includes the MC (asterisk). Bar = 60 μm . e. In stage II oocytes the XNOA 36 transcript is almost undetectable and in stage IV–VI (f) is localised in the germinal vesicle. The bar in (e) indicates 120 μm and in (f) 500 μm g. Control hybridisation using a XNOA33 sense riboprobe. Bar = 170 μm .

Extensive analysis of serial sections of oocytes deriving from 9 females showed that, starting from oocytes of about 100 μm , XNOA 36 RNA is located throughout the cytoplasm along a filamentous network (Fig. 3a) ($n = 424$). In stage I oocytes of 180–200 μm ($n = 140$), the most intensely labelled region is located beside the ovarian tissue from which the oocyte is pendant (hylum) (Fig. 3b–c). The mRNA distributes in a gradient-like fashion along a network which extends from the oocyte periphery to the interior of the cytoplasm and appears tightly linked to the MC on its way to the cortex. Sections exposed to sense XNOA 36 probe are not stained (Fig. 3d).

Serial sections of the oocyte photographed in Fig. 3b, exposed to an α -spectrin antisense probe show that this mRNA is segregated in the same oocyte sector that includes the MC, as XNOA 36 mRNA (Fig. 3f). The α -spectrin hybridisation signal is also located around the MC (Fig. 3g). This labelling is specific as

indicated by the absence of signal in sections incubated with an α -spectrin sense probe (Fig. 3e).

In 250–270 μm oocytes ($n = 46$), both mRNAs are segregated in the oocyte half opposite the hylum, as observed in sections parallel to, or coinciding with, the virtual A/V axis. The MC is positioned between the labelled and unlabelled regions of the oocyte (Fig. 4a,b,c). Moreover, we observed strings of young oocytes *in vivo*, and found that the position of the MC with respect to the hylum is stage-dependent: while in 30% of the oocytes with a diameter of 220–230 μm ($n = 65$) this position is random, in the rest of the oocytes (70%) the MC is positioned in the territory around the hylum. In oocytes with a diameter ranging between 250 and 280 μm ($n = 125$), the MC is positioned along the future A/V, approximately parallel to the gonadal walls.

Later in oogenesis the polarised localisation of XNOA 36 RNA is no longer detectable (see Fig. 2).

The distribution pattern of α -spectrin mRNA with respect to the MC in stage I oocytes, as described in this work, is in apparent conflict with previously reported data (Carotenuto et al., 2000). However, in earlier experiments, (using a DNA probe), the reciprocal MC and α -spectrin mRNA localisation patterns were not strictly determined as a function of the oocyte size. On the contrary, here, a α -spectrin riboprobe was used and serial sections of staged oocytes were obtained, taking account of the virtual A/V axis.

To further demonstrate that the two mRNAs are segregated in the same half of the oocyte, double *in situ* hybridisation experiments were performed. The distribution patterns of the two mRNAs overlap (Fig. 4d) in particular around the MC (Fig. 4e).

XNOA 36 mRNA localisation in stage I oocytes is cytoskeleton-dependent

To perturb the cytoskeleton, oocytes were exposed to cytochalasin B, which inhibits the polymerisation of monomeric actin, or to a two-step treatment (ice followed by incubation with nocodazole), which destroys acetylated and non-acetylated microtubules (Kloc et al., 1996; Gard et al., 1997; Chang et al., 2004). After processing by histological techniques, sections were incubated with riboprobes specific to either of the two transcripts (Fig. 5a–f). Here, the experiments were designed to evaluate the possible association of cytoskeleton components with XNOA 36 and α -spectrin mRNAs. Moreover, by disturbing the cytoskeleton, we aimed at challenging the association between the two mRNAs. The observations were carried out in oocytes where the distribution of the mRNAs is still homogeneous in the cytoplasm i.e. at early stages of cytoskeleton-mRNA segregation (diameter of about 200 μm). In oocytes treated with cytochalasin B, XNOA 36 mRNA distribution changes with respect to untreated oocytes (Fig. 5a,b). The transcript is in fact absent in the bulk of the cytoplasm, yet concentrated at the oocyte periphery (Fig. 5b). In oocytes incubated in ice-nocodazole XNOA 36 mRNA is mainly present in discrete territories at the oocyte periphery and is only partially located in the cytoplasm (Fig. 5c). Here, the filaments decorated by XNOA 36 mRNA in untreated oocytes are almost completely absent (compare Fig. 5c with Fig. 5a).

Oocytes treated with cytochalasin B and exposed to a α -spectrin antisense riboprobe show no major changes in the transcript distribution, with respect to untreated oocytes, except for a sparser presence of the hybridisation label in the oocyte periphery (Fig. 5e, compare with Fig. 5d). Oocytes incubated in ice-nocodazole and exposed to the same riboprobe again do not differ significantly from the untreated oocytes (Fig. 5f, compare with Fig. 5d). Sections of oocytes treated with cytochalasin B or ice-nocodazole do not show hybridization signals when incubated

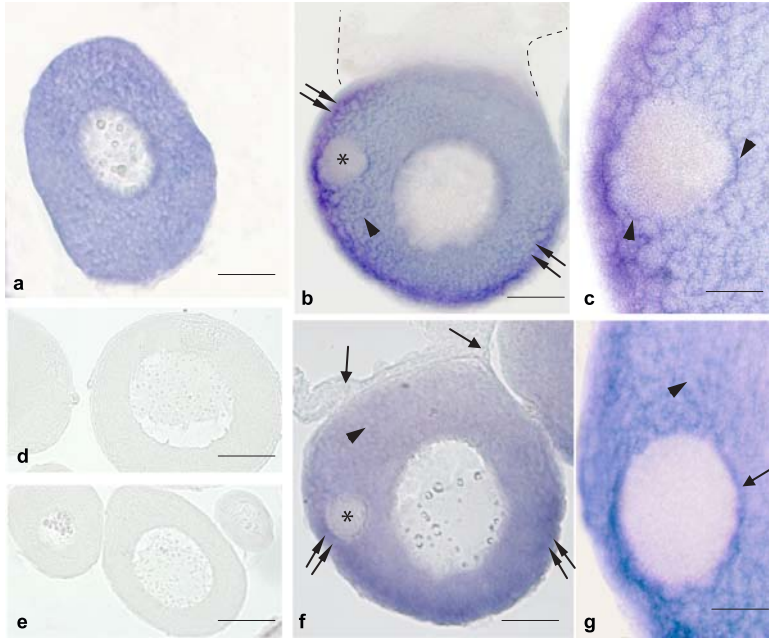


Fig. 3. *In situ* hybridisation on sectioned specimen, showing XNOA 36 (a-c) and spectrin (f-g) mRNA localisation in stage 1 oocytes. **a.** Oocyte of 130 µm. A continuous network decorated by XNOA 36 encompasses the whole oocyte. Bar= 37 µm. **b.** Oocyte of 180-200 µm. XNOA 36 mRNA is distributed along a filamentous network (arrowhead) and is mainly restricted to a spatial domain including the MC (asterisk). The most intensely labelled region is at the oocyte periphery (double arrows). The broken lines delineate the ovarian hylum. Bar= 47 µm. **c.** Higher magnification of a detail of figure **b**. The MC rim is partially decorated by XNOA 36 mRNA (arrowheads). Bar= 15 µm. **d-e.** Control sections hybridized with a sense XNOA 36 (**d**) or α -spectrin (**e**) riboprobe. The bar in (**d**) indicates 65 µm and in (**e**) 80 µm. **f-g.** Serial section of the same oocyte shown in **b**, hybridized with an α -spectrin antisense riboprobe. The α -spectrin mRNA is enriched in the sector of the oocyte including the MC (asterisk) where also XNOA 36 mRNA is mostly restricted. Bar= 46 µm. In a serial section shown at higher magnification (**g**) a ring of α -spectrin mRNA is present at the periphery of the MC (small arrow). Arrowhead= network decorated by α -spectrin mRNA. Bar=15 µm.

with XNOA 36 or α -spectrin sense riboprobes (Fig. 5'a-d'). Therefore, while the distribution pattern of the XNOA 36 transcript is strongly affected by drugs altering the cytoskeleton, α -spectrin mRNA is not influenced to the same extent, indicating that the two mRNAs, in spite of their co-localisation, probably utilise different cell components for distribution in the cell.

To investigate whether the distribution of XNOA 36 mRNA correlates with the distribution of cytoskeletal proteins, immunofluorescence experiments were performed on frozen sections of the same sets of oocytes utilised for *in situ* hybridisation (Fig. 5g-o). Upon cytochalasin B treatment and incubation of the sections with anti-cytokeratin antibodies, most of the immunoreactivity is concentrated in the MC and in aggregates surrounding the germinal vesicle (Fig. 5h), in contrast to control, i.e. oocytes unexposed to the drug, where a filamentous network is seen, extending from the cortex to the nuclear envelope (Fig. 5g). Upon ice-nocodazole treatment, few cytokeratin-containing filaments are found in the cytoplasm (Fig. 5i). Cytochalasin B-treated oocytes exposed to anti-acetylated tubulin antibodies (Gard et al., 1995) show a different fluorescence pattern from that of control oocytes (Fig. 5j), in particular due to the presence of immunoreactive perinuclear aggregates (Fig. 5k). In oocytes treated with ice-nocodazole, the anti-acetylated tubulin signal is barely detectable (Fig. 5l). In cytochalasin B-treated oocytes exposed to anti-spectrin antibodies, the immunofluorescence is mostly

located at the oocyte periphery, while few fibres are in the cytoplasm (Fig. 5n), in contrast to control oocytes where an extended network is present (Fig. 5m). In sections of ice-nocodazole-treated oocytes incubated with anti-spectrin antibodies, the immunofluorescence is again located mostly at the oocyte periphery as well as in aggregates (Fig. 5o). Control sections of treated oocytes incubated uniquely with anti-rabbit IgGs (for anti-spectrin immunostaining) or anti-mouse IgG (for anti-tubulin and anti-cytokeratin immunostaining) did not result in aspecific staining (Fig. 5'). These data indicate that in oocytes treated with ice-nocodazole or cytochalasin B, the spectrin protein becomes restricted to the oocyte periphery in the same manner as the XNOA 36 transcript.

XNOA 36 mRNA co-localises with the cytoskeletal protein spectrin

Alternating serial sections of stage I oocytes were exposed to an XNOA 36 riboprobe, to anti- β -spectrin antibodies or to both reagents (Fig. 6). Fig. 6a is a cross section of the oocyte, with respect to the A/V axis, the MC being at the centre of the section where it is bisected by the localisation domain of XNOA 36 mRNA. A serial section of the same oocyte (Fig. 6b) shows high levels of β -spectrin in the MC. Moreover, the immunostaining is concentrated at one side of the oocyte, particularly in the

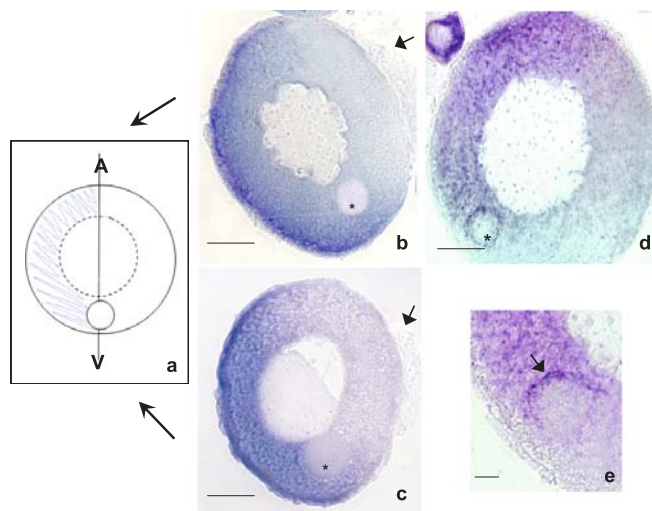


Fig. 4. *In situ* hybridisation on sectioned specimen, showing XNOA 36 and α -spectrin mRNA localisation in stage 1 oocytes of about 270 μ m. In (a) is indicated a schematic view of the localisation of XNOA 36 and α -spectrin mRNAs with respect to the virtual A/V axis, as determined by the position of the MC. XNOA 36 (b) as well as α -spectrin (c) mRNAs are labelled by BM purple staining. Both mRNAs are segregated in the half of the oocyte opposite to the hylum (arrow). The MC (asterisk) is positioned at the boundary between the labelled and unlabelled regions of the oocyte. The bar in (b) indicates 58 μ m, and in (c) 63 μ m. d. Double label *in situ* hybridisation showing the localisation of XNOA 36 mRNA (detected through BM-purple staining) and α -spectrin mRNA (detected through Vector black). The two hybridisation signals overlap (reddish-purple staining) and sites of co-localisation are seen, in particular around the MC (asterisk). Bar = 52 μ m. e. Detail of panel d showing at higher magnification the hybridisation signals at the MC periphery (arrow). Bar = 10 μ m. (For interpretation of the references in colour in this figure legend, the reader is referred to the web version of the article.)

peripheral cytoplasm. The regions of highest concentration of the β -spectrin protein and XNOA 36 mRNA are coincident (Fig. 6c). Their overlap is consistently found in subsequent serial sections (Fig. 6d,e,f). In all these sections the restriction of the XNOA 36 transcript to the half of the oocyte parallel to the virtual A/V axis is accompanied by similar segregation of the β -spectrin protein, as summarised by the drawing in Fig. 6g.

On the basis of the above results we sought to find out whether spectrin protein and XNOA 36 mRNA are physically associated. To address this question, we used anti- β -spectrin antibodies in immunoprecipitation experiments (IPs) and tested the immunoprecipitated material after SDS-PAGE, whereas panel 7b shows the RT-PCR products obtained from the same samples using XNOA 36 (Fig. 7 lanes A–B, D–E) or p27^{BBP}/eIF6 (Fig. 7b lane F) specific primers. p27^{BBP}/eIF6 mRNA encodes a protein with housekeeping features previously reported in *Xenopus* oogenesis (Donadini et al., 2001; Carotenuto et al., 2005). Only the IgG band is visible in the sample where the oocyte extract was exposed to pre-immune rabbit IgGs (Fig. 7, panel a, lane B), and no proteins are precipitated in the absence of IgGs (Fig. 7, panel a, lane C). In lane D of panel a, where the oocyte extract was immunoprecipitated with anti- β -spectrin antibodies, two major bands corresponding to proteins of about 239 and 100 kDa are present. These proteins are further demonstrated to be able to cross-react with anti- β -spectrin antibodies, by western blot analysis (Fig. 7 panel a, lane E) (see also Carotenuto et al., 2009). In the RT-PCR reaction performed on the RNA extracted from the sample immunoprecipitated with anti- β -spectrin antibodies, the expected amplification product was obtained, as confirmed also by using nested primers. This product was also

obtained when the immunoprecipitate was digested with DNaseI, while it was absent when the reverse transcriptase enzyme was omitted, indicating that it is generated by an RNA template (Fig. 7 panel b, lanes C–D–E). When the RT-PCR was performed using p27^{BBP}/eIF6 specific primers, no amplification product was found (Fig. 7 panel b, lane H). Finally, the amplification product is missing in all control IP samples (Fig. 7 panel b, lanes F–G). These data indicate that the spectrin protein is physically associated to XNOA 36 mRNA.

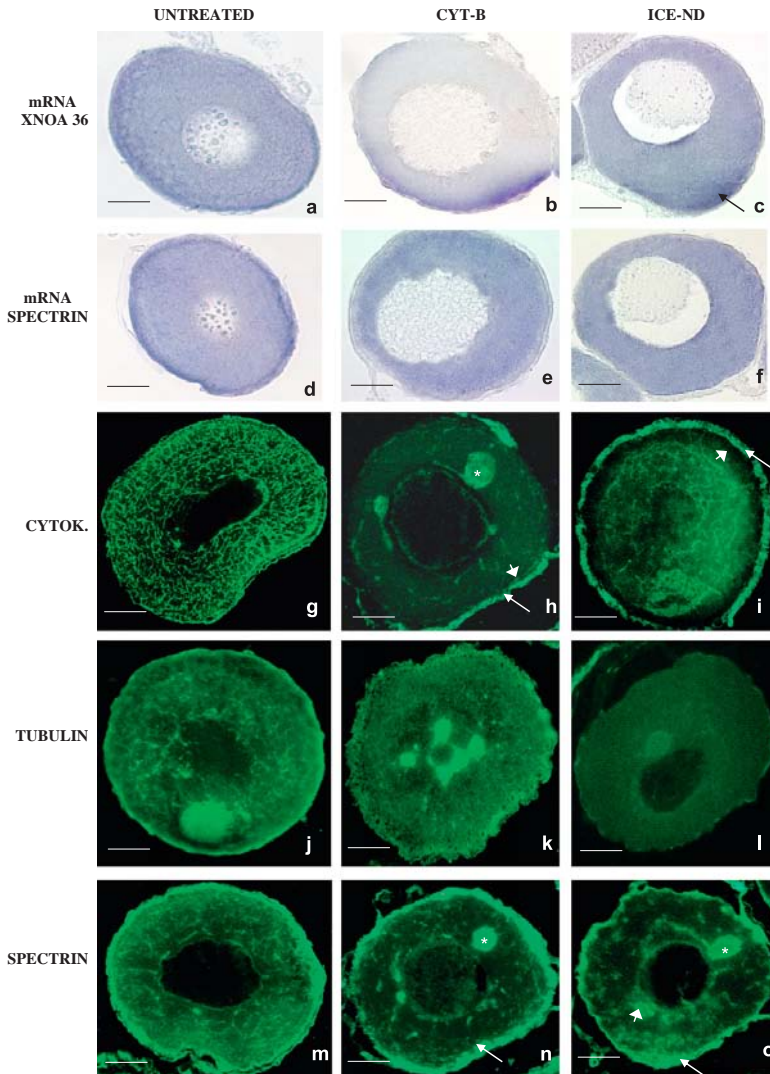
Discussion

We cloned a *X. laevis* cDNA encoding NOA 36, a highly conserved zinc finger protein with a predicted molecular mass of 36 kDa that has hitherto been studied only in humans (Bolivar et al., 1999). We analysed the localisation pattern of XNOA 36 mRNA in *X. laevis* oogenesis, as this transcript, while present throughout *X. laevis* embryogenesis, displays a characteristic stage-specific distribution in oogenesis, undergoing gradual segregation in the cytoplasm of stage I oocytes. In *Drosophila*, the segregation of several mRNAs governing embryonic polarity is established during oogenesis mainly thanks to microtubules (reviewed in Riechmann and Ephrussi, 2001). In contrast, in eggs of different species such as *C. elegans* (Kemphues et al., 1988) and *Styela* (Conklin, 1905; reviewed in Sardet et al., 2005) transcript segregation through association of the mRNAs with the cytoskeleton (actin and/or microtubules) occurs only following sperm activation. In *X. laevis*, microtubule-dependent mRNA localisation occurs during oogenesis at stage III (Yisraeli et al., 1990). mRNAs remain tightly anchored to the vegetal cortex, thanks to the actin-based cytoskeleton until the end of oogenesis (Alarcón and Elinson, 2001). Microtubules are also implicated in cortical

rotation, which occurs after sperm penetration and is responsible for the displacement of positional information cues established during oogenesis (Ancel and Vitemberger 1948; Houliston and Elinson, 1991).

In *X. laevis* stage I oocytes, most maternal transcripts are distributed in the entire cytoplasm, and a subset of them is recruited to the MC by a cytoskeleton-independent mechanism (Kloc et al., 1996; Chang et al., 2004). In contrast, the localisation pattern of the XNOA 36 transcript in late stage I oocytes (of 180–250 μm) displays a series of really unusual features: 1) it peaks at

the oocyte cortex and decorates a cytoplasmic network with a gradient-like distribution decreasing toward the inner cytoplasm; 2) it transiently segregates in about half of the oocyte; 3) it is almost undetectable in the oocyte region that is in contact with the ovarian hylum. Moreover, it largely disappears from the oocyte cytoplasm in later stages of oogenesis, suggesting that the XNOA 36 gene product accomplishes a specific function during early oogenesis. Considering the virtual A/V axis, the transcript accumulates in a domain that is parallel to this axis, yet only in one half of the oocyte. Localisation of the α -spectrin transcript is



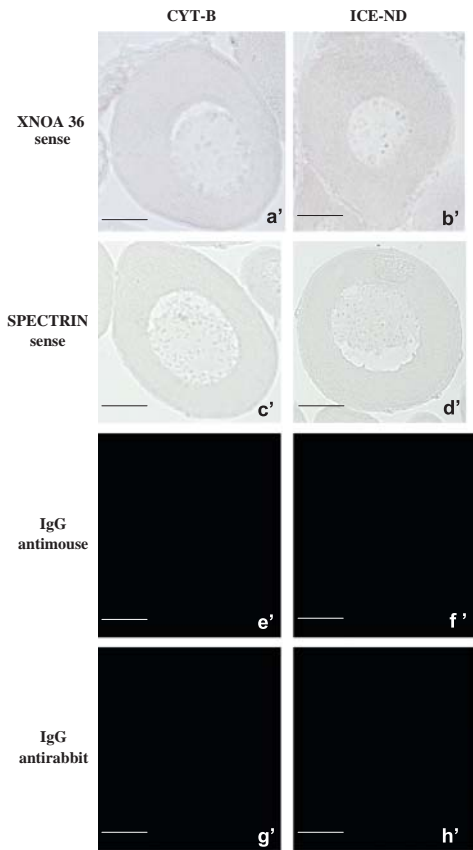


Fig. 5. (Continued)

practically identical to that of XNOA 36 mRNA, its edge coinciding with the A/V axis. The two mRNAs co-localise, i.e. are in the same half of the oocyte, as shown by double in situ localisation

experiments. We also showed that, in late stage I oocytes, the MC is at the boundary of the oocyte sector defined by XNOA 36 and α -spectrin mRNAs, having its outermost portion marked by the two transcripts. Therefore our experiments indicate that, upon reaching the size of about 250 μ m, the oocyte A/V is approximately parallel to the gonadal walls.

Despite the overlap of their localisation domains in the oocyte, α -spectrin and XNOA 36 RNAs do not appear to identify the same filamentous network. In fact, only XNOA 36 mRNA is dislocated by cytochalasin B or ice/nocodazole treatments, suggesting that the distribution of the two mRNAs is differently accomplished. Immunofluorescence experiments of the treated oocytes using anti-cytokeratin, anti-tubulin and anti- β -spectrin antibodies indicated that only the localisation of the spectrin protein is perturbed in a pattern similar to that of XNOA 36 mRNA. In situ localisation of the XNOA 36 transcript coupled with anti-spectrin immunostaining showed that XNOA 36 mRNA co-localises with spectrin. Moreover, immunoprecipitation experiments indicated that these molecules form a protein-RNA complex. Therefore, the spectrin-containing cytoskeleton, i.e. the actin-based cytoskeleton (Bennett and Gilligan, 1993; Morrow et al., 1991; Ryabova et al., 1994) may account for the network we found to be decorated by XNOA 36 mRNA.

Alpha/ β -spectrin heterodimers are found in *X. laevis* oocytes where at least two β -spectrin isoforms of 239 and 100 kDa respectively are present (Carotenuto et al., 2009), in addition to one form of α -spectrin (Giebelhaus et al., 1988). Carotenuto et al. (2000), using anti- α -spectrin antibodies cross-reacting with α - and β -spectrin (Di Stasi et al, 1991), showed that this heterodimer has a polarised distribution in the same stage of oogenesis where our data indicate co-localisation between XNOA 36 mRNA and β -spectrin protein. These observations are in agreement with the idea that the spectrin-based skeleton is a key player in establishing and/or maintaining cell shape and polarisation (Lee et al., 1999). In *X. laevis* oocytes, the first localisation of spectrin is in the oogonia, in the so-called pre-MC where, together with Xsirts, it is found in a structure called the spectrosome, asymmetrically located at one side of the cell. In stage I oocytes, the protein spectrin is present throughout the MC where it was hypothesised to be associated with both Xsirts and Xwnt11 (Kloc et al, 1998). Moreover, at this stage of growth, spectrin gradually localises in a filamentous network that particularly surrounds and permeates the MC, as also shown in this paper, together with cytokeratin and tubulin (Gard and Klymkowsky, 1998; Gard, 1999). The cytoskeletal network where XNOA 36 mRNA is located appears to hold the MC during its migration to the cortex. The MC reaches the cortex at stage II (Heasman et al., 1984). At present it

Fig. 5. Distribution of XNOA 36 or α -spectrin mRNAs (a-f) and of selected cytoskeleton proteins (g-o) in sections of oocytes of about 200 μ m treated with cytochalasin B (Cyt.-B) or ice-nocodazole (ICE-ND). **a-c.** *In situ* hybridisation with an antisense XNOA 36 riboprobe. **a.** Untreated oocyte. Bar = 46 μ m. **b.** Cytochalasin-B treated oocyte. Virtually all hybridisation signal is found at the periphery of the oocyte. Bar = 43 μ m. **c.** Oocyte incubated in ice-nocodazole. The filaments decorated by XNOA 36 mRNA are almost completely absent and most of the transcript is concentrated at the oocyte periphery, in discrete territories (arrow). Bar = 46 μ m. **d-e.** *In situ* hybridisation with an antisense α -spectrin riboprobe. **d.** Untreated oocyte. Bar = 48 μ m. **e.** Cytochalasin-B treated oocyte. The hybridisation signal is similar to that seen in the untreated control, except for a rim of staining at the oocyte periphery stronger in untreated control. Bar = 46 μ m. **f.** Oocyte incubated in ice-nocodazole. No major changes are observed in the distribution of the α -spectrin mRNA compared to untreated oocytes. Bar = 47 μ m. **g-i.** Cytokeratin immunolocalisation. **g.** Untreated oocyte showing a meshwork of immunoreactive fibres. Bar = 41 μ m. **h.** In cytochalasin B-treated oocytes, cytokeratin is mostly concentrated in the MC (asterisk) and in aggregates surrounding the germinal vesicle. Arrow=somatic tissue. Short arrow= peripheral cytoplasm. Bar = 43 μ m. **i.** Oocyte treated with ice-nocodazole. Cytokeratin is found in few cytoplasmic filaments. Bar = 41 μ m. **j-k.** Acetylated tubulin immunolocalisation. **j.** Untreated oocyte. Bar = 39 μ m. **k.** Cytochalasin B-treated oocyte, showing the presence of immunoreactive perinuclear aggregates, not observed in untreated oocytes. Bar = 39 μ m. **l.** In oocytes treated with ice-nocodazole, virtually no fluorescent signal is found. Bar = 41 μ m. **m-n.** Spectrin immunolocalisation. **m.** Untreated oocyte, showing a cortical spectrin network also extending in the cytoplasm. Bar = 41 μ m. **n.** Cytochalasin B-treated oocyte. The immunofluorescence is mostly located at the oocyte periphery (arrow), and only few fibres are seen in the cytoplasm. Asterisk= mitochondrial cloud, stained as well by the anti-spectrin antibody. Bar = 43 μ m. **o.** In ice-nocodazole-treated oocytes, the spectrin immunofluorescence is again located mostly at the oocyte periphery (arrow) as well as in aggregates (short arrow) and in the MC (asterisk). (o). Bar = 44 μ m. **Fig. 5'. Negative controls for Fig. 5 experiments.** **a'.** Sections of cytochalasin B-treated oocytes exposed to sense XNOA 36 probe. Hybridisation signals are absent. Bar = 51 μ m. **b'.** ice-nocodazole-treated oocytes exposed to sense XNOA 36 probe: hybridisation signals are absent. Bar = 56 μ m. **c'-d'.** Oocytes exposed to α -spectrin sense probe following treatment with cytochalasin B (c') or with ice-nocodazole (d'). Hybridisation signals are absent. Bar = 54 μ m in (c') and 55 μ m in (d'). **e'-f'.** Sections of oocytes incubated with cytochalasin B (e') or ice-nocodazole (f') exposed to anti-mouse IgGs with omission of primary antibodies (for anti-cytokeratin or anti-tubulin immuno-staining). The immuno-staining is absent. Bars = 56 μ m. **g'-h'.** Sections of oocytes incubated with cytochalasin B (g') or ice-nocodazole (h') exposed to anti-rabbit IgGs with omission of primary antibodies (for anti-spectrin immuno-staining) (h'). The immuno-staining is absent. Bars = 56 μ m.

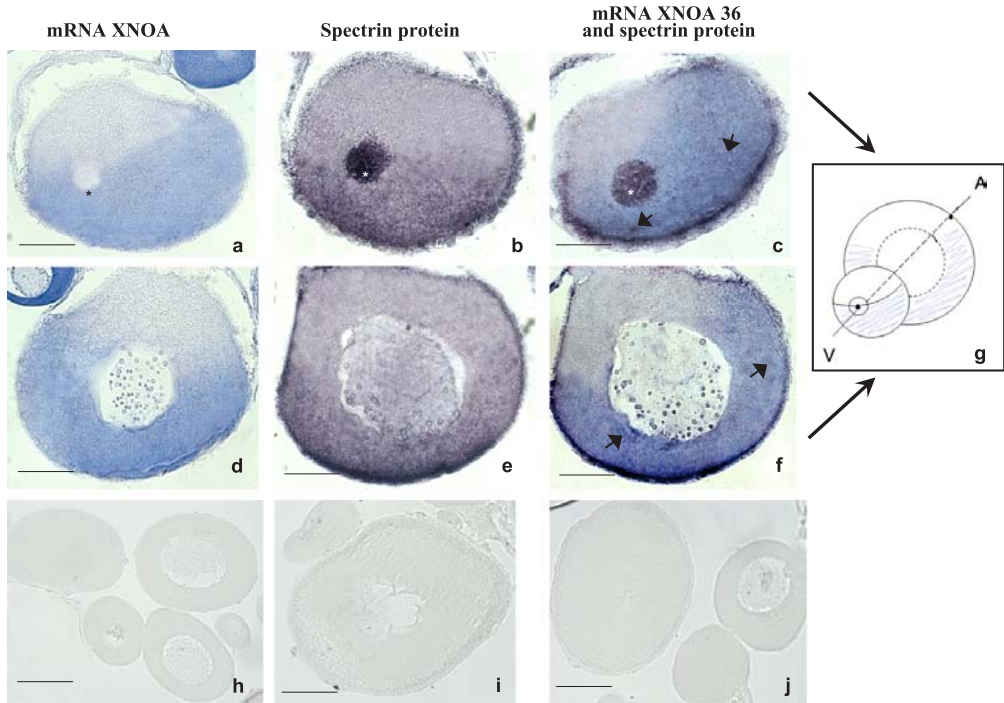


Fig. 6. Distribution of XNOA 36 mRNA (BM-purple label) (a,d), spectrin protein (Vector-black label) (b,e) or both (c,f) in alternating serial sections of a stage I oocyte. a–c. The localisation domains of the XNOA 36 mRNA and the spectrin protein coincide and bisect the MC (asterisk) located at the centre of the sections. d–f. Their localisations and overlaps are consistently found in subsequent serial sections. The bar indicates 69 μm in (d), 65 μm in (e) and (f). In figures c and f double incubation, a dominance of brown colour in the cortical region is observed, corresponding to spectrin localisation, while for the rest of the cytoplasm BM-purple staining (XNOA 36 mRNA) is darker than in Figs. 6a and 6d and the presence of a delicate network of brown staining (spectrin) is indicated (small arrows). In panel (g) a drawing is shown to better describe the distribution pattern of the two molecules with respect to the A/V axis. h. Control *in situ* hybridisation with a sense XNOA 36 probe. Bar = 120 μm . i. Control immunostaining using preimmune serum. Bar = 77 μm . j. Coupled *in situ* hybridisation and immunostaining controls. Bar = 95 μm .

is not known what forces drive the MC into the cortex, in oocytes where contractile activity is acquired only after maturation (Johnson and Capco, 1997). We speculate that, in late stage I oocytes, the asymmetric withdrawal of the cytoskeleton containing XNOA 36 mRNA might supply the force needed to drag the MC towards the cortex. On this point, it should also be considered that the described localisation pattern of the spectrin–mRNA complex is transient and it is no longer detected in oocytes following stage I of growth. In *Homo sapiens*, XNOA 36 is known to be associated with centromeres during metaphase (Bolivar et al., 1999). The specific role of XNOA 36 mRNA and protein in combination with the cytoskeletal network remains to be ascertained.

A fascinating hypothesis might be that the spatial relationship observed between spectrin and XNOA 36 RNAs and the MC signals a novel coordinate of the oocyte on the A/V axis. However, we doubt that the two oocyte halves anticipate a dorso-ventral (D/V) symmetry or a left/right (L/R) symmetry. Indeed, the D/V axis is known to be established as a consequence of the cortical rotation and of Xwnt-11 signalling occurring after fertilisation (Tao et al., 2005; Kofron et al., 2007). The L/R symmetry is also dependent upon the Wnt signalling pathway (Nascone and Mercola, 1997). Concerning the segregation of the spectrin–XNOA 36 mRNA complex in one half of the oocyte, better understanding will

probably be gained if the nature of the asymmetrical signal governing this cytoskeleton-based phenomenon is uncovered. Except for the MC, the only other asymmetry related to the oocyte is external, i.e. the position of the hylum, where the oocyte surface is in contact with thecal connective tissue and close to the external ovarian epithelium, rather than to the inner ovarian epithelium which surrounds the rest of the oocyte. Our data show that the hylum is in contact with the region of the 180–280 μm oocyte that is devoid of the XNOA 36-containing cytoskeleton network. It is plausible that extracellular signals are sent from this region to the oocyte, causing specific rearrangements of the actin-based cytoskeleton, eventually leading to mRNA segregation (see Cohen, 2005) into the region of the oocyte opposite the signal. Several data suggest that matrix stiffness could regulate the equilibrium between storage and release of matrix-bound growth factors (Wipff et al., 2007; Wells and Discher, 2008). In *Xenopus* oocytes it has been shown that changes in external “mechanical tone” exerted on the oocyte by somatic tissue may regulate mechano-sensitive release of chemicals (Maroto and Hamill, 2001). We hypothesise that, upon reaching a 120–150 μm growth threshold, the oocyte provokes tension on the external somatic tissues that in turn liberates factor(s) acting on the cytoskeleton. This putative signal spreading from the hylum would remodel the

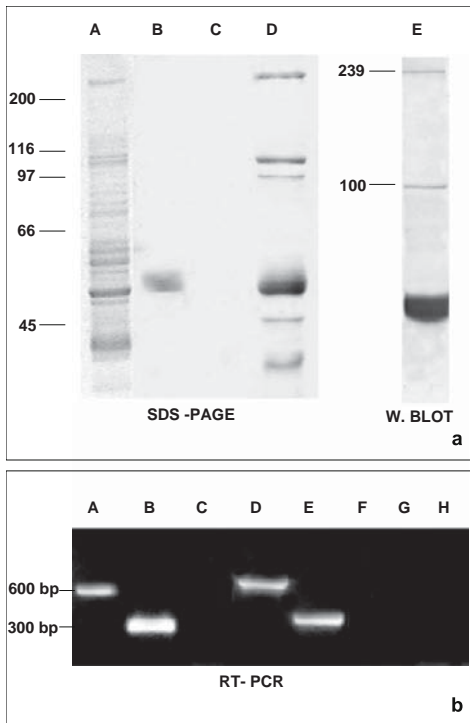


Fig. 7. SDS PAGE (panel a) and RT-PCR (panel b) analyses of macromolecular complexes immunoprecipitated with anti- β spectrin antibodies from stage I oocytes. **A.** Crude oocyte lysate. **B.** Oocyte lysate immunoprecipitated with pre-immune serum: only the IgG band is present. **C.** Oocyte lysate incubated with Sepharose beads in absence of IgGs: no immunoprecipitated proteins are found. **D.** Oocyte lysate immunoprecipitated with anti- β -spectrin antibodies: several silver-stained bands are present. Western blot analysis of these immunoprecipitated proteins is shown in the right part of panel a: two major bands of about 239 and 100 kDa are recognized by anti- β -spectrin antibodies. In panel b RT-PCR products generated by using XNOA 36 specific primers are shown. A band of the expected size was obtained (A), and its identity was confirmed by using nested primers (B). These RT-PCR products were also obtained when the oocyte lysate was digested with DNaseI following the IP experiment (D,E). On the contrary, the amplification products were absent when the reverse transcriptase enzyme was omitted (C) as well as in control IP samples obtained with pre-immune serum (F) or in the absence of IgGs (G). When the RT-PCR was performed using specific primers for the p27^{BBP}/elF6 transcript, no amplification product was found in the β -spectrin immunoprecipitated sample (H). In both panels Mr markers are indicated on the left.

oocyte cytoskeleton, exerting a major impact on the localisation of cytoskeleton-associated mRNAs.

Acknowledgements

We are grateful to Drs C. Romano, L. Dove, M.G. Agostinelli for help in the laboratory, to Dr C. Malva, IGB, CNR Napoli for helpful suggestions and to Mark Walters for revision of the manuscript. We also wish to thank Dr. J. Bolivar at the Department of Biochemistry and Molecular Biology, University of Cadiz, Puerto Real, Cadiz, Spain. This research was partly covered by PRIN 2003 funding awarded to C. Campanella, by Regione Campania L.5 funds and partly funded by AMRA scrl.

References

- Alarcón, V.B., Elinson, R.P., 2001. RNA anchoring in the vegetal cortex of the *Xenopus* oocyte. *J. Cell Sci.* 114, 1731–1741.
- Ancel, P., Vitemberger, P., 1948. Recherches sur le déterminisme de la symétrie bilatérale dans l'oeuf des amphibiens. *Bull. Biol. Fr. Belg.* 31 (Suppl.), 1–48.
- Bennett, V., Gilligan, D.M., 1993. The spectrin-based skeleton and micron-scale organization of the plasma membrane. *Annu. Rev. Cell Biol.* 9, 27–66.
- Birsoy, B., Wylie, C., Heasman, J., 2005. Vg1 is an essential signaling molecule in *Xenopus* development. *Development* 133, 15–20.
- Bolivar, J., Diaz, I., Iglesias, C., Valdivia, M., 1999. Molecular cloning of a zinc finger autoantigen transiently associated with interphase nucleolus and mitotic centromeres and midbodies. *J. Biol. Chem.* 274, 36456–36464.
- Carotenuto, R., Vaccaro, M.C., Capriglione, T., Petrucci, T.C., Campanella, C., 2000. alpha-Spectrin has a stage-specific asymmetrical localisation during *Xenopus* oogenesis. *Mol. Reprod. Dev.* 55, 229–239.
- Carotenuto, R., De Marco, N., Biffo, S., Wilding, M., Vaccaro, M.C., Marchisio, P.C., Capriglione, T., Russo, G.L., Campanella, C., 2005. Phosphorylation of p27^{BBP}/elF6 and its association with the cytoskeleton are developmentally regulated in *Xenopus* oogenesis. *Cell. Mol. Life Sci.* 62, 1641–1652.
- Carotenuto, R., Petrucci, T.C., Correias, I., Vaccaro, M.C., De Marco, N., Dale, B., Wilding, M., 2009. Protein 4.1 and its interaction with other cytoskeletal proteins in *Xenopus laevis* oogenesis. *Eur. J. Cell Biol.* 88, 343–356.
- Chang, P., Torres, J., Lewis, R.A., Mowry, K.L., Houliston, E., King, M.L., 2004. Localization of RNAs to the mitochondrial cloud in *Xenopus laevis* oocytes through entrapment and association with endoplasmic reticulum. *Mol. Biol. Cell* 15, 4669–4681.
- Cohen, R.S., 2005. The role of membranes and membrane trafficking in RNA localisation. *Biol. Cell* 97, 5–18.
- Conklin, E.G., 1905. Organ forming substances in eggs of ascidian. *Biol. Bull.* 8, 205–230.
- Di Stasi, A.M., Gallo, V., Ceccarini, M., Petrucci, T.C., 1991. Neuronal fodrin proteolysis occurs independently of excitatory amino acid-induced neurotoxicity. *Neuron* 6, 445–454.
- Donadini, A., Giodini, A., Sanvito, F., Marchisio, P.C., Biffo, S., 2001. The human ITGB4BP gene is constitutively expressed in vitro, but highly modulated in vivo. *Gene* 266, 35–43.
- Dumont, J.N., 1972. Oogenesis in *Xenopus laevis* (Daudin). I. Stages of oocyte development in laboratory maintained animals. *J. Morphol.* 136, 153–179.
- Gard, D.L., Affleck, D., Error, B.M., 1995. Microtubule organisation, acetylation, and nucleation in *Xenopus laevis* oocytes: II. A developmental transition in microtubule organisation during early diplotene. *Dev. Biol.* 168, 189–201.
- Gard, D.L., 1999. Confocal microscopy and 3-D reconstruction of the cytoskeleton of *Xenopus* oocytes. *Microsc. Res. Tech.* 44, 388–414.
- Gard, D.L., Klymkowsky, M.W., 1998. Intermediate filament organisation during oogenesis and early development in the clawed frog *Xenopus laevis*. In: Herrmann, H., Harris, J.R. (Eds.), *Subcellular Biochemistry: Intermediate Filaments*. Plenum Press, pp. 35–69.
- Gard, D.L., Cha, B.J., King, E., 1997. The organization and animal-vegetal asymmetry of cytokeleton filaments in stage VI *Xenopus* oocytes is dependent upon F-actin and microtubules. *Dev. Biol.* 184, 95–114.
- Giebelhaus, D.H., Eib, D.W., Moon, R.T., 1988. Anti-sense RNA inhibits expression of membrane skeleton protein 4.1 during embryonic development of *Xenopus*. *Cell* 53, 601–615.
- Harland, R.M., 1991. In situ hybridization: an improved whole-mount method for *Xenopus* embryos. *Methods Cell Biol.* 36, 685–695.
- Heasman, J., Quarumby, J., Wylie, C.C., 1984. The mitochondrial cloud of *Xenopus* oocytes: the source of germinal granule material. *Dev. Biol.* 105, 458–469.
- Houliston, E., Elinson, R.P., 1991. Evidence for the involvement of microtubules, endoplasmic reticulum and kinesin in cortical rotation of fertilized frog eggs. *J. Cell Biol.* 114, 1017–1028.
- Johnson, J., Capco, D.G., 1997. Progesterone acts through protein kinase C to remodel the cytoplasm as the amphibian oocyte becomes the fertilization-competent egg. *Mech. Dev.* 67, 215–226.
- Kemphues, K.J., Priess, J.R., Morton, D.G., Cheng, N.S., 1988. Identification of genes required for cytoplasmic localisation in early *C. elegans* embryos. *Cell* 52, 311–320.
- King, M.L., Messitt, T.J., Mowry, K.L., 2005. Putting RNAs in the right place at the right time: RNA localisation in the frog oocyte. *Biol. Cell* 97, 19–33.
- Kloc, M., Larabell, C., Etkin, L.D., 1996. Elaboration of the messenger transport organizer pathway for localisation of RNA to the vegetal cortex of *Xenopus* oocytes. *Dev. Biol.* 180, 119–133.
- Kloc, M., Larabell, C., Chan, A.P., Etkin, L.D., 1998. Contribution of METRO pathway localized molecules to the organisation of germ cell lineage. *Mech. Dev.* 75, 81–93.
- Kloc, M., Etkin, L.D., 1998. Apparent continuity between the messenger transport organizer and late RNA localisation pathways during oogenesis in *Xenopus*. *Mech. Dev.* 73, 95–106.
- Kloc, M., Zearfoss, N.R., Etkin, L.D., 2002. Mechanisms of subcellular mRNA localization. *Cell* 108, 533–544.
- Kloc, M., Bilinski, S., Dougherty, M.T., Brey, E.M., Etkin, L.D., 2004. Formation, architecture and polarity of female germline cyst in *Xenopus*. *Dev. Biol.* 266, 43–61.
- Kloc, M., Etkin, L.D., 2005. RNA localization mechanisms in oocytes. *J. Cell Sci.* 118, 269–282.



Contents lists available at ScienceDirect

Methods

journal homepage: www.elsevier.com/locate/ymeth

Review Article

Multiple-Particle-Tracking to investigate viscoelastic properties in living cells

Lara Selvaggi^b, Marinella Salemme^a, Carmen Vaccaro^a, Giuseppe Pesce^b, Giulia Rusciano^b, Antonio Sasso^b, Chiara Campanella^a, Rosa Carotenuto^{a,*}

^a Department of Structural and Functional Biology, University of Naples Federico II, via Cinthia, 80126 Napoli, Italy

^b Physics Department, University of Naples Federico II, via Cinthia, 80126 Napoli, Italy

ARTICLE INFO

Article history:

Accepted 21 December 2009

Available online xxx

Keywords:

Xenopus laevis

Oocytes

Multiple-Particle-Tracking

Brownian motion

Mitochondrial cloud

Endogenous granules

ABSTRACT

Cell mechanical properties play an important role in determining many cellular activities. Passive microrheology techniques, such as Multiple-Particle-Tracking (MPT) give an insight into the structural rearrangements and viscoelastic response of a wide range of materials, in particular soft materials and complex fluids like cell cytoplasm in living cells. The technique finds an important field of application in large cells such as oocytes where, during their growth, several organelles and molecules are displaced in specific territories of the cell instrumental for later embryonic development. To measure cell mechanics, cells are usually deformed by many techniques that are slow and often invasive. To overcome these limits, the MPT technique is applied. Probe particles are embedded in the viscoelastic sample and their properties are extracted from the thermal fluctuation spectra measured using digital video-microscopy. The Brownian motion of a probe particle immersed in a network is directly related to the network's mechanical properties. Particles exhibit larger motions when their local environments are less rigid or less viscous. The mean-square-displacement (MSD) of the particle's trajectory is used to quantify its amplitude of motions over different time scales.

© 2009 Elsevier Inc. All rights reserved.

1. Introduction

1.1. Overview of microrheology techniques

Traditional rheology measurements, important for industrial application, have given valuable insight into the structural rearrangements and mechanical response of a wide range of materials, in particular soft materials and complex fluids. However, conventional mechanical techniques are not always well-suited for all systems. In particular, conventional rheometers provide a measurement of the averaged bulk response but do not allow for local measurements in inhomogeneous systems. To address these issues, a new class of measurement techniques has emerged. These have come to be called microrheology methods and probe the material response on micrometer length scales, using micro-liter sample volumes [1,2]. These methods typically use embedded micro-sized mechanical probes to locally deform the medium, and information is extracted from their motion.

Microrheology techniques are usually classified as active and passive, depending on whether the strain is recovered after an externally applied stress or on whether the medium deformation are caused by the thermal energy $k_B T$, respectively. Passive techniques, like Multiple-Particle-Tracking (MPT), Laser Particle Track-

ing (LPT) and Diffusing Wave Spectroscopy (DWS), are typically more useful for measuring low values of predominantly viscous moduli, whereas active techniques, like Magnetic Tweezers (MT) and Atomic Force Microscopy (AFM), can extend the measurable range to samples containing significant amounts of elasticity. Active techniques involve the use of optical or magnetic forces to move probe particles and apply local stress to complex materials. Although active measurements can be extremely useful, especially in stiff materials where large stresses are necessary to obtain a measurable strain, large particles are required to apply sufficiently well-controlled forces to the material, preventing the application of this technique to very small length scales.

To measure cell mechanics, cells are usually deformed by many techniques [3]. Whole-cell deformations use torsion pendulum [4], parallel plates [5], and micropipette aspiration [6]. Smaller mechanical probes of cells include micro-needles [7,8], cell pokers [9] and atomic force microscopy [10,11]. Magnetic forces are applied to particles within living cells [12–14], and attached to the surface of living cells [15,16]. So far, optical forces are only applied to deforming soft sub-cellular structures, such as plasma membrane [17,18]. Mechanical measurements using direct deformations are slow and often invasive. Deformations can be so large as to be non-linear. To overcome these limits, passive microrheology techniques are used.

Particle tracking techniques directly derive from the experimental studies of Perrin about Brownian motion and are probably

* Corresponding author. Fax: +39 081679233.

E-mail address: rosa.carotenuto@unina.it (R. Carotenuto).

Expression of XNOA 36 in the mitochondrial cloud of *Xenopus laevis* oocytes

M.C. Vaccaro², M. Wilding³, B. Dale³, C. Campanella² and R. Carotenuto¹

Department of Structural and Functional Biology, University of Naples 'Federico II'; and Centre for Assisted Fertilization, Clinica Villa del Sole, Naples, Italy

Date submitted: 27.10.10. Date accepted: 21.01.11

Summary

In *Xenopus laevis* oocytes a mitochondrial cloud (MC) is found between the nucleus and the plasma membrane at stages I–II of oogenesis. The MC contains RNAs that are transported to the future vegetal pole at stage II of oogenesis. In particular, germinal plasm mRNAs are found in the Message Transport Organiser (METRO) region, the MC region opposite to the nucleus. At stages II–III, a second pathway transports Vg1 and VegT mRNAs to the area where the MC content merges with the vegetal cortex. Microtubules become polarized at the sites of migration of Vg1 and VegT mRNAs through an unknown signalling mechanism. In early meiotic stages, the centrioles are almost completely lost with their remnants being dispersed into the cytoplasm and the MC, which may contain a MTOC to be used in the later localization pathway of the mRNAs. In mammals, XNOA 36 encodes a member of a highly conserved protein family and localises to the nucleolus or in the centromeres. In the *Xenopus* late stage I oocyte, XNOA 36 mRNA is transiently segregated in one half of the oocyte, anchored by a cytoskeletal network that contains spectrin. Here we found that XNOA 36 transcript also localises to the nucleoli and in the METRO region. XNOA 36 protein immunolocalization, using an antibody employed for the library immunoscreening that depicted XNOA 36 expression colonies, labels the migrating MC, the cytoplasm of stage I oocytes and in particular the vegetal cortex facing the MC. The possible role of XNOA 36 in mRNA anchoring to the vegetal cortex or in participating in early microtubule reorganization is discussed.

Keywords: Cytoskeleton, Microtubules, Mitochondrial cloud, Oocyte, *Xenopus laevis*

Introduction

In *Drosophila melanogaster*, microtubule reorganisation induced by the early signal of the TGF α homologue Gurken underlies antero-posterior (A/P) polarisation in the oocyte and later its dorso/ventral (D/V) axis that will be inherited by the embryo (Schüpbach & Wieschaus, 1986; Neuman-Silberberg & Schüpbach, 1996; Roth, 2003). In *Xenopus*, the oocyte acquires a radial organisation along a primary coordinate, i.e. the animal–vegetal axis (A/V) that

dictates the perspective A/P planning of the embryo. At early stages of oogenesis (stages I and II), a mitochondrial cloud (MC) is located between the germinal vesicle (GV) and the plasma membrane (Heasman *et al.*, 1984). The MC is rich in active mitochondria (Wilding *et al.*, 2001) and gathers nuclear messages destined to be transported within the MC to the future vegetal pole at late stage II of oogenesis (Kloc *et al.*, 1996). Germinal plasm RNAs are found in the message transport organiser (METRO) region, the MC endoplasmic reticulum rich region opposite to the nucleus. Other messengers are Xwnt11 mRNA implicated in the determination of D/V (Tao *et al.*, 2005) and part of Vg1 mRNA (Kloc *et al.*, 1996). Messengers destined to be transported to the vegetal cortex may first assemble with proteins in the nucleus (Kress *et al.*, 2004). The localisation of some mRNA into the MC occurs through a diffusion/entrapment mechanism into the MC endoplasmic reticulum (Chang *et al.*, 2004). Later, at stages II–III, a second pathway takes care of the transportation of other mRNAs including

¹All correspondence to: Rosa Carotenuto, Department of Structural and Functional Biology, University of Naples Federico II, Complesso Universitario Monte Sant'Angelo, Via Cinthia, I-80126, Napoli, Italy. Tel: +39 081 679195. Fax: +39 081 679233. e-mail: rosa.carotenuto@unina.it

²Department of Structural and Functional Biology, University of Naples 'Federico II', Italy.

³Centre for Assisted Fertilization, Clinica Villa del Sole, Naples, Italy.

Vg1mRNA and VegT mRNA to the site where the MC content has merged to the vegetal cortex. Vg1 and VegT are implicated in endoderm and mesoderm specification (Thomsen & Melton, 1993; Zhang *et al.*, 1998). A polarized organisation of microtubules and related kinesins initiates at the site of Vg1 and VegT mRNA migration to the cortex (Yisraeli *et al.*, 1990; and see Kloc & Etkin, 1998; King *et al.*, 2005). At present, the signal that causes the microtubule reorganisation is unknown. By stages III–IV, the microtubules become fully organised as an orderly crown that links the oocyte cortex to the germinal vesicle (Klymkowsky *et al.*, 1987; Gard *et al.*, 1995, 1997).

In the oogonia, a primordial MC is found that gives a polarised organisation to the cell. In this structure, centrioles, spectrin and the endoplasmic reticulum-rich fusome are located in addition to microtubules that radiate from the centrioles. The latter supposedly constitutes an interphase microtubule organisation centre (MTOC) active in the oogonia (Kloc *et al.*, 2004). In early meiotic stages, the centrioles are almost completely lost, their remnants are dispersed into the cytoplasm and the MC where γ -tubulin was localised (Kloc & Etkin, 1998), although this point remains controversial (Gard, 1999). It was hypothesised that the MC may contain a MTOC to be used in the late mRNAs pathway (Kloc & Etkin, 1998).

Previous data showed that, in the late stage I oocytes (250 μ m oocytes), a transient XNOA 36 mRNA segregation occurs in a zone of the oocyte surrounding the MC and opposite to the ovarian hilum with the MC located between the XNOA 36 mRNA labelled region and the unlabelled region. The XNOA 36 mRNA is localised or anchored in the oocyte through a cytoskeletal network that contains spectrin. XNOA 36 encodes a member of a highly conserved protein family displaying characteristic CXXC motifs putatively involved in the formation of zinc-finger structures of the C2–C2 type (Bolivar *et al.*, 1999; Vaccaro *et al.*, 2010). NOA36 was first one to be isolated in *Homo sapiens* as an autoimmune antigen in a patient suffering from rheumatoid arthritis and was found in the nucleolus in G1/G2 or was associated with centromeres (Bolivar *et al.*, 1999). Recent data report that NOA36 (or ZN330) is a pro-apoptotic factor and associates dynamically to the outer mitochondrial membrane (de Melo *et al.*, 2009).

The *Xenopus laevis* NOA36 cDNA was isolated, using an anti-Gurken monoclonal antibody (anti-DrosGu), by immunoscreening of an expression library of stage I–III *Xenopus laevis* oocytes. The nucleotides sequence of the isolated XNOA 36 cDNA shows no homologies to Gurken cDNA, and the deduced amino acid sequences of Gurken and XNOA 36 do not share sequences longer than five amino acids (Vaccaro *et al.*, 2010).

In this paper we found that XNOA 36 transcript localises, in addition to its cytoplasmic localisation, in the nucleus and in a sector of the MC that eventually coincides with the METRO region facing the vegetal cortex. Moreover, we studied XNOA 36 protein immunolocalization, using the anti-DrosGu antibody employed for the library immunoscreening that depicted XNOA 36 expression colonies (Vaccaro *et al.*, 2010). We found that, in stage I oocytes, the antibody labels the nucleoli, the migrating MC and the peripheral cytoplasm, in particular the vegetal cortex facing the MC. The possible role of XNOA 36 is discussed.

Material and methods

Animals and oocytes

Adult *X. laevis* females were obtained from Rettili (Varese, Italy). They were kept and utilized at the Department of Structural and Functional Biology, the University of Naples Federico II, according to the guidelines and policies dictated by the University Animal Welfare Office and in agreement with European Community laws. Groups of oocytes at various stages of oogenesis were excised from the ovaries of females anaesthetized with MS222 (Sigma). The growth stages of the *X. laevis* oocyte are: stage I (50–300 μ m), stage II (300–450 μ m), stage III (450–600 μ m), stage IV (600–1000 μ m), stage V (1000–1200 μ m) and stage VI (1200–1300 μ m) (Dumont, 1972).

In situ hybridisation on sections

XNOA 36 cDNAs were used as templates to synthesise digoxigenin-labelled antisense and sense probes, using digoxigenin-labelled UTP and T3 and T7 RNA polymerase according to the manufacturer's recommendations (Roche RNA T3-SP6 transcription and labelling kit).

X. laevis oocytes were fixed in 2% PFA, 250 mM NaCl, 5% acetic acid for 50 min at room temperature, dehydrated in ethanol and processed for embedding in paraffin according to standard techniques. The 7- μ m thick paraffin sections were placed on Superfrost Plus slides (Carlo Erba) and were hybridized overnight at 60 °C in 40% formamide, 1 \times Denhardt's solution, 5 \times SSC, 200 μ g/ml tRNA (Sigma) and 100 ng of sense or antisense digoxigenin-labelled RNA on each slide. Slides were washed in 0.5 \times SSC, 20% formamide for 1 h at 60 °C, and exposed to RNase A at 37 °C for 30 min. After two washes in 0.5 \times SSC, 20% formamide, for 30 min at 60 °C, they were incubated overnight in anti-digoxigenin-alkaline phosphatase (AP)-conjugated antibody (Roche) diluted 1:2000 in 2% blocking reagent solution (Roche). After several washes in 1 \times PBS, 0.1% Tween 20, the detection was

performed using BM purple (Roche) (for more details see Vaccaro *et al.*, 2001).

Confocal microscopy

Small clusters of stage I–II oocytes were fixed in 2–4% PFA in PBS and extracted in a Hepes buffer containing glycol hexylene according to Klymkowsky *et al.* (1987). The samples were then incubated in anti-DrosGu antibody. The antibody was purchased by the Developmental Studies Hybridoma Bank, maintained by the University of Iowa, developed under the auspices of the National Institute of Child Health and Human Development of NIH, Department of Biological Sciences, Iowa City, IA 52242. This antibody recognizes an epitope of *Drosophila melanogaster* Gurken encompassing amino acids 53–185 upstream of the EGF domain (Nilson & Schüpbach, 1999). Control samples were performed by omitting primary antibody in the experimental trial. The secondary antibodies were BODIPY and Texas Red (H+L) goat anti-mouse IgG (Molecular Probes). After washing in PBS, the samples were directly immersed in glycerol/PBS 1:9 (v/v). Optical sections 1- μ m thick were obtained using an Olympus Fluoview confocal microscope based on Olympus IX70 inverted microscope equipped with an argon/krypton laser. Unless differently specified, each image was derived from an average of 10 optical sections at 1 μ m intervals.

Results and Discussion

In situ hybridisation on sections

Extensive analysis of serial sections of oocytes derived from nine females showed a small amount of the XNOA 36 transcript in the GV and in the MC, in addition to the major cytoplasmic localisation previously described (Vaccaro *et al.*, 2010). In particular, in Fig. 1a, the hybridisation signal is observed in the nucleoli and around the nuclear envelope, at a site where the MC is associated with the GV. As some signal is also in the MC, Fig. 1a suggests a passage of XNOA 36 mRNA from the GV to the MC. Kress *et al.* (2004) showed the mRNAs destined to be transported to the vegetal cortex may assemble with proteins in the nucleus through *cis*-acting RNA sequences and that this event is essential for final localisation of the mRNA. The nucleolus localisation is in agreement with data of Bolivar *et al.* (1999), as well as its association with mitochondria (de Melo *et al.*, 2009). In later stages of growth (starting from 140 μ m large oocytes) a little hybridisation signal is partially present at the periphery of the MC (Fig. 2b). This finding is also evidence in oocytes of about 200–250 μ m (Fig. 1c–e), of XNOA 36 mRNA

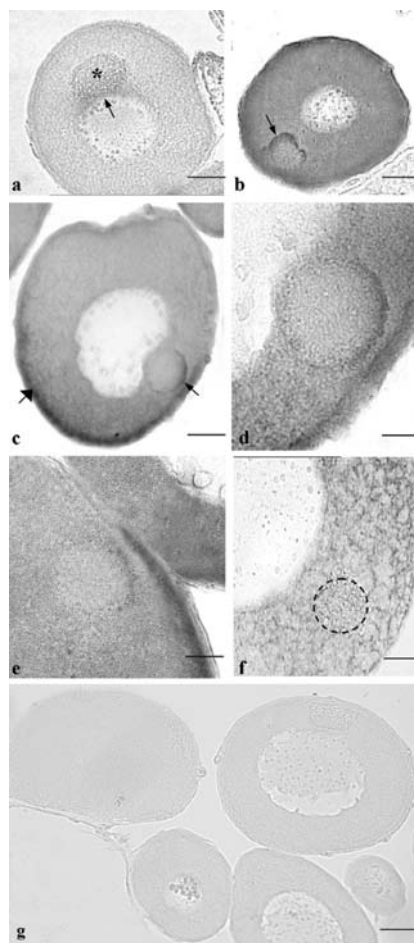
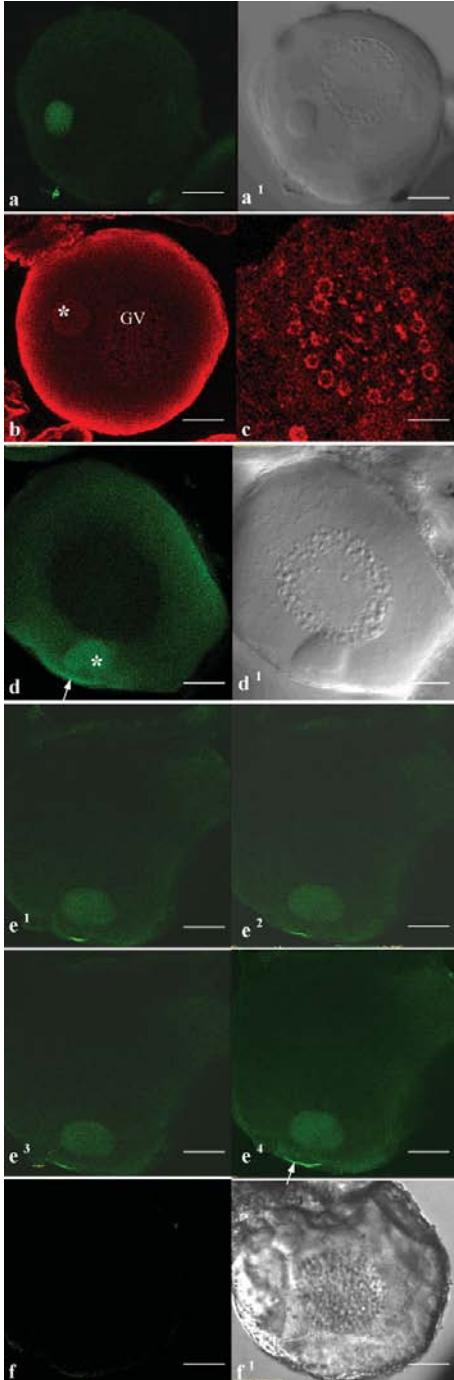


Figure 1 *In situ* hybridisation of oocyte sections. (a) A 130 μ m oocyte is shown, where the hybridisation signal of XNOA 36 mRNA is located in the nucleoli, around the nuclear envelope and in the mitochondrial cloud (MC) (asterisk). In particular we observe a site where the MC is associated with the nuclear envelope (small arrow). As some signal is also in the MC, this figure suggests a passage from the germinal vesicle (GV) to the MC. Bar = 26 μ m. (b) In this 140 μ m-large oocyte some hybridisation signal is partially present at the periphery of the MC (small arrow). Bar = 30 μ m. (c–e) A similar localisation is also evident in the oocytes of about 200–250 μ m, being XNOA 36 mRNA located in the region recognisable as the METRO territory (small arrow). The large arrow indicates the mRNA localisation in the cortex, including the region facing the MC. (d,e) Magnification of (c). Bar in (c) = 35 μ m, in (d) = 11 μ m, in (e) = 17 μ m. (f) The MC (bordered by interrupted lines) of this 250 μ m oocyte is not labelled by the riboprobe. Bar = 30 μ m. (g) Section incubated with sense-probe showing absence of labelling. Bar = 40 μ m.



being located in the region recognisable as the METRO territory (Fig. 2c–e) as it faces the cortex where it will eventually collapse (Kloc *et al.*, 1996) and as it co-localises with a typically METRO-located mRNA, i.e. the *Xcat-2* mRNA (Vaccaro, personal communication). The absence of the signal in most of the MC is shown in Fig. 1f showing an oocyte of 250 µm, about the same size as the oocyte in Fig. 1e (see also Vaccaro *et al.*, 2010). In Fig. 1g the section was incubated with the sense-riboprobe and the hybridization signal is absent. In the METRO region several germ-plasm mRNAs are located such as *Xcat-2* (Mosquera *et al.*, 1993), *Xdaz1* (Houston & King, 2000), *DEADSouth* (MacArthur *et al.*, 2000) as well as *Xwnt11*, (Ku & Melton, 1993) and *Xlsirt* (Kloc *et al.*, 1998) (see King *et al.*, 2005 for a review). Previous data indicated that *XNOA 36* mRNA co-immunoprecipitates with spectrin that is notoriously present in the cytoplasm as well in the MC, in particular in the germ plasm (Kloc *et al.*, 1998; Vaccaro *et al.*, 2010), suggesting that this mRNA is anchored through the spectrin-related cytoskeleton in this MC zone.

Confocal microscopy

Anti-DrosGu immunofluorescence is present in the entire MC of oocytes of 190–200 µm, where the MC is halfway between the cortex and the GV (Fig. 2a,a¹). The association of the *XNOA 36* protein with mitochondria

Figure 2 Confocal microscopy showing the immunofluorescence of anti-DrosGu-stained oocytes. (a) The immunofluorescence is present in the whole mitochondrial cloud (MC) of oocytes of 190–200 µm, whereas the MC is approximately halfway between the cortex and the germinal vesicle (GV). The immunofluorescence is mildly present at the periphery of the oocyte, in contrast to the bright signal present in the MC. Single optical sections of 3 µm. (a¹) Simultaneous differential interference contrast (DIC) image of the oocyte labelled in (a). Bar = 40 µm. (b) Oocyte of about 220 µm, in which several optical sections are pooled together in a single image (15 sections of 1 µm). A bright immunofluorescence is evident at the periphery MC = asterisk; GV = germinal vesicle. Bar = 44 µm. (c) The germinal vesicle contains nucleoli showing a rim of fluorescence at their periphery. Bar = 80 µm. (d) Oocyte of 250 µm, the MC is fluorescent (asterisk). The periphery of the oocyte is similarly fluorescent, however the cortex facing the migrating MC is particularly bright if compared with the rest of the oocyte periphery (small arrow). (d¹) Simultaneous DIC image of the oocyte in (d). Bar = 30 µm. (e¹–e³) Single optical sections of an oocyte of about 270 µm, pooled together in (e²), in which the cortex facing the MC is more fluorescent than the rest of the oocyte periphery. Bar = 25 µm. (f) Control section showing no immunofluorescence staining. (f¹) DIC of the oocyte shown in (f). Bar = 40 µm.

can be also predicted by the PSORTII program (see Vaccaro *et al.*, 2010). In Fig. 2a (one optical section of 1 μm) the anti-DrosGu immunofluorescence is mildly present at the periphery of the oocyte, in contrast to the bright signal present in the MC. The peripheral signal is evident in figures in which several optical sections are pooled together in a single image as in Fig. 2b (oocyte of about 220 μm , 15 optical sections of 1 μm), in agreement with previous data for XNOA 36 mRNA distribution indicating that this mRNA is highly concentrated at the oocyte periphery (Vaccaro *et al.*, 2010). However, it was previously reported that XNOA 36 mRNA is located in the hemisphere of the 250/270 μm oocyte opposite to the hilum, while this situation does not appear to be the case for the immunofluorescence staining such as the one shown in Fig. 2d,d¹,e, suggesting that diffusion of the newly translated protein has occurred. Nucleoli display immunofluorescence at their periphery (Fig. 2c), in agreement with the hybridisation signal in Fig. 1.

In oocytes of 250 μm , the MC is also quite fluorescent (Fig. 2d). The immunofluorescence distribution is conserved also in larger oocytes, as indicated in Fig. 2e¹-e⁴, showing optical sections of an oocyte of about 270 μm . Interestingly, in our confocal micrographs the cortex facing the migrating MC is particularly fluorescent if compared with the rest of the oocyte cortex, suggesting that this localised enrichment of the protein may be due to diffusion of XNOA 36 from the MC (Fig. 2e and see also Fig. 2d).

Taken together these data indicate that XNOA 36 mRNA is located in the nucleoli, in agreement with Bolivar *et al.*'s (1999) findings and in the portion of the MC corresponding to the METRO region. The XNOA 36 protein is also found in the nucleoli, in addition to its location in the cytoplasm periphery. The MC contains an extensive network of endoplasmic reticulum that was suggested to contribute to RNAs to the MC region and maintains a close association with RNA (Heasman *et al.*, 1984). Chang *et al.* (2004) showed that a particular endoplasmic reticulum (ER) domain is placed in the MC to provide support for mRNA immobilization and that this subdomain of ER is continuous with cytoplasmic and cortical networks. Accordingly, XNOA 36 mRNA translation might not necessarily occur within the MC, but be transported into the MC following translation in the ER cisternae penetrating into the MC. The fact that XNOA 36 protein is particularly concentrated in the oocyte cortex facing the MC is of specific interest. Prediction of XNOA 36 subcellular localisation, made with the PSORT II program, indicates the following: 73.9% nuclear, 17.4% cytoplasmic, 4.3% cytoskeletal and 4.3% mitochondrial, with the putative mitochondrial targeting sequence located in the N-terminal region

(see also Vaccaro *et al.*, 2010). As the cortex is notoriously rich in cytoskeletal proteins (Alarcon & Elinson, 2001) including spectrin (Vaccaro *et al.*, 2010), it can be hypothesized that XNOA 36 interacts with the cytoskeleton, participating in the anchorage of the MC and its mRNAs in the future vegetal pole. Moreover, according to Kloc & Etkin (1998) the MC contains and releases residual centriole proteins such as γ -tubulin, which could be used in the late mRNAs pathway as a MTOC. As in mammals XNOA 36 associates with centromeres (Bolivar *et al.*, 1999), we hypothesize that XNOA 36 may associate with residual centriole protein of the MC playing a role in early microtubule reorganization. This process starts at the vegetal cortex where the MC disaggregates and then spreads to the rest of the oocyte (Gard, 1999) cortex where XNOA 36 is also located (Vaccaro *et al.*, 2010).

Acknowledgements

We are grateful to Drs F. Graziani and S. Gigliotti for suggestions and to Dr M.G. Agostinelli and C. De Angelis for helping in the experimental procedures. Granted by Regione Campania L. 5 2007.

References

- Alarcon, V.B. & Elinson, R.P. (2001). RNA anchoring in the vegetal cortex of the *Xenopus* oocyte. *J. Cell Sci.* **114**, 1731-41.
- Bolivar, J., Diaz, I., Iglesias, C. & Valdivia, M. (1999). Molecular cloning of a zinc finger autoantigen transiently associated with interphase nucleolus and mitotic centromeres and midbodies. *J. Biol. Chem.* **274**, 36456-64.
- Chang, P., Torres, J., Lewis, R.A., Mowry, K.L., Houliston, E. & King, M.L. (2004). Localization of RNAs in the mitochondrial cloud in *Xenopus laevis* oocytes through entrapment and association with endoplasmic reticulum. *Mol. Biol.* **15**, 4669-81.
- de Melo, I.S., Iglesias, C., Benítez-Rondán, A., Medina, F., Martínez-Barberá, J.P. & Bolivar, J. (2009). NOA36/ZNF330 is a conserved cysteine-rich protein with proapoptotic activity in human cells. *Biochim. Biophys. Acta.* **12**, 1876-85.
- Dumont, J.N. (1972). Oogenesis in *Xenopus laevis* (Daudin). I. Stages of oocyte development in laboratory maintained animals. *J. Morph.* **136**, 153-80.
- Gard, D.L. (1995). Axis formation during amphibian oogenesis: reevaluating the role of the cytoskeleton. *Curr. Top. Dev. Biol.* **30**, 215-52.
- Gard, D.L. (1999). Confocal microscopy and 3-D reconstruction of the cytoskeleton of *Xenopus* oocytes. *Micro. Res. Tech.* **44**, 388-414.
- Gard, D.L., Cha, B.-J. & King, E. (1997). The organization and animal-vegetal asymmetry of cyokeratin filaments in stage VI *Xenopus* oocytes is dependent upon F-actin and microtubules. *Dev. Biol.* **184**, 95-114.

- Heasman, J., Quarmby, J. & Wylie, C.C. (1984). The mitochondrial cloud of *Xenopus* oocytes: the source of germinal granule material. *Dev. Biol.* **105**, 458–69.
- Houston, D.W. & King, M.L. (2000). Germ plasm and molecular determinants of germ cell fate. In: *Current Topics in Developmental Biology* (eds Peterson R. & Schatten G.) pp. 155–182. New York: Academic Press.
- King, M.L., Messit, T.J. & Mowry, K.L. (2005). Putting RNAs in the right place at the right time: RNA localization in the frog oocyte. *Biol. Cell.* **97**, 19–33.
- Kloc, M., & Etkin, L.D. (1998). Apparent continuity between the messenger transport organizer and late RNA localization pathways during oogenesis in *Xenopus*. *Mech. Dev.* **73**, 95–106.
- Kloc, M., Larabell, C. & Etkin, L.D. (1996). Elaboration of the messenger transport organizer pathway for localisation of RNA to the vegetal cortex of *Xenopus* oocytes. *Dev. Biol.* **180**, 119–30.
- Kloc, M., Bilinski, S., Dougherty, M.T., Brey, E.M. & Etkin, L.D. (2004). Formation, architecture and polarity of female germline cyst in *Xenopus*. *Dev. Biol.* **266**, 43–61.
- Klymkowsky, M.W., Maynell, L.A. & Polson, A.G. (1987). Polar asymmetry in the organization of the cortical cytokeratin system of *Xenopus laevis* oocytes and embryos. *Development* **100**, 543–57.
- Kress, T.L., Yoon, Y.J. & Mowry, K.L. (2004). Nuclear RNP complex assembly initiates cytoplasmic RNA localization. *J. Cell Biol.* **165**, 203–11.
- Ku, M. & Melton, D.A. (1993). Xwnt11: a maternally expressed wnt gene. *Development* **119**, 1161–73.
- MacArthur, H., Houston, D.W., Bubunenko, M., Mosquera, L. & King, M.L. (2000). DEAD_{South} is a germ plasm specific DEAD-box RNA helicase in *Xenopus* related to eIF4A. *Mech. Dev.* **95**, 291–5.
- Mosquera, L., Forristall, C., Zhou, Y. & King, M.L. (1993). An mRNA localized to the vegetal cortex encodes a protein with a nanos-like zinc finger domain. *Development* **117**, 377–86.
- Neuman-Silberberg, F.S. & Schüpbach, T. (1996). The *Drosophila* TGF- α -like protein Gurken: expression and cellular localization during *Drosophila* oogenesis. *Mech. Dev.* **59**, 105–13.
- Nilson, T.L.A. & Schüpbach, T. (1999). EGF receptor signaling in *Drosophila* oogenesis. *Curr. Top. Dev. Biol.* **44**, 203–43.
- Roth, S. (2003). The origin of dorsoventral polarity in *Drosophila*. *Phil. Trans. R. Soc. Lond. B Biol. Sci.* **358**, 1317–29.
- Schüpbach, T. & Wieschaus, E. (1986). Germline autonomy of maternal-effect mutations altering the embryonic body pattern of *Drosophila*. *Dev. Biol.* **113**, 443–8.
- Tao, Q., Yokota, C., Puck, H., Kofron, M., Birsoy, B., Yan, D., Asashima, M., Wylie, C.C. & Heasman, J. (2005). Maternal Wnt11 activates the canonical wnt signaling pathway required for axis formation in *Xenopus* embryos. *Cell* **120**, 857–71.
- Thomsen, G.H. & Melton, D.A. (1993). Processed Vg1 protein is an axial mesoderm inducer in *Xenopus*. *Cell* **74**, 433–41.
- Vaccaro, M.C., De Santo, M.G., Caputo, M., Just, M., Tian, J.D., Gong, H., Lennarz, W.J. & Campanella, C. (2001). Primary structure and developmental expression of DP ZP2, a vitelline envelope glycoprotein homolog to ZP2, in *Discoglossus pictus*, one of the oldest living anuran species. *Mol. Rep. Dev.* **59**, 133–43.
- Vaccaro, M.C., Gigliotti, S., Graziani, F., Carotenuto, R., De Angelis, C., Tussellino, M. & Campanella, C. (2010). A transient asymmetry of XNOA 36 mRNA and associated spectrin network bisects stage I oocytes along the future A/V axis in *Xenopus laevis*. *Eur. J. Cell Biol.* **89**, 525–36.
- Yisraeli, J.K., Sokol, S. & Melton, D.A. (1990). A two-step model for the localization of maternal mRNA in *Xenopus* oocytes: involvement of microtubules and microfilaments in the translocation and anchoring of Vg1 mRNA. *Development* **108**, 289–98.
- Wilding, M., Carotenuto, R., Infante, V., Dale, B., Marino, M., Di Matteo, L., Campanella, C. (2001). Confocal analysis of the activity of mitochondria contained within the 'mitochondrial cloud' during oogenesis of *Xenopus laevis*. *Zygote* **9**, 347–52.
- Zhang, J., Houston, D. W., King, M. L., Payne, C., Wylie, C. & Heasman, L. (1998). The role of maternal VegT in establishing the primary germ layers in *Xenopus* embryos. *Cell* **94**, 515–24.

The vitelline envelope and jelly coats of *D. pictus* egg

The source of inspiration for our research came from the seminal works by Chiaki Katagiri, Jerry Hedrick and Bill Lennarz (SUNY, Stony Brook, New York) on the role of vitelline envelope glycoproteins in *Xenopus*, *Rana* and *Bufo* fertilization. When we started this investigation, we had already collected a tremendous amount of ultrastructural information about sperm-VE and sperm-plasma membrane interaction. We were convinced that *D. pictus* could offer a good model for this study. Mariangela Caputo, Carmen Vaccaro and Enzo Infante embarked on painstaking studies on the subject. Mariangela de-



Fig. 20. 1988. At the Sapporo meeting organized by Chiaki Katagiri. From the left, Chiaki, Kazufumi Takamune, next to me Laurinda Jaffe, Daniel Danilchik, Karol Hedrick, Jerry Hedrick. In the first row Michel Charbonneau on the left and on the far right Rick Elinson and Yasuhiro Iwao.



Fig. 21. 1997. At the next Symposium in Sapporo on the Molecular and Cell Biology of Egg and Embryo and Egg coats, at dinner with Vic Vacquier, Rosaria De Sanctis, Rosaria Pinto, W.J. Swanson, Bill Lennarz, Paolo Gasparini, Motonori Hoshi.

scribed the changes occurring in the VE during the transition of the oocyte in the oviduct, changes that made the VE able to interact with sperm. In particular, a glycoprotein of 61 kDa is further glycosylated and undergoes a shift of its apparent Mr from 61 to 63 kDa. In Bill Lennarz's laboratory, Carmen determined the primary structure of the 63 kDa glycoprotein of VE, and found that is homolog of mouse ZP2. Enzo, together with Mariangela and Carmen, studied the sperm-binding activity of the main glycoproteins in the envelope and found that gp 63 and gp75 are glycoforms of the same polypeptide and are able to specifically bind sperm. Following fertilization these glycoproteins change their glycosylation characteristics. An F-layer forms similarly to other anuran species. Eventually, Mariangela studied the importance of sulphate groups in spermatozoa binding, the final part of her PhD thesis. She demonstrated that these groups are present in gp75 glycoconjugates and probably located in O-linked chains.

In studying *D. pictus*, one of the oldest living anuran species we were able to demonstrate that the basic mechanisms of envelope conversion from CE to VE and then from VE to FE are quite conserved during evolution in

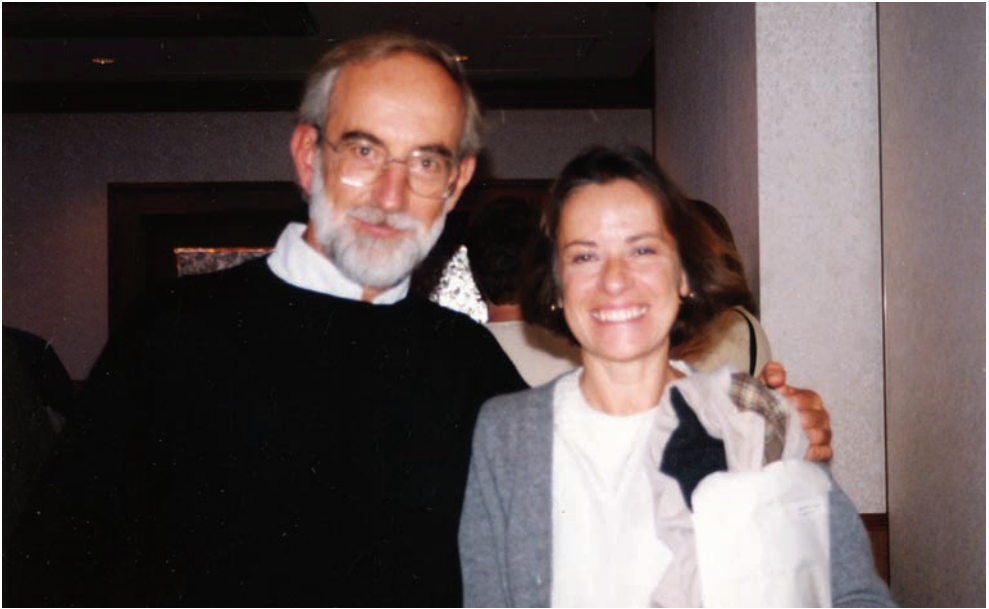


Fig. 22. At the 1997 Sapporo Symposium with Vic.



Fig. 23. At the 1997 Sapporo Symposium with Loise Epel, Chiaki, Paolo Gasparini, Mineko Katagiri.



Fig. 24. 1998. In my lab, from left Carmen Vaccaro, Rosa Carotenuto, Annarita Cimmino, Stefania Riccio, Enzo Infante, Mariangela Caputo.



Fig. 25. 1998. At Chia Laguna meeting. From left Mariangela, Roberta Amirante, Enzo, Shin-Ichi Abe.

amphibians. It was a pleasure to present these data at the Meeting in “ Fertilization in *Xenopus* and other amphibians Amphibian” (a satellite of the 7th International *Xenopus* Conference) at Chia Laguna, organized in 1998 by Gianni Bernardini and myself.

When I became full Professor, I spent four years at the University of L’Aquila (1986-1991) where I met Silvestro Duprè and his young researchers Giusi Pitari and Giovanni Maurizi. With them and with Carlo Fusco, my first student there, we performed experiments based on the expertise of Silvestro in oxidative-reduction reactions and on the fact that the jelly coats of the *D. pictus* egg is dissolved by DTT or DTE. We found that, following fertilization, a natural dissolution of the jelly plug occurs, caused by exocytosis of vacuoles and PAS-positive granules: the egg becomes a full sphere and rotates in the space created by plug liquefaction. This striking phenomenon had been filmed some time before by Riccardo and I was able to show it at a Congress in Sapporo, Japan. Plug dissolution involves peroxidase activity and oxidative opening of disulphide bonds.



Fig. 26. 1989. Giusi Pitari and Giovanni Maurizi, in Silvestro Duprè laboratory at L’Aquila.

Post-fertilization changes in *Discoglossus pictus* (Anura) eggs result in the formation of a capsular chamber where the egg rotates

CHIARA CAMPANELLA^{1*}, FILOMENA AMORE², GIUSEPPINA PITARI¹, CARLO FUSCO¹, GIOVANNI MAURIZI¹ and SILVESTRO DUPRÉ³

¹Dipartimento di Scienze e Tecnologie Biomediche e di Biometria, Collemaggio, L'Aquila, ²Dipartimento di Biologia Evolutiva e Comparata, Università di Napoli, Napoli and ³Dipartimento di Scienze Biochimiche, Università di Roma La Sapienza, Roma, Italy

ABSTRACT *Discoglossus pictus* is one of the few anurans with an egg where a capsular chamber forms as a consequence of fertilization; the egg with its vitelline envelope rotates in this chamber according to gravity. We investigated the formation of the capsular chamber through various experimental cytochemical and ultrastructural approaches, and found that it is the product of plug liquefaction. The plug is a lens-shaped jelly coat typical of *Discoglossus*, and covering only part of the egg animal half. About 15 min after fertilization, granular material coming from the egg enters the plug, which gradually dissolves and, once liquefied, reorganizes itself around the entire egg, thus forming the chamber. This process goes through stages of rearrangement of the 25-Å- and 250-Å-thick filaments which constitute the plug matrix. The material entering the plug derives from the exocytosis of two vacuole types, with electron transparent and granular PAS-positive contents. Liquefaction of the plug correlates with the reduction of disulfide bonds present in its matrix. Furthermore, *in vitro* tests showed that the substances released from the egg are active in selectively dissolving only the plug, and lose activity upon boiling.

KEY WORDS: Anuran egg, capsular chamber, jelly liquefaction, thiol groups

Introduction

Amphibian eggs are endowed with the vitelline envelope (VE) and several jelly layers. In anurans, cortical granule (CG) exocytosis takes place a few min following fertilization. As a consequence, the VE lifts from the egg surface and is transformed into the fertilization envelope (FE) (for a review, see Schmell et al., 1983). The perivitelline space enlarges and the egg becomes free to rotate in this space according to gravity. Rotation is essential for correct embryonic development. Information for dorsality resides in the vegetal and equatorial regions of the egg. If, during grey crescent formation, such regions are not positioned according to gravity, the embryo dorsal axis does not form correctly (for a review, see Wakahara, 1989).

In urodele eggs, CG's are absent, and the VE as well as the perivitelline space does not appear to change upon fertilization. The so-called capsular chamber forms from transformation of the innermost jelly layer, (J_1) (Salthe, 1963). This change occurs independently of fertilization in *Pleurodeles*; large granules are present in J_1 , which slowly dissolves upon ovideposition in the water (Jego

et al., 1986). As a consequence of J_1 transformation, the egg rotates together with its VE in the capsular chamber.

However, urodeles and anurans do not always show distinct patterns of egg investment transformation. Indeed, among anurans, capsular chambers form in the eggs of genera belonging to the same superfamily, *Discoglossidae* (*Alytes* and *Discoglossus*) or to evolutionarily distant families, *Leptodactylinae* (*Eleuterodactylus*) and *Pipidae* (*Pipa*), indicating that this process has developed independently of evolutionary trends (Wintrebert, 1928; Salthe, 1963).

The animal hemisphere of the *D. pictus* egg has a large depression, the *concavity*; at its center there is a small indentation, the *dimple*, which is filled with a fibrillar electron-dense material (Hibbard, 1928; Campanella, 1975). The central portion of the

Abbreviations used in this paper: J_1 , jelly 1; J_2 , jelly 2; J_3 , jelly 3; FE, fertilization envelope; D1, dimple 1; D2, dimple 2; D3, dimple 3; DTNB, 5,5'-dithiobis (2-nitrobenzoic acid).

*Address for reprints: Dipartimento di Biologia Evolutiva e Comparata, Università di Napoli, via Mezzocannone n.8, 80134 Napoli, Italy. FAX: 81-552.7807.

0214-6282/92/\$03.00

© UBC Press
Printed in Spain

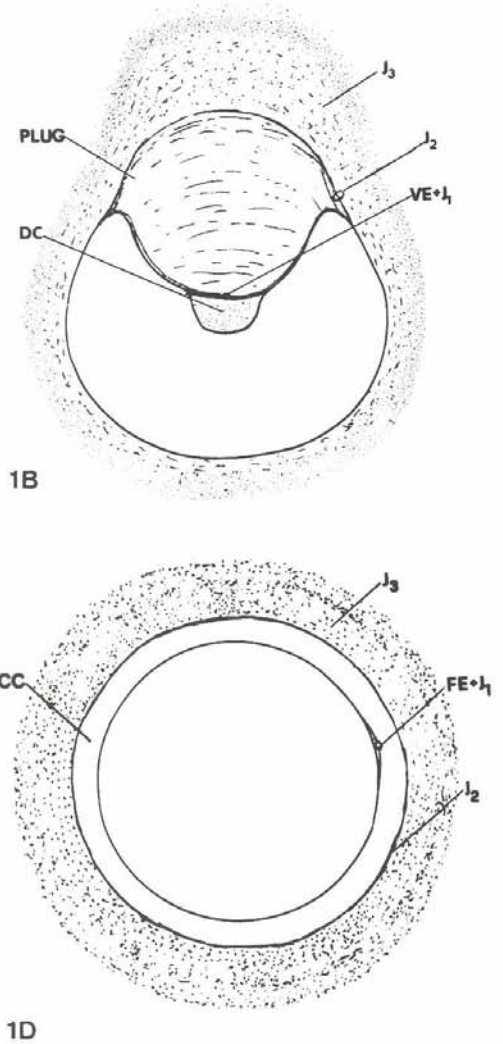
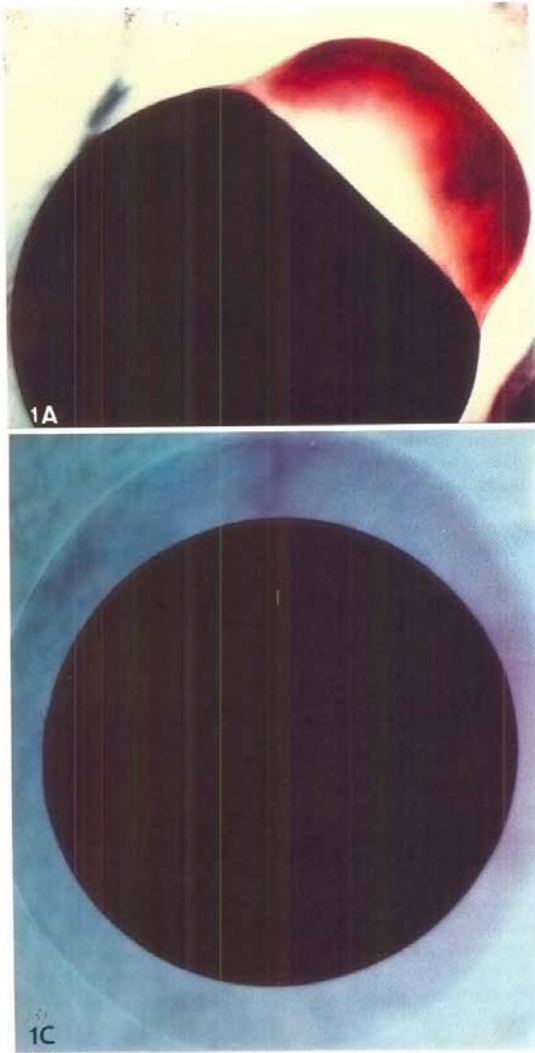


Fig. 1. Egg of *Discoglossus pictus* vitally stained with toluidine blue. J_3 =jelly 3; J_2 =jelly 2; J_1 =jelly 1; VE= vitelline envelope. (A) Unfertilized uterine egg. The plug is purple. (x48). (B) Schematic drawing of a longitudinal section of a *D. pictus* egg. D= dimple. The plug is sitting at the center of the animal hemisphere, in the concavity, which is typical of the eggs belonging to the genus *Discoglossus*. (C) Capsular chamber in a fertilized egg. The chamber is violet and externally delimited by J_2 (x50). (D) Schematic drawing corresponding to Fig. 1C and showing the capsular chamber. FE= Fertilization Envelope.

dimple, D1, is the site where fertilization occurs, whereas D2 and D3 are the dimple lateral walls (Talevi and Campanella, 1988). The concavity forms during the passage through the oviduct, because of the gradual deposition of the jelly plug. In oviposited eggs, the lens-shaped plug is surrounded by a thin jelly coat, J_2 , and the more

conspicuous J_3 . The presence of the plug at the animal hemisphere and of J_3 , which is three-fold thicker on the plug, gives the egg a typical asymmetrical configuration (Fig. 1). The plug sits on J_1 , which together with the VE constitutes the innermost egg envelopes (Ghiara, 1960; Denis-Donini and Campanella, 1977).

The plug has the specific characteristic of causing convergence of sperm on the dimple (Talevi and Campanella, 1988; Talevi, 1989).

At present the cytological as well as the physio-chemical basis of the capsular chamber formation is unknown in anurans.

This paper describes the formation of the capsular chamber in *Discoglossus pictus* and analyzes the factors involved in this process.

Results

Description of the capsular chamber formation

In *D. pictus* eggs, about 4 min after fertilization the dimple regresses, and a few minutes later, the concavity disappears (Campanella *et al.*, 1986; Campanella, 1991).

A total of sixty eggs from 15 females were inseminated and scored for these changes. While dimple disappearance can be easily determined only in dejellied eggs, the changes in the concavity can be depicted also in jellied eggs as they involve a more superficial region of the animal hemisphere (see Talevi and Campanella, 1988). The concavity regression depended upon modifications of the plug; it started 7 to 20 min after fertilization. This delay varied according to the egg clutches. The process is described in Figs. 2 and 3. Under incident light microscope, a sudden lifting could be observed at the center or the limits of the concavity (Fig. 2A,B) which extended to the rest of this region in about five min (Fig. 2C). Under the compound microscope, the first stage of this phenomenon appeared to be a sudden contraction of the concavity and a concomitant release of granular material from the egg (Fig. 2). This was followed by relaxation and lifting of the concavity and a loss of viscosity of the plug matrix. Several large globules (5-10 μm in diameter) could be seen in the plug. They migrated towards J_2 , at the plug boundary, with a velocity increasing with the loss of plug viscosity.

Plug liquefaction was accomplished in about 20 min and was also indirectly revealed by a gradual shift of the sperm bundle which had been spanning the plug since insemination (compare Fig. 2D with E).

A space, the capsular chamber, formed all around the egg because of the expansion of the plug-derived material (Fig. 1B) and changes that will be described below. The egg positioned itself in the chamber according to gravity.

The temporal relationship between egg material entering the plug and plug matrix dissolution clearly suggests that such material contains factor(s) which cause its liquefaction.

Cytological and ultrastructural observations of egg sections

In sections of eggs fixed at early stages of the reaction (10 min after fertilization), the cortex of the concavity (see Fig. 1B) contained PAS-positive granules, about 1.5 μm in diameter (Fig. 3A,B). At this stage, some of the granules as well as PAS-negative clouds were found outside the egg in the perivitelline space at the concavity (Fig. 3B). The latter contained a fibrillar matrix, the dimple content (see Fig. 1B), which had spread to the entire concavity as a result of dimple regression.

PAS-positive granules were not cortical granules because the latter had been exocytosed from the dimple within 2-3 min following activation (see Campanella *et al.*, 1988); this exocytosis will be here referred to as "primary exocytosis".

Ultrathin sections of eggs fixed at the beginning of the reaction

showed two types of vacuoles in the regressed dimple both at the peripheral cytoplasm and close to the plasma membrane. One type included about 0.4 μm large vacuoles with little electron-dense content and a small invagination of the limiting cytomembrane (Fig. 4A, B). The second type included 1.3- μm -large vacuoles with sparse fibrillar contents (Fig. 4A); because of their size and ultrastructural features, they might correspond to the PAS-positive granules. Both types of vacuoles could be seen along the whole egg periphery.

Several cases of vacuole exocytosis could be depicted due to the presence of invaginations containing a matrix dissimilar from that present on the egg surface and of hybrid membranes deriving from vacuole membranes and the oolemma (Fig. 4A,B,C) (see Campanella *et al.*, 1986). The exocytosed material was either granular (Fig. 5) or electron-transparent (Figs. 4 and 5B) and could be seen on the egg surface, in VE-J1 (Fig. 5C and D), as well as in the plug where it was concentrated in spherical, 3-4 μm large aggregates (Fig. 5B).

In eggs fixed when plug liquefaction became evident, most vacuoles had been exocytosed. Correspondingly, the plug matrix, which was made of alternating layers of thin and coarse fibers (Fig. 5B), had profoundly changed. The coarse-fiber layers had disaggregated, the fine filament layers had wound into globules up to 10 μm in diameter (Fig. 6), i.e., of the same size as those depicted under the compound microscope.

During this process, J_1 appeared largely unaffected despite some loosening of its matrix (see Fig. 5B and D). Both J_2 and J_3 were morphologically unaltered. However, during the final stages of the capsular chamber formation, J_3 was redistributed over J_2 in a more homogeneous fashion than in the unfertilized egg (Fig. 1B), as observed in *in vivo* conditions.

In conclusion, exocytosis is involved in the plug liquefaction process and two kinds of vacuoles appear to contain factors causing this phenomenon. This exocytosis will be here referred to as "secondary exocytosis".

Involvement of disulfide-bond reduction in plug liquefaction

It is known from laboratory practice that amphibia jelly coats are dissolved by thiols such as DTT or cysteine, because of the presence in the jelly of disulfide bonds (Gusseck and Hedrick, 1971). This observation suggests that a disulfide-bond reduction in plug proteins might be involved in plug dissolution.

Table 1 shows the results of SH-and-S-S content dosage of plug proteins obtained in three different experiments.

Following fertilization the content of free thiol groups became 4 to 10 times higher, whereas the content in disulfides dropped in a similar way. Similar trends were obtained when the concentrations were referred either to the egg or protein concentration.

Sonication of plugs completely solubilized the proteins of fertilized eggs, whereas parts of the plug proteins deriving from unfertilized eggs were less soluble; the less soluble proteins were richer in -SH groups. The data in Table 1 concern the total protein fraction, and are very similar before and after TCA precipitation; the contents in thiols or disulfides of the supernatant after TCA precipitation is below detection limits (<0.5nmol).

Denaturation with urea had a minor effect on free thiol group concentration, whereas it allowed the determination of a larger number of disulfide bonds.

The plug might be contaminated by a small amount of J_3 during manual dissection. The determination of thiol and disulfide content of J_3 was performed on unfertilized and fertilized eggs. Results did not change following fertilization; the amount of free thiol groups

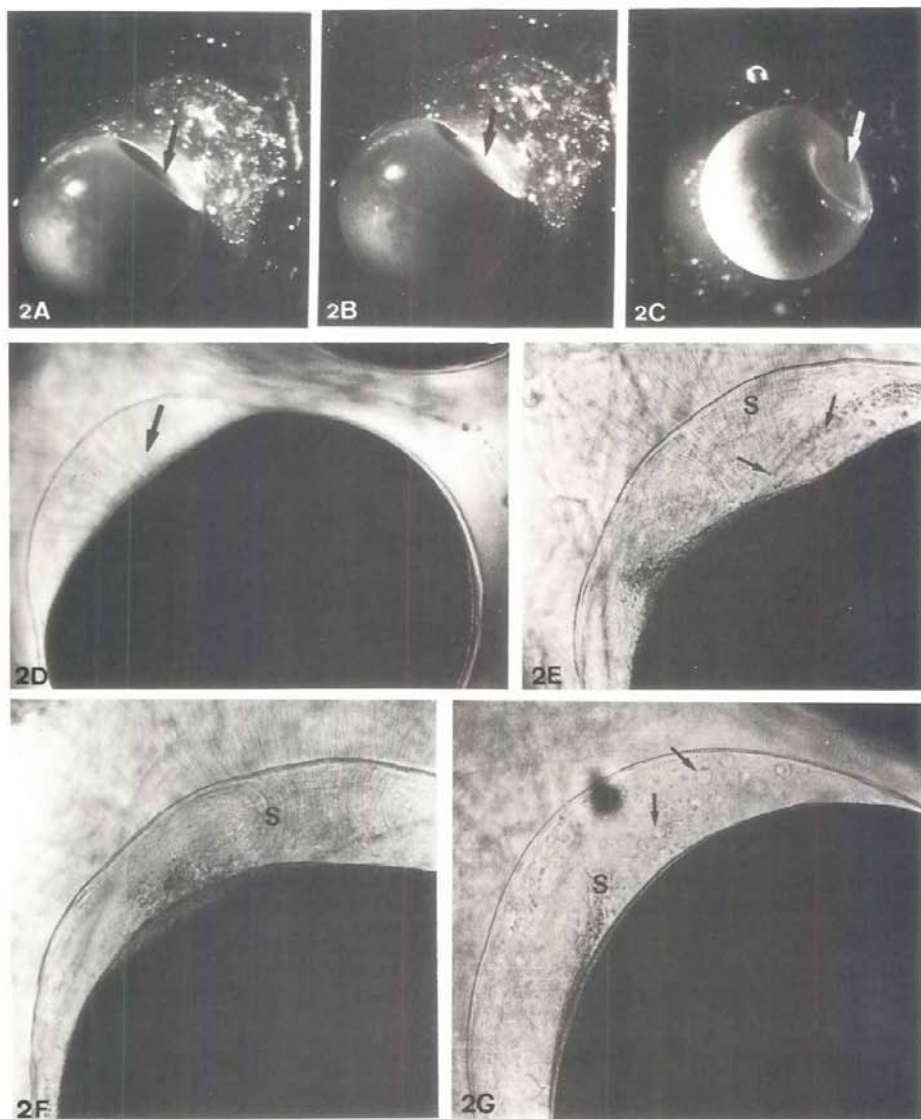


Fig. 2. Eversion of the concavity. (A-C) Sequence depicting the eversion of the concavity at the animal hemisphere (arrow at incident light during the capsular chamber formation. (x20). (D) Freshly inseminated eggs, under the compound microscope. The arrow indicates the spermatozoa converging on the plug. (x46). (E) Egg 18 min after fertilization. Granular material (small arrow) enters the plug, which starts liquefying. S= spermatozoa. (x55). (F) Five min from the onset of the reaction, plug liquefaction takes place, as indirectly evidenced by the sperm (S) shift, the expansion of the space occupied by the plug and the changes in the plug matrix. (x55). (G) At the final stage of liquefaction herein indicated, large globules can be seen in the liquefied plug (small arrow). S= spermatozoa. (x55).

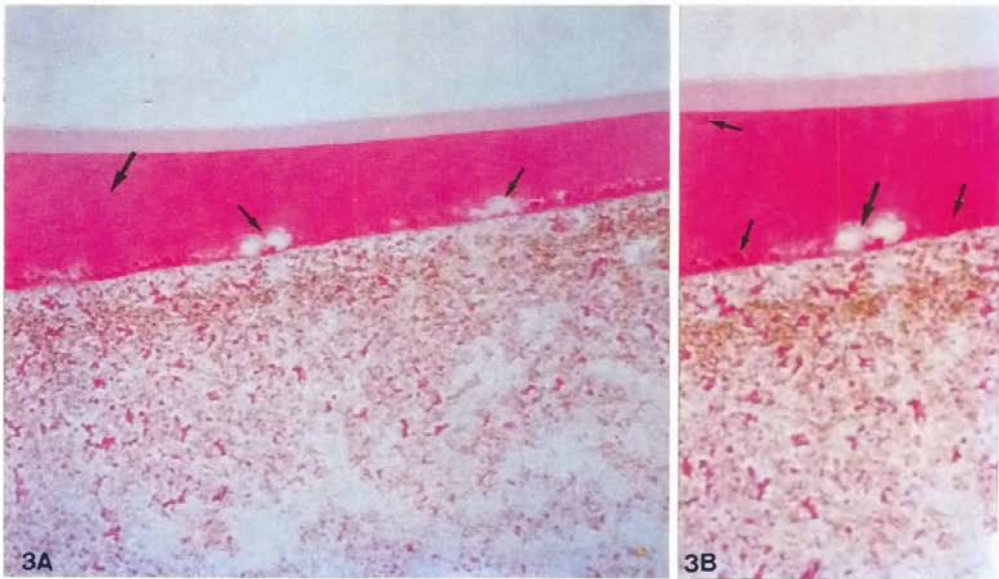


Fig. 3. Resin-embedded sections stained with PAS. (A) Egg at the onset of the plug liquefying reaction. The extracellular material indicated by the arrow is the dimple content (DC) which occupies most of the concavity, i.e., an area larger than the dimple of unfertilized eggs. The DC is very intensely PAS-positive. On the egg surface (small arrows) one can see several unstained areas which depict PAS-negative material derived from the egg. In the concavity, such granules were also found in the bulk of the cytoplasm for 1/3 of the egg depth. On the periphery of the rest of the egg, PAS-positive granules were located in the cortex as well as in a 200- μ m-thick belt (data not shown) ($\times 320$). **(B)** At a larger magnification, PAS-positive granular material can be seen in the egg peripheral cytoplasm, on the egg surface and in the DC (small arrows). The arrow indicates PAS-negative material. ($\times 1000$).

was negligible (<0.15 nmol/egg; <5 nmol/mg protein) and the concentration of disulfides was about 1 nmol/egg (about 40 nmol/mg protein). Therefore, contamination of plugs by J_3 , if present, did not alter the experimental data in Table 1. These data indicate that plug liquefaction correlates with disulfide-bond reduction. The latter does not involve the most conspicuous egg jelly layer, J_3 .

In vitro tests

In order to ascertain the biological activity of the material exocytosed from the egg, the following experimental procedure was performed.

Clutches of eggs were inseminated and scored for timing the arousal of plug liquefaction. Thereafter sets of 10 eggs were inseminated and readily immersed in 5 mM dithiothreitol (DTT), 0.1 M NaCl, 0.01 M Tris-HCl buffer, pH 8.0. The outermost jelly layers were removed in about 5 min by chemical treatment and with the help of fine forceps. Following several rinses, the eggs, endowed only with the VE-J1 complex, were placed in fresh 1/10 Ringer before the secondary exocytosis had occurred. Fifty min later, the Ringer (about 150 μ l) where the eggs were soaking (*egg Ringer*) was transferred to a new dish. A freshly dissected plug of unfertilized egg, partially surrounded by VE-J1 and J_2 , was immersed in the egg Ringer together with a piece of J_3 as control and observed for changes in its matrix. In all the experiments (10 tests), the plug dissolved about 30 min later, while the other jelly coats did not

change. This indicates that the exocytosed material present in the egg Ringer has the specific ability to liquefy only the plug matrix. Egg Ringer collected upon soaking of the eggs 20 min following insemination was not effective in plug dissolution, while this ability was found in egg Ringer collected between 45-60 min after insemination, indicating that under the experimental conditions here used, it takes longer for the reaction to be accomplished (see previous paragraph) than under natural conditions.

Similar results were obtained with egg Ringer from artificially (A23187) activated eggs; when dissected plugs were challenged with egg Ringer produced by these activated eggs, they were dissolved as in the fertilization experiments. As controls, Ringer was tested, recovered either at the time of primary exocytosis (see Materials and Methods) or from unactivated eggs soaking for at least 60 min; neither sample was active. Furthermore we could determine that the egg Ringer loses its activity as a result of heating at 90°C for 5 min.

In a second group of experiments, following jelly removal, A23187 exposure, primary exocytosis occurrence and rinsing, the eggs were placed in a quartz cuvette containing fresh 1/10 Ringer and the surrounding solutions read at the spectrophotometer at 280 nm against a blank of Ringer containing an equal amount of dejected, unactivated eggs. In the 3 experiments performed, measurements indicated that within a few minutes, an approximately ten-fold increase in absorption occurred, followed by stabilization of

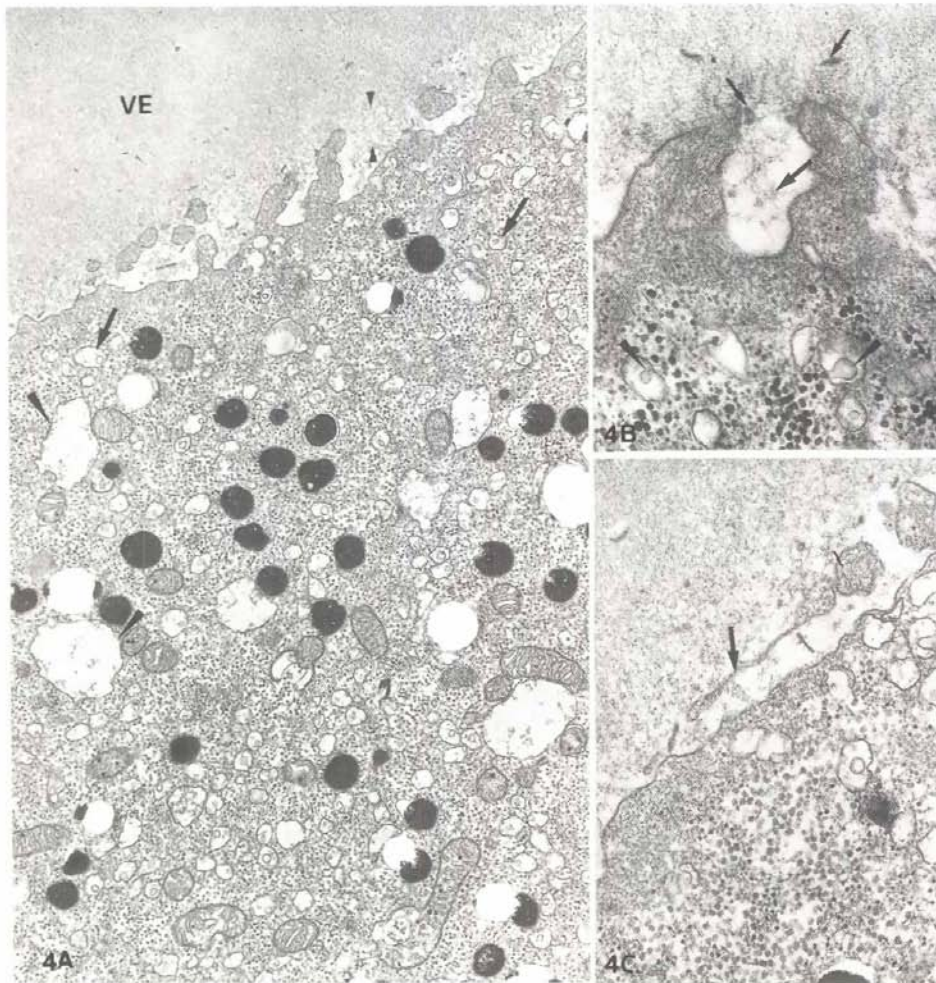


Fig. 4. Vacuoles involved in exocytosis. (A) Two classes of vacuoles can be seen in the dimple about 12 min after fertilization. They are located at the egg periphery, and especially beneath the plasma membrane. One is 0.4 μm large and is characterized by a small intravacuolar invagination of the limiting cytomembrane (arrows). The second vacuole is about 1.3 μm large and has sparse fibrillar content (arrowheads). On the egg surface, hybrid membranes are present, deriving from the exocytotic process. VE=vitelline envelope typically made of interwoven fibers. A shallow perivitelline space (arrowheads) containing fibro-granular matrix was located between the VE and the egg plasma membrane. (x18,500). **(B)** Example of vacuole exocytosis. The invagination contains a sparse matrix (arrow) different from that present on the egg surface and similar to that in the vacuoles. Hybrid membranes deriving from the vacuole membrane and the colemma are also found (small arrows). In *D. pictus* eggs, earlier stages of exocytosis are hardly found, as already indicated in previous papers (Talevi et al., 1985; Campanella et al., 1986). The arrowheads show internal invaginations of the 0.4- μm vacuoles. (x21,600). **(C)** Electron-transparent material is observed on the egg surface where large hybrid membranes are also present (arrow). The latter can be interpreted as deriving from multiple fusions of small vacuoles. (x35,000).

these values. Fig. 7 shows the time course of this process for three different experiments, followed at 280 nm; the egg suspension was shaken before each record. Assuming an average absorption

coefficient $A^{1\%}_{1\text{cm}}=15$ at 280 nm, about 1 μg protein per egg was liberated in the medium after 20 min. The absorption of the solution of untreated eggs, taken as control, was almost constant for 20

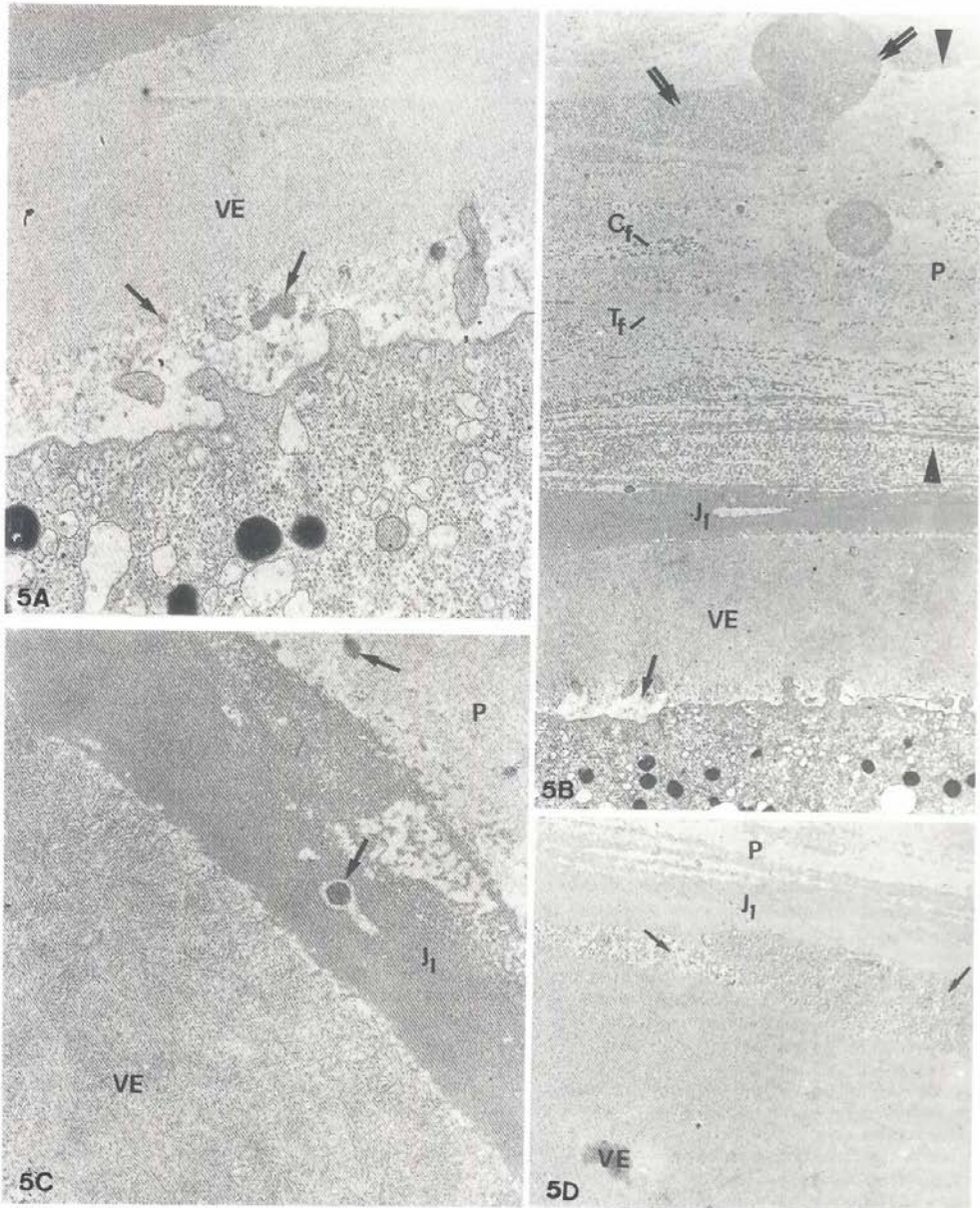


Fig. 5. Exocytosed material on the egg surface and investments. (A) Small aggregates of electron-dense material (arrows) can be observed next to the plasma membrane. (x27,000). (B) The exocytosed material is also present in electron-transparent regions (arrow) on the egg surface; in the plug (P), it is found in the shape of aggregates of fibro-granular material (double arrows). One can observe J_1 tightly packed and electron-dense constituents, as well as the alternating layers of coarse (Cf) and thin fibers (Tf) of the plug. (x9,000). (C and D) The exocytosed aggregates (arrows) are found in J_1 and in the plug (P). In D, a large mass of electron-dense material (small arrows) is present between VE and J_1 . In this layer, some loosening of its matrix occurs during plug liquefaction. (C= x40,000; D= x9,000).

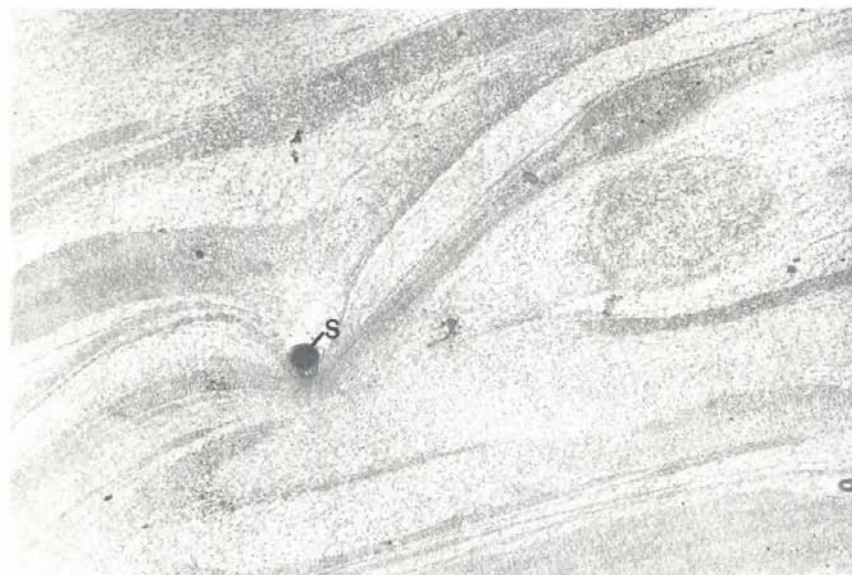


Fig. 6. Plug transformation during liquefaction. About 20 min after fertilization, the plug matrix layers of coarse fibers have disaggregated, the fine filament layers have wound up into globules up to 10 μm in diameter. S = sperm tail in cross section. ($\times 14,000$).

min. The raw material extruded from the egg following activation showed a free thiol content below the detection limits (<0.3 nmol-S-S per egg); after TCA precipitation the supernatant had about 6 nmol-S-S per egg, the proteic fraction about 30 nmol-S-S per egg. This fraction could be cross-contaminated with residues of the dissolved plug.

Discussion

We investigated the capsular chamber formation through *in vivo* observations, cytochemical and ultrastructural analysis as well as tests for protein and thiol group determinations. The results revealed new findings: (1) plug liquefaction occurs at fixed times following fertilization and is caused by substances released from the egg; (2) the phenomenon is temporally correlated with the exocytosis of two types of vacuoles containing at least two kinds of substances, one being PAS-positive; (3) plug liquefaction occurs through the reduction of disulfide bonds present in the plug gelatinous matrix; (4) the substances released from the egg contain components whose denaturation by heating determines a loss of the plug-liquefying activity.

Within 20 min from fertilization or activation an intraovular signal causes egg contraction and extrusion from the egg of substances which provoke plug liquefaction. The nature of the signal is unknown, but its effects can be discussed, as follows.

The timing of changes occurring in the plug suggests that coarse fibers are the first target of the exocytosed material, and fine filament layers get organized in large globules before dissolution. Other jelly layers do not show similar changes in plug matrix conversion. Accordingly, *in vitro* experiments the egg Ringer does not dissolve J_1 , J_2 and J_3 , indicating that the process which causes

plug liquefaction is highly specific for this jelly coat.

The capsular chamber may form all around the egg because a thin layer containing the plug matrix is present over the entire egg surface (data not shown). This indicates that during the passage through the oviduct, the plug matrix is deposited all around the egg as a thin layer except for the animal hemisphere portion surrounding and including the dimple where this jelly is deposited forming the conspicuous plug. The mechanism underlying this selectivity in jelly deposition will be the subject of a separate publication.

The material released from the egg, and then found on the egg surface as well as next to both sides of VE-J1, is contained in two types of vacuoles located along the entire periphery of the egg. One class of vacuoles can be easily detected under the light microscope because of its size (about 1.3 μm) and PAS-positivity. In the unfertilized egg, vacuoles with similar characteristics are present in the deeper region of the peripheral cytoplasm next to the endoplasmic reticulum clusters (Campanella *et al.*, 1988). Therefore it can be inferred that, following primary exocytosis, they have reached a more superficial position. Their sparse content and size make them similar to the acidic granules of the sea-urchin egg (Lee and Epel, 1983).

The second type of vacuoles — 0.4 μm large — is clearly detectable only in thin sections. In *D. pictus* unfertilized eggs, vacuoles similarly characterized by cytomembrane invaginations exocytose during "primary exocytosis" (Campanella *et al.*, 1986). The observed PAS-negative clouds of exocytosed material appear to correspond to the electron-transparent material observed under the electron microscope and may well derive from such vacuoles as no PAS-positivity was detected on granules smaller than 1 μm . However, cytochemistry on thin sections is needed to draw conclusions on this point.

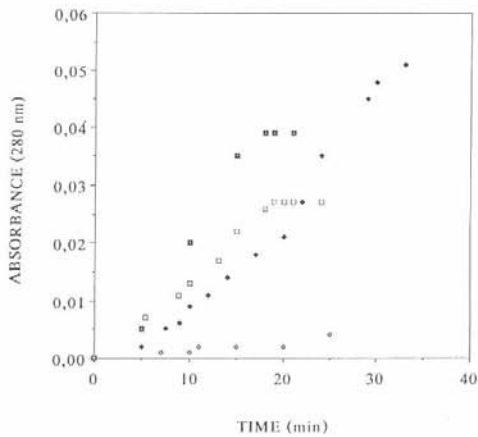


Fig. 7. Absorbance time course at 280 nm of solutions containing dejellied eggs activated by A23187. Three sets of experiments are reported. The eggs were placed in 1 ml 1/10 Ringer in the quartz cuvette after primary exocytosis had occurred. Blanks contained equal amounts of unactivated dejellied eggs; = 24 eggs; = 40 eggs; = 20 eggs; = blank of experiment.

Disulfide bridges are important intramolecular constituents of the amphibian jelly coat (Katagiri, 1963; Gussek and Hedrick, 1971). We have here shown that there is a clear increase of sulfhydryl groups in plugs examined at various stages of dissolution. Differences evidenced among the three sets of experiments may be related to the different conditions of jelly hydration, which, in turn, may be associated with seasonal conditions; eggs obtained from the ovisac in September-October are often surrounded by highly hydrated jelly. Data referring to fertilized eggs may be underestimated, because part of the dissolved plug was probably lost during collection.

The role of interchain-S-S bonds in stabilizing structural proteins and maintaining insolubility or higher levels of viscosity is well known. For example, acetylcystein liquefies mucus by acting directly on disulfide bonds of mucoproteins and thus lowering mucus viscosity.

It would be interesting to study whether the capsular chamber formation in *Pleurodeles waltii* (Jego *et al.*, 1986) shares some similarities with the process here described in *D. pictus*; the granules which dissolve in *Pleurodeles* innermost jelly layer might be active in the reduction of disulfide bonds.

The secondary exocytosis product contains the factors active in plug liquefaction; neither the egg Ringer of unactivated eggs nor the primary exocytosis product shares this activity with the egg Ringer.

As there is a precise temporal coincidence between vacuole exocytosis and the onset of plug dissolution, it can be concluded that vacuole content causes plug dissolution. However, it cannot be ruled out that other substances released from the egg through different mechanisms, may participate in this process.

Proteins probably rich in disulfide bridges are present in the "egg

Ringer". The fact that the activity of egg exudate was lost by boiling, strongly suggests that proteins are among the active factors causing plug dissolution. Studies are in progress to determine the nature of such proteins.

Early post-fertilization changes are well known to occur in the J_1 of other anuran eggs following CG exocytosis at the time of fertilization envelope (FE) formation (Wyrick *et al.*, 1974; Yoshizaki, 1984, 1989; Katagiri, 1987; Bakos *et al.*, 1990). Furthermore, at advanced stages of embryonic development, the hatching enzyme is secreted by a specific region of the embryo and causes dissolution of the jelly envelope (Carroll and Hedrick, 1974; Yamasaki *et al.*, 1990). To our knowledge, the present paper is the first to describe early post-fertilization changes in a jelly layer of anuran eggs, unrelated to FE formation and involving an exocytotic process.

Materials and Methods

Adult *Discoglossus pictus* males and females were captured near Palermo in Spring and kept in aquarium at 18°C. Gametes were collected and insemination was performed as previously described (Talevi and Campanella, 1988).

Composition of solutions used. Ringers (mM): 111.0 NaCl, 2.0 KCl, 1.3 CaCl₂, 0.8 MgSO₄; Hepes 25.0, pH 7.6. 10% Ringers (mM): 11.1 NaCl, 0.2 KCl, 0.13 CaCl₂, 0.08 MgSO₄; Hepes 2.5, pH 7.6.

Miscology

The eggs were observed at various post-fertilization stages under both a Zeiss stereomicroscope and a Leitz Orthomat compound microscope. Upon positioning of the egg, with a lateral view of the dimple and the concavity, plug dissolution sequence was followed. Photographs were made using Ilford Pan F film.

Some eggs were fixed at different times following fertilization. For light microscopy the samples were fixed in Carnoy's fixative, embedded in methyl methacrylate (JB-4 by Polyscience) and sectioned with a Reichert-Jung 2040/Autocut microtome. Four-micron thick sections were stained with PAS. Photographs were made using Ilford Pan F, Kodacolor, Ektachrome films. For electron microscopy the eggs were fixed in glutaraldehyde and embedded in Epon, as previously described (Talevi and Campanella, 1988).

Sulfhydryl and disulfide group determination, in vitro tests, protein assay

Eggs were washed in 1 mM HCl. Plugs from unfertilized eggs were manually dissected from the rest of the jelly coats. Similarly, plugs of

TABLE 1

CONCENTRATION OF THIOLS AND DISULFIDE GROUPS IN PLUGS AND J_1 FRACTIONS OF UNFERTILIZED AND FERTILIZED EGGS OF *DISCOGLOSSUS*

| | Experiment I | | Experiment II | | Experiment III | | jelly J_1 | |
|--------------------------|--------------|------|---------------|------|----------------|------|-------------|------|
| | plug | | plug | | plug | | u | f |
| eggs | u | f | u | f | u | f | u | f |
| µg protein/egg | 14 | 27.1 | 28 | 13.6 | 25 | 4.0 | 25 | 15 |
| -SH (nmol/egg)* | 0.26 | 2.60 | 0.20 | 2.80 | 0.30 | 0.85 | <0.13 | <0.1 |
| -S-S- (nmol/egg)* | 1.35 | 0.14 | 0.80 | 0.45 | 0.95 | 0.18 | 0.9 | 0.7 |
| -SH (nmol/mg protein)* | 15 | 94 | 15 | 207 | 60 | 246 | <5 | <6 |
| -S-S- (nmol/mg protein)* | 79 | 5 | 71 | 33 | 180 | 46 | 43 | 49 |

*Figures refer to data obtained after urea denaturation; u, unfertilized; f, fertilized.

fertilized eggs were manually removed at various stages of liquefaction. J_3 from unfertilized and fertilized eggs were also dissected from the egg and utilized as controls.

About twenty plugs or five J_3 were sonicated with an exponential tip sonicator (Lab Line Instr. Melrose, Il., U.S.A.) in ice for 20 sec at 40 W power, in 1 mM EDTA in order to solubilize the gelatinous matrix at a low pH and to avoid reoxidation of free sulfhydryl groups.

Titration with 5,5'-dithiobis (2-nitrobenzoic acid) (DTNB) (Ellman, 1959) was performed either on the sonicated solution as such or after TCA precipitation. The solution added with TCA (11% final concentration) was centrifuged after 15 min in the cold, and both the precipitate and the supernatant were collected. The proteic precipitate was dissolved in water by sonication.

For *in vitro* tests, aliquots of unfertilized eggs were de-jelled by the DTT treatment, rinsed in 1/10 Ringer, and immersed in 50 μ M A23187 for 2 min, then rinsed again. In the next 3-4 min there was contraction of the dimple followed by its disappearance, thus indicating that activation, including primary exocytosis, had occurred (Talevi et al., 1985; Campanella et al., 1986). About 15 min later, the eggs underwent secondary exocytosis, as evidenced by the transient whitening of the regressed dimple region. The activity of the Ringers containing "primary exocytosis" or "secondary exocytosis" products was tested on dissected plugs.

Tests for -SH were performed as follows. Samples (100-500 μ l) were adjusted to pH 8.5 by addition of diluted NaOH and Tris buffer, pH 8.5 (0.1 M final concentration) DTNB (1 mM in a final volume of 3.0 ml) was added, and absorption at 412 nm was recorded until constant values were reached (about 20 min).

To evaluate the concentration of disulfide groups, neutralized samples were first added with NaBH_4 (1-2 mg) and allowed to react for 30 min at room temperature. The solution was then acidified with 1 M HCl to destroy the reagent excess, brought to pH 8.5 with NaOH and Tris buffer pH 8.5 and added with DTNB as above. The amount of -SH groups was calculated by using the value $\Sigma = 13,600 \text{ M cm}$ (Ellman, 1959). The amount of -S-S- groups was calculated from the difference between the two sets of data. Determinations were in duplicate.

In some tests the solution, either as such or after TCA precipitation, was heated at 60°C in the presence of 6M urea before being processed further.

Proteins were determined by the Bio-Rad method, using BSA as standard protein.

Acknowledgments

We would like to thank Messrs G. Falcone and G. Argenzio for skilful micrograph printing. This paper is dedicated to Prof. G. Ghiara whose interest in *D. pictus* embryology represents a source of continuous inspiration and encouragement. The electron microscopy part of this research was carried out at the CIRUB of the University of Naples.

Supported by a 60% grant of the Italian MURST and by C.N.R. grant 91/654.

References

- BAKOS, M.A., KUROSKY, A. and HEDRICK, J.L. (1990). Physicochemical characterization of progressive changes in the *Xenopus laevis* egg envelope following oviductal transport and fertilization. *Biochemistry* 29: 609-615.
- CAMPANELLA, C. (1975). The site of spermatozoon entrance in the unfertilized egg of *Discoglossus pictus* (Anura): an electron microscope study. *Biol. Reprod.* 12: 439-447.
- CAMPANELLA, C. (1991). Fertilization in amphibians. *Symposium on the Evolution of Terrestrial Vertebrates* (Ed. G. Ghiara et al.). Selected Symposium and Monographs, U.Z.I. 4, Mucchi, Modena, pp. 205-224.
- CAMPANELLA, C., TALEVI, R., ATRIPALDI, U. and QUAGLIA, L. (1986). The cortical endoplasmic reticulum and its possible role in activation of *Discoglossus pictus* (Anura) eggs. In *Molecular and Cellular Biology of Fertilization* (Ed. J.L. Hedrick). Plenum Publish. Co., pp.185-203.
- CAMPANELLA, C., TALEVI, R., KLING, D. and NUCCITELLI, R. (1988). The cortical reaction in the egg of *Discoglossus pictus*: a study of the change in the endoplasmic reticulum at activation. *Dev. Biol.* 130: 108-119.
- CARROLL, E.J. and HEDRICK, J.L. (1974). Hatching in the toad *Xenopus laevis*: morphological events and evidence for a hatching enzyme. *Dev. Biol.* 38: 1-13.
- DENIS-DONINI, S. and CAMPANELLA, C. (1977). Ultrastructural and lectin binding changes during the formation of the animal dimple in oocytes of *Discoglossus pictus* (Anura). *Dev. Biol.* 61: 140-152.
- ELLMAN, G.L. (1959). Tissue sulfhydryl groups. *Arch. Biochem. Biophys.* 82: 70-77.
- GHIARA, G. (1960). Osservazioni sugli strati superficiali e corticali di ovociti e di uova di *Discoglossus pictus* (Oth) e di altre specie di Anfibi. *Arch. Zool. Ital.* 45: 9-92.
- GUSSEK, D.J. and HEDRICK, J.L. (1971). A molecular approach to fertilization. I. Disulfide bonds in *Xenopus laevis* jelly coat and a molecular hypothesis for fertilization. *Dev. Biol.* 25: 337-347.
- HIBBARD, H. (1928). Contribution à l'étude de l'ovogenèse chez *Discoglossus pictus*. *Ott. Arch. Biol.* 38: 251-326.
- JEGO, P., LERIVRAY, H., CHESNEL, A. and CHARBONNEAU, M. (1986). Urodele egg jelly and fertilization. In *The Molecular and Cellular Biology of Fertilization* Vol. 207 (Ed. J.L. Hedrick). Plenum Publ. Corp., pp. 205-230.
- KATAGIRI, C. (1963). On the fertilizability of the frog egg. III. Removal of egg envelopes from unfertilized egg. *J. Fac. Sci. Hokkaido Univ. Ser. VI.* 15: 202-211.
- KATAGIRI, C. (1987). Role of oviductal secretions in mediating gamete fusion in Anuran Amphibian. *Zool. Sci.* 4: 1-14.
- LEE, H.C. and EPEL, D. (1983). Changes in intracellular acidic compartments in sea urchin after activation. *Dev. Biol.* 98: 446-454.
- SALTHE, S.N. (1963). The egg capsules in the Amphibia. *J. Morphol.* 113: 161-171.
- SCHMELL, E.D., GULYAS, B.J. and HEDRICK, J.L. (1983). Egg surface changes during fertilization and the molecular mechanism of the block to polyspermy. In *Mechanism and Control of Animal Fertilization* (Ed. J.F. Hartman). Academic Press, NY, pp. 365-413.
- TALEVI, R. (1989). Polyspermic eggs in the anuran *Discoglossus pictus* develop normally. *Development* 105: 123-130.
- TALEVI, R. and CAMPANELLA, C. (1988). Fertilization in *Discoglossus pictus*. I. Sperm egg interactions in distinct regions of the dimple and occurrence of a late stage of sperm penetration. *Dev. Biol.* 130: 524-535.
- TALEVI, R., DALE, B. and CAMPANELLA, C. (1985). Fertilization and activation potentials in *Discoglossus pictus* (Anura) eggs: a delayed response to activation by pricking. *Dev. Biol.* 111: 316-323.
- YAMASAKI, H., KATAGIRI, C. and YOSHIZAKI, N. (1990). Selective degradation of specific components of fertilization coat and differentiation of hatching gland cells during the two phase hatching of *Bufo japonicus* embryos. *Dev. Growth Differ.* 32: 65-72.
- YOSHIZAKI, N. (1984). Immunoelectron microscopy demonstration on the pre-fertilization layer in *Xenopus* eggs. *Dev. Growth Differ.* 26: 191-195.
- YOSHIZAKI, N. (1989). Immunoelectron microscopic demonstration of cortical granule lectins in coelomic, unfertilized and fertilized eggs of *Xenopus laevis*. *Dev. Growth Differ.* 31: 325-330.
- WAKAHARA, M. (1989). Specification and establishment of dorsal-ventral polarity in eggs and embryos of *Xenopus laevis*. *Dev. Growth Differ.* 31: 197-207.
- WINTREBERT, P. (1928). Les changements de forme des membranes et de l'oeuf de *Discoglossus pictus* après la ponte. *Comp. Rend. Soc. Biol.* 72: 799-801.
- WYRICK, R.E., NISHIHARA, T. and HEDRICK, J.L. (1974). Agglutination of jelly coat and cortical granule components and the block to polyspermy in the amphibian *Xenopus laevis*. *Proc. Nat. Acad. Sci.* 71: 2067-2071.

Jelly plug dissolution in *Discoglossus pictus* eggs (Anura) involves peroxidase-like activity and oxidative opening of disulphide bonds

G. Pitari¹, S. Dupré², C. Fusco¹, G. Maurizi¹ and C. Campanella¹

Università dell'Aquila and Università di Roma 'La Sapienza', Italy

Summary

In amphibian eggs the formation of a capsular chamber is one of the most striking events occurring either upon oviposition or after fertilisation. In the egg of the anuran *Discoglossus pictus* a capsular chamber forms following fertilisation or activation; the egg with its vitelline envelope rotates in this chamber according to gravity. Previous work showed that the chamber is the product of plug dissolution. The plug is a lens-shaped jelly coat, typical of *Discoglossus*, covering only part of the animal hemisphere. Its dissolution is caused by material released from the egg about 15 min after fertilisation through exocytosis of at least two types of vacuoles. Liquefaction of the plug correlates with the reduction of disulphide bonds present in the jelly matrix. In this study we investigated the nature of the substances released from the egg and some changes occurring in the plug during liquefaction. SDS-PAGE showed that the proteic profile of the plug changes dramatically after fertilisation, confirming proteic cleavage in the plug matrix during its dissolution. Through *in vitro* tests and electrophoretic analysis of the Ringer solution in which the egg exudate was collected, an increase in the activity of the solution was determined in the presence of hydrogen peroxide, and peroxidase activity was depicted in the egg exudate. The presence of free thiol groups and cysteic acid residues (or cysteine sulphonic acid) in the plugs of activated eggs was established, suggesting that during plug dissolution some disulphide bonds are oxidatively opened. This suggests that enzyme(s) with peroxidase activity are released following fertilisation. We surmise that such enzymes are contained in the intraovular vacuoles the exocytosis of which triggers the onset of plug liquefaction. The possible release of hydrogen peroxide from the egg is discussed.

Keywords: Anuran eggs, Disulphide bonds, Peroxidase activity, Plug dissolution

Introduction

Post-fertilisation events occurring between fertilisation envelope formation and grey crescent segregation have been scantily investigated in amphibians. Among such events, one of the most striking is the formation of capsular chambers in urodeles and some anuran families.

Capsular chamber formation in *Discoglossus pictus*

(Anura) eggs has been described as a post-fertilisation event leading to changes in the jelly coat as well as in egg shape and position within its envelopes (Campanella *et al.*, 1992). A fertilisation envelope is not elevated in the egg of such species; therefore chamber formation is essential for the egg to rotate and for ensuring correct development of the embryo (Kao & Elinson, 1988; Wakahara, 1989). The chamber forms because of the dissolution of the plug, the lens-shaped gelatinous coat located in the animal hemisphere concavity of the *D. pictus* egg (Hibbard, 1928; Ghiara, 1960; Salthe, 1963). During this process the animal half is relieved of plug pressure and becomes spherical. About 15 min after insemination, exocytosis of two types of vacuoles with electron-transparent and granular periodic acid–Schiff (PAS)-positive content

All correspondence to: C. Campanella, Dipartimento di Biologia Evolutiva e Comparata, Università di Napoli, 80134 Napoli, Italy.

¹ Dipartimento di Scienze e Tecnologie Biomediche e di Biometria, Università dell'Aquila, Collemaggio, 67100 L'Aquila.

² Dipartimento di Scienze Biochimiche, Università di Roma 'La Sapienza', Rome, Italy.

occurs. The released material enters the plug, triggering its transition from solid to liquid. During dissolution, the plug matrix reorganises itself around the entire egg, thus forming the chamber (Campanella *et al.*, 1992).

Preliminary tests were performed on the Ringer solution in which the egg exudate was collected (egg Ringer) following activation of dejellied eggs. The presence of a plug-liquefying activity was determined, specifically acting on disulphide bonds present in the plug matrix. Indeed, reduction of disulphide bonds by egg Ringer has not been found in jelly coats other than the plug (Campanella *et al.*, 1992).

There are no data on the mechanism of capsular chamber formation in amphibian eggs; in particular, the biochemical implications and specificity of this event are unknown. In the present study the nature of the substances triggering plug liquefaction was studied. An increase in the activity of egg Ringer was determined in the presence of hydrogen peroxide, and peroxidase-like activity was depicted in the egg exudate. Furthermore, the presence of free thiol groups and cysteic acid (or cysteine sulphinic acid) residues in the plugs from activated eggs was established, suggesting that during plug dissolution some disulphide bonds are oxidatively opened.

Materials and methods

Adult *Discoglossus pictus* males and females were collected near Palermo, Italy, during spring and autumn, and kept in aquaria at room temperature. Gametes were collected, and insemination performed as previously described (Talevi & Campanella, 1988).

Amphibian Ringer composition is as follows (in mmol/l): NaCl, 110.0; CaCl₂, 1.3; KCl₂, 2.0; MgSO₄, 0.8; Hepes, 25.0; final pH 7.8.

In vitro tests

Eggs were dejellied by 5 mmol/l dithiothreitol (DTT) in Tris-HCl 50 mmol/l, NaCl 100 mmol/l, pH 8.0 (dejelling solution) for about 5 min at 20°C, and rinsed in Ringer. In this solution the plug and the outermost jelly coat J₃ are dissolved, while the next jelly coat J₂ first breaks into pieces and then dissolves. As a result, the eggs are surrounded by only the vitelline envelope (VE) and the innermost jelly coat J₁, which can be eliminated only after a more prolonged exposure to the dejelling solution. As a general control, untreated eggs were soaked for at least 60 min in Ringer, and then the Ringer was collected. Experimental eggs were activated by exposure to 50 µmol/l A23187 dissolved in Ringer for 2 min and rinsed again. In the next 3–4 min contraction of the dimple followed by its disappearance indicated activation, including

cortical granule exocytosis (primary exocytosis) (Talevi *et al.*, 1985; Campanella *et al.*, 1986). The Ringer containing the product of primary exocytosis was then collected, and the eggs were rinsed and transferred into new dishes. About 15–20 min later the eggs underwent the secondary exocytosis which triggers plug liquefaction (Campanella *et al.*, 1992). The Ringer containing such an egg exudate (the egg Ringer) was recovered and challenged with freshly dissected plugs to test its activity; plug dissolution was accomplished in about 40 min. Under natural conditions this process is accomplished in 20 min. The reason for this difference is unknown (Campanella *et al.*, 1992).

Preparation of samples and electrophoresis on polyacrylamide gel

The gelatinous extracellular plug partially surrounded by J₁ + VE and J₂ was manually dissected out from unfertilised (Fig. 1) and fertilised eggs at various stages of plug liquefaction. Plugs were transferred to 'sample buffer' containing mercaptoethanol, as described below, where they readily dissolved, while J₁ + VE and J₂ were not, and could be removed. Alternatively, when sample buffer without mercaptoethanol was used, the plugs were solubilised by sonication with an exponential tip Sonicator (Lab Line Instr., Melrose, IL, USA) in ice for 20 s at 40 W power in 0.1 mol/l Tris-HCl at low pH to avoid reoxidation of free sulphhydryl groups.

In order to collect J₁, DTT-treated eggs were further exposed for about 30 s to 0.6 mol/l KCl dissolved in 1:10 Ringer. By this treatment J₁s were fully solubilised; they were then dialysed against 0.1 mol/l Tris-HCl, pH 6.5, and concentrated with an Amicon Centricon (10 000 cut) by low-speed centrifugation.

The primary exocytosis Ringer, the secondary exocytosis Ringer and the Ringer of untreated eggs from several egg aliquots were pooled, added to 0.05% Triton X-100 and concentrated using an Amicon Centricon.

Protein concentration was measured with the Pierce microanalytic assay (Pierce Chemical Co.), using bovine serum albumin (BSA) as standard. We estimated that each egg produced egg Ringer containing about 0.2–0.5 µg protein and that each plug contained at least 5 µg protein.

Electrophoresis sample buffer, containing 1.5 mol/l mercaptoethanol, 0.013 mol/l sodium dodecyl sulphate (SDS), 0.9 mol/l glycerol and 0.001% bromophenol blue in 1.25 mol/l Tris-HCl, pH 6.8, was added to the samples, which were then boiled for 2 min. Alternatively, the same buffer lacking mercaptoethanol was used. The samples were run in 6%, 7.5% or 12% SDS-PAGE (polyacrylamide gel electrophoresis) using the Tris-glycine buffer system (Laemmli, 1970) and

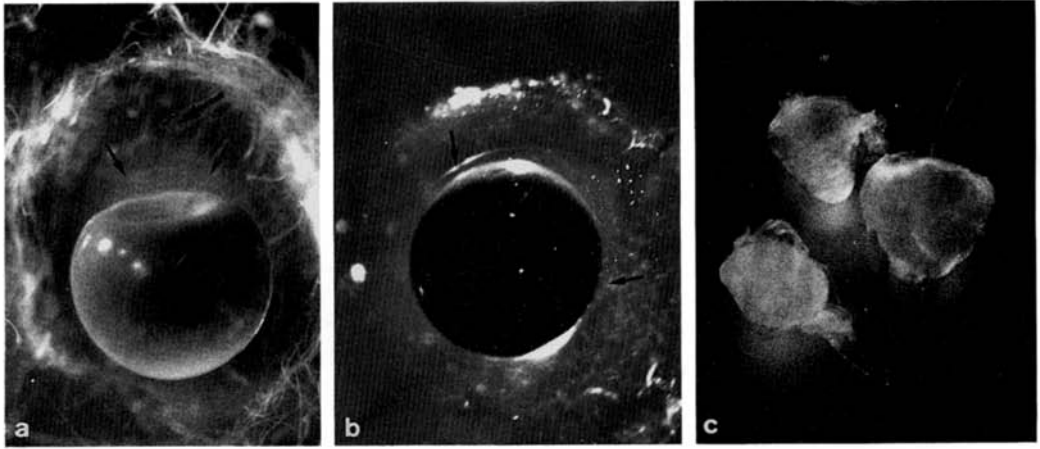


Figure 1 Isolated and *in situ* jelly plugs before and after capsular chamber formation ($\times 18$). (a) Freshly inseminated egg. A whitish mass of sperm surrounds the egg gelatinous coat. The small arrows indicate the plug boundary, which corresponds to J_2 . The large arrow indicates spermatozoa in the plug. (b) Egg about 30 min after insemination. The arrows indicate J_2 delimiting the capsular chamber. (c) Manually isolated plugs.

stained with Coomassie blue, silver staining, or PAS (Kapitany & Zebrowski, 1973). Five to eight micrograms of proteins were charged for each lane.

For the determination of catalase activity on polyacrylamide gels, samples were added with sample buffer containing 0.5 mol/l Tris-HCl, pH 6.8, 0.9 mol/l glycerol and 0.001% bromophenol blue and run at 4°C in a 7.5% gel in the absence of SDS and using 2 U bovine catalase (Sigma) as a control. The gels were then rinsed and exposed in sequence to 3.53 mol/l hydrogen peroxide, distilled water, 1% potassium ferricyanide and 0.5 mol/l ferric chloride (see Barja de Quiroga *et al.*, 1985).

Analytical techniques

Solutions of dissolved plugs were divided into small glass tubes and freeze-dried after the addition of known amounts of norleucine as internal standard.

Quantitative amino acid analyses were carried out on 1.5–20 μ g proteins hydrolysed in 0.2 ml 6 mol/l HCl at 110°C for 24 h in sealed evacuated tubes. The solution was then 'vacuum'-dried over NaOH and the residue dissolved in the buffer used for the amino acid analysis run; turbid solutions were filtered through a glass filter. Cysteine/cystine content as determined either after hydrolysis in the presence of 0.2 mol/l dimethylsulphoxide (DMSO) (Spencer, 1969) or after oxidation with performic acid (Hirs, 1967).

The amino acid composition of hydrolysed proteins was determined using a Pharmacia 4151 Alpha Plus instrument.

Electron microscopy

Unfertilised and fertilised eggs were fixed and embedded as previously described (Campanella *et al.*, 1992).

Results

Plug liquefaction activity

Previous data (Campanella *et al.*, 1992) indicated that egg Ringer activity causes a marked increase in free sulphhydryl group content in the plug matrix that starts at about 10–15 min after egg insemination and is lost upon boiling. Fig. 2 shows that the plug matrix is composed of thin and coarse filaments that gradually disappear after fertilisation. Since it was demonstrated by the foregoing observations that the beginning of plug dissolution is a very rapid phenomenon, the present aim was to identify enzymic activity in the egg Ringer.

Following secondary exocytosis the egg Ringer was collected and tested for activity on manually dissected plugs under control or experimental conditions. Timing for total plug dissolution was about 40 min (see also Campanella *et al.*, 1992). Dissolution activity was also tested in the presence of added compounds; the results in Table 1 summarise five sets of experiments utilising eggs from six females. NADPH and reduced glutathione are both components of the system, operating in many cells, which maintains thiol groups in their reduced state; their addition had no

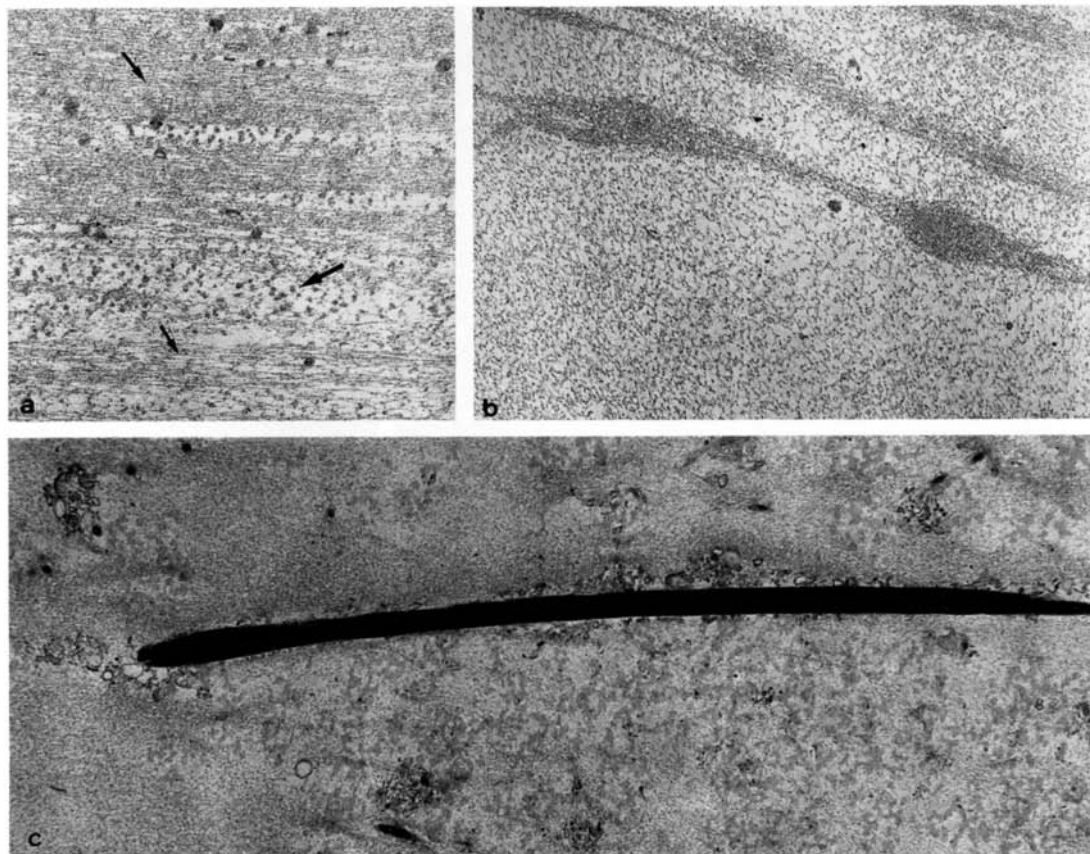


Figure 2 Thin sections of the jelly plug. (a) Unfertilised egg plug showing alternating layers of thin fibres (small arrows) and coarse fibres (arrow) ($\times 18\,000$). (b) Dissolving plug, about 20 min after fertilisation. The coarse fibres have disappeared, the thin fibres have collapsed ($\times 12\,000$). (c) Capsular chamber content. Some fibres are still present in the plug matrix, while flocculent material has appeared. The long electron-dense rod is part of the head nucleus of a spermatozoon lying parallel to the egg surface. It is surrounded by many vesicles thus indicating that it has undergone the acrosome reaction and is now degenerating ($\times 4\,000$).

effect on the dissolution activity of the egg Ringer. A specific trypsin inhibitor, SBTI, also had no effect. PMSF, a protease inhibitor which may react also with sulphhydryl groups at high concentrations, inhibited plug liquefaction. Strong inhibition was obtained with bromopyruvate. A dramatic increase in the dissolution rate occurred upon addition of $10\ \mu\text{mol/l}$ hydrogen peroxide, plugs being dissolved in about 1 min. The addition of 100 U catalase inhibited this process and up to 3 h were required to complete dissolution.

Electrophoretic analysis of plugs and egg products

SDS-PAGE analyses of proteins present in plugs of unfertilised eggs and eggs undergoing secondary

exocytosis showed some changes in the electrophoretic pattern of the plug during its dissolution. The presence of variable amounts of glycoproteins not entering the running gel was also observed.

Solubilised plugs from unfertilised eggs contained a prominent 37 kDa band and higher-molecular-weight proteins (Fig. 3, lane a). In the presence of mercaptoethanol, the pattern showed the disappearance of some of these proteins and the appearance of some lower-molecular-weight proteins including a 36 kDa band (lane b). This is in accordance with the high number of disulphide bonds reported in the plug (Campanella *et al.*, 1991); probably many of them are interchain bonds. In dissolving plugs of fertilised eggs less proteic bands were present either with mercaptoethanol (Fig. 3, lane

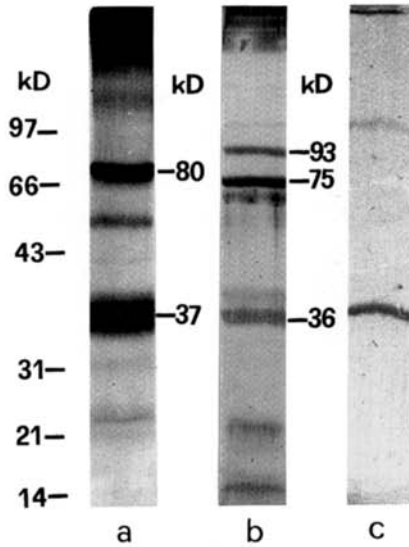


Figure 3 Plug electrophoretic analysis through 7.5% SDS-PAGE, silver stain. On the left are the molecular weight standards. (a) In the absence of mercaptoethanol, a high-molecular-weight protein and two prominent bands of 37 and 80 kDa are present. (b) In the presence of mercaptoethanol, several bands are separated, including proteins of about 36, 75 and 93 kDa. (c) About 20 min after fertilisation only two bands (under reducing conditions) are detectable in the liquefying plugs.

Table 1 Effect of the addition of some compounds to egg Ringer on the dissolution of isolated plugs

| Addition | Concentration | Effect |
|-------------------|-------------------|------------|
| NADPH | 5 μ mol/l | None |
| Glutathione | 5 μ mol/l | None |
| SBTI | 50 ng/200 μ l | None |
| PMSF | 2 mmol/l | Inhibition |
| Bromopyruvic acid | 2.5 μ mol/l | Inhibition |
| Hydrogen peroxide | 5 μ mol/l | Activation |
| Catalase | 100 U/200 μ l | Inhibition |

SBTI, soybean trypsin inhibitor; PMSF, Phenylmethanesulfonylfluoride.

Tested compounds at the given concentration were added to egg Ringer, collected as described in 'Materials and methods'. A 100–200 μ l aliquot of this solution was added to four isolated plugs and dissolution time was monitored. Inhibition means a dissolution time of more than 2 h; activation a time of less than 10 min.

c, where two proteins are present in plugs collected 20 min after insemination) or without mercaptoethanol (data not shown), indicating that both disulphide opening and protein cleavage are involved in plug dissolution.

A comparison was made between protein composition of egg Ringer, products of primary exocytosis, Ringer of untreated eggs (control Ringer) and J_1 , the only jelly coat remaining on the egg after dejellifying (Fig. 4). Comparable amounts of samples (see 'Materials and methods') were examined electrophoretically (7.5% and 10% polyacrylamide) and stained, as indicated below. On silver staining the primary exocytosis product appeared to contain a single band of about 68 kDa, the egg Ringer a main band of 29 kDa and other higher-molecular-weight proteins (37, 70 and 98 kDa), while the control Ringer was composed of three bands (31, 56 and 70 kDa). The electrophoretic protein pattern of J_1 included a protein of 70 kDa. The presence of a 70 kDa band in control Ringer, egg Ringer and J_1 suggests that at least one component of J_1 slowly diffused in the medium, probably as a result of previous DTT treatment for egg dejellifying. Indeed, the band of DTT absorbance was depicted spectrophotometrically in the egg Ringer (data not shown), thus indicating that some DTT might have stuck to J_1 , in spite of thorough rinsing of the eggs following exposure to this chemical.

Upon staining the gels with PAS, the main positive in all samples was found in high-molecular-weight components not entering the lower gel (6% or 12% acrylamide).

Aliquots of the egg Ringer and the primary exocytosis product were applied to polyacrylamide gels in the absence of SDS for determination of catalase activity. Enzymic activity, visualised as yellowish staining on a green background (Fig. 5, lane c) was positive in the egg Ringer but not in the primary exocytosis product and corresponded to the lane containing catalase and applied on the same gel as control (Fig. 5, lane a).

Amino acid analysis of egg Ringer of dissolved plugs

Four sets of experiments were carried out starting with isolated plugs (between 4 and 9 for each assay) at an initial concentration of 4 plugs per millilitre.

Standards were obtained by dissolving plugs by addition of 5 mmol/l DTT, 0.1 mol/l NaCl and 0.01 mol/l Tris-HCl buffer, pH 8.0; after 5 min a clear solution was obtained, which was stored at -20°C until use.

Assays in the presence of egg Ringer were obtained by adding 4–9 freshly dissected plugs to the Ringer containing the secondary exocytosis products of 10–20 eggs, obtained by the procedure described in 'Material and methods'. After about 40 min the dissolution was complete and the clear solution was processed further as described in the experimental section. Solutions were sometimes gelatinous, probably owing to the

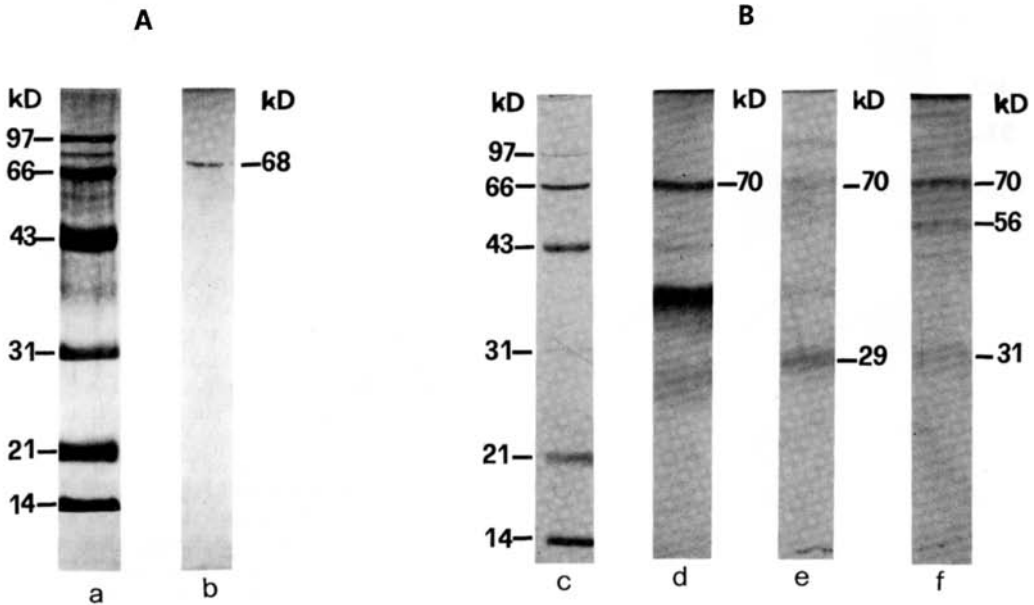


Figure 4 (a) and (b) 10% SDS-PAGE under reducing conditions, silver stain. (a) Protein standards; (b) primary exocytosis products; (c) protein standards; (d) J₁; (e) egg Ringer (secondary exocytosis products); (f) control Ringer. The primary exocytosis product consists of a single band of about 68 kDa. The other three samples share a band of 70 kDa. The egg Ringer also contains a main band of 29 kDa and a few minor bands; the control Ringer contains proteins of about 31 and 56 kDa.

Table 2 Amino acid analysis of plugs after dissolution with dithiothreitol (DTT) or with egg Ringer

| | Plugs + DTT | Plugs + egg Ringer |
|---------------|----------------|-----------------------|
| Aspartic acid | 7.1 ± 0.5 | 11.2 ± 1.7 |
| Threonine | 18.7 ± 5.5 | 21.2 ± 4.2 |
| Serine | 8.2 ± 1.6 | 8.3 ± 0.2 |
| Glutamic acid | 5.2 ± 0.3 | 7.0 ± 0.6 |
| Proline | 6.8 ± 1.4 | 7.6 ± 1.4 |
| Glycine | 4.9 ± 0.7 | 5.9 ± 0.7 |
| Alanine | 3.8 ± 0.9 | 4.3 ± 1.0 |
| Half cystine | ND | 1.7 ± 1.2 |
| Valine | 5.1 ± 0.6 | 4.3 ± 0.7 |
| Methionine | 4.5 ± 3.5 | 2.1 ± 1.7 |
| Isoleucine | 5.1 ± 0.6 | 2.2 ± 1.5 |
| Leucine | 5.6 ± 1.4 | 5.9 ± 1.3 |
| Tyrosine | 1.2 ± 0.9 | 2.1 ± 0.4 |
| Phenylalanine | 3.7 ± 0.9 | 3.1 ± 0.9 |
| Histidine | 2.0 ± 0.6 | 2.3 ± 0.2 |
| Lysine | 6.9 ± 1.6 | 5.3 ± 0.7 |
| Arginine | 0.9 ± 0.6 | 2.1 ± 0.5 |

ND, not determined.

Amino acids are given as a percentage of the total. Data are the average ± SD of four determinations. Analyses were carried out with 1.5–20 µg proteins.

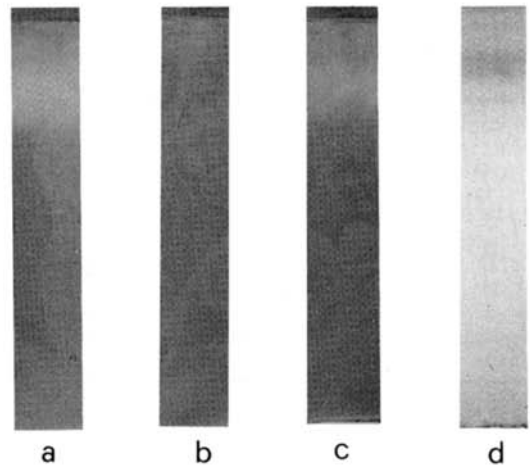


Figure 5 Determination of catalase activity in PAGE in the absence of SDS. Enzymic activity, visualised as a yellowish staining on a green background, is found in the egg Ringer (lane c), while it is absent in the primary exocytosis products (lane b). Lane a, catalase; lane d, egg Ringer stained with silver.

presence of glycoproteins; amino acid analysis was carried out on the supernatant, collected after centrifugation.

Table 2 reports the amino acid composition

Table 3 Sulphur-containing amino acid analysis of plugs after dissolution in various conditions

| Experiment no. | Conditions plugs dissolved with | Sulphur-containing amino acids | | |
|----------------|---------------------------------|--------------------------------|--------------|------------|
| | | Cysteic acid | Half cystine | Methionine |
| I | DTT | 0 | 0 | 3.2 |
| | Egg Ringer | 0.4 | 1.1 | 1.3 |
| | Egg Ringer + performic acid | 8 | 0 | 0 |
| II | DTT | 0 | 0 | 3.2 |
| | Egg Ringer | 3.8 | 0 | 0.9 |
| III | DTT | 0 | 0 | 9.3 |
| | Egg Ringer | 0.3 | 2.9 | 5.0 |
| | Egg Ringer + DMSO | 7.2 | 0 | 0 |
| IV | DTT | 0.5 | 0 | 1.0 |
| | Egg Ringer | 1.2 | 2.7 | 1.2 |

DMSO, dimethylsulphoxide; DTT, dithiothreitol.

Amino acids are given as a percentage of total amino acids as determined by amino acid analysis.

expressed as a percentage of the total. The compositions of the standard plugs (plugs dissolved with DTT) and plugs dissolved with egg Ringer were slightly different, a few amino acids (aspartic acid, methionine glutamic acid, isoleucine, tyrosine and arginine) being present in different amounts. We did not determine the amino acid composition of egg Ringer; it was, however, low (about 4–10 µl/ml), and about 10–20 times less than the protein concentration of the plug.

The high content of oxyamino acids is remarkable, comprising about 25% of the total. The high amount of galactosamine (0.5–1.2 µmol/mg protein, corresponding to about 8% of the total, calculated without taking into account the instability of galactosamine during acid hydrolysis) and the traces of glucosamine, also identified during amino acid analysis, indicate the presence of glycosylated proteins.

The reported amino acid composition cannot be ascribed to one specific protein. As reported above, plugs contained several bands including a main protein of 37 kDa.

Table 3 shows the analysis of sulphur-containing amino acids. Hydrolysates of egg Ringer-dissolved plugs contained small amounts of cysteic acid, which was not present in DTT-dissolved plugs. We cannot exclude the presence of cysteine sulphinic acid which failed to separate from cysteic acid during amino acid analysis, instead of cysteic acid. However, the oxidative activity of the egg Ringer most probably accounts for the presence of the most oxidised form. Oxidation with DMSO or performic acid showed the presence of half-cystines in an amount largely exceeding cysteic acid.

The utilisation of egg Ringer also lowered the amount of methionine recovered (Table 3).

Discussion

The formation of the capsular chamber in *D. pictus* has aroused interest in the sudden release of granular material causing plug liquefaction (Campanella *et al.*, 1992). In this study we have demonstrated peroxidase activity of this material, similar to that which has been found in invertebrate eggs, and raise new questions on the presence and role of such enzymes and hydrogen peroxide in other eggs.

Plug consistency and volume are mostly due to the high hydration of its matrix, which is composed of glycoproteins as well as acidic polysaccharides rich in sialic acid and sulphates (see Bellini & Campanella, 1974). In this study SDS-PAGE and amino acid analysis confirm the presence of large amounts of glycoproteins, and indicate that of amino sugars. Further studies are needed to identify the polysaccharide constituents of the plug.

Protein determination of the plug was carried out because we were interested in the reduction of disulphide bonds which occurs upon fertilisation (Campanella *et al.*, 1992) and therefore in the identification of proteins in the plug where such an event might occur. Electrophoretic analysis under reducing conditions shows bands with apparent molecular weights of 93, 75 and 36 kDa in the plug. Recently, prominent bands of about 30 kDa and higher-molecular-weight proteins have been separated through SDS-PAGE in the jelly coat of another frog, *Lepidobatrachus laevis* (Carroll *et al.*, 1991).

The protein pattern of the plug before and after fertilisation gives some insights into the dissolution process of this jelly coat, because it shows the disappearance of some proteins. This may be due either

to the opening of the interproteic disulphide bonds or/and to proteolytic activities, as suggested by the inhibition of plug dissolution by PMSF. The involvement of disulphide bridges is demonstrated by the titration of thiols and disulphides already reported in plugs of unfertilised and fertilised eggs (Campanella *et al.*, 1992) and suggested also by the different electrophoretic patterns in the presence or absence of mercaptoethanol.

The data on amino acid analyses show, as expected, that the amino acid composition of proteins in the plug after treatment with egg Ringer is rather similar to that after exposure to DTT. The most peculiar difference is observed in sulphur-containing amino acids. After the dissolution of plugs by egg Ringer a small, significant amount of cysteic acid is formed, which is absent in DTT-dissolved plugs and accounts for about one-twentieth of the total half-cystine as determined after performic acid oxidation or by hydrolysis in the presence of DMSO. The dissolution of the plug is thus related to the disappearance of disulphide bonds (Campanella *et al.*, 1992), the appearance of free sulphhydryl groups with the finding that egg Ringer activity is accelerated by the addition of hydrogen peroxide, inhibited by the addition of catalase and some sulphhydryl reagents, indicate that the opening of some of the disulphide bonds is an oxidative, peroxidase-like process; it does not appear to be the more usual thiol-mediated reduction involving an NADP-dependent system, as suggested by the data reported in Table 1.

Following fertilisation in the sea urchin hydrogen peroxide is released from the egg similarly to peroxidase (ovoperoxidase), which was reported to be contained in the cortical granules (Foerder *et al.*, 1977). As a consequence, the transformation of the VE into the fertilisation envelope occurs because of the formation of tyrosine cross-linkages contained in proteolyasin. This molecule is released from cortical granules and bound to the VE (Weidman *et al.*, 1985; for a review see Somers & Shapiro, 1989). In *D. pictus*, peroxidase activity demonstrated in the egg Ringer indicates that this enzyme is released from the egg after fertilisation in frogs also. The cortical granule products (primary exocytosis) are distinguishable from those present in the egg Ringer (secondary exocytosis) in both the proteic profile and the different activity with respect to the isolated plug. We surmise that the reported enzyme activity is present in the vesicles exocytosed after fertilisation.

The presence of a 70 kDa band in control Ringer, egg Ringer and J₁ suggests that components of J₁ slowly diffuse in the medium, probably as a result of the previous DTT treatment for egg dejellying. The 70 kDa band is not found in samples of the primary exocytosis product probably because the latter was

collected before much J₁ had diffused in the Ringer. Interestingly, the innermost jelly layer of anuran embryos has been reported to diffuse in the medium in more advanced stages of development, when it is exposed to the external medium, during early stages of release of hatching enzyme (Carroll & Hedrick, 1974).

Our results indicate that though post-fertilisation peroxidase release is similar in echinoderms and amphibians, it has quite opposite effects. Whereas in sea urchin eggs ovoperoxidase activity, together with hydrogen peroxide, is responsible for the *hardening* of the VE, tyrosine residues being the targets (Foerder & Shapiro, 1977), in *D. pictus* a similar enzymatic process involves the *liquefaction* of the plug, however disulphide bonds are affected. Furthermore, the release of peroxidase occurs at different stages of egg activation and from distinct organelles in these two egg types. In the sea urchin the enzyme is released from cortical granules, i.e. at the onset of egg activation, while in *D. pictus* it is exocytosed from typical vacuoles several minutes after cortical granule exocytosis has occurred (Campanella *et al.*, 1986). It would be interesting to investigate whether, and when, peroxidase is released from the egg and involved in egg-coat transformation in anuran species where no capsular chamber forms.

As previously reported (Campanella *et al.*, 1992), after fertilisation only the plugs are dissolved, not J₁ and J₃, which also contains disulphide bonds. Therefore the process of oxidative opening seems to be quite specific for some disulphide bridges in the plug and is not equivalent to the *in vitro* disulphide reduction operated by DTT, which leads to a more aspecific dissolution of most gelatinous egg components.

In sea urchin eggs the production of hydrogen peroxide in a 'respiratory burst' is caused by NADPH:O₂ oxidoreductase. Moreover, the molecular events responsible for hydrogen peroxide production appear to constitute the intraovular clock determining the time of the release of such a substance from the egg from 2 to 8 min post-fertilisation (Foerder *et al.*, 1978; Heinecke & Shapiro, 1989). In anurans, no oxidative burst occurs after fertilisation (see Monroy, 1967). Further studies are needed to demonstrate the release of hydrogen peroxide from *D. pictus* eggs and the molecular events underlying its production.

Acknowledgements

We are grateful to Ms Gianna Rossi and Drs Rosa Carotenuto and Pina Romano for laboratory help. We thank Professor D. Barra for amino acid analysis and Dr R. Talevi for suggestions. This work was supported by a 60% grant from the Italian MURST and CNR grant 1991/654.

References

- Barja de Quiroga, G., Gil, P. & Alonso-Bedate, M. (1985). Catalase enzymatic activity and electrophoretic patterns in adult amphibians: a comparative study. *Comp. Biochem. Physiol.* **80B**, 853–8.
- Bellini, L. & Campanella, C. (1974). Dati istochimici sulle gelatine ovalari e sull'ovidutto in *Discoglossus pictus* in rapporto alla fecondazione. *Boll. Zool.* **41**, 438.
- Campanella, C., Talevi, R., Atripaldi, U. & Quaglia, L. (1986). The cortical endoplasmic reticulum and its possible role in activation of *Discoglossus pictus* (Anura) eggs. In: *Molecular and Cellular Biology of Fertilisation*, ed. J.L. Hedrick, pp. 185–203. New York: Plenum Publishing Co.
- Campanella, C., Amore, F., Pitari, G., Fusco, C., Maurizi, G. & Dupré, S. (1992). Post-fertilization changes in *Discoglossus pictus* (Anura) eggs result in the formation of a capsular chamber where the egg rotates. *Int. J. Dev. Biol.* (in press).
- Carroll, E.J. & Hedrick, J.L. (1974). Hatching in the toad *Xenopus laevis*: morphological events and evidence for a hatching enzyme. *Dev. Biol.* **38**, 1–13.
- Carroll, E.J., Wei, S.H., Nagel, G.M. & Ruibal, R. (1991). Structure and macromolecular composition of the egg and embryo jelly coats of the anuran *Lepidobatrachus laevis*. *Dev. Growth Differ.* **33**, 37–43.
- Foerder, C.A. & Shapiro, B.M. (1977). Release of ovoperoxidase from sea urchin eggs hardens the fertilization membrane with tyrosine crosslinks. *Proc. Natl. Acad. Sci. USA* **74**, 4214–18.
- Foerder, C.A., Klebanoff, B.M. & Shapiro, B.M. (1978). Hydrogen peroxide production, chemiluminescence and the respiratory burst of fertilization: interrelated events in early sea urchin development. *Proc. Natl. Acad. Sci. USA* **75**, 3183–7.
- Giara, G. (1960). Osservazioni sugli strati superficiali e corticali di ovociti e di uova di *Discoglossus pictus*. *Arch. Zool. Ital.* **45**, 9–92.
- Heinecke, J.W. & Shapiro, B.M. (1989). Respiratory burst oxidase of fertilization. *Proc. Natl. Acad. Sci. USA* **86**, 1259–63.
- Hibbard, H. (1928). Contribution a l'étude de l'ovogénèse chez *Discoglossus pictus*. *Oth. Arch. Biol.* **38**, 251–326.
- Hirs, J.M. (1967). Performic acid oxidation. *Methods Enzymol.* **11**, 197–9.
- Kao, M. & Elinson, R. P. (1988). The entire mesodermal mantle behaves as Speman's organizer in dorso-anterior enhanced *Xenopus laevis* embryos. *Dev. Biol.* **127**, 64–77.
- Kapitany, R.A. & Zebrowski, E.J. (1973). A high resolution PAS stain for polyacrylamide gel electrophoresis. *Anal. Biochem.* **56**, 361–9.
- Laemmli, U.K. (1970). Cleavage of structural proteins during assembly of the head of bacteriophage T₄. *Nature* **227**, 680–5.
- Merril, C.R., Goldman, D., Sedman, S.A. & Ebert, M.H. (1981). Ultrasensitive stain in polyacrylamide gels shows regional variation in cerebro-spinal fluid proteins. *Science* **211**, 1437–1438.
- Monroy, A. (1965). *Chemistry and Physiology of Fertilization*. New York: Holt, Reinhart & Winston.
- Salthe, S.N. (1963). The egg capsule in the Amphibia. *J. Morphol.* **113**, 161–71.
- Somers, C.E. & Shapiro, B.M. (1989). Insights into the molecular mechanisms involved in sea urchin fertilization envelope assembly. *Dev. Growth Differ.* **31**, 1–7.
- Spencer, M.A. (1969). A new convenient method for estimation of total cystine–cysteine in proteins. *Anal. Biochem.* **32**, 185–7.
- Talevi, R. & Campanella, C. (1988). Fertilization in *Discoglossus pictus*. I. Sperm–egg interactions in distinct regions of the dimple and occurrence of a late stage of sperm penetration. *Dev. Biol.* **130**, 524–35.
- Talevi, R., Dale, B. & Campanella, C. (1985). Fertilization and activation potentials in *Discoglossus pictus* (Anura) eggs. *Dev. Biol.* **130**, 524–35.
- Wakahara, M. (1989). Specification and establishment of dorso-ventral polarity in eggs and embryos of *Xenopus laevis*. *Dev. Growth Differ.* **31**, 197–207.
- Weidman, P.J., Kay, E.S. & Shapiro, B.M. (1985). Assembly of the sea urchin fertilization membrane: isolation of proteoliasin, a calcium-dependent ovoperoxidase binding protein. *J. Cell Biol.* **100**, 938–46.

Following Passage Through the Oviduct, the Coelomic Envelope of *Discoglossus pictus* (Amphibia) Acquires Fertilizability Upon Reorganization, Conversion of gp 42 to gp 40, Extensive Glycosylation, and Formation of a Specific Layer

MARIANGELA CAPUTO, VINCENZO INFANTE, RICCARDO TALEVI,
MARIA CARMEN VACCARO, ROSA CAROTENUTO, AND
CHIARA CAMPANELLA*

Dipartimento di Biologia Evolutiva e Comparata, Università di Napoli, Napoli, Italy

ABSTRACT This paper describes the morphological and biochemical changes in *Discoglossus pictus* coelomic oocyte envelope (CE) following passage through the oviduct. As in other anurans, in this species, the transformation of the envelope into vitelline envelope (VE) leads to the acquisition of fertilizability and involves the cleavage of a glycoprotein. In addition, several features, typical of *Discoglossus pictus*, were observed. A new layer, VE-D, forms underneath the VE region facing the site of sperm entrance, the dimple. In the VE, arrowhead-like bundles of fibrils are perpendicularly oriented toward the dimple. Ultrastructural observations and staining with UEA-I suggested that VE-D might have a role in supporting sperm penetration into the dimple by orienting VE bundles and exposing sugar residues such as fucose. In 'in vitro' tests, VE binding of sperm occurs only if sperm are exposed to A23187, in agreement with previous data (Campanella et al., 1997: *Mol Reprod Dev* 47:323–333). Sperm binding occurs all over the VE. Accordingly, extracts of the VE covering the animal or the vegetal hemisphere have the same affinity to lectins (DBA, DSA, GNA, MAA, SBA, SNA, UEA-I, WGA). The CE contains six main glycoproteins. Peptide mapping indicated that during CE transformation into VE, gp 42 shifts to an apparent M_r of 40 and gp 61 is converted to an apparent M_r of 63 kDa. Lectin blot analyses showed extensive changes in cross-reactivity of most glycoproteins during the CE→VE transition. The fact that DBA and UEA-I stain gp 63 rather than gp 61 and that this change is related only to gp 63, suggested that O-glycosylation and terminal fucose might be acquired by gp 63 in preparation of fertilization. Gp 63 has recently been cloned (Vaccaro et al., submitted) and shown to exhibit high homology to *Xenopus* gp 69/64, a VE sperm ligand (Tian et al., 1997a: *J. Cell Biol.* 136: 1099–1108; Tian et al., 1997b: *Dev Biol* 187:143–153), and to ZP2 of mammals. *Mol. Reprod. Dev.* 58:318–329, 2001. © 2001 Wiley-Liss, Inc.

Key Words: vitelline envelope; amphibian oocytes; sperm binding; oligosaccharide chains

INTRODUCTION

In anurans, the envelope of the oocytes collected from the coelom (CE) is not penetrable by spermatozoa (Elinson, 1971; Brun, 1974). It is well known that this ability is acquired during the transit of the oocyte through the oviduct uppermost portion (*pars recta*, PR) simultaneously with changes in physicochemical and ultrastructural characteristics (Grey et al., 1977; Katagiri, 1987; Larabell and Chandler, 1989; Hedrick and Nishihara, 1991). PR secretion causes the exposure of sperm binding sites because of its sublytic action on the envelope (Cabada et al., 1978; Miceli et al., 1978a,b, in *Bufo arenarum*; Takamune et al., 1986, in *Bufo japonicus*; Gerton and Hedrick, 1986a; Tian et al., 1997a and b, in *Xenopus*). *Pars recta* proteases have been identified in *Bufo japonicus* (Takamune and Katagiri, 1987), *Bufo arenarum* (Miceli et al., 1980) and in *Xenopus* (*oviductin*, Bakos et al., 1990; Hardy and Hedrick, 1992). Oviductin is a serine protease that processes a glycoprotein of 43 kDa present in the CE into a 41 kDa glycoprotein (Gerton and Hedrick, 1986a), probably by acting at both the N- and the C-termini of gp 43 (Kubo et al., 1999). Gp 43 is a major CE glycoprotein that has an important role in CE transformation into the oviposited egg envelope (VE). The conversion gp 43→gp 41 uncovers a second glycoprotein, gp 64/69 that acts as sperm ligand (Tian et al., 1997a,b, 1999). Cloning of gp 69/64 has shown that this molecule is homologous to

*Correspondence to: Prof. Chiara Campanella, Dipartimento di Biologia Evolutiva e Comparata, Università di Napoli Federico II, Via Mezzocannone 8, 80134, Napoli, Italy.
E-mail: Campanella@dgbm.unina.it

Received 31 July 2000; Accepted 5 September 2000

the ZP2 of the mouse *zona* (Tian et al., 1999), which is able to bind sperm by a secondary binding (Bleil and Wassarman, 1988). Cloning of *Xenopus* gp 43 has revealed that this molecule is part of the ZPC family of glycoproteins and is homologous to the ZP3 (Kubo et al., 1997; Yang and Hedrick, 1997), which, in mouse, is responsible for sperm binding to the *zona* (Bleil and Wassarman, 1983). Recent data showed that in *Xenopus* gp 41 have sperm binding activity (Vo and Hedrick, 2000). That fact that in *Xenopus* both gp 69/63 and gp 41 act as sperm ligands indicate that sperm interaction with the egg envelope is a complex binding event involving several molecules, as suggested also in mammals fertilization (McLeskey et al., 1998).

These functional and biochemical data are paralleled by morphological evidence. The structure of the CE consists of a random and irregular network with broad channels, while that of the VE is a tight network of regularly arranged fiber bundles. The 43 gp proteolytic cleavage may interfere with protein domains that hold the CE fibrils in bundles, thereby allowing the bundles to rearrange and intermix with small fibrils present in the envelope (Larabell and Chandler, 1989).

In *Bufo japonicus*, a PR 66 kDa trypsin-like enzyme processes gps 40 and 52 of the CE to gps 36 and 39 of the VE, respectively (Takamune et al., 1986; Takamune and Katagiri, 1987). Interestingly, in *Bufo*, gps 36 and 39 may have sperm binding activity (Omata and Katagiri, 1996). More complex changes occur in *Lepidobatrachus laevis*, where a 56/53 kDa doublet of the CE is absent from the VE, and a CE 68 kDa glycoprotein shifts to 66 kDa in the VE (Peavy and Carroll, 1993).

These data show that, in amphibians, specific hydrolysis occurring during the CE→VE conversion is an important step allowing sperm binding to the envelope. However, it is improbable that this single proteolytic event might be responsible for all of the extensive changes occurring in the CE during the transit through the oviduct (Larabell and Chandler, 1989). More work is necessary for a complete understanding of the molecular changes occurring in the CE during its structural and functional transformation.

In this paper, we studied the morphological and the basic biochemical changes occurring during the CE→VE transition in *Discoglossus pictus* oocytes. In this species, several aspects of sperm-egg interaction are known which are still to be determined in other amphibian species. Therefore, it may be useful to carry out an investigation on *D. pictus* for a general understanding of sperm-VE binding in anurans.

The most evident characteristic of *D. pictus* egg is the distinct polarity of the egg and of the overlying jelly envelopes (Talevi and Campanella, 1988; Campanella et al., 1997; Maturi et al., 1998). Following insemination, sperm converge through the gelatinous *plug* into the *dimple*, the fertilization site, located at the center of the animal half. Sperm are as long as the jelly layers' thickness (2.33 mm). Their arrival at the egg surface coincides with the end of their motility. The acrosome reaction in the outermost jelly coat (J3) and sperm

penetration through the VE into the egg has been described elsewhere (Campanella et al., 1997).

Our results indicate that, during the passage through the oviduct, the CE reshapes, a shift of a CE gp of 42 kDa into a 40 kDa gp occurs, and the envelope acquires the ability to bind sperm. A second layer (VE-D) forms below the VE, only in correspondence with the dimple region, and a lectin specific for terminal fucose, UEA-I, stains exclusively the VE domain where this layer is present. Moreover, using several lectins, we found that most VE glycoproteins change in their lectin binding activity following passage through the oviduct. In particular, gp 63, a VE component which is homologous to gp 69/64 (personal communication), undergoes relevant changes as a consequence of the CE→VE transformation.

MATERIALS AND METHODS

Animals and Gametes

Adult *Discoglossus pictus* males and females were captured in the neighborhood of Palermo (Italy). They were injected in the dorsal lymphatic sac with 200–250 U of Profasi HP (Serono, Rome, Italy) in Amphibian Ringer (111 mM NaCl; 1.3 mM CaCl₂; 2 mM KCl; 0.8 mM MgSO₄; 5 mM HEPES pH 7.8). About 5 hr later, the females were anesthetised with MS222, and then their oocytes were removed from the body cavity. In some females, the oviduct full of oocytes was excised and separated into *pars recta*, medium, and lower portions for ultrastructural studies. Uterine eggs were obtained 18 hr after hormone injection. Twenty-four hours following hormone treatment, the seminal vesicles became filled with semen (sperm and seminal fluid) that can be collected by squeezing the abdomen, or by pricking the seminal vesicles after opening the abdomen of the males anesthetised with MS222 (Sigma St. Louis, MO) (see Campanella and Gabbiani, 1979).

Insemination was performed by addition of a drop of semen to coelomic oocytes or uterine eggs in 1/10 Ringer.

Microscopy

Coelomic oocytes, portions of the oviducts, and uterine eggs were fixed in 2.5% glutaraldehyde in 0.2 M phosphate buffer as previously described (Denis-Donini and Campanella, 1977) with a few modifications. Namely, the jelly layers were manually removed from the egg to improve fixative penetration. Alternatively, the eggs were cut in halves, 1 hr after immersion in the fixative. Embedding in Epon 812 followed dehydration in graded ethanol at 4°C. Thin sections were cut with diamond knives, stained with uranyl acetate and lead citrate, and examined in a Philips EM-300 microscope at the C.I.R.U.B. of the University of Naples.

For fluorescence microscopy, eggs were fixed, frozen, and sectioned, as previously described (Tatone et al., 1993). The sections were incubated with DIG-labeled *Galanthus nivalis* agglutinin (GNA) or DIG-labeled *Maackia amurensis* agglutinin (MAA), revealed with anti-DIG-FITC-conjugated (Roche Molecular Biochem-

icals, Mannheim, Germany) (for more details see Maturi et al., 1998). *Ulex europaeus* agglutinin I conjugated with fluorescein (UEA-I-FITC) (Sigma) was also used. After incubation for 45 min, the sections were extensively rinsed in PBS and mounted in 90% glycerol in PBS. The level of fluorescence was compared with that in control sections treated with UEA-I preincubated with 1 mg/ml fucosyl-lactose (Oxford Glycosystem Ltd., Abingdon, UK). Furthermore, eggs fixed in 95% alcohol were stained with DAPI for scoring sperm head attachment to the envelopes. Photographs were taken with a Leitz UV microscope using Ektachrome 64 T.

Sperm Binding Assays

Sperm suspensions as recovered from the seminal vesicle were diluted in 1/10 Ringer to provoke complete unraveling of the sperm bundles and sperm ejection from the bundles (Campanella and Gabbiani, 1979).

The sperm suspension was treated with 25 μ M A23187 (Sigma) for 2 min to induce the acrosome reaction (Gualtieri et al., 1996), and then washed twice in 1/10 Ringer. The binding assay was performed by the addition of groups of 10 coelomic eggs or fully dejellied eggs to untreated sperm or to calcium ionophore-treated sperm suspension and 15 min incubation at room temperature under gentle rocking. The sperm-exposed eggs were then washed by allowing them to fall through a 15 cm tall tube filled with 1/10 Ringer. The eggs with bound sperm quickly fell to the bottom of the well, while unbound free sperm settled more slowly. The unbound sperm in the buffer could, therefore, be separated from those bound to the eggs by swiftly aspirating the buffer above the eggs (see Tian et al., 1997a,b). The eggs were further rinsed in 1/10 Ringer, and the binding was monitored under a compound microscope.

Preparation of CE and VE

After transfer of coelomic oocytes into HB (25 mM HEPES pH 7.5 containing 900 mM glycerol; 0.02 mM NaN_3 ; 1 mM ATP; 1 mM DTT; 5 mM EGTA; 2 mM TAME, 5 mg/ml SBTI, 5 μ g/ml aprotinin, and 10 μ M E64), the CEs were manually removed and rinsed until clean. Uterine eggs were first dejellied in dejelling buffer (100 mM NaCl, 5 mM DTE; 50 mM Tris-HCl pH 8.5) and then transferred into HB for manual removal of the VE. After extensive rinsing and a brief centrifugation at a low speed to pellet the envelopes, the VEs were treated with 0.6 M KI for few minutes to remove the innermost jelly layer J1 and resuspended in 1/10 Ringer (see Pitari et al., 1993).

Solubilization of the CEs and the VEs was obtained in 1/10 Ringer containing 2% SDS and heating at 95°C for at least 2 min. After centrifugation at 14,000g for 10 min, the samples were processed for electrophoresis.

Protein Determination, SDS-PAGE, and Gel Staining

Protein concentration of the samples was determined with the BCA or Micro BCA Protein Assay Reagent

(Pierce Chemical Company, Rockford, IL). Fifteen micrograms of soluble proteins of CE or VE were applied on each lane of the gels. Samples were prepared for SDS-PAGE, by addition of sample buffer (Laemmli, 1970) and heating at 40°C for a few minutes (nonreducing conditions) or by heating for a few minutes in sample buffer containing 5% β -mercaptoethanol (reducing conditions). Protein samples were analyzed by SDS-PAGE using Laemmli's Tris-glycine buffer system (Laemmli, 1970). The running gel contained either 5 or 10% acrylamide. Gradients of 10–12% or 10–15% acrylamide were also utilized. M_r standards were the following: 200; 116; 97,500; 66,200; 45,000; 31,000; 21,500 Da (Bio-Rad, Hercules, CA) and the spectrin dimer (220 and 240 kDa) prepared from human erythrocyte ghosts, according to Marchesi (1971).

After fixation in methanol/acetic acid, gels were stained with either Coomassie blue or the silver method.

Peptide Mapping

The coelomic and vitelline envelopes were analyzed by peptide mapping using a modification (Bordier and Crettol-Jarvinen, 1979) of the limited proteolysis procedure of Cleveland et al. (1977). CE and VE components were separated on a 10% acrylamide SDS slab gel, under reducing conditions, for optimal band resolution. The first dimension gels were sealed on the top of a second dimension SDS gradient gel at 15–20% acrylamide and overlaid with 10 μ g *Staphylococcus aureus* V8 protease. CE gps 42 and 61 and gps 40 and 63 were similarly analyzed. Bands of single glycoproteins were cut out from the first dimension gels of the whole envelope homogenate, equilibrated for 30–60 min with 0.1% SDS, 62.5 mM Tris-HCl, pH 6.8 and stored at 4°C in a sealed dry tube up to 2 days or used immediately. About 3–4 excised bands were loaded for each well and were overlaid with the V8 protease.

The electrophoreses were interrupted for 1–2 hr when the proteins were in the stacking gel to allow extensive proteolysis. The peptide maps were stained with either the silver method or Coomassie blue.

Western Blot and Lectin Blot Detection on Nitrocellulose

Proteins subjected to SDS-PAGE were electrophoretically transferred onto nitrocellulose sheets overnight at 180 mA (for more details, see Tatone et al., 1993). A glycan detection kit (Roche) for carbohydrate and protein detection was used according to the manufacturer's instructions. Biotin-labeled *Triticum vulgare* agglutinin (WGA) (Sigma), UEA-I, *Glycine max* agglutinin (SBA) (Oxford Glycosystems), *Arachis hypogea* agglutinin (PNA), *Dolichos biflorus* agglutinin (DBA), *Concanavalin A* agglutinin (ConA) were used. Transferred proteins were first blocked in 2% BSA in PBS, and then exposed to the biotin-labeled lectin, followed by incubation in Avidin-AP (Sigma). Negative control runs were performed by adding sugars specific for each lectin: UEA-I preincubation with 5 mg/ml fucoidan (Sigma) or 1 mg/ml 2-fucosyl-lactose (Oxford Glyco-

Systems) inhibited the reaction (partial inhibition with fucosyl-lactose). WGA preincubation with 0.2 M *N*-acetyl-glucosamine (Sigma), SBA and DBA preincubation with 0.2 M *N*-acetyl-galactosamine (Sigma) inhibited lectin cross-reactivity (partial inhibition for DBA).

DIG-labeled MAA, GNA, *Datura stramonium* agglutinin (DSA), *Sambucus nigra* agglutinin (SNA), and *Galanthus nivalis* agglutinin (GNA) were part of a DIG Glycan differentiation Kit (Roche) and were utilized following the manufacturer's instructions. Positive controls were run for the DIG-labeled lectins according to the DIG Glycan differentiation Kit, i.e. carboxypeptidase Y for GNA, transferrin for SNA, fetuin for MAA and DSA, asialofetuin for PNA.

RESULTS

Ultrastructural Observations

The coelomic oocytes of *D. pictus* have a typical marker of polarity, the *germinative area*, located at the animal half center and where the CE is far from the oocyte surface (see Fig. 1). Previous work showed that, during the passage through the oviduct, the oocyte undergoes relevant changes. The germinative area invaginates to form the cup-shaped dimple, which is filled with glycoproteins. Therefore, in the uterine egg, the VE covers the whole egg plasma membrane except the region of the dimple where it spans the pit (see Denis-Donini and Campanella, 1977; Andreuccetti and Campanella, 1980).

In this paper, we studied the ultrastructure of the CE and its transformation into VE. Figure 1a shows a CE section at the germinative area level. The space between the envelope and the oocyte surface appears to be occupied by sparse granular material of about 50 nm in diameter. CE is made of interlaced fibrils and electron-dense granules (Fig. 1, inset). The fibril bundles are parallel or perpendicular to the egg surface, forming a meshwork interrupted by large channels. More loosely arranged fibrils and granules are located at the inner aspect of the CE (Fig. 1).

Figure 1b depicts the PR walls, where at least two kinds of secretory cell can be observed. During the passage through the PR, the apposition of electron-dense material or granular content modifies the arrangement of CE fibrils. In fact, the transforming envelope shows more tightly interwoven fibrils compared to the CE (Fig. 1c). Moreover, in front of the forming dimple, there is a further layer (VE-D) with granules and small fibrils that are not interwoven.

In the VE of the uterine egg, the tightly interwoven fibril bundles have a specific organization. In front of the dimple, some of these bundles 0.02 μ m in thickness are arranged with an arrowhead-like pattern pointing to the egg surface (Fig. 2a). This orientation is not observed in the VE located elsewhere around the egg, where the VE-D is absent (Fig. 2b). The VE-D is characterized by small fibrils and granules of about 50 nm in diameter and is clearly distinguishable from the under-

lying dimple content, which also contains granules of similar electron-density and size (Fig. 2a).

Sperm Binding Assays

Upon insemination of coelomic oocytes, sperm did not bind the CE, as expected. The same result was obtained by pretreating sperm with 25 μ M A23187 to induce the acrosome reaction. When uterine eggs were completely dejellied and inseminated, sperm exposed to A23187 readily bound the VE, while untreated sperm did not. The binding occurred all around the VE (Fig. 3), although to a lesser extent in the vegetal half (data not shown). Quantitative studies of this binding cannot be performed, as previously reported (Maturi et al., 1998).

SDS-PAGE Patterns of CE and VE

The bands present in the SDS-PAGE profiles of CE and VE have the same relative concentration as each lane is loaded with the same amount of total protein. All of the proteins are glycoproteins, as they stain with the DIG Glycan/protein double labeling kit (data not shown). Under non-reducing conditions, the CE pattern shows six glycoproteins with a following apparent M_r of 118, 106, 75, 61, 42 and 38/36 kDa, the latter two appearing as a doublet in gels loaded with as low as 5–10 μ g of total protein. The 118, 106, 42 and 38/36 bands are particularly conspicuous (Fig. 4). After passage through the oviduct, the envelope pattern shows some changes in the electrophoretic profile. The 42 kDa disappears and a 40 kDa band is now present in the VE. Furthermore, while a 61 kDa band is observed in the CE, a band of about 63 kDa is found in the VE (Fig. 4 and Table 1). High molecular mass bands up to 200 kDa are detectable only by silver staining or glycan staining blotting in the VE and the CE (see Fig. 7).

A band of 150 kDa is clearly present under reducing conditions in the CE and the VE. SDS-PAGE of VE manually separated in animal and vegetal halves showed that these bands are localized in the whole envelope, i.e., there is no difference in the electrophoretic patterns of the VE covering the animal or the vegetal half (Fig. 5), indicating that VE-D does not contain specific major proteins.

Peptide Mapping

The peptide maps of the whole VE show a specifically recognizable pattern for each VE component (Fig. 6A,B). Similar results were obtained for the peptide maps of the whole CE (data not shown).

Single bands excised from the gels were also analyzed. The polypeptides produced by V8 proteolysis of CE gp 61 and VE gp 63 were compared. The two peptide maps appear identical, the only difference lying in a peptide that is present in the gp 61 map and absent from the gp 63 one (asterisk in Fig. 6C). Similarly, the peptide maps of CE gp 42 and VE gp 40 are identical, except for two polypeptides that are present only in the gp 42 map (asterisks in Fig. 6D), while smaller peptides are generated from gp 40 by V8 digestion (arrowheads in Fig. 6D). These data suggested that gp 61 is con-

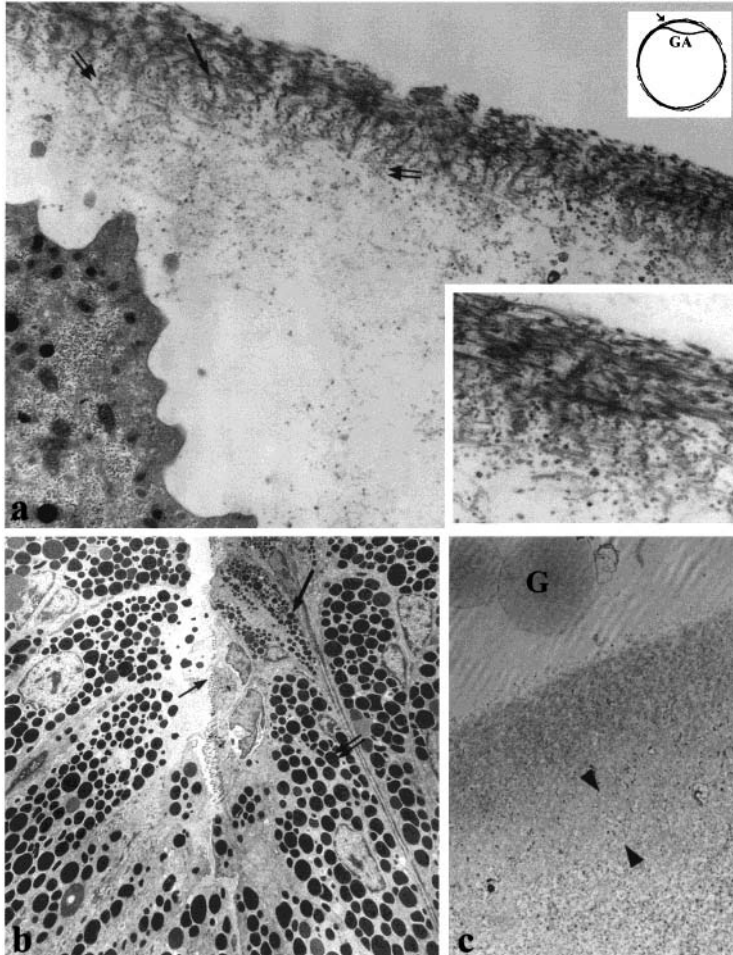


Fig. 1. Ultrathin sections stained with lead citrate and uranyl acetate. (a) Lateral view of the germinative area (GA) of a coelomic oocyte, at the site indicated by the small arrow in the drawing (upper right inset). The coelomic envelope is made of interlaced fibrils and electron-dense granules (arrow). The fibril bundles are interrupted by large channels. More loosely arranged fibrils and granules are located at the inner aspect of CE (double arrow). In the germinative area content sparse granules are present (small arrow). Magnification = 5200 ×. Lower right inset = detail of CE. Magnification = 9000 ×.

(b) PR walls. The large secretory cells, full of electron-dense granules (double arrow) occupies most of the epithelium. Smaller cells, with irregularly shaped granules (arrow) are located next to the ciliated cells (small arrow). Magnification = 2000 ×. (c) Oocyte in the PR lumen. Two granules (G) are seen next to the transforming envelope where the channels have disappeared and the fibers are tightly interwoven. A new layer is seen below the transforming envelope, VE-D (arrowheads). Magnification = 5700 ×.

verted into gp 63 and gp 42 into gp 40 during CE →VE conversion.

Lectin Blots and Section Staining

Analysis of carbohydrate moieties of the envelope components was performed by lectin-blotting, utilizing ConA, DBA, DSA, GNA, MAA, PNA, SBA, SNA, UEA-I, and WGA, the sugar specificity of which is indicated in Table 2. In particular, blotting with PNA and DBA

was performed for general identification of O-linked sugar chains (Schachter and Brockhausen, 1992) and blotting with ConA and GNA was used for identification of N-linked sugar chains (Shibuya et al., 1998).

Interestingly, when CE and VE components are electrophoretically separated under reducing or non-reducing conditions, blotted, and incubated with the overmentioned lectins, differences in the reactivity to

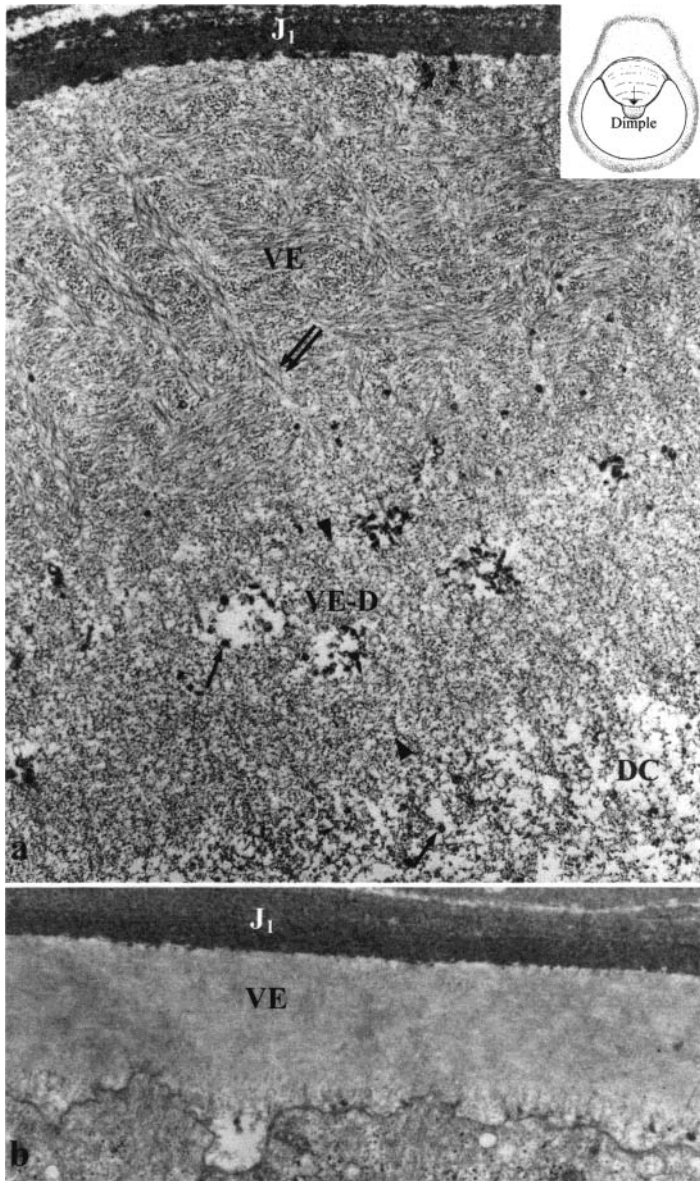


Fig. 2. Ultrathin sections of oviposited eggs, stained with lead citrate and uranyl acetate. (a) Envelope region facing the dimple at the site indicated by the arrow in the *D. pictus* egg drawing (inset). J₁, jelly layer 1; VE, vitelline envelope where arrowhead-like fibers oriented toward the dimple can be seen (double arrows). VE-D, this layer is present only in the region facing the dimple. It contains

granules (arrows) similar to those present in the dimple content (DC) and fibers. The dimple content has a granular and fibrillar composition morphologically dissimilar from VE-D. Magnification = 22,000 ×. (b) VE covering the egg in a region outside the dimple. Magnification = 19,000 ×.

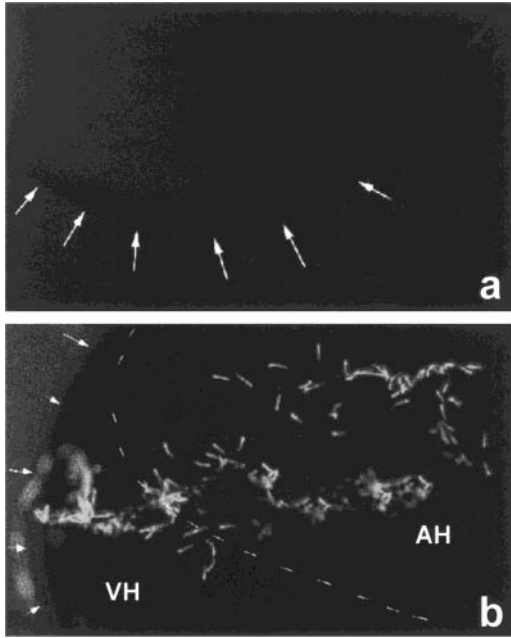


Fig. 3. Dejellied uterine eggs fixed and stained with DAPI. (a) There is no sperm binding, when eggs are inseminated with untreated sperm. The arrows point to the egg boundary. (b) Sperm binding occurs when sperm are exposed to A23187. Sperm bind to the VE covering the animal (AH) and the vegetal half (VH). The dashed line separates the two halves. The arrows point to the egg boundary. Magnification = 50 ×. [Color figure can be viewed in the online issue, which is available at www.interscience.wiley.com]

lectins are observed within the CE and VE corresponding bands (see Fig. 7a and Table 3). In the SBA blot, CE gp 61 is practically unreactive, while VE gp 63 is reactive, and the same occurs for gp 106 (Table 3). These differences in the CE and VE blots are particularly sharp in the samples run under reducing condi-

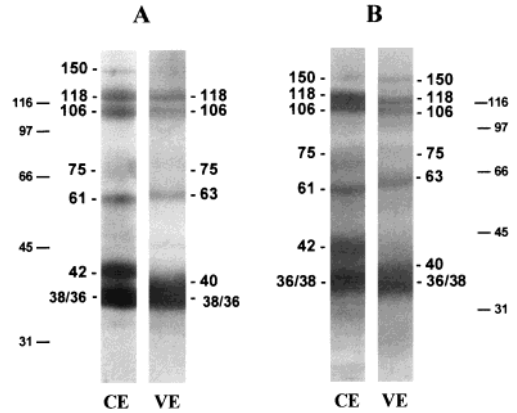


Fig. 4. SDS PAGE of CE and VE in the absence (A) or presence (B) of mercaptoethanol, in gels containing 10% acrylamide and Coomassie blue stained. Six main bands of 118,106,75, 61, 42, 38/36 kDa, as well as a minor band of 150 kDa, are present in the CE. In the VE, the bands have an apparent M_r of 118, 106, 75, 63, 40, 38/36 kDa. The band of 150 is also present. The addition of mercaptoethanol does not change the pattern of CE and VE gels. However, the 150 kDa band is better resolved in the presence of mercaptoethanol. Reference M_r are indicated. All the numbers are expressed in kDa.

tions (Fig. 7a). UEA-1 cross-reactivity on gp 61 is mild in CE blots and becomes more evident on gp 63 in VE blots. In DBA WGA blots, VE gp 63 is reactive, in contrast to CE gp 61. These differences are not shared by the other glycoproteins, or in some cases, they are even opposite. In fact, in the WGA and UEA-I blots, gp 106 is particularly reactive in the CE and slightly reactive in the VE, while it is similarly reactive in CE and VE DBA blots (Table 3, Fig. 7).

In GNA blots, VE gp 63 reactivity is enhanced with respect to CE gp 61. Moreover, in SNA blots, gps 118, 106, 40 are reactive in the VE, while the whole CE electrophoretic pattern is unreactive to that lectin. On the whole, six changes in reactivity to lectins occur during gp 61→63 transformation and only one (acquisition of reactivity to SNA) for the gp 42→40 transition.

TABLE 1. Apparent M_r of CE and VE Glycoproteins Separated by SDS-PAGE Under Reducing and Nonreducing Conditions (M_r in kDa)

| CE(-Me) High molec. mass bands | VE(-Me) High molec. mass bands | CE(+Me) High molec. mass bands | VE(+Me) High molec. mass bands |
|--------------------------------------|--------------------------------------|--------------------------------------|--------------------------------------|
| 150 ^a | 150 ^a | 150 | 150 |
| 118 | 118 | 118 | 118 |
| 106 | 106 | 106 | 106 |
| 75 | 75 | 75 | 75 |
| / | 63 | / | 63 |
| 61 | / | 61 | / |
| 42 | / | 42 | / |
| / | 40 | / | 40 |
| 38/36 | 38/36 | 38/36 | 38/36 |

^aThis band is better resolved in reducing conditions.

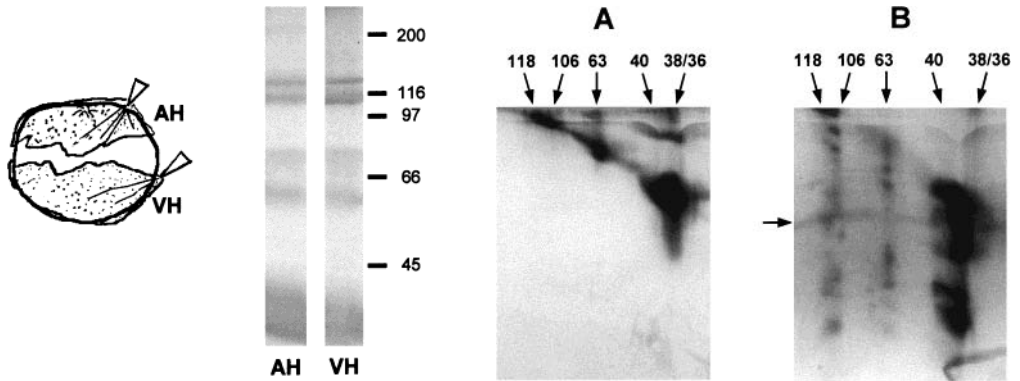


Fig. 5. The two 10% acrylamide gels contain extracts of VE bisected in animal (AH) and vegetal (VH) halves, as indicated in the drawing. AH and VH have identical electrophoretic patterns. Reference M_r are indicated and expressed in kDa.

Table 3 summarizes the data obtained for VE and CE glycoproteins. Although no reactivity to Con A is found, most glycoproteins cross-react with GNA, indicating the presence of high mannose N-linked sugar chains (Shibuya et al., 1998). With PNA, the bands were not reactive (data not shown). However, the presence of O-linked sugar chains can be hypothesized in gps 106, 75, 63, 38/36 because of the reactivity of these bands with DBA. In particular, in the VE, the 63 kDa band appears to contain N-linked glycans, sialic acid, Gal β 1-4GlcNAc, GlcNAc β 1-4GlcNAc, GalNAc α 1-3GalNAc, and fucose. Gp 40 contains N-linked glycans, sialic acid, α e β GalNAc, and Gal β 1-4GlcNA.

To check possible asymmetrical localization of VE glycoproteins due to egg polarization, lectin blots, and histological staining were performed. By lectin blotting, no differences were found in the reactivity for the tested lectins between the two halves of the dissected VE. Figure 8 shows a selection of results related to UEA-I, DBA, SBA, and WGA. By contrast, following exposure of frozen sections of uterine eggs to UEA-I-FITC, the VE was not stained except for the region facing the dimple (Fig. 9a,b). This cross-reactivity is due to the innermost rim of the envelope, corresponding to the VE-D (Fig. 9c,d). MAA-FITC and GNA-FITC were also utilized as they cross-react in the blots with several VE gps. For these lectins, in the sections, staining occurs along the whole envelope (data not shown).

DISCUSSION

The present paper describes the morphological and biochemical changes in *D. pictus* CE following passage through the oviduct. Along with envelope reorganization, a specific layer, VE-D, is deposited underneath the VE region facing the dimple. The main glycoproteins of the CE are six. During CE transformation into VE, gp 42 shifts to an apparent M_r of 40 kDa, and extensive changes in cross-reactivity to lectins occur in all enve-

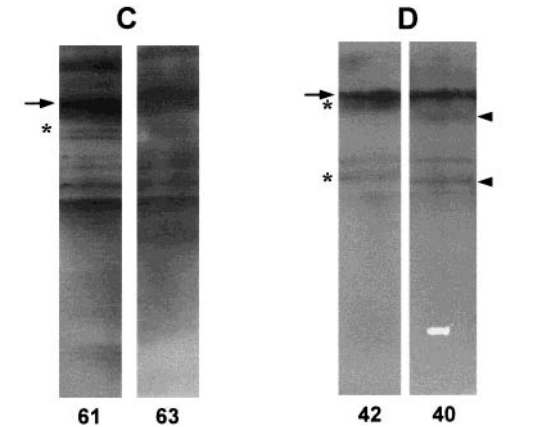


Fig. 6. A, B: VE peptide maps in the absence (A) or presence (B) of V8 protease. In B, following V8 digestion, each VE component has a specific peptide map. Arrow, V8 protease band. C, D: Peptide maps of the single envelope glycoproteins excised from a first dimension gel of total VE proteins and run in second dimension in 10% acrylamide (C) gp 61 and gp 63. (D) gp 42 and gp 40. The arrow indicates the V8 protease band. In (C) the asterisk indicates a peptide of gp 61, which is missing in gp 63. In (D) the asterisks indicate two peptides of gp 42 which are missing in gp 40, where two peptides of lower M_r are present (arrowheads). The numbers are expressed in kDa.

TABLE 2. Lectin Specificity

| Lectins | Specificity |
|---------|----------------------------|
| UEA-I | α L-Fuc |
| GNA | Man α 1-3 Man |
| DSA | Gal β 1-4 GlcNAc |
| SBA | α e β GalNAc |
| WGA | GlcNAc β 1-4 GlcNAc |
| PNA | Gal β 1-3 GalNAc |
| MAA | NeuNAc α 2-3 Gal |
| SNA | NeuNAc α 2-6 Gal |
| Con A | α -Man |
| DBA | GalNAc α 1-3 GalNAc |

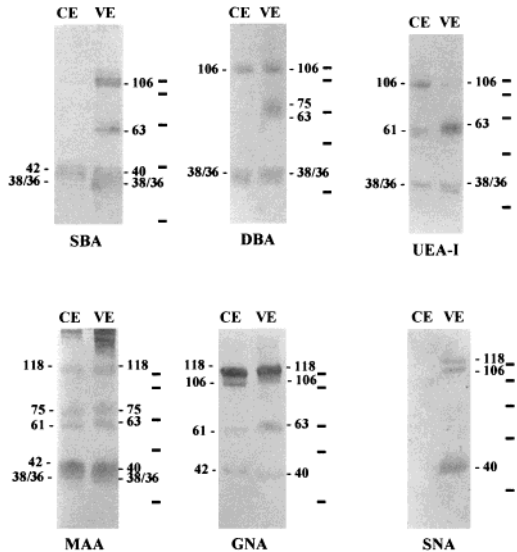


Fig. 7. Selection of CE and VE lectin blots. The utilized lectins are indicated (SBA, DBA, UEA-I, MAA, GNA, SNA). All except SBA blot derive from electrophoresis of samples prepared in the absence of mercaptoethanol. The bars indicate standard M_r of 116, 97, 66, 45, and 31 kDa. The high molecular mass glycoproteins are evident in the MAA blots. The numbers are expressed in kDa.

lope glycoproteins but gp 38/36. Furthermore, CE gp 61 is converted to an apparent M_r of 63 kDa in the VE. These findings indicate that extensive and unexpected events concur to the transformation of CE into VE.

D. pictus CE is a loose matrix of interwoven fibrils, similar to that described in *Xenopus laevis* (Grey et al., 1977; Larabell and Chandler, 1989), *Bufo arenarum* (Mariano et al., 1984), and *Rana pipiens* (Yoshizaki and Katagiri, 1981). In addition, at the inner aspect of the CE, loosely arranged fibers and granules are present, most probably constituting the initial substratum for the VE-D deposition. During the transit of the oocyte through the PR, the ultrathin sections showed the apposition of secretory granules to the CE and the redistribution of its constituents, similarly to what hap-

pens in other species (i.e., in *Rana pipiens*; Yoshizaki and Katagiri, 1981). VE ultrastructure is made of highly compact interwoven fibril bundles (for *Rana* and *Bufo* VE, see Yoshizaki and Katagiri, 1981; Mariano et al., 1984). At the dimple level, the arrowhead-like bundles of fibrils are perpendicularly oriented to the egg. In addition, this orientation is evident only where the VE-D is present, suggesting that this layer might be instrumental in positioning the arrowhead-like bundles.

In *D. pictus*, the initial stimulus for the acrosome reaction is triggered by the outermost jelly layer, J3 (Campanella et al., 1997). Two to three seconds after contact with J3, sperm become fully embedded in the jelly layers, their tip having reached the VE. These initial stages of VE penetration are not related to an evident release of enzymes from the sperm acrosome, as is indicated by ultrastructural observations. The thin sperm tip starts its penetration into the VE perpendicularly to the egg (Campanella et al., 1997), i.e., with the same orientation of the arrowhead-like bundles. We surmise that the bundle oriented perpendicularly to the egg might be sites of low-resistance for the penetrating sperm.

In *D. pictus*, sperm do not bind to the CE before or after exposure to A23187. This treatment triggers the acrosome reaction, replacing the action of J3 (Campanella et al., 1997; Gualtieri et al., 1997; Maturi et al., 1998). The lack of sperm binding to the CE can be related to the described structural organization of the CE. Sperm do bind to the VE, demonstrating that the passage through the oviduct confers fertilizability to the envelope, as in other anuran species (Katagiri, 1987; Nishihara and Hedrick, 1991). Interestingly, our observations indicate that sperm binding sites are present all over the envelope. SDS-PAGE and lectin blots on bisected envelope extracts demonstrate that there is no difference in the protein electrophoretic pattern, and affinity for lectins is the same along the whole VE. This provides additional evidence to previous data showing that molecules specific for sperm binding to the *D. pictus* egg are located on the dimple plasmalemma rather than in the VE (Maturi et al., 1998). In *Xenopus* as well, sperm binding occurs all over the envelope (Tian et al., 1997a), though sperm enter the egg only at the animal hemisphere. In histological

TABLE 3. Lectin Blotting Reactivity of CE and VE Glycoproteins

| Lectins | CE glycoproteins | VE glycoproteins |
|---------|----------------------------------|----------------------------------|
| SBA | 42, 38/36 | 106, 63, 40, 38/36 |
| DBA | 106 ^a , 38/36 | 106, 75, 63, 38/36 |
| MAA | H.m.w.b., 118, 75, 61, 42, 38/36 | H.m.w.b., 118, 75, 63, 40, 38/36 |
| GNA | 118, 106, 61, 42 | 118, 106, 63, 40 |
| DSA | 106, 75, 61, 42 | 106, 75, 63, 40 |
| SNA | / | 118, 106, 40 |
| UEA-I | 106, 61, 38/36 | 106, 63, 38/36 |
| WGA | 118, 106 | 118, 106, 63 |

^aIn bold are shown the glycoproteins strongly reactive to lectins. H.m.w.b.: high molecular weight bands.

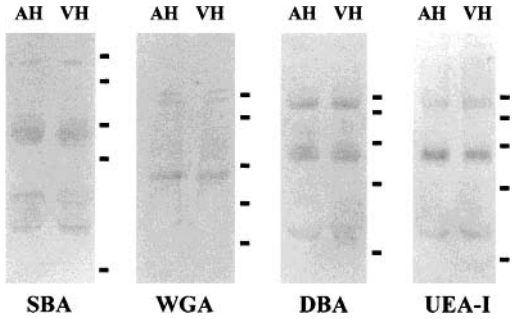


Fig. 8. Lectin blots of VEs bisected in animal (AH) and vegetal (VH) halves. The utilized lectins are SBA, WGA, DBA, and UEA-I. No differences in reactivity to lectins are found between the two hemispheres. Reference *M_r* (116, 97, 66, 45, 31 kDa) are indicated by the bars.

sections of *D. pictus* egg, lectins stain the VE all around the egg homogeneously. However, UEA-I does not stain the VE but only the VE-D, in contrast to the lectin blotting results where UEA-I has affinity for gp 106, gp 63, gp 38/37 in the bisected envelopes. For SDS-PAGE, the envelopes are solubilized, while under experimental conditions for microscopy, VE structure is preserved and terminal fucose may be masked and unavailable to UEA-I. We surmise that the VE-D may have a specific molecular organization compared to the VE, which renders fucose available to UEA-I staining. Thus, the VE-D might have a role in supporting sperm

penetration into the dimple by orienting VE bundles and exposing sugar residues such as fucose.

Binding to the VE occurs only if sperm have undergone the acrosome reaction, in contrast to *Bufo* and *Xenopus* where most probably binding with unreacted sperm (primary binding) occurs (Yoshizaki and Katagiri, 1982; Tian et al., 1997a; Vo and Hedrick, 2000). Interestingly, in the newt *Cynops phyllorhogaster*, the acrosome reaction is induced by the jelly, and acrosome-reacted sperm bind to the VE (secondary binding) (Nakai et al., 1999). In *D. pictus*, the present data suggest that, under physiological conditions, sperm bind to the VE when the hybrid vesicles are shed from the acrosome and uncover the inner acrosome membrane, i.e., around 30 sec following insemination. The occurrence of a late stage of sperm binding was earlier shown in ultrathin sections (Campanella et al., 1997).

The *D. pictus* CE electrophoretic pattern (main bands of 118, 106, 75, 61, 42, 38/36 kDa and a minor band of 150 kDa) is made of glycoproteins. In *D. pictus* oviposited eggs, the VE pattern appears to have undergone several changes when compared to the CE pattern, in samples under reducing and non-reducing conditions. Peptide mapping profile of the CE 42 kDa and the VE 40 kDa bands indicate that the latter derives from the former, suggesting that their difference lies in two peptides of smaller size in the map of gp 40. Therefore, it appears that the proteolytic cleavage of a glycoprotein, i.e. the main structural transformation of the envelope leading to the acquisition of fertilization, is also present in *D. pictus*, one of the oldest living frogs (Ford and Cannatella, 1993). A

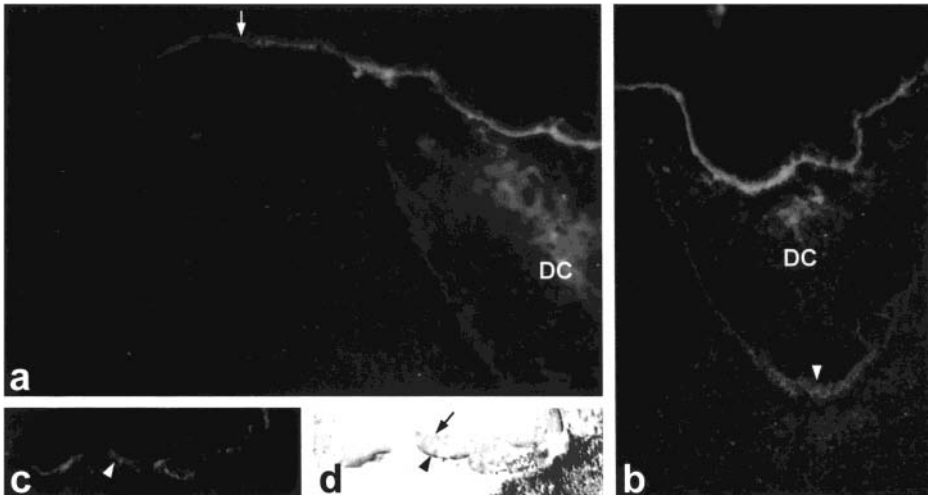


Fig. 9. Frozen sections of the dimple region in uterine eggs incubated with UEAI-FITC. (a) Lateral view of the dimple in a longitudinal section. (b) Central view of the dimple in a longitudinal section. The staining is on the envelope in the region facing the dimple (b) and gradually decreases over the VE borders, as indicated by the arrow in (a). DC, dimple content; arrowhead, dimple bottom. Magni-

fication = 300 ×. (c) UEAI stained envelope. (d) Corresponding phase contrast. Arrowheads in (c) and in (d) indicate the UEAI stained VE-D. The arrow in (d) points to VE. Magnification = 500 ×. [Color figure can be viewed in the online issue, which is available at www.interscience.wiley.com]

second shift, gp 61–63, is strongly suggested by the peptide map of the two glycoproteins. The peptide missing in VE gp 63 would suggest a proteolytic cleavage of gp 61, which, however, is not consistent with the increase in the apparent M_r of this glycoprotein in the VE.

Lectin blot analysis revealed that, in the VE, all of the CE bands but gp 38/36 change reactivity to at least one of the lectins utilized. The change in reactivity of the bands is specific for each glycoprotein of the VE SDS-PAGE pattern, and this argues against possible artifactual conditions of lectin blotting. It can be suggested that enzymes being derived from PR secretion might proteolytically cut gp 42, as occurs in *Xenopus* (Hardy and Hedrick, 1992) and *Bufo* (Takamune and Katagiri, 1987). The PR constituents may be similarly responsible for the changes in the glycosylation of VE constituents. Interestingly, Yoshizaki and Katagiri (1981, 1982) showed that, in *Rana japonica*, the VE fibers are strongly stained for carbohydrates of oviductal origin, but the CE is not. In *D. pictus*, the shift of the apparent M_r of 61–63 kDa may be caused by an increase in net positive charge due to the acquired polysaccharide chains and the consequent decrease in mobility throughout the gel. This hypothesis would imply that the amount of gp 63 glycans are larger in size than those gained by the other glycoproteins with an apparent M_r remaining unchanged during the transit through the oviduct. This is suggested by the fact that gp 63 undergoes the highest number of changes (six) in reactivity to lectins, with respect to the other VE components (Table 3). These data, however, give no information on the amount of the carbohydrates acquired.

The affinity to SNA acquired by VE gps 118, 106, and 40 suggests that sialic acids may play a role in the redistribution of fibers occurring in the CE→VE transformation, as seen in other systems (Rutishauser, 1990).

The fact that, following passage through the oviduct, only gp 63 acquires a strong stainability by DBA and UEA-I, leads to the attractive hypothesis that *O*-glycosylation and terminal fucose are specifically gained by this molecule in preparation of fertilization. Gp 63 has recently been cloned showing high homology to *Xenopus* gp 69/64, the VE sperm ligand, and to mammalian ZP2 (personal communication). The ability of gp 69/64 to bind sperm to the VE depends upon oligosaccharide chains (Tian et al., 1997a). Vo and Hedrick (2000) suggested that *N*-acetylglucosamine and fucose residues are involved in sperm binding to *Xenopus* VE. Both in *Bufo arenarum* and in *Bufo japonicus*, the relevance of carbohydrate moieties in sperm binding to the VE has been stressed (Valz-Gianinet et al., 1991; Omata and Katagiri, 1996). According to Omata and Katagiri (1996), in *B. japonicus*, DBA binding oligosaccharides of gps 39 and 36 are likely to be the binding component. Much experimental evidence indicates that *O*-glycosylation is the prerequisite for sperm binding ability in the envelope of several eggs (Florman and Wassarman, 1985; Yurewicz et al., 1992; Dhume and Lennarz, 1995; Focarelli and Rosati, 1995) and that fucose is similarly

important in this process (see Maturi et al., 1998; Vo and Hedrick, 2000). More work is needed to ascertain the role of gp 63 and of its oligosaccharide chains in this function.

ACKNOWLEDGMENTS

We are grateful to Drs. G. Maturi, S. Russo and D. Capobianco for help in the laboratory and Drs. A. Cirillo for editing the manuscript. We also thank Dr. W.J. Lennarz, Dr. Rosati and Dr. Focarelli for critical reading of the manuscript. Supported by M.U.R.S.T.'s P.R.I.N. 1999.

REFERENCES

- Andreuccetti P, Campanella C. 1980. Origin and cytochemistry of the animal dimple granules in *Discoglossus pictus* (Anura) eggs. *J Embryol Exp Morph* 56:239–252.
- Bakos M, Korosky A, Hedrick JL. 1990. Enzymatic and envelope converting activities of pars recta oviductal fluid from *Xenopus laevis*. *Dev Biol* 138:169–176.
- Bleil JD, Wassarman PM. 1983. Sperm–egg interactions in the mouse: sequence of events and induction of the acrosome reaction by a zona pellucida glycoprotein. *Dev Biol* 95:317–324.
- Bleil JD, Wassarman PM. 1988. Galactose at the non-reducing terminus of O-linked oligosaccharides of mouse egg zona pellucida glycoprotein is essential for the glycoprotein's sperm receptor activity. *Proc Natl Acad Sci USA* 85:6778–6782.
- Bordier A, Crettol-Jarvinen J. 1979. Peptide mapping of heterogeneous protein samples. *J Biol Chem* 254:2565–2567.
- Brun C. 1974. Studies on fertilization in *Xenopus laevis*. *Biol Reprod* 12:439–447.
- Cabada MO, Mariano MI, Raisman JS. 1978. Effect of trypsin inhibitors and concanavalin A on the fertilization of *Bufo arenarum* coelomic oocytes. *J Exp Zool* 204:409–416.
- Campanella C, Gabbiani G. 1979. Motile properties and localization of contractile proteins in the spermatozoon of *Discoglossus pictus*. *Gamete Res* 2:163–175.
- Campanella C, Carotenuto R, Infante V, Maturi G, Atripaldi U. 1997. Sperm–egg interaction in the painted frog (*Discoglossus pictus*): an ultrastructural study. *Mol Reprod Dev* 47:323–333.
- Cleaveland DW, Fisher SG, Kirschner MW, Laemmli UK. 1977. Peptide mapping by limited proteolysis in sodium dodecyl sulfate and analysis by gel electrophoresis. *J Biol Chem* 252:1102–1106.
- Denis-Donini S, Campanella C. 1977. Ultrastructural and lectin binding changes during the formation of animal dimple in oocytes of *Discoglossus pictus* (Anura). *Dev Biol* 61:140–152.
- Dhume ST, Lennarz, WJ. 1995. The involvement of O-linked oligosaccharide chains of the sea urchin egg receptor for sperm in fertilization. *Glycobiology* 5:11–17.
- Elinson RP. 1971. Fertilization of partially jellied and jellyless oocytes of the frog *Rana pipiens*. *J Exp Zool* 176:415–428.
- Florman H M, Wassarman PM. 1985. O-linked oligosaccharides of mouse egg ZP3 account for its sperm receptor activity. *Cell* 41:313–324.
- Focarelli R, Rosati F. 1995. The 220 kD vitelline coat glycoprotein mediates sperm binding in the polarized egg of *Unio elongatulus* through O-linked oligosaccharides. *Dev Biol* 171:606–614.
- Ford LS, Cannatella DC. 1993. The major clades of frog. *Herp Monogr* 7:94–117.
- Gerton GL, Hedrick JL. 1986a. The coelomic envelope to vitelline envelope conversion in eggs of *Xenopus laevis*. *J Cell Biochem* 30:341–350.
- Gerton GL, Hedrick JL. 1986b. The vitelline envelope to fertilization envelope conversion in eggs of *Xenopus laevis*. *Dev Biol* 1–7.
- Grey RD, Working PK, Hedrick JL. 1977. Alteration of structure and penetrability of the vitelline envelope after passage of eggs from coelom to oviduct in *Xenopus laevis*. *J Exp Zool* 201:73–83.
- Gualtieri R, Andreuccetti P. 1996. Localization of egg-surface carbohydrates and fertilization in *Discoglossus pictus* (Anura). *Cell Tissue Res* 283:173–181.

Primary Structure and Developmental Expression of Dp ZP2, a Vitelline Envelope Glycoprotein Homolog of Mouse ZP2, in *Discoglossus pictus*, One of the Oldest Living Anuran Species

M.C. VACCARO,¹ M.G. DE SANTO,¹ M. CAPUTO,¹ M. JUST,¹ J.D. TIAN,¹ H. GONG,² W.J. LENNARZ,² AND C. CAMPANELLA^{1*}

¹Dipartimento di Biologia Evolutiva e Comparata, Napoli, Italy

²Department of Biochemistry and Cell Biology and the Institute for Cell Biology and Developmental Biology, SUNY at Stony Brook, Stony Brook, New York

ABSTRACT A glycoprotein of the *Xenopus* vitelline envelope, gp 69/64, which mediates sperm binding, is closely related to the components of ZPA family, such as the mouse zona pellucida ZP2. To test the generality of these findings, we studied *Discoglossus pictus*, a species evolutionary distant from *Xenopus* and identified as a protein of 63 kDa in the vitelline envelope. Preliminary studies suggest that this protein may bind sperm at fertilization. We found that the 63-kDa protein is glycosylated and contains both N- and O-linked chains. We have cloned the cDNA encoding the *Discoglossus* protein of 63 kDa (Dp ZP2) by screening a *Discoglossus* cDNA library using *Xenopus* gp 69/64 cDNA as a probe. Analysis of the deduced sequence of *Discoglossus* protein revealed 48% identity with *Xenopus* gp 69/64 and 37–40% identity with mouse ZP2. The sequence conservation included a ZP domain, a potential furin cleavage site and a putative transmembrane domain. The N-terminus region of Dp ZP2 was 40% identical to the corresponding region of *Xenopus* gp 69/64 which has been shown to be essential for sperm binding to the VE. Although, as of yet, there is no evidence for sperm binding at the Dp ZP2 N-terminus, it is interesting that in this region three potential O-glycosylation sites are conserved in both species, in contrast to N-glycosylation sites. It was found that the Dp ZP2 mRNA is expressed in stage 1 oocytes and in the follicle cells surrounding the oocyte. Similarly, in *Xenopus* oocytes, the gp 69/64m RNA, was found in the oocytes, as well as in the somatic cells. *Mol. Reprod. Dev.* 59: 133–143, 2001. © 2001 Wiley-Liss, Inc.

Key Words: oogenesis; ZP domain; follicle cells; sperm binding

binding before progression of the sperm to the egg plasma membrane. In particular, two glycoproteins of *Xenopus* envelope, gp 43 and gp 69/64, have a key role in the envelope modifications that occur during acquisition of VE penetrability by sperm at fertilization (reviewed in Hedrick and Nishihara, 1991; see also Tian et al., 1997a). Investigations on *Xenopus* VE gp 41 or its coelomic form gp 43, have revealed homology between this glycoprotein and the ZPC family (Kubo et al., 1997; Yang and Hedrick, 1997). Recently, *Xenopus* gp 69/64 has been cloned and its sequence shown to be closely related to the components of the ZPA family, such as the mouse zona pellucida ZP2. It appears that in all the vertebrate ZP glycoproteins studied so far, there is high sequence similarity in a specific domain, the ZP domain (Kubo et al., 1997; Yang and Hedrick, 1997), which is also found in the extracellular matrix of some somatic tissues (Bork and Sander, 1992). Although the amount of structural information is increasing rapidly, at present we cannot yet assign specific physiological roles to the various segments that compose the ZP molecules. In particular, the chemical differences, other than primary amino acid sequences, that render the envelope glycoproteins functional in binding of sperm of homologous species have not been elucidated. Therefore, more comparative studies are needed to understand the structural similarities and differences between the ZP proteins and their role in binding sperm to the egg envelope.

Discoglossidae is considered one of the oldest anuran families (see Elinson, 1986). It is part of the Archeobatrachia group (Ford and Cannatella, 1993), together with the Pipidae family that includes *Xenopus laevis*.

INTRODUCTION

The vitelline envelope (VE) of the amphibian egg not only protects the egg and the embryo from environmental injuries until hatching, but also contains molecules that mediate the initial stage in sperm

Grant sponsor: NSF; Grant sponsor number: 1BN9728656; Grant sponsor: MURST PRIN.

*Correspondence to: Prof. Chiara Campanella, Dipartimento di Biologia Evolutiva e Comparata, Università di Napoli Federico II, Via Mezzocannone 8, 80134, Napoli, Italy.
E-mail: Campanella@dgbm.unina.it

Received 28 July 2000; Accepted 27 October 2000

However, while Discoglossidae diverged early from a common amphibian ancestor, the divergence of Pipidae occurred later in evolution (Ford and Cannatella, 1993). Eggs of several Discoglossidae species are characterized by an unusual jelly arrangement and by a highly specialized site of sperm entrance. In the most widespread species, *Discoglossus pictus*, in addition to the outer jelly layers which surround the egg completely, there is a plug of jelly which indents the animal half of the egg. At the base of this depression, there is a small cup-shaped pit, the *dimple*, which is the only site where sperm can fuse with the egg and can activate development (Campanella, 1975; Talevi and Campanella, 1988). At the dimple surface, specific glycoproteins are found that 'in vitro' function as sperm receptors (Maturi et al., 1998). The VE surrounds the whole egg, and in the region of the dimple it spans the pit. Despite these novel features, recent data indicate that, in this species, many features of the VE are shared with evolutionary distant anurans. Thus, the envelope, which forms during oogenesis, after ovulation cannot be penetrated by sperm. This coelomic form of the envelope acquires the ability to bind sperm following conformational and biochemical changes that occur during its passage through the oviduct. As observed in *X. laevis* (Gerton and Hedrick, 1986a) and in *Bufo japonicus* (Takamune et al., 1986), the *D. pictus* 42-kDa protein (43 and 52/40 kDa in respective species) undergoes limited proteolysis. In addition, the SDS PAGE profile of the VE proteins of the uterine *D. pictus* egg is quite similar to that of the *X. laevis* VE (120, 112, 69, 64, 41, and 37 kDa), as it is composed of bands of 118, 106, 75, 63, 40, and 37/38 kDa (Caputo et al., 2001). The protein of 63 kDa has been shown to undergo changes in Mr as a result of fertilization (Infante et al., 1998).

It has been reported that, in the *X. laevis* VE, gp 69/64 mediates sperm-egg binding and periodate-sensitive moieties presumed to be glycans are essential for the binding to occur (Tian et al., 1997a, b). During fertilization, limited proteolysis cleaves this component into two proteins of 66/61 kDa (Gerton and Hedrick, 1986b) by removing 27 amino acids from the N-terminus, thereby eliminating sperm binding ability (Tian et al., 1999). Moreover, the gp69 and gp64 glycoproteins are two glycoforms of the same polypeptide, having approximately the same number of N-linked oligosaccharide chains, but differing in the extent of O-glycosylation. Comparison between gp69/64 and members of the ZPA family indicate that the highest sequence similarity between the *X. laevis* and mammalian ZPAs is in the C-terminal half of the molecule that contains the ZP domain (Tian et al., 1999).

To test the generality of some of these findings, in this paper we have cloned and sequenced the cDNA encoding *D. pictus* 63-kDa protein, because preliminary experiments had suggested that this protein may bind spermatozoa during the fertilization process (Infante et al., 1998). Screening of a *D. pictus* oocyte cDNA library was performed utilizing *Xenopus* gp64/69 cDNA

as a probe. Analysis of the sequence of the *D. pictus* protein revealed regions of high sequence similarity with *Xenopus* gp 69/64 and with mammalian ZP2. Because of this homology, the *D. pictus* 63-kDa protein is named Dp ZP2. It was found that the Dp ZP2 mRNA is expressed early in oogenesis and its expression is turned off in the vitellogenic oocyte. Interestingly, somatic cells surrounding the oocyte also express Dp ZP2. Similarly, in situ hybridization using *Xenopus* gp 69/64 antisense RNA on *Xenopus* oocytes, indicates that a similar distribution occurs for the expression of gp 69/64.

MATERIALS AND METHODS

Animals and Gametes

Adult *D. pictus* females were captured in the neighborhood of Palermo (Italy). Adult *X. laevis* females were obtained from Rettilli (Varese, Italy). Groups of oocytes at various stages of oogenesis were excised from the ovaries of females anaesthetized with MS222 (Sigma Chemical Co, St. Louis, MO, USA). To obtain eggs, *D. pictus* females were injected in the dorsal lymphatic sac with 200–250 units of Profasi HP (Serono, Rome, Italy) in Amphibian Ringer (111 mM NaCl, 1.3 mM CaCl₂, 2 mM KCl, 0.8 mM MgSO₄, 25 mM Hepes, pH 7.8), while *X. laevis* females were injected with 500 UI of Profasi HP. Uterine eggs were collected 18 hr after hormone injection.

The stages of *X. laevis* oocyte growth stages (Dumont, 1972) are: stage 1 (50–300 µm); stage 2 (300–450 µm); stage 3 (450–600 µm); stage 4 (600–1,000 µm); stage 5 (1,000–1,200 µm); stage 6 (1,200–1,300 µm). For *D. pictus* the stages were as follows (Carotenuto, unpublished): stage 1 (50–300 µm); stage 2 (300–500 µm); stage 3 (500–750 µm); stage 4 (750–1,000 µm); stage 5 (1,000–1,500 µm); stage 6 (1,500–1,800 µm).

SDS PAGE and Protein or Lectin Blot

Vitelline envelopes were manually dissected from the eggs and prepared as previously described (Tian et al., 1997a). VE components were separated by SDS PAGE and transferred to nitrocellulose sheets overnight at 180 mA. Lectin blotting was performed as described in Maturi et al., 1998. Briefly, transferred proteins were first blocked in 2% BSA in PBS and then exposed to biotin-labeled *Dolichos biflorus agglutinin* (DBA) (Sigma), followed by incubation in Avidin-AP (Sigma). *Galanthus nivalis agglutinin* (GNA) was part of a DIG Glycan differentiation Kit (Roche). Negative controls consisted of the addition of 0.2 M D-mannose or 0.2 M N-acetyl-galactosamine to GNA and DBA, respectively.

Cloning and Sequencing of DpZP2 cDNA

Unidirectional cDNA library in pBK-CMV phagemid vector (ZAP Express cDNA cloning kit, Stratagene) was constructed using poly (A)⁺ mRNA isolated from *D. pictus* oocytes. The oocyte cDNA library was plated at a density of 3×10^4 PFU/150 mm plate and membranes (Hybond N-Amersham) were screened by standard

hybridization methods using a random primed ^{32}P labeled (GIBCO-BRL and NEN, respectively) *X. laevis* gp 69/64 cDNA as a probe in a solution of 0.5 M NaH_2PO_4 , 7% SDS, 1% BSA, 1 mM EDTA at 55°C. Washes were performed at high stringency and filters were exposed to Kodak XAR5 Film.

Since the initial cDNA clones identified lacked the 5' end of the coding sequence, RACE using *D. pictus* oocytes total RNA with specific primers was performed according to Frohman (1994). RNA was reverse transcribed with SuperScript II RT-polymerase (Gibco-BRL, Paisley, UK) and PCR was performed using HiFidelity Taq (Roche, Mannheim, Germany) to minimize errors in replication.

The library clone encoding the 3' half of the transcript and including the ZP domain was sequenced in both directions manually with the Sequitherm Excel II kit (Epicentre) using the Perkin-Elmer gene Amp PCR system 2,400 and ^{35}S -dATP (NEN). The 5'RACE product, which contain the first 1,200 bp of the entire Dp ZP2 sequence, was sequenced by Research Genetics (Huntsville, AL). All sequence information was processed using MacVector Software.

Hybridization of cDNA Probe to RNA Blots

For analysis of mRNA, total RNA from *D. pictus* tissues (ovaries, heart, liver, oviduct and testis) or *X. laevis* (ovaries, liver, heart, oviduct) was isolated using a Trizol kit (Gibco, BRL). Twenty micrograms of total RNA from each organ was separated on 1% formaldehyde agarose gel and blotted on a nylon membrane (Roche). For *D. pictus* tissues, Dp ZP2 cDNA (the 3' half of the transcript) probe was labeled with the random primer DNA labeled kit (Roche) and ^{32}P -labeled dCTP (NEN). For *X. laevis* tissues, gp69/64 cDNA full length was similarly labeled. RNA blots were hybridized in a mixture of 0.5 M NaH_2PO_4 , 7% SDS, 1% BSA, 1 mM EDTA at 60°C. The filters were washed at 60°C in $2 \times \text{SSC}$, 2% SDS, $0.2 \times \text{SSC}$, 0.2% SDS before exposure to X-ray film.

In Situ Hybridization on Sections

The following probes were utilized: 5'RACE fragment of DpZP2 and the first 1,031-bp fragment of the gp69/64 cDNA where the ZP region was eliminated by digestion with restriction enzymes Sma I at the 5' side and EcoRV at the 1,031 bp position. Both probes were cloned into pBluescript II KS vector (Stratagene, La Jolla, CA). The orientation of the insert was determined by digestion with restriction enzymes. The construct with 5' RACE fragment was cut with Eco RV and Bam HI and the construct with gp69/64 fragment was digested with BamHI and Xho I and used as template to synthesize digoxigenin-labeled antisense and sense, with digoxigenin-labeled UTP and, respectively, T3 and T7 RNA polymerase, according to the manufacturer recommendations (Roche).

D. pictus and *X. laevis* oocytes were fixed in 2% FAD, 250 mM NaCl, 5% acetic acid for 1 hr at 4°C and processed for embedding in paraffin according to

standard techniques. Following attachment onto Superfrost Plus slides (Merck), the 5–6 μm thick sections were deparaffinized in xylene and rehydrated in graded ethanols. Sections were then fixed in 4% paraformaldehyde in PBS, washed in PBS and digested with proteinase K (Roche) (10 $\mu\text{g}/\text{ml}$ in 20 mM Tris/HCl pH 7.2, containing 1 mM EDTA) at 37°C. After re-fixing with 4% paraformaldehyde, the sections were rinsed in PBS and incubated in 0.1 M Tris/glycine buffer. The sections were hybridized overnight at 60°C in 40% formamide, $1 \times$ Denhardt's solution, $5 \times \text{SSC}$, 200 $\mu\text{g}/\text{ml}$ tRNA (Sigma) and 100 ng of sense or antisense digoxigenin-labeled RNA on each slide. The slides were exposed to $0.5 \times \text{SSC}$, 20% formamide for 1 hr at 60°C and to the following treatments: (1) NTE (10 mM Tris-HCl pH 7.0, 0.5 M NaCl, 5 mM EDTA) at 37°C for 15 min; (2) NTE containing RNase A at 37°C for 30 min; (3) NTE at 37°C for 15 min; (4) $0.5 \times \text{SSC}$, 20% formamide at 60°C for 30 min; (5) 2% Roche blocking solution in 100 mM maleic acid, 150 mM NaCl, pH 7.5 for 30 min. Sections were incubated overnight in anti-digoxigenin alkaline phosphatase conjugated antibody (Roche), diluted 1: 2000 in 2% Roche blocking solution containing 100 mM maleic acid and 150 mM NaCl, pH 7.5. Following washing in 0.1% Tween-20, 0.5 mg/ml levamisole (Sigma), sections were incubated at room temperature in the developing solution, BM purple color substrate (Roche) in 2% Tween-20 and 1 mM levamisole. After stopping the reaction in 1 mM EDTA in PBS, sections were mounted in PBS-glycerol and observed on a Leitz Photomicroscope. Photographs were taken using a Kodacolor ASA 100 film.

Antibody Staining

An antiserum against *X. laevis* gp 69/64 components (Tian et al., 1997a) was used to immunolocalize the glycoproteins of *D. pictus* VE. Anti-gp 69/64 strongly reacts with *X. laevis* gp 69/64 and to a minor extent with other VE components including gp 41 (see Tian et al., 1997a). Similarly, it reacts with *D. pictus* 63 kDa protein and proteins of lower Mr (Infante et al., 1998). Sections of the same samples utilized for in situ hybridization were used as previously described (Carotenuto et al., 2000). Briefly, paraffin sections of *X. laevis* and of *D. pictus* oocytes were: (1) immersed in coplin jars containing 0.01 M buffer citrate pH 6 in a microwave oven for 3×7 min to expose potential antibody binding sites (Gown et al., 1993); (2) exposed to 0.3% H_2O_2 for quenching of endogenous peroxidase activity; (3) incubated first in goat antiserum and then in 10 mM Tris-HCl, pH 7.4, containing 1% BSA, 0.3% Triton X-100, 1% gelatin, 0.02 M glycine, 5% NaCl; (4) reacted to gp69/64 antiserum diluted in PBS containing 1% BSA and 0.3% Triton X-100 or, alternatively, to rabbit pre-immune serum or IgG as controls (Sigma). Antibody binding was detected by biotinylated anti-rabbit IgG raised in goat, followed by incubation with Vectastain ABC reagent (Vector laboratories,

Burlingame, CA) and by DAB development. The sections were mounted in PBS/glycerol.

RESULTS

Vitelline Envelope Protein of 63 kDa Is Glycosylated

In the cases studied, such as in *Bufo* and *Xenopus*, the proteins of the VE are glycosylated and their oligosaccharide chains are believed to have an important role in binding sperm (Omata and Katagiri, 1996; Tian et al., 1997a, b). To ascertain if this post-translation modification had occurred also in *D. pictus* 63 kDa protein, lectin blots were performed. In Fig. 1 are shown GNA and DBA blots of the total VE proteins after gel electrophoresis. GNA is a lectin specific for nonreducing terminal mannosyl residues present on high-mannose-type N-linked chains (Shibuya et al., 1988). DBA recognizes *N*-acetylgalactosamine α 1,3-*N*-acetyl galactosamine units found in O-linked glycans (Schachter and Brockhausen, 1992). The 63-kDa protein cross reacts with both lectins, suggesting that it contains both N-linked and O-linked glycans, similarly to other VE glycoproteins. More informations related to VE reactivity to lectins are available in Caputo et al. (2001).

D. pictus gp 63 Is a ZP2 Homolog

Because preliminary data suggested that gp 63 was able to bind sperm and was similar in size to *X. laevis* gp 69/64, we used *X. laevis* gp 69/64, a homolog of mammalian ZP2 proteins as a probe to screen an oocyte library and identified a homolog in *D. pictus* gp 63. Sequencing of the clone isolated from the *D. pictus* cDNA library as well as a 5' RACE fragment, revealed that the full-length Dp ZP2 cDNA contained 2,230 bp with an opening reading frame (ORF) of 2,094 nucleotides. The 5' and 3' untranslated regions flanking the coding sequence consisted of 89 nt from the start MET and 29 nt from the stop codon to the polyA tail, respectively. A polyadenylation site (AATAAA) is 14

nt upstream of the poly(A) tail and 9 nt after the stop codon (TGA) (underlined in Fig. 2). The ORF encodes a polypeptide chain of 697 residues with a calculated mass of 77,243 Da. The calculated mass is significantly larger than the apparent mass of the mature glycosylated gp 63, as in the case of *X. laevis* gp 69/64 (Tian et al., 1999). At the N-terminus, a possible cleavage site was predicted to be present between residues 36 and 37, applying the algorithm of Von Heijne (1986) (Figs. 2 and 3). Analysis using the Kyte-Doolittle algorithm, identified a hydrophobic domain 36 amino acids long (Fig. 3), as expected for a signal peptide. However, according to the algorithm of Von Heijne it is unclear if this sequence is a potential signal peptide. A second strong domain of hydrophobicity is present in the C-terminal domain (residues 668–684), followed by positively charged residues (Fig. 3), as in many transmembrane domains (Kyte and Doolittle, 1982). A domain with strong ZP-like sequence identity is located between residues 403 to 617. A potential furin cleavage site, RXK/RR (RKRR), is found between this ZP-domain and the highly hydrophobic domain.

A search of the GenBank revealed that the sequence of Dp ZP2 cDNA is very similar to that of the *X. laevis* gp 69/64 and to the mouse zona pellucida glycoprotein ZP2 (Fig. 4). In fact, most of the conserved sequence is located in the C-terminal half of the sequence, where the ZP domain is located. Moreover, as shown in Figs. 2 and 4, the polypeptide chains are similar in length and have a C-terminal hydrophobic domain and a furin-like protease cleavage site immediately after the ZP domain (Fig. 4); these features are characteristic of ZP2 proteins. Eighteen cysteine residues of the Dp ZP2 are located at conserved positions in all the ZP2s of the compared species (*X. laevis*, man, pig, rabbit, and dog). The entire deduced amino acid sequence of Dp ZP2 cDNA is 48% identical to *X. laevis* gp 69/64 and 37–40% to ZP2s of the above-mentioned mammalian species. In particular, in the C-terminal ZP domain, the identity reached 61% with *X. laevis* and 50–55% with ZP2s of the mammalian species. For the N-terminal half preceding the ZP-domain, the sequence identity is 40%, with *X. laevis* and 28–31% with mammalian ZP2s, (see Fig. 4). When the N-terminus of human ZP2 was compared with that of other mammalian species, the homologies were much higher, being 64% (canis), 59% (pig), 65% (rabbit), and 51% in the mouse.

The Dp ZP2 putative amino acid N-terminal sequence (positions 132–185) was aligned with the corresponding gp 69/64 fragment of *X. laevis* that has been shown to be necessary for sperm binding to the VE in this species (Tian et al., 1999) (Fig. 5). The sequences of the first 30 amino acids of the two species are 50% identical. In this region sequence, one potential N-glycosylation site [NCS] is found in Dp ZP2 that is absent in *X. laevis* gp 69/64. In contrast, in the same region, the sequence of both species contains several Thr and Ser residues that could serve as species-specific potential O-glycosylation sites that function in sperm binding. Among these residues, one

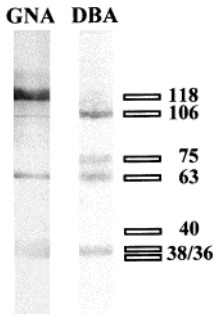


Fig. 1. Lectin blots of *D. pictus* VE proteins. The apparent molecular weight and position of the main proteins of the VE are indicated. The 63-kDa band reacts with GNA and DBA. Similarly, other proteins are reactive with one of both lectins.

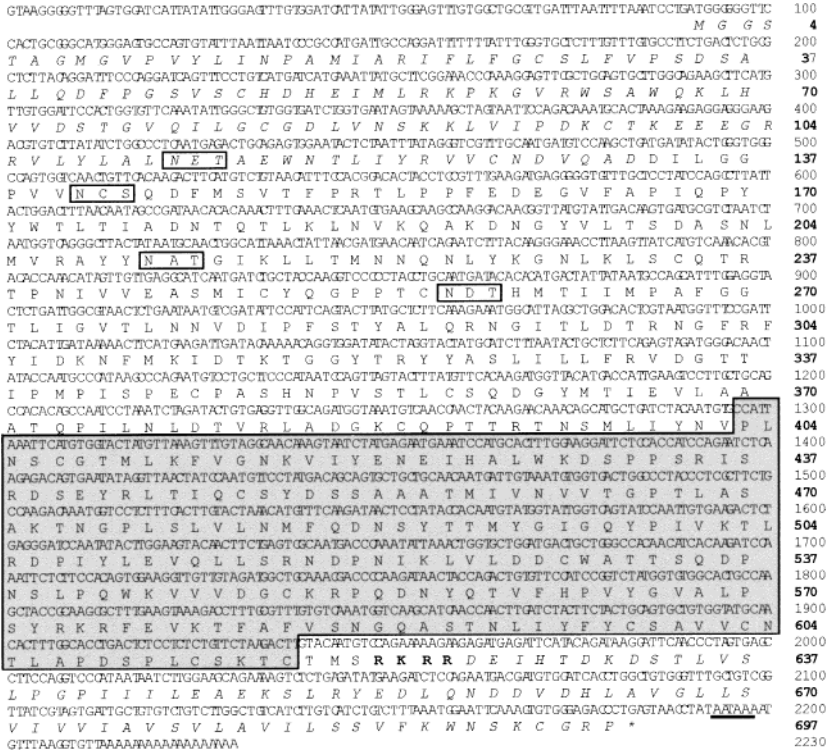


Fig. 2. cDNA sequence and translated single-letter amino acid sequence of Dp ZP2. The polyadenylation site (AATAAA) is underlined and the ZP-domain is boxed in gray. The putative carboxy and amino terminal prosequences are italicized with the potential furin cleavage site (RKRR) in bold face. The possible mature protein is in normal type. The four putative N-glycosylation sites are boxed.

Thr and two Ser/Thr residues are at the same position in *D. pictus* and in *X. laevis* (Fig. 5).

The entire deduced amino acid sequence of Dp ZP2 is 34% identical to *X. laevis* gp37 and 14% identical to *X. laevis* gp 43.

Dp ZP2 Expression

Northern blot analysis of total RNA isolated from *D. pictus* ovary, liver, heart, oviduct, and testis, detected a single 2.5-kb band only in the ovary in *D. pictus*. Similarly, the analysis of *X. laevis* mRNA revealed a single band of 2.5 kb in the RNA blot of the ovary, while in liver, heart, and oviduct RNA blots there was no signal. These results indicate that expression of the DpZP2 and of the gp69/64 cDNA transcript was localized to the ovary (Fig. 6).

In Situ Hybridization and Anti-gp 69/64 Immunolocalization

Discoglossus pictus. *D. pictus* ovarian sections were exposed to the sense and antisense transcripts of DpZP2 5'RACE fragment that do not contain the ZP

domain. The digoxigen-labeled antisense was found to hybridize to the oocytes, starting from oocytes of about 80 μm in diameter. The mRNA was located throughout the cytoplasm with a strong hybridization signal in stage 1 oocytes (Fig. 7). From stage 2 up to the end of oogenesis, the signal was absent from the cytoplasm. In addition, the hybridization probe was localized in the follicle cells surrounding the oocytes. This localization, appears early in the stage 1 oocytes (Fig. 7e). The mRNA localization occurred in all of the samples that we observed and was specific, as control sections incubated with sense riboprobe indicate (Fig. 7f). In sections incubated with anti-*X. laevis* gp64/69 antibody, the VE stained as a thin peripheral rim in late stage 1 oocytes, and as a more substantial layer in older stages (Fig. 8a). In stages 1 and 2, the immunostaining is also present in the cytoplasm, as tiny uniformly distributed spots. The follicle cells are stained as well (Fig. 8b). Figure 8c is a control section incubated with rabbit IgG as first antibody.

Xenopus laevis. *X. laevis* ovarian sections were exposed to sense and antisense transcripts of a gp69/64 cDNA fragment in which the ZP region was eliminated.

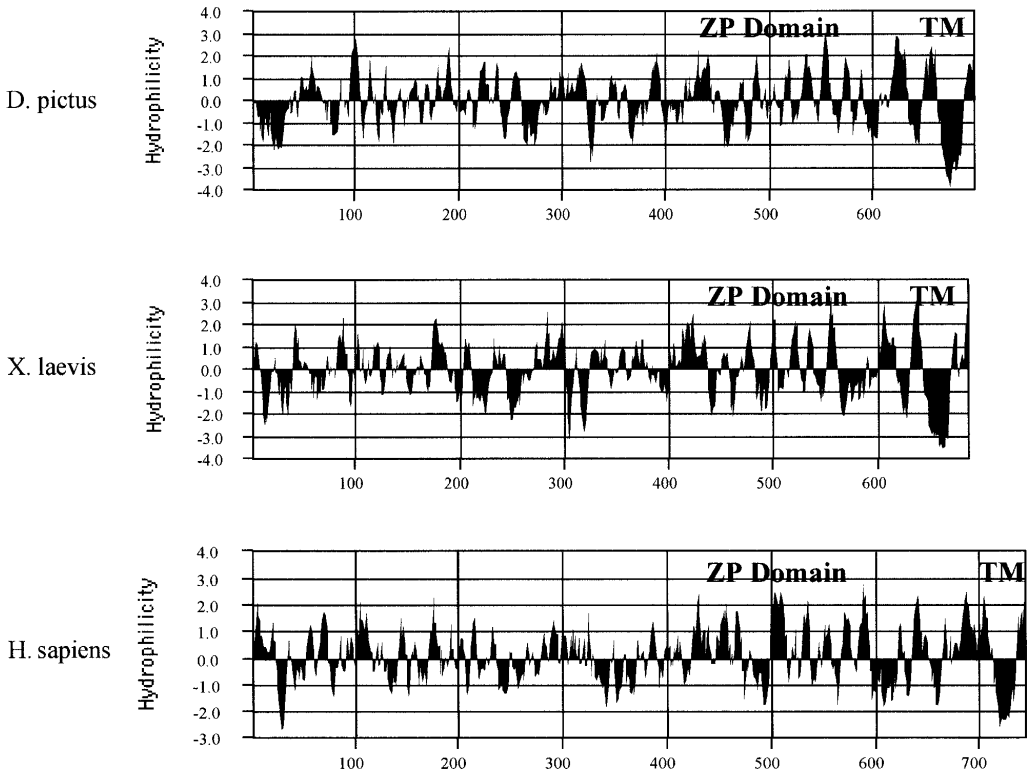


Fig. 3. Comparison of hydrophilicity plots of *D. pictus* Dp ZP2, human ZP2 and *X. laevis* gp 69/64. The plots were made using the Kyte-Doolittle algorithm and aligned at the conserved ZP domain. A C-terminal hydrophobic domain (TM) is present in all the three sequences.

Similar to *D. pictus*, the probe specifically hybridized to the oocytes starting from oocytes of about 60 μm , peaked in oocytes of 150–250 μm , and it was absent starting from stage 2 oocytes. (Fig. 9). In the follicle the hybridization was found as well (Figs. 9c and 9d). Control sections, incubated with sense riboprobe, did not show any hybridization signal (Fig. 9b). In oocyte sections incubated with anti-gp 64/69, immunostaining was observed as spots throughout the cytoplasm of stage 1 oocytes, and in the later stages it was clearly evident at the oocyte surface. The follicle cells were also labeled by the antibody (Figs. 9 f–h).

DISCUSSION

Earlier studies in *D. pictus* suggested that gp 63 in the VE of the mature egg is responsible for binding of sperm to the envelope and that the Mr of this glycoprotein changes as a result of fertilization (Infante et al., 1998). In vitro studies and ultrastructural observations showed that sperm bind to the VE and that fibrils are detectable between the VE and sperm in the process of VE penetration (Campanella et al., 1997; Infante et al., 1998). In this study, we have isolated the

cDNA of the *D. pictus* gp 63/ZP2 using the cDNA encoding for *X. laevis* gp 69/64 as a probe. The deduced amino acid sequence for the *D. pictus* glycoprotein was found to be 48% identical to *X. laevis* gp 69/64 and 37–40% identical to mammalian ZP2. Northern blots and in situ hybridization studies indicated that Dp Zp2 mRNA is expressed in previtellogenic oocytes. The probe localized in follicle cells as well, suggesting the possible involvement of somatic cells in the assembly of the VE. In *X. laevis* oocytes a similar localization was found.

Among the conserved sequence characteristics are a putative site for cleavage by a furin-like protease, a putative C-terminal transmembrane domain (Kyte and Doolittle, 1982) and 18 cysteine residues all present at conserved positions. Furthermore, the hydrophathy plots of mammalian and amphibian proteins are similar to each other. These data are consistent with the hypothesis that mammalian and amphibian envelopes have similar molecular constituents. Kubo et al. (1997) and Yang and Hedrick (1997) showed that, for ZPC, the identity can be extended to medaka VE, as several sequences are available for the ZP3 homolog of

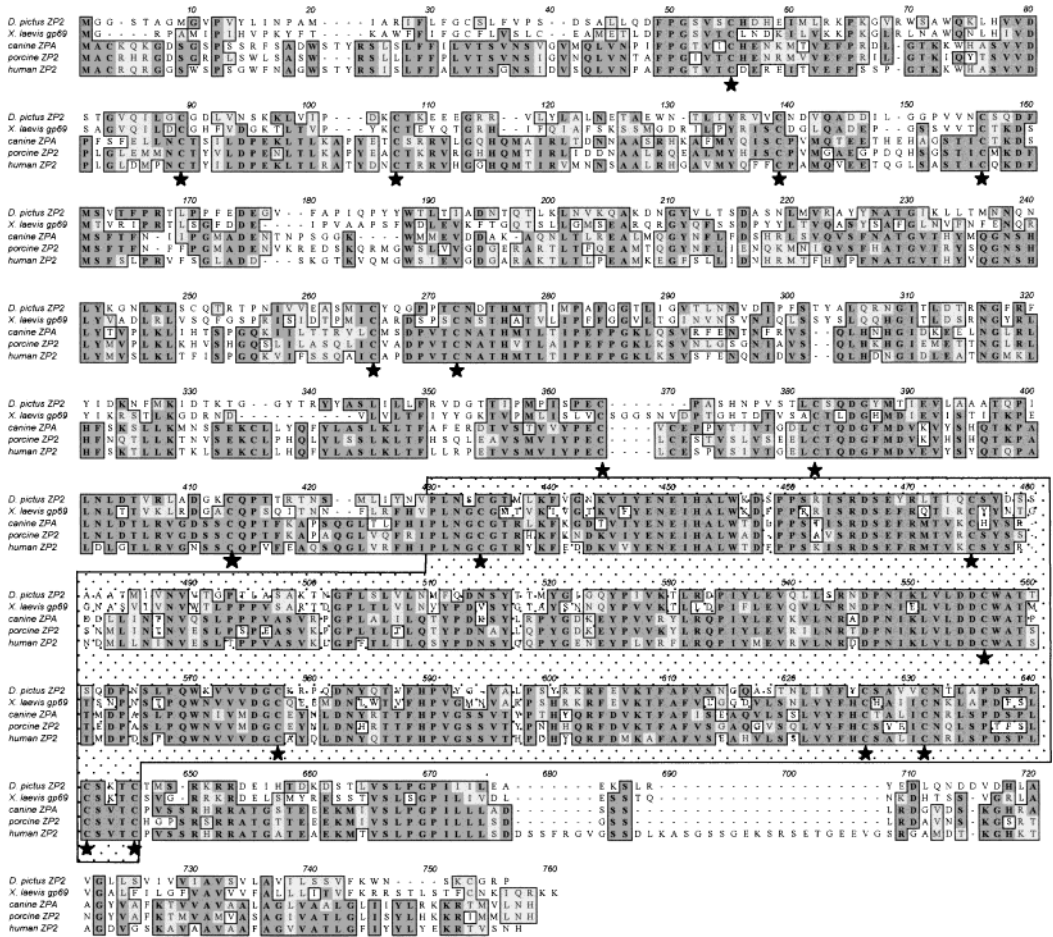


Fig. 4. Clustal formatted alignment of *D. pictus* Dp ZP2, *X. laevis* gp 69/64, dog ZPA, pig ZP2, and human ZP2. Residues in bold indicate a conserved amino acid in 3 of the 5 aligned sequences and when boxed in medium gray depict the identical amino acid in the conserved position. The conserved ZP domain is boxed. Each of the 18 conserved cysteines is indicated by a star.

this species (Lyons et al., 1993; Murata et al., 1995; Chang et al., 1996; Del Ciacco et al., 1998). ZP-domains are also present in the extracellular coat of somatic cells (Bork and Sanders, 1992). Comparative studies aimed at understanding the basis of sperm-egg interaction

may therefore contribute to the identification of ancestral molecules that served as precursors for both extracellular matrix proteins and sperm binding proteins.

In the present study, the focus was a comparison between *X. laevis* and *D. pictus* ZP2. In contrast to the



Fig. 5. Alignment of Dp ZP2 sequence at positions 132–185 with corresponding fragment of gp 69/64. One potential N-glycosylation site [NCS] (underlined and in bold) is present only in the *D. pictus* sequence. Three potential O-glycosylation sites (in bold) are found at corresponding positions in the sequence of both species. Species-

specific potential O-glycosylation sites are underlined. In the gp 69/64 sequence, site 1 is the N-terminus of the proteolytically processed form after fertilization, and site 2 is the N-terminus generated by treatment of eggs with crude type-I collagenase (see Tian et al., 1999).

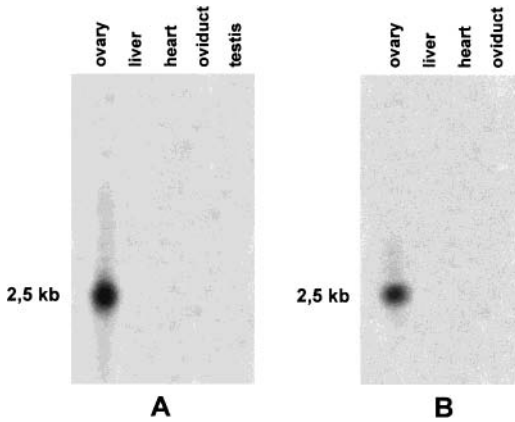


Fig. 6. Northern blot analysis of total RNA isolated from *D. pictus* and *X. laevis* tissues. **A**, Dp ZP2 cDNA was used to probe ovaries, liver, heart, oviduct and testis. A single 2.5-kb band is present only in the ovary RNAs. **B**, *X. laevis* gp 69/64 cDNA was used to probe ovaries, liver, heart, and oviduct. A single 2.5-kb band is found only in the ovary RNA.

situation in mammals, prior to this study information on the VE glycoproteins involved in sperm binding in amphibian species other than *X. laevis* was not available. Although the amphibians appear to have a monophyletic origin, their marked diversification during evolution and/or environmental adaptations may have given rise to different strategies of fertilization.

Discoglossus diverged early during evolution not only from *Rana* and *Bufo* (*Neobatrachia*), but also from *Xenopus* (*Archeobatrachia*) (Ford and Cannatella, 1993). Indeed, fertilization in this species has several morpho-functional features (cf. Introduction) quite dissimilar from those of the above mentioned species (Elinson, 1986).

However, the finding that Dp ZP2 cDNA has strong homology with *X. laevis* gp 69/64 cDNA supports the thesis that molecules containing ZP-domains constitute the common basis of sperm-VE interaction. We found that the N-terminus preceding the ZP domain in mammals share identities ranging from 65 to 51, while between *X. laevis* and the corresponding *D. pictus* deduced sequence was only 40% identical, suggesting more diversification in this region between amphibian species than among the compared mammalian species.

Information on the N-terminal sequence of the mature gp 63 present in the VE of *D. pictus* egg and the Mr of the deglycosylated protein are not yet available. However, it can be hypothesized that, because the calculated mass of the deduced amino acid sequence is larger than the apparent mass of the mature glycosylated gp 63, post-translational changes occur during passage through the secretory pathway. These changes include N- and O-linked oligosaccharide chains addition, as indicated by GNA and DBA lectin blots in our work, together with N- and C-terminal proteolysis and processing. With respect to the C-terminus, the sequence RXK/RR present between the ZP domain and the putative transmembrane domain could be the site of cleavage of the protein from

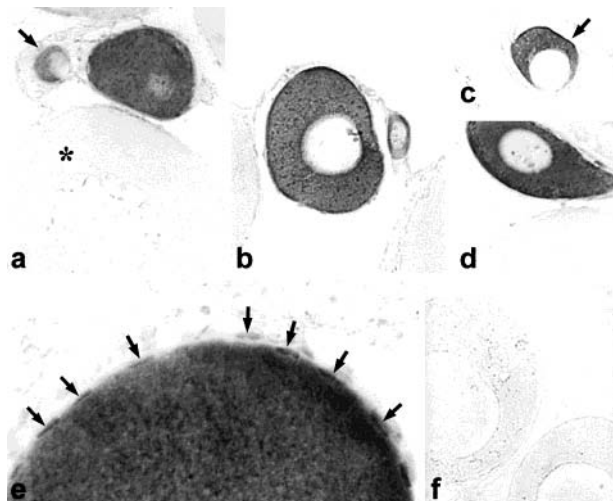


Fig. 7. In situ hybridization on *D. pictus* oocytes sections, utilizing as probes the sense and antisense transcripts of the 5' RACE, stages 1 and 2 oocytes. In stage 1 oocytes, the hybridization signal is strong, but is practically absent starting from 300- μ m oocytes (asterisk). The arrows indicate oocytes of 80–100 μ m in early stage 1, where the hybridization signal is already present. **a** and **b**, $\times 140$; **c** and **d**, $\times 280$;

e, the follicle cells located at the surface of a stage 1 oocyte are also labeled (arrows). $\times 320$; and **f**, control section incubated with sense riboprobe showing stage 1 oocytes; no hybridization signal is found. [Color figure can be viewed in the online issue, which is available at www.interscience.wiley.com]

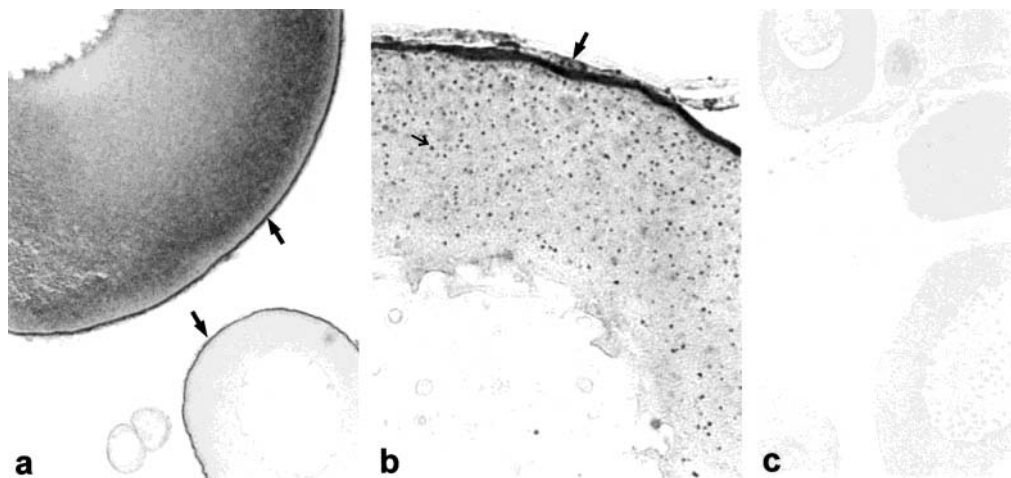


Fig. 8. Immunostaining with anti-gp 69/64 antiserum on *D. pictus* oocytes. **a**, the stain is on the VE (arrows) surrounding the two large oocyte (late stage 1 and stage 4). It should be noted that the brown color of the oocyte cytoplasm is the pigment typical of the animal half ($\times 140$); **b**, follicle cells on the surface of a stage 1 oocyte. The arrow

indicate follicle cells where the staining is clearly evident ($\times 500$); and **c**, control section stained with pre-immune serum. The immunostain is absent ($\times 140$). [Color figure can be viewed in the online issue, which is available at www.interscience.wiley.com]

hydrophobic anchor. This motif was shown to be a signal for furin-catalyzed precursor cleavage within the constitutive secretory pathway (Hosaka et al., 1991) and was first reported in ZPs by Yurewicz et al. (1993). In *X. laevis* gp 69/64, when deglycosylated, the size is that predicted for cleavage at the furin site (Tian et al., 1999).

Twenty-seven residues of the mature gp 69/64 of *X. laevis* gp 69/64 N-terminus were shown to be eliminated after fertilization and to be essential for sperm binding to VE in *X. laevis*. This conclusion was based on the facts that the isolated truncated glycoprotein is inactive as an inhibitor of sperm-egg binding and, in the FE of fertilized eggs, it is unreactive to polyclonal antibody against the mature gp 69/64 (Tian et al., 1999). In *D. pictus* deduced sequence, the first 30 amino acids domain within residues 132–185 is not proved yet to be the N-terminus of DpZP2, but it shares 50% identity with the corresponding sequence of gp 69/64. Some potential O-glycosylation sites are located in the latter sequence, three of them being in conserved positions in Dp ZP2 and in gp 69/64. The latter finding may be of interest, as it was suggested for gp 69/64 that the presence of O-glycosylation is essential for its role of binding to sperm (Tian et al., 1997a). This requirement has been demonstrated in mammals (Blail et al., 1988) and in other species (reviewed by Rosati, 1995, and Dhume et al., 1996). However, in the case of *D. pictus*, as of yet there is no direct or indirect evidence for sperm binding at the N-terminus.

Recently, it was shown that, in addition to gp69/64, gp 41 has sperm binding activity. This binding is proposed to be dependent on the N-linked oligosaccharide chains of gp41 (Vo and Hedrick, 2000).

In *D. pictus*, it has been shown by ultrastructural analysis that the acrosome reaction occurs in the outermost jelly layer, and that thin VE fibrils attach to the acrosome-reacted sperm a few minutes post-insemination. Moreover, sperm bind to the VE only after they had been treated with Ca ionophore (Campanella et al., 1997; Caputo et al., 2001). These data suggest that the binding between sperm and VE is a secondary binding. *X. laevis* sperm has an acrosome cap with sparse electron-dense contents (Bernardini et al., 1986). Recent data suggest that these sperm contain trypsin and chymotryptic activities (Mizoke et al., 1999). However, up to now, it is not clear if in *X. laevis* enzymes are located in the acrosome cap and if the sperm even undergo an acrosome reaction. According to our present knowledge, *X. laevis* sperm bind to the VE in a jelly coat-independent primary binding event, but only if jelly is present can sperm penetrate the VE and, subsequently, fertilize the egg (Tian et al., 1997a).

In the present work, we used for our 'in situ' hybridization *D. pictus* and *X. laevis* probes where the ZP domain was eliminated in order to exclude possible interference in the hybridization with other ZP-containing VE glycoproteins. We found that in *D. pictus*, the Dp ZP2 mRNA is abundantly present in stage 1. The mRNA production appears to be restricted to stage 1 oocytes. Dp ZP2 mRNA was found also in the follicle cells surrounding stage 1 oocytes. Similarly, in *X. laevis*, gp 69/64 mRNA was found only in stage 1 oocytes and related follicle cells. In both species, the VE proteins appeared scattered throughout the oocyte cytoplasm of stages 1 and 2 oocytes, suggesting that proteins do not preferentially accumulate in particular regions of the

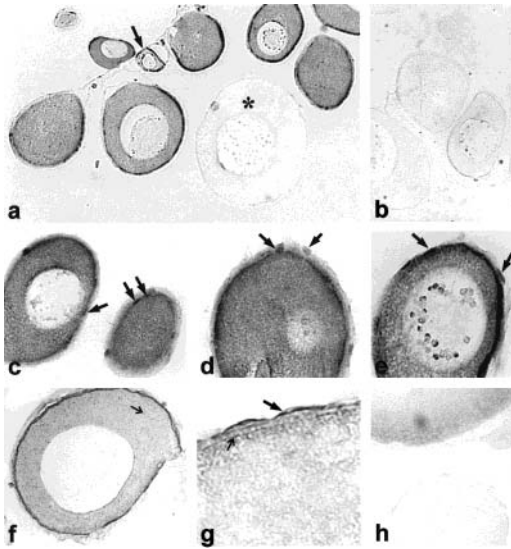


Fig. 9. a–e, Hybridization of *X. laevis* oocyte sections utilizing sense and antisense transcripts of gp69/64 1,031-bp fragment. In a, c, d, and e, the hybridization signal with the antisense riboprobe is strong in stage 1 oocytes, but was absent in early stage 2 oocytes (asterisk). The arrow indicates a 80- μ m oocyte. a, $\times 100$; in c, d and e the arrows indicate the follicle cells where the hybridization signal is present; c, $\times 200$; d and e, $\times 350$; b, section incubated with sense riboprobe; hybridization is absent; $\times 100$; f, g and h, immunostaining utilizing anti-gp 69/64 on *X. laevis* oocyte sections. In f, the staining is at the 200- μ m oocyte periphery and in tiny spots in the cytoplasm (small arrow), $\times 150$; g, the follicle cells covering the very thin layer of forming VE (small arrow) are stained (arrow), $\times 400$; and h, control section exposed to pre-immune antiserum: the immunostaining is absent, $\times 150$. [Color figure can be viewed in the online issue, which is available at www.interscience.wiley.com]

oocyte before secretion into the space between the oocyte surface and the follicle cells. The latter are stained by anti-gp 69/64 antiserum. Expression of DpZP2 mRNA and gp 69/64 mRNA does not occur in somatic tissue, such as oviduct, liver and heart or testis of either *D. pictus* or *X. laevis*. The liver in lower vertebrates (i.e., some teleosts) produces chorionic proteins that migrate through the bloodstream to the oocytes (Murata et al., 1997). By northern blot analysis we excluded the participation of liver in VE formation, and therefore it can be concluded that only the follicle cells of *D. pictus* and *X. laevis*, along with the oocyte, function in formation of the VE envelope by expressing Dp ZP2 and gp69/64.

Begovac and Wallace (1989) showed that VE glycoproteins originate in the follicle cell of the pipefish. In mammals, the zona pellucida (ZP) components of mouse are synthesized in the oocyte, whereas in the rabbit follicle cells also participate in the formation of the ZP (Lee and Dunbar, 1993; Wolgmuth et al., 1984). In *X. laevis*, it has been reported that the VE is primarily a product of the oocyte with little, if any, contribution

from the follicle cells (Pinto et al., 1985; Yamagimachi et al., 1989). In particular, gp 43 transcripts have been localized up to stage 2 oocyte cytoplasm and not to the somatic cells surrounding the oocytes (Kubo et al., 1997). Taken together, these data suggest that the VE glycoproteins are transcribed at an early stage of oogenesis, yet their transcription may follow different timing, i.e., stage 1 for gp 69/64 and up to stage 2 for gp 43. Moreover, the production of gp 69/64 is confined to follicle cells in the same stage, suggesting a contribution of these cells to the formation of the envelope at early stage of oogenesis.

ACKNOWLEDGMENTS

We are grateful to Drs. T. Capriglione, R. Carotenuto, and G. Odierna for suggestions and to Ms. D. Capobianco for help in the laboratory. A special thanks to Dr. Rita Marino of the Anton Dohrn Zoological Marine Station of Napoli and to Mr. G. Falcone for assistance. Work in the laboratory of Dr. W.J. Lennarz was supported by NSF grant #IBN9728656 and in the laboratory of Dr. Campanella by a MURST PRIN grant.

REFERENCES

- Begovac PC, Wallace RA. 1989. Major vitelline envelope proteins in pipefish oocytes originate within the follicle and are associated with the ZP3 layer. *J Exp Zool* 251:56–73.
- Bernardini G, Stipani R, Melone G. 1986. The ultrastructure of *Xenopus* Spermatozoon. *J Ultr Mol Struc Res* 94:188–194.
- Bleil JD, Wassarman PM. 1988. Galactose at the non reducing terminus of O-linked oligosaccharides of mouse egg zona pellucida glycoprotein is essential for the glycoprotein's sperm receptor activity. *Proc Natl Acad Sci USA* 85:6778–6782.
- Bork P, Sander C. 1992. A large domain common to sperm receptors ZP2 and ZP3 and TGF-type III receptor. *FEBS Lett* 300:237–240.
- Campanella C. 1975. The site of spermatozoa entrance in *Discoglossus* (Anura) unfertilized egg: an electron microscope study. *Biol.Reprod* 12:439–447.
- Campanella C, Carotenuto R, Infante V, Maturi G, Atripaldi U. 1997. Sperm-egg interaction in the painted frog (*Discoglossus pictus*): an ultrastructural study. *Mol Reprod Dev* 47:323–333.
- Caputo M, Infante V, Carotenuto R, Campanella C. 1999. Vitelline envelope in *Discoglossus pictus* fertilization. 7th International Xenopus Conference. Proceedings of the Satellite Workshop. 'Fertilization in Xenopus and other Amphibia', Chia Laguna September 1998 p. 11.
- Caputo M, Infante V, Carotenuto R, Talevi R, Campanella C. 2001. Following passage through the oviduct, the coelomic envelope of *Discoglossus pictus* (Amphibia) acquires fertilizability upon reorganization, conversion of gp42 to gp40, extensive glycosylation and formation of a specific layer. *Mol Reprod Dev* 58:318–329.
- Carotenuto R, Vaccaro MC, Capriglione T, Petrucci TC, Campanella C. 2000. Alpha-spectrin has a stage-specific asymmetrical localization during *Xenopus* oogenesis. *Mol Reprod Dev* 55:229–239.
- Chang YS, Wang SC, Tsao CC, Huang FL. 1996. Molecular cloning, structural analysis, and expression of carp ZP3 gene. *Mol Reprod Dev* 44:295–304.
- Del Ciacco L, Vanoni C, Bonsignorio D, Duga S, Mosconi G, Santucci A, Cotelli F. 1998. Identification and spatial distribution of mRNA encoding the gp49 component of the gilthead sea bream, *Sparus aurata*, egg envelope. *Mol Reprod Dev* 49:58–69.
- Dhume ST, Stears RL, Lennarz WJ. 1996. Sea urchin egg receptor for sperm: the oligosaccharide chains stabilize sperm binding. *Glycobiology* 6:59–64.
- Dumont JN. 1972. Oogenesis in *Xenopus laevis* (Daudin). I. Stages of oocyte development in laboratory maintained animals. *J Morphol* 136:153–180.

Vitelline Envelope gps 63 and 75 Specifically Bind Sperm in “In Vitro” Assays in *Discoglossus pictus*

VINCENZO INFANTE, MARIANGELA CAPUTO, STEFANIA RICCIO, ANNA DE FILIPPIS, ROSA CAROTENUTO, MARIA CARMEN VACCARO, AND CHIARA CAMPANELLA*

Dipartimento di Biologia Evolutiva e Comparata, Università di Napoli, Napoli, Italy

ABSTRACT In *Xenopus*, conflicting data related to sperm–vitelline envelope (VE) binding suggest that further experiments should be performed to study the role of VE glycoproteins in sperm binding. In this article, we studied the VE of *Discoglossus pictus*, where gp63, the product of the *Dp ZP2* gene, has high molecular identity to *Xenopus* gp69/64 and to mouse ZP2 and only A23187-treated sperm bind to VE. Sperm bind to VE all over the egg, yet a sperm tuft was found only in the animal half of the egg, where the dimple, the site of fertilization, is located and an intense immunostain was detected in VE by an antiserum directed against gp69/64. The same antiserum inhibited sperm binding to VE. Sperm binding to beads coated with gp63, gp40, or gp75 was in the range of 62–70% for gp63-beads, 67–75% for 75 beads, and about 20% for BSA beads and gp40-coated beads. Soluble purified gp63 and gp75 competitively inhibited binding of sperm to gp63-coated beads. Similarly, the same glycoproteins inhibited sperm binding to gp75-coated beads. SDS–polyacrylamide gels (PAGE) of FE and comparison of VE and FE peptide maps showed that gp63 undergoes a minor shift to about 62 kDa in FE. In sperm binding assays with beads coated with FEs gp62, there was no binding. Following fertilization, in the region of the dimple, an F-layer is formed as well as an alteration of the VE structure. Lectin blots of the FE showed that the FE and in particular gp62 acquires a stronger affinity to *Maackia amurensis* agglutinin (MAA) with respect to VEs gp63. These results indicate that gps 63 and 75 are the sperm binding glycoproteins of *D. pictus* VE, where major post-fertilization changes occur as in other anuran species. *Mol. Reprod. Dev.* 68: 213–222, 2004. © 2004 Wiley-Liss, Inc.

Key Words: vitelline envelope; amphibians eggs; sperm binding; glycoproteins; ZpA

INTRODUCTION

In the vitelline envelope (VE) of amphibian eggs, glycoproteins have been extensively studied and are thought to act at fertilization. In the case of *Xenopus laevis* VE, gp69/64 was reported to be a sperm ligand (Tian et al., 1997a,b, 1999) homolog of components of the

ZPA family, such as the mouse *zona pellucida* ZP2 which is able to bind sperm by a secondary binding (Bleil and Wassarman, 1988).

Glycoproteins gp69 and gp64 undergo post-fertilization limited proteolysis and reduce their apparent molecular weight to 66 and 61 kDa, respectively (Gerton and Hedrick, 1986), by cutting 27 amino acids at the N-terminus and thereby eliminating sperm binding ability (Tian et al., 1997a,b, 1999). In another anuran genus, namely *Bufo*, two glycoproteins of similar Mr (65 and 61 kDa) are similarly processed following fertilization (Lindsay et al., 1988). The *X. laevis* gp69 and gp64 glycoproteins are two glycoforms of the same polypeptide, having approximately the same number of N-linked oligosaccharide chains, but differing in the extent of O-glycosylation. O-linked polysaccharide chains were suggested to be instrumental for sperm binding in *X. laevis*, as in mammalian and invertebrate envelope glycoproteins (Bleil and Wassarman, 1988; Dhume and Lennarz, 1995; Focarelli and Rosati, 1995) and may reside in the 27 amino acids domain where potential glycosylation sites are present (Tian et al., 1997a,b, 1999).

Investigations into *Xenopus* VE gp41 or its coelomic form gp43, have shown homology between this glycoprotein and the ZPC family (Kubo et al., 1997; Yang and Hedrick, 1997) which, in mouse, is responsible for sperm binding to the *zona* (Bleil and Wassarman, 1983). In the coelomic envelope (CE), gp43 is a major glycoprotein that covers gp64/69. Upon CE transformation into the oviposited egg envelope VE, the envelope becomes able to bind to sperm (Gerton and Hedrick, 1986), gp43 is converted to gp41 and gp69/64 becomes available to sperm (Tian et al., 1997a,b, 1999).

More recently, it was shown that in *Xenopus*, gp41 has sperm binding activity more relevant than gp69/64. This binding is held to be dependent on the N-linked oligosaccharide chains of gp41 (Vo and Hedrick, 2000). In *Bufo bufo japonicus*, gps 36 and 39, probably homo-

Grant sponsor: MIUR PRIN 1999.

*Correspondence to: Prof. Chiara Campanella, Dipartimento di Biologia, Evolutiva e Comparata, Università di Napoli Federico II, via Mezzocannone 8, 80134, Napoli, Italy.

E-mail: chiara.campanella@unina.it

Received 22 July 2003; Accepted 13 November 2003

Published online in Wiley InterScience (www.interscience.wiley.com). DOI 10.1002/mrd.20063

logs of *X. laevis* gp41, may have sperm binding activity based on *Dolicus biflorus* agglutinin binding oligosaccharides (Omata and Katagiri, 1996). These data suggest that further investigation should be undertaken to explore the role of glycoprotein homologs of *X. laevis* gp69/64 or gp41 in the fertilization of other amphibians.

In *Discoglossus pictus*, a glycoprotein of 63 kDa has been sequenced and cloned (Vaccaro et al., 2001), exhibiting high homology to *Xenopus* gp69/64, and to the mammalian ZP2. The role of this glycoprotein in sperm binding has not yet been investigated.

During transit in the oviduct, in this species as for all anuran envelopes, the transformation of the envelope leads to the acquisition of fertilizability and involves the cleavage of a glycoprotein, gp42, to gp40 (Caputo et al., 2001). Reasonably, although not proved, this glycoprotein corresponds functionally to *X. laevis* gp41. In *D. pictus*, 'in vitro' sperm binding to VE occurs only following the acrosome reaction (Campanella et al., 1997; Caputo et al., 2001). The main question we addressed in this article was whether gp63 or gp40 is able to bind sperm. Further questions arose from the specific organization of the *D. pictus* egg and the general understanding of the changes occurring at fertilization in this species.

The *D. pictus* egg has a distinct polarity of the egg and of the thick overlaying jelly envelopes (Campanella, 1975; Talevi and Campanella, 1988). Sperm touch the outermost jelly layer, J3, where the acrosome reaction is triggered and converged through the gelatinous plug and the VE to the dimple, the fertilization site, located at the center of the animal half. Sperm stop moving when they reach the egg surface (Campanella et al., 1997). The route for sperm entrance includes a specific layer VE-D, formed during the transit of the oocyte in the oviduct, and located underneath the VE region facing the dimple. In the corresponding domain of VE, arrowhead-like bundles of fibrils are perpendicularly oriented toward the dimple, and are probable sites of low resistance for penetrating sperm (Caputo et al., 2001).

Following fertilization the cortical granules located in the dimple are exocytosed and the envelope becomes impermeable to sperm (Campanella et al., 1988 and unpublished data). As a further impediment to sperm entry, a capsular chamber forms as a consequence of plug dissolution. Peroxidase released from the egg causes oxidative opening of disulphide bonds in the plug (Campanella et al., 1992; Pitari et al., 1993).

Our results indicate that, by comparing peptide mapping of gp63 with that of the other glycoproteins of the VE (118, 106, 75, 63, 40, and 38/36), gp75, and gp63 peptide maps are similar. Sperm bind to both gp63 and gp75-coated beads, while for gp40-coated beads the binding percentage was as low as BSA-coated beads. Following fertilization gp63 transforms into three bands, a glycoprotein of 62 kDa being the most prominent. There was no sperm binding to beads coated to gp62. At fertilization, VE undergoes changes including the formation of an F-layer, as described for *Xenopus* (Greve and Hedrick, 1978) and other anurans (cfr.

Elinson, 1886). Preliminary data of these experiments were published elsewhere (Infante et al., 1998).

MATERIALS AND METHODS

Animals and Gametes

Adult *Discoglossus pictus* males and females were captured in the neighborhood of Palermo (Italy). They were injected in the dorsal lymphatic sac with 200–250 U of Profasi HP (Serono, Rome, Italy) in Amphibian Ringer (111 mM NaCl; 1.3 mM CaCl₂; 2 mM KCl; 0.8 mM MgSO₄; 5 mM HEPES, pH 7.8). Uterine eggs were obtained 18 hr after hormone injection. Twenty-four hours following hormone treatment, the semen (sperm and seminal fluid) was collected from the seminal vesicles (cfr. Caputo et al., 2001). Insemination was performed by adding a drop of semen to eggs immersed in 1/10 Ringer.

Microscopy

Fertilized eggs were fixed 2–6–10–20 min after insemination in 2.5% glutaraldehyde in 0.2 M phosphate buffer as previously described (Campanella et al., 1988). Dehydration in graded ethanol at 4°C was followed by embedding in Epon 812. Thin sections were cut with diamond knives, stained with uranyl acetate and lead citrate and examined in a Philips EM-300 microscope at the C.I.S.M.E. of the University of Naples.

For fluorescence microscopy, uterine eggs were fixed, frozen, and sectioned, as previously described (Tatone et al., 1993). The sections were incubated with an antiserum directed against *X. laevis* gp69/64, that cross-reacts with *D. pictus* gp63 and partially with lower Mr gps of the VE electrophoretic pattern components (Tian et al., 1997a and cfr. Vaccaro et al., 2001) (a gift from Dr W. J. Lennarz, SUNY, NY). After incubation for 60 min, sections were extensively rinsed in PBS and exposed to FITC-conjugated anti-rabbit IgGs for 30 min, rinsed in PBS, and mounted in 90% glycerol in PBS. The level of fluorescence was compared with that in control sections, where the first antibody was omitted.

Photographs were taken under a Zeiss Axioskop microscope equipped with a Progress 3800 color video camera and KS300 image analysis software.

Preparation of Eggs and VE

Eggs were first dejellied in dejelling buffer (100 mM NaCl, 5 mM DTE; 50 mM Tris-HCl, pH 8.5). Then, VE and FE were manually removed and, after extensive rinsing and brief centrifugations at low speed, were exposed to 0.6 M KI for a few minutes to remove the innermost jelly layer J1 (cfr. Caputo et al., 2001). The envelopes were transferred into HB (25 mM HEPES, pH 7.5 containing: 900 mM glycerol; 0.02 mM NaN₃; 1 mM ATP; 1 mM DTT; 5 mM EGTA; 2 mM TAME; 5 mg/ml SBTI; 5 µg/ml aprotinin; and 10 µM E64). VEs and FEs were dissolved in 1/10 Ringer containing 2% SDS and heated at 95°C for at least 2 min. After centrifugation at 14,000g for 10 min, the samples were processed for electrophoresis.

Protein Determination, SDS-PAGE, and Gel Staining

Protein concentration of the samples was determined with the BCA or Micro BCA Protein Assay Reagent (Pierce Chemical Company, Rockford, IL). Fifteen micrograms of soluble proteins of VE or FE were applied on each lane of the gels. Samples were prepared for SDS-PAGE by addition of sample buffer and heating at 40°C for a few minutes (nonreducing conditions) or by heating for a few minutes in sample buffer containing 5% β -mercaptoethanol (reducing conditions). Protein samples were analyzed by SDS-PAGE using Laemmli's Tris-glycine buffer system. The running gel contained either 5 or 10% acrylamide. Gradients of 10–12% or 10–15% acrylamide were also utilized. Mr standards were the following: 200; 116; 97.5; 66.2; 45; 31; 21.5 kDa (Biorad, Hercules, CA). After fixation in methanol/acetic acid, gels were stained with either Coomassie blue or the silver method.

Lectin Blot Detection on Nitrocellulose

Proteins subjected to SDS-PAGE were electrophoretically transferred to nitrocellulose sheets overnight at 180 mA (for more details, see Tatone et al., 1993).

Biotin-labeled *Ulex europaeus* agglutinin I (UEA-I), *Glycine max* agglutinin (SBA) (Oxford Glycosystems, St. Louis, MO), *Dolichos biflorus* agglutinin (DBA) were used. Transferred proteins were first blocked in 2% BSA in PBS, and then exposed to the biotin-labeled lectin, followed by incubation in Avidin-AP (Sigma, Abingdon, UK). Negative control runs were performed by adding sugars specific for each lectin: UEA-I pre-incubation with 5 mg/ml fucoidan (Sigma) or 1 mg/ml 2-fucosyl-lactose (Oxford GlycoSystems) inhibited the reaction (partial inhibition with fucosyl-lactose). SBA and DBA pre-incubation with 0.2 M *N*-acetyl-galactosamine (Sigma) inhibited the lectin cross-reactivity (partial inhibition for DBA).

DIG-labeled MAA, *Datura stramonium* agglutinin (DSA), *Sambucus nigra* agglutinin (SNA), and *Galanthus nivalis* agglutinin (GNA) were part of a DIG Glycan differentiation Kit (Roche) and were utilized following the manufacturer's instructions. Positive controls were run for the DIG-labeled lectins according to the DIG Glycan differentiation Kit, i.e., transferrin for SNA, fetuin for MAA and DSA, asialofetuin for PNA.

Peptide Mapping

The VEs and FEs were analyzed by peptide mapping using a modification (Bordier and Crettol-Jarvinen, 1979) of the limited proteolysis procedure of Cleaveland et al. (1977). Glycoproteins were separated on a 10% acrylamide SDS slab gel, under reducing conditions, for optimal band resolution. Bands of single glycoproteins were cut out from the first dimension gels of the whole envelope homogenate, equilibrated for 30–60 min with 0.1% SDS, 62.5 mM Tris-HCl, pH 6.8, and stored at 4°C in a sealed dry tube up to 2 days or used immediately. About 3–4 excised bands were loaded for each well and

overlaid with 10 [p1] μ g of *Staphylococcus aureus* V8 protease, sealed on the top of a second dimension SDS gradient gel at 15–20% acrylamide. The electrophoreses were interrupted for 12 hr when the proteins were in the stacking gel to allow extensive proteolysis. The peptide maps were stained with either the silver method or Coomassie blue.

Electroelution

VE and FE glycoproteins (gp118, gp75, gp63, gp62, and gp40) were separated by SDS-PAGE, visualized by staining with 0.3 M CuCl₂. The area of the selected bands was cut out and the gel slices were electroeluted with 25 mM Tris-HCl, pH 8.3 containing 1.44% glycine. Electroeluted proteins were dialyzed at 4°C against distilled water and stored at –20°C after concentration in a Savant speed vacuum concentrator. The protein content and purity of each sample was checked by SDS-PAGE.

Sperm-Egg Binding Assay

Sperm suspensions as recovered from the seminal vesicle were diluted in 1/10 Ringer to provoke complete unraveling of the sperm bundles and sperm ejection from the bundles. Sperm are motile for about 14 sec (Campanella and Gabbiani, 1979). The sperm suspension was then treated with 0.25 μ M A23187 (Sigma) for 2 min, because the previous work showed that dejected, unfertilized eggs bind to sperm, if sperm are pre-treated with Ca²⁺ ionophore to induce the acrosome reaction (Gualtieri and Andreuccetti, 1996; Caputo et al., 2001) and then washed in 1/10 Ringer. As a general control for testing sperm binding ability to VE, groups of fully dejected eggs were added to calcium ionophore-treated sperm and incubated for 15 min at room temperature under gentle rocking. The sperm-exposed eggs were then washed (cfr. Caputo et al., 2001), so as to separate unbound sperm from those bound to the eggs. Following fixation in 95% alcohol, the samples were either directly observed under a microscope with incident light or stained with DAPI for scoring sperm head attachment to the envelopes. Photographs were taken under a Zeiss microscope. In inhibition assays, the antiserum against *Xenopus* gp69/64 was used as well as an antiserum against *Unio elongatus* gp273 (a gift of Dr. F. Rosati, University of Siena, Italy). This serum reacts with gp273, the sperm-binding glycoprotein of *Unio* (Focarelli and Rosati, 1995), but does not cross-react with *D. pictus* VE component in Western blots (data not shown). A minimum of three assays on 20–30 eggs were performed for each serum dilution used.

The binding assay (see Maturi et al., 1998) considers the fact that when sperm come out of the bundles, they may get entangled because of their length (2.33 mm) and the resulting suspension of spermatozoa is therefore rather uneven. As a consequence, it is impossible to give an appropriate value to quantitative counts of sperm bound/egg (or sperm bound/beads, for the experiment in the paragraph below), i.e., it cannot be established whether a larger number of bound sperm means a

greater ability of the VE to bind sperm or more spermatozoa available to the egg. Therefore, we measured successful sperm collision (binding) with eggs under gentle rocking, in terms of percentage of eggs with sperm, without considering the number of sperm/egg. One or two males were used per experiment.

Sperm-Beads Binding Assay

About 100 gp63 bands were electroeluted yielding 150 μg of protein, 40 bands of gp40 for a total of 360 μg , 130 bands of gp75 for a total of 100 μg . The eluted glycoproteins as well as commercial BSA were adsorbed on polystyrene beads of 350 μm (Polysciences, Warrington, PA). Adsorption to the beads was performed as suggested by the supplier, utilizing 0.1 M borate buffer, pH 8.5, and blocking in 1% BSA. Generally, equimolar amounts of gps 63, 75, 40, or BSA were added to 120 μl of borate buffer containing about 800 beads. In the assay, sperm were smeared on microslides, further diluted in 10% Ringer and ionophore treated. Following rinsing in 1/10 Ringer, about 30 glycoprotein-coated beads were released on the spermatozoa and incubated for 5 min with gentle rocking in Petri dishes. Beads were then removed from the dishes and observed under a light transmission microscope for a first score of sperm attachment. The microslide carrying the beads was shaken by moving the microscope translation table. Sperm attachment to the beads that had resisted such treatment was assessed as sperm binding. A minimum of three experiments were performed for each binding experiment.

For competition assays, eluted glycoproteins were diluted in 1/10 Ringer and then pre-incubated with A23187-treated sperm for 15 min. The sperm-binding assay was subsequently performed as described.

RESULTS

Inhibition Assays With Antibodies

To investigate the physiological role of gp63 in sperm binding, inhibition assays were first performed by pre-treating eggs with increasing dilutions of *Xenopus* anti-gp69/64. A23187-treated sperm were used for the assays. Figure 1 indicates that the anti-serum inhibits binding starting from the dilution of 2 mg/ml, in contrast to anti-rabbit-IgG and *Unio* anti-gp273 anti-serum, that were not inhibitory over the dilutions of 1, 2, 4, 10 mg/ml (data not shown). Interestingly, in inseminated *D. pictus* dejected eggs, although binding occurs all over VE, tufts of sperm are observed only at the animal half of the egg, around the dimple region (Fig. 2a). Egg sections exposed to anti-gp69/64 antibodies, show that in the VE the immuno-staining is more intense in the animal side than in the vegetal side of the egg (Fig. 2b,c).

Comparison Between Peptide Maps Reveals Similarity Between gp63 and gp75

By comparing peptide maps of gp118, 106, 75, 40, and 38/36 to that of gp63, it was found that gp75 peptide map was similar to that of gp63 (Fig. 3): the gp75 pattern has one polypeptide absent and one band more conspicuous

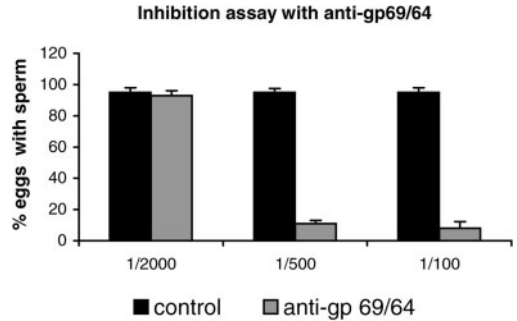


Fig. 1. Quantification of the mean percentage of inhibition of sperm-vitelline envelope (VE) binding by anti-gp69/64 of *Xenopus laevis*. A dramatic inhibition of the binding occurred starting from the serum dilution 1/500 v/v, compared to the binding in untreated eggs.

with respect to the gp63 pattern (Fig. 3). In the VE, gp75 is the glycoprotein with the Mr closest to gp63, yet with different reactivity to lectins (Caputo et al., 2001). If gp63 and gp75 are two glycoforms of the same protein, gp63 and gp75 peptides may migrate with different relative mobility in SDS-PAGE because of their specific glycosylation.

Competition Assays of Sperm-VE Binding Using gp63, gp75, and gp40

Electroeluted gps 118, 75, 63, and 40 were utilized in this assay for competing with the binding of spermatozoa to fully dejected eggs. In the experimental assays, the spermatozoa were pre-incubated with increasing concentrations of the electroeluted glycoproteins (Fig. 4). While for the control experiments, where reacted sperm were exposed to the sole 1/10 Ringer, the DAPI staining showed binding over 96% eggs (average value), for both gp63 and 75 competition assays the binding was impaired, in a dose-dependent fashion. By contrast, gps40 and 118 did not change the percentage of eggs with bound sperm of control experiments (Fig. 4 and data not shown). Figure 5 indicates DAPI stained eggs. In Figure 5a, a control egg is shown with bound sperm, while Figure 5b shows an egg exposed to sperm treated with the highest gp63 concentration.

Binding and Competition Assays on Beads Coated With gp75, gp63, or gp40

The electroeluted gps 75, 63, or 40 were adsorbed on polystyrene beads. The adsorption was checked by boiling the beads in sample buffer and analyzing by SDS-PAGE the released protein in each binding experiment (Fig. 6), to estimate the amount of bound glycoprotein/ bead. By knowing the concentration of the glycoprotein in the eluate before and after the adsorption and the number of 350 μm -beads/volume unit, the amount of bound glycoprotein/bead was estimated to be in the range of 0.0075 μg (i.e., 7.2×10^{10} molecules, in the case of gp63) and of 2 $\mu\text{g}/\text{cm}^2$. Commercial BSA was adsorbed

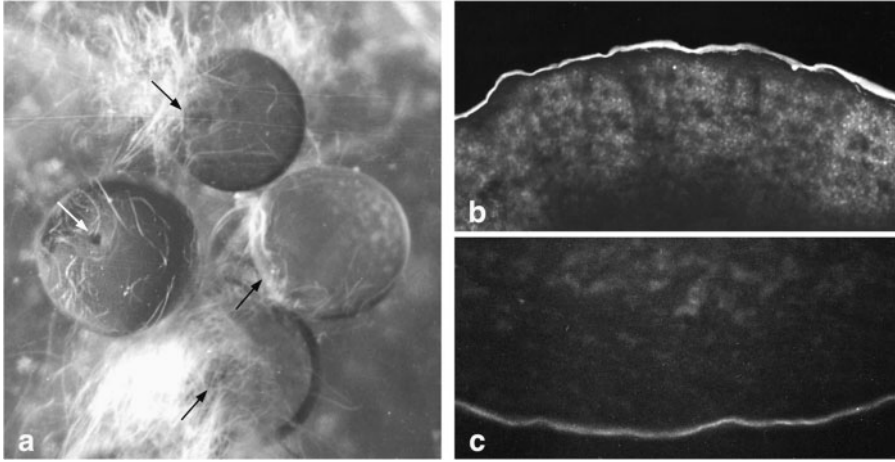


Fig. 2. a: Inseminated dejellied eggs. The arrows indicate the dimple region, where tufts of sperm bundles stick to the VE. Magnification 25 \times . b, c: Frozen sections of uterine eggs incubated with anti-gp69/64 of *Xenopus laevis*. The immunostain is located in the VE of the egg animal half (arrow) (b) and has lower intensity in the vegetal half of VE (arrow) (c). Magnification 310 \times .

on beads and utilized as control in sperm binding experiments. Upon exposure of gp63-beads, sperm stuck to the beads. The mean percentage of beads with sperm was about 62% (Fig. 7). Similar results were obtained for gp75-beads, where the mean percentage of beads with sperm was 67% (Fig. 7). In parallel experiments, using BSA-beads or the gp40-beads, the mean percentage of beads with sperm was about 22 for BSA-beads and 17 for gp40-beads (Fig. 7).

The 63 and 75gp bands eluted from SDS-PAGE were also tested for their ability to inhibit sperm binding to beads coated with corresponding or sister glycoprotein. Eluted gp40 was also used in these competition experi-

ments. Figure 8 reports the percentage of binding between gp63-beads and sperm in the presence of soluble gps 63, 75, or 40 (Fig. 8a). In the control experiment (sperm binding in Ringer) the mean percentage of beads with sperm was approximately 70. When soluble gp63 was used, the percentage of beads with sperm decreased on increasing the soluble glycoprotein concentration, indicating that sperm binding might be inhibited in a dose-dependent manner. Sperm-bead binding was also significantly affected by soluble gp75 that at 8×10^{-5} mM concentration lowered the binding to 30%. Surprisingly, when soluble gp40 was used in these competition assays, the percentage of beads with sperm showed a similar drop, while BSA did not affect binding (data not shown). For the gp75-beads, similar reciprocal results were

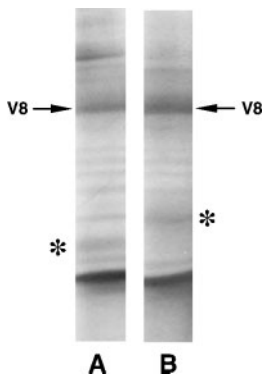


Fig. 3. Peptide maps of gp63 (A) and of gp75 (B). The arrows indicate the level of migration of V8 enzyme. The maps are identical with two exceptions marked by the asterisks. In (A), a band is present that is not found in (B). On the other hand, (B) has a more intense and thicker band than (A).

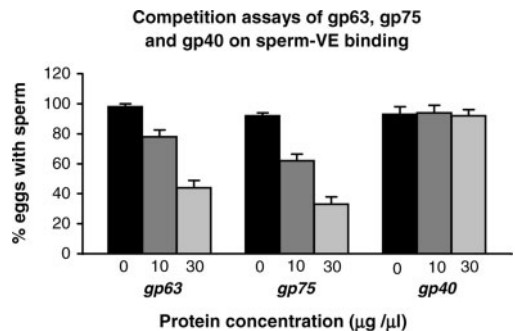


Fig. 4. These competition assays were performed using fully dejellied eggs and sperm pre-treated with the indicated concentrations of gps 63, 75, and 40. Bars represent standard deviation. The dose-dependent inhibition of sperm binding to eggs is evident for gp63 and gp75-treated sperm and is absent in the case of gp40-exposed sperm.

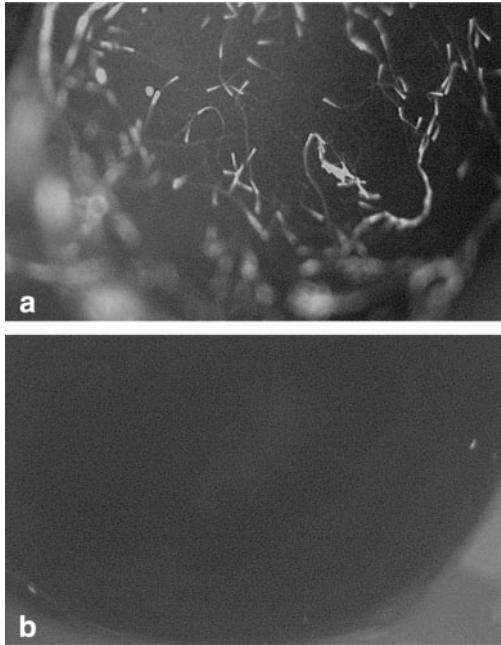


Fig. 5. Dejellied uterine eggs fixed and stained with DAPI. **a:** There is sperm binding, when eggs are inseminated with sperm exposed only to A23187. **b:** Sperm binding did not occur when sperm are exposed to A23187 and to 30 µg/ml gp63. Magnification 70×.

obtained, using soluble gp75 or 63 (Fig. 8b). When gp40 was used, a sharp decrease in the percentage of beads with sperm was noted at gp40 concentrations as low as 8×10^{-8} mM. The value dropped to 13% at 8×10^{-7} mM and to 10% at 8×10^{-5} mM, yet at 8×10^{-4} mM increased back to 20%, indicating for gp40 no dose-dependent inhibition of sperm binding to gp75-beads. In the control assay, the mean percentage of beads with sperm was approximately 75 (Fig. 8b).

Conversion of VE to FE

The FE electrophoretic pattern was analyzed both under reducing and nonreducing conditions and compared to the VE pattern. The glycoproteins present in the SDS-PAGE of VE and FE have the same apparent Mr with one exception. In the FE pattern, gp63 has disappeared, while a band of 62 kDa as well as two minor bands of 58 and 67 kDa are present, under reducing conditions (Fig. 9a). To investigate the probable conversion of gp63 into gp62, the polypeptides produced by the V8 proteolysis of the two glycoproteins were compared. The two peptide maps appear identical (Fig. 9b), indicating conversion of gp63 to gp62. As expected, it was found that, when sperm are exposed to dejellied fertilized eggs, they do not bind to FE (data not shown). When the binding assay was performed on beads coated with FE

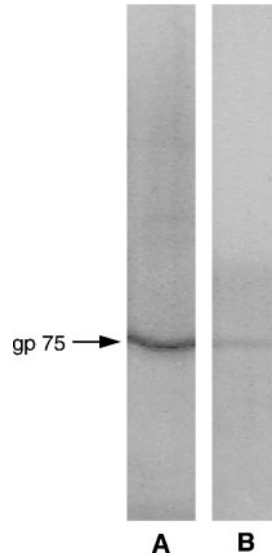


Fig. 6. Example of the estimation of adsorption of a VE glycoprotein on beads, by SDS-PAGE. Electroeluted gp75 used for adsorption to polystyrene beads (A) and as recovered in the supernatant after adsorption to the beads (B).

gp62, the sperm binding percentage was similar to BSA-beads (Fig. 10).

Ultrastructural observations were performed on fertilized eggs fixed approximately 10 min following fertilization. The exocytosis of vacuoles responsible for plug liquefaction occurred, based on the jelly plug transformation in large globules (Fig. 11, see Campanella et al., 1992). The VE appears modified as it has lost the orderly organization of its fiber bundles. A heavy electron-dense and thin F-layer is present between the envelope and the innermost jelly layer, J1. In J1 and the F-layer, a site of

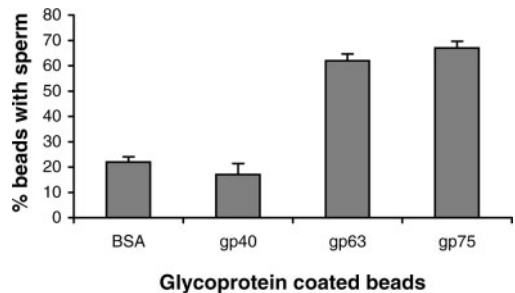


Fig. 7. Quantification of the mean percentage of BSA-beads, gp40-beads, gp63-beads, gp75-beads with bound sperm. Bars represent standard deviation. Glycoproteins gp63 and gp75 beads exhibit 62% and 67% of binding with sperm, respectively, while corresponding values for BSA and gp40-beads were 22% and 17%.

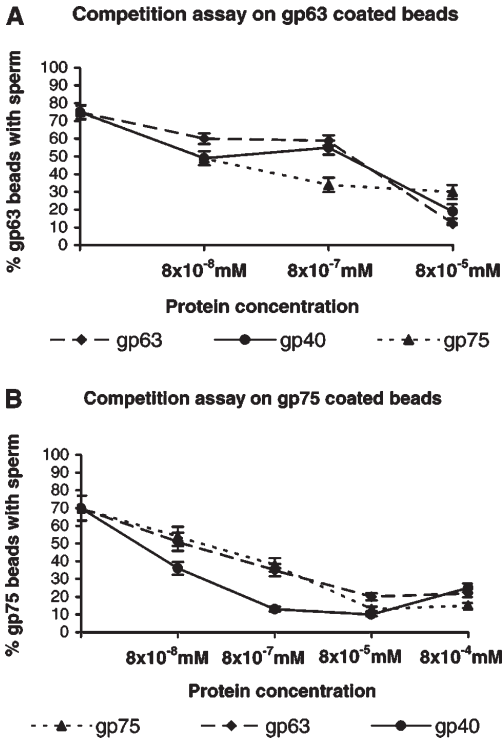


Fig. 8. Competition assays on glycoprotein-coated beads. **A:** For the gp63-beads, a dose-dependent inhibition of sperm binding to beads was observed when the soluble glycoprotein is gp63 or gp75. A similar inhibition of binding was observed when gp40 was used, particularly at the concentration of 10⁻⁸ and 10⁻⁵ mM. **B:** For gp75-beads, a similar dose-dependent inhibition action of gp75 and gp63 was observed, while for gp40 random inhibition of sperm binding on gp75-beads occurred. Bars represent standard deviation.

sperm passage is seen as a hole surrounded by remnants of sperm membranes involved in the acrosome reaction (Fig. 11).

FE glycoprotein cross-reactivity to lectins DBA, UEA-I, MAA, SBA, DSA was studied to learn whether major changes of glycosylation occur as a consequence of fertilization. Interestingly, changes in reactivity were found in gps 118, 106, 62, and higher Mr glycoproteins of FE, that sharply increase reactivity with MAA, with respect to corresponding VE glycoproteins. For DBA, UEA-I, SBA, and DSA, no change of reactivity was found in the envelope as a result of fertilization. Figure 12 shows MAA and UEA-I blots of FE and VE.

DISCUSSION

In this article, we investigated the role of gp63, the product of DpZp2 gene homolog of *X. laevis* gp69/64 (Vaccaro et al., 2001), and showed remarkable functional similarities among the glycoproteins of the two

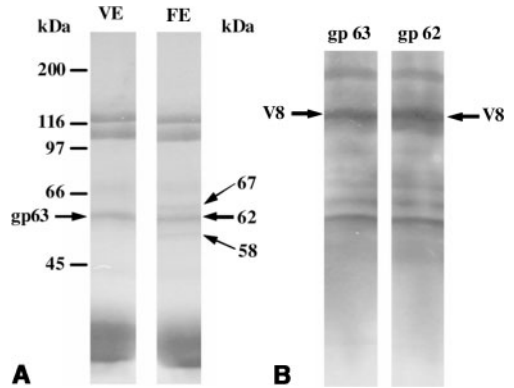


Fig. 9. A: SDS-PAGE of VE and FE in the presence (B) of mercaptoethanol, in gels containing 10% acrylamide and Coomassie blue stained. By comparing the gels the 6 main bands of 118,106, 75, 63, 40, 38/36 kDa may be observed in the VE gel, while in the FE gel, at the level of 63 kDa, the gp63 is absent and three bands of 67, 62, and 58 kDa are found. Reference Mr are indicated and the numbers of FE are expressed in kilo Daltons (kDa). **B:** peptide maps of gp63 and gp62. The V8 protease level of migration is indicated. The two maps are identical.

species. Moreover, thanks to the comparison of peptide maps, it was found that gp75 of *D. pictus* shares structural similarities to gp63, suggesting that gp63 and gp75 are two glycoforms of the same protein, as in *Xenopus* gps 69 and 64 (Tian et al., 1999a,b). The two glycoproteins are indeed differently glycosylated because gp75 has affinity to MAA, DBA, DSA, and gp63, in addition to these lectins, also to *Triticum vulgaris* agglutinin (WGA), SBA, DSA GNA, UEA-I (Caputo et al., 2001). However the possibility cannot be denied that also the protein backbone of these glycoproteins is different because of the absence in the gp75 peptide map of a band present in the that of gp63.

Eggs pre-treated with anti-*X. laevis* gp69/64 suggested a role of gp63 in sperm-VE interaction. Competition assays either with gp63 or gp75 on fully dejected eggs showed that the two glycoproteins are involved in

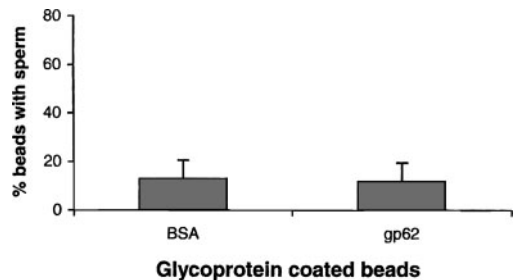


Fig. 10. Binding assay between BSA or gp62-beads and sperm. The mean percentage of beads with sperm is 13% for the BSA-beads and 12% for gp62-beads. Bars represent standard deviation.

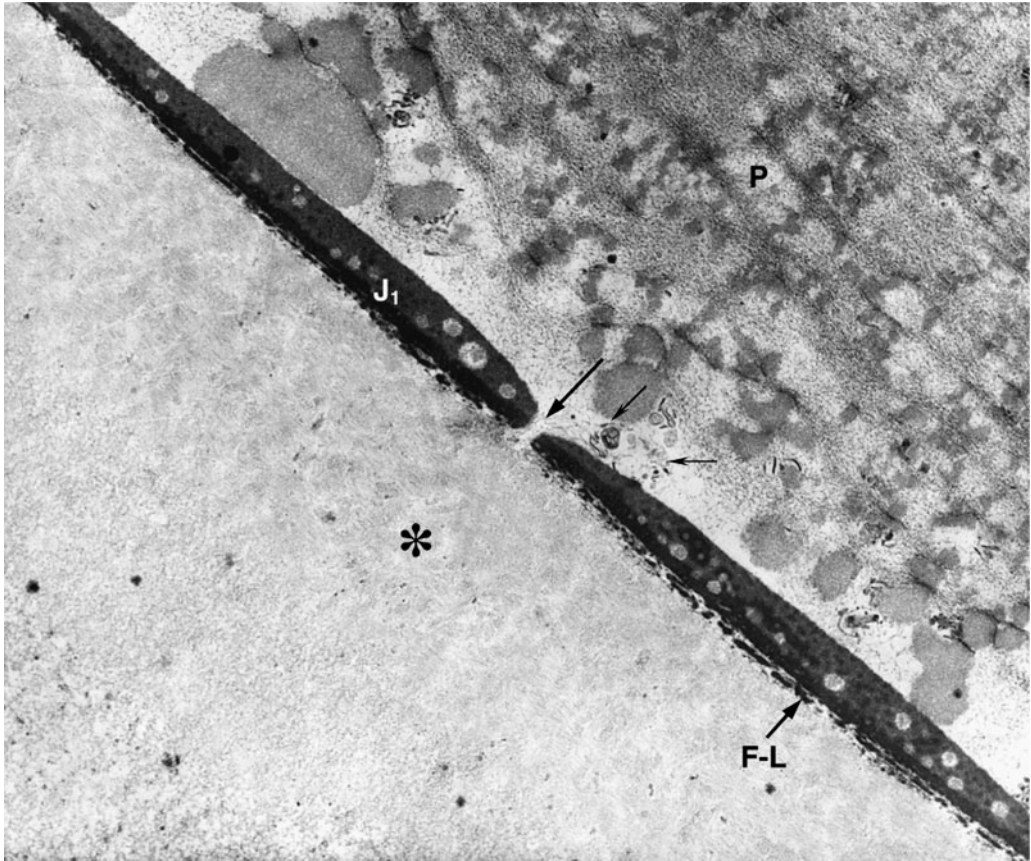


Fig. 11. Ultrathin section of an egg fixed 10 min following fertilization. The asterisk indicates the transformed VE, where the fibers are randomly oriented. An electron-dense F-layer (F-L) is located between the innermost jelly layer (J_1) and the envelope. The arrow indicates the site of passage of a spermatozoon and small arrows the remnants of membranes released by sperm during the acrosome reaction. Over J_1 the jelly plug in the process of dissolution (P) is indicated. Magnification 12,500 \times .

sperm-VE binding. Immobilization of glycoproteins on polystyrene beads indicated that sperm indeed bound to gp63 and to gp75 and that the binding did not occur for the immobilized gp40. The specificity of the binding was proved by the dose-dependent competition of sperm binding on the beads by the soluble glycoproteins. Interestingly, sperm binding competition by gp75 occurred on gp63-beads and vice versa, probably because of the hypothesized structural similarities between the two glycoproteins. However, the percentage of beads with bound sperm never achieved 100%, suggesting that gp63 and gp75 are both required for the observed 96–98% sperm binding to dejelled eggs. Moreover, soluble gp40 competed in a fashion similar to dose-dependence on gp63-beads-sperm binding and in a dose-independent way on gp75 beads-sperm binding. However, immobi-

lized gp40 does not bind sperm, nor is it able to inhibit sperm binding to VE. Indeed, the interaction of gp40 with sperm appears to consist not in a binding ability, but in influencing the binding. Glycoprotein gp40 is prominent in the pattern of *D. pictus* VE proteins (Caputo et al., 2001). It may co-operate or sterically interfere with the sperm binding to VE gp63 and 75. Interestingly, according to Vo and Hedrick (2000), in *X. laevis*, VE glycoproteins, including ZPC, ZPA do interact synergistically to promote sperm-VE binding. However, in our findings, in contrast to the results obtained by these authors in *X. laevis*, only gp63 and gp75 are able to bind sperm specifically.

In this article, anti-*X. laevis* gp69/64 staining of *D. pictus* VE strongly suggests that gp63 is more concentrated in the animal side of the VE, i.e., close to

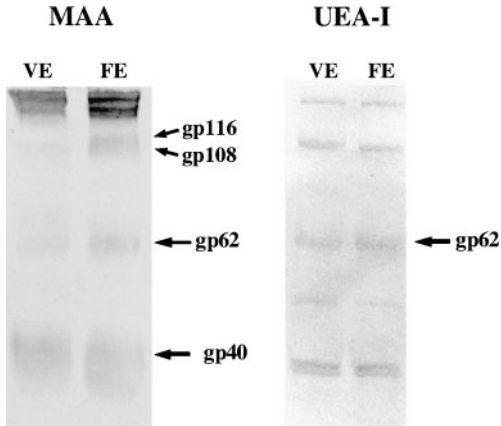


Fig. 12. Selection of VE and FE lectin blots. The lectins utilized are UEA-I and MAA. While for UEA-I blots there are no differences in the intensity of reactivity in VE and FE blots, in the MAA blot of FE there is a stronger reactivity of gps 116, 108, and 62 to the lectin than in the corresponding bands of the VE blot. Furthermore, high molecular mass glycoproteins are particularly reactive in the MAA blot of FE.

the region where the dimple is located and where tufts of sperm bind VE. These data add further information to the biochemical and structural basis responsible for the polarized organization of *D. pictus* VE with respect to the fertilization process (Talevi et al., 1985; Talevi and Campanella, 1988; Caputo et al., 2001). Indeed, the VE region facing the dimple appears to contain putative canals for sperm passage (Caputo et al., 2001) as well as a larger amount of sperm ligands, with respect to the rest of the VE.

Spermatozoa are able to bind VE only following the acrosome reaction, indicating that the molecules that interact with the envelope are located either in the acrosome content or at the inner acrosome membrane (Campanella et al., 1997; Caputo et al., 2001). In a previous article, ultrastructural observations showed that VE filaments are connected to the sperm inner acrosome membrane of *D. pictus* (Campanella et al., 1997). In contrast, in *X. laevis*, sperm-VE interact probably through a primary binding (Tian et al., 1999). A full comparison of the sperm-VE binding in the two species will be possible when the acrosome reaction will be studied in *X. laevis*.

Glycoprotein gp63 undergoes minor changes in electrophoretic mobility following fertilization. The band of approximately 62 kDa of the FE SDS-PAGE pattern, when immobilized on beads, does not bind sperm, similar to what was observed for gp66 and gp61 of *X. laevis* FE (Gerton and Hedrick, 1986; Tian et al., 1997a,b) and for gp62 and gp58 of *Bufo japonicus* (Lindsay et al., 1988). The envelope undergoes structural changes as a result of the exocytosis of the dimple cortical granules (Campanella et al., 1988) and a typical F-layer is formed between the innermost jelly layer and

the transformed envelope (Grey et al., 1977; Greve and Hedrick, 1978; Hedrick and Nishihara, 1991). In addition, it appears that in the FE and in particular in gp62, more sialic acid is found following fertilization, suggesting that the cortical granules content (Andreuccetti and Campanella, 1980) provides FE and the sperm ligand(s) with this sugar, thus contributing to the process that renders the envelope impermeable to sperm. In *D. pictus*, glycosylation events also appear to accompany the oviducal transformation of gp63 and gp75, i.e., during the transformation of the coelomic envelope into the VE, indicating that specific studies are necessary in the future to determine the role of oligosaccharide chains in sperm binding.

These observations show strong similarities between the events that occur in the dimple at fertilization and those found at the egg surface in other anurans (Elinson, 1986). Interestingly, previous data showed that in *D. pictus* the prevention of polyspermy by the outer coat lies not only in the FE barrier as in anuran species (Campanella, unpublished observations), but also in the plug liquefaction and capsular chamber formation (cfr. Elinson, 1986; Campanella et al., 1992).

ACKNOWLEDGMENTS

We thank Paolo Paglierucci, Maria Lucido, Clementina Diglio, Loredana Tretola, and Luigi Palmiero for participating in some of the experiments in preparation for their Master Thesis and to Giuseppe Falcone for image elaboration.

REFERENCES

- Andreuccetti P, Campanella C. 1980. Origin and cytochemistry of the animal dimple granules in *Discoglossus pictus* (Anura) eggs. *J Embryol Exp Morphol* 56:239–252.
- Bleil JD, Wassarman PM. 1983. Sperm-egg interactions in the mouse: Sequence of events and induction of the acrosome reaction by a zona pellucida glycoprotein. *Dev Biol* 95:317–324.
- Bleil JD, Wassarman PM. 1988. Galactose at the nonreducing terminus of O-linked oligosaccharides of mouse egg zona pellucida glycoprotein is essential for the glycoprotein's sperm receptor activity. *Proc Natl Acad Sci USA* 85:6778–6782.
- Bordier A, Crettol-Jarvinen J. 1979. Peptide mapping of heterogeneous protein samples. *J Biol Chem* 254:2565–2567.
- Campanella C. 1975. The site of spermatozoa entrance in *Discoglossus* (Anura) unfertilized egg: An electron microscope study. *Biol Reprod* 12:439–447.
- Campanella C, Gabbiani G. 1979. Motile properties and localization of contractile proteins in the spermatozoon of *Discoglossus pictus*. *Gamet Res* 2:163–175.
- Campanella C, Talevi R, Kline D, Nuccitelli R. 1988. The cortical reaction in the egg of *Discoglossus pictus*: A study of the changes of endoplasmic reticulum at activation. *Dev Biol* 130:108–119.
- Campanella C, Amore F, Pitari G, Fusco C, Maurizi G, Dupre S. 1992. Post-fertilization changes in *Discoglossus pictus* (Anura) eggs result in the formation of a capsular chamber where the egg rotates. *Int J Dev Biol* 36:413–422.
- Campanella C, Carotenuto R, Infante V, Maturi G, Atripaldi U. 1997. Sperm-egg interaction in the painted frog (*Discoglossus pictus*): An ultrastructural study. *Mol Reprod Dev* 47:323–333.
- Caputo M, Infante V, Talevi R, Vaccaro MC, Carotenuto R, Campanella C. 2001. Following passage through the oviduct, the coelomic envelope of *Discoglossus pictus* acquires fertilizability upon reorganization, degradation of gp42, extensive glycosylation and the formation of a specific layer. *Mol Rep Dev* 58:318–329.

- Cleaveland DW, Fisher SG, Kirschner MW, Laemmli UK. 1977. Peptide mapping by limited proteolysis in sodium dodecyl sulfate and analysis by gel electrophoresis. *J Biol Chem* 252:1102–1106.
- Dhume ST, Lennarz WJ. 1995. The involvement of O-linked oligosaccharide chains of the sea urchin egg receptor for sperm in fertilization. *Glycobiology* 5:11–17.
- Elinson RP. 1886. Fertilization in Amphibians: The ancestry of the block to polyspermy. *Int Rev Cytol* 101:59–100.
- Focarelli R, Rosati F. 1995. The 220-kDa vitelline coat glycoprotein mediates sperm binding in the polarized egg of *Unio elongatus* through o-linked oligosaccharides. *Dev Biol* 171:606–614.
- Gerton GL, Hedrick JL. 1986. The vitelline envelope to fertilization envelope conversion in eggs of *Xenopus laevis*. *Dev Biol* 116:1–7.
- Greve LC, Hedrick JL. 1978. An immunohistochemical localization of the cortical granule lectin in unfertilized and fertilized egg. *Gamete Res* 1:13–18.
- Grey RD, Working PK, Hedrick JL. 1977. Alteration of structure and penetrability of the vitelline envelope after passage of eggs from oolite to oviduct in *Xenopus laevis*. *J Exp Zool* 201:73–83.
- Gualtieri R, Andreuccetti P. 1996. Localization of egg-surface carbohydrates and fertilization in *Discoglossus pictus* (Anura). *Cell Tissue Res* 283:173–181.
- Hedrick JL, Nishihara T. 1991. Structure and function of the extracellular matrix of anuran eggs. *J Electron Microscop Tech* 17:319–335.
- Infante V, Caputo M, Carotenuto R, De Santo MG, Campanella C. 1998. In *Discoglossus pictus* (Anura) egg, does the structural polarization correspond to a vitelline envelope functional and biochemical polarity? The second symposium on the molecular and cell biology of egg and embryo-coats, sapporo. *Zygote(Suppl 1)*:124.
- Kubo H, Kawano T, Tsubuki S, Kawashima S, Katagiri C, Suzuki A. 1997. A major glycoprotein of *Xenopus* egg vitelline envelope, gp41, is a frog homolog of mammalian ZP3. *Dev Growth Differ* 39:405–417.
- Lindsay LL, Yamasaki H, Hedrick JL, Katagiri C. 1988. Egg envelope conversion following fertilization in *Bufo japonicus*. *Dev Biol* 130:37–44.
- Maturi G, Infante V, Carotenuto R, Focarelli R, Caputo M, Campanella C. 1998. Specific Glycoconjugates are present at the oolemma of the fertilization site in the egg of *Discoglossus pictus* (Anurans) and bind spermatozoa in an in vitro assay. *Dev Biol* 204:210–223.
- Omata S, Katagiri C. 1996. Involvement of carbohydrate moieties of the toad egg vitelline coat in binding with fertilizing sperm. *Dev Growth Differ* 38:663–672.
- Pitari G, Duprè S, Fusco C, Maurizi G, Campanella C. 1993. Jelly plug dissolution in *Discoglossus pictus* eggs (Anura) involves peroxidase-like activity and oxidative opening of disulfide bonds. *Zygote* 1:61–69.
- Talevi R, Campanella C. 1988. Fertilization in *Discoglossus pictus*. I: Regionalization of sperm-egg interaction site and occurrence of a late stage of sperm penetration. *Dev Biol* 130:524–535.
- Talevi R, Dale B, Campanella C. 1985. Fertilization and activation potentials in *Discoglossus pictus* eggs: A delayed response to activation by pricking. *Dev Biol* 111:316–323.
- Tatone C, Carotenuto R, Colonna R, Chaponnier C, Gabbiani G, Giorgi M, Campanella C. 1993. Spectrin and ankyrin-like proteins in the egg of *Discoglossus pictus* (Anura): Identification and localization in the site of sperm entrance versus the rest of the egg. *Dev Growth Differ* 35:161–171.
- Tian JD, Gong H, Thomsen GH, Lennarz WJ. 1997a. Gamete interactions in *Xenopus laevis*: Identification of sperm binding glycoproteins in the egg vitelline envelope. *J Cell Biol* 136:1099–1108.
- Tian JD, Gong H, Thomsen GH, Lennarz WJ. 1997b. *Xenopus laevis* sperm-egg adhesion is regulated by modifications in the sperm receptor and the vitelline envelope. *Dev Biol* 187:143–153.
- Tian JD, Gong H, Thomsen GH, Lennarz WJ. 1999. *Xenopus laevis* sperm receptor gp 69/64 glycoprotein is a homolog of the mammalian sperm receptor ZP2. *Proc Natl Acad Sci USA* 96:829–834.
- Vaccaro MC, De Santo MC, Caputo M, Just M, Tian JD, Gong H, Lennarz WJ, Campanella C. 2001. Primary structure and developmental expression of DpZP2, a vitelline envelope glycoprotein homolog of mouse ZP2, in *Discoglossus pictus*, one of the oldest living anuran species. *Mol Reprod Dev* 59:133–143.
- Vo LH, Hedrick JL. 2000. Independent and hetero-oligomeric-dependent sperm binding to egg envelope glycoprotein zpc in *Xenopus laevis*. *Biol Reprod* 62:766–774.
- Yang JC, Hedrick JL. 1997. cDNA cloning and sequence analysis of the *Xenopus laevis* egg envelope glycoprotein gp 43. *Dev Growth Differ* 39:457–467.

Sulphated glycoconjugates are powerful inhibitors of spermatozoa binding to the vitelline envelope in amphibian eggs

Mariangela Caputo, Stefania Riccio, Paolo Paglierucci, Loredana Tretola, Clementina Diglio, Rosa Carotenuto, Nadia De Marco and Chiara Campanella¹

Dipartimento di Biologia Evolutiva e Comparata, Università di Napoli Federico II, Napoli, Italy

Background information. In amphibians, the role of sulphated glycans has not been determined in spermatozoa–egg interaction, although they are known to be involved in other systems. In previous studies, it was found that, in *Discoglossus pictus*, a VE (vitelline envelope) glycoprotein of 63 kDa exhibits high homology to *Xenopus laevis* gp69/gp64 and to ZP2 of mammals. gp63 and a glycoprotein of 75 kDa are both capable of binding the spermatozoa in *in vitro* assays and, having similar peptide maps and different glycosylation, are probably two glycoforms of the same protein.

Results. In the present study, binding assays performed by treating dejellied eggs with metaperiodate suggest that hydroxy groups of sugars are not directly involved in spermatozoa–vitelline envelope binding. Competition assays between dejellied eggs and spermatozoa preincubated with dextran, dextran sulphate or fucoidan indicated that sulphated oligosaccharides have an inhibitory effect on spermatozoa binding. In similar competition assays, Le^x (Lewis^x) trisaccharide 3′-sulphate inhibited spermatozoa binding to VE in contrast with 3′-sialyl-Le^x tetrasaccharide. Assays performed with gp75- or gp63-coated beads and spermatozoa treated with fucoidan or dextran sulphate indicated that sulphated oligosaccharides competitively inhibit spermatozoa binding to gp75-coated beads, yet not to gp63-coated beads. Finally, solubilized VE digested with N-glycosidase F retains the inhibitory activity in spermatozoa–VE binding assays in contrast with VE treated with α -N-acetylgalactosaminidase.

Conclusion. It was concluded that VE sulphate groups are involved in spermatozoa binding. These groups are present in gp75 glycoconjugates and are probably located in O-linked glycoconjugates.

Introduction

The molecules responsible for egg envelope–spermatozoa binding are glycoconjugates and have selective properties with respect to spermatozoa according to their molecular components. In mammals, O-linked

polysaccharide chains possess suitable properties for spermatozoa binding, whereas the polypeptide backbone is capable of eliciting the spermatozoa acrosome reaction (Bleil and Wassarman, 1988). Studies on the spermatozoa–egg interaction in sea urchin indicated that a jelly coat glycoconjugate, rich in fucose sulphate, is the acrosome reaction inducer (SeGall and Lennarz, 1979; Vilela-Silva et al., 1999; Gunaratne et al., 2003). For a 350 kDa glycoprotein at the egg surface/VE (vitelline envelope), O-linked sulphated oligosaccharides bind the spermatozoa with low affinity, followed by a high-affinity interaction with

¹To whom correspondence should be addressed (email chiara.campanella@unina.it).

Key words: *Discoglossus pictus*, fertilization, fucoidan, polysaccharide chain.
Abbreviations used: BCA, biconchonic acid; DAPI, 4,6-diamidino-2-phenylindole; DIG, digoxigenin; DSA, *Datura stramonium* agglutinin; GNA, *Galanthus nivalis* agglutinin; VE, vitelline envelope; PNGase F, N-linked glycosidase F.

the protein backbone (Dhume and Lennarz, 1995). O-glycans containing fucose and/or sulphated fucose are involved in spermatozoa–VE binding in the mollusc *Unio elongatus* (Focarelli and Rosati, 1995; Capone et al., 1999), in ascidians and in mammals (see Miller and Ax, 1990; Oehninger, 2001). Interestingly, sulphate fucose was also shown to be involved in the spermatozoa–zona-free hamster interaction (Dravland and Mortimer, 1988). In humans and *U. elongatus*, spermatozoa selectin-like molecules are involved in binding to the zona (Oehninger, 2001) or to the VE (Focarelli et al., 2003) respectively. In *U. elongatus*, gp273, the VE ligand, contains a Lewis-like structure with fucose as determinant (Focarelli et al., 2003).

Therefore fucose or fucose sulphate in O-linked oligosaccharides may interact at various stages of spermatozoa–egg recognition, at the external coats or at the egg surface, before or after the acrosome reaction.

In the amphibian *Xenopus laevis*, the VE gp69/gp64 is a homologue to components of the ZPA family (Tian et al., 1997a, b) such as the mouse *zona pellucida* ZP2, which is capable of binding the spermatozoa by a secondary binding (Bleil and Wassarman, 1988). gp69/gp64 display adhesive properties with respect to the spermatozoa (Tian et al., 1997a, b). According to Vo and Hedrick (2000), in addition to gp69/gp64, gp41, a component of the ZPC family, has spermatozoa-binding activity. The gp69 and gp64 glycoproteins are two glycoforms of the same polypeptide and have approximately the same number of N-linked oligosaccharide chains, but differ in the extent of O-glycosylation. The gp69/gp64 binding motif may reside in a 27 amino acid domain where potential O-glycosylation sites are present (Tian et al., 1997a, b, 1999). In *Bufo*, VE carbohydrate moieties appear to be involved in binding to the fertilizing spermatozoa (Omata and Katagiri, 1996). Yet, in amphibians, the role of terminal fucose and sulphated glycans in spermatozoa–VE binding remains to be established.

In *Discoglossus pictus*, fucose was found in glycoconjugates selectively located at the plasma membrane of the dimple, the site of spermatozoa entry, the presence of fucose being associated with spermatozoa binding for the first time (Denis-Donini and Campanella, 1977). 'In vitro' assays later showed that these fucose-rich glycoconjugates (Gualtieri and

Andreuccetti, 1996) are capable of specifically binding the spermatozoa (Maturi et al., 1998; Talevi and Campanella, 1988). In *D. pictus* VE, gp75 and gp63 display adhesive properties with respect to spermatozoa. Indeed, competition assays and peptide maps showed that gp63 and gp75 interact with spermatozoa in *D. pictus* VE and that they may represent two glycoforms of the same protein (Caputo et al., 2001; Infante et al., 2004). Consistently, the two gps have differences in lectin affinity, with only gp63 cross-linking *Ulex europaeus* agglutinin I. This finding suggests that the terminal gp63's fucose residues recognized by this lectin plan an important role in binding the spermatozoa.

In *D. pictus*, binding of spermatozoa to VE occurs only after the acrosome reaction (A23187-exposed spermatozoa; Gualtieri and Andreuccetti, 1996; Caputo et al., 2001). Binding occurs all over the egg, although it is more abundant in the animal than in the vegetal half of the egg (Infante et al., 2004). The 63 kDa glycoprotein cDNA (DpZP2) was sequenced and cloned (Vaccaro et al., 2001) and shown to exhibit high homology to *X. laevis* gp69/gp64 and to ZP2 of mammals.

In the present study, we investigated whether, in *D. pictus* VE, fucose and/or sulphate groups are involved in spermatozoa–VE binding and whether they are present in gp63 or gp75, using competition assays. Surprisingly, we found that sulphates by themselves have a major role in spermatozoa–VE binding, irrespective of whether they are borne by fucose, dextran or Le^x oligosaccharides. They appeared to be located in the gp75, where fucose is absent, probably in O-linked oligosaccharide chains.

Results

Metaperiodate pretreatment and binding assay

Dejellied eggs, i.e. deprived of jelly layers J1, J2, J3 and the jelly plug, were treated with sodium metaperiodate and incubated with acrosome-reacted spermatozoa. After washing to remove the unbound spermatozoa, the eggs were fixed and stained with DAPI (4,6-diamidino-2-phenylindole). Comparison of the number of eggs having bound spermatozoa in the treated eggs versus untreated eggs showed that binding of spermatozoa was not affected by the treatment (results not shown). Therefore it appears that hydroxy groups are not directly involved in spermatozoa–VE binding.

Competition assays between dejellied eggs and fucoidan-, dextran sulphate- or dextran-treated spermatozoa

Having undergone the acrosome reaction after exposure to the calcium ionophore A23187, spermatozoa were incubated with fucoidan and then added to dejellied eggs. The results indicated a dose-dependent competition of fucoidan on spermatozoa–VE binding. As shown in Figure 1(a), for untreated spermatozoa, a high percentage of eggs having bound spermatozoa occurred, whereas the binding percentage obtained with fucoidan-treated spermatozoa decreased by approx. 20% already at the fucoidan concentration of 0.005 mg/ml. There were practically no eggs with bound spermatozoa at the concentration of 5 mg/ml. Figure 1(b) is an example of an egg having bound spermatozoa, when spermatozoa were not exposed to fucoidan, and Figure 1(c) shows an egg exposed to spermatozoa treated with 5 mg/ml fucoidan. Figure 1(d) depicts a spermatozoon in the VE. The plasma membrane and the outer acrosome membrane are in the process of vesiculation and only the outermost acrosome component is present in the acrosome cap (see Campanella et al., 1997).

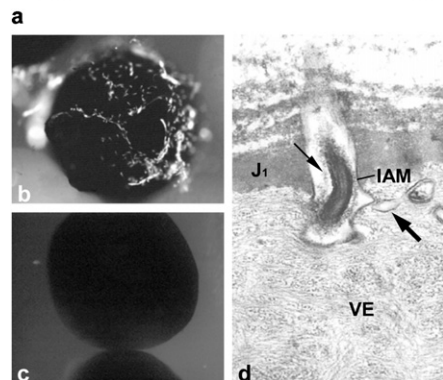
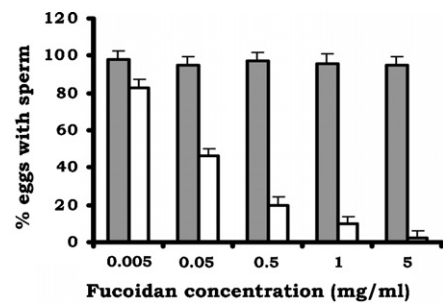
To investigate whether the inhibitory effect of fucoidan was due to fucose or SO_4^{2-} groups, the acrosome-reacted spermatozoa were treated with dextran or dextran sulphate and then incubated with dejellied eggs. Binding percentages are shown in Figure 2. For dextran-treated spermatozoa, a high percentage of eggs with spermatozoa bound to VE along the whole range of concentrations was observed. In contrast, the percentage of eggs with bound spermatozoa in the dextran sulphate-treated spermatozoa assays was 35% lower at the concentration of 0.0005 mg/ml and abolished at 0.5 mg/ml (Figure 2).

Competition assays between spermatozoa and fucoidan- or dextran sulphate-treated eggs

Since, in the competition assays, the competing sugars cannot be completely washed away from the spermatozoa, further experiments were needed to determine whether, in our experiments, receptive molecules interacting with sugars are located on the spermatozoa or on eggs. To this end, dejellied eggs were exposed to fucoidan or dextran sulphate and then rinsed before spermatozoa–egg incubation. No spermatozoa binding inhibition was found (Figure 3), indicating that the above-mentioned SO_4^{2-} groups

Figure 1 | Competition assays with fucoidan

(a) Spermatozoa–VE binding significantly decreases in a fucoidan dose-dependent way. Grey bar, spermatozoa unexposed to fucoidan; white bar, fucoidan-exposed spermatozoa. Bars represent S.D. (b) Egg in an experiment where eggs were incubated with spermatozoa unexposed to fucoidan and (c) Egg in an experiment where eggs were incubated with spermatozoa treated with 5 mg/ml fucoidan. In (b), spermatozoa are bound to the VE surrounding the egg, whereas, in (c), the spermatozoa are absent. $x = 14$. (d) Ultrathin section of an inseminated egg, where a spermatozoon is shown in the innermost jelly coat (J1) and in the VE. The spermatozoon is surrounded by its inner acrosome membrane (IAM) and the acrosome is empty except for some of its outermost components (small arrow). The large arrow indicates vesicles derived from vesiculation of the spermatozoon plasma membrane and outer acrosome membrane. $x = 14000$.



are located on the VE and that fucoidan and dextran sulphate interact with receptive molecules on the spermatozoa.

Figure 2 | Competition assays with dextran and dextran sulphate

Spermatozoa treatment with dextran (white bars) before the addition of dejellied eggs results in a high percentage of eggs with bound spermatozoa over the entire range of concentrations tested. In contrast, on spermatozoa exposure to dextran sulphate (grey bars), the percentage of eggs with bound spermatozoa decreased in a dose-dependent way. Bars represent S.D.

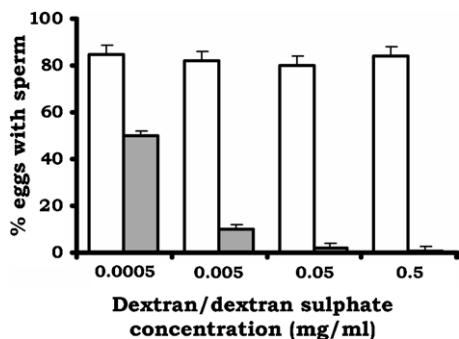
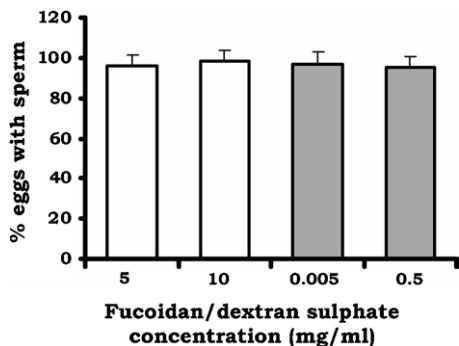


Figure 3 | Binding assay between spermatozoa and fucoidan/dextran sulphate-pretreated eggs

White bar, fucoidan; grey bar, dextran sulphate. Egg pretreatment with these glycans does not interfere with spermatozoa binding to VE. Bars represent S.D.

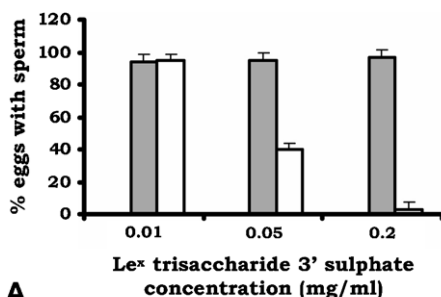


Competition assays between dejellied eggs and Le^x trisaccharide 3'-sulphate- or 3'-sialyl- Le^x tetrasaccharide-treated spermatozoa

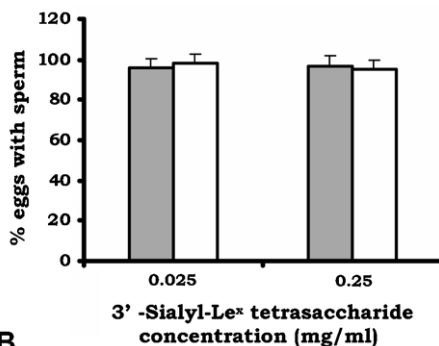
Competition binding assays with Le^x trisaccharide 3'-sulphate and 3'-sialyl- Le^x tetrasaccharide sugars

Figure 4 | Competition assays with Le^x trisaccharide 3'-sulphate and 3'-sialyl- Le^x tetrasaccharide

(A) When spermatozoa were exposed to Le^x trisaccharide 3'-sulphate, spermatozoa binding to VE was inhibited in a dose-dependent manner. In contrast, (B) spermatozoa pretreatment with 3'-sialyl- Le^x tetrasaccharide did not, in practice, change the percentage of eggs with bound spermatozoa in the control assays. Grey bars, control binding assay with untreated spermatozoa; white bar, pretreatment assays.



A



B

were performed by incubating spermatozoa with one of these oligosaccharides before exposure to dejellied eggs. Le^x trisaccharide 3'-sulphate inhibited spermatozoa-VE binding by approx. 60 and 100% at sugar concentrations 0.05 mg/ml and 0.2 mg/ml respectively (Figure 4a). Conversely, 3'-sialyl- Le^x tetrasaccharide was not inhibitory at the concentrations used (Figure 4b), confirming the role of SO_4^{2-} groups in spermatozoa-VE binding in contrast with CO_2H^- groups.

Competition assays with fucoidan- and dextran sulphate-treated spermatozoa on beads-gp63 and/or beads-gp75

Since both gp63 and gp75 of VE specifically bind to the spermatozoa (Infante et al., 2004), we supposed that sulphated sugars are present in one or both of the glycoproteins. Accordingly, we performed assays on gp63 and gp75 immobilized on polystyrene beads utilizing spermatozoa pretreated with fucoidan or dextran sulphate.

Electroeluted gp63 and gp75 were adsorbed on beads. To estimate the amount of bound glycoprotein/ bead, adsorption was checked by boiling the beads in sample buffer and the released protein was analysed by SDS/PAGE in each binding experiment. By knowing the concentration of the glycoprotein in the eluate before and after adsorption and the number of 350 μm beads/vol., the amount of bound glycoprotein/ bead was estimated to be in the range of 0.0075 μg (i.e. 7.2×10^{10} molecules) and of 2 $\mu\text{g}/\text{cm}^2$. Commercial BSA was adsorbed on beads and used as control in spermatozoa-binding experiments.

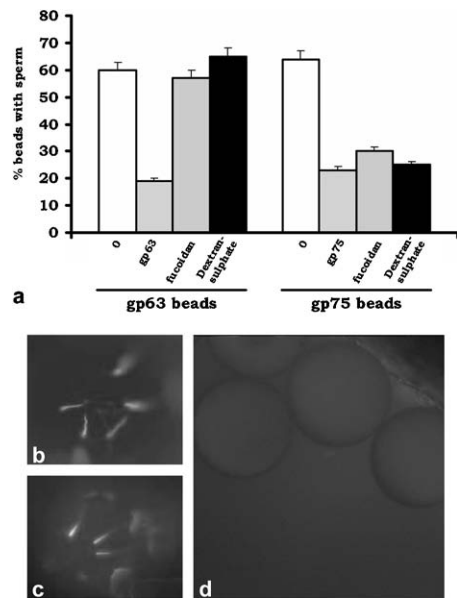
Spermatozoa were preincubated with fucoidan or dextran sulphate and exposed to gp63 beads (Figure 5). The binding of fucoidan- and dextran sulphate-incubated spermatozoa in the range of sugar concentrations used was almost the same as the binding of the unincubated spermatozoa (60, 58 and 65% respectively). Spermatozoa treated with soluble gp63 (0.5 mg/ml) underwent significantly lower adhesion to gp63 beads (20% eggs with bound spermatozoa). Similar assays were performed with gp75 beads (Figure 5a). Binding of spermatozoa to gp75 beads was significantly affected by treating the spermatozoa with fucoidan or dextran: it decreased to 30–25% with respect to control untreated spermatozoa (64% binding; Figures 5a and 5b). Only 23% of the beads had bound spermatozoa when the latter were incubated with gp75 (0.5 mg/ml).

Competition assays with solubilized VEs treated with PNGase F (N-linked glycosidase F) or α -N-GalNAcase (α -N-acetylgalactosaminidase)

Preliminary experiments showed that addition of 40 or 20 μg of solubilized VEs per 200 μl of reacted spermatozoa suspension in a final volume of 1 ml produced an inhibition of the order of 70–60%. To investigate the involvement of VE's N-linked sugar

Figure 5 | Competition assays between the spermatozoa exposed to fucoidan or dextran sulphate and gp63 beads/gp75 beads

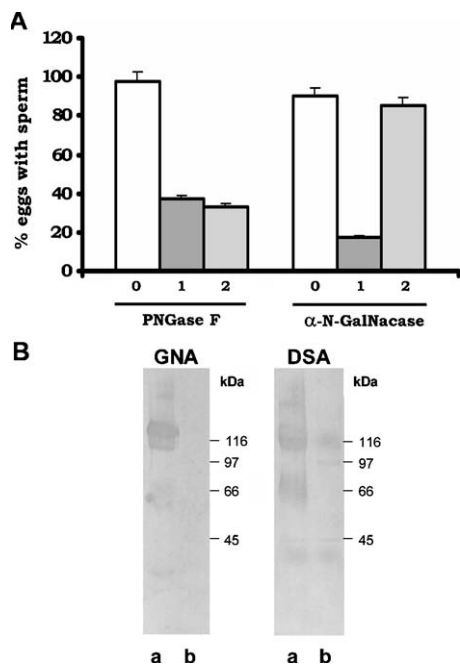
(a) 0, untreated spermatozoa. The concentrations of fucoidan (1, 5 and 10 mg/ml) and dextran sulphate (0.5, 1 and 2 mg/ml) used for spermatozoa preincubations gave practically identical results and therefore they were pooled together in a single bar. Data indicate that both sulphated glycans do not interfere upon spermatozoa adhesion to gp63 beads, whereas they exert a strong inhibition on the binding of spermatozoa–gp75 beads. (b, c) gp75 beads exposed to untreated spermatozoa: spermatozoa adhere to the beads. (d) gp75 beads exposed to fucoidan-incubated spermatozoa: the spermatozoa do not bind to the beads. Bead size is 350–400 μm .



chains in spermatozoa binding, solubilized VEs were exposed to increasing concentrations of PNGase F. Previous work showed that lectin blots of solubilized VEs clearly cross-linked GNA (*Galanthus nivalis* agglutinin), a Man α 1–3 Man-specific lectin, detecting N-linked sugars (Caputo et al., 2001). In the present study, when solubilized VEs were exposed to PNGase F in the ratio 1 unit/4 μg of VEs, no cross-linking occurred with GNA, in contrast with untreated VE

Figure 6 | Enzyme-treated VEs

(A) Competition assays using solubilized VEs digested by PNGase F or α -N-GalNAcase. 0, untreated spermatozoa; 1, spermatozoa treated with soluble VEs; 2, enzyme-digested VEs. In the PNGase F assay, the inhibitory action of solubilized VE in spermatozoa–VE binding (38% binding) is not removed by the digestion of VE by the enzyme (35% binding). In the α -N-GalNAcase assay, the inhibitory action of solubilized VE in spermatozoa–VE binding (13% binding) is removed by the enzyme (85% binding). (B) Lectin blot of solubilized VEs. a, untreated VEs; b, PNGase F-treated VEs. In the GNA blot, the PNGase F-treated VEs lose their cross-reactivity to the lectin, whereas in the DSA blot, the cross-reactivity is partially retained by some of the VE glycoprotein.



blots (Figure 6). In addition, VE blots were similarly exposed to the Gal β 1–4GlcNAc-specific DSA (*Datura stramonium* agglutinin). In this case, the lectin cross-linking of VE glycoproteins was only partially eliminated by the PNGase F treatment (Figure 6). In parallel competition trials, reacted spermatozoa

suspensions were incubated with 40 μ g of VEs previously treated with PNGase F (1 unit/4 μ g of VEs) and then used in spermatozoa–VE competition assays over dejellied eggs. The results show that PNGase F treatment did not eliminate the competing ability of soluble VEs on spermatozoa–VE binding (Figure 6). In contrast, in the spermatozoa–VE competition assay where α -N-GalNAcase was used for VE digestion, an enzyme/VE ratio as low as 0.03 unit/1 μ g was sufficient for abolishing VE inhibitory action. In these experiments, the proportion of eggs having bound spermatozoa was 85%, whereas the proportion with untreated VEs was 12% (Figure 6). α -N-GalNAcase is capable of cleaving terminal α 1– α 3-linked GalNAc from glycoconjugates as well as GalNAc-Ser/Thr i.e. it acts on GalNAc O-linked to the peptide backbone (see Schachter and Brockhausen, 1992). Although we cannot discriminate between the two actions of the enzyme, overall the results of PNGase F and α -N-GalNAcase indicate that determinants for binding are not located in N-linked oligosaccharide chains, but rather on O-linked chains.

Discussion

Competition assays performed on dejellied eggs or on immobilized gp63 and gp75 indicate that VE-sulphated sugars are essential for the occurrence of spermatozoa–VE binding in *D. pictus*. Indeed, competition trials utilizing three kinds of sulphated sugars (fucoidan, dextran sulphate and Le^x trisaccharide 3'-sulphate) showed a dose-dependent inhibition of VE–spermatozoa binding. Inhibition did not occur if unsulphated dextran or 3'-sialyl-Le^x tetrasaccharide was used. 3'-Sialyl-Le^x tetrasaccharide/Le^x trisaccharide 3'-sulphate competition assays, in addition, indicated that sulphate-negative charges specifically act on the interaction in contrast with negative charges carried by carboxylic groups. Moreover, these experiments indicated that the presence of fucose did not affect competitively spermatozoa–VE binding. Consistently, for *D. pictus*, previous studies (Infante et al., 2004) showed no cross-reactivity with anti-*U. elongatus* gp273 antibodies. The latter recognize glycans containing a Lewis-like structure with fucose as the determinant (Focarelli et al., 2003). Moreover, metaperiodate trials support the conclusion that, in spermatozoa–VE binding, sugar radicals such as hydroxy groups are not implicated.

VE digestion by PNGase F and by α -N-GalNAcase suggests that the sugars carrying sulphate groups are located in O-linked chains, as shown both in the sea urchin (Dhume and Lennarz, 1995) and in *U. elongatus* (Capone et al., 1999). In the amphibian *Cynops pyrrhogaster*, heparan sulphate-like molecules located on acrosome-reacted spermatozoa are responsible for spermatozoa binding to the uterine envelope of this species. A protein of approx. 70 kDa purified from the envelope appears to bind to the heparan sulphate-like molecules expressed on spermatozoa (Nakai et al., 1999). In contrast, in the present study, sulphates appeared to be part of the VE glycoconjugates, as suggested by binding assays with eggs pretreated with sulphated sugars. In particular, competition assays using immobilized gp63 or gp75 strongly suggest that SO_4^{2-} groups are present on gp75 glycoconjugates, whereas gp63, its fucose-containing glycoform, has no SO_4^{2-} groups involved in spermatozoa binding.

In most cases (see Miller and Ax, 1990; Oehninger, 2001; Focarelli et al., 2003), in spermatozoa–egg interaction, fucose has been found to have a dominant role, in particular in its sulphated form. However, in some cases, as in rabbit spermatozoa–zona interaction, sulphate groups are the determinants carried by the carbohydrate moiety which are important for binding to occur (O’Rand et al., 1988). In human, porcine and mouse spermatozoa–zona interaction, acrosin, a spermatozoa acrosome enzyme, appears to bind to sulphated polysaccharides of the *zona pellucida* (Moreno et al., 1998; Howes and Jones, 2002). This binding is inhibited by sulphated but not by desulphated polymers (Williams and Jones, 1990). Moreover, in bovine reproductive biology, sulphate glycoconjugates not containing fucose are known to modulate spermatozoa adhesion to the oviductal epithelium (Talevi and Gualtieri, 2001). In the sea urchin *Strongylocentrotus purpuratus*, sulphates play a critical role in determining the binding activity of VE on spermatozoa. Desulphated fucoidan has no activity, but resulphation of fucoidan restores the inhibition of *bindin*-induced agglutination (De Angelis and Glabe, 1987). In the same species, a two-step model was hypothesized for spermatozoa–egg surface interaction (Dhume and Lennarz, 1995), i.e. (i) an ionic weak binding involving sulphate groups of O-linked oligosaccharide chains, part of the 350 kDa glycoprotein, and (ii) a high-affinity binding involving one or more domains of the 350 kDa poly-

peptide chain in the second step. Moreover, sulphate groups appear to modulate the activity of some oligosaccharide chains in VE–spermatozoa interaction, since binding efficiency is proportional to the presence of sulphate groups (Dhume and Lennarz, 1995). In *D. pictus*, gp75 and gp63 are the two glycoproteins displaying adhesive properties to spermatozoa, but only one, gp75, contains sulphate groups, on the basis of indirect yet compelling evidence in the present study. It may be postulated that, similar to the sea urchin, multistep binding may occur in this system, where sulphate groups in gp75 oligosaccharide chains provide initial adhesion, and gp63 and gp75 protein backbones provide second binding. In *S. purpuratus* jelly coats, sulphate positions 2-O- and 4-O- in the saccharide chains of the sulphated α -L-fucan determine spermatozoa cell recognition (Vilela-Silva et al., 1999) and later, in embryos, dermatan sulphate bearing high amounts of O-4- and O-6-disulphated galactosamine units are essential for development to occur (Vilela-Silva et al., 2001). In *D. pictus* VE, further studies are required to determine whether specific positions of sulphate groups are similarly needed in gp75 sugar chains for adhering to a spermatozoa.

Materials and methods

Animals and gametes

Adult male and female *D. pictus* were injected in the dorsal lymphatic sac with 200–250 units of Profasi HP (Serono, Rome, Italy) in Amphibian Ringer (111 mM NaCl, 1.3 mM CaCl_2 , 2 mM KCl, 0.8 mM MgSO_4 and 5 mM Hepes, pH 7.8). Uterine eggs were obtained 18 h after hormone injection. The semen (spermatozoa and seminal fluid) was collected from the seminal vesicles (see Caputo et al., 2001) 24 h after hormone treatment. Standard control insemination was performed by the addition of a drop of semen to eggs immersed in 1/10 Ringer.

Preparation of VE

Eggs were first de jellyed in dejellying buffer (100 mM NaCl, 5 mM dithioerythritol and 50 mM Tris/HCl, pH 8.5). VEs were then manually removed and transferred into HB (25 mM Hepes, pH 7.5, containing 900 mM glycerol, 0.02 mM NaN_3 , 1 mM ATP, 1 mM dithiothreitol, 5 mM EGTA, 2 mM *N*-*p*-tosyl-arginine methyl ester, 5 mg/ml soya-bean trypsin inhibitor, 5 $\mu\text{g}/\text{ml}$ aprotinin and 10 μM E64). After extensive rinsing and brief centrifugations at low speed, VEs were exposed to 0.6 M KI for a few min to remove the innermost jelly layer J1 (see Caputo et al., 2001) and, after extensive rinsing in 1/10 Ringer, dissolved in 2% (w/v) SDS by heating at 95°C for at least 2 min. After centrifugation at 14 000 g for 10 min, the samples were processed for electrophoresis or binding assays.

Protein determination, SDS/PAGE and gel staining

Protein concentration of the samples was determined with the BCA (bicinchoninic acid) or Micro BCA Protein Assay Reagent (Pierce, Rockford, IL, U.S.A.); 15 µg of the VE-soluble proteins was applied on each lane of the gels. Samples were prepared for SDS/PAGE by the addition of sample buffer and heating at 40°C for a few minutes. Protein samples were analysed by SDS/PAGE using Laemmli's Tris/glycine buffer system. The running gel contained 10% (w/v) acrylamide. Molecular-mass standards were the following: 200, 116, 97.5, 66.2, 45, 31 and 21.5 kDa (Bio-Rad, Hercules, CA, U.S.A.). After fixation in methanol/acetic acid, gels were stained with either Coomassie Blue or silver.

Lectin blot detection on nitrocellulose

Proteins subjected to SDS/PAGE were electrophoretically transferred on to nitrocellulose sheets by the method of Towbin et al. (1979) overnight at 180 mA (for more details, see Infante et al., 2004). DIG (digoxigenin)-labelled DSA and GNA were part of a DIG glycan differentiation kit (Roche, Mannheim, Germany) and were utilized according to the manufacturer's instructions. Positive controls were run for the DIG-labelled lectins according to the DIG glycan differentiation kit, i.e. fetuin for DSA.

Electroelution

VE glycoproteins (gp63 and gp75) were separated by SDS/PAGE and visualized by staining with 0.3 M CuCl₂. The area of the selected bands was cut out and the gel slices were electroeluted with 25 mM Tris/HCl (pH 8.3) containing 1.44 mM glycine. Electroeluted proteins were dialysed at 4°C against distilled water and stored at -20°C after concentration in a speed vacuum concentrator Savant. The protein content and purity of each sample were checked by SDS/PAGE and/or the BCA protein assay method.

Metaperiodate-binding assays

After dejelling, groups of approx. 10–15 eggs were exposed to sodium metaperiodate (25, 50 and 100 mM) in Ringer at 18–20°C for 15 min. Five assays for each metaperiodate concentration were performed. In some experiments, after metaperiodate treatment, eggs were further incubated with sodium borohydride (20 mM) to stabilize the transformation of oligosaccharide hydroxy groups into aldehyde groups. Treated eggs were then used for the spermatozoa–egg binding assays.

Spermatozoa–egg binding and competition assays

Spermatozoa suspensions as recovered from the seminal vesicle were diluted in 1/10 Ringer to provoke complete unravelling of the spermatozoa bundles and spermatozoa ejection from the bundles. Spermatozoa are motile for approx. 14 s (see Maturi et al., 1998). The spermatozoa suspension was then treated with 0.25 µM A23187 (Sigma) for 2 min, because previous work showed that dejellied, unfertilized eggs bind to the spermatozoa if spermatozoa are pretreated with this Ca²⁺ ionophore to induce acrosome reaction (Gualtieri and Andreuccetti, 1996; Caputo et al., 2001) and then washed with 1/10 Ringer. As a general control for testing the binding ability of the spermatozoa to VE, groups of fully dejellied eggs were added to calcium ionophore-

treated spermatozoa and incubated for 15 min at room temperature (22°C) under gentle rocking. The spermatozoa-exposed eggs were then washed to separate the unbound spermatozoa from those bound to the eggs (see Caputo et al., 2001). The samples were either directly observed under a compound microscope or, after fixation in 95% (v/v) ethanol, stained with DAPI for counting spermatozoa head attachment to the VEs under a Zeiss Axioskop microscope equipped with a Progress 3800 colour video camera and KS300 image analysis software.

The binding assay (see Maturi et al., 1998) considers the fact that, when spermatozoa come out of the bundles, they may get entangled because of their length (2.33 mm), and the resulting suspension of spermatozoa is, therefore, rather uneven. As a consequence, it cannot be established whether more bound spermatozoa (or spermatozoa-bound beads, for the experiment in the next section) means a greater ability of the VE to bind the spermatozoa or more spermatozoa available for the egg. Therefore we measured successful spermatozoa collision (binding) with eggs under gentle rocking in terms of percentage of eggs with spermatozoa, without considering the number of spermatozoa/egg.

In competition assays, acrosome-reacted spermatozoa were treated with fucoidan at the concentrations of 0.005, 0.05, 0.5, 1 and 5 mg/ml and with dextran or dextran sulphate at the concentrations of 0.0005, 0.005, 0.05 and 0.5 mg/ml. Alternatively, spermatozoa were pretreated with Le^x trisaccharide 3'-sulphate at the concentrations of 0.01, 0.05 and 0.2 mg/ml or with 3'-sialyl-Le^x tetrasaccharide at 0.025 and 0.25 mg/ml. The spermatozoa suspension was then incubated with groups of 10–15 eggs for 15 min to allow spermatozoa binding under gentle rocking.

In a further set of experiments, groups of approx. 10–15 eggs were treated with fucoidan at the concentrations of 5 and 10 mg/ml or dextran sulphate at the concentrations of 0.005 and 0.5 mg/ml, washed to remove competing sugars and mixed with acrosome-reacted spermatozoa. A minimum of three assays was performed for each sugar dilution used. The eggs were stained with DAPI for counting spermatozoa at the VE surface.

For ultrastructural observation, fertilized eggs were fixed at 2, 6, 10 and 20 min after insemination in 2.5% (v/v) glutaraldehyde in 0.2 M phosphate buffer as described previously (Talevi and Campanella, 1988). Dehydration in graded ethanol at 4°C was followed by embedding in Epon 812. Thin sections were cut with diamond knives, stained with uranyl acetate and lead citrate and examined in a Philips EM-300 microscope at the CISME (Centro Interdipartimentale di Servizio per la Microscopia Elettronica) of the University of Naples Federico II.

Spermatozoa–bead binding and competition assays

The electroeluted glycoproteins as well as commercial BSA were adsorbed on polystyrene beads of 350–400 µm (Polysciences, Warrington, PA, U.S.A.). Adsorption on the beads was performed as suggested by the supplier, utilizing 0.1 M borate buffer (pH 8.5) and blocking in 1% BSA. In the assay, spermatozoa were smeared on microslides, further diluted in 10% (v/v) Ringer and treated with Ca²⁺ ionophore. After rinsing in 1/10 Ringer, approx. 100 glycoprotein-coated beads were released on the spermatozoa and incubated for 15 min in Petri dishes under gentle rocking.

For competition assays, reacted spermatozoa were preincubated with 0.5 mg/ml of eluted gp63 or gp75 in 1/10 Ringer,

with fucoidan at the concentration 1, 5 and 10 mg/ml or dextran sulphate at the concentration of 0.5, 1 and 2 mg/ml for 15 min. After a 10-fold dilution with 1/10 Ringer, the spermatozoa-binding assay was performed by mixing the treated spermatozoa suspension with groups of approx. 100 gp63 or gp75 beads and maintaining for 15 min under gentle rocking. After several rinses in 1/10 Ringer, beads with bound spermatozoa were directly observed under a compound microscope to count spermatozoa attachment or stained with DAPI and observed under a UV microscope.

PNGase F and α -N-GalNAcase assays

N-linked sugar chains were released from solubilized VEs on incubation with PNGase F (glycopeptidase F) from *Flavobacterium meningosepticum* (Sigma) in the ratio of 5 units of PNGase F/20 μ g of VE. Incubation was performed in 500 mM sodium phosphate, 12.5 mM EDTA and 5 M glycerol (pH 7.2) for 16 h at 37°C. In control experiments, the VE was incubated in an enzyme boiled at 100°C. The enzyme/ μ g of solubilized VE ratio mentioned above was calibrated by exposing increasing concentrations of VE to fixed unit numbers of enzymes, blotting the digested VE and exposing the blot to GNA or DSA. The ratio 5 units of PNGase F/40 μ l VE ratio was optimal for eliminating Man α 1- α 3 Man of N-linked sugars and it was used for spermatozoa-VE competition assays. In these assays, 200 μ l of reacted spermatozoa suspensions was incubated with the PNGase F-exposed envelopes. The suspension was further diluted to 1 ml and used in spermatozoa-VE competition assays over dejellied eggs.

α -N-GalNAcase (from chicken liver; Sigma) cleaves terminal α 1- α 3-linked GalNAc from glycoconjugates as well as GalNAc-Ser/Thr. The incubation of VEs with the enzyme was performed overnight at 37°C in 0.1 M phosphate-citrate buffer (pH 3.6). In competition assays, 200 μ l of reacted spermatozoa suspensions was incubated with the enzyme-exposed envelopes (0.03 unit of α -N-GalNAcase/1 μ g of solubilized VE). The pH of the α -N-GalNAcase-exposed VE suspension was neutralized before adding to spermatozoa suspension. The suspension was further diluted to 1 ml and used in competition assays between spermatozoa and dejellied eggs. In control experiments, VEs were incubated in 100°C-boiled enzyme.

Acknowledgements

We thank Professors F. Rosati and R. Focarelli for helpful discussions, Dr M. Walkers for a critical reading of this paper, Mr G. Falcone for image elaboration, A. De Filippis and L. Iannone for help in the laboratory. C.C. was supported by MIUR (Ministero dell'Istruzione, dell'Università e della Ricerca Scientifica; Programmi di Ricerca Scientifica di Rilevante Interesse Nazionale 1999).

References

Bleil, J.D. and Wassarman, P.M. (1988) Galactose at the nonreducing terminus of O-linked oligosaccharides of mouse egg zona pellucida glycoprotein is essential for the glycoprotein's sperm receptor activity. *Proc. Natl. Acad. Sci. U.S.A.* **85**, 6778-6782

Campanella, C., Carotenuto, R., Infante, V., Maturi, G. and Atripaldi, U. (1997) Sperm-egg interaction in the painted frog (*Discoglossus pictus*): an ultrastructural study. *Mol. Reprod. Dev.* **47**, 323-333

Capone, A., Rosati, F. and Focarelli, R. (1999) A 140 kDa glycoprotein from the sperm ligand of the vitelline coat of the freshwater bivalve *Unio elongatus*, only contains O-linked oligosaccharide chains and mediates sperm-egg interaction. *Mol. Reprod. Dev.* **54**, 203-207

Caputo, M., Infante, V., Talevi, R., Vaccaro, M.C., Carotenuto, R. and Campanella, C. (2001) Following passage through the oviduct, the coelomic envelope of *Discoglossus pictus* acquires fertilizability upon reorganization, degradation of gp42, extensive glycosylation and the formation of a specific layer. *Mol. Reprod. Dev.* **58**, 318-329

De Angelis, P.L. and Glabe, C.G. (1987) Polysaccharides structural features that are critical for the binding of sulfated fucans to *bindin*, the adhesive protein from sea urchin sperm. *J. Biol. Chem.* **262**, 13946-13952

Denis-Donini, S. and Campanella, C. (1977) Ultrastructural and lectin binding changes during the formation of the animal dimple in oocytes of *Discoglossus pictus* (Anura). *Dev. Biol.* **61**, 140-152

Dhume, S.T. and Lennarz, W.J. (1995) The involvement of O-linked oligosaccharide chains of the sea urchin egg receptor for sperm in fertilization. *Glycobiology* **5**, 11-17

Dravland, J.E. and Mortimer, D. (1988) Role of fucose-sulphate-rich carbohydrates in the penetration of zona-pellucida-free hamster eggs by hamster spermatozoa. *Gamete Res.* **21**, 353-358

Focarelli, R. and Rosati, F. (1995) The 220-Kda vitelline coat glycoprotein mediates sperm binding in the polarized egg of *Unio elongatus* through O-linked oligosaccharides. *Dev. Biol.* **171**, 606-614

Focarelli, R., Capone, A., Ermini, L., Del Buono, F., La Sala, G.B., Balasini, M. and Rosati, F. (2003) Immunoglobulins against gp273, the ligand for sperm-egg interaction in the Mollusk Bivalve *Unio elongatus*, are directed against charged O-linked oligosaccharide chains bearing a Lewis-like structure and interact with epitopes of the human zona pellucida. *Mol. Reprod. Dev.* **64**, 226-234

Gualtieri, R. and Andreuccetti, P. (1996) Localization of egg-surface carbohydrates and fertilization in *Discoglossus pictus* (Anura). *Cell Tissue Res.* **283**, 173-181

Gunaratne, H.M.M.J., Yamagaki, T., Matsumoto, M. and Hoshi, M. (2003) Biochemical characterization of inner sugar chains of acrosome reaction-inducing substance in jelly coat of starfish eggs. *Glycobiology* **13**, 567-580

Howes, L. and Jones, R. (2002) Interaction between zona pellucida glycoproteins and sperm proacrosome/acrosin during fertilization. *J. Reprod. Immunol.* **53**, 181-192

Infante, V., Caputo, M., Riccio, S., De Filippis, A., Carotenuto, R., Vaccaro, M.C. and Campanella, C. (2004) Vitelline Envelope gps 63 and 75 specifically bind sperm in 'in vitro' assays in *Discoglossus pictus*. *Mol. Reprod. Dev.* **68**, 213-222

Maturi, G., Infante, V., Carotenuto, R., Focarelli, R., Caputo, M. and Campanella, C. (1998) Specific glycoconjugates are present at the oolemma of the fertilization site in the egg of *Discoglossus pictus* (Anurans) and bind spermatozoa in an *in vitro* assay. *Dev. Biol.* **204**, 210-223

Miller, D.J. and Ax, R.L. (1990) Carbohydrates and fertilization in animals. *Mol. Reprod. Dev.* **26**, 184-198

Moreno, R.D., Sepulveda, M.S., de Ioannes, A. and Barros, C. (1998) The polysulphate binding domain of human proacrosin/acrosin is involved in both the enzyme activation and spermatozoa-zona pellucida interaction. *Zygote* **7**, 105-111

Nakai, S., Watanabe, A. and Onitake, K. (1999) Sperm surface heparin/heparan sulfate is responsible for sperm binding to the uterine envelope in the newt, *Cynops pyrrhogaster*. *Dev. Growth Differ.* **41**, 101-107

Oehninger, S. (2001) Molecular basis of human sperm-zona pellucida interaction. *Cells Tissues Organs* **168**, 58-64

- Omata, S. and Katagiri, C. (1996) Involvement of carbohydrate moieties of the toad egg vitelline coat in binding with fertilizing sperm. *Dev. Growth Differ.* **38**, 663–672
- O'Rand, M.G., Widgren, E.E. and Fisher, S.J. (1988) Characterization of the rabbit sperm membrane autoantigen, RSA, as a lectin-like zona binding protein. *Dev. Biol.* **129**, 231–240
- Schachter, H. and Brockhausen, I. (1992) The biosynthesis of serine (threonine)-N-acetylgalactosamine-linked carbohydrate moieties. *Glycoconjugates. Composition, Structure and Function* (Allen, H.J. and Kisailus, E.C., eds), pp. 165–198, Marcel Dekker, New York
- SeGall, G.K. and Lennarz, W.J. (1979) Chemical characterization of the component of the jelly coat from sea urchin eggs responsible for the induction of the acrosome reaction. *Dev. Biol.* **71**, 33–48
- Talevi, R. and Campanella, C. (1988) Fertilization in *Discoglossus pictus*. I: Regionalization of sperm-egg interaction site and occurrence of a late stage of sperm penetration. *Dev. Biol.* **130**, 524–535
- Talevi, R. and Gualtieri, R. (2001) Sulfated Glycoconjugates are powerful modulators of bovine sperm adhesion and release from the oviductal epithelium in vitro. *Biol. Reprod.* **64**, 491–498
- Tian, J.D., Gong, H., Thomsen, G.H. and Lennarz, W.J. (1997a) Gamete interactions in *Xenopus laevis*: identification of sperm binding glycoproteins in the egg vitelline envelope. *J. Cell Biol.* **136**, 1099–1108
- Tian, J.D., Gong, H., Thomsen, G.H. and Lennarz, W.J. (1997b) *Xenopus laevis* sperm-egg adhesion is regulated by modifications in the sperm receptor and the vitelline envelope. *Dev. Biol.* **187**, 143–153
- Tian, J.D., Gong, H., Thomsen, G.H. and Lennarz, W.J. (1999) *Xenopus laevis* sperm receptor gp 69/64 glycoprotein is a homolog of the mammalian sperm receptor ZP2. *Proc. Natl. Acad. Sci., U.S.A.* **96**, 829–834
- Towbin, H., Staehelin, T. and Gordon, J. (1979) Electrophoretic transfer of proteins from polyacrylamide gels to nitrocellulose sheets: procedure and some applications. *Proc. Natl. Acad. Sci. U.S.A.* **76**, 4350–4354
- Vaccaro, M.C., De Santo, M.C., Caputo, M., Just, M., Tian, J.D., Gong, H., Lennarz, W.J. and Campanella, C. (2001) Primary structure and developmental expression of DpZP2, a vitelline envelope glycoprotein homolog of mouse ZP2, in *Discoglossus pictus*, one of the oldest living anuran species. *Mol. Reprod. Dev.* **59**, 133–143
- Vilela-Silva, A.C.E.S., Alves, A.P., Valente, A.P., Vacquier, V.D. and Mourao, P.A.S. (1999) Structure of the sulfated α L fucan from the egg jelly coat of the sea urchin *Strongylocentrotus purpuratus*: patterns of preferential 2 O and 4 O sulfation determine sperm cell recognition. *Glycobiology* **9**, 927–933
- Vilela-Silva, A.C.E.S., Werneck, C.C., Valente, A.P., Vacquier, V.D. and Mourao, P.A.S. (2001) Embryos of the sea urchin *Strongylocentrotus purpuratus* synthesize dermatan sulfate enriched in 4-O- and 6-O-disulfated galactosamine units. *Glycobiology* **11**, 433–440
- Vo, L.H. and Hedrick, J.L. (2000) Independent and hetero-oligomeric-dependent sperm binding to egg envelope glycoprotein ZPC in *Xenopus laevis*. *Biol. Reprod.* **62**, 766–774
- Williams, R.M. and Jones, R. (1990) Specific binding of sulphated polymers to ram sperm acrosin. *FEBS Lett.* **270**, 168–172

Received 2 August 2004; accepted 16 September 2004

Published as Immediate Publication 29 April 2005, DOI 10.1042/BC20040092

Eif6 in *Xenopus* oogenesis and embryogenesis

At end of the 1990s, a new change occurred in our scientific life. Pier Carlo Marchisio (DIBIT, Saint Raphael Hospital, Milan) was looking for a model where the function of p27BBP/eif6 could be tested in multicellular organisms and suggested we took charge of this project. We were immediately intrigued by this proposal for several reasons, one of them being that Rosa had demonstrated that spectrin surrounds nucleoli similarly to eif6 that is indeed involved in 60S biogenesis and also interacts with the cytoskeleton. That was the time when our Ministry of Public Education decided to support research through nation projects called PRIN, cancelling the previous method of funding. We successfully presented a joint project for the PRIN call in 2000.

In 2003 Pier Carlo and Stefano Biffo (DIBIT, Saint Raphael Hospital, Milan), showed that eif6 impedes the joining of 40S and 60S subunits, regulated by protein kinase C. Our first paper was on the stage-dependent phosphorylation and relationship with the cytoskeleton during *Xenopus* oogenesis/beginning of development. During prophase I, eif6 is little cytoskeleton-bound and is a single protein of 27kDa. Following maturation induced by progesterone or protein kinase C, a serine-phosphorylated 29kDa appears and is kept throughout development. Similarly, eif6 becomes linked to the cytokeratin-rich embryo cytoskeleton, suggesting that the CK fibres are a reservoir of unphosphorylated eif6-60S to be called into action according to functional changes. The latter result was attained because of Rosa and Martin Wilding's (Centre for Reproduction, Villa del Sole, Naples) striking confocal microscope pictures. Moreover, at that time Nadia De Marco was already working in my group and devoted considerable energy and skill to the success of this manuscript and to all the papers related to eif6.

Our next challenge was to explore the role of eif6 in *Xenopus* embryogenesis. This was an attractive yet difficult field as we knew little about techniques needed for performing RNA injections. Giuseppina Barsacchi and Irma Nardi's groups in Pisa helped us with their usual warmth and kindness in this transitional stage. Carmen cloned *Xenopus* eif6 and localized its mRNA distribution during embryogenesis. Next, Nadia, while acquiring considerable skill in research and ability to programme her work, over-expressed eif6 by injection in one blastomere of a two cell-stage embryo, and found several ab-



Fig. 27. 2007. In my office at the Department of Structural and Functional Biology. From left to right, Francesca Nunziata, Loredana Chierchia, Mariano Bernardo, Luigi Iannone, Carmen, Rosa, Nadia De Marco, Luisa Doveve and Ludovica Zampini.

normalities that were in part described in her PhD thesis. She first studied the ability of *eif6* to act as an anti-apoptotic factor acting upstream of *bcl-2*. That paper is one of the most interesting research papers produced in my laboratory. Stefano Biffo, who had followed and supported our work, was really enthusiastic about it: the understanding of *eif6* in a multicellular organism was a real breakthrough. Stefano's enthusiasm encouraged the two of us to respond to comments made, or criticism levelled, I should say, by reviewers. Finally, the paper was accepted by *Cell Death and Differentiation* with an impact factor higher than 9.0.

The next steps were to investigate the two other phenotypes of the over-expressors, i.e. a delay in eye formation and an oedema linked to pronephros malfunctioning. The first phenotype was remarkably described in a paper by Nadia who showed that *eif6* is necessary for eye formation below threshold

levels. We then addressed the study of igf signalling, because eye formation is strictly depending upon it. In 2006 an important paper by Peter Klein and co-workers showed that kermit/gipc2 binds to igfr and is able to sustain igf/akt signalling towards eye morphogenesis. We found that eif6 interacts with gipc2 as well as with igfr and sustains the signalling through the igf/pi3k/akt pathway. Nadia and Margherita Tussellino, the last PhD student graduated in my lab, are currently working (in collaboration with Luca Tamagnone, University of Turin) on the interesting possibility that semaphorins/plexins are an important part of igf signalling active both in the eye and the pronephros, two organs where eif6 appears to regulate gipc2. The oedema/pronephros phenotype was also studied and is the subject of the last paper we are publishing, which bears the hallmark of Margherita's research skills.



Fig. 28. 2009. Rosa, Nadia and Margherita Tussellino.

Research Article

Phosphorylation of p27^{BBP}/eIF6 and its association with the cytoskeleton are developmentally regulated in *Xenopus* oogenesis

R. Carotenuto^a, N. De Marco^a, S. Biffo^b, M. Wilding^c, M. C. Vaccaro^a, P. C. Marchisio^d, T. Capriglione^a, G. L. Russo^e and C. Campanella^{a,*}

^a Dipartimento di Biologia Strutturale e Funzionale, Università di Napoli Federico II, Napoli (Italy), Fax + 39 081 2535035, e-mail: chiara.campanella@unina.it

^b Dipartimento di Scienze dell'Ambiente e della Vita, Università del Piemonte Orientale, Alessandria (Italy)

^c Centro per la Biologia della Riproduzione, Clinica Villa del Sole, Napoli (Italy)

^d DIBIT e Università Vita-Salute San Raffaele Milano, (Italy)

^e CNR, Istituto Scienze dell'Alimentazione Avellino (Italy)

Received 7 April 2005; received after revision 11 May 2005; accepted 25 May 2005
Online First 30 June 2005

Abstract. p27^{BBP}/eIF6 is an evolutionarily conserved regulator of ribosomal function. It is necessary for 60S biogenesis and impedes improper joining of 40S and 60S subunits, regulated by protein kinase C or Efl1p. No data on p27^{BBP}/eIF6 during early development of Metazoa are available. We studied the distribution, post-translational changes and association with the cytoskeleton of p27^{BBP}/eIF6 during *Xenopus* oogenesis and early development. Results indicate that p27^{BBP}/eIF6 is present throughout oogenesis, partly associated with 60S subunits, partly free and with little cytoskeleton bound. During prophase I, p27^{BBP}/eIF6 is detected as a single band of 27-kDa. Upon maturation induced by progesterone or protein kinase C, a serine-phosphorylated 29 kDa isoform appears and

is kept throughout development to the neurula stage. Confocal microscopy showed that the distribution of p27^{BBP}/eIF6 and its association with the cytoskeleton varies according to oogenesis stages. Briefly, in stage 6 oocytes, p27^{BBP}/eIF6 has a limited dot-like distribution, and does not co-localize with cytokeratin, whereas upon maturation it spreads throughout the cytoplasm. After fertilization, a large fraction coalesces around cytomembranes and a cytochalasin B-sensitive co-localization with cytokeratin occurs. RNase removes p27^{BBP}/eIF6 from the cytokeratin fibres. Developmental data suggest a role of p27^{BBP}/eIF6 in controlling ribosomal availability or regulating cross-talk between ribosomes and the cytoskeleton.

Key words: *Xenopus*; meiosis; oocyte; 60S; p27^{BBP}/eIF6; phosphorylation; cytokeratin.

The protein p27^{BBP}/eIF6 is an evolutionarily conserved factor necessary for 60S biogenesis in yeast and mammals [1–3]. It is partly associated with 60S and nucleolus associated in all cells [1, 4]. p27^{BBP}/eIF6 was recently shown to prevent improper joining of the 40S and 60S subunits for 80S assemblage [5]. This activity is regulated by Efl1p

in yeast [6] and by protein kinase c (PKC) phosphorylation in mammalian cells [5]. Biochemical work has shown that p27^{BBP}/eIF6 can also bind to $\beta 4$ integrin [1, 2]. Although in $\beta 4$ integrin-expressing epithelial cells, p27^{BBP}/eIF6 is present at the hemidesmosomes, its ability to associate with intermediate filaments in the nuclear matrix is independent of $\beta 4$. No data are available for multicellular organisms, in vivo, during their functional and/or developmental changes. Studies on the in vivo localization of

* Corresponding author. R. Carotenuto and N. De Marco contributed equally to the paper

p27^{BBP}/eIF6 in a developing system may help to evaluate its role and the significance of its association with the cytoskeleton (CSK) and/or phosphorylation.

In this paper, p27^{BBP}/eIF6 was studied in *Xenopus laevis* oogenesis and early development. This model, where $\beta 4$ is lacking [7], has a differentiation program in which both the timing of translation and that of CSK organization are known. Moreover, the *Xenopus* oocyte is among the cells with the largest amount of ribosomes. During oocyte meiosis, two major changes governed by PKC activation occur [8, 9]: the first meiotic reactivation with germinal vesicle breakdown (prophase-metaphase I transition), and the second reactivation after fertilization (metaphase II-telophase II transition). In prophase I oocytes, large amounts of ribosomes accumulate and translation is blocked [10–14]. Blocks are removed by progesterone at maturation when translation increases [see ref. 15].

The CSK also changes during oogenesis and development. In the germinal vesicle, cytoskeletal proteins are found among nucleoli [16, 17]. The oocyte membrane and cytoplasm are characterized by a rich actin-based cytoskeleton. Vimentin and cytokeratin are found in bundles at the peripheral cytoplasm and in radii spanning the cytoplasm [see refs. 18, 19]. Following germinal vesicle breakdown at maturation, the phosphorylation cascade disrupts this organization. Later, in fertilized eggs, the cytokeratin assembles back into peripheral fibres, starting from the vegetal half, together with a thin network throughout the blastomere periphery and cytoplasm [8, 9, 20–23].

In this paper, the data indicate that post-translational changes and distribution of p27^{BBP}/eIF6 are regulated during oogenesis and early development. Following treatment with progesterone or with the tumour-promoting agent (TPA), a serine-phosphorylated form of p27^{BBP}/eIF6 was detected, indicating that at the first meiosis resumption, p27^{BBP}/eIF6 acquires a potential role in protein synthesis regulation. The distribution of p27^{BBP}/eIF6 changes concomitantly with the CSK reorganization that follows maturation and fertilization. Accordingly, data show that after fertilization, p27^{BBP}/eIF6 associates with the CSK.

Materials and methods

Animals

Adult *X. laevis* females were obtained from 'Rettili' Varese, Italy. They were kept and utilized at the Department of Structural and Functional Biology, University of Naples, Federico II, according to the guidelines and policies dictated by the University Animal Welfare Office and in agreement with international rules.

Oocytes at various stages of oogenesis were excised from the ovaries of females anaesthetized with MS222 (Sigma St. Louis, M.). The *X. laevis* oocyte growth stages (Dumont) are: st. 1 (50–300 μm); st. 2 (300–450 μm); st. 3

(450–600 μm); st. 4 (600–1000 μm); st. 5 (1000–1200 μm); st. 6 (1200–1300 μm). Previtellogenic oocytes (sts 1–2) have a large centrally-located germinal vesicle. A flat monolayer of follicle cells surrounds the oocyte, projecting thin villi (macrovilli) in the highly folded oocyte surface. Larger oocytes are vitellogenic and acquire polarization of their constituents. Pigment marks the animal hemisphere where the germinal vesicle is located. The oocytes, surrounded by follicle cells and thecae over the vitelline envelope, represent a functional unit, the follicle.

To obtain eggs, *X. laevis* females were injected in the dorsal lymphatic sac with 500 units of Profasi HP (Serono, Rome, Italy) in Amphibian Ringer (111 mM NaCl, 1.3 mM CaCl₂, 2 mM KCl, 0.8 mM MgSO₄, 25 mM Hepes, pH 7.8). Fertilized eggs, embryos at 2–4 blastomeres and at neurula stage (st. 19, Nieuwkoop and Faber) were obtained by standard in vitro insemination methods.

Antibodies

p27^{BBP}/eIF6 immunostaining was revealed with a rabbit polyclonal antiserum previously described [1], or with a mouse monoclonal recognizing an epitope between amino acids 135 and 200. Rabbit antibodies against the ribosomal protein L5 were prepared as in Nadano et al. [24] and utilized at 1:200 (v/v) dilution. Anti-pan-cytokeratin monoclonal antibody (Sigma C2931), cross-reacting with type I cytokeratin (K18) and type II cytokeratins (K8) of *Xenopus* oocytes [see ref. 25] and polyclonal rabbit anti-phosphoserine (Zymed Laboratories, San Francisco, Calif.) were also utilized at 1:200 (v/v) dilution.

For Western blots of maturation markers, polyclonal rabbit antibody against *Xenopus* Mos (anti-XeMos antibody Sc-86; Santa Cruz Biotechnology, Heidelberg, Germany) and anti-phospho-MAP kinase monoclonal antibody (9106S; New England Biolabs, Beverly, Mass.) were both used at 1:1000 (v/v) dilution.

Sample preparation for SDS-PAGE and Western blot

Oocytes and embryos (neurula stage) were homogenized in a HEPES buffer pH 7.5 containing 900 mM glycerol, 0.02 mM Na₃N, 1 mM ATP, 1 mM DTT, 5mM EGTA (buffer I) and the following protease inhibitors (Sigma): 2 mM TAME, 5 mg/ml SBTI, 5 $\mu\text{g}/\text{ml}$ aprotinin and 10 μM E64. Unfertilized and fertilized (about 1 h after insemination) eggs were similarly homogenized following removal of the vitelline envelope and the jelly coats. For Maturation Promoting Factor (MPF) activity assays, oocytes were homogenized in buffer I without ATP and containing phosphatase inhibitors (2 mM NAF, 50 mM β -glycerol-phosphate, 1 mM sodium vanadate), in addition to a cocktail of protease inhibitors. After centrifugation at 15,000 g for 40 min at 4 °C, protein concentration was determined in the supernatants with the BCA protein assay reagent (Pierce, Rockford, Ill.). After boiling in sample buffer with β -mercaptoethanol, aliquots of 30–60 μg of

proteins were analysed through SDS PAGE (10, 12 or 15% polyacrylamide), utilizing molecular mass standards (200, 116, 97, 45, 31, 21 or 14 kDa) (Bio-Rad, Hercules, Calif.). Oocytes for anti-p27^{BBP}/eIF6 and anti-XeMos/anti-p42/44MAP kinase Western blots were separated on 4–12% NuPage precast gradient gels (Invitrogen, Life Technologies, Carlsbad, Calif.), using Invitrogen SeeBlue plus 2 pre-stained Mr standards (188, 98, 62, 38, 28, 17, 14, 6 or 3 kDa). Proteins were detected by Coomassie staining. Western blotting on nitrocellulose membrane was performed as previously reported [26], using alkaline phosphatase (AP)-conjugated antibodies. Blotting was also performed on Millipore Immobilon-P transfer membrane (Millipore, Bedford, Mass.), utilizing Protein A-peroxidase-linked and chemiluminescence (ECL) Western Blotting Detection Reagent (Amersham Biosciences, Little Chalfont, UK). In some experiments, the same Immobilon-P membrane was used again after exposure to Restore Western Blot Stripping Buffer (Pierce). For Mos and MAP kinase detection, the membranes were incubated with anti-XeMos or with anti-phospho-MAP kinase antibodies, followed by incubation with anti-rabbit or anti-mouse horseradish peroxidase-conjugated IgGs, respectively (Amersham Biosciences).

In vitro maturation Cdc2 and MAP kinase assays

To induce maturation, stage 6 oocytes were excised from the ovaries and de-theated in low-strength saline Steinberg's solution (58 mM NaCl, 0.67 mM KCl, 0.3 mM Ca(NO₃)₂, 0.8 mM MgSO₄, 4.6 mM Tris-HCl pH 7.4). Aliquots of 50 oocytes were incubated for 10–60 min in 32 μM progesterone in OR2 (82.5 mM NaCl, 2.5 mM KCl, 1 mM CaCl₂, 1 mM Na₂HPO₄, 1 mM MgCl₂, 5 mM Hepes, 3.8 mM NaOH, pH 7.4). Similarly, about 50 oocytes were exposed to 150 nM TPA (Sigma) in Ringer (TPA stock solution in DMSO) up to 6 h. As controls, 50 oocytes were incubated in OR2 or in 0.3 M DMSO in Ringer. About 95% of oocytes matured following progesterone treatment, and 78% of oocytes as a result of TPA exposure. Oocytes were also sampled at increasing times following progesterone treatment (0 h; 2 h; 3.5 h; 6 h; 16 h), white spot occurring about 6 h after hormone exposure. Disappearance of the germinal vesicle was also checked by dissecting the oocytes before homogenization. Moreover, previous experimentation showed that about 14 h following 'white-spot' appearance the oocytes are at M-II stage [27]. For staging the progesterone-induced signalling cascade, MPF kinase and MAP kinase activities were assayed. Here some informations about Cdc2 kinase (the catalytic subunit of MPF), *mos* RNA, Mos kinase. Cdc2 kinase, peaks in metaphase I (M-I) and metaphase II (M-II). Translation of maternal *mos* RNA begins shortly after progesterone addition and is maximal in the mature oocyte. Mos kinase starts a phosphorylation cascade leading to the activation of MAP kinase [see ref.

28]. MPF kinase activity was determined by measuring the enzymatic activity of Cdc2 [see ref. 29]. The radioactivity incorporated in the peptide substrate was determined using phosphocellulose paper (Whatman P81). MAP kinase (p42/44MAP kinase; Amersham Biosciences kit RPN84) was assayed following the manufacturer's instructions with some modifications. Briefly, 5 μl of cell lysate (corresponding to 20 μg of total proteins) were added to a reaction mixture containing 10 μl of substrate buffer and 15 μl of [³²P]ATP (50 μM; 5,000 cpm/pmol). The reaction was incubated for 60 min at 30°C, and the amount of phosphorylated peptide was determined as for the Cdc2 kinase assay.

Cytochalasin treatment

Two-cell embryos were exposed to 20 or 50 μM cytochalasin B for 90 min and processed for confocal microscopy parallel to control embryos. Early studies showed that tritiated cytochalasin B does not penetrate into the *Xenopus* egg before first cleavage and cytochalasin B enters the eggs through the unpigmented surface area in the furrow [see ref. 30]. Exposure to the drug was preferred to injection into the egg as it allows an even distribution of the drug in the cell.

Immunoprecipitation

Samples were homogenized in buffer I with the addition of 100 mM NaF and a protease inhibitor cocktail (Sigma P8340), prior to centrifugation at 15,000 g for 45 min. Alternatively, 20 mM Tris-HCl 7.5, 20 mM NaCl, 0.1% NP-40, 10% glycerol and protease inhibitors (buffer II) were used as homogenization buffer. The A431 cell line was used as positive control. Undiluted polyclonal anti-p27^{BBP}/eIF6 or preimmune serum was exposed to supernatants (1:75 v/v) for 1 h under constant agitation. Protein A-Sepharose Cl4B (Pharmacia Biotech) was added to the sample (1:3 v/v) and kept under agitation for 30 min. Following several rinses in buffer I, the recovered precipitates were boiled in sample buffer under reducing conditions.

Phosphatase treatment

Eggs were homogenized in buffer II with the addition of 100 mM phosphatase inhibitor NaF (Sigma P8340), prior to centrifugation. Supernatants containing 600 μg of proteins were immunoprecipitated with polyclonal anti-p27^{BBP}/eIF6 or preimmune serum, for 1 h under constant agitation and exposed to Protein A-Sepharose Cl4B as indicated above. Following several rinses in buffer II, without NaF, the recovered precipitates were suspended in phosphatase buffer (10 mM Tris-HCl, pH 8.5 at 37°C, 10 mM MgCl₂) and treated with 4 U of calf intestinal alkaline phosphatase (New England Biolabs) for 30 min, at room temperature. After treatment and rinsing, beads were resuspended in sample buffer before electrophoresis.

Sucrose gradients

Sucrose gradients were performed according to Ceci et al. [5], modified by a short centrifugation to avoid yolk interference as in Cardinali et al. [31].

Confocal microscopy

Small clusters of previtellogenic oocytes were fixed in 2–4% paraformaldehyde in PBS and extracted in a Hapes buffer containing glycol hexylene [20]. Fully grown oocytes, eggs, fertilized eggs and two-cell embryos were similarly fixed in paraformaldehyde in PBS, omitting the extraction step, according to Gard et al. [18]. The samples were bisected along the equator to separate animal and vegetal halves for the optimization of antibody penetration. All the samples were incubated in anti-p27^{BBP}/eIF6 or in anti-pan-cytokeratin, using rabbit IgG as controls for the purified antibody and PBS for monoclonal antibody. The secondary antibodies were BODIPY FL-conjugated

anti-rabbit goat IgG for anti-p27^{BBP}/eIF6 and Texas Red-conjugated anti-mouse goat antibodies for anti-pan-cytokeratin. For double localization, the samples were incubated with anti-p27^{BBP}/eIF6 and anti-pan-cytokeratin followed by exposure to both secondary antibodies. Some samples of fertilized eggs were exposed for 30 min after methanol fixation to 10 or 20 U of RNase from bovine pancreas (Roche, Mannheim, Germany) in 1× SSC.

An Olympus Fluoview (Olympus, Segrate, Italy) confocal microscope, based on an Olympus IX-70 inverted microscope, was used for all experiments. A Kr/Ar laser was used to produce the excitation laser lines at 488 and 568 nm. Fluorescence emission wavelengths were separated by a 530-nm dichroic mirror followed by passage through a 510- to 550-nm bandpass filter (green fluorescence emission) or a 585-nm longpass filter (red fluorescence emission). Images were then collected in a photomultiplier. Laser power and photomultiplier settings

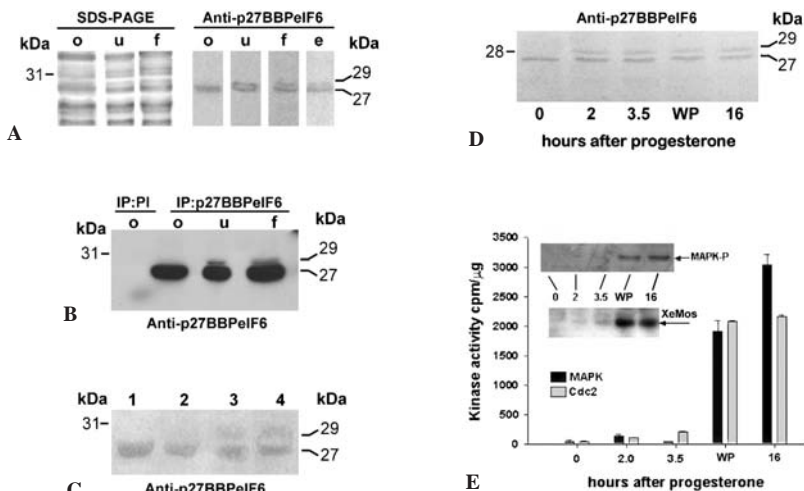


Figure 1. p27^{BBP}/eIF6 distribution in oocytes and in eggs. (A) Left: SDS-PAGE (10% polyacrylamide) of oocytes (o), unfertilized (u) and fertilized (f) egg supernatant. Right: Western blotting with monoclonal anti-p27^{BBP}/eIF6 antibody and AP-conjugated secondary antibodies. A 27-kDa band cross-reacting with the antibody is present in oocytes, unfertilized and fertilized eggs and embryos (neurula) (e). In unfertilized and fertilized eggs and embryos a second band of 29 kDa cross-reacts with the same antibody. (B) Supernatants of oocytes, unfertilized and fertilized eggs immunoprecipitated with anti-p27^{BBP}/eIF6 polyclonal antibodies. The immunoprecipitates were run on 10% polyacrylamide gels, blotted, incubated with the same antibodies and revealed by Protein A-peroxidase-ECL. As control, oocyte supernatant was immunoprecipitated with pre-immune serum (PI). While in the control oocytes, no band was detected, the 27-kDa band was found in the three samples immunoprecipitated by anti-p27^{BBP}/eIF6, and the 29-kDa band was found in the u and f eggs. (C) St. 6 oocytes treated with TPA or progesterone and utilized for SDS-PAGE (15% polyacrylamide) and Western blot with anti-p27^{BBP}/eIF6 and secondary AP-conjugated antibodies. The original gels used for this Western blot were charged with 60 mg for each well and over-run to improve band separation. Lane 1, untreated oocytes; lane 2, TPA exposed oocytes and (lane 3) related control; lane 4, progesterone-exposed oocytes. The 29-kDa band appears in both progesterone- and TPA-exposed oocytes. (D) Western blot of a gel loaded with equal protein amounts of oocytes collected at times 0, 2, 3.5, the white-spot stage (WP) and 16 h following progesterone treatment (M-II). The 29-kDa protein was immunodetected 2 h following progesterone exposure. (E) Markers of oocyte maturation. The same oocyte samples used for the experiments in D were utilized in these assays. At the indicated times after progesterone induction, oocytes were lysed and 20 mg of supernatants assayed to measure Cdc2 and MAP kinase activities (graph). WP, white spot. Alternatively, 40 mg of the same samples was separated on SDS-PAGE, blotted to nitrocellulose and probed with anti-*Xenopus* Mos (XeMos) or anti-phospho-MAP kinase (MAPK-P). Immunoreactivity was detected by ECL plus.

were kept constant for all experiments. Experiments were standardized by using sections spaced at 1- μ m intervals using a $\times 60/1.25$ NA UPlanFl fluorescence objective (Olympus). Images were processed by the confocal software and Adobe Photoshop.

Analysis of confocal images

Confocal images were analyzed to examine the extent of p27^{BBP}/eIF6 along cytokeratin fibres or in the whole cytoplasm. The analysis was performed using the confocal software. Graphs of localization on cytokeratin filaments were analysed by recording green fluorescence along a fibre of cytokeratin traced by the confocal software. Because cytokeratin fibres were of variable lengths, diverse traces were accumulated to form a total of 50 μ m of cytokeratin fibre length. Areas of p27^{BBP}/eIF6 were defined as peaks of green fluorescence greater than 2000 fluorescence units (background fluorescence averaged 500 fluorescence units). For each analysis (a minimum of three samples), ten single confocal sections were superimposed to provide the images used in the analysis. Peaks of p27^{BBP}/eIF6 fluorescence were again recorded over 2000 fluorescence units in an area of interest of the egg cytoplasm, defined by the confocal software analysis program. Here, single confocal slices were used to measure the number of peaks. Where indicated, peripheral areas immediately under the egg plasma membrane were measured and internal areas were measured 40 μ m from the plasma membrane, as visualized by the confocal section.

Results

p27^{BBP}/eIF6 protein is in the oocytes and is modified after progesterone or TPA-induced oocyte maturation

Supernatants of previtellogenic and vitellogenic oocytes (meiotic prophase I), unfertilized eggs (meiotic metaphase II), early zygotes (meiotic telophase II-first cleavage cycle) displayed a band of approximately 27 kDa by SDS-PAGE and Western blotting, using either monoclonal or polyclonal anti-p27^{BBP}/eIF6 antibodies and AP-conjugated secondary antibodies. In unfertilized and fertilized eggs, a second band of about 29 kDa cross-reacted with the same antibodies. The two bands were maintained throughout development to the neurula stage (fig. 1A). Similar results, i.e. the presence of a 27-kDa band and a 29-kDa band, were obtained by immunoprecipitation of total extract of unfertilized eggs and fertilized eggs with anti-p27^{BBP}/eIF6 (fig. 1B). These samples were ECL-developed. We noted that during immunoprecipitation, the 29-kDa band was less efficiently recovered, suggesting differential localization leading to antigenic masking. We hypothesized that the 29-kDa band is a developmentally regulated post-translational modification of p27^{BBP}/eIF6.

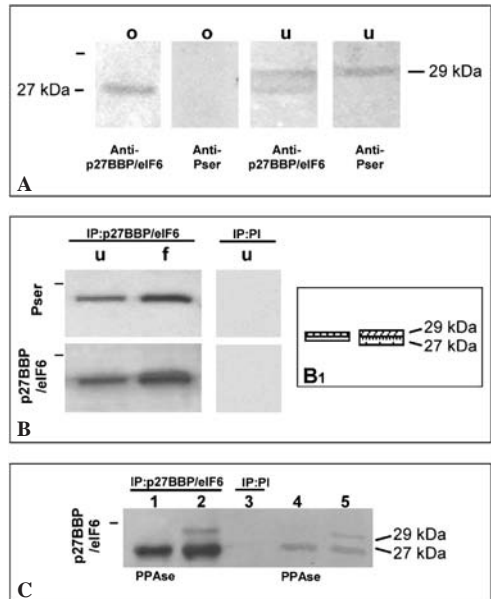


Figure 2. (A) Western blot of oocytes (o) and unfertilized eggs (u) exposed to anti-phosphoserine (anti-Pser) or to anti-p27^{BBP}/eIF6, as indicated, and revealed by AP-conjugated secondary antibodies. In the unfertilized eggs, the 29-kDa band cross-reacts with anti-p27^{BBP}/eIF6 and anti-phosphoserine. B. Western blot of unfertilized (u) and fertilized (f) egg supernatants immunoprecipitated with anti-p27^{BBP}/eIF6 or with preimmune serum. The blot was first incubated with anti-phosphoserine and revealed by protein A-peroxidase-ECL. The same blot, after stripping, was incubated with p27^{BBP}/eIF6 and similarly revealed, showing that the upper part of the band of u and f cross-reacts with anti-phosphoserine, as reconstructed in B1. In B, pre-immune serum-precipitated (PI) unfertilized eggs are also shown as negative control. (C) Western blots of unfertilized egg supernatants immunoprecipitated with anti-p27^{BBP}/eIF6 or with preimmune serum. Following immunoprecipitation, some samples were treated with calf intestinal alkaline phosphatase (PPase). The blotted 15% gel was run over the front line to improve resolution of the 29-kDa protein. The blots were incubated with anti-p27^{BBP}/eIF6 and revealed by protein A-peroxidase-ECL. Lane 1, immunoprecipitate treated with PPase; lane 2, untreated immunoprecipitate; lane 3, Preimmune serum-precipitated sample; lane 4, total lysate treated with PPase; lane 5, untreated total lysate. The small bar on the left panels indicates the 31-kDa Mr standard.

In vitro maturation of st. 6 oocytes was induced by progesterone or TPA (PKC agonist) treatment [32]. Mature oocytes extracted and probed with a monoclonal p27^{BBP}/eIF6 antibody (fig. 1C) showed the 29-kDa band in progesterone- and TPA-stimulated but not in untreated oocytes. To determine at what stage the 29-kDa band appears along the progesterone-induced pathway, hormone-exposed samples were monitored until several hours after 'white-spot' appearance, run in SDS-PAGE and analysed for p27^{BBP}/eIF6 (fig. 1D). Data indicated that the 29-kDa

band was visible already 2 h following progesterone exposure. In aliquots of the same oocyte samples, Mos and MAPK onset, as well as MAPK and Cdc2 activities were determined (fig. 1E). A comparison of figures 1D and 1E shows that the 29-kDa band was found when the maturation markers started to appear and MAPK and Cdc2 activities were at an initial stage, suggesting that p27^{BBP}/eIF6 undergoes a post-translational change during oocyte maturation.

The 29-kDa band cross-reacts with anti-phosphoserine and disappears following phosphatase treatment

Western blotting showed that the 29-kDa band cross-reacted with anti-phosphoserine (fig. 2A) but not with anti-phosphothreonine (data not shown). We immunoprecipitated p27^{BBP}/eIF6 and probed it for phosphoserine. Data showed that the 29-kDa band immunoprecipitated by anti-p27^{BBP}/eIF6 was recognized by phosphoserine antibodies (fig. 2B). Furthermore, the 29-kDa band was not recovered by immunoprecipitation with anti-p27^{BBP}/eIF6, if extracts were previously incubated with phosphatase (fig. 2C). Thus, data suggest that p27^{BBP}/eIF6 is phosphorylated by a PKC pathway during oocyte maturation.

Protein localization varies according to meiotic stage

In toto confocal microscopy of oocytes showed immunostaining both in the whole nucleoplasm and in strings surrounding the nucleoli (fig. 3a, b). In previtellogenic oocytes, the immunostaining was evenly distributed (fig. 3a). In vitellogenic oocytes, anti-p27^{BBP}/eIF6 immunostaining was clearly present in follicle cells, in the macrovilli of the follicle cells and at the oocyte periphery both in the animal and vegetal hemispheres (fig. 3c, d). However, at the final stages of oocyte growth, this protein acquired a rather polarized distribution, like other molecules and organelles [see ref. 18, 33]. In the animal half, small dots of the immunostain were concentrated at the oocyte surface and in a peripheral layer of 15–20 µm, while sparsely distributed in the cytoplasm bulk (fig. 3c, d). In the vegetal hemisphere, p27^{BBP}/eIF6 distribution in the peripheral layer was not evident and the immunofluorescent dots were even less abundant (fig. 3e).

In unfertilized eggs, the immunostain was spread across the cytoplasm from the periphery to the bulk of the cytoplasm in the animal half (fig. 3g, h). Immunofluorescent dots were detected in the vegetal half and surrounded the numerous yolk platelets appearing as pearl strings (arrow in fig. 3i). One hour after fertilization, abundant immunofluorescent dots were found in the animal half. Some of them were concentrated in a fluorescent shell around cytoplasmic organelles, such as yolk platelets (fig. 3k, l). In the vegetal half, the fluorescence pattern was similar, although dots were sparsely present in the cytoplasm (fig. 3m, n). The immunostaining was specific (fig. 3f, j).

p27^{BBP}/eIF6 binds 60S subunits, partially overlaps with cytokeratin and is functionally linked to the CSK

In mammalian cells, p27^{BBP}/eIF6 is associated with the CSK. In addition, in yeasts and mammals, it is partially linked to 60S ribosomal subunits [1, 2, 5]. In *Xenopus*, immunoprecipitation of p27^{BBP}/eIF6 leads to co-precipitation of ribosomal protein L5 (fig. 4a), suggesting that, at least part of p27^{BBP}/eIF6 is bound to 60S subunits. Similarly, in ribosome profiles, p27^{BBP}/eIF6 sedimented with the ribosomes, peaking at 60S–80S, was absent on polysomes and was present in the soluble phase (fig. 4b). Since this analysis excludes cytoskeletal bound p27^{BBP}/eIF6, we conclude that p27^{BBP}/eIF6 is present on 60S, absent from polysomes (as in yeasts and mammals), but also present in other compartments (soluble and insoluble).

To gain information about the CSK association of p27^{BBP}/eIF6, which eludes ribosomal analysis, samples were incubated with anti-cytokeratin and anti-p27^{BBP}/eIF6 antibodies and observed by confocal microscopy. In st. 6 oocytes, some overlap of fluorochromes was recorded in the follicle cells and oocyte membranes and in the surrounding thecae. Furthermore, anti-p27^{BBP}/eIF6-stained dots were found mostly in the peripheral cytoskeletal network delimited by bundles cross-reactive with anti-cytokeratin antibodies (fig. 5a). Figure 5b is a control section where staining is absent. In unfertilized eggs, practically no overlap was observed of the two antibodies (fig. 5c). In the animal halves of fertilized eggs, cytokeratin was organized in short bundles immersed in the cytoplasm. Figure 5d indicates contiguity or overlap between cytokeratin and p27^{BBP}/eIF6, particularly around the yolk platelets. In corresponding vegetal halves (fig. 5e, f), the thick bundles of cytokeratin were spread across the zygote periphery and co-localized with p27^{BBP}/eIF6. The protein was spot-like and decorated the cytokeratin bundles, acquiring a yellow fluorescence (BODIPY FL and Texas Red fluorescence), in contrast to the green fluorescence (BODIPY FL-labelling) of p27^{BBP}/eIF6 dispersed in the cytoplasm (fig. 5f). A frequency trace of the p27^{BBP}/eIF6 localization on cytokeratin fibres in oocytes and fertilized eggs is shown in figure 5i (I, II, III). In samples treated with 20 U RNase (fig. 5g, h), sites of co-localization appeared to be sparser than in the untreated eggs. Indeed, comparison of the frequency trace of RNase-treated fertilized eggs versus the trace of corresponding untreated samples strongly suggests that the sites of co-localization decreased following RNase treatment (compare fig. 5i IV, with 5i II and III). In this sense, p27^{BBP}/eIF6 fluorescence peaks were higher in control images than in RNase-treated samples, with no distinction between the peripheral and the internal cytoplasm (table 1).

In cleaving embryos, cytokeratin and p27^{BBP}/eIF6 were mixed in the cytoplasm and appeared to colocalize in particular at the blastomere periphery (fig. 6a). In embryos exposed to cytochalasin B at the two-cell stage, we found

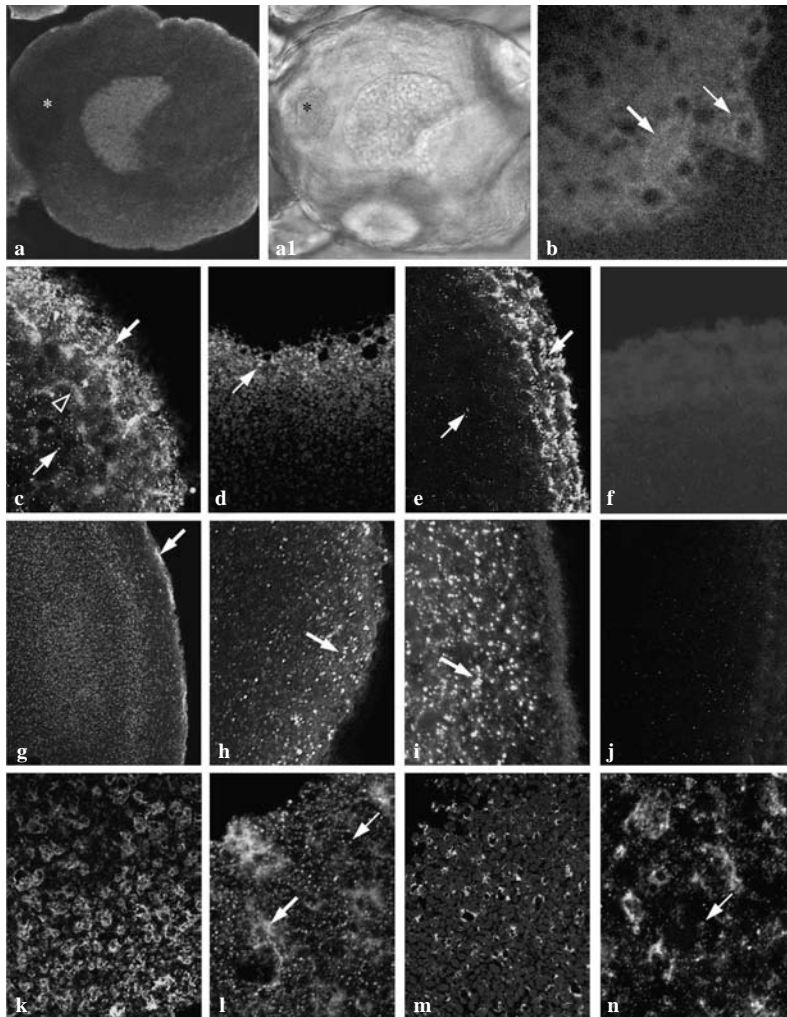


Figure 3. Confocal immunolocalization of p27^{BBP}/eIF6 in oocytes and unfertilized and fertilized eggs with BODIPY-conjugated secondary antibodies. Each image was elaborated using three optical sections 1- μ m thick. Stage 2 oocyte showing a general cross-reactivity to the antibody in the germinal vesicle (a) that is evident in thin chains (b, large arrow) that surround nucleoli (small arrow). The mitochondrial cloud is indicated with an asterisk (a) and in the corresponding phase contrast image (al): it is not immunoreactive. a, al, \times 230; b \times 1000. (c) Tangential view of the animal hemisphere of a st. 5 oocyte. The large arrow points to the theca and follicle cells whose boundaries are immunoreactive. The arrowhead indicates the articulated peripheries of the oocyte and the follicle cells that are cross-reactive, similar to the small dots in the peripheral cytoplasm (small arrow); \times 500. (d) Animal half of an oocyte where the somatic cells were removed. The immunoreactive dots (small dots) are present in a layer of 15–20 μ m; \times 500. (e) Vegetal half of the same oocyte shown in c, where the large arrow points to the somatic tissue and the small arrow to the sparse immunoreactive dots in the peripheral cytoplasm; \times 500. (f) Control image of the vegetal half of the oocyte where no staining is present; \times 500. (g) Optical section of the animal hemisphere taken at the equator of an unfertilized egg. The immunofluorescence is relevant at the egg periphery (large arrow) and is also widespread in the rest of the cytoplasm; \times 70. (h) The animal half periphery shows a high concentration of immunoreactive dots that may fuse together (large arrow); \times 850. (i) Vegetal half of the same egg as in h, showing that the immunoreactive dots form a string of pearls around organelles such as yolk platelets (large arrow); \times 850. (j) Control image of an egg animal half; the immunostain is absent; \times 850. (k) Tangential view of the animal hemisphere of a fertilized egg, showing an immunoreactive rim around cytoplasmic organelles, \times 300. At a higher magnification (l) (\times 1000) in addition to the fluorescence around the organelles (large arrow), immunoreactive dots are abundantly present (small arrow). (m, n) Corresponding views of the vegetal side of the fertilized egg where the immunoreactive dots (small arrow) are less concentrated than in the animal half (compare l with n). m \times 300, n, \times 1000.

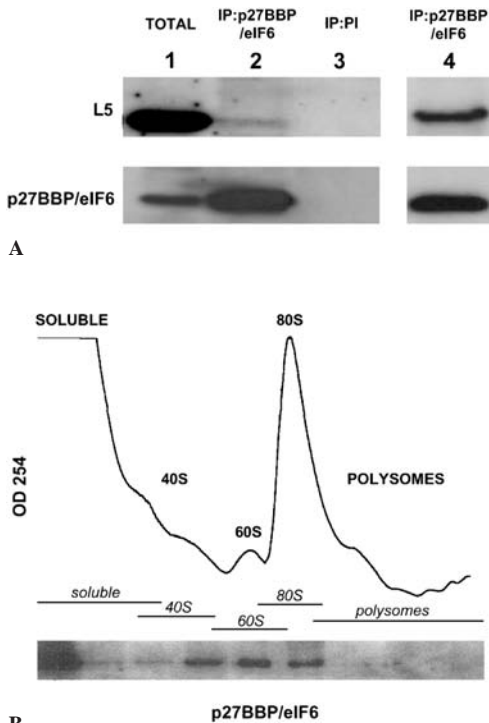


Figure 4. p27^{BBP}/eIF6 association with ribosomes. (A) Oocyte supernatant immunoprecipitated with anti-p27^{BBP}/eIF6, blotted and incubated with anti-L5 or anti-p27^{BBP}/eIF6, as indicated. The blots were ECL-revealed. 1, stage 4–6 oocytes total supernatant; 2, anti-p27^{BBP}/eIF6-immunoprecipitated oocyte supernatant; 3, oocyte supernatant immunoprecipitated with preimmune serum; 4, anti-p27^{BBP}/eIF6-immunoprecipitated A431 mammalian cells, as positive control. On the anti-p27^{BBP}/eIF6-immunoprecipitated supernatant of oocytes (2), a band immunoreactive with anti-L5 is detectable. (B) Sucrose gradient analysis. Fractions from unfertilized eggs were separated on 15–50% sucrose gradients. Gradient fractions were collected while the optical density profile at 254 nm was monitored (upper panel). Aliquots of each fraction were used for immunoblotting with anti-p27^{BBP}/eIF6 (lower panel).

Table 1. Distribution of p27^{BBP}/eIF6 after RNase treatment of fertilized eggs.

| | No RNase | RNase | <i>p</i> |
|-----------|-------------------------|-------------------------|----------|
| Periphery | 0.77 ± 0.12 (n = 60) | 0.4 ± 0.02 (n = 60) | <0.001 |
| Internal | 0.39 ± 0.01 (n = 60) | 0.23 ± 0.04 (n = 60) | <0.001 |

Values represent the mean ± SD of peaks of green fluorescence per 100 μm² of cytoplasm. Data were collected using ten analyses of at least three separate experiments. Internal regions are 40 μm inside the egg cytoplasm.

that, as expected, the cleaving furrows had disappeared (fig. 6b). Here, the cytokeratin localization was strongly affected, being located mostly at the embryo periphery. p27^{BBP}/eIF6 followed this distribution (fig. 6b). In an optical section taken from the equator, in the animal half, the finely intermingled co-localization of both proteins at the cell periphery could be observed (fig. 6c). Figure 6d is a control sample where the immunostain is absent.

Taken together, the data indicate that p27^{BBP}/eIF6 associates with the CSK according to the developmental stage. In addition, association with the CSK is impaired by RNase treatment (see Discussion).

Discussion

We studied p27^{BBP}/eIF6 localization and post-translational modifications during oogenesis and early embryonic stages in *X. laevis*. Three properties have been described in the past for p27^{BBP}/eIF6: association with 60S and ribosomes in yeasts and mammals [4, 2]; PKC-dependent modifications coincident with translation in human cancer [5]; association with intermediate filaments in mammalian cells [1, 34]. We observed that these properties are also present in *Xenopus*. However, our data, the first in an in vivo multicellular and developing system, suggest that these properties are developmentally regulated.

The association of p27^{BBP}/eIF6 with ribosomes has been observed in yeasts and mammals. Here we confirm findings from these systems. Importantly, we observe that p27^{BBP}/eIF6 is excluded from polysomes in line with the notion that p27^{BBP}/eIF6 must be released from 60S to start translation [see ref. 5]. Additionally, we noted that, unlike yeasts, the amount of p27^{BBP}/eIF6 not bound to ribosomes is higher [see ref. 5]. This observation suggests that during evolution, p27^{BBP}/eIF6 may have acquired novel functions. We observe for the first time in vivo a developmental change of p27^{BBP}/eIF6 electrophoretic mobility. In vitro maturation experiments coupled with Western blotting showed that, upon oocyte stimulation by progesterone, a major post-translation change of p27^{BBP}/eIF6 takes place, i.e. a higher-Mr band of 29 kDa appears, as a result of its de novo serine phosphorylation. The 29-kDa band is also observed in developing embryos, indicating that it is produced as well by the zygotic genome. One interesting possibility is that the kinase involved is PKC as shown in mammalian cells [5] and this may have a major functional role in oocyte maturation. In *Xenopus* oocytes, progesterone is known to act synergistically to [35] or via [9] PKC. In this work, the 29-kDa protein appears before the ‘white-spot’ stage, suggesting that during oogenesis, p27^{BBP}/eIF6 phosphorylation occurs at the onset of the major Mos/MPF activation events. No direct evidence is yet available that the observed phosphorylation in serine is caused by PKC. However, the fact that the 29-kDa pro-

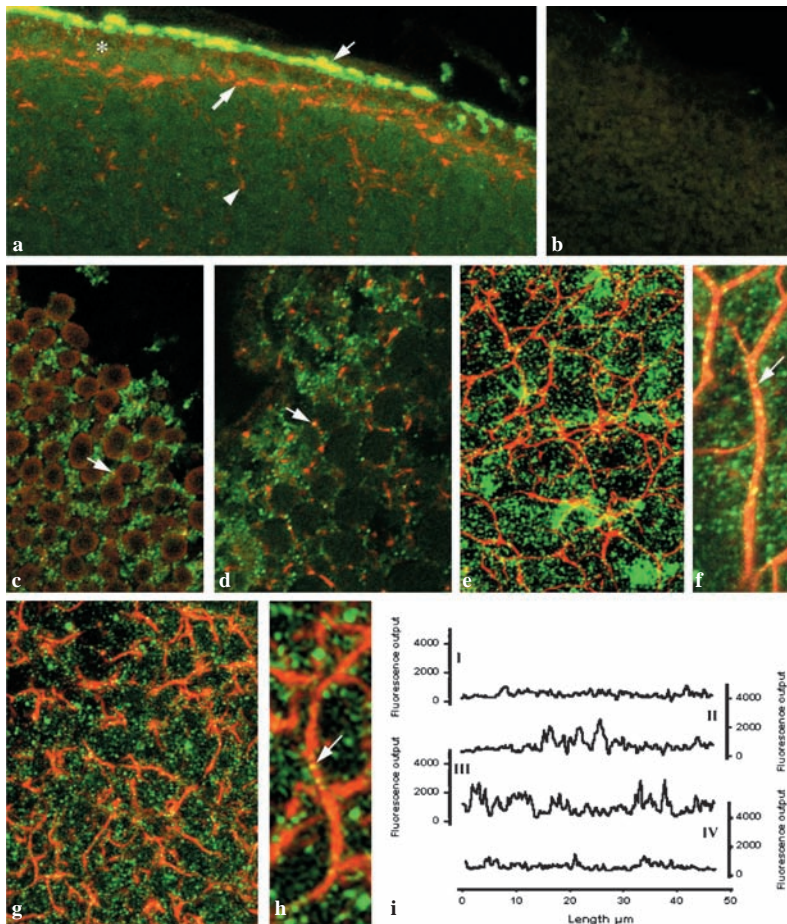


Figure 5. Confocal immunoco-localization of p27^{BBP}/eIF6 and cytokeratin in st. 6 oocytes and unfertilized and fertilized eggs. The secondary antibodies were BODIPY-conjugated anti-rabbit goat IgG for anti-p27^{BBP}/eIF6 and Texas Red-conjugated anti-mouse goat antibodies for anti-pan cytokeratin. Images were elaborated as indicated in figure 4. (a) Animal half of a st. 6 oocyte. Note a co-localization of both antibodies in the somatic tissue (small arrow). Anti-p27^{BBP}/eIF6-stained dots (asterisk) are embedded in the peripheral network of the CSK delimited by anti-cytokeratin antibody-stained fibres (large arrow). The arrowhead shows the 'radii' of the CSK where no co-localization was found with anti-p27^{BBP}/eIF6 antibodies. $\times 350$ (b) Control st. 6 oocyte, incubated with pre-immune serum. The staining is absent. $\times 350$. (c) Animal half of an unfertilized egg, at the equator. The cytoplasmic organelles are surrounded by an anti-cytokeratin cross-reacting ring (in red), where little or no co-localization (in yellow) with anti-p27^{BBP}/eIF6 (in green) is present (small arrow). $\times 1000$. (d) Animal half of a fertilized egg, at the equator. Cytokeratin surrounds the organelles as short bundles where some co-localization (in yellow) of the two antibodies occurs (arrow). $\times 1200$. (e) Vegetal half of a fertilized egg. The optical section shows the conspicuous peripheral cytoskeletal network that forms in this region following fertilization. $\times 1100$. (f) Higher magnification of the vegetal half of a fertilized egg. A dot-like localization of p27^{BBP}/eIF6 is spread throughout the cytoplasm, on the cytokeratin-containing fibres (arrow) and on the thinner CSK network branching from the large one. $\times 1700$. (g) Vegetal half of a fertilized egg, treated with 20 U RNase. $\times 1100$. (h) Detail of the sample shown in g. Little co-localization of p27^{BBP}/eIF6 and cytokeratin is seen (arrow). $\times 1700$. (a-h) Each figure was elaborated using 15 optical sections. (i) Graphs are a representative example of the confocal green fluorescence (p27^{BBP}/eIF6) output measured by following a trace of cytokeratin fibres (red fluorescence). The top trace (I) shows the periphery of the animal half of the oocyte, the central trace (II) is the periphery of the animal half of the fertilized egg and the lower trace (III) is the periphery of the vegetal half of the fertilized egg. IV is a trace of green fluorescence along a cytokeratin fiber after treatment of fertilized eggs (vegetal half) with 20 U RNase. The trace is recorded in an area 40 μm from the periphery of the egg. All traces are measured along a total of 50 μm cytokeratin fibres.

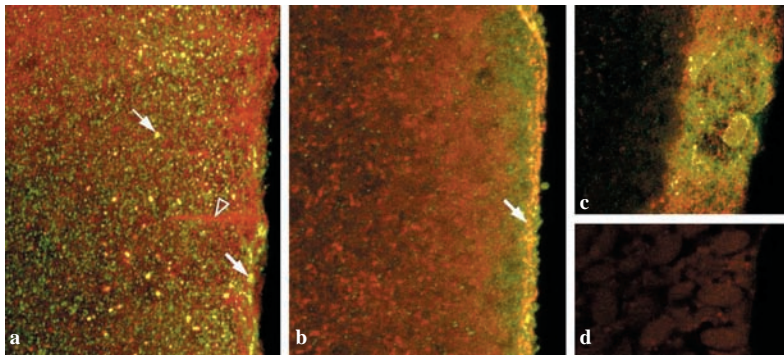


Figure 6. Confocal immunocolocalization of p27^{BBP}/eIF6 and cytokeratin in cytochalasin B-treated embryos. The secondary antibodies were the same as indicated for figure 5. Images were elaborated as indicated in figures. 3 and 5. (a) Untreated cleaving embryo, animal side, at the equator. Cytokeratin and p27^{BBP}/eIF6 appear to co-localize both at the blastomere membranes (large arrow) and in the cytoplasmic dots (small arrow). Arrowhead cleavage furrow. $\times 900$; (b) Cognate embryo where cleavage could not occur as a consequence of cytochalasin B exposure. The optical section was taken at the embryo equator. Most p27^{BBP}/eIF6 is at the membrane, where co-localization with cytokeratin is evident (arrow). $\times 760$. (c) Detail of the co-localization of cytokeratin and p27^{BBP}/eIF6 in a tangential view of a cytochalasin B-treated embryo. $\times 900$. (d) Control sample of cleaving embryo. The immunostain is absent. $\times 900$.

tein is produced in the oocyte by TPA treatment argues in favour of this hypothesis. Furthermore, in *Xenopus*, two potential PKC phosphorylation sites in Ser were found in p27^{BBP}/eIF6 cDNA [M. C. Vaccaro et al., unpublished data]. In vitro and in cancer cells, PKC-mediated phosphorylation of p27^{BBP}/eIF6 is part of the major biological role of p27^{BBP}/eIF6 in mammals. In fact, PKC-mediated phosphorylation of p27^{BBP}/eIF6 results in its release from 60S and translation [5]. Data in this paper suggest the first example where phosphorylation of p27^{BBP}/eIF6 is functional to the regulation of translation along a developmental pathway. Indeed, p27^{BBP}/eIF6 phosphorylation of *X. laevis* oocytes occurs following removal of the meiotic translation block at maturation, a time when the regulation of protein synthesis is orchestrated by new mechanisms [36]. Accordingly, we found a higher concentration of immunofluorescent dots, in the animal half compared to the vegetal half after fertilization, and the activity in protein synthesis of the animal half is higher than in the vegetal half of *Xenopus* fertilized eggs [37]. Moreover, the coalesced configuration of p27^{BBP}/eIF6 around cytoplasmic organelles and its co-localization with the CSK occur after maturation, when the phosphorylated and the unphosphorylated forms of p27^{BBP}/eIF6 are both present throughout the cytoplasm and the cytoskeleton is sharply rearranged [see ref. 20]. In contrast, in the oocyte at prophase arrest, when only the unphosphorylated form is found, confocal microscopy showed that p27^{BBP}/eIF6 colocalizes with the CSK in the follicle cells but not with the oocyte cytoplasmic CSK [see ref. 18]. Indeed, in the animal half, p27^{BBP}/eIF6 is segregated in a layer, intermingled but not co-localizing with a cytoskeletal network located therein [18, 19].

In yeast, phosphorylation in serine of Tif6p, the homologue of p27^{BBP}/eIF6, by casein kinase 1 was found to regulate p27^{BBP}/eIF6 nucleocytoplasmic distribution [38], suggesting that this event may be similarly involved in regulating protein distribution in *Xenopus* oocytes. This event being mediated by casein kinase 1, it is unlikely to reflect the PKC-stimulated appearance of the 29-kDa band, although further studies would be required to reach a definitive conclusion.

The p27^{BBP}/eIF6 co-localization with the CSK filament network is, strikingly, developmentally regulated. It occurs in fertilized eggs over spots aligned along the bundle axis, while dots reactive uniquely with anti-p27^{BBP}/eIF6 are spread throughout the cytoplasm. Cytochalasin B experiments and confocal microscopy suggest a functional association of p27^{BBP}/eIF6 with the CSK. On the other hand, RNase depletion of the anti-p27^{BBP}/eIF6-reacting spots on cytokeratin fibres, as indicated by fluorescence frequency analysis, strongly suggests that some of the p27^{BBP}/eIF6 is linked to RNA bound to those fibres. One should note that, in our experiments, enzymatic treatment is apparently effective in removing p27^{BBP}/eIF6 also from RNase-sensitive sites throughout the cytoplasm. The actual role of p27^{BBP}/eIF6 binding to the CSK is unclear, especially where $\beta 4$ integrin is absent. We propose the following hypothesis. In eukaryotic cells, the majority of mRNAs and polyribosomes have been shown to be associated with the cytoskeleton [reviewed in ref. 39]. In cell-free extracts, 40S and 60S ribosomes bind to intermediate filaments at the N-terminal head domain of cytokeratin [40, 41]. As p27^{BBP}/eIF6 binds to 60S in eukaryotic cells [2], the intriguing possibility exists that p27^{BBP}/eIF6 on cytokeratin filaments observed in this study indicates

sites where p27^{BBP}/eIF6 binds to 60S, forming 60S-p27^{BBP}/eIF6 complexes. If this is correct, then in early embryogenesis, 60S-p27^{BBP}/eIF6 may be stored at the cytoskeleton and made available for use according to cellular needs. Ceci et al. [5] showed that p27^{BBP}/eIF6 binds to the 60S subunits when it is not phosphorylated by PKC. Therefore the cyokeratin-linked RNA-p27^{BBP}/eIF6 complexes may represent a storage of inactive 60S in *Xenopus* eggs. Our next step will be to analyse cyokeratin-p27^{BBP}/eIF6 binding under various experimental conditions.

Acknowledgements. We are grateful to G. Falcone for image processing and to V. Monfrecola for technical assistance. This work was supported by a PRIN grant to C. C., S. B and P. C. M and by an ABCD fellowship to N. D. M. This study was carried out under the auspices of the Italian MIUR Centre of Excellence in Physiopathology of Cell Differentiation (PCM).

- Biffo S., Sanvito F., Costa S., Preve L., Pignatelli R., Spinardi L. et al. (1997) Isolation of a novel $\beta 4$ integrin binding protein (p27^{BBP}) highly expressed in epithelial cells. *J. Biol. Chem.* **272**: 30314–30321
- Sanvito F., Piatti S., Villa A., Bossi M., Lucchini G., Marchisio P. C. et al. (1999). The $\beta 4$ integrin interactor p27^{BBP}/eIF6 is an essential nuclear matrix protein involved in 60s ribosomal subunit assembly. *J. Cell Biol.* **144**: 823–838
- Basu U., Si K., Warner J. R. and Maitra U. (2001) The *Saccharomyces cerevisiae* TIF6 gene encoding translation initiation factor 6 is required for 60S ribosomal subunit biogenesis. *Mol. Cell Biol.* **21**: 1453–1462
- Si K. and Maitra U. (1999). The *Saccharomyces cerevisiae* homologue of mammalian translation initiation factor 6 does not function as a translation initiation factor. *Mol. Cell Biol.* **19**: 1416–1426
- Ceci M., Gaviraghi C., Gorrini C., Marchisio P. C. and Biffo S. (2003). Assembly of 80S ribosomes requires phosphorylation-dependent release of p27^{BBP}/eIF6 from 60S subunits. *Nature* **426**: 580–584
- Senger B., Lafontaine D. L., Graindorge J. S., Gadal O., Camasses A., Sanni A. et al. (2001). The nucleolar Tif6p and Efl1p are required for a late cytoplasmic step of ribosome synthesis. *Mol Cell.* **8**: 1363–1373
- De Simone D. W. and Hynes R. O. (1988). *Xenopus laevis* integrins: structural conservation and evolutionary divergence of integrin beta subunits. *J. Biol. Chem.* **263**: 5333–5340
- Capco D. G., Tutnick J. M. and Bement W. M. (1992). The role of protein kinase C in reorganization of the cortical cytoskeleton during the transition from oocyte to fertilization-competent egg. *J. Exp. Zool.* **264**: 395–405
- Johnson J. and Capco D. G. (1997). Progesterone acts through protein kinase C to remodel the cytoplasm as the amphibian oocyte becomes the fertilization-competent egg. *Mech. Dev.* **67**: 215–226
- Bouvet P. and Wolffe A. P. (1994). A role for transcription and FRGY2 in masking maternal mRNA within *Xenopus* oocytes. *Cell* **77**: 931–941
- Stutz A., Conne B., Huarre J., Gubler P., Volkel V., Flandin P. et al. (1998). Masking, unmasking and regulated polyadenylation cooperate in the translational control of a dormant mRNA in mouse oocytes. *Genes Dev.* **12**: 2535–2548
- Richter J. D. (1999). Cytoplasmic polyadenylation in development and beyond. *Microbiol. Mol. Biol. Rev.* **63**: 446–456
- Moor C. H. de and Richter J. D. (1999). Cytoplasmic polyadenylation elements mediate masking and unmasking of cyclin B1 mRNA. *EMBO J.* **18**: 2294–2903
- Mendez R., Barnard D. and Richter J. D. (2002). Differential mRNA translation and meiotic progression require Cdc2-mediated CPEB destruction. *EMBO J.* **21**: 1833–1844.
- Davidson E. H. (1986). *Gene Activity in Early Development*. 3rd ed., Academic Press, New York
- Bremer J. W., Busich H. and Yeoman L. C. (1981) Evidence for a species of nuclear actin distinct from cytoplasmic and muscle actins. *Biochemistry* **20**: 2013–2017
- Carotenuto R., Maturi G., Infante V., Capriglione T., Petrucci T. and Campanella C. (1997). A novel protein cross-reacting with antibodies against spectrin is localized in the nucleoli of amphibian oocytes. *J. Cell Sci.* **110**: 2683–2690
- Gard D. L., Cha B. J. and King E. (1997). The organization and animal-vegetal asymmetry of cyokeratin filaments in stage 6 *Xenopus* oocytes is dependent upon F-actin and microtubules. *Dev. Biol.* **184**: 95–114
- Gard D. L. and Klymkowsky M. W. (1998). Intermediate filament organization during oogenesis and early development of the clawed frog, *Xenopus laevis*. In: *Subcellular Biochemistry*, vol. 31: Intermediate Filaments, pp. 35–70. Herman H. and Harris W. A. (eds), Plenum, New York
- Klymkowsky M. W., Maynell L. A. and Polson A. G. (1987). Polar asymmetry in the organization of the cortical cyokeratin system of *Xenopus laevis* oocytes and embryos. *Development* **100**: 543–557
- Klymkowsky M. W. and Maynell L. A. (1989). MPF-induced breakdown of cyokeratin filament organization in the maturing *Xenopus* oocyte depends upon the translation of maternal mRNAs. *Dev. Biol.* **134**: 479–485
- Klymkowsky M. W., Maynell L. A. and Nislow C. (1991). Cyokeratin phosphorylation, cyokeratin filament severing and the solubility of the maternal Vg1. *J. Cell Biol.* **114**: 787–797
- Klymkowsky M. W. and Karnovsky A. (1994). Morphogenesis and the cytoskeleton: studies of the *Xenopus* embryo. *Dev. Biol.* **165**: 372–348
- Nadano D., Ishihara G., Aoki C, Yoshinaka T., Irie S. and Sato T. A. (2000). Preparation and characterization of antibodies against human ribosomal proteins: heterogeneous expression of S11 and S30 in a panel of human cancer cell lines. *Jpn. J. Cancer Res.* **9**: 802–810
- Franz J. K and Franke W. W. (1986). Cloning of cDNA and amino acid sequence of a cyokeratin expressed in oocytes of *Xenopus laevis*. *Proc. Natl. Acad. Sci. USA.* **83**: 6475–6479.
- Maturi G., Infante V., Carotenuto R., Focarelli R., Caputo M. and Campanella C. (1998). Specific glycoconjugates are present at the oolemma of the fertilization site in the egg of *Discoglossus pictus* (Anurans) and bind spermatozoa in an in vitro assay. *Dev. Biol.* **204**: 210–223
- Campanella C., Andreuccetti P., Taddei C. and Talevi R. (1984). The modifications of cortical endoplasmic reticulum during 'in vitro' maturation of *Xenopus laevis* oocytes and its involvement in cortical granule exocytosis. *J. Exp. Zool.* **229**: 283–294
- Tunquist B. J. and Maller J. L. (2003). Under arrest: cyotostatic factor (CSF)-mediated metaphase arrest in vertebrate eggs. *Genes Dev.* **17**: 683–710
- Russo G., Kyozyuka K., Antonazzo L., Tosti E. and Dale B. (1996). Maturation promoting factor in ascidian oocytes is regulated by different intracellular signals at meiosis I and II. *Development* **122**: 1995–2003
- Bluemink J. G. (1978). Use of cytochalasins in the study of amphibian development. *Front. Biol.* **46**: 113–142
- Cardinali B, Carissimi C, Gravina P and Pierandrei-Amaldi P. (2003). La protein is associated with terminal oligopyrimidine mRNAs in actively translating polysomes. *J Biol Chem.* **278**: 35145–35151
- Stith B. J. and Maller J. L. (1987). Induction of meiotic maturation in *Xenopus* oocytes by 12-O-tetradecanophorbol 13 acetate. *Exp. Cell Res.* **169**: 514–523

Expression of p27^{BBP}/eIF6 is Highly Modulated During *Xenopus laevis* Embryogenesis

MARIA CARMELA VACCARO,* MARTA CUCCARO, NADIA DE MARCO, AND CHIARA CAMPANELLA

Department of Structural and Functional Biology, University of Naples Federico II, Complesso Universitario Monte Sant'Angelo, Palazzina D, Napoli, Italy

ABSTRACT Protein p27^{BBP}/eIF6 is necessary for ribosomal function of all cells. Previous data showed that from mammals to yeast p27^{BBP}/eIF6 is involved in the biogenesis of ribosomal subunit 60S and its association with the 60S prevents premature 80S formation regulated by PKC signaling, indicating that phosphorylation of p27^{BBP}/eIF6 is needed for translation to occur. While in vitro p27^{BBP}/eIF6 is constitutively expressed, and it has a high level of expression in cycling cells, in vivo its expression varies according to tissues and appears regulated by factors up to now unknown. p27^{BBP}/eIF6 has never been investigated in developing organisms where its upregulation can be correlated with tissue growth and differentiation. In this study we have sequenced p27^{BBP}/eIF6 cDNA and studied its expression during development of *Xenopus laevis*, as the first step for studying its regulation. The amino acid sequence is highly conserved with two putative PKC phosphorylation sites in serine, one site being typical of *Xenopus*. At the end of gastrulation, the p27^{BBP}/eIF6 riboprobe localizes in the neural plate and in the paraxial mesoderm. In particular, from stage 24, a clear-cut localization occurs in the perspective head. In embryos exposed to teratogens, the localization of p27^{BBP}/eIF6 riboprobe varies according to the change of head size caused by the treatment. p27^{BBP}/eIF6 expression is particularly evident in differentiating olfactory pits, the lens, otic vesicles, and in branchial arches. Features of particular interest are p27^{BBP}/eIF6 high level of expression in the eye field, and in the mid-hindbrain-boundary, two regions with high proliferative activity. Altogether, data indicate that a modulated expression of p27^{BBP}/eIF6 occurs in developing anlagen in addition to a basal level of expression, and may suggest a correlation between p27^{BBP}/eIF6 and proliferative activity. Moreover, the *X. laevis* cDNA isolation and characterization offer new hints for further studies in relation to potential p27^{BBP}/eIF6 phosphorylation. *Mol. Reprod. Dev.* 73: 482–490, 2006.

© 2006 Wiley-Liss, Inc.

Key Words: embryonic development; serine phosphorylation; brain; eyes; mid-hindbrain transition; somites

INTRODUCTION

Mammalian p27^{BBP}/eIF6 protein interacts with the cytoskeleton and the β 4 integrin cytodomain in epithelial cells (Biffo et al., 1997). However, its most conserved function derives from its participation in 60S biogenesis and its association with the 60S ribosomal subunit. First, it is essential for the biogenesis of 60S (Sanvito et al., 1999); second, when bound to 60S, p27^{BBP}/eIF6 inhibits its interaction with 40S ribosomal subunits to form 80S (Si and Maitra, 1999; Ceci et al., 2003). Recently, it was shown in vitro and in cancer cells that p27^{BBP}/eIF6 release from 60S depends upon PKC phosphorylation (Ceci et al., 2003). In synthesis, p27^{BBP}/eIF6 is necessary for ribosomal function of all cells. However, since overexpression of p27^{BBP}/eIF6 inhibits 80S formation in the absence of PKC regulation (Ceci et al., 2003), its level must be tightly regulated.

The promoter of ITGB4BP, the gene encoding for the human p27^{BBP}/eIF6 protein, has features of house-keeping genes. Accordingly, in 'in vitro' cycling cells the steady-state levels of p27^{BBP}/eIF6 mRNA and protein are high, the protein is stable and is downregulated only upon prolonged serum starving (Donadini et al., 2001). However, the scenarios of p27^{BBP}/eIF6 expression are variable in 'in vivo' conditions. p27^{BBP}/eIF6 decreases in cells committed to apoptotic cell death and is highly expressed during the progression of some human cancer, its overexpression corresponding to mRNA upregulation (Sanvito et al., 2000). In mammalian normal tissues, p27^{BBP}/eIF6 levels are variable among cells. Moreover, high steady state levels of p27^{BBP}/eIF6 protein and mRNA can be rapidly induced, in response to external events such as the rupture of the epithelial barrier (Wood et al., 1999) or differentiative events such as mast cell activation (Cho et al., 1998; Oh et al., 2001)

Grant sponsor: P.R.I.N.

*Correspondence to: Maria Carmela Vaccaro, Department of Structural and Functional Biology, University of Naples Federico II, Complesso Universitario Monte Sant'Angelo, Palazzina D, Napoli, Italy. E-mail: chiara.campanella@unina.it

Received 1 July 2005; Accepted 18 November 2005

Published online 19 January 2006 in Wiley InterScience

(www.interscience.wiley.com).

DOI 10.1002/mrd.20449

indicating that in vivo the gene is tightly regulated (Donadini et al., 2001). The molecular mechanisms underlying these regulations are completely unknown. At the light of the recent data on the role of p27^{BBP}/eIF6 in ribosome maturation (Ceci et al., 2003), it appears that more studies are needed to establish whether, in normal cells, conditions such as cell proliferation or specific steps of cell differentiation coincide with high levels of p27^{BBP}/eIF6 expression, in relationship to an increased need of protein synthesis regulation.

p27^{BBP}/eIF6 expression has never been evaluated in embryogenesis, a process where cells actively cycle before/during various differentiation fates and high expression of the protein may occur along selected pathways. As first step of a project aiming to study p27^{BBP}/eIF6 regulation during development, in this study we have sequenced p27^{BBP}/eIF6 cDNA and studied p27^{BBP}/eIF6 expression during the embryogenesis of *Xenopus laevis*. In this system, p27^{BBP}/eIF6 undergoes phosphorylation in serine at first meiotic resumption, constituting an example where phosphorylation of p27^{BBP}/eIF6 may take part in protein synthesis regulation in vivo (Carotenuto et al., 2005). Data in this study show that the messenger is present throughout embryogenesis, as analyzed by RT-PCR. Moreover, high expression levels of p27^{BBP}/eIF6 occur in the neural plate and paraxial mesoderm, from the beginning of their patterning and later in embryogenesis in developing anlagen, in agreement with the proposed role of p27^{BBP}/eIF6 in regulating protein synthesis (Ceci et al., 2003; Carotenuto et al., 2005). In particular, p27^{BBP}/eIF6 can be included among the molecules highly expressed in regions where high cell proliferation occurs, such as the eye field and the midbrain-hindbrain boundary.

MATERIALS AND METHODS

Collection of Embryos

Adult *X. laevis* females were obtained from 'Rettilli' Varese, Italy. To obtain eggs, *X. laevis* females were injected in the dorsal lymphatic sac with 500 units of Profasi BP (Serono, Rome, Italy) in Amphibian Ringer (111 mM NaCl, 1.3 mM CaCl₂, 2 mM KCl, 0.8 mM MgSO₄, 25 mM HEPES, pH 7.8). Testes were removed from males anaesthetized with MS122 (Sigma Chemical Co, St. Louis, MO). Uterine eggs were inseminated by a sperm suspension obtained by macerating testes in 1/10 of Ringer. Embryos were staged according to the normal table of *X. laevis* development (Nieuwkoop and Faber, 1994).

Isolation and Sequence Analysis of *X. laevis* p27^{BBP}/eIF6 cDNA

The *X. laevis* p27^{BBP}/eIF6 sequence deposited in EST Bank with accession number AW767577, corresponds to the 5' region of cDNA. The remaining sequence was obtained by 3' rapid amplification of cDNA ends using the System for Rapid Amplification of cDNA ends (Invitrogen Life Technologies, Carlsbad, CA). The cDNA synthesis was performed according to the manufac-

turer's recommendations with 5 µg of total RNA extracted from embryo stage 19 using the following gene specific forward primer RACE 1: 5'-AGAAGCTTC-TACAGTGTGTTTGAA-GG-3' and forward nested primer RACE 2: 5'-GCCTTTAGTAACCAAGGAGGCC-3'. The cDNA amplified was cloned into pDRIVE vector (Qiagen, Valentia, CA) and sequenced in both directions by PRIMM (Naples, Italy). All sequence information was processed using BLAST, TM prediction, and ScanProsite program; the multiple alignments were generating with ClustalW. The complete sequence was deposited in Gene bank with accession number AY383654.

RNA Extraction and Nonquantitative RT-PCR

Total RNA was extracted from several embryonic stages with TRI Reagent (Sigma). RT-PCR was performed with a Titan one-step system (Roche, Mannheim, Germany) using 1 µg of total RNA and the *X. laevis* p27^{BBP}/eIF6 gene-specific oligonucleotide, primer forward: 5'-GTGTG-TCGCTTGAGTGAGGA-3' and primer reverse: 5'-CAGTTGCTCGTGAAGTCCA-3'. The reaction was performed according to the manufacturer's recommendations using the Perkin-Elmer gene Amp PCR system 2400.

Sample Preparation for SDS-PAGE and Western Blot

Embryos were homogenized in HEPES buffer pH 7.5 containing 900 mM glycerol, 0.02 mM NaN₃, 1 mM ATP, 1 mM DTT, 5 mM EGTA, and the following protease inhibitors (Sigma): 2 mM TAME, 5 mg/ml SBTI, 5 µg/ml aprotinin, and 10 µM E64. After centrifugation at 15,000g for 40 min at 4°C, protein concentration was determined in the supernatants with the BCA protein assay reagent (Pierce, Rockford, IL). After boiling in sample buffer with β-mercaptoethanol, aliquots of 30–60 µg of proteins were submitted to SDS-PAGE separation in 15% polyacrylamide, utilizing molecular mass standards (200, 116, 97, 45, 31, 21, or 14 kDa) (Bio-rad, Hercules, CA). Western blotting on nitrocellulose membrane was performed as in Carotenuto et al. (2005), using a rabbit polyclonal antiserum against p27^{BBP}/eIF6 C-terminus or a mouse monoclonal antibody recognizing an epitope between p27^{BBP}/eIF6 aa 135 and 200, followed by incubation in alkaline phosphatase (AP)-conjugated antibodies. Both anti-p27^{BBP}/eIF6 antibodies are a gift of P.C. Marchisio and S. Biffo (DIBIT and University Vita-Salute San Raffaele Milano, Italy).

In situ Hybridization

Embryos were fixed in MEMFA 1X and stored in absolute ethanol. The full-length *X. laevis* p27^{BBP}/eIF6 was obtained by RT-PCR and cloned into pDRIVE vector (Qiagen). p27^{BBP}/eIF6 sense and antisense digoxigenin labeled RNA probes were synthesized with RNA T7 or SP6 polymerases (Roche). Fluorescein labeled RNA probes of X-Otx2 (kindly supplied by M. Pannese,

Ospedale San Raffaele DIBIT, Milan, Italy), Xrx1, and XFGF8 (generously supplied by R. Vignali e M. Andreazzoli, University of Pisa, Italy) were synthesized with T3, T7, or SP6 RNA polymerases (Roche).

Whole mount was carried out as described by Harland (1991) with the following modifications: the anti-DIG-alkaline phosphates conjugated antibody (Roche) was preadsorbed against *X. laevis* embryo powder before incubation. AP detection was performed with BM-purple color substrate (Roche) and after staining, the embryos were bleached and cleared in benzyl alcohol: benzylbenzoate (1:2).

For double whole mount in situ hybridization, the embryos were hybridized simultaneously with both a digoxigenin- and a fluorescein-labeled probe under standard conditions. After detection of the first probe with BM-purple, the AP was inactivated in 100 mM glycine pH 2.2 and 0.1% Tween-20, then the embryos were blocked in MAB (100 mM maleic acid, 150 mM NaCl, pH 7.5) and blocking reagent. Following incubation with the second antibody, anti-fluorescein-alkaline phosphates conjugated antibody (Roche), the AP reaction was performed with magenta-Phos (Sigma) or BCIP (5-bromo-4-chloro-3-indolylphosphate) (Sigma).

For the in situ hybridization on sections, the embryos were fixed in 4% formaldehyde at room temperature, followed by overnight 30% w/v sucrose treatment at 4°C. After embedding in tissue tek, the samples were frozen and cryostat sectioned to a thickness of 9–10 µm. Sections were placed on Superfrost Plus slides (Carlo Erba) and processed as previously described (Vaccaro, 2003), utilizing p27^{BBP}/eIF6 cDNA as probe.

Retinoic Acid and Lithium Chloride Treatment

Thirty two-cells cleaving embryos were dejelled in Ringer pH 9.00 containing β-mercaptoethanol and exposed to 1 µM or 10 µM retinoic acid (all-trans RA, Sigma) in 1% DMSO until neurula (st.14), (see Durston et al., 1989; Papalopuli et al., 1991). After several rinses, the embryos were raised in 1/10 Ringer, together with untreated sibling embryos to monitor the stage of development. In a second group of experiments, 32-cells embryos were treated with 0.3 M LiCl for 10 min (see Kao and Elinson, 1988; Pannese et al., 1995), extensively rinsed and grown in 1/10 Ringer.

RESULTS

Isolation and Analysis Sequence of *X. laevis*

Full-length *X. laevis* p27^{BBP}/eIF6 cDNA was isolated from embryos RNA by 3' rapid amplification of cDNA end. The complete sequence is 1084 bp containing an open reading frame (ORF) of 245 amino acids (Fig. 1a). The size was confirmed by Northern blot analysis (data not shown). In the ORF, the nucleotide sequence shows 78% identity with the p27^{BBP}/eIF6 in mammals (*H. sapiens* and *M. musculus*). By contrast no identity is found in the *X. laevis* 3' Untranslated Region (UTR) of 279 bases which is AU-rich with the particular motif UUUUUU, located 93 nucleotides downstream of the

common polyadenylation hexanucleotide AAUAAA. Analysis in the Embnet database UTR site shows that this motif is the typical consensus sequence of the cytoplasmatic polyadenylation elements (CPE).

Xenopus deduced amino acid sequence is highly conserved in living organism and shares 92% identity with the mammalian sequence (*H. sapiens* and *Mus musculus*), 72% with *S. cerevisiae*, 75% with *D. melanogaster*, and 62% with *C. elegans*. In the mentioned organisms, the homology is related to the whole sequence, with a percentage of identity in the protein C-terminus region smaller than the N-terminus (Fig. 1b). *Xenopus* p27^{BBP}/eIF6 has one potential transmembrane domain in the N-terminus region (position 21–40) (Fig. 1a), two potential N-glycosylation sites, NNIT (position 74–77), and NTTD (position 75–78) (Fig. 1a) and two potential protein kinase C phosphorylation sites, 91 SvR and 235 SmR (Fig. 1a–b).

p27^{BBP}/eIF6 Expression in Embryo Development

RT-PCR analysis showed that p27^{BBP}/eIF6 messenger is present throughout embryonic development, from first cleavage to tadpole (Fig. 2a). Parallel Western blots indicate that both p27^{BBP}/eIF6 isoforms of 27 and 29 kDa are present in samples of the same stages, in agreement with data previously reported by Carotenuto et al. (2005), where it was shown that p29 is a phosphorylated form of p27^{BBP}/eIF6.

Stages 12.5–24

The expression pattern of p27^{BBP}/eIF6 gene was studied by whole mount in situ hybridization in embryos, starting from stage 12.5 where the signal was found in the neural plate and was particularly evident in the anteriormost region (Fig. 3a). Xotx2 and Xrx1 probes were used for double hybridization with p27^{BBP}/eIF6 to mark the anteriormost extension of p27^{BBP}/eIF6 expression. Xrx1 controls proliferation and neurogenesis, and at the end of gastrulation is expressed in the anterior neural plate in territories fated to give rise to the retina, diencephalons and part of the telencephalon, while Xotx2, expressed in the prospective anterior neuroectoderm, is repressed in the area of Xrx1 expression (Andreazzoli et al., 2003). Double in situ hybridization with Xrx1 and p27^{BBP}/eIF6 showed overlap of the probes in particular in the eye field area, labeled by sharp Xrx1 expression (Fig. 3b). Double in situ hybridization with Xotx2 and p27^{BBP}/eIF6 probes overlaps anteriorly: Xotx2 surrounds part of the anterior p27^{BBP}/eIF6 expression (Fig. 3c,d). Moreover, p27^{BBP}/eIF6 signal overcomes anteriorly Xotx2 expression (Fig. 3d), where the cement gland field is located, as reported by other authors (Gammil and Sive, 1997; Wardle et al., 2002). In later development p27^{BBP}/eIF6 is similarly expressed all along the antero-posterior axis of the embryo (Fig. 3e,f,h). At stage 24, p27^{BBP}/eIF6 mRNA is found in the developing brain area, in particular in the eye primordia, anlagen of otic, and olfactory vesicles, as well as in the somites (Fig. 3h,i). Starting from this stage, p27^{BBP}/eIF6 mRNA is constantly

a

| | | |
|------------------------|---|----|
| <i>X. laevis</i> | MAVRFASFENNNEIGCFAKLTNTYCLVAIGGSENFYSVFEGEELSETIPVHHASIAIGCRIIG | 60 |
| <i>H. sapiens</i> | MAVRFASFENNNEIGCFAKLTNTYCLVAIGGSENFYSVFEGEELSDTIPVHHASIAIGCRIIG | 60 |
| <i>D. melanogaster</i> | MALRVQFENNDDIGVFTKLTNTYCLVAIGGSETFYSAFEAEELGDTIPVHHANVGGCRIIG | 60 |
| <i>S. cerevisiae</i> | MATRTPQFENNEIGVFEKLTNTYCLVAVGGSENFYSAFEAEELGDAEIPVHTTIAIGTRIIIG | 60 |

b

| | | |
|-------------------|--|----|
| <i>C. elegans</i> | MALRVVDYEGSNDVGVFCTLTNSYCLVGVGGTQNFYSILEAEELSDLIPVHHTSIASTRIVG | 60 |
|-------------------|--|----|

*

| | | |
|------------------------|--|-----|
| <i>X. laevis</i> | RMCVGNRHGLMVPNNITDQELQHMNRNSLPD SVRI QQRVEERLSALGNVIAICNDYVALVHPD | 120 |
| <i>H. sapiens</i> | RMCVGNRHGLMVPNNITDQELQHIRNSLPD TVQIR RVEERLSALGNVITCNDYVALVHPD | 120 |
| <i>D. melanogaster</i> | RLTVGNRNGLLVFNSTTDEELQHLRNSLPD AVKIR VEERLSALGNVIAICNDYVALVHPD | 120 |
| <i>S. cerevisiae</i> | RMTAGNRRLVPTQTDDQELQHLRNSLPD SVKIQ RVEERLSALGNVITCNDYVALVHPD | 120 |
| <i>C. elegans</i> | RLTVGNRHGLMVPNATDQELQHLRNSLPD EVAIR FRVDERLSALGNVIAICNDHVAIVHAE | 120 |

*

| | | |
|------------------------|---|-----|
| <i>X. laevis</i> | LDRETEEILADVLKVEVFRQTIAEQVLVGSYCAFSNOGGLLHPKTSIEDQDELSSLLQVP | 180 |
| <i>H. sapiens</i> | LDRETEEILADVLKVEVFRQTIVADQVLVGSYCVFSNOGGLVHPKTSIEDQDELSSLLQVP | 180 |
| <i>D. melanogaster</i> | LDKETEEIIADVLKVEVFRQTIADNSLVGSYAVLSNOGGMVHPKTSIQDQDELSSLLQVP | 180 |
| <i>S. cerevisiae</i> | IDRETEELISDVLGVEVFRQTISGNILVGSYCSLSNOGGLVHPQTSVQDQELSSLLQVP | 180 |
| <i>C. elegans</i> | ISAETEALVEVLKVEVFRVSLAQNSLVGSYCILSSNGCLVAARTPPETQREIAALLQIP | 180 |

*

| | | |
|------------------------|---|-----|
| <i>X. laevis</i> | LVTGTVNRGSEVIAAGMVVNDWCAFCGLDITSTELSVIESVFKLSDAH-PSTIAT SMR GS | 239 |
| <i>H. sapiens</i> | LVAGTVNRGSEVIAAGMVVNDWCAFCGLDITSTELSVVSVFKLNEAQ-PSTIAT SMR DS | 239 |
| <i>D. melanogaster</i> | LVAGTVNRGSEVLAAGMVVNDWLSFVGMNTTATEISVIESVFKLNQQAQ-BATVTTKLRRAA | 239 |
| <i>S. cerevisiae</i> | LVAGTVNRGSSVVGAGMVVNDYLAVTGLDITAPELSVIESIFRLQDAQ-PESISGNLRDT | 239 |
| <i>C. elegans</i> | VVAGTCNRGSELIGAGMVVNDWVAFCGLDITSTELSVVSVIFKLGEGQAFPTSISNQLRDT | 240 |

*

| | | |
|------------------------|--------|-----|
| <i>X. laevis</i> | LIDSLT | 245 |
| <i>H. sapiens</i> | LIDSLT | 245 |
| <i>D. melanogaster</i> | LIEDMS | 245 |
| <i>S. cerevisiae</i> | LIETYS | 245 |
| <i>C. elegans</i> | LIESML | 246 |

Fig. 1. a: Deduced amino acid sequence of the cDNA of *X. laevis* p27^{BBP}/eIF6 (EST Bank with accession number AY 383654). The potential transmembrane domain in the N-terminus region (position 21–40) are evidenced, the potential protein kinase C phosphorylation sites are in boldface and the potential glycosylation sites (NNTT and NTTD) are underlined. **b:** Clustal formatted alignment of *X. laevis*

p27^{BBP}/eIF6 with *H. sapiens*, *D. melanogaster*, *S. cerevisiae* and *C. elegans* homologs. The perfectly conserved position are evidenced, the potential protein Kinase C phosphorylation site typical to *X. laevis* or common to mammalian are marked respectively by symbol * and symbol ω.

localized in the differentiating epidermis (Fig. 3g). p27^{BBP}/eIF6 hybridization signal is specific, as indicated by the absence of signal, when the sense riboprobe is used (Fig. 3g).

Stages 32–36

As development proceeds, the head localization becomes more evident. At stages 32 and 35–36, the p27^{BBP}/eIF6 mRNA is found in this region, with a clear-cut boundary at the trunk limit (Fig. 4). In particular, the riboprobe is localized in the brain, otic vesicle, periphery of the lens area and more faintly, in the optic cup (Fig. 4a). To further check the specificity of the riboprobe localization in the head, in addition to control sense riboprobe (Fig. 4b), we have used teratogens, such as retinoic acid (RA) and lithium chloride. Depending upon dosage, RA diminishes or impairs the head formation, on the basis of its well-known action on *Hox* genes (Durstont et al., 1989; Papalopulu et al., 1991). In embryos treated with 10 μM RA, the head is strongly reduced in size, the cephalon is rudimental or absent and p27^{BBP}/eIF6 expression has a sharply reduced extension, according to the change in the head size (Fig. 4c). Conversely, embryos treated with 0.3 M LiCl, with opposite action on the embryos (see Kao and Elinson, 1988), display sharp reduction of the trunk and oversized head where high expression of p27^{BBP}/eIF6 occurs (Fig. 4d).

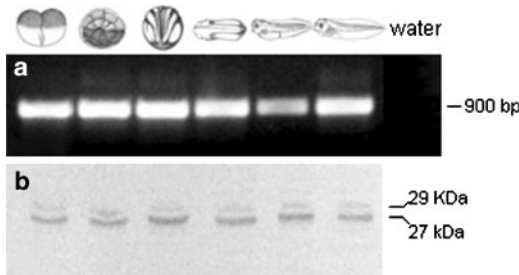


Fig. 2. Not quantitative RT-PCR analysis and Western blot of *X. laevis* p27^{BBP}/eIF6 in embryos of the stages: 2, 8, 14, 24, 41, 45. **a:** We have amplified 900 bp of complete p27^{BBP}/eIF6 cDNA from the total RNA of the indicated embryos stage. In the lane 'water', total RNA was not added. **b:** The two p27^{BBP}/eIF6 isoforms of 27 and 29 kDa are present in all the examined stages.

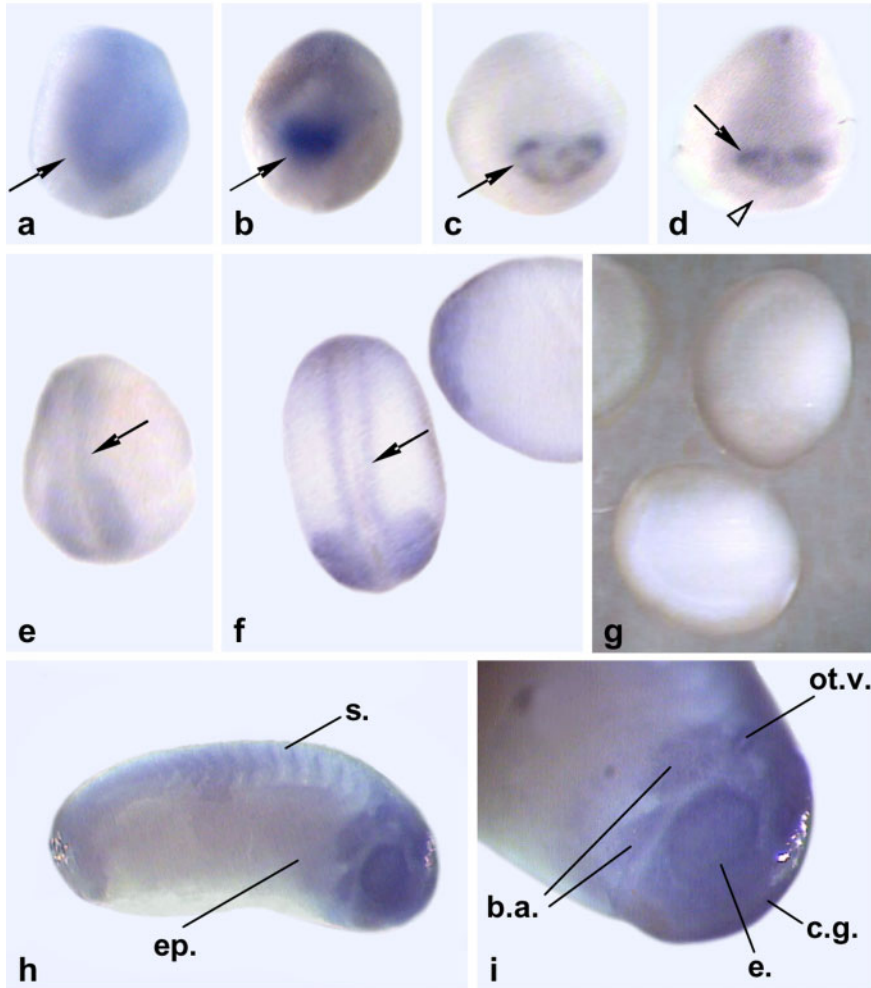


Fig. 3. Whole mount in situ hybridization of stages 12.5–24 embryos. **a:** Stage 12.5 embryo. Using p27^{BBP}/eIF6 antisense probe the hybridization signal is present in the neural plate, whose anteriormost portion is indicated by the arrow. **b:** At the same stage, double in situ hybridization with Xrx1 and p27^{BBP}/eIF6 riboprobes shows that p27^{BBP}/eIF6 expression occurs in the eye field marked by Xrx1 expression (arrow). **c:** Stage 12.5 embryo labeled by Xotx-2 riboprobe, showing the ring-like expression that surrounds the eye field (arrow). **d:** The same embryo as in C labeled with p27^{BBP}/eIF6 in addition to Xotx-2 riboprobe. p27^{BBP}/eIF6 label surrounds Xotx-2

expression (arrow). The arrowhead indicates that p27^{BBP}/eIF6 is further expressed anteriorly to the eye field. A,B,C = 13x. **e, f:** p27^{BBP}/eIF6 expression in stage 14 and 19 embryos, respectively, occurs in the whole neural tube and surrounding axial mesoderm (arrow) x = 14. **g:** Whole mount in situ hybridization using sense probe in stage 19 embryos: the signal is absent. x = 14. **h, i:** p27^{BBP}/eIF6 messenger in stage 24 is present in the somites (s), anlagen of otic vesicles (ot. v.), and optic vesicles (e.). The anlagen of cement gland (c.g.) is stained h = 16x; i = 32x. [See color version online at www.interscience.wiley.com.]

In a dorsal view of the embryo, the hybridization becomes evident in the forebrain, midbrain, and hindbrain and a strong signal is present in the midbrain posterioriormost region (Fig. 4e). In order to investigate whether the labeled region is coincident with the MHB (midbrain-hindbrain boundary), the constriction in the neural tube at the junction between these two brain

regions, sibling embryos were hybridized with the riboprobe of a marker of this region, FGF8 (Riou et al., 1998) (Fig. 4f) or double labeled with p27^{BBP}/eIF6 and FGF8 riboprobes. Figure 4g indicates that the domain of higher p27^{BBP}/eIF6 expression coincides with that of FGF8. p27^{BBP}/eIF6 signal gradually decreases in the hindbrain and in the spinal cord is

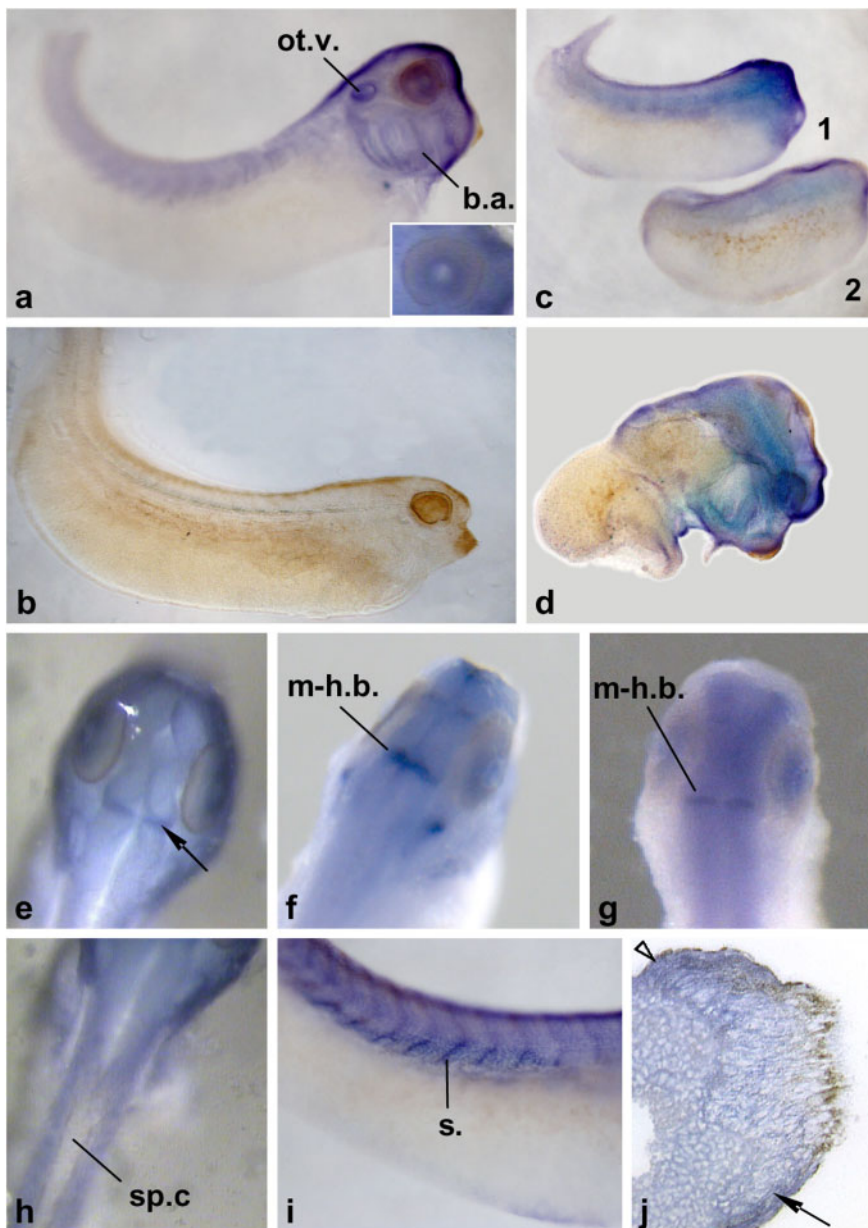


Fig. 4. Expression of *X. laevis* p27^{BBP}/eIF6 messenger in stage 35/36 embryos. **a:** Lateral view of embryos indicating the signal in the somites, branchial arches (b.a.), otic vesicle (o.v.), lens, and retina areas (insert). The cement gland (c.g.) is practically unstained. **b:** Control embryo with sense probe. a–b = 10x. **c:** Embryos treated with 10 μ M RA: the head was strongly reduced in size in embryo 1 and practically absent in embryo 2. An high p27^{BBP}/eIF6 expression is found in the head remnant x = 6. **d:** Embryos treated with 0.3 M LiCl, with sharp reduction of the trunk and oversized head where high expression of p27^{BBP}/eIF6 occurs, in particular in the eye x = 6. **e–h:** Dorsal view of the embryo. **e:** The signal is evident in the brain; in particular a strong

signal is present in the midbrain posteriormost region (arrow). **f:** Embryo labeled by the FGF-8 riboprobe. The middle brain-hindbrain boundary is labeled (m-h.b.). **g:** Double hybridization with p27^{BBP}/eIF6 and FGF-8 riboprobes, showing coincident labeling at the middle brain-hindbrain boundary (m-h.b.). **h:** p27^{BBP}/eIF6 riboprobe signal is absent in the spinal cord (sp.c.). **e–h** = 15x. **i:** Lateral view of an embryo showing hybridization signal in the somites s = 20x. **j:** Cement gland section hybridized with the p27^{BBP}/eIF6 riboprobe. The label is present in particular in the lateral cells (arrow). Arrowhead = epithelial cells x = 100. [See color version online at www.interscience.wiley.com.]

absent (Fig. 4h), while still present in the somites (Fig. 4i). In the developing cement gland p27^{BBP}/eIF6 riboprobe was better depicted in sections than in 'whole mounts.' The hybridization is evident in the whole region of the gland, in particular in the lateral boundaries (Fig. 4j).

Stage 41–45

At stage 41, the trunk keeps a faint localization of the messenger and in the head the strong hybridization is restricted to the anteriormost region where the riboprobe labels the forebrain and midbrain, as well as the pharynx region and the branchial arches (Fig. 5a,b). At stage 45, the hybridization, while still notable in the forebrain, is faintly present in the MDH region and absent in the hindbrain. The label is particularly evident around the lens, in the olfactory pits, branchial arches, and in the miotomes (Fig. 5c,d,e). Figure 5f is a sample exposed to the sense riboprobe, and no label is found.

DISCUSSION

Donadini et al. (2001) reported that, in contrast to in vitro cycling cells, human p27^{BBP}/eIF6 expression is regulated in normal cells, suggesting that p27^{BBP}/eIF6, in addition to being expressed at basal level, consistent with the characteristics of the ITGB4BP promoter, can be modulated according to tissue needs. According to Ceci et al. (2003) and as tested during oocyte maturation in *Xenopus* (Carotenuto et al., 2005), phosphorylation of p27^{BBP}/eIF6 has an important role in protein synthesis regulation. Therefore, in embryogenesis, major expression and post-translation modification of p27^{BBP}/eIF6 are expected to occur according to increased need of protein synthesis regulation along tissue differentiation and proliferation. Data in this study on the pattern of expression of total p27^{BBP}/eIF6

during embryonic development appear to be in agreement with this expectation. Moreover, *X. laevis* cDNA isolation and characterization offer new hints in relation to potential p27^{BBP}/eIF6 phosphorylation.

While in the ORF the nucleotide sequence has high identity with that of mammalian species, *X. laevis* has a specific 3'UTR of 279 bases, with a CPE domain UUUUUUAU, located downstream of the polyadenylation site. CPE elements have been reported to have the general sequence UUUUUUAU. However the U-rich motif is not identical in all mRNAs, and its position is variable with respect to AAUAAA (Kuhl and Wedlich, 1995; Richter, 1991). The CPE domain is potentially capable of stimulating elongation of the poly(A) tail that regulates translation activation of maternal messenger during oocyte maturation and early development (Fox et al., 1989; Varnum et al., 1992; Hake and Richter, 1994).

The p27^{BBP}/eIF6 deduced amino acid sequence shares high identity with the protein of all the studied organisms and, in particular, 92% percentage of identity was found for mammals. The identity is less strict in the C-terminus region and high in the N-terminus, a characteristic that accompanies all the studies on p27^{BBP}/eIF6 sequence homology (Biffo et al., 1997). Regarding the two potential sites of protein kinase C phosphorylation depicted in the N-terminus region, the position S 235 is the same as in p27^{BBP}/eIF6 of mammalian species, and, interestingly, site S 91 is typical of *Xenopus*. In connection, in this species a major phosphorylation in serine was found at oocyte maturation undergoing a new form of p27^{BBP}/eIF6 of 29 kDa. The latter was hypothesized to be phosphorylated by endogenous PKC (Carotenuto et al., 2005). The presence of two potential sites of PKC phosphorylation, may lead to speculation that in *Xenopus* there is a more articulate

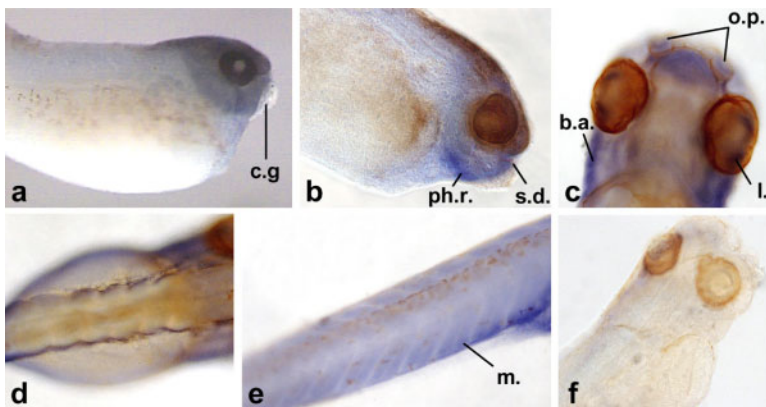


Fig. 5. a: In a stage 41 embryo the strong hybridization signal of the head is restricted to the anteriormost region where some hybridization is in the eye. In the somites a faint localization is found. c.g. = cement gland $\times 8$. b: This stage 41 embryo shows riboprobe labels in the brain, pharynx region (ph. r.), and stomodeum opening (st.) $\times 10$. c–e: Dorsal views of a stage 45 embryo: the hybridization is in the optic cup,

around the lens (l) and in the forebrain, in the olfactory pits (o.p.). A mild hybridization is present in the branchial arches (b.a.). d: The hindbrain is unstained. e: The signal is in the miotomes (m.) $\times 12$. f: There is no signal in the embryo hybridized with sense probe $\times 8$. [See color version online at www.interscience.wiley.com.]

regulation of p27^{BBP}/eIF6 activity than found in mammals where p27^{BBP}/eIF6 impedes improper joining of 40S and 60S subunits, and PKC phosphorylation of p27^{BBP}/eIF6 allows the formation of 80S and protein synthesis to occur (Ceci et al., 2003). However, much work should be done to ascertain the functional meaning of the two potential sites of p27^{BBP}/eIF6 phosphorylation during *Xenopus* embryogenesis.

The hybridization analysis conducted in this study throughout *Xenopus* embryogenesis indicates that p27^{BBP}/eIF6 earliest expression is in the neural plate, and includes the telencephalon and diencephalon area and in particular the eye field. As the p27^{BBP}/eIF6 mRNA is expressed also anteriorly to *Xrx1* and *Xotx2* sites of expression, it may be concluded that p27^{BBP}/eIF6 mRNA is probably located as well in the cement gland field (see Gammil and Sive, 1997; Wardle et al., 2002). p27^{BBP}/eIF6 highest expression undergoes progressive modulation and regionalization along embryogenesis in developing neuroectoderm and dorsal mesoderm derivatives, that is, in the brain, sensory organs, epidermis, somites, and cement gland. The high expression levels observed in the head are tightly linked to the brain region, as shown by using teratogens (retinoic acid and LiCl). It has been reported that genes encoding some ribosomal proteins, such as 60S ribosomal protein 29 (Gawantka et al., 1998), have an expression pattern similar to the above p27^{BBP}/eIF6 pattern, suggesting that p27^{BBP}/eIF6 is expressed in several embryonic anlagen according to its role of linker of 60S, and its involvement in ribosome maturation.

Moreover, there are some features of specific interest. In the first place we should note the high level of p27^{BBP}/eIF6 expression in the MHB region. In vertebrates, this zone is an important signaling center for patterning the midbrain and anterior hindbrain, and for the formation and maintenance of the MHB region itself. In MHB a complex genetic network of expression exists, that includes *pax-2* (Lun and Brand, 1998), *XEN-2*, *XWnt-1* (Hemmati-Brivanlou et al., 1991; Eizema et al., 1994), *XHRI* (Shinga et al., 2001), as well as the signaling of members of the FGF family (*XFGF3*, *XFGF8*, *EFGF*, Lee et al., 1997; Riou et al., 1998). It appears that, in the MHB region, during embryogenesis and in particular at stage 35–41 an active proliferation occurs, needing regulation of protein synthesis, in agreement with the level of expression of p27^{BBP}/eIF6 we have described. Accordingly, it appears that p27^{BBP}/eIF6 expression decreases around stage 45, when most of the mesencephalon and hindbrain cell proliferation and patterning has occurred. In contrast, in the forebrain, p27^{BBP}/eIF6 expression is still high at this stage, probably in agreement with the formation of cerebellum hemispheres, beginning at stage 43.

Second, p27^{BBP}/eIF6 expression is comprehensive of the whole neuro-ectoderm territory and in particular, it is always present in the eye field starting from its early formation to the differentiation of retina and lens. The early p27^{BBP}/eIF6 expression in the eye field is consistent with the presence in the same region of several gene

activities related to proliferation including *Xrx1* that we showed colocalizing with p27^{BBP}/eIF6. Therefore, p27^{BBP}/eIF6 can be included among the genes active during retina and lens formation. In conclusion, this study shows that p27^{BBP}/eIF6 expression is modulated during embryogenesis in differentiating anlagen and preliminarily may suggest that this protein may be included among markers of regions in active proliferation.

ACKNOWLEDGMENTS

We are grateful to S. Biffo, Barbara Di Benedetto, and Rosa Carotenuto for suggestions, M. G. Agostinelli and D. Calabresi for assistance with this research during the preparation of their Master Thesis, and Giuseppe Falcone for image processing and to Mark Walters for critical reading of the manuscript. This work was supported by a P.R.I.N. grant to C.C.

REFERENCES

- Andreazzoli M, Gestri G, Cremisi F, Casarosa S, Dawid IB, Barsacchi G. 2003. *Xrx1* controls proliferation and neurogenesis in *Xenopus* anterior neural plate. *Development* 130:5143–5154.
- Biffo S, Sanvito F, Costa S, Preve L, Pignatelli R, Spinardi L, Marchisio PC. 1997. Isolation of a novel beta4 integrin-binding protein p27(BBP) highly expressed in epithelial cells. *J Biol Chem* 272: 30314–30321.
- Carotenuto R, Vaccaro MC, De Marco N, Wilding M, Biffo S, Marchisio PC, Capriglione T, Campanella C. 2005. p27BBP/IF6 is phosphorylated and associated with the cytoskeleton in relation to the stages of oogenesis in *Xenopus laevis*. *In Cell Mol Life Sci* 62:1641–1652.
- Ceci M, Gaviraghi C, Gorrini C, Sala LA, Offenhauser N, Marchisio PC, Biffo S. 2003. Release of eIF6 (p27BBP) from the 60S subunit allows 80S ribosome assembly. *Nature* 426:579–584.
- Cho SH, Cho JJ, Kim LS, Vliagoftis H, Metcalfe DD, Oh CK. 1998. Identification and characterization of the inducible murine mast cell gene, *imc-415*. *Biochem. Biophys Res Commun* 252:123–127.
- Donadini A, Giodini A, Sanvito F, Marchisio PC, Biffo S. 2001. The human *ITGB4BP* gene is constitutively expressed in vitro, but highly modulated in vivo. *Gene* 266:35–43.
- Durston AJ, Timmermans JPM, Hage WJ, Hendriks HFJ, de Vries NJ, Heideveld M, Nieuwkoop PD. 1989. Retinoic acid causes an anteroposterior transformation in the developing central nervous system. *Nature* 340:140–144.
- Eizema K, Koster JG, Stegeman BI, Baarends WM, Lanser PH, Destree OH. 1994. Comparative analysis of engrailed-1 and Wnt-1 expression in the developing central nervous system of *Xenopus laevis*. *Int J Dev Biol* 38:623–632.
- Fox CA, Sheets MD, Wickens MP. 1989. Poly(A) addition during maturation of frog oocytes: Distinct nuclear and cytoplasmic activities and regulation by the sequence UUUUUUU. *Genes Dev* 3:2151–2162.
- Gammil LS, Sive H. 1997. Identification of the *Otx2* target genes and restrictions in ectodermal competence during *Xenopus* cement gland formation. *Development* 124:471–481.
- Gawantka V, Pollet N, Delius H, Vingron M, Pfister R, Nitsch R, Blumenstock C, Niehrs C. 1998. Gene expression screening in *Xenopus* identifies molecular pathways, predicts gene functional and provides a global view of embryonic patterning. *Mech Dev* 77:95–141.
- Hake LE, Richter JD. 1994. CPEB is a specificity factor that mediates cytoplasmic polyadenylation during *Xenopus* oocyte maturation. *Cell* 79:617–627.
- Harland RM. 1991. In situ hybridisation: An improved whole mount method for *Xenopus* embryos. *Meth Cell Biol* 36:675–685.

- Hemmati-Brivanlou A, de la Torre JR, Holt C, Harland RM. 1991. Cephalic expression and molecular characterization of *Xenopus* En-2. *Development* 111:715–724.
- Kao KR, Elinson RP. 1988. The entire mesodermal mantle behaves as Spemann's organizer in dorsoanterior enhanced *Xenopus laevis* embryos. *Dev Biol* 127:64–77.
- Kuhl M, Wedlich D. 1995. XBIU-cadherin NBNA contains cytoplasmic polyadenylation elements and is polyadenylated during oocyte maturation in *Xenopus laevis*. *Biochim Biophys Acta* 1262:95–98.
- Lee SM, Danielian PS, Fritzsche B, McMahon AP. 1997. Evidence that FGF8 signalling from the midbrain-hindbrain junction regulates growth and polarity in the developing midbrain. *Development* 124:959–969.
- Lun K, Brand M. 1998. A series of no isthmus (noi) alleles of the zebrafish pax2.1 gene reveals multiple signaling events in development of the midbrain-hindbrain boundary. *Development* 125:3049–3062.
- Nieuwkoop PD, Faber J. 1994. Normal table of *Xenopus laevis* (Daudin). Amsterdam: North Holland.
- Oh CK, Filler SG, Cho SH. 2001. Eukaryotic translation initiation factor-6 enhances histamine and IL-2 production in mast cells. *J Immunol* 166:3606–3611.
- Pannese M, Polo C, Andreazzoli M, Vignali R, Kablar B, Barsacchi G, Boncinelli E. 1995. The *Xenopus Ems* genes identify presumptive dorsal telencephalon and are induced by head organizer signals. *Development* 121:707–720.
- Papalopulu N, Clarke JD, Bradley L, Wilkinson D, Krumlauf R, Holder N. 1991. Retinoic acid causes abnormal development and segmental patterning of the anterior hindbrain in *Xenopus* embryos. *Development* 113:1145–1158.
- Richter JD. 1991. Translational control during early development. *Bioessays* 4:179–183.
- Riou JF, Delarue M, Mendez AP, Boucaut JC. 1998. Role of fibroblast growth factor during early midbrain development in *Xenopus*. *Mech Dev* 78:3–15.
- Sanvito F, Piatti S, Villa A, Bossi M, Lucchini G, Marchisio PC, Biffo S. 1999. The beta4 integrin interactor p27(BBP/eLF6) is an essential nuclear matrix protein involved in 60S ribosomal subunit assembly. *J Cell Biol* 144:823–837.
- Sanvito F, Vivoli Gambini S, Santambrogio G, Catena M, Viale E, Veglia F, Donadini A, Biffo S, Marchisio PC. 2000. Expression of a highly conserved protein p27BBP, during the progression of human colorectal cancer. *Cancer Res* 60:510–516.
- Shinga J, Itoh M, Shiokawa K, Taira S, Taira M. 2001. Early patterning of the prospective midbrain-hindbrain boundary by the HES-related gene XHR1 in *Xenopus* embryos. *Mech Dev* 109:225–239.
- Si K, Maitra U. 1999. The *Saccaromyces cerevisiae* homologue of mammalian translation initiation factor 6 does not function as translation initiation factor. *Mol Cell Biol* 19:1416–1426.
- Vaccaro MC. 2003. Sequencing and characterization of the *Xenopus laevis* ribosomal protein L34 cDNA. *Gene* 318:163–167.
- Varnum SM, Humey CA, Wormington WM. 1992. Maturation-specific deadenylation in *Xenopus* oocytes requires nuclear and cytoplasmic factors. *Dev Biol* 153:283–290.
- Wardle FC, Wainstock DH, Sive HL. 2002. Cement gland-specific activation of the Xag1 promoter is regulated by co-operation of putative Ets and ATF/CREB transcription factors. *Development* 129:4387–4397.
- Wood LC, Ashby MN, Grunfeld C, Feingold KR. 1999. Cloning of murine translation initiation factor 6 and functional analysis of the homologous sequence YPR016c in *Saccaromyces cerevisiae*. *J Cell Biol* 274:11653–11659.

Erratum

M.C. Vaccaro et al. Expression of p27^{BBP}/eIF6 is Highly Modulated During *Xenopus laevis* Embryogenesis. Mol Reprod Dev 73:482–490, 2006. DOI: 10.1002/mrd.20449

The above-mentioned paper contained an error. The correct Figure 1a,b is published below.

a

```

MAVRASFENNNEIGCFAKLTNTYCLVAIGGSENFYSVFEGELSETIPVVHASIAGCRIIG 60
RMCVGNRHGLMVPNNTTDQELQHMRNSLPDSVRIQRVEERLSALGNVIACNDYVALVHPD 120
LDRETEEILADVLRKVEVFRQTIAEQVLVGSYCAFNSNOGGLLHPKTSIEDQDELSSLLQVP 180
LVTGTVNRGSEVIAAGMVVNDWCAFCGLDTTSTELSVIESVFKLSDAHPSTIATSMRGSL 240
IDSLT 245

```

b

| | | |
|------------------------|---|-----|
| <i>X. laevis</i> | MAVRASFENNNEIGCFAKLTNTYCLVAIGGSENFYSVFEGELSETIPVVHASIAGCRIIG | 60 |
| <i>H. sapiens</i> | MAVRASFENNNEIGCFAKLTNTYCLVAIGGSENFYSVFEGELSDTIEVVHASIAGCRIIG | 60 |
| <i>D. melanogaster</i> | MALRVQFENNDDIGVFTKLTNTYCLVAIGGSENFYSFAEAELGDTIEVVHANVGGCRIIG | 60 |
| <i>S. cerevisiae</i> | MATRTQFENSNEIGVFSKLTNTYCLVAVGGSENFYSFAEAELGDAIPIVHTTIA TR IIG | 60 |
| <i>C. elegans</i> | MALRVVDYEGNSDVGVECTLTNSYCLVGVGGTQNFYSILEAESDLIRVVHTSI ASTR IVG | 60 |
| * | | |
| <i>X. laevis</i> | RMCVGNRHGLMVPNN <u>TTDQELQ</u> HMRNSLPD SVRI QRVEERLSALGNVIACNDYVALVHPD | 120 |
| <i>H. sapiens</i> | RMCVGNRHGLMVPNN <u>TTDQELQ</u> HMRNSLPD TVQIR RVVEERLSALGNVTT CNDY VALVHPD | 120 |
| <i>D. melanogaster</i> | RLTVGNRRGLLVPN <u>STTDEELQ</u> HLRNSLPDAVKIYRVEERLSALGNVIACNDYVALVHPD | 120 |
| <i>S. cerevisiae</i> | RMTAGNRRGLLVPTQ TTDQELQHLRNSLPDSVKIQRVEERLSALGNVICNDYVALVHPD | 120 |
| <i>C. elegans</i> | RLTVGNRHGLMVPNN <u>TTDQELQ</u> HLRNSLPD EVAIR RVDERLSALGNVIACNDHVAI VHAE | 120 |
| ◻ | | |
| <i>X. laevis</i> | LDRETEEILADVLRKVEVFRQTIAEQVLVGSYCAFNSNOGGLLHPKTSIEDQDELSSLLQVP | 180 |
| <i>H. sapiens</i> | LDRETEEILADVLRKVEVFRQTIVADQVLVGSYCVFSNOGGLVHPKTSIEDQDELSSLLQVP | 180 |
| <i>D. melanogaster</i> | LDKETEELIADVLRKVEVFRQTIA DN SLVGSYAVLSNOGGMVHPKTSIQDQDELSSLLQVP | 180 |
| <i>S. cerevisiae</i> | IDRETEELISDVLGVEVFRQTISGNILVGSYCSLSNOGGLVHPQTSVQDQDELSSLLQVP | 180 |
| <i>C. elegans</i> | ISAETEIQALVEVLRKVEVFRVSLAQNSLVGSY CILSSNG CLVAART PPETQR EIAALLQIE | 180 |
| ◻ | | |
| <i>X. laevis</i> | LVTGTVNRGSEVIAAGMVVNDWCAFCGLD TTSTEL SVIESVFKLSDAH PSTIAT SMR GSL | 239 |
| <i>H. sapiens</i> | LVAGTVNRGSEVIAAGMVVNDWCAFCGLD TTSTEL SVIESVFKLNEAQ PSTIAT SMR GSL | 239 |
| <i>D. melanogaster</i> | LVAGTVNRGSEVLAAGMVVNDWLSFVGMNTTATEISVIESVFKLNQQA PATV TTKLRAA | 239 |
| <i>S. cerevisiae</i> | LVAGTVNRGSSVVGAGMVVNDYLAVTGLD TTAPE LSVIESIERLQDQA PES ISGNLRDT | 239 |
| <i>C. elegans</i> | VVAGTCNRGSELI GAG MVVNDWVAF CG LD STSTEL SVIESIEFKL EGQA RTSIS NQL RDT | 240 |
| ◻ | | |
| <i>X. laevis</i> | LIDSLT | 245 |
| <i>H. sapiens</i> | LIEDSL | 245 |
| <i>D. melanogaster</i> | LIEDMS | 245 |
| <i>S. cerevisiae</i> | LIE TY S | 245 |
| <i>C. elegans</i> | LIE S ML | 246 |

Fig. 1. a: Deduced amino acid sequence of the cDNA of *X. laevis* p27^{BBP}/eIF6 (EST Bank with accession number AY 383654). The potential transmembrane domain in the N-terminus region (position 21–40) are evidenced, the potential protein kinase C phosphorylation sites are in boldface and the potential glycosylation sites (NNTT and NTTD) are underlined. **b:** Clustal formatted alignment of *X. laevis*

p27^{BBP}/eIF6 with *H. sapiens*, *D. melanogaster*, *S. cerevisiae* and *C. elegans* homologs. The perfectly conserved position are evidenced, the potential protein Kinase C phosphorylation site typical to *X. laevis* or common to mammalian are marked respectively by symbol* and symbol◻.

p27^{BBP}/eIF6 acts as an anti-apoptotic factor upstream of Bcl-2 during *Xenopus laevis* development

N De Marco¹, L Iannone², R Carotenuto¹, S Biffo^{3,4}, A Vitale⁵ and C Campanella^{*1}

p27^{BBP}/eIF6 (β 4-binding protein/eukaryotic initiation factor 6) regulates the joining of 40S and 60S ribosomal subunits, on receptor for activated C kinase 1 binding and protein kinase C phosphorylation in serine 235. In *Xenopus*, p27^{BBP}/eIF6 is abundantly expressed in the majority of the embryonic anlagen. Although p27^{BBP}/eIF6 abundance may be required for a general regulation of protein synthesis, our data suggest that p27^{BBP}/eIF6 may target the translation of specific mRNAs. We injected Xp27^{BBP}/eIF6 mRNA in one blastomere of two-cell-stage embryos and obtained a bent phenotype, the curvature being lateral with respect to the embryo antero-posterior axis. The injected side had fewer apoptotic cells than the uninjected side, whereas cell proliferation appeared unaffected. Accordingly, in Xp27^{BBP}/eIF6 morphants, endogenous apoptosis increased. Injection of Xp27^{BBP}/eIF6 point mutants indicated that the anti-apoptotic action of Xp27^{BBP}/eIF6 requires the conserved S235. The bent phenotype was also obtained with B-cell lymphoma gene-2 (Bcl-2) overexpression and was rescued by Bcl-2-associated X protein (Bax)/Xp27^{BBP}/eIF6 co-injection. In addition, embryos overexpressing Xp27^{BBP}/eIF6 had a higher amount of Bcl-2 and an unchanged amount of Bax with respect to controls. In Xp27^{BBP}/eIF6 morphants, Bcl-2 levels were unaffected and Bax levels were higher than in the controls. Thus, we propose that Xp27^{BBP}/eIF6 is part of a mechanism acting on the specific translation of messengers regulating cell survival. In particular, we suggest that Xp27^{BBP}/eIF6 may regulate the translation of factors upstream of Bcl-2/Bax.

Cell Death and Differentiation (2010) 17, 360–372; doi:10.1038/cdd.2009.128; published online 25 September 2009

Protein p27^{BBP}/eIF6 (β 4-binding protein/eukaryotic initiation factor 6) is a highly conserved regulator of ribosomal function. It regulates the binding of 40S and 60S ribosomal subunits¹ and is necessary for the biogenesis of 60S and cell growth in organisms as diverse as yeast^{2–4} and mammals.⁵ In the latter, p27^{BBP}/eIF6 null mice are lethal before implantation, whereas heterozygous mice, which present 50% reduction of p27^{BBP}/eIF6 levels in all tissues, show a decrease in body mass.⁵ p27^{BBP}/eIF6, when bound to 60S, act as factors preventing 40S and 60S subunits from joining in the 80S assemblage. The assemblage of 80S is regulated by Efl1p in yeast cells³ and by receptor for activated C kinase 1 (RACK1)/protein kinase C (PKC) signaling in mammals. In particular, in mammalian cells, on PKC phosphorylation of serine 235, p27^{BBP}/eIF6 is released from 60S to start translation.⁶ Accordingly, a serine phosphorylated isoform of p27^{BBP}/eIF6 has been found in *Xenopus laevis*,⁷ in which two potential PKC phosphorylation sites have been found, that is, 235 SmR in common with mammals and 91SvR specific to *X. laevis*.^{8,9}

Although p27^{BBP}/eIF6 is an essential gene,¹⁰ its expression is variable. p27^{BBP}/eIF6 mRNA and protein levels are high in rapidly proliferating tumoral cells and low in cells committed to apoptosis.¹¹ In normal mammalian tissues, p27^{BBP}/eIF6 levels are variable among cell types, suggesting that *in vivo* its expression is tightly regulated.^{10,12}

During *Xenopus* embryogenesis, chains of induction bring to the construction of the body anlagen through proliferation, apoptosis and differentiation. In this system, a modulated expression of p27^{BBP}/eIF6 occurs in developing anlagen in addition to a basal level of expression. In particular, p27^{BBP}/eIF6 mRNA is abundant in the eye field and in the mid-hindbrain boundary, two regions with high proliferation levels.^{8,9} Recently, the study of p27^{BBP}/eIF6 has gained new interest because this protein seems to regulate the translation of specific mRNAs such as β -catenin mRNA, thus modulating the fundamental signaling of the Wnt/ β -catenin pathway.¹³ Moreover, it has been proposed that p27^{BBP}/eIF6 functions in miRNA-mediated post-transcriptional silencing because it is part of RNA-induced silencing complex (RISC)

¹Department of Structural and Functional Biology, University of Naples Federico II, Naples, Italy; ²AMRA Center of Competence, University of Naples Federico II, Naples, Italy; ³Department of Science and Advanced Technology, University of Eastern Piedmont, 'Amedeo Avogadro', Alessandria, Italy; ⁴DIBIT and University Vita-Salute San Raffaele Milan, Milan, Italy and ⁵TIGEM, Naples, Italy

*Corresponding author: C Campanella, Department of Structural and Functional Biology, University of Naples Federico II, Naples, Italy.

Tel: + 39 081 679200; Fax: + 39 081 679233; E-mail: chiara.campanella@unina.it

Keywords: p27^{BBP}/eIF6; *Xenopus laevis*; apoptosis; Bcl-2/Bax

Abbreviations: A-P, antero-posterior axis; Bax, Bcl-2-associated X protein; Bcl-2, B-cell lymphoma gene-2; BrdU, 5-bromo-2'-deoxyuridine; BSA, bovine serum albumin; D-V, dorsoventral axis; DAPI, 4'-6-diamidino-2-phenylindole; DTT, dithiothreitol; e, eye; EGTA, ethylene glycol tetraacetic acid; enc, encephalon; end., endoderm; GFP, green fluorescent protein; H, head; HEPES, N-2-hydroxyethylpiperazine-N-2-ethanesulfonic acid; HUA, hydroxyurea and aphidicolin; i.s., injected side; m, mitome; mo, morpholino; nc, notochord; ot.v, otic vesicle; p27^{BBP}/eIF6, β 4-binding protein/eukaryotic initiation factor 6; PARP, poly (ADP-ribose) polymerase; PBS, phosphate-buffered saline; ph, pharynx; pH3, phospho histone 3; PKC, protein kinase C; RACK1, receptor for activated C kinase 1; SBTI, soybean trypsin inhibitor; SDS-PAGE, SDS-polyacrylamide gel electrophoresis; sp.c., spinal cord; RT-PCR, reverse transcriptase-PCR; T, tail; TAME, N₂-(p-toluene sulfonyl)-L-arginine methyl ester; Tris, hydroxymethyl aminomethane

Received 28.11.08; revised 24.6.09; accepted 03.8.09; Edited by P Bouillet; published online 25.9.09

and as such, in *Caenorhabditis elegans*, it specifically represses the translation of LIN-14 and LIN-28 mRNAs without an effect on the general translation.¹⁴ In other experimental systems, p27^{BBP}/eIF6 is not necessary for miRNA-based translational repression.¹⁵ To reveal whether p27^{BBP}/eIF6 has a qualitative role in gene expression, we studied the effects of ectopic overexpression of p27^{BBP}/eIF6 in *X. laevis* development

The analysis of a mutated phenotype stemming out from our study has highlighted a novel function for p27^{BBP}/eIF6: its potential role as an apoptosis inhibitor. Apoptosis is physiologically required for normal development during *Xenopus* embryogenesis, where it occurs with a reproducible pattern, starting from late gastrulation.¹⁶ In addition to its general role in controlling the cell number in developing anlagen, apoptosis participates in the process of neural determination,¹⁷ and is essential for several processes including the removal of the tail in anurans during metamorphosis and of the interdigital membrane in the developing vertebrate limb.¹⁸ Here, we show that p27^{BBP}/eIF6 although overexpression does not induce an increase in cell number, it does induce a decrease in apoptotic nuclei. A similar effect is seen by B-cell lymphoma gene-2 (Bcl-2) overexpression.

p27^{BBP}/eIF6 overexpressing embryos showed an increase of Bcl-2 that was not found in p27^{BBP}/eIF6 morphants. In addition, although p27^{BBP}/eIF6 overexpression did not modify the levels of Bcl-2-associated X protein (Bax) expression, in the morphants, Bax mRNA and protein levels are higher than in the controls, suggesting that p27^{BBP}/eIF6 may be upstream in the same apoptotic pathway. Moreover, the S235A p27^{BBP}/eIF6 mutant lacked an anti-apoptotic function, indicating that S235A is the site responsible for this function and suggesting that the anti-apoptotic role of p27^{BBP}/eIF6 relies on its ribosome anti-associative function.

Results

p27^{BBP}/eIF6 overexpression causes bending of the embryo. We injected Xp27^{BBP}/eIF6 mRNA (from 100 pg to 500 pg) together with green fluorescent protein (GFP) mRNA (300 pg) in one blastomere of the two-cell-stage *X. laevis* embryos to investigate the effects of its overexpression. Given that the first cleavage plane divides the embryo in two symmetrical halves, in these experiments the uninjected side can be considered as the natural control of each test. Xp27^{BBP}/eIF6 expression was controlled by immunofluorescence or western blot analysis with a specific anti-p27^{BBP}/eIF6 antibody and consistently indicated that the injected part was expressing more protein as opposed to the uninjected part (Figure 1). Two days after injection, about 40% of st.28 embryos showed a marked bending lateral with respect to the antero-posterior axis of the embryo and the embryos became ring-shaped. The external, concave side derived from the injected blastomere, as this side was marked by GFP fluorescence ($n=80$) (Figures 2a–c). This phenotype was transient and recovered at stage 35.

Control experiments showed that the single injection of GFP mRNA at the concentration described above did not produce bent embryos or defective phenotypes

(see Figure 2a). When Xp27^{BBP}/eIF6 mRNA was injected before cleavage, at one-cell stage, no bending occurred in st.28 embryos (Figures 2d and e), indicating that the bent phenotype occurs when the mRNA is injected only on one side of the embryo. Previous data have shown that the endogenous Xp27^{BBP}/eIF6 is abundantly expressed in somites.^{8,9} Accordingly, to investigate whether the bending might be due to defects of number, position or dimension of the somite metameric pattern, we performed whole-mount immunohistochemistry using an antibody directed against the myotome protein 12/101, a somite marker. No difference or defect was observed in the somites between the injected and the control side (Figure 2f), suggesting that the bent phenotype was because of an unbalanced number of cells with respect to the embryo symmetry plane.

p27^{BBP}/eIF6 overexpression does not increase proliferation. As Xp27^{BBP}/eIF6 is particularly abundant in territories showing high proliferation,^{8,9} we asked ourselves whether p27^{BBP}/eIF6 overexpression causes an increase in cell number on the injected side. First, we counted the nuclei number in 4'-6-diamidino-2-phenylindole (DAPI)-stained p27^{BBP}/eIF6 overexpressors. In Figures 3a–d, counts were performed in serial sections of embryos ($n=15$, $P<0.05$), in areas of 3000 μ^2 settled through the Leica, Wetzlar, Germany, Laser Microdissection LMD V6.5 software. The number of cells was higher on the side of injection compared with the uninjected side (Figure 3d), whereas in embryos injected with GFP alone ($n=15$, $P<0.05$), there was no difference between the number of nuclei counted on the injected and uninjected sides of the embryo (Figure 3e–h).

The embryos injected with Xp27^{BBP}/eIF6 were then tested for 5-bromo-2'-deoxyuridine (BrdU) incorporation. At 2 h after BrdU injection (see Viczian *et al.*¹⁹), the embryos were fixed and cryostat-sectioned. We further stained the serial sections with antibodies against BrdU or phospho histone 3 (pH3), markers of mitotic cells. No difference was detected in BrdU-positive cells on the injected side compared with the uninjected side (Figures 3j). Counts of pH3-positive nuclei in embryos entirely sectioned showed no significant difference in the number of cycling cells between the control and injected side ($n=30$, $P<0.05$) (Figure 3k and l). Taken together, these results suggest that p27^{BBP}/eIF6 overexpression does not lead to an increase of cells in the S phase. Therefore, the observed increase in cell numbers leading to the bent phenotype may be due to differences in the cell survival rates on the two sides of the embryo, rather than proliferation.

Overexpression of p27^{BBP}/eIF6 reduced endogenous apoptosis in embryos. During *Xenopus* development, apoptosis is first detected at gastrulation and later in development, during the tailbud stage when it is found in the developing brain, eyes, spinal cord and tail.²⁰ The TUNEL assay has proved to be effective and specific for detecting apoptosis in *Xenopus* embryos^{16,20} as in other systems.²¹ We thus compared the incidence of TUNEL-positive nuclei on the side of the embryos overexpressing p27^{BBP}/eIF6 compared with the control side. The labeled apoptotic nuclei were largely on the control side, whereas the injected side showed little apoptosis, as observed in whole-mount

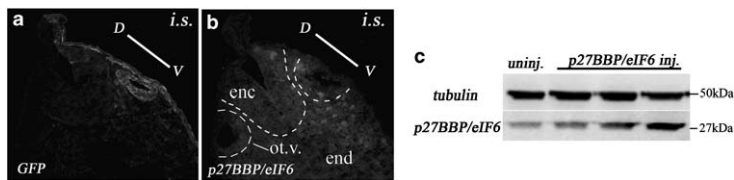


Figure 1 Xp27^{BBP}/eIF6 overexpression. In serial cross-sections of Xp27^{BBP}/eIF6 and GFP-injected embryos, the injected side is immunostained with anti-GFP (a) and with anti-p27^{BBP}/eIF6 antibodies (b). In the latter case, the lower level of immunostaining is on the uninjected side indicating the w.t. expression of Xp27^{BBP}/eIF6. enc, encephalon; ot.v, otic vesicle; end, endoderm. (c) Western blot with anti-p27^{BBP}/eIF6 antibody indicates the major presence of protein in p27^{BBP}/eIF6-injected embryos with respect to uninjected embryos. Three sets of injected embryos were used in the blot. Normalization was performed with anti- α -tubulin antibody. D-V, dorsoventral axis. The injected side is indicated (i.s.)

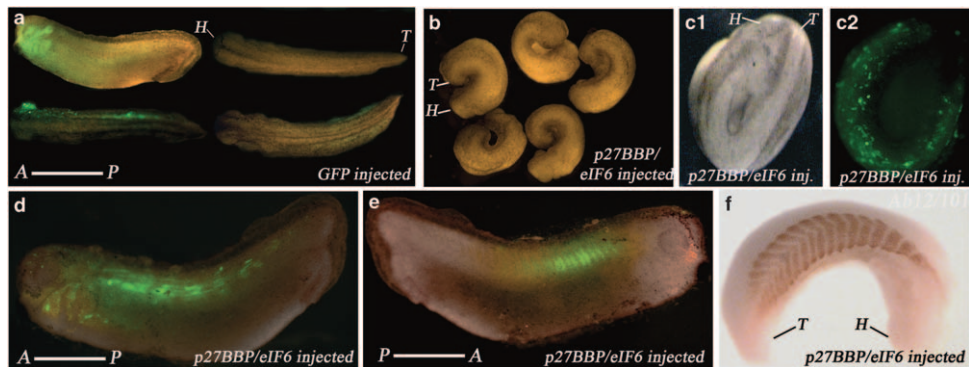


Figure 2 Effects of Xp27^{BBP}/eIF6 overexpression. Compared with GFP-injected embryos (a) (lateral and dorsal view), 40% of the Xp27^{BBP}/eIF6 overexpressing embryos showed a bent phenotype at st.28 (b), the side deriving from the injected blastomere being the external and concave side (c1) marked by GFP fluorescence (c2). When Xp27^{BBP}/eIF6 injection was performed at one-cell stage (d–e), no bending occurred in the embryos, suggesting that the bent phenotype occurs when Xp27^{BBP}/eIF6 is overexpressed only on one side of the embryos. Micrographs of the two sides (d–e) of the same embryo are given. Whole-mount immunohistochemistry with 12/101 antibody showed no defects in size, number and morphology of the somite metameric pattern (f). H, head; T, tail; D-V, dorsoventral axis

embryos and related sections (Figures 4a and b). We made counts of TUNEL-positive nuclei in sections of injected embryos fixed at stage st.28 and entirely sectioned (Figures 4c and d). We found a significantly lower percentage of apoptotic nuclei on the Xp27^{BBP}/eIF6-injected side compared with the control side ($n = 30$, $P < 0.05$) (Figure 4e). We did not see differences in control embryos, either uninjected or injected uniquely with GFP mRNA ($n = 15$, $P < 0.05$) (Figure 4f).

Caspase 3 is a polypeptide of 32 kDa that releases an active peptide of 18 kDa on cleavage.²² During apoptosis, the 116 kDa form of the poly (ADP-ribose) polymerase (PARP1) is cleaved to form a peptide of 85 kDa.²³ We carried out western blots to analyze the executioner caspase 3 and PARP1 cleavage. Xp27^{BBP}/eIF6-injected embryos showed less active caspase 3 and more uncleaved PARP1 than did uninjected or GFP-injected embryos (Figure 4g and h).

These results indicate that Xp27^{BBP}/eIF6 overexpression exerts an anti-apoptotic action contrasting the physiologically occurring apoptosis during *X. laevis* embryogenesis.

We further checked whether p27^{BBP}/eIF6 downregulation of apoptosis depended on cell cycling, by treating the injected embryos with hydroxyurea and aphidicolin (HUA), which inhibits DNA synthesis in the early S phase of the cell cycle.²⁴ Despite the decline in cell proliferation as shown by anti-pH3 staining of HUA-treated embryos, we observed a decrease in the number of apoptotic cells on the side overexpressing Xp27^{BBP}/eIF6 (Figures 5a–c). We conclude that the anti-apoptotic effect of Xp27^{BBP}/eIF6 is independent of cell cycling.

Downregulation of Xp27^{BBP}/eIF6 increases endogenous apoptosis. We injected Xp27^{BBP}/eIF6 morpholino (7.5 ng) together with GFP mRNA (200 pg) in one blastomere of a two-cell-stage *X. laevis* embryos to investigate the effects of p27^{BBP}/eIF6 downregulation. As a control, a mispaired morpholino (7.5 ng) was injected together with GFP mRNA (200 pg) to distinguish the specific effects of Xp27^{BBP}/eIF6 morpholino injection. The p27^{BBP}/eIF6 downregulation was monitored by immunofluorescence or western blot analysis with the anti-p27^{BBP}/eIF6 antibody (data not shown).

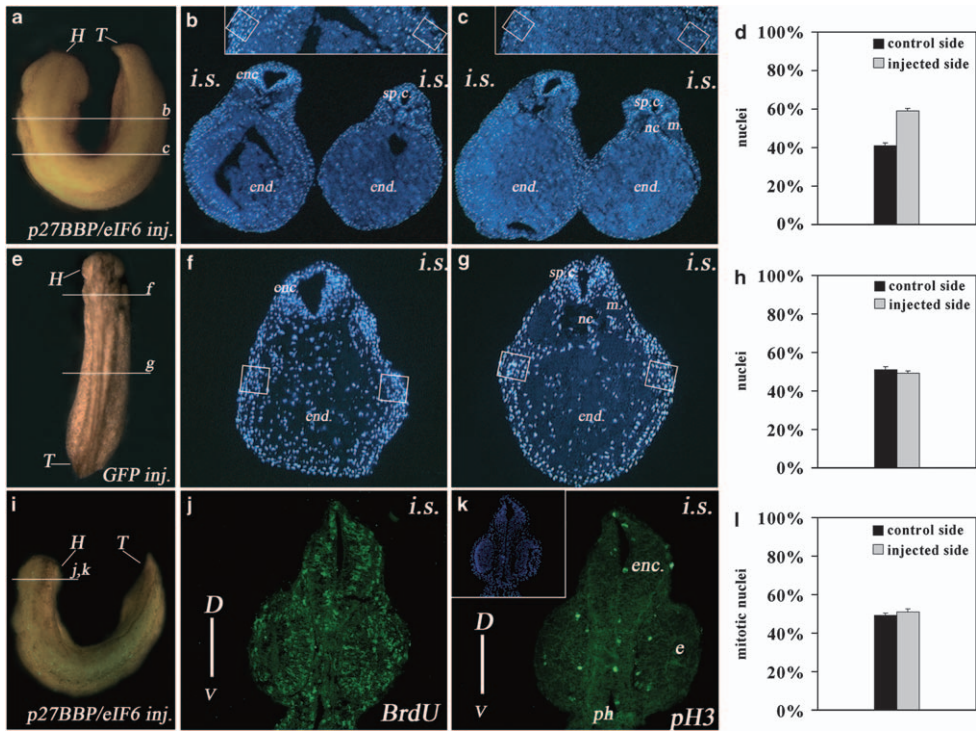


Figure 3 Proliferation assays on Xp27^{BBP}/eIF6 overexpressing embryos. DAPI staining was carried out in bent embryos overexpressing Xp27^{BBP}/eIF6 (a-c). Panels b and c show embryo sections cut as shown in a. DAPI-stained nuclei were counted in 3000 μ^2 areas, as indicated in panels b and c insets. The nuclei number is higher on the injected side than on the uninjected side (d). The counts are statistically significant ($n = 15$, $P < 0.05$). (e-g) DAPI staining in embryos injected uniquely with GFP. Counts of nuclei in sections cut as shown in (e) indicate no differences in cell number between the uninjected and the GFP-injected side (h) ($n = 15$, $P < 0.05$). (i-l) Panels j and k are sections of Xp27^{BBP}/eIF6 overexpressors cut as shown in (i). (j-k) Immunolocalization of anti-BrdU and anti-pH3 antibodies on the serial section of an Xp27^{BBP}/eIF6-overexpressing embryo (injected with BrdU at st.28). No difference was detected in BrdU- or pH3-positive cells (k) on the injected side, compared with cells of the uninjected side. Nuclei are contrasted with DAPI (inset in k). (l) Counts of pH3-positive nuclei on a section of Xp27^{BBP}/eIF6-overexpressing embryos showed no difference in cells in mitosis between the injected and control sides ($n = 30$, $P < 0.05$). D-V, dorsoventral axis. The injected side is indicated (i.s). enc, encephalon; e, eye; ph, pharynx; sp.c., spinal cord; nc, notochord; end., endoderm; m, miotome

Although the morpholino control injection did not produce defective phenotypes (Figure 6a), about 50% of st.28 morpholino-injected embryos showed a bent phenotype symmetrical to the phenotype obtained by Xp27^{BBP}/eIF6 overexpression, as the embryos were bent with the concave, external side opposite to the injected side (Figure 6b). TUNEL assay showed a major percentage of apoptotic nuclei on the morpholino-injected side compared with the uninjected one ($n = 20$, $P < 0.05$) (Figures 6c,d and g), thus confirming the anti-apoptotic role of Xp27^{BBP}/eIF6.

In eIF6^{+/-} adult mice, specific organs, that is, the liver and fat body, display reduction of cell proliferation.⁵ Thus, we asked whether in Xp27^{BBP}/eIF6 morphants a general decrease in cell proliferation could be observed. Data show that embryos injected with Xp27^{BBP}/eIF6 morpholino and GFP on the one side and with mispaired morpholino

(Figures 6e and f) on the opposite side had no differences in the number of anti-pH3-positive nuclei ($n = 20$, $P < 0.05$) (Figure 6h). It should be noted, however, that specific counts in hepatocytes and fat cells could not be performed in adult *Xenopus* to parallel the eIF6^{+/-} mice observations.⁵ Indeed, in *Xenopus* embryos, liver cells differentiate at stage 46,²⁵ when the bent phenotype had recovered and fat cells appear following metamorphosis (see Rot-Nikcevic and Wassersug²⁶).

S235A mutant loses the anti-apoptotic function. *X. laevis* p27^{BBP}/eIF6 cDNA has two serine embedded in a PKC consensus phosphorylation site: one is serine 235 and is conserved in mammals, and the other is serine 91 and is typical of *Xenopus*.^{8,9} In mammalian cells, translation occurs when p27^{BBP}/eIF6 is released from 60S following

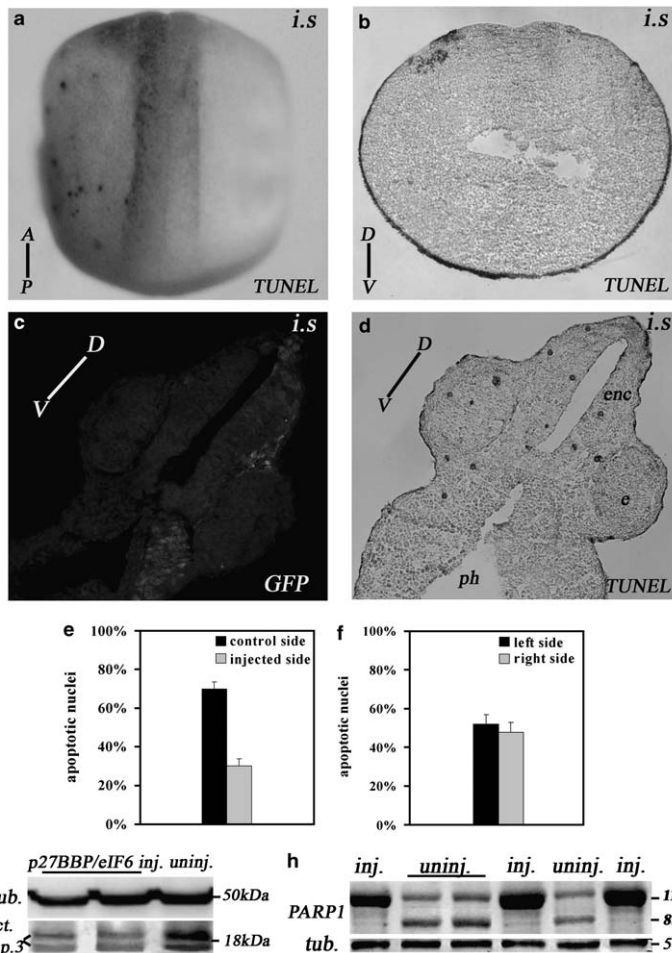


Figure 4 Apoptosis assays on embryos overexpressing Xp27^{BBP}/eIF6. (a) Whole-mount TUNEL staining was performed on Xp27^{BBP}/eIF6-injected st.19 embryo (neural plate stage). (b) Cross paraffin section taken from the anteriormost part of the TUNEL-stained embryo showed in a. (c) st.28 embryo overexpressing Xp27^{BBP}/eIF6, as observed by anti-GFP staining. (d) TUNEL staining on section of same embryo. Enc, encephalon; e, eye; ph, pharynx. The injected side showed less apoptosis compared with the control side, as counted in (e). Differences between injected and control sides are statistically significant ($n = 30$, $P < 0.05$). (f) TUNEL-labeled nuclei were counted in uninjected embryos and no significant difference in apoptotic nuclei was observed between the left and right sides ($n = 15$, $P < 0.05$). In the ordinates of panels e and f histograms, as well as in histograms of subsequent figures, the percentages are reported of apoptotic cells with respect to the total number of counted apoptotic cells (100%). (g and h) Western blots of st.28 Xp27^{BBP}/eIF6-injected and uninjected embryos exposed to anti-active caspase 3 specific for the cleaved form (g) or to anti-PARP1 (h) antibodies. Xp27^{BBP}/eIF6 overexpressing embryos showed less active caspase 3 (18 kDa) and cleaved PARP1 (85 kDa) compared with the uninjected ones. Normalization was performed with an anti- α -tubulin antibody. In the caspase 3 western blot, the effect of Xp27^{BBP}/eIF6 was underestimated because lysates were used, deriving from experiments in which the injection was performed in one blastomere of stage 2 embryos, thereby containing both the injected and control sides. In the PARP1 western blots, lysates were used, deriving from the injection of one-cell embryo. A-P, antero-posterior axis; D-V, dorsoventral axis

phosphorylation in Ser235 through the RACK1-PKC pathway. S235A mutants impair RACK1/PKC-mediated phosphorylation.⁶ We performed injections of p27^{BBP}/eIF6 single mutants (S235A or S91A) into one blastomere of two-cell-stage *Xenopus* embryos. The mutant's overexpression was

confirmed by immunofluorescence or western blot analysis with anti-p27^{BBP}/eIF6 antibody (data not shown). When we injected S235A mRNA, the embryos did not show the bent phenotype ($n = 70$) (Figure 7a1), as for embryos injected uniquely with GFP (Figure 7a2). TUNEL assay and counts of

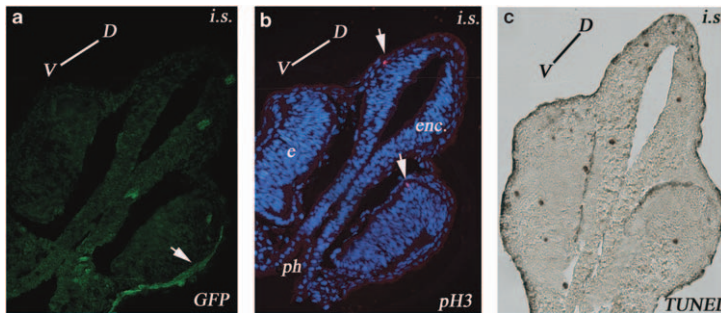


Figure 5 Embryos injected with Xp27^{BBP}/eIF6 were treated with HUA at st.28 and the effects of such treatment on apoptosis were analyzed. (a) The injected side of the embryos is labeled with GFP (arrow). (b) Section of the same embryo as in panel a exposed to anti-pH3 and DAPI. The HUA treatment dramatically reduced anti-pH3 staining (arrows). Enc, encephalon; e, eye; ph, pharynx. (c) TUNEL staining showed a decrease in positive nuclei on the Xp27^{BBP}/eIF6-injected side compared with the control side, indicating that apoptosis inhibition is independent from cell cycling. A-P, antero-posterior axis. The injected side is indicated (i.s.)

apoptotic nuclei indicated no difference in apoptotic nuclei between the injected and control sides ($n=30$, $P<0.05$) (Figure 7c; data not shown). When we injected S91A mRNA, st.28 embryos showed the ring-shaped phenotype ($n=90$) (Figure 7b) and a decrease in TUNEL-stained nuclei on the injected side ($n=30$, $P<0.05$) (Figure 7d; data not shown). We then carried out western blots to analyze caspase 3 activation and PARP1 cleavage in these samples. In S235A mRNA-injected-embryos, the levels of active caspase 3 and cleaved PARP1 were unaffected compared with uninjected embryos (Figures 7e and f). S91A mRNA-injected-embryos instead showed a decrease of active caspase 3 and cleaved PARP1 compared with uninjected and S235A mRNA-injected-embryos (Figures 7e and f).

Taken together, these results indicate that Ser 235 is the site responsible for the anti-apoptotic function of p27^{BBP}/eIF6.

Xp27^{BBP}/eIF6 regulation of Bcl-2/Bax levels. Members of the Bcl-2 family are key regulators in apoptosis, acting either as pro- or anti-apoptotic factors. Bcl-2 and Bax proteins are part of the core apoptotic machinery. At the functional level, Bcl-2 inhibits apoptosis whereas Bax promotes it, although the final decision of a cell to execute the cell death program depends on the balance among all the proteins of the apoptotic machinery.^{27,28} In *X. laevis* early embryogenesis, Bcl-2 mRNA injection dramatically inhibits apoptosis, whereas Bax mRNA injection moderately promotes it.²⁹

When we injected 300 pg of mRNA encoding Bcl-2 in one blastomere of two-cell-stage embryos, at st.28 these embryos showed the same ring-shaped phenotype as the one observed with Xp27^{BBP}/eIF6 overexpression, being the external side of the embryos marked by GFP fluorescence (Figure 8a and b, embryos injected uniquely with GFP). TUNEL staining and counts of apoptotic nuclei showed that the Bcl-2 overexpression strongly inhibits apoptosis, as expected,²⁹ whereas pH3 immunofluorescence and counts of mitotic nuclei showed that proliferation is unaffected (data not shown).

To investigate whether p27^{BBP}/eIF6 alters the level of endogenous Bcl-2 and Bax proteins, we carried out western blots, using anti-Bcl-2 and anti-Bax antibodies. Embryos overexpressing Bcl-2 showed an increase of Bcl-2 protein levels compared with uninjected embryos or embryos uniquely expressing GFP (Figure 8c), whereas Xp27^{BBP}/eIF6 levels were unaffected (data not shown). Embryos overexpressing p27^{BBP}/eIF6 also showed an increase of Bcl-2 but not of Bax protein levels, with respect to uninjected embryos (Figures 8c and d). In contrast, p27^{BBP}/eIF6 morphants showed an increase of Bax but not of Bcl-2 protein levels compared with uninjected embryos or embryos expressing mispaired morpholino control (Figure 8e). Then, we carried out analysis of Bcl-2 and Bax mRNA levels in p27^{BBP}/eIF6 overexpressors and morphants to investigate whether p27^{BBP}/eIF6 similarly regulates Bcl-2/Bax expression. In Xp27^{BBP}/eIF6-overexpressing embryos, the level of Bcl-2 mRNA increased, whereas the Bax level was unaffected. In morphants, an increase of Bax mRNA occurred, whereas Bcl-2 was unaffected (Figure 8f).

Further, we carried out experiments to rescue the p27^{BBP}/eIF6-induced phenotype by co-injecting Xp27^{BBP}/eIF6 mRNA (300 pg) and Bax mRNA (300 pg or 1 ng), together with the GFP mRNA (300 pg). The phenotypes of the injected embryos were not bent, similar to the embryos injected uniquely with GFP (Figure 9a). In addition, a small percentage (2–3%) of the injected embryos ($n=60$) were bent with the concave, external side opposite to the injected side (Figure 9b). This phenotype was symmetrical to the phenotype obtained by Bcl-2 overexpression and identical to the phenotype obtained by p27^{BBP}/eIF6 downregulation. Western blots using anti-p27^{BBP}/eIF6 or anti-Myc antibodies on extracts of embryos injected with Xp27^{BBP}/eIF6/bax mRNAs indicated that the embryos were successfully expressing both proteins (data not shown). pH3 immunofluorescence and counts of mitotic nuclei showed that Bax overexpression had no effects on cell proliferation (data not shown). TUNEL staining and counts of apoptotic nuclei showed that co-injection of Bax mRNA and Xp27^{BBP}/eIF6 reversed the

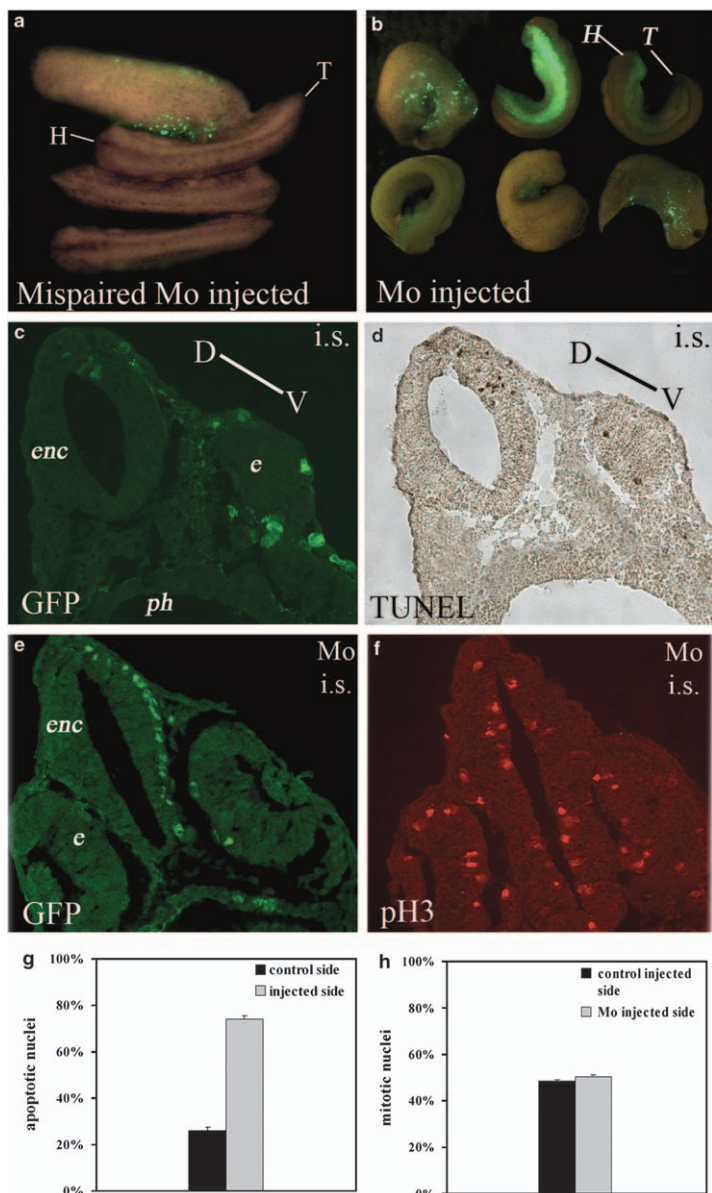


Figure 6 Effects of Xp27^{BBP}/eIF6 downregulation. (a) Control embryos injected with mispaired morpholino and GFP (lateral and dorsal views). (b) Morpholino-injected embryos have an inverted phenotype with respect to the one obtained by Xp27^{BBP}/eIF6 overexpression. In fact, the injected side marked by GFP fluorescence is the internal side of the bent embryo. (c and d) Sections of morpholino-injected embryo, in (c) GFP immunofluorescence on the injected side, in (d) TUNEL and counts of labeled nuclei. Apoptotic cells are more abundantly present on the injected side (i.s.) ($n=20$, $P<0.05$). (e and f) Embryos injected with morpholino and GFP on one side (Mo i.s.) and with mispaired morpholino on the opposite side. (f and h) Counts of pH3-positive nuclei show no difference in mitotic cells between the two sides of the embryo ($n=20$, $P<0.05$). H, head; T, tail; enc, encephalon; e, eye; ph, pharynx; D-V, dorsoventral axis

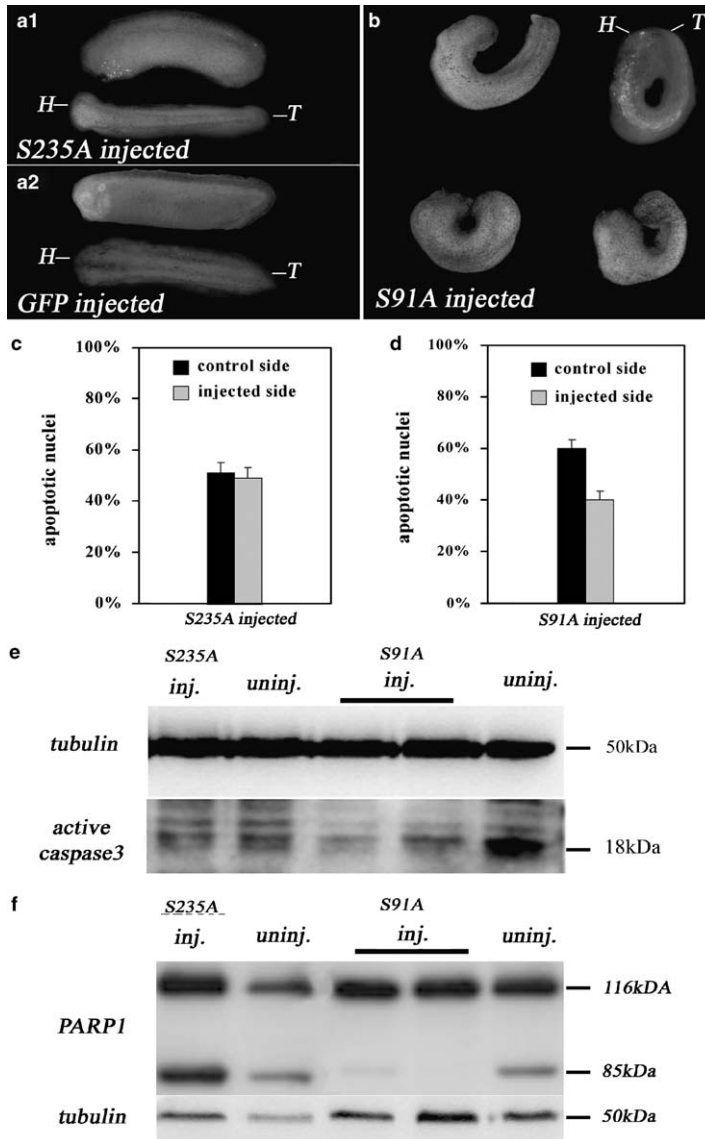


Figure 7 Effects of Xp27^{BBP}/eIF6 mutant overexpression. (a1) S235A-injected embryos displaying non-bending as for embryos injected uniquely with GFP (a2) (lateral and dorsal views). (b) In all, 38% of S91A-injected embryos ($n=90$) showed the curve-shaped phenotype as the one caused by Xp27^{BBP}/eIF6 w.t. overexpression, with the external concave side marked by GFP. H, head; T, tail. (c) In S235A-injected embryos ($n=70$), counts of TUNEL-positive nuclei indicate no difference in apoptosis between the injected and control sides ($n=30$, $P<0.05$). (d) TUNEL staining and counts of apoptotic nuclei showed a decrease in apoptosis on the injected side, compared with the control side ($n=30$, $P<0.05$). (e) S91AmRNA-injected embryos showed a decrease of active caspase 3 (18 kDa) compared with uninjected and S235A mRNA-injected embryos. (f) S91A-injected embryos showed more intact PARP1 compared with uninjected and S235A-injected embryos. Normalization was performed with the anti- α -tubulin antibody. In the caspase 3 western blot, the effect of Xp27^{BBP}/eIF6 was underestimated because lysates were used, deriving from experiments in which the injection was performed in one blastomere of stage 2 embryos, thus containing both the injected and control sides. In the PARP1 western blots, lysates were used, deriving from the injection of the one-cell embryo

inhibition of apoptosis produced by injecting Xp27^{BBP}/eIF6 alone, as the number of apoptotic cells on the injected side was higher than on the uninjected side ($n = 30$, $P < 0.05$) (Figures 9c–e). When we co-injected the mRNA of S235A-mutated Xp27^{BBP}/eIF6 with Bax mRNA, the number of embryos ($n = 48$) showing a symmetrical phenotype increased to 5 (data not shown). Altogether, these data indicate that Bax is able to reverse the anti-apoptotic

action of p27^{BBP}/eIF6 and suggest that p27^{BBP}/eIF6 acts upstream of Bcl-2/Bax machinery in apoptosis control.

Discussion

p27^{BBP}/eIF6 function in regulating protein synthesis⁶ may explain why it is abundant in growing or differentiating tissues. In fact, high expression of p27^{BBP}/eIF6 is expected to occur according to the increased need of protein synthesis regulation along differentiation, cell growth and proliferation. Major expression of Xp27^{BBP}/eIF6 was indeed observed during *X. laevis* embryonic development, in particular in the trunk region and in the brain.^{8,9} Major expression of p27^{BBP}/eIF6 is similarly reported for a variety of somatic cells (see Donadini *et al.*¹⁰). Moreover, a study by Sanvito *et al.*¹¹ showed that in cells progressing to malignancy, p27^{BBP}/eIF6 is extremely overexpressed while being downregulated in tissues progressing to apoptosis.

Here, we studied a phenotype resulting from overexpressing Xp27^{BBP}/eIF6 in *X. laevis* embryos and found that Xp27^{BBP}/eIF6 is involved in protection from apoptosis, thus lending support to the predictions of Sanvito *et al.*¹¹ for cells progressing to apoptosis. We did not observe an increase in cell proliferation following p27^{BBP}/eIF6 overexpression, implying that endogenous Xp27^{BBP}/eIF6 suffices for cell cycle progression. In conditions of Xp27^{BBP}/eIF6 downregulation, our mitosis assays in Xp27^{BBP}/eIF6 morphants did not show differences in cell proliferation with respect to control conditions. The situation is different from what is observed in eIF6^{+/-} adult mice, where a decrease of 50% in the levels of all tissues was accompanied by a reduction in cell proliferation in the liver, fat cells and cultured fibroblasts.⁵ The difference in these two observations may be due to several reasons: (i) the different way in which eIF6 was depleted, chronic in mice *versus* acute in *Xenopus*; (ii) different organs and time points analyzed; (iii) species-specific differences. It is, however, possible that eIF6 depletion may affect the translation of different classes of mRNA in different tissues, depending on the relative abundance of each mRNA, and that the phenotypic effects are the result of reaching thresholds that may vary among tissues.

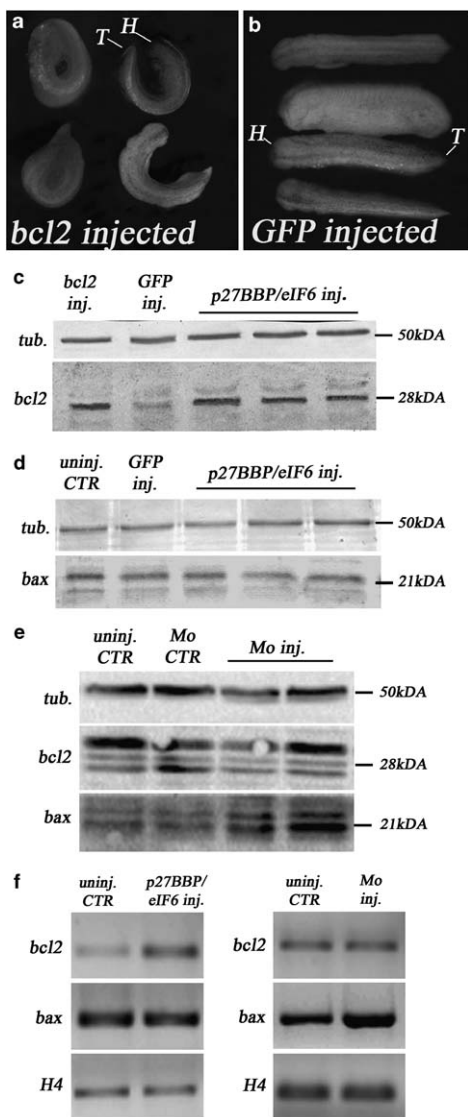


Figure 8 Effects of Xp27^{BBP}/eIF6 on the Bcl-2/Bax levels. (a) In all, 50% of embryos unilaterally injected with Bcl-2 mRNA show at st.28 the same bent phenotype as the one caused by Xp27^{BBP}/eIF6 overexpression, with the external side marked by GFP ($n = 60$). (b) Control embryos injected uniquely with GFP, lateral and dorsal views. (b–e) Western blots with anti-Bcl-2 or anti-Bax antibodies. Three sets of Xp27^{BBP}/eIF6-injected embryos (st.28) were used in the blots in panels c and d. (c) Bcl-2 or Xp27^{BBP}/eIF6-injected-embryos showed an increase of Bcl-2 protein compared with uninjected embryos. (d) The level of Bax was unaffected in embryos overexpressing Xp27^{BBP}/eIF6, as well as in uninjected embryos. (e) Levels of Bcl-2 and Bax were analyzed in embryos injected with p27^{BBP}/eIF6 morpholino or mispaired morpholino control. An increase of Bax but not of Bcl-2 protein levels was shown, compared with uninjected embryos or embryos expressing mispaired morpholino. Normalization was performed with the anti- α -tubulin antibody. (f) Analysis of Bcl-2 and Bax mRNA levels in p27^{BBP}/eIF6 overexpressors and morphants, compared with levels in uninjected embryos. In Xp27^{BBP}/eIF6-overexpressing embryos, the level of Bcl-2 mRNA increased, whereas the Bax mRNA level was unaffected. In morphants, an increase of Bax mRNA occurred, whereas Bcl-2 mRNA was unaffected. Normalization was performed using H4 primers. These data underestimate the effect of Xp27^{BBP}/eIF6 because entire embryos were used for the blots and RT-PCR preparation

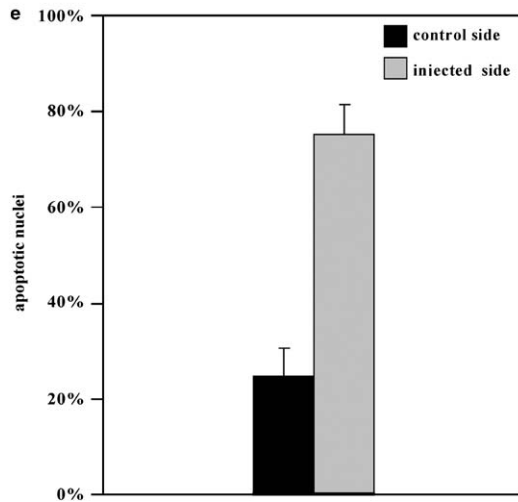
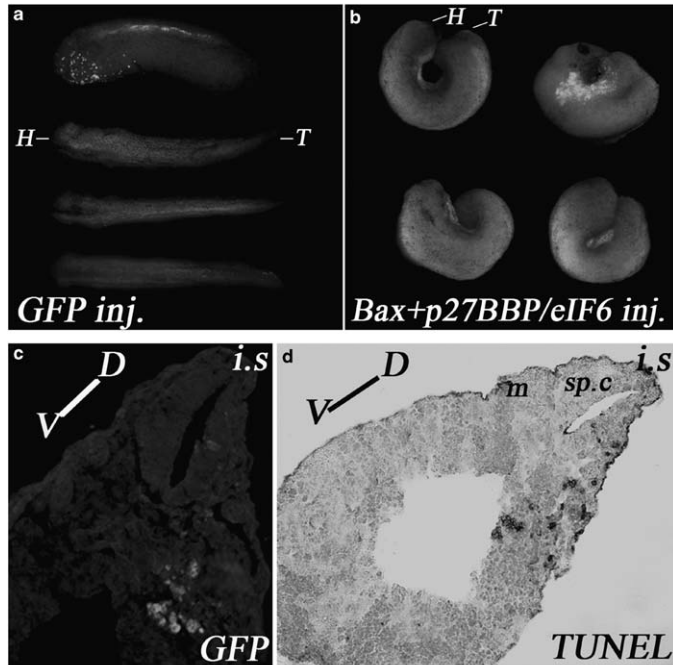


Figure 9 Bcl-2-associated X protein (Bax) rescues embryos injected with Xp27^{BBP}/eIF6. (a) Control embryos injected uniquely with GFP (lateral and dorsal views). Embryos ($n = 60$) co-injected in one blastomere at two-cell stage with Xp27^{BBP}/eIF6 and Bax are not curved, yet in 2–3% of the co-injected embryos, an inverted phenotype with respect to the one obtained by injecting only Xp27^{BBP}/eIF6 is observed. The embryos were bent, but the external side originated from the uninjected blastomere (b). H, head; T, tail. (c–e) On the injected side, marked by GFP (c), TUNEL staining (d) and counts (e) showed that the labeled apoptotic nuclei are more abundant on the injected side, compared with the control side ($n = 30$, $P < 0.05$). m, mitome; sp.c., spinal cord; A-P, antero-posterior axis. The injected side is indicated (i.s)

In many vertebrates, apoptosis is needed for the correct development of embryonic structures of several organisms, both at the beginning of embryogenesis and in the morphogenesis of anlagen, such as the limb and kidney, as well as the nervous system.^{30,31} In *X. laevis*, apoptosis is active in the embryo starting at the beginning of gastrulation and its spatio-temporal pattern has been thoroughly described until the tadpole stage.²⁰ Cell death and cell survival are regulated by complex and interacting signals. Data by Finkielstein *et al.*³² and Yeo and Gautier¹⁷ have indicated that, in *X. laevis*, after MBT, Bcl-2 and Bax balance and downstream caspase activation are the main mechanisms involved in the control of apoptosis. These step-by-step controlled mechanisms converge eventually to a yes-or-no result that can be experimentally reverted. Accordingly, our data indicate that Xp27^{BBP}/eIF6 overexpression is able to shift the program of cell death to cell survival, as shown by TUNEL staining, caspase 3 activation and PARP1 cleavage. Consistently, p27^{BBP}/eIF6 loss-of-function experiments elicit an increase in apoptosis accompanied by reversal of the phenotype. By overexpressing the mRNA of the anti-apoptotic factor Bcl-2, a bent phenotype was found as in the embryos injected with Xp27^{BBP}/eIF6 mRNA, and consistent differences in apoptotic cell number were detected between the injected and uninjected sides of the embryos. Xp27^{BBP}/eIF6 appears to be upstream in the Bcl-2 apoptotic pathway because Xp27^{BBP}/eIF6 overexpressing embryos show an increase of Bcl-2 mRNA and protein, which does not occur in Xp27^{BBP}/eIF6 morphants. Consistently, although Xp27^{BBP}/eIF6 overexpressing embryos do not increase Bax expression, Xp27^{BBP}/eIF6 morphants have higher levels of Bax mRNA and protein. When Bax mRNA was co-injected with Xp27^{BBP}/eIF6 mRNA, the bent phenotype recovered and a low occurrence was observed of the reverted phenotype, the same phenotype obtained in Xp27^{BBP}/eIF6 downregulation experiments. We reasoned that this result is a compromise balance between the anti-apoptotic action of Xp27^{BBP}/eIF6 and the pro-apoptotic action of Bax. In favor of this hypothesis, when mutated Xp27^{BBP}/eIF6 mRNA (lacking anti-apoptotic function) was co-injected with Bax, the number of embryos with reverted phenotypes increased. Altogether, these data indicate that p27^{BBP}/eIF6 may act by shifting the balance between pro- and anti-apoptotic factors in favor of cell survival and strongly suggest that Xp27^{BBP}/eIF6 acts through an upstream, yet unknown, regulator of the Bcl-2/Bax balance. Moreover, in Xp27^{BBP}/eIF6 overexpressors, the decrease in apoptosis also occurred when the cell cycle was stopped, following HUA exposure, indicating that the reduction in apoptosis levels was independent from cell cycling as in untreated *Xenopus* embryos.¹⁷

In mammalian cultured cells, on PKC phosphorylation on serine 235, p27^{BBP}/eIF6 is released from 60S, the 80S forms and translation is started, whereas the S235 mutant binds the 60S but cannot be released.⁶ In a lentiviral rescue experiment, the S235 mutant did not recover translation downstream of the growth factors, whereas the w.t. did.⁵ Together, the data suggested that the regulated release of p27^{BBP}/eIF6 from 60S positively affects translation, whereas the mutant does not. In other terms, the current understanding is that the regulated anti-association activity of w.t. p27^{BBP}/eIF6

may positively affect translation, whereas the S235 mutant does not. Yet it is not known whether p27^{BBP}/eIF6 anti-association activity equally affects the translation of all mRNAs or is somewhat selective. Two potential PKC phosphorylation sites are present in Xp27^{BBP}/eIF6 cDNA, that is, 235 SmR as in mammals and 91SvR typical of *X. laevis*.^{8,9} In *X. laevis*, we also know that p27^{BBP}/eIF6 is associated with 60S polysome fractions and that a serine phosphorylated isoform of p27^{BBP}/eIF6, consequent on PKC phosphorylation, is present all along embryogenesis. This finding suggests a highly conserved function of Xp27^{BBP}/eIF6, depending on phosphorylation, in regulating the availability of active ribosomes to the translation machinery.⁷ Therefore, in our trials, it appeared of special interest to learn which of the two potential sites of Xp27^{BBP}/eIF6 phosphorylation was responsible for the anti-apoptotic function of Xp27^{BBP}/eIF6. Our data indicate that the site is serine 235 SmR. In fact, it is on injection of the 235 SmR mutant, and not of the 91SvR mutant, that straight st.28 embryos are obtained, in contrast to the bent phenotype obtained by injection of Xp27^{BBP}/eIF6 w.t. Our data suggest that the anti-apoptotic function of Xp27^{BBP}/eIF6 depends on its role in regulating protein synthesis, if we correctly hypothesize that also in *X. laevis* the 235 SmR site is PKC-phosphorylated to allow joining of the 40S–60S subunits. In other words, the specific role of w.t. Xp27^{BBP}/eIF6 in favoring cell survival would require that its proper function be that of a regulator of protein synthesis affecting the translation of mRNAs involved in apoptosis, in contrast to the S235 mutant. Xp27^{BBP}/eIF6 seems to be part of a mechanism acting at translation and reverting cell death to cell survival, thus regulating the apoptotic process during normal development and giving way to a new interpretation for the major presence of this protein in embryonic anlagen. In particular, considering the conditions that our Xp27^{BBP}/eIF6 gain-of-function and loss-of-function experiments brought to a specific regulation of the Bcl-2/Bax levels, it will be important to establish the nature of the factor(s) regulating this balance and the involvement of p27^{BBP}/eIF6 in regulating its translation.

Materials and Methods

Animals. Adult *X. laevis* females were obtained from 'Rettili' (Varese, Italy). They were kept and used at the Department of Structural and Functional Biology, the University of Naples, Federico II, according to the guidelines and policies dictated by the University Animal Welfare Office and in agreement with European Community laws.

To obtain eggs, *X. laevis* females were injected in the dorsal lymphatic sac with 500 units of Gonase (AMSA, Rome, Italy) in Amphibian Ringer (111 mM NaCl, 1.3 mM CaCl₂, 2 mM KCl, 0.8 mM MgSO₄, 25 mM *N*-2-hydroxyethylpiperazine-*N'*-2-ethanesulfonic acid (HEPES), pH 7.8). Fertilized eggs and embryos were obtained by standard insemination methods and staged according to Nieuwkoop and Faber.³³

Microinjections. To generate pCS2p27^{BBP}/eIF6, the cDNA cloned in pDrive^{8,9} was subcloned into the *Bam*HI/*Xho*I sites of the pCS2⁺ vector. The complete coding sequence of XbCl-2 was obtained by reverse transcriptase (RT)-PCR, using the primers forward: 5'-ACAATGGAGGGCAGCAGTAG-3' and reverse: 5'-TTGCAGAACTTCTGGGTGT-3', on the basis of the sequence of the *Xenopus* homolog of Bcl-2, XR11 (Accession Nos. X82461). The PCR products were cloned into the pCRLI vector (Invitrogen, Life Technologies, Carlsbad, CA, USA) and subsequently subcloned into the *Bam*HI/*Xho*I sites of the pCS2⁺ vector. The full-length clone was

completely sequenced. The pCS2MTXBax plasmid was kindly offered by JL Maller (University of Colorado, School of Medicine, USA).

Capped synthetic RNAs were generated by *in vitro* transcription using the Sp6 Message Machine Kit (Ambion, Austin, TX, USA).

The p27^{BSP}/eIF6 antisense morpholino used was 5'-GCGGACGGCCATGTTGG CTTCTTAG-3' (Gene Tools LLC, Philomath, OR, USA). The mispaired morpholino control used was 5'-GCCGACcGCCATcTTGcCTTcTaAG-3' (Gene Tools LLC). pCS2MTGFP mRNA was always co-injected to label the injected side.

RNAs were injected into the animal hemisphere of a single cell of one- and two-cell embryos using a Drummond 'Nanoject' apparatus (Drummond "Nanoject II" Cat.N.3-000-204). The amounts injected ranged between 100 pg to 1 ng, in most cases 200–300 pg. In particular, for samples destined to western blots of Parp1, injection was performed in one-cell embryos using 500 pg Xp27^{BSP}/eIF6 to better visualize the difference in Parp1 cleavage between injected and uninjected embryos. During injection, embryos were cultured in 3% Ficoll in 0.1% Ringer. The phenotype of the injected embryos was scored when the uninjected embryos reached stage 28. The samples were photographed at the Leica MZ16F UV stereomicroscope, equipped with a Leica DFC 300F camera and IM50 image manager software.

RNA extraction and RT-PCR. Total RNA was extracted from st.19 embryos using Tri Reagent (Sigma, St Louis, MO, USA) according to the manufacturer's recommendations. RT-PCR was carried out using the Super Script VILO cDNA synthesis kit (Invitrogen, Carlsbad, CA, USA) and primers to detect Bcl-2 (forward: 5'-ACAATGGAGGGCAGCAGTAG-3' and reverse: 5'-TGCAGAACTTCCTGG GTGT-3'), Bax (forward: 5'-AGGCATCTCCCAACAGAGTG-3' and reverse: 5'-CC TCCAGATGGCAAGAGAGG-3') or H4 (forward: 5'-CGGGATAACATTCAGG GTA-3' and reverse: TCCATGCGCGTAACTGTC-3').

PCR site-directed mutagenesis. Site-directed mutagenesis to generate S235A and S91A was performed as in De Marco *et al.*³⁴ The following oligonucleotides were used to introduce the S235A mutation into pCS2p27^{BSP}/eIF6 wild type: 5'-CCTAGTACTATTGCCACCGCCATGAGGGGCTCCCTC-3' and 5'-GAGG GAGCCCTCATGGCGTGGCAATAGTACTAGG-3'. The following oligonucleotides were used to introduce the S91A mutation into pCS2 p27^{BSP}/eIF6 wild type: 5'-GAA ACAGCTGCCCGCAGCCGCTGCGCAATTACAGAGAG-3' and 5'-CTCTCTGAATTCGC ACGGCGTGGGCAAGCTGTTTC-3'.

The DNA sequence of the mutants was confirmed by sequence analysis.

Sample preparation for SDS-PAGE and western blot. Embryos were homogenized in HEPES buffer pH 7.5 containing 900 mM glycerol, 0.02 mM Na₃N, 1 mM ATP, 1 mM DTT, 5 mM ethylene glycol tetraacetic acid (EGTA) (buffer I) and the following protease inhibitors (Sigma): 2 mM N_ε-(p-toluene sulfonyl)-L-arginine methyl ester (TAME), 5 mg/ml soybean trypsin inhibitor (SBTI), 5 μg/ml aprotinin and 10 μM E64. Protein concentration was determined in the supernatants following centrifugation (15 000 × g for 40 min at 4 °C) with the BCA protein assay reagent (Pierce, Rockford, IL, USA). After boiling in sample buffer with 1 mM DTT, aliquots of 40 μg of proteins were analyzed through SDS-polyacrylamide gel electrophoresis (PAGE) 8% or 15% polyacrylamide using standard Tris glycine buffer and using molecular mass standards (200, 116, 97, 45, 31, 21 or 14 kDa) (Bio-rad, Hercules, CA, USA). Western blotting on nitrocellulose membrane was carried out as in Matur *et al.*³⁵ Incubation with the antibodies was carried out using an anti-p27^{BSP}/eIF6 antibody (1:1000 dilution v/v),¹ rabbit anti-Caspase 3 Active, specific for the cleaved form of caspase (1:400 dilution, v/v) (Sigma C8487), mouse anti- α -tubulin (1:500 dilution, v/v) (Sigma), anti-PARP H-250 polyclonal antibody (1:500 dilution, v/v) (Santa Cruz Biotechnology, Heidelberg, Germany), anti-Bcl-2 monoclonal antibody (1:250 dilution, v/v) (Santa Cruz Biotechnology) and polyclonal anti-Bax (1:200 dilution, v/v) (Calbiochem, Darmstadt, Germany). Antibody binding was detected with secondary anti-mouse or anti-rabbit IgGs coupled with horseradish peroxidase (Pierce) and revealed with the enhanced chemiluminescence kit (Pierce).

BrdU and HUA experiments. Xp27^{BSP}/eIF6 overexpressing embryos were injected at st.28 with BrdU (Roche, Mannheim, Germany) in the gut, fixed 2 h later and cryostat-sectioned. Preliminary experiments showed that at this stage cell division occurs in a few minutes (see also Viczian *et al.*¹⁵). Sections were washed with 2 N HCl for 45 min and then neutralized with several phosphate-buffered saline (PBS) washes. The mouse anti-BrdU antibody (Sigma) was added at 1:500 dilution and the sections were incubated at 4 °C overnight. Staining was completed by incubation with BODIPY FL goat anti-mouse IgG (Invitrogen). To block DNA synthesis, embryos were incubated in a solution of 20 mM HUA (Sigma) and

150 μM aphidicolin (Sigma) in 0.1 × Ringer as described in Harris and Hartenstein.²⁴ Aphidicolin was diluted from 10 mg/ml stock in dimethyl sulfoxide. Embryos were kept in HUA at 16 °C for 5 h until fixation.

TUNEL staining. TUNEL staining for the identification of apoptotic cells was carried out using the ApoTag Peroxidase *In situ* Apoptosis Detection Kit (Chemicon International, Inc., Temecula, CA, USA) in accordance with the manufacturer's instructions. Counts of TUNEL-positive nuclei in sections of fixed embryos were reported in histograms in which the ordinates indicate percentages of apoptotic cells with respect to the total number of counted apoptotic cells (100%). The data were statistically validated by PAIRED *t*-test analysis.

The whole-mount TUNEL staining protocol was performed as described in Hensley and Gautier.¹⁶ Detection and chromogenic reaction was carried out as in Harland.³⁶ The embryos were blocked in 20% goat serum, followed by incubation with the anti-digoxigenin antibody coupled to alkaline phosphatase (Roche). Staining was developed using BM-purple (Roche). Embryos were viewed following dehydration in methanol and mounting in benzyl benzoate/benzyl alcohol 2:1. Whole mounts were photographed at the Leica MZ 16F. Some embryos were cleared, paraffin-embedded and sectioned.

Immunofluorescence. *X. laevis* embryos were fixed in 4% formaldehyde at 4 °C and stored in 100% methanol at -20 °C. Frozen sections of 10-μm thickness were obtained for immunofluorescence after embedding and freezing in Killik (Bio Optica, Milan, Italy). Nonspecific background was blocked by incubating the sections for 30 min in normal goat serum 3% in PBS, 0.5% BSA, 0.1% Tween before exposure to O/N at 4 °C to rabbit anti-p27^{BSP}/eIF6,^{1,7} rabbit anti-GFP (Molecular Probe, Milan, Molecular probes-Invitrogen) or to polyclonal anti-pH3 antibody (UPSTATE, Lake Placid, NY, USA), diluted 1:500 in PBS containing 0.5% BSA and 0.1% Tween. Staining was completed by incubating the samples with anti-rabbit goat IgG BODIPY FL-conjugated or Texas-Red-conjugated (Molecular Probe), followed by nuclei counterstaining with DAPI and mounting in PBS/glycerol (9:1, v/v). Sections were observed and photographed using a Leica CTR 6500 UV microscope equipped with a Leica application suite.

The number of anti-pH3-positive nuclei counted in sections of fixed embryos was reported in histograms in which the ordinates indicate percentages of labeled cells with respect to the total number of labeled cells (100%) counted in an embryo entirely sectioned. All the data are statistically validated by PAIRED *t*-test analysis.

Immunohistochemistry. Whole-mount antibody staining was performed following standard procedures for indirect immunohistochemistry using an anti-muscle ATPase monoclonal antibody 12f10/1 at 1:10 dilution. This antibody was developed by Dr JP Brookes (Department of Biochemistry and Molecular Biology, University College London, London, UK), obtained from the Developmental Studies Hybridoma Bank (under the auspices of the National Institute of Child Health and Human Development, NIH) and maintained at the University of Iowa, Department of Biological Sciences, Iowa City, IA, USA. The protocol was completed by incubating the samples with the biotinylated secondary antibody and the avidin-biotinylated peroxidase complex (Vector Laboratories, Inc, Burlingame, CA, USA). The reaction product was visualized by incubation in diaminobenzidine (Vector Laboratories).

Acknowledgements. We are grateful to Professor PG Marchisio for reading the paper and to Drs Amalia De Angelis and Margherita Tussellino for assistance. Special thanks go to Dr Graciiana Diez Roux for carefully reading the paper and contributing with critical suggestions. This work was partially funded by AMRA Scarl, by a Grant of the Italian Ministry of University and Research (P.R.I.N. 1997) to CC and by a Grant of the 'Compagnia di San Paolo' ('Integration of spatial and biochemical clues during brain development' Project) to CC.

1. Biffo S, Sanvito F, Costa S, Preve L, Pignatelli R, Spinardi L *et al.* Isolation of a novel $\beta 4$ integrin binding protein (p27^{BSP}) highly expressed in epithelial cells. *J Biol Chem* 1997; **272**: 30314–30321.
2. Basu U, Si K, Warner JR, Maitra U. The Saccharomyces cerevisiae TIF6 gene encoding translation initiation factor 6 is required for 60S ribosomal subunit biogenesis. *Mol Cell Biol* 2001; **21**: 1453–1462.
3. Senger B, Lafontaine DL, Grandjean JS, Gadal O, Camasses A, Sanni A *et al.* The nuclear Tif6p and E11p are required for a late cytoplasmic step of ribosome synthesis. *Mol Cell* 2001; **8**: 1363–1373.

4. Sanvito F, Piatti S, Villa A, Bossi M, Lucchini G, Marchisio PC *et al*. The beta4 integrin interactor p27^{BBP}/eIF6 is an essential nuclear matrix protein involved in 60S ribosomal subunit assembly. *J Cell Biol* 1999; **144**: 823–837.
5. Gandin V, Miluzio A, Barbieri A, Magri L, Kiyokawa H, Marchisio PC. eIF6 is rate limiting for translation, growth and transformation. *Nature* 2006; **445**: 684–688.
6. Ceci M, Gaviraghi C, Gorini C, Sala LA, Offenhauser N, Marchisio PC *et al*. Release of eIF6 (p27^{BBP}) from the 60S subunit allows 80S ribosome assembly. *Nature* 2003; **426**: 579–584.
7. Carotenuto R, De Marco N, Biffo S, Wilding M, Vaccaro MC, Marchisio PC *et al*. Phosphorylation of p27^{BBP}/eIF6 and its association with the cytoskeleton are developmentally regulated in *Xenopus* oogenesis. *Cell Mol Life Sci* 2005; **62**: 1641–1652.
8. Vaccaro MC, Cuccaro M, De Marco N, Campanella C. Isolation and expression pattern of p27^{BBP}/eIF6 cDNA in *Xenopus laevis* embryos. *Mol Reprod Dev* 2006a; **73**: 485–490.
9. Vaccaro MC, Cuccaro M, De Marco N, Campanella C. Isolation and expression pattern of p27^{BBP}/eIF6 cDNA in *Xenopus laevis* embryos ERRATUM. *Mol Reprod Dev* 2006b; **73**: 1612.
10. Donadini A, Giodini A, Sanvito F, Marchisio PC, Biffo S. The human ITGB4BP gene is constitutively expressed *in vitro*, but highly modulated *in vivo*. *Gene* 2001; **266**: 35–43.
11. Sanvito F, Vivoli F, Gambini S, Santambrogio G, Catena M, Viale E *et al*. Expression of a highly conserved protein, p27^{BBP}, during the progression of human colorectal cancer. *Cancer Res* 2000; **60**: 510–516.
12. Vreugde S, Ferrai C, Miluzio A, Hauben E, Marchisio PC, Crippa M *et al*. Nuclear myosin VI enhances RNA polymerase II dependent transcription. *Mol Cell* 2006; **23**: 749–755.
13. Ji Y, Shah S, Soanes K, Islam MN, Hoxter B, Biffo S *et al*. Eukaryotic initiation factors 6 selectively regulates Wnt signalling and β -catenin protein synthesis. *Oncogene* 2008; **27**: 755–762.
14. Chendrimada TP, Finn KJ, Ji X, Baillat D, Gregory RI, Liebhaber SA *et al*. MicroRNA silencing through RISC recruitment of eIF6. *Nature* 2007; **447**: 823–829.
15. Eurialio A, Huntzinger E, Izaurralde E. GW182 interaction with Argonaute is essential for miRNA-mediated translation repression and mRNA decay. *Nat Struct Mol Biol* 2008; **15**: 346–353.
16. Hensley C, Gautier J. A developmental timer that regulates apoptosis at the onset of gastrulation. *Mech Dev* 1997; **69**: 183–195.
17. Yeo W, Gautier J. A role for programmed cell death during early neurogenesis in *Xenopus*. *Dev Biol* 2003; **260**: 31–45.
18. Jacobson MD, Weil M, Raff MC. Programmed cell death in animal development. *Cell* 1997; **88**: 347–354.
19. Viczian AS, Vignali R, Zuber ME, Barsacchi G, Harris WA. Xotx5b and Xotx2 regulate photoreceptor and bipolar fates in the *Xenopus* retina. *Development* 2003; **130**: 1281–1294.
20. Hensley C, Gautier J. Programmed cell death during *Xenopus* development: a spatio-temporal analysis. *Dev Biol* 1998; **238**: 36–48.
21. Gavrieli Y, Sherman Y, Ben-Sasson SA. Identification of programmed cell death *in situ* via specific labeling of nuclear DNA fragmentation. *J Cell Biol* 1992; **119**: 493–501.
22. Kaufmann SH, Lee SH, Meng XW, Loegering DA, Kottke TJ, Henzing AJ *et al*. Apoptosis-associated caspase activation assays. *Methods* 2008; **44**: 262–272.
23. Yuan J, Shaham S, Ledoux S, Ellis HM, Horvitz HR. The *C. elegans* cell death gene *ced-3* encodes a protein similar to mammalian interleukin-1 beta-converting enzyme. *Cell* 1993; **75**: 641–652.
24. Harris WA, Hartenstein V. Neuronal determination without cell division in *Xenopus* embryos. *Neuron* 1991; **6**: 499–515.
25. Zorn AM, Mason J. Gene expression in the embryonic *Xenopus* liver. *Mech Dev* 2001; **103**: 153–157.
26. Rot-Nikcevic I, Wassersug RJ. Arrested development in *Xenopus laevis* tadpoles: how size constrains metamorphosis. *J Exp Biol* 2004; **207**: 2133–2144.
27. Adams JM, Cory S. Life-or-death decisions by the Bcl-2 protein family. *Trends Biochem Sci* 2001; **26**: 61–66.
28. Cory S, Adams JM. The Bcl2 family: regulators of the cellular life-or-death switch. *Nat Rev Cancer* 2002; **2**: 647–656.
29. Tribulo C, Aybar MJ, Sánchez SS, Mayor R. A balance between the anti-apoptotic activity of Slug and the apoptotic activity of *msx1* is required for the proper development of the neural crest. *Dev Biol* 2004; **275**: 325–342.
30. Coles HS, Burne JF, Raff MC. Large-scale normal cell death in the developing rat kidney and its reduction by epidermal growth factor. *Development* 1993; **118**: 777–784.
31. Burek MJ, Oppenheim RW. Programmed cell death in the developing nervous system. *Brain Pathol* 1996; **6**: 427–446.
32. Finkielstein CV, Lewellyn AL, Maller JL. The midblastula transition in *Xenopus* embryos activates multiple pathways to prevent apoptosis in response to DNA damage. *Proc Natl Acad Sci USA* 2001; **98**: 1006–1011.
33. Nieuwkoop PD, Faber J. *Normal Table of Xenopus laevis*. Daudin, Amsterdam: North Holland, 1967.
34. De Marco N, Buono M, Troise F, Diez-Roux G. Optineurin increases cell survival and translocates to the nucleus in a Rab8-dependent manner upon an apoptotic stimulus. *J Biol Chem* 2006; **281**: 16147–16156.
35. Maturi G, Infante V, Carotenuto R, Focarelli R, Caputo M, Campanella C. Specific glycoconjugates are present at the oolemma of the fertilization site in the egg of *Discoglossus pictus* (Anurans) and bind spermatozoa in an *in vitro* assay. *Dev Biol* 1998; **204**: 210–223.
36. Harland RM. *In situ* hybridisation: an improved whole mount method for *Xenopus* embryos. *Meth Cell Biol* 1991; **36**: 675–685.

In *X. laevis* embryos high levels of the anti-apoptotic factor p27BBP/eIF6 are stage-dependently found in BrdU and TUNEL-reactive territories

N. De Marco¹, C. Campanella² and R. Carotenuto²

Department of Structural and Functional Biology, University of Naples Federico II, Naples, Italy

Date submitted: 19.01.10. Date accepted: 22.03.10

Summary

p27BBP/eIF6 ($\beta 4$ binding protein/eukaryotic initiation factor 6) is a highly conserved protein necessary for cell life. In adult eIF6 mice, a 50% decrease in the protein levels in all tissues is accompanied by a reduction in cell proliferation only in the liver, fat cells and cultured fibroblasts. During *X. laevis* embryogenesis expression of p27BBP/eIF6 is abundant in high proliferative territories. However, in *Xenopus* cell proliferation appears unaffected following p27BBP/eIF6 over-expression or down-regulation. Indeed, p27BBP/eIF6 is an anti-apoptotic factor acting upstream of Bcl2 that reduces endogenous apoptosis. We studied p27BBP/eIF6 protein localization in wild type embryos and compared it to proliferation and apoptosis. At the beginning of embryogenesis, high levels of p27BBP/eIF6, proliferation and apoptosis overlap. In later development stages high proliferation levels are present in the same regions where higher p27BBP/eIF6 expression is observed, while apoptosis does not appear specifically concentrated in the same sites. The higher presence of p27BBP/eIF6 would appear related to an increased need of apoptosis control in the regions where cell death is essential for normal development.

Keywords: Apoptosis, p27BBP/eIF6, Proliferation, TUNEL, *Xenopus laevis*

Introduction

In building an embryo, complex mechanisms operate to increase, model and attribute specific traits to developing anlagen. Proliferation and apoptosis are the main sculptors acting in this process. In *Xenopus laevis* embryogenesis, apoptosis controls the absolute cell number and its occurrence is regulated in time and during development, starting from the beginning of gastrulation (Hensey & Gautier, 1997). Bcl-2 and Bax balance and activation of downstream caspases are the main mechanisms involved in the control of apoptosis in this organism (Finkielstein *et al.*, 2001; Yeo & Gautier, 2003). It was recently suggested that apoptosis may be further modulated during *X. laevis* development

through p27BBP/eIF6 ($\beta 4$ binding protein/eukaryotic initiation factor 6), which inhibits cell death by acting upstream of Bcl2 (De Marco *et al.*, 2010).

p27BBP/eIF6 is a highly conserved protein necessary for cell life (Sanvito *et al.*, 1999; Gandin *et al.*, 2008). It regulates translation by preventing the interaction of 40S ribosomal subunits with 60S subunits through its binding to 60S ribosomes. In mammalian cells, upon PKC phosphorylation in serine 235, p27BBP/eIF6 is released from 60S to start translation (Ceci *et al.*, 2003; Miluzio *et al.*, 2009). This phosphorylative event may occur downstream of extra-cellular signalling such as insulin/growth factors indicating that p27BBP/eIF6 is a 60S-associated initiation factor able to modulate translation *in vivo* (Gandin *et al.*, 2008). The 235 SmR potential PKC phosphorylation site is also found in *Xenopus* p27BBP/eIF6 cDNA, in which a serine phosphorylated isoform has been reported as well (Carotenuto *et al.*, 2005; Vaccaro *et al.*, 2006a,b).

Significantly, p27BBP/eIF6 appears to be selective in regulating translation of certain mRNAs, as in the case of β -catenin (Ji *et al.*, 2008) and of a factor acting

¹All correspondence to: N. De Marco. Department of Structural and Functional Biology, University of Naples Federico II, Naples, Italy. Tel: +39 081 679189. Fax: +39 081 679233. e-mail: nademarc@unina.it

²Department of Structural and Functional Biology, University of Naples Federico II, Naples, Italy.

upstream of Bcl-2 (De Marco *et al.*, 2010). Moreover, its expression is variable among cell types (Donadini *et al.*, 2001) and p27BBP/eIF6 mRNA and protein levels are high in rapidly proliferating cancer cells and low in cells committed to apoptosis (Sanvito *et al.*, 2000).

During *Xenopus* embryogenesis, modulated expression of p27BBP/eIF6 occurs in developing anlagen in addition to a basal level of expression. In particular, p27BBP/eIF6 mRNA is abundant in the eye field and in the mid-hindbrain boundary, two regions with high proliferation levels suggesting a correlation between p27BBP/eIF6 and proliferative activity (Vaccaro *et al.*, 2006a,b). In *Xenopus* embryos, following p27BBP/eIF6 ectopic over-expression or down-regulation, cell proliferation appears unaffected (De Marco *et al.*, 2010), suggesting that under these experimental conditions, cell proliferation and apoptosis inhibition are uncoupled events. However, at present it is not known whether, during development of wild type embryos, the higher presence of p27BBP/eIF6 coincides with high activity of cell proliferation or low apoptosis levels, suggesting the existence of complex physiological co-ordination of such events.

In this paper we performed immunofluorescence with anti-p27BBP/eIF6-specific antibody, BrdU injection and TUNEL staining to investigate the correlation of p27BBP/eIF6 protein localization with proliferation and apoptosis levels in developing *Xenopus* embryos. Our data indicate that p27BBP/eIF6 is present throughout embryogenesis. However, the presence of this protein varies according to the sites where high proliferative activity occurs. Cell death appears variously associated to proliferative evidence and p27BBP/eIF6 localization. Indeed, at the beginning of embryogenesis a high concentration of p27BBP/eIF6 is correlated with high levels of both apoptosis and proliferation. Late in development, greater presence of p27BBP/eIF6 is always coincident with high mitotic activity whereas cell death decreases and is ubiquitously present.

Material and methods

Animals

Adult *Xenopus laevis* females were obtained from 'Rettili' Varese, Italy. They were kept and utilized at the Department of Structural and Functional Biology of the University of Naples, Federico II, according to the guidelines and policies dictated by the University Animal Welfare Office and in agreement with international rules.

To obtain eggs, *X. laevis* females were injected in the dorsal lymphatic sac with 500 units of Gonase (AMSA)

in amphibian Ringer's solution (111 mM NaCl, 1.3 mM CaCl₂, 2 mM KCl, 0.8 mM MgSO₄, 25 mM HEPES, pH 7.8). Fertilized eggs and embryos were obtained by standard insemination methods (see De Marco *et al.*, 2010) and staged according to Nieuwkoop & Faber (1967).

Immunofluorescence

X. laevis embryos were fixed in 4% formaldehyde at 4°C and stored in 100% MeOH at -20°C. For *in toto* immunofluorescence after incubation in hydrogen peroxide/methanol 1:2 (v/v) for about 2 days, the samples were incubated with rabbit anti-p27BBP/eIF6 antibody (Biffo *et al.*, 1997; Carotenuto *et al.*, 2005) or polyclonal anti-pH3 antibody (UPSTATE) diluted 1:500 PBS/0.5%BSA/0.1% Triton X-100. The secondary antibody was goat anti-rabbit IgG BODIPY FL-conjugated (Molecular Probes). The embryos were then dehydrated in graded methanol and cleared in benzyl alcohol/benzyl benzoate 1:2 (v/v). Whole mounts were photographed with a Leica MZ 16F. For immunofluorescence on frozen section 10 μm-thick sections were obtained after embedding and freezing in Killik (Bio Optica). Non-specific background was blocked by incubating the sections for 30 min in normal goat serum 3% in PBS, 0.5% BSA, 0.1% Tween, prior to exposure O/N at 4°C to rabbit anti-p27BBP/eIF6 diluted 1:500 in PBS containing 0.5% BSA and 0.1% Tween. Staining was completed by incubating the samples with anti-rabbit goat IgG BODIPY FL-conjugated (Molecular Probes), followed by nuclei counter-staining with DAPI and mounting in PBS/glycerol (9:1, v/v). Sections were observed and photographed with a Leica CTR 6500 UV microscope equipped with the Leica application suite.

TUNEL staining

TUNEL staining to identify apoptotic cells was performed using ApopTag Peroxidase In Situ Apoptosis Detection Kit (Chemicon), in accordance with the manufacturer's instructions. The whole-mount TUNEL staining protocol was performed as described in Hensey & Gautier (1997). Detection and chromogenic reaction were carried out according to Harland (1991). The embryos were blocked in 20% goat serum, followed by incubation with anti-digoxigenin antibody coupled to alkaline phosphatase (Roche). Staining was developed using BM-purple (Roche). Embryos were viewed following dehydration in methanol. Whole mounts were photographed on a Leica MZ 16F.

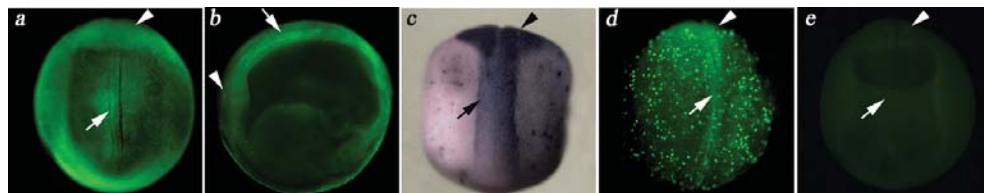


Figure 1 *In toto* immunofluorescence with anti-p27BBP/eIF6 antibody of stage 14 embryo, dorsal (a) and lateral (b) view. Staining is relevant in the neural plate (arrow) and in the anteriormost region indicated by the arrowhead. (c) Apoptosis detected by *in toto* TUNEL assay at stage 14 embryo. A strong signal is present in the neural plate (arrow) with the most intense staining corresponding to the anteriormost portion (arrowhead). (d) immunofluorescence with anti-pH3 antibody. At the early neurula stage numerous mitotic cells are present in the whole embryo. The strongest staining is localized in the developing neuroepithelium (arrow for posteriormost and arrowhead for anteriormost neuroepithelium). (e) *In toto* immunofluorescence using only secondary antibody BODIPY-conjugates anti-rabbit goat IgG. Staining is absent.

BrdU experiments

Embryos were injected with BrdU (5-bromo-2'-deoxyuridine, Roche) in the gut, fixed 2 h later and cryostat sectioned. Preliminary experiments showed that cell division occurs in a few minutes (see also Viczian *et al.*, 2003). Sections were washed with 2 N HCl for 45 min and then neutralized with several PBS washes. The mouse anti-BrdU antibody (Sigma) was added at 1:500 dilution and the sections were incubated at 4°C overnight. Staining was completed by incubation with BODIPY FL goat anti-mouse IgG (Invitrogen, Molecular Probes).

Results

Stage 14

p27BBP/eIF6 localization was studied by *in toto* immunofluorescence in stage 14 embryos. The immunostaining was highly concentrated in the neural plate along the anteroposterior axis of the embryo and in the anteriormost region in territories fated to develop eyes and part of the encephalon (Fig. 1a,b). Apoptosis was detected by *in toto* TUNEL-staining. Labelled cells were found in the dorsal region where they appear to mark the neural plate, being highly concentrated at its anterior edge (Fig. 1c). We performed immunostaining with an antibody against phosphorylated histone H3, which specifically recognizes mitotic chromosomes. High levels of cell proliferation were present in whole embryos and were mostly localized in the developing neural plate (Fig. 1d). The immunostaining was specific, as indicated by the absence of a signal, when the primary antibody was absent (Fig. 1e). Therefore, at the beginning of embryogenesis, high levels of p27BBP/eIF6, proliferation and apoptosis are coincident.

Stage 24

At tailbud stage p27BBP/eIF6 *in toto* immunofluorescence was detected throughout the developing brain, otic and optic vesicles, branchial arches and somites (Fig. 2a). In particular, the pattern of p27BBP/eIF6 distribution was studied during brain and eye formation. At stage 24, the neural tube is fully formed and differentiated into forebrain, midbrain and hindbrain. The optic vesicle has evaginated from the prosencephalon and makes contact with the overlying epidermis. The retina consists of a single population of neuroepithelial cells (Nieuwkoop & Faber, 1967; Holt *et al.*, 1988; Eagleson *et al.*, 1995). Immunofluorescence was performed, as well, on embryo frozen sections. Extensive p27BBP/eIF6 labelling was observed in all brain regions and in the undifferentiated cells of the optic stalk, presumptive retinal pigment epithelium and neural retina (Fig. 2b,c). BrdU and TUNEL experiments were performed on serial section of stage 24 embryos. BrdU labelling showed mitotic cell throughout the brain and eye. Indeed, at this stage most of the cells are still actively proliferating. However, TUNEL assay showed diffuse staining in the developing brain and eye and no tissue-specific localizations were found (Fig. 2e). The immunostaining was specific (Fig. 2f,g). Therefore while the greater presence of p27BBP/eIF6 and proliferation are coincident, apoptosis diminishes in the brain and eyes and does not appear to have specific localizations.

Stage 32

The general pattern of the brain and connected sensorial placodes is established at about stage 28 (Nieuwkoop & Faber, 1967). At stage 32, the eye cup is formed and cells are being generated in the central retina while some cells continue to divide in the ciliary

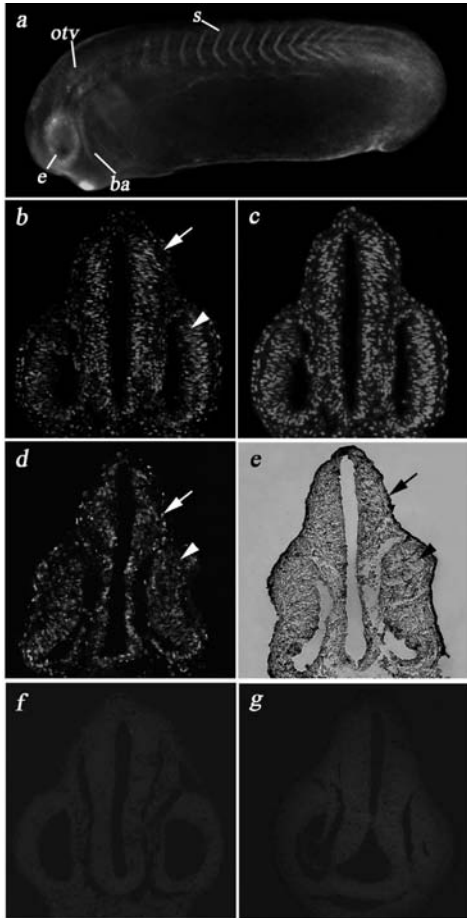


Figure 2 (a) At stage 24, *in toto* immunofluorescence shows the presence of p27BBP/eIF6 in somites (s), branchial arches (ba) and in the anlagen of optic (e) and otic (otv) vesicles. (b) immunofluorescence with anti-p27BBP/eIF6 antibody on a section of a stage 24 embryo. The protein is abundant in developing brain (arrow) and retina (arrowhead). (c) DAPI staining of section (b). BrdU immunolocalization (d) and TUNEL assay (e) was performed in serial cross-sections of stage 24 embryos. High proliferation rates are present in developing brain (arrow) and eye (arrowhead), while apoptosis levels are reduced compared with earlier stages of neurulation both in brain and in retina (e). Immunofluorescence controls using only anti-rabbit goat IgG BODIPY-conjugates as control for anti-p27BBP/eIF6 immunofluorescence (f) and anti-mouse goat IgG BODIPY-conjugates as control for anti-BrdU immunofluorescence (g). Staining is absent.

marginal zone (CMZ), the most peripheral region of the retina (Straznický & Gaze, 1971; Wetts *et al.*, 1989). High levels of p27BBP/eIF6 were expressed in the brain, otic vesicle, optic cup as well as in branchial arches and somites (Fig. 3a). In particular, anti-p27BBP/eIF6 immunostaining detected high concentrations of the protein in more restricted regions than in earlier stages. Indeed the stain was segregated in the dorsal region of the brain and in the CMZ (Fig. 3b,f,i). BrdU and TUNEL experiments on serial sections of stage 32 embryos showed that higher proliferation and apoptosis rates were found in the dorsal with respect to the ventral region of the brain (Fig. 3d,e,h,j). In the eye, many cells were post-mitotic and the majority of the BrdU immunostaining was found in the CMZ, while TUNEL-positive nuclei were detected in the whole developing retina including the CMZ (Fig. 3d,e,j,k). Taken together, these data show that in the brain the levels of p27BBP/eIF6, proliferation and apoptosis are nearly overlapping. In contrast, in the eye the TUNEL reaction is found in the whole retina and does not appear specifically concentrated in the same sites where strong localization of both anti-BRDU and anti-p27BBP/eIF6 immunostaining was found.

Stage 45

In the stage 45 brain, p27BBP/eIF6 immunofluorescence was abundant in the subependymal layer (Fig. 4a), cell division and apoptosis were localized as well in the subependymal layer as revealed by intense BrdU and TUNEL signals close to the ventricle (Fig. 4c,d). At the same stage, the retina is fully laminated, with three distinct nuclear layers separated by two plexiform layers where retinal cell types can be distinguished by morphological and cytological criteria (Straznický & Gaze, 1971). In the mature retina p27BBP/eIF6 was localized in the CMZ (Fig. 4e), where high proliferative activity was demonstrated by the presence of BrdU staining (Fig. 4g). TUNEL signal was detected in all layers of the retina including the CMZ (Fig. 4h). Therefore, at stage 45, higher p27BBP/eIF6 presence, proliferation and apoptosis are fully overlapping in the brain. However, in the eye high levels of p27BBP/eIF6 and mitosis are restricted to the CMZ while cell death is widespread and not layer-specific as in previous stages.

Discussion

In adult eIF6^{+/-} mice, while the eIF6 level is 50% lower in all tissues, the cell proliferation rate is largely unchanged except for a reduction in the liver, fat cells and cultured fibroblasts (Gandin *et al.*, 2008). In contrast, in p27BBP/eIF6 morphants of *Xenopus laevis*,

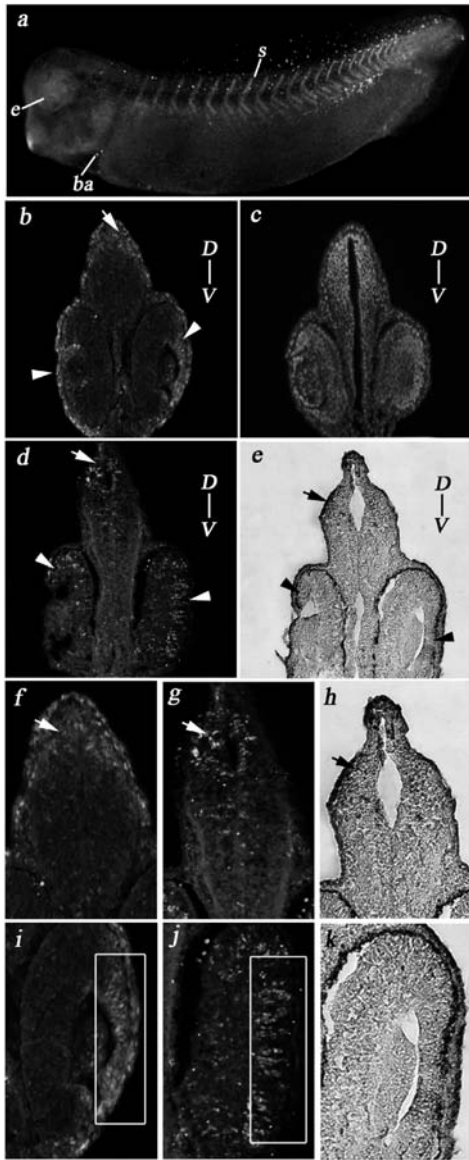


Figure 3 p27BBP/eIF6 localization in stage 32 embryos. (a) A strong signal is present in somites (s), branchial arches (ba) and developing eye (e). (b) Immunofluorescence on sections shows that p27BBP/eIF6 label is more abundant in dorsal region of the brain (arrow) and in ciliary marginal zone of the eye (arrowhead). (c) DAPI staining of section (b). Immunostaining with anti-BrdU antibody (d) and TUNEL

cell proliferation levels are unchanged with respect to controls (De Marco *et al.*, 2010). It should be observed that the conditions of down-regulation experiments are not fully comparable in the mouse and the frog. Indeed, in eIF6^{+/-} mice, p27BBP/eIF6 haploidy is genetically fixed and leads to chronic depletion of eIF6 in contrast to *Xenopus* p27BBP/eIF6 morphants where depletion is acute. Moreover, different organs and time-points were analyzed (Gandin *et al.*, 2008; De Marco *et al.*, 2010). In the opposite condition, i.e., when p27BBP/eIF6 is over-expressed, the data available for *Xenopus* embryogenesis indicate that any increase in cell proliferation occurs in p27BBP/eIF6 over-expressors. Yet in these experimental conditions, the induced high levels of p27BBP/eIF6 expression were found to reduce endogenous apoptosis, acting upstream of Bcl2 (De Marco *et al.*, 2010).

In the present paper we studied p27BBP/eIF6 protein localization in wild-type embryos and compared it to proliferation and apoptosis, in light of the recent data on the role of p27BBP/eIF6 as an anti-apoptosis factor and taking into consideration that in natural conditions high levels of p27BBP/eIF6 expression occur in developing anlagen of *Xenopus laevis* (Vacarro *et al.*, 2006a,b). We focused on brain and eye development because they are excellent models for studies of cellular proliferation and differentiation. Indeed, these organs have reproducible stereotypic pattern of cell division and apoptosis required for their morphogenesis (Eagleson *et al.*, 1995; Hensey & Gautier, 1998; Yeo & Gautier, 2003).

Immunofluorescence data showed that high levels of p27BBP/eIF6 protein are present in the neural tube and the presumptive eye field from the start of neurulation. Similarly, high proliferation levels were observed in the majority of cells of stage 14 embryos and these rates are greatest in antero-dorsal areas i.e. coincident with the localization of p27BBP/eIF6.

assay (e) on serial sections of a stage 32 embryo show that proliferation and apoptosis are overlapping in the brain. In contrast, in the eye anti-BRDU immunostaining is restricted to CMZ, while TUNEL staining is diffuse in the whole retina. (f) Higher magnification of the brain showed in b. Most anti-p27BBP/eIF6 immunostaining is next to the ventricle in dorsal region of the brain (arrow). (g, h) Details of parts (d) and (e) respectively show that BrdU and TUNEL assays stain the same sites (arrows) strongly labelled by anti-p27BBP/eIF6 antibody. (i) Higher magnification of eye showed in section (b). High levels of p27BBP/eIF6 are present in CMZ (square). (j) detail of section (d) shows a strong localization of mitotic cells in CMZ (square) overlapping with p27BBP/eIF6 immunostaining. (k) detail of section (e) shows that apoptotic cells are diffuse in all developing retina including CMZ. D-V, dorsoventral axis.

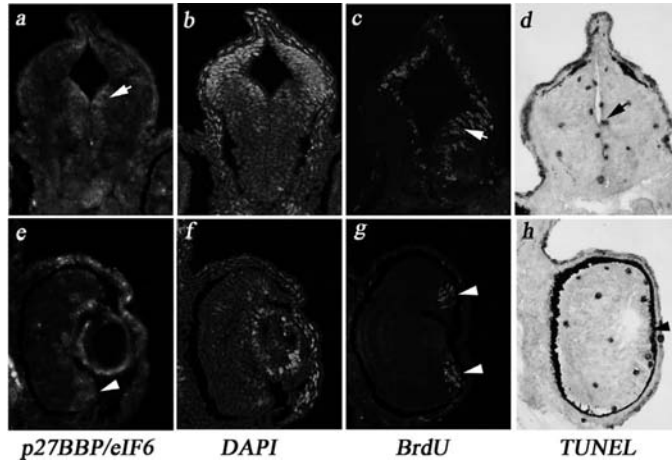


Figure 4 p27BBP/eIF6 (a); DAPI staining (b); BrdU immunofluorescence (c); and TUNEL assay (d) in brain of stage 45 embryo. Most p27BBP/eIF6, BrdU and TUNEL signals are close to the brain ventricle (arrow). In the fully laminated retina p27BBP/eIF6 (e) and BrdU (g) staining is restricted to CMZ (arrowhead), whilst the TUNEL signal (h) is present in the whole retina. (f) DAPI staining.

In these embryos, dorsal embryonic regions are also heavily labelled with TUNEL assay, in agreement with previous studies where a possible interaction was suggested between apoptosis and proliferation in regulating the physiological number of cells within the developing neuroectoderm (Yeo & Gautier, 2003).

At stage 24, high levels of proliferation are present in the same regions where p27BBP/eIF6 major expression is observed, while cell death was considerably reduced compared with earlier stages of neurulation. This finding may be because, at this stage, p27BBP/eIF6 activity as a modulator of apoptosis becomes evident.

In later stages of development (stages 32–45) when the brain acquires most of its form and structure (Nieuwkoop & Faber, 1967), the cell proliferation rate and p27BBP/eIF6 presence are restricted to specific areas of the brain. Indeed, the BrdU-detected mitoses localize in selected areas such as the subependymal layer of CNS and the CMZ of the eye, a perpetually self-renewing proliferative neuroepithelium at the perimeter of the retina in amphibians and fish (Straznicky & Gaze, 1971; Johns, 1977; Reh & Kljavin, 1989; Wetts *et al.*, 1989). Apoptosis is similarly localized, but it is more widespread and not restricted to the same areas highly reactive with anti-p27BBP/eIF6 and anti-BrdU antibodies. We surmise that high levels of p27BBP/eIF6 are required for fine regulation of apoptosis which appears to play a pivotal role in the morphogenesis of the brain (Hensley &

Gautier, 1998). Indeed, apoptosis regulates primary neurogenesis at the level of neuronal determination (Yeo *et al.*, 2003).

In conclusion this study shows that high levels of p27BBP/eIF6 are present in highly proliferative regions, where apoptosis is also physiologically required for normal development. We hypothesize that p27BBP/eIF6 finely regulates the development machinery in stages of neural differentiation and organogenesis by acting through its ability to switch the apoptotic Bcl-2-Bax balance to cell survival.

Acknowledgements

This work was funded by a Grant of the Italian Ministry of University and Research (P.R.I.N. 1997) to C.C. and by a Grant of the 'Compagnia di San Paolo' (Integration of spatial and biochemical clues during brain development) to C.C.

References

- Biffo, S., Sanvito, F., Costa, S., Preve, L., Pignatelli, R., Spinardi, L. & Marchisio, P.C. (1997). Isolation of a novel $\beta 4$ integrin binding protein (p27BBP) highly expressed in epithelial cells. *J. Biol. Chem.* **272**, 30314–21.
- Carotenuto, R., De Marco, N., Biffo, S., Wilding, M., Vaccaro, M.C., Marchisio, P.C., Capriglione, T., Russo, G.L. & Campanella, C. (2005). Phosphorylation of p27BBP/eIF6 and its association with the cytoskeleton are

- developmentally regulated in *Xenopus* oogenesis. *Cell. Mol. Life Sci.* **62**, 1641–52.
- Ceci, M., Gaviraghi, C., Gorrini, C., Sala, L.A., Offenhauser, N., Marchisio, P.C. & Biffo, S. (2003). Release of eIF6 (p27BBP) from the 60S subunit allows 80S ribosome assembly. *Nature* **426**, 579–84.
- De Marco, N., Iannone, L., Carotenuto, R., Biffo, S., Vitale, A. & Campanella, C. (2010). p27(BBP)/eIF6 acts as an anti-apoptotic factor upstream of Bcl-2 during *Xenopus laevis* development. *Cell Death Differ.* **17**, 360–72.
- Donadini, A., Giodini, A., Sanvito, F., Marchisio, P.C. & Biffo, S. (2001). The human *ITGB4BP* gene is constitutively expressed *in vitro*, but highly modulated *in vivo*. *Gene* **266**, 35–43.
- Eagleson, G., Ferreira, B. & Harris, W.A. (1995). Fate of the anterior neural ridge and the morphogenesis of the *Xenopus* forebrain. *J. Neurobiol.* **28**, 146–58.
- Finkielstein, C.V., Lewellyn, A.L. & Maller, J.L. (2001). The midblastula transition in *Xenopus* embryos activates multiple pathways to prevent apoptosis in response to DNA damage. *Proc. Natl. Acad. Sci. USA* **98**, 1006–11.
- Gandin, V., Miluzio, A., Barbieri, A., Magri, L., Kiyokawa, H., Marchisio, P.C. & Biffo, S. (2008). eIF6 is rate limiting for translation, growth and transformation. *Nature* **455**: 684–8.
- Harland, R.M. (1991). In situ hybridization: an improved whole mount method for *Xenopus* embryos. *Meth. Cell. Biol.* **36**, 675–685.
- Hensley, C. & Gautier, J. (1997). A developmental timer that regulates apoptosis at the onset of gastrulation. *Mech. Dev.* **69**, 183–95.
- Hensley, C. & Gautier, J. (1998). Programmed cell death during *Xenopus* development: a spatio-temporal analysis. *Dev. Biol.* **203**, 36–48.
- Holt, C.E., Bertsch, T.W., Ellis, H.M. & Harris, W.A. (1988). Cellular determination in the *Xenopus* retina is independent of lineage and birth date. *Neuron* **1**, 15–26.
- Ji, Y., Shah, S., Soanes, K., Islam, M.N., Hoxter, B., Biffo, S., Heslip, T. & Byers, S. (2008). Eukaryotic initiation factor 6 selectively regulates Wnt signalling and β -catenin protein synthesis. *Oncogene* **27**, 755–62.
- Johns, P.R. (1977). Growth of the adult goldfish eye. III. Source of the new retinal cells. *J. Comp. Neurol.* **176**, 343–57.
- Miluzio, A., Beugnet, A., Volta, V. & Biffo, S. (2009). Eukaryotic initiation factor 6 mediates a continuum between 60S ribosome biogenesis and translation. *EMBO Rep.* **10**, 459–65.
- Nieuwkoop, P.D. & Faber, J. (1967). *Normal table of Xenopus laevis*. Daudin. Amsterdam, North Holland.
- Reh, T.A. & Kljavin, I.J. (1989). Age of differentiation determines rat retinal germinal cell phenotype: induction of differentiation by dissociation. *J. Neurosci.* **9**, 4179–89.
- Sanvito, F., Piatti, S., Villa, A., Bossi, M., Lucchini, G., Marchisio, P.C. & Biffo, S. (1999). The beta4 integrin interactor p27(BBP/eIF6) is an essential nuclear matrix protein involved in 60S ribosomal subunit assembly. *J. Cell. Biol.* **144**, 823–37.
- Sanvito, F., Vivoli, F., Gambini, S., Santambrogio, G., Catena, M., Viale, E., Veglia, F., Donadini, A., Biffo, S. & Marchisio, P.C. (2000). Expression of a highly conserved protein, p27BBP, during the progression of human colorectal cancer. *Cancer Res.* **60**, 510–16.
- Straznicky, K. & Gaze, R.M. (1971). The growth of the retina in *Xenopus laevis*: an autoradiographic study. *J. Embryol. Exp. Morphol.* **26**, 67–79.
- Vaccaro, M.C., Cuccaro, M., De Marco, N. & Campanella, C. (2006a). Isolation and expression pattern of p27 BBP/eIF6 cDNA in *Xenopus laevis* embryos. *Mol. Reprod. Dev.* **73**, 485–490.
- Vaccaro, M.C., Cuccaro, M., De Marco, N. & Campanella, C. (2006b). Isolation and expression pattern of p27 BBP/eIF6 cDNA in *Xenopus laevis* embryos. *ERRATUM Mol. Reprod. Dev.* **73**, 1612.
- Viczian, A.S., Vignali, R., Zuber, M.E., Barsacchi, G. & Harris, W.A. (2003). Xotx5b and Xotx2 regulate photoreceptor and bipolar fates in the *Xenopus* retina. *Development* **130**, 1281–94.
- Wetts, R., Serbedzija, G.N. & Fraser, S.E. (1989). Cell lineage analysis reveals multipotent precursors in the ciliary margin of the frog retina. *Dev. Biol.* **136**, 254–63.
- Yeo, W. & Gautier, J. (2003). A role for programmed cell death during early neurogenesis in *Xenopus*. *Dev. Biol.* **260**, 31–45.



Contents lists available at ScienceDirect

Differentiation

journal homepage: www.elsevier.com/locate/diff

Eukaryotic initiation factor 6 (eif6) overexpression affects eye development in *Xenopus laevis*

N. De Marco^{a,*}, M. Tussellino^a, A. Vitale^b, C. Campanella^a

^a Department of Structural and Functional Biology, University of Naples Federico II, Naples, Italy

^b TIGEM, Naples, Italy

ARTICLE INFO

Article history:

Received 19 November 2010

Received in revised form

27 April 2011

Accepted 2 May 2011

Available online 20 May 2011

Keywords:

eif6

Eye

Brain

Apoptosis

Xenopus laevis

bcl2

ABSTRACT

The translation initiation factor eif6 has been implicated as a regulator of ribosome assembly, selective mRNA translation and apoptosis. Many of these activities depend upon the phosphorylation of eif6 serine 235 by PKC. Previous data showed that eif6 binds to the 60S ribosomal subunit when unphosphorylated, inhibiting assembly with the 40S subunit. Phosphorylation of Ser235 releases eif6 from the 60S subunit and allows assembly. eif6 acts as an anti-apoptotic factor via regulation of the bcl2/bax balance and acts selectively upstream of bcl2. This activity also depends upon phosphorylation of eif6 Ser235. One of the consequences of *eif6* overexpression in *Xenopus* embryos is aberrant eye development. Here we evaluate the eye phenotype and show that it is transient. We show that the whole eye, particularly the retina layers, of the embryos injected with *eif6*-encoding mRNA recover by stage 42. Embryos over-expressing *eif6* have normal expression of anterior- and brain-specific markers, indicating that outside the eye field, other neural regions appear unaffected by the *eif6* injection. No eye defect was detected when morpholinos were used to reduce eif6 protein synthesis. We tested how two known pathways of eif6 function with respect to alteration of eye development. We found that injection of *bcl2* did not produce the eye phenotype and *eif6*-bax co-injection did not rescue the eye defect, suggesting that the eye phenotype is not bearing on the anti-apoptotic role played by eif6 is not linked to its role as an anti-apoptotic factor. We also determined that PKC-dependant phosphorylation of Ser235 in eif6 is not required to produce defective eye development. These results indicate that the aberrant eye phenotype, produced by *eif6* overexpression, is not directly linked to the PKC-regulated effects of eif6 on translation and ribosomal subunit interaction or on eif6 anti-apoptotic properties.

© 2011 International Society of Differentiation. Published by Elsevier Ltd. All rights reserved.

1. Introduction

P27^{BBP}/eif6 (β4 binding protein/eukaryotic initiation factor 6) or eif6¹ is a protein necessary for cell life and is highly conserved from yeast to *Homo sapiens* (Sanvito et al., 1999; Gandin et al., 2008). Eif6 binds to the 60S ribosomal subunit when it is unphosphorylated, inhibiting assembly with the 40S subunit. In mouse cells, Ceci et al. (2003) showed that, upon PKC phosphorylation of serine 235, Eif6 is released from the 60S ribosomal subunit and translation can initiate. In *Xenopus*, eif6 is similarly present in the 60S subunits. In this system, immunoprecipitation of eif6 leads to co-precipitation of ribosomal protein L5. In ribosome profiles, eif6 sediments with ribosomes, peaks at

60–80S and is absent in polysomes. Moreover, the Ser235 PKC phosphorylation site is also found in *Xenopus eif6* cDNA, and a serine-phosphorylated isoform of eif6 is detectable in embryo lysates (Carotenuto et al., 2005; Vaccaro et al., 2006).

PKC phosphorylation may occur downstream of extra-cellular signalling such as insulin/growth factors, indicating that Eif6 is able to modulate translation *in vivo* upon specific or integrating stimulation (Gandin et al., 2008). Significantly, EIF6 appears to be selective in regulating the translation of certain mRNAs, as in the case of β-catenin (Ji et al., 2008). This intriguing selectivity in regulating translation is not fully understood, but it may entail the above-mentioned phosphorylation of Ser235 and/or a role associated with mi-RNAs. EIF6 is, in fact, part of the RISC (RNA-induced silencing complex), which also contains the 60S ribosomal subunit and may inhibit translation by blocking ribosome recycling on selected target mRNAs (Chendrimada et al., 2007; Ji et al., 2008). However, in other systems, eIF6 does not appear to be necessary for mi-RNA-based translation repression (Eulalio et al., 2008).

The *Xenopus laevis* embryo is a useful model to explore the selectivity of eif6 action. In this embryo, a modulated expression of *eif6* occurs in the developing anlagen, in addition to a base level of

Abbreviations: PKC, protein kinase C; RISC, RNA-induced silencing complex; bcl2, B-cell CLL/lymphoma 2; GFP, green fluorescent protein; DAPI, 4',6-diamidino-2-phenylindole

* Corresponding author. Tel.: +39 081 679189; fax: +39 081 679233.

E-mail address: nademarc@unina.it (N. De Marco).

¹ We use official names (www.ncbi.nlm.nih.gov/sites/gquery) for each gene or protein according to the species to which they refer.

expression. In particular, *eif6* mRNA is abundant in the dorsal mesoderm, in the eye field and the mid-hindbrain boundary (Vaccaro et al., 2006). Overexpression of *eif6* in the *Xenopus* embryo produces two altered phenotype features: a bending of the embryo along the right/left axis and a defect in eye formation. While no data are available for the eye defect, previous experimentation indicated that, in *eif6* overexpressors, the bending is due to a decrease of apoptosis in the injected side (De Marco et al., 2010a). In *Xenopus* embryogenesis, apoptosis controls the absolute cell number and its timing is regulated during development (Hensley and Gautier, 1997). *eif6* inhibits cell death by acting upstream of *bcl2*, suggesting that apoptosis may be further modulated during *X. laevis* development by fine tuning this protein. The anti-apoptotic action of *eif6* requires the conservation of Ser235. As *eif6* overexpression causes an increase in both the mRNA and the protein levels of *bcl2*, it was concluded that *eif6* acts through an unknown factor that selectively acts upstream of *bcl2* (De Marco et al., 2010a,b).

In this paper, we found that *eif6* overexpression affects eye development. We investigated whether the defect in the eye correlates with the observed decrease in apoptosis occurring in the injected side of the embryo (De Marco et al., 2010a). Indeed, Yeo and Gautier (2003) demonstrated that apoptosis regulates primary neurogenesis at the level of neuronal determination, indicating that apoptosis is essential for proper morphogenesis of neural tube-derived organs. We therefore hypothesised that the reduction in cell death due to *eif6* overexpression may correlate to the eye defect in morphogenesis. In contrast, our data indicate that the altered eye phenotype caused by *eif6* overexpression cannot be mimicked by *bcl2* overexpression. Moreover, we show that in embryos injected with *eif6* morpholino the eye phenotype does not differ from that of w.t. embryos while, following injection of different dosages of *eif6*, it was found that even a minor increase in *eif6* level produces altered eye phenotypes. Therefore, we concluded that for proper eye development the *eif6* level should be kept within or below the physiological range. Embryos injected with *eif6* mutated in Ser235 showed the altered eye phenotype, suggesting that the eye defect is not related to *eif6* impairment of ribosomal subunit association through PKC phosphorylation (Ceci et al., 2003).

2. Materials and methods

2.1. Animals

Adult *Xenopus laevis* females were obtained from Rettili, Varese, Italy. They were kept and utilised at the Department of Structural and Functional Biology at the University of Naples Federico II, according to the guidelines and policies dictated by the University Animal Welfare Office and in agreement with international regulations.

To obtain eggs, *X. laevis* females were injected in the dorsal lymphatic sac with 500 units of Gonase (AMSA, Rome, Italy) in Amphibian Ringer (111 mM NaCl, 1.3 mM CaCl₂, 2 mM KCl, 0.8 mM MgSO₄, 25 mM Hepes, pH 7.8). Fertilised eggs and embryos were obtained by standard insemination methods and staged according to Nieuwkoop and Faber (1967).

2.2. Microinjections

The pCS2eif6, pCS2bcl2 and pCS2S235A plasmids were used, as described in De Marco et al. (2010a). The pCS2MTXBax plasmid was kindly offered by JL Maller (University of Colorado, School of Medicine, USA). The pCS2βgal was generously supplied by M. Ori (University of Pisa, Italy). Capped synthetic RNAs were generated by *in vitro* transcription using the Sp6 Message Machine kit (Ambion, Austin, TX, USA). The *eif6* antisense morpholino used

was 5'-GCGGACGGCCATGTTGGCTTCTTAG-3' (Gene Tools LLC, Philomath, OR, USA). The mispaired morpholino control used was 5'-GcGACcGCCATcTTGcCTTcTAAG-3' (Gene Tools LLC). pCS2MTGFP or pCS2βgal mRNA was always co-injected to label the injected side. RNAs were injected into the animal hemisphere of a single cell of one- or two-cell embryos using a Drummond 'Nanoject' apparatus. During injection, embryos were cultured in 3% Ficoll in 0.1% Ringer. The phenotype of the injected embryos was scored when the un-injected embryos reached stage 35/36. The samples were photographed with a Leica MZ 16F UV stereo-microscope, equipped with a Leica DFC 300F camera and IM50 image manager software.

2.3. In situ hybridisation

In situ hybridisation was performed as described (Vaccaro et al., 2006). Antisense digoxigenin-labelled RNA probes of *rax*, *pax6*, *six3*, *sox2*, *rbpms*, *nrl*, *fgf8* (generously supplied by R. Vignali, M. Andreazzoli, University of Pisa, Italy and S. Casarosa, University of Trento, Italy) and *otx2*, *en2*, *egr2* (kindly supplied by M. Pannese, Ospedale San Raffaele DIBIT, Milan, Italy) were synthesised with RNA T7 or SP6 polymerases (Roche, Mannheim, Germany). β-galactosidase activity was visualised in embryos using Red-Gal (Biosynth, Staad, Switzerland). Sections were observed and photographed using a Leica 6500 microscope. Whole mounts were photographed with a Leica MZ 16F.

2.4. Immunofluorescence

X. laevis embryos were fixed in 4% formaldehyde at 4 °C and stored in 100% methanol at 20 °C. Frozen sections of 10 mm thickness were obtained for immunofluorescence after embedding and freezing in Killik (Bio Optica, Milan, Italy). Non-specific background was blocked by incubating the sections for 30 min in normal goat serum 3% in PBS, 0.5% BSA, 0.1% Tween before exposure overnight at 4 °C to rabbit anti-Eif6 (1:500 dilution v/v; generous gift of P.C. Marchisio and S. Biffo, DIBIT, Milan, Italy) and rabbit anti-GFP (1:500 dilution v/v; Invitrogen). Staining was completed by incubating the samples with BODIPY FL-conjugated or Texas-Red-conjugated anti-rabbit goat IgG (Invitrogen, Life Technologies, Carlsbad, CA, USA); nuclei were counter-stained with DAPI. Sections were observed and photographed using a Leica CTR 6500 UV microscope equipped with a Leica application suite.

2.5. TUNEL staining

TUNEL staining for the identification of apoptotic cells was carried out using the ApopTag Peroxidase *In situ* Apoptosis Detection Kit (Chemicon International, Inc., Temecula, CA, USA) in accordance with the manufacturer's instructions.

2.6. Western blot

For western blot experiments the embryos were injected on both sides of the two-cell stage and harvested until stage 28. Embryos were homogenised in HEPES buffer pH 7.5 containing 900 mM glycerol, 0.02 mM Na₃N, 1 mM ATP, 1 mM DTT, 5 mM ethylene glycol tetraacetic acid (EGTA) and protease inhibitors as described in De Marco et al. (2010a). Western blotting on nitrocellulose membrane was carried out as in De Marco et al. (2010a). Antibody incubation was carried out using rabbit anti-Eif6 antibody (1:1000 dilution v/v), mouse anti-β catenin (1:500 dilution v/v; Santa Cruz Biotechnology, inc.), mouse anti-Bcl2 (1:250 dilution v/v; Santa Cruz Biotechnology, inc.), mouse anti-myc (1:1000 dilution v/v; Sigma) and mouse anti-α-tubulin (1:500 dilution, v/v; Sigma, St. Louis, MO, USA). Antibody binding

was detected with secondary anti-mouse or anti-rabbit IgGs coupled with horseradish peroxidase (Pierce, Rockford, IL, USA) and revealed with the enhanced chemiluminescence kit (Pierce).

2.7. RNA extraction and RT-PCR

Total RNA was extracted from batches of five embryos using Tri Reagent (Sigma) according to the manufacturer's recommendations. RT-PCR was performed using the Super Script VIL0 cDNA synthesis kit (Invitrogen Life Technologies) and primers for β -catenin (forward: AGATGCAGCAACTAACAGGA and reverse: GTACTGCATTTGAGCCATCT) *hsth4* (forward: CGGGATAACATTACAGGTA and reverse: TCCATGGCGTAACTGTC).

3. Results and discussion

3.1. Overexpression of *eif6* affects eye development

The endogenous *eif6* mRNA and corresponding protein are constantly present in the eye field during its early formation and

in the neuroectoderm region (Vaccaro et al., 2006; De Marco et al., 2010b). Our preliminary results indicated that *eif6* mRNA, injected into a blastomere at the onset of development (stage 2), interferes with eye formation; in stage 35 the eye of the injected side displays an altered morphogenesis. However, at stage 42, the eye recovers in all the observed cases, suggesting that the eye phenotype is due to a delay in eye morphogenesis. In this study, we injected *eif6* mRNA (100 pg to 400 pg), together with GFP mRNA (300 pg) or β -galactosidase mRNA (400 pg), into a blastomere of the two-cell stage *X. laevis* embryo to investigate the effects of *eif6* overexpression on eye development. In these experiments, the uninjected side can be considered to be the natural control of each assay because the first cleavage plane divides the embryo into two symmetrical halves. When injected embryos were scored at stage 35 we observed that eye formation was markedly affected with high dosages of the injected mRNA. Indeed, in 70% ($n=98$) of embryos receiving 400 pg of *eif6* mRNA, the eye derived from the injected blastomere was reduced in size or apparently absent (Fig. 1a–f). Even when we injected the blastomere with a lower dosage (100 pg) of the mRNA, 50% ($n=90$) of the embryos showed a defective eye phenotype.

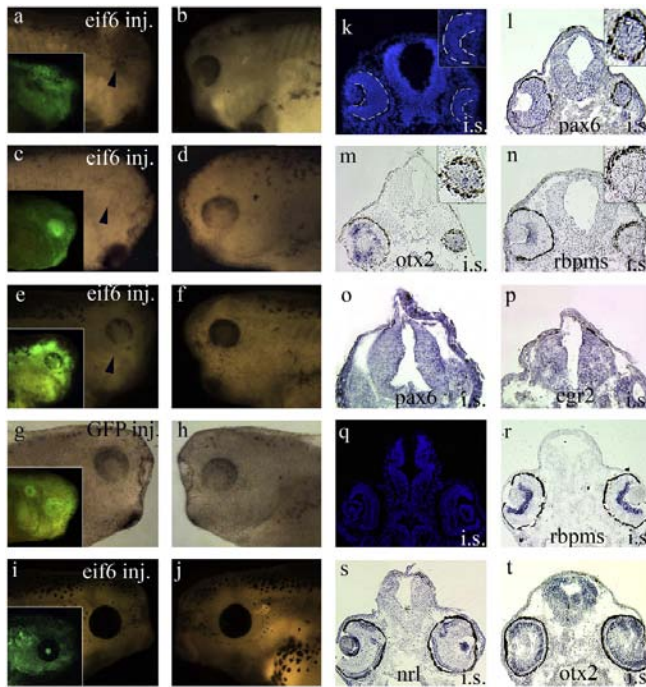


Fig. 1. Effects of *eif6* overexpression on eye formation. (a)–(f) Three different embryos injected with 400 pg *eif6* mRNA and 300 pg GFP mRNA into one blastomere of the two-cell stage and harvested at stage 35. Micrographs of the two sides (a and b; c and d; e and f) of the same embryos are shown: (a), (c), and (e) are the injected sides. The *eif6* overexpressors showed a range of the defective eye phenotype (arrowheads in a, c, e). The injected sides were marked by GFP fluorescence (inset in a, c, e). (g) GFP-injected side (fluorescence in the inset) and uninjected side (h) of the same embryo: overexpression of GFP alone did not affect eye development. (i)–(j) Micrographs of the two sides of the *eif6*-injected embryo harvested at stage 42. The eye of the injected side marked by GFP fluorescence (inset in i) recovers normal morphology. (k)–(p) Cryostat sections of stage 35 *eif6*-injected embryos showed a reduced eye in the injected side. Magnification of reduced eye in insets of figures k–n. (k) DAPI staining. Dasher lines border the entire thickness of neural retinas. The eye marker *pax6* (l) was present in both injected and uninjected eye. However the retina layer markers showed a difference between injected and uninjected eye. Indeed, in the small injected eye *otx2* (m) was diffuse and not localised in the central retina as in the uninjected eye. *rbpm5*, (n) becomes evident only in the uninjected side. The encephalon structures were morphologically normal, forebrain (o) and midbrain (l) were labelled with *pax6*, hindbrain (p) was marked by *egr2*. (q)–(t) Cryostat sections of stage 42 *eif6*-injected embryos. (q) DAPI staining shows a normal stratification of retina in the injected eye compared to the control eye. (r)–(t) *In situ* hybridisation with *rbpm5*, *nrl*, an outer nuclear layer marker and *otx2*, showed no difference between injected and uninjected eye, indicating that the recovered retina is structurally similar to the control retina. i.s.: *eif6*-injected side.

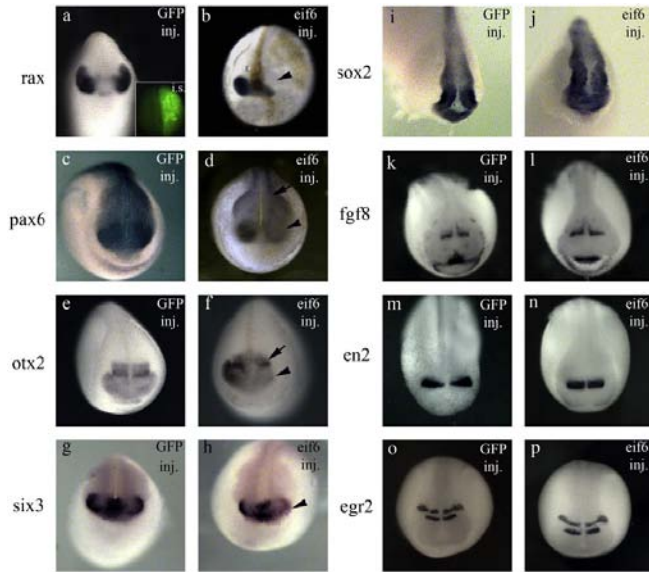


Fig. 2. *eif6* overexpression specifically inhibits eye development. (a)–(j) Embryos were injected with *eif6* (400 pg) and *fgal* (400 pg) or *GFP* (400 pg) alone into one blastomere of the two-cell stage and harvested at the neurula stage. Whole mount *in situ* hybridisations were performed for *rax* (a), (b), *pax6* (c), (d), *otx2* (e), (f), *six3* (g), (h) and *sox2* (i), (j), *fgf8* (k), (l), *en2* (m), (n), *egr2* (o), (p). *GFP* overexpression did not affect the expression of *rax* (a), *pax6* (c), *otx2* (e), *six3* (g), *sox2* (i), *fgf8* (k), *en2* (m), *egr2* (o). Inset in (a) shows diffusion of GFP fluorescence in the whole injected side (i.s.) of a neurula. *eif6* overexpression specifically reduced *rax* (b), *pax6* (d), *otx2* (f) and *six3* (h) expression within the presumptive eye field (arrowheads), while neural expression of the same markers was unaffected (arrows). (j) No expression difference was found for the specific neural markers *sox2*, *fgf8*, *en2*, *egr2* between the *eif6*-injected and un-injected side.

Control experiments showed that a single injection of *GFP* mRNA at the concentration of 400/700 pg did not produce defective phenotypes (Fig. 1g and h). At stage 42, when the retina is mature, the eye of the *eif6*-injected side appeared morphologically similar to that of the control side (Figs. 1i and j). In vertebrates, the mature retina is organised into three distinct cellular layers: the outer nuclear layer (ONL), the inner nuclear layer (INL) and the ganglion cell layer (GCL). *nrl* can be used as a marker of the ONL, *otx2* as a marker of the INL and *rbpms* as a marker of the GCL. These layers organise gradually during retinogenesis. At stage 35 the GCL is in the process of differentiation and the INL starts segregating into the central portion of the retina (see Decembrini et al., 2006). We performed *in situ* hybridisations with the early eye field marker *pax6* and retinal differentiation markers (*otx2*, *rbpms*) on frozen sections of *eif6* overexpressors at stages 35 (Fig. 1k–n). While *pax6* is evenly distributed in the eye anlagen of both sides of the embryo (Fig. 1i), *otx2* and *rbpms* localise in the expected sites in the un-injected side of the embryo (Fig. 1m and n) in contrast to the delayed eye of the injected side, where the markers are sparsely distributed or have not yet appeared. The retinal pigment epithelium (RPE) is evident in both sides of the embryo. Moreover, *in situ* analysis of the brain markers *pax6* (expressed in the brain and in the eye) at the forebrain and midbrain level, and *egr2* (hindbrain and neural crest) at the hindbrain level, indicate that the brain is morphologically normal in *eif6* overexpressors (Fig. 1o and p). *In situ* analyses of *rbpms*, *otx2*, *nrl* expression were also performed to ascertain whether anatomical recovery of the eye at stage 42 correlates with the correct structure of the retina. Indeed, the *eif6*-injected side displays identical *in situ* hybridisation

patterns, in both the *eif6*-injected eye and in the un-injected side (Fig. 1q–t).

To characterise the eye phenotype further we performed *in situ* hybridisation in stage 19 embryos with *rax*, *pax6*, *otx2* (forebrain and eye marker), *six3* (eyes and ventral forebrain), *sox2* (a general neural marker), *fgf8*, *en2* (mid/hindbrain boundary markers) and *egr2*. Moreover we injected β -galactosidase as a tracer (Fig. 2b and d) to check whether the injected RNA was in more than just the eye field. The β -galactosidase activity was measured *in situ* (red) followed by whole-mount hybridisation. In the injected side, the expression of *rax* (75%, $n=80$ Fig. 2b) was strongly reduced in the eye field of the experimental side compared to the control side, consistent with the eye phenotype observed at stage 35 in the *eif6*-injected side. Furthermore, expressions of *pax6* (70%, $n=80$ Fig. 2d), *otx2* (65%, $n=60$ Fig. 2f) and *six3* (71%, $n=30$ Fig. 2h) were reduced in the presumptive eye domain, in contrast to the prosencephalon and spinal cord regions, which were unaffected (Fig. 2). Importantly, the reduction in the expression of the eye field markers we detected is also consistent with a delay in RPE pigmentation at stage 35 (see Westenskow et al., 2009). We examined the expression of the specific neural marker *sox2* ($n=30$ Fig. 2j), *fgf8* ($n=30$ Fig. 2l), *en2* ($n=30$ Fig. 2n) and *egr2* ($n=30$ Fig. 2p) and found no difference between the injected and un-injected side. Therefore, outside the eye field, other neural regions appear unaffected by *eif6* injection.

To study the endogenous function of *eif6* in eye development, we performed loss-of-function experiments injecting *eif6* morpholino antisense oligonucleotides (7.5 ng, $n=60$) or mispaired morpholino control (7.5 ng, $n=60$) together with *GFP* mRNA (200 pg) into a blastomere of a two-cell-stage embryo as

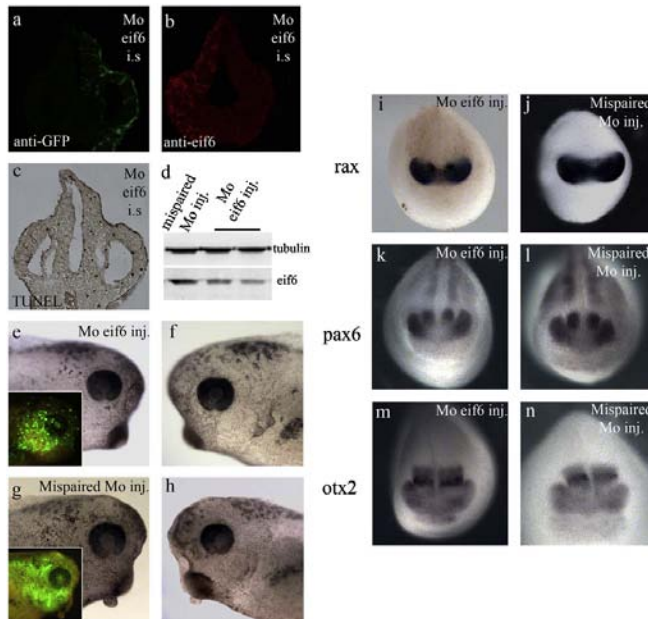


Fig. 3. Effects of *eif6* downregulation. (a), (b) Serial cross-sections of stage 28 *eif6*-direct morpholino and *GFP*-injected embryo were immunostained with anti-*GFP*, with anti-*eif6* antibodies and with TUNEL assay. The lower level of *eif6* immunostaining (b) is present in the injected side (i.s.) marked by *GFP* (a). An increase of apoptotic nuclei is evident in the injected side (c). (d) Western blot with anti-*eif6* antibody indicates that the level of protein in *eif6* morpholino-injected embryos was lower than that in mispaired morpholino-injected embryos. Three sets of injected embryos were used in the blot. Normalisation was performed with anti- α -tubulin antibody. (e)–(h) Experimental and control side of the same embryo injected with *eif6*-direct morpholino (e), (f) or control mispaired morpholino (g), (h) in one blastomere at the two-cell stage and harvested at stage 35. No eye difference was evident between the injected side (e), (g) marked by *GFP* fluorescence (inset) and the un-injected side (f), (h). (i)–(n) *In situ* hybridisation of morpholino (i, k, m) or mispaired morpholino (j, l, n) injected embryos at the neurula stage. The expression of anterior markers *rax* (i), (j), *pax6* (k), (l) and *otx2* (m), (n) was not affected by depletion of *eif6*.

described in De Marco et al. (2010a). The *eif6* downregulation was monitored by immunofluorescence (Fig. 3a and b) or western blot analysis with the anti-*Eif6* antibody (Fig. 3d). Surprisingly, unilateral injection of *eif6* morpholino did not cause apparent eye defects (Fig. 3e and f), while a curvature of the embryo occurred, as expected, because of an increase of apoptosis in the injected side (data not shown and Fig. 3c), in agreement with De Marco et al. (2010a). Consistently, the expressions of *rax* ($n=40$), *pax6* ($n=40$) and *otx2* ($n=40$) were unchanged in the *eif6* morpholino-injected side compared to those in the un-injected side (Fig. 3i–n).

Our results indicate that *eif6* overexpression reduces eye size in early developing embryos, which recover and form normal sized eyes by stage 42. The eye development is delayed as a result of *eif6* overexpression and *eif6* downregulation, at the concentration tested, does not produce eye defects.

It should also be considered that the reduction of *eif6* level produced by the used dosage of *eif6* morpholino may be not sufficient to generate an eye phenotype. Higher dosages of *eif6* morpholino antisense oligonucleotides were not employed because they produced aspecific phenotypes (data not shown; for a review see Heasman, 2002).

Altogether, it appears that *eif6* levels below a physiological threshold are sufficient for the correct timing of eye morphogenesis, while levels over this threshold induce the abnormality observed in ectopically expressed *eif6*. Accordingly, it can be hypothesised that *eif6* overexpression affects the translation of

different classes of mRNA in different tissues, depending upon the relative abundance of each mRNA, and that the phenotypic effects are the result of reaching thresholds that may vary among tissues. A tissue-specific, dose-dependent effect of *Eif6* was demonstrated in *Eif6*^{+/-} mice, where a 50% decrease in the levels of protein in all tissues was accompanied by a tissue-specific effect, i.e., a mass reduction and impaired G1/S phase progression in only the liver and adipose tissue (Gandin et al., 2008).

3.2. The role of *eif6* in eye formation is independent of its anti-apoptotic function

During *X. laevis* embryogenesis, apoptosis presents a stereotypical, reproducible pattern. At the neurula plate stage, apoptosis is detected exclusively within the presumptive neuroectoderm. In particular, apoptosis regulates primary neurogenesis at the level of neuronal determination (Yeo and Gautier, 2003). At later stages, apoptosis remains localised to specific brain regions and is always abundant in the developing eye. At the neurula stage, the apoptosis pattern is known to overlap with expression of *Pax6*, the eye master gene (Hirsch and Harris, 1997). *Pax6* is expressed throughout eye development, as well as in cells destined to form part of the brain, suggesting that cell death here plays a role in the eye placode and brain (Hensey and Gautier, 1998).

We hypothesised that reduction in cell death due to *eif6* overexpression could cause the described eye defect. Indeed, we

previously reported that a decrease of apoptosis occurs in *eif6* overexpressors (De Marco et al., 2010a) including the eye territory (data not shown). Because *eif6* is an anti-apoptotic factor acting upstream of *bcl2* (De Marco et al., 2010a), we injected 300 pg of *bcl2*, together with 300 pg of *GFP* mRNA, into a blastomere of a two-cell stage embryo. *bcl2* overexpression was examined by western blot analyses, which consistently indicated that *bcl2*-injected embryos showed more protein compared to

GFP-injected embryos (Fig. 4a). The *bcl2*-injected embryos displayed the bent phenotype (data not shown) and a TUNEL reduction in the injected side, including the eye (Fig. 4b and c). At the neurula stage, the eye-markers, *rax* ($n=40$), *pax6* ($n=40$) and *otx2* ($n=40$), had similar expressions in the injected and uninjected sides, and consistently, at stage 35, the eyes of these embryos appeared morphologically normal (Fig. 4d–i and data not shown). Moreover, to investigate whether normal expression of eye markers is restored at neurula stage by pro-apoptotic agents, we co-injected *eif6* and *bax*. In Fig. 4j and k, the *bax*-injected side shows an increase of apoptosis, including the eye territory, as observed by TUNEL experiments (see also De Marco et al., 2010a). Fig. 4l indicates that, in *bax* overexpressors, the myc-tagged *bax* protein appears. In *bax*-*eif6*- β -gal co-injected neurulae, normal expression of *rax* is not restored in the injected side (Fig. 4m).

Our data show that the delay in eye morphogenesis caused by *eif6* overexpression does not appear related to the previously reported anti-apoptotic action of *eif6* upstream of *bcl2* (De Marco et al., 2010a).

3.3. Ser235 phosphorylation site is not required to produce the eye phenotype

In mammalian cells, translation occurs when Eif6 is released from the 60S ribosomal subunit following phosphorylation on Ser235 through the RACK1–PKC pathway. S235A mutants are impaired in the RACK1/PKC-mediated phosphorylation (Ceci et al., 2003). In *Xenopus*, the Ser235 site is conserved and may be reasonably considered the target of PKC phosphorylation leading to initiation of translation, as shown in mammalian cells (Ceci et al., 2003).

Previous data showed that Ser235 is necessary for the *eif6* apoptotic function, leading to the conclusion that *eif6* acts as a regulator of protein synthesis affecting the translation of mRNAs involved in apoptosis (De Marco et al., 2010a). However, in *Xenopus* *eif6* activity in regulating translation via PKC phosphorylation was not fully investigated (see Carotenuto et al., 2005).

In the present study, we test the known action of *eif6* in inhibiting the translation of β -catenin in mammalian cells (Ji et al., 2008). We found that the same holds true for β -catenin in our system and that Ser235 is necessary for this function (Fig. 5a and b). Accordingly, we hypothesised that the eye defect was correlated to the *eif6* activity in regulating translation via PKC phosphorylation.

In contrast with the above hypothesis, embryos injected with S235A mRNA produced defective eye phenotypes at the tadpole stage, as occurs in embryos injected with wild type *eif6* (Fig. 5c–h). Indeed, 70% of embryos injected with 400 pg of S235A ($n=55$) and 45% of embryos injected with 100 pg of S235A ($n=98$) showed the eye phenotype (from reduction in size to an apparently absence in the whole-mount samples). Also in these embryos the eye recovers at stage 42. At the neurula stage, a reduction in *rax* ($n=50$), *pax6* ($n=50$) and *otx2* ($n=50$) expressions in the injected side was observed (Fig. 5i–n). The data are consistent with those shown in Fig. 1, using w.t. *eif6*. They indicate that the PKC phosphorylation site is not involved in the production of the eye phenotype, suggesting that *eif6* acts through a mechanism unrelated to the control of the association of the 60S and 40S ribosomal subunits (Ceci et al., 2003). Further studies should investigate whether, in our system, *eif6* mediates mRNA translational repression, as was shown to occur during *C. elegans* development (Chendrimada et al., 2007). Interestingly, Wnt- β -catenin controls differentiation of RPE in vertebrate development (Westenskow et al., 2009). However, our data (Fig. 5) lead to conclude that this signalling is not involved in the generation of

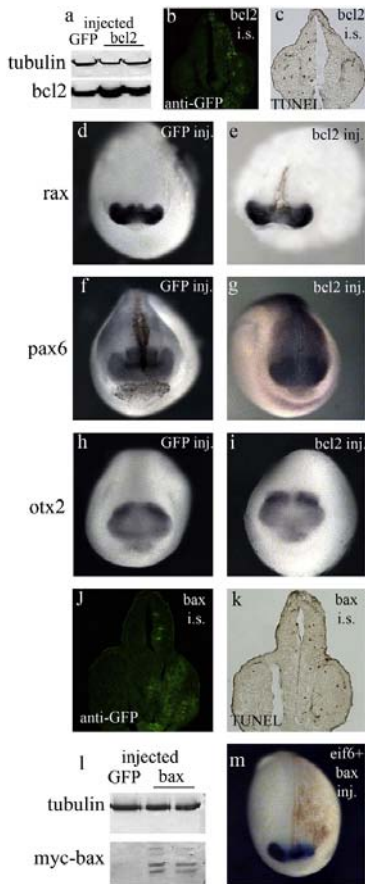


Fig. 4. Apoptosis reduction is not involved in the eye defect. Embryos were injected with *bcl2* (300 pg) and *GFP* (200 pg) or *GFP* (400 pg) alone in one blastomere of the two-cell stage. (a) Western blot with anti-Bcl2 antibody indicates the greater presence of protein in *bcl2*-injected embryos with respect to *GFP*-injected embryos. Two sets of *bcl2*-injected embryos were used in the blot. Normalisation was performed with anti- α -tubulin antibody. *GFP* immunofluorescence (b) and TUNEL staining (c) on sections of *bcl2*-injected embryo. The injected side, marked by *GFP* fluorescence, showed fewer apoptotic nuclei compared with the control side. At the neurula stage, whole mount *in situ* hybridisations were performed for *rax* (d), (e), *pax6* (f), (g) and *otx2* (h), (i). *bcl2* overexpression did not reduce *rax* (e), *pax6* (g) or *otx2* (i) expression in the injected side compared to the control side. (j)–(l) Embryo were injected with myc-*bax* (1 ng) and *GFP* (200 pg). The injected side, marked by *GFP* (j) showed an increase of TUNEL-positive nuclei (k). Western blot with anti-myc antibody indicates the presence of exogenous *bax* in the injected embryos (l). *bax*-*eif6* co-injection does not restore normal expression of *rax* (m).

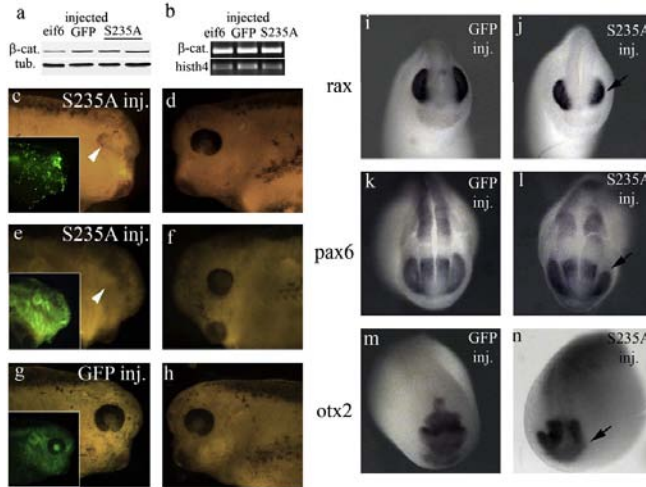


Fig. 5. Effects of mutant S235A overexpression. Embryos injected with *eif6* mutant S235A (300 pg) and *GFP* (200 pg) or *GFP* alone (400 pg) in one blastomere of the two-cell stage were harvested at stage 35 (a)–(h) or at the neurula stage (i)–(n). (a) In the Western blots using anti-β-catenin antibody, *eif6* or *GFP*-injected embryos and two sets of *S235A*-injected embryos were used. A decrease in β-catenin level was found only in *eif6* overexpressors. Normalisation was performed with the anti-tubulin antibody. (b) RT-PCR analysis showed that β-catenin mRNA level was unaffected in *eif6* and *S235A* overexpressors compared with *GFP*-injected embryos. Normalisation was performed using *histH4* primers. (c)–(h) Micrographs of the two sides (c and d; e and f; g and h) of the same stage 35 embryo are given. *S235A* overexpressors show a reduction in eye size (arrowheads) of the injected side (c), (e), marked by *GFP* fluorescence (inset), compared to the uninjected side (respectively d, f), (g), (h) Injection of *GFP* alone (fluorescence in inset of Figure e) did not affect eye development. (i)–(n) Whole mount *in situ* hybridisations were performed for *rax* (i), (j), *pax6* (k), (l) and *otx2* (m), (n) on *GFP* (i, k, m) or *S235A* (j, l, n) overexpressing embryos at neurula stage. The expression of the eye marker *rax* (j), *pax6* (l) and *otx2* (n) was inhibited in the eye field (arrows) of the *S235A*-injected side.

the eye phenotype induced by *eif6* overexpression. Indeed, *S235A* overexpressors present eye defects without a reduction of β-catenin translation.

In this paper, we showed that the effect of *eif6* overexpression is related to the morphogenesis of the eye and does not affect the surrounding tissue. Moreover, we found that *eif6* morpholino has no effect on eye morphogenesis at the concentration tested. Therefore, the levels of *eif6* appear to be highly regulated during development and instrumental for proper morphogenesis of the eye placode. Because eye formation is regulated by Igf signalling (Richard-Parpaillon et al., 2002; Pera et al., 2001; Wu et al., 2006) and *Eif6* is able to modulate the translation of specific mRNA upon stimulation of a growth factor such as Igf (Gandin et al., 2008), future experimentation should investigate in particular whether a relationship exists between Igf signalling and the regulation of *eif6* steady-state in proper eye morphogenesis.

Acknowledgements

We thank S. Biffo for suggestions, A. Gadaleta and A. Liberti for laboratory assistance, M. Walters for reviewing the manuscript and AMRA Scarl for using AMRA instruments. Our research was funded by a Grant from the *Compagnia di San Paolo* ('Integration of spatial and biochemical clues during brain development' Project) to C.C.

References

Carotenuto, R., De Marco, N., Biffo, S., Wilding, M., Vaccaro, M.C., Marchisio, P.C., Capriglione, T., Russo, G.L., Campanella, C., 2005. Phosphorylation of p27B^{BP}/

eif6 and its association with the cytoskeleton are developmentally regulated in *Xenopus* oogenesis. *Cell. Mol. Life Sci.* 62, 1641–1652.
 Ceci, M., Gaviraghi, C., Gorrini, C., Sala, L.A., Offenhäuser, N., Marchisio, P.C., Biffo, S., 2003. Release of *eif6* (p27^{B^{BP}}) from the 60S subunit allows 80S ribosome assembly. *Nature* 426, 579–584.
 Chendrimada, T., Finn, K.J., Ji, X., Bailat, D., Gregory, R.I., Liebhaber, S.A., Pasquinelli, A.E., Shiekhattar, R., 2007. MicroRNA silencing through RISC recruitment of *eif6*. *Nature* 447, 823–828.
 Dicembrini, S., Andreazzoli, M., Vignali, R., Barsacchi, G., Cremisi, F., 2006. Timing the generation of distinct retinal cells by homeobox proteins. *PLoS Biol.* 4, e272.
 De Marco, N., Iannone, L., Carotenuto, R., Biffo, S., Vitale, A., Campanella, C., 2010a. p27(BBP)/*eif6* acts as an anti-apoptotic factor upstream of Bcl-2 during *Xenopus laevis* development. *Cell Death Differ.* 17, 360–372.
 De Marco, N., Campanella, C., Carotenuto, R., 2010b. *X. laevis* embryos high levels of the anti-apoptotic factor p27B^{BP}/*eif6* are stage-dependently found in BrdU and TUNEL-reactive territories. *Zygote* 27, 1–7.
 Eulalio, A., Huntzinger, E., Izaurralde, E., 2008. GW182 interaction with Argonaute is essential for miRNA-mediated translational repression and mRNA decay. *Nat. Struct. Mol. Biol.* 15, 346–353.
 Gandin, V., Miluzio, A., Barbieri, A., Magri, L., Kiyokawa, H., Marchisio, P.C., Biffo, S., 2008. *eif6* is rate limiting for translation, growth and transformation. *Nature* 455, 684–688.
 Heasman, J., 2002. Morpholino oligos: making sense of antisense? *Dev. Biol.* 243, 209–214.
 Hensy, C., Gautier, J., 1997. A developmental timer that regulates apoptosis at the onset of gastrulation. *Mech. Dev.* 69, 183–195.
 Hensy, C., Gautier, J., 1998. Programmed cell death during *Xenopus* development: a spatio-temporal analysis. *Dev. Biol.* 203, 36–48.
 Hirsch, N., Harris, W.A., 1997. *Xenopus* Pax-6 and retinal development. *J. Neurobiol.* 32, 45–61.
 Ji, Y., Shah, S., Soanes, K., Islam, M.N., Hoxter, B., Biffo, S., Heslip, T., Byers, S., 2008. Eukaryotic initiation factor 6 selectively regulates Wnt signalling and β-catenin protein synthesis. *Oncogene* 27, 755–762.
 Nieuwkoop, P.D., Faber, J., 1967. Normal Table of *Xenopus laevis*. Daudin, Amsterdam, North Holland.
 Pera, E.M., Li, W.O., De Robertis, E.M., S.Y., 2001. Neural and head induction by insulin-like growth factor signals. *Dev. Cell* 1, 655–665.
 Richard-Parpaillon, L., Héligon, C., Chesnel, F., Boujard, D., Philpott, A., 2002. The IGF pathway regulates head formation by inhibiting Wnt signaling in *Xenopus*. *Dev. Biol.* 244, 407–417.

Involvement of the eukaryotic initiation factor 6 and *kermit2/gipc2* in *Xenopus laevis* pronephros formation

MARGHERITA TUSSELLINO, NADIA DE MARCO*, CHIARA CAMPANELLA and ROSA CAROTENUTO

Department of Structural and Functional Biology, University of Naples Federico II, Naples, Italy

ABSTRACT The translation initiation factor Eif6 has been implicated as a regulator of ribosome assembly, selective mRNA translation and apoptosis. Many of these activities depend upon the phosphorylation of eif6 Serine 235 by protein kinase C (PKC). Eif6-60S is probably part of the RNA-induced silencing complex (RISC). *eif6* over-expression in *Xenopus* embryos causes aberrant eye development. *kermit2/gipc2* morphants have an eye phenotype similar to that of the *eif6* over-expressors. Eye formation is regulated by insulin growth factor (IGF) signalling. *eif6* interacts with the IGF receptor (IGFR) and *kermit2/gipc2*, which also binds to *igfr*. *eif6* over-expression in *Xenopus* causes also the formation of antero-ventral oedema, suggesting a malfunction of the excretory system. Here we evaluated the pronephros phenotype. The oedema grows into the nephrocoel, expanding its boundary and is accompanied by a strong reduction of the pronephros. The three main components of the pronephros are severely impaired in *eif6* over-expressors, while are not affected in *eif6* morphants. Conversely, *gipc2* depletion induces the oedema phenotype and reduction of the pronephros, while *gipc2* overexpression does not. p110*, a constitutively active p110 subunit of the PI3 kinase partially recovers the oedema phenotype. We also determined that PKC-dependent phosphorylation of Ser235 in *eif6* is not required to produce defective pronephroi. These results indicate that the levels of *eif6* are highly regulated during development and instrumental for proper morphogenesis of the pronephros. Moreover, it appears that for proper pronephros development the *gipc2* level should be kept within or over the physiological range and that the oedema phenotype is partly due to the inhibition of IGF signalling.

KEY WORDS: *pronephros*, *Xenopus laevis*, eukaryotic initiation factor 6, *kermit2/gipc2*

Eif6 (eukaryotic initiation factor 6) is a protein essential for cell survival that plays important roles in ribosome biogenesis and translation (see Ceci *et al.*, 2003). In particular, it is associated with the plasma membrane where it interacts with $\beta 4$ integrin as well as the cytoskeleton (Biffo *et al.*, 1997). Eif6 can be regulated by extracellular signals, such as IGF (Gandin *et al.*, 2008), and is itself a regulator of translation at the 60S ribosomal subunit. When unphosphorylated, it impedes the joining of the 60S with the 40S ribosomal subunit. When phosphorylated by PKC, Eif6 separates from the 60S subunit. As a consequence, ribosomal subunits 60S and 40S may join, allowing mRNA translation to occur (Ceci *et al.*, 2003). Eif6-60S is probably part of the RISC (RNA-induced silencing complex) and as such may regulate the availability of mRNAs for translation (Chendrimada *et al.*, 2007). Because EIF6 appears to act selectively on specific mRNAs (Ji

et al., 2008; De Marco *et al.*, 2010), the study of this protein in embryogenesis is quite appealing because it may help to explain steps of anlagen determination or differentiation.

We previously showed that, in *Xenopus laevis*, *eif6* is a factor regulating apoptosis upstream of *bcl-2/bax* (De Marco *et al.*, 2010). Moreover, *eif6* over-expression causes a delay in eye develop-

Abbreviations used in this paper: Akt, serine/threonine-protein kinase; β gal, β -galactosidase; *Clenk*, chloride channel Kb; *cdh16*, human cadherin-16; Eif6¹, eukaryotic initiation factor 6; IGF, insulin growth factor; *Igfr*, insulin growth factor receptor; *gipc2*, GAIIP interacting protein, C terminus; *tlx1*, LIM homeobox 1; miR, microRNA; *myod1*, myogenic differentiation 1; *nplh1*, nephrin; p110*, protein 110 (subunit of the PI3 kinase); pi3/kinase, phosphatidylinositol 3-kinase; RISC, RNA-induced silencing complex; S235A, *eif6* mutated in serine 235; *slc5a9*, solute carrier family 5 (sodium/glucose cotransporter), member 9.

*Address correspondence to: Nadia De Marco, Department of Structural and Functional Biology, University of Naples Federico II, Naples, Italy. Tel: +39-081-679189. Fax: +39-081-679233. e-mail: nademarc@unina.it

Note 1: We use official names (www.ncbi.nlm.nih.gov/sites/gquery) for each gene or protein according to the species to which they refer.

Accepted: 24 April 2012. Final, author-corrected PDF published online: 21 May 2012.

ment, evident at stage 35, independent of the *eif6*-regulated apoptosis. Analyses of *eif6* over-expressors and morphants led to the conclusion that eye morphogenesis is achieved only at a tightly regulated level of *eif6* (De Marco *et al.*, 2011). In *Xenopus*, eye formation is regulated by *igf* signalling (Pera *et al.*, 2001; Wu *et al.*, 2006), and *eif6* is able to modulate the translation of specific mRNA upon stimulation of growth factors such as *Igf* (Gandin *et al.*, 2008). Recently, it was found that *eif6* interacts with *igf* receptor (*igfr*) and *kermit2/gipc2* (GAIP interacting protein, C terminus) (Wu *et al.*, 2006; De Marco *et al.*, in preparation), which also binds to *igfr* (Booth *et al.*, 2002). *gipc2* morphants have an eye phenotype similar to that of the *eif6* gain-of-function embryos (Wu *et al.*, 2006; De Marco *et al.*, in preparation). It should be mentioned that the *gipc2* protein is a powerful modulator of signals as it interacts not only with *igfr* but also with a variety of molecules implicated in cell signalling, such as semaphorins-F

and 4C (Wang *et al.*, 1999), and integrins (Spicer *et al.*, 2010) (see Wu *et al.*, 2006, for detailed references).

In addition to the above-mentioned effects, *eif6* over-expression in *Xenopus* causes the formation of antero-ventral oedema, suggesting a malfunction of the excretory system. Importantly, Wu *et al.*, (2006) showed that a *gipc2* riboprobe labels *X. laevis* pronephroi, where *igfr* is expressed as well (Groigno *et al.*, 1999). The connections existing between *eif6* and *gipc2* prompted us to investigate whether these two proteins have a role in the pronephros formation, highlighting the interesting possibility that they act along the *igf* pathway.

The pronephros is the embryonic kidney, present and fully functional in amphibian tadpoles. It originates mostly from the intermediate mesoderm. At metamorphosis, the pronephros regresses, and its function is replaced by the adult mesonephros. Importantly, as many events regulating pronephros induction, patterning and differentiation have been revealed, it is now evident that the genetic programs underlying pronephros formation are conserved across evolution, being similarly present in the kidneys of higher vertebrates (Vize *et al.*, 1997; Jones, 2005). *Xenopus* pronephros is composed of the pronephric corpuscle, with the glomus as the filtration unit, the pronephric tubules and the pronephric duct. The filtration chamber of the pronephros is the nephrocoel, initially contiguous to the coelom. Later, the nephrocoel and the coelom will separate into two distinct cavities. Splanchnic mesoderm surrounds the glomus (Vize *et al.*, 1997). Convoluted pronephric tubules are composed of ciliated nephrostomes and connecting tubules linked to a common tubule which joins the pronephric duct. The first histological indication of pronephric development occurs around stage 21 when cells begin to condense away from the intermediate mesoderm below somites 3 to 5. These cells will form the main body of the pronephros. At about the same time, below somites 5 to 7, a similar cellular condensation occurs that will give rise to the pronephric duct. The primordia of these two structures fuse, and the body of the pronephros forms a lumen.

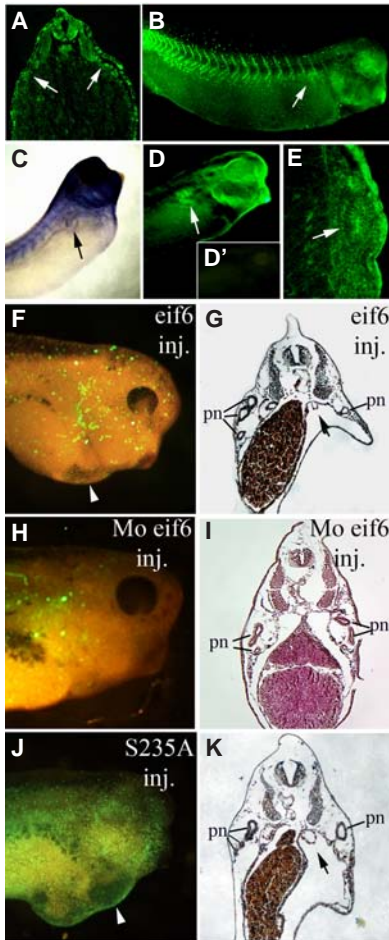


Fig. 1. The pronephros phenotype in *eif6* overexpressors. (A-E) *eif6* mRNA and protein are expressed in the pronephros (arrows) of stages 24, 32 and 38 *Xenopus laevis* embryos. (A,B) Immunofluorescence using anti-*Eif6* antibody of section (A) or whole mount (B) of respectively stage 24 and stage 32 embryos indicating that *eif6* is present in the pronephros as well as in most tissues; the arrows indicate the pronephros Anlagen. (C) Whole mount in situ hybridisation using *eif6* antisense probe (stage 38). (D,E) Immunofluorescence with anti-*Eif6* antibody of whole mounts (D) or sections (E) of stage 38 embryo. (D') Whole mount immunofluorescence using only secondary antibody BODIPY-conjugates as negative control. Staining is absent. (F) Oedema formation (arrowhead) is present in embryos injected with 400 pg of *eif6* and 300 pg of GFP into one blastomere at the two-cell stage and harvested at stage 38. (G) Histology with haematoxylin and eosin on the embryonic sections showed in (F). A reduction of pronephric tubules is evident. The arrow indicates that the glomus is not surrounded by the splanchnic mesoderm, as the oedema has grown in the nephrocoel, expanding the splanchnic mesoderm boundary (see also K). (H) A stage 38 embryo injected with *eif6* morpholino: there is no oedema. (I) A section of the same embryo stained with haematoxylin and eosin. *eif6* depletion did not produce oedema. (J,K) Embryos injected with 400 pg of S235A and 300 pg of GFP show the oedema (arrowhead). (J) The pronephric reduction is evident in the histological section of embryo shown in (K). The arrow indicates that the glomus is not surrounded by the splanchnic mesoderm. pn, pronephros.

In this study, we found that the oedema phenotype is present in *eif6* over-expressors and *gipc2* morphants and is due to a defect of the pronephros. Indeed, *in situ* hybridisation showed that the three main components of the pronephros are severely impaired in *eif6* over-expressors, while in *eif6* morphants the oedema is absent. Conversely, *gipc2* depletion induces the oedema phenotype and *gipc2* gain-of-function has no effect on the pronephros. A constitutively active p110 subunit (p110*) of the PI3 kinase partially recovers the oedema phenotype, suggesting that the oedema is at least partly due to the inhibition of the igf signalling. Therefore, the interplay between *igf*, *eif6* and *gipc2* appears to be relevant during pronephric development.

Results

The pronephros phenotype in *eif6* gain-of-function and *gipc2* loss-of-function embryos

Anti-*eif6* immunostaining shows the pronephric anlagen in stage 24 and 32 embryos (Figs. 1A-B). The pronephros of stage 38 embryos is marked by *eif6* riboprobe in *eif6* whole mount *in situ* hybridisation, (Fig. 1C, and see Vaccaro *et al.*, 2006) as well as by anti-*eif6* immunostaining (Fig 1D,D',E). It should be observed that *eif6* is present in most tissues at various level in agreement with previous data (Biffo *et al.*, 1997; Vaccaro *et al.*, 2006) (Figs. 1). Overall, 65% of the embryos injected with *eif6* (400 pg; n=91) displayed oedema in the antero-ventral region, a condition often caused by impaired osmoregulatory function of the pronephros. Indeed, upon sectioning, we found a strong reduction of the pronephric tubules in the injected side. Moreover, in contrast to the uninjected side, the splanchnic mesoderm delineating the nephrocoel does not surround the glomus. The oedema grew into the nephrocoel, expanding its boundary (Figs. 1F,G). The *eif6* morpholino does not cause oedema. Accordingly, in *eif6* loss-of-function embryos, the pronephros of the injected side was not affected (Figs. 1H,I).

Previous data showed that, in *X. laevis*, PKC-dependent phosphorylation of Ser235 is necessary for regulating both translation and the anti-apoptotic activities of *eif6*, but it is not

required for proper eye development (De Marco *et al.*, 2010). Here, by injecting the mutated form of *eif6*, S235A, the oedema and pronephric reduction are present as well (Figs. 1J,K), indicating that phosphorylation of Ser235 in *eif6* is not required to produce defective pronephros development. Therefore, the aberrant kidney phenotype produced by *eif6* over-expression is not directly linked to the PKC-regulated effects on translation and ribosomal subunit interaction. This finding is similar to what we have found for the eye phenotype in *eif6* over-expressors (De Marco *et al.*, 2011). As *gipc2* depletion leads to an eye defect similar to *eif6* over-expression (Wu *et al.*, 2006; Marco *et al.*, 2011), we investigated the involvement of *gipc2* in the pronephros phenotype. We injected *gipc2*-morpholino (40 pg, n=82) and found that in 65% of the morphants, oedema develops similar to the oedema found in *eif6* over-expressors but not in the embryos injected with *gipc2* mismatch-morpholino (Fig. 2). The phenotype appears at stage 32, when the pronephros starts functioning, and is particularly evident at stage 38 in both *gipc2* morphants and in *eif6* over-expressors (Fig. 2). It should be mentioned that *gipc2* over-expressors do not display oedemas (data not shown and see Wu *et al.*, 2006).

***eif6* over-expression and *gipc2* depletion affect pronephros markers**

The primordia of the pronephros starts forming at stage 21 (see Vize *et al.*, 1997). Whole mount *in situ* hybridisation of stage 22 *eif6* over-expressors using *lhx1*, an early marker of the pronephros anlagen (Agrawal *et al.*, 2009) was performed. Staining shows that the pronephric anlagen of the injected side is markedly less extended with respect to the contra-lateral uninjected side (70% n=60) (Fig. 3A,B). It should be noted that, according to Wu *et al.*, (2006), although the pronephros is not marked by *gipc2* *in situ* hybridisation before stage 33, *gipc2* is maternally detected and expressed throughout early development. At stage 22 of *gipc2* morphants, the injected side shows little evidence of the pronephric anlagen (66% n=60) (Fig. 3C). Previous data showed that the *gipc2* morpholino phenotype can be rescued by coinjection of *gipc2* RNA lacking the morpholino

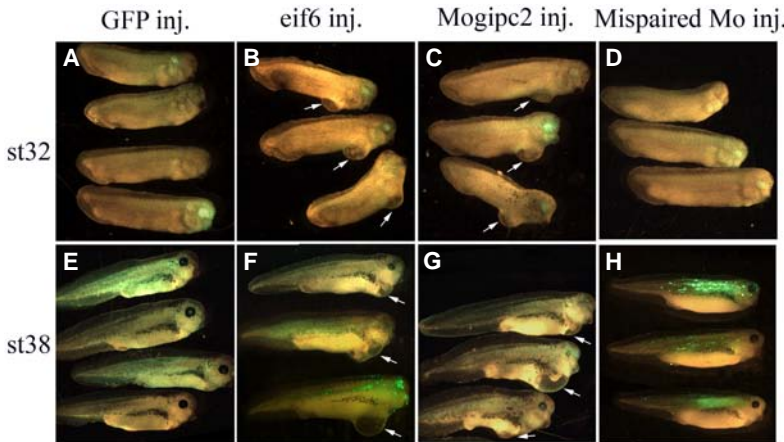
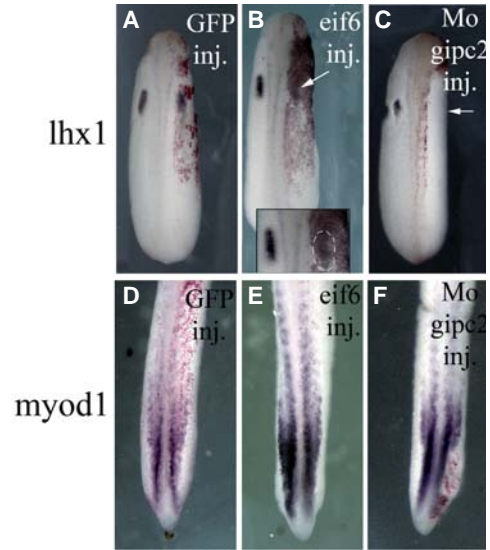


Fig. 2. Oedema phenotype in *eif6* overexpressors and in *gipc2* loss-of-function embryos. (A-D) Stage 32 and stage 38 embryos (E-H) injected into one blastomere at the two-cell stage with 400 pg of GFP alone (A,E), 400 pg of *eif6* and 300 pg of GFP (B,F), 40 ng of *gipc2* morpholino and 300 pg of GFP (C,G) or 40 ng of *gipc2* mismatched morpholino and 300 pg of GFP (D,H). In the *eif6* over-expressors (B,F) and *gipc2* morphants (C,G), the oedema phenotype (arrow) appears at stage 32 and increases at stage 38.

Fig. 3. *eif6* over-expression and *gipc* depletion affect *lhx1* expression. Embryos injected into one blastomere at the two-cell stage with GFP (A,D), *eif6* (B,E) and *gipc2* morpholino (C,F). β gal mRNA was co-injected for tracing lineage (stained red). (A-C) Embryos were cultured until stage 22 and whole mount *in situ* hybridised for expression of *lhx1*, an early marker of the pronephric anlagen. Injection of the GFP alone had no effect on *lhx1* expression (A). *eif6* over-expression (B) and *gipc2* depletion (C) inhibited most pronephric anlagen formation (arrow). The white lines in the inset of (B) surround the reduced pronephric anlagen. (D-F) Embryos were cultured until stage 25-26 and whole mount *in situ* hybridised for expression of *myod1*, a marker of differentiating muscle. No difference in the *myod1* expression pattern was found in the *eif6* over-expressors (E) and *gipc2* morphants (F).



target sequence (Wu et al., 2006). This phenotype is not related to the closely positioned paraxial mesoderm. Indeed, embryos fixed at stage 25/26 and hybridised with *myod1*, have identical hybridisation patterns in the injected and uninjected side, both in the case of *eif6* over-expressors (n=50) and *gipc2* morphants (n=50) (Figs. 3D-F).

The pronephros is organised along its proximal-distal axis in a manner that is highly similar to the metanephric nephron, thus allowing the use of molecular markers of metanephric terminal differentiation for the identification of various segments (Zhou and Vize, 2004). By using nephrin (*nphs1*) as marker of the glomus (see Jones, 2005), it can be seen that at stage 38 the glomus of the injected side appears reduced when compared to the uninjected side in *eif6* over-expressors (78% n=70) (Figs. 4B,B') and *gipc2* morphants (78% n=60) (Figs. 4C,C'). The proximal tubule marker *slc5a9* (Zhou and Vize, 2004) shows that this region is partially affected by *eif6* over-expression (Figs. 4E,E') (60% n=70) as well as by *gipc2* depletion (62% n=70) (Figs. 4F,F'). Whole mount *in situ* hybridisation was performed using a *clcnkb* or *cdh16* riboprobe, both markers of intermediate and distal tubules and the duct. In

eif6 over-expressors, the pronephric anlagen of the injected side is markedly less developed with respect to the counter-lateral uninjected side (81% both *clcnkb* n=65 and *cdh16* n=70) (Figs. 4H,H',K,K'). Very similar hybridisation patterns are obtained in the injected side of *gipc2* morphants (Fig. 4I,I',L,L').

It is known that *eif6* interacts with *igr* and *gipc2* and that *gipc2* binds to *igr*, leading to the activation of the tyrosine kinase pi3/akt kinase pathway (Wu et al., 2006; De Marco et al., in prepara-

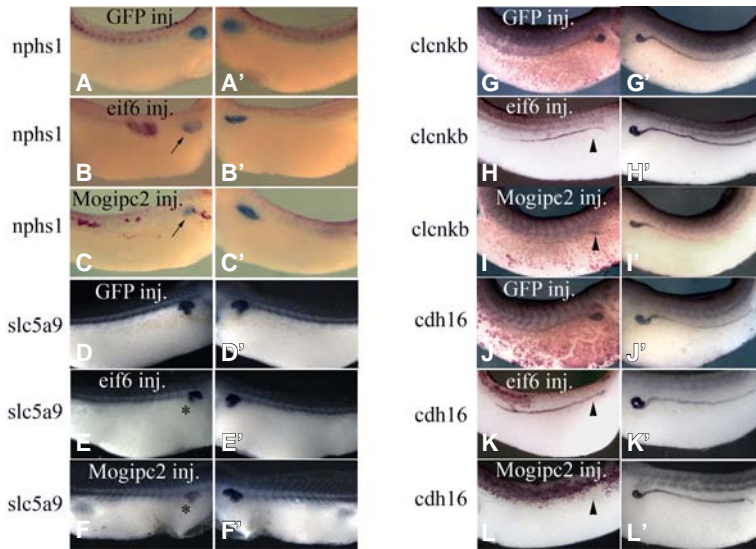


Fig. 4. Whole mount *in situ* hybridisation for markers of terminal pronephros differentiation. Stage 38 embryos injected with GFP alone (A,D,G,J), *eif6* (B,E,H,K) or *gipc2* morpholino (C,F,I,L). Micrographs of the two sides of the same embryos are shown (A,A', B,B', etc.). Co-injection of (D-F) GFP mRNA as tracer, and (G-I) β gal mRNA (stained red). It should be observed that the red stained tissue distributed in the most superficial tissues is often partially removed during manipulation. The glomus, (arrow) marked by nephrin; proximal tubule (asterisk), marked by *slc5a9*; intermediate and distal tubule domain (arrowhead), marked by *clcnkb* and *cdh16*, respectively, were reduced in *eif6* over-expressors and in *gipc2* morphants.

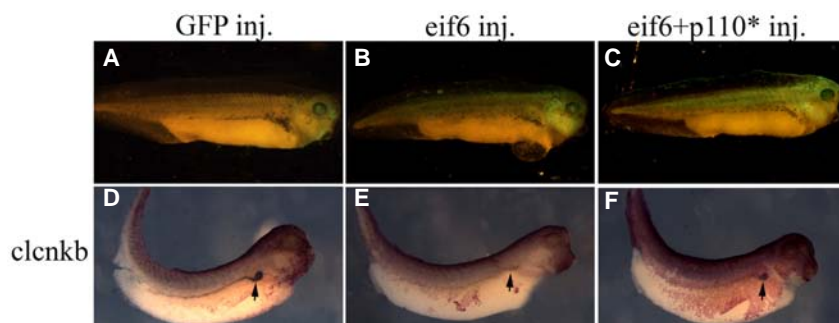


Fig. 5. p110* partially recovers the phenotype in eif6 overexpressors. (A-F) Stage 38 embryos injected into one blastomere at the two-cell stage with 400 pg of GFP only (A,D), 400 pg of eif6 and 300 pg of GFP (B,E), or 400 pg of eif6, 300 pg of GFP and 1 ng of p110* (C,F). (D-F) Whole mount in situ hybridisation for *clcnkb*, an intermediate and distal tubule marker (arrow). p110* partially recovers the oedema phenotype (C) and *clcnkb* expression (F).

ration). To investigate whether the pronephric defect from eif6 over-expression is related to a decrease in akt phosphorylation/activation, we used a constitutively active p110 subunit (p110*) of the pi3 kinase, which is upstream of akt and downstream of igf1r. Indeed, when we coinjected embryos with eif6 and p110* and compared to eif6 over-expressors, a partial rescue of the oedema phenotype and *clcnkb* marker expression was obtained (72% n=60) (Fig 5). Thus, p110* partially recovers the oedema phenotype, suggesting that this phenotype is at least partly due to the inhibition of the pi3 kinase/akt pathway.

Discussion

In conclusion, our results indicate that in *Xenopus* eif6 over-expression produces an aberrant kidney phenotype that is not directly linked to the pkc-regulated effects of eif6 on translation and ribosomal subunit interaction. This finding is in contrast to eif6 anti-apoptotic function and to the translation of *b-catenin* that require the conserved S235 in *Xenopus* embryogenesis (De Marco *et al.*, 2010, 2011). Our data suggest that eif6 regulates *gipc2* levels in *Xenopus* embryogenesis through a different mechanism. In fact, for the kidney phenotype, eif6 may act through RISC (Chendrimada *et al.*, 2007; De Marco *et al.*, 2011) down-regulating *gipc2* translation. Indeed, analyses of the 3'UTR of *gipc2* through the miRBase (www.mirbase.org) and miRanda (www.microrna.org) programs depict binding sites for miRNAs implicated in kidney and eye development. Examples of miRNA regulation include the following: the miR-30 family (Agrawal *et al.*, 2009), which appears to regulate *Xenopus* pronephros development; miR467e*, which is implicated in eye development of the mouse (Karali *et al.*, 2010); and miR-532-5p, which is involved in kidney cancer and human retinoblastoma (Hoon and Kitago, 2010).

In embryos injected with eif6 morpholino, the pronephros does not differ from that of w.t. embryos, leading us to speculate that the levels of eif6 are highly regulated during development and instrumental for proper morphogenesis of the pronephros. This finding is in agreement with previous data on eif6 activity in eye development (De Marco *et al.*, 2011). On the other hand, this result also suggests that *gipc2* expression beyond threshold levels is necessary for pronephric formation.

Is igf signalling involved in the pronephric formation? *gipc2* binds to igf and is involved in the maintenance of igf/pi3k/akt stimuli. Embryos coinjected with *gipc2* morpholino and p110* partially recover the defective eye phenotype of *gipc2* morphants (Wu *et al.*, 2006).

This finding is in agreement with our findings showing a partial rescue of the pronephric defect upon coinjection of eif6 and p110*. In *Xenopus*, igf (Groigno *et al.*, 1999) as well as the adaptor proteins of the igf substrate family (IRS-1 family) are expressed in the pronephros. However, it has not been determined whether IRS-1 acts through the pi3k/akt pathway. Because two organs, the eye and pronephros, are regulated by eif6 and *gipc2* (this paper and De Marco *et al.*, in preparation), the question can be raised as to whether any other anlagen development is also dependent upon the interaction of these two molecules. Comparing the major expression patterns of *gipc2* and eif6 suggests that this could be the case (Vaccaro *et al.*, 2006; Wu *et al.*, 2006). Further studies should establish the functionality of these colocalisations and whether eif6 and *gipc2* interactions are required for igf signalling. As the *gipc2* protein is a potential interactor not only of igf but also of a variety of molecules implicated in cell signalling, we hypothesise that during *Xenopus* embryogenesis the eif6/*gipc2* partnership is a crucial step for anlagen development. In fact, eif6 may regulate the *gipc2* levels, consequently leading to organ-specific downstream-signalling events.

Materials and Methods

Animals

Adult *Xenopus laevis* females were obtained from Nasco (Fort Atkinson, Wisconsin, USA). They were kept and utilised at the Department of Structural and Functional Biology of the University of Naples, Federico II, according to the guidelines and policies dictated by the University Animal Welfare Office and in agreement with international rules. To obtain eggs, *X. laevis* females were injected in the dorsal lymphatic sac with 500 units of Gonase (AMSA) in amphibian Ringer's solution (111 mM NaCl, 1.3 mM CaCl₂, 2 mM KCl, 0.8 mM MgSO₄, and 25 mM Hepes, pH 7.8). Fertilised eggs and embryos were obtained by standard insemination methods (see De Marco *et al.*, 2010) and staged according to Nieuwkoop and Faber.

Microinjections

The pCS2eif6 and pCS2S235A plasmids were used as described in De Marco *et al.*, (2010). The pCS2p110* plasmid was a generous gift of Laurent Kodjabachian (Université de la Méditerranée, France). The pCS2p1gal was kindly supplied by M. Ori (University of Pisa, Italy). Capped synthetic RNAs were generated by *in vitro* transcription using the Sp6 Message Machine kit (Ambion, Austin, TX, USA). *gipc2* antisense morpholino (5'-AGAGGCATCTTTCTTCAGCGAAGG-3'), eif6 antisense morpholino (5'-GCGGACCGCCATGTTGCGCTTCTTAG-3') and the mismatched morpholino control (5'-GCGGACCGCCATcTTGcCTTcTaAG-3') were purchased from Gene Tools LLC, Philomath, OR, USA. pCS2MTGFP or

pCS2 β gal mRNA was always co-injected to label the injected side. RNAs were injected into the animal hemisphere of a single cell of one- or two-cell embryos using a Drummond 'Nanoject' apparatus. During injection, embryos were cultured in 3% Ficoll in 0.1% Ringer. The phenotype of the injected embryos was scored when the uninjected embryos reached stage 32 or 38. The samples were photographed with a Leica MZ16F UV stereomicroscope, equipped with a Leica DFC 300F camera and IM50 image manager software.

Immunofluorescence and histology

X. laevis embryos were fixed in 4% formaldehyde at 4°C and stored in 100% MetOH at -20°C. For *in toto* immunofluorescence, the samples were incubated in hydrogen peroxide/methanol 1:2 (v/v) for about 2 days, then incubated with rabbit anti-Eif6 antibody (a gift of PC Marchisio and S. Biffo, DIBIT, Milan, Italy) diluted 1:500 in PBS/0.5%BSA/0.1% Triton X-100. The secondary antibody was goat anti-rabbit IgG BODIPY FL conjugated (Molecular Probes). Next, the embryos were dehydrated in graded methanol and cleared in benzyl alcohol/benzyl benzoate 1:2 (v/v). Whole mounts were photographed with a Leica MZ 16F. Frozen 10 μ m-thick sections were obtained after embedding and freezing in Killik (Bio Optica). For histology, sections were stained with haematoxylin and eosin. For immunofluorescence, non-specific background was blocked by incubating the sections for 30 min in normal goat serum, 3% in PBS/0.5% BSA/0.1% Tween, prior to exposure O/N at 4°C to rabbit anti-Eif6 (generous gift of P.C. Marchisio and S. Biffo, DIBIT, Milan, Italy) diluted 1:500 in PBS/0.5% BSA/0.1% Tween. Staining was completed by incubating the samples with anti-rabbit goat IgG BODIPY FL-conjugated (Molecular Probes) and mounting in PBS/glycerol (9:1, v/v). Sections were observed and photographed with a Leica CTR 6500 UV microscope equipped with the Leica application suite.

In situ hybridisation

In situ hybridisation was performed as described previously (Vaccaro et al., 2006). Antisense digoxigenin-labelled RNA probes of *lhx1*, *myod1* (a gift from M. Ori, University of Pisa, Italy) *slc5a9*, *clcnkb*, *cdh16* (generously supplied by O. Wessely, LSU, New Orleans, USA) and *nphs1* (courtesy of European *Xenopus* Resource Centre, University of Portsmouth) were synthesised with RNA T7 or SP6 polymerases (Roche, Mannheim, Germany). β -galactosidase activity was visualised in embryos with Red-Gal (Biosynth, Staad, Switzerland). Sections were observed and photographed using a Leica 6500 microscope. Whole mounts were photographed with a Leica MZ16F.

Acknowledgments

We thank S. Biffo for suggestions, Valentina Magnin and Valentina Abete for laboratory assistance. The research was funded by a grant from the Compagnia di San Paolo ('Integration of spatial and biochemical clues during brain development' Project) to C.C. We thank AMRA Scarl for the use of AMRA instruments. We apologize for work not cited in this article due to an upper limit on the permitted number of citations.

References

AGRAWAL R, TRAN U, WESSELY O (2009). The miR-30 miRNA family regulates *Xenopus* pronephros development and targets the transcription factor *Xlim1*

Lhx1. *Develop.* 136: 3927-3936.

- BIFFO S, SANVITO F, COSTAGEA S, PREVE L, PIGNATELLI R, SPINARDI L, MARCHISIO PC (1997). Isolation of a Novel I4 Integrin Binding Protein (p27BBP) Highly Expressed in Epithelial Cells. *J. Biol. Chem.* 272: 30314-30321.
- BOOTH RA, CUMMINGS C, TIBERI M, LIU XJ (2002). GIPC participates in G protein signaling downstream of insulin-like growth factor 1 receptor. *J. Biol. Chem.* 277: 6719-6725.
- CECI M, GAVIRAGHI C, GORRINI C, SALA LA, OFFENHAUSER N, MARCHISIO PC, BIFFO S (2003). Release of eIF6 (p27^{BBP}) from the 60S subunit allows 80S ribosome assembly. *Nature* 426: 579-584.
- CHENDRIMADA T, FINN KJ, JI X, BAILLAT D, GREGORY RI, LIEBHABER SA, PASQUINELLI AE, SHIEKHATTAR R (2007). MicroRNA silencing through RISC recruitment of eif6. *Nature* 447: 823-828.
- DE MARCO N, IANNONE L, CAROTENUTO R, BIFFO S, VITALE A, CAMPANELLA C (2010). p27(BBP)/eIF6 acts as an anti-apoptotic factor upstream of Bcl-2 during *Xenopus laevis* development. *Cell Death Differ.* 17: 360-372.
- DE MARCO N, TUSSELLINO M, VITALE A, CAMPANELLA C (2011). Eukaryotic initiation factor 6 (eif6) over-expression affects eye development in *Xenopus laevis*. *Diff.* 82: 108-115.
- GANDIN V, MILUZIO A, BARBIERI A, MAGRI L, KIYOKAWA H, MARCHISIO PC, BIFFO S (2008). eIF6 is rate limiting for translation, growth and transformation. *Nature* 455: 684-688.
- GROIGNO L, RICHARD-PARPAILLON L, BOUJARD D (1999). Expression pattern of insulin receptor mRNA during *Xenopus laevis* embryogenesis. *Mech. of Dev.* 86: 151-154.
- HOON D S, KITAGO M (2010). Use of miR-532-5p as cancer markers and therapeutic targets. *United States Patent Application Publication No.* US2011/0158975 A1.
- JI Y, SHAH S, SOANES K, ISLAM MN, HOXTER B, BIFFO S, HESLIP T, BYERS S (2008). Eukaryotic initiation factor 6 selectively regulates Wnt signalling and β -catenin protein synthesis. *Oncogene* 27: 755-762.
- JONES EA (2005). *Xenopus*: A Prince among models for pronephric kidney development. *J. Am. Soc. Nephrol.* 16: 313-321.
- KARALI M, PELUSO I, GENNARINO VA, BILIO M, VERDE R, LAGO G, DOLLÉ P, BANFI S (2010). miRNeye: a microRNA expression atlas of the mouse eye. *BMC Genomics* 11: 715.
- PERA EM, LI, WESSELY, O, LI SY AND DE ROBERTIS EM (2001). Neural and head induction by insulin-like growth factor signals. *Dev. Cell.* 1: 655-665.
- SPICER E, SUCKERT C, AL-ATTAR H, MARSDEN M (2010). Integrin alpha5beta1 function is regulated by XGIPC/kermi2 mediated endocytosis during *Xenopus laevis* gastrulation. *PLoS One* 5, e10665.
- VACCARO M, CUCCARO M, DE MARCO N, CAMPANELLA C (2006). Expression of p27BBP/eif6 is highly modulated during *Xenopus laevis* embryogenesis. *Mol Reprod Dev* 73: 482-490 Erratum in: *Mol Reprod Dev* (2006). 73: 1612.
- VIZE PD, SEUFERT DW, CARROLL TJ, WALLINGFORD JB (1997). Model systems for the study of kidney development: use of the pronephros in the analysis of organ induction and patterning. *Dev Biol* 188: 189-204.
- WANG LH, KALB RG, STRITTMATTER SM (1999) A PDZ protein regulates the distribution of the transmembrane semaphorin, M-SemF. *J. Biol. Chem.* 274: 14137-14146.
- WU J, O'DONNELL M, GITLER AD, KLEIN PS (2006). Kermit 2/XGIPC, an IGF1 receptor interacting protein, is required for IGF signaling in *Xenopus* eye development. *Development* 133: 3651-3660.
- ZHOU X, VIZE PD (2004). Proximo-distal specialization of epithelial transport processes within the *Xenopus* pronephric kidney tubules. *Dev. Biol.* 271: 322-338.

Final remarks

I often think of my past students. Their personalities and their work in my lab remain vivid in my memory. I remember their attitudes to tackling new work, solving problems and their readiness to admit mistakes or use observations to back up their learning, in such very different ways according to their personalities. I also remember their eyes while we were talking, or while they were learning for the first time the remarkable phenomena that occur during animal development. They taught me that a teacher should have a great sense of responsibility in education during the difficult transition from young adult to adult. This is the part of my academic life I miss and the reason I still think that learning, teaching and working in a lab at University is a great opportunity for teachers and students alike.

I would like to mention two people who were particularly important for me and for my work in Naples. Peppe Falcone was our department's photographer: in the old days of developing negatives, Peppe was able to work miracles with his exposure camera, and then develop and print photos. With his attitude towards his work and his ability to penetrate into the research of others, Peppe set an outstanding example of quality and dedication. He was quite attracted by digital techniques, and adopted them with so much ability that he became the top expert in this field at the University of Naples. When we were working together on images I had the chance to discuss many things related to life in general or to academia. He was a real master of life. He died suddenly one day in September. The day before we had worked together on an eif6 paper and he had sent me his last file: "All the work by Falcone".

Annamaria Cirillo was as beautiful as she was intelligent. She was taking care of the English style and grammar of our publications. Upon her arrival in department, responding to our impelling calls, she used to sit with her cigarette at the computer and immediately to scan with her intelligent green eyes the text in the screen. I remember in particular when I needed to review an important manuscript on August 3rd, a time during the summer recess when nobody was around in the Department and the conditioners were out of use. She came without a murmur and did a fantastic job. She used to concede from time to time breaks for the two of us at the computer. In these intervals she used to talk about her major interests: fighting for the rights of

people, and in particular, for Rom in Naples. She was one of the few entrusted with communicating with the local Rom, especially in matters concerning their health and children's education. She was adored by them and invited to their country of origin for a wedding. Annamaria told me about the joy, the colours, the music of that people on that occasion. One day she failed to turn up to a meeting we had. She had found out she was suffering from severe lung cancer, a tragedy for her and her family. I will never forget the way she hugged her daughters, while lying in bed, hoping to see them just a little more. A big piece of my heart is there, with Annamaria.

As a final remark, I would like to point out how delighted I am by the lack of boundaries in the scientific community. Every time I send an e-mail to a colleague, even if I do not know her or him personally, I receive prompt answers and quite often we exchange probes, antibodies and so on. To me it feels as natural as communicating with one's own brothers and sisters, which gives me the wonderful sense of the universality of knowledge.



Finito di stampare nel mese di settembre 2012
presso Officine Grafiche Francesco Giannini & Figli S.p.A. – Napoli